

Geological Survey of Canada Open File 5344

Mineral and Energy Resource Assessment of the Greater Nahanni Ecosystem Under Consideration for the Expansion of the Nahanni National Park Reserve, Northwest Territories

Edited by D.F. Wright, D. Lemkow, and J.R. Harris

2007



Natural Resources Canada Ressources naturelles Canada

Canada

Geological Survey of Canada
Open File 5344

MINERAL AND ENERGY RESOURCE ASSESSMENT OF THE GREATER NAHANNI ECOSYSTEM UNDER CONSIDERATION FOR THE EXPANSION OF THE NAHANNI NATIONAL PARK RESERVE, NORTHWEST TERRITORIES

D. F. Wright, D. Lemkow, and J. R. Harris

Geological Survey of Canada, Earth Sciences Sector, 601 Booth Street, Ottawa, Ontario K1A 0E8

D. F. Wright, D. Lemkow, and J. R. Harris
2007: Mineral and Energy Resource Assessment of the Greater Nahanni Ecosystem Under Consideration for the Expansion of the Nahanni National Park Reserve, Northwest Territories; Geological Survey of Canada, Open File 5344, 1 DVD.

Open files are products that have not gone through the Geological Survey of Canada's formal publication process.

Cover illustration
Stream sediment sampling in the Greater Nahanni Ecosystem, courtesy of the Geological Survey of Canada

©Her Majesty the Queen in Right of Canada 2007
Available from:
Geological Survey of Canada
601 Booth Street
Ottawa, Ontario K1A 0E8

TABLE OF CONTENTS

Executive Summary

D.F. Wright, J.R. Harris, D. Lemkow, and H. Falck 1

Introduction . . . . .

Study Area . . . . .

Mineral and Energy Resource Assessment (MERA 2) Results . . . . .

Introduction

H. Falck, D. Lemkow, D.F. Wright, and J.R. Harris, ... 7

History of the Nahanni MERA Process 7

The National MERA Process and Methodology 8

Physiography of the MERA 2 Study Area 10

Regional Geology 11

MERA 2 Fieldwork and Data Synthesis 11

Organization of this Report and Responsibilities of the Authors 23

Acknowledgments 24

References 25

PART 1

REGIONAL STUDIES

Spring Geochemistry: A Tool for Mineral Exploration in the South Nahanni River Basin of the Mackenzie Mountains, Northwest Territories

Marie-Eve Caron, Stephen E. Grasby, and M. Cathryn Ryan

Abstract 31

Introduction 31

Geological Setting 31

Hydrogeochemical Exploration Background 34

Methods 35

Results and Discussion 39

Conclusions 46

Acknowledgements 47

References 47

Appendix 1. Description of bedrock geology from which MERA 2 springs discharge. 51

Appendix 2. Field parameters from MERA 2 springs. 52

Appendix 3. Major ions from spring waters. 54

Appendix 4. Trace elements from the MERA 1 and 2 samples. 56

Appendix 5. Isotopes of MERA 2 samples. 68

Appendix 6. Number of times springs were sampled for MERA 1 and 2. 70

Appendix 7. Summary of anomalous springs for MERA 1 and 2. 71

Appendix 8. Summary of MERA 2 spring sample numbers and names 74

Stream Sediment Geochemistry in the Proposed Extension to the Nahanni Park Reserve

M. W. McCurdy, R. J. McNeil, P. W. B. Friske, S. J. A. Day, and R. S. Wilson

Introduction 75

Physiographic and Ecological Features of the Study Area 75

Surficial Geology 75

Factors Affecting Geochemical Dispersion 76

Sample Collection and Analytical Techniques 77

Presentation of Data 78

Discussion 92

Acknowledgements 92

References 92

Appendix 1. Sample collection, analytical techniques, and laboratories 95

Evaluation of Airborne Radiometric and Magnetic Data in the Vicinity of Nahanni National Park, Northwest Territories, Canada

B. W. Charbonneau

Introduction 99
Geophysical Surveys 100
Comparison of Geophysics with Geology and Mineral Occurrences 101
Summary - All Survey Blocks 119
Acknowledgements 121
References 121

Quaternary Geology and Glacial Limits of the Nahanni National Park Reserve and Adjacent Areas, Northwest Territories, Canada

A. Duk-Rodkin, D. Huntley, and R. Smith

Quaternary Geology 125
Acknowledgments 129

PART 2

MINERAL DEPOSIT STUDIES

Isotope Geochemistry of the Prairie Creek Carbonate-Hosted Zinc-Lead-Silver Deposit, Southern Mackenzie Mountains, Northwest Territories

S. Paradis

Abstract 131
Introduction 132
Exploration and Mining History 132
Regional Geological Setting 134
Geology of the Prairie Creek Deposit Area 135
Mineralization 137
Isotope Geochemistry 143
Discussion and Synthesis 160
Acknowledgements 163
References 163
Appendix 1. Geological characteristics of the representative samples in the Prairie Creek area 167

Geochemical Investigation of High-Grade Quartz-Scheelite Veins of the Cantung Mine, Northwest Territories

Jason Yuvan, Kevin Shelton, and Hendrik Falck

Abstract 177
Introduction 177
Rationale for Study 178
Questions Addressed 178
Geology 179
Fluid Inclusions in Veins and Aplites 183
Oxygen Isotope Compositions of Veins and Aplites 187
Isotope Thermometry 188
Conceptual Model 188
Conclusions 188
References 189

A Review of the Late Cretaceous Little Nahanni Pegmatite Group and Associated Rare Element Mineralization in the Selwyn Basin Area, Northwest Territories

Elspeth M. Barnes, Lee A. Groat, and Hendrik Falck

Abstract 191
Introduction 191
Location 193
Previous Work 193
Geology 194

Structure 195
Characteristics of the Pegmatites 195
Whole Rock Geochemistry 196
Geochronology 197
Discussion 197
Conclusion 199
Acknowledgements 200
References 200

The Potential for Intrusion-Related Mineralization within the South Nahanni River MERA Area, Selwyn and Mackenzie Mountains, Northwest Territories

Kirsten L. Rasmussen, James K. Mortensen, Hendrik Falck, and Thomas D. Ullrich

Introduction 203
Field Observations 203
Geochronological, Geochemical, and Geophysical Classification of Plutonic Suites 210
Lead-Isotope Compositions of Intrusions and Mineral Occurrences 221
Metallogenic Considerations 223
Fluorine, Chlorine, and Sulphur Analysis of Igneous Apatite and Biotite 227
Summary of Intrusive Characteristics that are Favourable for Intrusion-Related Mineralization within the Nahanni MERA Area 233
Acknowledgements 237
References 237
Appendix 1. Mineral deposit types and styles present in the Nahanni MERA area 241
Appendix 2. Intrusive textures from polished and stained slabs for most of the intrusions in the Nahanni MERA area 245
Appendix 3. Analytical methods 262
Appendix 4. Apatite compositions for intrusions in the Nahanni MERA area 266
Appendix 5. Biotite compositions for intrusions in the Nahanni MERA area. 273

Radiogenic Isotope Studies of Pb-Zn Mineralization in the Howards Pass Area, Selwyn Basin

Brian L. Cousens

Introduction 279
Radiogenic Isotopes and Ore Deposits 280
Project Goals 280
Field Work and Laboratory Techniques 280
Study of Sediment Provenance using Sm-Nd Isotope Systematics 284
Study of the Roles of Seawater and Hydrothermal Fluids in Carbonate Formation 287
Pb Isotopic Composition of Sulphides and Host Rocks, Howards Pass 288
Summary 290
Acknowledgements 291
References 291

PART 3

MINERAL POTENTIAL MODELLING

Modelling Mineral Potential for the Greater Nahanni Ecosystem Using GIS-Based Analytical Methods

J.R. Harris, D. Lemkow, D.F. Wright, and H. Falck

Abstract 293
Introduction 293
Deposit Models 300
Applied Methodology 310
Final Model 316
Discussion and Summary 321
Acknowledgements 322
References 322

APPENDICES

Appendix 1. A review of the bed geology of the Nahanni River region and its context in the Northern Cordillera

H. Falck 327

Appendix 2. Morphological and compositional analysis of placer gold in the South Nahanni River drainage, Northwest Territories

K.L. Rasmussen, J.K. Mortensen, and H. Falck 367

Appendix 3. Spring geochemistry: A tool for mineral exploration in the South Nahanni River Basin, NWT

M-E. Caron 381

GIS Database

Appendix 4. Digital geoscience database: A contribution to the mineral and energy resource assessment of the Greater Nahanni Ecosystem, Northwest Territories

D. Lemkow, J.R. Harris, and T. Slack 549

EXECUTIVE SUMMARY

D.F. Wright[1], J.R. Harris[1], D. Lemkow[1], and H. Falck[2]
1. Geological Survey of Canada, 601 Booth Street, Ottawa, Ontario K1A 0E8
2. Northwest Territories Geoscience Office, P.O. Box 1500, Yellowknife, Northwest Territories X1A 2R3

INTRODUCTION

In October 2002, then Prime Minister Jean Chrétien and Heritage Minister Sheila Copps announced the "Action Plan to Protect Canada's Natural Heritage". The Action Plan recommended that by 2008 Parks Canada should establish ten new national parks and five new national marine conservation areas, in addition to expanding three national parks. Expansion and formalization of the Nahanni National Park was made a priority. Parks Canada commenced discussion with local aboriginal people and stakeholders, and by 2003 entered into a Memorandum of Understanding (MOU) with the Deh Cho First Nations (DCFN) to work cooperatively on studying the addition of lands to the park reserve and defining a new park boundary for amendment to the *Canada National Parks Act*.

In 2004 as part of the MOU, a Mineral and Energy Resource Assessment (MERA) feasibility study, as defined by federal government policy, was initiated by the Geological Survey of Canada, Natural Resources Canada. The purpose of MERA was to ensure that the economic and strategic significance of any mineral potential and non-renewable energy resources in the area be duly considered in the national park establishment process.

The Nahanni National Park Reserve (NNPR) was set aside under the *National Parks Act* in 1976; it predated and was therefore excluded from the MERA process. In 1983, three areas were proposed for the expansion of the NNPR: the Ragged Ranges, Tlogotsho Plateau, and the Nahanni Karst of the Ram Plateau. An initial Nahanni MERA (MERA 1, Fig. 1) was initiated with fieldwork and studies conducted by the Geological Survey of Canada between 1985 and 1987. The expansion process, however, was delayed for 15 years, with MERA 1 being completed and published in 2003. The 2003, MOU identified a possibly larger expansion study area, the Greater Nahanni Ecosystem, and thus a second Nahanni MERA (MERA 2) was initiated in 2004 to complement and expand upon MERA 1.

STUDY AREA

The Greater Nahanni Ecosystem MERA 2 study area covers over 39,000 km^2 of the South Nahanni River watershed in the Mackenzie Mountains in the southwestern corner of the Northwest Territories (Fig. 1). The area extends from the headwaters, beginning at the border of the Northwest Territories and Yukon in the Selwyn Mountains, to the Mackenzie Plain and Liard Basin, where the South Nahanni River flows into the Liard River.

The South Nahanni River crosses the structural grain of the eastern Selwyn Mountains and southern Mackenzie Mountains. These mountains expose mainly sedimentary rocks that, in very general terms, including Neoproterozoic (ca. 800 Ma) to Late Cretaceous (ca. 100 Ma) platformal to shale basin sedimentary strata. Older rocks were intruded by minor Devonian (35 Ma) granitoid rocks and all were folded and thrust faulted during the Jurassic (ca. 170 Ma) to Cretaceous collision of an island arc with western North America. During this collision, the Selwyn and westernmost Mackenzie Mountains were intruded by large Cretaceous granitoid batholiths. Comprehensive and right-lateral strike-slip adjustments continued throughout the Tertiary (ca. 40 Ma) to the present, as recent earthquakes in the Nahanni region demonstrate. This area was also the boundary region between mountain and continental glaciations, preserving an ice-free corridor during the last ice age.

MINERAL AND ENERGY RESOURCE ASSESSMENT (MERA 2) RESULTS

This MERA 2 report identifies approximately 12% of the entire study area as moderate to high in mineral potential, with restricted areas of very high potential. These conclusions are consistent with previously published, aerially or topically restricted resource assessments.

MERA 2 confirms and extends the areas that were identified in MERA 1 as having high or very high mineral resource potential. Although the hyrdocarbon resource potential published in MERA 1 was not formally re-evaluated for this study, the findings have been reaffirmed by recent research and industry results, and as such are incorporated into the final MERA 2 results.

Field surveys and laboratory studies for MERA 2 improved geological and geochemical knowledge and resolved uncertainties presented in MERA 1, thereby improving confidence and accuracy in the MERA 2

Wright, D.F., Harris, J.R., Lemkow, D., and Falck, H., 2007, Executive Summary, *in* Mineral and Energy Resource Assessment of the Greater Nahanni Ecosystem Under Consideration for the Expansion of the Nahanni National Park Reserve, Northwest Territories, (eds.) D.F. Wright, D. Lemkow, and J.R. Harris; Geological Survey of Canada, Open File 5344, p.1-6.

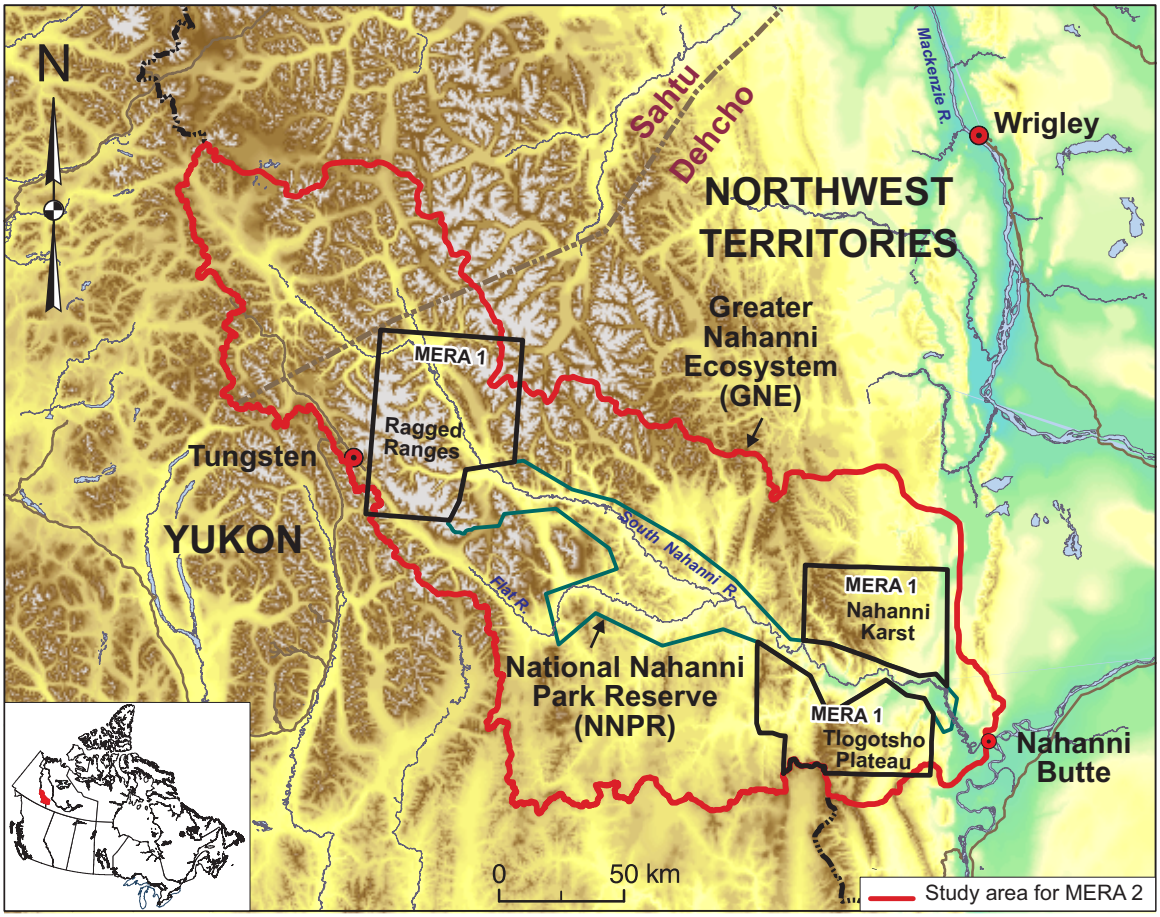


Figure 1. Index and regional geographic context of the Nahanni Mera 2 study area. The MERA 1 study areas are Nahanni Karst, Ragged Ranges, and the Tlogotsho Plateau.

geographical information system (GIS) calculations of regional mineral potential.

Various types of data were acquired for this resource assessment:

1) bedrock geology was updated and integrated,
2) mineral occurrences information was collected (ranging from showings to mined deposits; 40 sites were visited and 5 major deposit studies are included in this report),
3) combined airborne radiometric and magnetic surveys results (16,000 line kilometres were flown in three areas, which were chosen to help resolve potential boundary issues related to important mineral occurrences),
4) stream sediment and water geochemical survey data (2764 sediment and 2327 water samples were analyzed, with over 1500 of these being new samples), and
5) spring water geochemical survey analyses (79 new springs were sampled).

The newly collected and existing data were statistically and spatially analyzed using combined knowledge- and data-driven techniques, and were integrated in a GIS database to produce mineral-potential maps. Four potential maps were generated using four composite mineral deposit models, which were designed to represent most of the many mineral deposit types that are known to occur or are likely to be present in the MERA 2 study area.

1) SEDEX model (stratiform shale-hosted sedimentary-exhalative zinc-lead-silver) - the largest of several SEDEX occurrences in the area is the Howards Pass zinc-lead prospect.
2) 'Carbonate-fault' model (carbonate-hosted zinc-lead-silver associated with major faults) - based on the Prairie Creek advanced prospect.
3) 'Intrusion-related' model (mineralization, including skarn, rare metals and gemstones, associated with the Cretaceous plutons) - includes the world-class Cantung skarn tungsten mine and the Little Nahanni Pegmatite Group lithium prospect.
4) Carlin-type gold (lode and/or derived placer gold) - deposits of this type have not yet been found in the study area, but placer gold deposits with poly-

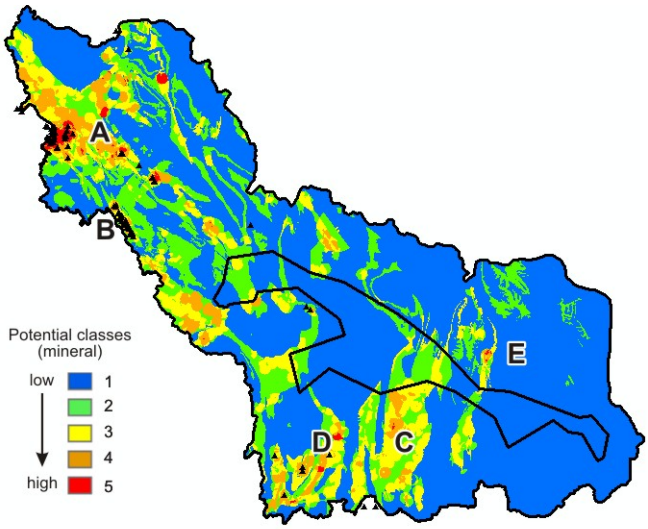


Figure 2. Simplified five-class SEDEX map that was incorporated in the final additive potential map (Fig. 6). The areas of highest potential are indicated by single unique capital letters and are explained in the text.

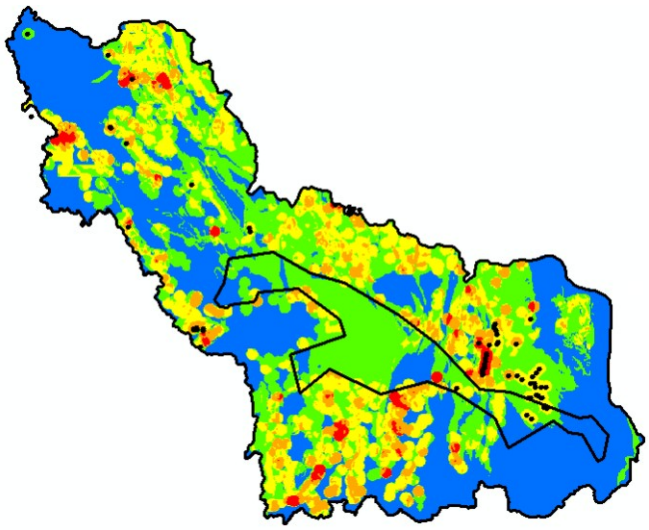


Figure 3. Simplified five-class carbonate-fault map that was incorporated in the final additive potential map (Fig. 6). The areas of highest potential are indicated by single unique capital letters and are explained in the text.

metallic signatures (eg. Selena Creek) are thought to be good indicators of its presence.

Twenty one areas with the highest assessed mineral potential are summarized by these deposit models; three areas of high potential for hydrocarbon are also noted:

SEDEX Model

Area A, in the northwest section of the study area, contains some of the Howards Pass deposits (Fig. 2). The high-potential area containing these deposits forms the northwest part of a southeast-northwest-trending linear zone within the study area, which is informally known as the 'zinc corridor'. This corridor extends from the northwest end of the existing park reserve and the Flat River Valley to the Howards Pass deposits.

Area B is a separate subparallel strand of this zinc corridor,, which contains a high-potential zone northwest of the Cantung deposit.

Area C represents a broad area of relatively high potential in the Meilleur River Embayment of the Selwyn Basin, which hosted by the Road River Group but partially masked by the younger Besa River Formation. This area along the western edge of the Tlogotsho Plateau is generally under-explored due to its remoteness but was previously highlighted by the Nahanni MERA 1. The Meilleur River Embayment had earlier been identified as an important eastern extension of the Selwyn Basin. Despite the lack of exploration interest, this MERA 2 study has quantitatively reinforced evidence that the Meilleur River Embayment has relatively high potential for the presence of undiscovered SEDEX deposits based on the favourable stream sediment, stream water, and spring-water geochemistry, the presence of northeasterly growth faults associated with the Leith Ridge basement structure, and the favourable rock units throughout the area.

Area D in the vicinity of the Selena Creek deposit, represents an area of relatively high potential, very much like that of Area C and underlain by the Road River Group within the Selwyn Basin proper. This area is characterized by rolling vegetated hills with little exposure except where dissected by deep canyons. Some zinc showings have been identified by the limited exploration efforts in this area. The regional northeasterly trend of high mineral potential from the Prairie Creek to Meilleur River areas continues toward the southwest into this area, parallel to the deep-seated Leith Ridge structure.

Area E represents the northeastern extension of the Leith Ridge trend established by areas C and D, into the MacDonald Platform. The potential of Area E is enhanced by the growth fault accompanying the carbonate-shale facies change that trends northerly along the Prairie Creek sub-embayment of the Meilleur River Embayment. Stream sediment, stream water, and spring water geochemical data further support this designation.

Carbonate-Fault Model

A large area around the Prairie Creek deposit (Area F, Fig. 3), which contains many fault-related prospects, has been classified as high potential based on the carbonate-fault model. This rating is supported by favourable stream sediment chemistry, a high density of mapped faults, and the presence of diagenetically altered limestone and dolostone units (Manetoe Facies).

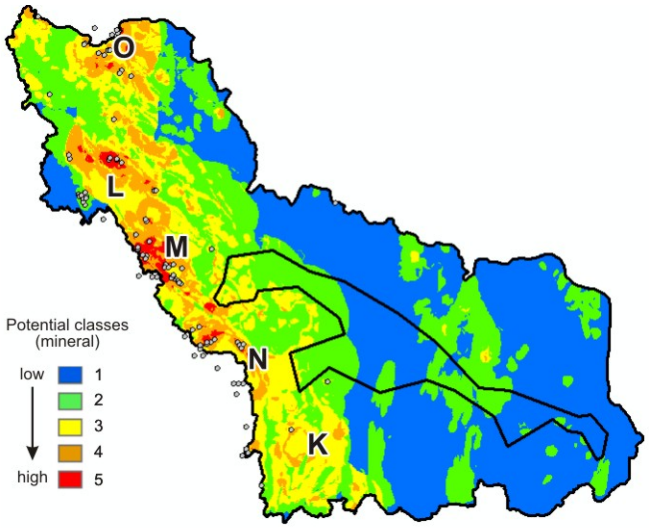


Figure 4. Simplified five-class intrusion-related map incorporated in the final additive potential map (Fig. 6). The areas of highest potential are indicated by single unique capital letters and are explained in the text.

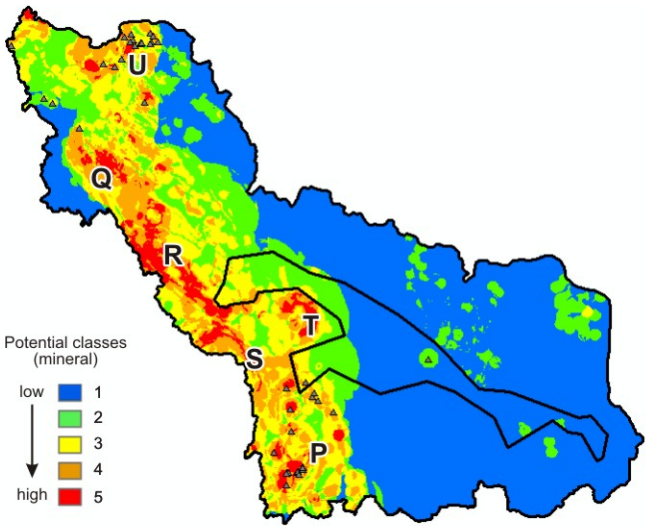


Figure 5. Simplified five-class Carlin-type map incorporated in the final additive potential map (Fig. 6). The areas of highest potential are indicated by single unique capital letters and are explained in the text.

The Broken Skull area (Area G) is in the vicinity of the Broken Skull Fault, which is interpreted as a reactivated growth fault due to lithological changes that occur across it. The presence of a number of anomalous hot springs in this area, combined with geochemistry that is suggestive of mantle fluids, supports the inference that this fault is long-lived and deep-seated. This area is also characterized by anomalous stream sediment geochemistry.

Area H, in the vicinity of the Selena Creek deposit, is classified as high in potential due to anomalous sediment geochemistry, favourable rock units, and the presence of a number of north-trending faults. This area contains some known SEDEX prospects and also has high potential for intrusion-related mineralization, which may reflect some overlaps in the genetic models. The plutons in this vicinity may have acted as heat sources for remobilizing mineralized fluids along major faults.

Areas I (Howards Pass) and J (southeast of Cantung) are located along the western strand of the zinc corridor, and are defined here primarily by anomalous stream sediment geochemistry, favourable basinal shale packages, and a high density of faults.

A southeast-northwest-trending divide is apparent between high-potential zones F and G in strata of the Mackenzie Platform, and areas H, I, and J within the Selwyn Basin which may reflect an overlap of the intrusion-related model with SEDEX parameters. There are some examples of carbonate-fault occurrences in the southwestern area, but most of these show evidence of higher temperatures, which favours classification as intrusion-related instead.

Intrusion-Related Model

Area K, around and to the north of Selena Creek (Fig. 4), is identified as high in potential by virtue of its proximity to the "McLeod and Big Charlie plutons", intersecting carbonate units, anomalous geochemistry (particularly stream sediment), anomalies in spring waters, and anomalous geophysical signatures. This area also contains a number of skarn occurrences.

Area L-M-N is a broad zone of high potential related directly to the Tay River plutonic suite. Its favourability is supported in part by anomalous stream sediment geochemistry, as well as carbonate units within the pluton buffers.

Area O is centred near O'Grady Lakes/Moose Ponds, covering the O'Grady Batholith of the Tombstone Plutonic Suite and a number of high-ranking intrusion-related mineral prospects. In addition to anomalous stream sediment geochemistry, the pluton-buffered areas also contains favourable carbonate units and several intrusion-related anomalies represented by pathfinder elements in spring waters.

Carlin-Type Model

An expansive area of high potential occurs in the vicinity of the Selena Creek placer deposit (Area P, Fig. 5). This area has been classified as high potential based on a series of placer gold showings, favourable pathfinder elements (As, Sb, Hg, Ti, and Ba accompanying Au and Ag), favourable rock units, proximity to plutons, and its position at the southern end of a regional trend of existing gold prospects and deposits extending to Alaska.

The linear zinc corridor (Area Q-R-S), which contains both the Howards Pass and the Cantung regions,

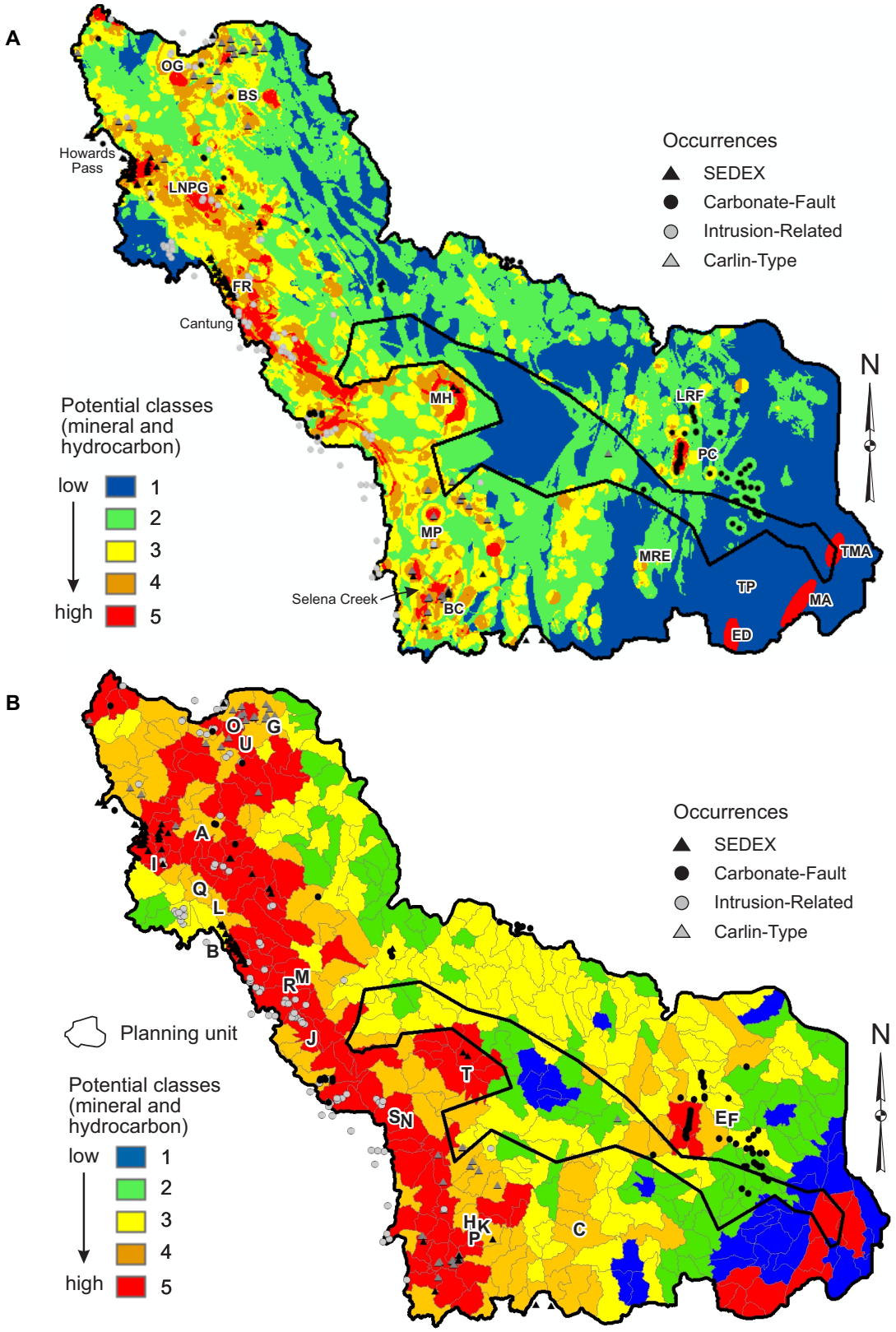


Figure 6. Final additive mineral-potential maps. Mineral occurrences by type are shown for reference. **A)** Continuous potential map generated by combining the maximum values of the individual potential maps for each deposit model as well as the map for hydrocarbons potential; BC = Big Charlie pluton, BS =Broken Skull River area, ED = Etanda Dome, FR = Flat River, LNPG = Little Nahanni Pegmatite Group, LRF = Leif Ridge Fault, MA = Mattson Anticline, MH = Mount Hamilton pluton, MP = McLeod pluton, MRE = Meilleur River Embayment, OG = O'Grady Batholith, PC = Prairie Creek, TMA = Twisted Mountain Anticline, and TP = Tlogotsho Plateau. **B)** Resource potential apportioned to park planning units using the MAX operator (the maximum value from each of the five normalized potential maps, based on a cell-to-cell basis). See text for explanation. Unique letters refer to deposit model areas of interest as described in the Mineral and Energy Resource Assessment (MERA 2) Results section.

is divided and partly overlapped by an area with high potential for Carlin-type Au mineralization. The high potential rating of this intersecting area is based on its proximity to plutons, a high density of anticlines, and a trend of numerous occurrences that includes the world-class Cantung mine. This area illustrates an overlap in parameters with the intrusion-related model.

The high-potential rating of Area T is a result of the intersection of the Mount Hamilton pluton buffer with favourable carbonate lithology, anomalous geochemical data from stream sediment, stream water, and springs, as well as the presence of minor placer gold occurrences.

Area U, around and to the east of the O'Grady Batholith, is similar to Area T with the added influence of favourable structural parameters, such as faults parallel to the Broken Skull River.

Hydrocarbons

Etanda Dome (ED), Mattson Anticline (MA), and Twisted Mountain Anticline (TMA) (Fig. 6) have high gas potential.

Composite Resource Potential

The final composite resource potential map (Fig. 6) integrates the mineral-potential maps for the four deposit-models (Figs. 2-5) plus the hydrocarbon-potential map from MERA 1. This overall non-renewable resource-potential map captures the highest values of all areas in the five component maps. For example, if the SEDEX model indicates high potential but the model for the other four resource types indicates low potential, the overall resource potential is high.

Caveats

The results of this Nahanni MERA 2 are based on the best information and resource analogues currently available. They reflect the present knowledge of the geology and models for deposit types known or thought to be important in the Nahanni Park area, and the combined data- and knowledge-driven weighting system and integration methods used to combine the various evidence maps. The process still has subjective steps. Although the new data have improved the confidence in the results, the geological knowledge is never finite and the likelihood of future geoscience advances always incorporates uncertainties into any resource-potential analysis. Thus, there will always be a need for new geoscience knowledge as future land-use issues arise.

Stakeholders are encouraged to comment and provide any new or overlooked information to Danny Wright (Geological Survey of Canada, MERA Working Group Co-Chair).

INTRODUCTION TO THE NAHANNI MINERAL AND ENERGY RESOURCE ASSESSMENT (MERA 2)

H. Falck[1], D. Lemkow,[2], D.F. Wright[2], and J.R. Harris[2]
1. Northwest Territories Geoscience Office, P.O. Box 1500, Yellowknife, Northwest Territories X1A 2R3
2. Geological Survey of Canada, 601 Booth Street, Ottawa, Ontario K1A 0E8

HISTORY OF THE NAHANNI MERA PROCESS

In 1972, a 4766 km^2 section along part of the South Nahanni and Flat Rivers in the Northwest Territories was designated as the Nahanni National Park Reserve. In 1978, the UNESCO World Heritage Committee determined that the area should be placed on the World Heritage List as an exceptional natural site forming part of the heritage of Mankind (Tate, 2004). Whereas this designation recognized the significance of the greater Nahanni River Region, it did not provide either legislative protection or recognition of the area as a National Park.

By the early 1980s, Parks Canada, the federal agency responsible for management of National Parks re-examined the issues surrounding the park status and identified a need for expansion. A new federal government policy had been established in 1980 to guide the process of establishing a national park and under this policy it was mandated that an assessment of the non-renewable resources of an area be conducted prior to formal establishment of a National Park, north of latitude 60ºN.

> *"It is the policy of the Department of Indian Affairs and Northern Development to ensure that an inventory of the non-renewable natural resource potential of areas in the Yukon and Northwest Territories be compiled prior to their formal establishment as new national parks. The fundamental qualities of the area which recommend it for national park status will be taken into account in any land use activities associated with compiling the inventory. Parks Canada will cooperate with other federal agencies responsible for carrying out such inventories."*
>
> - Government of Canada, 1995

The existing Nahanni National Park Reserve was exempted from this policy along with other previously established national parks. In 1983, Parks Canada proposed the addition of three adjacent land packages to ensure the protection of adjacent unique landscapes. These areas, the Ragged Ranges, Nahanni Karst (Ram Plateau area) and the Tlogotsho Plateau, became the study areas for a Mineral and Energy Resource Assessment (MERA) conducted by the Geological Survey of Canada. Fieldwork for this first Nahanni MERA (MERA 1) was conducted during the summers of 1985, 1986 and 1987 and preliminary reports were published. The finalization of MERA 1 (Jefferson and Spirito, 2003) was postponed however due to other MERA priorities, and MERA 1 was overtaken by two factors: the Deh Cho and Sahtu land claims, and the change in approach for establishing national parks to one emphasizing ecological integrity.

In October 2002, then Prime Minister Jean Chrétien and Heritage Minister Sheila Copps announced the Action Plan to Protect Canada's Natural Heritage. The Action Plan recommended that Parks Canada establish ten new national parks and five new national marine conservation areas in addition to expanding three national parks by 2008. The expansion and formalization of the Nahanni National Park was one of the prime candidate areas. Parks Canada commenced discussion with local aboriginal people and stakeholders, and by 2003 entered into a Memorandum of Understanding with the Deh Cho First Nations (DCFN) to work cooperatively on studying the addition of the lands to the park reserve (e.g. Fig. 1)

The border of the study area for the expanded Park was designated as the Greater Nahanni Ecosystem (GNE) (Fig. 1), comprising the entire watershed of the South Nahanni and Flat Rivers and a section of the Ram River watershed in the Karst lands. A new MERA was required as part of the feasibility studies for the proposed expansion because of the larger area being considered than had been assessed by the Nahanni MERA 1.

This report complements and expands upon the MERA 1 Open File (Jefferson and Spirito, 2003). Though all the data collected during the MERA 1 study were included in modelling the mineral potential and is part of the digital GIS database there are detailed reports for the specific areas studied during MERA 1 that are not included in this report including the petroleum resource assessment and mineral occurrence and deposit descriptions.

Falck, H., Lemkow, D., Wright, D.F., and Harris, J.R., 2007, Introduction to the Nahanni Mineral and Energy Resource Assessment (MERA2),, *in* Mineral and Energy Resource Assessment of the Greater Nahanni Ecosystem Under Consideration for the Expansion of the Nahanni National Park Reserve, Northwest Territories, (ed.) D.F. Wright, D. Lemkow, and J.R. Harris; Geological Survey of Canada, Open File 5344, p. 7-29.

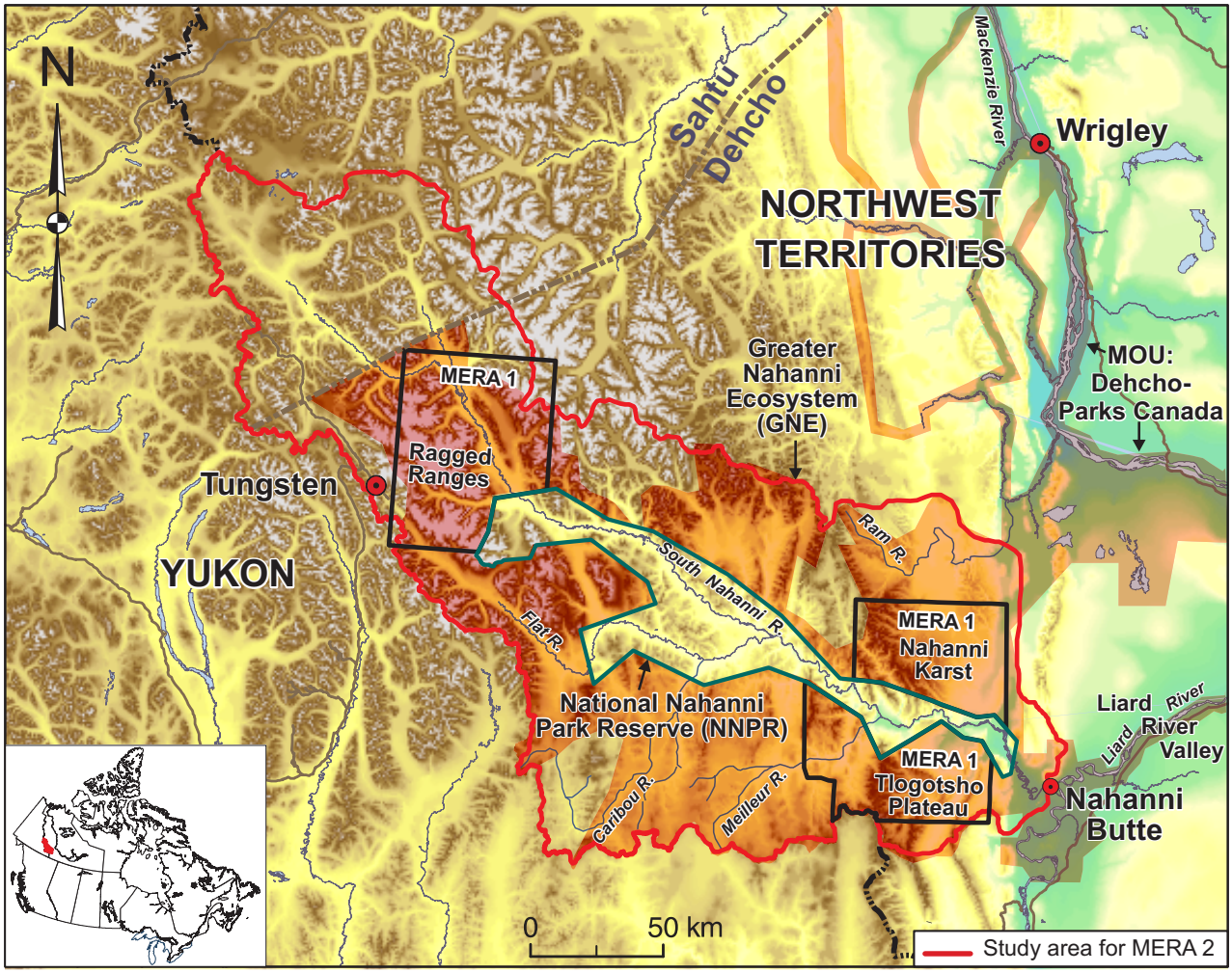


Figure 1. Context of the Greater Nahanni Ecosystem in the regional geography of western Canada, the Memorandum of Understanding (MOU) between the Deh Cho First Nation and Parks Canada, the boundary between the Sahtu and Deh Cho First Nations, and the study areas of MERA 1 (Jefferson and Spirito, 2003).

THE NATIONAL MERA PROCESS AND METHODOLOGY

The study of the economic and strategic significance of the mineral and energy resource potential within the Greater Nahanni Ecosystem was to be conducted using the MERA process as defined by federal government policy (Government of Canada, 1995). A MERA is conducted to ensure that, in making recommendations regarding the withdrawal of land for national park purposes, the Minister of the Department of Indian Affairs and Northern Development (DIAND) is advised on the balance between the values of the land with respect to park establishment criteria and the potential for the exploration, development and use of mineral and energy resources that may inhere in the land. The MERA process is the primary means whereby DIAND, Parks Canada, Natural Resources Canada (NRCan) and the territorial governments cooperate in conducting mineral and energy resource assessments of proposed federal protected areas on lands under federal jurisdiction north of latitude 60ºN.

Under the MERA Terms of Reference, NRCan's Geological Survey of Canada (GSC) is mandated to conduct the MERA. The MERA work plan and implementation are designed and guided by working and Senior MERA committees on a case-by-case basis for each study area. Approval to proceed with the second Nahanni MERA was received in 2004. The Geological Survey of Canada's approach to conducting a MERA is outlined in detail in Wright et al., (2004). Research data are collected to support the interpretation of the region's geology, geochemistry, and geophysics in terms of relevant mineral deposit models. Each mineral deposit type represents one or more commodities of potential economic interest. Where data are absent or insufficient to properly evaluate non-renewable resource potential, new geoscience information is collected by geological mapping, geochemical, and geophysical surveys. Utilizing experts' national and international knowledge of mineral deposit and hydrocarbon analogues (such as mineral deposit models and petroleum play histories), the compiled geoscientific

Table 1. Relative sizes of the MERA 2 study area, MERA 1 study areas, and the areas of New Brunswick and Nova Scotia.

	ACRES	HECTARES	AREA (km sq.)
Greater Nahanni Ecoregion	9851837	3986913	39869
Nahanni National Park Reserve	1195041	483618	4836
Ragged Ranges	998610	404125	4041
Nahanni Karst/Ram Plateau	504434	204138	2041
Tlogotsho Plateau	528067	213702	2137
New Brunswick[1]	18015888	7290800	72908
Nova Scotia[1]	13660920	5528400	55284

1. Source: http://www40.statcan.ca/l01/cst01/phys01.htm

data set is analyzed to produce an assessment of resource potential. More recently this has involved spatial analysis by knowledge-driven geographic information systems (GIS) in concert with other statistical techniques.

The assessments are generally conducted in two phases, an initial, preparatory phase where inventory is taken of the existing data and a preliminary internal report is written, and a second phase that typically involves new fieldwork to fill data gaps and concludes with the preparation and submission of a final public report (this Open File).

Phase 1 (6 months to 1 year)

Phase 1 includes the following stages.

1. The MERA study area is clearly defined; this area may extend outside of the proposed park expansion area in order to include relevant geoscience information.
2. Compilation of existing geoscience data from reports, maps and databases. This includes geochemical, geological, geophysical, surficial, and mineral deposits data. A gap analysis of the data is done.
3. Establish geologic domains and potential deposit types occurring in the area.
4. Define conceptual models for deposit types identified.
5. Prepare preliminary internal assessment report.
6. GSC personnel present the preliminary report through the MERA working group to the Senior MERA Committee. A decision is made as to whether additional information is required to improve or complete the resource assessment.

Phase 2 (1.5 to 2 years)

If additional information is required then the following are completed.

1. A work plan and budget are developed for the acquisition of the additional data and the completion of the resource assessment. This is presented to Senior MERA for approval. Specific areas are targeted that are in alignment with Phase 1, step 3. Fieldwork is conducted to collect data (usually geological, geophysical, or geochemical); this may also include visiting known mineral occurrences and follow-up laboratory analytical work.
2. The new data is integrated into existing data, using geospatial and geostatistical tools to normalize results over the study area. A reassessment of mineral and energy potential is undertaken.

A final report is submitted to the Senior MERA Committee and is released to the public for review and stakeholder consultations for 3 months prior to final decisions on the park boundary.

The second Nahanni MERA (MERA 2) project had the advantage of building upon the recently completed Nahanni MERA 1 (Jefferson and Spirito, 2003). MERA 1 demonstrated some of the data gaps in the region that the new project needed to address. The original Nahanni National Park Reserve was never assessed. MERA 1 examined three extensions to that reserve, totaling 8220 km^2 (Table 1). MERA 2 fieldwork was not conducted in the MERA 1 areas but the MERA 1 data were used in the MERA 2 analysis to provide a uniform, continuous and consistent evaluation compatible with the deposit models used in the MERA 2 study for the entire study area (excluding the existing Nahanni National Park Reserve). Whereas previous MERA projects (cf. Jefferson and Spirito, 2003 (Nahanni MERA 1); Anglin and Harrison, 1999 (North Bathurst Island); Jefferson et al., 1991 (Wager Bay - Ukkusiksalik)) had timeframes determined through negotiations between the members of the Senior MERA Committee, the Nahanni Park expansion MERA 2 timeframe was integrated with the Deh Cho Process and its associated land withdrawal.

The MERA methodology has been utilized consistently since its inception in the 1980s and has developed into an accepted approach recognized by the Government of Canada as a reliable technique that provides dependable results when used within the context of its qualitative nature (Scoates et al., 1986).

This report reviews existing data from published sources, including Nahanni MERA 1, presents results of field and laboratory studies conducted in 2004 and 2005, synthesizes the existing and new data, and interprets these data in a GIS. The mineral potential is assessed using a combined data- and knowledge-driven spatial analysis with reference to four composite mineral deposit models synthesized for the Nahanni River study area (incorporates some components from Eckstrand et al. 1995). The results have quantitative parameters but are still qualitative and relative within the context of the study area. This mineral potential assessment is considered to be at the Phase II level (Government of Canada, 1995) because of the significant addition of new data. The components of this Nahanni MERA 2 study are detailed below.

PHYSIOGRAPHY OF THE MERA 2 STUDY AREA

The study area for this MERA is defined as the Greater Nahanni Ecosystem (GNE) excluding the existing Nahanni National Park Reserve and the areas assessed during MERA 1 (Fig. 1). The GNE includes the South Nahanni River watershed and an adjacent section of the Ram River watershed in the karst lands to the northeast.

The GNE is located in the southwestern corner of the Northwest Territories. It covers approximately 39,000 square kilometres, from ice fields near the Yukon-Northwest Territories border, extending 540 kilometres eastward through the southern Mackenzie Mountains to the Liard River. The headwaters are in the height of land defined by the Northwest Territories / Yukon border in the Selwyn Mountains. Its waterways include the Little Nahanni River and its multiple tributaries in the Ragged Ranges, the O'Grady Lakes / Moose Ponds area, Virginia Falls, the Nahanni River deep canyons, the Flat River which has its source area to the south of the Little Nahanni headwaters, the Ram River and Prairie Creek and their deep canyons that drain Nahanni Karst and carry natural sources of lead and zinc in surface and ground waters, and mineral and thermal springs. The eastern limit of the Nahanni River watershed is defined by the height of land separating its tributaries from those that flow directly into the Liard River.

Information on flow dynamics, physiography, and chemical compositions of surface waters in this watershed are provided by Halliwell and Catto (1998). They have determined that the waters and/or natural fine particles of minerals suspended in the waters are regionally and naturally enriched in elements such as aluminum, cadmium, and zinc. Some of these elements are also elevated in the aquatic life that appears to have been sustained at these natural background levels. Geologically, this is understandable because the waters drain rocks that contain natural and regionally elevated contents of these elements that are released during normal weathering. The ecosystem is built upon this geological foundation, so all life that draws its nutrients from plants, groundwaters and surface waters will reflect the regional and local compositions of the bedrock. Interestingly a number of the cold and hot springs in the region that contain salts, also contain elevated metals (see Jefferson and Spirito, 2003), and there are abundant signs that large animals come to these springs (such as Meilleur River hot springs) to drink, thereby enhancing the process of enriching their bodies in these elements.

The study area transects the southern Mackenzie Mountains and lies just north of the Liard Plain that is situated along the Yukon - British Columbia border and is most complex in Ragged Ranges. Details and illustrations of the bedrock geology are provided in Appendix 1 (Falck, 2007). In general, shaly rocks form wooded and grassy slopes on the backs of, and at the feet of mountain ridges (e.g. Yohin Ridge and Nahanni Butte extending up to Little Doctor Lake area; also mountain pastures in Ragged Ranges). Sandstone, limestone and dolostone form cliffs and extensive ridges.

Extensive karst topography comprising solution channels, gushing cold springs from underground drainage, caves and sinkholes, some containing beautiful isolated small lakes (poljes), is developed in the naturally soluble carbonate rocks of the region, particularly in the Nahanni Karst (Ram Plateau) area, but also in carbonates found in Ragged Ranges, due to dissolution of the carbonates by rainwater and snow-melt. The spectacular gorges of the Nahanni River and its tributaries are also hosted by dolomite and limestone that preserve evidence of ancient dolomitization, brecciation and solution collapse ("Manetoe Facies" of Morrow et al., 1990). These processes created oil and gas reservoirs some 350 million years ago.

Granite plutons with their mantles of thermally altered sedimentary rocks core the highest peaks (2700 m) in Logan Mountains of the Ragged Ranges, some of which still support alpine glaciers, as well as ice-cored rock glaciers. The Logan Mountains are an attractive destination for mountaineers (e.g. Hubbard, 1957), and the Cirque of the Unclimbables formed a backdrop for filming part of the Clan of the Cave Bear film. Caribou use the mountain pastures for their summer range.

Active alpine glaciation has sculpted the mountain peaks and valleys, producing high-elevation cirques, and U-shaped valleys with lateral and terminal moraines in the Ragged Ranges. Much of the glacial till along the east side of Nahanni Karst and Tlogotsho Plateau is terminal moraine from the Laurentide ice sheet. Tills and glaciolacustrine clay deposits border or

mantle valley floors within the Nahanni River Basin. Eastward, in the Liard River valley, drumlin fields are oriented northwest-southeast in the northern half of the area and east-west in the southern half of the area. The various glacial deposits have been locally reworked into ancient and modern river sands and gravels, some of which contain minor amounts of placer gold. The silt and clay fractions reworked from these tills continue to be carried downstream, suspended in the turbulent Nahanni waters. River erosion is actively changing the shapes of the stream beds and banks in the Nahanni River Basin, in places destroying man-made edifices such as the Nahanni Butte Ranger Station.

A range of high- and low-volume, cold, warm, and hot springs are associated with fracture systems and locally produce geological structures such as the picturesque tufa mounds of the famous Rabbitkettle Hot Springs, as well as providing soothing bathing pools. The distribution, classification and chemical composition of spring waters are described and interpreted in Caron et al. (2007) and in Hamilton et al. (2003).

REGIONAL GEOLOGY

The geology underlying the study area (Fig. 2) is the product of major tectonic and depositional events that affected the entire Canadian Cordillera and in some cases the western half of North America. The regional geology of the Nahanni area is summarized in this section and a comprehensive review is in Falck (2007). The digital GIS geology map from Okulitch (in press a, b) is in Appendix 4 (Lemkow et al., 2007).

The South Nahanni River transects the eastern fringes of the Selwyn Mountains and the southern Mackenzie Mountains. The rocks forming these mountains are mainly sedimentary, deposited in a huge Neoproterozoic delta (800 million years ago (Ma)) that was covered by a carbonate platform similar to today's Bahamas, and then buried by mud and sand in a deep basin similar to the present day Gulf of Mexico. These sediments recorded the dawn of animal life (580 Ma exposures in the Vampire Ranges) and fluctuating platformal and shale basin conditions until compression from the Pacific Oceanic plate during the "Antler" mountain-building shed conglomerate into the Devono-Mississippian shale basin (ca. 380-310 Ma) from the west (Gordey et al., 1987). Relatively quiescent basinal shale and platformal carbonate deposition resumed until the Jurassic (170 Ma). By this time, plate tectonics had carried a volcanic island arc (similar to Indonesia) into collision against North America. This slow but intense compression pushed sheets of sedimentary rocks toward the east, causing them to fold and slide over each other along thrust faults. Sand and mud shed from these young mountains formed a delta over the present Tlogotsho Plateau, which faced an interior seaway extending down to the present location of Texas. At the same time, deeply buried rocks to the west became hot enough to melt, resulting in the rise of giant inverted tear-drops of granite that formed the Cretaceous (about 100 Ma) intrusions. These form the peaks of the Ragged Ranges and are surrounded by baked sedimentary rocks, called hornfels. The Cretaceous intrusions (formerly the Selwyn Plutonic Suite, Gordey and Anderson, 1993) comprise 3 suites: Tombstone, Tungsten and Tay River (Mortenson et al., 2000; Hart et al., 2004, 2005; Heffernan, 2004; Barnes et al., 2007; Rasmussen et al., 2007a). A cluster of over 200 coarse-grained, sub-vertical, granitic pegamtitic dykes (Late Cretaceous offshoots from the Cretaceous intrusions) form the L-i, Cs-, Ta-, Nb-, and S-enriched Little Nahanni Pegmatite Group (Barnes et al., 2007). Compression and lateral shearing by the colliding plate has continued with right-lateral strike-slip faults, through the Tertiary (ca. 40 Ma) to the present (Hyndman et al., 2005b), as illustrated by the Nahanni Earthquake of 1985 (described by Wetmiller et al., 1988 and Hyndman et al., 2005a). Whereas plate tectonics raised the mountains, it was the massive ice sheets during the ice age (2 Ma to 10,000 years ago) and their alpine glacier remnants that have carved the spectacular spires of the Ragged Ranges. The interaction between the Laurentide Ice sheets centred over Hudson's Bay and the Cordilleran Mountain Ice sheets, as well as subsequent melt water lakes and outwash plains control the morphology of many of the valley floors (cf. Duk-Rodkin et al., 2007). The melt waters and present day precipitation also dissolved the limestone of the mountains to form the caves and intricate landforms of the karst terrain. The advancing and retreating of the glaciers also permitted an 'ice-free' corridor following the Mackenzie Valley, which is believed by many to have been critical for man's arrival to the Americas.

The NNPR and proposed park expansion areas lie mainly within the large Meilleur River Embayment of the Selwyn Basin but also include a major zig-zag carbonate-shale facies change that outlines the boundary between basinal shales and the MacDonald Platform to the east and northeast (Fig. 2). The Prairie Creek Embayment forms a northerly trending appendage to the Meilleur River Embayment. The Cretaceous intrusions of the Ragged Ranges transect some of the stratigraphic facies changes. These geological entities are the framework for beautiful scenery, natural habitat and mineral deposits in the region.

MERA 2 FIELDWORK AND DATA SYNTHESIS

The existing data sets from MERA 1, NORMIN (Department of Indian Affairs and Northern

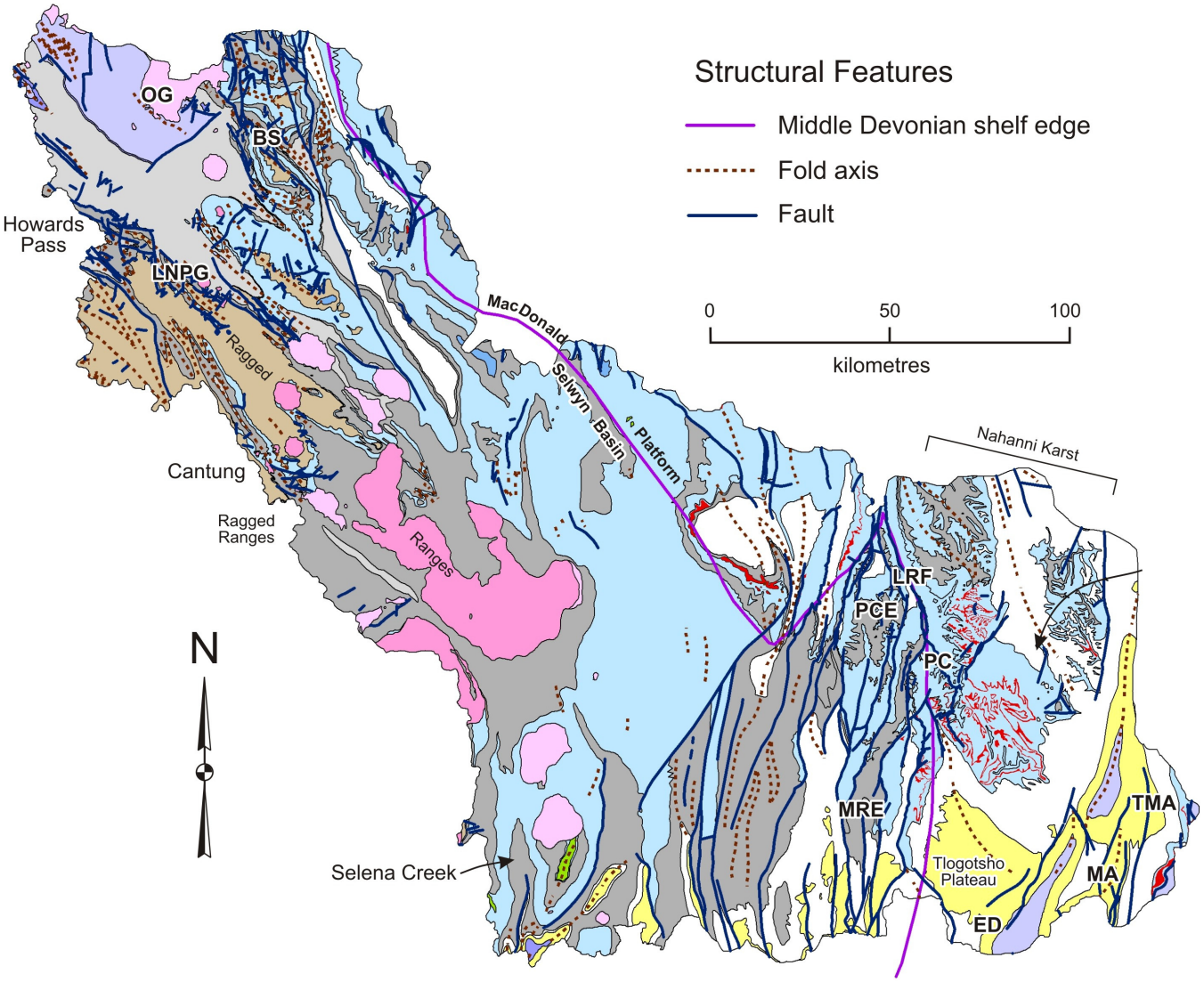


Figure 2. Generalized geology of the Nahanni MERA 2 study area (from Okulitch, in prep., a, b). BS = Broken Skull River area, ED = Etanda Dome, FR = Flat River, LNPG = Little Nahanni Pegmatite Group, LRF = Leif Ridge Fault, MA = Mattson Anticline, MRE = Meilleur River Embayment, OG = O'Grady Batholith, PC = Prairie Creek, PCE = Prairie Creek Embayment, and TMA = Twisted Mountain Anticline. See opposite page for legend.

Development), and the Geological Survey of Canada (e.g. National Geochemical Reconnaissance surveys and 1:250,000 scale geological maps) were augmented by the following:

1. 1:500,000 scale geological synthesis (Fig. 2; Okulitch, in prep. a,b).
2. National Geochemical Reconnaissance of stream sediments and waters over the entire study area not covered by MERA 1 with some calibration overlap (Fig. 3A).
3. Airborne radiometric/magnetic surveys (Fig. 3B).
4. Spring water geochemistry (Fig. 3C), with new samples collected in areas not covered by MERA 1, some calibration overlap, all data compiled, and statistically reinterpreted.
5. Mineral occurrences (Fig. 3D; Barnes et al., 2007; Cousens, 2007; Rasmussen et al., 2007a; Yuvan et al., 2007).

A summary of each data type is provided below. All fieldwork for Nahanni MERA 2 was completed during the summers of 2004 and 2005.

Geological Compilation

The geological base map used in this study (Fig. 2) is after Okulitch (in prep. a,b) and the regional geological context is reviewed by Falck (2007). The original sources are helicopter reconnaissance surveys from the 1960s to the 1980s published in formats ranging from memoirs with 1:250,000 scale colour maps, geological descriptions, and interpretations, to Open File maps printed as black line copies of sepia maps with minimal legends and virtually no stratigraphic or paleontologi-

LEGEND

CRETACEOUS INTRUSIONS

Tay River, and Tombstone suites; grandodiorite to quartz monzonite (LKgd, LKmzg, CEKgd, Kgd, Kqm, Kdi)

Tungsten suite: biotite + muscovite + garnet + tourmaline grandiorite to quartz monzonite (CEKgd, Lkgd, Kqm)

Transitional to deep basinal

LATE DEVONIAN to EARLY MISSISSIPPIAN

Siliceous shale, minor siltstone, sandstone, and conglomerate (Earn Group and Portrait Lake Formation) (DCE-p, DCE, DE-PL)

Platform to intracratonic basin

TRIASSIC to CRETACEOUS

Shale to sandstone (KSu, KSk, KL, KSc, KGr, TrJL)

CARBONIFEROUS to PERMIAN

Mainly shale and siltstone: cherty (PF, CPMC, CPT)

EARLY CARBONIFEROUS

Coal-bearing sandstone and shale (Mattson Fm) overlying dolomitic limestone, with minor shale and siltstone (CM, CFG, CF, CPr, CYC, CY)

MIDDLE DEVONIAN to CARBONIFEROUS

Predominantly shale: (Besa River and Horn River, and Fort Simpson formations) (DCBR, mDHR, uDs, DHlc, uDFS, uDpc, uDspc)

MIDDLE DEVONIAN to CRETACEOUS

Diagenetic shelf facies, dolostone, and hydrothermal dolomite (Manetoe, Presqu'ile, and Grizzly Bear) (Pp, PM, PGB)

MIDDLE DEVONIAN

Calcareous bioclastic shale, minor limestone and dolostone (mDFH, mDF)

Limestone, minor dolostone and calcareous shale (MDN, mDL, lmDGB, lmDA, lmDAL, lmDNa, MDHN, MDFHN, MDHe)

CAMBRIAN to EARLY DEVONIAN

Calcareous graptolitic shale, minor quartz arenite, and thin basal conglomerate (Road River Formation) (SDD-cd, SRR, SDSa, SDRR, P-DRR, ODRR-h, COR, ICGL, ICBR)

Dolostone with minor limstone and quartz arenite (Whittaker and Broken Skull formations) (lDSo, lDD-CM, lDD-V, SD-RR, OSW, OH, mOSu, COBS, SDD, O-DWD, C-SBW, COBSu, uCH, mCA, mCR, lCSe, C-Sh, lmDC)

Mafic volcanic rocks (Sunblood and Sekwi formations) (mOSuv, lCSev)

NEOPROTEROZOIC

WINDERMERE SUPERGROUP

Sandstone, siltstone, and shale (ECV, ECH, ECH-N, ECH-Y)

Dolostone, minor limestone, minor shale (ER, EGt, Esh, nPK)

Figure 2 continued. Legend for the geological map of the Nahanni MERA 2 study area shown on the opposite map.

cal analysis (e.g. Roots et al., 1969). Some of the mapping was by geologists familiar with stratigraphy to the south and west in the mountains (e.g. Gordey and Anderson, 1993) whereas other geologists extrapolated geology from petroleum wells in the Interior Platform (Morrow and Cook, 1987). The issue of duplicated nomenclature is compounded by the complex nature of the transition from the MacDonald carbonate platform in the east to the Meilleur River Embayment, a shale-dominated sub-basin of the larger Selwyn Basin to the west. Correlation of stratigraphic terminology was begun by Table 3.1 of Jefferson et al. (2003a).

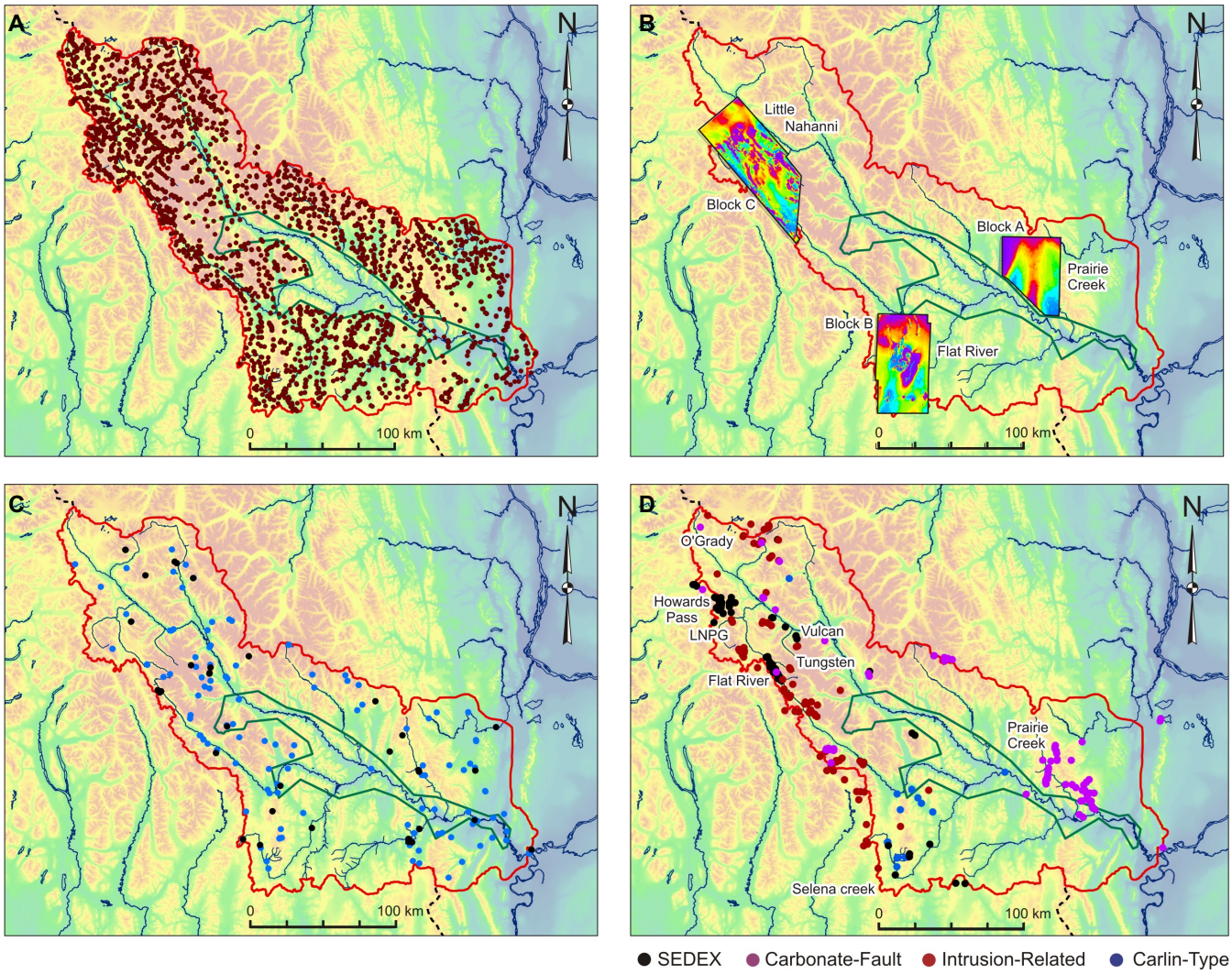


Figure 3. Locations of data collected and compiled for Nahanni MERA 2. The Greater Nahanni Ecosystem is outlined in red, the existing Nahanni National Park Reserve in green, and the MERA 1 study areas in black. **A)** Stream sediment and water sample sites (McCurdy et al., 2007). **B)** Total field magnetic surveys (Charbonneau, 2007). Low magnetic field is represented by cool colours and high by warm colours. **C)** Spring water sample sites (Caron et al., 2007). **D)** Mineral occurrences (Department of Indian Affairs and Northern Development, 2006).

As a contribution to the National Geological Atlas of Canada, compilation of the Redstone Sheet 1:1,000,000 scale map (NTS 95) included the eastern three quarters of the study area (Okulitch in prep. a) and a comprehensive stratigraphic legend. In order to complete the western coverage of the MERA 2 study area, Okulitch (in prep. b) integrated the eastern portion of the Ross River 1:1,000,000 sheet (NTS 105). The complete geology compilation was converted into shapefiles using ESRI's ArcMap (Lemkow et al., 2007) as the primary base for mineral potential modelling.

National Geochemical Reconnaissance Stream Sediment and Water Survey

A stream sediment survey (Fig. 3A) utilized the National Geochemical Reconnaissance (NGR) program's protocol for the MERA 2 project (Friske et al., 2006; McCurdy et al., 2007). Canada's NGR program has involved reconnaissance-scale drainage sediment and water sampling by the Geological Survey of Canada since 1973. The elemental analyses collection includes fifty or more variables in both sediment and water from a combination of inductively coupled plasma mass spectrometry (ICP-MS), inductively coupled plasma atomic-emission spectrometry (ICP-AES), ion chromatography, instrumental neutron activation analysis (INAA) and specific element methods. Regional geochemical surveys typically consist of lake or stream sediment surveys, or till surveys which utilize chemical analyses combined with special interpretative skills to 'see through' cover to the bedrock beneath. Geochemical sampling of stream sediments, stream waters and soils offers a representative analysis of all the rocks upstream and within the catchment basin feeding the stream being sampled.

Geochemical surveys in the study area prior to MERA 2 are summarized in Spirito and Jefferson (2003). These include samples collected regionally at watershed junctions with the aim of covering large prospective areas, as well as focused, detailed soil sampling surveys on the watersheds that can be used as training areas or have anomalies that require follow-up.

For the purposes of MERA 2, a broad multi-element survey with a uniformly high level of quality and data integrity was essential to provide confidence. The most important characteristic of NGR surveys is its nationally standardized, consistent and structured sampling routine. The standard density is 1 sample per 13 km^2 in order to ensure efficient coverage in survey areas of 1000 km^2 or greater. The stream sediment samples are taken from first or second order streams following the methodology outlined in McCurdy et al. (2007). Samples collected in older previous surveys (763 from Goodfellow (1982); the same 763 samples reanalyzed by Friske et al. (1999); and 415 from Spirito and Jefferson (2003) were examined and geochemically reanalysed with current laboratory methods to ensure compatibility. From Day et al. (2005), 10 sample data sets were used as-is. During the MERA 2 field and laboratory project, three blocks of samples (697, 857, and 22) were collected and geochemically analyzed to complete the coverage of the study area. In total, data from 2764 sample sites were analysed for the MERA 2 study. A preliminary assessment of mineral potential based on metal values 2, 5, and 10 times the median is included in the paper by McCurdy et al. (2007) but is not used in the GIS modelling of mineral potential because their median and calculated elevated value ranges for pathfinder elements did not take into account the effects of rock type. Only raw geochemical data were used in the GIS analysis wherein the influences of rock types on background versus anomalous geochemical ranges were calculated. Geochemical data used in the GIS analysis are archived in the GIS database (Lemkow et al., 2007).

Combined Airborne Radiometric and Magnetic Surveys

Regional airborne geophysical surveys (Fig. 3B) provide unbiased and consistent scientific information that cannot be obtained over large areas in any other way. Similar surveys have been used throughout Canada and worldwide for several decades, to improve mapping of bedrock and surficial geology, structures and in exploration for a wide range of commodities (Galbraith and Saunders, 1983; Maurice and Charbonneau, 1987; Shives et al., 1995; Ford et al., 1998; Shives et al., 2000). The large size of the study area, the short times lines and no publicly available regional surveys for the study area, made the airborne geophysical surveys critical to the assessment. A number of different geophysical approaches were considered.

A combined radiometric and magnetic survey was decided as the best compromise between the amount and suitability of information collected compared to the cost and logistical difficulties of conducting the survey. Because of the costs, it was not possible to fly a survey over the entire region, therefore, three survey blocks were identified on the basis of known mineral potential under the premise that the geophysical signatures of known mineral occurrences have not been documented and that the indicators could be used to identify results that were anomalous with respect to the mapped geology. Block A (Virginia Falls) covers the Prairie Creek Embayment of Selwyn Basin, including the Prairie Creek Mine area. Block B (Flat River and Coal River) covers the Caribou Creek area, the southernmost extent of the exposed Cretaceous intrusions and the Selena Creek polymetallic placer gold showings that are suggestive of Carlin-type lode gold source. Block C (Frances Lake and Little Nahanni River) covers the middle part of the Selwyn Plutonic Suite from the upper Flat River valley and Cantung to the Lened deposit, including the Little Nahanni Pegmatite Group.

The helicopter-borne surveys were conducted by Sander Geophysics Limited, Ottawa, in 2004 and 2005 under the technical supervision of the Radiation Geophysics Section, Geological Survey of Canada. All surveys were conducted using a Eurocopter AS 350B-3 helicopter flown at 135 m nominal terrain clearance along lines spaced at 500 m intervals. A total of 16,000 line kilometres were flown distributed as follows: Block A - 4000 km; Block B - 5000 km; and Block C - 7000 km (Fig. 3B).

Four channels of information were collected and include measurements of magnetic field and the natural radioactivity of potassium, uranium and thorium. The magnetic field changes proportionally to the ferromagnetic mineral content. Magnetic surveys are important for identifying the rock types and tracing their structure in areas where standard mapping cannot (Shives et al., 1995). Some mineral deposits are characterized by elevated magnetic susceptibility; others by decreased magnetic signal. Trace amounts of radioactive elements are present in different proportions in every rock type. Gamma ray spectrometry records the geochemical concentrations of potassium, uranium and thorium in the upper 30 cm of the Earth's surface, including rocks and surficial deposits such as soil, alluvium and till. Gamma rays do not penetrate water, snow, or ice, so the measurements must be taken under dry summer conditions (Shives et al., 1995). MERA 2 survey results are summarized in Charbonneau (2007) and the data are published by Carson et al. (2007a,b,c).

These results were also incorporated into the mineral potential modelling of Harris et al. (2007) and included in the GIS database (Lemkow et al., 2007)

Spring Water Geochemistry Survey

Geochemistry and hydrogeology of the abundant springs in the area (Fig. 3C) were studied by Caron et al. (2007). The primary goal of this study was to identify areas of anomalous metal concentrations by analysing samples of groundwater discharge obtained by standard field sampling and laboratory analytical procedures. The survey also characterized the natural background concentrations of a variety of chemical constituents that could be used to detect environmental impacts if any development were to take place in the future. The greater Nahanni watershed stream waters, sediments, fish, and caribou have been documented to have naturally elevated levels of zinc, cadmium, copper, and iron (Halliwell and Catto, 2003). These are NOT a result of the limited human impacts, exemplifying the importance of documenting and understanding the natural levels of trace constituents in surficial materials before making land use decisions.

During the MERA 1 study, Hamilton et al. (2003) collected 127 water samples from 92 different spring locations. They used geological context and major element characteristics with several statistical methods to classify the springs into genetic groups, within which they determined background and anomalous metal contents, and from which they inferred potential for a range of mineral deposit types. The MERA 1 primary data were combined with the 95 samples collected in MERA 2 (Caron et al., 2007) taken from 79 different locations (16 of these springs were re-sampled by MERA 2) to provide a total of 222 samples from155 springs. Caron et al. (2007) re-evaluated all of the primary data, using reverse logic in a method applied elsewhere to determine the environmental impact of geology and mineral deposits on groundwater systems. From this they inferred anomalous versus background spring waters but did not interpret them in terms of mineral deposit types. Harris et al. (2007) recompiled the primary data from both spring studies and took into account their respective interpretations of anomalousness to generate a study-wide data set of anomalous springs. This set of anomalous springs included only those springs that could be confidently assigned to one of the four composite deposit models that were used for mineral potential analysis (Table 1 of Harris et al., 2007)

MERA 2 analytical data obtained from the spring water sampling program include cations and trace elements, anions, alkalinity, $\delta^{34}S$ analysis in sulphates, $\delta^{34}S$ analysis of sulphides, dissolved inorganic carbon (DIC) $\delta^{13}C$ analysis, silica, and $\delta^{18}O$ and $\delta^{2}H$. Field data included sulphide concentration, electrical conductivity, temperature, total dissolved gas pressure, and total dissolved oxgen. The methodology, analytical details, and data are presented in Caron et al. (2007) and Caron (2007), and the raw data sets are in Lemkow et al. (2007).

Mineral Occurrences

Initial examination of the mineral occurrences (Fig. 3D) was based on NORMIN.DB, a database including references to geology and mineral exploration in the Northwest Territories (Department of Indian Affairs and Northern Development, 2006). A mineral commodity occurrence, (defined as an economic or potentially economic concentration of a mineral commodity ranging from showing to economic deposit) is entered into the NORMIN.DB only if a commodity has actually been found in a bedrock sample and classified according to set threshold values.

The MERA 2 study data sets were augmented by companies working in the area including Canadian Zinc, North American Tungsten, and Pacifica Resources. Additional information was collected from the Yukon Minfile database (Deklerk and Traynor, 2005). The NORMIN data in the MERA 2 study area were based initially on a compilation by MERA 1 using CANMINDEX, the Archer Cathro Database and other sources (Jefferson et al., 2003b). Information from Barnes et al. (2007), Cousens (2007), Paradis (2007), Rasmussen et al. (2007a), and Yuvan et al. (2007) was also reviewed and incorporated into the final MERA 2 database (Lemkow et al., 2007).

Using the compiled information Harris et al. (2007) developed a customized resource assessment method for the MERA 2 the study area. The mineral occurrences were grouped into four synthetic deposit models for the GIS analysis: (Figs. 4-7)

1. SEDEX (stratiform shale-hosted sedimentary-exhalative Zn-Pb-Ag; the largest of several SEDEX occurrences is the Howards Pass zinc-lead prospect.
2. ‘Carbonate-fault’ (carbonate-hosted zinc-lead-silver associated with major faults); this model is based on the Prairie Creek advanced prospect,
3. ‘Intrusion-related’ (includes skarn, rare metals and gemstones) mineralization associated with the Cretaceous plutons includes the world-class Cantung skarn tungsten mine and the Little Nahanni Pegmatite Group lithium prospect,
4. Carlin-type gold as lode and/or derived placer. Carlin-type deposits have not yet been found in the study area, but placer gold deposits with polymetallic signatures (eg. Selena Creek) are thought to be good indicators of its presence.

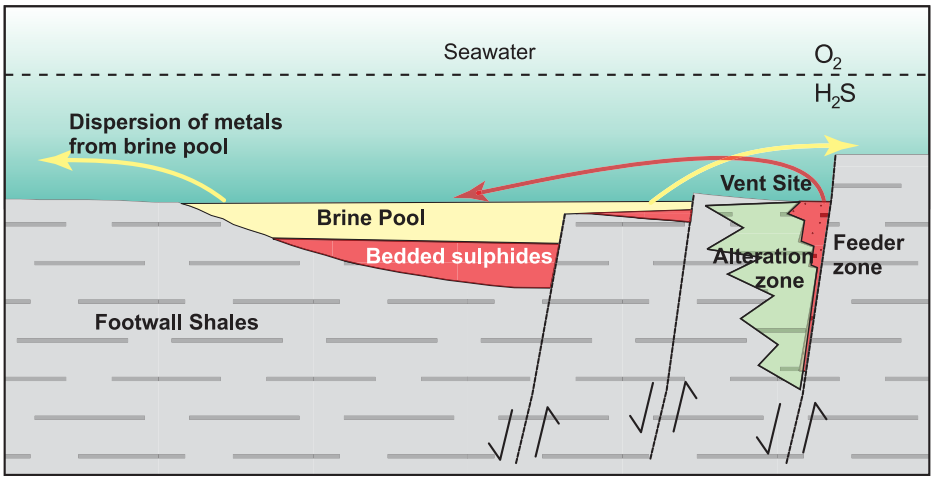


Figure 4. Genetic model for stratiform hosted zinc lead deposits (after Goodfellow and Lydon, 2007).

Research projects were developed to help define geological controls as well as to examine unresolved geological issues outlined in MERA 1 pertaining to the larger mineral deposits in the area that could improve determination of the regional mineral potential. Mineral occurrences were prioritized for forty site visits in the 2005 field season under MERA 2, but none were re-described because the descriptions in NORMIN and Jefferson and Spirito (2003) were found to be accurate.

Sediment-hosted stratabound copper, glaciogenic iron formation, porphyry copper-molybdenum, and volcanic redbed copper were considered by Jefferson and Spirito (2003) and Lariviere et al. (2006), but no examples of these styles of mineralization have been identified within the study area. These mineral deposit types were considered of low potential as their distributions are tied to specific host rocks (Little Dal, Coates Lake, and Rapitan groups) that do not crop out within the study area. The 'Nick' stratiform exhalative Ni-PGE sulphide type documented elsewhere in the Selwyn Basin by Hulbert et al. (1992) was noted as possibly being present by Jefferson and Spirito (2003) but geochemical results of the MERA 2 study included no nickel or PGE anomalies. Hydrocarbons were fully assessed in the 2003 MERA 1 (Osadetz et al., 2003) and were incorporated in Harris et al. (2007).

Following is a brief description of the four main deposit models with reference to the research that was done under this MERA, and included in this Open File. For more information on the models and the mineral potential modelling, refer to Harris et al. (2007).

SEDEX (Stratiform Shale-Hosted Sedimentary Exhalative Zn-Pb-Ag)

The origins of the Nahanni area sediment-hosted deposits are related to extensional tectonism during the deposition of fine-grained deep-water sediments in the Selwyn Basin (Lydon, 1995; Leach et al., 2005) (Fig. 4). Basinal fluids were expelled along marginal faults into a rift basin. The restricted basin had a stratified water column restricting oxygen circulation allowing preservation of precipitated metals. The dense fluids ponded in topographic lows forming concentrations of base metal sulphide minerals. Because the zinc-lead-silver deposits are hosted only in specific stratigraphic intervals, identifying which sets of fine-grained black rocks are favourable helps to better constrain where the metal-rich strata might occur elsewhere in the study area. Cousens (2007) examined the Ordovician-Silurian Road River Group that hosts the large zinc-lead-silver accumulations in the Howards Pass area and compared them with similar strata throughout the region using rare earth signatures and Pb isotopes. Paradis (2007) examined the Prairie Creek deposits, which are a composite of three different deposit types (SEDEX, Mississippi Valley-type (MVT), and veins); and form the basis for the Carbonate-Fault model (see below). Jefferson and Spirito (2003) also recognized the early Devonian SEDEX potential that may be exemplified by the Vulcan prospect.

'Carbonate-Fault' (Carbonate-Hosted Zinc-Lead-Silver Associated with Major Faults)

The fault-controlled parts of carbonate-hosted zinc-lead-silver deposits in the study area, exemplified by the Prairie Creek deposit, are exceptionally silver-rich compared to pure SEDEX or pure MVT deposits elsewhere. Three distinct forms of zinc-lead±silver sulphide accumulations have been identified by Canadian Zinc Corporation (2001) at Prairie Creek: stratabound massive sulphide (essentially a deep SEDEX fringe in calcareous shale that is silver-poor), classic dolomitic karst or breccia-hosted MVT deposits in the Devonian Manetoe Facies (Morrow et al., 1990), and 1 to 3 m thick quartz-carbonate-sulphide veins along north-northeast-trending structures (Jefferson and Spirito,

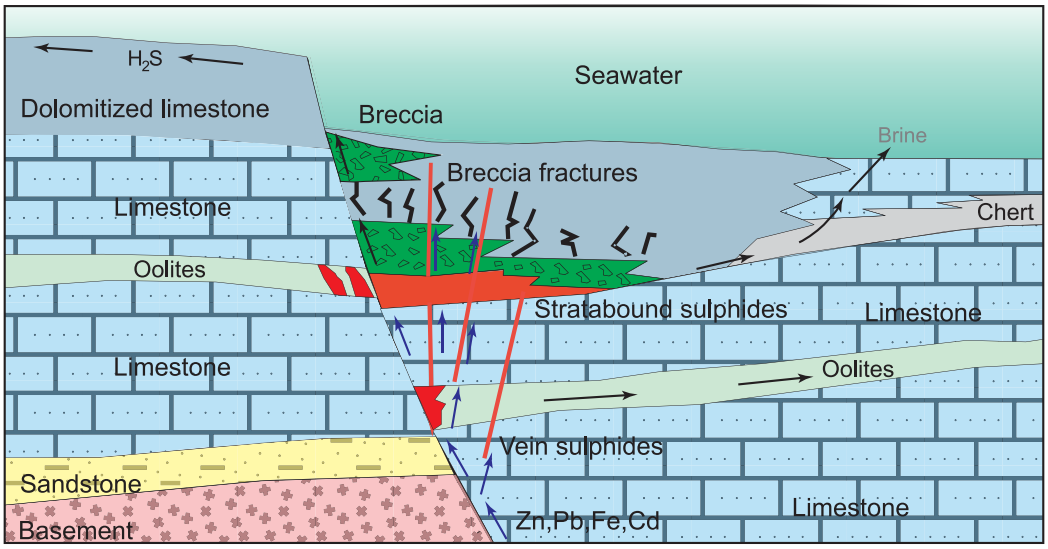


Figure 5. A genetic model for carbonate-hosted zinc lead silver deposits after Wilkinson et al. (2005) and Paradis (2007).

2003, Dewing et al., 2006; Paradis, 2007). The zinc-lead sulphide minerals partially replace dolomite units, fill open-spaces in more limestone-rich strata or form veins, vein networks and breccias developed preferentially in competent carbonate layers but also extend locally into shale-dominated beds. One genetic model (Fig. 5) is that basinal fluids were expelled along faults into the margin of a carbonate platform. Reaction with and replacement of permeable carbonate horizons allowed improved fluid movement and increased metal precipitation. Hydrostatic pressure fluctuations due to tectonic activity enhanced the permeability through vein and breccia formation.

'Intrusion-Related' (Includes Skarn, Rare Metals and Gemstones)

The intrusion-related deposit model comprises a diverse suite of elements and precious stones that are concentrated in a large variety of intrusions and their adjacent strata, in two basic components:

1. elements concentrated in minerals that crystallized directly from the magma,.
2. elements concentrated in favourable host rocks and marginal phases of the plutons during their intrusion and crystallization (some examples in Fig. 6).

The first component includes two deposit types: rare metals such as Li, Nb and Ta in the Little Nahanni Pegmatite Group (LNPG) (Barnes et al., 2007); and gem-quality tourmaline in pegmatite phases of the O'Grady batholith (showing ID 105INE0023 in NORMIN.db; Department of Indian Affairs and Northern Development, 2006; and Rasmusen et al., 2007a).

The second component includes the gemstone emerald, and a wide suite of metals such as copper, gold, bismuth, tungsten, lead, and zinc in a broad spectrum of additional deposit types. This component involves fluids that mobilized, transported, and concentrated metals. The fluid and metals could have been derived from the magma directly, from dehydration and metamorphism of host rocks or from meteoric or groundwater (Sillitoe and Thompson, 1998; Hart, 2005; Meinert et al., 2005). The thermal energy from the magma allowed the fluids, commonly a chloride brine, to dissolve and carry small quantities of metals as it moved until the temperature, pressure and/or acidity of the fluid changed. At sites of such changes metal-bearing minerals can precipitate from solution and if enough accumulate, an economic deposit may be formed. The specific deposit type was determined by local factors.

Three studies were undertaken by MERA 2 to better define the sources and tectonic settings of four Intrusion-Related deposit types: skarn tungsten, rare metal pegmatites, precious metals and base metal skarns. Yuvan et al. (2007) examined a series of high-grade tungsten-bearing quartz veins from the two deposits at the Cantung mine, to better characterize the nature of the fluids that mobilized the metals. Barnes et al. (2007) focused on the rare earth –bearing Little Nahanni Pegmatite Group that intrudes the Neoproterozoic Hyland Group (formerly termed 'Grit Unit') underlying the Selwyn Basin.

Rasmussen et al. (2007a,b) provided the geological framework for the above as well as precious metal and base metal skarn deposits. They examined the regional geochemistry and geochronology of plutons in the Mackenzie and Selwyn mountains of southwestern Northwest Territories and southeastern Yukon. These intrusions form the easternmost extent of the Tintina Gold Province, an elongate belt of Cretaceous plutons

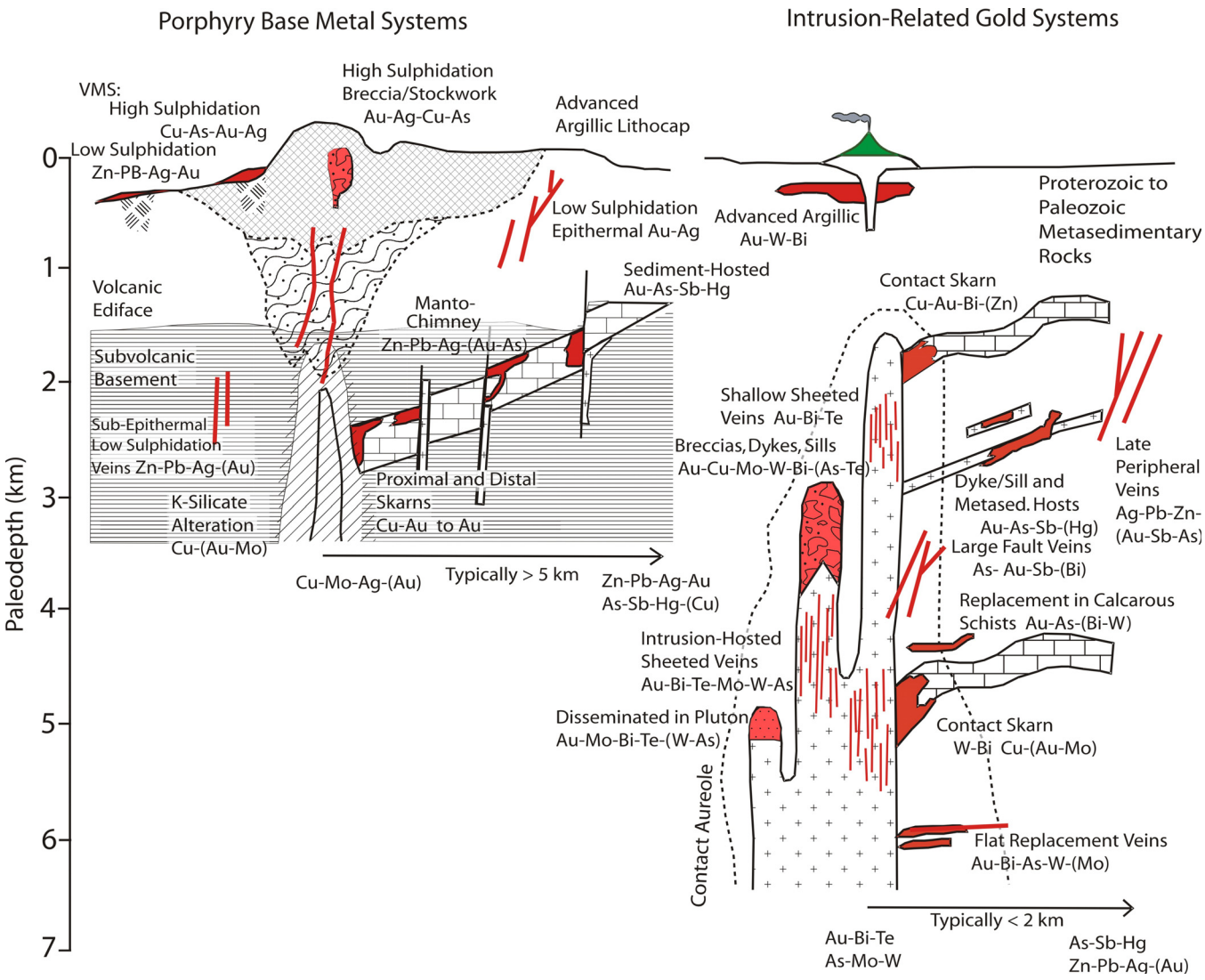


Figure 6. Genetic model for porphyry base metal and intrusion-related gold deposits (from Lang et al., 2000).

extending southeast from Alaska through the Yukon to the study area that is defined by metalliferous to non-metalliferous suites of peraluminous to metaluminous radiogenic character respectively (Gordey and Anderson, 1993; Smith, 2000). Rasmussen et al. (2007a) used the classifications of Hart et al. (2004, 2005) to subdivide the plutons in the MERA 2 study area into three suites: Tay River, Tungsten, and Tombstone. Collectively these were formerly known as the Selwyn Plutonic suite (Gordey and Anderson, 1993).

The gemstone component of the intrusion-related deposit model was not studied in detail for MERA 2. Table 1 of Rasmussen et al. (2007a) placed tourmaline (B-elbaite) in the Tombstone suite and Be-emerald in association with the Tungsten suite. They also mentioned the specific setting of elbaite in the O'Grady Batholith (after Ercit et al., 2003). The quartz vein-hosted emerald (chromium-rich beryl) occurrence in the Lened pluton contact-skarn rocks was documented by Groat et al. (2003) and Marshall et al. (2004).

Carlin-Type Gold as Lode and/or Derived Placer Deposits

Placer gold deposits have experienced the longest recorded exploration history in the Nahanni region. Since the 1920s, prospectors have hunted for placer gold in the Caribou River valley, in the southwest part of the study area. Even now, little is known about the gold and its possible sources. A number of potential lode gold sources have been suggested:

1. Intrusion-hosted veins or disseminations in skarn or siliceous contact aureoles (Spirito et al., 1988; Jefferson et al., 2003b; Rasmussen et al., 2007a).
2. A Carlin-type gold lode source from a disseminated sedimentary host rock (e.g. Richards, 1989; Rowan, 1989; Poulsen, 1996; Jefferson et al., 2003b; Cline et al., 2005; Emsbo et al., 2006) (Fig. 7).

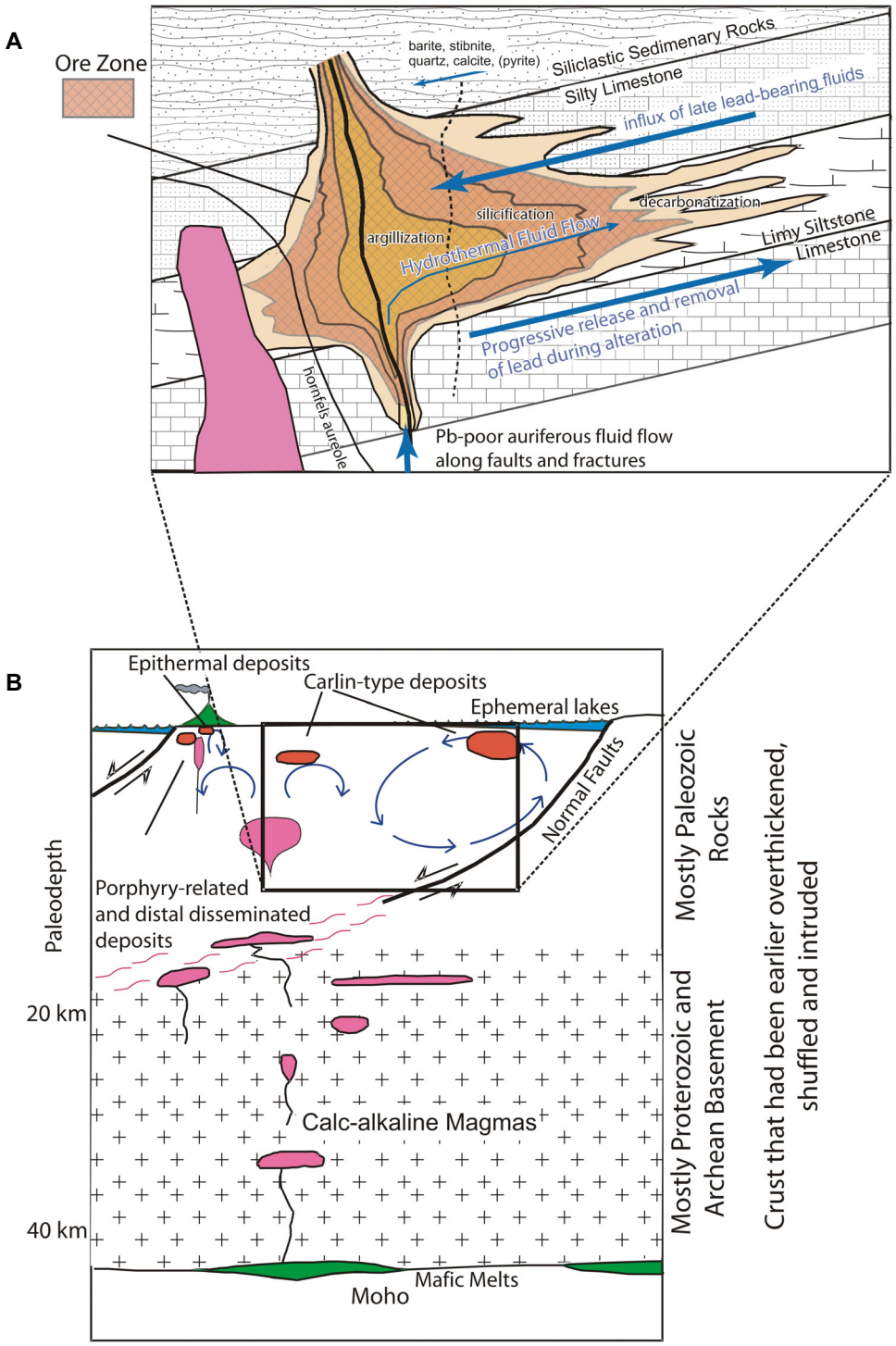


Figure 7. Genetic model for Carlin-type gold deposits. **A)** Crustal setting of fine-grained disseminated gold deposits in the Nevada area (from Howard, 2003). **B)** Detail of gold-bearing fluids interacting with permeable 'dirty' carbonate units resulting in an alteration halo and gold deposition (from Tosdal et al., 2003).

3. Tetrahedrite-bearing sulphide veins (Spirito et al., 1988; Jefferson and Paré, 1991; Jefferson et al., 2003b) that may in places crosscut fault-controlled base metal mineralization such as Prairie Creek (Paradis, 2007).
4. Glacially transported gold derived from the east, sourced in orogenic quartz veins of the Slave craton (Spirito et al., 1988; Jefferson and Spirito, 2003; Rasmussenet al, 2007b).

The possibility of multiple sources of gold for placer occurrences can not be discounted as there is a lack of statistically valid data available to ascertain similarities or dissimilarities between the placer gold and gold from specific lodes sources. Rasmussen et al. (2007b)

Table 2. Explanation of mineral and energy potential rating categories used in previous MERA studies.

RATING	POTENTIAL	CRITERIA
1	Very high	Geological environment is very favourable Significant deposits[1] are known Presence of undiscovered deposits is very likely
2	High	Geological environment is very favourable Occurrences are known Presence of undiscovered deposits is likely
3	Moderate to high	Intermediate between moderate and high potential Reflects greater uncertainty due to fewer data
4	Moderate	Geological environment is favourable Occurrences may or may not be known Presence of undiscovered deposits is possible
5	Low to moderate	Intermediate between low and moderate potential Reflects greater uncertainty due to fewer data or inferred greater depth of buried resources
6	Low	Some aspects of the geological environment are favourable but are limited in extent Occurrences generally not known Presence of undiscovered deposits is unlikely
7	Very low	Geological environment is unfavourable No occurrences[2] are known Presence of undiscovered deposits is very unlikely

determined that the composition of placer grains from the eastern part of the study areas overlaps with gold grain compositions from the western part of the study area. The latter have been interpreted as derived from intrusion-related lode sources (Rasmussen et al., 2007a,b). The discovery of new placer deposits and outcrops containing anomalous gold suggests that future work may be able to resolve this question (Carne, 2007).

The Carlin-type model is included as one of the four used in the overall mineral potential anlaysis. Carlin-type gold has not yet been identified in bedrock in the study area. The possibility of its presence has been suggested by similar trace element signature and tectonic regime to those of northern Nevada (Richards, 1989; Rowan, 1989; Poulsen, 1996; Emsbo et al., 2006). In the type Nevada region, most large Carlin-type gold deposits are hosted by basinal sedimentary host-rocks in a distal back-arc environment affected by deep-seated structures. Carlin-type deposits are spatially and temporally associated with either Cretaceous plutonism or younger Eocene magmatism. Poulsen (1996) noted that the association of gold with specific Tombstone suite intrusions through Yukon-Alaska, including the Tombstone suite intrusions that crops out in the study area, is analogous to the relationship identified in the Carlin-type area (Hart et al., 2005; Gabrielse et al., 2006; Rasmussen et al., 2007a).

Mineral Potential Modelling

The new and existing geoscience data were compiled into a spatial database (Lemkow et al., 2007). These data were used by Harris et al. (2007) as 'evidence' layers (geological controls) to produce mineral potential maps for each of the four mineral deposit types described above using a GIS-based modified knowledge-driven approach. Evidence maps included favourable rock units, structural features, geochemistry (from stream sediments, stream waters, and spring waters) and mineral occurrences. An overall mineral potential map was generated by combining the information from the four mineral potential maps plus the hydrocarbon potential (determined in the MERA 1 study).

The GIS method of assigning mineral potential ratings in this report differs from all previous MERA reports. The previous standard was to assign resource potential ratings to assessment domains defined by distinctive combinations of geological and geochemical characteristics. The ratings were qualitative, from 1 (very high) to 7 (very low), based on presence or absence of parameters for each possible published mineral deposit type (Table 2). Ratings in the present report were generated as five relative classes in a GIS by assigning weights to evidence layers such as specific lithologic units, chemistry, proximity to structural controls, geophysical anomalies (where present) and proximity to mineral deposits, using geological knowledge

Table 3. Summary of evidence layers used by the geographical information system (GIS) integration method (Harris et al., 2007) for four composite mineral deposit models. The GIS was used to generate five-class relative-potential maps by dividing the continuous-potential maps into five categories from high to low, based on natural breaks in their distribution functions. These ratings apply only in relative terms to the Nahanni study area and have no relationship to previous MERA mineral and energy potential rating categories shown in Table 2.

Sediment-Hosted Base Metal (SEDEX) Deposits Evidence Map (17 evidence maps)
Favourable rock units
Structural features (carbonate-shale facies change, proximity to volcanics, growth faults, and faults)
Geochemistry pathfinder elements
pH
Springs with anomalous SEDEX element signatures
Mineral occurrences with SEDEX characteristics
Carbonate-Fault (carbonate-hosted base metals associated with major faults) Deposits Evidence Map (15 evidence maps)
Favourable rock units
Structural features (carbonate-shale facies change, proximity to growth faults, and faults)
Geochemistry pathfinder elements
Springs with anomalous carbonate-fault element signatures
Mineral occurrences with carbonate-fault characteristics
Intrusion-Related Deposit Evidence Map (14 evidence maps)
Favourable rock units
Structural features (faults)
Geochemistry pathfinder elements
Springs with anomalous intrusion-related element signatures
Mineral occurrences with intrusion-related characteristics
Carlin-Type/Placer-Type Deposits Evidence Map (20 evidence maps)
Favourable rock units
Structural features (proximity to volcanics, growth faults, and faults, anticlines)
Geochemistry pathfinder elements
pH
Springs with anomalous Carlin-type element signatures
Placer gold occurences
Lode gold mineral occurences
Airborne gamma-ray spectrometry
Overall Mineral Potential Map
Integrates the above four deposit model maps plus hydrocarbon assessment by Osatetz et al. (2003)

(Harris et al., 2007). The evidence layers used to model the four different deposit types are summarized in Table 3. The advantage of the GIS method is that it integrates large amounts of spatial data using consistent quantitative methods. The process is auditable, reproducible, and more effective at delineating the favourable areas. It also made possible for the first time, digital transformation of the geologically oriented resource potential ratings into park planning units. The results of Harris et al. (2007) are reproduced in the Executive Summary (Wright et al., 2007).

Confidence in this Assessment

Each assessment and its products are influenced by the availability and quality of data at an appropriate scale and the amount of time for the analysis to be conducted. Furthermore all resource assessments are sensitive to new work and research and thus have a distinct shelf-life. Ten years may be the longest that an assessment can be valid (Jefferson and Spirito, 2003). New geological knowledge may reveal rocks with significantly different potentials than were identified earlier. Changes to technology or economics may influence the demand on elements not previously considered to have any significance.

The information presented here, based on integration of new field and laboratory studies with existing knowledge, aims to improve the confidence in this assessment for policy-makers to design national parks while minimally compromising future non-renewable resource development. The mineral potential maps produced in the Nahanni MERA 2 are a reflection of the present knowledge base with respect to different deposit models known or thought to be important in the study area represented by a limited number of evidence maps that have been combined using a subjective weighting system and integration method. The entire process is a modified knowledge-driven approach and the mineral potential maps generated represent a ‘best estimate’ given the limitations discussed above. These maps are expected to change in various areas over time, given increased exploration and scientific knowledge and the advancement of mineral deposit models. Ideally re-evaluation at regular intervals could address such changes.

Individual papers present data and assess for mineral potential and geological relationships from their individual perspectives. The GIS paper takes these results into consideration and provides the definitive mineral potential based on a holistic analysis of all of the data.

If sufficient quantitative information on the amount of estimated metals is available, the assessment can be expressed in current dollar values of recoverable metals in the ground for each deposit type (Cox and Singer, 1986; Grunsky et al., 1994; selected references to

Mineral Resource Assessment in British Columbia, (http://www.em.gov.bc.ca/mining/geolsurv/Minpot/mpref.htm)). The federal MERA process is designed for regional-scale assessment of areas with low data density, and therefore restricts itself to qualitative relative rating schemes (Tables 2, 3). The interdepartmental MERA working groups convey the economic and strategic implications of qualitative mineral and energy resource assessments to stakeholders and decision makers by means of public consultations that include examples of mines in other parts of Canada or the world that may be represented in the area of interest.

ORGANIZATION OF THIS REPORT AND RESPONSIBILITIES OF THE AUTHORS

The Executive Summary (Wright et al., 2007) provides a high-level précis of the entire Nahanni MERA 2 with a focus on key results. This paper describes the MERA process, the generalized geological context, and defines four mineral deposit models for the various components of the Nahanni MERA 2. In addition to the authors, contributions were incorporated from M. Burgess, C.W. Jefferson, and A. Okulitch. The primary results of the MERA 2 studies are presented in a series of papers grouped as follows: Part 1. Regional Surveys, Part 2. Mineral Deposit Studies, and Part 3. Modelling. Appendix 1 (Falck, 2007) provides background information on the regional geology of the study area and supplements the mineral deposit studies. Appendix 4 (Lemkow et al., 2007) archives all data collected and generated during the MERA 2 as a digital, georeferenced, 2-D geoscience database.

Part 1. Regional Studies

Caron et al. (2007) present the results of a regional geochemical study of spring waters. It incorporates and reinterprets data from MERA 1 spring studies, generates a list of anomalous springs and shows that this type of study can be effective for identifying mineralized zones as well as important environmental baseline data in under-explored areas. The primary results were incorporated and re-processed statistically in the GIS analysis (Harris et al., 2007), in terms of the four mineral deposit models for Nahanni MERA 2.

A regional stream sediment and water survey over the entire study area (McCurdy et al., 2007) provides a complete uniform layer of geochemical data critical for modelling mineral potential as well as important environmental baseline data.

Charbonneau (2007) summarizes key results of the combined, helicopter-borne, gamma ray spectrometric and total field magnetic surveys flown over three representative mineral potential areas where the results are most likely to assist in resolving park boundary issues. In each area, geophysical anomalies express bedrock lithological units and alteration systems related to mineral potential.

Duk-Rodkin et al. (2007) provide an overview of the Quaternary geology and glacial limits. Such information is vital to understanding the current landscape, transport of geochemical media, and the setting of placer gold deposits.

Part 2. Mineral Deposit Studies

Paradis (2007) investigates the geology and chemistry associated with the Prairie Creek mine - the representative locality for the ‘carbonate-fault (carbonate-hosted zinc-lead-silver associated with major faults) deposit model. The results of this study provide crucial information for modelling this type of deposit in the study area.

The Cantung mine is the only operating mine in the study area and is an important world source of tungsten. Yuvan et al. (2007) define a possible process and geological environment for this component of the intrusion-related deposit model for other portions of the study area.

Barnes et al. (2007) update knowledge of the Late Cretaceous Little Nahanni Pegmatite Group. This rare metal pegmatite occurrence is another facet of the intrusion-related model.

Rasmussen et al. (2007a) review the evolution and classification of the Cretaceous plutonic suites, and related gold metallogeny as a fundamental framework and additional facet for both the Intrusion-Related and Carlin-Type gold models. Information on geochronology, geochemistry, geophysics, Pb-Isotopes and magmatic fluid compositions was included.

Cousens (2007) uses an isotopic approach to the origin and potential for discovery of additional SEDEX deposits in the Howards Pass area.

Part 3. Mineral Potential Modelling

Harris et al. (2007) present favourability maps for four composite mineral deposit models and an overall synthesis. The GIS and quantitative spatial analysis methods critically integrated all information collected during the course of the Nahanni MERA 1 and 2 projects and generated the final mineral potential assessment. The final resource potential map included the hydrocarbon resource assessment from MERA 1 (Osadetz et al., 2003) and was transformed into catchment basin planning units used by Parks Canada.

Appendices

Appendix 1 (Falck, 2007) is an overview of the regional geology including crustal structure of the study area and its relevance to metallogeny. Guidance and reviews were provided by A. Okulitch and C.W. Jefferson.

Appendix 2 (Rasmussen et al., 2007b) presents the results of a morphological and compositional analysis of gold grains in the South Nahanni River drainage. This previously published paper was part of their study of the intrusion-related deposit model for MERA 2.

Appendix 3 (Caron, 2007) provides additional analytical results and information on springs not presented in Caron et al. (2007).

Appendix 4 (Lemkow et al., 2007) archives all digital data collected as part of the MERA 2 study, compiled into a current, internally consistent, georeferenced, digital database suitable for use in Geographic Information Systems. This database will allow future users to view and analyse data.

ACKNOWLEDGEMENTS

Funding was provided by Parks Canada, Department of Indian Affairs and Northern Development, and Natural Resources Canada with logistical support from the Northwest Territories Geoscience Office. NSERC support was provided to the graduate students through Dr. Cathryn Ryan, University of Calgary for Marie-Eve Caron, and Dr. Jim Mortensen, University of British Columbia, for Kirsten Rasmussen. National Science Foundation funding support was also provided through Dr. Kevin Shelton, University of Missouri for Jason Yuvan.

We are extremely grateful to the personnel of Canadian Zinc Corporation, for all of the logistical support and especially to Alan Taylor, for the geological information on the Prairie Creek deposit. Canadian Zinc Corporation is also thanked for the access to the property, drill cores and underground tours of the deposit.

Pacifica Resources Ltd, in particular Jason Dunning, John J. O'Donnell, and Geoff Newton were very generous with their time and knowledge of the Howards Pass deposits. The logistical support, accommodations and helicopter support, that they provided, as well as, access to the property and drill core were invaluable.

North American Tungsten Ltd. and especially Dave Tenney are thanked for the access to the site, housing, food and use of the facilities and equipment at Cantung. Dennis Bergen, Shawn Horte, Matt Kochtubajda, Peter Mason, and Joe Clarke all contributed immensely through discussions, data and files. The tours underground and of the open pit, access to the exploration files and core were important for understanding the formation of skarn deposits.

Brad Wilson of Alpine Gems is thanked for access to the Stargazer Claims and all of the discussions regarding gems and their potential in the Nahanni Region. Bernard Gaboury and True North Gems Ltd. are thanked for the visit to their property allowing comparison with Yukon Emeralds. Heather Neufeld is also thanked for all of her insights into the Regal Ridge property.

Dave White of Aurora Geosciences Ltd. is thanked for his mineral occurrence research, discussions, and unpublished report on the NORMIN database.

Kirsten Rasmussen is especially thanked all of the assistance in the field to H. Falck, and for her organizational skills in field season preparation and wrap up. Fieldwork was greatly assisted by Jim Mortensen, Kevin Shelton, Jason Yuvan, Suzanne Paradis, Al Doherty, Bob Hodder, Duncan McBean, Mike Power, Lee Groat, Lara Lewis, Steve Grasby, Marie-Eve Caron, Melanie Myden, Laurie Fichter, Jessica Jumbo, and Elspeth Barnes.

The field logistics were efficient and effective due to the efforts of Glen Sibbeston, Colin Monroe, Great Slave Helicopters, Jacques Harvey, South Nahanni Airways, Susan Sibbeston, Bannockland B+B, Arctic Sunwest Charters, Trans North Helicopters, Alkan Air, and Prism Helicopters.

Acme Analytical Laboratories Ltd. conducted the major and trace element analyses. Thanks are extended to Dave Lentz, University of New Brunswick for the loans of standards. G.G. Hatch Isotope Laboratories of the University of Ottawa performed the sulphur isotope analyses. Bill Davis of the geochronology laboratories of the GSC did most of the Sr isotope analyses on the carbonates. Brian L. Cousens of the Herzberg Laboratories of Carleton University performed the Pb analyses on sulphides and some Sr isotope analyses on carbonates. O and C isotope analyses on carbonates were done at the Delta Lab of GSC in Quebec City. Sm-Nd analyses were carried out by Vishal Gupta, Integrated Sciences Program, Carleton University. Sample preparation and lab chemistry were ably handled by Anatoliy Franchuk and Jacqueline Dohaney, and assistance in the mass spectrometry lab was provided by E.A. Spencer. John Blenkinsop was maintained the Triton at peak efficiency.

Conversations with Charlie Jefferson, Wayne Goodfellow, Rob Shives, Luke Ootes, Andrew Okulitch, John Kerswill, Dan Marshall, Steve Piercey, Dan Kontak, Velma Sterenberg, Donald Rotherham, Rob Roman, and Craig Hart were very helpful in the initial design of the project. GIS-support and satellite imagery provided by Kelly Pierce, Helmut Epp and Todd Slack were very useful especially the programming for Pocket PC Arcpad interconnection with GPS navigation.

Grateful acknowledgment goes to the following for their substantial improvements to various papers in the overall MERA 2 report: Andrea Mills, Edith Martel, Peter Hannigan, Kevin Shelton, Andrew Okulitch, and

Margo Burgess. The editorial and technical support of Elizabeth Ambrose and Sue Davis were essential to complete the overall report. The entire report, including all components except the digital database, was critically reviewed by Charlie Jefferson; this substantial contribution and the resulting improvements and refinements deserve special mention.

The following are thanked for critically reviewing manuscripts.

M. Burgess	Geological Survey of Canada
B. Daneshfar	Agriculture and Agri-Food Canada and University of Ottawa
R.G. Garrett	Geological Survey of Canada
W.D. Goodfellow	Geological Survey of Canada
P. Hannigan	Geological Survey of Canada
C. Jefferson	Geological Survey of Canada
D. Kerr	Geological Survey of Canada
J. Kerswill	Geological Survey of Canada
D. Kontak	Laurentian University
D. Lentz	University of New Brunswick
E. Martell	Government of the Northwest Territories
B. Mayer	University of Calgary
A. Mills	Government of the Northwest Territories
A. Okulitch	Geological Survey of Canada
R. Shives	Geological Survey of Canada

REFERENCES

Anglin, C.D. and Harrison, J.C.
1999: Mineral and energy resource assessment of Bathurst Island area, Nunavut (parts of NTS 68G, 68H, 69A, 69B and 79A); Geological Survey of Canada, Open File 3714, p. 250 p.

Barnes, E.M., Groat, L.A., and Falck, H.
2007: A review of the Late Cretaceous Little Nahanni Pegmatite Group and associated rare-element mineralization in the Selwyn Basin area, Northwest Territories, *in* Mineral and Energy Resource Assessment of the Greater Nahanni Ecosystem Under Consideration for the Expansion of the Nahanni National Park Reserve, Northwest Territories, (ed.) D.F. Wright, D. Lemkow, and J.R. Harris; Geological Survey of Canada, Open File 5344, p. 191-202.

Canadian Zinc Corporation
2001: Prairie Creek mine, Northwest Territories, Scoping Study; Internal report, Canadian Zinc Corporation, January 29, 2001, 185 p.

Carne, R.C.
2007: Farms Out Mac Gold Project; Atac Resources Ltd. Tue Feb 27, 2007 http://www.atacresources.com/s/NewsReleases.asp?ReportID=180879&_Type=News-Releases&_Title=Atac-Resources-Ltd.-Farms-Out-Mac-Gold-Project

Caron, M-E.
2007: Spring geochemistry: A tool for mineral exploration in the South Nahanni River basin of the Mackenzie Mountains, Northwest Territories, Appendix 3 *in* Mineral and Energy Resource Assessment of the Greater Nahanni Ecosystem Under Consideration for the Expansion of the Nahanni National Park Reserve, Northwest Territories, (ed.) D.F. Wright, D. Lemkow, and J.R. Harris; Geological Survey of Canada, Open File 5344, p. 381-547 (M..Sc. Thesis, University of Calgary, Alberta, 152 p.)

Caron, M-E., Grasby, S.E., and Ryan, M.C.
2007: Spring geochemistry: A tool for exploration in the South Nahanni River basin of the Mackenzie Mountains, Northwest Territories, *in* Mineral and Energy Resource Potential of the Proposed Expansion to the Nahanni National Park Reserve, North Cordillera, Northwest Territories, (ed.) H. Falck, D.F. Wright, and J. Harris; Geological Survey of Canada, Open File 5344, p. 31-73.

Carson, J.M., Dumont, R., Potvin, J., Buckle, J., Shives. R.B.K., and Harvey, B.
2007a: Geophysical Series - NTS 95F - Virginia Falls, Northwest Territories; Geological Survey of Canada, Open File 5154, 1 CD-ROM.
2007b: Geophysical Series – NTS 95D and 95E – Flat River, Northwest Territories; Geological Survey of Canada, Open File 5160, 1 CD-ROM.
2007c: Geophysical Series – NTS 105H and 105I – Little Nahanni River, Northwest Territories; Geological Survey of Canada, Open File 5164, 1 CD-ROM.

Charbonneau, B.W.
2007: Evaluation of airborne radiometric and magnetic data in the vicinity of the Nahanni National Park Reserve, Northwest Territories, Canada, *in* Mineral and Energy Resource Assessment of the Greater Nahanni Ecosystem Under Consideration for the Expansion of the Nahanni National Park Reserve, Northwest Territories, (ed.) D.F. Wright, D. Lemkow, and J.R. Harris; Geological Survey of Canada, Open File 5344, p. 99-123.

Cline, J., Hofstra, A., Muntean, J., Tosdal, R.M., and Hickey, K.A.
2005: Carlin-type gold deposits in Nevada: Critical geologic characteristics and viable models, *in* Economic Geology 100th Anniversary Volume: 1905-2005, (ed.) J.W. Hedenquist, J.F.H. Thompson, R.J. Goldfarb, and J.P. Richards; Society of Economic Geologists, p. 451-484.

Cousens, B.
2007: Radiogenic isotope studies of Pb-Zn mineralization in the Howards Pass area, Selwyn Basin, *in* Mineral and Energy Resource Assessment of the Greater Nahanni Ecosystem Under Consideration for the Expansion of the Nahanni National Park Reserve, Northwest Territories, (eds.) D.F. Wright, D. Lemkow, and J.R. Harris; Geological Survey of Canada, Open File 5344, p. 281-294.

Cox, D.P. and Singer, D.A. (eds.)
1986: Mineral Deposit Models; United States Geological Survey Bulletin 1693, 379 p.

Day, S.J.A., Lariviere, J.M., Friske, P.W.B., Gochnauer, K.M., MacFarlane, K.E., McCurdy, M.W. and McNeil, R.J.
2005: National Geochemical Reconnaissance (NGR): Regional stream sediment and water geochemical data, Macmillan Pass - Sekwi Mountain, Northwest Territories; Geological survey of Canada, Open File 4949.

Deklerk, R. and Traynor, S. (comp.)
2005: Yukon MINFILE 2005 - A database of mineral occurrences; Yukon Geological Survey, CD-ROM.

Department of Indian Affairs and Northern Development (DIAND)
2006: NORMIN.DB, The Northern Minerals Database; Northwest Territories GeoscienceOffice, Yellowknife, Northwest Territories.

Dewing, K., Sharp, R.J., Ootes, L., Turner, E.C., and Gleeson, S.
2006: Geological assessment of known Zn-Pb showings, Mackenzie Mountains, Northwest Territories, *in* Current Research 2006-A4, Geological Survey of Canada, 12 p.

Duk-Rodkin, A., Huntley, D., and Smith, R
2007: Quaternary geology and glacial limits of the Nahanni National Park Reserve and adjacent areas, Northwest Territories, Canada, *in* Mineral and Energy Resource Assessment of the Greater Nahanni Ecosystem Under Consideration for the Expansion of the Nahanni National Park Reserve, Northwest Territories, (ed.) D.F. Wright, D. Lemkow, and J.R. Harris; Geological Survey of Canada, Open File 5344, p. 125-130.

Eckstrand, O.R., Sinclair, W.D., and Thorpe, R.I. (ed.)
1995: Geology of Canadian Mineral Deposit Types; Geological Survey of Canada, no. 8, 633 p., (also Geological Society of America, The Geology of North America, v. P-1).

Emsbo, P., Groves, D.I., Hofstra, A.H., and Bierlein, F.P
2006: The giant Carlin gold province: a protracted interplay of orogenic, basinal, and hydrothermal processes above a lithospheric boundary; Mineralium Deposita, v. 41, p. 517-525.

Ercit, T.S., Groat, L.A., and Gault, R.A.
2003: Granitic pegmatites of the O'Grady batholith, NWT - a case study of the evolution of the elbaite subtype of rare element pegmatite; Canadian Mineralogist, v.41, p. 117-137.

Falck, H.
2007: A review of the bedrock geology of the Nahanni River region and its context in the Northern Cordillera, Appenidx 1 *in* Mineral and Energy Resource Assessment of the Greater Nahanni Ecosystem Under Consideration for the Expansion of the Nahanni National Park Reserve, Northwest Territories, (ed.) D.F. Wright, D. Lemkow, and J.R. Harris; Geological Survey of Canada, Open File 5344, p. 327-366.

Ford, K.L., Shives, R.B.K., and Charbonneau, B.W.
1998: Application of airborne gamma-ray spectrometry to geological mapping: Mineral exploration and land-use planning, *in* Proceedings of the 10th Latin American Geological Congress (Symposium on Airborne Geophysics and Geochemistry in the Prospecting for Minerals); p 131-150.

Friske, P.W.B., McCurdy, M.W., Day, S.J.A., and Durham, C.C.
1999: Reanalysis of stream sediments from the Little Nahanni River map sheet (105I), Yukon and Northwest Territories; Geological Survey of Canada, Open File 3772, 1 CD-ROM.

Friske P.W.B., McNeil R.J., McCurdy M.W., Wilson, R.S., and Day S.J.A.
2006: Geochemical data from a National Geochemical Reconnaissance stream sediment and water Survey in the Yukon portion of the Flat River map area, southeast Yukon Territory (Part of NTS 95E); Yukon Geological Survey Open File 2006-18 (also Geological Survey of Canada, Open File 5329, 1CD-ROM).

Gabrielse, H., Murphy, D.C., and Mortensen, J.K.
2006: Cretaceous and Cenozoic dextral orogen-parallel displacements, magmatism, and paleogeography, north-central Canadian Cordillera, *in* Paleogeography of the North American Cordillera: Evidence for and Against Large-Scale Displacements, (ed.) J.W. Haggart, R.J. Enkin, and J.W. Monger; Geological Association of Canada, Special Paper 46, p. 255-276.

Galbraith, J.H. and Saunders, D.F.
1983: Rock classification by characteristics of aerial gamma-ray measurements; Journal of Geochemical Exploration, v. 18, p. 49-73.

Goodfellow, W.D.
1982: Geochemical Stream Sediment and Water, Nahanni, Yukon and District of Mackenzie, Maps and Data; Geological Survey of Canada, Open File 868, 156 p.

Goodfellow, W.D. and Lydon, J.W.
2007: Sedimentary exhalative (SEDEX) deposits, *in* Mineral Deposits of Canada: A Synthesis of Major Deposit Types, District Metallogeny, the Evolution of Geological Provinces, and Exploration Methods, (ed.) W.D. Goodfellow; Geological Association of Canada, Mineral Deposits Division, Special Publication No. 5, p. 163-183.

Gordey, S.P., Abbott, J.G., Tempelman-Kluit, D.J., and Gabrielse, H.
1987: "Antler" clastics in the Canadian Cordillera; Geology, v. 15, p. 103-107.

Gordey, S.P. and Anderson, R.G.
1993: Evolution of the Northern Cordilleran Miogeocline, Nahanni Map Area (105I), Yukon and Northwest Territories; Geological Survey of Canada, Memoir 428, 214 p.

Government of Canada
1995: Terms of Reference, Mineral and Energy Resource Assessment (MERA) of Proposed National parks in Northern Canada; commissioned and approve by the Senior MERA committee, Governments of Canada, Yukon and Northwest Territories, Ottawa; 8 p. website http://www.nrcan.gc.ca/smm/pdf/meratxte.pdf

Groat, L.A., Mulja, T., Mauthner, M.H.F., Ercit, T.S., Raudsepp, M. Gault, R.A., and Follo, H.A.
2003: Geology and mineralogy of the Little Nahanni rare-element granitic pegmatites, Northwest Territories; Canadian Mineralogist, v. 41, p. 139-160.

Grunsky, E.C. Massey, N.W.D., and Kilby, W.E.
1994: Mineral resource assessment in British Columbia, the Mineral Potential Project; Nonrenewable Resources, v. 3, p. 271-283.

Halliwell, D.R. and Catto, S.
2003: How and why is aquatic quality changing at Nahanni National Park Reserve, NWT, Canada?; Environmental Monitoring and Assessment, v. 88, p. 243-281.

Hamilton, S.M,. Michel, F.A, Jefferson, C.W., and Power-Fardy, D.
2003: Spring water geochemistry and hydrogeology for mineral resource assessment of the South Nahanni River region, *in* Non-Renewable Mineral and Energy Resource Potential of the Proposed Extensions to Nahanni National Park Reserve, Northern Cordillera, Northwest Territories, (ed.) C.W. Jefferson and W. Spirito; Geological Survey of Canada, Open File 1686, p. 5-1 to 5-40.

Harris, J.R., Lemkow, D., Wright, D.F., and Falck, H.
2007: Modelling mineral potential for the Greater Nahanni Ecosystem using GIS-based analytical methods, *in* Mineral and Energy Resource Assessment of the Greater Nahanni Ecosystem Under Consideration for the Expansion of the Nahanni National Park Reserve, Northwest Territories, (eds.) D.F. Wright, D. Lemkow, and J.R. Harris; Geological Survey of Canada, Open File 5344, p. 295-328.

Hart, C.J.R.
2005: Classifying, distinguishing and exploring for intrusion-related gold systems, *in* The Gangue, Geological Association of Canada Mineral Deposits Division, Newsletter, October 2005, v. 87, p.1-9.

Hart, C. J.R., Goldfarb, R.J., Lewis, L.L., and Mair, J.L.
2004: The northern cordilleran mid-Cretaceous plutonic province: Ilmenite/magnetite-series granitoids and intrusion-related mineralization; Resource Geology, v. 54, p. 253-280.

Hart, C.J.R., Mair, J.L., Goldfarb, R.J., and Groves, D.I.
2005: Source and redox controls on metallogenic variations in intrusion-related ore systems, Tombstone-Tungsten belt, Yukon Territory, Canada; Geological Society of America, Special Papers, v. 389, p. 339-356.

Heffernan, R.S.
2004: Temporal, Geochemical, Isotopic and Metallogenic Studies of mid- Cretaceous Magmatism in the Tintina Gold Province, Southeastern Yukon and Southwestern Northwest Territories, Canada; M.Sc. thesis, University of British Columbia, Vancouver, British Columbia, 83 p.

Howard, K.A.
2003: Crustal structure in the Elko-Carlin region, Nevada, during Eocene gold mineralization: Ruby-East Humboldt metamorphic core complex as a guide to the deep crust; Economic Geology, v. 98, p. 249-268.

Hubbard, D.
1957: Logan Mountains, N.W.T.; 1955 Canadian Alpine Journal, v. XL, p. 21-47.

Hulbert, L.J., Gregoire, C.D., Paktunc, D., and Carne, R.C.
1992: Sedimentary nickel, zinc and platinum-group-element mineralization in Devonian black shales at the Nick Property, Yukon, Canada: A new deposit type; Canadiun Institute of Mining, Metallurgy and Petroleum, Exploration and Mining Geology, v. 1, p. 39 - 62.

Hyndman, R.D., Cassidy, J.F., Adams, J., Rogers, G.C., and Mazzotti, S.
2005a: Earthquakes and seismic hazard in the Yukon-Beaufort-Mackenzie; Canadian Society of Exploration Geologists (CSEG), Recorder, May 2005, p. 32-66.

Hyndman, R.D., Flueck, P., Mazzotti, S., Lewis, T.J., Ristau, J., and Lucinda, L.
2005b: Current tectonics of the northern Canadian Cordillera; Canadian Journal of Earth Sciences, v. 42, p. 1117-1136.

Jefferson, C.W.
2003: Mineral resource assessment of the Tlogotsho Plateau, Nahanni Karst, Ragged Ranges and adjacent areas under consideration for expansion of Nahanni National Park Reserve, N.W.T, *in* Non-Renewable Mineral and Energy Resource Potential of the Proposed Extensions to Nahanni National Park Reserve, Northern Cordillera, Northwest Territories, (ed.) C.W. Jefferson and W. Spirito; Geological Survey of Canada, Open File 1686, p. 7-1 to 7-11.

Jefferson, C.W. and Pare, D.
1991: New placer gold anomalies in the northern Liard Range – southern Ram Plateau area, South Nahanni River region, District of Mackenzie, Northwest Territories, *in* Current Research, Part E; Geological Survey of Canada, Paper 91-1E, 4 p.

Jefferson, C.W. and Spirito, W. (ed.)
2003: Non-Renewable Mineral and Energy Resource Potential of the Proposed Extensions to Nahanni National Park Reserve, Northern Cordillera, Northwest Territories; Geological Survey of Canada, Open File 1686, 253 p.

Jefferson, C.W., Smith, J.E.M., and Hamilton, S.M.
1991: Preliminary Account of the Resource Assessment Study of Proposed National Park, Wager Bay - Southampton Island Areas, District of Keewatin; Geological Survey of Canada, Open File 2351, 47 p.

Jefferson, C.W., Spirito, W.A. and Hamilton, S.M.
2003a: Geological setting, *in* Non-Renewable Mineral and Energy Resource Potential of the Proposed Extensions to Nahanni National Park Reserve, Northern Cordillera, Northwest Territories, (ed.) C.W. Jefferson and W. Spirito; Geological Survey of Canada, Open File 1686, p. 3-1 to 3-21.

Jefferson, C.W., Spirito, W.A., Hamilton, S.M., and Power-Fardy, D.
2003b: Mineral occurrences and geochemical anomalies, South Nahanni River Region, *in* Non-Renewable Mineral and Energy Resource Potential of the Proposed Extensions to Nahanni National Park Reserve, Northern Cordillera, Northwest Territories, (ed.) C.W. Jefferson and W. Spirito; Geological Survey of Canada, Open File 1686, p. 6-1 to 6-18.

Lang, J.R., Baker, T., Hart, C.J.R., and Mortensen, J.K.
2000: An exploration model for intrusion-related gold systems; Society of Economic Geologists Newsletter, no. 40, January 2000, p. 1 and 6-15.

Lariviere, J.M., Eddy, B.G., Udell, A., and Slack, T.
2006: Mackenzie Valley Mineral Potential Map; Northwest Territories Geoscience Office, Open File 2006-03, scale 1:1 500 000.

Leach, D.L., Sangster, D.F., Kelley, K.D., Large, R.R., Garven, G., Allen, C.R., Gutzmer, J., and Walters, S.
2005: Sediment-hosted lead-zinc deposits: A global perspective, *in* Economic Geology 100th Anniversary Volume: 1905-2005, (ed.) J.W. Hedenquist, J.F.H. Thompson, R.J. Goldfarb, and J.P. Richards; Society of Economic Geologists, p. 561-607.

Lemkow, D., Harris, J.R., and Slack, T.
2007: Digital geoscience database: A contribution to the Mineral and Energy Resource Assessment of the greater Nahanni ecosystem, Northwest Territories, Appendix 4 *in* Mineral and Energy Resource Assessment of the Greater Nahanni Ecosystem Under Consideration for the Expansion of the Nahanni National Park Reserve, Northwest Territories, (ed.) D.F. Wright, D. Lemkow, and J.R. Harris; Geological Survey of Canada, Open File 5344.

Lydon, J.W.
1995: Sedimentary exhalative sulphides (SEDEX), *in* Geology of Canadian Mineral Deposit Types, (ed.) O.R. Eckstrand, W.D. Sinclair, and R.I. Thorpe; Geological Survey of Canada, no. 8, p. 130-152 (also Geological Society of America, The Geology of North America)

Marshall, D.D., Groat, L.A., Falck, H., Giuliani, G., and Neufeld, H.
2004: The Lened Emerald prospect, Northwest Territories, Canada: Insights from fluid inclusions and stable isotopes, with implications for northern Cordilleran Emerald; Canadian Mineralogist, v. 42, p. 1523-1539.

Maurice, Y.T. and Charbonneau, B.W.
1987: U and Th Concentration processes in Canadian granitoids: Their detection by airborne gamma-ray spectrometry and their relationship to granophile mineralization; Revista Brasileira de Geociências, v. 17, p. 644-646.

McCurdy, M.W., McNeil, R.J., Friske, P.W.B., Day, S.J.B, and Wilson, R.S.
2007: Stream sediment geochemistry in the proposed extension to the Nahanni Park Reserve, *in* Mineral and Energy Resource Potential of the Proposed Expansion to the Nahanni National Park Reserve, North Cordillera, Northwest Territories, (ed.) D.F. Wright, D. Lemkow, and J. Harris; Geological Survey of Canada, Open File 5344, p. 75-98.

Meinert, L.D., Dipple, G.M., and Nicolescu, S.
2005: World skarn deposits, *in* Economic Geology 100th Anniversary Volume: 1905-2005, (ed.) J.W. Hedenquist, J.F.H. Thompson, R.J. Goldfarb, and J.P. Richards; Society of Economic Geologists, p. 299-336.

Morrow, D.W. and Cook, D.G.
1987: The Prairie Creek Embayment and Lower Paleozoic Strata of the Southern Mackenzie Mountains; Geological Survey of Canada, Memoir 412, 195 p.

Morrow, D.W., Cumming, G.L., and Aulstead, K.L.
1990: The Gas-Bearing Devonian Manetoe Facies, Yukon and Northwest Territories; Geological Survey of Canada, Bulletin 400, 54 p.

Mortensen, J.K., Hart, C.J.R., Murphy, D.C, and Heffernan, S.
2000: Temporal evolution of Early and mid-Cretaceous magmatism in the Tintina Gold Belt, *in* The Tintina Gold Belt:

Concepts, Exploration and Discoveries, (ed.) J. Jambor; British Columbia and Yukon Chamber of Mines, Special Volume 2, p. 49-57.

Okulitch, A.
in prep a: Geology of the Redstone River Area; National Earth Science Series, Geological Atlas, National Resources Canada, Map NP-9/10-G, 1:1 000 000 scale.

in prep b: Geology of the Ross River Area,;National Earth Science Series, Geological Atlas, National Resources Canada, scale 1:1 000 000.

Osadetz K.G., Chen, Z., and Morrow, D.W.
2003: Petroleum resource assessment of the Tlogotsho Plateau, Nahanni Karst and adjacent areas under consideration for expansion of the Nahanni National Park Reserve, Northern Cordillera and District of Mackenzie, *in* Non-Renewable Mineral and Energy Resource Potential of the Proposed Extensions to Nahanni National Park Reserve, Northern Cordillera, Northwest Territories, (ed.) C.W. Jefferson and W. Spirito; Geological Survey of Canada, Open File 1686, p. 8-1 to 8-36.

Paradis, S.
2007: Isotope geochemistry of the Prairie Creek carbonate-hosted zinc-lead-silver deposit, southern Mackenzie Mountains, Northwest Territories, *in* Mineral and Energy Resource Assessment of the Greater Nahanni Ecosystem Under Consideration for the Expansion of the Nahanni National Park Reserve, Northwest Territories, (ed.) D.F. Wright, D. Lemkow, and J.R. Harris; Geological Survey of Canada, Open File 5344, p. 131-176.

Parks Canada
2003: Memorandum of understanding between the Parks Canada Agency as represented by the Minister of Canadian Heritage and Deh Cho First Nations as represented by Deh Cho First Nations Grand Chief respecting the expansion of Nahanni National Park Reserve of Canada; http://www.dehchofirstnations.com/documents/resource_management/nahanni_expansion_mou_final.pdf); (accessed October 22, 2007).

Poulsen, K.H.
1996: Carlin-type gold deposits and their potential occurrence in the Canadian Cordillera; in, Cordillera and Pacific margin, *in* Current Research, Part A; Geological Survey of Canada, Paper 1996-A, p. 1-9.

Rasmussen, K.L., Mortensen, J.K., Falck, H. and Ullrich, T.D.
2007a: The potential for intrusion-related mineralization within the South Nahanni River MERA area, Selwyn and Mackenzie Mountains, Northwest Territories, *in* Mineral and Energy Resource Assessment of the Greater Nahanni Ecosystem Under Consideration for the Expansion of the Nahanni National Park Reserve, Northwest Territories, (ed.) D.F. Wright, D. Lemkow, and J.R. Harris; Geological Survey of Canada, Open File 5344, p. 203-244.

Rasmussen, K.L., Mortensen, J.K., and Falck, H.
2007b: Morphological and compositional analysis of placer gold in the South Nahanni River drainage, Northwest Territories, Appendix 2 *in* Mineral and Energy Resource Assessment of the Greater Nahanni Ecosystem Under Consideration for the Expansion of the Nahanni National Park Reserve, Northwest Territories, (ed.) D.F. Wright, D. Lemkow, and J.R. Harris; Geological Survey of Canada, Open File 5344 p. 367-380 (also Yukon Exploration and Geology 2006, (ed.) D.S. Emond, L.L. Lewis, and L.H. Weston; Yukon Geological Survey, p. 237-250).

Richards, B.G.
1989: Report on the Selena Creek placer property, Nahanni Mining Division, Northwest Territories, Latitude: 60º55'N; Longitude: 126º40'W; unpubl. Report for Sirius Resource Corporation and Verdstone Gold Corporation; Dynamin Engineering Limited, Vancouver, August 1989, 19 p.

Roots, E.F., Blusson, S.L., and Gabrielse, H.
1969: Geology, Coal River, Yukon Territory-District of Mackenzie; Geological Survey of Canada, Preliminary Map 11-1968.

Rowan, L.
1989: Similarities of geological environment and potential for Carlin-style mineralization at Selena Creek; unpubl. memorandum, Indian and Northern Affairs Canada Assessment Files, November 27, 1989.

Scoates, R.F.L., Jefferson, C.W., and Findlay, D.C.
1986: Northern Canada mineral resource assessment, *in* Prospects for Mineral Resource Assessment on Public Lands, (ed.) S.M. Cargill and S.B. Green; United States Geological Survey, Proceedings of the Leesburg Workshop, Circular 980, p. 111-139.

Shives, R.B.K., Ford, K.L., Charbonneau, B.W.
1995: Applications of gamma Ray Spectrometry Magnetic/VLF-EM Surveys Workshop Manual; Geological Survey of Canada, Open File 3061, 82 p.

Shives, R.B.K., Charbonneau, B.W., and Ford, K.L.
2000: The detection of potassic alteration by gamma-ray spectrometry – recognition of alteration related to mineralization; Geophysics, v. 65, p. 2001-2011.

Sillitoe, R.H. and Thompson, J.F.H.
1998: Intrusion-related vein gold deposits: types, tectono-magmatic settings and difficulties of distinction from orogenic gold deposits; Resource Geology, v. 48, p. 237-250.

Smith, M.
2000: The Tintina Gold Belt: An emerging gold district in Alaska and Yukon, *in* The Tintina Gold Belt: Concepts, exploration, and discoveries; British Columbia and Yukon Chamber of Mines, Special Volume 2, p. 1-3.

Spirito, W.A. and Jefferson, C.W.
2003: Regional surficial geochemistry, *in* Non-Renewable Mineral and Energy Resource Potential of the Proposed Extensions to Nahanni National Park Reserve, Northern Cordillera, Northwest Territories, (ed.) C.W. Jefferson and W. Spirito; Geological Survey of Canada, Open File 1686, p. 4-1 to 4-79.

Spirito, W.A., Jefferson, C.W., and Pare, D.,
1988: Comparison of gold, tungsten and zinc in stream silts and heavy mineral concentrates, South Nahanni resource assessment area, District of Mackenzie, *in* Current Research, Part E; Geological Survey of Canada, Paper 88-1E, p. 117-126.

Tate, D.P.
2004: Expanding Nahanni National Park Reserve – the contributions of research, consultation and negotiation, *in* Making Ecosystem Based Management Work, Connecting Managers and Researchers, (ed.) N.W.P. Munro, P. Deardon, T.B.Herman, Beazley, K., and S. Bondrup-Nielsen; Proceedings of the Fifth International Conference on Science and Management of Protected Areas, 11-16 May 2003, Wolfville, Nova Scotia, Canada.

Tosdal, R.M., Cline, J. S., Fanning, C.M., and Wooden, J.L.
2003: Lead in the Getchell-Turquoise Ridge carlin-type gold deposits from the perspective of potential igneous and sedimentary rocks sources in northern Nevada; Implications for fluid and metal sources; Economic Geology, v. 98, p.1189-1211.

Wetmiller, R.J., Horner, R.B., Hasegawa, H.S., North, R.G., Lamontagne, M., Weichert, D.H., and Evans, S.G.
1988: An analysis of the 1985 Nahanni earthquakes; Bulletin of the Seismological Society of America, v. 78, p. 590-616.

Wilkinson, J.J., Eyre, S.L., and Boyce, A.J.
2005: Ore-forming processes in Irish-type carbonate-hosted Zn-Pb deposits; Evidence from mineralogy, chemistry, and isotopic composition of sulfides at the Lisheen Mine; Economic Geology, v. 100, p. 63-86.

Wright, D.F., Jefferson, C.W., Burgess, M.M., and Lapalme, L.A.
2004: Canada's MERA process and the role of Earth sciences; Geological Survey of Canada, Open File 4732, 1 CD-ROM.

Yuvan, J., Shelton, K., and Falck, H.
2007: Geochemical investigations of the high-grade quartz-scheelite veins of the Cantung mine, Northwest Territories, *in* Mineral and Energy Resource Assessment of the Greater Nahanni Ecosystem Under Consideration for the Expansion of the Nahanni National Park Reserve, Northwest Territories, (ed.) D.F. Wright, D. Lemkow, and J.R. Harris; Geological Survey of Canada, Open File 5344, p. 177-190.

SPRING GEOCHEMISTRY: A TOOL FOR MINERAL EXPLORATION IN THE SOUTH NAHANNI RIVER BASIN OF THE MACKENZIE MOUNTAINS, NORTHWEST TERRITORIES

Marie-Eve Caron[1], Stephen E. Grasby[2], and M. Cathryn Ryan[1]
1. Department of Geology and Geophysics, University of Calgary, 2500 University Drive Northwest, Calgary, Alberta T2N 1N4
2. Geological Survey of Canada, 3303-33 Street Northwest, Calgary, Alberta T2L 2A7

ABSTRACT

Geochemical data from 155 spring locations within the remote 37,000 km^2 South Nahanni River basin of the Mackenzie Mountains, Northwest Territories, were used to evaluate the economic mineral potential of the region, an area proposed for a national park designation. Trace element analyses were evaluated using three different approaches (the sum of trace element concentrations as a percentage of total dissolved solids, identifying individual anomalously high trace elements, and the inverse use of the Ficklin Diagram). Two out of the three approaches detected the two known deposits of the area, Prairie Creek and Tungsten, but not with the same method in each case, indicating that a multi-pronged approach is best. The springs were determined to be elevated in trace elements in comparison to waters related to mining deposits around the world. Silica geothermometry determined the average depth of circulation of the springs to be 2.1 km for warm or hot springs, and ranging from 4.7 km to less than 200 m for the entire dataset, which is indicative of the accessibility of the predicted mineralized zones. These simple statistical and graphing methods can successfully identify mineralized zones quickly and efficiently in a largely under-explored area.

INTRODUCTION

Nahanni National Park Reserve was first designated by the Canadian Government in 1976 to protect the South Nahanni River basin, which flows through the Mackenzie Mountains, Northwest Territories (Fig. 1). It became a World Heritage Site in 1978 when three areas were chosen for possible future expansion: the Ragged Range, the Tlogotsho Plateau, and the Nahanni Karst (Fig. 1). In consequence, a Mineral and Energy Resource Assessment (MERA 1) was conducted in those areas (Jefferson and Spirito, 2003) including examination of spring waters (Hall et al., 1988; Hamilton et al., 1991; Timlin, 1991). A recent proposal to include the entire watershed of the South Nahanni River in the National Park Reserve has triggered a second, larger MERA study (MERA 2). This work forms one component of the MERA 2 study, which also includes airborne geophysics, stream sediment and stream water sampling, and hard-rock geology exploration.

The primary goal of this study is to assess the economic mineral potential of the South Nahanni River basin by examining the geochemistry of groundwater discharge for evidence of mineralization. A secondary benefit of this study is the possibility of determining an environmental baseline of aqueous geochemical data. Given that Nahanni waters, sediments, fish, and caribou have naturally elevated metals levels (Halliwell and Catto, 2003), it is important to characterize the natural background concentrations of a variety of chemical constituents that could be used to detect environmental impacts if any development were to occur in the future.

Dissolved constituents in spring water are used as geochemical tracers in an attempt to elucidate the types and locations of mineral deposits in the South Nahanni River basin. In particular, major ions are used to group springs with associated rock types, trace elements are studied in order to predict the type of mineral deposits that exist, and geothermometers are applied to estimate depth of circulation of springs. Stable isotopes help as tools to predict the origin of the waters.

GEOLOGICAL SETTING

The South Nahanni River basin encompasses two main geological regions: 1) the relatively flat eastern region, which is characterized by broadly folded karstic terrain, shallowly incised topography, and inferred faults; and 2) the mountainous western region with more complex structure (including igneous intrusions of the Cretaceous Selwyn Plutonic Suite) and strong glacially eroded terrain (Fig. 2).

The Mackenzie Mountains comprise mainly sedimentary rocks, including Neoproterozoic (ca. 800 Ma) to Late Cretaceous (ca. 100 Ma) platformal to basinal shale sedimentary strata. Older rocks were intruded by minor Devonian (350 Ma) granitoid rocks and all were folded and thrust faulted during the collision of an island arc with western North America, from the Jurassic (ca. 170 Ma) to Cretaceous. During this collisional event, the Selwyn and westernmost Mackenzie Mountains were intruded by major Cretaceous granitoid batholiths, which are interpreted to be a result of syn- to post-collisional partial melting of miogeoclinal

Caron, M-E., Grasby, S.E., and Ryan, M.C., 2007, Spring geochemistry: A tool for exploration in the South Nahanni River basin of the Mackenzie Mountains, Northwest Territories, *in* Mineral and Energy Resource Assessment of the Greater Nahanni Ecosystem Under Consideration for the Expansion of the Nahanni National Park Reserve, Northwest Territories, (eds.) D.F. Wright, D. Lemkow, and J.R. Harris; Geological Survey of Canada, Open File 5344, p. 31-74.

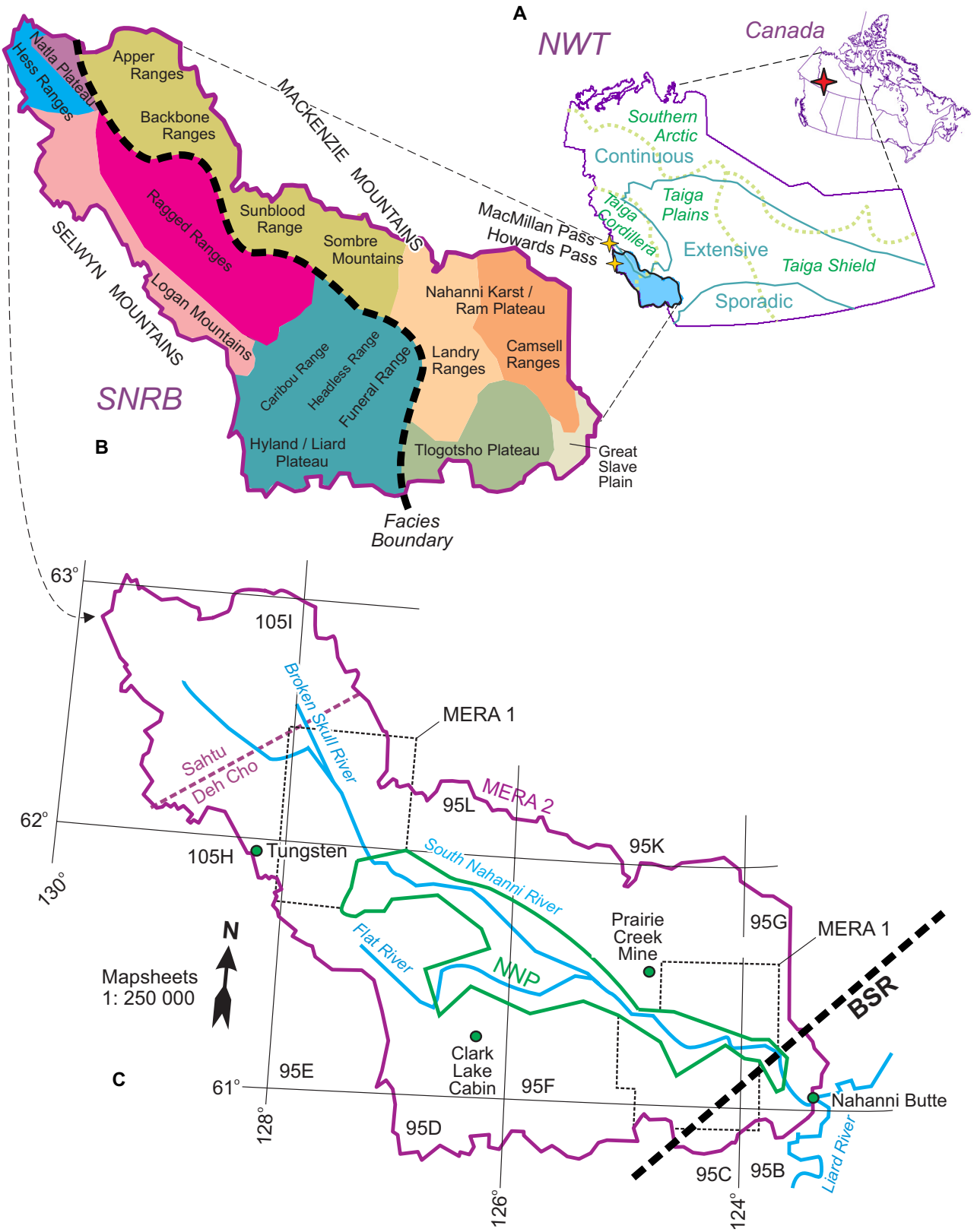


Figure 1. Location and description of the South Nahanni River basin. **A)** Northwest Territories permafrost zones (bold font and solid lines; Natural Resources Canada, 1995), ecozones (italic font and dashed lines; Wiken, 1986; Canadian Council on Ecological Areas and Environment Canada, 2006), with the South Nahanni River basin highlighted in blue and MacMillan Pass and Howards Pass mineral deposit locations marked with stars. **B)** South Nahanni River basin physiographic regions (Mathews, 1986) with the platformal carbonate / basinal shale facies boundary as described by Gabrielse et al. (1965). **C)** South Nahanni River basin map sheets, Sahtu/Deh Cho First Nations groups, waterways, infrastructure, and current Nahanni National Park (NNP) boundary. Mineral and Energy Resource Assessment (MERA) 1 and 2 areas are marked as dotted boxes and as the outline of the watershed, respectively. Beaver River Structure (BSR), as proposed by Morrow and Miles (2000), is marked with a dashed line.

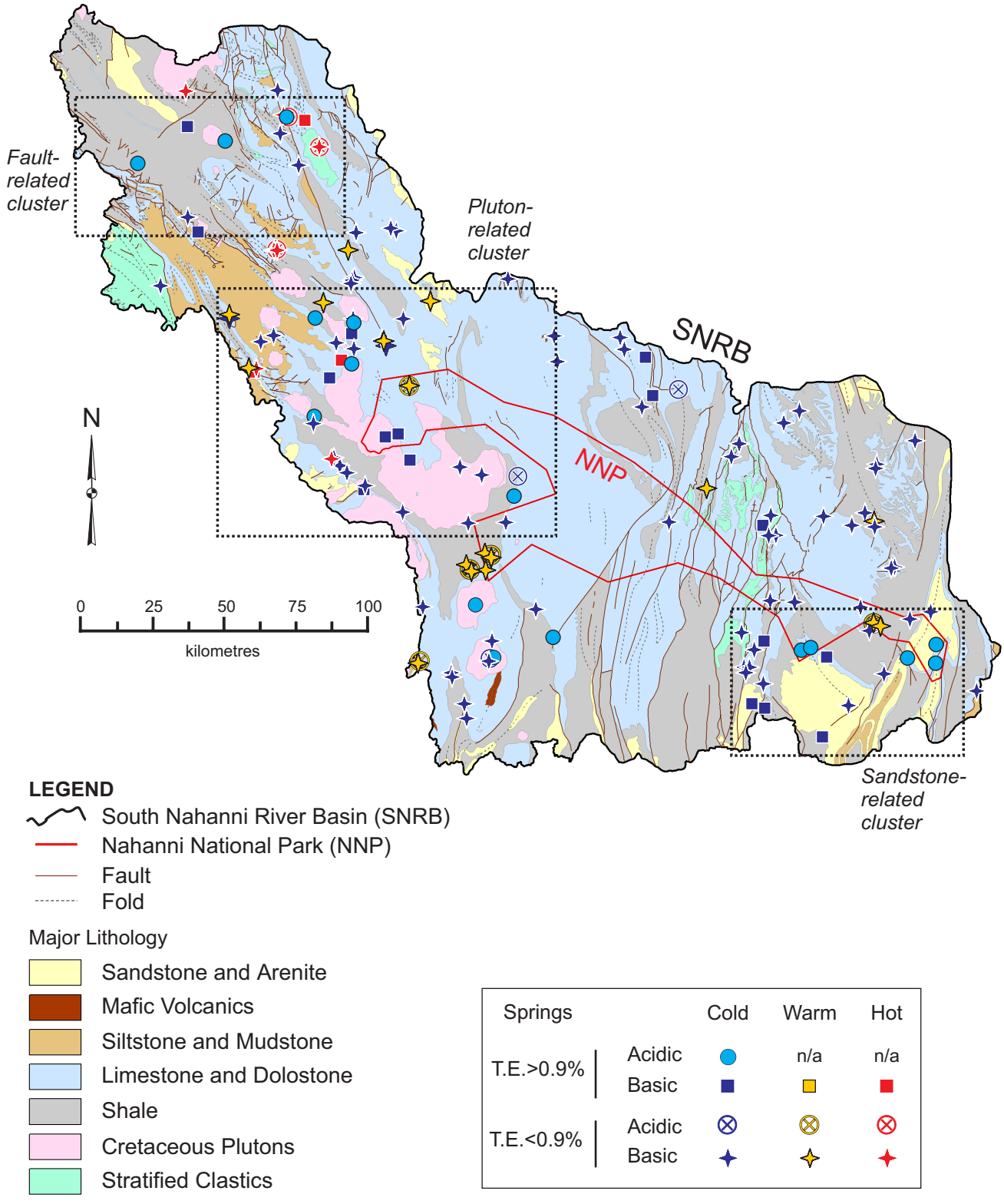


Figure 2. Major bedrock lithological groupings based on Okulitch (in prep.), overlaid with MERA 1 and 2 springs, Nahanni National Park (NNP) boundary, major faults and folds, and outlined by the current proposed park expansion area of the South Nahanni River basin (SNRB). Springs discharge mostly near faults, folds, and/or contacts between major bedrock types. Springs are symbolized for temperature, pH, and total trace elements as described in Figure 4. Springs with elevated total trace elements (T.E.>0.9%) cluster in three groups: sandstone-related, pluton-related, and fault-related. Lithological units are described in further detail in Appendix 1.

strata within the thickened crustal material (Woodsworth et al., 1991). Most of the mid-Cretaceous intrusions have relatively restricted mineralogies, classified as biotite-hornblende-bearing, biotite-bearing, and biotite-muscovite-bearing plutons (Anderson, 1983). Compressive and right-lateral strike-slip adjust-

ments continued throughout the Tertiary (ca. 40 Ma) and continue into the present (e.g. the 1985 Nahanni earthquake) in the South Nahanni River basin (Gendzwill, 1994; Hyndman et al., 2005). This complex geological setting is summarized and illustrated using major lithological groupings such as shale, carbonate, and plutons, which are explained in further detail in Appendix 1, and selected faults and folds (Fig. 2).

HYDROGEOCHEMICAL EXPLORATION BACKGROUND

Previous spring geochemistry research in the MERA 1 report (Hamilton et al., 2003) focused on statistical means of classifying springs based on geochemical properties. Whereas this approach is successful at sorting springs into groups of similar characteristics, this may or may not imply similar hydrogeochemical history of the spring water; although Hamilton et al. (2003) made the direct interpretation that the geochemical properties record the hydrogeological history. From these classifications, high metal content springs where identified as a group. However, as this classification is based on major ions as well as trace elements, there was no clear assessment of the variability of trace elements in waters across the entire study area. Whereas springs with 'high' or 'anomalous' metal concentrations are discussed in the MERA 1 study, some of the terms are defined by diagrams for which generative software and the time to experiment were not available to the authors of this study. For these reasons, this project developed a new geochemical exploration approach that can more quickly and simply identify mineralized zones in an area as large as Vancouver Island, British Columbia, given a limited budget and a total of four weeks of field work (split over two field seasons). Naturally discharging groundwaters (i.e. springs) of the South Nahanni River basin were sampled and analyzed for indicators of mineralization in the local bedrock, using one of the largest data sets of springs known in the literature. The methodology, focusing on the trace element geochemistry, was adapted from previous studies that largely focused on the environmental impact assessment of mines. To ensure consistency of results through both MERA 1 and 2 reports, we reinterpreted data reported by Hamilton et al. (2003) using the methods described herein.

> *"An important next step in the development of geoenvironmental mineral-deposit models will be the shift to watershed- or ecosystem-based focus, where the deposits are considered not only in the context of their geology, but also in the context of their surrounding watersheds."*
>
> *— Plumlee, 1999*

Ideally, mineral resource assessments at a regional or watershed scale are the first reconnaissance step in exploration and mine development (Plumlee and Logsdon, 1999). More detailed subregional environmental or prospect evaluations should follow, for example, determining local subwatershed delineations, climate, stream chemistry, rock units, faults, and fractures that may control flow, mine prospects, unmined deposits, extent of metal mobility away from mineralized areas, and biological/ecological data, i.e., potential receivers of impacts (Plumlee and Logsdon, 1999). This approach is considered to be a holistic one. Geochemical characterization of entire ecosystems has been recommended to better understand mine impacts, pre- and post-mining. It has even been recommended to map world-wide geochemical patterns in many overlapping mediums to better understand our planet, one watershed at a time (Fortescue et al., 1992; Smith and Huyck, 1999).

The current South Nahanni River basin study is well aligned with these ideal development practices as it represents one of the largest compilations of spring geochemistry in the literature. The collected data could be used as part of a baseline study in an impact assessment if development were to occur because the South Nahanni River basin is currently an area with little or no human impact.

Geochemical mapping is a common tool for regional reconnaissance, especially for large, under-explored areas such as the South Nahanni River basin. Commonly used media include stream sediments (e.g. Avila et al., 2005), lakes (e.g. base metal exploration in the northern Canadian Shield, Cameron, 1978), and stream water samples (Mingqi et al., 1995; Kelley and Taylor, 1997; Banks et al., 2004; Olias et al., 2004; Tosiani et al., 2004). Groundwater is another useful medium because it also is known to reflect bedrock geochemistry, in particular during winter stream base flow seasons (Whitfield et al., 1996) and shallow (<50 m) wells (Deering et al., 1983). The usefulness of groundwater as a reconnaissance tool for large areas, such as the South Nahanni River basin, is confirmed by Deering et al. (1983), where regional geochemical trends were more significant at the regional (approximately 19 000 km^2) than local (approximately 100 km^2) scale in shallow ground waters near mineral deposits. Hydrogeochemical prospecting has generally been restricted to areas with developed well networks. In Australia, water analysis from wells has been used as an effective exploration tool to map out anomalies in groundwater chemistry (Giblin, 2001; de Caritat and Kirste, 2005). Similarly, one hundred shallow wells (<50 m) were linked to Mississippi Valley-type deposits via elevated strontium concentrations, which were sampled in a 19 000 km^2 area rich in carbonate and evaporite (Deering et al., 1983).

Hydrochemical prospecting is not a new idea; broad discussions can be found in Runnells (1984), and

Table 1. Field measurements conducted.

Parameter Measured	Instrument Used
pH	Orion 290A meter; ThermoOrion Perphect ROSS 8202BN electrode
Electrical Conductivity (EC)	Conductivity meter Orion 125; conductivity cell
Eh (redox potential)	Orion 290A meter; ThermoOrion 9678BN combination redox electrode
Dissolved Oxygen (DO)	ThermoOrion DO meter 830A, probe included
GPS Location	Garmin 12CX (hand held)
Temperature	Recorded from DO, pH, and EC meters
Sulphide concentration	Orion 900200 D/junc. ref. electrode; Orion 9416BN sulphide electrode

groundwater sampling and anomaly determination techniques have been described in detail in Giblin (2001). Mineral deposit models and their related geochemistry are well established (i.e. Cox and Singer, 1986; Seal and Foley, 2002). More recently, hydrogeochemistry has also been incorporated into these discussions (Plumlee et al., 1994; du Bray, 1995; Plumlee, 1999; Wanty et al., 2006). There are several primary factors affecting deposit-drainage water chemistry: extent of exposure of the deposit, grade of mineralization, amount of carbonate rocks (which buffers pH and reduces the tendency for minerals to be dissolved), and proportion of Fe-sulphides in the ore (Kelley and Taylor, 1997). Sometimes hydrogeochemical data have been incorporated into regional geochemical descriptions, with natural water being one of the foci that also include soils, sediments, and mine drainage (e.g. King, 1995; Miller, 2002).

One of the most directly applicable hydrogeochemical ore deposit models is the Ficklin Diagram (Plumlee et al., 1994; Plumlee, 1999), which will be used here to infer local mineralized zones of the South Nahanni River basin, but is normally utilized to predict environmental impact of mineral deposits, such as acid-consuming or -producing tendencies. This is done by plotting the sum of six key sulphide-related metals versus pH, and comparing the spring geochemistry to fields of mine waters of known deposits. Most other hydro-geochemical studies have also been designed to predict environmental impacts of mines (Plumlee and Logsdon, 1999), rather than for exploration purposes. The United States Geological Survey has done extensive surveys of stream and spring samples in watersheds close to mined regions in order to improve the understanding of the local processes and environmental impacts (Miller, 2002; Wanty et al., 2006). Local studies have found significant geochemical trends, such as the Mississippi Valley-type deposits that were associated with anomalous Pb-Zn concentrations (>20 ppb) in 143 spring samples over zones approximately 100 km^2 in size (Steele and Dilday, 1985). There are many more examples from around the world in the literature describing local, environmentally oriented, hydrogeochemical studies that include, but are not limited to, Cu-Ni mines in Minnesota (Siegel and Ericson, 1980); Cu mines in Sweden (Sanden et al., 1997); Pb-Zn ore deposits in New Brunswick (Leybourne et al., 1998); Au, Cu-Mo, and Au-bearing iron-skarn deposits in Wrangell - St. Elias National Park in Alaska (Eppinger et al., 2000); antimony deposits in Denali National Park in Alaska (Eppinger et al., 2002); Pit Lake inflows of high-grade Cu-Zn-Ag-Mn veins in Montana (Pellicori et al., 2005); groundwater samples from sulphide mine tailings in northern Manitoba (Sidenko and Sherrif, 2005); acid mine drainage in Japan (Ohkuni et al., 2004); an abandoned mine in Colorado (Verplanck et al., 2004); and Ag- and Au-rich veins that have been mined since 1548 in Mexico (Carrillo-Chavez et al., 2003).

METHODS

Field Methods

Previously known springs were located using reports such as Brandon (1965), Souther and Halstead (1973), Crandall and Sadlier-Brown (1978), Hamilton et al. (1988), Hamilton (1990), and Jefferson and Spirito (2003). A total of 16 spring locations from the MERA 1 report were resampled (Appendix 6). Other springs sampled during the MERA 1 study (Hamilton, 1990; Jefferson and Spirito, 2003) were included, where possible, in many of the analyses in order to provide consistent anomaly detection across the two MERA regions. MERA 1 data lack silica data suitable for aqueous geothermometry, so circulation depths for those springs were not assessed. New spring locations were found by sighting from a helicopter in the summer months (June, July, and August of 2004 and 2005). A bare patch of ground within a vegetated area, a spot of colouring (usually a red or white zone of precipitate, or a bright green patch of algae), and creeks flowing out of mountains or starting from nowhere were some of the visual clues used. Creeks starting from below patches of snow or ice were avoided since their main source was likely freshly melted water, although a few were sampled simply for comparison. At each spring, a global positioning system (GPS) location was

Table 2. Summary of sample descriptions.

Sample Purpose	Amount (ml)	Bottle Material*	Filtered (0.45 mm)	Additive
Anions	125	HDPE	Yes	No
Cations and Trace Elements	125	HDPE	Yes	Ultra pure nitric acid – HNO_3(aq)
Alkalinity	125	HDPE	Yes	No
Sulphate Isotopes	250	HDPE	Yes	Barium chloride - $BaCl_2{\cdot}2H_2O$(s)
Sulphide Isotopes	1000	Amber PET	No	Cadmium acetate - $(CH_3COO)_2Cd{\cdot}2H_2O$(s)
DIC Isotopes	60	Amber Glass	Yes	Mercuric chloride - HgCl(s)
Silica	10	HDPE	Yes	50 ml of doubly distilled water
O and H Isotopes	30	HDPE	Yes	Paraffin wax on lid
Dissolved Gases	2 x 125	Amber Glass with Septum Lid	No	No
Free Gases	2 x 125	Amber Glass with Septum Lid	No	No
Sulphide	30	HDPE	No	30 mL of Sulphur-Anti-Oxidant-Buffer (SAOB)

*HDPE = High density polyethylene
**PET = Polyethylene terephthalate

obtained, and Eh, pH, electrical conductivity, dissolved oxygen, and temperature were measured as close to the outlet as possible (Table 1, Appendix 2).

In total, 95 samples were obtained for MERA 2. The analyzed water samples included 7 laboratory duplicates, 5 field duplicates, 1 field triplicate, 1 trip blank, and 1 laboratory blank. Ten of the water samples were surface water, one was direct mine water, three were seeps, and the rest were springs. An additional 127 MERA 1 sample data sets were added to the 95 MERA 2 data for characterizing the regional geochemistry, background concentrations, and to provide a consistent assessment of anomalies. Accounting for field duplicates and triplicates, 79 different spring locations were sampled in MERA 2 and 92 in MERA 1. MERA 2 resampled 16 MERA 1 springs, bringing the total of number of different springs sampled to 155 (for resampling overlap, see Appendix 6). A number of spring localities included one or more outlets within a 100 m radius, each of which were sampled but typically showed similar water geochemistry and therefore were counted as one site for the GIS analysis.

A typical, complete water sample included cations and trace elements (samples field-acidified to a pH of less than 2 with ultra pure nitric acid, HNO_3), anions, alkalinity, $\delta^{34}S$ analysis in sulphates (field precipitation of $BaSO_4$ by adding barium chloride, $BaCl_2{\cdot}2H_2O$), $\delta^{34}S$ analysis in sulphides only if they were detectable by smell (CdS(s) was precipitated by adding cadmium acetate, $(CH_3COO)_2Cd{\cdot}2H_2O$(s)), silica (with a dilution factor of 6 to inhibit precipitation, using doubly distilled water), and $\delta^{18}O$ and $\delta^{2}H$ (lids sealed tightly with paraffin wax to prevent evaporation) (Table 2).

Between each spring sampling, the filter apparatus was rinsed with distilled water once and with filtered sample water three times. Cation sample bottles were rinsed three times with filtered sample water before being used, and the anion and alkalinity bottles were rinsed once. The samples were kept in coolers and fridges until laboratory analysis. Samples were also taken of any mineral precipitates present for X-ray diffraction and $\delta^{13}C$ analysis of $CaCO_3$(s).

Table 3. Methods and limits of detection for trace elements.

(METHOD ICPES-120) Element	Limit of determination (ppb)	(METHOD ICPMS-120) Element	Limit of determination (ppb)
Al	5.5	Ag	0.2
As	12	Al	0.5
B	9.5	As	1
Ba	0.6	Ba	0.5
Be	0.1	Be	1
Ca	2.8	Bi	0.2
Cd	0.3	Cd	0.5
Co	3.1	Co	0.2
Cr	29	Cr	2
Cu	0.4	Cs	0.2
Fe	1.9	Cu	0.5
Li	0.6	Ga	0.2
K	12	Hg	0.2
Mg	1.1	In	0.2
Mn	0.2	Mn	0.2
Na	12.1	Mo	0.5
Ni	1.6	Ni	1
Pb	9.4	Pb	0.2
Sc	0.3	Rb	0.2
Se	23.8	Sb	0.2
Si	3.3	Se	2
Sr	0.2	Tl	0.2
Ti	0.4	U	0.2
V	1	V	0.2
Zn	0.32	Zn	2

Table 4. Summary of isotope methods.

Isotope	Accuracy and Precision	Standard	Preparation Process	Instrument Type	Method	Machine Name
$\delta^{34}S$ in sulphides and sulphates	+/-0.7‰	V-CDT[1]	chemical oxidation and gas generation	EA-C-IRMS[3]	Coplen and Krouse, 1998	Carlo Erba *NA 1500* elemental analyzer interfaced to a magnetic-sector mass analyzer
$\delta^{18}O$ in sulphates	+/-0.5‰	V-SMOW[2]	chemical oxidation and gas generation	TC/EA-C-IRMS[3]		Carlo Erba *NA 1500* elemental analyzer interfaced to a magnetic-sector mass analyzer
$\delta^{2}H$ in H_2O	+/-2‰	V-SMOW[2]	Zn or Cr reduction	D-IRMS[4]	Freidman, 1953; Coleman et al., 1982; Gehre et al., 1996; Donnelly et al., 2001; Nelson and Dettman, 2001	Micromass 602
$\delta^{18}O$ in H_2O	+/-0.2‰	V-SMOW[2]	equilibriation with CO_2	D-IRMS[4]	Epstein and Mayeda, 1953; Sofer, 1972; O'Neil et al., 1975; Horita et al., 1993	Micomass SIRA II

1. Canyon Diablo Troilite
2. Standard Mean Ocean Water
3. Continuous Flow-Isotope Ratio Mass Spectrometry
4. Dual Inlet-Isotope Ratio Mass Spectrometry

Laboratory Methods

Alkalinity was measured using an Orion 960 Autotitrator with $H_2SO_{4(aq)}$ and an ROSS pH electrode. Anions, cations, and trace elements were analyzed at the Geological Survey of Canada Laboratories in Ottawa (results of major ion and trace element analyses are listed in Appendices 3 and 4, respectively). Anions were measured using Ion Chromatography (IC-110). The cations and trace elements were measured using Inductively Coupled Plasma emission spectrometry / mass spectrometry (ICP-ES / ICP-MS 120). The limits of detection for the anions, cations, and trace elements are listed in their respective tables, and are also listed for trace elements in Table 3. Analytical error in concentration measurements was estimated to be 3% for major ions and 7% for trace elements. Ninety percent of MERA 2 samples were found to have a charge balance less than 10% and the rest less than 20%, indicating good sample quality. The terms 'major ions' and 'trace elements' are used throughout this report, even though they may not be representative of their respective element concentrations in particular springs. For example, when total trace elements add up to more than 10% of total dissolved solids in a sample, they are not 'trace' elements anymore, but for simplicity will still be referred to as such. In this report, major ions are therefore Na, K, Ca, Mg, Cl, HCO_3, and SO_4, whereas everything else is considered trace elements.

Oxygen and deuterium isotopes in water were analyzed by the Geological Survey of Canada Laboratory in Quebec, and sulphur and oxygen isotopes in sulphate were analyzed at the University of Calgary Isotope Laboratory using continuous flow and dual inlet isotope ratio mass spectrometry. Stable isotope composition ($^{18}O/^{16}O$, D/H, $^{34}S/^{32}S$) are expressed in the usual δ notation:

$$\delta(‰) = [(R_{sample} - R_{standard})/(R_{standard})] \times 10^3$$

where R is the ratio of heavy to light isotope abundances. Table 4 summarizes the isotope laboratory's methods from the University of Calgary Isotope Laboratory, and results are shown in Figure 3. Appendix 5 lists all isotope-related analyses as described in Caron (2007).

Trace Element Data Analysis

Given the range of potential deposit types within the large study area, and the variability in water/rock interaction, a broad range of geochemical signatures indicating water flow through mineral deposits could develop. To address this, a multi-pronged approach was developed to detect mineralized zones through indicator or anomalous springs in the South Nahanni River basin. Our assumption is that no single method can detect all potential deposit types. Instead we use three different methods (total trace elements, individual trace elements, and a Ficklin diagram) of detection. Detection by any one method is considered sufficient condition to classify a spring as anomalous. Detection by more than one method provides additional support but does not imply a stronger likelihood of a deposit being present.

Our approach was tested by assessing the two known major deposits in the region, the Tungsten and Prairie Creek mines, as well as other deposits from around the world. MERA 1 and 2 data were combined to determine background levels of total and individual trace elements in the South Nahanni River basin; MERA 1 samples were also reanalyzed to provide a consistent definition of anomalous spring waters throughout the South Nahanni area (see Appendix 6 for frequency of sampling and replicates for MERA 1 and 2). A summary of the number of springs identified with elevated total or individual trace elements (i.e. 'anomalous') is included in Appendix 7.

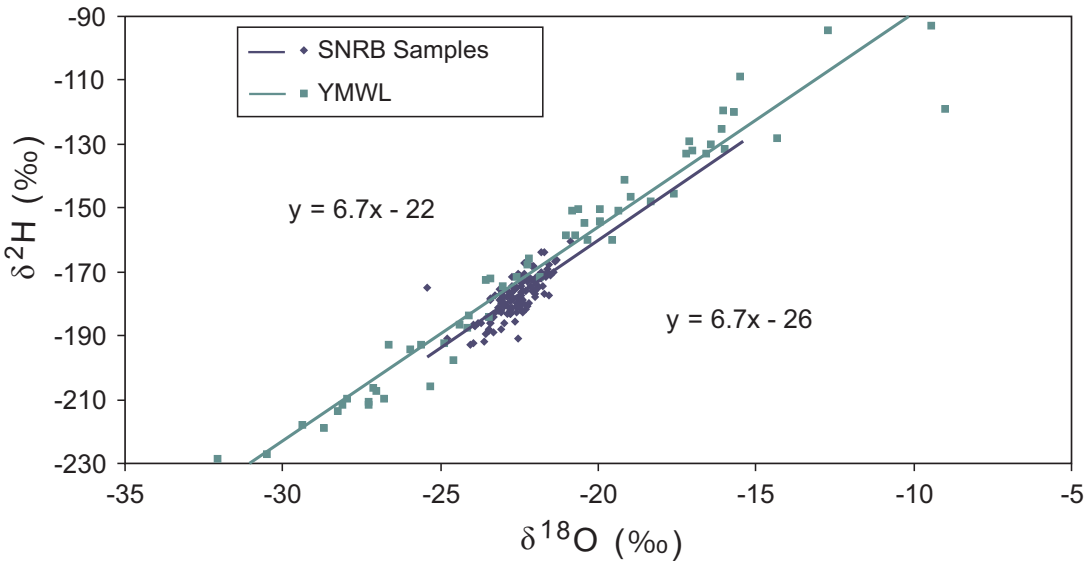


Figure 3. Hydrogen and oxygen stable isotopes of the South Nahanni River basin (SNRB) springs showing a parallel linear trend to the Yellowknife Meteoric Water Line (YMWL; International Atomic Energy Agency / World Meteorological Organisation, 1998).

Total Trace Elements

Total trace element concentrations were normalized after Giblin (2001) by dividing them each by the total dissolved solids (TDS), and were labelled as 'anomalous' if they were above the average of the South Nahanni River basin (0.9%). These anomalous springs were then plotted on a Piper diagram (Fig. 4), where geochemical groupings were identified and linked to major ions, pH, temperature, and a bedrock geology map. This method can detect a variety of potential deposit types because it lumps all the trace elements into one parameter. It may also be an indicator to the size of the deposit.

Individual Trace Elements

Anomalously high individual trace elements were identified and counted for each spring by using averages and standard deviations. Descriptive statistical results (minimum, maximum, average, and average plus 1 standard deviation of concentrations) were plotted for each trace element in the South Nahanni River basin springs, and anomalous trace elements were identified using six different approaches, depending on the element and its distribution. For example, some elements are only detected in a few springs (e.g. Ag); therefore all springs with detectable concentrations are considered anomalously high in that element, even if their concentrations are below average. On the other hand, some elements are very common (e.g. Cu or Zn) and therefore need a higher cut-off to be defined as 'anomalous'.

Cut-off values were used for each element: 50%, 100%, and 150% of the average, and the average plus 50%, 100%, and 150% of the standard deviation. The aim was to find the approximately fifteen most anomalous springs (about the 7th percentile) for each element.

A large variety of combinations and permutations of anomalous elements in the environment can indicate different mineral deposits. For example, a possible deposit is indicated as a sedimentary exhalative deposit (SEDEX) if Ag is seen in combination with Cu, Au, Zn, Sn, Pb, As, Sb, S, C, NH_3, Ba, Mn, and Fe (Cox and Singer, 1986). As another example, sedimentary manganese deposits leave a geochemical signature of Ba, Mn, P, and Pb (du Bray, 1995). However, though these anomalies may be found in rocks, they may not correspond to the same anomalies in water, depending on the pH, Eh, and salinity. Geochemical signatures from deposit models by Cox and Singer (1986) have, on average, nine anomalous elements, although some have as few as one or as many as nineteen.

Ficklin Diagram

A Ficklin diagram, where pH is plotted versus the sum of the concentrations of six key sulphide-related metals, was used to characterize spring waters with high mineralization potential (Plumlee et al., 1994). This method allows for the comparison of spring waters of the South Nahanni River basin with mine waters from known mineral deposits in Colorado (n = 50) (Plumlee et al., 1994). The higher the pH of the water, the more buffered the system is, and the higher the sum of the six key metal concentrations, the higher the base metal content of the deposit (Plumlee, 1999). This method is largely restricted to identifying sulphide-related mineral deposits and has limited use for other deposit types.

Geothermometry Approach

Chemical species, such as silica, K, or Na, are buffered by temperature-dependent mineral reactions. Chemical geothermometers can be applied to estimate the reservoir temperature if the water in which they are dis-

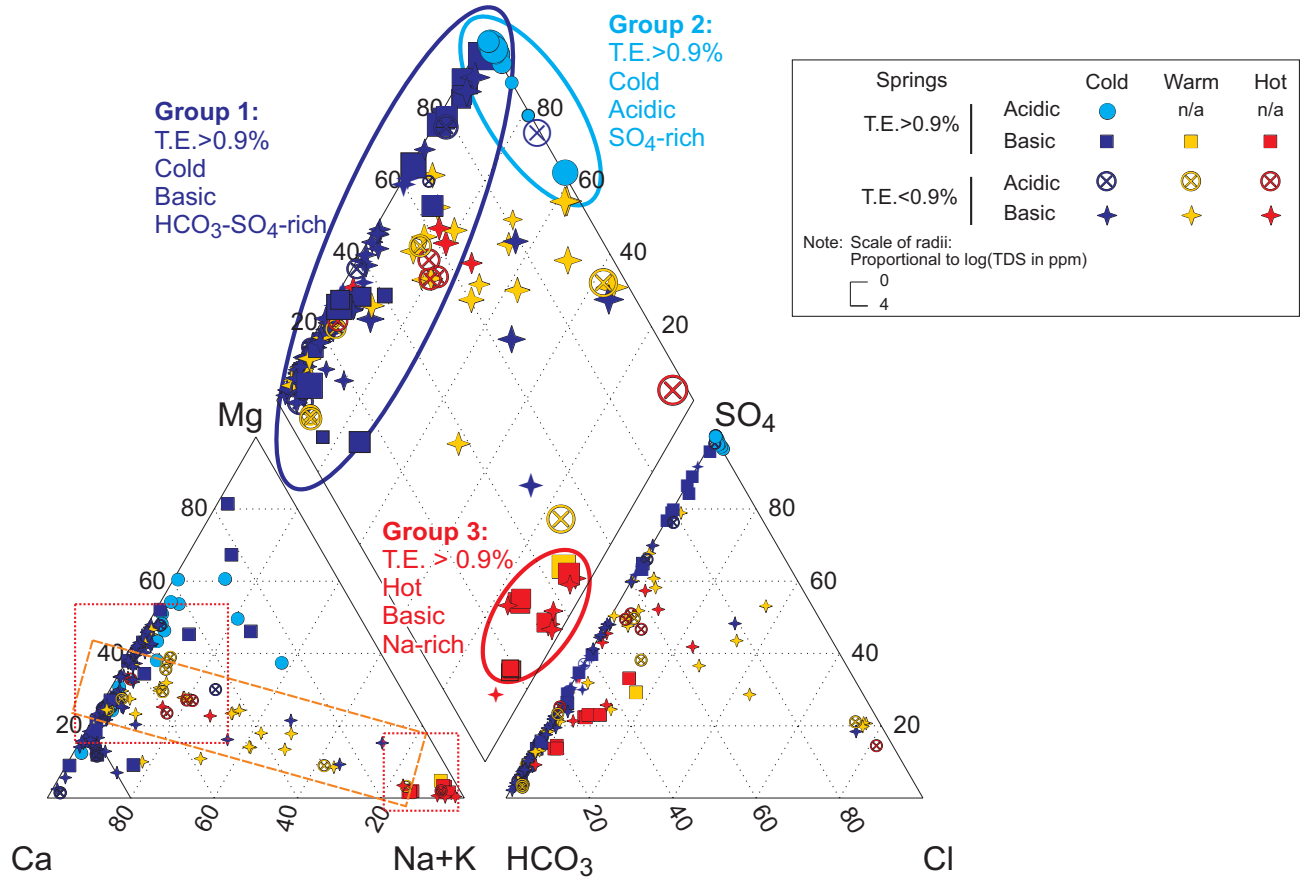


Figure 4. Piper plot of the South Nahanni River basin springs' major ions. Springs with anomalously high trace element percentages (T.E.>0.9%) have filled symbols and fall into three distinct groups: 1) cold, basic, and HCO_3-SO_4-rich; 2) cold, acidic, and SO_4-rich; and 3) hot, basic, and Na-rich. There are no anomalous warm springs (except for the Tungsten mine water drainage), and no anomalous acidic hot springs (n/a). Dotted rectangles in the lower left-hand triangle highlight the linear trend of warm springs from Ca to Na richness, and the two clusters of hot springs: Ca-rich on the left and Na-rich on the right. These symbols are used in other figures throughout this report.

solved discharges at surface relatively quickly, without re-equilibrating to lower temperature conditions (Fournier and Truesdell, 1973; Truesdell, 1976; Tonani, 1980; Armorsson, 1983; D'Amore et al., 1987; Nieva and Nieva, 1987; Giggenbach, 1988; Kharaka and Mariner, 1989; Tole et al., 1993; Pang and Reed, 1998).

Silica geothermometry (chalcedony version) was deemed most appropriate for the South Nahanni River basin springs, as was used in the southern Cordillera and discussed by Grasby and Hutcheon (2001). Since low-temperature Na/K ratios are more controlled by mineral dissolution rather than chemical equilibrium, they may cause erroneous results (Mutlu and Gulec, 1998) and are slow to equilibrate in low-temperature settings. Generally speaking, high-temperature reservoirs (>100ºC) are usually studied with the quartz geothermometer, and low temperature (<100ºC) with chalcedony (Fournier, 1981). The method of plotting select mineral solubilities at different temperatures (Pang and Reed, 1998) was also applied to 5 warm springs (Caron, 2007). The Solmineq88 program (Kharaka et al., 1988) was used to create geothermometry graphs and solubility diagrams (see Caron, 2007, for more detail).

RESULTS AND DISCUSSION

Linking Major Ions and Isotopes to the Local Geology

A broad range of spring characteristics is observed within the study area (thermal, acidic, saline, high pCO_2, and combinations thereof); although stable isotope data indicate that they are all meteoric in origin (Fig. 3). The springs are classified into basic geochemical types, where each group can be associated with dominant rock types and processes of water-rock interaction. The major processes include sulphide oxidation, carbonate dissolution, and deep circulation near faults and plutons. Typical characteristics include metalliferous, cold, low pH, and high-sulphate springs associated with shale and pyritic sandstone; cold, basic springs with calcium-carbonate-dominated geochemistry, variable total dissolved solids, with only a few detectable trace elements; and hot or warm, sodium-bicarbonate dominated springs with variable flow rates, low total dissolved solids, high pH, and include some high-pCO_2 springs in association with plutons and faulting.

Predicting Mineralization Types Using Trace Element Concentrations

Total Trace Elements

The South Nahanni River basin's MERA 2 total trace element data are listed in Table 5 in increasing order and normalized to total dissolved solids after Giblin (2001). This provides an easy way to determine which springs have anomalously high trace elements, possibly indicating economic potential. In this study, springs indicating the greatest economic potential have above-average total trace element concentrations as a percentage of total dissolved solids (>0.9%).

On a major-ion Piper diagram, springs with greater than 0.9 % total trace elements cluster into three distinct groups (Fig. 4). When temperature and pH are also added as factors, three groups can be defined: Group 1 - a sulphate-bicarbonate linear distribution, with basic (pH ~8), and cold (<12ºC) springs that discharge from carbonate and shale; Group 2 - sulphate-rich, acidic (pH ~3), and cold (<12ºC) springs that discharge mostly from shale; and Group 3 – sodium bicarbonate-dominated, basic, and hot (>40ºC) springs that discharge near plutons. Only the coldest and hottest waters of the South Nahanni River basin are defined as anomalous by the total trace elements method, whereas springs with moderate temperatures between 12 to 40ºC have total trace elements below 0.9%. Anomalous total trace elements occur in both acidic and basic waters, suggesting that pH is not a dominant influence on detection of anomalies.

From the MERA 2 study, these correspond to Glacier Lake, Cathedral, Softie, and Sombre (Group 1); Orange Creek, Bougere, Interpluton, Cotton, Overflow, and Red Mini (Group 2), and Nahanni Headwaters (Group 3).

Two main features of these groups will be important for potential environmental impact of development: buffering capacity and relative depth of circulation as indicated by surface temperature. The anomalous hot and cold basic spring groups both have relatively higher alkalinity and are dominantly associated with carbonate, whereas the cold acidic spring group tends to be more SO_4-rich and associated with shale. The hot and cold basic springs have more buffering capacity, and their exploitation would have a lower risk of acid mine drainage than the cold acidic group, which has little to no internal buffering capacity. The temperature of the anomalous basic and acidic cold springs suggests that the mineralized zone is not as deeply buried and potentially more accessible for exploration and extraction purposes.

Overall, the Na-rich hot springs have significantly higher values of total trace elements (average is 1.13 ± 0.16%) than Ca-rich springs (0.31 ± 0.15%). Na-rich hot springs tend to originate from plutonic rock (Hole in-the-Wall), near a contact with plutonic rock (Nahanni North and Nahanni Headwaters) or from the Flat River Valley (West Cantung, Cantung East, and Cantung, a.k.a. Tungsten mine water), which is bordered on each side by plutons and likely underlain by them as well. These same Na-rich hot springs were described as having a 'granitic' influence, as opposed to the others as having a 'sedimentary' origin (Crandall and Sadlier-Brown, 1978). It is therefore likely that the Na-rich waters in hot springs originate from the plutons or the alteration halo near the plutons, indicating higher potential in those areas.

Comparing the anomalous springs with the geology map simplified from Okulitch (in prep) allows for the delineation of three main clusters: 1) pluton-related anomalous springs (Selwyn Plutonic Suite); 2) sandstone-related anomalous springs (Mattson Formation); and 3) anomalous springs near major faults and fractures, mostly on the western side of the basin near the Flat River Valley and Broken Skull River (Fig. 2).

The pluton-related anomalous springs are not necessarily discharging directly from the plutons themselves, but instead often within a certain radius around them and usually within 5 km of the contact with the country rock. Contact aureoles of metamorphism have been documented by Blusson (1968) up to 1.6 km (1 mile) in diameter from where these anomalous springs discharge. The Tungsten mine is located within one of these halos of deformation (Blusson, 1968). The anomalousness of the springs clustered near the Mattson Formation can be explained by the pyritic nature of the sandstone and its coal deposits south of the basin (Stott, 1982; sandstone group in Fig. 2). Lastly, the cluster of anomalous springs near faults and fractures may be explained by the observed presence of mineralization in these types of structures in other places in the basin (e.g. Morrow and Miles, 2000).

Individual Trace Elements

Cut-off values to identify 'anomalousness' in individual trace elements were determined using background values from the combined analysis of MERA 1 and 2 springs (Fig. 5). The cut-off values are listed in Table 5, along with comparable concentrations in mining-related waters from around the world. The South Nahanni River basin values are quite conservative in comparison, indicating the high potential of the region (Table 5). Geochemical signatures for deposit models from Cox and Singer (1986) have, on average, 9 anomalous elements, although some have as few as 1 or as many as 19. For the purposes of this study, the authors considered springs with 3 or more anomalous elements to have the most economic potential. These are, in decreasing order, Orange Creek (15), Bougere (8),

Table 5. Trace elements and their cut-off values used to determine 'anomalousness', compared to select deposit-related waters.

	Fe	Al	Mn	Ni	Cu	Zn	Pb	Cd	Co	Cr
Criteria Cut-Off Used to Determine Anomalousness in SNRB	>10,000	>7,500	>880	>300	>15	>622	>2	>5	>31	>1
Criteria Statistic Description	ave+ 0.5 stdev	ave+ 0.5 stdev	ave+ 0.5 stdev	ave+ 0.5 stdev	1.5*ave	ave	ave	ave	1.5*ave	ave
Leybourne et al., 1998	6 to 4,600	2 to 281	11 to 440	1 to 6	1 to 7.8	2-2,300	0.2-530	0.5- 6.1	0-2.7	0.2-2.7
Kennecott Site (Eppinger et al., 2000)	10	10 to 50	0.01 to 15	0.01-1	0.2-80	0.05	0.05-0.1	0.01	0.01-0.1	0.2-0.8
Bremner Site (Eppinger et al., 2000)	10	2 to 30	0.04-80	0.01-10	0.3-20	0.03-10	0.02	0.01-0.2	0.01-7	0.2
Gold Hill Site (Eppinger et al., 2000)	10	2 to 100	0.003-1	0.4-1	0.2-8	0.03-4	0.03-0.2	0.01	0.02-0.05	0.2
Orange Hill and Bond Creek Sites (Eppinger at al., 2000)	10-3,000	10-100,000	0.007-15,000	0.01-200	0.2-20,000	20-20,000	0.03-10	0.1-100	0.01-900	0.3-3
Nabesna Site (Eppinger et al., 2000)	10-1,500,000	0.003-100,000	0.005-7,000	0.01-100	0.3-30,000	20-7,000	0.03-150	0.01-100	0.01-900	0.2-30
Siegel and Ericson, 1980	0-67,000	0-280	10-26,000	1-120	0.6-190	3.9-620	0.1-18	0-8.4	0.1-46	0-5.5
Pellicori et al., 2005	1,450-311,000	<300-42,700	1,300-6,500	n/a	<2-13,400	1,100-114,000	n/a	n/a	n/a	n/a
Sidenko and Sherriff, 2005	1,200,000	n/a	n/a	3,000	45	300	n/a	n/a	n/a	n/a
Ohkuni et al., 2004	9,500									
Big Colorado Mine (Verplanck et al., 2004)	892-242	210	n/a	1	0.44	17	0.01	0.074	0.9	n/a
Carrillo-Chavez et al., 2003	3 to 80	n/a	n/a	n/a	10-100	30-800	1 to 10	n/a	n/a	n/a

	Cs	Mo	As	Li	Rb	Sr	Ba	U	V	B	Sb
Criteria Cut-Off Used to Determine Anomalousness in SNRB	>3.5	>12	>16	>266	>23	>4,200	>231	>15	>1	>350	>0.9
Criteria Statistic Description	0.5*ave	ave+ 1.5 stdev	ave+ 0.5 stdev	ave+ 0.5 stdev	ave+ 0.5 stdev	ave+ stdev	ave+ stdev	ave+ 1.5 stdev	ave	ave	ave*0.5
Leybourne et al., 1998	n/a	0.5-19	13-110	2-1,800	0.34- 3.7	2.1-610	12-550	0.01-0.92	0.01-0.18	n/a	n/a
Kennecott Site (Eppinger et al., 2000)	n/a	0.07-20	0.1-8	0.05-2	n/a	30-300	0.6-40	0.07-0.8	0.6-2	30-100	0.01
Bremner Site (Eppinger et al., 2000)	n/a	0.2-1.5	0.1-1.5	0.04-1	n/a	40-100	2-30	0.2-0.3	0.07	5	0.01
Gold Hill Site (Eppinger et al., 2000)	n/a	0.1-0.9	0.1-2	1 to 9	n/a	10-300	3-30	0.01-0.3	0.05	4-200	0.01-0.2
Orange Hill and Bond Creek Sites (Eppinger at al., 2000)	n/a	0.07-200	0.1-0.3	1-40	n/a	200-6,000	3-80	0.4-20	0.05	4-80	0.01-70
Nabesna Site (Eppinger et al., 2000)	n/a	0.03-20	0.1-5,000	0.03-20	n/a	15-1,000	0.01-40	0.03-40	0.06-20	4-200	0.01-1
Siegel and Ericson, 1980	n/a	n/a	n/a	n/a	n/a	n/a	n/a	n/a	n/a	n/a	n/a
Pellicori et al., 2005	n/a	n/a	8-750	n/a	n/a	n/a	n/a	n/a	n/a	n/a	n/a
Ohnuki et al., 2004	n/a	n/a	90	n/a	n/a	n/a	n/a	n/a	n/a	n/a	n/a
Big Colorado Mine (Verplanck et al., 2004)	n/a	n/a	n/a	8	n/a	8	0.03	n/a	n/a	n/a	n/a
Carrillo-Chavez et al., 2003	n/a	n/a	7 to 20	n/a	n/a	n/a	n/a	n/a	n/a	n/a	n/a

	Tl	Ga	Se	Br	Ag	Be	Sc	Ti	Bi	In
Criteria Cut-Off Used to Determine Anomalousness in SNRB	>0.07	>0	>0	>0	>0	>0	>0	>0	>0	>0
Criteria Statistic Description	ave*0.5	anything detectable	anything detectable	anything detectable	anything detectable	anything detectable	anything detectable	anything detectable	anything detectable	anything detectable
Leybourne et al., 1998	n/a	n/a	n/a	n/a	n/a	n/a	n/a	0.05-1.52	n/a	n/a
Kennecott Site (Eppinger et al., 2000)	n/a	n/a	n/a	n/a	0.05	0.02	0.02	0.04	n/a	n/a
Bremner Site (Eppinger et al., 2000)	n/a	n/a	0.1	n/a	0.005	0.02	0.02-0.5	0.07	n/a	n/a
Gold Hill Site (Eppinger et al., 2000)	n/a	n/a	0.2-3	n/a	0.004-0.07	0.02	0.02-1	0.05-0.9	n/a	n/a
Orange Hill and Bond Creek Sites (Eppinger at al., 2000)	n/a	n/a	0.1-7	n/a	0.006-0.02	0.02-2	0.03-20	0.05-10	n/a	n/a
Nabesna Site (Eppinger et al., 2000)	n/a	n/a	0.1-9	n/a	0.004-1	0.02-0.9	0.06-10	0.05-200	n/a	n/a

Description of References

Eppinger et al., 2000 — *Kennecott stratabound copper mines (Alaska)*

Eppinger et al., 2000 — *Bremner Disctrict Historic Mine gold polytmetallic veins (Alaska)*

Eppinger et al., 2000 — *Gold Hill gold placer mines (Alaska)*

Eppinger et al., 2000 — *Orange Hill and Bond Creek undisturbed porphyry copper-molybdenum deposits (Alaska)*

Eppinger et al., 2000 — *Nabesna Historic Mine gold-bearing iron skarn deposits (Alaska)*

Leybourne et al., 1998 — *undisturbed Zn-Pb massive sulphide deposits, Bathurst Mining Camp (New Brunswick)*

Siegel and Ericson, 1980 — *Cu-Ni mining region (Minnesota)*

Pellicori et al., 2005 — *Berkeley Pit Lake of high-grade Cu-Zn-Pb-Ag-Mn veins (Montana)*
- *-largest Superfund complex in US in terms of areal extent*
- *-mined from 1870 to 1982*
- *-320 million tons of ore, >700 million tons of waste rock*
- *-10,000 km of interconnected mine workings*
- *-lake is 220 m deep with 110 billion litres of acidic mine water*
- *-concentrations shown here are from the monitoring wells around the pit lake*

Sidenko and Sherrif, 2005 — *Groundwater samples from within two sulphide mine tailings (northern Manitoba)*

Ohkuni et al., 2004 — *Acid mine discharge water (Japan)*

Verplanck et al., 2004 — *Abandoned Big Colorado mine water (Colorado)*

Carrillo-Chavez et al., 2003 — *Silver and gold exploitation from low-sulphidation quartz and calcite-rich epithermal veins since 1548 (Mexico)*

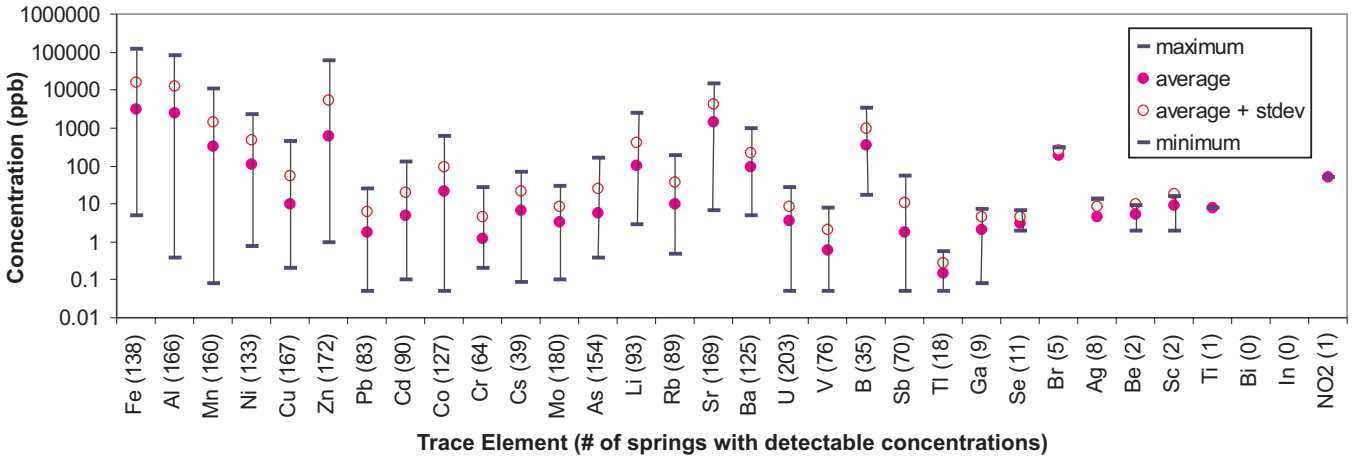


Figure 5. Trace element statistics for South Nahanni River basin springs: maximum, minimum, average, and sum of average plus 1 times the standard deviation concentrations (stdev) for all MERA 1 and 2 springs. The number next to each element refers to the total number of springs with detectable concentrations of that element. Some elements are very common (e.g. Cu and Zn) whereas some elements are uncommon (e.g. Ag). Correspondingly, different cut-off values were used to determine anomalousness for each element, which are listed and compared to deposit-related waters in Table 5.

Kraus (7), Nahanni headwaters (7), Prairie Creek mine shaft (7), Brimstone (6), Persistent (6), Broken Skull (5), Nahanni North (5), West Cantung (5), Wrigley (5), Galena (4), Grizzle Bear (4), Hole-in-the-Wall (4), Wildmint (4), Cimitar (3), Glacier Lake (3), and Meilleur River (3).

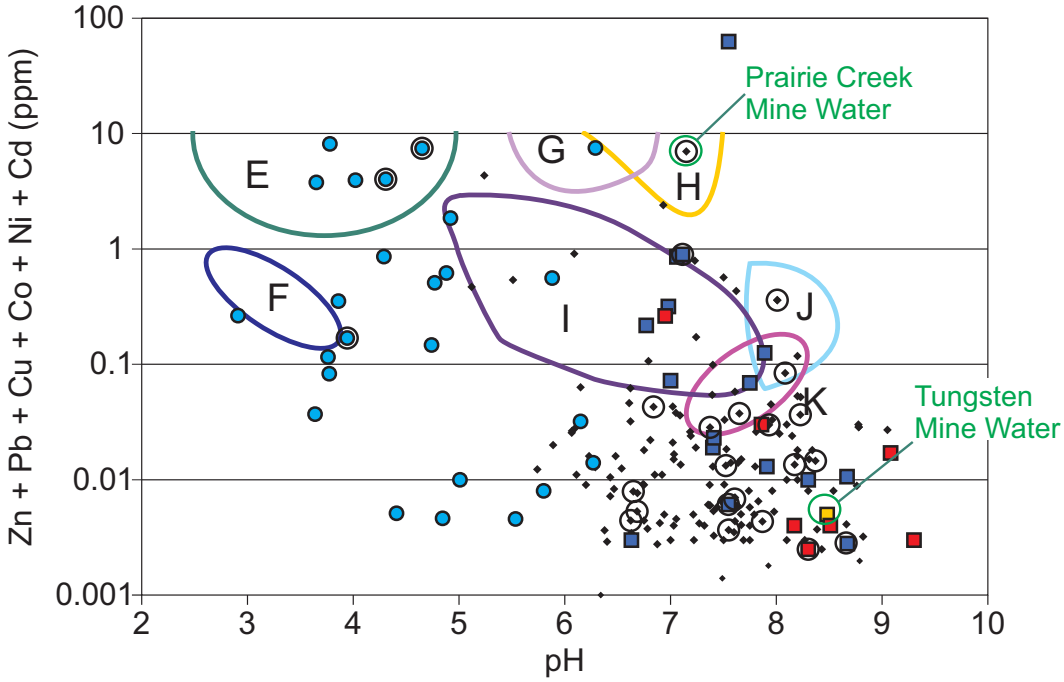
Both known deposits of the South Nahanni River basin have positively identified trace elements with this method, demonstrating its usefulness for a variety of deposit types (a summary of the deposits and their associated waters can be found in Table 6). For example, Tungsten mine water (MERA 1 sample # 86-020) is anomalous in Ag, and Stinky Drift (a sulphide-smelling seep from inside a mine shaft at the Tungsten mine) is anomalous in Tl. Comparatively, the hot spring flowing next to the Tungsten mine (i.e. West Cantung) has five anomalous trace elements: Cs, Li, V, B, and Ga. Prairie Creek mine water is anomalously elevated in seven elements (Cu, Zn, Pb, Cd, Sb, Tl, and Se) and two nearby creeks are anomalous in Pb (Harrison Creek) and Sb (Prairie Creek).

Ficklin Diagram

The Ficklin diagram was designed specifically to predict environmental impacts of mining, i.e., the buffering capacity of an area and its potentially released trace element concentrations using six indicator metals, for different deposit types, for both natural and man-made acid drainage (Plumlee, 1999). In the South Nahanni River basin, this approach was adapted by using the natural environmental conditions to predict the deposit types (Fig. 6). As a test of internal consistency, Prairie Creek mine water from the eastern side of the South Nahanni River basin plots exactly in the correct type of deposit in Figure 6, demonstrating the usefulness of this approach. Above, the sum of the six key metals where known deposits exist (>0.3), mostly cold springs are found, and springs with available sulphide-oxidation data plot in or around delineated fields. Non-sulphide-related Tungsten mine water does not plot in any area defined by Plumlee et al. (1994), demonstrating the method's limitations for identifying non-sulphidic deposits or those at low metal concentrations (below 0.03 of the sum of six key metals).

Table 6. Testing the multi-method approach using the two known deposits (Tungsten and Prairie Creek) of the South Nahanni River basin with MERA 1 and 2 samples.

Sample	Total Trace Elements	Individual Trace Elements	Ficklin Diagram Group	Geochemical Group
Tungsten mine water	1.00%	Ag	n/a	3
Stinky Drift	0.16%	Tl	n/a	n/a
West Cantung	1.42%	Cs, Li, V, B, Ga	n/a	3
Prairie Creek mine water	0.81%	Cu, Zn, Pb, Cd, Sb, Tl, Se	H	n/a
Prairie Creek	0.14%	Sb, NO_2	IJK	n/a
Harrisson Creek	0.08%	Pb	n/a	n/a
Galena	0.13%	Pb, U, Tl, Se	J	n/a
Galena (lab dup)	0.13%	U, Tl	J	n/a



Ficklin Groups E - K

E Pyrite + base metal-rich polymetallic veins and disseminations in wallrock with low acid-buffering capacity

F Pyrite-rich, base metal-poor veins and disseminations in wallrock with low acid-buffering capacity

G Pyrite + base metal-rich polymetallic veins that are carbonate-rich or occur in wallrock altered to contain carbonate

H Pyrite + base metal-rich, polymetallic replacements and veins in carbonate-rich sediments

I Polymetallic veins with moderate to low pyrite and base metal content that are carbonate-rich or occur in carbonate-rich wallrock

J Pyrite-poor polymetallic replacements in carbonate-rich sediments

K Pyrite-poor, Au-Te veins and breccias with carbonate gangue

- Total Trace Elements < 0.9 %
- Group 1: Cold and Basic
- Group 2: Cold and Acidic
- Group 3: Hot and Basic
- Mine Water
- Sulphide Oxidation

Figure 6. Ficklin diagram showing MERA 1 and 2 springs grouped by total trace elements greater than 0.9% with the same symbols as in Figure 4. Springs showing sulphide oxidation as indicated by $\delta^{18}O_{SO_4}$ and $\delta^{34}S_{SO_4}$ values are circled (Caron, 2007). Many springs fall into fields labeled E-K, as delineated from mine water drainage geochemistry from known mineral deposits in Colorado (Plumlee et al., 1994; descriptions listed above). Increasing buffering capacity increases with pH towards the right, and sulphide-related base metal content increases towards the top. Prairie Creek mine waters plot in the expected field and are successfully identified with this method. Tungsten's deposit is not detected with this method.

The anomalous springs in MERA 2, as determined from the Ficklin diagram (Fig. 6), include Bougere and Orange Creek from Group E; Cotton and Red Mini from Group F; Prairie Creek mine shaft from Group H; Selena, Cimitar, Wrigley, Glacier Lake, and Muddy from Group I; Galena from Group J; Mel's Pool, Sibbeston, and Cowgirl from Group K; and Smurf and Prairie Creek from the overlap of Groups I, J, and K.

Relative Accessibility of Mineralized Zones Using Silica Geothermometry

Combining geothermometer-estimated spring reservoir temperatures and geothermal gradients can be a useful tool for determining approximate depth of water circulation. An estimate of the geothermal gradient in the Mackenzie Mountains is approximately 23ºC/km (Hyndman et al., 2005). Normal geothermal gradients of the Cordillera, even in low heat-flow settings, are sufficient for thermal springs to develop (Grasby and Hutcheon, 2001). Warmer springs, therefore, are assumed to flow more deeply than colder springs and this method can help quantify this depth difference and hopefully pinpoint the spring circulation depth to a particular rock unit and/or lithology, which can be useful in predicting the location of mineralized zones underground.

The average depth of circulation of the analyzed springs in the South Nahanni River basin is 2.1 km, the deepest being 4.7 km at Brimstone Spring and the shallowest being near 0.2 km at Cotton. Corresponding

Table 7. Summary of anomalous springs for the MERA 2 study. Anomalous spring means interpreted as anomalous by at least one of three MERA 2 methods. '% trace elements' = total trace elements as a percentage of total dissolved solids. Ficklin diagram groups are described and shown in Figure 6. Geochemical groups are from the Piper diagram, Figure 4. Depth of circulation was estimated from Si-geothermometry using a quartz chalcedony geothermometer. Springs are listed in nested order of decreasing geochemical grouping, decreasing number of individual anomalous trace elements (each row listed in decreasing order of anomalousness), and decreasing % trace elements.

Spring	Anomalous Spring	% Trace Elements	# of Anomalous Elements	List of Anomalous Elements	Ficklin Diagram Group	Geochemical Group	Estimated Depth of Circulation (km)
Glacier Lake	x	4.87	3	Fe, Zn, Tl	I	**1**	1.4
Cathedral	x	1.41	1	Sr		**1**	<0.2
Softie	x	1.13				**1**	<0.2
Sombre	x	1.59				**1**	<0.2
Sombre (field dup)	x	1.60				**1**	<0.2
Orange Creek	x	4.00	15	Al, Mn, Ni, Cu, Zn, Cd, Co, Cr, Li, U, Tl, Ga, Be, Sc, Ti	E	**2**	<0.2
Bougere	x	8.20	8	Al, Mn, Ni, Cu, Zn, Co, Ga, Ag	E	**2**	1.3
Interpluton	x	3.04	1	Ga		**2**	<0.2
Cotton	x	4.47			F	**2**	0.2
Overflow	x	3.33				**2**	
Red Mini	x	4.63			F	**2**	0.9
Nahanni Headwaters	x	0.93	7	Cs, Mo, As, Li, B, Sb, Ga		**3**	4.4
Prairie Creek Mine Shaft	x	0.81	7	Cu, Zn, Pb, Cd, Sb, Tl, Se	H		<0.2
Kraus (Clausen)	x	0.39	7	Cr, Cs, Li, Rb, Sr, V, B			2.3
Brimstone	x	0.73	6	Fe, Mn, Cr, Rb, Se, Be			4.7
Tulita	x	0.57	6	Cs, Li, Ba, B, Br, Sc			1.5
Persistent (lab dup)	x	0.26	6	Cd, Cs, As, Rb, Ba, Tl			n/a
Persistent	x	0.26	6	Cd, Cs, As, Rb, Ba, Tl			n/a
Ekwi	x	0.03	6	Cr, Cs, Li, Rb, B, Tl			2.3
West Cantung	x	0.60	5	Cs, Li, V, B, Ga			3.2
Wrigley	x	0.51	5	Mo, U, V, Tl, Se	I		<0.2
Broken Skull's Upper Pool	x	0.38	5	Pb, Cs, Rb, B, Br			2.7
Nahanni North (Lened Creek)	x	0.28	5	Cs, Mo, Li, B, Ga			3.6
Broken Skull's Lower Pool	x	0.39	4	Cs, Rb, B, Br			2.7
Hole in the wall	x	0.37	4	Mo, As, V, Ga			3.7
Grizzle Bear	x	0.22	4	Cr, Cs, Rb, Br			2.8
Galena	x	0.13	4	Pb, U, Tl, Se	J		<0.2
Wildmint	x	0.09	4	Cs, Li, B, Ga			2.9
Cimitar	x	0.63	3	Sr, U, Tl	I		<0.2
Broken Skull	x	0.37	3	Cs, Rb, B			2.7
Meilleur River	x	0.28	3	Cs, Rb, Br			3.1
Sibbeston	x	0.31	2	Tl, Ga	K		<0.2
Smurf	x	0.15	2	V, Se	IJK		<0.2
Prairie Creek	x	0.14	2	Sb, NO_2	IJK		<0.2
Galena (lab dup)	x	0.13	2	U, Tl	J		<0.2
Cowgirl	x	0.08	2	V, Tl	K		<0.2
Tabletop		0.63	1	Cr			2.3
Red Steel		0.63	1	Se			<0.2
Sculpin		0.61	1	Sr			0.3
Mineral Lake		0.48	1	Cr			0.5
South Redstone		0.45	1	Cr			2.7
Quickie		0.38	1	Se			<0.2
Stinky Drift		0.16	1	Tl			1.2
Flat Fruit		0.14	1	Cs			0.9
Veil		0.13	1	Se			<0.2
Big Veil		0.13	1	Se			<0.2
Champagne Creek		0.12	1	Se			<0.2
Cordes Vertes		0.11	1	Cr			n/a
Deca		0.09	1	Cr			0.8
Harrison Creek		0.08	1	Pb			<0.2
Grasby		0.08	1	Se			n/a
Crack		0.04	1	V			<0.2
Mossy (lab dup)		0.69					<0.2
Mossy		0.68					<0.2
Clark Lake		0.53					<0.2
Clark Lake (lab dup)		0.53					<0.2
Ram Plateau		0.53					<0.2
Jacson		0.49					<0.2

Table 7 continued.

Spring	Anomalous Spring	% Trace Elements	# of Anomalous Elements	List of Anomalous Elements	Ficklin Diagram Group	Geochemical Group	Estimated Depth of Circulation (km)
Brigade		0.39					<0.2
Darkness		0.33					<0.2
Redstone Junction #1		0.30					2.0
Waterfall		0.30					<0.2
Stinky		0.28					n/a
Mel's Pool		0.27			K		<0.2
Selena		0.27			I		<0.2
Meltwater		0.26					<0.2
Champagne		0.23					n/a
Champagne (dup)		0.21					n/a
Cartman		0.19					<0.2
Dookie (field trip)		0.19					<0.2
Dookie (field dup)		0.18					<0.2
Moore's		0.18					3.3
Corridor Creek		0.17					<0.2
Caribou		0.16					<0.2
Dookie		0.16					<0.2
Caribou River		0.15					<0.2
Half Spring		0.13					<0.2
Rabbitkettle		0.12					1.1
Chance		0.12					<0.2
Cowboy		0.12					<0.2
Champagne Creek (dup)		0.12					<0.2
Cascade		0.10					<0.2
Cascade (lab dup)		0.10					<0.2
Blue Bells (field dup)		0.09					<0.2
Descente		0.08					<0.2
Blue Bells		0.08					<0.2
Tiny		0.07					<0.2
Muddy		0.07			I		0.9
Karst		0.07					<0.2
Clearwater Creek		0.06					<0.2
Boulder		0.03					<0.2
North Cantung (Zenchuck Creek)		0.01					1.3

Ficklin Diagram Groups (Plumlee et al., 1994)

E Pyrite- and base metal-rich polymetallic veins and disseminations in wallrock with low acid-buffering capacity
F Pyrite-rich, base metal-poor veins and disseminations in wallrock
G Pyrite- and base metal-rich polymetallic veins that are carbonate-rich or occur in wallrock altered to contain carbonate
H Pyrite- and base metal-rich, polymetallic replacements and veins in carbonate-rich sediments
I Polymetallic veins with moderate to low pyrite and base metal content that are carbonate-rich or occur in carbonate-rich wallrock
J Pyrite-poor polymetallic replacements in carbonate-rich sediments
K Pyrite-poor, Au-Te veins and breccias with carbonate gangue

temperatures at depth range from 5.5 to 108ºC, with an average of 48ºC. These are considered minimum estimates of the system's highest temperatures since dilution and re-equilibration of waters would only lower the calculated temperatures (Grasby and Hutcheon, 2001) and advective heat flow along faults would lower the geothermal gradient (Forster and Smith, 1988). All other springs are assumed to flow at less than 200 m in depth due to cold temperatures and low silica concentrations.

The estimates of depth of circulation obtained via Si-geothermometry compare favourably to other work done on some of the previously analyzed springs. A previous analysis of the Kraus Hot Spring, using a combination of the understanding of the local geology and a tritium age of 30 ± 10 years old, predicted the depth of circulation as being 1.5 km (Brandon, 1965), which is within the same range of the estimate of 2.3 km from this study. Similarly, Rabbitkettle Hot Springs were estimated to circulate approximately 1 km at depth by Gulley (1993), similar to the estimate of 1.1 km from this study. High pCO_2 springs of the Flat River Valley were estimated to flow 3 to 5 km at depth by Hamilton (1990), similar to the estimated 4.7 km depth of circulation for Brimstone by this study but different from the estimated 0.9 km for Flat Fruit by this study, both high pCO_2 springs. It is possible that Flat Fruit's deep fluids mixed with a larger component of fresh meteoric waters than Brimstone, diluting the Si concentrations.

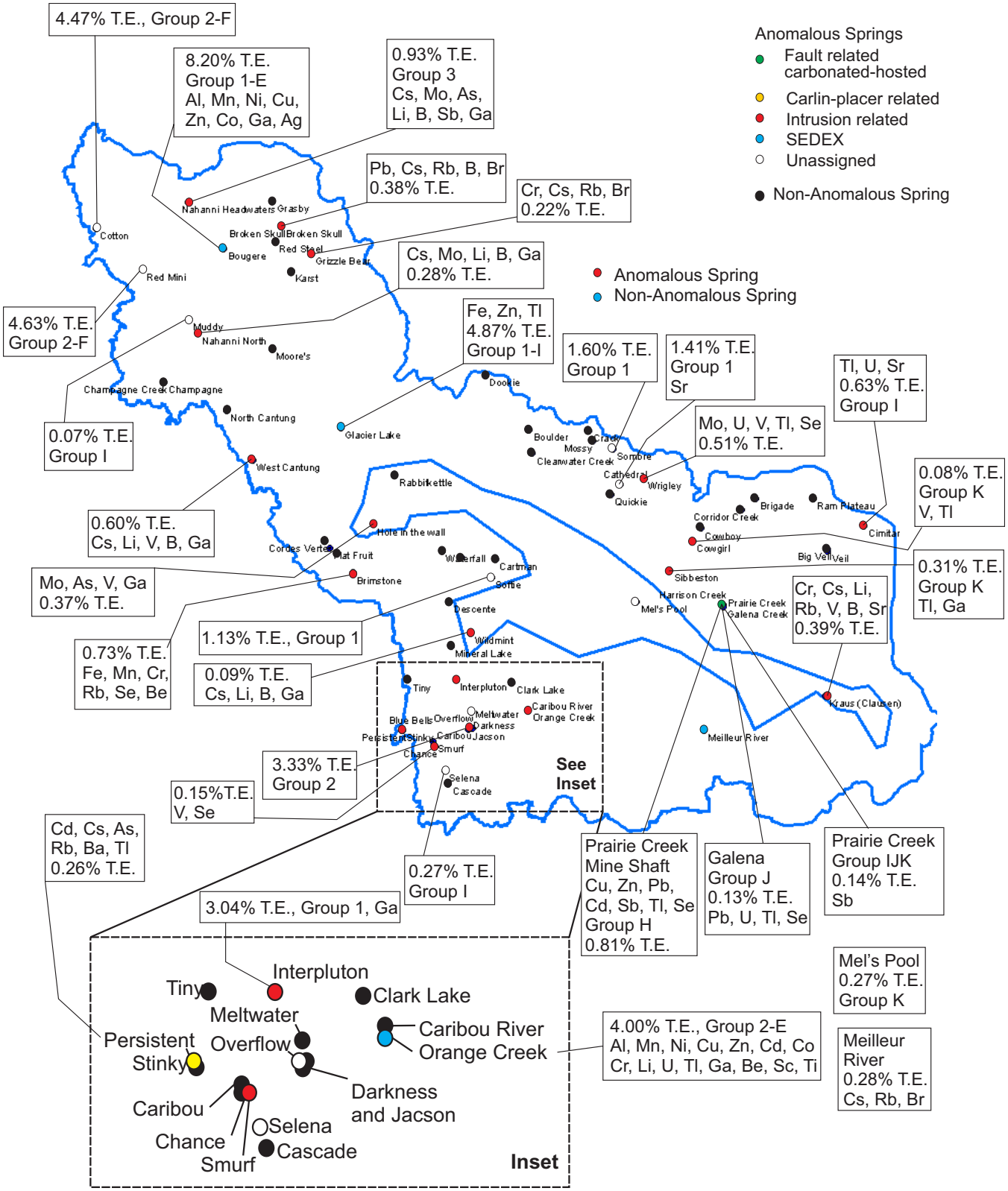


Figure 7. Summary of anomalous MERA 2 springs as determined from individual anomalous trace elements, % total trace element (T.E.). Geochemical groups are from the Piper diagram (Group 1-3; Fig. 4), and the Ficklin diagram groups (Group E-K; Fig. 6) for each spring, when applicable.

CONCLUSIONS

Table 7 summarizes the MERA 2 springs discussed in this report in decreasing order of geochemical grouping, individual anomalous trace elements, and total trace elements as a percentage of total dissolved solids (the complete data set of MERA 1 and 2 samples are

presented in a similar table in Appendix 7). Ficklin diagram groupings and estimated depth of circulation (or relative accessibility) are also included in the table. These results are summarized on the map in Figure 7. Results identify 84 springs (excluding duplicates) from the MERA 1 and 2 study areas that are deemed to have anomalous trace element characteristics as detected by one or more of the three methods used here. Reinterpretation of the MERA 1 data using the present methods reclassified 16 samples of the MERA 1 study from background levels to anomalous (Appendix 7). Nineteen samples from 18 springs that MERA 1 classified as having high metal content (but not anomalous), are classified as anomalous by these methods. Five samples from 4 springs that MERA 1 classified as having anomalous metal content are here classified as background (including Tungsten mine water and White Aster hot spring). This reassessment of data also made numerous changes to the identification of which particular metals have statistically anomalous concentrations within MERA 1 spring waters. Each spring with anomalous economic metal content according to MERA 1 and/or MERA 2 was assigned by Harris et al. (2007) to one or more of four mineral deposit models for the final GIS analysis of mineral potential.

This study demonstrates that three simple statistical and graphing methods can successfully identify mineralized zones quickly and efficiently in a largely underexplored area using spring geochemistry. The methods include summing trace element concentrations as a percentage of total dissolved solids, identifying individual anomalously high trace elements from background concentrations, confirming their identities by comparing them with mine waters from known deposits around the world, and using a Ficklin diagram (Plumlee et al., 1994). The two currently known world-class deposits of the South Nahanni River basin (Tungsten and Prairie Creek; Fig. 1C) were successfully detected using these three methods combined. No single approach is suitable, however, for detecting anomalous metal concentrations related to the diverse suite of deposit types found in the South Nahanni basin. Overall, the large sample size used in the analyses allows for a regional, watershed-based understanding of the South Nahanni River basin geochemistry and its related mineral potential.

The methods developed in this work are adaptable for a variety of geological terrains, which can be used for future MERA (or similar) assessments, in addition to regional geochemical prospecting and environmental baseline studies. Springs are an excellent tool for regional geochemical studies because they are relatively easy and inexpensive to sample, and are natural groundwater 'outcrops' that retain characteristics of the rocks they flow through. 'Anomalous' springs, elevated in total or individual trace elements above background concentrations, can be used as indicators to the overall elevated mineral potential of the region, and ideally guide future field work and/or decision making. The Ficklin diagram can be adapted for the purpose of mineral exploration, aside from its original purpose of predicting environmental impacts (as designed by Plumlee et al., 1994). A multi-method approach can successfully identify mineralized zones quickly and efficiently in a large, under-explored area, whereas single methods of data analysis can result in major world-class deposits going undetected.

ACKNOWLEDGEMENTS

The writers would like to acknowledge the contribution of a number of organizations and individuals to the paper. Funding was provided by Parks Canada and the Geological Survey of Canada through the MERA process. Analyses were carried out by the Geological Survey of Canada in Calgary by their laboratories in Quebec and Ottawa, and the University of Calgary Isotope Laboratory. Great Slave Helicopters supplied safe and friendly transportation. Staff at Canadian Zinc's Prairie Creek mine provided hospitable accommodation. Support from Melanie Myden, Hendrik Falck, Danny Wright, Kirsten Rasmussen, Glenn Sibbeston, and Andrew Okulitch.was greatly valued. GIS helpers include Paul Wozniak, Kelly Pierce, and Todd Slack. This report was improved through helpful comments of reviewers Bernhard Meyer and Charlie Jefferson. Field assistance of Melanie Meyden is greatly appreciated.

REFERENCES

Anderson, R.G.
1983: Selwyn plutonic suite and its relationship to tungsten skarn mineralization, southeastern Yukon and District of Mackenzie, *in* Current Research, Part B; Geological Survey of Canada, Paper 83-1B, p. 1151-1163.

Armorsson, S.
1983: Chemical equilibria in Icelandic geothermal systems. Implications for chemical geothermometry investigations; Geothermics, v. 12, p. 119-128.

Avila, P.F., Santos Oliveira, J.M., Ferreira da Sila, E., and Cardoso Fonseca, E.
2005: Geochemical signatures and mechanisms of trace elements dispersion in the area of the Vale das Gatas mine (Northern Portugal); Journal of Geochemical Exploration, v. 85, p. 17-29.

Banks, D., Markland, H., Smith, P.V., Mendez, C., Rodriguez, J., Huerta, A., and Saether, O.M.
2004: Distribution, salinity and pH dependence of elements in surface waters of the catchment areas of the Salars of Coipasa and Uyuni, Bolivian Altiplano; Journal of Geochemical Exploration, v. 84, p. 141-166.

Blusson, S.L.
1968: Geology and Tungsten Deposits near the Headwaters of Flat River, Yukon Territory and southwestern District of Mackenzie, Canada; Geological Survey of Canada, Paper 67-22, 77 p.

Brandon, L.V.
1965: Groundwater and Water Supply in the District of Mackenzie, Yukon Territory, and Adjoining Parts of British Columbia; Geological Survey of Canada, Paper 64-39, 102 p.

Cameron, E.M.
1978: Hydrogeochemical methods for base metal exploration in the northern Canadian Shield; Journal of Geochemical Exploration, v. 10, p. 219-243.

Caron, M-E.
2007: Spring Geochemistry: A Tool for Mineral Exploration in the South Nahanni River Basin, NWT; M.Sc. thesis, University of Calgary, Calgary, Alberta, 155 p. (also Appendix 3 *in* Mineral and Energy Resource Assessment of the Greater Nahanni Ecosystem Under Consideration for the Expansion of the Nahanni National Park Reserve, Northwest Territories, (ed.) D.F. Wright, D. Lemkow, and J.R. Harris; Geological Survey of Canada, Open File 5344, p. xx-xx).

Carrillo-Chavez, A., Morton-Bermea, O., Gonzalez-Partida, E., Rivas-Solorzano, H., Oesler, G., Garcia-Meza, V., Hernandez, E., Morales, P., and Cienfuegos, E.
2003: Environmental geochemistry of the Guanajuato Mining District, Mexico; Ore Geology Reviews, v. 23, p. 277-297.

Canadian Council on Ecological Areas and Environment Canada
2006: Ecozones of Canada; available online at http://www.ccea.org/ecozones. First published by Wiken, 1986. Last updated 2006. Last accessed on Apr. 8, 2006.

Coleman, M.L., Shepherd, T.J., Durham, J.J., Rouse, J.E., and Moore, G.R.
1982: Reduction of water with zinc for hydrogen isotope analysis; Analytical Chemistry, v. 54, p. 993-995.

Coplen, T.B. and Krouse, H.R.
1998: Sulphur isotope data consistency improved; Nature, v. 392, p. 32.

Cox, D.P. and Singer, D.A. (ed.)
1986: Mineral Deposit Models; United States Geological Survey, Bulletin 1693, 379 p.

Crandall, J.T. and Sadlier-Brown, T.L.
1978: Data on geothermal areas: Cordilleran Yukon, Northwest Territories, and adjacent British Columbia; Department of Energy, Mines and Resources, Open File, 78-1, 80 p.

D'Amore, F., Fancelli, R., and Caboi, R.
1987: Observations on the application of chemical geothermometers to some hydrothermal systems in Sardinia; Geothermics, v.16, p. 271-282.

de Caritat, P. and Kirste, D.
2005: Hydrogeochemistry applied to mineral exploration under cover in the Curnamona Province; MESA Journal, v. 37, p. 13-17.

Deering, M.F., Mohr, E.T., Sypniewski, B.F., and Carlson, E.H.
1983: Regional hydrogeochemical patterns in ground water of northwestern Ohio and their relation to Mississippi Valley-type mineral occurrences; Journal of Geochemical Exploration, v. 19, p.225-241.

Donnelly, T., Waldron, S., Tait, A., Dougans, J., and Bearhop, S.
2001: Hydrogen isotope analysis of natural abundance and deuterium-enriched waters by reduction over chromium on-line to a dynamic dual inlet isotope; Rapid Communications in Mass Spectrometry, v. 15, p. 1297-1303.

du Bray, E.A. (ed.)
1995: Preliminary Compilation of Descriptive Geoenvironmental Mineral Deposit Models; United States Geological Survey, Open-File Report, 95-831, 272 p.

Eppinger, R.G., Briggs, P.H., Rosenkrans, D., and Ballestrazze, V.
2000: Environmental Geochemical Studies of Selected Mineral Deposits in Wrangell-St.Elias National Park and Preserve, Alaska; United States Geological Survey, Professional Paper, 1619, 47 p.

Eppinger, R.G., Briggs, P.H., Crock, J.G., Meier, A.L., Sutley, S.J., and Theodorakos, P.M.
2002: Environmental-geochemical study of the Slate Creek antimony deposit, Kantisha Hills, Denali National Park and Preserve, Alaska, *in* Studies of the U.S. Geological Survey of Alaska, 2000, (ed.) F.H. Wilson and J.P. Galloway; United States Geological Survey, Professional Paper 1662, p. 123-141.

Epstein, S. and Mayeda, T. K.
1953: Variation of O^{18}/O^{16} ratio in natural waters; Geochimica et Cosmochimica Acta, v. 4, p. 213-224.

Forster, C. and Smith, L.
1988: Groundwater Flow Systems in Mountainous Terrain: 2. Controlling factors; Water Resources Research, v. 24 p.1011-1023.

Fortescue, J.A.C., Bolivar, S.L., and Heier, K.S.
1992: Landscape geochemistry: Retrospect and prospect – 1990. Critical Comments; Applied Geochemistry, v. 7, p. 1-57.

Fournier, R.O.
1981: Application of water geochemistry to geothermal exploration and reservoir engineering, *in* Geothermal Systems: Principles and Case Histories, (ed.) L. Rybach and L.J.P. Muffler; John Wiley and Sons Limited, New York, p. 109-143.

Fournier, R.O. and Truesdell, A.M.
1973: An empirical Na–K–Ca geothermometer for natural waters; Geochimica et Cosmochimica Acta, v. 43, p. 1543–1550.

Freidman, I.
1953: Deuterium content of natural water and other substances; Geochimica et Cosmochimica Acta, v. 4, p. 89-103.

Gabrielse, H., Roddick, J.A., and Blusson, S.L.
1965: Flat River, Glacier Lake, and Wrigley Lake, District of Mackenzie and Yukon Territory; Geological Survey of Canada, Paper 64-52, 30 p.

Gehre, M., Hoefling, R., Kowski, P., and Strauch, G.
1996: Sample preparation device for quantitative hydrogen isotope analysis using chromium metal; Analytical Chemistry, v. 68, p. 4414-4417.

Gendzwill, D.J.
1994: Earthquakes and a review of seismicity in the Canadian North; Musk-Ox, v. 40, p. 31-46.

Giblin, A.
2001: Groundwaters: Geochemical Pathfinders to Concealed Ore Deposits; Commonwealth Scientific and Industrial Research Organisation Exploration and Mining, Australia, 79 p.

Giggenbach, W.F.
1988: Geothermal solute equilibria. Derivation of Na-K-Mg-Ca geoindicators; Geochimica et Cosmochimica Acta, v. 52, p. 2749-2765.

Grasby, S.E. and Hutcheon, I.
2001: Controls on the distribution of thermal springs in the southern Canadian Cordillera; Canadian Journal of Earth Sciences, v. 38, p. 427-440.

Gulley, A.L.
1993: Rabbitkettle Hotsprings, Nahanni National Park Reserve, N.W.T.: A Hydrogeological Study; M.Sc. thesis, Carleton University, Ottawa, Ontario, 178 p.

Hall, G.E.M., Jefferson, C.W., and Michel, F.A.
1988: Determination of W and Mo in natural spring waters by ICP-AES (Inductively Coupled Plasma Atomic Emission Spectrometry) and ICP-MS (Inductively Coupled Plasma Mass Spectrometry): Application to South Nahanni River Area, Northwest Territories, Canada; Journal of Geochemical Exploration, v. 30. p. 63-84.

Halliwell, D.R. and Catto, S.
2003: How and why is aquatic quality changing at Nahanni National Park Reserve, NWT, Canada?; Environmental Monitoring and Assessment, v. 88, p. 243-281.

Hamilton, S.M.
1990: The Application of Spring Water Geochemistry and Hydrogeology to a Non-Renewable Resource Assessment of the South Nahanni River Area, NWT; M.Sc. thesis, Carleton University, Ottawa, Ontario, 169 p.

Hamilton, S.M., Michel, F.A., and Jefferson, C.W.
1988: Groundwater geochemistry, South Nahanni resource assessment area, District of Mackenzie, *in* Current, Part E; Geological Survey of Canada, Paper 88-1E, p. 127-136.
1991: CO_2-rich ground waters of the Flat River Valley, NWT, *in* Northern Hydrology: Selected Perspectives 1990, (ed.) T.D. Prowse and C.S.L. Ommanney; Proceedings of the Northern Hydrology Symposium, 10-12 July 1990, Saskatoon, Saskatchewan.

Hamilton, S.M., Michel, F.A., Jefferson, C.W., and Power-Fardy, D.
2003: Spring water geochemistry and hydrogeology for mineral resource assessment of the South Nahanni River region, *in* Non-Renewable Mineral and Energy Resource Potential of the Proposed Extensions to Nahanni National Park Reserve, Northern Cordillera, Northwest Territories, (ed.) C.W. Jefferson, and W. Spirito; Geological Survey of Canada, Open File 1686, p. 5-1 to 5-40.

Harris, J.R., Lemkow, D., Wright, D.F., and Falck, H.
2007: Modelling mineral potential for the Greater Nahanni Ecosystem using GIS-based analytical methods, *in* Mineral and Energy Resource Assessment of the Greater Nahanni Ecosystem Under Consideration for the Expansion of the Nahanni National Park Reserve, Northwest Territories, (eds.) D.F. Wright, D. Lemkow, and J.R. Harris; Geological Survey of Canada, Open File 5344, p. 293-326.

Health and Welfare Canada
1992: Guidelines for Canadian Recreational Water Quality; Federal-Provincial Working Group on Recreational Water Quality of the Federal-Provincial Advisory Committee on Environmental and Occupational Health, Health and Welfare Canada, Government of Canada.

Health Canada
2006: Guidelines for Canadian Drinking Water Quality Summary Table; Federal-Provincial-Territorial Committee on Drinking Water, Health Canada, Government of Canada.

Horita, J., Wesolowski, D., and Cole, D.
1993: The activity-composition relationship of oxygen and hydrogen isotopes in aqueous salt solutions: I. Vapor-liquid water equilibration of single salt solutions from 50 to 100°C; Geochimica et Cosmochimica Acta, v. 57, p. 2797-2817.

Hyndman, R.D., Flueck, P., Mazzotti, S., Lewis, T.J., Ristau, J., and Leonard, L.
2005: Current tectonics of the northern Canadian Cordillera; Canadian Journal of Earth Sciences, v. 42, p. 1117-1136.

Jefferson, C.W. and Spirito, W.A. (ed.)
2003: Mineral and Energy Resource Assessment of the Tlogotsho Plateau, Nahanni Karst, Ragged Ranges and Adjacent Areas Under Consideration for Expansion of Nahanni National Park Reserve, Northwest Territories; Geological Survey of Canada, Open File 1686, 1 CD-ROM.

Kelley, K.D. and Taylor, C.D.
1997: Environmental geochemistry of shale-hosted Ag-Pb-Zn massive sulfide deposits in northwest Alaska: Natural background concentrations of metals in water from mineralized zones; Applied Geochemistry, v. 12, p. 397-409.

Kharaka, Y.K., Gunter, W.D., Aggarwal, P.K., Perkins, E.H., and Debraal, J.D.
1988: SOLMINEQ.88: A Computer Program for Geochemical Modeling of Water-Rock Interactions; United States Geological Survey, Water Resources Investigation Report 88-4227, 420 p. (also Alberta Research Council, Information Series, No. 104).

Kharaka, Y.K., Mariner, R.H.
1989: Chemical geothermometers and their application to formation waters from sedimentary basins; in Thermal History of Sedimentary Basins, (ed.) N.D. Naeser and T. McCulloch; Springer Verlag, New York, p. 99-117.

King, T.V.V. (ed.)
1995: Environmental Considerations of Active and Abandoned Mine Lands: Lessons from Summitville, Colorado; United States Geological Survey, Bulletin 2220, 43 p.

Leybourne, M.I., Goodfellow, W.D., and Boyle, D.R.
1998: Hydrogeochemical, isotopic, and rare earth element evidence for contrasting water-rock interactions at two undisturbed Zn-Pb massive sulphide deposits, Bathurst Mining Camp, N.B., Canada; Journal of Geochemical Exploration, v. 64, p. 237-261.

Mathews, W.H.
1986: Physiographic Map of the Canadian Cordillera; Geological Survey of Canada, Map 1701A, scale 1:5 000 000

Miller, W.R.
2002: Influence of Rock Composition on the Geochemistry of Stream and Spring Waters from Mountainous Watersheds in the Gunnison, Uncompahgre, and Grand Mesa National Forests, Colorado; United States Geological Survey, Professional Paper 1667, 58 p.

Mingqi, W., Tianxiang, R., Yinhan, L., and Shuxing, L.
1995: Stream water, an ideal medium for rapidly locating polymetallic mineralization in forest-swamp terrain: a case study in the Da Hinggan Mts., northern Heilongjiang, China; Journal of Geochemical Exploration, v. 55 p. 257-264.

Morrow, D.W. and Miles, W.C.
2000: The Beaver Structure: A cross-strike discontinuity of possible crustal dimensions in the southern Mackenzie Fold Belt, Yukon and Northwest Territories, Canada; Bulletin of Canadian Petroleum Geology, v. 48, p. 19-29.

Mutlu, H. and Gulec, N.
1998: Hydrogeochemical outline of thermal waters and geochemistry applications in Anatoia (Turkey); Journal of Volcanology and Geothermal Research, v. 85, p. 495-515.

Nelson, S.T. and Dettman D.
2001: Improving hydrogen isotope ratio measurements for on-line chromium reduction systems; Rapid Communications in Mass Spectrometry, v.15, p. 2301-2306.

Nieva, D. and Nieva, R.
1987: Developments in geothermal energy in Mexico: Part 12. A cationic composition geothermometer for prospecting of geothermal resources; Heat Recovery Systems and CHP, v. 7, p. 243-258.

Natural Resources Canada
1995: Canada Permafrost; The National Atlas of Canada, Map MCR 4177, (5th edition), scale 1: 7 500 000, Last accessed on Apr. 8, 2006.

Ohkuni, T., Sakamoto, F., Kozai, N., Ozaki, T., Yoshida, T., Narumi, I., Wakai, E., Sakai, T., and Francis, A.
2004: Mechanisms of arsenic immobilization in a biomat from mine discharge water; Chemical Geology, v. 212, p. 279-290.

Okulitch, A.V. (comp.)
in prep: Bedrock Geology, Redstone River, Yukon and Northwest Territories; Geological Survey of Canada, Map NP-9/10-G,

scale 1:1 000 000 (National Earth Science Series, Geological Atlas).

Olias, M., Nieto, J.M., Sarmiento, A.M., Ceron, J.C., and Canovas, C.R.
2004: Seasonal water quality variations in a river affected by acid mine drainage: The Odiel River (South West Spain); Science of the Total Environment, v. 333, p. 267-281.

O'Neil, J.R., Adami, L.H., and Epstein, S.
1975: Revised value for the O^{18} fractionation factor between CO_2 and H_2O at 25°C;United States Geological Survey, Journal of Research, v. 3, p. 623-624.

Pang, Z-H. and Reed, M.
1998: Theoretical chemical thermometry on geothermal waters: Problems and methods; Geochimica et Cosmochimica Acta, v. 62, p.1083-1091.

Pellicori, D.A., Gammons, C.H., and Poulson, S.R.
2005: Geochemistry and stable isotope composition of the Berkeley Pit Lake and surrounding mine waters, Butte, Montana; Applied Geochemistry, v. 20, p. 2116-2137.

Plumlee, G.S.
1999: The environmental geology of mineral deposits, *in* The Environmental Geochemistry of Mineral Deposits, Part A: Processes, Techniques and Health Issues, (ed.) L. H. Filipek and G. S. Plumlee; Society of Economic Geologists, Reviews in Economic Geology, v. 6A, p. 71-116.

Plumlee, G.S. and Logsdon, M.J.
1999: An earth-system toolkit for environmentally friendly mineral resource development, *in* The Environmental Geochemistry of Mineral Deposits, Part A: Processes, Techniques and Health Issues, (ed.) L. H. Filipek and G. S. Plumlee; Society of Economic Geologists, Reviews in Economic Geology, v. 6A, p. 1-27.

Plumlee, G.S., Smith, K.S., and Ficklin, W.H.
1994: Geoenvironmental Models of Mineral Deposits and Geology-Based Mineral-Environmental Assessments of Public Lands; United States Geological Survey, Open-File 94-203, 9 p.

Runnells, D.D.
1984: Workshop 3: Hydrochemistry in mineral exploration; Journal of Geochemical Exploration, v. 21, p. 129-131.

Sanden, P., Karlsson, S., Duker, A., Ledin, A., and Lundman, L.
1997: Variations in hydrochemistry, trace metal concentration and transport during a rain storm event in a small catchment; Journal of Geochemical Exploration, v. 58, p. 145-155.

Seal II, R.R. and Foley, N.K. (ed.)
2002: Progress on Geoenvironmental Models for Selected Mineral Deposit Types; United States Geological Survey, Open File Report, 02-195, Chapters A-L.

Sidenko, N.V. and Sherriff, B.L.
2005: The attenuation of Ni, Zn and Cu, by secondary Fe phases of different crystallinity from surface and ground water of two sulfide mine tailings in Manitoba, Canada; Applied Geochemistry, v. 20, p. 1180-1194.

Siegel, D.I. and Ericson, D.W.
1980: Hydrology and Water Quality of the Copper-Nickel Study Region, Northeastern Minnesota; United States Geological Survey, Water-Resource Investigation, 80-739, 87 p.

Smith K.S. and Huyck, H.L.O.
1999: An overview of the abundance, relative mobility, bioavailability, and human toxicity of metals, *in* The Environmental Geochemistry of Mineral Deposits, Part A: Processes, Techniques and Health Issues, (ed.) L. H. Filipek and G. S. Plumlee; Society of Economic Geologists, Reviews in Economic Geology, v. 6A, p. 29-70.

Sofer, Z. and Gat, J.R.
1972: Activities and concentrations of oxygen-18 in concentrated aqueous salt solutions: Analytical and geochemical implications; Earth and Planetary Science Letters, v. 15, p. 232-238.

Souther, J.G. and Halstead, E.C.
1973: Mineral and Thermal Waters of Canada; Geological Survey of Canada, Paper 73-18, 62 p.

Steele, K.F. and Dilday, T.F.
1985: Hydrogeochemical exploration for Mississippi Valley-type deposits, Arkansas, USA; Journal of Geochemical Exploration, v. 23, p.71-79.

Stott, D.F.
1982: Lower Cretaceous Fort St. John Group and Upper Cretaceous Dunvegan Formation of the Foothills and Plains of Alberta, British Columbia, District of Mackenzie and Yukon Territory; Geological Survey of Canada, Bulletin 328, 124 p.

Timlin, R.P.
1991: The hydrogeochemistry and isotope geochemistry of three travertine precipitating springs in the Flat River valley, Northwest Territories; B.Sc. thesis, Carleton University, Ottawa, Ontario, 68 p.

Tole, M.P., Armannsson, H., Pang, Z., and Armorsson, S.
1993. Fluid/ mineral equilibrium calculations for geothermal fluids and chemical geothermometry; Geothermics, v. 22, p. 17-37.

Tonani, F.
1980: Some remarks on the application of geochemical techniques exploration; Proceedings of Advances in European Geothermal Research, 2nd Symposium, Strasboug, p. 428-443.

Tosiani, T., Loubet, M., Viers, J., Valladon, M., Tapia, J., Marrero, S., Yanes, C., Ramirez, A., and Dupre, B.
2004: Major and trace elements in river-borne materials from the Cuyuni basin (southern Venezuela): Evidence for organo-colloidal control on the dissolved load and element redistribution between the suspended and dissolved load; Chemical Geology, v. 211, p. 305-334.

Truesdell, A.H.
1976: Geochemical techniques in exploration, *in* Proceedings, 2nd United Nations Symposium on the Development and Use of Geothermal Resources; San Francisco, v. 53-79.

Verplanck, P.L., Nordstrom, D.K., Taylor, H.E., and Kimball, B.A.
2004: Rare earth element partitioning between hydrous ferric oxides and acid mine water during iron oxidation; Applied Geochemistry, v. 19, p. 1339-1354.

Wanty, R.B., Berger, B.R., Tuttle, M.L., Briggs, P.H., Meier, A.L., and Crock, J.G.
2006: Hydrogeochemical Investigations in the Osgood Mountains, North-Central Nevada; United States Geological Survey, Bulletin 2210-B, 25 p.

Whitfield, P.H., Whitley, W., Wade, N.L., and Regnier, R.
1996: Controls on chemistry of Yukon streams during winter baseflow, *in* Proceedings of the Hydro-Ecology Workshop on the Arctic Environmental Strategy Action on Water; Banff, May 1996.

Wiken, E.B.
1986: Terrestrial Ecozones of Canada; Environment Canada, Ecological Land Classification, Series No. 19, 26 p.

Woodsworth, G.J., Anderson, R.G., and Armstrong, R.L.
1991: Plutonic regimes, *in* Geology of the Cordilleran Orogen in Canada, (ed.) H. Gabrielse and C.J. Yorath; Geological Survey of Canada, Geology of Canada, no. 4, p. 491-531.

Appendix 1. Description of bedrock geological units from which MERA 2 springs discharge, based on Okulitch (in prep). Major lithology is keyed to legend in Figure 2; MERA 2 springs marked with an asterisk do not occur in the South Nahanni River basin. Also note that not all units occurring in the South Nahanni River basin are listed in the table.

Major Grouping	Geology Unit	Unit Description	Associated Springs
Limestone / Dolostone	mOSu	Sunblood Formation: dolostone, limestone	Wildmint, Clearwater Creek, Cascade, Cartman
	OSW	Whittaker Formation: lower grey limestone, middle white quartzite, upper dark grey cherty dolostone	South Redstone*, Prairie Creek Mine Shaft, Harrison Creek, Prairie Creek, Galena Creek
	PM	Manetoe Facies: grey coarse-grained massive vuggy diagenetic dolostone	Kraus (Clausen)
	SDRR	Root River Formation: light yellowish grey dolostone	Mel's Pool
	COBS	Broken Skull Formation: dolostone, limestone; basal sandstone, sandy dolostone	Dookie, Boulder
	COR	Rabbitkettle Formation: wavy banded silty limestone; platy impure limestone, siltstone, limestone	Brimstone, North Cantung, Glacier Lake, Stinky Drift, Tiny
	CSH	Haywire Formation: dolomitic, cherty, and argillaceous limestone	Moore's, Grizzle Bear
	lCSe	Sekwi Formation: limestone, calcareous silstone, sandstone, sandy and silty dolostone, argillite, minor quartzite and limestone	West Cantung, Blue Bells, Persistence, Stinky
	lmDC	Camsell, Sombre, Bear Rock, Arnica, Natla, Grizzly Bear, Funeral, Headless, Landry, Hume and Nahanni formations: limestone, dolostone, shale, siltstone, and sandstone	Tabletop*, Meilleur River, Sibbeston, Sombre, Wrigley, Cowgirl, Mossy, Crack
	lmDA	Arnica Formation: dolostone: finely crystalline thick-bedded grey finely porous	Sculpin*
	mCR	Rockslide Formation: dark grey sooty argillaceous limestone and calcareous siltstone, shale	Grasby
	mDHN	Headless and Nahanni formations: grey shale and limestone / bioclastic limestone	Veil, Big Veil, Cimitar
	PLD	Little Dal Group: basal varicloured mudstone, subordinate sandstone; grainstone, lime mudstone, stromatolotic biostromes and bioherms passing northwards in lime rhythmites, shale, siltstone; dolomitic grainstone, laminite, stromatolites, calcareous siltite all interbedded with dolostone and minor gypsum and local breccia; gypsum, anhydrite, minor quartz sandstone, siltstone, claystone; red, green and grey shale, very fine-grained sandstone, peritidal carbonate; dolomitic stromatolitic peritidal carbonate, mudrock; basaltic lava	Ekwi*, Deca*
Cretaceous Plutons	Kqm	Hole-in-the-Wall Batholith, Selwyn Plutonic Suite: quartz, monzonite, granodiorite	Hole-in-the-Wall, Waterfall, Half Spring
	LKmzg	Tombstone Plutonic Suite: biotite monzogranite	Overflow, Jacson, Darkness, Interpluton, Seep, Meltwater
	LKgd CEKgd, Kgd	Selwyn Plutonic Suite, Tay River Plutonic Suite, and mid-Cretaceous granodiorite unit	Hole-in-the-Wall, Overflow, Jacson, Darkness,
Shale	CPMC	Mount Christie: burrowed, interbedded greenish grey cherty shale and green shale; thin to medium bedded, light grey-green to black chert; black siliceous slate and siltstone; minor quartzite, limestone and dolostone; locally abundant, large grey barite nodules	Nahanni Headwaters
	DCBR	Besa River Formation: shale: dark grey, pyritic, siliceous; calcareous shale, siltstone, calcareous siltstone, silty limestone and limestone	Smurf, Clark Lake, Selena, Caribou, Chance, Orange Creek, Caribou River
	DCE	Earn Group (marine): chert, cherty mudstone, black shale, silty shale, argillite	Tulita*, Cotton, Red Mini, Muddy, Red Steel, Bougere
	mDF	Funeral Formation: grey thin-bedded argillaceous bioclastic shale	Corridor Creek, Broken Skull, Brigade
	ODRR	Road River Formation: black calcareous graptolitic shale, grey argillaceous limestone	Mineral Lake, Cordes Vertes, Rabbitkettle, Flat Fruit, Descente, Softie, Karst
	uDFS	Fort Simpson Formation: green and grey shale, siltstone, limestone	Cowboy, Ram Plateau, Cathedral, Quickie
Siltstone/ Mudstone	ECv	Vampire Formation: siltstone, grey fine-grained sandstone	Nahanni North
Stratified Clastics	ECH	Hyland Group: lower dark shale and slate, gritty quartzite, calcarenite, quartz pebble conglomerate; upper sandstone, maroon green and buff shale and slate	Champagne, Champagne Creek
	PCssc	Neohadrynian and/or Lower Paleozoic: grey to brown fine-grained sandy dolostone, medium- to coarse-grained sandstone	Redstone Junction #1*
Sandstone/ Arenite	CM, KGr KSc, Ksk, ICBR, ICGL, TrJL, uDs	Mattson Formation: arenite shale, sandy limestone, coal; Sikanni, Garbutt, Scatter, Backbone Ranges, Gull Lake, and Jones Lake formations: sandstone, some conglomerate, and mudstone; Upper Devnonian sandstone unit	n/a; MERA 1 springs only
Mafic Volcanics	ICSev, mOSuv	Sekwi and Sunblood formations: mafic volcanics	n/a

Appendix 2. Field parameters from MERA 2 springs (2003-2005 field seasons).

Informal Name of Water Sample	Water Type	UTM Zone	Easting (m)	Northing (m)	Year Sampled	Sulphide[1] (ppm)	Eh[2] (mV)	pH[2]	EC[3] (mS/cm)	T[4] (°C)	TDGP[5] (% sat'n)	DO[6] (ppm)
CCME Drinking Water Guideline						**≤0.05***	**n/a**	**6.5-8.5***	**n/a^**	**≤15***	**n/a**	**n/a**
CCME Recreation Water Guideline								**6.5-8.5**		**≤30**		
Tulita	spring	09V	457358.49	7075425.69	2004	45.45	nd	7.05	966.00	24.65	101.30	0.65
Sculpin	spring	09V	484585.25	7089846.74	2004	0.04	nd	7.03	2.43	17.05	104.50	0.52
Deca	spring	09V	527633.28	7113365.17	2004	0.89	125.00	7.10	40,800.00	21.60	126.60	2.2
Ekwi	spring	09V	537293.69	7104065.83	2004	0.03	10.40	6.69	18,300.00	40.80	127.10	0.23
Mineral Lake	spring	09V	622470.06	6806504.69	2004	n/a	(57.50)	6.68	776.00	18.30	105.10	0.13
Brimstone	spring	09V	583173.11	6830760.98	2004	0.11	11.50	5.89	8,200.00	6.20	113.60	2.1
Cordes Vertes	spring	09V	571387.59	6841734.95	2004	0.04	88.00	7.22	600.00	8.20	97.00	8.2
Tabletop	spring	10V	355312.53	7030439.74	2004	0.02	76.70	7.67	827.00	38.50	101.50	2.7
South Redstone	spring	10V	352412.30	7033921.27	2004	0.03	97.50	7.51	767.00	51.20	137.90	nd
Redstone Junction #1	spring	10V	365505.79	7047713.36	2004	0.09	139.70	7.36	1,274.00	15.40	104.90	3.4
Cotton	spring	09V	474514.23	6951212.93	2004	0.12	365.70	3.77	0.10	12.45	nd	7.0
Red Mini	spring	09V	493635.05	6937403.69	2004	0.12	402.50	3.94	143.70	4.15	nd	9.9
Muddy	spring	09V	512709.47	6920297.80	2004	0.14	130.30	6.84	342.00	2.25	98.70	9.3
Grasby	spring	09V	539902.76	6967577.54	2004	0.13	44.90	7.27	455.00	3.20	100.20	9.6
Red Steel	spring	09V	542373.96	6952471.06	2004	0.10	92.40	6.65	127.30	0.80	99.80	10.4
Bougere	spring	09V	523354.34	6948112.66	2004	0.34	344.00	4.31	547.00	2.70	102.00	10.5
Champagne	spring	09V	505561.89	6895664.37	2004	0.15	115.00	6.43	436.00	5.85	100.70	6.4
Champagne Creek	surface	09V	505561.89	6895664.37	2004	0.13	nd	nd	nd	nd	nd	nd
Broken Skull Upper Pool (2003)	spring	09V	544140.76	6958546.67	2003	nd	nd	nd	nd	nd	nd	nd
North Cantung / Zenchuck Creek	spring	09V	530148.61	6887223.23	2003	n/a	124.20	7.61	367.00	20.90	nd	nd
Moore's	spring	09V	544845.13	6911991.50	2003	n/a	(191.10)	6.75	871.00	48.20	nd	nd
Nahanni North / Lened Creek	spring	09V	516599.88	6915433.14	2003	34.00	(363.00)	8.66	579.00	56.10	nd	nd
Nahanni Headwaters	spring	09V	508210.84	6964253.26	2003	n/a	(149.00)	8.30	503.00	63.60	nd	nd
Broken Skull	spring	09V	544140.76	6958546.67	2003	20.00	(159.80)	6.38	2,200.00	46.40	nd	nd
Grizzle Bear	spring	09V	556331.44	6949262.49	2003	n/a	(79.30)	6.78	1,371.00	42.60	nd	nd
Glacier Lake	spring	09V	573551.51	6884820.47	2003	n/a	(203.50)	7.11	944.00	3.50	nd	nd
Rabbitkettle	spring	09V	595449.10	6868956.47	2003	n/a	nd	5.74	1,896.00	21.10	nd	nd
Kraus / Clausen	spring	10V	443147.32	6791496.54	2003	61.00	nd	6.54	11,870.00	36.70	nd	nd
Meilleur River	spring	10V	397575.60	6778381.38	2003	25.00	nd	6.63	1,845.00	36.90	nd	nd
Wildmint	spring	09V	629391.33	6812338.62	2003	43.00	nd	6.63	1,243.00	30.00	nd	nd
Stinky Drift	spring	09V	541638.39	6869583.84	2003	nd	nd	8.76	1,013.00	16.60	nd	nd
Hole in the wall	spring	09V	589112.54	6849730.52	2003	n/a	nd	8.43	211.00	40.20	nd	nd
Flat Fruit	spring	09V	573499.03	6839392.88	2003	n/a	nd	6.29	4,030.00	9.30	nd	nd
West Cantung	spring	09V	541638.39	6869583.84	2003	nd	nd	8.39	460.00	41.30	nd	nd
Prairie Creek Mine Shaft	mine	10V	404598.00	6825669.00	2005	0.46	149.00	7.15	1,185.00	1.40	nd	n/a
Harrison Creek	surface	10V	404760.00	6825676.00	2005	0.63	136.10	8.23	645.00	8.20	nd	n/a
Prairie Creek	surface	10V	404733.00	6825262.00	2005	0.67	160.00	8.08	498.00	9.10	nd	n/a
Broken Skull Upper Pool (2005)	spring	09V	544140.76	6958546.67	2005	0.26	112.00	7.18	1,346.00	27.90	nd	6.26
Broken Skull Lower Pool (2005)	spring	09V	544140.76	6958546.67	2005	7.91	(286.00)	6.46	1,340.00	46.30	nd	0.8
Cowboy	spring	10V	396251.00	6854569.00	2005	0.74	230.00	7.87	352.00	1.25	nd	11.4
Sibbeston	spring	10V	384613.00	6838707.00	2005	0.78	235.00	7.65	340.00	16.90	nd	4.62
Corridor Creek	seep	10V	411544.00	6861536.00	2005	0.20	197.00	8.82	265.00	3.80	nd	10.96
Veil	spring	10V	444167.00	6845930.00	2005	0.64	203.20	8.17	414.00	4.80	nd	11.04
Big Veil	spring	10V	443995.00	6846719.00	2005	n/a	254.00	8.37	446.00	4.80	nd	7.89
Galena	spring	10V	404768.00	6824888.00	2005	0.49	235.30	8.01	779.00	2.30	nd	3.64
Sombre	spring	10V	363265.00	6884608.00	2005	0.50	228.50	8.67	169.40	0.30	nd	11.28
Wrigley	spring	10V	374780.00	6873478.00	2005	0.69	258.00	6.15	624.00	2.50	nd	7.83
Mel's Pool	waterfall	10V	371922.00	6826904.00	2005	0.27	2.62	7.53	138.00	2.70	nd	12.46

Appendix 2 continued.

Informal Name of Water Water Sample	Water Type	UTM Zone	Easting (m)	Northing (m)	Year Sampled	Sulphide[1] (ppm)	Eh[2] (mV)	pH[2]	EC[3] (mS/cm)	T[4] (°C)	TDGP[5] (% sat'n)	DO[6] (ppm)
CCME Drinking Water Guideline						**≤0.05***	**n/a**	**6.5-8.5***	**n/a^**	**≤15***	**n/a**	**n/a**
CCME Recreation Water Guideline								**6.5-8.5**		**≤30**		
Cowgirl	spring	10V	393366.00	6849954.00	2005	n/a	178.00	7.37	463.00	2.00	nd	7.72
Brigade	spring	10V	417004.00	6865784.00	2005	0.43	2.89	7.55	576.00	3.30	nd	10.19
Ram Plateau	waterfall	10V	438705.00	6865933.00	2005	0.29	3.08	7.52	134.40	2.60	nd	11.63
Cimitar	spring	10V	457861.00	6855539.00	2005	n/a	5.80	6.79	1,960.00	11.90	nd	0.27
Cathedral	spring	10V	365815.00	6871064.00	2005	0.22	3.91	7.55	473.00	2.00	nd	10.79
Mossy	spring	10V	355469.00	6887488.00	2005	0.24	3.69	7.61	409.00	1.40	nd	8.38
Crack	spring	10V	354083.00	6891379.00	2005	n/a	(1.50)	7.83	279.00	4.00	nd	7.15
Quickie	seep	10V	362240.00	6867252.00	2005	n/a	2.11	7.98	453.00	7.00	nd	10.25
Clearwater Creek	surface	09V	646454.00	6881852.00	2005	0.15	309.50	8.66	292.00	5.80	nd	10.81
Dookie	surface	09V	626201.00	6909591.00	2005	0.11	282.50	8.78	298.00	4.10	nd	10.15
Boulder	spring	09V	644261.00	6890647.00	2005	n/a	258.40	8.79	158.90	0.80	nd	11.4
Overflow	spring	09V	633581.00	6776726.00	2005	0.00	311.50	4.85	4.90	1.70	nd	10.28
Smurf	spring	09V	619206.00	6770435.00	2005	n/a	289.30	7.39	354.00	2.70	nd	10.47
Clark Lake	spring	09V	646722.00	6795048.00	2005	n/a	53.10	7.49	473.00	3.30	nd	2.77
Jacson	spring	09V	632059.00	6776080.00	2005	n/a	280.10	6.87	13.10	1.80	nd	11.06
Darkness	spring	09V	632175.00	6776410.00	2005	n/a	291.50	6.40	22.80	1.00	nd	9.96
Selena	seep	09V	624764.00	6759725.00	2005	n/a	88.80	7.24	708.00	7.60	nd	3.3
Caribou	spring	09V	619689.00	6768728.00	2005	n/a	215.10	7.75	377.00	3.80	nd	10.09
Chance	spring	09V	619815.00	6768439.00	2005	n/a	399.50	7.66	431.00	2.00	nd	11.53
Interpluton	seep	09V	625583.00	6794379.00	2005	n/a	259.90	4.41	15.60	4.10	nd	9.75
Tiny	spring	09V	607475.00	6792433.00	2005	n/a	225.20	7.64	252.00	1.40	nd	11.41
Blue Bells	spring	09V	606845.00	6773246.00	2005	n/a	193.10	7.41	380.00	7.60	nd	6.51
Cascade	spring	09V	626373.00	6754797.00	2005	n/a	290.80	7.37	356.00	4.00	nd	8.86
Meltwater	seep	09V	632361.00	6782647.00	2005	n/a	264.40	7.44	63.10	3.70	nd	8
Waterfall	surface	09V	615834.00	6842094.00	2005	n/a	259.00	6.90	25.90	9.80	nd	8.97
Descente	spring	09V	620423.00	6823148.00	2005	n/a	278.10	7.49	56.50	0.80	nd	11.1
Softie	spring	09V	635352.00	6833829.00	2005	n/a	287.00	5.53	18.20	6.30	nd	6.31
Cartman	spring	09V	636224.00	6840955.00	2005	n/a	256.40	6.34	29.70	1.70	nd	10.74
Half Spring	spring	09V	623424.00	6840327.00	2005	n/a	242.60	7.60	155.40	4.50	nd	11.34
Orange Creek	surface	09V	653663.00	6785389.00	2005	n/a	218.80	4.65	3,260.00	1.90	nd	7.7
Caribou River	surface	09V	653624.00	6785282.00	2005	n/a	190.30	7.93	355.00	9.30	nd	12.75
Karst	spring	09V	549539.00	6942051.00	2005	n/a	285.10	7.93	163.30	3.70	nd	13
Persistent	spring	09V	607144.00	6773277.00	2005	n/a	127.00	6.07	661.00	20.50	nd	2.38
Stinky	spring	09V	607101.00	6773258.00	2005	2.32	(60.30)	6.74	761.00	24.10	nd	1

1. Sulphide concentration <1 ppm is considered negligible
2. Normalized to 25ºC
3. Electrical conductivity
4. Temperature
5. Total dissolved gas pressure (% saturation)
6. Dissolved oxygen

n/a = not applicable (no smell of sulphide)

nd = no data available (test not performed)

unstable reading

CCME Drinking Water Guidelines:
Federal-Provincial-Territorial Committee on Drinking Water. "Guidelines for Canadian Drinking Water Quality Summary Table". Health Canada, Government of Canada, March 2006.

CCME Recreation Guidelines:
Federal-Provincial Working Group on Recreational Water Quality of the Federal-Provincial Advisory Committee on Environmental and Occupational Health. "Guidelines for Canadian Recreational Water Quality". Health and Welfare Canada, Government of Canada, 1992.

*Aesthetic guideline only

n/a = guideline not available

^Total dissolved solids ≤500*

Appendix 3. Major ions from spring waters collected in the 2003, 2004, and 2005 field seasons (all units in ppm unless otherwise noted).

Name of Spring	Ca^{2+}	Mg^{2+}	K^{+}	Na^{+}	Si^{4+}	HCO_3^{-}	SO_4^{2-}	Cl^{-}	NO_3^{-}	F^{-} (ppb)	Charge
CCME Drinking Water Guideline	*n/a*	*n/a*	*n/a*	*<=200**	*n/a*	*n/a*	*<=500**	*<=250**	*45*	*1.5*	**Balance (%)**
Tulita	68	22	12	110	8.40	389.4	118.4	45.9	<0.05	2614	0.75
Sculpin	440	130	1.0	1.6	4.44	219.7	1495.1	<1	<0.50	<500	-3.0
Deca	270	59	5.2	420	5.40	261.3	943.9	471	<0.50	<500	-0.68
Deca (lab dup)	nd	nd	nd	nd	5.46	nd	nd	nd	nd	nd	nd
Ekwi	220	49	72	4800	12.0	663.3	1783.1	7503	<2.50	<2500	-7.0
Mineral Lake	120	29	2.8	6.4	4.32	327.3	78.3	1.59	<0.05	342	**10.7**
Brimstone	630	55	8.2	44	36	1813.0	69.3	4.09	<0.05	2710	9.8
Cordes Vertes	92	20	0.95	7.0	2.52	457.7	14.7	0.40	0.43	<50	-8.7
Tabletop	73	23	1.4	60	13.2	188.1	150.4	85.2	0.2	178	-2.6
South Redstone	77	21	1.3	48	15.6	172.1	162.3	68.5	0.15	157	-2.8
Redstone Junction #1	110	38	2.1	100	10.8	172.1	251.9	144	0.74	239	3.6
Cotton	0.93	1.2	0.27	0.27	3.72	0	15.6	0.1	<0.05	<50	**-15.1**
Red Mini	4.7	1.5	0.83	0.7	5.58	0	38.0	<0.1	<0.05	<50	**-10.4***
Muddy	37	15	1.7	1.4	5.58	79.9	99.0	<0.1	0.63	136	-2.9
Grasby	64	17	0.85	1.9	2.64	296.6	29.3	0.29	0.81	<50	-7.7
Red Steel	17	2	0.26	1.0	2.40	0.0	21.6	<0.1	1.21	<50	**12.4***
Bougere	2.8	37	0.32	0.29	7.20	0.0	278.7	<0.1	0.29	<50	0.87*
Champagne	83	1	1.6	2.4	2.58	223.0	52.7	<0.1	0.3	<50	-4.2
Champagne (field dup)	79	0.93	1.6	2.1	2.76	217.9	52.3	<0.1	0.3	<50	-5.8
Champagne Creek	72	0.57	1.6	0.96	2.22	168.8	55.8	0.10	0.12	<50	-2.7
Champagne Creek (lab dup)	72	0.58	1.6	0.97	nd	168.8	54.9	0.14	<0.05	<50	nd
North Cantung / Zenchuck Creek	26	14	0.56	0.58	4.92	200.9	8.64	0.21	729	197	**-16.6**
Moore's	74	23	4.1	2.2	21	278.9	73.4	0.48	<50	286	-2.8
Nahanni North / Lened Creek	1.6	0.059	1.1	76	25.8	146.0	57.4	1.11	157	2874	-2.9
Nahanni Headwaters	2.9	0.01	1.6	65	34.2	100.8	31.9	10.3	<50	8157	7.3
Broken Skull Upper Pool (2003)	160	50	32	56	15.6	386.5	344.5	22.0	<50	2250	4.1
Grizzle Bear	110	26	23	22	16.2	228.7	188.0	26.8	290	680	4.3
Glacier Lake	75	17	0.84	1.3	7.80	64.5	198.8	0.14	<50	436	0.17
Rabbitkettle	200	40	5.1	4.1	6.60	447.4	34.8	0.57	<50	235	0.91*
Kraus / Clausen	410	74	81	940	12.6	235.8	656.0	1695	<500	<500	3.1
Meilleur River	150	46	14	30	18.6	316.9	276.6	23.9	<50	467	5.3
Wildmint	17	2.5	1.2	130	16.8	186.7	114.2	29.4	6590	8310	3.6
Stinky Drift	130	26	2.8	1.5	7.80	346.0	29.4	0.30	208	291	-4.8*
Hole in the wall	1.6	0.061	0.63	26	25.8	72.3	5.74	1.14	<50	1876	-4.1
Flat Fruit	500	52	6.0	27	5.70	581.4	35.1	1.56	454	631	1.6*
West Cantung	8	1.2	1.2	57	21	140.0	31.5	5.89	<50	4997	-1.8
Prairie Creek Mine Shaft	150	65	1.1	0.91	1.86	315.4	396	0.39	0.41	<50	-2.0
Harrison Creek	75	39	0.79	0.91	1.50	222.6	161.1	0.19	1.04	<50	-0.09
Prairie Creek	58	23	0.47	1.8	1.32	193.3	74.8	<0.1	0.27	67.0	1.5
Broken Skull's Upper Pool (2005)	160	50	32	51	13.2	439.1	366.0	21.6	<0.05	1699	-0.94
Broken Skull's Lower Pool (2005)	160	49	31	50	15.0	440.0	363.8	21.2	<0.05	1771	-1.3
Cowboy	45	15	0.22	0.72	1.08	156.5	35.3	<0.1	0.56	<50	3.1
Sibbeston	44	16	0.58	1.3	4.74	168.2	29.8	0.91	0.77	1307	2.4
Corridor Creek	35	11	0.16	0.64	0.66	121.9	22.7	0.14	0.64	129	3.9
Veil	65	14	0.6	5.6	1.68	186.0	62.4	0.72	0.65	307	3.1
Big Veil	65	14	0.6	5.6	1.68	187.7	64.2	0.69	0.73	300	2.3
Galena	110	40	1.0	1.8	1.74	282.8	155.0	0.49	0.12	53.0	6.0
Galena (lab dup)	120	44	1.1	2.2	nd	282.8	144.2	0.58	0.1	<50	**12.0**
Sombre	22	8.3	0.067	0.040	0.17	94.5	4.2	<0.1	0.4	1193	4.2
Sombre (field dup)	22	8.2	0.080	0.040	bdl	94.6	4.1	<0.1	0.5	907	3.9
Wrigley	95	19	0.43	0.84	1.74	244.0	112.6	0.26	1.38	337	-0.16
Mel's Pool	27	4.1	0.17	0.35	1.56	73.4	1.3	<0.1	<0.05	<50	**16.2**
Cowgirl	70	14	0.23	0.49	1.38	190.4	64.9	0.18	0.58	66.0	2.0
Brigade	68	29	0.50	4.1	1.92	197.6	126.5	0.27	1.32	133	0.59
Ram Plateau	23	3.4	0.45	0.30	1.02	61.3	7.4	<0.1	<0.05	<50	**11.2**
Cimitar	370	63	2.5	13	4.32	287.3	780.2	14.6	<0.05	<500	6.4
Cathedral	55	19	0.31	6.1	1.08	178.1	73.2	0.17	0.96	370	1.3
Mossy	46	21	0.26	0.21	0.90	166.8	54.2	0.16	0.67	350	2.0
Mossy (lab dup)	51	24	0.34	0.33	nd	166.8	56.1	<0.1	0.5	333	7.5

Appendix 3 continued.

Name of Spring	Ca^{2+}	Mg^{2+}	K^{+}	Na^{+}	Si^{4+}	HCO_3^{-}	SO_4^{2-}	Cl^{-}	NO_3^{-}	F^{-} (ppb)	Charge
CCME Drinking Water Guideline	*n/a*	*n/a*	*n/a*	*<=200**	*n/a*	*n/a*	*<=500**	*<=250**	*45*	*1.5*	**Balance (%)**
Crack	34	15	0.14	0.16	0.84	136.3	14.8	0.14	0.51	86.0	7.0
Quickie	61	19	0.30	4.2	1.50	174.2	67.7	0.18	0.65	145	5.7
Clearwater Creek	39	12	0.32	0.27	0.96	111.9	37.8	0.14	0.46	<50	5.7
Dookie	30	17	0.19	0.099	0.96	97.6	62.9	<0.1	0.39	<50	-0.17
Dookie (field dup)	31	17	0.19	0.12	0.84	83.8	63.2	<0.1	0.39	<50	4.6
Dookie (field trip)	31	17	0.19	0.11	0.78	81.7	63.8	<0.1	0.38	<50	5.0
Boulder	20	7.4	0.089	0.07	0.53	75.8	5.5	0.11	0.54	<50	8.2
Overflow	0.66	0.078	0.11	0.54	1.14	4.0	<0.05	<0.1	<0.05	<50	0.08
Smurf	62	6.8	0.45	0.84	2.40	219.6	8.4	<0.1	<0.05	<50	-1.0
Clark Lake	81	11	0.64	0.35	2.04	186.6	21.4	0.14	<0.05	<50	**17.3**
Clark Lake (lab dup)	89	12	0.72	0.45	nd	186.6	21.3	<0.1	<0.05	<50	**21.9**
Jacson	1.4	0.13	0.20	0.51	1.08	5.7	0.3	<0.1	0.35	<50	1.1
Darkness	2.4	0.15	0.26	0.91	1.92	9.7	0.7	<0.1	0.76	<50	-2.0
Selena	130	14	0.77	1.2	2.22	188.2	130.5	0.15	<0.05	<50	**14.1**
Caribou	57	12	0.64	0.77	2.58	200.1	11.9	0.11	0.48	<50	4.6
Chance	67	13	0.49	0.66	2.46	180.6	17.6	0.11	0.77	<50	**14.3**
Interpluton	1.6	0.17	0.36	0.70	2.94	8.0	<0.05	<0.1	<0.05	<50	0.90
Tiny	38	7.7	1.2	0.62	2.22	127.0	2.55	<0.1	<0.05	<50	9.6
Blue Bells	43	20	1.8	2.2	3.30	186.6	11.9	0.70	0.72	451	8.2
Blue Bells (field dup)	42	20	1.8	2.2	3.30	187.6	11.9	0.71	0.79	456	7.3
Cascade	55	11	0.41	0.48	1.98	165.9	14.4	0.11	0.43	<50	9.7
Cascade (lab dup)	60	12	0.45	0.59	nd	165.9	13.7	<0.1	0.35	<50	**14.3**
Meltwater	9.4	0.27	0.78	0.47	1.74	36.6	0.56	<0.1	<0.05	<50	-7.0
Waterfall	3.1	0.17	0.74	0.81	2.16	14.2	0.20	<0.1	<0.05	<50	-3.1
Descente	4.9	1.8	0.39	0.63	2.52	19.5	7.97	<0.1	0.22	<50	-6.4
Softie	1.7	0.5	<0.02	1.1	4.02	8.9	<0.05	<0.1	<0.05	<50	8.7
Cartman	1.7	1.2	0.24	0.86	3.72	15.5	0.66	<0.1	<0.05	<50	-8.1
Half Spring	27	2.6	0.89	2.3	3.18	85.4	12.3	0.15	0.58	536	0.43
Orange Creek	380	170	1.6	0.89	4.44	0.0	1913	<0.5	<0.5	<500	-9.3
Caribou River	56	11	0.69	0.87	1.92	163.6	41.9	<0.1	0.14	<50	2.7
Karst	23	8.1	0.13	0.10	0.60	89.3	10.5	<0.1	0.3	<50	3.9
Persistent	79	34	8.4	12	nd	397.0	11.8	5.35	<0.05	1463	4.0
Persistent (lab dup)	83	38	9.3	13	6.6	397.0	11.1	4.97	<0.05	1443	8.0
Stinky	93	37	9.7	15	8.4	457.2	10.7	6.52	<0.05	1804	4.2
Field Blank (2005)	0.3	0.011	<0.02	<0.02	<0.06	nd	<0.05	<0.1	<0.05	<50	nd
Calgary Lab Blank (2005)	<0.005	<0.002	<0.02	<0.02	<0.06	nd	<0.05	<0.1	<0.05	<50	nd

CCME Drinking Water Guidelines:
Federal-Provincial-Territorial Committee on Drinking Water. "Guidelines for Candadian Drinking Water Quality Summary Table". Health Canada, Government of Canada, March 2006.

*Aesthetic guideline only

bdl = below detection limit

n/a = guideline not available

nd = no data

**Silica concentration was determined by diluting 10 ml of sample water with 50 ml of distilled water

The determined concentration of the diluted sample was multiplied by 6 for the reported values

Appendix 4A. Trace elements, Fe, Al, Mn, Ni, Cu, Zn, Pb, Cd, Co, and Cr (units in mg/L unless otherwise noted), from the MERA 1 and 2 samples; numbers in bold were determined to be anomalous.

	Fe	Al	Mn	Ni	Cu	Zn	Pb	Cd	Co	Cr
detection limit (MERA 2)	3	0.2	0.05	0.2	0.2	0.32	0.05	0.1	0.05	0.2
detection limit (MERA 1)	4	100	5	2	2	5	2	2	2	n/a
CCME Drinking Water Guideline (mg/L)	≤0.3*	n/a	≤0.05*	n/a	≤1.0*	<=5.0*	0.010	0.005	n/a[c]	0.05
Name of Spring					**MERA 2 Samples**					
Tulita	bdl	0.6	5.60	0.8	0.6	3	bdl	0.1	0.08	0.9
Sculpin	84	0.8	2.50	9.9	bdl	6	0.06	0.1	0.56	0.4
Deca	bdl	0.8	0.94	5.7	3.3	4	0.08	0.1	0.34	**4.4**
Ekwi	170	3.9	17.0	2.8	2.5	2	0.09	bdl	0.25	**2.9**
Mineral Lake	1300	0.4	12.0	3.9	0.2	1	bdl	bdl	0.21	**1.8**
Brimstone[1]	**15400**	120	**1340**	9.7	0.5	7	bdl	0.9	1.90	**6.9**
Cordes Vertes	13	0.8	0.25	2.2	0.3	2	0.05	0.3	0.13	**1.6**
Tabletop	bdl	0.7	0.08	1.2	0.4	2	bdl	0.4	0.06	**1.6**
South Redstone	bdl	1.1	0.08	1.2	1.3	6	0.42	0.1	0.07	**1.1**
Redstone Junction #1	bdl	0.6	0.10	2.0	0.8	3	0.06	0.1	0.11	2.5
Cotton	300	600	23.0	19.0	2.0	56	0.74	1.3	3.90	bdl
Red Mini	140	2000	94.0	70.0	14.0	72	0.23	2.2	11.0	bdl
Muddy	bdl	7.0	0.27	13.0	0.3	29	bdl	0.4	0.05	0.2
Grasby	bdl	0.7	bdl	1.3	bdl	1	bdl	1.8	0.08	0.6
Red Steel	5	12.0	0.28	1.9	0.7	3	bdl	2.3	bdl	0.2
Bougere	26	**24000**	**930**	**1300**	**28**	**2300**	0.22	4.4	**390**	bdl
Champagne	180	5.9	150	2.1	0.4	4	bdl	3.8	0.21	0.8
Champagne (dup)	150	9.9	120	1.9	0.3	2	bdl	2.8	0.18	0.6
Champagne Creek	28	22.0	1.10	1.6	0.3	2	bdl	4.2	0.11	0.4
Champagne Creek (dup)	28	19.0	1.00	1.4	0.2	2	bdl	3.8	0.10	0.3
North Cantung (Zenchuck Creek)	bdl	0.60	bdl	0.3	0.7	3	0.36	bdl	bdl	0.2
Moore's	110	39.0	14.0	1.0	0.7	2	0.43	0.1	0.20	0.3
Nahanni North (Lened Creek)	77	70.0	0.79	0.2	0.5	2	0.08	bdl	0.05	bdl
Nahanni Headwaters	5	24.0	0.23	bdl	0.5	2	bdl	bdl	bdl	0.4
Broken Skull	65	2.40	3.20	1.9	0.5	1	0.10	bdl	0.13	0.8
Grizzle Bear	14	0.60	26.0	1.2	0.2	2	0.05	bdl	0.30	**1.1**
Glacier Lake	**17000**	6.40	530	190	bdl	**679**	bdl	2.1	28.0	bdl
Rabbitkettle	10	0.40	4.50	4.0	bdl	8	bdl	bdl	0.29	0.8
Kraus (Clausen)	11	4.70	27.0	3.3	5.8	3	0.07	bdl	0.37	**27**
Meilleur River	17	5.10	14.0	2.0	0.3	2	bdl	bdl	0.13	0.8
Wildmint	bdl	1.50	49.0	1.2	0.8	1	0.07	0.1	0.26	1.2
Stinky Drift	23	3.40	1.20	1.6	bdl	7	0.12	bdl	0.12	0.6
Hole-in-the-Wall	17	36.0	0.37	bdl	0.4	2	bdl	0.1	bdl	0.4
Flat Fruit	9	2.70	94.0	6.3	0.9	5	0.05	0.1	0.47	bdl
West Cantung	34	4.00	0.79	bdl	0.5	3	bdl	0.2	bdl	0.4
Prairie Creek Mine Shaft	bdl	1.0	4.60	15.0	**16.0**	**6900**	**16.0**	**41**	0.46	0.2
Harrison Creek	bdl	2.0	0.11	1.9	0.8	30	**3.50**	0.3	0.08	0.2
Prairie Creek	bdl	1.3	0.36	2.0	0.7	80	0.82	0.2	0.06	bdl
Broken Skull's Upper Pool	5	4.6	11.0	2.1	1.2	20	**2.30**	0.2	0.27	0.4
Broken Skull's Lower Pool	120	4.1	5.10	2.8	0.5	4	0.64	0.2	0.19	0.6
Cowboy	bdl	1.8	0.05	1.3	0.2	2	0.48	0.3	0.05	0.2
Sibbeston	bdl	2.6	0.08	2.9	0.2	33	1.00	0.2	0.05	0.2
Corridor Creek	bdl	2.4	bdl	0.8	0.2	2	0.15	bdl	0.05	0.2
Veil	bdl	0.8	0.07	2.8	0.3	10	0.11	0.2	0.08	0.2
Big Veil	bdl	1.3	2.10	3.0	0.9	10	0.40	0.2	0.08	0.2
Galena	bdl	1.7	0.18	6.1	0.9	350	**2.60**	0.6	0.12	0.3
Galena (lab dup)	bdl	1.3	0.15	5.9	1.3	350	2.00	0.6	0.11	0.2
Sombre	bdl	4.4	0.09	0.3	bdl	2	0.50	bdl	bdl	bdl
Sombre (field dup)	bdl	5.0	0.18	0.6	0.3	9	0.65	0.1	bdl	bdl
Wrigley	bdl	0.9	0.16	20.0	0.5	42	0.27	0.2	0.11	0.4
Mel's Pool	130	62.0	1.50	4.8	2.4	10	0.78	0.3	0.13	0.2
Cowgirl	bdl	1.2	0.06	8.6	0.5	19	0.19	0.1	0.07	0.2
Brigade	bdl	0.9	0.08	1.2	0.2	2	0.19	bdl	0.07	bdl
Ram Plateau	120	72.0	1.30	3.1	5.6	4	0.29	0.1	0.16	0.3
Cimitar	840	3.5	150	37.0	0.2	64	0.24	0.1	4.90	0.4
Cathedral	11	7.2	0.44	1.3	0.2	4	0.44	0.1	0.07	0.3
Mossy	15	4.6	0.20	1.0	0.3	5	0.34	0.1	0.06	0.2
Mossy (lab dup)	4	4.4	0.20	1.0	0.5	5	0.33	0.1	0.06	bdl
Crack	bdl	2.8	0.10	1.7	0.3	4	0.34	0.1	0.05	0.2
Quickie	bdl	2.8	0.11	2.4	0.5	2	0.19	0.1	0.08	0.2
Clearwater Creek	bdl	14.0	1.40	1.4	0.2	2	0.26	0.1	0.15	bdl

Appendix 4A continued.

	Fe	Al	Mn	Ni	Cu	Zn	Pb	Cd	Co	Cr
detection limit (MERA 2)	3	0.2	0.05	0.2	0.2	0.32	0.05	0.1	0.05	0.2
detection limit (MERA 1)	4	100	5	2	2	5	2	2	2	n/a
CCME Drinking Water Guideline (mg/L)	≤0.3*	n/a	≤0.05*	n/a	≤1.0*	<=5.0*	0.010	0.005	n/a[c]	0.05
Dookie	bdl	40.0	220	14.0	0.4	4	0.54	0.1	11.0	bdl
Dookie (field dup)	18	46.0	220	14.0	0.4	3	0.22	bdl	11.0	bdl
Dookie (field trip)	bdl	70.0	220	14.0	0.4	3	0.10	bdl	11.0	bdl
Boulder	bdl	5.2	0.65	0.5	0.2	1	0.18	bdl	0.10	bdl
Overflow	31	170	1.90	0.3	0.6	3	0.52	0.1	0.10	bdl
Smurf	bdl	2.6	0.23	6.5	0.6	46	0.11	0.9	0.09	0.3
Clark Lake	1300	1.1	35.0	1.7	0.3	4	0.27	bdl	0.14	0.2
Clark Lake (lab dup)	1300	1.2	35.0	1.5	0.5	4	0.28	bdl	0.14	bdl
Jacson	bdl	26.0	0.37	bdl	0.4	2	0.35	bdl	bdl	bdl
Darkness	bdl	28.0	0.52	0.2	0.4	2	0.20	0.1	bdl	bdl
Selena	470	0.8	110	35.0	14.0	120	1.50	0.3	1.20	0.3
Caribou	150	2.3	0.95	1.3	0.2	4	0.08	0.1	0.08	0.4
Chance	bdl	1.9	0.10	1.4	0.3	3	0.14	0.1	0.09	0.4
Interpluton	57	340	1.20	0.3	1.3	3	0.34	0.1	0.06	bdl
Tiny	bdl	7.3	0.20	0.8	2.6	2	0.38	bdl	0.07	0.4
Blue Bells	bdl	2.0	0.09	0.8	0.3	4	0.17	bdl	0.06	0.3
Blue Bells (field dup)	bdl	2.2	0.13	0.8	0.2	2	0.21	bdl	0.06	0.3
Cascade	bdl	1.5	0.06	1.2	0.5	4	0.22	bdl	0.07	0.3
Cascade (lab dup)	bdl	1.1	0.06	1.1	0.6	4	0.22	bdl	0.07	0.2
Meltwater	18	54.0	0.31	0.3	3.9	1	0.50	bdl	0.07	bdl
Waterfall	10	26.0	0.94	bdl	0.9	3	0.22	0.1	bdl	bdl
Descente	bdl	6.2	0.17	bdl	0.2	1	0.10	0.1	bdl	bdl
Softie	96	58.0	3.40	0.4	0.9	3	0.08	0.1	0.09	bdl
Cartman	bdl	4.5	0.40	bdl	bdl	1	bdl	bdl	bdl	bdl
Half Spring	10	14.0	2.90	0.7	0.6	2	0.05	0.1	0.05	bdl
Orange Creek	bdl	**83000**	**11000**	**1900**	**430**	**4500**	0.99	**14**	**620**	**8.0**
Caribou River	26	78.0	13.0	9.4	1.1	18	0.14	0.4	0.81	0.2
Karst	bdl	12.0	0.51	0.5	0.2	1	0.05	bdl	0.05	bdl
Persistent	16	9.9	200	1.5	0.4	11	0.20	**12**	0.43	0.3
Persistent (lab dup)	14	9.7	200	1.4	0.4	12	0.19	**12**	0.42	0.3
Stinky	bdl	11.0	220	1.9	0.7	4	0.26	1.4	0.87	0.2
Field Blank	bdl	0.5	0.76	0.7	**18.0**	6	**7.40**	bdl	bdl	bdl
Calgary Lab Blank	bdl	0.2	bdl	0.3	**31.0**	4	**4.50**	0.1	bdl	bdl
MERA 1 Samples (as reported by Hamilton, 1990)										
86-1	129	100	13	<2	3	8		<2	<2	
86-4	361	600	12	<2	4	<5		3	3	
86-6	<20	100	<10	<2	<2	<5		<2	<2	
86-7	<20	bdl	<10	<2	3	<5		<2	<2	
86-9	33	bdl	<10	<2	<2	<5		<2	<2	
86-10	108		12	16	3	<5		<2	5	
86-11	<20	100	<10	<2	5	10		<2	<2	
86-12	<20	4100	135	101	10	366		5	28	
87-012B	<5	400	3	35	3	220	<5	5	<2	
87-12	60	3500	80	130	15	305	<5	5	13	
87-012C	103	800	45	75	3	445	<5	**10**	5	
86-13	<20	bdl	<10	<2	3	<5		<2	<2	
86-15	**14416**	200	430	173	<2	**652**		3	23	
86-17	**20766**	400	**1503**	<2	11	<5		3	<2	
87-17	58	100	**1498**	<2	3	8	<5	<2	<2	
86-18	<20	bdl	<10	<2	4	<5		<2	<2	
87-18	<5	bdl	3	<2	<2	<2	<5	<2	<2	
87-018B		bdl								
86-19	199	200	37	<2	<2	<5		<2	<2	
86-20	65	bdl	<10	<2	5	<5		<2	<2	
86-21	243	700	165	<2	4	<5		<2	<2	
86-22	33	bdl	<10	<2	4	<5		<2	<2	
86-23	<20	bdl	<10	<2	13	<5		<2	6	
86-24	<20	bdl	<10	<2	<2	<5		<2	<2	
86-25	147	7000	169	<2	<2	**3936**		<2	<2	
86-26	<20	bdl	<10	<2	<2	<5		<2	<2	
86-27	26	bdl	<10	<2	4	<5		<2	<2	
87-27	15	bdl	<2	<2	<2	5	<5	<2	<2	
86-28	<20	bdl	<10	<2	<2	<5		<2	<2	

Appendix 4A continued.

	Fe	Al	Mn	Ni	Cu	Zn	Pb	Cd	Co	Cr
detection limit (MERA 2)	3	0.2	0.05	0.2	0.2	0.32	0.05	0.1	0.05	0.2
detection limit (MERA 1)	4	100	5	2	2	5	2	2	2	n/a
CCME Drinking Water Guideline (mg/L)	≤0.3*	n/a	≤0.05*	n/a	≤1.0*	<=5.0*	0.010	0.005	n/a[c]	0.05
86-29	24	100	<10	<2	4	7		<2	13	
86-30	1710	200	15	<2	4	<5		<2	5	
86-31	<20	bdl	<10	<2	<2	<5		3	5	
86-32	460	200	23	<2	<2	<5		<2	3	
86-33	36	100	<10	11	13	<5		3	<2	
87-33	<5	bdl	<2	<2	<2	<2	<5	<2	<2	
87-34	<5	bdl	<2	<2	<2	<2	<5	<2	<2	
86-35	972	700	10	63	**16**	7		<2	**40**	
86-36	645		534	168	4	**640**		<2	**46**	
86-37	**19082**	200	425	8	3	306		<2	<2	
86-38	26	bdl	<10	<2	5	8		<2	<2	
86-40	65	300	<10	8	5	<5		3	<2	
86-41	440	500	<10	3	6	6		<2	<2	
86-42	5816	**8000**	225	273	**25**	**1488**		**39**	29	
86-43	138	200	30	<2	<2	5		<2	6	
86-44	91	100	<10	<2	3	<5		<2	<2	
86-45	57	bdl	<10	<2	4	6		<2	<2	
86-46	36	100	<10	<2	3	10		<2	<2	
86-47	72	200	<10	<2	3	13		<2	<2	
86-48	451	500	11	<2	5	<5		3	11	
86-49	**122307**	**28400**	856	233	<2	331		3	**50**	
86-50	91	300	16	23	<2	92		3	<2	
86-51	79	bdl	<10	<2	<2	8		<2	<2	
86-52	57	200	<10	<2	4	<5		<2	<2	
86-53	72	100	<10	4	3	8		<2	15	
87-53	5	bdl	<2	<2	<2	<2	<5	<2	<2	
86-54	3194	500	152	<2	4	19		<2	<2	
86-55	**15850**	300	587	125	6	412		<2	18	
86-56	33	300	34	16	4	<5		<2	8	
86-57	161	300	521	8	4	<5		<2	10	
86-58	28	200	158	<2	5	<5		<2	4	
87-58	<5	bdl	275	<2	<2	8	**8**	<2	<2	
86-59	480	100	157	<2	<2	<5		<2	3	
86-60	120	100	<10	8	6	<5		<2	3	
87-60	<5	bdl	<2	<2	3	<2	<5	<2	<2	
86-61	1817	bdl	123	3	6	<5		<2	<2	
86-62	9721	bdl	707	13	6	<5		<2	13	
86-63	852	600	75	4	**19**	30		3	6	
86-64	129	500	57	<2	**16**	13		3	<2	
87-64	163	200	85	<2	8	13	**25**	<2	<2	
86-65	136	100	<10	6	4	10		<2	6	
86-66	67	100	<10	3	9	40		<2	<2	
86-67	337	300	92	65	**448**	**61877**		**135**	9	
86-68	81	100	<10	<2	8	14		3	<2	
86-69	**51793**	**30300**	**1180**	115	6	86		<2	**58**	
86-70	2870	6900	**1294**	94	11	67		<2	**45**	
86-71	**21517**	**21500**	**1047**	103	**18**	187		<2	**46**	
86-072A	136	**43000**	**2824**	**2318**	14	**4977**		**34**	**170**	
86-072B	1402	**57200**	**5396**	**2311**	**49**	**5351**		**30**	**405**	
87-072B	470	**29200**	**3568**	**1120**	15	**2350**	**5**	**13**	**268**	
87-072BH		**28800**								
87-073A	10	100	15	**768**	<2	**1613**	**13**	3	<2	
87-073B	13	**15000**	**3818**	**1513**	3	**2713**	<5	**15**	**95**	
87-073C	<5	200	18	**633**	<2	155	<5	3	<2	
86-74	465	500	653	16	11	58		4	10	
86-75	337	bdl	<10	<2	9	36		<2	<2	
86-76	158	bdl	10	8	6	<5		<2	<2	
86-77	96	bdl	11	<2	10	23		<2	<2	
86-78	**63347**	100	**1180**	34	5	15		<2	18	
86-79	1942	bdl	101	<2	8	6		<2	4	
86-80	9820	3500	217	11	9	12		<2	5	
86-81	705	bdl	222	5	4	9		<2	<2	

Appendix 4A continued.

	Fe	Al	Mn	Ni	Cu	Zn	Pb	Cd	Co	Cr
detection limit (MERA 2)	3	0.2	0.05	0.2	0.2	0.32	0.05	0.1	0.05	0.2
detection limit (MERA 1)	4	100	5	2	2	5	2	2	2	n/a
CCME Drinking Water Guideline (mg/L)	≤0.3*	n/a	≤0.05*	n/a	≤1.0*	<=5.0*	0.010	0.005	n/a[c]	0.05
86-82	159	200	23	<2	9	44		<2	<2	
87-82	<5	bdl	3	<2	<2	18	<5	<2	<2	
87-82	H	bdl	0.1			<.1				
87-082B		bdl								
86-83	5179	300	437	<2	11	15		<2	4	
87-100	80	2900	108	38	8	98	<5	<2	3	
87-101	<5	bdl	<2	<2	<2	38	<5	<2	<2	
87-102	<5	bdl	<2	<2	<2	<2	<5	<2	<2	
87-103	6363	500	305	<2	<2	3	<5	<2	5	
87-104	<5	bdl	<2	<2	<2	<2	<5	<2	<2	
87-105	35	1100	48	13	3	50	<5	<2	3	
87-106	<5	bdl	<2	<2	<2	<2	<5	<2	3	
87-107	<5	bdl	<2	<2	3	565	<5	<2	<2	
87-108	65	800	83	<2	<2	10	<5	<2	<2	
87-109	5373	bdl	250	<2	<2	3	<5	<2	<2	
87-110	2013	bdl	190	<2	3	8	<5	<2	3	
87-111	10	bdl	<2	80	<2	353	<5	<2	<2	
87-112	**>20000**	200	**3098**	**303**	5	538	<5	<2	**60**	
87-112H		200								
87-113	18	bdl	<2	5	<2	28	<5	<2	<2	
87-114	<5	bdl	8	<2	<2	3	<5	<2	<2	
87-115	8	bdl	<2	<2	3	3	<5	<2	<2	
87-116	105	200	<2	<2	3	5	<5	<2	<2	
87-117	<5	bdl	<2	<2	<2	<2	<5	<2	<2	
87-118	<5	bdl	<2	<2	<2	10	<5	<2	<2	
87-119	<5	bdl	<2	<2	<2	10	**5**	<2	<2	
87-120	<5	bdl	<2	<2	<2	5	<5	<2	<2	
87-121	3763	**14700**	313	50	8	58	<5	<2	<2	
87-122	250	bdl	78	<2	3	3	**15**	<2	<2	
87-123	123	100	230	<2	8	8	**20**	<2	<2	
87-124	50	bdl	<2	<2	<2	<2	<5	<2	<2	
87-125	<5	bdl	<2	<2	<2	58	<5	<2	<2	
87-126	523	500	10	<2	3	10	<5	<2	<2	
87-127	33	bdl	10	<2	3	40	<5	<2	<2	
87-128	115	200	<2	<2	<2	5	<5	<2	3	
AVERAGE (PPM)	**3203**	**2602**	**326**	**112**	**10**	**622**	**2**	**5**	**21**	**1**
STANDARD DEVIATION	**12918**	**9846**	**1108**	**382**	**48**	**4791**	**4**	**16**	**78**	**4**
AVE+0.5*STDEV	**9662**	**7524**	**880**	**303**	**34**	**3017**	**4**	**13**	**60**	**3**
AVE+STDEV	**16121**	**12447**	**1434**	**495**	**58**	**5413**	**6**	**21**	**100**	**5**
MAX	**122307**	**83000**	**11000**	**2318**	**448**	**61877**	**25**	**135**	**620**	**27**
MIN	**5**	**0**	**0**	**1**	**0**	**1**	**0**	**0**	**0**	**0**
Criteria Cut-Off Used to Determine Anomalousness:	>10 000	>7500	>880	>300	>15	>622	>2	>5	>31	>1
Definition of Criteria (to obtain approximate top 15 springs):	ave+0.5 stdev	ave+0.5 stdev	ave+0.5 stdev	ave+ 0.5 stdev	1.5* ave	ave	ave	ave	1.5*ave	ave

bdl = below detection limit

nd = no data available

n/a = guideline not available

*Aesthetic Guideline Only

[c]Maximum 100 Platinum-Cobalt Units for Recreational Aesthetics of Colour

CCME Drinking Water Guidelines:

Federal-Provincial-Territorial Committee on Drinking Water. "Guidelines for Candadian Drinking Water Quality Summary Table". Health Canada, Government of Canada, March 2006.

CCME Recreation Guidelines:

Federal-Provincial Working Group on Recreational Water Quality of the Federal-Provincial Advisory Committee on Environmental and Occupational Health. "Guidelines for Canadian Recreational Water Quality". Health and Welfare Canada, Government of Canada, 1992.

Appendix 4B. Trace elements, Cs, Mo, as, Li, Rb, Sr, Ba, U, V, B, and Sb (units in mg/L unless otherwise noted), from MERA 1 and MERA 2 samples; numbers in bold were determined to be anomalous.

	Cs	Mo	As	Li	Rb	Sr	Ba	U	V	B	Sb
detection limit (MERA 2)	0.05	0.1	0.2	1	0.05	1	0.6	0.05	0.05	16	0.05
detection limit (MERA 1)	n/a	0.1	0.3	n/a	n/a	100	100	0.01/0.1	n/a	n/a	0.3
CCME Drinking Water Guideline (mg/L)	n/a	n/a	0.025	n/a	n/a	n/a	1.0	0.02	n/a	5	0.006
MERA 2 Samples											
Tulita	**7.50**	bdl	3.0	**910**	19.0	1500	**780**	0.13	0.27	**920**	bdl
Sculpin	bdl	0.6	0.9	15	1.20	**14000**	10	0.38	0.06	24	bdl
Deca	1.40	0.2	0.4	64	9.20	1900	22	0.40	1.00	130	bdl
Ekwi	**20.0**	0.2	0.9	**630**	**110**	3100	30	0.05	bdl	**800**	0.05
Mineral Lake	1.20	2.1	1.8	24	9.10	1300	47	2.80	0.25	37	bdl
Brimstone[1]	1.00	0.4	0.9	160	**33.0**	2400	110	0.63	0.19	25	0.05
Cordes Vertes	0.67	0.2	bdl	25	2.70	470	98	0.61	0.18	22	0.06
Tabletop	0.26	1.6	0.8	13	2.00	3700	44	0.67	0.51	18	bdl
South Redstone	0.42	1.6	1.8	13	1.90	2500	27	0.42	0.36	bdl	bdl
Redstone Junction #1	0.35	1.0	0.5	18	3.00	2400	31	0.88	0.62	28	bdl
Cotton	0.14	bdl	bdl	8	0.93	7	13	0.05	bdl	bdl	0.10
Red Mini	0.16	bdl	bdl	3	2.50	25	56	0.12	bdl	bdl	0.18
Muddy	0.09	0.2	bdl	17	4.50	79	19	0.54	0.05	bdl	bdl
Grasby	bdl	0.6	bdl	3	1.70	260	56	0.62	0.06	bdl	bdl
Red Steel	bdl	0.4	bdl	bdl	0.49	85	170	0.05	bdl	bdl	0.06
Bougere	0.39	bdl	bdl	150	0.66	8	37	0.48	bdl	bdl	bdl
Champagne	0.46	0.2	0.8	150	3.90	350	6.0	1.40	0.05	bdl	bdl
Champagne (dup)	0.43	0.1	0.8	130	3.80	310	6.0	1.40	bdl	bdl	bdl
Champagne Creek	0.39	0.1	1.0	16	3.90	270	5.2	1.50	0.05	bdl	bdl
Champagne Creek (dup)	0.37	0.1	0.8	17	3.60	270	5.0	1.60	0.05	bdl	bdl
North Cantung (Zenchuck Creek)	0.15	0.6	0.5	5	0.78	78	35	1.50	0.14	bdl	bdl
Moore's	1.60	1.4	2.6	25	9.90	470	120	1.50	0.25	48	0.18
Nahanni North (Lened Creek)	**11.0**	**16.0**	bdl	**500**	16.0	22	5.5	bdl	0.09	**600**	bdl
Nahanni Headwaters	**68.0**	**30.0**	**87.0**	**480**	18.0	71	4.6	bdl	0.15	**1600**	**1.3**
Broken Skull	**4.50**	0.1	1.2	92	**57.0**	3300	43	0.1	0.22	**380**	bdl
Grizzle Bear	**5.80**	0.2	5.1	110	**34.0**	1400	50	0.05	0.24	220	0.05
Glacier Lake	0.99	3.8	1.0	69	4.00	190	9.1	2.30	0.13	bdl	0.15
Rabbitkettle	0.56	2.9	0.3	38	9.80	620	180	6.30	bdl	34	0.78
Kraus (Clausen)	**65.0**	0.1	14.0	**1300**	**200**	**13000**	44	1.6	**8.3**	**1400**	bdl
Meilleur River	**4.40**	2.6	5.2	250	**28**	1600	44	2	0.32	230	bdl
Wildmint	**17.0**	0.4	0.7	**2500**	13	180	0.71	1.5	0.35	**3400**	bdl
Stinky Drift	0.47	1.5	0.9	16	8.10	1000	78	3.70	0.28	24	0.10
Hole in the wall	2.30	**19.0**	**19.0**	210	4.20	8	2.1	6.70	**7.00**	160	0.39
Flat Fruit	**4.50**	bdl	0.2	150	18.0	1700	160	1.30	0.05	110	bdl
West Cantung	**30.0**	11.0	1.7	**570**	17.0	38	160	1.20	**2.10**	**760**	0.24
Prairie Creek Mine Shaft	bdl	1.5	0.8	12	0.91	450	36	6.20	bdl	bdl	**56**
Harrison Creek	bdl	2.9	bdl	11	0.41	280	65	12.0	0.08	bdl	0.39
Prairie Creek	bdl	3.0	0.2	12	0.25	260	66	5.40	0.26	bdl	**0.95**
Broken Skull's Upper Pool	**4.00**	0.2	0.6	87	**55.0**	3500	53	0.15	0.26	**390**	0.06
Broken Skull's Lower Pool	**4.30**	0.1	1.1	85	**52.0**	3500	60	0.15	0.13	**390**	bdl
Cowboy	bdl	2.1	bdl	11	0.16	190	93	2.40	0.59	bdl	bdl
Sibbeston	bdl	3.0	2.2	10	0.83	680	81	3.40	0.96	bdl	1.00
Corridor Creek	bdl	0.9	bdl	11	0.08	290	20	1.10	0.09	bdl	bdl
Veil	bdl	4.6	0.3	19	0.36	320	83	4.90	0.11	bdl	0.07
Big Veil	bdl	4.7	0.3	18	0.37	320	83	4.90	0.12	bdl	0.11
Galena	bdl	1.9	0.3	13	0.90	320	54	**16.0**	0.09	bdl	0.74
Galena (lab dup)	bdl	1.9	0.2	14	0.92	330	54	**16.0**	0.10	bdl	0.73
Sombre	bdl	0.2	bdl	7	bdl	2000	97	0.98	bdl	bdl	bdl
Sombre (field dup)	bdl	0.2	bdl	5	bdl	2000	97	0.93	bdl	bdl	bdl
Wrigley	bdl	**26.0**	bdl	7	0.20	2200	120	**16.0**	**7.10**	bdl	0.39
Mel's Pool	bdl	1.6	0.5	2	0.08	52	21	0.18	0.43	bdl	0.16
Cowgirl	bdl	8.5	bdl	6	0.10	170	32	6.60	**3.60**	bdl	0.16
Brigade	bdl	3.5	bdl	15	0.40	1600	45	2.40	bdl	30	bdl
Ram Plateau	bdl	0.5	0.3	3	0.28	280	21	0.13	0.13	bdl	0.21
Cimitar	bdl	5.9	0.5	34	2.10	**8500**	13	**16.0**	0.06	29	bdl
Cathedral	bdl	3.7	bdl	6	0.23	**4600**	110	3.60	0.23	32	0.09
Mossy	bdl	0.8	bdl	3	0.15	1900	54	2.60	0.42	bdl	bdl
Mossy (lab dup)	bdl	0.8	bdl	9	0.15	2000	50	2.50	0.43	bdl	bdl
Crack	bdl	1.8	0.2	2	0.07	34	23	1.90	**2.70**	bdl	0.10
Quickie	bdl	11.0	0.2	6	0.15	1100	120	7.40	0.66	bdl	0.22
Clearwater Creek	bdl	2.3	bdl	4	0.36	82	11	2.50	0.07	bdl	0.12

Appendix 4B continued.

	Cs	Mo	As	Li	Rb	Sr	Ba	U	V	B	Sb
detection limit (MERA 2)	0.05	0.1	0.2	1	0.05	1	0.6	0.05	0.05	16	0.05
detection limit (MERA I)	n/a	0.1	0.3	n/a	n/a	100	100	0.01/0.1	n/a	n/a	0.3
CCME Drinking Water Guideline (mg/L)	n/a	n/a	0.025	n/a	n/a	n/a	1.0	0.02	n/a	5	0.006
Dookie	bdl	0.3	bdl	7	0.10	25	12	0.15	bdl	bdl	bdl
Dookie (field dup)	bdl	0.2	bdl	11	0.09	25	12	0.16	bdl	bdl	bdl
Dookie (field trip)	bdl	0.2	bdl	11	0.08	25	11	0.16	bdl	bdl	bdl
Boulder	bdl	0.1	bdl	7	0.05	11	3.3	0.14	bdl	bdl	0.05
Overflow	bdl	bdl	bdl	7	0.42	4	5.6	0.16	0.09	bdl	bdl
Smurf	bdl	4.2	0.7	9	0.62	160	210	2.40	**2.80**	bdl	0.82
Clark Lake	bdl	3.5	1.1	9	1.60	130	140	1.70	0.05	bdl	bdl
Clark Lake (lab dup)	bdl	3.6	1.1	14	1.60	130	150	1.60	0.05	bdl	bdl
Jacson	bdl	0.2	bdl	7	0.89	6	3.7	0.24	0.07	bdl	bdl
Darkness	bdl	0.4	bdl	7	0.96	11	3.5	1.60	0.10	bdl	bdl
Selena	bdl	7.4	4.1	10	0.61	370	78	6.90	bdl	24	0.29
Caribou	bdl	3.4	0.3	9	0.13	160	130	1.70	0.33	bdl	0.40
Chance	bdl	2.2	0.3	9	0.60	180	150	1.30	0.44	bdl	0.17
Interpluton	bdl	0.1	bdl	7	0.65	10	9.3	1.40	0.18	bdl	0.08
Tiny	bdl	0.5	0.5	8	0.51	84	24	0.85	0.29	bdl	0.11
Blue Bells	0.69	0.3	3.2	23	6.50	150	21	0.78	0.06	bdl	0.08
Blue Bells (field dup)	0.70	0.3	3.2	23	6.40	150	20	0.77	0.07	22	0.09
Cascade	bdl	0.9	0.4	8	0.41	130	92	0.85	0.12	bdl	0.22
Cascade (lab dup)	bdl	0.9	0.3	12	0.40	130	91	0.88	0.11	bdl	0.22
Meltwater	bdl	bdl	bdl	7	1.70	37	6.3	0.11	0.22	bdl	0.17
Waterfall	bdl	0.9	0.4	7	0.72	9	3.9	0.65	0.11	bdl	0.12
Descente	bdl	0.1	0.4	8	0.24	13	2.2	bdl	0.09	bdl	0.07
Softie	bdl	bdl	0.3	7	0.06	10	5.5	0.06	0.14	bdl	0.09
Cartman	bdl	0.1	0.2	7	bdl	8	2.1	bdl	0.12	23	0.07
Half Spring	bdl	2.9	0.3	13	0.24	110	9.6	3.80	0.15	bdl	0.10
Orange Creek	bdl	0.4	bdl	**280**	2.10	990	19	**26.0**	0.14	33	0.10
Caribou River	bdl	3.0	0.3	9	0.58	170	83	1.80	0.28	bdl	0.35
Karst	bdl	0.2	0.3	7	0.09	29	15	0.24	0.06	23	bdl
Persistent	**4.10**	0.7	**50.0**	87	**32.0**	650	**240**	0.87	0.07	90	0.10
Persistent (lab dup)	**4.10**	0.7	**51.0**	110	**32.0**	670	**260**	0.83	0.08	110	0.09
Stinky	**4.80**	0.3	**120**	100	**37.0**	770	**380**	1.00	0.14	110	0.07
Field Blank	bdl	bdl	bdl	7	bdl	bdl	1.2	bdl	bdl	bdl	bdl
Calgary Lab Blank	bdl	bdl	bdl	6	bdl	bdl	0.1	bdl	bdl	bdl	bdl
MERA 1 Samples (as reported by Hamilton, 1990)											
86-1		1.8	0.3			700	200	6.4			
86-4		0.2	1.4			bdl	bdl	0.4			
86-6		0.6	0.5			400	bdl	1.92			
86-7		0.7	<.2			100	bdl	0.84			
86-9		1.2	<.2			200	bdl	4.4			
86-10		7.3						14.2			
86-11		3.8	0.5			bdl	bdl	3.6			
86-12		0.6	0.8			bdl	bdl	4.4			
87-012B		3	<.3			bdl	bdl	1.7			0.4
87-12		1	<.3			bdl	bdl	1.6			<.3
87-012C		0.1	<.3			bdl	bdl	2.8			<.3
86-13		1	**32.9**			100	bdl	0.92			
86-15		2.1	1.4			200	bdl	2.38			
86-17		<.1	0.4			2900	200	0.6			
87-17		<.1	<.3			2300	100	0.5			<.3
86-18		8	1.8			bdl	200	0.92			
87-18		9.1	1.9			bdl	100	1.4			<.3
87-018B		9.9	1.8			bdl	100				<.3
86-19		8.1	5.2			100	bdl	0.96			
86-20		1.1	<.2			bdl	bdl	0.24			
86-21		0.4	**99.3**			**5600**	bdl	7.8			
86-22		2.5	0.7			200	200	1.2			
86-23		4	2.4			200	100	6.2			
86-24		8	0.3			200	100	5.7			
86-25		<.1	0.4			bdl	bdl	4			
86-26		4.3	1			200	200	2.8			
86-27		1.2	0.8			1200	100	2.4			
87-27		1.7	0.8			1000	bdl	3.8			0.4

Appendix 4B continued.

	Cs	Mo	As	Li	Rb	Sr	Ba	U	V	B	Sb
detection limit (MERA 2)	0.05	0.1	0.2	1	0.05	1	0.6	0.05	0.05	16	0.05
detection limit (MERA 1)	n/a	0.1	0.3	n/a	n/a	100	100	0.01/0.1	n/a	n/a	0.3
CCME Drinking Water Guideline (mg/L)	n/a	n/a	0.025	n/a	n/a	n/a	1.0	0.02	n/a	5	0.006
86-28		2	0.2			200	100	0.96			
86-29		0.6	0.5			1400	100	3.6			
86-30		1.6	1.2			1500	bdl	4			
86-31		0.9	0.3			1700	100	3.2			
86-32		1.4	2.4			500	100	1.64			
86-33		**19**	0.2			bdl	bdl	0.66			
87-33		**18.8**	0.3			bdl	bdl	1.3			<.3
87-34		9.5	2.1			bdl	bdl	**28**			<.3
86-35		<.1	0.5			300	bdl	0.44			
86-36		<.1						0.4			
86-37		0.4	2.2			500	bdl	4			
86-38		**30**	**163.5**			bdl	bdl	0.4			
86-40		<.1	1.5			4000	bdl	3.8			
86-41		0.1	0.8			4000	bdl	5.2			
86-42		<.1	0.6			200	100	3.2			
86-43		0.1	5.2			1800	bdl	5			
86-44		0.5	0.6			100	bdl	2.4			
86-45		<.1	0.3			bdl	bdl	0.24			
86-46		3.1	1.2			200	200	3.2			
86-47		3	0.6			300	bdl	3.4			
86-48		1.4	<.2			bdl	bdl	3.6			
86-49		<.1	<.2			700	bdl	4.4			
86-50		2.4	1			200	bdl	2.6			
86-51		0.6	0.6			bdl	bdl	2.8			
86-52		10	**23.7**			bdl	bdl	7.4			
86-53		**21**	**25.5**			bdl	bdl	7.2			
87-53		**20.3**	**20.9**			bdl	bdl	6.6			0.4
86-54		0.5	4			bdl	bdl	2			
86-55		1.7	0.9			800	100	6.6			
86-56		0.7	0.5			3300	bdl	4.68			
86-57		<.1	0.2			2500	bdl	3			
86-58		<.1	<.2			2000	200	1.44			
87-58		0.2	0.38			200		<.3			<.3
86-59		<.1	<.2			500	100	0.66			
86-60		**19**	0.5			bdl	bdl	0.27			
87-60		**17.8**				bdl	bdl	1.2			
86-61		0.6	0.5			100	bdl	0.74			
86-62		<.1	<.2			bdl	bdl	0.1			
86-63		0.2	7.2			**15000**	bdl	**15.6**			
86-64		<.1	1.4			**15300**	bdl	5.4			
87-64		0.7	0.3			**14100**	bdl	**15.2**			<.3
86-65		0.6	0.12			bdl		1.2			0.3
86-66		1.7	0.1			bdl		2			0.6
86-67		0.6	0.49			bdl		3.8			**49.6**
86-68		<.1	0.11			100		2			0.2
86-69		<.1	0.28			bdl		3			<.2
86-70		<.1	0.2			500	bdl	3.12			
86-71		<.1	1.3			1000	bdl	2.4			
86-072A		<.1	0.4			**5300**	bdl	5.4			
86-072B		0.8	1.9			**4500**	bdl	**26**			
87-072B		0.3				3200	bdl	13.2			
87-072BH						3100	bdl				
87-073A		0.4	1.32			bdl		<.3			<.3
87-073B		0.4	2.18			bdl		<.3			<.3
87-073C		0.3	1.36			bdl		<.3			<.3
86-74		0.8	0.8			3500	100	4.4			
86-75		0.3	0.3			bdl	bdl	2.4			
86-76		2.5	0.4			100	100	2.4			
86-77		2.7	3.4			200	**600**	4.6			
86-78		<.1	0.8			200	bdl	0.66			
86-79		<.1	1.5			bdl	bdl	0.92			

Appendix 4B continued.

	Cs	Mo	As	Li	Rb	Sr	Ba	U	V	B	Sb
detection limit (MERA 2)	0.05	0.1	0.2	1	0.05	1	0.6	0.05	0.05	16	0.05
detection limit (MERA 1)	n/a	0.1	0.3	n/a	n/a	100	100	0.01/0.1	n/a	n/a	0.3
CCME Drinking Water Guideline (mg/L)	n/a	n/a	0.025	n/a	n/a	n/a	1.0	0.02	n/a	5	0.006
86-80		<.1	0.4			bdl	bdl	0.44			
86-81		3.9	4.5			400	bdl	2.4			
86-82		4.5	10.9			1400	bdl	5			
87-82		4.6				1600	bdl	14			
87-82						1500	bdl				
87-082B		4.5				1500	bdl				
86-83		3	12.7			1700	bdl	5.4			
87-100		<.1	<.3			bdl	bdl	3.5			<.3
87-101		5.5	0.9			bdl	bdl	6.9			<.3
87-102		0.6	<.3			200	bdl	2.5			<.3
87-103		0.1	12.6			700	bdl	0.5			0.3
87-104		0.5	14.9			bdl	bdl	0.3			0.4
87-105		<.1	<.3			bdl	bdl	0.7			<.3
87-106		0.3	0.3			bdl	bdl	0.7			<.3
87-107		1.8	0.7			300	100	5.8			0.7
87-108		<.1	<.3			bdl	bdl	<.1			<.3
87-109		<.1	0.3			bdl	bdl	0.8			<.3
87-110		6	1.2			1300	bdl	**20**			<.3
87-111		11	<.3			800	bdl	**27.9**			<.3
87-112		0.2	7.7			3400	bdl				
87-112H						3400	bdl				
87-113		6.7	0.5			200	100	11.2			<.3
87-114		5.5	<.3			200	bdl	7.9			<.3
87-115		10.2	0.3			700	bdl	4.7			0.4
87-116		0.4	0.4			1100	bdl	14.4			<.3
87-117		1.1	<.3			bdl	bdl	1.4			<.3
87-118		1	<.3			bdl	bdl	1.4			<.3
87-119		1.1	0.4			bdl	200	3.1			0.4
87-120		1.4	<.3			200	100	6			<.3
87-121		<.1	<.3			bdl	bdl	2.5			<.3
87-122		0.3	2.4			2900	bdl	**16.8**			0.4
87-123		0.3	<.3			**12300**	bdl	6.6			<.3
87-124		4.6	0.5			bdl	**1000**	0.7			0.4
87-125		**15.3**	<.3			300	bdl	12.2			0.6
87-126		2.8	0.3			100	200	1.7			0.4
87-127		1.2	<.3			600	**300**	4.2			<.3
87-128		2.3	0.8			200	**300**	7.6			0.4
AVERAGE	**7**	**3**	**6**	**107**	**10**	**1459**	**97**	**4**	**1**	**351**	**1.79**
STANDARD DEVIATION	**15**	**5**	**20**	**318**	**26**	**2755**	**135**	**5**	**2**	**661**	**9**
AVE+0.5*STDEV	**15**	**6**	**16**	**266**	**23**	**2837**	**164**	**6**	**1**	**681**	**6.2**
AVE+STDEV	**22**	**9**	**26**	**425**	**36**	**4214**	**231**	**9**	**2**	**1012**	**10.6**
MAX	**68**	**30**	**164**	**2500**	**200**	**15300**	**1000**	**28**	**8**	**3400**	**56**
MIN	**0**	**0**	**0**	**3**	**0**	**7**	**5**	**0**	**0**	**18**	**0**
Criteria Cut-Off Used to Determine Anomalousness:	>3.5	>12	>16	>266	>23	>4200	>231	>15	>1	>350	>0.9
Definition of Criteria (to obtain approx. top 15 springs):	0.5*ave	ave+ 1.5stdev	ave+ 0.5stdev	ave+0.5 stdev	ave+0.5 stdev	ave+ stdev	ave+ stdev	ave+ 1.5stdev	ave	ave	ave*0.5

bdl = below detection limit

nd = no data available

n/a = guideline not available

*Aesthetic Guideline Only

[C]Maximum 100 Platinum-Cobalt Units for Recreational Aesthetics of Colour

CCME Drinking Water Guidelines:

Federal-Provincial-Territorial Committee on Drinking Water. "Guidelines for Candadian Drinking Water Quality Summary Table". Health Canada, Government of Canada, March 2006.

CCME Recreation Guidelines:

Federal-Provincial Working Group on Recreational Water Quality of the Federal-Provincial Advisory Committee on Environmental and Occupational Health. "Guidelines for Canadian Recreational Water Quality". Health and Welfare Canada, Government of Canada, 1992.

Appendix 4C. Trace elements, Ga, Se, Br, Ag, Be, Sc, Ti, Bi, In, NO_2 (units in mg/L unless otherwise noted), from MERA 1 and MERA 2 samples; numbers in bold were determined to be anomalous.

	Tl	Ga	Se	Br	Ag	Be	Sc	Ti	Bi	In	NO_2
detection limit (MERA 2)	0.05	0.05	2	50	0.05	1	1	1	0.05	0.05	50
detection limit (MERA 1)	n/a	n/a	n/a	n/a	2	n/a	n/a	n/a	n/a	n/a	n/a
CCME Drinking Water Guideline (mg/L)	n/a	n/a	0.01	n/a	n/a	n/a	n/a	n/a	n/a	n/a	3.2
Name of Spring					***MERA 2 Samples***						
Tulita	bdl	bdl	bdl	**317**	bdl	bdl	**2**	bdl	bdl	bdl	<500
Sculpin	bdl	bdl	bdl	<500	bdl	bdl	bdl	bdl	bdl	bdl	<500
Deca	bdl	bdl	bdl	<500	bdl	bdl	bdl	bdl	bdl	bdl	bdl
Ekwi	**0.10**	bdl	bdl	<2500	bdl	bdl	bdl	bdl	bdl	bdl	bdl
Mineral Lake	bdl	bdl	bdl	bdl	bdl	bdl	bdl	bdl	bdl	bdl	bdl
Brimstone[1]	bdl	bdl	**2**	bdl	bdl	**2**	bdl	bdl	bdl	bdl	bdl
Cordes Vertes	bdl	bdl	bdl	bdl	bdl	bdl	bdl	bdl	bdl	bdl	bdl
Tabletop	0.05	bdl	bdl	bdl	bdl	bdl	bdl	bdl	bdl	bdl	bdl
South Redstone	0.06	bdl	bdl	bdl	bdl	bdl	bdl	bdl	bdl	bdl	bdl
Redstone Junction #1	bdl	bdl	bdl	bdl	bdl	bdl	bdl	bdl	bdl	bdl	bdl
Cotton	0.05	bdl	bdl	bdl	bdl	bdl	bdl	bdl	bdl	bdl	bdl
Red Mini	0.06	bdl	bdl	bdl	bdl	bdl	bdl	bdl	bdl	bdl	bdl
Muddy	bdl	bdl	bdl	bdl	bdl	bdl	bdl	bdl	bdl	bdl	bdl
Grasby	bdl	bdl	**2**	bdl	bdl	bdl	bdl	bdl	bdl	bdl	bdl
Red Steel	bdl	bdl	**5**	bdl	bdl	bdl	bdl	bdl	bdl	bdl	bdl
Bougere	bdl	**0.08**	bdl	bdl	**14.00**	bdl	bdl	bdl	bdl	bdl	bdl
Champagne	bdl	bdl	bdl	bdl	bdl	bdl	bdl	bdl	bdl	bdl	bdl
Champagne (dup)	bdl	bdl	bdl	bdl	bdl	bdl	bdl	bdl	bdl	bdl	bdl
Champagne Creek	bdl	bdl	**2**	bdl	bdl	bdl	bdl	bdl	bdl	bdl	bdl
Champagne Creek (dup)	bdl	bdl	bdl	bdl	bdl	bdl	bdl	bdl	bdl	bdl	bdl
North Cantung (Zenchuck Creek)	bdl	bdl	bdl	bdl	bdl	bdl	bdl	bdl	bdl	bdl	nd
Moore's	bdl	bdl	bdl	bdl	bdl	bdl	bdl	bdl	bdl	bdl	nd
Nahanni North (Lened Creek)	bdl	**7.50**	bdl	bdl	bdl	bdl	bdl	bdl	bdl	bdl	nd
Nahanni Headwaters	bdl	**2.60**	bdl	bdl	bdl	bdl	bdl	bdl	bdl	bdl	nd
Broken Skull	bdl	bdl	bdl	bdl	bdl	bdl	bdl	bdl	bdl	bdl	nd
Grizzle Bear	bdl	bdl	bdl	**157**	bdl	bdl	bdl	bdl	bdl	bdl	nd
Glacier Lake	**0.58**	bdl	bdl	bdl	bdl	bdl	bdl	bdl	bdl	bdl	nd
Rabbitkettle	bdl	bdl	bdl	bdl	bdl	bdl	bdl	bdl	bdl	bdl	nd
Kraus (Clausen)	bdl	bdl	bdl	<500	bdl	bdl	bdl	bdl	bdl	bdl	nd
Meilleur River	bdl	bdl	bdl	**215**	bdl	bdl	bdl	bdl	bdl	bdl	nd
Wildmint	bdl	**1.50**	bdl	bdl	bdl	bdl	bdl	bdl	bdl	bdl	nd
Stinky Drift	**0.14**	bdl	bdl	bdl	bdl	bdl	bdl	bdl	bdl	bdl	nd
Hole-in-the-Wall	bdl	**4.90**	bdl	bdl	bdl	bdl	bdl	bdl	bdl	bdl	nd
Flat Fruit	bdl	bdl	bdl	bdl	bdl	bdl	bdl	bdl	bdl	bdl	nd
West Cantung	bdl	**1.70**	bdl	bdl	bdl	bdl	bdl	bdl	bdl	bdl	nd
Prairie Creek Mine Shaft	**0.37**	bdl	**7**	bdl	bdl	bdl	bdl	bdl	bdl	bdl	bdl
Harrison Creek	bdl	bdl	bdl	bdl	bdl	bdl	bdl	bdl	bdl	bdl	bdl
Prairie Creek	bdl	bdl	bdl	bdl	bdl	bdl	bdl	bdl	bdl	bdl	**52**
Broken Skull's Upper Pool	bdl	bdl	bdl	**149**	bdl	bdl	bdl	bdl	bdl	bdl	bdl
Broken Skull's Lower Pool	bdl	bdl	bdl	**145**	bdl	bdl	bdl	bdl	bdl	bdl	bdl
Cowboy	bdl	bdl	bdl	bdl	bdl	bdl	bdl	bdl	bdl	bdl	bdl
Sibbeston	**0.07**	**0.07**	bdl	bdl	bdl	bdl	bdl	bdl	bdl	bdl	bdl
Corridor Creek	bdl	bdl	bdl	bdl	bdl	bdl	bdl	bdl	bdl	bdl	bdl
Veil	bdl	bdl	**3**	bdl	bdl	bdl	bdl	bdl	bdl	bdl	bdl
Big Veil	bdl	bdl	**3**	bdl	bdl	bdl	bdl	bdl	bdl	bdl	bdl
Galena	**0.10**	bdl	**3**	bdl	bdl	bdl	bdl	bdl	bdl	bdl	bdl
Galena (lab dup)	**0.08**	bdl	bdl	bdl	bdl	bdl	bdl	bdl	bdl	bdl	bdl
Sombre	bdl	bdl	bdl	bdl	bdl	bdl	bdl	bdl	bdl	bdl	bdl
Sombre (field dup)	bdl	bdl	bdl	bdl	bdl	bdl	bdl	bdl	bdl	bdl	bdl
Wrigley	**0.13**	bdl	**2**	bdl	bdl	bdl	bdl	bdl	bdl	bdl	bdl
Mel's Pool	bdl	bdl	bdl	bdl	bdl	bdl	bdl	bdl	bdl	bdl	bdl
Cowgirl	**0.12**	bdl	bdl	bdl	bdl	bdl	bdl	bdl	bdl	bdl	bdl
Brigade	bdl	bdl	bdl	bdl	bdl	bdl	bdl	bdl	bdl	bdl	bdl
Ram Plateau	bdl	bdl	bdl	bdl	bdl	bdl	bdl	bdl	bdl	bdl	bdl
Cimitar	**0.32**	bdl	bdl	bdl	bdl	bdl	bdl	bdl	bdl	bdl	bdl
Cathedral	bdl	bdl	bdl	bdl	bdl	bdl	bdl	bdl	bdl	bdl	bdl
Mossy	bdl	bdl	bdl	bdl	bdl	bdl	bdl	bdl	bdl	bdl	bdl
Mossy (lab dup)	bdl	bdl	bdl	bdl	bdl	bdl	bdl	bdl	bdl	bdl	bdl
Crack	bdl	bdl	bdl	bdl	bdl	bdl	bdl	bdl	bdl	bdl	bdl
Quickie	bdl	bdl	**3**	bdl	bdl	bdl	bdl	bdl	bdl	bdl	bdl
Clearwater Creek	bdl	bdl	bdl	bdl	bdl	bdl	bdl	bdl	bdl	bdl	bdl

Appendix 4C continued.

	Tl	Ga	Se	Br	Ag	Be	Sc	Ti	Bi	In	NO_2
detection limit (MERA 2)	0.05	0.05	2	50	0.05	1	1	1	0.05	0.05	50
detection limit (MERA 1)	n/a	n/a	n/a	n/a	2	n/a	n/a	n/a	n/a	n/a	n/a
CCME Drinking Water Guideline (mg/L)	n/a	n/a	0.01	n/a	n/a	n/a	n/a	n/a	n/a	n/a	3.2
Dookie	bdl	bdl	bdl	bdl	bdl	bdl	bdl	bdl	bdl	bdl	bdl
Dookie (field dup)	bdl	bdl	bdl	bdl	bdl	bdl	bdl	bdl	bdl	bdl	bdl
Dookie (field trip)	bdl	bdl	bdl	bdl	bdl	bdl	bdl	bdl	bdl	bdl	bdl
Boulder	bdl	bdl	bdl	bdl	bdl	bdl	bdl	bdl	bdl	bdl	bdl
Overflow	bdl	bdl	bdl	bdl	bdl	bdl	bdl	bdl	bdl	bdl	bdl
Smurf	bdl	bdl	**3**	bdl	bdl	bdl	bdl	bdl	bdl	bdl	bdl
Clark Lake	bdl	bdl	bdl	bdl	bdl	bdl	bdl	bdl	bdl	bdl	bdl
Clark Lake (lab dup)	bdl	bdl	bdl	bdl	bdl	bdl	bdl	bdl	bdl	bdl	bdl
Jacson	bdl	bdl	bdl	bdl	bdl	bdl	bdl	bdl	bdl	bdl	bdl
Darkness	bdl	bdl	bdl	bdl	bdl	bdl	bdl	bdl	bdl	bdl	bdl
Selena	bdl	bdl	bdl	bdl	bdl	bdl	bdl	bdl	bdl	bdl	bdl
Caribou	bdl	bdl	bdl	bdl	bdl	bdl	bdl	bdl	bdl	bdl	bdl
Chance	bdl	bdl	bdl	bdl	bdl	bdl	bdl	bdl	bdl	bdl	bdl
Interpluton	bdl	**0.05**	bdl	bdl	bdl	bdl	bdl	bdl	bdl	bdl	bdl
Tiny	bdl	bdl	bdl	bdl	bdl	bdl	bdl	bdl	bdl	bdl	bdl
Blue Bells	bdl	bdl	bdl	bdl	bdl	bdl	bdl	bdl	bdl	bdl	bdl
Blue Bells (field dup)	bdl	bdl	bdl	bdl	bdl	bdl	bdl	bdl	bdl	bdl	bdl
Cascade	bdl	bdl	bdl	bdl	bdl	bdl	bdl	bdl	bdl	bdl	bdl
Cascade (lab dup)	bdl	bdl	bdl	bdl	bdl	bdl	bdl	bdl	bdl	bdl	bdl
Meltwater	bdl	bdl	bdl	bdl	bdl	bdl	bdl	bdl	bdl	bdl	bdl
Waterfall	bdl	bdl	bdl	bdl	bdl	bdl	bdl	bdl	bdl	bdl	bdl
Descente	bdl	bdl	bdl	bdl	bdl	bdl	bdl	bdl	bdl	bdl	bdl
Softie	bdl	bdl	bdl	bdl	bdl	bdl	bdl	bdl	bdl	bdl	bdl
Cartman	bdl	bdl	bdl	bdl	bdl	bdl	bdl	bdl	bdl	bdl	bdl
Half Spring	bdl	bdl	bdl	bdl	bdl	bdl	bdl	bdl	bdl	bdl	bdl
Orange Creek	**0.25**	**0.23**	bdl	<500	bdl	**9**	**16**	**8**	bdl	bdl	<500
Caribou River	bdl	bdl	bdl	bdl	bdl	bdl	bdl	bdl	bdl	bdl	bdl
Karst	bdl	bdl	bdl	bdl	bdl	bdl	bdl	bdl	bdl	bdl	bdl
Persistent	**0.10**	bdl	bdl	bdl	bdl	bdl	bdl	bdl	bdl	bdl	bdl
Persistent (lab dup)	**0.09**	bdl	bdl	bdl	bdl	bdl	bdl	bdl	bdl	bdl	bdl
Stinky	0.06	bdl	bdl	bdl	bdl	bdl	bdl	bdl	bdl	bdl	bdl
Field Blank	bdl	bdl	bdl	bdl	bdl	bdl	bdl	bdl	bdl	bdl	bdl
Calgary Lab Blank	bdl	bdl	bdl	bdl	bdl	bdl	bdl	bdl	bdl	bdl	bdl
MERA 1 Samples (as reported by Hamilton, 1990)											
86-1					<2						
86-4					<2						
86-6					<2						
86-7					<2						
86-9					<2						
86-10					<2						
86-11					<2						
86-12					<2						
87-012B											
87-12											
87-012C											
86-13					<2						
86-15					<2						
86-17					<2						
87-17											
86-18					<2						
87-18											
87-018B											
86-19					**3**						
86-20					**3**						
86-21					<2						
86-22					<2						
86-23					<2						
86-24					<2						
86-25					<2						
86-26					<2						
86-27					**4**						
87-27											

Appendix 4C continued.

	Tl	Ga	Se	Br	Ag	Be	Sc	Ti	Bi	In	NO_2
detection limit (MERA 2)	0.05	0.05	2	50	0.05	1	1	1	0.05	0.05	50
detection limit (MERA 1)	n/a	n/a	n/a	n/a	2	n/a	n/a	n/a	n/a	n/a	n/a
CCME Drinking Water Guideline (mg/L)	n/a	n/a	0.01	n/a	n/a	n/a	n/a	n/a	n/a	n/a	3.2
86-28					<2						
86-29					<2						
86-30					3						
86-31					<2						
86-32					<2						
86-33					<2						
87-33											
87-34											
86-35					<2						
86-36					<2						
86-37					<2						
86-38					<2						
86-40					<2						
86-41					<2						
86-42					<2						
86-43					<2						
86-44					<2						
86-45					<2						
86-46					<2						
86-47					<2						
86-48					<2						
86-49					<2						
86-50					<2						
86-51					<2						
86-52					<2						
86-53					<2						
87-53											
86-54					<2						
86-55					<2						
86-56					<2						
86-57					<2						
86-58					<2						
87-58											
86-59					<2						
86-60					<2						
87-60											
86-61					<2						
86-62					<2						
86-63					<2						
86-64					<2						
87-64											
86-65					<2						
86-66					<2						
86-67					3						
86-68					<2						
86-69					<2						
86-70					<2						
86-71					<2						
86-072A					4						
86-072B					<2						
87-072B											
87-072BH											
87-073A											
87-073B											
87-073C											
86-74					<2						
86-75					<2						
86-76					<2						
86-77					<2						
86-78					<2						
86-79					<2						

Appendix 4C continued.

	Tl	Ga	Se	Br	Ag	Be	Sc	Ti	Bi	In	NO_2
detection limit (MERA 2)	0.05	0.05	2	50	0.05	1	1	1	0.05	0.05	50
detection limit (MERA 1)	n/a	n/a	n/a	n/a	2	n/a	n/a	n/a	n/a	n/a	n/a
CCME Drinking Water Guideline (mg/L)	n/a	n/a	0.01	n/a	n/a	n/a	n/a	n/a	n/a	n/a	3.2
86-80					<2						
86-81					<2						
86-82					<2						
87-82											
87-82											
87-082B											
86-83					3						
87-100											
87-101											
87-102											
87-103											
87-104											
87-105											
87-106											
87-107											
87-108											
87-109											
87-110											
87-111											
87-112											
87-112H											
87-113											
87-114											
87-115											
87-116											
87-117											
87-118											
87-119											
87-120											
87-121											
87-122											
87-123											
87-124											
87-125											
87-126											
87-127											
87-128											
AVERAGE	**0.152**	**2.070**	**3.182**	**197**	**4.625**	**5.500**	**9.000**	**8.000**	**0.000**	**0.000**	**52.000**
STANDARD DEVIATION	**0.141**	**2.590**	**1.537**	**73**	**3.815**	**4.950**	**9.899**	**n/a**	**0.000**	**0.000**	**n/a**
AVE+0.5*STDEV	**0.222**	**3.365**	**3.951**	**233**	**6.532**	**7.975**	**13.950**	**n/a**	**0.000**	**0.000**	**n/a**
AVE+STDEV	**0.293**	**4.660**	**4.719**	**270**	**8.440**	**10.450**	**18.899**	**n/a**	**0.000**	**0.000**	**n/a**
MAX	**0.580**	**7.500**	**7.000**	**317**	**14.000**	**9.000**	**16.000**	**8.000**	**0.000**	**0.000**	**52.000**
MIN	**0.050**	**0.080**	**2.000**	**317**	**14.000**	**2.000**	**2.000**	**0.000**	**0.000**	**0.000**	**0.000**
Criteria Cut-Off Used to Determine Anomalousness:	> 0.07	>0	>0	>0	>0	>0	>0	>0	>0	>0	>0
Definition of Criteria (to obtain approximate top 15 springs):	ave*0.5	anything detectable	anything detectable	anything detectable	anything detectable	anything detectable	anything detectable	anything detectable	anything detectable	anything detectable	anything detectable

bdl = below detection limit

nd = no data available

n/a = guideline not available

*Aesthetic Guideline Only

[C]Maximum 100 Platinum-Cobalt Units for Recreational Aesthetics of Colour

CCME Drinking Water Guidelines:

Federal-Provincial-Territorial Committee on Drinking Water. "Guidelines for Candadian Drinking Water Quality Summary Table". Health Canada, Government of Canada, March 2006.

CCME Recreation Guidelines:

Federal-Provincial Working Group on Recreational Water Quality of the Federal-Provincial Advisory Committee on Environmental and Occupational Health. "Guidelines for Canadian Recreational Water Quality". Health and Welfare Canada, Government of Canada, 1992.

Appendix 5. Isotopes of MERA 2 samples. Gaseous springs are marked with a bubble (o). Note: 1.81E+03 signifies 1.81×10^3 or 1810 in scientific notation.

	WATER		AQ SULPHUR			AQ CARBON		FREE GASES		DISSOLVED GASES		TUFA	
	$\delta^{18}O_{H_2O}$	$\delta^{2}D_{H_2O}$	$\delta^{34}S_{SO_4}$	$\delta^{18}O_{SO_4}$	$[SO_4]$	$\delta^{13}C_{HCO_3(aq)}$	$[HCO_3]$	$\delta^{13}C_{CH_4}$	$\delta^{13}C_{CO_2}$	$\delta^{13}C_{CH_4}$	$\delta^{13}C_{CO_2}$	$\delta^{13}C_{CaCO_3}$	$\delta^{18}O_{CaCO_3}$
SAMPLE NAME Unit	‰	‰	‰	‰	ppm	‰	ppm	‰	‰	‰	‰	‰	‰
Precision and Accuracy	*0.04*	*0.4*	*0.3*	*0.5*		*0.2*		*0.5*	*0.5*	*0.5*	*0.5*	*0.2*	*0.2*
Prairie Creek Mine Shaft	-22.4	-173.6	12.8	-13.7	396	-19.9	315						
Harrison Creek	-23.1	-176.8	9.8	-12.7	161	-6.3	223						
Prairie Creek (downstream of mine)	-22.8	-176.4	8.2	-12.2	74.8	-3.8	193						
Broken Skull Upper Pool (2005) °	-23.1	-178.9	24.7	3.7	366	-4.3	439		-5.1		-8.5		
Broken Skull Lower Pool (2005)	-24.0	-186.5	25.4	3.4	364	0.5	440				-8.3		
Cowboy	-22.7	-176.0	-1.8	-14	35.3	-4.1	157						
Sibbeston	-22.0	-173.8	7.4	-5.9	29.8	-3.3	168				-13.8		
Corridor Creek	-23.0	-177.5	2.1		22.7	-1.2	122						
Veil	-22.4	-172.7	2.4	-7.9	62.4	-5.3	186				-16		
Big Veil	-21.8	-170.5	2.5	-6.8	64.2	-6.5	188				-16.2		
Galena Creek	-22.5	-176.2	10.4	-9.5	150	-6.9	283						
Sombre	-21.8	-164.0	5.4		4.15	2.9	94.5				-7.2		
Sombre (field dup)	-21.3	-166.2			4.13	5.5	94.6				-6.8		
Wrigley	-22.5	-178.3	16.6	-9.7	113	-8.9	244						
Mel's Pool	-21.4	-166.7			1.25	-8.0	73.4						
Cowgirl	-23.0	-175.3	5.6	-8.7	64.9	-6.6	190						
Brigade	-22.1	-172.4	1.4	-15.2	127	-5.8	198						
Ram Plateau	-21.8	-172.1	-11.3	-6.3	7.42	-7.2	61.3						
Cimitar	-21.9	-172.8	19.7	9.9	780	-9.5	287				-16.4		
Cathedral	-22.2	-174.4	5.7	-10.8	73.2	-5.9	178						
Mossy	-22.3	-175.9	11.3	-5.9	55.2	-4.0	167						
Crack	-22.7	-178.4	-3.7		14.8	-3.0	136						
Quickie	-21.8	-171.1		-8.3	67.7	-6.3	174						
Clearwater Creek	-25.4	-175.2	15.9	-11.7	37.8	-1.2	112						
Dookie	-23.1	-177.1	31.6	-11.7	62.9	2.0	97.6						
Dookie (field dup)	-23.1	-175.6	31.5	-12.3	63.2	0.7	83.8						
Dookie (field trip)	-23.3	-177.5	31.8	-11.9	63.8	0.5	81.7						
Boulder	-22.7	-174.4	1.7		5.47	2.6	75.8						
Overflow	-21.7	-163.9	6.3		0.00		4.0						
Smurf	-21.8	-174.5			8.37	-10.3	220						
Clark Lake	-21.9	-171.0	22.6	-7.1	21.4	-8.6	187						
Jacson	-20.9	-160.3			0.32		5.7						
Darkness	-22.1	-172.2	-8.2		0.73	-15.3	9.7						
Selena	-21.6	-167.9	20.8	-9.8	131	-8.3	188						
Caribou	-22.1	-174.9	12.4		11.9	-9.1	200						
Chance	-22.0	-172.8			17.6	-8.4	181					-6.5	-19.0
Interpluton Seep		-168.9			0.00		8.0						
Tiny	-22.7	-171.6			2.55	-11.0	127						
Blue Bells	-22.6	-175.0	18.3		11.9	-5.9	187				-15.2		
Blue Bells (field dup)	-22.8	-177.6	18.2		11.9	-5.1	188						
Cascade	-22.3	-173.2	6.7		14.1	-6.5	166				-16.9		
Meltwater	-22.3	-167.4			0.56	-9.8	36.6						
Waterfall	-23.4	-178.4			0.20		14.2						
Descente	-22.6	-170.9	4.0		7.97	-6.5	19.5						
Softie	-22.4	-172.8			0.00	-17.5	8.9						

Appendix 5 continued.

	WATER		AQ SULPHUR			AQ CARBON		FREE GASES		DISSOLVED GASES		TUFA	
SAMPLE NAME Unit	$\delta^{18}O_{H_2O}$ ‰	$\delta^{2}D_{H_2O}$ ‰	$\delta^{34}S_{SO_4}$ ‰	$\delta^{18}O_{SO_4}$ ‰	$[SO_4]$ ppm	$\delta^{13}C_{HCO_3(aq)}$ ‰	$[HCO_3]$ ppm	$\delta^{13}C_{CH_4}$ ‰	$\delta^{13}C_{CO_2}$ ‰	$\delta^{13}C_{CH_4}$ ‰	$\delta^{13}C_{CO_2}$ ‰	$\delta^{13}C_{CaCO_3}$ ‰	$\delta^{18}O_{CaCO_3}$ ‰
Precision and Accuracy	*0.04*	*0.4*	*0.3*	*0.5*		*0.2*		*0.5*	*0.5*	*0.5*	*0.5*	*0.2*	*0.2*
Cartman	-22.8	-176.5			0.66	-17.0	15.5						
Half Spring	-22.6	-185.6	10.5		12.3	-6.6	85.4						
Orange Creek	-21.7	-171.7	12.9	-15.1	1913.2	-8.06	0						
Caribou River	-21.8	-170.5	11.6	-12.7	41.88	-8.1	163.6						
Karst	-22.5	-171.1	7.7		10.482	1.45	89.27						
Persistent	-22.9	-178.0	14.4		11.48	-0.52	397						
Stinky	-23.2	-182.2	31.9		10.695	-1.89	457.2				-8.7		
Twitya	-24.1	-193.0	28.6	2.8	118.35	-9.31	389.4			-49.2	-17.8	-9.2	-26.2
Sculpin	-23.9	-192.3	24.0	13.7	1495.1	-2.35	219.7				-10.3	1.3	-21.8
Deca °	-23.5	-189.7	16.7	12.8	943.85	-1.84	261.3		-10.4		-9.5	2.2	-21.4
Ekwi	-23.6	-191.8	18.2	13.1	1783.1	-1.21	663.3				-8.1	2.5	-22.8
Mineral Lake	-22.8	-183.0	3.1	-7.4	78.25	-4.01	327.3				-12.5	-0.8	-20.2
Brimstone °	-23.2	-181.1	15.1	-2.9	69.3	3.0	1.81E+03		-3.3		-3.6	10.5	-18.1
Cordes Vertes	-22.5	-178.4	12.3		14.7	2.4	458				-5.8	2.1	-20.8
Tabletop	-23.0	-179.5	22.5	7.3	150	-2.9	188				-13.6	-2.5	-25.8
South Redstone	-22.5	-177.5	23.3	8.3	162	-5.3	172				-13.1	-3.3	-27
Redstone Junction #1	-22.6	-175.2	19.0	1.6	252	-5.6	172				-13.7	-3.5	-21.3
Cotton	-22.2	-172.0	19.2		15.6		0.0						
Red Mini	-22.8	-179.5	2.3	-10	38.0		0.0						
Muddy	-23.0	-178.2	1.5	-9.7	99.0	-9.8	79.9				-18.1		
Grasby	-23.1	-178.2	19.0	-6.8	29.3	-8.5	297				-17.0	-6.5	-19.7
Red Steel	-22.5	-174.6	12.2	-11.6	21.6	-14.1	0.0				-21.1		
Bougere	-22.4	-170.5	10.7	-7.2	279		0.0				-22.1		
Champagne °	-22.1	-168.2	18.3	-9.5	52.7	-2.6	223	-81.1	-2.7		-8.8		
Champagne ° (field dup)	-22.1	-168.3	18.3	-9.5	52.3	-2.1	218						
Champagne Creek	-22.0	-172.1	17.9		55.8	-5.3	169				-13.6		
North Cantung (Zenchuck Creek)	-22.4	-182.7			8.64	-15.7	201						
Moore's	-22.6	-182.9	13.6	-1.3	73.4	-6.3	279						
Nahanni North (Lened Creek)	-23.3	-188.7	11.9	-7.9	57.4	-12.6	146						
Nahanni Headwaters	-22.8	-181.1	8.1	-8.7	31.9	-8.9	101						
Grizzle Bear °	-23.5	-188.2	21.7	6.2	188	-4.0	229	-40.4	-6.18				
Glacier Lake	-23.1	-182.7	5.3	-6.9	199	-7.5	64.5					-3.8	-19.2
Rabbitkettle	-22.5	-181.6	7.7	2.5	34.8	-1.5	447						
Kraus (Clausen)	-21.7	-176.9	24.1	6.5	656	-8.5	236						
Meilleur River	-22.3	-181.6	11.8	-5.1	277	-10.1	317					-5.9	-24.1
Wildmint	-22.5	-190.9	16.5	-12.2	114	-6.2	187						
Stinky Drift	-22.3	-180.6	6.2	2.5	29.4	-4.9	346						
Hole in the wall	-22.6	-181.2			5.74	-15.1	72.3						
West Cantung	-22.5		19.4	-6.9	31.5	-9.5	140						
Broken Skull Upper Pool (2003) °	-23.5	-188.3	24.3	4.4	345	-3.5	387	1.8	-5.1				
Broken Skull Upper Pool (2004) °						-3.5		-0.1					
Flat Fruit (2003) °	-21.5	-177.4	11.1	4.8	35.1	1.6	581						
Flat Fruit (2004) °									-2.47				

Appendix 6. Number of times springs were sampled for MERA 1 and 2; all other springs were sampled once only. Does not include lab duplicates, triplicates, or field blanks. The 2003 sampling season was funded externally from MERA 2 but included for completion.

Spring	1986	1987	2003	2004	2005	Total
Rabbitkettle (001)	1		1			2
not named (012)	1	3				4
Glacier Lake (015)	1		1			2
not named (017)	1	1				2
Cantung West (018)	1	2	1			4
Cantung mine (019, 020)	2		1			3
Wildmint (027)	1	1	1			3
Moore's (032)	1		1			2
Nahanni North (033, 034)	1	2	1			4
Nahanni Headwaters (038)	1		1			2
Broken Skull (040, 041)	2		1		2	5
Grizzly Bear (043)	1		1			2
Cantung North (044)	1		1			2
Hole-in-the-Wall (052, 053)	2	1	1			4
Flat Fruit (058)	1	1	1			3
Cantung East (060)	1	1				2
Kraus (063, 064)	2	1	1			4
Prairie Creek mine (067)	1				1	2
Meilleur (072, 073)	2	5	1			8
White Aster (082)	1	3				4
Champagne				2		2
Sombre					2	2
Dookie					3	3
Blue Bells					2	2

Appendix 7. Summary of anomalous springs for MERA 1 and 2. MERA 1 anomalous = springs listed as anomalous in Table 5.12 of Hamilton et al. (2003). MERA 1 'high metals' = springs listed as 'high metals' in Table 5.12 of Hamilton et al. (2003). MERA 2 anomalous = MERA 2 and/or MERA 1 data interpreted as anomalous by at least one of three MERA 2 methods. '% trace elements' = total trace elements as a percentage of total dissolved solids. Ficklin diagram groups are described and shown in Figure 6. Geochemical groups are from the Piper diagram, Figure 4. Depth of circulation was estimated from Si-geothermometry using a quartz chalcedony geothermometer. Springs are listed in nested order of decreasing geochemical grouping, decreasing number of individual anomalous trace elements (each row listed in decreasing order of anomalousness), and decreasing % trace elements.

Spring	MERA 1 analysed	MERA 1 anomalous	MERA 1 'high metals'	MERA 2 anomalous	% trace elements	Number anomalous	List of anomalous trace elements	Ficklin diagram group	Geochemical group	Estimated depth of circulation (km)
86-072A (near Meilleur River)	x	x		x	2.16	8	Al, Mn, Ni, Zn, Cd, Co, Sr, Ag	G	**1**	
86-67 (Prairie Creek mine water)	x	x		x	4.68	5	Cu, Zn, Cd, Sb, Ag	H	**1**	
Glacier Lake				x	4.87	3	Fe, Zn, Tl	I	**1**	1.4
86-78	x		x	x	5.96	2	Fe, Mn	I	**1**	
86-15 (Glacier Lake)	x	x		x	2.78	2	Fe, Zn	I	**1**	
86-17	x			x	1.44	2	Fe, Mn		**1**	
86-35	x		x	x	1.14	2	Cu, Co	IJK	**1**	
86-37	x		x	x	2.28	1	Fe	I	**1**	
86-55	x		x	x	1.47	1	Fe	I	**1**	
Cathedral				x	1.41	1	Sr		**1**	<0.2
86-54	x			x	5.12			K	**1**	
86-62	x			x	4.89				**1**	
86-48	x			x	3.21				**1**	
87-012B	x			x	2.26			I	**1**	
Sombre (field dup)				x	1.60				**1**	<0.2
Sombre				x	1.59				**1**	<0.2
87-103	x		x	x	1.53				**1**	
86-4	x			x	1.20				**1**	
Softie				x	1.13				**1**	<0.2
87-109	x		x	x	1.05				**1**	
Orange Creek				x	4.00	15	Al, Mn, Ni, Cu, Zn, Cd, Co, Cr, Li, U, Tl, Ga, Be, Sc, Ti	E	**2**	<0.2
86-072B (near Meilleur River)	x	x		x	3.24	9	Al, Mn, Ni, Cu, Zn, Cd, Co, Sr, U	E	**2**	
Bougere				x	8.20	8	Al, Mn, Ni, Cu, Zn, Co, Ga, Ag	E	**2**	1.3
87-072B (near Meilleur River)	x	x		x	1.16	7	Al, Mn, Ni, Zn, Pb, Cd, Co	E	**2**	
86-71	x			x	3.07	5	Fe, Al, Mn, Cu, Co	F	**2**	
86-69 (Twisted Mountain)	x			x	5.59	4	Fe, Al, Mn, Co	F	**2**	
86-42	x	x		x	4.36	4	Al, Cu, Zn, Cd	E	**2**	
86-49	x		x	x	11.32	3	Fe, Al, Co		**2**	
86-36	x		x	x	1.17	2	Zn, Co	E	**2**	
86-70	x			x	1.01	2	Mn, Co	I	**2**	
87-121	x		x	x	3.85	1	Al	F	**2**	
86-25	x	x		x	3.52	1	Zn	E	**2**	
Interpluton				x	3.04	1	Ga		**2**	<0.2
87-072BH (near Meilleur River)	x	x		x	1.93	1	Al		**2**	
86-80	x		x	x	5.93				**2**	
Red Mini				x	4.63			F	**2**	0.9
Cotton				x	4.47			F	**2**	0.2
Overflow				x	3.33				**2**	
87-108	x			x	3.32				**2**	
87-100	x		x	x	2.43				**2**	
86-12	x	x		x	1.99				**2**	
87-105	x		x	x	1.30			IJK	**2**	
Nahanni Headwaters				x	0.93	7	Cs, Mo, As, Li, B, Sb, Ga		**3**	4.4
87-53 (Hole-in-the-Wall)	x		x	x	1.93	2	Mo, As		**3**	
86-53 (Hole-in-the-Wall)	x		x	x	1.72	2	Mo, As	K	**3**	
87-33 (Nahanni North)	x		x	x	0.92	1	Mo		**3**	
87-60 (Cantung East)	x		x	x	2.07	1	Mo		**3**	
86-52 (Hole-in-the-Wall)	x		x	x	1.71	1	As		**3**	
86-20 (Tungsten mine water)	x	x		x	1.00	1	Ag		**3**	
87-18 (West Cantung)	x	x		x	1.95				**3**	
87-18B (West Cantung)	x	x		x	1.90				**3**	
86-18 (West Cantung)	x	x		x	1.71				**3**	
Prairie Creek mine shaft				x	0.81	7	Cu, Zn, Pb, Cd, Sb, Tl, Se	H		<0.2
Kraus (Clausen)				x	0.39	7	Cr, Cs, Li, Rb, Sr, V, B			2.3
87-073B	x	x		x	0.73	6	Al, Mn, Ni, Zn, Cd, Co			
Brimstone				x	0.73	6	Fe, Mn, Cr, Rb, Se, Be			4.7
Tulita				x	0.57	6	Cs, Li, Ba, B, Br, Sc			1.5

Appendix 7 continued.

Spring	MERA 1 analysed	MERA 1 anomalous	MERA 1 'high metals'	MERA 2 anomalous	% trace elements	Number anomalous	List of anomalous trace elements	Ficklin diagram group	Geochemical group	Estimated depth of circulation (km)
Persistent (lab dup)				x	0.26	6	Cd, Cs, As, Rb, Ba, Tl			n/a
Persistent				x	0.26	6	Cd, Cs, As, Rb, Ba, Tl			n/a
Ekwi				x	0.03	6	Cr, Cs, Li, Rb, B, Tl			2.3
West Cantung				x	0.60	5	Cs, Li, V, B, Ga			3.2
Wrigley				x	0.51	5	Mo, U, V, Tl, Se	I		<0.2
Broken Skull's upper pool				x	0.38	5	Pb, Cs, Rb, B, Br			2.7
Nahanni North (Lened Creek)				x	0.28	5	Cs, Mo, Li, B, Ga			3.6
Broken Skull's lower pool				x	0.39	4	Cs, Rb, B, Br			2.7
Hole-in-the-Wall				x	0.37	4	Mo, As, V, Ga			3.7
Grizzle Bear				x	0.22	4	Cr, Cs, Rb, Br			2.8
87-112	x	x		x	0.15	4	Fe, Mn, Ni, Co	I		
Galena				x	0.13	4	Pb, U, Tl, Se	J		<0.2
Wildmint				x	0.09	4	Cs, Li, B, Ga			2.9
Cimitar				x	0.63	3	Sr, U, Tl	I		<0.2
Broken Skull				x	0.37	3	Cs, Rb, B			2.7
Meilleur River				x	0.28	3	Cs, Rb, Br			3.1
86-63	x			x	0.26	3	Cu, Sr, U	I		
87-64	x			x	0.18	3	Pb, Sr, U			
87-073A	x	x		x	0.15	3	Ni, Zn, Pb	H		
86-21	x	x			0.37	2	As, Sr			
87-122	x				0.31	2	Pb, U			
Sibbeston	x				0.31	2	Tl, Ga	K		<0.2
87-123	x				0.30	2	Pb, Sr			
86-64	x				0.25	2	Cu, Sr			
Smurf				x	0.15	2	V, Se	IJK		<0.2
Prairie Creek				x	0.14	2	Sb, NO_2	IJK		<0.2
Galena (lab dup)				x	0.13	2	U, Tl	J		<0.2
Cowgirl				x	0.08	2	V, Tl	K		<0.2
86-60	x				0.89	1	Mo			
87-012C	x	x		x	0.84	1	Cd	I		
87-124	x				0.79	1	Ba			
86-33	x				0.73	1	Mo			
Tabletop					0.63	1	Cr			2.3
Red Steel					0.63	1	Se			<0.2
Sculpin					0.61	1	Sr			0.3
86-30	x				0.54	1	Ag			
86-19 Tungsten mine water	x	x			0.53	1	Ag			
Mineral Lake					0.48	1	Cr			0.5
South Redstone					0.45	1	Cr			2.7
87-128	x				0.39	1	Ba			
Quickie					0.38	1	Se			<0.2
86-83	x				0.38	1	Ag			
86-77	x			x	0.31	1	Ba	K		
86-27	x				0.30	1	Ag			
87-17	x				0.25	1	Mn			
87-110	x				0.20	1	U			
Stinky drift					0.16	1	Tl			1.2
87-34	x		x		0.15	1	U			
87-58	x				0.15	1	Pb			
87-127	x				0.15	1	Ba			
87-119	x				0.14	1	Pb			
Flat Fruit					0.14	1	Cs			0.9
Veil					0.13	1	Se			<0.2
Big Veil					0.13	1	Se			<0.2
Champagne Creek					0.12	1	Se			<0.2
87-111	x	x			0.11	1	U			
Cordes Vertes					0.11	1	Cr			n/a
87-073C	x			x	0.11	1	Ni	I		
86-13	x		x		0.10	1	As			
Deca					0.09	1	Cr			0.8
Harrison Creek					0.08	1	Pb			<0.2
87-125	x	x		x	0.08	1	Mo	IJK		
Grasby					0.08	1	Se			n/a
Crack					0.04	1	V			<0.2
Mossy (lab dup)					0.69					<0.2
Mossy					0.68					<0.2
86-61	x				0.59					
Clark Lake					0.53					<0.2
Clark Lake (lab dup)					0.53					<0.2
Ram Plateau					0.53					<0.2
87-126	x				0.49					
Jacson					0.49					<0.2

Appendix 7 continued.

Spring	MERA 1 analysed	MERA 1 anomalous	MERA 1 'high metals'	MERA 2 anomalous	% trace elements	Number anomalous	List of anomalous trace elements	Ficklin diagram group	Geochemical group	Estimated depth of circulation (km)
86-11	x		x		0.46					
86-31	x				0.45					
Brigade					0.39					<0.2
86-41	x				0.39					
87-12	x				0.38					
86-79	x				0.37					
86-74	x			x	0.37			I		
86-29	x				0.37					
86-81	x				0.36					
86-40	x				0.35					
Darkness					0.33					<0.2
86-43	x				0.31					
86-32	x				0.31					
Redstone Junction #1					0.30					2.0
Waterfall					0.30					<0.2
86-50	x		x	x	0.30			IJK		
86-59	x				0.28					
Stinky					0.28					n/a
87-82B White Aster	x				0.27					
Mel's Pool				x	0.27			K		<0.2
Selena				x	0.27			I		<0.2
Meltwater					0.26					<0.2
86-57	x				0.25					
86-1 (Rabbitkettle)	x				0.25					
86-75	x		x	x	0.25			K		
87-107	x	x		x	0.24			I		
87-27	x				0.24					
Champagne					0.23					n/a
86-58	x				0.22					
86-82 White Aster	x	x			0.22					
Champagne (dup)					0.21					n/a
86-76	x				0.20					
86-9	x				0.20					
Cartman					0.19					<0.2
87-82 White Aster	x	x			0.19					
Dookie (field trip)					0.19					<0.2
86-44	x				0.18					
Dookie (field dup)					0.18					<0.2
86-56	x				0.18					
87-115	x				0.18					
86-10	x		x		0.18					
Moore's					0.18					3.3
Corridor Creek					0.17					<0.2
86-6	x				0.17					
86-46	x				0.17					
Caribou					0.16					<0.2
Dookie					0.16					<0.2
86-47	x				0.16					
Caribou River					0.15					<0.2
87-104	x				0.15					
86-26	x				0.15					
86-22	x				0.14					
87-116	x				0.14					
86-28	x				0.14					
86-7	x				0.14					
86-68	x				0.14					
Half Spring					0.13					<0.2
Rabbitkettle					0.12					1.1
Chance					0.12					<0.2
86-45	x				0.12					
Cowboy					0.12					<0.2
87-120	x				0.12					
Champagne Creek (dup)					0.12					<0.2
86-65	x			x	0.12			K		
87-112H	x				0.12					
87-113	x				0.11					
86-23	x				0.10					
86-24	x				0.10					
86-66	x		x	x	0.10			IJK		
Cascade					0.10					<0.2
Cascade (lab dup)					0.10					<0.2
Blue Bells (field dup)					0.09					<0.2
Descente					0.08					<0.2
87-114	x				0.08					

Appendix 7 continued.

Ficklin Diagram Groups (Plumlee et al., 1994)	
E	Pyrite- and base metal-rich polymetallic veins and disseminations in wallrock with low acid-buffering capacity
F	Pyrite-rich, base metal-poor veins and disseminations in wallrock with low acid-buffering capacity
G	Pyrite- and base metal-rich polymetallic veins that are carbonate-rich or occur in wallrock altered to contain carbonate
H	Pyrite- and base metal-rich, polymetallic replacements and veins in carbonate-rich sediments
I	Polymetallic veins with moderate to low pyrite and base metal content that are carbonate-rich or occur in carbonate-rich wallrock
J	Pyrite-poor polymetallic replacements in carbonate-rich sediments
K	Pyrite-poor, Au-Te veins and breccias with carbonate gangue

Appendix 8. Summary of MERA 2 spring sample numbers and names.

Sample ID	Spring Name	Sample ID	Spring Name
C-453852	Big Veil	C-420952	Hole-in-the-Wall
C-453882	Blue Bells	C-453880	Interpluton Seep
C-453883	Blue Bells (duplicate)	C-453875	Jacson
C-420979	Bougere	C-453893	Karst
C-453870	Boulder	C-420944	Kraus (Clausen)
C-453859	Brigade	C-453871	Meilleur
C-420968	Brimstone	C-420946	Meilleur River
C-453847	Brimstone	C-453857	Mel's Pool
C-420973	Broken Skull	C-453885	Meltwater
C-420933	Broken Skull	C-420967	Mineral Lake
C-453843	Broken Skull (lower pool)	C-420929	Moore's
C-453842	Broken Skull (upper pool)	C-453863	Mossy
C-453844	Broken Skull (upper pool)	C-420976	Muddy
C-453878	Caribou	C-420932	Nahanni Headwaters
C-453892	Caribou River	C-420930	Nahanni North (Lened Creek)
C-453889	Cartman	C-420927	North Cantung (Zenchuck Creek)
C-453884	Cascade	C-453891	Orange Creek
C-453862	Cathedral	C-453872	Overflow
C-420982	Champagne Creek	C-453841	Prairie Creek (downstream of mine)
C-420980	*Champagne I	C-453839	Prairie Creek mine shaft
C-420981	Champagne II	C-453894	Persistent (Last Minute)
C-453879	Chance	C-453865	Quickie
C-453861	Cimitar	C-420941	Rabbitkettle
C-453874	Clark Lake	C-453860	Ram Plateau
C-453866	Clearwater Creek	C-420975	Red Mini
C-420969	Cordes Vertes	C-420978	Red Steel
C-453850	Corridor Creek	C-420972	Redstone Junction #1
C-420974	Cotton	C-420964	Sculpin
C-453848	Cowboy	C-453877	Selena
C-453858	Cowgirl	C-453849	Sibbeston
C-453864	Crack	C-453873	Smurf
C-453876	Darkness	C-453888	Softie
C-420965	Deca	C-453854	Sombre I
C-453887	Descente	C-453855	Sombre II (duplicate)
C-453867	Dookie	C-420971	South Redstone
C-453868	Dookie (duplicate)	C-453895	Stinky
C-453869	Dookie (triplicate)	C-420970	Tabletop
C-420966	Ekwi	C-453881	Tiny
C-420953	Flat Fruit	C-420963	Tulita
C-453846	Flat Fruit	C-453845	Tungsten
C-453853	Galena Creek	C-453851	Veil
C-420937	Glacier Lake	C-453886	Waterfall
C-420977	Grasby	C-420957	West Cantung
C-420936	Grizzle Bear	C-420947	Wildmint
C-453890	Half Spring	C-453856	Wrigley
C-453840	Harrison Creek		

STREAM SEDIMENT GEOCHEMISTRY IN THE PROPOSED EXTENSION TO THE NAHANNI PARK RESERVE

M.W. McCurdy, R.J. McNeil, P.W.B. Friske, S.J.A. Day, and R.S. Wilson
Geological Survey of Canada, 601 Booth Street, Ottawa, Ontario K1A 0E8

INTRODUCTION

An evaluation of stream sediment and water data from parts of the South Nahanni watershed and Nahanni Karst region was one component of the 2004-2006 Nahanni Mineral and Energy Resource Assessment (MERA).

As part of this study, geochemical surveys were carried out during the 2004 and 2005 field seasons. Additional geochemical data for stream sediments and waters from surveys, between 1985 and 1987 (Jefferson et al., 2003), were integrated with data from two national geochemical reconnaissance surveys, Geological Survey of Canada (GSC) Open files 4016 (Friske et al., 2001) and 4949 (Day et al., 2005), to evaluate mineral potential in the proposed extension of the Nahanni Park Reserve (Fig. 1).

Sediments collected during the 1985 to 1987 surveys were reanalyzed by several methods in order to obtain data compatible with the current National Geochemical Reconnaissance data sets.

PHYSIOGRAPHIC AND ECOLOGICAL FEATURES OF THE STUDY AREA

The proposed extension to the Nahanni Park Reserve falls mainly within two terrestrial ecozones, the Taiga Plains Ecozone (Nahanni Plateau, Sibbeston Lake Plain) and the Taiga Cordillera Ecozone (Selwyn Mountains; Ecological Stratification Working Group, 1995). The study area rises topographically from southeast to northwest. Elevations range from 168 m ASL at the water aerodrome on the South Nahanni River at Nahanni Butte to 2380 m ASL in the Sapper Ranges of the Mackenzie Mountains. The valley of the South Nahanni River separates the Selwyn Mountains in the southwest from the Sapper Ranges to the northeast (Fig. 2).

The climate of the Taiga Plains Ecozone (Fig. 2) is characterized by short cool summers and long cold winters. The mean annual temperature is approximately -5ºC, mean daily temperatures in July range between 10 and 15ºC, and the mean winter temperature is -19.5ºC on the plateau and -1ºC on the lake plain. Precipitation ranges from 200 mm in the east to 500 mm in the west. These conditions are characteristic of a low sub-arctic ecoclimate; dry to semi-arid and cold.

Vegetation is dominated by open stands of black spruce with an understory of dwarf birch, Labrador tea, lichen, and moss. Drier and warmer sites have more white spruce, paper birch and some aspen. The transition from forest to alpine tundra occurs at 1050 to 1150 m.

Permafrost is extensive and discontinuous. Land use is limited to fishing, trapping, hunting, outdoor recreation, tourism and limited mining operations. At Prairie Creek (Fig. 2), the site of Pb-Ag-Zn mineralization, mining activity (underground development, bulk sampling, and surface drilling) was carried out between 1970 and 1982, but the site was abandoned in 1982 when world silver prices fell (Jefferson et al., 2003). Since 1991, surface drilling, underground sampling and mine rehabilitation operations have been carried out by Canadian Zinc Corporation at the site.

The climate of the Taiga Cordillera Ecozone (Fig. 2) varies with elevation. A summer mean temperature of 9.5ºC and winter mean of -19.5ºC is typical in major valley systems. Precipitation ranges from 600 mm at lower elevations to 750 mm at higher elevations. Vegetation is characteristic of alpine tundra at higher elevations (crustose lichens, mountain avens, dwarf willow, and ericaceous shrubs). Subalpine open-woodland vegetation consists of discontinuous open stands of stunted white spruce, with willow, dwarf birch, and northern Labrador tea, ground cover moss, and lichens. Permafrost is permanent and continuous. Elevations in this part of the study area reach a maximum of 2380 m ASL in the Sapper Ranges (Mackenzie Mountains) and 2275 m ASL (Mt. Wilson) in the Logan Mountains (Selwyn Mountains).

Land use is limited to hunting, trapping, ecotourism, and mining and mineral exploration (Ecological Stratification Working Group, 1995). Production commenced at the North American Tungsten Corporation Ltd. Cantung tungsten mine, Tungsten, Northwest Territories (Fig. 2), on September 1, 2005.

SURFICIAL GEOLOGY

Laurentide glaciation from the east reached as far as Virginia Falls and the lower Flat River, damming the South Nahanni River and causing the formation of a glacial lake covering an approximate maximum area of 900 km^2. Glaciolacustrine sediments up to 120 m thick can be found at various locations along the South Nahanni River. Local glaciers originated from various sources, including valley glaciers and local ice caps,

McCurdy, M.W., McNeil, R.J., Friske, P.W.B., Day, S.J.B, and Wilson, R.S., 2007, Stream sediment geochemistry in the proposed extension to the Nahanni Park Reserve, *in* Mineral and Energy Resource Potential of the Proposed Expansion to the Nahanni National Park Reserve, North Cordillera, Northwest Territories, (ed.) D.F. Wright, D. Lemkow, and J. Harris; Geological Survey of Canada, Open File 5344, p. 75-98.

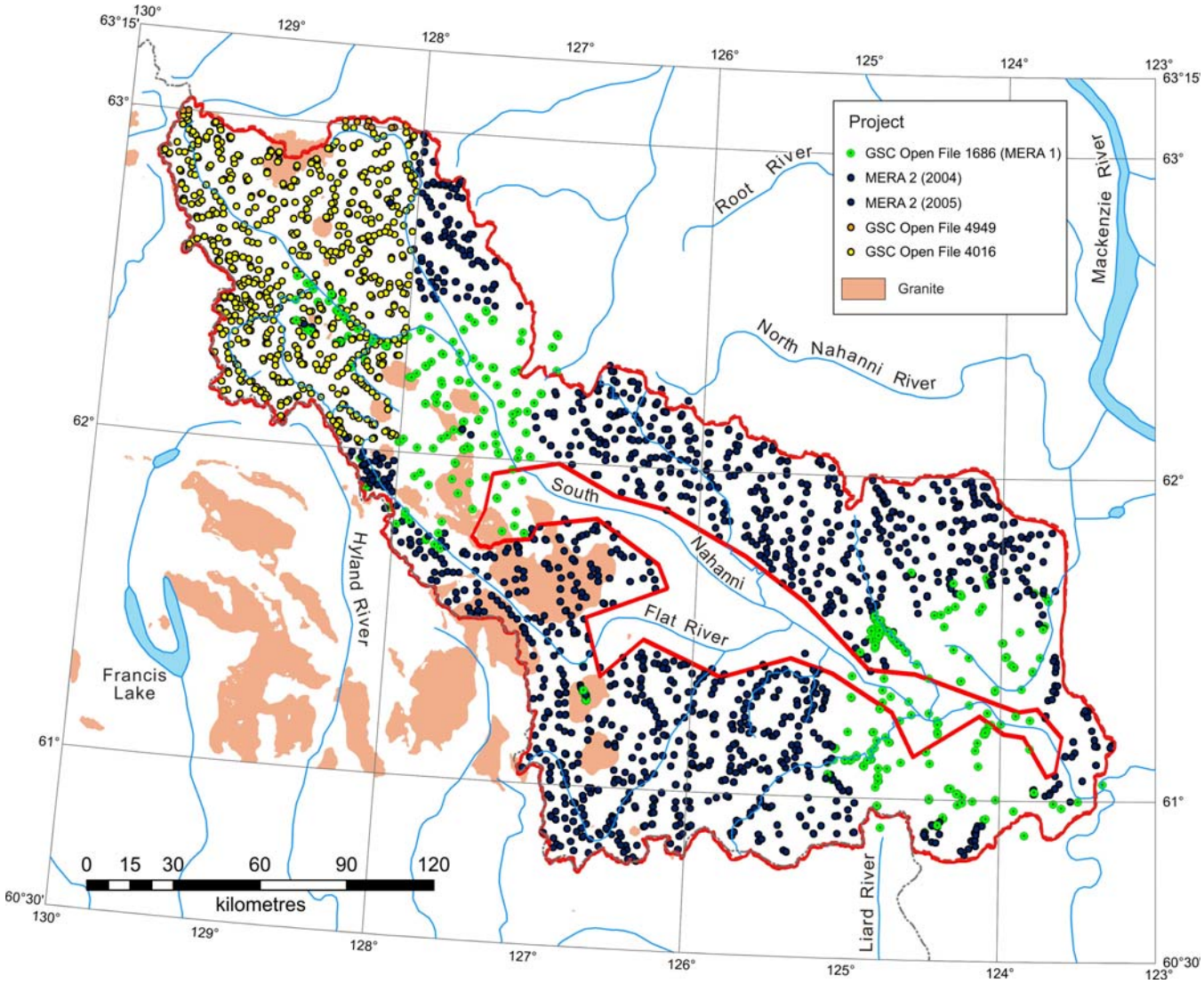


Figure 1. Sources of geochemical data used to evaluate mineral potential within the study area. Samples labelled MERA 2 are from this study during the field seasons of 2004 and 2005.

and Cordilleran ice sheets in the Selwyn Mountains (Duk-Rodkin, 2005).

Surface materials of the Taiga Plains (Fig. 2) consist mainly of glacial drift, colluvium, and organic deposits. Soils (luvisols, brunisols, gleysols) have developed on glacial till and lacustrine deposits (Ecological Stratification Working Group, 1995).

Steep, narrow valleys incise the Taiga Cordillera Ecozone (Fig. 2). Bare rock outcrop and rubble are present at higher elevations, and bare talus slopes are common: little bedrock is exposed below the tree line at about 1500 m. Soils (brunisols) have developed on alluvial, fluvioglacial, and morainal veneers and blankets (Ecological Stratification Working Group, 1995). The most common glacial deposits are tills that blankets or form a veneer over bedrock. Glaciofluvial deposits, consisting primarily of gravel, form kames, eskers, and planar deposits in most valleys. Glaciolacustrine deposits are present mainly in the South Nahanni River Valley, especially near Mt. Wilson. Bogs form in areas of poor drainage (Jackson, 1987).

FACTORS AFFECTING GEOCHEMICAL DISPERSION

The relative mobility of elements in surface environments is affected by climate and physiography, as well as biologic, anthropogenic, and geological factors (Plant and Raiswell, 1994).

Climate and altitude are major post-glacial factors affecting the dispersion of elements within the study area. Extreme cold at high altitudes prevents growth of plants and other organisms, and limits geochemical dispersion to mechanical processes of frost action, solifluxion, and wind-blasting. At lower altitudes within the study area and in periglacial zones, mountain tundra environments prevail. Plants grow in soil

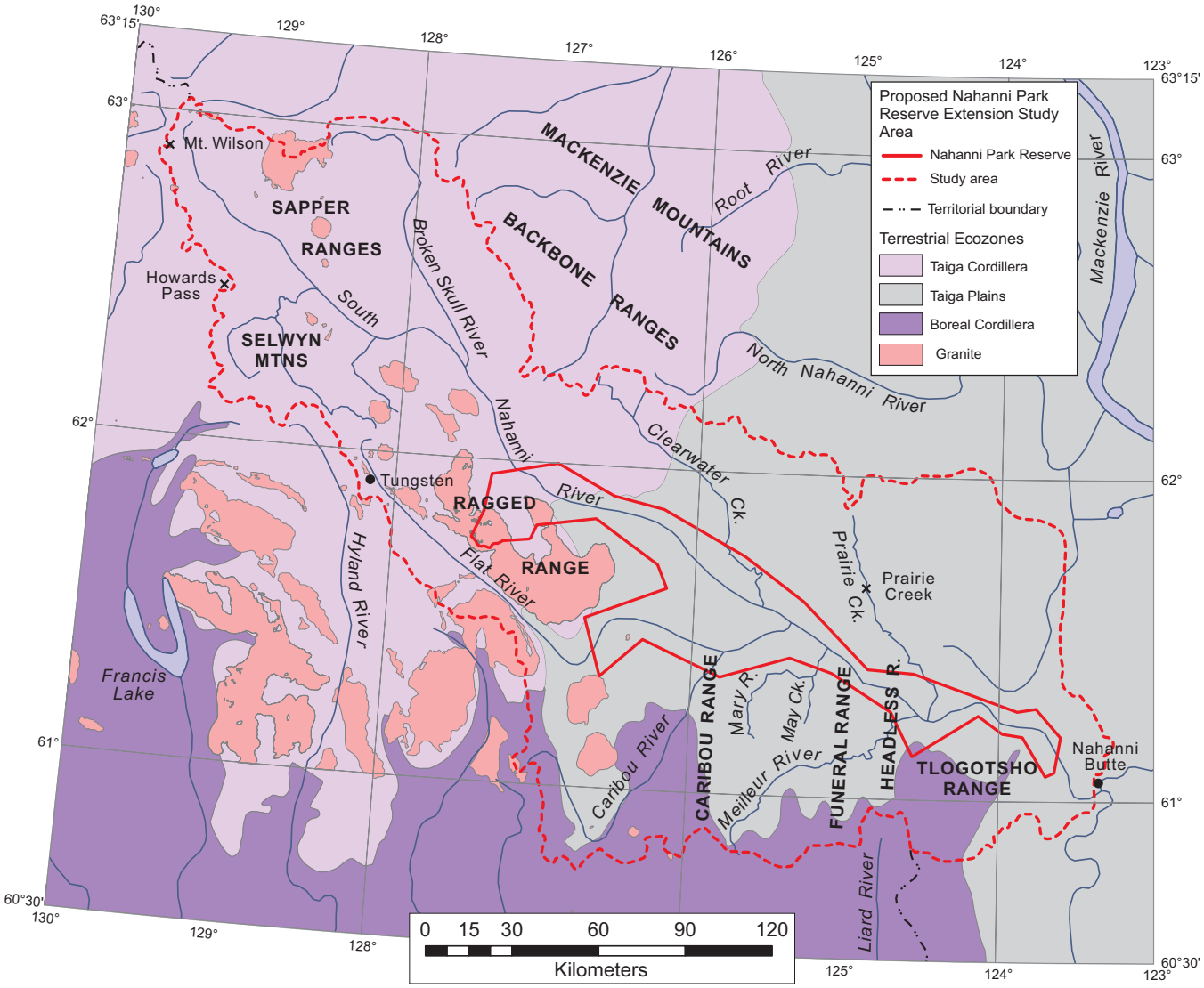


Figure 2. Drainage and physiography of the Nahanni National Park Reserve and proposed extension. Geology modified from Wheeler (1996) and Okulitch (in prep. a,b)

that impedes solifluxion and organic material accumulates. Under these conditions, limited hydromorphic dispersion is possible (Wilhelm and Artignan, 1994), however, stream sediments collected within these environments consist mainly of finely ground particles of rock from mechanical erosion. Hydromorphic dispersion tends to be localized in areas below breaks in slope and is normally subordinate to the detrital component (Wihelm and Artignan, 1994).

Tundra becomes taiga below a transition zone between 1050 to 1150 metres. Increasing average temperatures, plant diversity, and soil development, combined with decreasing permafrost coverage, result in an increased hydromorphic component in stream sediment samples, and potentially a wider dispersion of elements in the environment, mainly related to the formation and transport of metal-scavenging secondary oxides (Ottesen and Theobald, 1994).

The pH of stream waters, by controlling the dissolution and precipitation of elements in solution, also affects geochemical dispersion throughout the environment. In neutral to alkaline environments the chemical mobility of many metals, including Zn, Ag, and Pb, and to a lesser extent As and Cd, is severely restricted (Plant and Raiswell, 1994). Conversely, metals such as U, Mo, and V are relatively mobile. Figure 3 illustrates pH values from the various surveys used to evaluate mineral potential. As the pH of stream waters equals or exceeds 7.2 in in 85% of the streams sampled, the geochemical dispersion of many elements will be affected.

SAMPLE COLLECTION AND ANALYTICAL TECHNIQUES

Geochemical data from several sources were used to evaluate the mineral potential of the proposed extension of the Nahanni Park Reserve. Details of the col-

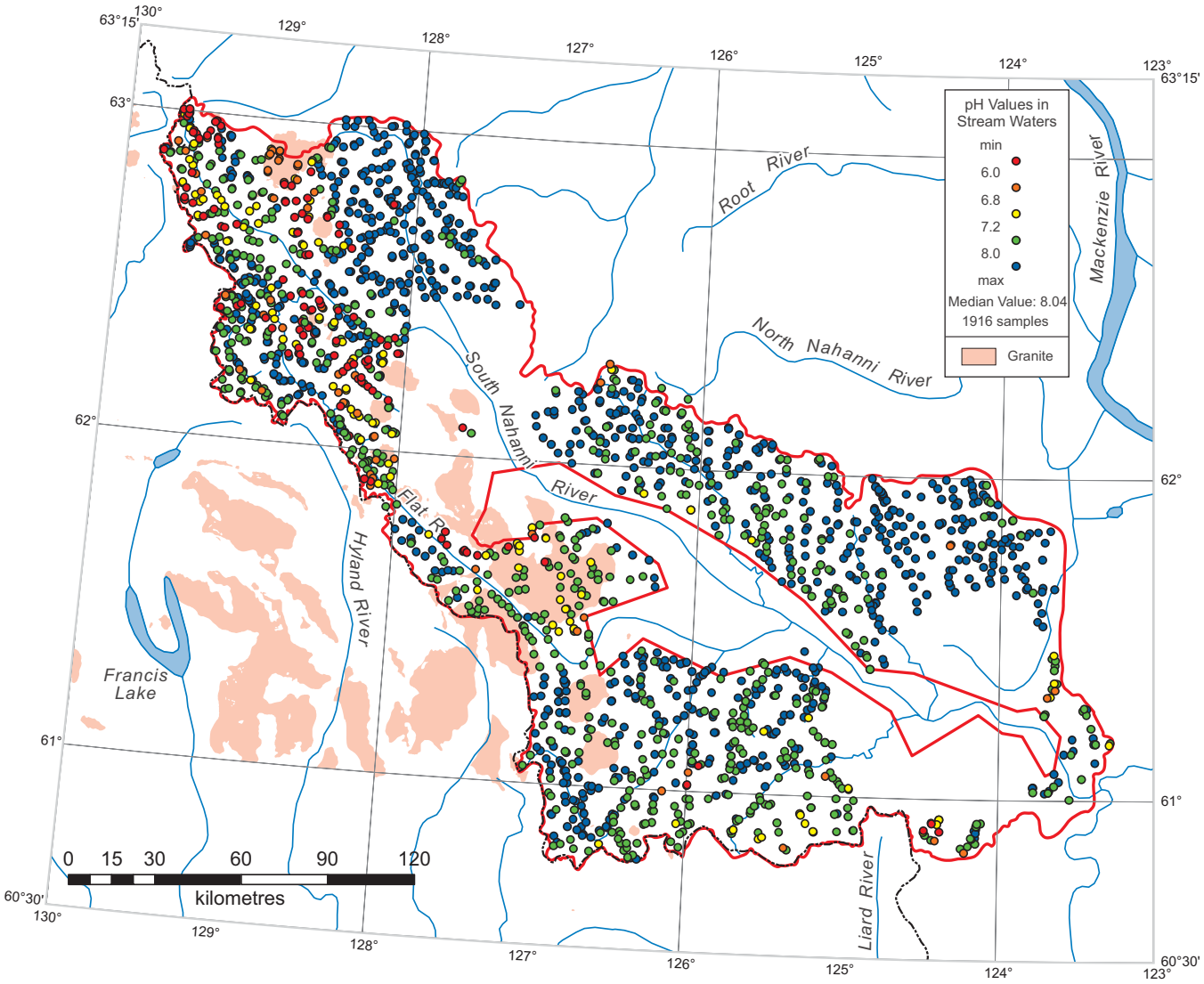


Figure 3. pH values of stream waters within the survey area.

lection, preparation, and analytical methods for each survey are described in Appendix 1.

Concentrations of Zn, Cu, Pb, Ni, Co, Ag, Cd, Mn, Fe, Mo, and V in stream sediments originally collected in 1981 and published in GSC Open File 4016 (Friske et al., 2001; Fig. 1) were determined in an open system using a mixture of HF-$HCLO_4$-HNO_3-HCL to decompose the less than 177 micron fraction. This attack is often described as a 'total' decomposition although refractory minerals such as cassiterite, wolframite, chromite, spinel, beryl, zircon, tourmaline, magnetite, and high concentrations of barite are not dissolved. Most oxides, sulphides, and silicates are put into solution with this type of acid digestion (Hall, 1991).

Samples of stream sediment collected after 1981 (MERA 2, Open files 1686 and 4949; Fig. 1) were analyzed (or reanalyzed) in an open system using hot aqua regia (a mixture of HCl and HNO_3) to decompose the less than 177 micron fraction. This method is often described as a 'partial' decomposition. Metals, such as Cu, Pb, and Zn sorbed onto clay minerals or in other readily decomposed stages, are put into solution and most sulphides, arsenides, selenides, tellurides, sulphosalts, and native Au, Pt, and Pd are dissolved (Hall, 1991).

PRESENTATION OF DATA

Data for individual and groups of elements are represented in two different ways. Differences in concentrations of individual elements in sediment are illustrated by assigning values at each site based on the position of the analytical value relative to the median value for all sites. The maximum symbol size is assigned to values greater than 10 times the median value. Portraying relatively high values as large, bold symbols and 'background' values with unobtrusive dots visually enhances elevated values on regional-scale maps. Decreasing levels of elemental concentrations at five, three, and two times median values are represented by succes-

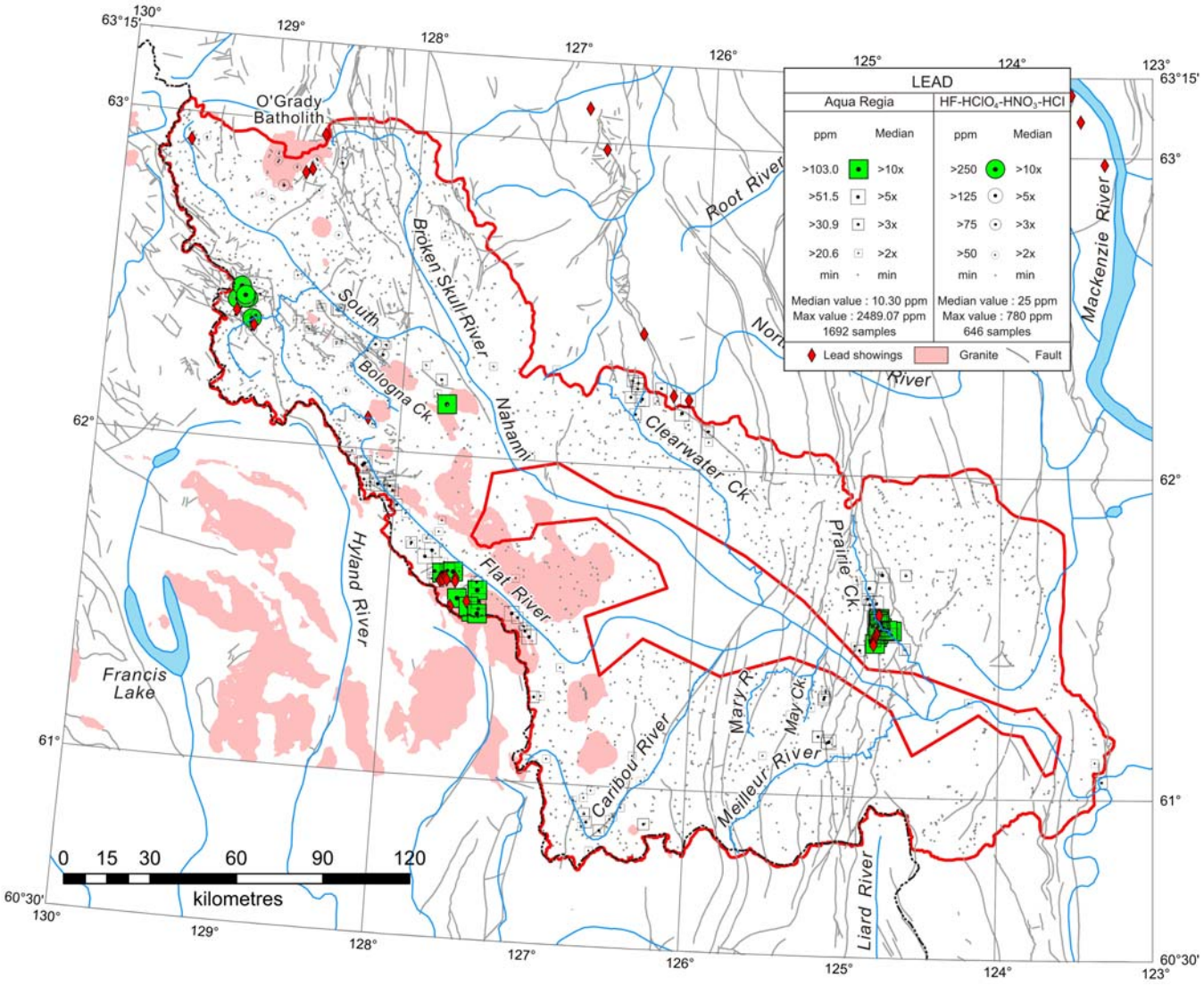


Figure 4. Single-element plot of lead in stream sediments. It is important to note that lead data published in GSC Open File 4016 (Friske et al., 2001; Fig. 1) were obtained using HF-HCl0_4-HNO_3-HCl to decompose samples, a 'near-total' digestion. All other samples were decomposed using aqua regia (HCl-HNO_3), a 'partial' digestion. See Appendix 1 for details.

sively smaller symbols. In the discussion of geochemical results, the following descriptive terms are used: the median value for a given element is considered as 'background', and 'anomalies' are described as weak (2 to 3 times median), moderate (3.1 to 5 times median), strong (5.1 to10 times median), or very strong (greater than 10 times median). To compare data from stream sediments collected in 1981 (Fig. 1) and decomposed in HF-$HClO_4$-HNO_3-HCl with samples decomposed in aqua regia, separate median values for each data set were calculated and used to plot maps.

Caveat: this report does not assess individual drainage basins using regression analysis to establish different background element contributions by different geological units to stream sediments. This was demonstrated by Spirito and Jefferson (2003) to be significant, and some apparent anomalies identified in this report could be influenced by a spatially dominant rock unit with high background values of that element in the catchment area.

Multi-element concentrations at specific sites are plotted as proportional pie charts. Individual analytical values of each element are reassigned with the number 0, 1, 2, or 3, depending on the relation to the median value of the concentrations of individual elements. Concentrations exceeding ten times the median concentration are assigned a value of 3, concentrations greater than five times median concentration and less than or equal to ten times the median value are assigned a value of 2, concentrations greater than two times median concentration and less than or equal to five times median concentration are assigned a value of 1. Concentrations less than or equal to two times the median value are assigned a value of 0. The total of these values is used to establish the size of the individual pie, and the maximum pie size represents three

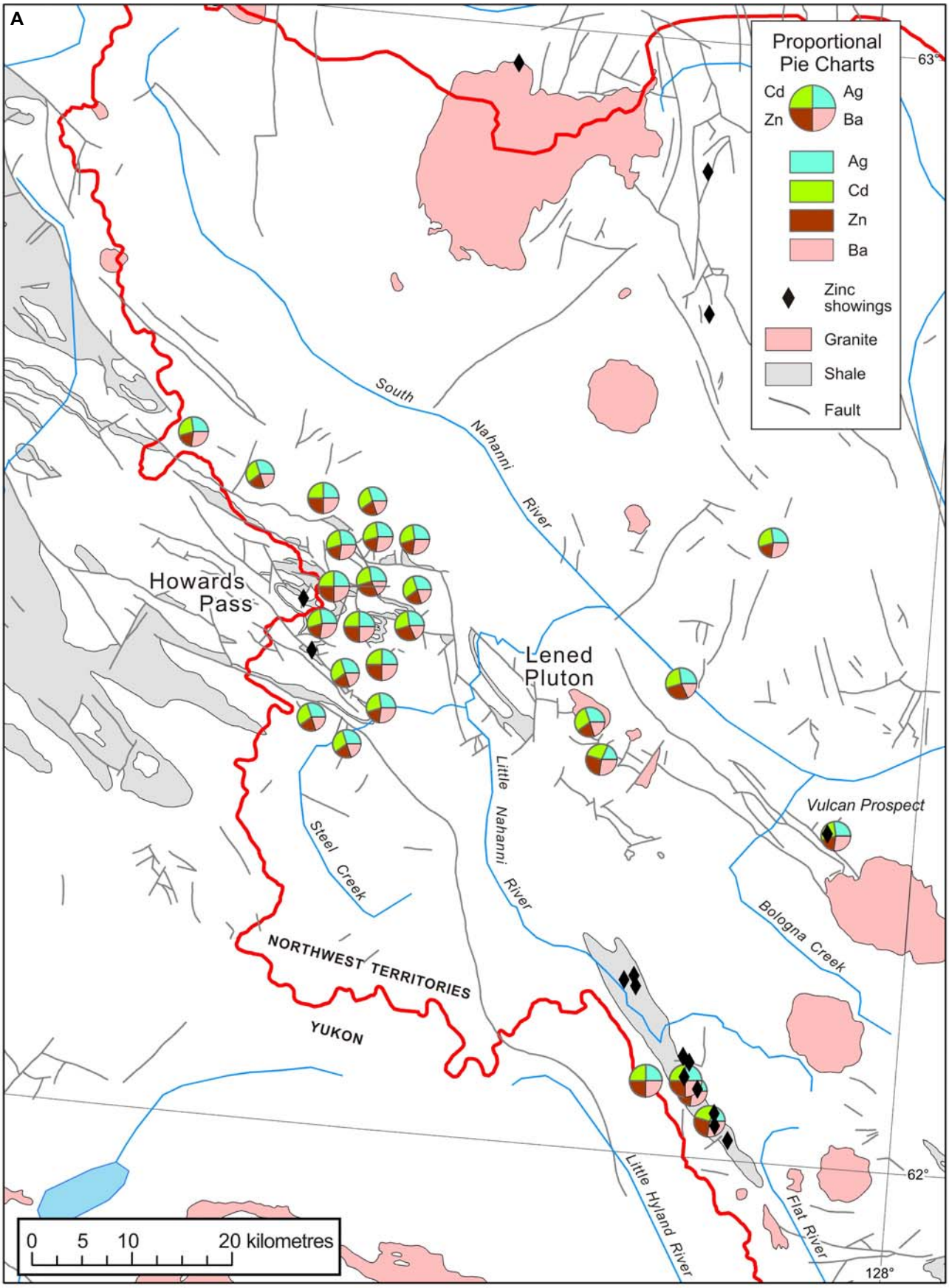
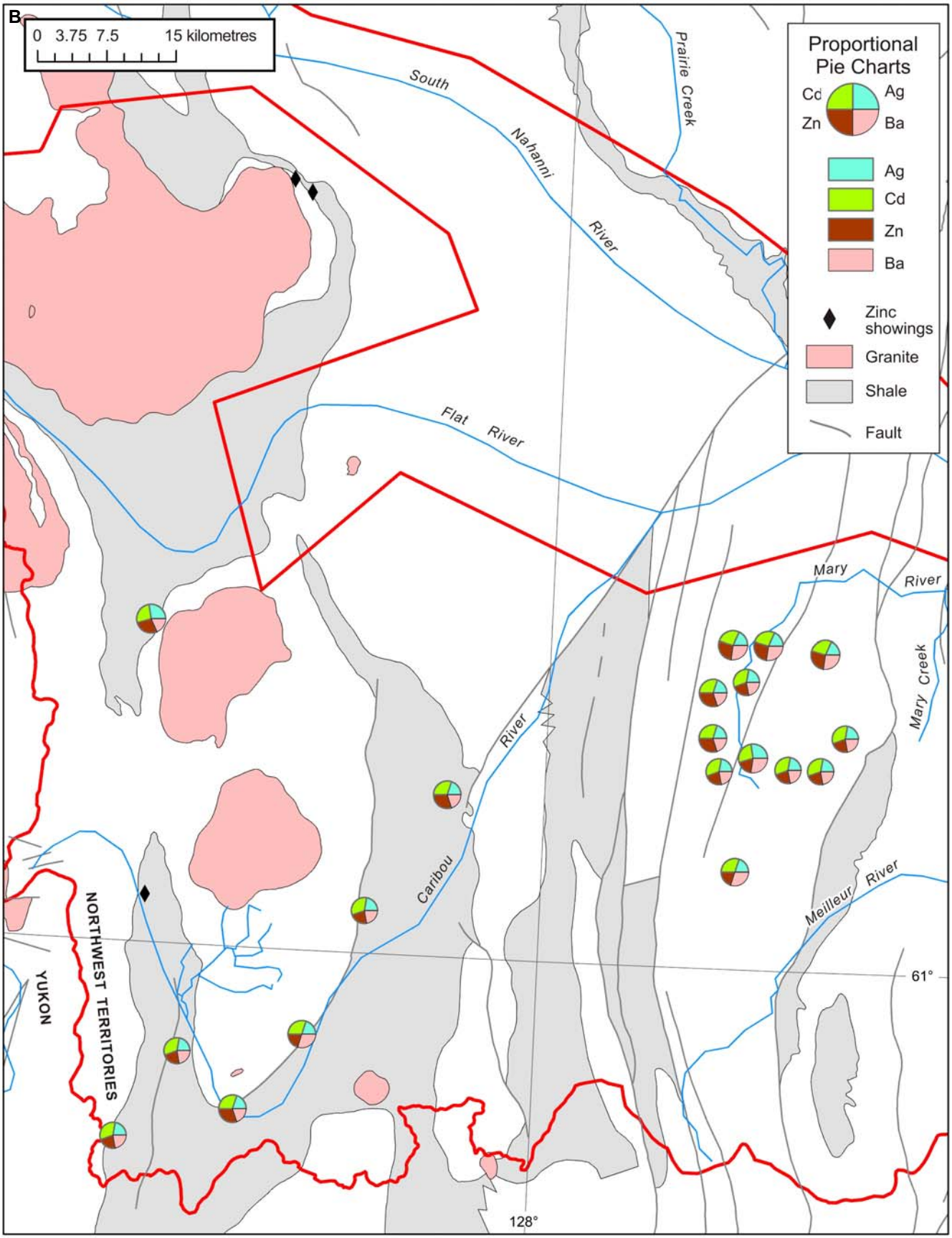


Figure 5. A) Multi-element plot of Ag-Ba-Cd-Zn at Howards Pass. Pie charts represent sites where the concentrations of Ag, Cd, Zn, and Ba are greater than five times their median value.



Figures 5 continued. B) Multi-element plot of Ag-Ba-Cd-Zn at Mary River.

times the total number of elements. The proportion of the total value within individual pies represented by any one element (each element is assigned a colour) is indicated by the size of the arc of each segment within the circle. Pie charts in Figures 5, 6, 9, and 12 indicate sites where concentrations of all elements represented exceed five times the median value.

Lead-Zinc-Silver

A single-element symbol map of lead in stream sediments suggests a restricted pattern of dispersion, with values greater than ten times the median concentrations of the two data sets around known showings along Prairie Creek, Bear Pass Creek, and at Howards Pass. Values between five and ten times the median concentrations are found in stream sediments from the headwaters of Clearwater Creek and the North Nahanni River, adjacent to the Cantung deposit and south of the O'Grady Batholith (Fig. 4).

Elevated lead values between five and ten times the median values are present south of May Creek in the drainage basin of the Meilleur River (Fig. 4). There are no recorded showings with lead as the primary commodity from this area. Given the limited mobility of lead in alkaline environments, these concentrations in stream sediments warrant further investigation.

Values of zinc in stream sediments exceeding ten times the median concentrations of the two data sets are located around known showings at Howards Pass, northwest of Cantung, southeast of the O'Grady Batholith, Prairie Creek, and the headwaters of the Caribou River. Areas of elevated zinc in stream sediment that are not found around recorded zinc showings are located adjacent to the Lened pluton (Fig. 5A), east and west of the upper reaches of the Broken Skull River, south of the junction of the Broken Skull River and South Nahanni River, west of the junction of the Caribou River and the Flat River, and within the drainage basin of the Mary River.

Within the drainage basins of the Caribou and Mary rivers, elevated Ag-Ba-Cd-Zn (Fig. 5B) was detected in stream sediments. This assemblage of elements can be characteristic of sediment-hosted Zn-Pb-Ag occurrences (MacIntyre, 1995). A similar pattern exists in the area east of Howards Pass (Fig. 5A), suggesting the potential for deposit types of a similar nature.

Patterns of distribution of silver are similar to zinc, with values in stream sediments exceeding the median values concentrated in the northwest, especially around Howards Pass, Mt. Wilson, and the O'Grady Batholith. Elevated silver concentrations are found also in stream sediments from the southwest part of the survey area, distributed throughout the catchment basins of the Mary, Caribou, and Meilleur rivers.

Geochemical dispersion in stream sediments around the deposit at Prairie Creek is constrained by a cold, dry climate and by pH values in stream waters often exceeding 8.0 (Fig. 6). The chemical mobility of Zn and Ag is severely reduced under these conditions, and Pb and Cd somewhat less so (Plant and Raiswell, 1994). Physical weathering and transport is thus the major source of dispersion of these metals. Only as a result of increased sample density around the deposit is it outlined by a multi-element array of elevated (greater than five times the median concentrations) Pb-Zn-Ag-Cd (Fig. 6). Uranium, mobile in alkaline environments, is also elevated at several sites.

Uranium

Jefferson and Spirito (2003) report low potential for both sandstone uranium and unconformity-associated uranium deposit types in their assessment of the Nahanni watershed. Within the survey area, only one showing is recorded in the Northern Minerals Database (NORMIN.DB, Department of Indian Affairs and Northern Development, 2001) with uranium as a primary commodity (DY 883; 105ISW012), listing in addition to U, Pb, Zn, P_2O5, and Ba hosted in Ordovician phospahtic shale (Gordey and Anderson, 1993) (Fig. 7). However, both Spirito and Jefferson (2003) and Hamilton et al. (2003) noted multiple element anomalies in stream sediments and waters of hot and cold springs, indicating the potential for stratiform sediment-hosted Pb-Zn deposits. Uranium concentrations in stream sediments are elevated in or adjacent to several granitoid bodies, as well as along faults in shale in the upper Meilleur River drainage basin (Fig. 7).

Average concentrations of uranium from a number of different sources are listed in Reimann and Caritat (1998) and provide a general idea of the differences in chemical composition of major rock types. Granitic/granodioritic rocks have relatively higher concentrations of uranium (4 ppm) than shale (3.2 ppm), sandstone (1.3 ppm), or limestone (1 ppm). The median concentration of U in stream sediments within the survey area analysed by Instrumental Neutron Activation analysis (INAA) is 4 ppm. Rose (1994) reports that values of less than 33 ppm uranium in stream sediments can be anomalous around magmatic-associated uranium deposits where background in stream sediment is 4 ppm.

Uranium concentrations in stream sediments exceeding ten times the median value of 4 ppm (INAA) in all stream sediments are shown in or adjacent to the O'Grady, Coal River, and Hole-in-the-Wall batholiths (Fig. 7). The highest value of uranium in stream sediment (157 ppm) is from Bologna Creek, draining a granitoid unit and in the same area as the above-noted shale-hosted uranium showing (Fig. 7).

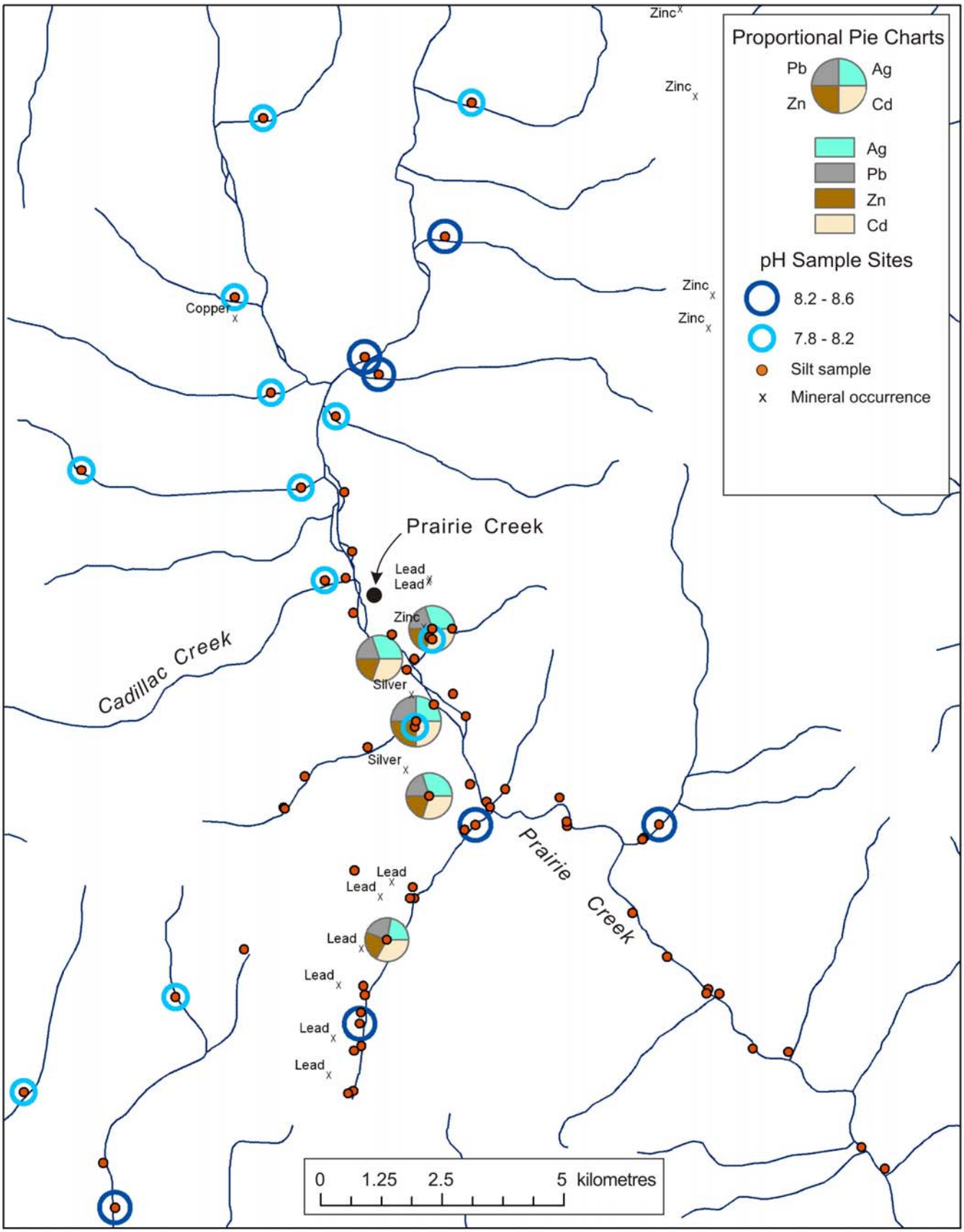


Figure 6. Multi-element plot of Ag-Pb-Zn-Cd around Prairie Creek, showing pH values of stream waters at sites sampled adjacent to the deposit.

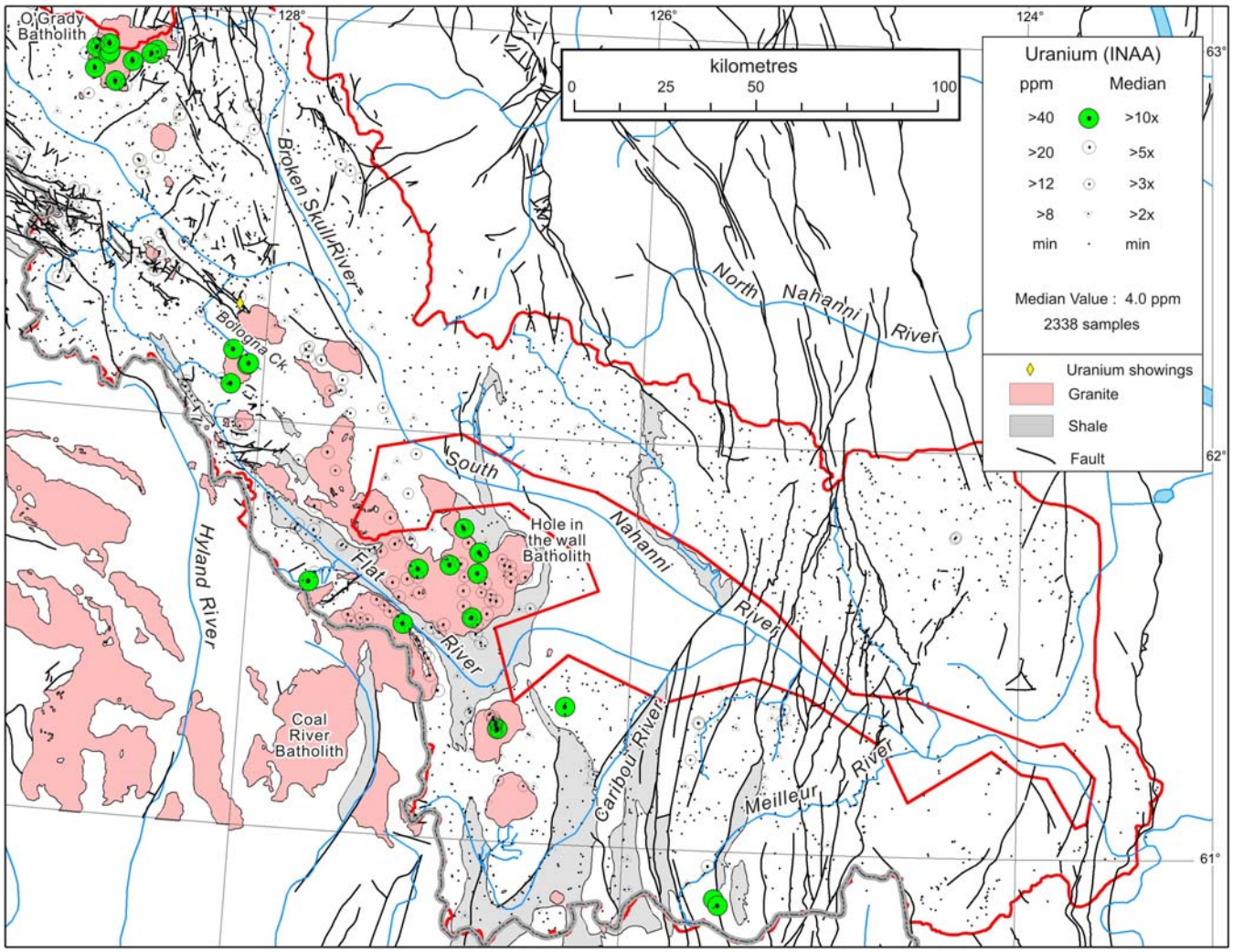


Figure 7. Uranium concentrations in stream sediments determined by Instrumental Neutron Activation analysis.

Elevated thorium values greater than five times the median value of 8.5 ppm (INAA) are associated with uranium over and adjacent to granitoid units. For deposits associated with magmatic rocks, thorium (usually in monazite) in stream sediment is a useful pathfinder element (Rose, 1994) that can suggest the presence of vein uranium. Uranium is relatively mobile in alkaline environments and can be extensively leached in oxidizing conditions, whereas thorium is immobile in most environments (Plant and Raiswell, 1994).

Uranium is not associated with thorium in the Meilleur River catchment basin. However, Mo, V, and Ni are associated with elevated values of uranium in stream sediments from this area. Elevated concentrations follow faults in Ordovician Road River shale, and are consistent with geochemical dispersion around uranium deposits with sedimentary and hydrothermal or groundwater associations (Rose, 1994) and with phosphatic uranium.

Gold

The NORMIN.DB (NORMIN records in this paper are from Department of Indian Affairs and Northern Development, 2001) lists ten placer- and one lode-gold showings within the boundaries of the survey area. Seven of these showings fall within the catchment basin of the Caribou River (Fig. 8). Most of these are placer showings on Selena Creek. Placer gold has also been reported on Bennett Creek (O95ESE0007) and McLeod Creek (095ESE0008). Lode gold is reported in basaltic volcanic rocks of the Sekwi Formation (095DNE0008: Chuck 1; Fig. 8).

All of these placer-gold showings are interpreted as derived from nearby lode-gold deposists (Rasmussen et al., 2007). Concentrations of gold exceeding ten times the median concentration (INAA) are present in stream sediments collected from a tributary of Hell Roaring Creek (Fig. 8) but the absence of other elevated elements in these samples suggests a more distal placer origin for these sites. Numerous placer gold-only showings were identified in eastern parts of the greater

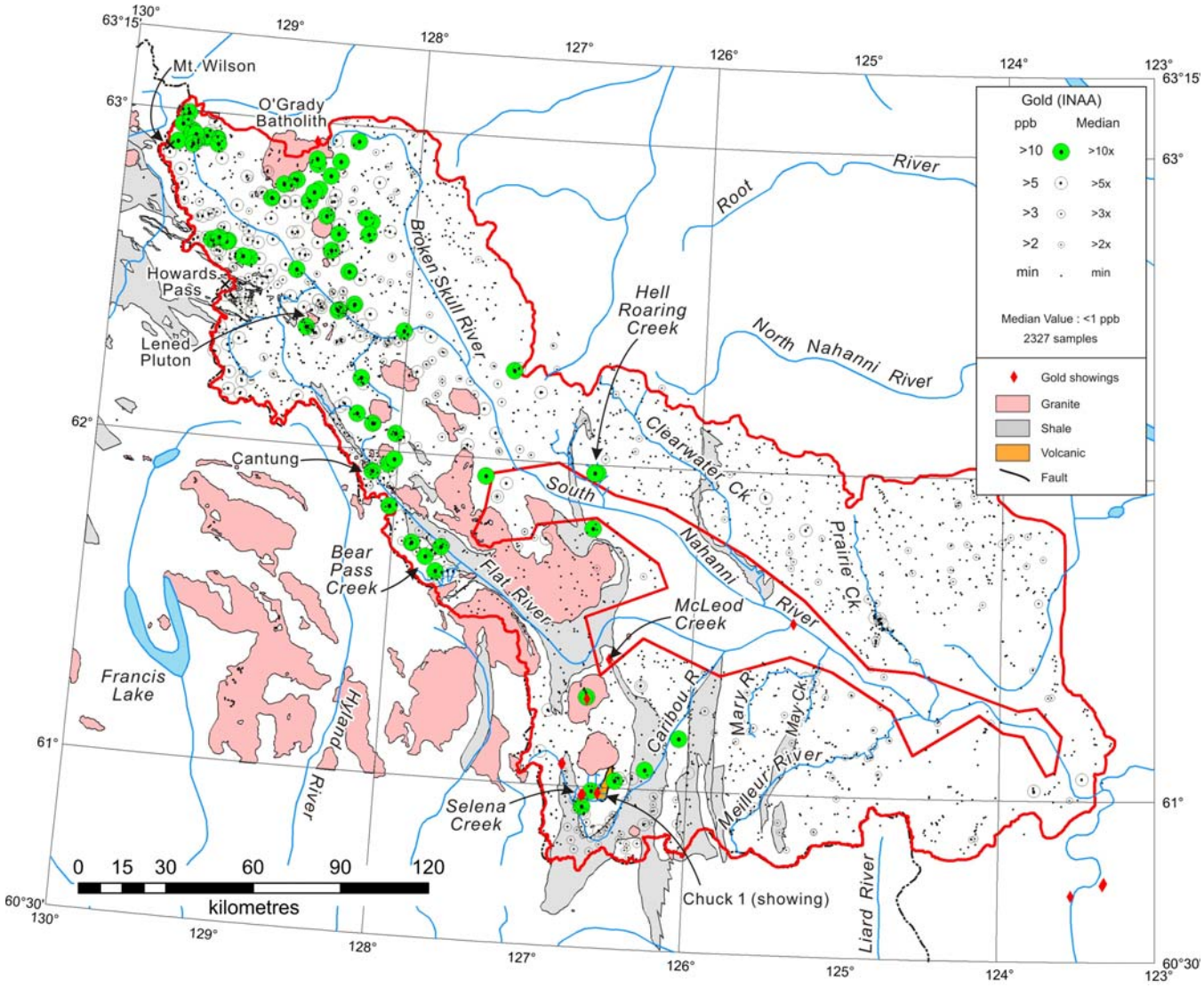


Figure 8. Gold concentrations in stream sediments determined by Instrumental Neutron Activation analysis.

Nahanni watershed by study of heavy mineral concentrations in coarse and fine fractions of stream sediments by Jefferson and Paré (1991) and Spirito and Jefferson (2003). They interpreted these as of distal Canadian Shield origin, reaffirmed by Rasmussen et al. (2007).

Gold concentrations in stream sediments are elevated relative to the total population throughout the intersection of the Tintina Gold Province (Rasmussen et al., 2006) and the proposed park extension. Areas of interest are suggested by concentrations of gold in stream sediment (determined by INAA) exceeding ten times the median value of 1 ppb, and include the upper headwaters and tributaries of the Broken Skull River and South Nahanni River, part of a zone of elevated gold values between the O'Grady Batholith and the Lened pluton. Gold is also elevated in stream sediments around Mt. Wilson, Howards Pass, Cantung, and Bear Pass Creek (Fig. 8).

Multi-element plots suggest several different styles of gold mineralization, and that a variety of different elements in addition to Au can be used as pathfinder elements for gold, including Ag, As, Bi, Cd, Cu, Hg, Mo, Sb, W, and U. The combination of Ag-As-Au-Sb highlights anomalies around Mt. Wilson, between the O'Grady Batholith and the Lened pluton, and around Bear Pass Creek (Fig. 9A) and is consistent with geochemical dispersion around sediment-hosted gold mineralization (Plant and Tarney, 1994). Boyle (1974) observed that these elements are associated with 'quartz veins, irregular bodies, saddles, and stockworks; quartz-sulphide veins and impregnation zones; silicified and pyritized zones; and disseminated gold-sulphide zones.' The combination of As-Au-Bi is elevated in stream sediments around Bear Pass Creek (Fig. 9B) and is characteristic of skarn gold mineralization (Ray, 1998).

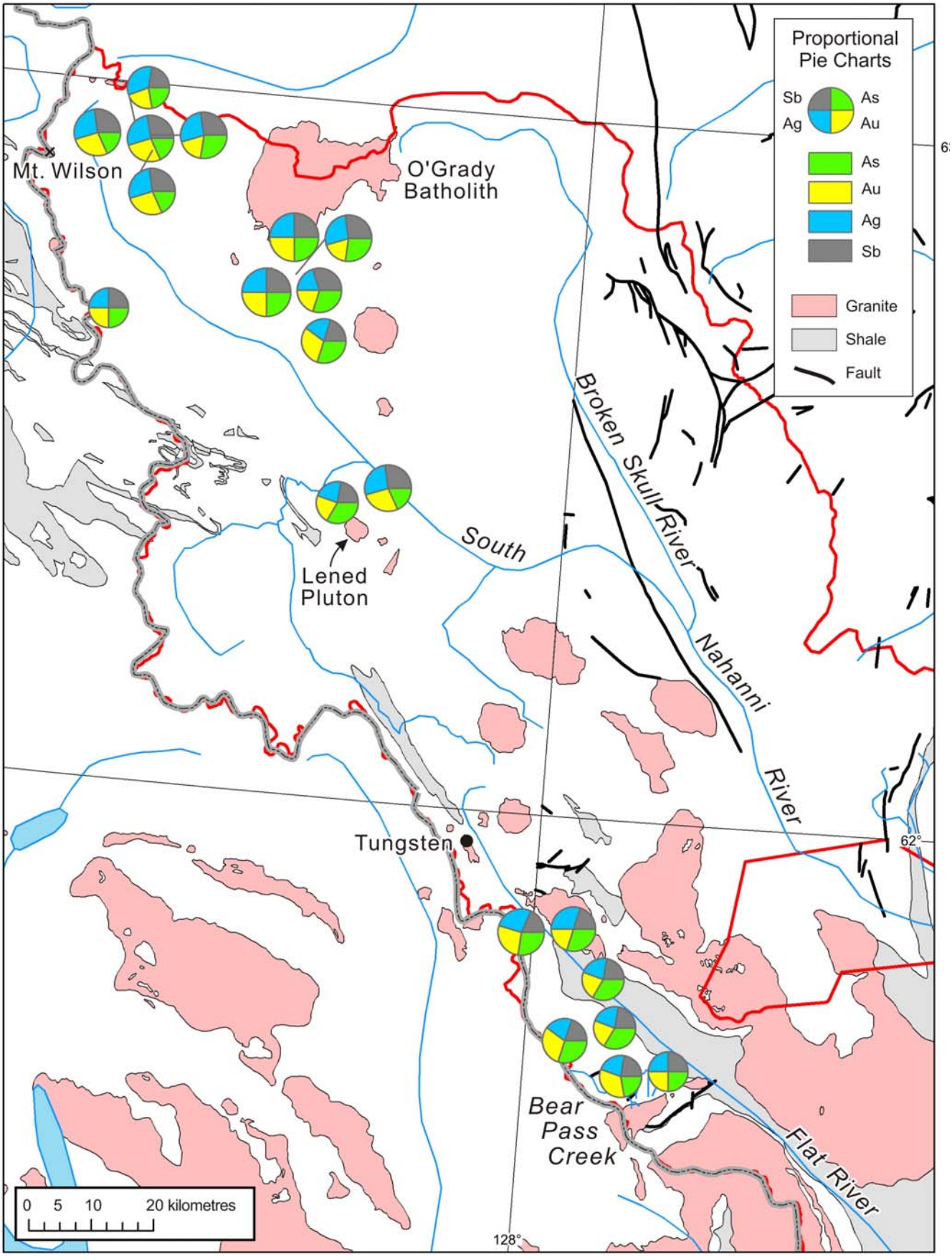


Figure 9. A) Multi-element proportional pie plots of Au and As-Ag-Sb showing sites where the concentrations of all of these elements are greater than five times their median value.

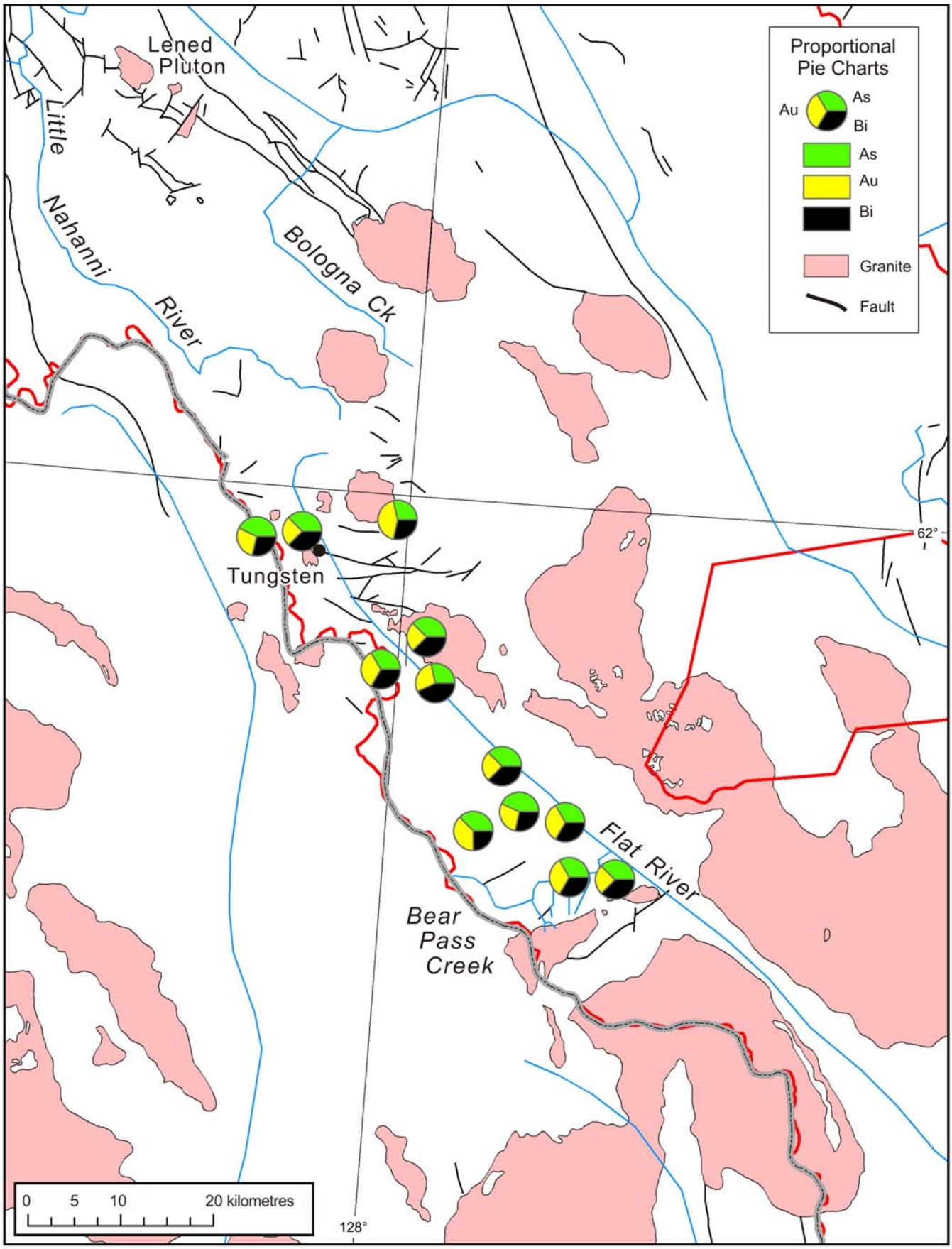


Figure 9 continued. B) Multi-element proportional pie plots of Au and As-Bi, representing sites where the concentrations of all of these elements are greater than five times their median value. .

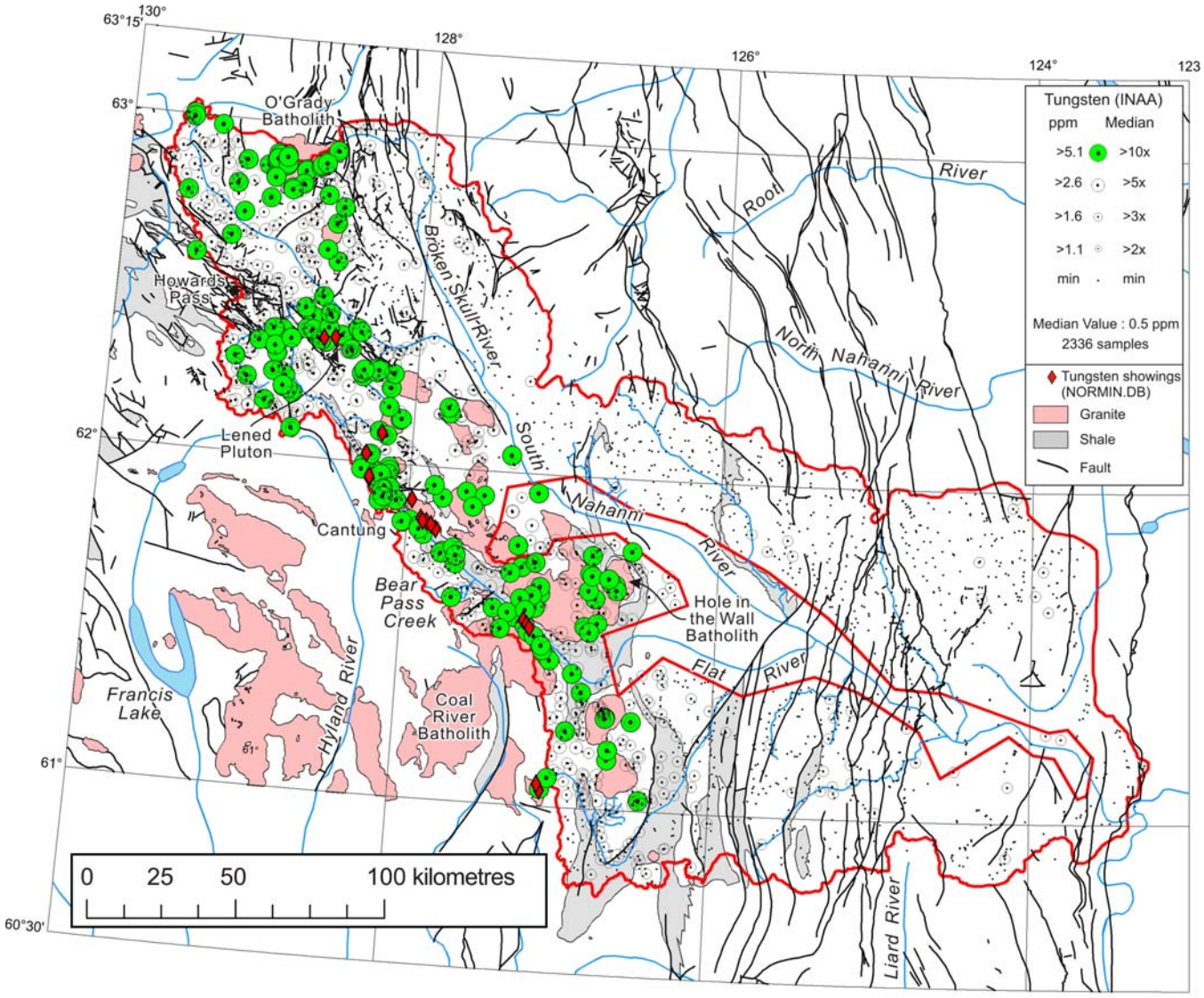


Figure 10. Tungsten concentrations in stream sediments determined by Instrument Neutron Activation analysis.

Tungsten

NORMIN.DB records 17 showings within the survey area listing tungsten as a primary commodity (Fig 10). Within this group are the Cantung mine, currently in production, located near the headwaters of the Flat River (NORMIN.DB 105HNE0006), and the Lened showing (Fig. 10), 50 km north of Tungsten, Northwest Territories, with estimated resources of 907,180 tonnes grading 1.0% WO_3 (NORMIN.DB 105ISE0003). Other areas with recorded showings are located 40 to 80 km southeast of Cantung. Showings are also present in the drainage basin of the Caribou River and southeast of Bear Pass Creek, along the Flat River (Fig. 10). In all cases, the mineralization is noted in skarn, and in all cases locations are recorded around the margins of mid-Cretaceous granitic to granodioritic intrusions of the Tintina Gold Province (Rasmussen et al., 2006).

Elevated values of tungsten (more than ten times the median value of 0.5 ppm in stream sediments by INAA, Fig. 10) fall entirely within the intersection of the Nahanni MERA study area and the Tintina Gold Province (Rasmussen et al., 2006) and, except for a cluster of elevated values west of the Lened showing, are found proximal to mapped intrusions. Geochemical response of tungsten around known occurrences is robust, indicating that tungsten itself can be used as a geochemical pathfinder despite the relative immobility of tungsten in most natural environments (Plant and Raiswell, 1994). Tungsten is also anomalous in spring waters of the Rae region (Hamilton et al., 2003). Areas with anomalous tungsten not near known occurrences include the O'Grady Batholith, Mt. Wilson, and the area west of the Lened showing noted above. In addition, there is further potential for tungsten around the margins of two large plutons, the Hole-in-the-Wall and Coal River batholiths (Fig. 10).

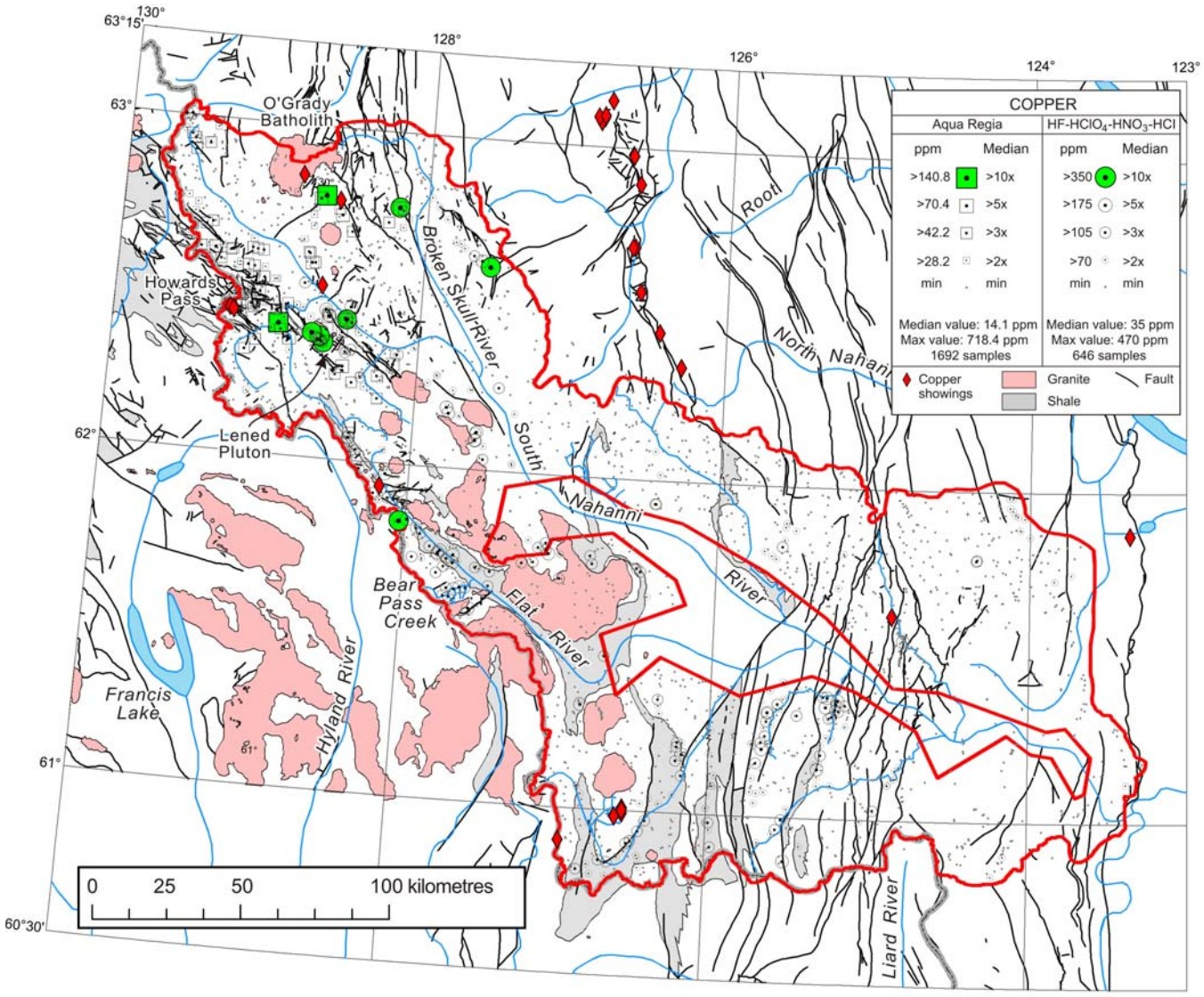


Figure 11. Single-element plot of copper in stream sediments. It is important to note that copper data published in GSC Open File 4016 (Friske et al., 2001; Fig. 1) were obtained using HF-HCl0_4-HNO_3-HCl to decompose samples, a 'near-total' digestion. All other samples were decomposed using aqua regia (HCl-HNO_3), a 'partial' digestion. See Appendix 1 for details.

Anomalous tungsten is generally associated with anomalous uranium in the vicinity of intrusive bodies and can be effectively used to delineate the margins of intrusions. Bismuth is associated with tungsten occurrences in the survey area (correlation coefficient for all sites is equal to 0.9) and a multi-element combination of W-U-Bi can be used to expand potential areas of interest. Other possible pathfinder elements include As, Cd, and Sn. In stream sediment, Cu is elevated around the Lened pluton and As is elevated in streams draining the Cantung deposit. Geochemical dispersion of Mo, sometimes used as a pathfinder for W skarns (Ray, 1995a), appears to be limited in the survey area.

Copper

Copper is listed as a primary commodity within the boundaries of the survey area at thirteen showings, including the deposits at Prairie Creek and Howards Pass as well as adjacent to Cantung along the north shoreline of the South Nahanni River, and in showings at the margins of the O'Grady Batholith (Fig. 11).

Copper values are elevated around the Lened pluton and north and southeast of Howards Pass (Fig. 11). Elevated Ag-Cd-Cu-Pb-Zn throughout these areas is consistent with geochemical dispersion around sediment-hosted Cu±Ag (Lefebure and Alldrick, 1996). Copper is essentially immobile in alkaline environments (Plant and Raiswell, 1994) and values from stream sediments collected around Prairie Creek are relatively subdued (Fig. 4).

A multi-element plot of As-Bi-Sb-W (Fig. 12A), which is consistent with geochemical dispersion around skarn copper showings (Ray, 1995b), suggests

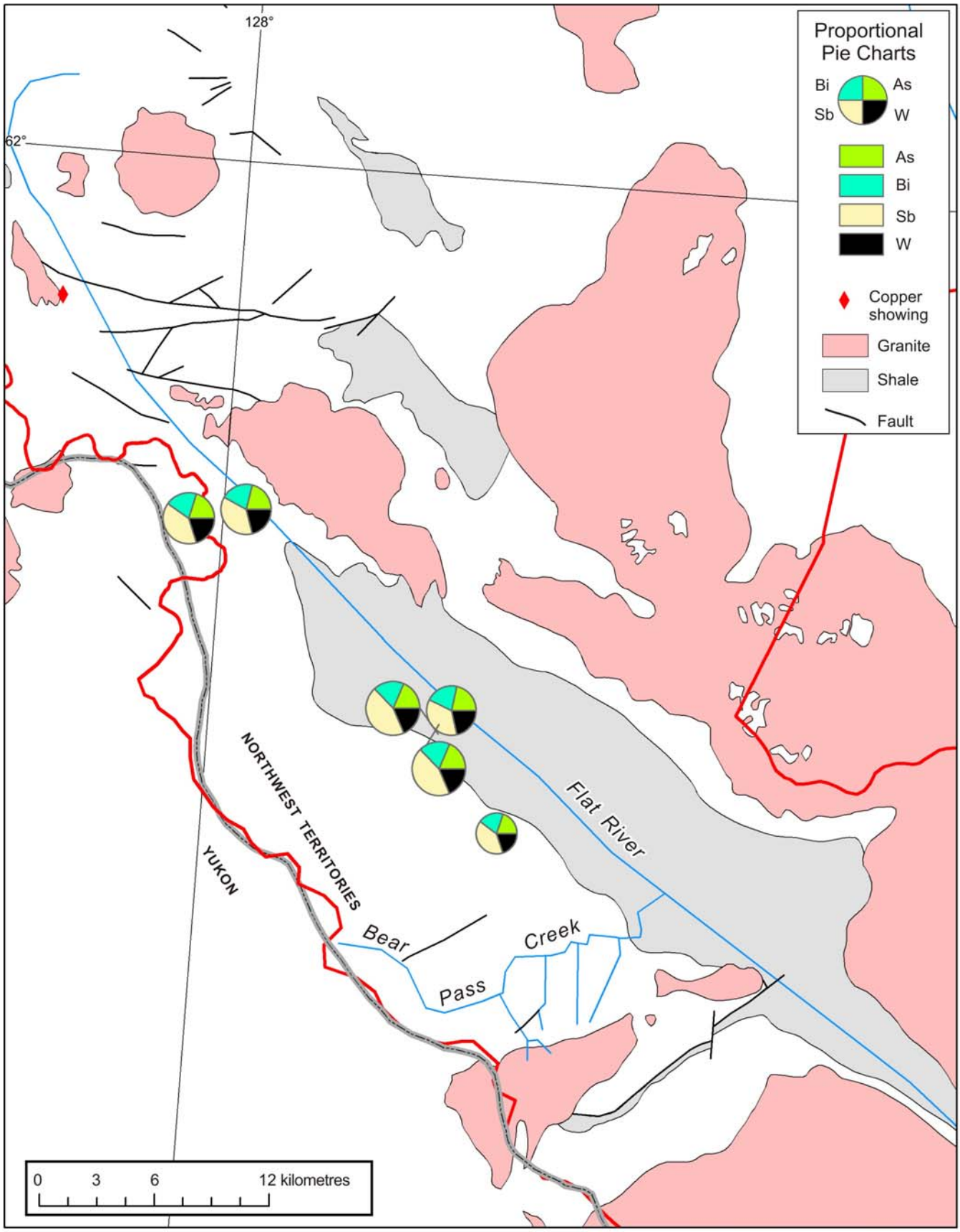


Figure 12. A) Multi-element plot of As-Bi-Cd-W. Dots represent sites where the concentrations of all of these elements are greater than five times their median value.

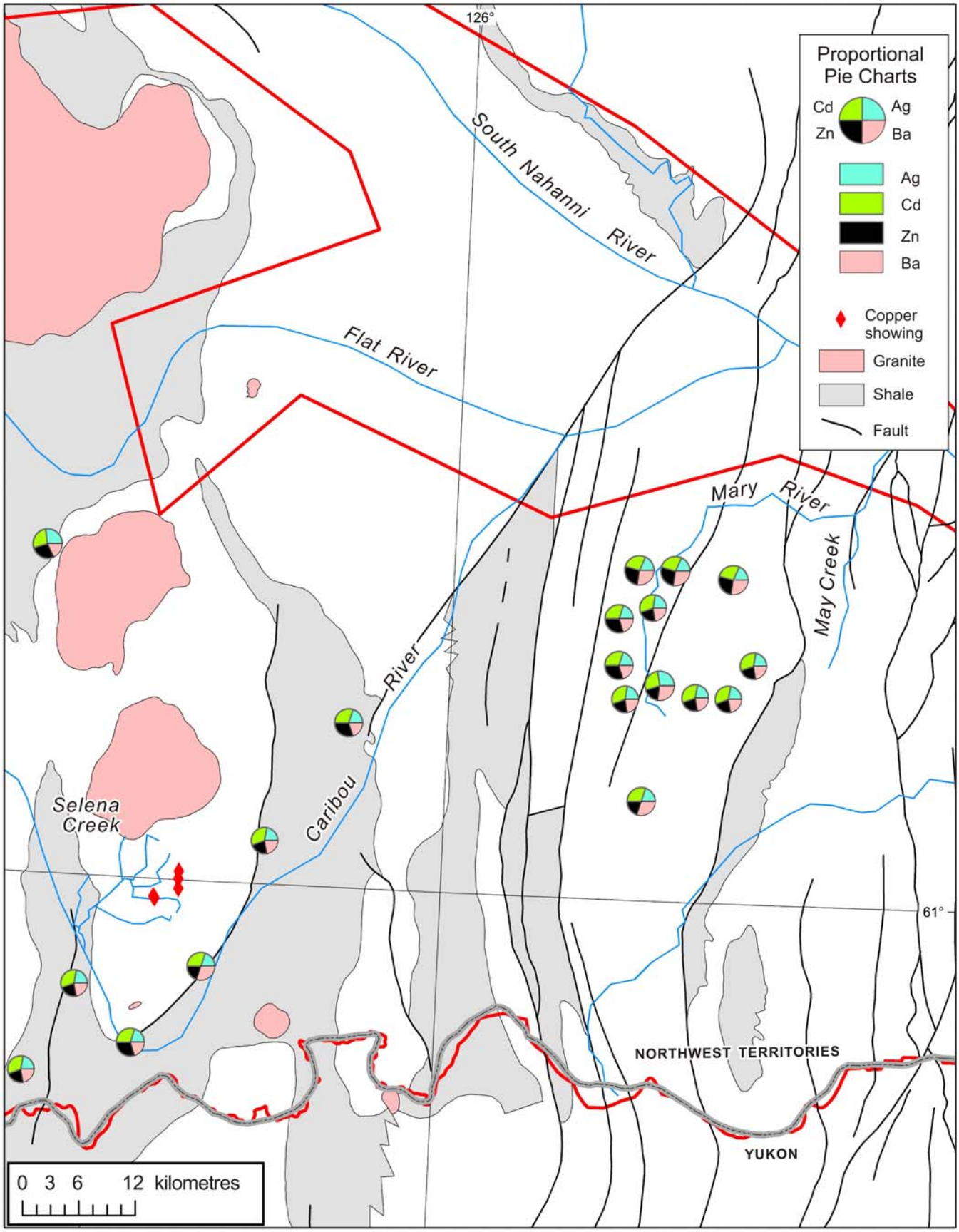


Figure 12 continued. B) Multi-element plot of Ag-Ba-Cd-Zn.

potential areas for further exploration north of Bear Pass Creek on the Flat River.

Copper values in stream sediments from the Caribou River headwaters are subdued, possibly due to alkaline stream waters. A multi-element plot of Ag-Ba-Cd-Zn (Fig. 12B) does highlight this area, as well as the upper reaches of the Mary River. This geochemical signature is not inconsistent with some types of sedimentary exhalative copper mineralization (Lydon, 1996).

DISCUSSION

Regional stream sediment surveys are used to quickly and economically evaluate mineral potential over large areas. Within the limits set by sample density, approximately one sample per 13 km^2,potential areas of mineralization are reduced to the size of the drainage basins of first-order (primary) or second-order (secondary) streams. Although the area for exploration is narrowed considerably, even a primary stream a few kilometres in length can drain a considerable area.

Recognizing the limits of a regional geochemical survey is an important factor to consider when interpreting data. To go beyond establishing in general the mineral potential of an area, it is necessary to understand how climate (including glacial history), physiography, surficial and bedrock geology, biology, and anthropogenic activity can affect element concentrations in stream sediments.

This study took a very simple numerical approach to statistical analysis and did not attempt to quantitatively adjust anomalous thresholds based on the proportion of rock types in the catchment basins. The MERA 1 study by Spirito et al. (2003) demonstrated how such quantitative analysis in a GIS provides a greater understanding of anomalies related to dominant bedrock type, but was based on a low density of sample sites and with slightly different analytical standards. The present study has a sample density and analytical methods that are consistent with national standards. The ideal would be to combine the methods of Spirito et al. (2003) with the complete data set of this study.

The regional geochemistry of the study area indicates that elevated concentrations of many elements, including U and W and to a lesser extent Ag, Au, Cu, and Zn, are associated with the granitic intrusive rocks in the western part of the survey area, from Mt. Wilson in the north to the Caribou River in the south. Elevated concentrations of Zn, Cu, and Ag are also associated with black shale, particularly the Ordovician Road River shale around Howards Pass and in the Mary River and Meilleur River drainage basins in the southern part of the survey area.

Concentrations of most elements of economic significance are generally low throughout the carbonate and dolomite rocks of the northeastern part of the survey area, with the exception of Prairie Creek. However, the mobility of most metals in alkaline surficial environments is restricted, and this may be a significant factor in the low concentrations of many elements in stream sediments in areas underlain by carbonates.

Whereas much of the mineral potential highlighted by stream sediment geochemistry is in areas of known showings, the geochemistry of the Caribou and Meilleur River drainage basins suggest that there are as yet undiscovered occurrences in these areas as well.

ACKNOWLEDGEMENTS

We would like to acknowledge the considerable assistance from many individuals who have helped us over the course of this project. In 2004, accommodations in the field were provided at the Canadian Zinc Corporation's Prairie Creek facility, under the direction of Alan Taylor and Dave Hart. Field assistance in 2004 was provided by Sarah Morgan, and Laurie Fichter. Doug Hladun, Trans-North Helicopters (Whitehorse, YT) was our pilot. In 2005, accommodation was provided at the North American Tungsten Corporation's Cantung mine site. Field assistance was provided by Alain Grenier, Jessica Jumbo, and Ryan Wilson. Glen Sibbeston, flying for Great Slave Helicopters, was our pilot.

We would very much like to thank Sue Davis for her assistance with the figures that accompany this report, and R.G. Garrett, for his expert review of the original manuscript.

REFERENCES

Boyle, R.W.
1974: Elemental Associations in Mineral Deposits and Indicator Elements of Interest in Geochemical Prospecting (revised); Geological Survey of Canada, Paper 74-45, 40 p.

Day, S.J.A., Lariviere, J.M., Friske, P.W.B., Gochnauer, K.M., MacFarlane, K.E., McCurdy M.W., and McNeil, R.J.
2005: National Geochemical Reconnaissance (NGR): Regional Stream Sediment and Water Geochemical Data, Macmillan Pass –Sekwi Mountains, Northwest Territories; Geological Survey of Canada, Open File 4949, 1 CD-ROM.

Department of Indian Affairs and Northern Development (DIAND)
2001: NORMIN.DB The Northern Minerals Database; Northwest Territories Geoscience Office, Yellowknife, Northwest Territories.

Duk-Rodkin, A.
2005: Quaternary geology and glacial limits of southern Mackenzie Mountains and foothills; American Geophysical Union, Fall Meeting 2005, Abstract #PP11B-1471.

Ecological Stratification Working Group
1995: A National Ecological Framework for Canada; Agriculture and Agri-Food Canada, Research Branch, Centre for Land and Biological Resources Research and Environment Canada, State of the Environment Directorate, Ecozone Analysis Branch, Ottawa/Hull. Report and national map at 1:7 500 000 scale.

Friske, P.W.B., McCurdy, M.W., and Day, S.J.A.
2001: Regional stream sediment and water geochemical data, eastern Yukon and western Northwest Territories; Geological Survey of Canada, Open File 4016, 1 CD-ROM.

Garrett, R.G.
1974: Field Data Acquisition Methods for Applied Geochemical Surveys at the Geological Survey of Canada; Geological Survey of Canada, Paper 74-52, 36 p.

Goodfellow, W.D.
1982: Regional Stream Sediment and Water Geochemistry of the Nahanni Map Area (NTS 105I), Yukon and N.W.T; Geological Survey of Canada, Open File 868, 157 p.

Gordey, S. and Anderson, R.G.
1993: Evolution of the Northern Cordilleran Miogeocline, Nahanni Map Area (105I), Yukon and Northwest Territories; Geological Survey of Canada Memoir 428, 214 p.

Hall, G.E.M.
1991: Analytical methods used in exploration geochemistry; Exploration Geochemistry Workshop, Geological Survey of Canada, Open File 2390, p. 8-1 - 8-90.

Hamilton, S.M., Michel, F.A., Jefferson, C.W., and Power-Fardy, D.
2003: Spring water geochemistry and hydrogeology for mineral resource assessment of the South Nahanni River Region, in Non-Renewable Mineral and Energy Resource Potential of the Proposed Extensions to Nahanni National Park Reserve, Northern Cordillera, Northwest Territories, (ed.) C.W. Jefferson, and W. Spirito; Geological Survey of Canada, Open File 1686, p. 5-1 to 5-40.

Jackson, L.E.
1987: Terrain Inventory and Quaternary History of Nahanni Map Area, Yukon Territory and Northwest Territories; Geological Survey of Canada, Paper 86-18, 23 p.

Jefferson, C.W. and Paré, D.
1991: New placer gold anomalies in the northern Liard Range - southern Ram Plateau area, South Nahanni River Region, District of Mackenzie, N.W.T., *in* Current Research, Part E; Geological Survey of Canada, Paper 91-1E, p. 1-4.

Jefferson, C.W. and Spirito, W.A. (ed.)
2003: Mineral and Energy Resource Assessment of the Tlogotsho Plateau, Nahanni Karst, Ragged Ranges and Adjacent Areas Under Consideration for Expansion of Nahanni National Park Reserve, Northwest Territories; Geological Survey of Canada, Open File 1686, 528 p.

Lefebure, D.V. and Alldrick, D.J.
1996: Sediment-hosted Cu±Ag±Co, *in* Selected British Columbia Mineral Deposit Profiles, Volume 2 – Metallic Deposits, (ed.) D.V. Lefebure and T. Hoy; British Columbia Ministry of Employment and Investment, Open File 1996-13, p. 13-16.

Lydon, J.W.
1996: Sedimentary exhalative sulphides (Sedex), *in* Geology of Canadian Mineral Deposit Types, (ed.) O.R. Eckstrand, W.K. Sinclair, and R.I. Thorpe; Geological Survey of Canada, Geology of Canada, no. 8, p. 130-152 (also Geological Society of America, The Geology of North America, v. P-1).

MacIntyre, D.
1995: Sedimentary exhalative Zn-Pb-Ag, *in* Selected British Columbia Mineral Deposit Profiles, Volume 1 – Metallics and Coal, (ed.) D.V. Lefebure and G.E. Ray; British Columbia Ministry of Energy of Employment and Investment, Open File 1995-20, p. 37-39.

Okulitch, A.
in prep a: Geology of the Redstone River Area; National Earth Science Series, Geological Atlas, National Resources Canada, Map NP-9/10-G, scale 1:1 million.

in prep b: Geology of the Ross River Area; National Earth Science Series, Geological Atlas, National Resources Canada, scale 1:1 million.

Ottesen, R.T. and Theobald, P.K.
1994: Stream sediments in mineral exploration, *in* Drainage Geochemistry, (ed.) M. Hale and J.A. Plant; Handbook of Exploration Geochemistry, v. 6, Elsevier Science, p. 147-184.

Plant, J.A. and Raiswell, R.W.
1994: Modifications to the geochemical signatures of ore deposits and their associated rocks in different surface environments, *in* Drainage Geochemistry, (ed.) M. Hale and J.A. Plant; Handbook of Exploration Geochemistry, v. 6, Elsevier Science, p. 73-109.

Plant, J.A. and Tarney, J.
1994: Mineral deposit models and primary rock geochemical characteristics, *in* Drainage Geochemistry, (ed.) M. Hale and J.A. Plant; Handbook of Exploration Geochemistry; v. 6, Elsevier Science, p. 11-72.

Rasmussen, K.L., Mortensen, J.K., and Falck, H.
2006: Geochronological and lithogeochemical studies of intrusive rocks in the Nahanni region, southwestern Northwest Territories and southeastern Yukon, *in* Yukon Exploration and Geology 2005, (ed.) D.S. Emond, G.D. Bradshaw, L.L. Lewis, and L.H. Weston; Yukon Geological Survey, p. 287-298

2007: The potential for intrusion-related mineralization within the South Nahanni River MERA area, Selwyn and Mackenzie Mountains, Northwest Territories, *in* Mineral and Energy Resource Potential of the Proposed Expansion to the Nahanni National Park Reserve, North Cordillera, Northwest Territories, (ed.) D.F. Wright, D. Lemkow, and J. Harris; Geological Survey of Canada, Open File 5344, p. 203-244.

Ray, G.E.
1995a: W skarns, *in* Selected British Columbia Mineral Deposit Profiles, Volume 1 – Metallics and Coal, (ed.) D.V. Lefebure and G.E. Ray; British Columbia Ministry of Energy, Employment and Investment, Open File 1995-20, p. 71-74.

1995b: Cu skarns, *in* Selected British Columbia Mineral Deposit Profiles, Volume 1 – Metallics and Coal, (ed.) D.V. Lefebure and G.E. Ray; British Columbia Ministry of Energy, Employment and Investment, Open File 1995-20, p. 59-60.

1998: Au skarns, *in* Geological Fieldwork 1997; British Columbia Ministry of Employment and Investment, Paper 1998-1, p. 24H-1 to 24H-4.

Reimann, C. and de Caritat, P.
1998: Chemical Elements in the Environment: Factsheets for the Geochemist and Environmental Scientist; Springer-Verlag, Berlin, 398 p.

Rose, A.W.
1994: Drainage geochemistry in uranium exploration, *in* Drainage Geochemistry, (ed.) M. Hale and J.A. Plant; Handbook of Exploration Geochemistry, v. 6, Elsevier Science, p. 559-599.

Spirito, W.A. and Jefferson, C.W.
2003: Regional surficial geochemistry, in Non-Renewable Mineral and Energy Resource Potential of the Proposed Extensions to Nahanni National Park Reserve, Northern Cordillera, Northwest Territories, (ed.) C.W. Jefferson and

W. Spirito; Geological Survey of Canada, Open File 1686, p. 4-1 to 4-79.

Stanton, R.E.
1966: Rapid Methods of Trace Analysis for Geochemical Applications; Edward Arnold (Publishers) Ltd., London, 96 p.

Wheeler, J.O., Hoffman, P.F., Card, K.D., Davidson, A., Sanford, B.V., Okulitch, A.V., and Roest, W.R.
1996: Geological map of Canada; Geological Survey of Canada, A Series Map 1860A, 1996; Scale 1: 5 000 000, 2 sheets.

Wilhelm, E. and Artignan, D.
1994: Drainage geochemistry in young folded mountain belts, *in* Drainage Geochemistry, (ed.) M. Hale and J.A. Plant; Handbook of Exploration Geochemistry, v. 6, Elsevier Science, p. 415-444.

APPENDIX 1. SAMPLE COLLECTION, ANALYTICAL TECHNIQUES, AND LABORATORIES

Stream Silts and Waters, 1981 (Goodfellow, 1982)

Collection Procedures and Sample Management

Stream sediment and water samples at 984 sites were collected at an average density of one sample per 12 km^2 throughout the 11,489 km^2 comprising the Nahanni map sheet (NTS 105I). For the purposes of sampling, preparation, and analytical control, sample numbers were divided into blocks of twenty, each block consisting of seventeen routine samples, one field duplicate, one blind duplicate, and one control reference standard. Further details can be obtained from Garrett (1974).

At GSC laboratories in Ottawa, field-dried stream sediment samples were air dried, sieved to minus 80 mesh (177 μm) and ball-milled to minus-150 mesh. Control reference and blind duplicate sample positions were filled during sample preparation. In the case of stream waters, the control reference positions were filled in the field with one of three control standards collected near base camp. The blind duplicates for stream waters were left blank.

Analytical Procedures

Stream Waters

The pH of stream waters was determined using a Radiometer TTT 81 digital pH meter.

Stream Sediments

Zn, Cu, Pb, Ni, Co, Ag, Cd, Mn, Fe, Mo, and V were determined by atomic absorption spectrophotometry after decomposition with a multi-acid total digestion. A 500 mg sample was leached over a period of four hours using a 5 ml aliquot of HF-HCl-HNO_3-$HClO_4$ (ratio 1:1:1:1). A final solution of 5% HCl was made up to a volume of 20 ml. All elements, with the exception of Mo, were atomized using an air-acetylene flame: a nitrous oxide-acetylene flame and a 1000 ppm Al solution as ionization buffer were used for Mo analyses. Background corrections were made on Ni, Cd, Ag, Pb, and Mo analyses.

F was determined using an ion selective electrode and total ionic strength adjustment buffer (TISAB). A 500 mg sample was fused with Na_2O_3-KNO_3 (9:1) at 800ºC for 10 minutes.

Ba was analysed by X-ray fluorescence using pressed powder disks.

A colourimetric method was used to determine the concentration of W in stream sediments. The sample was fused at 800ºC in nickel crucibles along with a mixture of Na_2CO_3, NaCl and $KN0_3$ (5:4:1) and the residue dissolved, with heating, in water. After cooling, an aliquot of this solution was mixed with stannous chloride, heated, and dithiol solution (zinc dithiol, hydrochloric acid, iso-amyl acetate) added. The solution was cooled and white spirit, a paraffin-derived organic

Table A-1. Summary of analytical data and methods for sediments.

ELEMENT	DETECTION	METHOD
SEDIMENTS		
Ag Silver	0.2 ppm	AAS
As Arsenic	0.4 ppm	HY-AAS
As Arsenic	0.5 ppm	INAA
Au Gold	2 ppb	INAA
Ba Barium	0.02 pct	XRF
Ba Barium	50 ppm	INAA
Br Bromine	0.5 ppm	INAA
Cd Cadmium	0.2 ppm	AAS
Ce Cerium	5 ppm	INAA
Co Cobalt	2 ppm	AAS
Co Cobalt	5 ppm	INAA
Cr Chromium	20 ppm	INAA
Cs Caesium	0.5 ppm	INAA
Cu Copper	2 ppm	AAS
Eu Europium	1 ppm	INAA
F Fluorine	20 ppm	ISE
Fe Iron	0.2 pct	AAS
Fe Iron	0.2 pct	INAA
Hf Hafnium	1 ppm	INAA
Hg Mercury	30 ppb	CV-AAS
La Lanthanum	2 ppm	INAA
LOI Loss-on-ignition	1.0 pct	GRAV
Lu Lutetium	0.02 ppm	INAA
Mn Manganese	2 ppm	AAS
Mo Molybdenum	2 ppm	AAS
Na Sodium	0.02 pct	INAA
Ni Nickel	2 ppm	AAS
P_2O_5 Phosphoric anydride	0.04 pct	COL
Pb Lead	2 ppm	AAS
Rb Rubidium	5 ppm	INAA
Sb Antimony	0.4 ppm	HY-AAS
Sb Antimony	0.1 ppm	INAA
Sc Scandium	0.2 ppm	INAA
Sm Samarium	0.1 ppm	INAA
Ta Tantalum	0.5 ppm	INAA
Tb Terbium	0.5 ppm	INAA
Th Thorium	0.2 ppm	INAA
U Uranium	1.0 ppm	NADNC
U Uranium	0.2 ppm	INAA
V Vanadium	20 ppm	AAS
W Tungsten	2 ppm	COL
W Tungsten	1 ppm	INAA
Yb Ytterbium	2 ppm	INAA
Zn Zinc	2 ppm	AAS
AuWt Sample Weight	0.01 g	-

AAS - atomic absorption spectrometry
COL - colorimetric methods
CV-AAS - cold vapour / atomic absorption spectrometry
FUS - fusion
GRAV - gravimetry
HY-AAS - hydride evolution followed by atomic absorption spectrometry
INAA - Instrumental Neutron Activation Analysis
ISE - ion selective electrode
NADNC - neutron activation followed by delayed neutron counting
XRF - x-ray fluorescence

solvent, added. The resulting colour of the solution was compared with a standard series (Stanton, 1966).

P_2O_5 was determined colourimetrically using the H_2SO_4 and ammonium molybdate method after sample decomposition using HNO_3-HCl-$HClO_4$.

Loss-on-ignition (LOI) was recorded as a measure of the weight percent loss of volatiles after igniting a known weight at 450ºC for four hours.

Uranium was determined by neutron activation analysis using delayed neutron counting on a 3 g sample. The flux density used was 2 x 1011 neutrons/cm^2/s to 1 x 1012 neutrons/cm^2/s.

For the determination of As, Sb, and Hg, a 750 ml sample was digested overnight in aqua regia (3 HCl: 1 HNO_3). It was then heated in a water bath for approximately four hours during which time the temperature was raised to 90ºC. The final volume was 15 ml. The hydride of the element was formed with a sodium borohydride reducing agent. Subsequently, As and Sb were measured by atomic absorption spectrophotometry using a silica tube heated to 900ºC. Mercury was determined similarly by measuring Hg vapour atomized in a silica tube heated to 100ºC.

Instrumental Neutron Activation Analysis (INAA)

Weighed and encapsulated samples were packaged for irradiation along with internal standards and international reference materials. Samples and standards were irradiated together with neutron flux monitors in a two megawatt pool-type reactor. After a seven-day decay period, samples were measured on a high-resolution germanium detector. Computer control was achieved with a Microvax II computer. Typical counting times were 500 seconds. Elements determined by INAA include: Ag, As, Au, Ba, Br, Cd, Ce, Co, Cr, Cs, Eu, Fe, Hf, Ir, La, Lu, Mo, Na, Ni, Rb, Sb, Sc, Se, Sm, Sn, Ta, Tb, Te, Th, U, W, Yb, Zn, and Zr. The sample weights were also reported. Data for Ag, Cd, Ir, Mo, Ni, Se, Sn, Te, Zn, and Zr were not published because of inadequate detection limits and/or precision.

Table A-1 provides a summary of lower detection limits and methods for elements determined in stream sediments.

MERA 1 Stream Silts 1985, 1986, and 1987; MERA 2 Stream Silts and Waters 2004 and 2005 and NGR Stream Silts and Waters 2004 (Day et al, 2005)

Sample Collection

Stream Sediments (Silts)

At each site a prelabelled Kraft paper bag (12.5 cm x 28 cm with side gusset) (Fig. A-1) was two-thirds filled with silt or fine sand collected from the active stream channel. In practice, the silt sample was collected after water samples were collected. Commonly, the sampler collected handfuls of silt from various points in the active stream channel while moving gradually upstream, normally over a distance of 5 to 15 m. If the stream channel consists mainly of clay, coarse material, or organic sediment from which suitable sample material is scarce or absent, moss mat from the stream channel, which commonly contains trapped silt, may be added to the sample. A field duplicate pair of silt samples, assigned sequential sample numbers, is collected within each block of 20 samples. The first sample of the pair is assigned a replicate status value of 10 and the second is assigned a replicate status value of 20. Routine (nonduplicate) field samples are assigned replicate status values of 0.



Figure A-1. Pre-labelled Kraft paper bags and plastic bottles were used to collect samples of stream silts and stream waters. Flagging tape with a sample site number was used to mark sample sites. Field observations were noted on preprinted water-resistant paper.

Stream Waters

Waters were sampled in midchannel, from flowing water where possible. At each site, water was collected in a 125-ml Nalgene high-density polyethylene bottle. Samples were collected after first rinsing bottles at least two times in flowing water before a final fill. Field duplicate pairs of water samples, assigned sequential sample numbers, were collected within each block of 20 samples. The first sample of each pair was assigned a replicate status value of 10 and the second was assigned a replicate status value of 20. Routine (nonduplicate) field samples were assigned replicate status values of 0.

Sample Preparation

Stream Sediments (Silts)

The Kraft paper bags containing the silt samples were placed into plastic bags, taped with electrical tape, and shipped directly to a commercial lab where they were

Table A-2. Elements in stream sediments determined by Instrumental Neutron Activation analysis.

ELEMENT	DETECTION
As Arsenic	0.5 ppm
Au Gold	2 ppb
Ba Barium	50 ppm
Br Bromine	0.5 ppm
Ce Cerium	5 ppm
Co Cobalt	5 ppm
Cr Chromium	20 ppm
Cs Cesium	0.5 ppm
Eu Europium	1 ppm
Fe Iron	0.2 pct
Hf Hafnium	1 ppm
La Lanthanum	2 ppm
Lu Lutetium	0.2 ppm
Mo Molybdenum	1 ppm
Na Sodium	0.02 pct
Ni Nickel	10 ppm
Rb Rubidium	5 ppm
Sb Antimony	0.1 ppm
Sc Scandium	0.2 ppm
Sm Samarium	0.1 ppm
Ta Tantalum	0.5 ppm
Tb Terbium	0.5 ppm
Th Thorium	0.2 ppm
U Uranium	0.2 ppm
W Tungsten	1 ppm
Yb Ytterbium	2 ppm

air-dried at temperatures below 40ºC and sieved through a minus 80 mesh (177 µm) screen. Control reference and duplicate samples were inserted into each block of twenty sample numbers.

Analytical Procedures

Stream Sediment (Silt) Analyses

Instrumental Neutron Activation Analysis (INAA)

Weighed and encapsulated samples, normally 30 g, were packaged for irradiation along with internal standards and international reference materials. Samples and standards were irradiated together with neutron flux monitors in a two-megawatt pool-type reactor. After a seven-day decay period, samples were measured with a high-resolution germanium detector. Typical counting times were 500 seconds. Elements determined by INAA are listed in Table A-2.

INAA data for Ag, Cd, Ir, Se, Sn, Te, Zn, and Zr were not published because of inadequate detection limits and/or precision.

Inductively Coupled Plasma Mass Spectrometry (ICP-MS) and Other Analyses

For determination of the 36 elements listed in Table A-3, a 1 g sample was leached with 6 ml of a mixture

Table A-3. Variables in stream silts determined by Inductively Coupled Plasma - Mass Spectrometry and other analytical methods.

VARIABLE	DETECTION LEVEL
Ag Silver	2 ppb
Al Aluminum	0.01 pct
As Arsenic	0.1 ppm
Ba Barium	0.5 ppm
Bi Bismuth	0.02 ppm
Ca Calcium	0.01 pct
Cd Cadmium	0.01 ppm
Co Cobalt	0.1 ppm
Cr Chromium	0.5 ppm
Cu Copper	0.01 ppm
F Fluorine (fusion/ion selective electrode)	10 ppm
Fe Iron	0.01 pct
Ga Gallium	0.1 ppm
Hg Mercury	5 ppb
K Potassium	0.01 pct
La Lanthanum	0.5 ppm
LOI Loss-on-ignition	1 pct
Mg Magnesium	0.01 pct
Mn Manganese	1 ppm
Mo Molybdenum	0.01 ppm
Na Sodium	0.001 pct
Ni Nickel	0.1 ppm
P Phosphorus	0.001 pct
Pb Lead	0.01 ppm
S Sulphur	0.01 pct
Sb Antimony	0.02 ppm
Sc Scandium	0.1 ppm
Se Selenium	0.1 ppm
Sn Tin ($LiBO_2$ Fusion)	1 ppm
Sr Strontium	0.5 ppm
Te Tellurium	0.02 ppm
Th Thorium	0.1 ppm
Ti Titanium	0.001 pct
Tl Thallium	0.02 ppm
U Uranium	0.1 ppm
V Vanadium	2 ppm
W Tungsten	0.1 ppm
Zn Zinc	0.1 ppm

of HCl, HNO_3, and distilled, deionized water (2:2:2 v/v) at 95°C for one hour. The sample solution was diluted with deionized water to 20 ml and analysed by inductively coupled plasma emission spectroscopy on a Jarell-Ash instrument and inductively coupled plasma mass spectroscopy on a Perkin-Elmer Elan instrument.

Loss-on-ignition was determined using a 1 g sample. The sample, weighed into a Leco® crucible, was placed into a 100ºC muffle furnace and brought up to 500°C for one hour. The oven was cooled to 100ºC and crucibles were transferred to a desiccator for cooling to

room temperature. The crucibles were reweighed and the difference was reported as loss-on-ignition.

Samples were prepared for analysis for tin by heating a 0.2 g sample mixed with 1.5 g of $LiBO_2$ flux in a muffle furnace for 15 minutes at 1050°C in a graphite crucible. The molten mixture was removed and immediately poured into 100 ml of 5% HNO_3. The solution was shaken for two hours and then an aliquot was poured into a test tube. Analytical values were determined using a Perkin-Elmer Elan 6000 ICP-MS.

Fluorine was determined using 0.25 gram sample aliquots weighed into Ni crucibles. One gram of sodium hydroxide was added and the mixture was fused at 600ºC in a muffle furnace. The fusion product was dissolved in a mixture of 7 ml of deionized water and 5 ml of 30% sulphuric acid. The solutions were transferred to plastic beakers and 5 ml of 30% ammonium acetate was added. The volume was made up to 90 ml with deionized water. The pH was tested and adjusted to 7.8 with either sodium hydroxide or sulphuric acid. Fluorine content was determined using a fluorine-selective ion electrode.

Water Analyses

The pH of stream waters was determined at the field base location using a Hanna Instruments Combo® waterproof tester with automatic temperature compensation, a range of 0.00 to +14.00 pH, resolution of 0.01 pH and an accuracy of ±0.05 pH. Meters were calibrated using commercial buffer solutions with pH values of 4.0, 7.0, and 10.0.

EVALUATION OF AIRBORNE RADIOMETRIC AND MAGNETIC DATA IN THE VICINITY OF THE NAHANNI NATIONAL PARK RESERVE, NORTHWEST TERRITORIES, CANADA

B.W. Charbonneau
Consultant, 2828 Grandeur Avenue, Ottawa, Ontario K2B 6Y9

INTRODUCTION

In Canada, mineral and energy resource assessment is required prior to designation of land as national parks, marine conservation and protected areas. Assessment may include studies of geological, geochemical, geophysical and mineral deposit characteristics (Jefferson and Spirito, 2003). This study provides improved geophysical understanding of important mineral occurrence areas within the Nahanni MERA 2 study area. This in turn contributes to the mineral deposit model knowledge base for the GIS synthesis of mineral potential (Harris et al., 2007).

Airborne geophysical surveys provide unbiased and regionally consistent scientific information that can be applied to environmental, geological, and resource-potential evaluation. For the current study, Parks Canada funded helicopter-borne surveys that were conducted by Sander Geophysics Limited, Ottawa, under the technical supervision of the Radiation Geophysics Section, Geological Survey of Canada, Natural Resources Canada. Magnetometer and gamma-ray spectrometer systems measured magnetic features within the underlying bedrock and near-surface concentrations of radioactive elements. These techniques have been described in numerous papers and basic textbooks (Telford et al., 1976; Nicolet and Erdi-Krausz, 2003). Gamma-ray spectrometry provides geochemical information by quantitatively mapping concentrations of potassium (K), uranium (U), and thorium (Th) in the upper 30 cm of the Earth's surface. Similar surveys have been used throughout Canada and worldwide for several decades to improve mapping of bedrock and surficial geology, structures, and in the exploration for a wide range of commodities (Galbraith and Saunders, 1983; Maurice and Charbonneau, 1987; Charbonneau and Legault, 1994; Shives et al., 1995, 1997, 2000; Charbonneau et al., 1997; Ford et al., 1998).

Three separate blocks were selected for evaluation in the peripheral zone surrounding the existing borders of Nahanni Park (Fig. 1). These areas were considered most likely to generate conflicts between mineral potential and park values. The geophysical data provide additional evidence to help refine the mineral potential and resolve possible planning issues. The corresponding names for Blocks A, B, and C referred to in this paper are shown in Table 1. Airborne geophysical surveys were flown over blocks A and B during the summer of 2004 and blocks B and C in 2005. Resulting data and maps have been published as Geological Survey of Canada Open Files at scales of 1:250,000 and 1:50,000 (Carson et al., 2007a,b,c).

The bedrock geology, mineral occurrences, and specific sites within the Nahanni study area are also illustrated in Figure 1. The following summary of geology is condensed from Jefferson et al. (2003). In general, a thick succession of sedimentary rocks was deposited on a Neoproterozoic carbonate platform (to 800 Ma), covered by an extensional continental margin sequence of platformal carbonate and glaciomarine to platformal clastic rocks (to 540 Ma), subsequently covered by a carbonate platform and marginal shale basin (540 to 350 Ma), buried by conglomerate, sandstone, and silicious to silty mudstone, and then draped by intercalated thin carbonate platform strata and sandy muddy coal measures. Mesozoic plate tectonic compression caused folding and thrust faulting that involved both basement and cover rocks. During and after the deformation, the more deeply buried rocks around the western margin of the study area were melted, forming granitic plutons. Recent glaciation and stream erosion has dissected these layers and structures to expose different parts of this geological history in various places.

The radioactive element and magnetic characteristics of the exposed bedrock lithological units contrast sufficiently to produce geophysical contrasts in all three survey blocks. Mineral occurrences known within Block A are limited to vein and replacement-style Zn-Pb-Ag (carbonate-fault model of Harris et al., 2007) on the Prairie Creek mine property. Blocks B and C contain mineral occurrences associated with granitic pluton, pegmatite, vein, and skarn settings (intrusion-related and Carlin-type of Harris et al., 2007), and with sedimentary exhalative (SEDEX) settings. These deposit styles have been shown elsewhere to respond well to both magnetic and gamma-ray spectrometric techniques, where associated alteration of the host rocks indirectly reflects the various mineralization processes.

The interpretations described in this report are based on visual examination of all airborne geophysical data

Charbonneau, B.W., 2007, Evaluation of airborne radiometric and magnetic data in the vicinity of the Nahanni National Park Reserve, Northwest Territories, Canada, *in* Mineral and Energy Resource Assessment of the Greater Nahanni Ecosystem Under Consideration for the Expansion of the Nahanni National Park Reserve, Northwest Territories, (ed.) D.F. Wright, D. Lemkow, and J.R. Harris; Geological Survey of Canada, Open File 5344, p. 99-123.

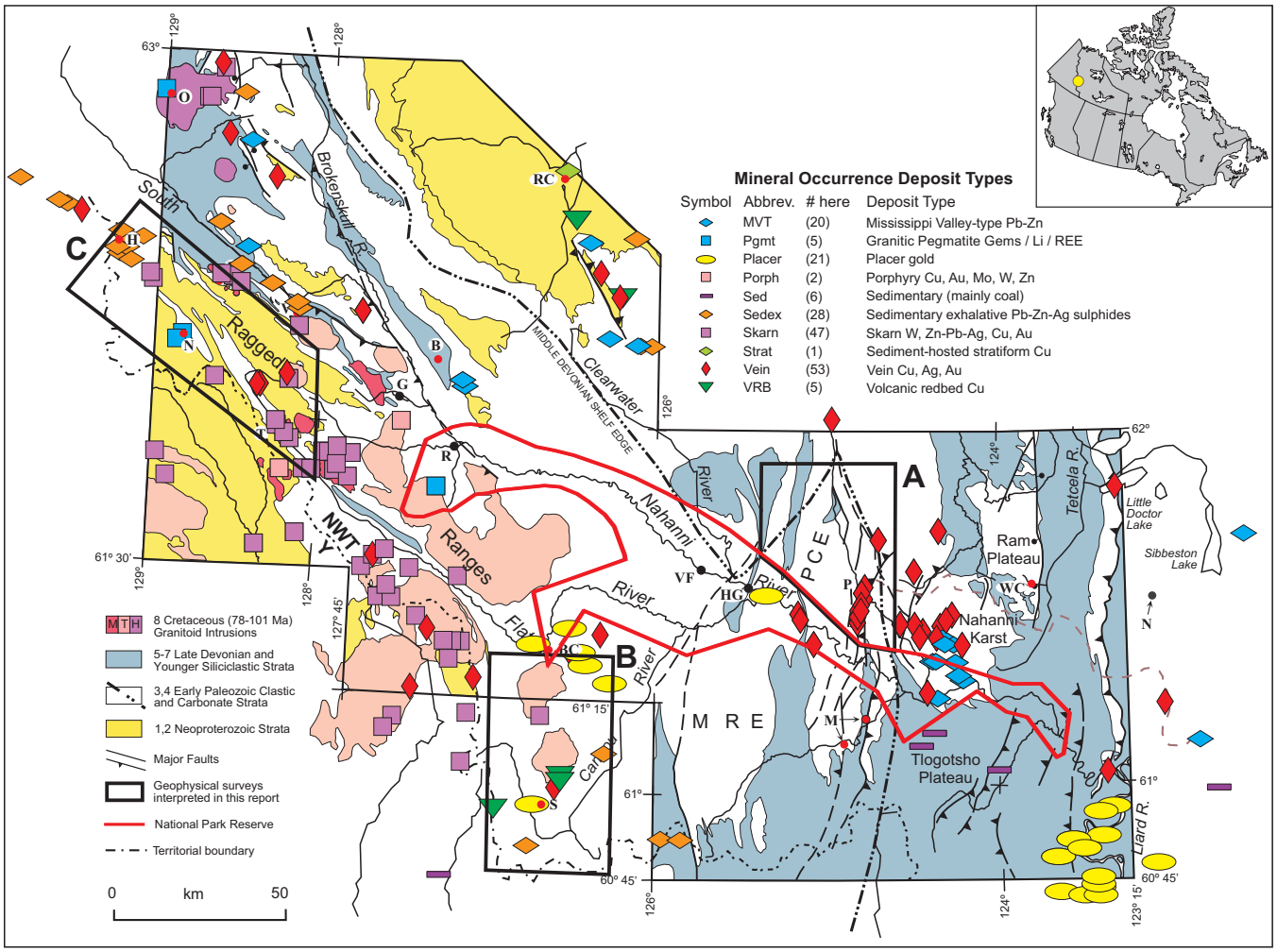


Figure 1. Location of Nahanni National Park showing geology, mineral occurrences, locations of airborne geophysical surveys (blocks A, B, and C), and important localities, from Jefferson and Spirito (2003). Abbreviations: MRE = Meilleur River Embayment, PCE = Prairie Creek Embayment, SS = Sombre Salient. Localities (black dots) and mineral sites (red dots) are: 1st, 2nd, 3rd = Canyons of Nahanni River; B = Broken Skull; BC = Bennett Creek placer gold; G = Glacier Lake, H = Howards Pass zinc-lead; HG = Hells Gate; L = Lened tungsten; M = Meilleur River hot springs; N = Nahanni Butte community; NWT = Northwest Territories; O = O'Grady gemstones; P = Prairie Creek silver-lead-zinc; R = Rabbitkettle hot springs; RC = Redstone copper; S = Selena Creek placer gold; T = Tungsten mine and hot springs; V = Vulcan zinc-lead; VF = Virginia Falls; WC = "Wretched Creek" (informal) placer gold; Y = Yukon.

generated from the three survey blocks, including 30 geophysical colour maps and approximately 451 stacked profiles. These full-scale, 1:50 000 and 1:250 000 products are provided in the publications listed in Table 1 and in the GIS database (Lemkow et al., 2007) that accompanies the MERA 2 report, of which this is a component. The original data may be examined by the reader to better understand the correlations presented between the new airborne geophysics and currently known geological and mineral-occurrences information. Highlights from a few of the complete set of maps and profiles available are depicted in the accompanying figures. Emphasis has been placed on determination of mineral potential within the surveyed areas by anomaly detection and through improved geological understanding. A separate, more rigorous interpretation using a multi-layered digital geographic information system and incorporating the recommended field follow-up should also be completed to resolve issues.

GEOPHYSICAL SURVEYS

The survey equipment and specifications are summarized below. All primary data are included in Lemkow et al. (2007) and Carson et al. (2007a,b,c). All surveys

Table 1. The corresponding Geological Survey of Canada Open File numbers for blocks A, B, and C referred to in this paper.

Survey Area Name	Corresponding GSC Open File
Block A	Virginia Falls, NTS 95F, Carson et al. (2007a)
Block B	Coal River, NTS 95D, and Flat River, NTS 95E, Carson et al. (2007b)
Block C	Frances Lake, NTS 105H, and Little Nahanni River, NTS 105I, Carson et al. (2007c)

were conducted using a Eurocopter AS 350B-3 helicopter flown at 135 m nominal terrain clearance along lines spaced at 500 m intervals. Flight operations were based in Prairie Creek, Ross River, Cantung, and Mactung. A total of 16,000 line kilometres were flown, distributed as follows: Block A - 4000 km; Block B - 5000 km; Block C - 7000 km.

The gamma-ray spectrometric system used 38 litres of on-board sodium iodide detectors and a cesium vapour magnetometer in a bird towed below the helicopter. Ground base stations provided magnetic total-field control. Real-time differential GPS navigation and radar altimeter ensured accurate flight path recovery. The survey data were compiled digitally and were subjected to a wide range of corrections and verification procedures. The final products (Carson et al., 2007a,b,c) include ten layers of digital data and colour map information (1:50 000 and 1:250 000 scale), including total radioactivity, potassium (K, %), equivalent uranium (eU, ppm), equivalent thorium (eTh, ppm), eU/eTh, eU/K, eTh/K, ternary radioactive element (K, eU, eTh), residual magnetic total field (nT), and calculated magnetic vertical gradient (nT/m). To improve interpretation, all digital data can be viewed as stacked geophysical profiles for each flight line, in order to highlight correlations between the variables.

The rugged topography in the study area (local relief exceeds 1000 m in each survey block) affected the survey flight logistics. To minimize the effect on data quality, a drape-surface was designed before the surveys were flown, based on aircraft performance and terrain models, and then used by the pilot to guide helicopter position during flight. Some deviations from ideal position were corrected by post-survey processing, but others cannot be corrected by routine procedures, and these may influence interpretation of the gamma-ray spectrometric data. The influential deviations include geometric terrain effects at the boundaries of steep, high-amplitude topographical changes. These effects are under investigation by Sprague et al. (in prep) using the new Nahanni airborne data.

For practical interpretation purposes, airborne radiometric patterns within the Nahanni surveys strongly reflect bedrock geological variation, with little topographic influence. Thus, terrain corrections should be of concern, primarily when examining the data in profile format, and only in specific locations.

COMPARISON OF GEOPHYSICS WITH GEOLOGY AND MINERAL OCCURRENCES

Block A

Geology and Mineral Occurrences

Block A geology (Fig. 2) is derived from Douglas and Norris (1976) and Morrow and Cook (1987). The pre-

Table 2. Geological units and mineral occurrences in area A, Prairie Creek (Figs. 2, 3).

	Formation	Morrow and Cook 1987 unit	Main lithology
10	Fort Simpson	UDS	dark shale, siltstone
9	Nahanni	MDN	dark grey limestone
8	Funeral	MDF	shale, grey limestone
7	Arnica	1mDab, ImDA	dolostone, limestone
6	Sombre	ImDsd, ImDs	dolostone
5	Cadillac	SDc	dolostone, siltstone,
4	Camsell	1Dc	dolostone, siltstone
3	Vera	1Dv	limestone, siltstone
2	Road River	SDR	shale, limestone
1	Whittaker	0SW3	dolostone, quartzite

D=Devonian S= Silurian O=Ordovician

dominant geological element is the Prairie Creek Embayment (labelled PCE in Fig. 1), which opens southwestward into the Meilleur River Embayment of the Selwyn Basin (MRE, Fig. 1). Known mineral occurrences sites (Canadian Zinc Corporation, 1999), which are located near faulting along the 30 km long Prairie Creek trend, are also indicated in Figure 2.

Ten geological formations have been mapped in the survey area, comprising Siluro-Devonian sedimentary rocks, and are summarized in Table 2.

Detailed maps of the surficial geology are not available for this area. The Surficial Materials Map of Canada (Fulton, 1995) indicates that the area is covered by thin rubble and colluvial silt derived from carbonates and fine clastics. Ford (1976) indicates this area escaped regional glaciation. For this reason, the airborne radiometric signatures associated with unconsolidated surficial materials can be interpreted as locally derived with no glacial transport effects.

The Prairie Creek mineral-occurrences trend is defined by the only known mineral occurrences within the map area, represented by eighteen base metal occurrences or deposits. The southern cluster of twelve dots defines the Prairie Creek Zone and includes the Prairie Creek mine. The six remaining occurrences to the north include the Rico, Zebra, Zulu, Horse, Joe, and Samantha showings.

Annomolous zinc (Zn), lead (Pb), silver (Ag), and copper (Cu) concentrations occur in sulphide-rich veins or massive lenticular bodies in fractures or stockworks (Fraser, 1996; Canadian Zinc Corporation, 1999; Jefferson and Spirito, 2003). The resource of Zone 3 at the Prairie Creek mine is estimated at 11.8 million tons grading 12.5% Zn, 10.1% Pb, 161 g/t Ag, and 0.47% Cu over a strike length of 2.1 kilometres. Mineralized veins are best developed in rocks within the Whittaker Formation and Road River Group, and to

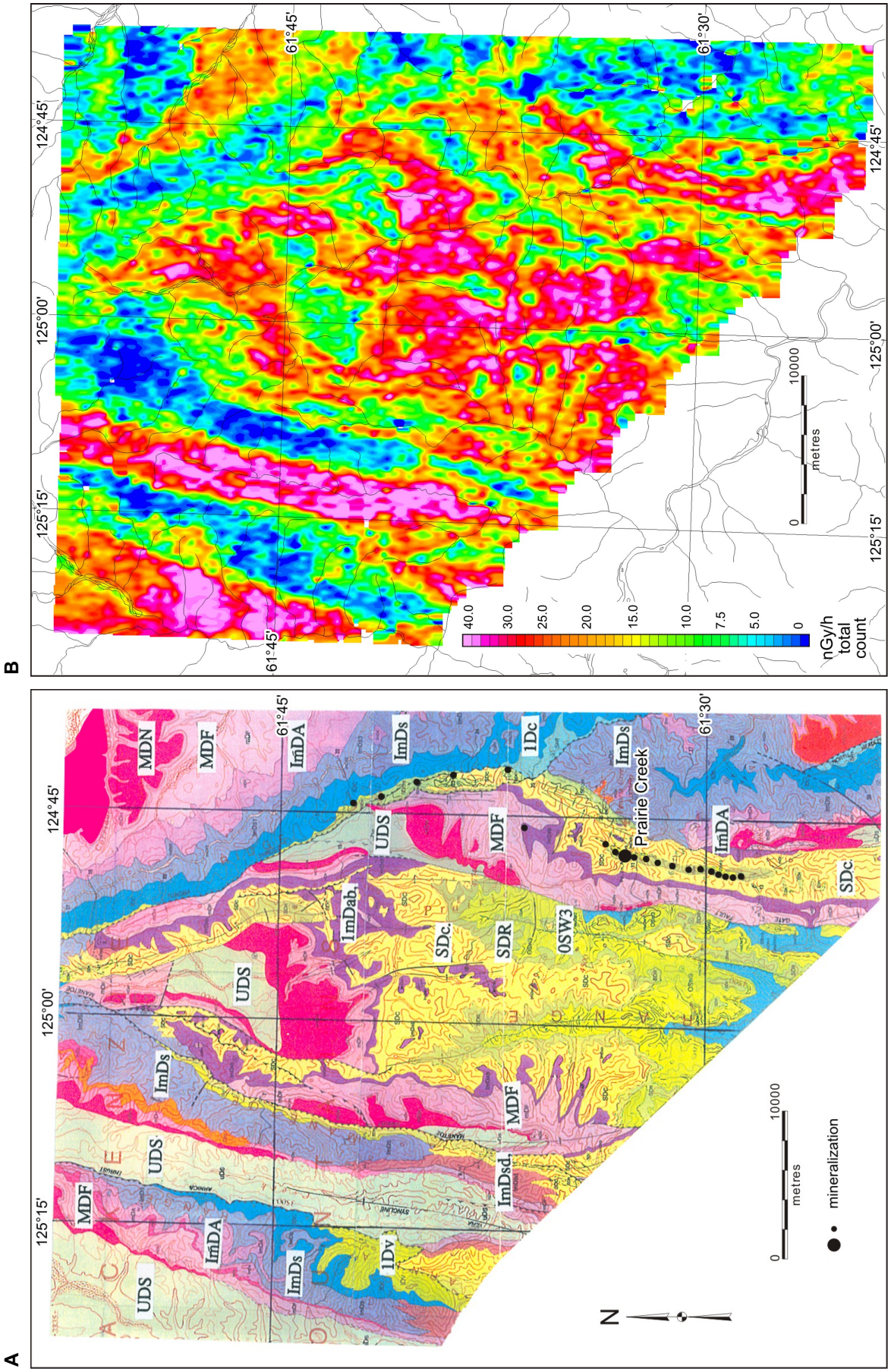


Figure 2. A) Geology and mineral occurrences (Table 2), Block A. **B)** Total radioactivity map, Block A.

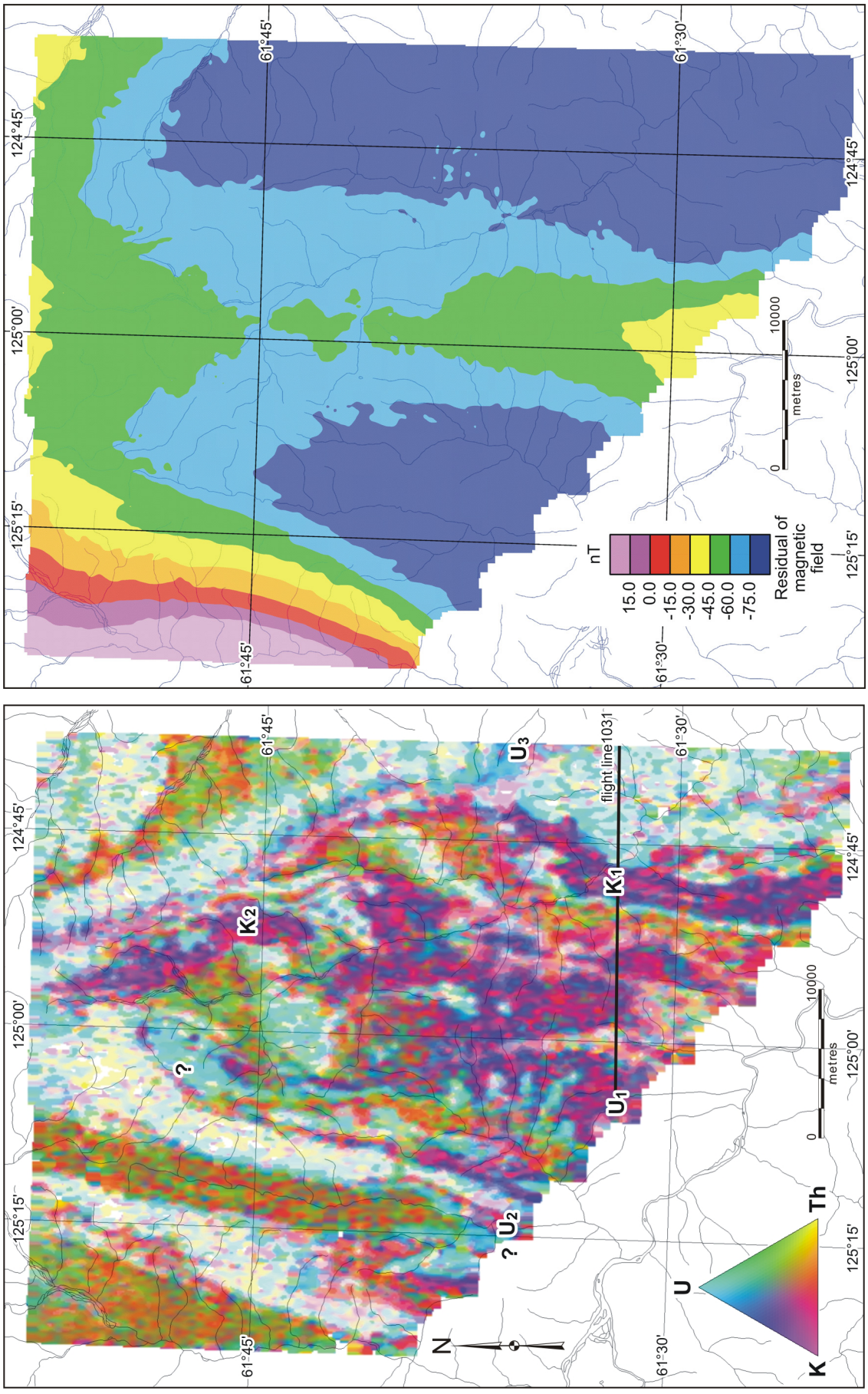


Figure 3. A) Ternary radioactive element map, Block A. 'Flight line 1031' label shows the location of the line 103100 profile shown in Figure 4. **B)** Total field magnetic patterns, Block A.

some extent in the Cadillac Formation, where hydrothermal fluids migrated from deep crustal faults. The presence of Ag suggests a plutonic relationship, although no granitic rock has been mapped in the immediate area.

Interpretation of Geophysics

Geology and total radioactivity for Block A are shown in Figure 2A and 2B, respectively. The survey was flown using 108 east-west oriented flight lines to cross the generally north-south-trending geological fabric. Total radioactivity levels are relatively low, ranging from 5 to 40 and averaging 20 nGy/h. This is less than one-half the intensity of terrestrial radiation worldwide, which averages about 45 nGy/h (Grasty et al., 1984). However, the low levels are appropriate for the rock types involved (Clarke et al., 1966; Killeen, 1979; Galbraith and Saunders, 1983) and show excellent correlation with the mapped lithological units: highest average total radioactivity (30-40 nGy/h) is over the Fort Simpson, Cadillac, and Road River units; intermediate values (10-20 nGy/h) are over the Vera, Funeral and Camsell formations; lowest values (<10 nGy/h) are associated with the Whittaker, Sombre, Arnica, and Nahanni formations.

The total radioactivity variations are caused by varying concentrations of potassium, uranium, and thorium within the rocks. These variations are indicated separately on the survey colour contour maps for K, eU, eTh, and related ratios, including the ternary radioactive element map. The ternary radioactive element map depicts the relative concentrations of K, U, and Th on a single map layer, where colour hue represents the relative abundance of the three elements (refer to ternary image colour triangle in Fig. 3A), and colour intensity is determined by the total radioactivity present (Broome et al., 1987). The contoured airborne concentration ranges are K (0.2-1.5%); eU (0.2-1.5 ppm); eTh (1-6 ppm). Actual corresponding bedrock values will be higher, due to averaging effects inherent in the airborne measurement process. Average ratio value ranges are eU/eTh (0.1-1.5); eU/K ($0.5x10^{-4}$ to $3x10^{-4}$); and eU/K ($2x10^{-4}$ to $6x10^{-4}$).

In Block A, higher K and Th values are associated with Fort Simpson Formation shale and siltstone, Cadillac Formation dolostone, siltstone, and shale, and Road River Group calcareous shale and shaly limestone. Intermediate K and eTh values overlie Funeral Formation shale and limestone, Vera Formation limestone and siltstone, and Camsell Formation dolostone and siltstone. Low K and eTh concentrations are associated with carbonate-dominated Sombre, Nahanni, Arnica, and Whittaker formations. Uranium patterns also reflect broad geological trends, but with less definition.

The lithology-related, relative and absolute variations in radioactive element concentrations described above generate a ternary map (Fig. 3A), which provides a pseudo-geological map of Block A (compare Fig. 3A with Fig. 2A). Departures from this strong positive correlation with known geology are indicated by two question marks in Figure 3A, where the typical, relatively K-rich character of the Cadillac Formation is not observed.

The effectiveness of the ternary map in indicating relative variations in radioactive elements can be seen by comparing the signatures over the Fort Simpson and Cadillac formations. The two units have similar total radioactivity values (high radioactivity) and cannot be distinguished on the total radioactivity map (Fig. 2B). However, the geochemical differences between the formations contrast sharply on the ternary map, where mottled green-yellow-red colours reflect mixed K, U, and Th in the Fort Simpson Formation, and bright red colours define the K-dominated Cadillac Formation.

Two areas (labelled K1 and K2, Fig. 3A) have been selected as examples of the signature of the Cadillac Formation along the Prairie Creek mineral occurrences trend. Although K alteration has not been reported within the Prairie Creek mine, Dawson (1995) considered the Prairie Creek zone to be of possible skarn affinity and elsewhere, Beaudoin and Sangster (1995) report narrow zones of phyllitic and sericitic alteration (sericite is a common form of K-bearing hydrothermal alteration mineral) in this style of deposit. Sedimentary-exhalative (SEDEX) deposits in southeast British Columbia (Sullivan) are known to have an envelope of sericite alteration (Leitch et al., 2000; Lowe et al., 2000; Turner et al., 2000). SEDEX-style deposits, such as those within the Howards Pass area, are marked by K enrichment (Goodfellow at al., 1983; Goodfellow and Jonasson, 1986). These facts suggest that K alteration may exist within the Prairie Creek style of deposit. Examples of the radioactive element signatures related to potassium alteration in several deposit styles has been described in Gandhi et al. (1996) and Shives et al. (1997, 2000). Field examination of the K1 and K2 areas is required to determine if the radioactive element anomalies relate to alteration or to lithological variation only.

The stacked profile presented in Figure 4 depicts data from a flight line passing 1 km south of the Prairie Creek mine (large dot on Fig. 2A, anomaly K1). The segment labelled ‘m’ is underlain by the Cadillac, Whittaker, and Road River units. The latter two units form a thin north-south-trending zone, and are mineralized in this location. Within the flanking Cadillac Formation, K concentrations are consistent with regional exposures of the formation (concentrations of up to 3% K, Fig. 4). K concentrations are lower

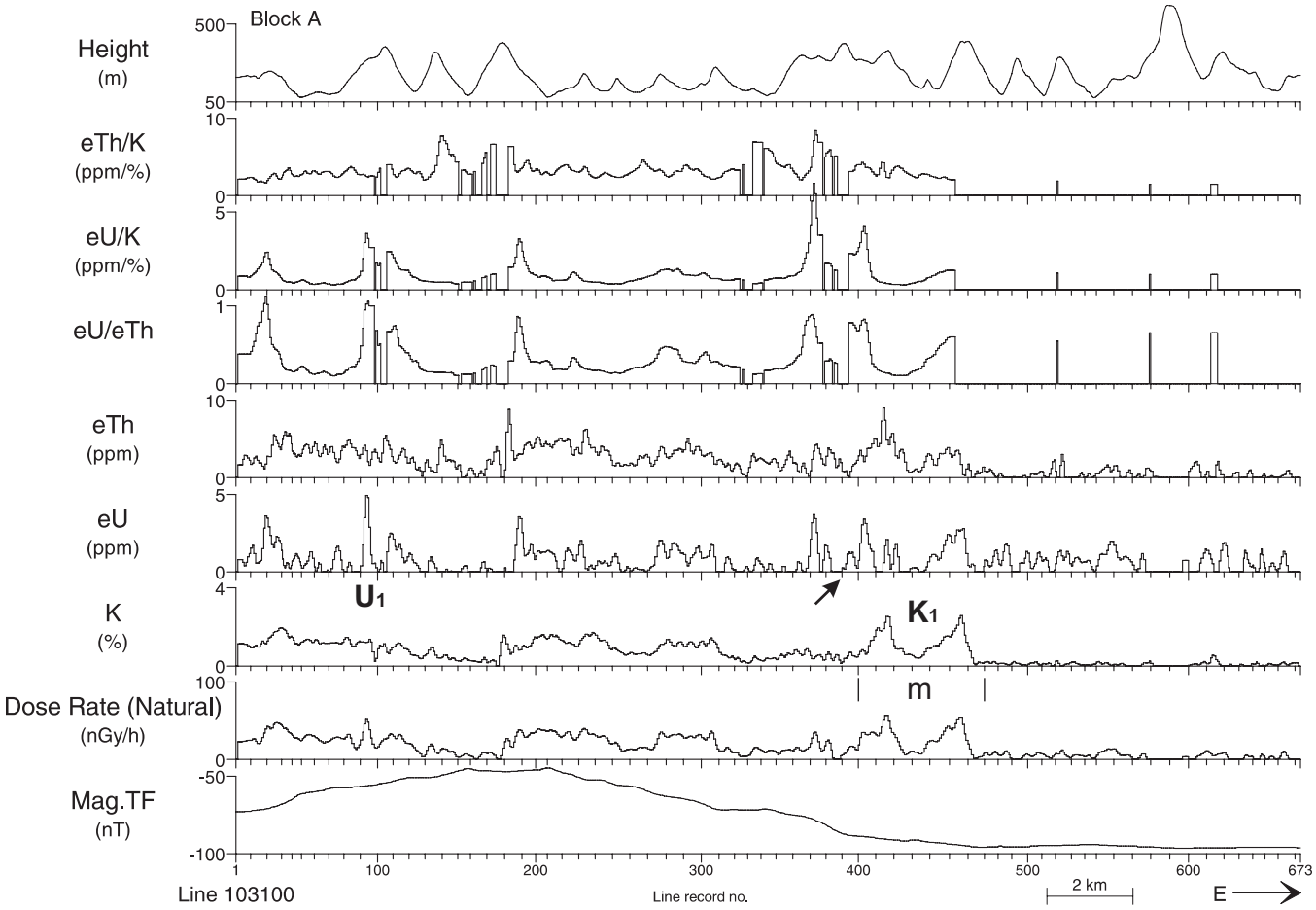


Figure 4. Stacked geophysical profile over the Prairie Creek mineral occurrence trend along line 103100. (Fig. 3A).

(~0.5%) over the mineralized parts of Whittaker and Road River units, creating a central low. Although this low includes a portion of Road River Group, which elsewhere contains relatively higher concentrations of K, a clear association between the mineral occurrences and K alteration (enrichment or depletion) cannot be established using the airborne data. Thorium concentrations in the Cadillac Formation west of the central low are higher than those in the same formation to the east, probably reflecting lithological variations.

Uranium anomalies in several areas within Block A are best observed on the stacked profiles. Where these are accompanied by increased U/Th ratio values, potential for U deposits may exist (Shives et al., 1995). Examples include three U anomalies on the western side of profile 1031 (Fig. 4, marked as U1) within the Road River Group, and two anomalies in the centre of the same profile, in Cadillac and Funeral formations. These areas should be field checked to evaluate their significance, especially where the U and U/Th ratio anomalies extend across adjacent flight lines. The latter include 5 ppm U occurrences labelled U2 (profile 1048, fiducial 940, Fort Simpson Formation) and U3 (profile 1047, fiducial 860, Camsell Formation) in Figure 3A.

The numerous eU anomalies may indicate the presence of U-enriched sediments, which are known to exist in the general area (Bell and Jones, 1979; Dawson, 1979). As uranium commonly serves as a pathfinder element, occurring in association with other elements of economic interest (Shives et al., 1995) including Pb, Zn, P, Ba, and others, several of these features should be carefully examined in the field to investigate their nature and possible significance to Pb-Zn or skarn deposits.

The magnetic total field map (Fig. 3B) for Block A depicts broad magnetic patterns, dominated by a north-south-trending, 10 km wide, 50 nT high, lying along the axis of the Prairie Creek embayment. This trend merges with a high magnetic trend of similar amplitude that extends across the northern boundary of the survey. The western edge of the survey overlies a band of higher amplitude residual total field values (100 nT). Boundaries between these relatively low-amplitude magnetic features are diffuse, suggesting the patterns are produced by deep-seated geological features. The relationship of these features to development of the Prairie Creek embayment is not known. Regional aeromagnetic and gravity data would provide a broader geophysical context for interpreting large-scale struc-

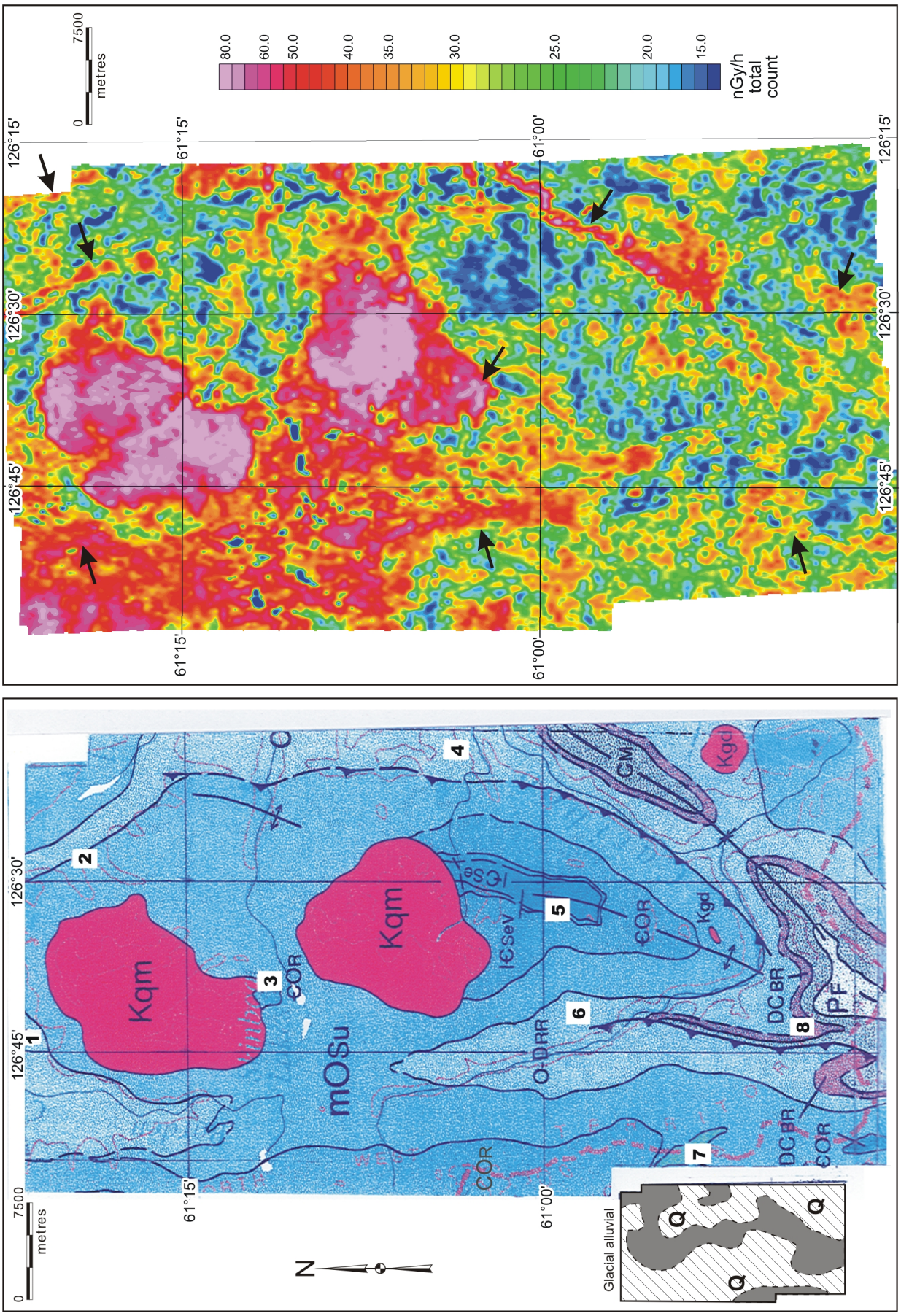


Figure 5. A) Geology (Table 3) and mineral occurrences (Table 4), Block B. **B)** Total radioactivity map, Block B.

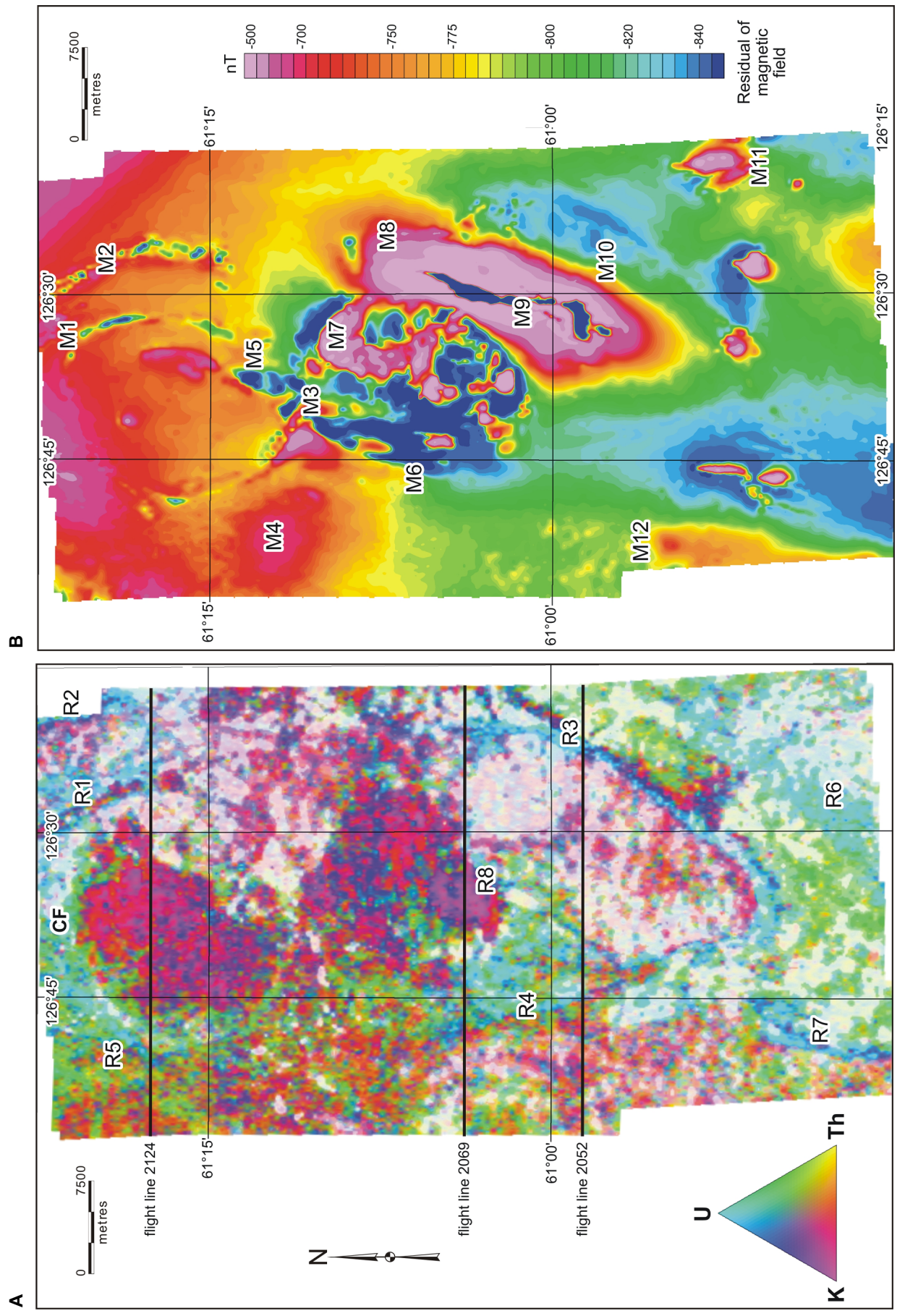


Figure 6. A) Ternary radioactive element map, Block B. **B)** Total field magnetic pattern, Block B.

tures within and beyond Block A, but these data do not exist in the area.

The calculated vertical gradient map (not shown) for Block A depicts a more complex pattern than the total field magnetic map. However, amplitudes are weak (0.01 nT/m) compared to gradient anomalies elsewhere over crystalline rocks (in the Canadian Shield, for example), which typically have gradient values exceeding 1.0 nT/m. As the noise level of the magnetic sensor used to collect the data is 0.02 nT, the calculated gradient anomalies lie at the extreme margin of detection. Correlation of the calculated vertical gradient patterns with geological contacts and faults may be fortuitous, as the magnetic boundaries are also marked by sharp topographic changes. These topographic changes offer more probable explanation for the weak gradient anomalies than the weak ferromagnetic contrasts within the geological units.

Block A Summary

Strong correlation of geophysical patterns with mapped geological units in Block A supports improved geological mapping in several areas. Elevated K concentrations within the Cadillac Formation near the Prairie Creek mineral occurrences are accompanied by Th/K ratio lows, suggesting that some of the potassium may be due to hydrothermal alteration, rather than a purely lithological variation. This possible distinction can be tested through focused ground spectrometric follow-up in the field. Moderate to weak U anomalies in Block A may indicate a potential for other sediment-hosted elements.

Mississippi Valley-style of base metal deposits east of survey Block A (Fig. 1) do not typically respond well to the type of airborne geophysical survey employed. Thus, Block A may overlie undetected deposits of this type.

Block B

The geology of the Caribou River Survey area (Fig. 5) is derived from Okulitch (in prep) and based on work by Gabrielse and Blusson (1969) and Gabrielse et al. (1973). Nine geological units have been mapped (Table 3). The sedimentary formations are intruded by Cretaceous quartz monzonite. The major structure in the area is the Caribou anticline, which is flanked by synclinal structures to the east and west. Two major faults are also mapped.

Mineral occurrences include a variety of commodities and deposit types. Eight of these are shown in Figure 5A (labelled 1-8) and are listed in Table 4. Further data on these occurrences can be found in Jefferson and Spirito (2003) and NORMIN.db (Department of Indian Affairs and Northern Development, 2001).

Table 3. Geological units of area B, Caribou River (Fig. 5A)

Map Notation	Formation	Rock Types
Q	Quaternary	glacial and alluvial deposits
Kqm	Selwyn Plutonic Suite	transitional granitic rocks (I to S)
PF	Fantasque Formation	dark grey chert
Cm	Mattson Formation	quartz arenite, shale siltstone, limestone
DcBr	Besa River Formation	pyritic calcareous shale, limestone, conglomerate, barite
O – D RR	Road River Formation	calcareous silty dolostone, pyrite, shale
mOSu	Sunblood Formation	dolostone, limestone, volcanics
C OR	Rabbitkettle Formation	silty limestone
C Se, Sev	Sekwi Formation	limestone, silty dolostone, quartzite, volcanics

E Cambrian O Ordovician D Devonian C Carboniferons
P Permian K Cretaceous Q Quaternary

Interpretation of Geophysics

The airborne geophysical survey comprises 139 east-west-oriented flight lines. The total radioactivity map (Fig. 5B) shows less correlation with the mapped regional bedrock geology than noted within Block A, reflecting weaker radioactive element contrasts in the bedrock units, and the attenuation effects of extensive glacial drift in Block B. Two large Cretaceous plutons are obvious exceptions, producing well defined highs within the northern part of the survey. Two smaller Cretaceous stocks in the southern part of the survey have radioactive element signatures that are indistinguishable from those of the surrounding sedimentary units.

Excluding the pluton bodies (average 50-80 nGy/h), total radioactivity ranges from approximately 20 to 40 nGy/h. Increased radioactivity (Fig. 5A) over more extensive glacial cover in the northwestern part of the survey area suggests the presence of debris derived from the nearby, larger plutons located northwest of the survey. The bedded sedimentary formations are not well defined by the total radioactivity map, which reflects only weakly the folding of units in the southern part of the survey area. Bedding-parallel linear anomalies are indicated by arrows in the northeast corner of

Table 4. Mineral occurrences in area B, Caribou River (Fig. 5A).

Name	Location Lat. x Long. (degrees, minutes)	Occurrence Type
1 Bennet CK	61, 22 x 126, 43	Au placer
2 Diamond/Mcleod	61, 20 x 126, 28	Au-Pb vein/placer
3 Skinboat/Rino	61, 20 x 126, 39	W-Mo Skarn
4 Solstice	61, 04 x 126, 16	Pb-Zn SEDEX
5 Stonemarten	60, 59 x 126, 31	Cu (volcanic redbed)
6 Selena CK	60, 57 x 126, 41	Au-Ba-Hg-Sn-W placer vein
7 Gabe	60, 54 x 126, 54	Volcanic-related Cu
8 Last	60, 48 x 126, 42	Ba blebs in argillite

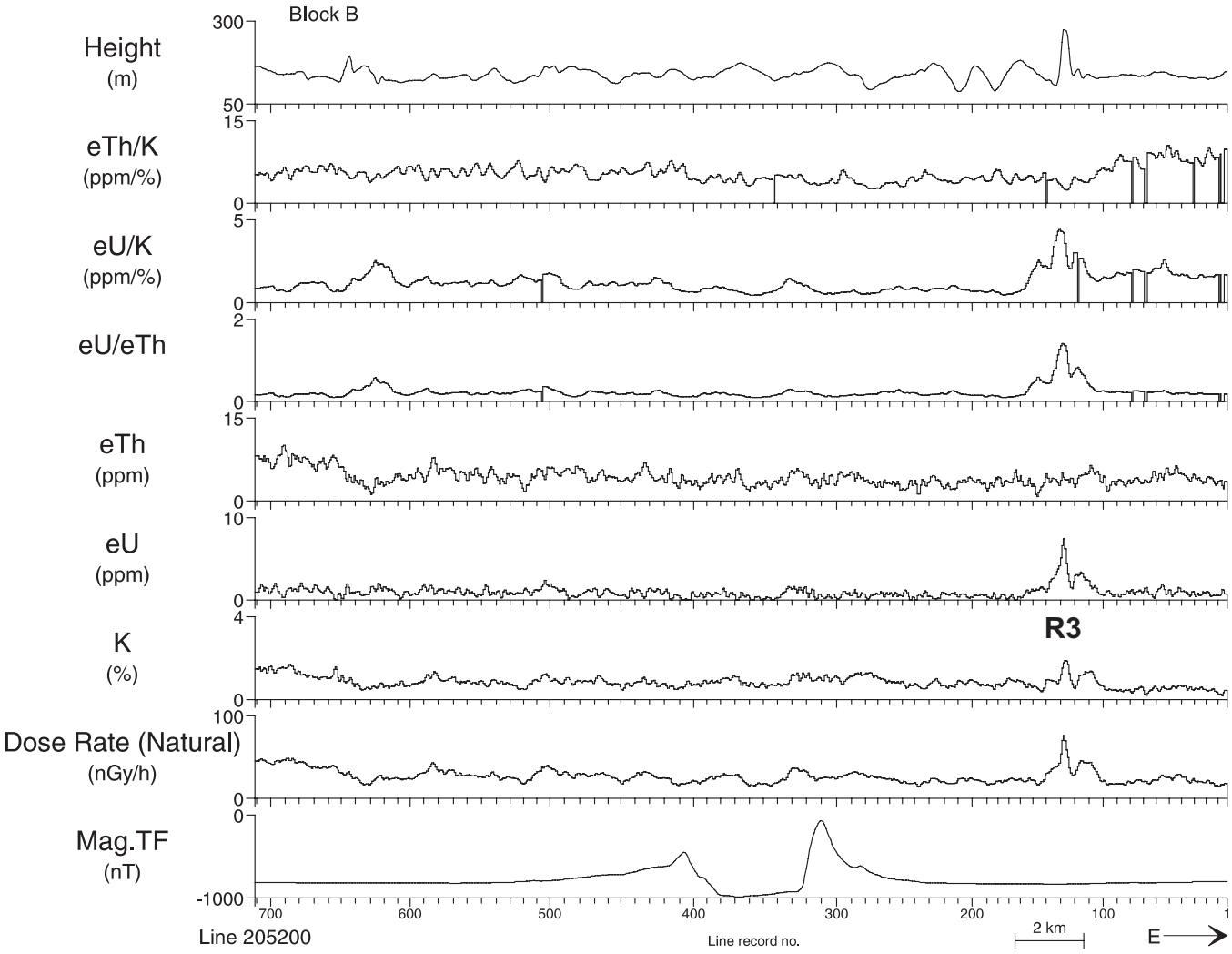


Figure 7. Stacked geophysical profile over uranium-enriched areas, Line 52, Block B.

the survey area and in the east-central and west-central areas (Fig. 5B). Weak linear trends are also apparent in the northwest, southwest, and southeast parts of the survey area. The total radioactivity anomalies in the east- and west-central parts of the survey correlate with portions of the Caribou River and may relate to glacial drift in the river valley. These features are best evaluated by examination of the ternary radioactive element and magnetic map (Fig. 6A,B), which are discussed below.

Patterns shown by the K, U, and Th maps (data and images in Lemkow et al., 2007; and Carson et al. 2007a,b,c) are similar to those on the total radioactivity maps: K concentrations range from 0.5 to 2.0% over the sedimentary formations, to more than 3% over the plutons; U ranges from 0.2 to 2.5 ppm over the sedimentary formations, to more than 4.0 ppm over the plutons; Th ranges from 2 to 10 ppm over the sedimentary formations, to greater than 15 ppm over the plutons.

The radioactive element ratio maps (data and images in Lemkow et al., 2007; and Carson et al. 2007a,b,c) show various patterns that could be of mineral exploration significance. The U/Th map indicates average values of 0.25 (approximate crustal average) with some well defined areas of greater than 0.50. The U/K map correlates closely with U/Th patterns, averaging 1.3×10^{-4} (crustal levels are 1.0×10^{-4}) with high values greater than 3.0 x 10-4. The Th/K map presents a much more diffuse pattern. Average levels are about 5 to 6×10^{-4} (crustal average ~4.0×10^{-4}). The strongest correlations noted are relatively high Th/K ratios over the belt of Permo-Carboniferous rocks in the southeast part of the survey (>8×10^{-4}) and a marked low over the central part of the southern of the two large plutons (Th/K <3×10^{-4}).

The linear radioactive element characteristics noted above are summarized and clearly evident on the ternary radioactive element map (Fig. 6A). The best defined patterns are dominated by blue (relatively high U) colours, labelled R1 to R7 (Fig. 6A). Anomaly R2 overlies the Sunblood Formation; the others overlie the Road River Group. Anomaly R3 also correlates with a major northeast-trending fault.

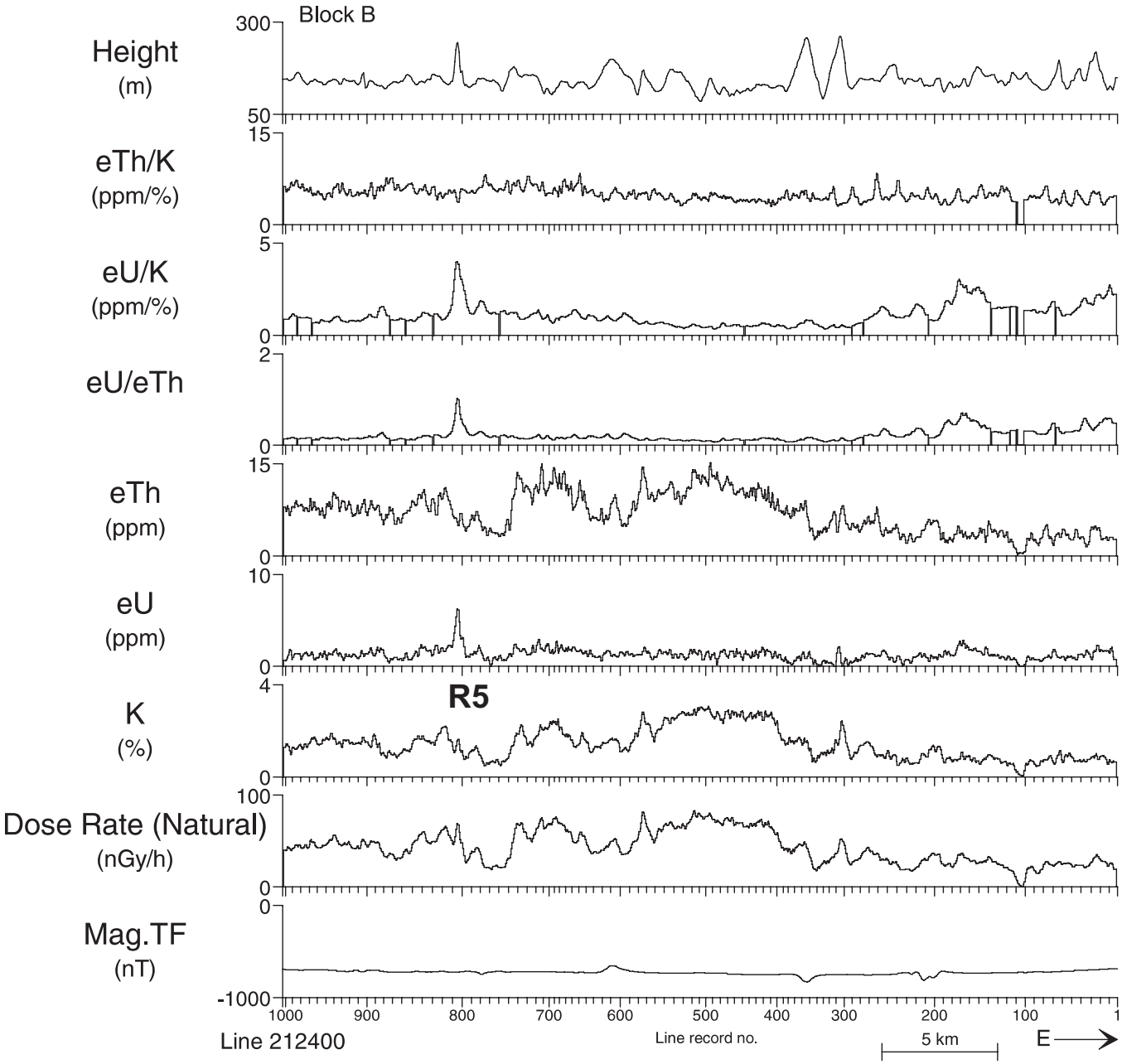


Figure 8. Stacked geophysical profile over uranium-enriched areas, Line 212400, Block B.

The uraniferous anomalies are much more sharply defined on the stacked geophysical profiles, by sharp high U and U/Th peaks. For example, Figure 7 shows the geophysical profile over anomaly R3 (flight line 52, fiducial 130) with greater than 8 ppm U, coincident with faulted Road River Group. In map view (Fig. 6A), this U anomaly can be traced to the north and south along the fault.

A strong U anomaly (R5, Fig. 6A) lies along flight line 124, near fiducial 800 (Fig. 8). The eastern (right-hand) side of the profile overlies two weakly U-enriched zones (R1, R2, Fig. 6A), which are characterized by high U/Th ratios. Anomalies R4, R6, and R7 are weak uranium anomalies, correlating with the basal Road River Group.

Within the southern part of the large southern pluton (R8, Fig. 6A), high K (relative to U and Th) indicates K enrichment that may be prospective for gold deposits. A close association has long been recognized between gold and potassic felsic intrusions (Wolfe, 1976). The Th/K ratio low found here is typical of gold deposits in similar settings elsewhere in Canada (Shives et al., 1997, 2000). This anomaly is shown in profile along flight line 69, fiducial 500, in Figure 9.

The belt of Permian to Carboniferous rocks in the southern part of the survey is clearly indicated by

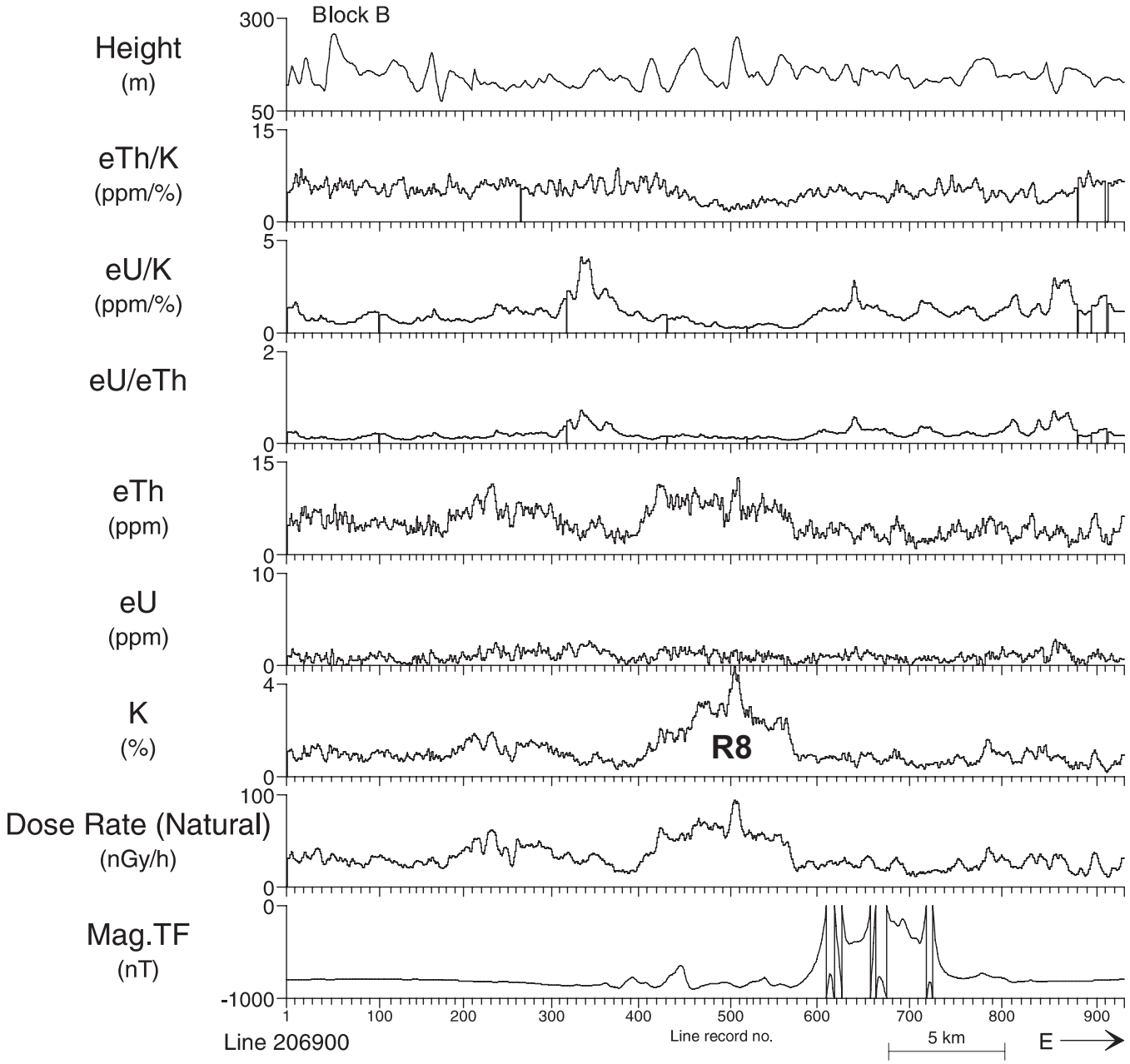


Figure 9. Stacked geophysical profile over the potassic pluton core, Line 69, Block B.

greenish hues on the ternary map (Fig. 6A), indicating relatively potassium-poor lithology.

The total field magnetic map (Fig. 6A) and the magnetic gradient map (not shown) define several features that may have significance to geological mapping and to mineral exploration. Twelve anomalies have been selected for discussion and have been labelled M1 to M12.

Anomalies M1 and M6 correspond with the two main pluton bodies. M1 is a narrow, curved low that defines the perimeter of the northern pluton, with local departures from the mapped contact. The main body of this pluton is weakly positive, suggesting some magnetic mineralogy. The peripheral low could be an oxidized boundary feature. Anomaly M6 is a well defined low of greater than 100 nT, which correlates only approximately with the mapped southern pluton boundary. Detailed examination suggests that the actual boundary of the intrusion extends further to the west, southwest, and east, perhaps masked by glacial cover. The explanation for the strong low over the southern pluton is not known, but may be related to primary oxide composition. Late-or post-magmatic alteration may have affected the magnetic character of this intrusion.

Anomaly M2 is a linear low corresponding partly with a belt of the Road River Group, but departing from the southern end of the belt. Anomalies M2 and

Table 5. Geological units of area C, Flat River (Figs. 10A, 13A).

	Name	Age	Lithology
Q	Glacial alluvial	Quaternary	unconsolidated surficial material
K	Granite	Cretaceous	Selwyn plutonic suite
Dmp	Prevost Lake Formation	Mississippian / Devonian	sandstone, conglomerate, shale
DP	Portrait Lake Formation	Devonian / Mississippian	wacke, pebbly mudstone
OSR	Road River Formation	Ordovician / Silurian	shale, chert
CSH	Haywire Formation	Cambrian / Silurian	dolostone, basalt, tuff
COR	Rabbitkettle Formation	Cambrian / Ordovician	limestone, some volcanics
CG	Gull Lake Formation	Cambrian	shale, siltstone, limestone
CS	Sekwi Formation	Cambrian	siltstone, limestone, volcanics
PCV	Vampire Formation	Late Proterozoic	siltstone
PCN	Narchella Formation	Late Proterozoic	shale, sandstone
PCY	Yusezu Formation	Late Proterozoic	sandstone, conglomerate

M1 are concentric and M2 is coincident with a circular element on the ternary radioactive element map (labelled CF, Fig. 6A). They probably relate to the intrusive history of the northern pluton. Uranium anomalies R1 and R5, and mineral occurrences 1, 2, and 3 (Table 4) lie along this feature. Anomaly M5 is a magnetic low that extends northerly from the southern pluton into sedimentary rocks of the Sunblood and Rabbitkettle formations.

Anomaly M3 is a well defined magnetic high (>300 nT) between the two large plutons in an area of glacial drift west of Skinboat Lakes. Anomaly M4 is a broad high west of the northern pluton, probably reflecting a buried, slightly magnetic pluton at depth.

Anomaly M7 is one of a number of high magnetic anomalies lying within the southern magnetic-low pluton. These anomalies exceed 300 nT (up to 1000 nT) and may indicate compositional zoning within the intrusion or the presence of altered, volcano-metasedimentary rafts of the Sekwi Formation. The latter appears to be the source of the magnetic-high feature labelled M8.

Anomaly M9 is a linear, 15 km long by 2 km wide magnetic low, which may be an altered or nonmagnetic volcano-sedimentary belt within anomaly M8. Anomaly M10 is a weak magnetic boundary that correlates with the major fault near Caribou Creek. Anomaly M11 is an east-west string of six well defined magnetic highs (>300 nT). Two of these have been mapped as Cretaceous plutons, suggesting the remaining four may also relate to small, unmapped intrusions. Anomaly M12 is a northerly weak magnetic trend associated with volcanic rocks in the Sunblood Formation.

The magnetic gradient map (data and images in Lemkow et al., 2007; and Carson et al. 2007a,b,c) further refines and sharpens the patterns described above, enhancing magnetic contacts. For example, the broad magnetic high (M8) over the Sekwi Formation volcanic unit is resolved into separate belts on the vertical gradient map and on the corresponding stacked profiles (Fig. 7). These data will support detailed mineral resource evaluation within the volcanic units in this area.

The geophysical patterns discussed above provide a number of correlations with known mineral occurrences, and suggest additional mineral potential in several areas:

1. The arcuate linear magnetic-low M2 corresponds in part with uraniferous zone R1 (Fig. 6A) and may be related to the Diamond Mcleod Au-Pb vein and placer occurrence, which is located on this feature. This 2 km wide anomaly exceeds 10 km in length and, if this correlation is valid, offers extended exploration potential. This arcuate feature is congruent with the curvature of the adjacent pluton and is possibly part of a larger circumferential structure, offering wider exploration significance.
2. Magnetic anomaly M3 occurs near the Skinboat/Rino (W polymetallic) skarn occurrence.
3. The magnetic highs within the southern pluton M7 may offer similar altered hornfels/skarn potential.
4. The Stonemarten Cu (volcanic redbed) occurrence lies along the distinct magnetic-low anomaly M9, suggesting potential along the entire length of this 12 km by 2 km feature.
5. The Gabe occurrence (volcanic-hosted Cu) lies along the weak north-trending magnetic anomaly M12 and this may suggest exploration potential along this feature.
6. The string of isolated magnetic anomalies M11 in the southern part of the survey offers potential to generate intrusion-related polymetallic skarns.
7. Skarn and vein-hosted mineral occurrences occur immediately west of the survey area. The seven distinct uranium highs noted on the ternary map

Table 6. Mineral occurrences in area C, Flat River (Figs. 10A, 13A).

Name	Location Lat x Long (degrees, minutes)	Occurrence Type
1 Cantung Mine	61, 57 x 128, 16	W-Cu-Zn-Mo skarn near granite in adjacent sediments (~10 Mt ~1.5% W)
2 Jay + others	62, 06 x 128, 13	Pb-Zn-Ag-Au vein skarn near granite contact with Vampire Formation sediments
3 Hat 1,2	62, 04 x 128, 23	Cu-Pb-Zn-Ag-Au vein in Rabbit Kettle Formation
4 Rotherham/Calia	62, 11 x 128, 52	L1 Cs Be pegmatite in Yusezu Formation
5 Lened	62, 22 x 128, 33	W Cu + gems in Rabbitkettle Formation near granite (~3/4 Mt at 1.17% W, 0.15% Cu)
6 Borovic	62, 24 x 128, 30	Ba sedex in Portrait Lake Formation
7 Golden Ram	62, 21 x 129, 01	Zn Pb Ag skarn in Rabbitkettle Formation
8 Cinq Group	62, 25 x 129, 13	Cu SEDEX, shales
9 Howards Pass E.	62, 28 x 129, 05	Pb-Zn-Ag-Cu SEDEX in black shale
10 Howards Pass Summit Lake, XY, others	62, 28 x 129, 11	Pb-Zn-Ag SEDEX in Road River shale ~473 Mt (proven and inferred) ~5% Zn, 2% Pb, and 9 g/t Ag

(Fig. 6A) should be investigated for similar deposit potential. In particular, anomaly R3 indicates very high uranium at the base of the Road River Group in proximity to a major fault (Fig. 7, flight line 52, fiducial 130).

8. The K-rich, low Th/K ratio core of the southern pluton (anomaly R8, Fig. 6A) may relate to bedrock sources of gold associated with the Selena Creek Au-Pb placer occurrences.

Block B Summary

The airborne gamma-ray spectrometric patterns within the Caribou River area correlate strongly with the mapped felsic intrusions. Less correlation is apparent over the older sedimentary formations, due to the combined effects of extensive glacial cover and subdued radioactive element contrasts between the bedrock lithologies.

A number of radioactive element (U and U/Th ratio) and magnetic features were noted that suggest mineral potential relating to a number of geological targets, such as faults, oxidized zones, skarn systems, formational units, subdivisions of plutons, and alteration systems related to plutons.

Block C

Block C covers twelve major geological units (Fig. 10A; Blusson, 1966; Gordey and Anderson, 1993), which are summarized in Table 5.

Northwest-trending Proterozoic strata underlie roughly 70% of the survey block. Structure is dominated by the northwest-trending, south-dipping thrust called the March Fault. There are also a great number of smaller faults. Major folds include the Fork Lake anticline, located southwest of the March Fault and the central, Flat Lakes syncline. Glacial/alluvial deposits lie along some of the major river valleys.

A variety of mineral deposits (Jefferson and Spirito, 2003) are summarized in Table 6 and labelled 1 to 10 on the geology map (Fig. 10A).

Interpretation of Geophysics

The total radioactivity map derived from 204 northeast-trending flight lines is shown in Figure 10B. The radioactive element patterns correlate well with the mapped geology. Total radioactivity ranges from 30 to more than 150 nGy/h, which is considerably higher than blocks A or B. Proterozoic formations Yusezu, Narchella, and Vampire have uniformly high values, averaging 70 to 120 nGy/h. The highest total radioactivity values relate to the Selwyn plutonic suite quartz monzonite, which averages greater than 150 nGy/h. Radioactivity in the younger Cambrian to Devonian/Mississippian sediments range from 40 to 80 nGy/h. Areas of lower values (20-40 nGy/h) relate to surficial deposits. Areas covered by glaciers (pale blue in Fig. 10A) have very low radioacitivy, at less than 20 nGy/h.

Average K, U, and Th values are summarized in Table 7. Although K, U, and Th map patterns (not illustrated) are similar to the total radioactivity trends, subtle relative concentration variations between the three

Table 7. Radioactive element variations over major rock types of area C, Flat River.

	K	U	Th
Granite	>4%	>6 ppm	>25 ppm
Younger formations	1-2%	2-3 ppm	5-10 ppm
Proterozoic formations	3-4%	3-6 ppm	15-25 ppm

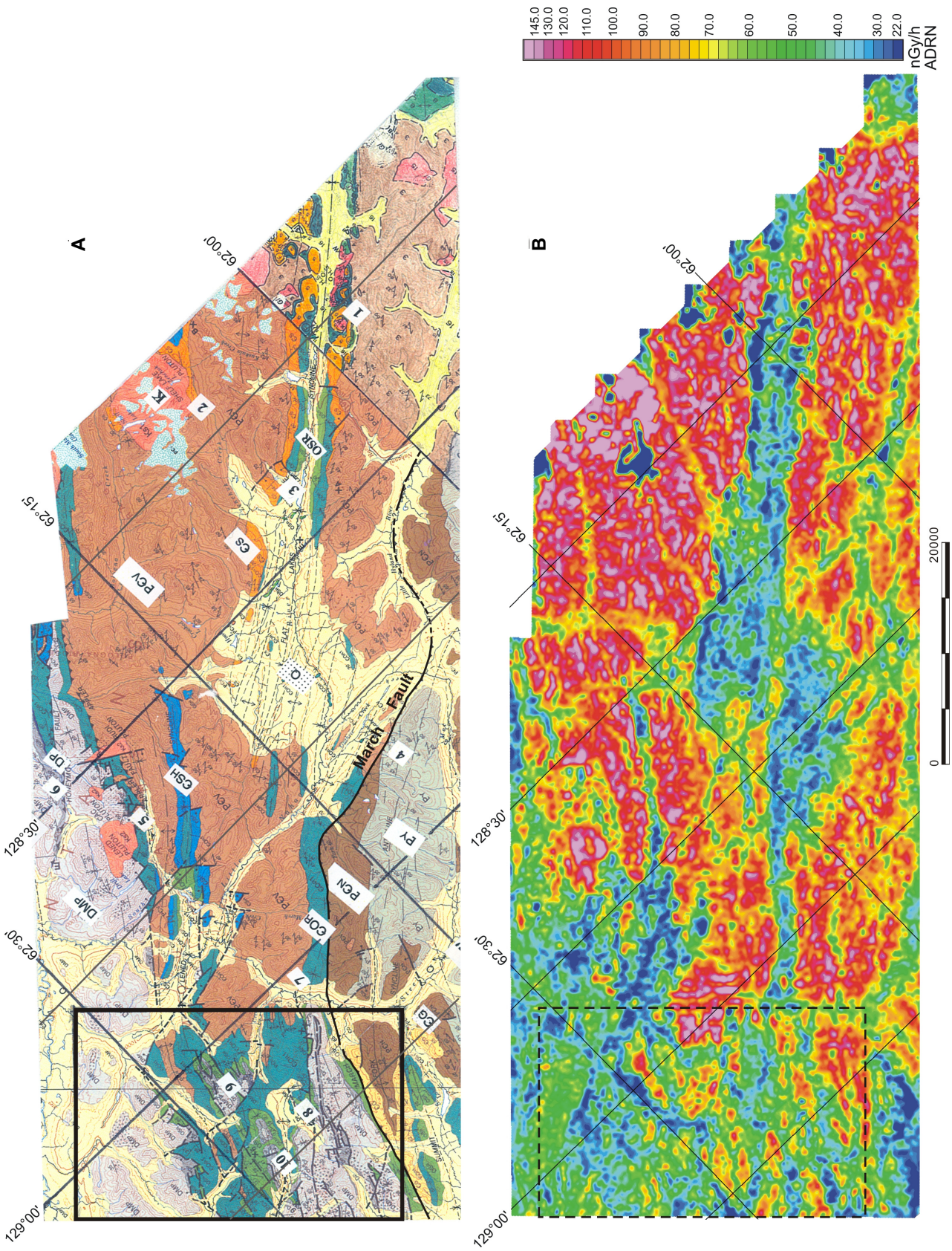


Figure 10. A) Geology (Table 5) and mineral occurrences (Table 6), Block C. **B)** Total radioactivity map, Block C. The dashed rectangle shows the location of Figure 13, in the Howards Pass area.

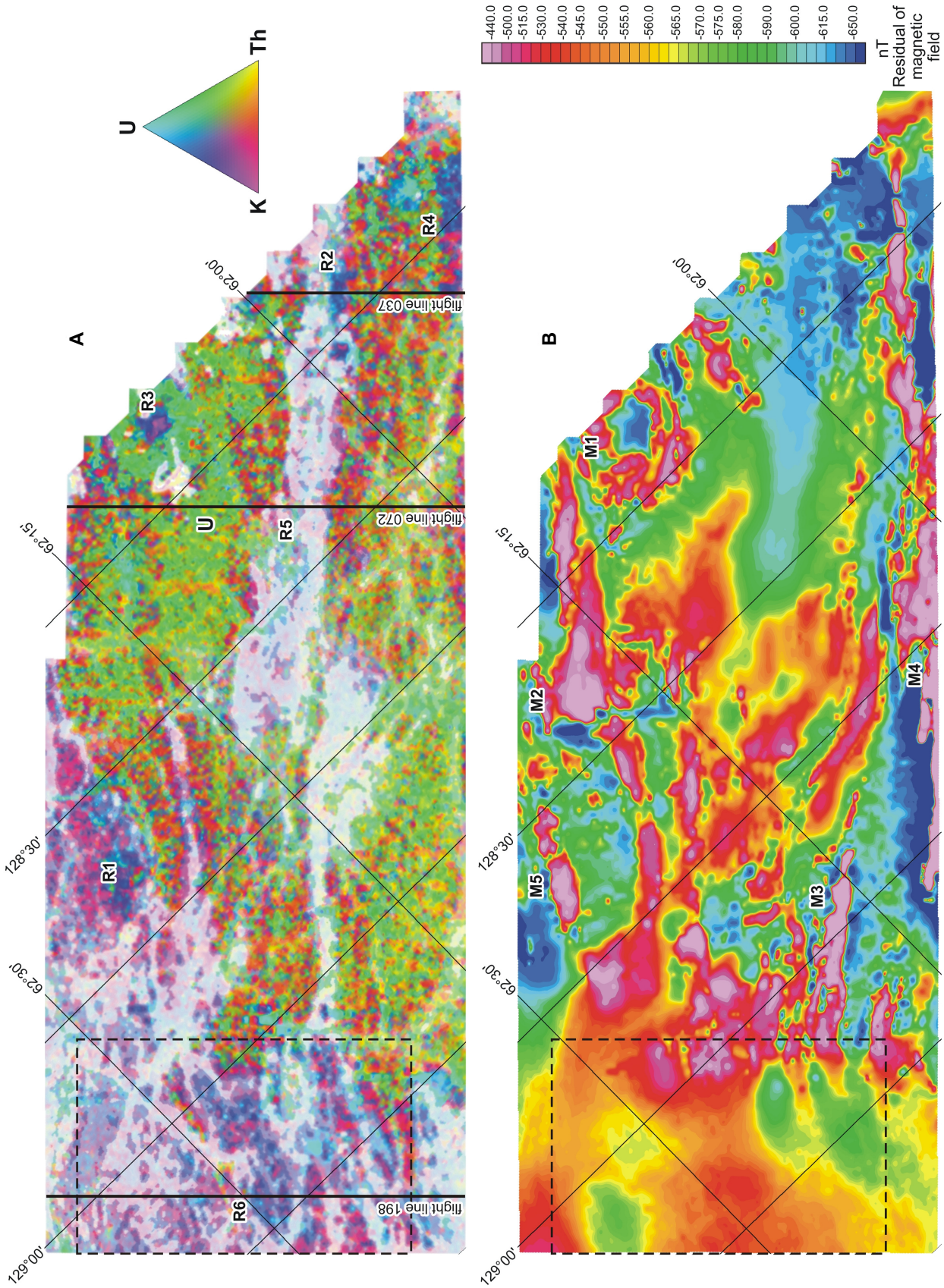


Figure 11. A) Ternary radioactive element map, Block C. **B)** Total field magnetic map, Block C.

elements generate significant anomalies on the corresponding ratio maps, indicating mineral potential.

The U/Th ratios average 0.2 over Proterozoic rocks, 0.3 or more over plutons and their margins, and variable, often higher values over younger sedimentary formations. Portions of the Ordovician-Silurian Road River Group and the Devonian-Mississippian formations have the highest U/Th ratio values.

U/K ratios reflect similar variations with lithology but with less distinct patterns than the U/Th map. Well defined Th/K ratio patterns are inverted relative to the U/Th map, with high values associated with Proterozoic sedimentary rocks, ($8x10^{-4}$, about twice crustal levels), low values ($3x10^{-4}$) over Cretaceous plutons, and low to midrange values (3 to $4x10^{-4}$) over the younger Cambrian to Mississippian sedimentary formations.

The above observations are reflected in the ternary radioactive element map (Fig. 11A). The Proterozoic formations are primarily green/yellow (indicating relatively similar proportions of U and Th, with less K) with local areas of red (K dominated) and blue (U dominated). The Cretaceous plutons are characterized by bluish purple ternary images (high U and U+K values). The younger sediments, Cambrian to Devonian/Mississippian in many places, are bluish/purple/reddish (respectively, higher U, mixed U+K, and higher K).

The total field magnetic map (Fig. 11B) shows a well defined array of anomalies with a range of approximately 300 nT. Weak magnetic patterns in the northwest result from burial of the Proterozoic magnetic source rocks by thick, younger sedimentary formations. Several linear magnetic anomalies are located within the Proterozoic and younger strata. Correlation of these anomalies with K patterns (red colours on ternary map) suggests the units may be arkosic sedimentary rocks containing iron oxides. The plutons have generally low magnetic values, with the exception of concentric, highly magnetic bands at the boundary of the large Shelf Lake pluton on the eastern boundary of the survey. The magnetic gradient map (not shown) refines the total field magnetic patterns, enhances contacts, and shows details that are consistent with the total field patterns.

The geophysical patterns discussed above provide a number of correlations with known mineral occurrences:

1. Anomalies R2 and R1 (Fig. 11A) are associated with the major tungsten polymetallic skarn Cantung and Lened deposits (labelled 1 and 5 respectively, Fig. 10A). The ternary map anomalies are bluish purple, indicating high U and K geochemistry. Anomaly R3 occurs over the polymetallic skarn/vein Jay prospect (occurrence 2, Fig. 10A), which is located on the periphery of the Shelf Lake pluton whose boundary is marked by concentric magnetic highs and lows indicating variations in magnetic character within the pluton or the development of contact hornfels rock. The pluton is zoned, with a K-rich core surrounded by a U-rich zone, in turn surrounded by a U+Th-rich outer zone. Anomaly R4 overlies a belt of tungsten/polymetallic skarn occurrences in the southeast corner of the survey, which is best developed to the east (Fig. 1). All of the skarn-related plutons are classified as peraluminous (Gordey and Anderson, 1993). These are commonly associated with Sn-W skarn deposits worldwide (Yeates et al., 1982), and typically have high U and U/Th ratios (Shives et al., 1995). Profile 037 (Fig. 12) illustrates the geophysical signature across the Cantung skarn area, near fiducial 300.
2. Anomaly R5 (occurrence 3, Fig. 11A) is defined by moderately low radioactivity (pale colour) but dominated by uranium (blue hue, high U/Th ratio), associated with skarn/vein-type mineral assemblages (Cu, Pb, Zn, Ag, and Au) at occurrences Hat 1 and 2. The low radioactive intensity here is consistent with the overburden cover.
3. The Rotherham/Cali Cs-Li pegmatite occurrence (4, Fig. 10A), is not distinguished on the radioactivity and magnetic maps, and has only a weak expression in the corresponding stacked radiometric profile data (not shown).
4. The most significant anomalies, labelled collectively as R6 on Figure 11A, overlie the Cambro-Ordovician and Silurian-Devonian Selwyn Basin in the northwest part of the survey, in the Howards Pass area (occurrence 10, Fig. 11A). The Howards Pass style of SEDEX deposit is well delineated by a high-K and high-U signature. Figure 13 illustrates a more detailed view of this area, where purple anomalies (Fig. 13B) clearly outline the Howards Pass (XY, Summit) and the Howards Pass East deposits (occurrences 9 and 10, respectively, Fig. 13A). A low Th/K ratio over the deposits (Fig. 13C) indicates K enrichment relative to Th. High U/Th ratios (Fig. 13D) indicate U enrichment, which in combination with the K produces the purple signature on the ternary map. These features are also shown on the stacked profile (see line 319800, Fig. 14) over the Howards Pass XY deposit. The Cinq deposit (occurrence 8) appears less potassic and more U rich (i.e. blue). Potassium enrichment, with associated low Th/K ratio, has been noted in the vicinity of the Sullivan SEDEX deposit in southeastern British Columbia (Lowe et al., 2000).

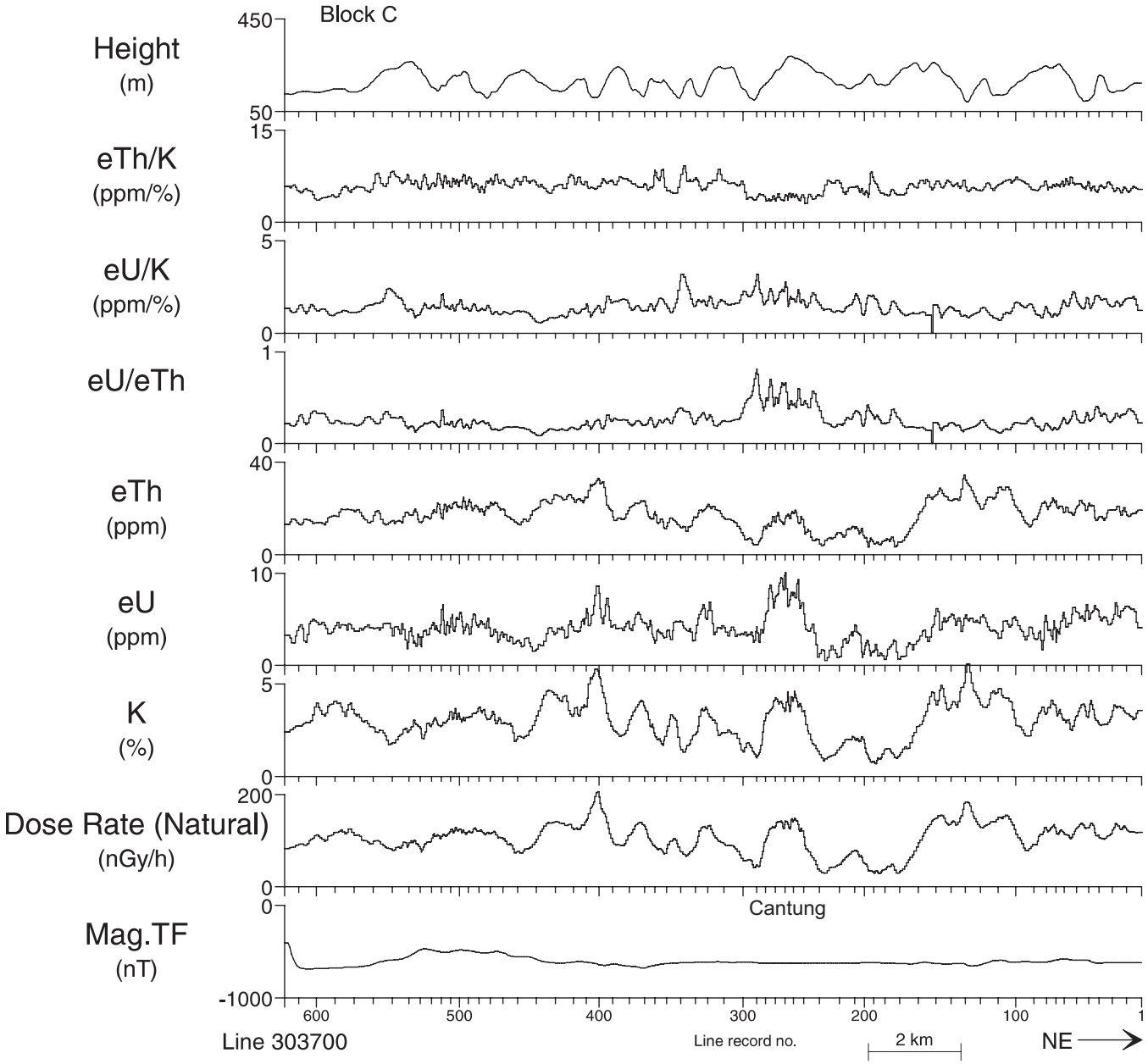


Figure 12. Stacked geophysical profile over the Cantung tungsten polymetallic skarn deposit, Block C.

5. The observed radioactive element signatures may provide an exploration model for SEDEX Pb-Zn deposits using airborne gamma-ray spectrometry. The model is based on K enrichment in footwall mudstone and uranium enrichment in overlying phosphatic shale, as described by Goodfellow et al. (1983) and Goodfellow and Jonasson (1986). Bell and Jones (1979) also described uranium-rich phosphatic shale units in the area. A number of similar anomalies occur elsewhere within the survey, providing exploration guidance. However, this tentative model requires further evaluation.
6. Several uranium anomalies within the Proterozoic rocks may have mineral potential significance. Flight line 72 (Fig. 15) crosses a 2 km wide area that approaches 10 ppm uranium at fiducial 450. The area can be expected to have localized enrichments much higher than 10 ppm because the airborne levels are averaged values relating to the broad area measured by the detectors. It is not known if these high uranium areas have any economic significance. As mentioned above, a number of uranium anomalies are obvious over the younger strata on the ternary map (as well as U and U-Th ratio maps) and should be examined in the field for uranium and related metal enrichments in possible SEDEX and skarn deposit settings.
7. A number of magnetic features could also provide exploration targets for intrusion-related, skarn-type deposits. These include the concentric zones

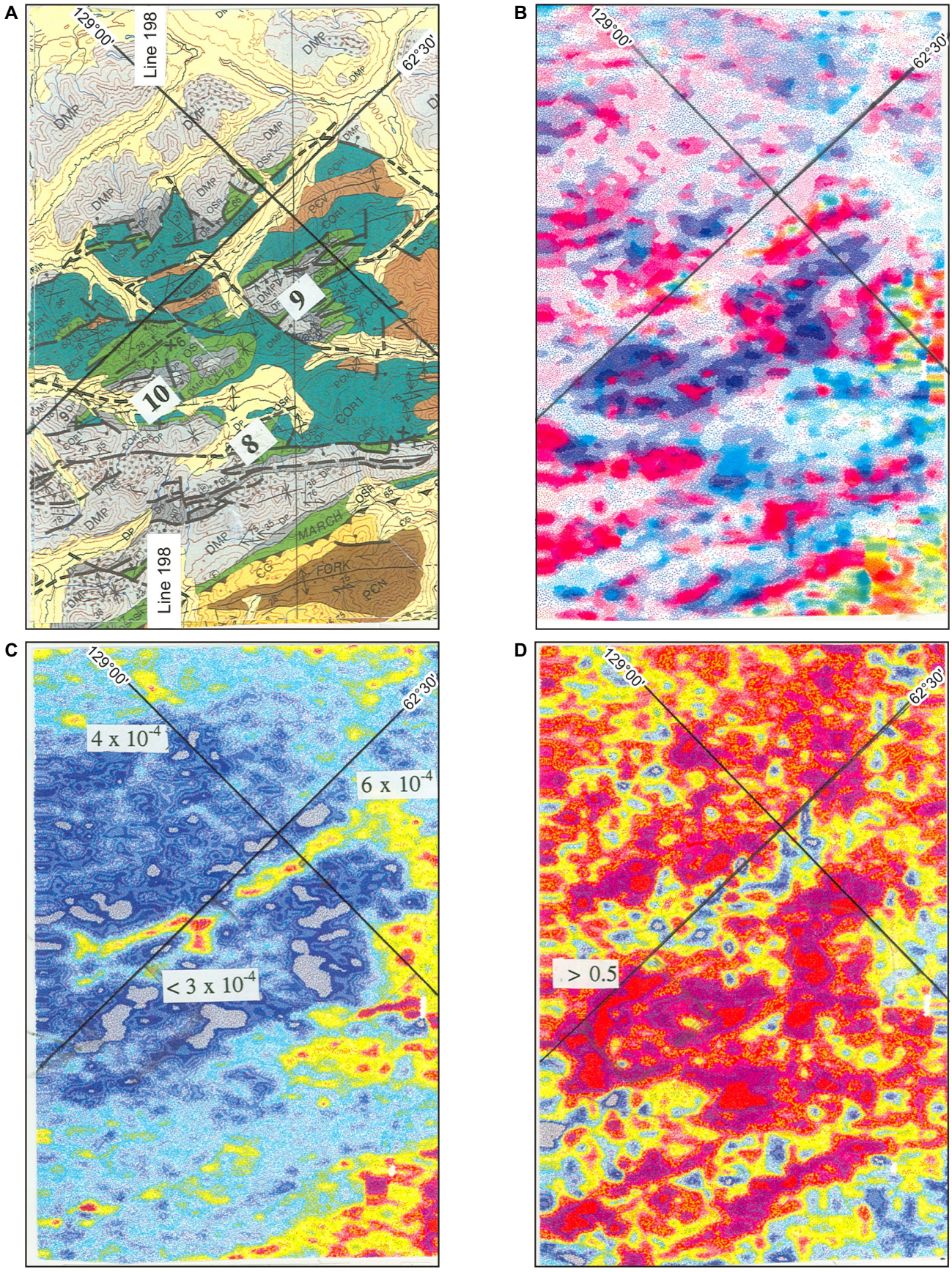


Figure 13. Geology and radiometric patterns, in the Howards Pass area, Block C. **A)** Geology and mineral occurrences. 'Line 198' labels indicate location of the line 319800 profile shown in Figure 14. **B)** Ternary radioelement map. **C)** Thorium/potassium ratio map. **D)** Uranium/thorium ratio map. The area of this figure is outlined in Figure 10.

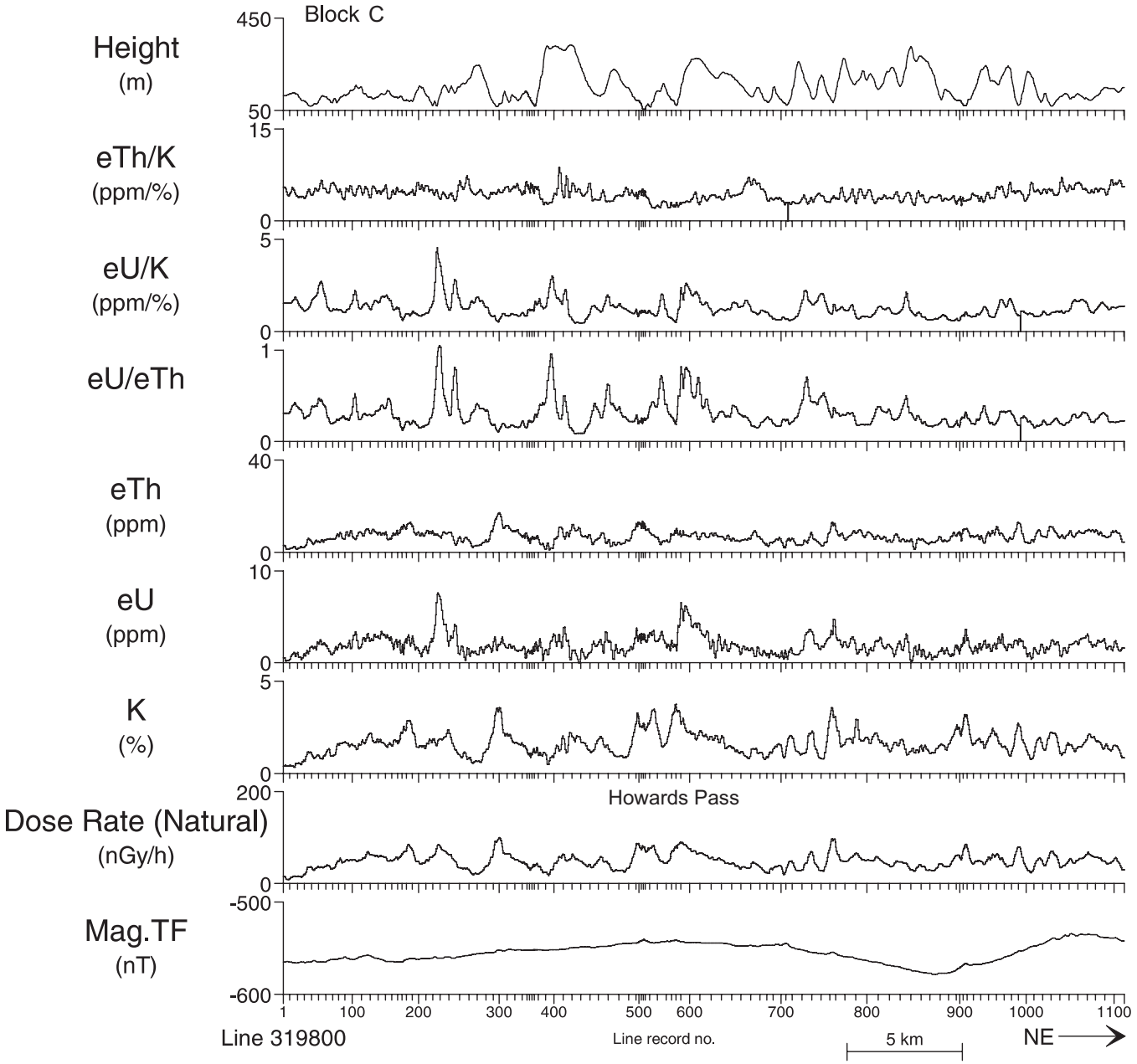


Figure 14. Stacked geophysical profile (line 319800, location shown in Fig. 13A) over the Howards Pass SEDEX camp, Block C.

around the Shelf Lake pluton (M1, Fig. 11B). Other relatively weak (~100 nT) magnetic features in Proterozoic rocks (M2, M3, and M4) and in Devonian sediments (M5) should also be investigated. A very weak broad magnetic high of less than 30 nT is noted in the general area of the Howards Pass deposits.

Summary Block C

The radiometric signatures in the Flat River survey Block C relate to the major geological subdivisions and to the known deposit styles, including pluton-related W polymetallic skarns and SEDEX Pb-Zn. Additional anomalies offer significant exploration guidance in several areas where mineral occurrences are currently unknown. A number of magnetic anomalies offer additional exploration targets.

SUMMARY – ALL SURVEY BLOCKS

Results of the combined, helicopter-borne, gamma-ray spectrometric and total field magnetic surveys flown over blocks A, B, and C demonstrate the value of these surveys to geological mapping and to mineral potential evaluation, providing regionally consistent geophysical and geochemical information. Localized, radioactive element and magnetic total field anomalies are related to bedrock contacts, unmapped lithological units, or alteration associated with various plutons and inferred mineralization systems. Ternary radioactive element patterns associated with the mineral occurrence trends

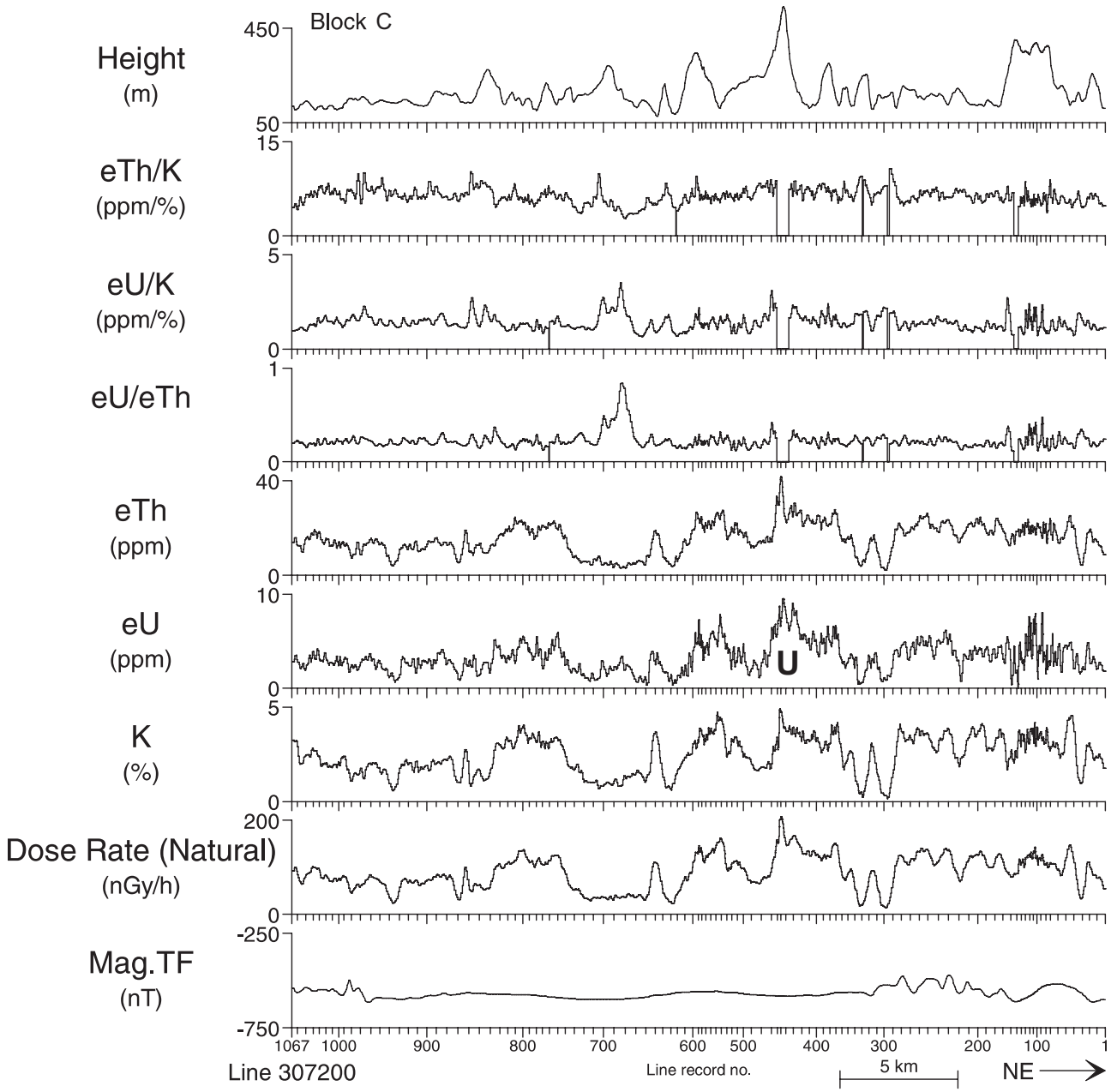


Figure 15. Stacked geophysical profile over high uranium Proterozoic sediments, Block C.

show distinct signatures in each of the three blocks surveyed: potassic rocks in Block A appear as bright red colour, U enrichment produces blue colours in Block B, and K+U enrichment in Block C generates purple ternary shades.

A clear airborne geophysical signature has not been recognized over the Prairie Creek prospects at the scale investigated, but detailed ground studies of the potassium patterns near the deposits may establish a relationship with alteration. Isolated uranium anomalies within Block A may provide guidance for related metals. Geophysical signatures in blocks B and C indicate undiscovered potential for skarn-related base metals, tungsten, and lode-gold deposits.

The following geophysical observations should be tested by field work and spatial analysis in a GIS to support full interpretation and establish how much confidence should be placed on mineral potential inferred from the geophysical surveys.

Block A

1. The relationship of bedrock K concentrations adjacent to the Prairie Creek Pb-Zn mineral occurrences should be investigated to determine if alteration has enhanced the K levels locally in the Cadillac Formation, or has reduced the K concentrations of the Road River Group.

2. Isolated areas of U enrichment over several formations should be checked in the field and sampled for related metals.

Block B

3. Several magnetic anomalies are located along pluton boundaries, inclusions, skarn zones, oxidized zones, and volcanic rocks. Some of the anomalies relate to known mineral occurrences.
4. Block B contains several high U and U/Th ratio anomalies within the Road River Group and near major faults. These should also be checked and sampled for associated pathfinder elements.
5. Potassic phases of the southern plutons should be investigated for gold and other metals.

Block C

6. One of several magnetic features relates to the Jay skarn occurrence; the others require field testing.
7. A number of discrete uranium anomalies in Proterozoic and younger strata should be investigated for uranium and other metals. High uranium levels over the plutons may warrant investigation for uranium itself.
8. Further investigation should be conducted on the signatures associated with the Howards Pass deposit styles, and comparison made with a number of new uranium and potassium anomalies.

The field examinations should include field procedures established by the Radiation Geophysics Section, Geological Survey of Canada, including scintillometry to guide calibrated, in situ spectrometric readings, magnetic susceptibility measurements, rock sample collection, geochemical analyses, and petrologic and mineralogical studies of selected samples. The field results should be used to better constrain a re-interpretation of the surveys and improve the resource assessment of the Nahanni Park region.

ACKNOWLEDGEMENTS

The author acknowledges the high quality of the helicopter-borne geophysical surveys conducted by Sander Geophysics Limited, despite very difficult terrain. Several Geological Survey of Canada employees are thanked for their contributions: John Carson and Regis Dumont provided radiometric and magnetic (respectively) quality control, contract monitoring, and supplied the author with maps or the airborne survey results; Rob Shives supervised the overall survey contracting process and offered many improvements to this manuscript; Susan Davis prepared the figures for this report; Dr. Danny Wright managed the Geological Survey of Canada's activities under the MERA Program, which was supported financially by Parks Canada.

The author values the experience and knowledge gained during a full career with the Geological Survey of Canada, working with many expert colleagues to conduct, process, interpret, follow-up, and apply airborne radiometric and magnetic data to diverse geological challenges.

REFERENCES

Beaudoin, G. and Sangster, D.F.
1995: Clastic metasediment-hosted vein silver-lead-zinc, *in* Geology of Canadian Mineral Deposit Types, (ed.) O.R. Eckstrand, W.D. Sinclair, and R.I. Thorpe; Geological Survey of Canada, Geology of Canada No. 8, p. 393-398.

Bell, R.T. and Jones, L.D.
1979: Geology of some uranium occurrences in western Canada, in Current Research Part A; Geological Survey of Canada, Paper 79-1A, p. 397-399.

Blusson, S.L.
1966: Geology Frances Lake Yukon territory and District of MacKenzie NTS 105 H; Geological Survey of Canada, Map 6.

Broome, J, Carson, J.M., Grant, J.A., and Ford, K.L.
1987: A modified ternary radioelement mapping technique and its application to the south coast of Newfoundland; Geological Survey of Canada, Paper 87-14, scale 1:500 000.

Canadian Zinc Corporation
1999: The Prairie Creek Information Memorandum; unpublished company report, 34 p.

Carson, J.M., Dumont, R., Potvin, J., Buckle, J., Shives. R.B.K., and Harvey, B.
2007a: Geophysical Series - NTS 95F - Virginia Falls, Northwest Territories; Geological Survey of Canada, Open File 5154, 1 CD-ROM.
2007b: Geophysical Series – NTS 95D and 95E – Flat River, Northwest Territories; Geological Survey of Canada, Open File 5160, 1 CD-ROM.
2007c: Geophysical Series – NTS 105H and 105I – Little Nahanni River, Northwest Territories; Geological Survey of Canada, Open File 5164, 1 CD-ROM.

Charbonneau, B.W. and Legault, M.I.
1994: Interpretation of airborne geophysical data for the Thor Lake area, Northwest Territories, *in* Studies of Rare-Metal Deposits in the Northwest Territories, (ed.) W.D. Sinclair and D.G. Richardson; Geological Survey of Canada, Bulletin 475, p. 17-31.

Charbonneau, B.W., Holman, P.B., and Hetu, R.J.
1997: Airborne gamma spectrometer-magnetic-VLF survey of northeastern Alberta, *in* Exploring for Minerals in Alberta; Geological Survey of Canada, Geoscience Contributions, Canada Alberta Agreement on Mineral Development 1992-1995, (ed.) R.W. MacQueen; Geological Survey of Canada, Bulletin 500, p. 117-132.

Clarke, S.P., Peterman, Z.E., and Heir Knut S.
1966 Abundances of uranium, thorium, and potassium, *in* Handbook of Physical Constants (Revised edition), (ed.) S.P. Clark, Jr.; Geological Society of America, Memoir 97, p. 521-542.

Dawson, K.M.
1979 Regional metallogeny of the northern Cordillera: Recent stratiform base metal discoveries in Yukon Territory and District of MacKenzie, *in* Current Research, Part A; Geological Survey of Canada, Paper 79-1A, p. 375-379.

1995: Skarn zinc-lead-silver, *in* Geology of Canadian Mineral Deposit Types, (ed.) O.R. Eckstrand, W.D. Sinclair, and R.I. Thorpe; Geological Survey of Canada, Geology of Canada No. 8, p. 448-459.

Department of Indian Affiars and Northern Development (DIAND)
2001: NORMIN.DB, The Northern Mineral Database; Northwest Territories Geoscience Office, Yellowknife, Northwest Territories.

Douglas, R.J.W. and Norris, D.K.
1976: Geology, Virginia Falls, District of Mackenzie NTS 95F; Geological Survey of Canada, Map 1378A, scale 1:250,000.

Ford, D.C.
1976: Evidence of multiple glaciation in South Nahanni National Park MacKenzie Mountains, Northwest Territories; Canadian Journal of Earth Science, v. 13, p. 1433-1445.

Ford, K.L., Shives, R.B.K., and Charbonneau, B.W.
1998: Application of airborne gamma-ray spectrometry to geological mapping, mineral exploration and land-use planning, *in* Proceedings, 10th Latin American Geological Congress (Symposium on Airborne Geophysics and Geochemistry in the Prospecting for Minerals); p 131-150.

Fraser, S.C.
1996: Geology and geochemistry of the Prairie Creek An, Pb, Ag deposit, southern MacKenzie Mountains, N.W.T.; M.Sc. thesis, University of Alberta, Edmonton, Alberta, 146 p.

Fulton, R.J. (compiler)
1995: Surficial Materials of Canada; Geological Survey of Canada, Map 1880A, scale 1:5000,000.

Gabrielse, H. and Blusson, S.L.
1969: Geology of Coal River Map Area, Yukon Territory and District of MacKenzie, NTS 95D; Geological Survey of Canada, Paper 68-38, 22 p.

Gabrielse, H., Blusson, S.L., and Roddick, J.A.
1973: Geology of Flat River, Glacier Lake, and Wrigley Lake Map Areas, District of MacKenzie and Yukon Territory; Geological Survey of Canada, Memoir 366, 268 p.

Galbraith, J.H. and Saunders, D.F.
1983: Rock classification by characteristics of aerial gamma–ray measurements; Journal of Geochemical Exploration, v. 18, p. 49-73.

Gandhi, S.S., Prasad, N., and Charbonneau, B.W.
1996: Geological and geophysical signatures of a large polymetallic exploration target at Lou Lake, southern Great Bear magmatic zone, NWT, *in* Current Research, Part E; Geological Survey of Canada, Paper 96-1E, p. 147-158.

Goodfellow, W.D. and Jonasson, I.R.
1986: Environment of formation of the Howards Pass (XY) Zn-Pb deposit, Selwyn Basin, Yukon, *in* Mineral Deposits of Northern Cordillera, (ed.) J.A. Morin; Canadian Institute of Mining and Metallurgy, Special Volume 37, p. 19-50.

Goodfellow, W.D., Jonasson, I.R., and Morganti, J.M.
1983: Zonation of chalcophile elements about the Howards Pass (XY) Zn-Pb deposit, Selwyn Basin, Yukon; Journal of Geochemical Exploration, v. 19, p. 503-542.

Gordey, S.P. and Anderson, R.G.
1993: Evolution of the Northern Cordilleran Miogeocline, Nahanni Map Area (105I), Yukon and Northwest Territories; Geological Survey of Canada, Memoir 428, 213 p.

Grasty R.L., Carson J.M., Charbonneau, B.W., Holman P.B.
1984: Natural Background Radiation in Canada; Geological Survey of Canada, Bulletin 360, 39 p.

Harris, J.R., Lemkow, D., Wright, D.F., and Falck, H.
2007: Modelling mineral potential for the Greater Nahanni Ecosystem using GIS-based analytical methods, *in* Mineral and Energy Resource Assessment of the Greater Nahanni Ecosystem Under Consideration for the Expansion of the Nahanni National Park Reserve, Northwest Territories, (eds.) D.F. Wright, D. Lemkow, and J.R. Harris; Geological Survey of Canada, Open File 5344, p. 293-326.

Jefferson, C.W. and Spirito, W.A. (ed.)
2003: Mineral and Energy Resource Assessment of the Tlogotsho Plateau, Nahanni Karst, Ragged Ranges, and Adjacent Areas under Consideration for Expansion of Nahanni National Park Reserve, Northwest Territories; Geological Survey of Canada, Open File 1686, 1 CD-ROM, 253 p.

Jefferson, C.W., Spirito, W.A., and Hamilton, S.M.
2003: Geological setting, Chapter 3 *in* Mineral and Energy Resource Assessment of the Tlogotsho Plateau, Nahanni Karst, Ragged Ranges, and Adjacent Areas under Consideration for Expansion of Nahanni National Park Reserve, Northwest Territories; Geological Survey of Canada, Open File 1686.

Killeen, P.G.
1979: Gamma-ray spectrometric methods in uranium exploration: Application and interpretation, *in* Geophysics and Geochemistry in the Search for Metallic Ores, (ed.) P.J. Hood; Geological Survey of Canada, Economic Geology Report 31, p. 163-230.

Leitch, C.H.B., Turner, R.J.W., Ross, K.V., and Shaw, D.R.
2000: Wallrock alteration at the Sullivan deposit, British Columbia, Canada, Chapter 34 *in* The Geological Environment of the Sullivan Deposit, British Columbia, (ed.) J.W. Lydon, T. Höy, J.F. Slack, and M.E. Knapp; Geological Association of Canada, Mineral Deposits Division, Special Paper No. 1, p. 633-651.

Lemkow, D., Harris, J.R., and Slack, T.
2007: Digital geoscience database: A contribution to the Mineral and Energy Resource Assessment of the greater Nahanni ecosystem, Northwest Territories, Appendix 4 *in* Mineral and Energy Resource Assessment of the Greater Nahanni Ecosystem Under Consideration for the Expansion of the Nahanni National Park Reserve, Northwest Territories, (ed.) D.F. Wright, D. Lemkow, and J.R. Harris; Geological Survey of Canada, Open File 5344.

Lowe, C., Brown, D.A., Best, M.E., and Shives, R.B.K.
2000: High resolution geophysical survey of the Purcell basin and Sullivan deposit: Implications for bedrock geology and mineral exploration, Chapter 20 *in* The Geological Environment of the Sullivan Deposit, British Columbia, (ed.) J.W. Lydon, T. Höy, J.F. Slack, and M.E. Knapp; Geological Association of Canada, Mineral Deposits Division, Special Paper No. 1, p. 355-369.

Maurice, Y.T. and Charbonneau, B.W.
1987: U and Th concentration processes in Canadian granitoids, their detection by airborne gamma ray spectrometry and their relationship to granophile mineralization; Revista Brasileira de Geociências, v. 17, p. 644-646.

Morrow, D.W. and Cook, D.G.
1987: The Prairie Creek Embayment and Lower Paleozoic Strata of the Southern MacKenzie Mountains; Geological Survey of Canada, Memoir 412, 195 p.

Nicolet, J.P. and Erdi-Krausz, G.
2003: Guidelines for Radioelement Mapping using Gamma Ray Spectrometry Data; Internaltional Atomic Energy Agency, Technical Document 1363, 171 p.

Okulitch, A.V. (compiler)
in prep: Bedrock Geology Redstone River, Northwest Territories, NP-9/10; Geological Survey of Canada, Open File, scale 1:1 000 000.

Shives, R.B.K., Ford, K.L., and Charbonneau, B.W.
1995: Applications of Gamma Ray Spectrometrometric-Magnetic-VLF-EM Surveys; Geological Survey of Canada; Open File 3061, 82 p.

Shives, R.B.K., Charbonneau, B.W., and Ford, K.L.
1997: The detection of potassic alteration by gamma ray spectrometry – Recognition of alteration related to mineralization, *in* Geophysics and Geochemistry at the Millennium: Proceedings of Exploration '97, Fourth Decennial International Conference on Mineral Exploration, Toronto, Canada, September 1997, (ed.) A.G. Gubins; p. 741-752.

2000: The detection of potassic alteration by gamma-ray spectrometry – Recognition of alteration related to mineralization; Geophysics, v. 65, p. 2001-2011.

Sprague K.B., Carson, J., and St. John Smith.
in prep: Combining Terrain and Detector Geometrical Sensitivity Corrections to Airborne Gamma-Ray Spectrometry Data.

Telford W.M., Geldart L.P., Sheriff, R.E., and Keys, D.A.
1976: Applied Geophysics; Cambridge University Press, London, England, 860 p.

Turner, R.J.W., Leitch, C.H.B., Ross, K.V., and Höy, T.
2000: District-scale alteration associated with the Sullivan deposit, British Columbia, Canada, Chapter 22 *in* The Geological Environment of the Sullivan Deposit, British Columbia, (ed.) J.W. Lydon, T. Höy, J.F. Slack, and M.E. Knapp; Geological Association of Canada, Mineral Deposits Division, Special Paper No. 1, p. 408-439.

Wolfe, W.J.
1976: Gold in Early Precambrian Superior Province Plutonic Rocks – The Relation of Geochemical Abundance and Concentration to Exploitable Levels; Ontario Ministry of Natural Resources, Geoscience Study 17, 6 p.

Yeates, A.N., Wyatt, B.W., and Tucker, D.H.
1982: Application of gamma-ray spectrometry to prospecting for tin and tungsten granites, particularly within the Lachlan Fold Belt, New South Wales; Economic Geology, v. 77, p. 1725-1738.

QUATERNARY GEOLOGY AND GLACIAL LIMITS OF THE NAHANNI NATIONAL PARK RESERVE AND ADJACENT AREAS, NORTHWEST TERRITORIES, CANADA

A. Duk-Rodkin, D. Huntley, and R. Smith
Geological Survey of Canada,3303-33 Street North West, Calgary, Alberta T2L 2A7

QUATERNARY GEOLOGY

The southern Mackenzie Mountain region has a complex glacial history. The region was glaciated by two ice masses from two different sources: the mountains to the west and the plains to the east. Stratigraphic and geomorphologic evidence indicate that the two glaciers occupied this region at different times during the Late Pleistocene (Fig. 1). The eastern continental ice sheet (Laurentide) advanced over the foothills and up major valleys reaching its maximum extent, ca. 30 ka. This took place when Cordilleran glaciers were in their initial stages of development. This pattern of glaciation is the same one that affected the central and northern Mackenzie Mountains in the Late Pleistocene. However, while areas north of the 64th parallel have an excellent geomorphic and pre-Late Pleistocene stratigraphic glacial record, the southern areas have an excellent geomorphic and stratigraphic Late Pleistocene record. Evidence of the older pre-Late Pleistocene glaciation has only been found in old glacial cirques north of the South Nahanni River watershed, in the Dahadinni Range; these are filled with Late Pleistocene Laurentide sediments.

Ice in the mountains was from three sources: valley glaciers from the Continental Divide; local ice caps that developed on mountain tops above the snow line during glaciation; and the Cordilleran ice sheets of the Cassiar and Selwyn mountains (Fig. 1B). Ice from the east (Laurentide) moved into the region as lobes and sub-lobes that followed the very irregular topography from foothills to mountains (Fig. 1A).

The two ice masses caused major changes to the landscape of the southern Mackenzie region. The Laurentide Ice Sheet blocked the drainage of the South Nahanni River causing the formation of a glacial lake, inundating an approximate maximum area of 900 km^2 with an outlet to the southwest into the Yukon and from there to the Pacific Ocean (Fig. 1B). Lacustrine sediments at various sites reach between 110 to 120 metres thick east of Virginia Falls (Figs. 1B, 2). These sediments have also been recorded up to 700 m in elevation along Wrigley Creek east of Virginia Falls (Figs. 3, 4, 5). The eastern ice sheet reached Virginia Falls and lower Flat River (Fig. 6). Shield granite erratics were found over 100 km west of the mountain front. Shield and less common non-shield glacial erratics can be seen at various elevations (Figs. 7, 8). During the retreat of the continental Laurentide Ice Sheet and advance of Cordilleran valley glaciers, glacial Lake Nahanni cut an outlet to the east at First Canyon. This outlet drained into a continuous northbound network of marginal meltwater channels joining the north-flowing drainage that eventually reached the Arctic Ocean. Further retreat of the ice sheet established the Mackenzie River where it is today.

Surficial deposits in the Nahanni Park area comprise mainly colluviated glacial sediments in areas that were covered by glaciers, colluvium blankets (that once covered or currently) covering bedrock slopes (sheetwash, rock falls, landslides), with present day development of cryogenic features on the flat mountain tops (stone and/or mud circles, solifluction lobes, and others). Alluvial flood-plain deposits developed along the Nahanni River and its tributaries. Fluvial deposits are found as glaciofluvial terraces and deltas from Cordilleran and/or continental provenance. Areas along the upper Flat River have extensive terraces and deltas that were built along the southwestern shores of glacial Lake Nahanni. Among the most important surficial features are landslides that developed on the glaciolacustrine sediments of the former Lake Nahanni and are now exposed along rivers, particularly the South Nahanni River (Fig. 2).

Neotectonic activity in the area is interpreted from exposures such as at Virginia Falls. Glaciolacustrine sediments of Lake Nahanni continue on the western side of the falls indicating that the falls most likely formed, or were tectonically reactivated in postglacial time. However, this observation is very preliminary and the stratigraphy of the lacustrine sediments needs further study to establish the lake sequence east and west of the falls in order to develop a better understanding of the Neotectonic events that affected the park area. Furthermore, glacial Lake Nahanni, with its history of outlets and shorelines, needs to be researched in detail before its extent and fluctuations due to continental and Cordilleran glaciers can be established.

Duk-Rodkin, A., Huntley, D., and Smith, R., 2007, Quaternary geology and glacial limits of the Nahanni National Park Reserve and adjacent areas, Northwest Territories, Canada, *in* Mineral and Energy Resource Assessment of the Greater Nahanni Ecosystem Under Consideration for the Expansion of the Nahanni National Park Reserve, Northwest Territories, (ed.) D.F. Wright, D. Lemkow, and J.R. Harris; Geological Survey of Canada, Open File 5344, p. 125-129.

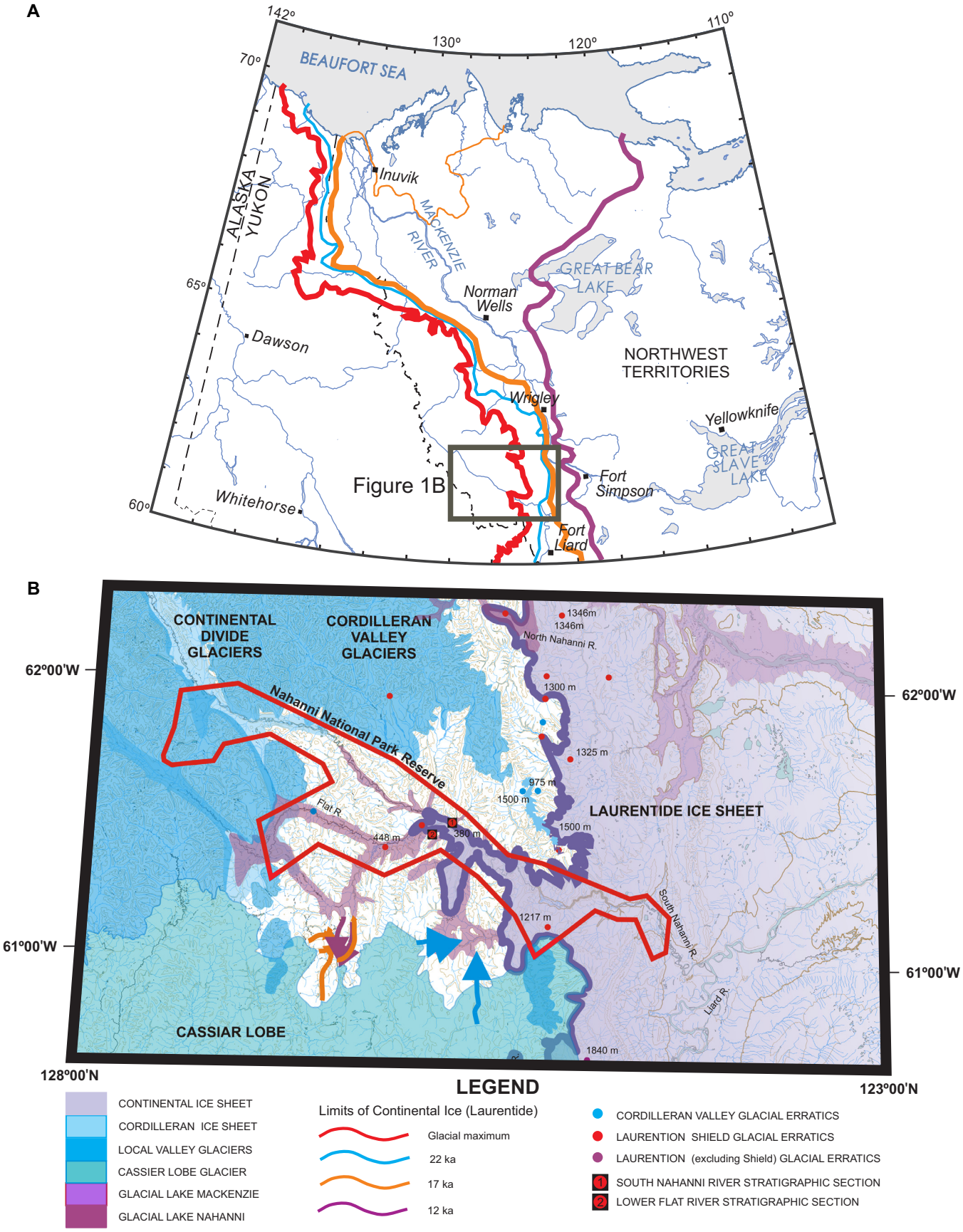


Figure 1. A) Location of the study area in relation to the Mackenzie Valley transportation corridor; also shown are the approximate limits of the Late Pleistocene Laurentide Ice Sheet. **B)** Pleistocene geology of the Nahanni area; also shown are the cross-section locations for the glacial lake sediments in the South Nahanni River (Fig. 2) and in the lower reach of the Flat River (Fig. 6).

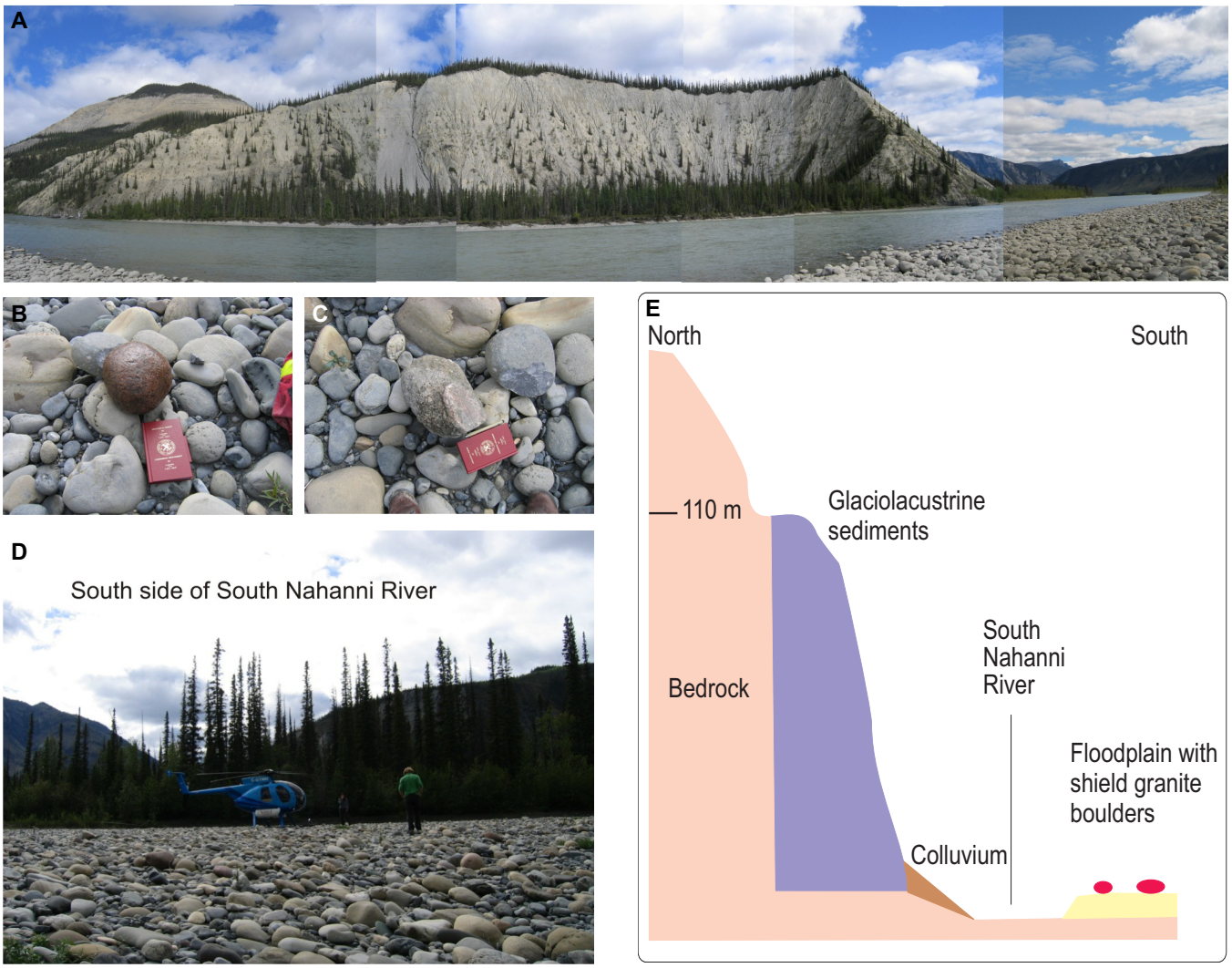


Figure 2. Glacial lake sediments in the South Nahanni River. **A)** Panoramic view of the north side of the South Nahanni River, showing 110 m of lacustrine sediments of Late Pleistocene glacial Lake Nahanni. **B, C)** Glacial boulders from the flood plain. **D)** Flood plain along the south side of the South Nahanni River. **E)** Cross-section of glacial Lake Nahanni.

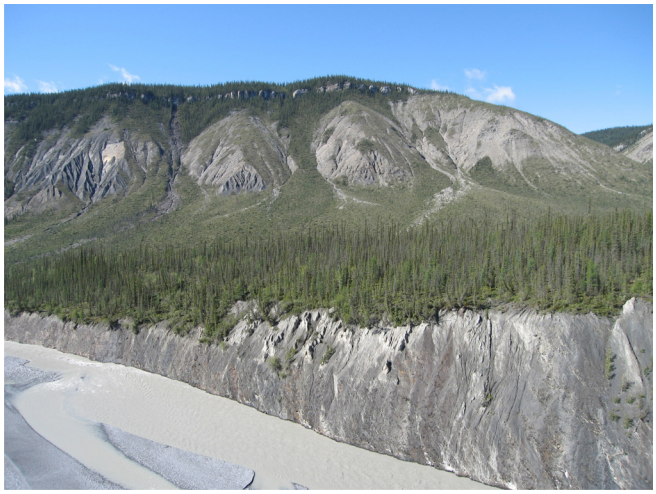


Figure 3. Lacustrine sediments (glacial Lake Nahanni) exposed on the eastern slope of lower Wrigley Creek, northern tributary to South Nahanni River



Figure 4. Lacustrine sediment (glacial Lake Nahanni) remnants along the eastern slopes of upper Wrigley Creek (Arnica Range), northern tributary to South Nahanni River.



Figure 5. Lacustrine sediments (glacial Lake Nahanni) exposed along the western slope of the upper Wrigley Creek, northern tributary to the South Nahanni River.

Figure 6. Glacial sediments in the lower reach of Flat River. **A, B)** Shield granite boulders in the flood plain. **C)** Schematic cross-section of glacial sediments.**D)** Laurentide meltout till, **E)** Laurentide outwash. **F)** Left side of Flat River opposite (G), looking downstream, showing flood plain. **G)** Panoramic view of the right side of Lower Flat River (looking downstream) near its confluence with the South Nahanni River, **H,I,J)** Granite boulders in melt out till.

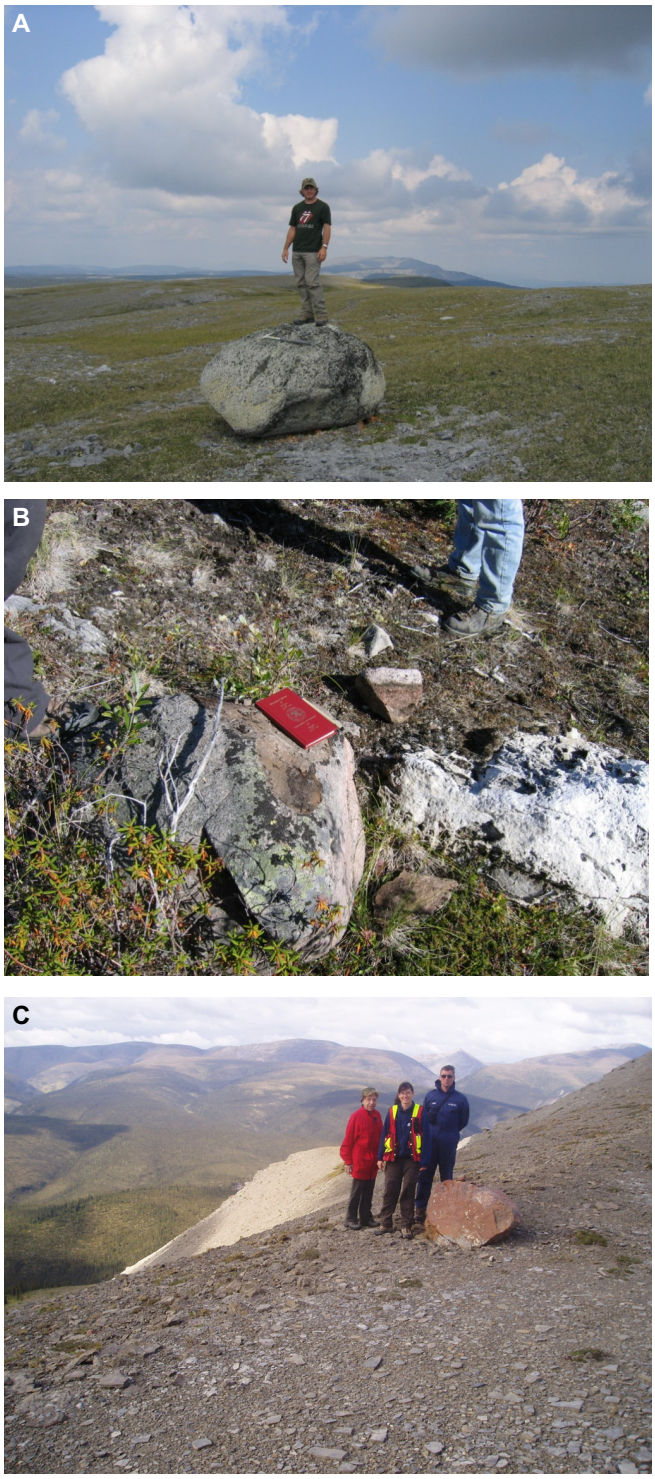


Figure 7. Shield erratics (granites) carried by the Laurentide Ice Sheet to various elevations.



Figure 8. Glacial erratic carried by the Laurentide Ice Sheet, of non-Shield origin.

ACKNOWLEDGMENTS

The authors would like to thank Parks Canada and the MERA process for support in accessing the park area and information on site locations for sampling. Thanks also go to D. Lemkow for editing, compiling, and reformatting.

ISOTOPE GEOCHEMISTRY OF THE PRAIRIE CREEK CARBONATE-HOSTED ZINC-LEAD-SILVER DEPOSIT, SOUTHERN MACKENZIE MOUNTAINS, NORTHWEST TERRITORIES

S. Paradis
Geological Survey of Canada, 9860 West Saanich Road, Sidney, British Columbia V8L 4B2

ABSTRACT

The Prairie Creek Zn-Pb-Ag deposit comprises three distinct types of carbonate-hosted sulphide mineralization that includes stratabound massive sulphide, classic Mississippi Valley-type (MVT), and quartz-carbonate-sulphide veins. The stratabound massive sulphides containing pyrite, sphalerite, and galena preferentially replaced the "Mottled Dolostone unit" of the Ordovician-Silurian Upper Whittaker Formation, but also formed within the "Lower and Upper Spar units" of the Upper Whittaker Formation. The MVT sulphides occur as open-space fillings of pyrite, sphalerite, and rare galena in a series of showings within the Silurian Root River dolostone. The quartz-carbonate-sulphide veins containing sphalerite, galena, chalcopyrite and tennantite-tetrahedrite fill fractures parallel to regional-scale faults crosscutting the Upper Whittaker Formation, Ordovician-Silurian Road River Formation, Silurian-Devonian Cadillac Formation, and Devonian Arnica Formation. The stratabound mineralization occurs over several stratigraphic levels for a strike length of 3 km and a thickness of ≤28 m. The vein-type sulphides are found along a 16 km long section of the north-south trending Prairie Creek Fault structure in twelve showings. Spatially, the stratabound sulphides are closely associated with the vein-type mineralization, fault structures, and regional north-south trending fold axis. However, the isotope data do not favour a genetic link between the stratabound sulphides and the vein sulphides.

Values of $\delta^{18}O_{PDB}$ for the mineralized dolomite associated with the stratabound sulphides range from -6.9 to -14.9‰ and values of $\delta^{13}C_{PDB}$ range from -2.3 to -4.7‰, similar to mineralized values of the Manetoe Facies in the Mackenzie Mountains of Yukon and Northwest Territories. The stratabound sulphides have similar $\delta^{18}O_{PDB}$ values but lower $\delta^{13}C_{PDB}$ values than the non-mineralized host dolostone of the Upper Whittaker Formation. $\delta^{18}O_{PDB}$ and $\delta^{13}C_{PDB}$ values for the quartz-carbonate-sulphide veins are slightly lower than the stratabound sulphides. The MVT showings have $\delta^{18}O_{PDB}$ values ranging from -17.6 to -10.7‰ and $\delta^{13}C_{PDB}$ values ranging from -7.2 to -1.0‰, which are similar to values for the Presqu'ile barrier of Alberta and Northwest Territories, and the Manetoe Facies. $^{87}Sr/^{86}Sr$ values of mineralized dolomite from the stratabound sulphides range from 0.7138 to 0.7239, which are similar to non-mineralized dolostone of the Upper Whittaker Formation. $^{87}Sr/^{86}Sr$ values for the quartz-carbonate-sulphide veins are variable and range from 0.70963 to 0.72848. These values are some of the most radiogenic values recorded in the northern Canadian Cordillera. They suggest that deep-circulating hydrothermal fluids were interacting with continental crust or derived siliciclastic rocks. $^{87}Sr/^{86}Sr$ values of mineralized dolomite from the Mississippi Valley-type showings range between 0.7105 and 0.7127, similar to Manetoe Facies, and overlapping the lighter values for the Robb Lake deposit in northeastern British Columbia.

Lead isotope values for the stratabound sulphides plot in a tight cluster below the "shale curve" with $^{206}Pb/^{204}Pb$ values ranging from 18.664 to 18.801 and $^{207}Pb/^{204}Pb$ values ranging from 15.640 to 15.663. These values overlap with the values of the Ordovician-Silurian SEDEX (sedimentary exhalative) deposits and the Devonian SEDEX deposits of the Selwyn Basin in Yukon. The quartz-carbonate-sulphide veins have $^{206}Pb/^{204}Pb$ values of 18.978 to 19.132 and $^{207}Pb/^{204}Pb$ values of 15.656 to 15.731 that form a linear array crosscutting the shale curve at 250 Ma. These data suggest that the stratabound sulphides and the vein sulphides are isotopically different and not genetically related. Lead isotope values from the Mississippi Valley-type sulphide occurrences plot in proximity to the stratabound sulphides, similar to values of the Silurian-Devonian MVT deposits of the Mackenzie Mountains and the northern Rocky Mountains.

Preliminary results on the sulphur isotopes of the Prairie Creek mineralization show their similarity with sulphides of the Selwyn Basin in Yukon and the Kechika Trough in northeastern British Columbia. The source of reduced sulphur in both cases was most likely bacterially reduced seawater sulphate.

The metallogenic model invoked for the stratabound sulphide mineralization at Prairie Creek is similar to the SEDEX deposits of the Selwyn Basin. The mineralization formed in a secondary rift-controlled sedimentary basin, the Prairie Creek Embayment, along the margin of the carbonate platform, which is adjacent to the Selwyn Basin. It is suggested that the stratabound sulphides formed by replacement of carbonates at the time or slightly later to the genesis of SEDEX deposits in the Selwyn Basin. Sulphides precipitated as a consequence of fluid mixing within dolomitic units. This process involved relatively high temperature (110-240°C), metal-bearing solutions derived from a basement-equilibrated fluid reservoir (carrying Zn, Pb, Fe, Cu) and cooler, saline (~10-23 wt.% NaCl) formation waters rich in bacteriogenic H_2S.

Paradis, S., 2007, Isotope geochemistry of the Prairie Creek carbonate-hosted zinc-lead-silver deposit, southern Mackenzie Mountains, Northwest Territories, *in* Mineral and Energy Resource Assessment of the Greater Nahanni Ecosystem Under Consideration for the Expansion of the Nahanni National Park Reserve, Northwest Territories; Geological Survey of Canada, Open File 5344, p. 131-176.

INTRODUCTION

The Prairie Creek Zn-Pb-Ag deposit, previously known as the Cadillac deposit, is located in platform carbonate rocks of the southern Mackenzie Mountains, in southwestern Northwest Territories (61°33'11.6"N and 124°47'33.2"W; 95F/10; Fig. 1). It comprises three distinct types of carbonate-hosted sulphide mineralization that include stratabound massive sulphides (SMS), Mississippi Valley-type, and quartz-carbonate-sulphide veins. The known sulphide occurrences in the Prairie Creek deposit area are listed in Table 1 and their locations are shown on Figure 2 (excluding South Gate which occurs south of the area shown on Fig. 2).

The deposit contains a geological resource of 11.8 million tonnes at 12.5% Zn, 10.1% Pb, and 0.4% Cu, 161 g/t Ag; the resource was calculated on 2.5 km of a 16 km mineralized trend (Canadian Zinc Corporation, 2001). The majority of the mineral resource occurs as vein-type mineralization and the remainder as stratabound massive sulphides in zone 3. The vein mineralization contains a measured and indicated mineral resource of 2.3 million tonnes grading 12.2% Zn, 12.5% Pb, 190 g/t Ag, and 0.4% Cu with an additional inferred resources of 9.1 million tonnes grading 10.5% Zn, 12.9% Pb, 171 g/t Ag, and 0.4% Cu (Canadian Zinc Corporation, 2004). The stratabound mineralization consists of a measured and indicated mineral resource of 1.25 million tonnes grading 10.6% Zn, 5.2% Pb, and 55.9 g/t Ag (Canadian Zinc Corporation, 2004).

The quartz-carbonate-sulphide veins and the stratabound sulphides occur within the Prairie Creek Embayment, a north-south paleo-depression filled by Ordovician to Devonian conformable platformal and basinal sediments. The veins are exposed in twelve showings along a north-south trending 16 km-long corridor crosscutting dolostones of the Upper Whittaker Formation, shales of the Road River Formation and dolostones and limestones of the Arnica Formation (Fig. 2). Approximately 7.5 km northwest of the Prairie Creek mine site, another north-south trending, subvertical quartz-carbonate-sulphide vein system is exposed at the North Gate showing (Fig. 2). Farther south, i.e. 25.8 km southwest of the Prairie Creek mine site, north-south trending, subvertical to west 60° dipping quartz-carbonate veins containing sporadic galena, sphalerite, malachite, and azurite occurred at the South Gate showing. The stratabound sulphides, which don't outcrop, occur as small lenses replacing the dolostones of the Upper Whittaker Formation in proximity to the Prairie Creek mine site. The MVT showings are exposed in the northern portion of the Prairie Creek property within the marginal carbonate sequence of the Root River Formation where typical sulphide textures include open-space filling of breccias, fractures and vugs.

This paper presents preliminary results of C, O, Sr, Pb, and S isotopes from the stratabound sulphides, quartz-carbonate-sulphide veins, and the Mississippi Valley-type sulphides and their carbonate host rocks. These results are compared to other sediment-hosted sulphide deposits of the Canadian Rocky Mountains, the Mackenzie Mountains and the Western Canada Sedimentary Basin (WCSB).

EXPLORATION AND MINING HISTORY

Sulphide mineralization was first noted in 1928 in the Prairie Creek area (NORMIN.DB, Canadian Zinc Corporation, 2006) however, limited exploration work was done until 1966 when Cadillac Resources Ltd. acquired the ground. Between 1966 and 1969, they explored and discovered quartz-carbonate-sulphide veins containing variable amounts of sphalerite, galena, pyrite, and tetrahedrite exposed in twelve zones along a north-south trend in dolostone of the Road River and Upper Whittaker formations (Thorpe, 1972).

In 1970, Penarroya Canada Ltd. optioned the property from Cadillac Resources Ltd. and completed some underground development in zone 3 and drilling in zones 6, 7, and 9. In the late 1970s, Cadillac terminated the option agreement with Penarroya. Between 1970 and 1980, Cadillac Resources Ltd. carried out extensive underground development of zone 3 at the 929.6 and 868.7 metre levels. In 1980, based on a feasibility study completed by Kilborn Engineering Ltd., Procan Exploration Company Ltd. agreed to finance the mine into production. By May 1982, the mine surface facilities were almost completed, and mine production was scheduled at an initial rate of 453.6 metric tonnes per day, when the price of silver collapsed and all the operations at Prairie Creek were suspended. Cadillac was forced into bankruptcy, and the property together with all other assets of Procan Exploration Company Ltd., were tied up in litigation until 1990. In 1991, Conwest Exploration Company Ltd. acquired the property and granted an option to San Andreas Resources Corporation to acquire a 60% interest in the property. Between 1991 and 1995, San Andreas completed 40,000 metres of surface diamond drilling and an underground exploration program, which expanded the inventory of known resources on the property. In 1992, stratabound sulphide mineralization was discovered while drilling to extend the vein resource at depth. In 1999, San Andreas Resources Corporation's name was changed to Canadian Zinc Corporation, and they started a grass-roots regional exploration program in the Prairie Creek Embayment. The company staked four claim blocks 7.5 km northwest of the Prairie Creek mine site, and did some prospecting and geochemical sampling that resulted in the discovery of a new vein showing (i.e. North Gate) and geochemical Zn anom-

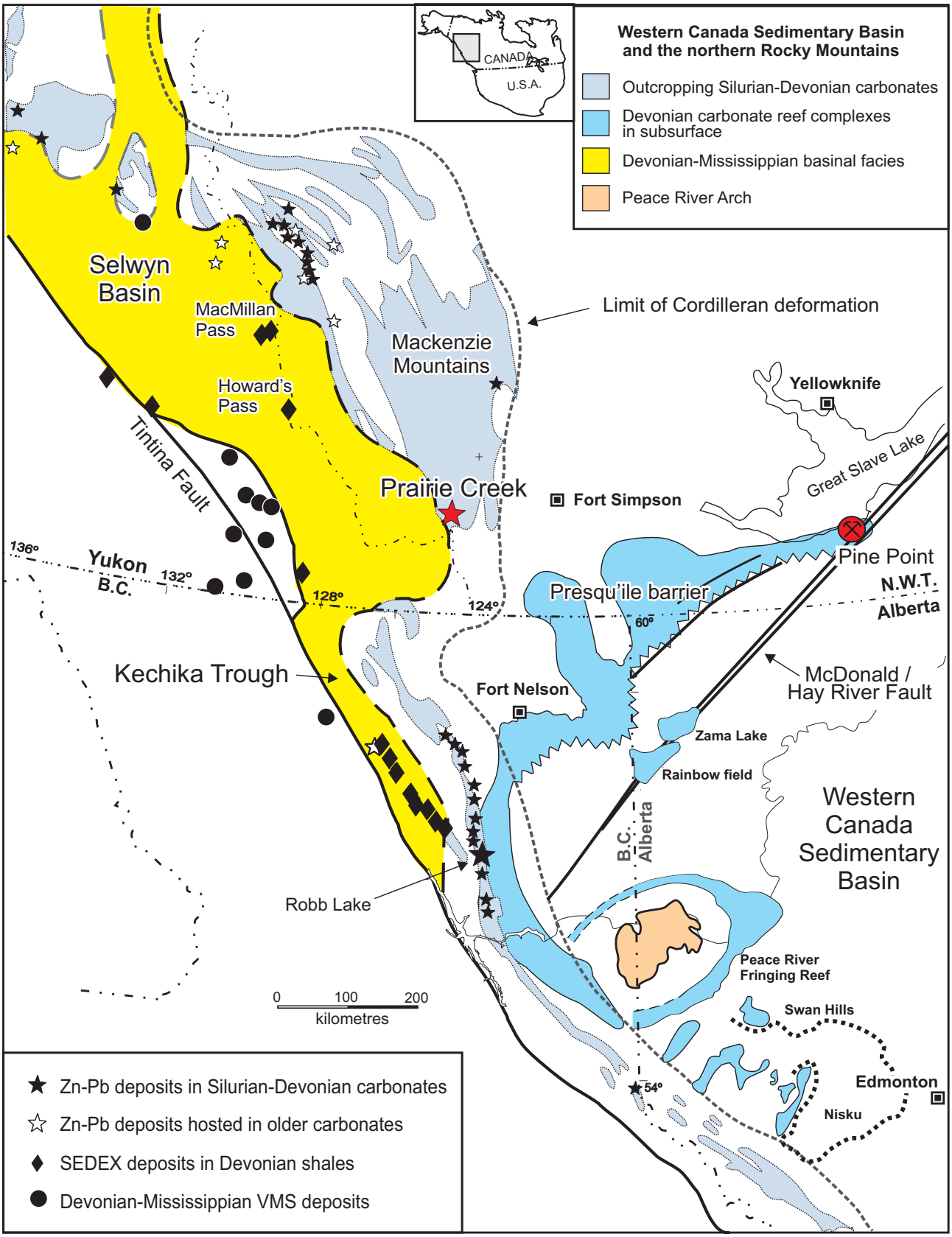


Figure 1. Location of the Prairie Creek Zn-Pb-Ag carbonate-hosted deposits, southern Mackenzie Mountains, Northwest Territories. Also shown are the location of other carbonate-hosted Zn-Pb deposits within the northern Canadian Rocky Mountains and the Western Canada Sedimentary Basin, the sedimentary exhalative (SEDEX) deposits within the Kechika Trough and the Selwyn Basin, and the volcanic-hosted massive sulphide (VHMS) deposits in the outermost continental margin. Diagram is compiled from Morrow et al. (1990), Olson et al. (1994), and Mossop and Shetsen (1994), and modified from Nelson et al. (2002).

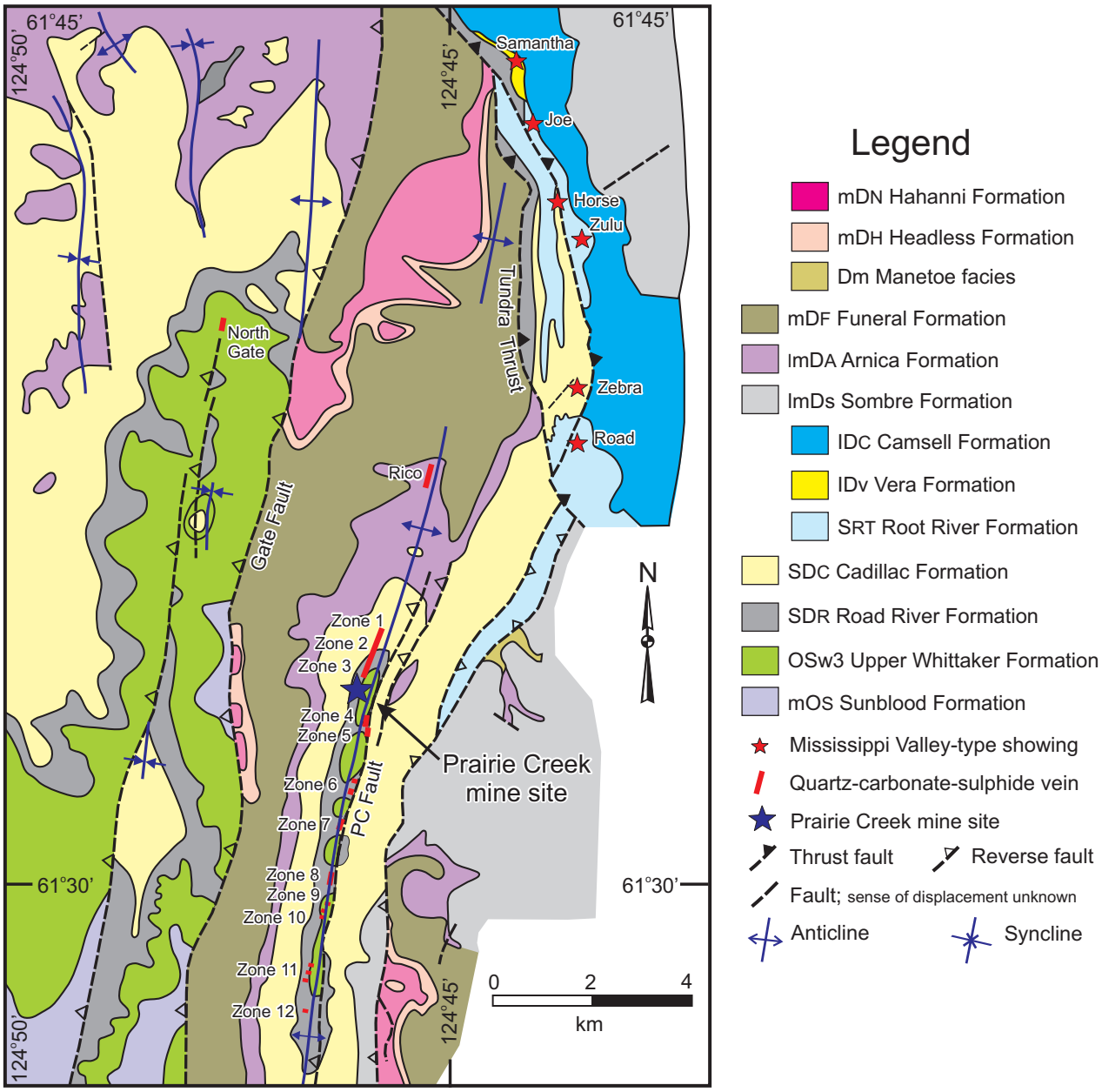


Figure 2. Geological map of the Prairie Creek deposit area showing the location of the mine site at zone 3, the various zones of the quartz-carbonate-sulphide veins, and the Mississippi Valley-type showings (from Morrow and Cook, 1987; Canadian Zinc Corporation, http://www.canadianzinc.com). According to Taylor (1995), the Zebra showing is hosted in a brecciated facies of the Cadillac Formation (i.e. Cadillac ET), which is a facies equivalent to the Root River Formation. The Samantha showing is associated with a 40°–trending and north-west-dipping normal fault, which brings the Vera Formation into contact with the Root River Formation. Showings from the Prairie Creek district are tabulated in Table 1.

alies over parts of the Upper Whittaker Formation (Canadian Zinc Corporation, 2004). In May 2000, Canadian Zinc Corporation performed a regional reconnaissance helicopter exploration program to assess the regional mining potential focused mainly in the northern sector of its property. Throughout 2001 to 2003, the company focused its efforts to advance the Prairie Creek deposit towards development, principally in the permitting process. In 2004, they carried out a surface and underground drill exploration program within 1000 metres of the Prairie Creek mine site facility. An underground and surface exploration and development program is planned for 2006 and 2007.

REGIONAL GEOLOGICAL SETTING

The Canadian Cordillera is characterized by imbricated and folded miogeoclinal and clastic wedge assemblages onlapping ancestral North American rocks. These Cambrian to Middle Devonian shelf strata are exposed in the northern Rocky Mountains of British Columbia and in the Mackenzie Mountains of eastern Yukon and western Northwest Territories.

In the southern Mackenzie Mountains, lower Paleozoic rocks record the development of a broad depositional shelf-edge margin where shallow water carbonates passed abruptly basinward to deeper water argillaceous limestone, shale, and dolostone (Morrow and Cook, 1987). The migration of this shelf edge was related to the evolution of the Root Basin in Paleozoic time, an intrashelf basin that occupied the southern Mackenzie Shelf, and to the development of the Prairie Creek Embayment at the southern entrance to the Root Basin (Morrow and Cook, 1987). The Prairie Creek Embayment is a north-south paleo-depression feature where thick accumulations of basinal sediments and platformal carbonates occurred during lower Paleozoic time. It is bounded to the east, north, and west by shallow-water platformal carbonates of the Mackenzie Mountains and to the south by basinal shales of the Selwyn Basin. Morrow and Cook (1987) suggested that during the lower Paleozoic, the embayment was a half-graben type structure controlled by a north-south trending westerly downthrowing fault. The embayment is presently bounded to the east by the east-dipping Tundra thrust fault, and 20 km to the west by the west-dipping Manetoe thrust fault (Morrow and Cook, 1987).

GEOLOGY OF THE PRAIRIE CREEK DEPOSIT AREA

A brief description of the main geological formations within the Prairie Creek Embayment is given here. For a detailed description, the reader is referred to Morrow and Cook (1987).

Morrow and Cook (1987) divided the lower Paleozoic strata into four ascending subdivisions: 1) Sunblood Platform, 2) Mount Kindle-Root River assemblage, 3) Prairie Creek assemblage, and 4) Funeral-Headless assemblage.

The Sunblood Platform consists solely of the middle Ordovician shallow water argillaceous limestone and dolostone of the Sunblood Formation. It is conformably overlain by basinal shales of the Road River Formation west of Prairie Creek, and unconformably overlain by dolostones of the Whittaker Formation in the Prairie Creek area.

The Late Ordovician to Devonian Mount Kindle-Root River assemblage consists of the Whittaker, Road River, and Root River formations. The Mount Kindle Formation, which is the shallow water reefal facies equivalent of the deeper water Whittaker Formation, is not present in the Prairie Creek area. Morrow and Cook (1987) divided the Whittaker Formation into three lithofacies: 1) a middle to upper Ordovician dark grey silty and sandy limestone (muOw1), 2) a middle to upper Ordovician fine-grained quartzite (muOw2), and 3) an upper Ordovician to Silurian laminated dark grey finely crystalline dolostone (OSw3), which hosts the stratabound sulphide mineralization at Prairie Creek. The lithofacies OSw3 has been subdivided into 7 subunits in the Prairie Creek deposit area by geologists of San Andreas Resources Corporation (see Table 2). The Silurian-Devonian Road River Formation comprises a sequence of graptolite-bearing shale and argillaceous bioclastic shaly dolostone conformably overlying the Whittaker Formation. West of Prairie Creek, the Road River Formation thickens considerably in excess of 1000 m, and passes conformably upward into the Vera Formation. Eastward, in the Prairie Creek area, the Road River Formation thins to 170 m and is conformably overlain by the Cadillac and Root River formations. The Silurian Root River Formation is believed to be the shelf equivalent of the basinal facies of the Cadillac Formation. It consists of light grey vuggy micritic dolostone.

The Silurian-Devonian Prairie Creek assemblage represents strata of greatest facies variation as well as greatest thickness and it records the inception and growth of the Prairie Creek Embayment (Morrow and Cook, 1987). It consists of the lower and upper Cadillac phases (Morrow, 1984; Morrow and Cook, 1987). The lower Cadillac phase, which marks the inception of the embayment in Early Devonian, comprises orange-weathering siltstone and megabreccia members of the Cadillac, Vera, and Camsell formations. The upper Cadillac phase, encompassing strata deposited in the Embayment throughout early Devonian time, comprises the Sombre and Arnica formations, and the pink shale member of the Cadillac Formation.

The middle Devonian Funeral-Headless assemblage, which records the disappearance of the Prairie Creek Embayment, is divided into two phases, a lower Funeral-Landry phase, and an upper Headless-Nahanni phase. The Funeral-Landry phase comprises shale and grey weathering massive limestone. The Headless-Nahanni phase consists of a recessive shale and argillaceous limestone overlain by a resistant limestone.

Structures

The lower Paleozoic sedimentary rocks of the southern Mackenzie Mountains are characterized by north- to northeast-trending structures. The folds are doubly-plunging, faulted anticlines and broad, flat-bottomed synclines, which presently expose Upper Devonian shales (Gabrielse et al., 1991). The anticlines are asymmetrical, and axial planes within these folds are shown to change dip. De Wit et al. (1973) suggest that these structures can be explained by transcurrent movements. Another characteristic of the Mackenzie Mountains is the sinuous arrangement of folds and thrust faults, with north-northeast fold axes.

Table 1. Major sulphide showings within the Prairie Creek area, Northwest Territories.

Showing	NORMIN #	Datum	UTM Northing	UTM Easting	Deposit Class	Formation	Host Lithology	Mineralization - Tonnage / Grades
Samantha - upper	095FNE0034	Nad 83	6843204.5	408890.0	MVT	Root River	Finely crystalline, fossiliferous dolostone	Gossanous zone in oxidized and silicified breccias.
Samantha - lower	095FNE0034	Nad 83	6842662.5	408600.5	MVT	Root River	Finely crystalline, fossiliferous dolostone	Galena, smectite, malachite/azurite accompany by white sparry dolomite cement in fractures, vugs, and other open cavity type settings. Best-grade samples trenches = 0.97% Cu, 9.55% Pb, 40.05% Zn, 180.4 g/t Ag over 3.65 m (Tremblay, 1981). Chip samples = 0.47% Cu, 20.65% Pb, 19.94% Zn, 164.5 g/t Ag over 3.65 m, and 0.05% Cu, 0.60% Pb, 31.84% Zn, 15.2 g/t Ag over 5.61 m (Tremblay, 1981).
Joe	095FNE0040	Nad 83	6840616.3	409164.1	MVT	Root River	Finely crystalline, fossiliferous dolostone	Gossanous zone consists of oxidized dolostone breccia, ferricrete, calcrete and locally smithsonite. One grab sample returned 0.18% Pb and 27.9% Zn (Taylor, 1995). Four soil samples returned best assay of 945 ppm Pb and 13.1% Zn.
Horse	095FNE0039	Nad 83	6839185.0	410100.0	MVT	Root River	Finely crystalline, fossiliferous dolostone	Fine-grained sphalerite is found associated with sparry dolomite cement within dolostone breccias. Soil geochemical survey identified anomalous Zn (<5550 ppm) and Pb (<481 ppm) in an area 800 m long by 50-300 m wide (NORMIN.DB).
Zebra - lower	095FNE0037	Nad 83	6842662.5	410801.2	MVT	Cadillac ET (~Root River)	Finely crystalline, fossiliferous brecciated dolostone	Pyrite, sphalerite, traces of galena, sparry and saddle dolomite cement as open-space fillings of fractures, vugs, and breccias observed over 650 m in strike. Best composite drilling intercept = 8.5 m at 2.8% Zn (Taylor, 1995).
Zebra - upper	095FNE0037	Nad 83	6833925.9	410027.5	MVT	Cadillac ET (~Root River)	Finely crystalline, fossiliferous vuggy dolostone	Pyrite-sphalerite occur as anastomosing vein-like system in vuggy dolostone and dolospar breccia.
Zulu	095FNE0038	Nad 83	6837372.0	410406.0	MVT	Root River	Finely crystalline, fossiliferous dolostone	3 areas (upper, main, lower). Upper=silicified spar breccia lenses host disseminated fine-grained sphalerite and pyrite. Main=coarse grained dolospar breccia with sphalerite and pyrite forming rims around dolostone fragments. Lower=disseminated sphalerite in sparry dolomite filling vugs and breccias.
Road	095FNE0035	Nad 83	6832497.5	410146.5	MVT	Root River	Finely crystalline, fossiliferous dolostone	Traces of galena in vug gy dolostone.
North Gate	N/A	Nad 83	6835732.6	400838.6	Veins	Upper Whittaker	Finely crystalline, fossiliferous dolostone	Quartz-carbonate-galena-sphalerite-malachite (with traces of tetrahedrite) vein.
South Gate	N/A	Nad 83	6807388.0	390411.3	Veins	Sunblood?	Finely crystalline, fossiliferous dolostone	Quartz-carbonate veins containing sporadic galena, sphalerite, malachite, and azurite.
Rico	095FNE0036	Nad 83	6831946.8	406649.5	Vein and stratabound sulphides	Arnica	Finely crystalline, nodular and banded cherty (silicified) dolostone	Quartz-carbonate-galena-sphalerite-malachite vein within a fault zone and a stratabound lens hosting patches of galena and/or traces of tetrahedrite in matrix of breccia (20% Pb, 8.9% Zn). Assay values from vein: 0.06% Cu, 14.46% Pb, 6.9% Zn, 63.8 g/t Ag over 1.1 m. Assay values from lens: 0.28% Cu, 35.23% Pb, 17.82% Zn, 219.6 g/t Ag over 1.1 m (Taylor, 1993).
Prairie Creek zone 1	095FNE0012	Nad 27	6827227	404926	Veins	Upper Whittaker [1]	Thin-bedded dark grey cherty dolostone	Two parallel galena-sphalerite veins. Assay values: 1544 g/t Ag, 61.75% Pb, 1.43% Zn, and 2.77% Cu (NORMIN.DB).
Prairie Creek zone 2	095FNE0001	Nad 27	6827166	404910	Veins	Upper Whittaker	Thin-bedded dark grey cherty dolostone	0.3 to 1 m thick, NNE-trending quartz-carbonate-galena-sphalerite-tetrahedrite-malachite veins exposed over 50 m. Best assay values: 13.25% Zn, 52.5% Pb, 1113.5 g/t Au, 0.062% Cd(NORMIN DB)
Prairie Creek zone 3	095FNE0013	Nad 83	6825979.8	404343.3	Veins and stratabound sulphides	Upper Whittaker	Thin-bedded dark grey cherty dolostone	Vein: Measured and indicated resources are 2.3 Mt grading 12.2% Zn, 12.5% Pb, 190 g/t Ag, 0.4% Cu; additional inferred resources are 8.1 Mt grading 10.5% Zn, 12.9% Pb, 171 g/t Ag, 0.4% Cu. Stratabound: Measured and indicated resources are 1.25 Mt grading 10.6% Zn, 5.2% Pb, 55.9 g/t Ag (Canadian Zinc Corporation, 2004).
Prairie Creek zone 5	095FNE0002	Nad 83	6825069.0	404794.8	Veins and stratabound sulphides	Upper Whittaker	Thin-bedded dark grey cherty dolostone	"Discovery zone": N-S trending, subvertical quartz-carbonate-galena-sphalerite-tetrahedrite vein. Stratabound massive sulphides intersected by drilling.
Prairie Creek zone 6	095FNE0003	Nad 83	6823154.6	404363.3	Veins and stratabound sulphides	Upper Whittaker and Road River	Upper Whittaker = thin-bedded dark grey cherty dolostone. Road River=dark grey graphitic, argillaceous bioclastic shaley dolostone.	N-S trending, subvertical quartz-carbonate-galena-sphalerite-malachite-tetrahedrite vein. Stratabound massive sulphides intersected by drilling.
Prairie Creek zone 7	095FNE0009	Nad 83	6822145.4	403910.8	Veins	Upper Whittaker and Road River	Upper Whittaker = thin-bedded dark grey cherty dolostone. Road River=dark grey graphitic, argillaceous bioclastic shaley dolostone.	N-S trending, subvertical quartz-carbonate-galena-sphalerite-malachite-tetrahedrite vein.
Prairie Creek zone 8	095FNE0010	Nad 83	6820721.3	403662.2	Veins	Upper Whittaker	Thin-bedded dark grey cherty dolostone (OSw3)	N-S trending, subvertical quartz-carbonate-galena-sphalerite-malachite-tetrahedrite vein.
Prairie Creek zone 9	095FNE0011	Nad 27	6819620	403519	Veins	Upper Whittaker	Thin-bedded dark grey cherty dolostone (OSw3)	N-S trending, subvertical quartz-carbonate-galena-sphalerite-malachite-tetrahedrite vein.
Prairie Creek zone 10	095FNE0004	Nad 83	6819071	402971	Veins	Upper Whittaker	Thin-bedded dark grey cherty dolostone	N-S trending, subvertical quartz-carbonate-galena-sphalerite-malachite-tetrahedrite vein.
Prairie Creek zone 11	095FNE0005	Nad 83	6817990	402867	Veins	Upper Whittaker	Thin-bedded dark grey cherty dolostone	N-S trending, subvertical quartz-carbonate-galena-sphalerite-malachite-tetrahedrite vein.
Prairie Creek zone 12	095FNE0006	Nad 83	6817218	402771	Veins	Upper Whittaker	Thin-bedded dark grey cherty dolostone	N-S trending, subvertical quartz-carbonate-galena-sphalerite-malachite-tetrahedrite vein.

[1]Upper Whittaker Formation has been divided into 7 units from the lower to the upper most: OSw3-1=grey massive dolostone; OSw3-2=mottled dolostone; OSw3-3=lower chert nodule dolostone; OSw3-4=lower spar unit; OSw3-5=upper chert nodule dolostone; OSw3-6=upper spar unit; OSw3-7=banded chert dolostone. Abbreviation: MVT=Mississippi Valley-type. All data is in UTM Zone 10, and NTS map sheet 95F10.

Table 2. Stratigraphy of the Whittaker Formation to the Arnica Formation in the Prairie Creek deposit area (modified from Earls, 1995; Fraser, 1996; and Canadian Zinc Corporation, 2001, 2004).

Unit	Formation	Thickness (m)	Description
lmDAb	Arnica	200-250	*Nodular and banded cherty dolostone:* Finely crystalline dark nodular and thick banded cherty (silicified) dolostone with quartz-carbonate crackle veining.
SDC	Cadillac	300-350	*Thin bedded silty dolostone, and calcareous siltstone and shale:* Orange weathering, minor debris flows (crinoidal).
SDR	Road River	230-280	*Argillaceous bioclastic shaly dolostone and shale:* Thin to thick bedding, graphitic, graptolites common, minor crinoids and brachiopods.
OSw3-7	Upper Whittaker	50-60	*Banded chert dolostone:* Well bedded chert interbedded with brownish grey dolostone.
OSw3-6	Upper Whittaker	10-25	*Upper spar unit:* Massive bioclastic dolostone with abundant white cm size sparry carbonate filling vugs and cavities.
OSw3-5	Upper Whittaker	55-100	*Upper chert nodule dolostone:* Massive to poorly bedded grey dolostone with occasional black cherty nodules.
OSw3-4	Upper Whittaker	10-24	*Lower spar unit:* Similar to upper spar unit but spars are more variable and less well developed in places.
OSw3-3	Upper Whittaker	40-60	*Lower chert nodule dolostone:* Similar to upper chert nodule dolostone.
OSw3-2	Upper Whittaker	20-30	*Mottled dolostone:* Fine-grained dolostone with spheroidal mottled texture in dolostone and cherty nodules.
OSw3-1	Upper Whittaker	20-50	*Massive dolostone:* Grey massive dolostone with minor chert nodules.
muOw2	Middle Whittaker	40-50	*Gritty dolostone:* interbedded with occasional siltstone and sandstone beds.
muOw1	Lower Whittaker	50-?	*Chert nodule dolostone:* Grey massive dolostone with minor cherty nodules.

Cook (1977) described three phases of deformation in the Prairie Creek Embayment. The earliest phase corresponds to regional north-south trending folding. These folds are cut by steeply dipping wrench faults that were subsequently rejuvenated as high-angle reverse faults (Morrow and Cook, 1987). The reverse faults are postdated by prominent north-trending flat thrust faults, which occur primarily in the platform carbonates flanking the embayment (Morrow and Cook, 1987), and are related to regional compression during the Laramide Orogeny.

Two major thrusts, the Tundra Thrust to the east (see Fig. 2), and the Manetoe Thrust 20 km to the west (not shown on Fig. 2), define the present margins of the Prairie Creek Embayment (Morrow and Cook, 1987). They juxtapose hanging-wall shallow-water shelf carbonates against footwall deeper water basinal sediments of the Embayment. The Tundra Thrust is a regional north-south trending structure, which dips approximately 45° to the east and in part places hanging-wall Road River shales against deeper water embayment units of the Funeral Formation (Morrow and Cook, 1987).

In the immediate area of the Prairie Creek mine site, faulting and folding axes trend north-south, resulting in windows of Road River shales cored by dolostones of the Upper Whittaker Formation being exposed along the core of the Prairie Creek anticline. The axial plane of the anticline plunges gently northward around the mine site and plunges southward. The Prairie Creek anticline is structurally bounded to the east by the Prairie Creek Fault and to the west by the Gate Fault (Fig. 2). These faults are presently north-south striking, reverse west-dipping (65-90°) structures that could have been originally normal faults (Earls, 1995; Fraser, 1996). The Prairie Creek Fault is a steeply dipping reverse fault that is up to 40 m in thickness and has a 1500 m displacement (Morrow and Cook, 1987). Earls (1995) suggests that the Prairie Creek Fault might have initially been a west-down throwing normal fault related to the formation of the Embayment, which would have been reactivated and reversed during the compressional event associated with the Laramide Orogeny.

MINERALIZATION

Deposit Types and Distribution

Three types of sulphide mineralization have been recognized in the Prairie Creek district, i.e. quartz-carbonate-sulphide veins, stratabound massive sulphide lenses, and MVT sulphide occurrences.

The stratabound massive sulphides form five lenses or bands (SD1, SD2, SD3, SD4, and SD5) that replaced the host dolostones of the Upper Whittaker Formation. They occur at different stratigraphic levels of the Ordovician-Silurian Upper Whittaker Formation, i.e. within the mottled dolostone (OSw3-2), the lower chert nodule dolostone (OSw3-3), the lower spar (OSw3-4) and upper spar (OSw3-6) units, the upper chert nodule dolostone (OSw3-5), and the banded chert dolostone (OSw3-7) of the Upper Whittaker Formation. The sulphides of the largest lens, SD1, preferentially replaced the mottled dolostone unit (OSw3-2; Fig. 3A, B). The stratabound sulphides have been located by drilling in zones 3, 4, 5, and 6, along the trend of the quartz-carbonate-sulphide vein system for a strike length of more than 3 km (Findlay, 2000). Spatially, they are closely associated with the sulphide vein system, the Prairie Creek Fault structure, and the regional north-south trending fold axis of the Prairie Creek anticline (Fig. 4).

The Prairie Creek stratabound sulphides have previously been compared to the Irish-type deposits (Earls, 1995; Findlay, 2000) because they share several characteristics, such as 1) they have simple mineralogy of

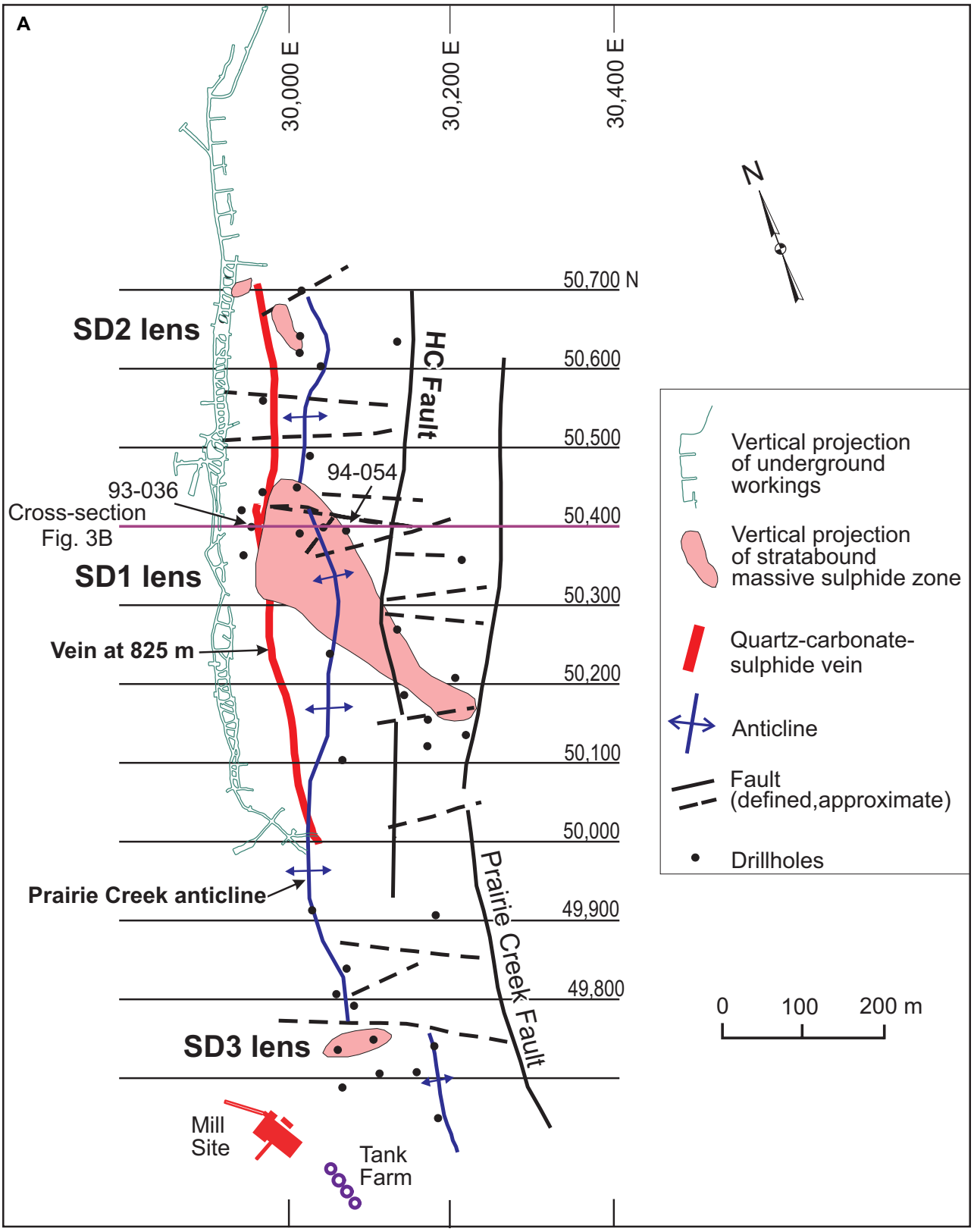


Figure 3. A) Plan view of the vertical projection of the stratabound lenses (SD1, SD2, SD3) and the position of the quartz-carbonate-sulphide vein at 825 m elevation (modified from Canadian Zinc Corporation, 2004).

sphalerite, galena, and iron oxides in a gangue of quartz and carbonates, 2) the sulphide and oxide minerals preferentially replaced the carbonate units, 3) the mineralization occurs along or immediately adjacent to faults that may have formed conduits for upward-migrating hydrothermal fluids, 4) the morphology of

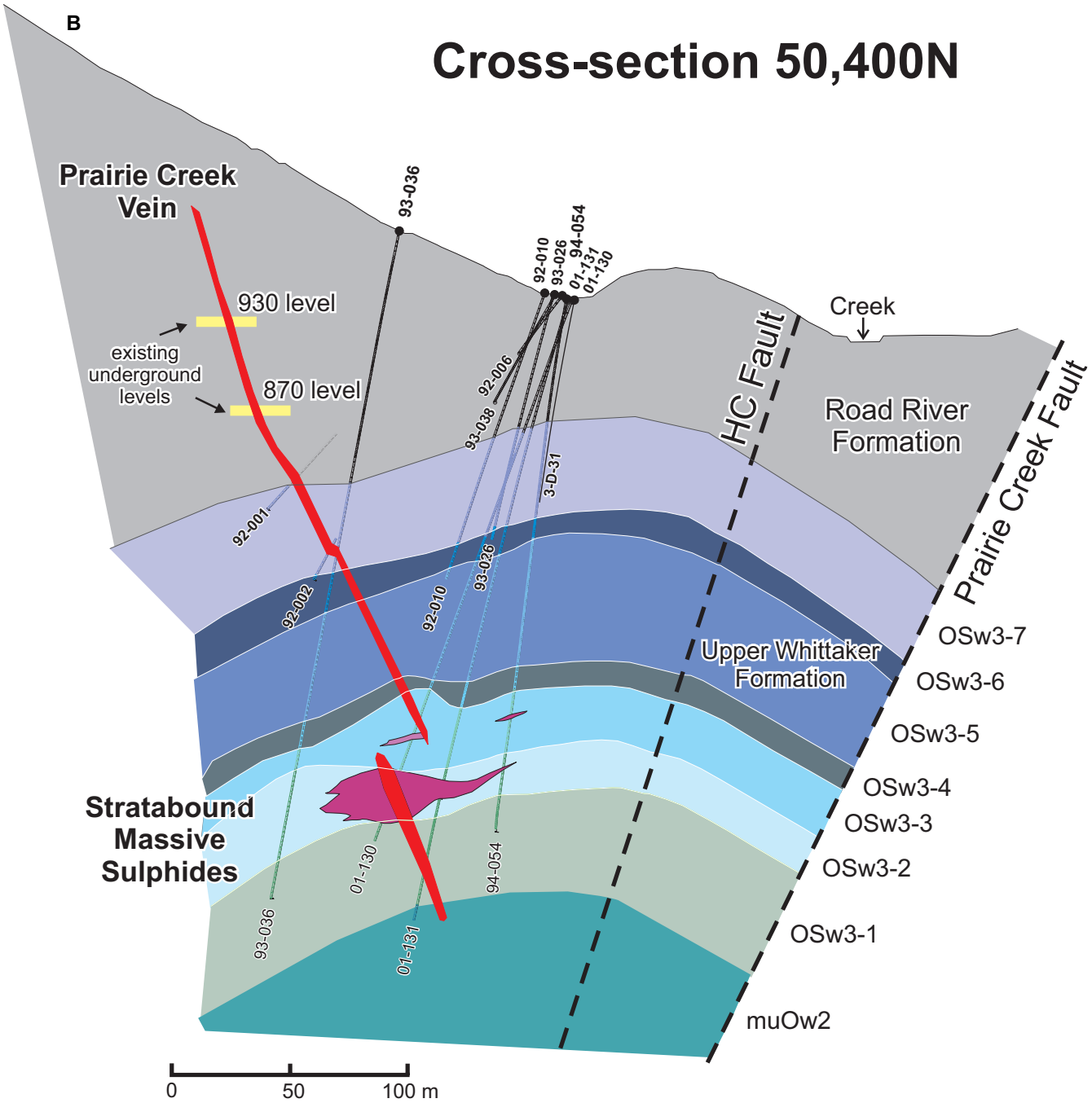


Figure 3 continued. B) Schematic cross-section 50,400 N illustrating two small lenses of stratabound mineralization in unit OSw3-3 (lower chert nodule dolostone), and a larger stratabound lens in unit OSw3-2 (mottled dolostone) of the Upper Whittaker Formation; the section is located on Figure 3A.

the deposits is stratabound with stacked lenses being concordant to slightly discordant to bedding, and 5) the mineralization display complex textures ranging from fine- to medium-grained aggregates of sulphides and oxides replacing the host carbonates to open-space fillings and rare layered sulphide textures.

The quartz-carbonate-sulphide veins fill fractures parallel to regional-scale faults crosscutting the Lower Paleozoic strata and the stratabound sulphides. The vein sulphides are best developed within dolostone of the Upper Whittaker and the argillaceous bioclastic shaly dolostone and shale of the Road River Formation. Also, although less well developed, they cut the thin bedded silty dolostone, calcareous siltstone and shale of the Cadillac Formation and the nodular and banded cherty dolostone of the Arnica Formation. The vein sulphides are found along a north-south trending 16 km long corridor. They occur close to the axial plane of the north-south doubly-plunging anticline, although they generally trend at an angle to the fold

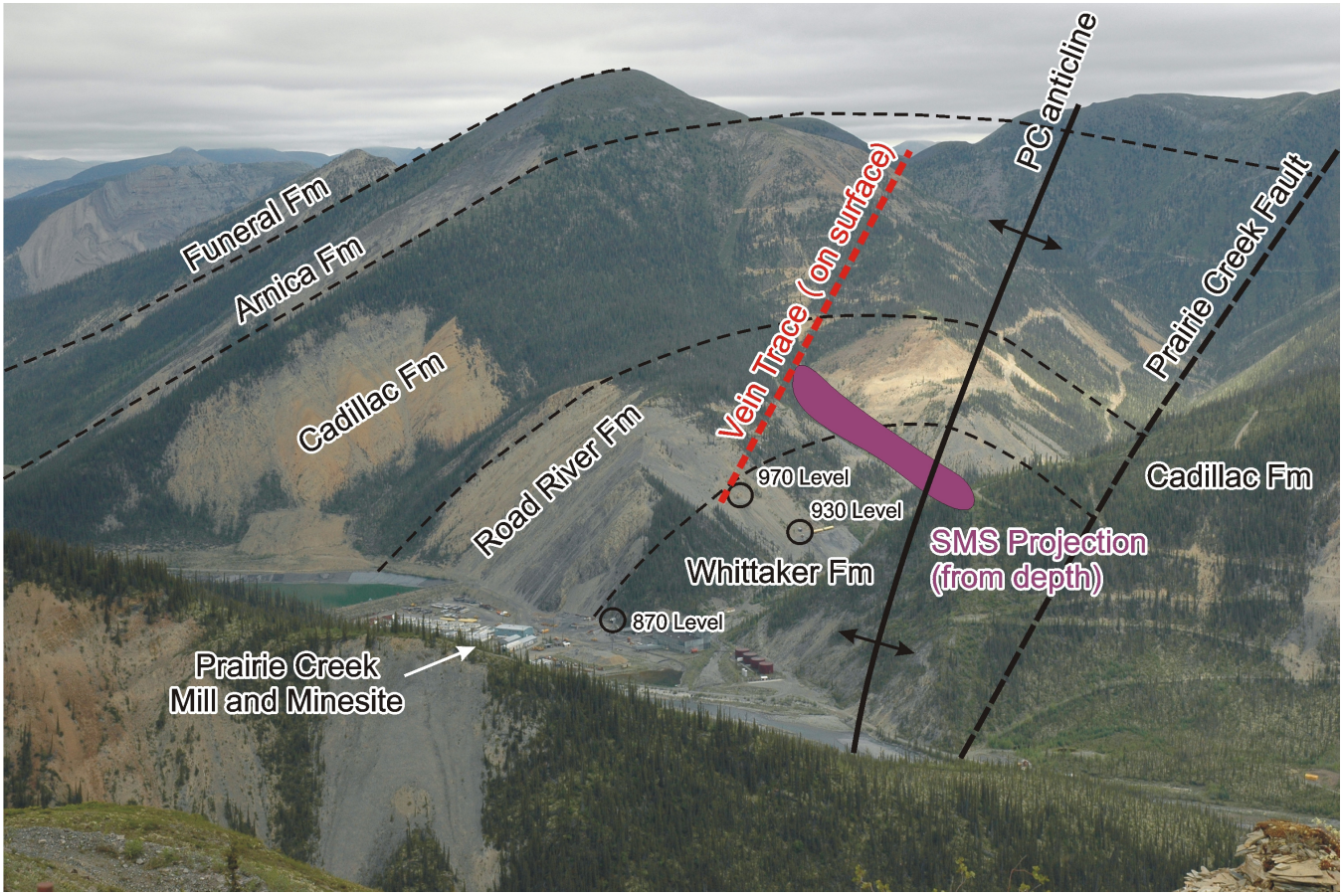


Figure 4. View looking north from zone 6 toward the Prairie Creek mill and mine site. The geological contacts and the formations, the surface projection of stratabound massive sulphide (SMS) SD1 lens and the quartz-carbonate-sulphide vein are outlined. Photo courtesy of Canadian Zinc Corporation.

axis and locally crosscut it (Fig. 2). The surface expressions of the veins are referred sequentially by numbered zones from zone 1 in the north to zone 12 in the south. As a result of exploration drilling, zones 1, 2, and 4 are included with zone 3, which is located at the Prairie Creek mine site (see Fig. 2). The Rico showing located 4 km north on strike of zone 3 is the northernmost known surface expression of the vein system. The South Gate showing located 25.8 km southwest of the mine site consists of sulphide veins parallel to a reverse fault zone, similar to the Prairie Creek Fault. The North Gate showing, located 7.5 km northwest of the mine site, consists of a north-south trending, subvertical quartz-carbonate-sulphide vein occupying dilatant fractures parallel to an unnamed regional-scale reverse fault (A. Taylor, Canadian Zinc Corporation, pers. comm., 2005). Regionally, the quartz-carbonate-sulphide veins strike approximately 320 to 360° and dip between 40 and 90° east (Canadian Zinc Corporation, 2004). In zones 3 to 12, the veins strike mostly 350 to 360° and have variable dips of 45 to 90°. In the underground workings at zone 3, conjugated vein sets related to the main vein strike 310° and 330 to 340° and dip subvertically (Jenks, 1982).

The MVT showings are hosted by the vuggy light grey dolostone of the Silurian Root River Formation (or facies equivalent) deposited in a shallow-water carbonate shelf setting. From north to south over a distance of approximately 12 km, the known surface showings are Samantha, Joe, Horse, Zulu, Zebra, and Road (Table 1; Fig. 2).

Morphology

Five stratabound sulphide lenses (i.e. SD1 to SD5) have been discovered so far by drilling. They consist of stacked intervals of massive sulphides replacing the dolostone units of the Upper Whittaker Formation. The sulphides are concordant to discordant to bedding. The lower contact is usually sharp and irregular and sulphides cut the strata at low to high angles (Fig. 5A). The upper contact is gradational to stringer-like (Fig. 5B). The geometry of the sulphide lenses is irregular consisting of multiple massive sulphide intervals concordant to discordant to bedding and separated by non-mineralized dolostone (Fig. 6). The largest stratabound lens, SD1, is an irregular elongated lens with a minimum lateral dimension of 400 m by 100 m and a maximum thickness of 28 m (Earls, 1995; Findlay, 2000).

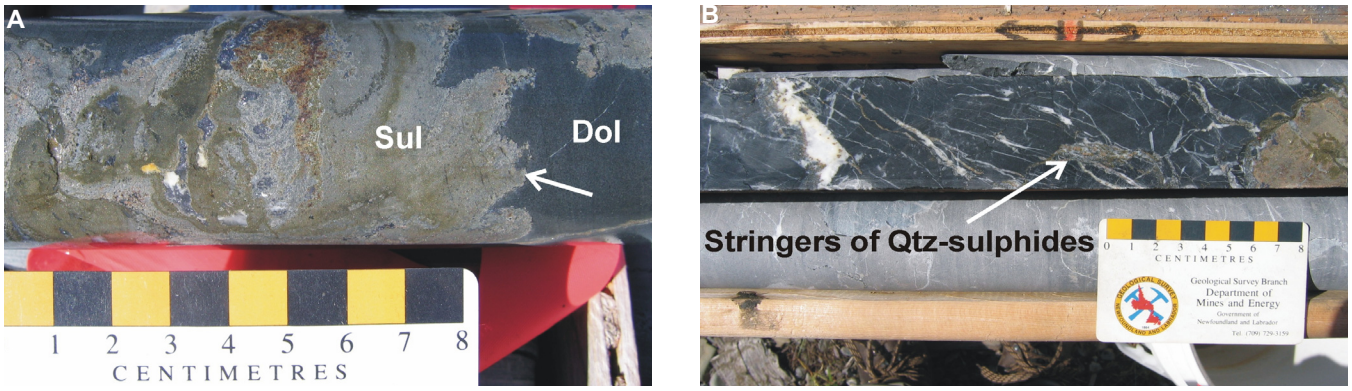


Figure 5. Photographs of the stratabound sulphides. **A)** DDH 94-64 at 191.0 m. Irregular deformed contact between the sulphide intersection and the host dolostone (arrow). **B)** DDH 92-19 at 289.5 to 289.8 m. Stringers of quartz-carbonate-sulphides at the upper contact of the stratabound sulphide section. Abbreviations: Dol=dolomite, Qtz=quartz, sul=sulphides.

It consists of multiple massive sulphide intervals 2 to 5 m thick separated by nonmineralized dolostone. Smaller lenses occur 200 m north (SD2) and 450 m south (SD3) of the main SD1 lens (Fig. 3A). Small intersections of stratabound massive sulphides are also found in lenses 5 (SD5) and 6 (SD4) where they replace and crosscut (stringer-type) various units of the Upper Whittaker Formation. The width of these intersections ranges from 0.2 to 1 m.

The vein sulphides are found discontinuously along a north-south trending 16 km long corridor along which twelve separate showings or zones have been identified (Fig. 2). They may represent exposure of a single vein system. The most extensive known vein is observed within the underground workings at zone 3 where it has a proven strike length of 940 m (Canadian Zinc Corporation: http://www.canadianzinc.com). In zone 3, the width of the sulphide veins is quite variable and range between <0.1 m to over 5 m (Fig. 7A, B), with an average width of 2.7 m (Canadian Zinc Corporation, 2004). In the other zones, the overall width of the veins varies from 0.6 to 6.1 m and average 4.5 m (Brophy, 1984; Figs. 8 and 9). Underground exposures of the main sulphide vein in zone 3 show that the hanging-wall rocks are sheared and crosscut by stringers of sulphides (Fig. 7C), whereas the footwall rocks are not. Layering, brecciation, and shearing within the main sulphide vein are the common textures (Fig. 9A, B, C). The well-developed layering, brecciation and shearing suggest that movement accompanied by largely brittle deformation was ongoing throughout most of the vein emplacement. Formation of the vein fault system likely occurred during the latest stages of, or even after, development of the anticline, because it crosscuts the anticline axis and is not folded (Findlay, 2000).

MVT sulphide mineralization ranges from open-space fillings of breccias, fractures, and vugs to disseminated clusters of crystals that occupy intergranular pore spaces. Sulphide-hosting structures are most commonly zones of highly brecciated sparry dolomite within the host dolostone (Fig. 10A). The breccias range from more or less concordant thin and narrow tabular structures and pods, controlled by individual strata, to slightly discordant structures. According to Alan Taylor, Canadian Zinc Corporation (pers. comm., 2005), the showings occur discontinuously at approximately the same stratigraphic level along the 12 km long north-northwest-trend (Fig. 2). This linear pattern suggests a tectonic control. At some showings, such as Zebra and Samantha, sulphide mineralization is associ-



Figure 6. Drill core intersection of the stratabound sulphides within zone 3 (DDH 01-130 at 307.7 to 322 m) illustrating the distribution of massive sulphide sections and non-mineralized mottled dolostone of the Upper Whittaker Formation. The top and bottom contacts of a sulphide intersection are outlined by red lines. The top contact is irregular and diffuse (dashed red line), whereas the bottom contact is sharp (solid red line).

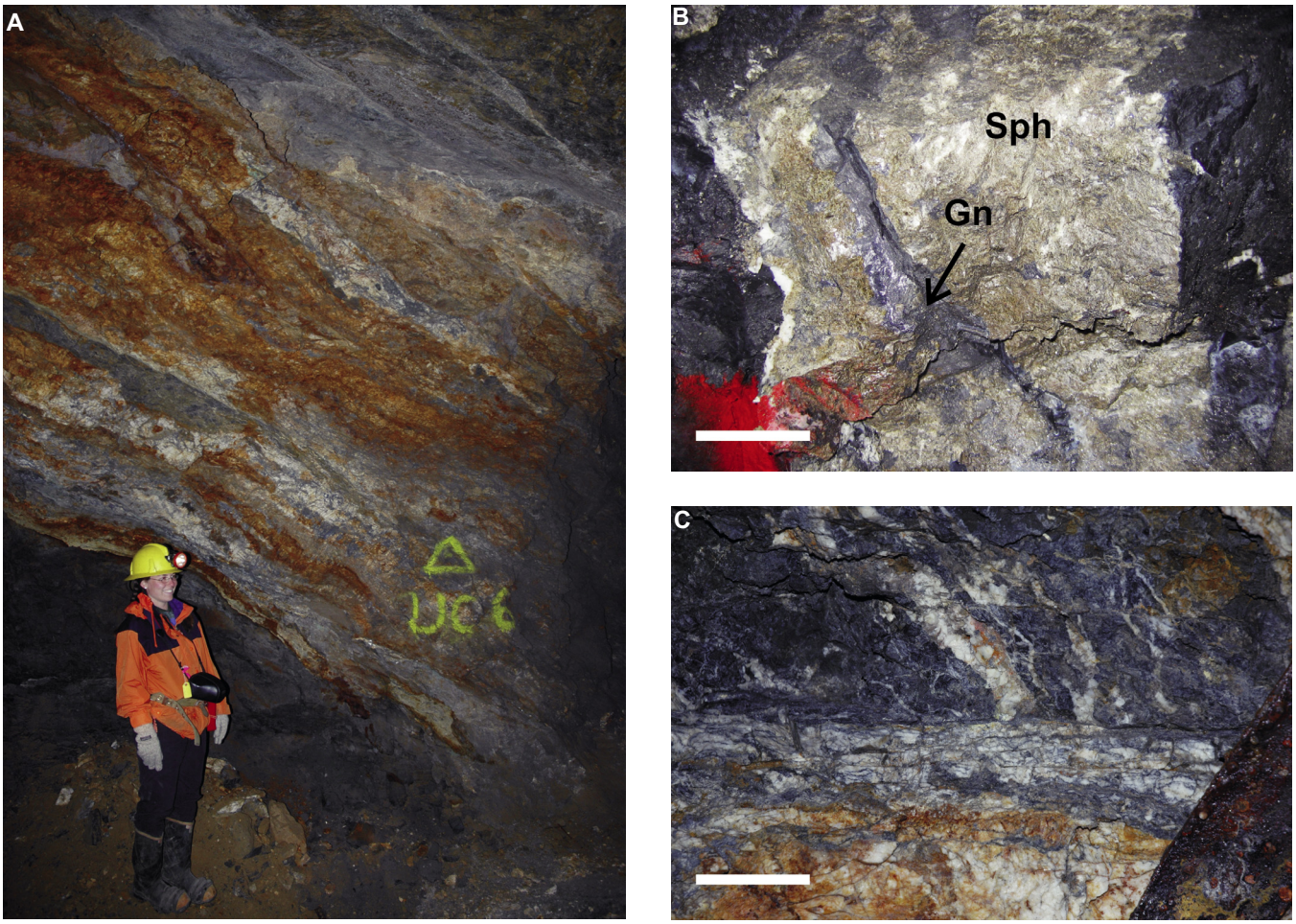


Figure 7. Underground exposures of the quartz-carbonate-sulphide veins of zone 3 at the 930 m level. **A)** Sharp contact between the main vein and the footwall dolostone of the Upper Whittaker Formation (lower left corner). **B)** Coarse-grained sphalerite crystals crosscut by coarse-grained galena vein and veinlets. Scale bar = 5 cm. **C)** Brecciated and sheared contact between the vein and the hanging-wall rocks; note the orthogonal veins to the main vein. Scale bar = 5 cm.

ated with low-angle normal faults (Taylor, 1995). Several carbonate-hosted Zn-Pb showings in the Mackenzie Mountains of the Northwest Territories and Yukon appear to be structurally controlled, with a secondary stratigraphic control (Dewing et al., 2006). The dimension of individual MVT sulphide bodies is impossible to measure due to lack of exposures, drilling information, and the morphology of MVT bodies that are typically irregular and of variable shape.

Mineralogy and Textures

The stratabound sulphides contain pyrite, sphalerite, galena, and trace amount of tetrahedrite-tennantite in a gangue of quartz, dolomite, and calcite. The textures are complex ranging from complete to partial replacement of the dolostone by fine- to coarse-grained massive aggregates of pyrite and yellowish to pinkish sphalerite and galena to fine-grained laminated sulphides (Fig. 11A, B, C). When the sulphides replace the mottled dolostone unit (OSw3-2), remnants of irregular siliceous patches of dolostone are often observed (Fig. 11B). These siliceous dolostone patches form characteristic nodules that are partially replaced along the rims and fractures by fine- to medium-grained yellowish sphalerite. Broad bands of fine-grained massive aggregates of pyrite and sphalerite and occasional fine-grained well-developed laminae of pyrite and sphalerite are noted within SD1 and SD4 (Fig. 11C). More often, chaotic convoluted banding of sulphides is the typical texture observed in the stratabound zones (Fig. 11D). Occasional open-space cavity-fill textures typical of MVT style mineralization are observed within SD1 and SD2 (Fig. 11E). Veinlets of coarse-grained yellowish to reddish sphalerite crosscut the massive aggregates of fine-grained pyrite and pinkish sphalerite (Fig. 11F). Sheared sulphides and brecciated sulphides are common within the stratabound zones. The brecciated sulphides consist of fragmented grains of pyrite and sphalerite infilled by galena and subsequently by white sparry carbonates. The sheared sulphides appear as fine-scale streaky laminations of pyrite and sphalerite.

The mineralogy of the veins is dominantly sphalerite and galena with lesser pyrite and tetrahedrite-tennantite

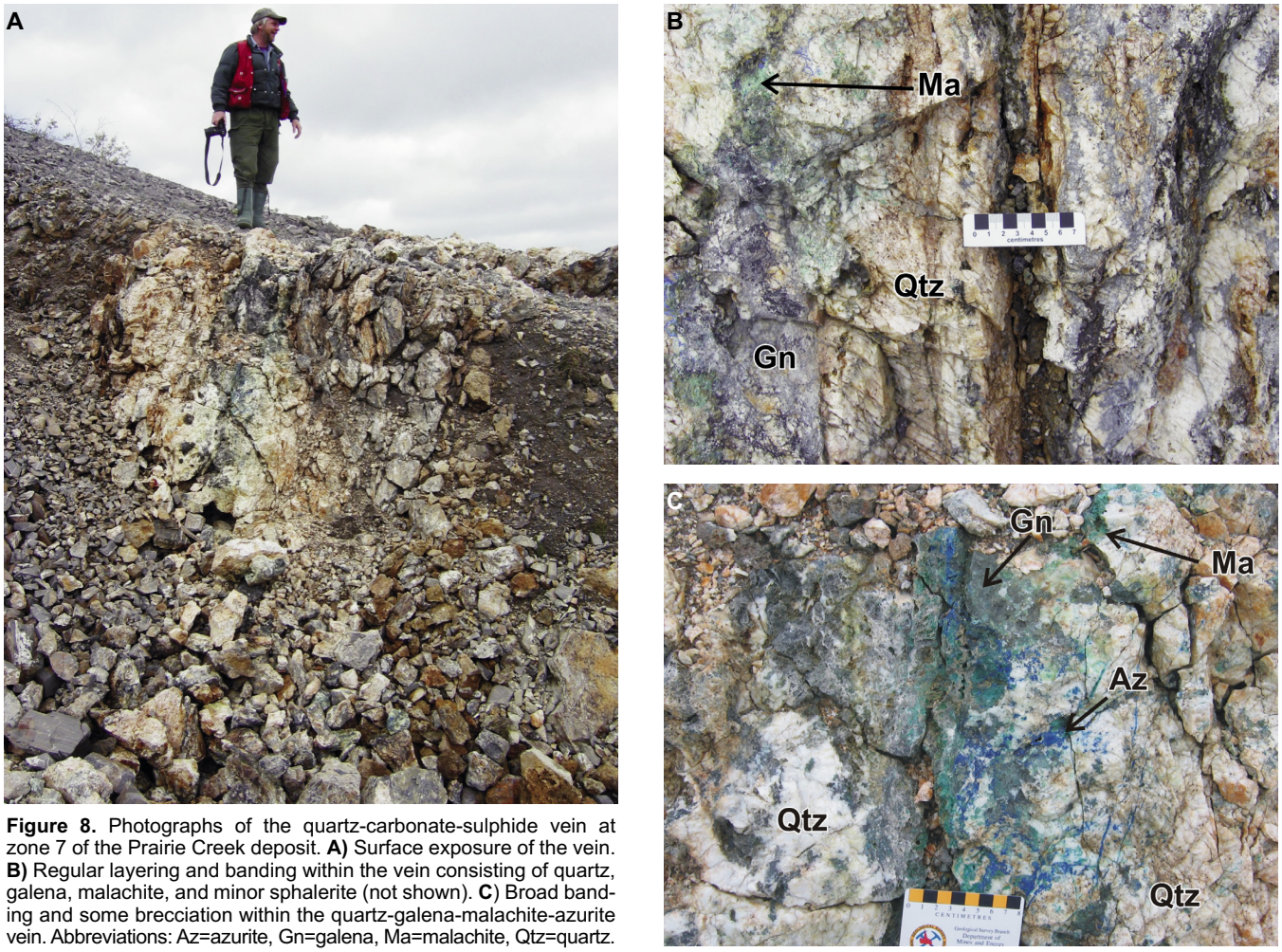


Figure 8. Photographs of the quartz-carbonate-sulphide vein at zone 7 of the Prairie Creek deposit. **A)** Surface exposure of the vein. **B)** Regular layering and banding within the vein consisting of quartz, galena, malachite, and minor sphalerite (not shown). **C**) Broad banding and some brecciation within the quartz-galena-malachite-azurite vein. Abbreviations: Az=azurite, Gn=galena, Ma=malachite, Qtz=quartz.

as massive aggregates to disseminations in quartz, calcite, and rare dolomite gangue (Fig. 12A, B). The sulphides are occasionally oxidized to cerussite, smithsonite, malachite, and azurite (Fig. 8B, C). Sphalerite is medium- to coarse-grained (0.2-2 cm), tan to yellowish-grey crystals intermixed with or crosscut by coarse-grained galena (0.5-2 cm) and fine- to coarse-grained pyrite (Figs. 7C, 12A, B). Tetrahedrite-tennantite forms small anhedral grains (<2 mm) in sphalerite and galena (Fig. 12C, D). Quartz is the main gangue mineral of the vein sulphides. Dolomite and calcite fill the fractures in the quartz crystals and the remaining open spaces. Textures within the veins are layering, brecciation and shearing. The vein sulphides are locally undeformed to strongly sheared and brecciated (Fig. 12E, F).

The MVT sulphides occur as breccias, veins, and vug-fillings of pyrite, sphalerite, and rare galena (Fig. 10). The pyrite and sphalerite form colloform textures rimming dolostone fragments in open-space breccias filled by sparry and saddle white dolomite (Fig. 10C). They also form fine- to medium-grained aggregates in the sparry dolomite cement and crustiform pyrite-sphalerite veinlets crosscutting the rusty weathered dolostone.

ISOTOPE GEOCHEMISTRY

Sampling and Analytical Methods

Representative samples of the three different types of sulphide mineralization and their host rocks were collected for isotopic analyses from surface and drill-cored intervals. A list of the samples is given in Appendix 1. Samples previously collected by Fraser (1996) from the Prairie Creek deposit and by Paradis et al. (in press) from outcrops in the Rocky Mountains, the Manetoe Facies in the Mackenzie Mountains, and the WCSB are included for comparison. Carbon, oxygen, and strontium isotope analyses of the Prairie Creek samples are presented in Table 3. Lead and sulphur isotope analyses are given in Tables 4 and 5, respectively. Examination of the samples was done by petrographic microscopy.

Carbon, Oxygen, and Strontium Isotopes

Carbon and oxygen isotope analyses were completed on 28 calcite and dolomite crystals of various carbonate cements and fracture-filling calcite and dolomite of the different ore types. Analyses were done at the



Figure 9. Photographs of the quartz-carbonate-sulphide vein exposure at zone 8 of the Prairie Creek deposit. **A)** Regular layering and banding within the main vein. **B)** Sample consisting mostly of quartz and smithsonite. **C)** Quartz-carbonate-sulphide breccia showing the subangular and angular fragments of quartz in a gangue of quartz, carbonates, and sulphides. Abbreviations: Qtz=quartz, Sm=smithsonite.

Delta-Lab of the Geological Survey of Canada in Québec City. Samples were drilled and hand picked from rock slabs using 100 µm-diameter drill bits. Carbon and oxygen isotopic compositions were determined on 10 to 20 mg of powdered sample by analysis of CO_2 generated by reaction with 3 ml of 100% phosphoric acid (McCrea, 1950). Digestion was done at 25°C. All dolomite and calcite samples were subjected to a two-stage procedure whereby CO_2 from any possible calcite was produced after the first 3 to 5 hours of reaction and then frozen in a breakseal vessel. After 72 hours, the remaining CO_2 from dolomite was sealed in a second breakseal vessel. Only the results from the 2nd stage of the analysis are reported for dolomite. The evolved CO_2 gas was analysed for $^{18}O/^{16}O$ and $^{13}C/^{12}C$ using a PRISM III isotope ratio mass spectrometer. Results are reported in conventional per mil notation (‰) relative to Vienna NBS-19 standard (VPDB), and corrected for ^{17}O as described in Craig (1957). No correction for acid fractionation was made for dolomite (Friedman and O'Neil, 1977). Precision, based on replication of international and internal standards, is ±0.1‰. Strontium isotope analyses were done by B. Cousens on dolomite and calcite at the Isotope Geochemistry and Geochronology Research Facility (IGGRF) of Carleton University, and by B. Davis at the geochronology laboratories of the Geological Survey of Canada. Splits of powder samples used for C and O isotope analyses were treated for Sr separation by standard ion exchange techniques. Mass spectrometry was performed on a Thermo Finnigan Triton TI thermal ionization mass spectrometer. Isotope ratios were normalized to $^{86}Sr/^{88}Sr = 0.11940$ to correct for fractionation and are presented relative to a value of 0.708043 for the NIST Standard Reference Material Eimer and Amend (E&A) $SrCO_3$. Uncertainty in $^{87}Sr/^{86}Sr$ is expressed as ±2 sigma of the mean, equivalent to two standard errors (2σ).

Results

Host dolostone of the Upper Whittaker Formation has $\delta^{18}O_{PDB}$ and $\delta^{13}C_{PDB}$ values ranging from -5.8 to -10.2‰ and 0.5 to -2.0‰, respectively (Table 3, Fig. 13A). Values for dolostone of the Root River Formation form a separate group with $\delta^{18}O_{PDB}$ and $\delta^{13}C_{PDB}$ values ranging from -5.4 to -7.2‰ and 0.6 to 1.7‰,

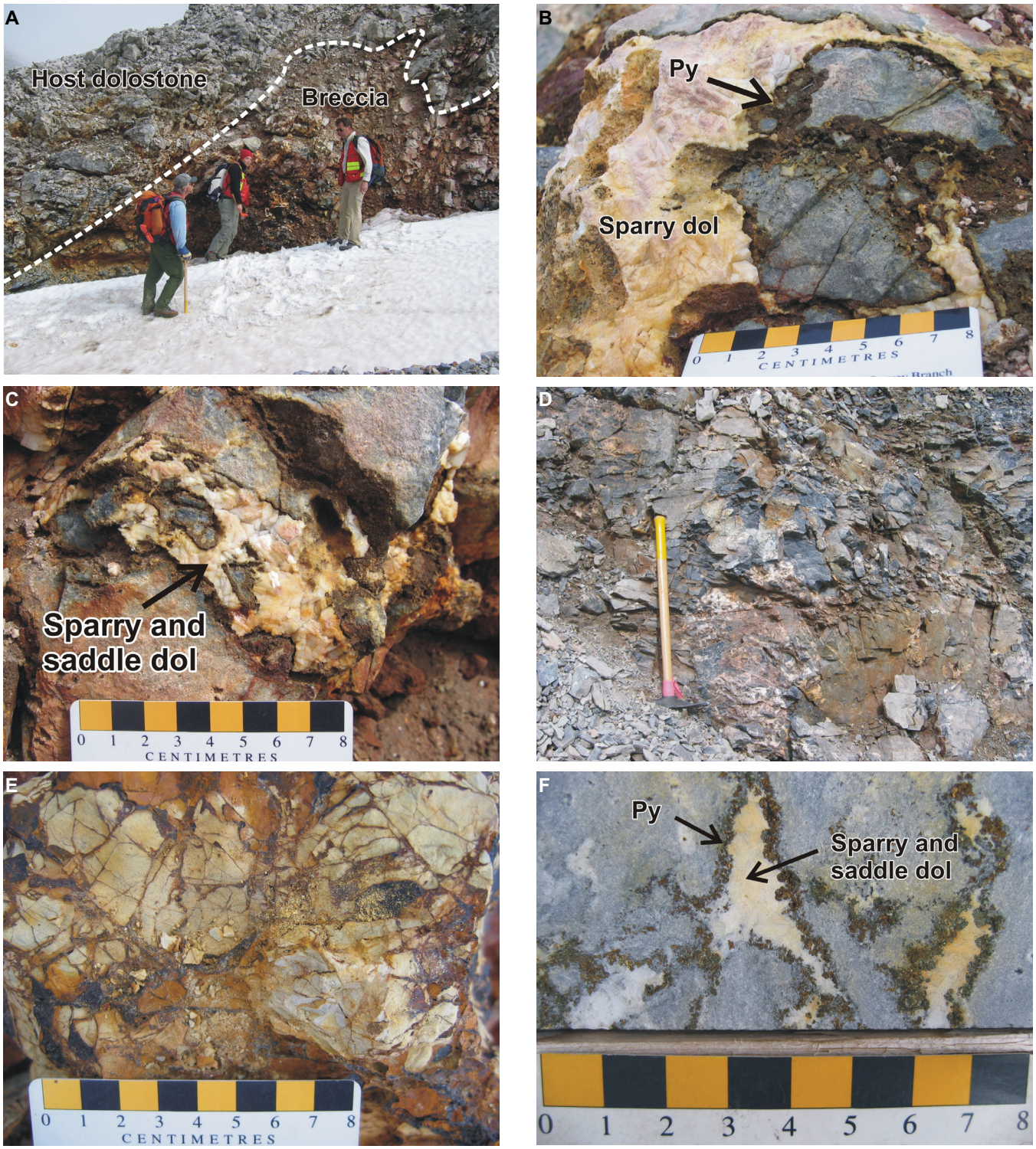


Figure 10. Photographs of the Mississippi Valley-type sulphides in the Prairie Creek area. **A)** Surface exposure of a south-facing cliff of the Zebra showing; note the irregular nature of the contact between the mineralized crackle and mosaic breccia and the host dolostone of the Root River Formation. **B)** Sparry white dolomite and pyrite fill fractures within the dolostone of the Zebra showing. **C.** Fractures filled by sparry and saddle dolomite of the Zebra showing; note the colloform pyrite and sphalerite rimming the fragments and rimming the walls of the vein. **D)** Sparry dolomite cemented breccia of the Upper Zebra showing. **E)** Highly oxidized breccia with bleached dolostone fragments cemented by oxidized sulphides from the Upper Samantha showing. **F)** DDH 94-80 at 220 m - Drill-core photograph showing the colloform pyrite with trace amount of sphalerite lining cavities filled by coarse-grained saddle dolomite. Abbreviations: Dol=dolomite, Py=pyrite.

respectively (except for one value of -6.4 $\delta^{18}O_{PDB}$ and -1.4 $\delta^{13}C_{PDB}$). The carbon and oxygen values of the Upper Whittaker dolostone are similar to estimated Ordovician marine carbonate values of Veizer et al. (1999). Those of the Root River Formation are similar to estimated Silurian marine carbonate values of Veizer

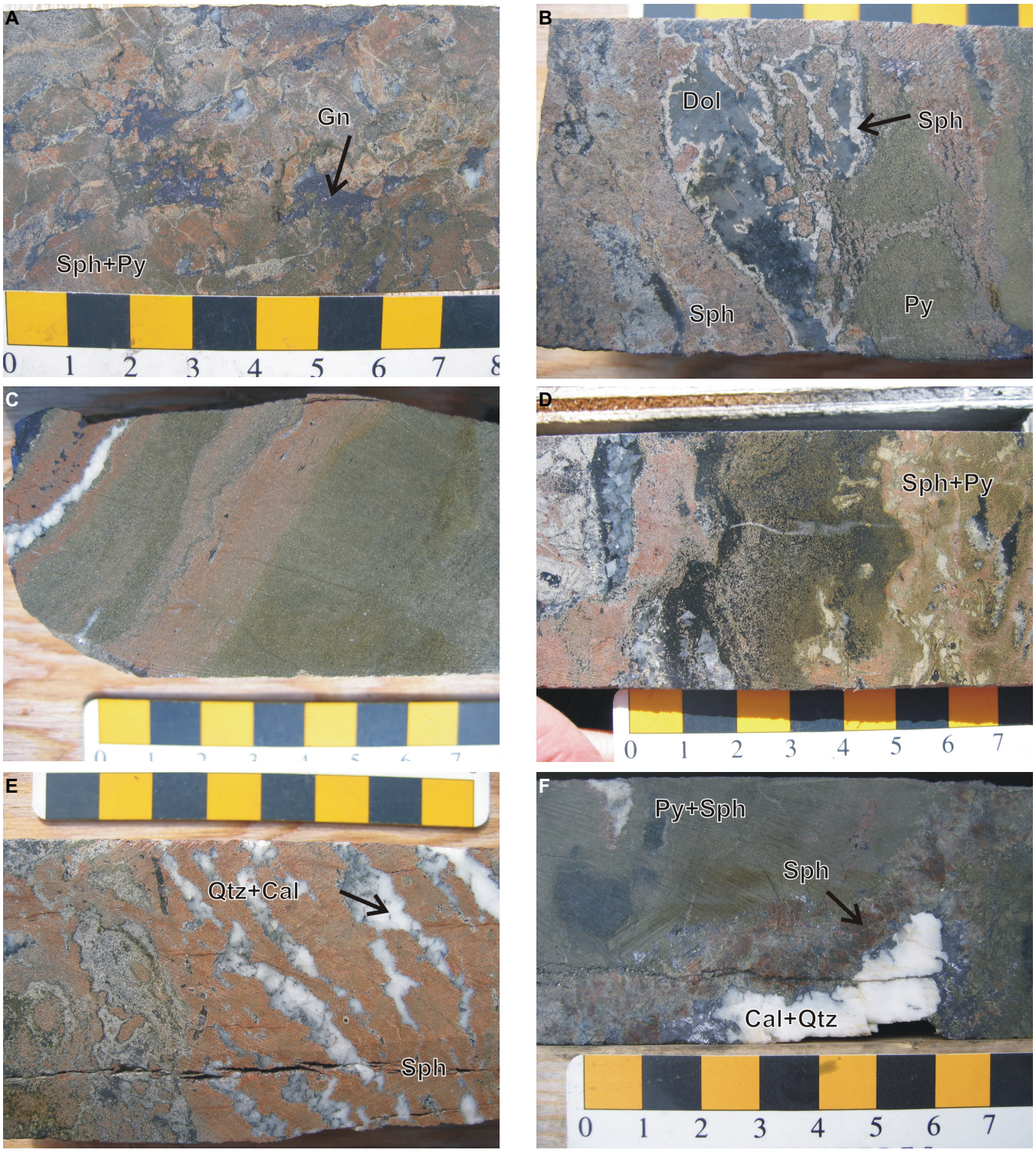


Figure 11. Photographs of the stratabound sulphides. **A)** DDH 94-82 at 482.5 m. Massive sulphide drill-core intercept consisting of chaotic fine-grained mixed aggregate of sphalerite (pinkish) and pyrite (brass colour) and interstitial galena (dark blue). This constitutes a complete replacement of the host dolostone. **B)** DDH 93-26 at 293 m. Sulphide intercept with siliceous remnants of mottled dolostone showing replacement by pale yellowish sphalerite along the rims. **C)** DDH 93-26 at 285.2 m. Fine-grained aggregates of pyrite (brass colour) and sphalerite (pinkish) forming nice centimetre-thick bands. **D)** DDH 93-25 at 254.5 m. Chaotic convoluted banded sulphides showing broadly defined bands rich in sphalerite and others rich in pyrite. **E)** DDH 93-26 at 290.6 m. Open-space cavity-filled texture. **F)** DDH 04-150 at 239.55 m. Fine-grained massive aggregate of pyrite with lesser sphalerite crosscut by a vein of coarse-grained red sphalerite. The remaining cavities in the vein are filled first by galena and second by sparry calcite and quartz. Abbreviations: Cal=calcite, Dol=dolomite, Gn=galena; Py=pyrite, Qtz=quartz, Sph=sphalerite.

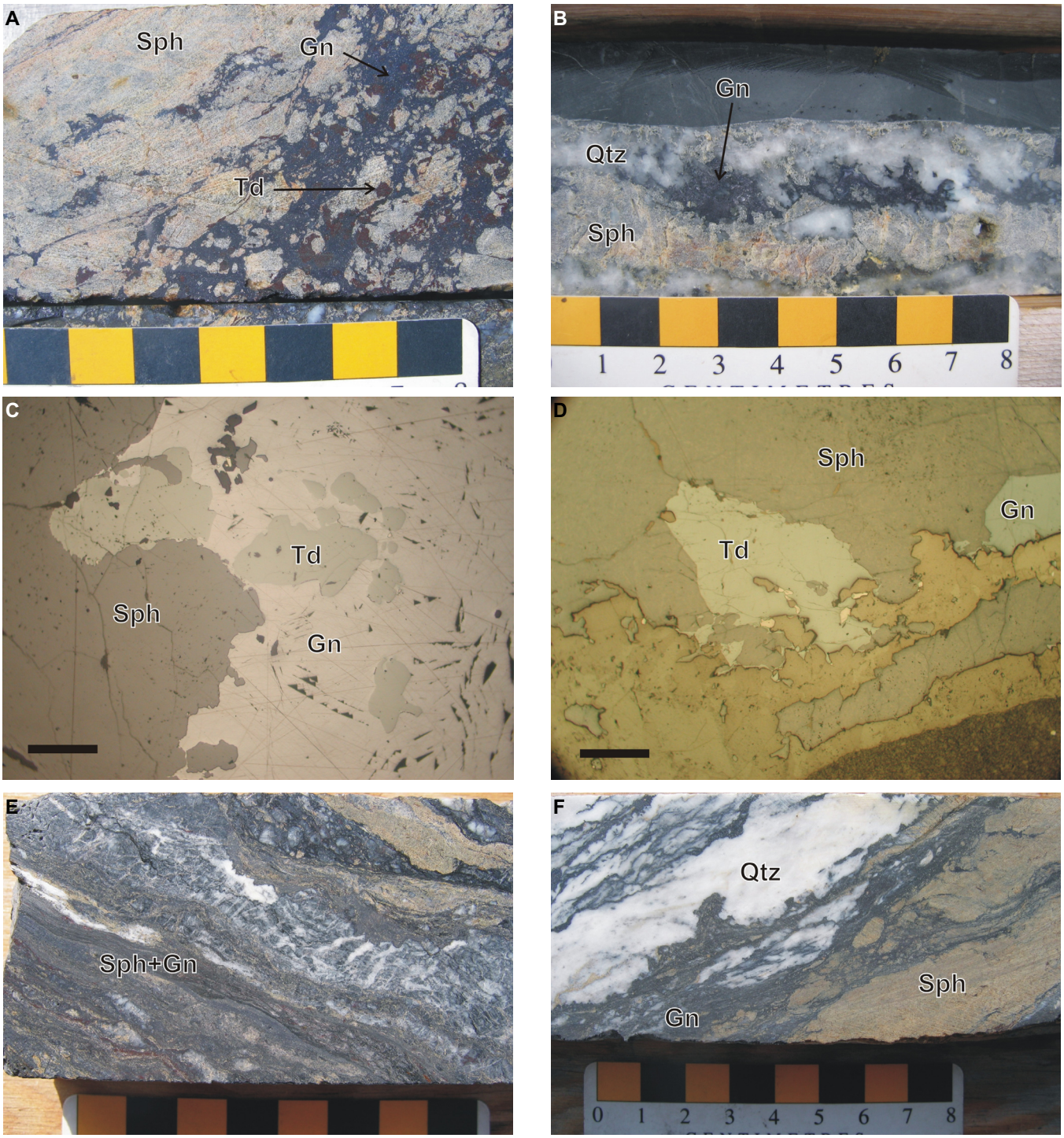


Figure 12. Photographs of the quartz-carbonate-sulphide veins. **A)** DDH 92-19 at 237.9 m. Sheared sulphides consisting of pale pinkish sphalerite and interstitial galena and tetrahedrite. **B)** DDH 01-130 at 181.6 m. Undeformed vein of quartz, sphalerite, and galena. **C)** DDH 95-122 at 765.6 m. Microphotograph (reflected light) of an aggregate of sphalerite, galena, and tetrahedrite; note that the tetrahedrite is enclosed in the galena; scale bar=1 mm. **D)** DDH 01-130 at 182 m. Microphotograph (reflected light) of anhedral tetrahedrite grain and galena grain enclosed in sphalerite; scale bar=1 mm. **E)** DDH 95-95 at 420.1 m. Strongly sheared and laminated quartz-carbonate-sulphide section consisting of red and tan coloured sphalerite, galena, and quartz. Calcite veinlets occur orthogonal to the main direction of shearing. **F)** DDH 01-133 at 309 m. Strongly sheared section of the quartz-carbonate-sulphide vein. Abbreviations: Gn=galena, Py=pyrite, Qtz=quartz, Sph=sphalerite, Td=tetrahedrite-tennantite.

et al. (1999). $^{87}Sr/^{86}Sr$ values for the non-mineralized Upper Whittaker dolostone are variable. They range from 0.7096 to 0.7267 and increase in values in proximity to the stratabound sulphide mineralization (Fraser, 1996). All the Upper Whittaker host dolostones (except sample PC-R3 located west of Gate Fault) plot above the Sr isotope ratio of 0.7120 (Fig. 13B, C), which defines the "Maximum Sr Isotope Ratio of

Table 3. Oxygen, carbon, and strontium isotope values of various carbonates from the various deposit-types of the Prairie Creek area, Northwest Territories.

Drill hole # / zone / showing	Depth (m) min-max	Datum	UTM Northing	UTM Easting	Host formation	Unit / lithology	Carbonate texture	Mineral Phase	Descriptions / Comments	$\delta^{13}C$ (PDB)	$\delta^{18}O$ (PDB)	$\delta^{18}O$ (SMOW)	$^{87}Sr/^{86}Sr$	error, 2σ	Ref.
PC-95-124	309.9	Nad 27	6824601.7	405041	Upper Whittaker	Stratabound sulphides at contact with OSw3-7	mg dolomite	Dolomite	Blebs of mg dolomite in sulphide section.	-2.39	-7.38	23.25			1
PC-01-130	269.3	Nad 27	6826335.0	405042	Upper Whittaker	Stratabound sulphides - OSw3-3	vug-filling	Dolomite	Dolostone with vugs rimmed by pyrite and filled by dolomite.	-2.86	-9.31	21.26	0.71899	0.00003	1
PC-01-130	313.5	Nad 27	6826335.0	405042	Upper Whittaker	Stratabound sulphides - OSw3-2	mg dolomite	Dolomite	Dolomite occurs as gangue filling spaces in the fg aggregate of sulphides.	-3.63	-12.19	18.30			1
PC-01-130	317.2	Nad 27	6826335.0	405042	Upper Whittaker	Stratabound sulphides - OSw3-2	mg dolomite	Dolomite	Dolomite occurs as veinlets in the fg aggregate of sulphides.				0.71716	0.00002	1
PC-01-132	320.8	Nad 27	6826405.5	405004	Upper Whittaker	Stratabound sulphides - OSw3-2	recrystallized dolostone	Dolomite	Recrystallized dolostone within the sulphide section.	-3.24	-9.75	20.81			1
PC-04-150	237.2	Nad 27	6825981.0	404343	Upper Whittaker	Stratabound sulphides - OSw3-2	sparry dolomite (±calcite)	Dolomite	Cg white sparry dol replaced by fg aggregate of sulphides.	-2.30	-8.10	22.50	0.72390	0.00009	1
PC-92-16	310.6	Nad 27	6826316.0	404962	Upper Whittaker	Stratabound sulphides - OSw3-3	mg dolomite	Dolomite	Blebs of mg dolomite in sulhidep section.	-2.60	-8.36	22.25	0.71419	0.00002	1
PC-92-16	310.6	Nad 27	6826316.0	404962	Upper Whittaker	Stratabound sulphides - OSw3-3	mg dolomite	Dolomite	Blebs of mg dolomite in sulphide section.				0.71556	0.00001	1
PC-92-19	289.5-289.8	Nad 27	6826398.8	405009	Upper Whittaker	Stratabound sulphides - OSw3-3 or OSw3-2	cg sparry dolomite	Dolomite	Veinlets of cg white sparry dol cutting the fg aggregate of sulphides.	-3.10	-9.00	21.50	0.71586	0.00001	1
PC-92-19	314	Nad 27	6826398.8	405009	Upper Whittaker	Stratabound sulphides - OSw3-3 or OSw3-2	cg sparry dolomite	Dolomite	White sparry dol forms bands and veinlets; resemble open-space filling texture.				0.71890	0.00001	1
PC-93-23	249.7	Nad 27	6826202.1	405005	Upper Whittaker	Stratabound sulphides - OSw3-2	sparry dolomite	Dolomite	White sparry dolomite forms bands within the fg sulphide aggregate and resembles zebra texture.				0.71379	0.00002	1
PC-93-23	249.7	Nad 27	6826202.1	405005	Upper Whittaker	Stratabound sulphides - OSw3-2	sparry dolomite	Dolomite	White sparry dol forms bands within the fg sulphide aggregate and resembles zebra texture.	-2.80	-8.30	22.30	0.71890	0.00001	1
PC-94-82	496.1	Nad 27	6825981.0	405212	Upper Whittaker	Stratabound sulphides - OSw3-4	siliceous dolostone	Dolomite	Siliceous dolostone in fg aggregate of sulphides.	-4.74	-14.94	15.46			1
PC-94-64	285.7	Nad 27	6823154.6	404363	Upper Whittaker	Lower spar dolostone - OSw3-4	sparry dolomite in vugs	Dolomite	White dol spars and some quartz as filling of vugs; loc sulphide stringers.	-19.86	-13.42	17.07	0.71543	0.00001	1
PC-94-64	329.5	Nad 27	6823154.6	404363	Upper Whittaker	Mottled dolostone - OSw3-2	sparry dolomite in vugs	Dolomite	Sparry dolomite as vug-fillings and veinlets.	-1.98	-14.24	16.19	0.71857	0.00001	1
PC-94-64	329.5	Nad 27	6823154.6	404363	Upper Whittaker	Mottled dolostone - OSw3-2	sparry dolomite in vugs	Dolomite	Sparry dolomite as vug-fillings and veinlets.				0.71949	0.00001	1
PC-92-19	274.7	Nad 27	6826398.8	405009	Upper Whittaker	Lower spar dolostone - OSw3-4	yellowish dolomite in vugs	Dolomite	Cg yellowish dolomite and cg clear dolomite fill large vugs.	-1.77	-10.52	20.02			1
PC-92-19	274.7	Nad 27	6826398.8	405009	Upper Whittaker	Lower spar dolostone - OSw3-4	cg clear dolomite in vugs	Dolomite	Cg yellowish dolomite and cg clear dolomite fill large vugs.	-2.72	-10.32	20.22	0.72263	0.00002	1
PC-94-77 (Zebra)	73.3-73.4	Nad 27	6833291.0	410801	Cadillac ET (~Root River)	MVT-type sulphides	white saddle dolomite	Dolomite	Vugs and cavities fill by sparry dolomite and rimmed by pyrite.	-3.40	-16.00	14.40	0.71231	0.00001	1
PC-94-77 (Zebra)	73.3-73.4	Nad 27	6833291.0	410801	Cadillac ET (~Root River)	MVT-type sulphides	white saddle dolomite	Dolomite	Vugs and cavities fill by sparry dolomite and rimmed by pyrite.				0.71244	0.00004	1
Road showing	surface	Nad 83	6832497.5	410147	Root River	MVT-type sulphides	saddle dolomite	Dolomite	Vugs filled with saddle dolomite	-2.70	-15.70	14.70	0.71268	0.00001	1
Samantha - lower showing	surface	Nad 83	6842662.5	408600	Root River	MVT-type sulphides	saddle dolomite	Dolomite	Dolostone fragments enclosed in a sparry dolomite cement.				0.71065	0.00001	1
Zebra - lower showing	surface	Nad 83	6833291.0	410801	Cadillac ET (~Root River)	MVT-type sulphides	saddle dolomite	Dolomite	Breccia with dolostone fragments and colloform sp (weathered) and galena and sparry dolomite filling the spaces.				0.71184	0.00002	1
Zone 5	surface	Nad 83	6825069.0	404795	Upper Whittaker	Quartz-carbonate-sulphide veins in OSw3-5	mg dolomite	Dolomite	Dolomite gangue in brecciated quartz-sulphide vein.	-3.65	-15.30	15.20	0.72524	0.00004	1
Zone 6	surface	Nad 83	6823154.6	404363	Cadillac	Quartz-carbonate-sulphide veins	cg sparry dolomite	Dolomite	Cg saddle dolomite gangue in vein.	-6.30	-14.60	15.80	0.70963	0.00002	1
Zone 8-1	surface	Nad 83	6820721.3	403662	Cadillac	Quartz-carbonate-sulphide veins	Smithsonite	Smithsonite	Bands of smithsonite alternating with bands of quartz ±sulphides.				0.72538	0.00002	1
PC-01-130	258.6	Nad 83	6826335.0	405042	Upper Whittaker	Quartz-carbonate-sulphide veins in OSw3-3	mg dolomite	Dolomite	Mg dolomite gangue in sulphide-rich vein.	-2.68	-12.16	18.32	0.72848	0.00001	1
North Gate showing	surface	Nad 83	6835732.6	400839	Upper Whittaker	Quartz-carbonate-sulphide veins	cg calcite	Calcite	Cg calcite fill spaces in quartz-sulphide vein.	-2.30	-14.60	15.80	0.72138	0.00002	1

Table 3 continued.

Drill hole # / zone / showing	Depth (m) min-max	Datum	UTM Northing	UTM Easting	Host formation	Unit / lithology	Carbonate texture	Mineral Phase	Descriptions / Comments	$\delta^{13}C$ (PDB)	$\delta^{18}O$ (PDB)	$\delta^{18}O$ (SMOW)	$^{87}Sr/^{86}Sr$	error, 2σ	Ref.
PC-01-130	258.6	Nad 83	6826335.0	405042	Upper Whittaker	Quartz-carbonate-sulphide veins in OSw3-3	cg calcite	Calcite	Cg calcite fill spaces in quartz-sulphide vein.	-1.50	-30.70	-0.80	0.71578	0.00002	1
PC-01-132	288.5	Nad 83	6826405.5	405004	Upper Whittaker	Quartz-carbonate-sulphide veins in OSw3-3	cg calcite	Calcite	White coarse-grained (>2cm) calcite crystals in quartz-sulphide vein.	-1.20	-26.80	3.20	0.71756	0.00001	1
PC-04-159	480.6	Nad 83	6825981.0	404343	Upper Whittaker	Quartz-carbonate-sulphide veins	cg calcite	Calcite	Large blebs of cg white calcite within the aggregate of cg galena.	-2.64	-23.06	7.09			1
PC-01-130	297.3	Nad 83	6826335.0	405042	Upper Whittaker	Stratabound sulphides in OSw3-3	cg calcite	Calcite	Agg of cg sphalerite, galena, and calcite; calcite seems to be associated with sulphides (possibly contemporaneous).	-2.39	-20.47	9.67	0.72396	0.00006	1
PC-04-150	239.5	Nad 83	6825981.0	404343	Upper Whittaker	Stratabound sulphides in OSw3-2	cg calcite	Calcite	Cg calcite filling remaining spaces in sulphide section.	-4.80	-14.00	16.50	0.73070	0.00003	1
PC-93-27	231.6-231.7	Nad 83	6826126.4	405092	Upper Whittaker	Stratabound sulphides in OSw3-2	cg calcite	Calcite	Calcite-dolomite-quartz stringers.	-4.34	-14.61	15.80			1
PC-93-25	251.9	Nad 83	6826203.1	405006	Upper Whittaker	Stratabound sulphides in OSw3-2	cg calcite	Calcite	Coarse sparry calcite (fragments?) is completely surrounded by galena; and galena seems to cut the calcite.	-5.00	-14.00	16.40	0.73173	0.00001	1
PC-95-103	110	Nad 83	6825694.8	404838	Upper Whittaker	Stratabound sulphides at contact of OSw3-3 and OSw3-2	cg calcite vugs	Calcite	Chips of coarse-grained calcite in vugs	-4.20	-13.30	17.20	0.73189	0.00001	1
PC-94-82	469.6	Nad 83	6825981.0	405212	Upper Whittaker	Stringer/stratabound sulphides in OSw3-4	cacite vein	Calcite	Calcite veinlets cutting stringers of quartz-sulphides.	-1.18	-27.18	2.84	0.71537	0.00001	1
PC-06	207.5	Nad 27	N/A	N/A	Upper Whittaker	Chert nodule dolostone - OSw3-5	fg cx dolostone matrix	Dolomite	Massive light grey dolostone with cherty nodular zones.	-0.50	-9.27	21.30	0.71787	0.00000	2
PC-08	239	Nad 27	6826287.6	405024	Upper Whittaker	Lower spar unit - OSw3-4	fg cx dolostone matrix	Dolomite					0.71378	0.00004	2
PC-08	239.4	Nad 27	6826287.6	405024	Upper Whittaker	Lower spar unit - OSw3-4	fg cx dolostone matrix	Dolomite		-0.30	-7.33	23.30			2
PC-08	269.5	Nad 27	6826287.6	405024	Upper Whittaker	Lower spar unit - OSw3-4	fg cx dolostone matrix	Dolomite		-0.50	-9.37	21.20			2
PC-08	272	Nad 27	6826287.6	405024	Upper Whittaker	Lower spar unit - OSw3-4	fg cx dolostone matrix	Dolomite					0.72099	0.00004	2
PC-08	282.9	Nad 27	6826287.6	405024	Upper Whittaker	Mottled dolostone - OSw3-2	fg cx dolostone matrix	Dolomite		-1.00	-8.89	21.70			2
PC-08	283	Nad 27	6826287.6	405024	Upper Whittaker	Mottled dolostone - OSw3-3	fg cx dolostone matrix	Dolomite					0.72125	0.00002	2
PC-08	298.9	Nad 27	6826287.6	405024	Upper Whittaker	Chert nodular dolostone (possible mottled dolostone)	fg cx dolostone matrix	Dolomite		-2.00	-9.86	20.70			2
PC-08	308.0 to 308.1	Nad 27	6826287.6	405024	Upper Whittaker	Chert nodular dolostone (possible mottled dolostone)	fg cx dolostone matrix	Dolomite		0.50	-8.11	22.50	0.71443	0.00002	2
PC-11	201.2	Nad 27	6826289.7	405051	Upper Whittaker	Lower spar unit - OSw3-4	fg cx dolostone matrix	Dolomite		0.20	-7.24	23.40			2
PC-11	208.4	Nad 27	6826289.7	405051	Upper Whittaker	Lower spar unit - OSw3-4	fg cx dolostone matrix	Dolomite		-0.40	-6.65	24.00			2
PC-11	253.5	Nad 27	6826289.7	405051	Upper Whittaker	Lower nodular dolostone - OSw3-3	fg cx dolostone matrix	Dolomite		0.10	-6.07	24.60			2
PC-11	260.9	Nad 27	6826289.7	405051	Upper Whittaker	Lower nodular dolostone - OSw3-3	fg cx dolostone matrix	Dolomite		-1.00	-7.82	22.80			2
PC-11	260.9 dup	Nad 27	6826289.7	405051	Upper Whittaker	Lower nodular dolostone - OSw3-3	fg cx dolostone matrix	Dolomite		-1.00	-8.01	22.60			2
PC-11	290.5	Nad 27	6826289.7	405051	Upper Whittaker	Lower nodular dolostone - OSw3-3 or mottled dolostone - OSw3-2	fg cx dolostone matrix	Dolomite		0.00	-8.50	22.10			2
PC-13	76.2	Nad 27	6826289.6	405021	Upper Whittaker	Interbedded chert/dolostone - OSw3-7	fg cx dolostone matrix	Dolomite		-0.40	-5.98	24.70			2
PC-13	103	Nad 27	6826289.6	405021	Upper Whittaker	Interbedded chert/dolostone - OSw3-7	fg cx dolostone matrix	Dolomite		0.10	-5.78	24.90			2
PC-13	303.9	Nad 27	6826289.6	405021	Upper Whittaker	Chert nodule dolostone - OSw3-1	fg cx dolostone matrix	Dolomite					0.72673	0.00033	2
PC-13	303.9 dup	Nad 27	6826289.6	405021	Upper Whittaker	Chert nodule dolostone - OSw3-1	fg cx dolostone matrix	Dolomite					0.72605	0.00002	2
PC-13	312.9	Nad 27	6826289.6	405021	Upper Whittaker	Dolostone - OSw3-1	fg cx dolostone matrix	Dolomite	Rubble, well fractured; numerous calcite stringers.	-0.20	-9.86	20.70			2
PC-14	76.9	Nad 27	6826289.6	405021	Road River	Road River Formation	fg cx dolostone matrix	Dolomite	Well laminated, bedded, fg shaley calcareous sediment.	-0.60	-6.07	24.60			2
PC-14	245.5	Nad 27	6826289.6	405021	Upper Whittaker	Lower spar unit - OSw3-4	fg cx dolostone matrix	Dolomite		-0.70	-9.27	21.30	0.72121	0.00004	2
PC-28	107.8	Nad 27	N/A	N/A	Upper Whittaker	Upper chert nodule dolostone - OSw3-5	brecciated fg dolostone matrix	Dolomite	Tectonic breccia with angular clasts of dolomite ranging in size from <1 mm to 5 cm in a white grey quartz cement.	-0.30	-10.24	20.30			2
PC-28	160.6	Nad 27	N/A	N/A	Upper Whittaker	Upper chert nodule dolostone - OSw3-5	fg cx dolostone matrix	Dolomite		-0.04	-6.85	23.80			2
PC-28	280.7	Nad 27	N/A	N/A	Upper Whittaker	Lower chert nodule dolostone	fg cx dolostone matrix	Dolomite		-0.50	-8.89	21.70			2

Table 3 continued.

Drill hole # / zone / showing	Depth (m) min-max	Datum	UTM Northing	UTM Easting	Host formation	Unit / lithology	Carbonate texture	Mineral Phase	Descriptions / Comments	$\delta^{13}C$ (PDB)	$\delta^{18}O$ (PDB)	$\delta^{18}O$ (SMOW)	$^{87}Sr/^{86}Sr$	error, 2σ	Ref.
PC-40	302.2 outcrop	Nad 27	6825981.0	404343	Upper Whittaker	Mottled dolostone - OSw3-2	fg cx dolostone matrix	Dolomite		-0.50	-8.89	21.70			2
PC-R3	west of Gate Fault	Nad 27	N/A	N/A	Upper Whittaker		fg cx dolostone matrix	Chert nodule dolomite		-0.50	-7.33	23.30	0.70958	0.00002	2
PC-08	273.5	Nad 27	6826287.6	405024	Upper Whittaker	Stratabound sulphides	cg gangue dolomite	Dolomite	Fragments of quartz-carbonates in vein	-2.30	-6.85	23.80			2
PC-11	261.3	Nad 27	6826289.7	405051	Upper Whittaker	Stratabound sulphides	cg gangue dolomite	Dolomite	5 cm white sparry calcite caps a sulphide section.	-2.90	-8.50	22.10	0.72387	0.00002	2
PC-13	290.7	Nad 27	6826289.6	405021	Upper Whittaker	Stratabound sulphides	cg gangue dolomite	Dolomite	Crystalline carbonate bands interlayered with sulphide section.	-2.50	-7.92	22.70			2
PC-13	290.7	Nad 27	6826289.6	405021	Upper Whittaker	Stratabound sulphides	cg gangue dolomite	Dolomite	Bands and veinlets of cg dolomite in the sulphide section.	-2.50	-7.04	23.60			2
PC-14	289.3	Nad 27	6826289.6	405021	Upper Whittaker	Stratabound sulphides	cg gangue dolomite	Dolomite	<10% cg gangue dolomite within sulphide zone.	-3.30	-8.50	22.10	0.72136	0.00003	2
PC-21	273.5	Nad 27	6826239.3	405010	Upper Whittaker	Stratabound sulphides	cg gangue dolomite	Dolomite	Cg dolomite gangue in sulphide zone.	-3.30	-7.04	23.60			2
Zebra showing	Surface	Nad 83	6833925.9	410027	Cadillac ET (~Root River)	MVT-type sulphides	dolomite cement	Dolomite		-2.10	-13.54	16.90			2
Zebra showing	Surface	Nad 83	6833925.9	410027	Cadillac ET (~Root River)	MVT-type sulphides	dolomite cement	Dolomite	Zebra dolomite cement adjacent to colloform sphalerite.	-7.20	-17.62	12.70			2
Zebra showing	Surface	Nad 83	6833925.9	410027	Cadillac ET (~Root River)	MVT-type sulphides	dolomite cement	Dolomite		-4.90	-16.36	14.00			2
Zulu showing	Surface	Nad 83	6837372.0	410406	Cadillac ET (~Root River)	MVT-type sulphides	dolomite cement	Dolomite	Dolomite cement	-3.30	-13.54	16.90			2
Zebra showing	181	Nad 83	6833925.9	410027	Cadillac ET (~Root River)	MVT-type sulphides	dolomite cement	Dolomite	1-15% vugs lined with coarse white dolomite and euhedral pyrite.	-2.00	-12.67	17.80			2
Zebra showing	208A	Nad 83	6833925.9	410027	Cadillac ET (~Root River)	MVT-type sulphides	dolomite cement	Dolomite		-1.00	-10.73	19.80			2
Zebra showing	242	Nad 83	6833925.9	410027	Cadillac ET (~Root River)	MVT-type sulphides	dolomite cement	Dolomite	Local zones of breccia development containing variable sparry dolomite, pyrite, and sphalerite.	-1.60	-13.64	16.80			2
Zebra showing	208B	Nad 83	6833925.9	410027	Cadillac ET (~Root River)	MVT-type sulphides	cg dolomitic host rock	Dolomite	Cg dolomite in brecciated zebbra texture.	1.50	-5.39	25.30			2
Zebra showing	287	Nad 83	6833925.9	410027	Cadillac ET (~Root River)	MVT-type sulphides	cg dolomitic host rock	Dolomite	Small 1-3 mm seams and wisps of green marker mudstone in gray dolostone.	1.70	-6.85	23.80			2
Zebra showing	46	Nad 83	6833925.9	410027	Cadillac ET (~Root River)	MVT-type sulphides	cg dolomitic host rock	Dolomite		1.00	-7.24	23.40			2
Zebra showing	Surface	Nad 83	6833925.9	410027	Cadillac ET (~Root River)	MVT-type sulphides	bleached dolomite	Dolomite	Heavily bleached dolomite.	1.00	-5.39	25.30			2
Zebra showing	Surface	Nad 83	6833925.9	410027	Cadillac ET (~Root River)	MVT-type sulphides	host dolomite	Dolomite	Cg dolomitic host rock	0.60	-5.68	25.00			2
Zebra showing	Surface	Nad 83	6833925.9	410027	Cadillac ET (~Root River)	MVT-type sulphides	host dolomite	Dolomite	Zebra host dolomite	1.20	-6.36	24.30			2
Zulu showing	Surface	Nad 83	6837372.0	410406	Cadillac ET (~Root River)	MVT-type sulphides	host dolomite	Dolomite		-1.40	-6.36	24.30			2
Zebra showing	Surface	Nad 83	6833925.9	410027	Cadillac ET (~Root River)	MVT-type sulphides	host dolomite	Dolomite		0.93	-5.81		0.70934	0.00003	2
Zebra showing	Surface	Nad 83	6833925.9	410027	Cadillac ET (~Root River)	MVT-type sulphides	Saddle dolomite	Saddle dolomite		-4.73	-15.84		0.71052	0.00002	2
Zone 8	Surface	Nad 83	6820721.3	403662	Cadillac	Calcite veins	Calcite veining	Calcite	Unmineralized calcite veins	2.90	-8.59	22.00			2
PC-13	289	Nad 27	6826289.6	405021	?	Calcite veins	Calcite veining	Calcite	Unmineralized calcite veins	-4.00	-20.04	10.20			2
PC-41	103.4	Nad 27	6823154.6	404363	?	Calcite veins	Calcite veining	Calcite	Unmineralized calcite veins	-15.50	-10.63	19.90			2
PC-40	299.7	Nad 27	6825981.0	404343	?	Calcite veins	Calcite veining	Calcite	Unmineralized calcite veins						2
3-C-21	180.44	Nad 27	N/A	N/A	?	Calcite veins	Calcite veining	Calcite	Unmineralized calcite veins	-2.30	-11.89	18.60			2

Abbreviations: agg=aggregates, cg=coarse grained, conc=concentration, cx=coarse crystalline, diss=disseminated, dol=dolomite, dup=duplicate, fg=fine grained, mg=medium grained, N/A = Not available, occ=occasional.
All data in UTM zone 10. Ref (References) 1 = This study; 2 = Fraser (1996)

Table 4. Lead isotope values for the various deposit-types of the Prairie Creek area, Northwest Territories.

Drill hole # / sample # / showing	Depth (m) min-max	Datum	UTM Northing	UTM Easting	Host formation	Unit	Type of sulphides	Descriptions	Mineral phase	$^{206}Pb/^{204}Pb$	$^{207}Pb/^{204}Pb$	$^{208}Pb/^{204}Pb$	Ref.
PC-08	273.5	Nad 27	6826287.6	405024.1	Upper Whittaker	OSw3-2	Stratabound	Fg pyrite with cherty bands and zones of dissemineated cg pyrite with spars. Fine sphalerite and galena in the groundmass.	Galena	18.664	15.640	38.727	2
PC-08	281.5	Nad 27	6826287.6	405024.1	Upper Whittaker	OSw3-2	Stratabound	Numerous quartz-calcite-sulphide veins.	Galena	18.698	15.652	38.793	2
PC-08	281.5B	Nad 27	6826287.6	405024.1	Upper Whittaker	OSw3-2	Stratabound	Numerous quartz-calcite-sulphide veins.	Galena	18.681	15.646	38.748	2
PC-11	263.3	Nad 27	6826289.7	405051.3	Upper Whittaker	OSw3-2	Stratabound	Massive pyrite and sphalerite with irregular discontinuous calcite bands and voids; minor galena around higher sphalerite-rich intervals (5% sphalerite, 1% galena, 33% pyrite).	Galena	18.676	15.641	38.745	2
PC-12	269.2	Nad 27	6826264.2	405018.8	Upper Whittaker	OSw3-2 ?	Stratabound	Fg to cg galena in a groundmass of fg pyrite and sphalerite. The fg pyrite and sphalerite is occ banded and graded.	Galena	18.690	15.640	38.769	2
PC-12	274.7	Nad 27	6826264.2	405018.8	Upper Whittaker	OSw3-2 ?	Stratabound	Weakly banded fg pyrite, interval rich in black cherty/jasperoid nodules variably replaced by sphalerite, cg galena in sphalerite cement.	Galena	18.723	15.653	38.778	2
PC-13	290.7	Nad 27	6826289.6	405020.8	Upper Whittaker	OSw3-2	Stratabound	Cavity fill sulphides: well banded red framboidal sphalerite and some galena band.	Galena	18.770	15.656	38.807	2
PC-13	290.7	Nad 27	6826289.6	405020.8	Upper Whittaker	OSw3-2	Stratabound	Solution cavity fill-style banded massive sulphides - massive to well banded fg pyrite, sphalerite, lesser galena interlayered with black pyritic siliceous bands, nodules, and crystalline carbonate bands.	Galena	18.718	15.654	38.775	2
PC-14	289.3	Nad 27	6826289.6	405020.8	Upper Whittaker	OSw3-2	Stratabound	Massive medium grained framboidal red-brown sphalerite (60%), galena (15%), pyrite (5%) and quartz. Stringers at 25° CA.	Galena	18.708	15.662	38.806	2
PC-14	289.6	Nad 27	6826289.6	405020.8	Upper Whittaker	OSw3-2	Stratabound	Massive mg framboidal red-brown sphalerite (60%), galena (15%), pyrite (5%) and quartz. Stringers at 25° CA.	Galena	18.801	15.663	38.861	2
PC-17B	312.4	Nad 27	6826316.9	404956.4	Upper Whittaker	OSw3-3	Stratabound	Roughly banded fine-grained pyrite (45%), grey tan fg sphalerite (25%) and chert (25%) at 65-75° CA.	Galena	18.700	15.655	38.763	2
PC-27	213	Nad 27	6826126.4	405092.0	Upper Whittaker	OSw3-2	Stratabound		Galena	18.689	15.655	38.768	2
PC-27	226.4	Nad 27	6826126.4	405092.0	Upper Whittaker	OSw3-2	Stratabound	Broken, rubbly MVT?-style mineralized fragments mixed with sul/chert. Galena in rubbly fragments much higher conc (40%) than usual within a pyrite-sphalerite groundmass.	Galena	18.687	15.650	38.752	2
PC-35	224	Nad 27	6826084.0	405065.5	Upper Whittaker	OSw3-2	Stratabound	Dol with diss galena followed by massive galena -pyrite bands at 40° CA, followed by rare massive sulphide rubble of "MVT" style.	Galena	18.773	15.655	38.822	2
PC-95-103	110	Nad 27	6825694.8	404837.6	Upper Whittaker	Contact of OSw3-3 & OSw3-2	Stratabound	Chips of galena.	Galena	18.679	15.657	38.760	1
PC-94-82	496.1	Nad 27	6825981.0	405212.4	Upper Whittaker	OSw3-4	Stratabound	High grade sphalerite-pyrite-galena and sparry dolomite; upper contact at 70° CA; lower contact irregular but sharp at 80-90° CA.	Galena	18.689	15.659	38.772	1
PC-95-124	309.9	Nad 27	6824601.7	405040.5	Upper Whittaker	OSw3-7	Stratabound	Chips of massive sulphide; from 309.9 to 311.2 section consists of fg massive aggregate of pyrite with pink sphalerite, and galena+quartz in veinlets or vugs.	Galena	18.717	15.681	38.847	1
PC-04-150	239.5	Nad 27	6825981.0	404343.0	Upper Whittaker	OSw3-2	Stratabound	Sulphide section with some open space filling textures: Aggegates of fg pyrite+sphalerite replacing cherty dolostone; coarse sphalerite and pyrite rimmed by fg agg of pyrite+sphalerite; galena and calcite fills the remaining spaces.	Galena	18.690	15.660	38.770	1
PC-01-130	313.5	Nad 27	6826335.0	405042.0	Upper Whittaker	OSw3-2	Stratabound	Bands of fg pyrite in agg of fg pinkish sphalerite + fg pyrite; galena and calcite fills the remaining spaces.	Galena	18.682	15.662	38.776	1
PC-94-64 (1)	207.6	Nad 27	6823154.6	404363.3	Upper Whittaker	OSw3-6	Stratabound	Stratabound sulphides (sphalerite-galena-pyrite); sample 1=galena (<2% sphalerite).	Galena	18.703	15.687	38.857	1

Table 4 continued.

Drill hole # / sample # / showing	Depth (m) min-max	Datum	UTM Northing	UTM Easting	Host formation	Unit	Type of sulphides	Descriptions	Mineral phase	$^{206}Pb/^{204}Pb$	$^{207}Pb/^{204}Pb$	$^{208}Pb/^{204}Pb$	Ref.
PC-11	261	Nad 27	6826289.7	405051.3	Upper Whittaker	OSw3-2 or OSw3-3	Stratabound	Gangue dolomite within lower nodular dolostone (OSw3-3) or within the mineralized zone.	Dolomite	18.934	15.669	38.981	2
PC-13	290	Nad 27	6826289.6	405020.8	Upper Whittaker	OSw3-2	Stratabound	Solution cavity fill-style banded massive sul:massive to well banded fg pyrite, sphalerite, lesser galena interlayered with black pyritic siliceous bands, nodules, and crystalline carbonate bands.	Dolomite	18.703	15.647	38.778	2
PC-13 (rerun)	290.7	Nad 27	6826289.6	405020.8	Upper Whittaker	OSw3-2	Stratabound	Solution cavity fill-style banded massive sulphide: massive to well banded fg pyrite, sphalerite, lesser galena interlayered with black pyritic siliceous bands, nodules, and crystalline carbonate bands.	Dolomite	18.692	15.646	38.751	2
PC-14	289.3	Nad 27	6826289.6	405020.8	Upper Whittaker	OSw3-2	Stratabound	<10% dolomite within sulphide zone.	Dolomite	18.885	15.663	38.934	2
PC-21	273.5	Nad 27	6826239.3	405009.9	Upper Whittaker	OSw3-2	Stratabound		Dolomite	18.869	15.666	38.935	2
Rico showing	Surface	Nad 83	6831946.8	406649.5	Arnica		Veins		Sphalerite	19.132	15.685	39.097	2
Rico showing	Surface	Nad 83	6831946.8	406649.5	Arnica		Veins		Galena	19.042	15.675	39.040	2
#8 zone	Surface	Nad 27	6820721.3	403662.2	Cadillac		Veins	#8 zone vein near Prairie Creek Fault.	Smithsonite	19.018	15.679	39.060	2
#8 zone	Surface	Nad 27	6820721.3	403662.2	Cadillac		Veins	#8 zone vein near Prairie Creek Fault (rerun)	Smithsonite	19.010	15.676	39.067	2
PC-11	286.4	Nad 27	6826289.7	405051.3	Upper Whittaker	OSw3-1 or OSw3-2	Veins	N/A	?	19.003	15.667	39.031	2
1 (#3 drift)	Under-ground	Nad 27	NA	NA	NA		Veins	N/A	Galena	19.020	15.672	39.050	3
2 (#6 drift)	Under-ground	Nad 27	NA	NA	NA		Veins	N/A	Galena	19.027	15.675	39.066	3
3 (#9 drift)	Under-ground	Nad 27	NA	NA	NA		Veins	N/A	Galena	19.028	15.675	39.084	3
4 (#11 drift)	Under-ground	Nad 27	NA	NA	NA		Veins	N/A	Galena	19.037	15.677	39.081	3
5 (#20 drift)	Under-ground	Nad 27	NA	NA	NA		Veins	N/A	Galena	19.017	15.673	39.062	3
6 (#31 drift)	Under-ground	Nad 27	NA	NA	NA		Veins	N/A	Galena	19.025	15.674	39.072	3
7 shear	Surface	Nad 27	NA	NA	NA		Veins	N/A	Galena	19.018	15.677	39.066	3
8 shear	Surface	Nad 27	NA	NA	NA		Veins	N/A	Galena	19.027	15.674	39.075	3
9 #8 showing	Surface	Nad 27	6820721.3	403662.2	Cadillac		Veins	N/A	Galena	19.012	15.675	39.060	3
45670-1	Surface	Nad 27	NA	NA	NA		Veins	N/A	Galena	19.019	15.667	39.035	3
45669-2	Surface	Nad 27	NA	NA	NA		Veins	N/A	Galena	19.025	15.659	39.024	3
? Drift	Under-ground	Nad 27	NA	NA	NA		Veins	N/A	Galena	19.036	15.681	39.100	3
6295	Surface	Nad 27	NA	NA	NA		Veins	N/A	Galena	19.009	15.656	39.015	3
076294-3	Surface	Nad 27	NA	NA	NA		Veins	N/A	Galena	19.030	15.669	39.033	3
076294-2	Surface	Nad 27	NA	NA	NA		Veins	N/A	Galena	19.023	15.667	39.045	3
076294-1	Surface	Nad 27	NA	NA	NA		Veins	N/A	Galena	19.019	15.668	39.054	3
10	Surface	Nad 27	NA	NA	NA		Veins	N/A	Galena	19.030	15.674	39.054	3
11	Surface	Nad 27	NA	NA	NA		Veins	N/A	Galena	19.025	15.673	39.060	3
12	Surface	Nad 27	NA	NA	NA		Veins	N/A	Galena	19.030	15.660	38.978	3
13	Surface	Nad 27	NA	NA	NA		Veins	N/A	Galena	19.035	15.672	39.053	3
14	Surface	Nad 27	NA	NA	NA		Veins	N/A	Galena	19.044	15.676	39.069	3
15	Surface	Nad 27	NA	NA	NA		Veins	N/A	Galena	19.036	15.669	39.031	3

Table 4 continued.

Drill hole # / sample # / showing	Depth (m) min-max	Datum	UTM Northing	UTM Easting	Host formation	Unit	Type of sulphides	Descriptions	Mineral phase	$^{206}Pb/^{204}Pb$	$^{207}Pb/^{204}Pb$	$^{208}Pb/^{204}Pb$	Ref.
17	Surface	Nad 27	NA	NA	NA		Veins	N/A	Galena	19.021	15.674	39.075	3
PC-93-50	176	Nad 27	6825981.0	404343.0	Road River		Veins	Chips of galena from mineralized vein (sphalerite-galena-quartz-calcite).	Galena	19.015	15.673	39.034	1
North Gate vein-2	surface	Nad 83	6835732.6	400838.6	Upper Whittaker		Veins	Massive sphalerite (tan colour) with traces of galena and tetrahedrite in quartz-calcite vein. Cg calcite fill spaces. The cg sphalerite+galena is associated with quartz-calcite vein.	Galena	18.982	15.672	39.008	1
South Gate vein	surface	Nad 83	6807388.0	390411.3	Sunblood?		Veins	Various samples of massive galena with some sphalerite and malachite in quartz matrix (no calcite); sample of galena has traces of malachite.	Galena	18.978	15.685	39.071	1
5-3	surface	Nad 83	6825069.0	404794.8	Upper Whittaker	OSw3-5	Veins	Boulder of mineralized vein: Massive galena with some quartz fragments; the aggregate of galena contains fg pyrite and quartz.	Galena	19.040	15.696	39.117	1
6-1	surface	Nad 83	6823154.6	404363.3	Cadillac		Veins	Sample of mineralized vein: Quartz vein with some stringers of galena; traces of malachite in the quartz.	Galena	19.048	15.704	39.147	1
8-3	surface	Nad 83	6820721.3	403662.2	Cadillac		Veins	Sulphide-rich vein with bands of quartz, and bands of smectite; galena present.	Galena	19.051	15.714	39.173	1
PC-95-125 (Rico showing)	760	Nad 27	6827849.6	405628.9	Road River		Veins	Quartz-galena±sphalerite vein with calcite blobs (calcite is late versus quartz and galena); darker sulphides (tetrahedrite?) with galena.	Galena	19.047	15.710	39.164	1
PC-01-130	182	Nad 27	6826335.0	405042.0	Upper Whittaker	OSw3-5	Veins	Sulphide-rich vein cutting core at ~10° CA; vein of cg pale sphalerite with cg galena in the centre. Section 181.6 to 183.1: coarse 5 cm wide sphalerite-galena vein stringers subparalleling CA, honey colour sphalerite 50%, galena 30%, and carbonates 20%.	Galena	18.989	15.694	39.064	1
PC-04-159	480.6	Nad 27	6825981.0	404343.0	Upper Whittaker		Veins	Cg calcite associated with cg galena.	Galena	19.069	15.731	39.235	1
PC-15	101.7	Nad 27	6826316.0	404962.3	Road River		Breccia	Tectonic breccia	Galena	18.695	15.653	38.782	2
Zebra showing	Surface	Nad 83	6833291.0	410801.2	Cadillac ET (~Root River)		MVT	N/A	Dolomite	19.288	15.697	38.972	2
Zebra showing	Surface	Nad 83	6833291.0	410801.2	Cadillac ET (~Root River)		MVT	N/A	Dolomite	19.283	15.700	38.844	2
Samantha showing	Surface	Nad 83	6842662.5	408600.5	Root River		MVT	N/A	Sphalerite	18.739	15.647	38.816	2
Zebra showing	Surface	Nad 83	6833291.0	410801.2	Cadillac ET (~Root River)		MVT	N/A	Sphalerite	18.581	15.641	38.566	2
Zulu showing	Surface	Nad 83	6837372.0	410406.0	Root River		MVT	N/A	Sphalerite	18.664	15.656	38.552	2

Abbreviations: agg=aggregates, CA=core axis, cg=coarse grained, coll=colloform, conc=concentration, cx=coarse crystalline, diss=disseminated, dup=duplicate, fg=fine grained, mg=medium grained, occ=occasional, N/A=Not available, sul=sulphides. References: 1 = this study, 2 = Fraser (1996) and 3 = Morrow and Cumming (1982)

Table 5. Sulphur isotope values for the various deposit types of the Prairie Creek area, Northwest Territories.

Drill hole # / zone / showing	Depth (m) min-max	Datum	UTM Northing	UTM Easting	Host formation	Unit	Type of sulphides	Descriptions	Mineral phase	$\delta^{34}S_{(‰\ CDT)}$ pyrite	$\delta^{34}S_{(‰\ CDT)}$ galena	$\delta^{34}S_{(‰\ CDT)}$ sphalerite	%S	Ref.
PC-92-16	310.6	Nad 27	6826316.0	404962.3	Upper Whittaker	OSw3-3	Stratabound	Mixture of framboidal sphalerite and mg galena.	Galena		17.6		14.57	1
PC-92-19	315.2	Nad 27	6826398.8	405008.6	Upper Whittaker	OSw3-3 or OSw3-2	Stratabound	Cg galena adjacent to intervals of white crystalline dolomite.	Galena		19.85		13.82	1
PC-93-23	249.7	Nad 27	6826202.1	405004.5	Upper Whittaker	OSw3-2	Stratabound	Aggregate of fg pyrite, sphalerite, and mg galena.	Pyrite	20.38			51.76	1
PC-93-23	249.7	Nad 27	6826202.1	405004.5	Upper Whittaker	OSw3-2	Stratabound	Aggregate of fg pyrite, sphalerite, and mg galena.	Galena		20.38		14.02	1
PC-93-25	251.9	Nad 27	6826203.1	405005.8	Upper Whittaker	OSw3-2	Stratabound	Cg galena enclosing cg calcite and reddish sphalerite grains.	Galena		20.34		13.41	1
PC-93-35	228.0-228.2	Nad 27	6826084.0	405065.5	Upper Whittaker	OSw3-2	Stratabound	Massive fg aggregates of pyrite and sphalerite with occ galena.	Pyrite	12.56			42.36	1
PC-93-35	228.0-228.2	Nad 27	6826084.0	405065.5	Upper Whittaker	OSw3-2	Stratabound	Massive fg aggregates of pyrite and sphalerite with occ galena.	Pyrite	12.7			41.87	1
PC-94-64	207.6	Nad 27	6823154.6	404363.3	Upper Whittaker	OSw3-6	Stratabound	Fg aggregates of pyrite-sphalerite-galena.	Galena		21.23		21.8	1
PC-95-65	432.9	Nad 27	6825981.0	404343.0	Upper Whittaker	OSw3-4?	Stratabound	Aggregate of fg pyrite in dolomite cement; the whole forming poorly defined bands.	Pyrite	24.19			41.28	1
PC-94-82	496.1	Nad 27	6825981.0	405212.4	Upper Whittaker	OSw3-4	Stratabound	Aggregate of fg pyrite and sphalerite with interstitial galena.	Pyrite	18.59			47.5	1
PC-94-82	496.1	Nad 27	6825981.0	405212.4	Upper Whittaker	OSw3-4	Stratabound	Aggregate of fg pyrite and sphalerite with interstitial galena.	Galena		21.3		13.48	1
PC-95-103	110	Nad 27	6825694.8	404837.6	Upper Whittaker	At contact of OSw3-3 & OSw3-2	Stratabound	Galena in open-space filling.	Galena		20.32		13.71	1
PC-95-103	110.3	Nad 27	6825694.8	404837.6	Upper Whittaker	At contact of OSw3-3 & OSw3-2	Stratabound	Aggregate of fg pinkish to red sphalerite and pyrite, streaks of galena and minor sparry dolomite and pyrobitumen. Sphalerite may have traces of pyrite.	Sphalerite			23.81	33.79	1
PC-95-103 (dup)	110.3	Nad 27	6825694.8	404837.6	Upper Whittaker	At contact of OSw3-3 and OSw3-4	Stratabound	Aggregate of fg pinkish to red sphalerite and pyrite, streaks of galena and minor sparry dolomite and pyrobitumen.	Sphalerite			23.57	32.35	1
PC-95-124	309.9	Nad 27	6824601.7	405040.5	Upper Whittaker	OSw3-7	Stratabound	Aggregate of fg pyrite and pinkish sphalerite; galena and quartz occur as veinlets and vug-fillings.	Pyrite	23.79			48.2	1
PC-01-130	269.3	Nad 27	6826335.0	405042.0	Upper Whittaker	OSw3-3	Stratabound	Fg pyrite (±pinkish sphalerite) rims vugs in dolostone.	Pyrite	22.87			55.3	1
PC-01-130	295.9	Nad 27	6826335.0	405042.0	Upper Whittaker	OSw3-3	Stratabound	Aggregate of cg sphalerite and galena cut by calcite.	Sphalerite			19.68	33.56	1
PC-01-130 (dup)	295.9	Nad 27	6826335.0	405042.0	Upper Whittaker	OSw3-3	Stratabound	Aggregate of cg sphalerite and galena cut by calcite.	Sphalerite			19.3	31.28	1
PC-01-130	295.9	Nad 27	6826335.0	405042.0	Upper Whittaker	OSw3-3	Stratabound	Aggregate of cg sphalerite and galena cut by calcite.	Galena		17.3		13.16	1
PC-01-130	313.5	Nad 27	6826335.0	405042.0	Upper Whittaker	OSw3-2	Stratabound	Bands of fg pyrite and fg pinkish sphalerite; galena and calcite fill the remaining spaces.	Galena		19.32		13.76	1
PC-04-150	237.2	Nad 27	6825981.0	404343.0	Upper Whittaker	OSw3-2	Stratabound	Fg pyrite replacing the sparry and cherty dolomite.	Pyrite	24.28			42.78	1
PC-04-150	238.15	Nad 27	6825981.0	404343.0	Upper Whittaker	OSw3-2	Stratabound	Fg aggregate of pyrite and sphalerite; minor galena and sparry dolomite.	Sphalerite			19.82	32.07	1
PC-92-15	332.5	Nad 27	6826316.0	404962.3	Upper Whittaker	OSw3-2	Veins	Fg to mg pyrite and minor galena in quartz vein.	Pyrite	20.97			53.95	1
PC-92-19	237.9	Nad 27	6826398.8	405008.6	Upper Whittaker	OSw3-5	Veins	Galena crosscutting yellowish tan colour sphalerite in quartz matrix.	Galena		18.11		13.05	1
PC-92-19	237.9	Nad 27	6826398.8	405008.6	Upper Whittaker	OSw3-5	Veins	Yellowish tan color sphalerite crosscut by galena in quartz matrix.	Sphalerite			20.41	33.62	1
PC-93-50	176	Nad 27	6825981.0	404343.0	Road River		Veins	Cg galena in quartz-carbonate-sulphide vein.	Galena		16.69		13.33	1
PC-93-50	176.4	Nad 27	6825981.0	404343.0	Road River		Veins	Tan colour sphalerite in quartz-carbonate-sulphide vein.	Sphalerite			19.22	32.05	1
PC-95-122	765.5	Nad 27	6827664.6	405587.7	Road River		Veins	Cg galena and yellowish tan colour sphalerite in quartz vein.	Galena		18.32		13.34	1
PC-95-122	765.5	Nad 27	6827664.6	405587.7	Road River		Veins	Yellowish tan colour sphalerite and cg galena in quartz vein.	Sphalerite			20.95	33.87	1
PC-95-125	760	Nad 27	6827849.6	405628.9	Road River		Veins	Galena and minor sphalerite in quartz-calcite vein.	Galena		18.64		13.18	1
PC-95-125	762	Nad 27	6827849.6	405628.9	Road River		Veins	Cg dark tan colour sphalerite in galena-tetrahedrite-quartz vein.	Sphalerite			19.91	31.63	1
PC-01-130	182	Nad 27	6826335.0	405042.0	Upper Whittaker	OSw3-5	Veins	Cg galena and tan colour sphalerite in quartz-carbonate-sulphide vein.	Galena		22.85		13.57	1
PC-01-130	182	Nad 27	6826335.0	405042.0	Upper Whittaker	OSw3-5	Veins	Cg tan colour sphalerite and galena in quartz-carbonate-sulphide vein.	Sphalerite			24.06	32.01	1
PC-01-130	257.5	Nad 27	6826335.0	405042.0	Upper Whittaker	OSw3-3	Veins	Fg to mg pyrite in quartz-carbonate-sphalerite-galena vein.	Pyrite	21.81			52.49	1

Table 5 continued.

Drill hole # / zone / showing	Depth (m) min-max	Datum	UTM Northing	UTM Easting	Host formation	Unit	Type of sulphides	Descriptions	Mineral phase	$\delta^{34}S_{(‰\ CDT)}$ pyrite	$\delta^{34}S_{(‰\ CDT)}$ galena	$\delta^{34}S_{(‰\ CDT)}$ sphalerite	%S	Ref.
PC-04-159	482.1	Nad 27	6825981.0	404343.0	Upper Whittaker		Veins	Cg reddish tan sphalerite and traces of galena in quartz-carbonate-sulphide vein.	Sphalerite			20.53	33.16	1
PC-04-159	480.6	Nad 27	6825981.0	404343.0	Upper Whittaker		Veins	Cg galena in quartz-calcite-sulphide vein.	Galena		17.92		13.44	1
Rico-4	Surface	Nad 83	6831946.8	406649.5	Arnica		Veins	Cg yellowish tan color sphalerite in quartz-carbonate-galena vein.	Sphalerite			16.87	33.12	1
Rico-3	Surface	Nad 83	6831946.8	406649.5	Arnica		Veins	Fg galena intergrown with cg sphalerite in quartz-carbonate-sulphide vein.	Galena		15.36		11.92	1
8-3	Surface	Nad 83	6820721.3	403662.2	Upper Whittaker		Veins	Galena and smithsonite in banded quartz-carbonate-sulphide vein.	Galena		17.14		14.12	1
5-3	Surface	Nad 83	6825069.0	404794.8	Upper Whittaker	OSw3-5	Veins	Galena and fg pyrite in brecciated quartz vein.	Galena		18.16		12.31	1
5-3 (dup)	Surface	Nad 83	6825069.0	404794.8	Upper Whittaker	OSw3-5	Veins	Galena and fg pyrite in brecciated quartz vein.	Galena		17.73		12.62	1
5-2	Surface	Nad 83	6825069.0	404794.8	Upper Whittaker	OSw3-5	Veins	Brecciated sphalerite and quartz in aggregates of galena.	Sphalerite			20.16	31.17	1
6-1	Surface	Nad 83	6823154.6	404363.3	Upper Whittaker		Veins	Stringers of galena with traces of malachite in quartz-sulphide vein.	Galena		17.96		13.33	1
7-1	Surface	Nad 83	6822145.4	403910.8	Upper Whittaker		Veins	Galena in quartz vein.	Galena		17.36		11.02	1
930-2 ct 11	Mine site	Nad 27	6825973	404825	?		Veins	Cg galena partially replacing sphalerite.	Galena		17.82		13.72	1
Underground level 930 ct 22	Mine site	Nad 27	6825973	404825	?		Veins	Cg pale tan to grey sphalerite enclosing galena crystals.	Sphalerite			20.4	32.54	1
North Gate - 2	Surface	Nad 83	6835732.6	400838.6	Upper Whittaker		Veins	Cg pale tan colour sphalerite and traces of galena and tetrahedrite.	Sphalerite			13.14	33.57	1
N-Gate	Surface	Nad 83	6835732.6	400838.6	Upper Whittaker		Veins	Cg pale tan colour sphalerite and traces of galena and tetrahedrite.	Galena		18.45		17.78	1
N-Gate	Surface	Nad 83	6835732.6	400838.6	Upper Whittaker		Veins	Cg pale tan colour sphalerite and traces of galena and tetrahedrite.	Sphalerite			20.06	33.87	1
South Gate vein	Surface	Nad 83	6807388.0	390411.3	Sunblood?		Veins	Cg massive aggregalenate of galena and minor sphalerite.	Galena		9.82	19.61	13.41	1
PC-94-80 (Zebra showing)	220	Nad 27	6833291.0	410801.2	Cadillac ET (~Root River)		MVT	Pyrite rimming walls of vugs filled by saddle dolomite.	Pyrite	13.79			48.96	1
Zebra-2 (lower showing)	Surface	Nad 83	6833291.0	410801.2	Cadillac ET (~Root River)		MVT	Breccia cemented by saddle dolomite cements and colloform sphalerite and pyrite mantled dolostone fragments.	Sphalerite			13.61	30.93	1
Samantha-2 (lower trench)	Surface	Nad 83	6842662.5	408600.5	Root River		MVT	Cg massive aggregates of galena and minor sphalerite.	Galena		13.06		13.7	1
Samantha-2 (lower trench) (dup)	Surface	Nad 83	6842662.5	408600.5	Root River		MVT	Cg massive aggregates of galena and minor sphalerite.	Galena		13.06		13.39	1
PC-94-62	300.1	Nad 27	6822986.0	404356.6	Upper Whittaker	OSw3-2	Fg muddy pyrite	Fg pyrite aggregates in host dolostone.	Pyrite	3.05			39.37	1
PC-11	269	Nad 27	6826289.7	405051.3	Upper Whittaker		Stratabound	NA	Sphalerite			22.2		2
PC-35	224	Nad 27	6826084.0	405065.5	Upper Whittaker		Stratabound	NA	Galena		20.0			2
PC-12	274.8	Nad 27	6826264.2	405018.8	Upper Whittaker		Stratabound	NA	Pyrite	23.8				2
PC-12	274.8	Nad 27	6826264.2	405018.8	Upper Whittaker		Stratabound	NA	Pyrite	23.9				2
PC-13	274.8	Nad 27	6826289.6	405020.8	Upper Whittaker		Stratabound	NA	Pyrite	22				2
PC-21	273.5	Nad 27	6826239.3	405009.9	Upper Whittaker		Stratabound	NA	Pyrite	21.6				2
Rico	Surface	Nad 83	6831946.8	406649.5	Arnica		Veins	NA	Sphalerite			17		2
3050 level	Underground workings	Nad 27	6825722.0	404747.0	Upper Whittaker		Veins	NA	Sphalerite			20		2
#8 zone	Surface	Nad 83	6820721.3	403662.2	Cadillac		Veins	NA	Sphalerite			19.1		2

Abbreviations: cg=coarse grained, ct=crosscut, conc=concentration, cx=coarse crystalline, diss=disseminated, dup=duplicate, fg=fine grained,mg=medium grained, occ=occasional, N/A = Not available.
All data is in UTM zone 10. References: 1 = this study, 2 = Fraser (1996).

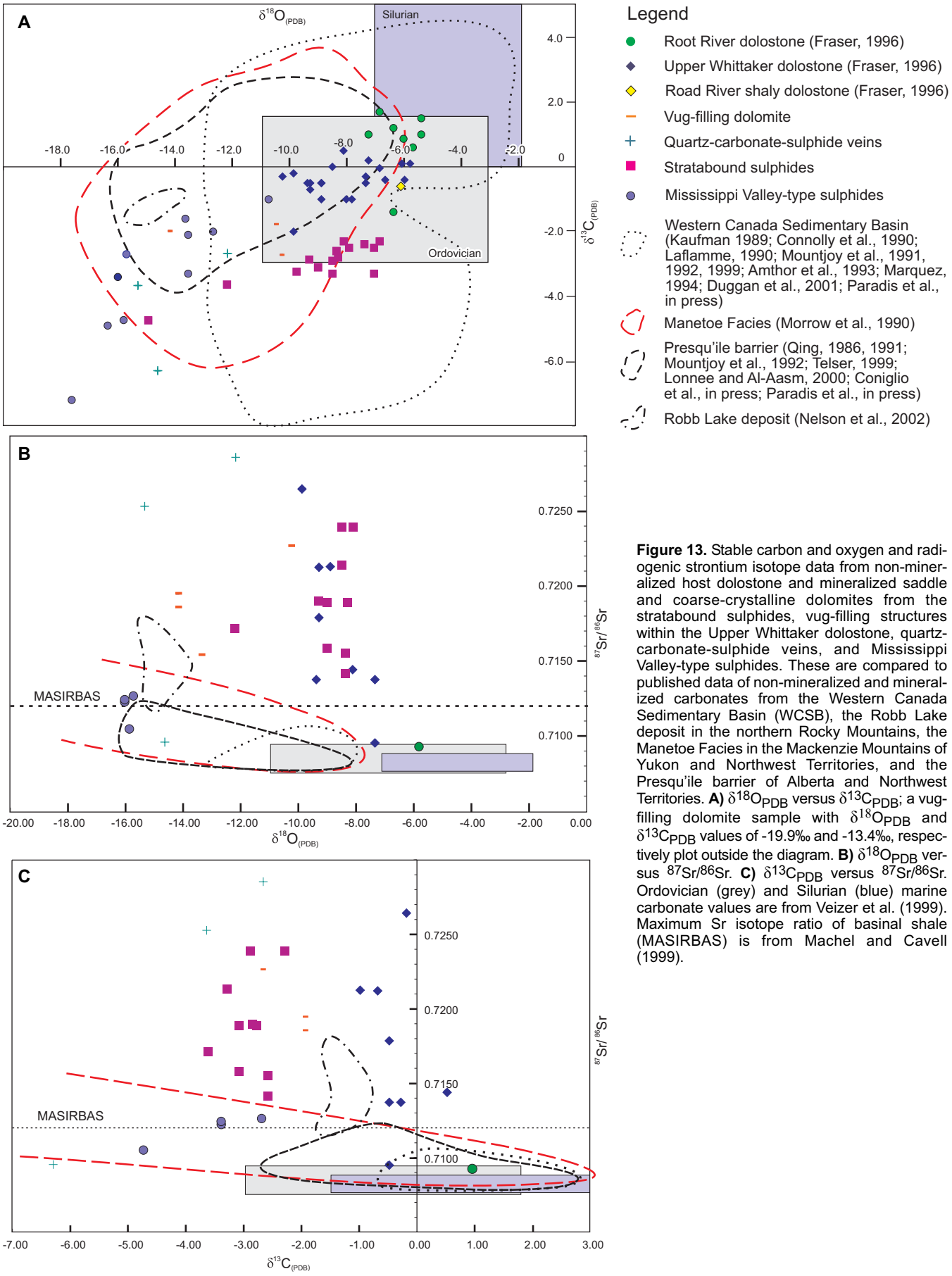


Figure 13. Stable carbon and oxygen and radiogenic strontium isotope data from non-mineralized host dolostone and mineralized saddle and coarse-crystalline dolomites from the stratabound sulphides, vug-filling structures within the Upper Whittaker dolostone, quartz-carbonate-sulphide veins, and Mississippi Valley-type sulphides. These are compared to published data of non-mineralized and mineralized carbonates from the Western Canada Sedimentary Basin (WCSB), the Robb Lake deposit in the northern Rocky Mountains, the Manetoe Facies in the Mackenzie Mountains of Yukon and Northwest Territories, and the Presqu'ile barrier of Alberta and Northwest Territories. **A)** $\delta^{18}O_{PDB}$ versus $\delta^{13}C_{PDB}$; a vug-filling dolomite sample with $\delta^{18}O_{PDB}$ and $\delta^{13}C_{PDB}$ values of -19.9‰ and -13.4‰, respectively plot outside the diagram. **B)** $\delta^{18}O_{PDB}$ versus $^{87}Sr/^{86}Sr$. **C)** $\delta^{13}C_{PDB}$ versus $^{87}Sr/^{86}Sr$. Ordovician (grey) and Silurian (blue) marine carbonate values are from Veizer et al. (1999). Maximum Sr isotope ratio of basinal shale (MASIRBAS) is from Machel and Cavell (1999).

Basinal Shale" (MASIRBAS; Machel and Cavell, 1999) in the Cordillera. They are also higher than Ordovician-Silurian marine carbonates (0.7078-0.70950; Veizer et al., 1999). Sample PC-R3 of Fraser (1996) taken from the Upper Whittaker Formation west of the Gate Fault has a $^{87}Sr/^{86}Sr$ ratio similar to the Root River dolostone and is within the range of values published for the Western Canada Sedimentary Basin (WCSB), Presqu'ile barrier, and other dolostones of the northern Rocky Mountains. Only one sample from the Root River dolostone was analyzed for $^{87}Sr/^{86}Sr$ and it gives a value of 0.7093, which is slightly higher from that of Silurian marine carbonates (0.7079-0.7088; Veizer et al., 1999). All the other host dolostone samples are significantly more radiogenic than the Western Canada Sedimentary Basin (WCSB), Presqu'ile barrier, and other dolostones of the northern Rocky Mountains.

Sparry dolomite associated with the stratabound sulphide mineralization has $\delta^{18}O$ values ranging from -6.9 to -14.9‰ and $\delta^{13}C_{PDB}$ values ranging from -2.3 to -4.7‰ (Fig. 13A). These values are depleted in ^{13}C compared to the host dolostone values of the Upper Whittaker Formation. Except for two samples, the $\delta^{18}O$ values are similar to the host dolostone. The two samples have low $\delta^{18}O$ values of -12.2 and -14.9‰. Oxygen and carbon isotope values for the stratabound sulphides resemble the values of the mineralized dolomite of the Manetoe Facies, especially the $\delta^{18}O_{PDB}$ and $\delta^{13}C_{PDB}$ values of -14.0 to -12.8‰ and -3.8 to -2.2‰, respectively (Paradis et al., in press). $^{87}Sr/^{86}Sr$ ratios of the sparry dolomites from the stratabound sulphides range from 0.7138 to 0.7239 (Table 3) and are significantly more radiogenic than Ordovician-Silurian marine carbonates (0.7078-0.70950; Veizer et al., 1999). The values are similar to the host dolostone of the Upper Whittaker Formation that are in proximity to the stratabound zones, but they are higher than the host dolostone away from sulphide mineralization. On the $\delta^{18}O_{PDB}$ vs. $^{87}Sr/^{86}Sr$ cross plot (Fig. 13B), the mineralized dolomites from the stratabound sulphides plot in a field with higher $^{87}Sr/^{86}Sr$ values than of the WCSB, Presqu'ile barrier, and Manetoe Facies. The mineralized dolostones of the Robb Lake deposit have slightly lower $^{87}Sr/^{86}Sr$ ratios to the sparry dolomites from the Prairie Creek stratabound sulphides. The same relationship is observed on the $\delta^{13}C_{PDB}$ versus $^{87}Sr/^{86}Sr$ cross plot (Fig. 13C).

Only three dolomite samples from quartz-carbonate-sulphide veins were analyzed for oxygen, carbon and strontium isotopes. Their isotopic composition is variable with $\delta^{18}O$ values of -12.2 to -15.3, $\delta^{13}C_{PDB}$ values of -2.7 to -6.3, and $^{87}Sr/^{86}Sr$ values of 0.70963 to 0.72848 (Table 3; Fig. 13A, B, C).

Mineralized sparry dolomites from the Prairie Creek MVT showings have $\delta^{18}O$ values ranging from -17.6 to -10.7‰ and $\delta^{13}C$ values ranging from -7.2 to -1.0‰ (Fig. 13A, Table 3) with a broad co-variance between the $\delta^{13}C$ and $\delta^{18}O$ values. These values are more negative than the Root River host dolostone, but they are similar to values published for the Manetoe Facies and the Presqu'ile barrier (Fig. 13A). Strontium isotope values from the Prairie Creek MVT dolomites range between 0.7105 and 0.7127 (Table 3). These $^{87}Sr/^{86}Sr$ values are slightly more radiogenic than Silurian marine carbonates (0.7079-0.7088; Veizer et al., 1999), but they are similar to the Manetoe Facies, and they overlap the lighter values for the Robb Lake deposit.

Lead Isotopes

Lead isotopic analyses were performed on clean cubes of galena at the Isotope Geochemistry and Geochronology Research Facility (IGGRF) of Carleton University. All samples were processed for Pb isotopic analysis using standard anion exchange techniques, followed by thermal ionization mass spectrometry (details by Cousens, 1996). All Pb mass spectrometer data are corrected for fractionation using NIST SRM981. The average ratios measured for NIST SRM981 are $^{206}Pb/^{204}Pb=16.891\pm0.011$, $^{207}Pb/^{204}Pb=15.430\pm0.014$, and $^{208}Pb/^{204}Pb=36.505\pm0.048$ (2σ), based on 40 runs between September 1992 and March 1996. The fractionation correction is +0.13%/amu (based on the values of Todt et al., 1984, 1996).

New lead isotope analyses of galena from the stratabound and the vein sulphides are presented in Table 4. Lead isotope analyses from Fraser (1996) and Morrow and Cumming (1982) are also included for comparison; analyses from the MVT showings are also included.

Lead isotopic investigation of mineral occurrences in the study area was undertaken in order to assess the possible sources for Pb, place constraints on the possible timing of mineralization, and in particular, determine whether the stratabound and the vein sulphides are genetically related (i.e. are the vein sulphides remobilized from the stratabound sulphides). Lead isotope analyses are plotted on the "shale curve" of Godwin and Sinclair (1982), a growth curve unique to the ancient western margin of North America.

Results

In Figure 14A, the stratabound sulphides (except for two samples) plot in a tight cluster below the shale curve of Godwin and Sinclair (1982) with $^{206}Pb/^{204}Pb$ values of 18.664 to 18.801 and $^{207}Pb/^{204}Pb$ values of 15.640 to 15.663, and above the average crustal evolution curve of Stacey and Kramers (1975). The shale curve of Godwin and Sinclair (1982) is a growth curve unique to the ancient western margin of North America. It was constructed using leads from well

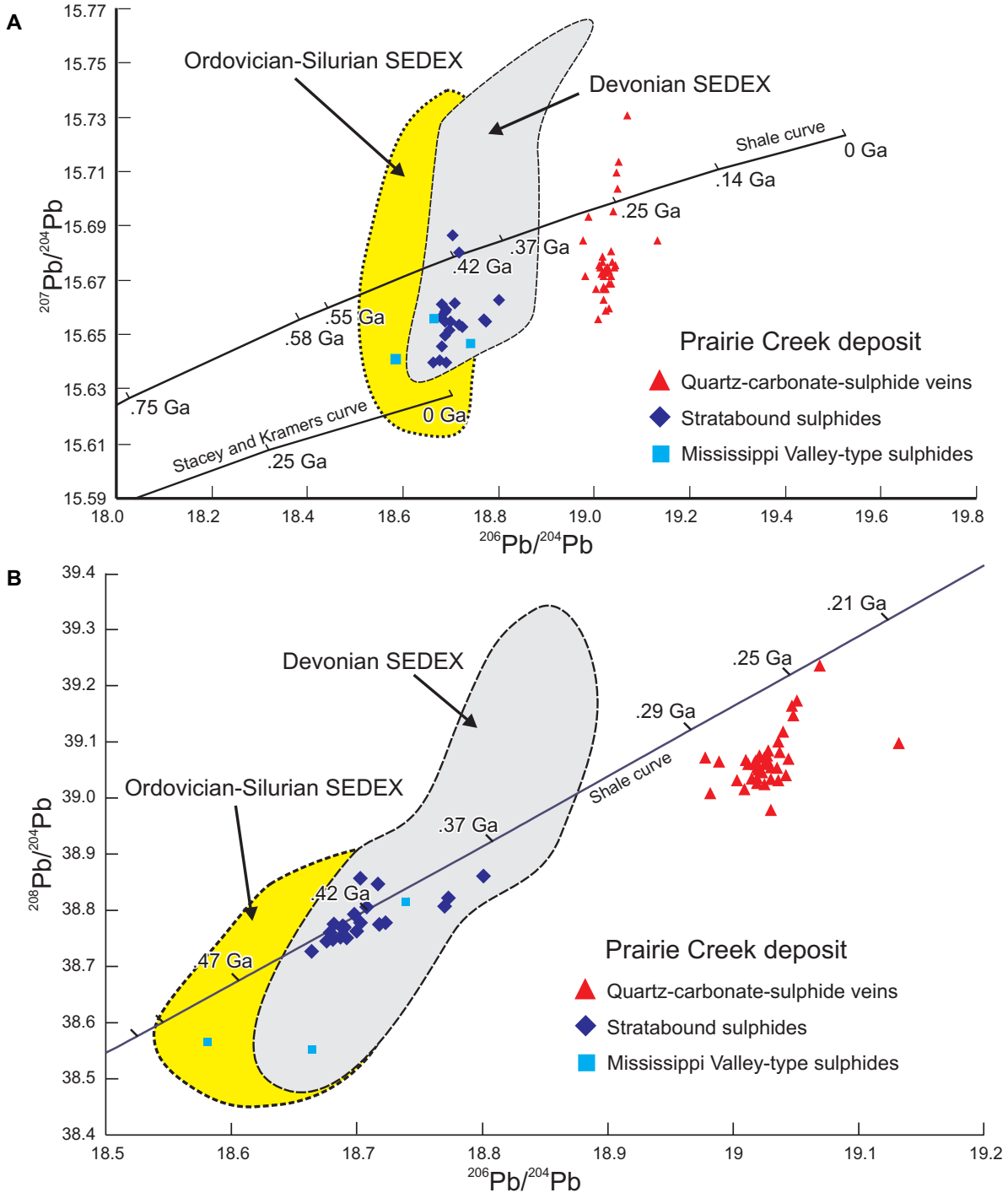


Figure 14. Lead isotopic data from the stratabound sulphides, quartz-carbonate sulphide veins, and Mississippi Valley-type sulphides from the Prairie Creek deposit. **A)** $^{207}Pb/^{204}Pb$ versus $^{206}Pb/^{204}Pb$. **B)** $^{208}Pb/^{204}Pb$ versus $^{206}Pb/^{204}Pb$. These plots include new data from the Prairie Creek occurrences (see Table 4 for data) and data from Morrow and Cumming (1982) and Fraser (1996). Ordovician-Silurian SEDEX deposits and Devonian SEDEX deposits from the Selwyn Basin (data from Godwin et al., 1988; Cousens, 2006) are shown for comparison with Prairie Creek. The data is compared to the average crustal evolution curve of Stacey and Kramers (1975) and to the shale curve of Godwin and Sinclair (1982).

dated SEDEX deposits of the Canadian Cordillera ranging in age from middle Proterozoic to Mississippian. The Prairie Creek data indicate that the lead was derived from an upper crustal source with higher U/Pb values than that of the Stacey and Kramers (1975) growth curve.

In the $^{207}Pb/^{204}Pb$ versus $^{206}Pb/^{204}Pb$ (Fig. 14A) and $^{208}Pb/^{204}Pb$ vs $^{206}Pb/^{204}Pb$ diagrams (Fig. 14B), the stratabound and vein sulphides plot in separate clusters, with stratabound sulphides crosscutting the shale curve at around 420 Ma. They also show variations in both $^{207}Pb/^{204}Pb$ and $^{208}Pb/^{204}Pb$ that are

large relative to variations in $^{206}Pb/^{204}Pb$. In both figures, the Prairie Creek stratabound sulphides isotopically overlap with the values of the Ordovician-Silurian SEDEX deposits and the Devonian SEDEX deposits of the Selwyn Basin.

The Prairie Creek quartz-carbonate-sulphide veins form a linear array crosscutting the shale curve at 250 Ma. Values of $^{206}Pb/^{204}Pb$ range from 18.978 to 19.132 and $^{207}Pb/^{204}Pb$ values range from 15.656 to 15.731. A sphalerite sample from the Rico showing has a slightly more elevated $^{206}Pb/^{204}Pb$ value of 19.132. Fraser (1996) explained this high value to post-crystallization contamination due to the highly fractured and brecciated nature of the sphalerite.

Only three MVT sphalerite and two dolomite samples were analysed by Fraser (1996) and none by the author. The sphalerites have $^{206}Pb/^{204}Pb$ values between 18.581 and 18.739 and $^{207}Pb/^{204}Pb$ values between 15.641 and 15.656, which plot in proximity to the stratabound sulphides but show a wider range of $^{206}Pb/^{204}Pb$ values. These values resemble the Ordovician-Silurian MVT values of the Mackenzie Mountains but are different than the radiogenic lead trend of the Devonian "Cordilleran Carbonate Lead", which characterizes the Mississippi Valley-type Zn-Pb occurrences of the northern Rocky Mountains and the Mackenzie Mountains (see Nelson et al., 2002; and Paradis et al., in press).

Sulphur Isotopes

Sulphur isotope analyses were performed on clean sulphide powders of pyrite, galena, and sphalerite at the G.G. Hatch Isotope Laboratories of the University of Ottawa. Samples are weighed into tin capsules with tungstic oxide (or vanadium pentoxide) and then loaded into a VarioEL III elemental analyzer to be flash combusted at 1800°C. Released gases are carried by helium through the Vario to be cleaned and separated. SO2 gas is carried into the DeltaPlus isotope ratio mass spectrometer (Thermo Finnigan, Germany) for analysis. The analytical precision of $\delta^{34}S_{CDT}$ values is 0.2‰ (2σ).

Results

The sulphur isotope results are listed in Table 5 and illustrated in Figure 15. Sulphur isotope analyses from Fraser (1996) are also included in Table 5 for comparison.

The $\delta^{34}S$ values of all sulphides within the different mineral deposit types at Prairie Creek are positive. Values of $\delta^{34}S$ in stratabound sulphides are isotopically heavy, ranging between 12.6 and 24.3‰ (average 20.1‰). They range from 12.6 to 24.3‰ (average 19.9‰) in pyrite, 17.3 to 21.2‰ (average 19.7‰) in galena, and 19.3 to 23.8‰ (average 21.2‰) in sphalerite (Fig. 15A). No isotopic trend is observed within

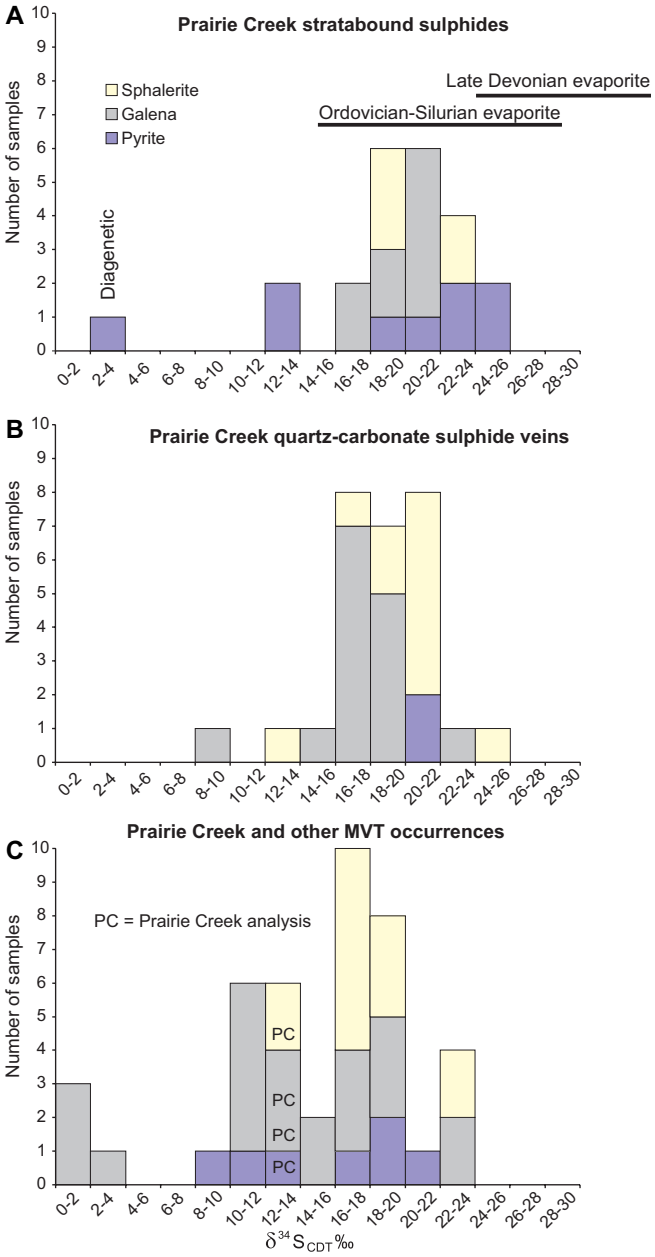


Figure 15. Histograms of sulphur isotope values of sphalerite, galena, and pyrite from the **A)** stratabound sulphides, **B)** quartz-carbonate sulphide veins, and **C)** Mississippi Valley-type (MVT) sulphides from the Prairie Creek deposit. Sulphur isotopes for other MVT deposits in the Canadian Cordillera and WCSB are plotted in **(C)** for comparison purposes. The range of values for Ordovician-Silurian and Late Devonian evaporite in the Western Canada Sedimentary Basin (Claypool et al., 1980) are plotted for reference.

the stratabound zones and no correlation can be made between $\delta^{34}S$ values and mineral textures and paragenetic position. This may be an artifact of the small amount of data analyzed in this study. Additional analyses using in situ laser technique in polished blocks (planned study) may give more information on the sulphur zonation and trend.

The sulphides from the stratabound zones at Prairie Creek are not in isotopic equilibrium; therefore, geothermometers cannot be used to calculate temperature

of sulphide precipitation. If isotopic equilibrium is attained in coprecipitating sulphur-bearing minerals, the difference in $\delta^{34}S$ values between mineral pairs is primarily a function of temperature, and pyrite always has the highest $\delta^{34}S$ values, with sphalerite next highest, and galena the lowest (Ohmoto and Goldhaber, 1997). Reversals in this sequence are used as evidence for a lack of isotopic equilibrium between coexisting mineral pairs.

The $\delta^{34}S$ values for the vein sulphides range from 9.8 to 24.1‰ (average 18.6‰). They range from 21.0 to 21.8‰ (average 21.4‰) in pyrite, 9.8 to 22.9‰ (average 17.5‰) in galena, and 13.1 to 24.1‰ (average 19.6‰) in sphalerite (Fig. 15B). No isotopic trend is observed along the north-south corridor. Some of the sulphide minerals from the same vein samples are in isotopic equilibrium, therefore calculated fractionation temperatures using sphalerite-galena pairs and the geothermometer of Ohmoto and Rye (1979) give temperatures between 250 and 350°C.

The $\delta^{34}S$ values for the MVT sulphides range from 13.1 to 13.8‰ (average 13.4‰; Fig. 15C). A single pyrite sample giving a value of 13.8‰ was analysed. Galena and sphalerite in the MVT showings have values of 13.1‰ and 13.6‰, respectively. They are different than those of the stratabound and vein sulphides, but they fall in the range of values for other MVT deposits in the Cordillera and the WCSB, such as Robb Lake, Pine Point, and mineralized carbonates of the Manetoe Facies and the WCSB (Fig. 15C).

The ranges of sulphur isotope data from the vein and stratabound galena and sphalerite are overall similar. Sphalerite and galena have a slightly broader range of values in the vein system than in the stratabound sulphides, whereas pyrite in the stratabound zones has a broader isotopic signature than the vein sulphides. For comparison, the range of $\delta^{34}S$ values of SEDEX deposits of the Kechika Trough of northeastern British Columbia, the Howards Pass XY deposit and MacMillan Pass Jason deposit of the Selwyn Basin in Yukon are illustrated in Figure 16. The $\delta^{34}S$ values for the Prairie Creek sulphides fall in the lower range of those of the Kechika Trough but they are quite similar to those of the Selwyn Basin. It is interesting to note that the negative $\delta^{34}S$ values, which are present in some deposits of the Selwyn Basin and the Irish-type deposits of Ireland (-44 to +14; Anderson, 1990; Hitzman and Beaty, 1997), have not been obtained at Prairie Creek. Another interesting fact is the occurrence of barite associated with the sulphides of the Selwyn Basin and the Irish-type deposits, and its absence at Prairie Creek.

The source of reduced sulphur in the Prairie Creek quartz-carbonate-sulphide veins and stratabound sulphides is most likely bacterial-reduced seawater sulphate, as it is for SEDEX deposits of the adjacent Selwyn Basin (Goodfellow, 2004). However, without knowing the age of the sulphide mineralization at Prairie Creek, the author can only speculate that the source of reduced sulphur could have been Ordovician-Silurian or Devonian SO_4. Also the fairly heavy $\delta^{34}S$ values of sulphides in the stratabound zones (ranging from 12.6 to 24.3‰) suggest a small to complete bacteriogenic reduction of marine sulphate in the sediments or water column. The fluid inclusion homogenization temperatures of sphalerite and dolomite from the stratabound zones range from 112 to 225°C (average 130°C) and 165 to 221°C (average 188°C), respectively (Fraser, 1996). This is evidence that the sulphur was produced by bacteriogenic means. Further work is required to improve the interpretation of the sulphur isotope data.

DISCUSSION AND SYNTHESIS

Coarse-grained sparry dolomite and saddle dolomite cements are often associated with sulphide mineralization in the northern Rocky Mountains and the Mackenzie Mountains (Morrow et al., 1986; Morrow, 1998; Nelson et al., 2002; Paradis et al., in press). These dolomites have often been called "hydrothermal" (e.g. Davies, 1997; Berger and Davies, 1999; Reimer et al., 2001). They form regionally extensive bodies of hydrothermal dolomite in the southern part of the Mackenzie Mountains, the northern Rocky Mountains, and the northern part of the WCSB, especially north of the Peace River Arch. An example is the Manetoe saddle dolomite Facies, which is interpreted as "hydrothermal-type white dolomite that formed in the subsurface at shallow depths in Late Devonian to Carboniferous time" and is the product of regional hydrothermal fluid flow (Morrow and Aulstead, 1995; p. 279). Elsewhere in the Cordillera, hydrothermal dolomites are not always as widespread, and they are restricted to small zones where fluids appear to have ascended via faults and fractures.

In this study, the term "hydrothermal dolomites" applies to the sparry and saddle dolomites that are closely associated with sulphide mineralization of the stratabound zones, quartz-carbonate-sulphide veins, and MVT bodies. These dolomites are assumed to be the products of interaction of relatively high-temperature hydrothermal fluids with surrounding carbonate rocks. It follows the definition and criteria of Machel and Lonnee (2002).

Therefore, assuming that sulphide mineralization and hydrothermal dolomites are coeval and syngenetic in each deposit types, we discuss their isotopic signature, linkages and trends, and then discuss the results in terms of mineralizing systems.

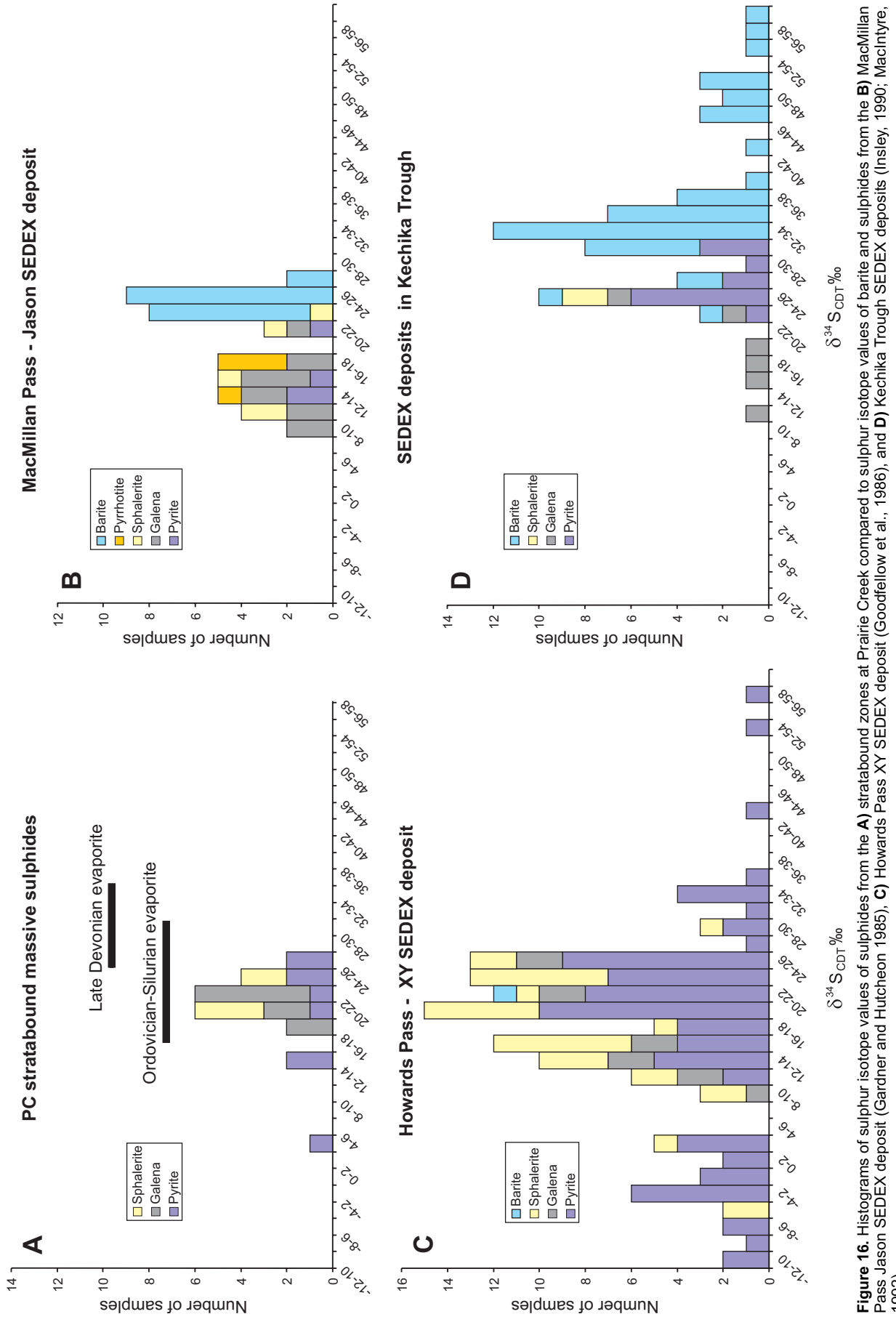


Figure 16. Histograms of sulphur isotope values of sulphides from the **A)** stratabound zones at Prairie Creek compared to sulphur isotope values of barite and sulphides from the **B)** MacMillan Pass Jason SEDEX deposit (Gardner and Hutcheon 1985), **C)** Howards Pass XY SEDEX deposit (Goodfellow et al., 1986), and **D)** Kechika Trough SEDEX deposits (Insley, 1990; MacIntyre, 1992).

Oxygen, Carbon, and Strontium Isotopes

Mineralized dolomite associated with the stratabound sulphides and the non-mineralized dolostone of the Upper Whittaker Formation have similar O and Sr isotopic values but the $\delta^{13}C_{PDB}$ values of the stratabound sulphides are lower than the host dolostone (Fig. 13), which can be attributed to oxidation of hydrocarbons. The $\delta^{18}O_{PDB}$ and $\delta^{13}C_{PDB}$ values of the hydrothermal dolomites associated with the vein sulphides and the MVT sulphides are lower than their host dolostones and the Ordovician and Silurian marine carbonates (Fig. 13). This relationship expressed as broad linear trends is also observed elsewhere in the Cordillera and WCSB, such as Robb Lake, Manetoe Facies, and Presqu'ile barrier (Nelson et al., 2002; Paradis et al., in press). It is generally attributed to increase in temperature. Fraser (1996) obtained homogenization fluid inclusion temperatures of 112 to 225°C (average 130°C) for the stratabound sulphides, 110 to 240ºC (average 163°C) for the vein sulphides, and 155 to 220°C (average 199°C) for the MVT sulphides at Prairie Creek.

$^{87}Sr/^{86}Sr$ values of mineralized dolomite from the stratabound sulphides and quartz-carbonate-sulphide veins are similar to values from non-mineralized dolostone of the Upper Whittaker Formation. These values are some of the most radiogenic values recorded in the northern Canadian Cordillera. They suggest that deep-circulating hydrothermal fluids were interacting with continental crust or derived siliciclastic rocks. $^{87}Sr/^{86}Sr$ values of mineralized dolomite from the Mississippi Valley-type showings are similar to the Manetoe Facies, overlap the lighter values of the Robb Lake deposit, and are slightly higher than Ordovician or Silurian marine carbonates.

In summary, the $\delta^{18}O_{PDB}$ and $\delta^{13}C_{PDB}$ values from hydrothermal dolomites of the stratabound, vein and MVT sulphides resemble those for late-stage hydrothermal dolomites of the Manetoe Facies, and the Presqu'ile barrier, particularly the western part of the barrier. Strontium isotopes are more radiogenic compared to Robb Lake, the Manetoe Facies, and the western Presqu'ile barrier. They compare to some of the highest values of hydrothermal carbonates associated with SEDEX mineralization from the Selwyn Basin (Goodfellow et al., 1986; Goodfellow and Rhodes, 1991; Turner, 1991). This characteristic is consistent with the geological setting of the stratabound and vein sulphides of the Prairie Creek deposit within the Prairie Creek Embayment; the Embayment being a half-graben type structure where thick accumulations of basinal sediments and platformal carbonates were deposited during lower Paleozoic time. It was located at the western carbonate edge, a location where deeply circulating high temperature fluids would have encountered mainly siliciclastic rocks.

Lead Isotopes

Most of the lead isotope values for the Prairie Creek stratabound sulphides plot in a tight cluster below the "shale curve" and two samples plot on or slightly above the "shale curve" of Godwin and Sinclair (1982), forming a trend crosscutting the curve at 420 Ma (i.e. Early Devonian; Fig. 14). The quartz-carbonate-sulphide veins plot in a separate cluster to the stratabound sulphides and form a linear trend that intersects the shale curve in the Triassic age range (about 250 Ma; Fig. 14). The MVT sulphides plot below the shale curve, and they overlap in isotopic composition with the stratabound sulphides. From these data, the following observations can be made:

The stratabound sulphides and the quartz-carbonate-sulphides veins formed at different time in the geological history. They are not genetically related and the vein sulphides cannot come from remobilized lead (and zinc) from the stratabound sulphides.

The Prairie Creek stratabound sulphide values overlap with values of the Ordovician-Silurian SEDEX deposits and the Devonian SEDEX deposits of the Selwyn Basin. The stratabound sulphides form a broad linear trend that intersects the shale curve in the Devonian age range, suggesting that the sulphide mineralization formed at around that time. The Devonian was an important period for the formation of SEDEX deposits in the western margin of North America (Goodfellow et al., 1993). We suggest that the stratabound sulphides at Prairie Creek formed during the Devonian time and that their formation was contemporaneous to the formation of SEDEX deposits of Selwyn Basin and Kechika Trough.

The stratabound sulphides form a cluster on or close to the shale curve. The shale curve, a growth curve unique to the ancient western margin of North America, indicates the Pb isotopic evolution of sediments deposited on the western margin of North America that were derived primarily from upper crustal rocks of the western Canadian Shield (Godwin and Sinclair, 1982). Therefore, the stratabound sulphide values indicate source(s) of lead are primarily derived from upper crustal rocks of the western Canadian Shield or Proterozoic sedimentary rocks.

The lead composition overlap between the stratabound sulphides and the MVT sulphides suggests that both may have a common lead source. The lead isotope values of the Prairie Creek MVT sulphides are some of the least radiogenic lead of the Cordilleran carbonate-hosted Zn-Pb occurrences. They have a similar signature to the Ordovician-Silurian MVT deposits of

the Mackenzie Mountains and the northern Rocky Mountains, but differ fundamentally from the Devonian "Cordilleran carbonate lead" trend (see Nelson et al., 2002; Paradis et al., in press).

Prairie Creek Mineralized System

The geological setting of the Prairie Creek deposit and preliminary results from its isotopic data suggest that the stratabound sulphides share many geological and geochemical characteristics with the SEDEX deposits of the Selwyn Basin. Some of these characteristics are 1) simple mineralogy (i.e. sphalerite, galena, and iron oxides), 2) occurrence along or immediately adjacent to faults that may have formed conduits for upward-migrating hydrothermal fluids, 3) similar Sr and Pb isotope values with deposits of the Selwyn Basin, and 4) ore fluid temperatures and salinities in the range of 110 to 240°C and 10 to 23 wt.% NaCl equivalent. Differences include the ubiquitous presence of barite in the SEDEX deposits and its absence at Prairie Creek, and $\delta^{34}S$ values, which range between -11.8 and +57‰ in the Selwyn deposits (Goodfellow et al., 1986), and between +16 and +24‰ at Prairie Creek.

Therefore, the genetic model we propose for stratabound sulphide mineralization at Prairie Creek resembles the SEDEX deposits of the Selwyn Basin. Mineralization at Prairie Creek formed in a secondary rift-controlled sedimentary basin along the margin of the carbonate platform, which is adjacent to the Selwyn Basin. The stratabound sulphides at Prairie Creek preferentially replaced the stratigraphically lowest carbonate unit during Early Paleozoic time.

The author does not have an absolute age constraint on the formation of sulphide mineralization at Prairie Creek. However, the similarity in Pb isotope values between Devonian SEDEX deposits of the Selwyn Basin and the stratabound sulphides at Prairie Creek imply a roughly contemporaneous age of mineralization. Similar hydrothermal fluids rising along basement structures to the site of ore deposition would have independently mineralized the anoxic shale basin of the Selwyn Basin and the adjacent shale-carbonates subbasin of the Prairie Creek Embayment.

Goodfellow et al. (1993) have also argued for a connection between the northern Cordilleran SEDEX deposits and the Zn-Pb carbonate-hosted deposits, based on the spatial association of the platform margin carbonate-hosted Zn-Pb deposits with the rifted margins of the anoxic basin, the similarity of metal ratios, and the similar heavy and variable sulphur isotope values. They envisaged a mixing model, in which reduced and sulphur-bearing fluids circulating in porous and permeable carbonates encountered metal-bearing fluids that rose along basement structures to the site of ore deposition. The Prairie Creek Fault and other unnamed northeast-trending faults are likely candidates for this role.

ACKNOWLEDGEMENTS

Field and analytical work on the Prairie Creek deposit were conducted as part of a Mineral and Energy Resource Assessment (MERA) in the Nahanni watershed and a small portion of the Nahanni Karst, an area of nearly 40,000 km^2 in the Mackenzie Mountains. The Mineral and Energy Resource Assessment (MERA) process was established in 1980 to ensure an inventory of non-renewable resource potential before creation of new national parks north of 60˚. These assessments are conducted for areas where the Federal Government administers the resources and they follow the published MERA Terms of Reference viewable at http://nrcan.gc.ca/mms/poli/mera_e.htm. Support from Hendrik Falck and Danny Wright of the Geological Survey of Canada during the course of this study was appreciated.

We are extremely grateful to all the personnel of Canadian Zinc Corporation and more specifically to Alan Taylor, who provided invaluable geological information on the Prairie Creek deposit and its district. Canadian Zinc Corporation is also thanked for giving us access to the property, allowing us to sample the drill core and providing pertinent geological information on the deposit.

G.G. Hatch Isotope Laboratories of the University of Ottawa performed the sulphur isotope analyses. Bill Davis of the geochronology laboratories of the GSC did most of the Sr isotope analyses on the carbonates. Brian L. Cousens of the Herzberg Laboratories of Carleton University performed the Pb analyses on sulphides and some Sr isotope analyses on carbonates. O and C isotope analyses on carbonates were done at the Delta Lab of the Geological Survey of Canada in Québec City. We are grateful to Peter Hannigan of the Geological Survey of Canada who reviewed the preliminary version of the manuscript; its suggestions greatly improved the manuscript.

REFERENCES

Amthor, J.E., Mountjoy, E.W., and Machel, H.G.
1993: Subsurface dolomites in Upper Devonian Leduc Formation buildups, central part of Rimbey-Meadowbrook reef trend, Alberta, Canada; Bulletin of Canadian Petroleum Geology, v. 41, p. 164-185.

Anderson, I.K.
1990: Ore Depositional Processes in the formation of the Navan Zn-Pb deposit, Co. Meath, Ireland; Ph.D thesis, University of Strathclide, Glasgow, Scotland, 290 p.

Berger, Z. and Davies, G.
1999: The development of linear hydrothermal dolomite (HTD) reservoir facies along wrench or strike slip fault systems in the Western Canada Sedimentary Basin; Canadian Society of Petroleum Geologists, Reservoir, v. 26, p. 34-38.

Brophy, J.A. (ed.)
1984: Contributions to the geology of the Northwest Territories, Volume 1; Department of Indian Affairs and Northern Development, Northwest Territories, EGS Open File 1984-06.

Canadian Zinc Corporation
2001: Prairie Creek mine, Northwest Territories, Scoping Study; Internal report, Canadian Zinc Corporation, January 29, 2001, 185 p.
2004: Annual information form. Internal report, Canadian Zinc Corporation. 41 p.
2006: http://www.canadianzinc.com/prairie/history.shtml

Claypool, C.E., Hosler, W.T., Saki, I.R. and Zak, I.
1980: The age curves for sulphur and oxygen isotopes in marine sulphates and their mutual interpretation; Chemical Geology, v. 28, p. 199-260.

Coniglio, M., Morrow, D.W. and Wilson, N.
in press: Reassessment of Middle Devonian dolomites, Presqu'ile barrier, Northwest Territories; *in* Potential for Carbonate-Hosted Lead-Zinc Mississippi Valley-Type Mineralization in Northern Alberta and Southern Northwest Territories, (ed.) P.K. Hannigan; Geoscience Contributions, Targeted Geoscience Initiative, Geological Survey of Canada, Bulletin 591.

Connolly, C.A., Walter, L.M., Baadsgaard, H., and Longstaffe, F.J.
1990: Origin and evolution of formation waters, Alberta Basin, Western Canada Sedimentary Basin. I. Chemistry. Applied Geochemistry, v. 5, p. 375-395.

Cook, D.G.
1977: Two stages of faulting, Virginia Falls map-area, District of Mackenzie; Report of Activities, Part A, Geological Survey of Canada, Paper 77-1A, p. 113-115.

Cousens, B.L.
1996: Magmatic evolution of Quaternary mafic magmas at Long Valley Caldera and the Devils Postpile, California: Effects of crustal contamination on lithospheric mantle-derived magmas; Journal of Geophysical Research. B, Solid Earth and Planets, v. 101, p. 27,673-27,689.
2007: Radiogenic isotope studies of Pb-Zn mineralization in the Howards Pass area, Selwyn Basin, *in* Mineral and Energy Resource Assessment of the Greater Nahanni Ecosystem Under Consideration for the Expansion of the Nahanni National Park Reserve, Northwest Territories, (eds.) D.F. Wright, D. Lemkow, and J.R. Harris; Geological Survey of Canada, Open File 5344, p. 279-292.

Craig, H.
1957: Isotopic standards for carbon and oxygen and correction factors for mass spectrometric analysis of carbon dioxide; Geochimica et Cosmochimica Acta, v. 12, p. 133-149.

Davies, G.R.
1997: Hydrothermal Dolomite (HTD) Reservoir Facies: Global Perspectives on Tectonic-Structural and Temporal Linkage between MVT and SEDEX Pb-Zn Ore Bodies, and Subsurface HTD Reservoir Facies; Short Course Notes, Canadian Society of Petroleum Geologists, Graham Davies Geological Consultants, 167 p.

de Wit, R., Gronberg, E.C., Richards, W.B., and Richmond, W.O.
1973: Tathlina area, District of MacKenzie; *in* The Future Petroleum Provinces of Canada – Their Geology and Potential, (ed.) R.G. McCrossan; Canadian Society of Petroleum Geologists, Memoir 1, p. 187-212.

Dewing, K., Sharp, R.J., Ootes, L., Turner, E.C., and Gleeson, S.
2006: Geological Assessment of Known Zn-Pb Showings, Mackenzie Mountains, Northwest Territories; Geological Survey of Canada, Current Research 2006-A4, 12 p.

Duggan, J.P., Mountjoy, E.W., and Stasiuk, L.D.
2001: Fault-controlled dolomization at Swan Hills Simonette oil field (Devonian), deep basin west-central Alberta, Canada; Sedimentology, v. 48, p. 301-323.

Earls, G.
1995: A Review of the Prairie Creek Deposit, NWT, Canada; Internal Report, San Andreas Resources Corporation, 36 p.

Findlay, A.
2000: Geology and Exploration Potential of the Stratabound Massive Sulphides, Prairie Creek Mine, NWT;. Internal Report, Canadian Zinc Corporation, 17 p.

Fraser, S.C.
1996: Geology and Geochemistry of the Prairie Creek Zn, Pb, Ag Deposits, Southern Mackenzie Mountains, NWT; M.Sc. thesis, University of Alberta, Edmonton, Alberta, 146 p.

Friedman, I. and O'Neil, J.R.
1977: Compilation of stable isotope fractionation factors of geochemical interest; *in* Data of Geochemistry, Chapter KK, (ed.) M. Fleischer; United States Geological Survey, Professional Paper 440-KK, 12 p.

Gabrielse, H., Monger, J.W.H., Wheeler, J.O., and Yorath, C.J.
1991: Part A. Morphogeological belts, tectonic assemblages, and terranes; *in* Geology of the Cordilleran Orogen in Canada, (ed.) H. Gabrielse and C.J. Yorath; Geological Survey of Canada, No. 4, p. 15-28.

Gardner, H.D. and Hutcheon, I.
1985: Geochemistry, mineralogy and geology of the Jason Pb-Zn deposits, Macmillan Pass, Yukon, Canada; Economic Geology, v. 80, p. 1257-1276.

Godwin, C.I. and Sinclair, A.J.
1982: Average lead isotope growth curves for shale-hosted zinc-lead deposits, Canadian Cordillera; Economic Geology, v. 77, p. 675-690.

Godwin, C.I., Gabites, J.E., and Andrew, A.
1988: Lead table: A galena lead isotope data base for the Canadian Cordillera, with a guide to its use by explorationists; A contribution to the Canada/British Columbia Mineral Development Agreement, 1985-1990, British Columbia Ministry of Energy, Mines, and Petroleum Resources, Paper 1988-4, 188 p.

Goodfellow, W.D.
2004: Geology, genesis, and exploration of SEDEX deposits, with emphasis on the Selwyn Basin, Canada; *in* Sediment-Hosted Lead-Zinc Sulphide Deposits: Attributes and Models of some Major Deposits in India, Australia and Canada, (ed.) M. Deb and W.D. Goodfellow; Narosa Publishing House, New Delhi, India, p.24-99.

Goodfellow, W.D., and Rhodes, D.
1991: Geological setting, geochemistry and origin of the Tom stratiform Zn-Pb-Ag-barite deposits; *in* Mineral Deposits of the Northern Canadian Cordillera, Yukon-Northeastern British Columbia (Field Trip 14), Guidebook: International Association on the Genesis of Ore Deposits, Eighth Symposium, (ed.) J.G. Abbott and R.J.W. Turner; Geological Survey of Canada, Open File 2169, p. 177-241.

Goodfellow, W.D., Jonasson, I.R., and Morin, J.A.
1986: Environment of formation of the Howards Pass (XY) Zn-Pb deposit, Selwyn Basin, Yukon; *in* Mineral Deposits of Northern Cordillera, (ed.) J.A. Morin; Canadian Institute of Mining and Metallurgy, Special Volume 37, p. 19-50.

Goodfellow, W.D., Lydon, J.W., and Turner, R.J.W.
1993: Geology and genesis of stratiform sediment-hosted (SEDEX) Zn-Pb-Ag sulphide deposits; *in* Mineral Deposit Modeling, (ed.) R.V. Kirkham, W.D. Sinclair, R.I. Thorpe, and J.M. Duke; Geological Association of Canada, Special Paper 40, p. 201-251.

Hitzman, M.W. and Beaty, D.W.
1997: The Irish Zn-Pb-(Ba-Ag) orefield; *in* Carbonate-Hosted Lead-Zinc Deposits, (ed.) D.F. Sangster; Society of Economic Geologists, Special Publication No. 4, p. 112-143.

Insley, M.W.
1990: Sedimentology and geochemistry of the Driftpile Ba-Fe-Zn-Pb Mineralization, Northeastern British Columbia; Ph.D. thesis, Royal Holloway and Bedford New College, University of London, England, 377 p.

Jenks, J.D.
1982: Report on the Cadillac Property including Regional Exploration Work – Summer 1981; Procan Exploration Company, 17 p.

Kaufman, J.
1989: Sedimentology and Diagenesis of the Swan Hills Formation (Middle-Upper Devonian), Rosevear Field, Alberta, Canada; Ph.D. thesis, State University of New York, Stony Brook, New York, 427 p.

Laflamme, A.K.
1990: Replacement Dolomitization in the Upper Devonian Leduc and Swan Hills Formations, Caroline Area, Alberta, Canada; M.Sc. thesis, McGill University, Montreal, Quebec, 138 p.

Lonnee, J. and Al-Aasm, I.S.
2000: Dolomitization and fluid evolution in the Middle Devonian Sulphur Point Formation, Rainbow South Field, Alberta: petrographic and geochemical evidence; Canadian Petroleum Geology, Bulletin 48, p. 262-283.

Machel, H.G. and Cavell, P.A.
1999: Low-flux, tectonically-induced squeegee fluid flow ("hot flash") into the Rocky Mountain foreland basin; Canadian Petroleum Geology, Bulletin 47, p. 510-533.

Machel, H.G., and Lonnee, J.
2002. Hydrothermal dolomite – A product of poor definition and imagination; Sedimentary Geology, v. 152, p. 163-171.

McCrea, J.M.
1950: On the isotopic chemistry of carbonates and a paleothermometer scale; Journal of Chemical Physics, v. 18, p. 849-857.

MacIntyre, D.G.
1992: Geological setting and genesis of sedimentary exhalative barite and barite-sulfide deposits, Gataga district, northeastern British Columbia; Exploration and Mining Geology, v. 1, p. 1-20.

Marquez, X.M.
1994: Reservoir Geology of Upper Devonian Leduc buildups, Deep Alberta Basin; Ph.D. thesis, McGill University, Montreal, Quebec, 312 p.

Morrow, D.W.
1984: Sedimentation in Root Basin and Prairie Creek Embayment; Siluro-Devonian, Northwest Territories; Bulletin of Canadian Petroleum Geology, v. 32, p.162-189.
1998: Regional subsurface dolomitization: Models and constraints; Geoscience Canada, v. 25, p. 57-70.

Morrow, D.W. and Aulstead, K.L.
1995: The Manetoe Dolomite – A Cretaceous-Tertiary or a Paleozoic event? Fluid inclusion and isotopic evidence; Bulletin of Canadian Petroleum Geology, v. 43, p. 267-280.

Morrow, D.W. and Cook, D.G.
1987: The Prairie Creek Embayment and Lower Paleozoic strata of the southern Mackenzie Mountains; Geological Survey of Canada, Memoir 412, 195 p.

Morrow, D.W. and Cumming, G.L.
1982: Interpretation of lead isotope data from zinc-lead mineralization in the northern part of the western Canadian Cordillera; Canadian Journal of Earth Sciences, v. 19, p. 1070-1078.

Morrow, D.W., Cumming, G.L., and Aulstead, K.L.
1990: The gas-bearing Devonian Manetoe Facies, Yukon and Northwest Territories; Geological Survey of Canada, Bulletin 400, 54 p.

Morrow, D.W., Cumming, G.L., and Koepnick, R.B.
1986: Manetoe Facies - a gas-bearing, megacrystalline, Devonian dolomite, Yukon and Northwest Territories, Canada; American Association of Petroleum Geologists, Bulletin 70, p. 702-720.

Mountjoy, E.W., Amthor, J.E., and Machel, H.G.
1991: Burial dolomitization of the Upper Devonian Rimbey-Meadowbrook reef trend, central Alberta, Canada; American Association of Petroleum Geologists, Bulletin 75, p. 641.

Mountjoy, E.W., Machel, H.G., Green, D., Duggan, J., and Williams-Jones, A.E.
1999: Devonian matrix dolomites and deep burial carbonate cements: a comparison between the Rimbey-Meadowbrook reef trend and the deep basin of west-central Alberta; Bulletin of Canadian Petroleum Geology, v. 47, p. 487-509.

Mountjoy, E.W., Qing, H., and MacNutt, R.H.
1992: Strontium isotopic composition of Devonian dolomites, Western Canada Sedimentary Basin: Significance of sources of dolomitizing fluids; Applied Geochemistry, v. 7, p. 59-75.

Mossop, G. and Shetsen, I. (comp.)
1994: Geological Atlas of the Western Canada Sedimentary Basin; Canadian Society of Petroleum Geologists and Alberta Research Council, 510 p.

Nelson, J., Paradis, S., Christensen, J., and Gabites, J.
2002: Canadian Cordilleran Mississippi Valley-type deposits: A case for Devonian-Mississippian back-arc hydrothermal origin; Economic Geology, v. 97, p. 1013-1036.

NORMIN.DB – http://www.nwtgeoscience.ca/normin/

Ohmoto, H. and Goldhaber, M.B.
1997: Sulfur and carbon isotopes; *in* Geochemistry of Hydrothermal Ore Deposits, 2nd Edition; (ed.) H.L. Barnes; New York, John Wiley and Sons, p. 517-612.

Ohmoto, H. and Rye, R.O.
1979: Isotopes of sulfur and carbon; *in* Geochemistry of Hydrothermal Ore Deposits, 2nd Edition; (ed.) H.L. Barnes; New York, John Wiley and Sons, p. 509-567.

Olson, R.A., Dufresne, M.B., Freeman, M.E., Eccles, D.R., and Richardson, R.J.H.
1994: Regional Metallogenic Evaluation of Alberta; Alberta Geological Survey Open File 1994-8, 50 p.

Paradis, S., Turner, W.A., Coniglio, M., Wilson, N., and Nelson, J.L.
in press: Stable and radiogenic isotopic signatures of mineralized Devonian carbonates of the Northern Rocky Mountains and the Western Canada Sedimentary Basin; *in* Potential for Carbonate-Hosted Lead-Zinc Mississippi Valley-Type Mineralization in Northern Alberta and Southern Northwest Territories: Geoscience Contributions, Targeted Geoscience Initiative, (ed.) P.K. Hannigan; Geological Survey of Canada, Bulletin 591.

Qing, H.
1986: Diagenesis and Sedimentology of Rainbow F and E Build-Ups (Middle Devonian), Northwestern Alberta; M.Sc. thesis, McGill University, Montreal, Quebec, 154 p.

1991: Diagenesis of Middle Devonian Presqu'ile Dolomite Pine Point, NWT and Adjacent Subsurface; Ph.D. thesis, McGill University, Montreal, Quebec, 292 p.

Reimer, J.D., Hudema, T., and Viau, C.
2001: TSR-HTD ten years later: an exploration update, with examples from western and eastern Canada; Canadian Society of Petroleum Geologists Annual Convention, p. 276-279.

Stacey, J.S. and Kramers, J.D.
1975: Approximation of terrestrial lead isotope evolution by a two-stage model; Earth and Planetary Science Letters, v. 26, p. 207-221.

Taylor, A.B.
1995: Geological Summary of the Northern Sector Pb-Zn Trend on the Prairie Creek Property, NWT; Internal Report, San Andreas Resources Corporation, 31 p.

Telser, H.
1999: Significance of Inclusion Fluid Chemistry for the Origin of the Pine Point Mineralization, NWT; M.Sc. thesis, University of Leoben, Leoben, Austria, 99 p.

Thorpe, R.I.
1972: Mineral Exploration and Mining Activities, Mainland Northwest Territories, 1966 to 1968; Geological Survey of Canada, Paper 70-70, 139 p.

Todt, W., Cliff, R.A., Hanser, A., and Hofmann A.W.
1984: ^{202}Pb-^{205}Pb spike for Pb isotopic analysis; Terra Cognita., v. 4, p. 209.

Todt, W., Cliff, R.A., Hanser, A., and Hofmann A.W.
1996: Evaluation of a 202Pb-205Pb double spike for high-precision lead isotope analysis; *in* Earth Processes: Reading the Isotopic Code, (ed.) A. Basu and S.R. Hart; Geophysical Monograph Series., v. 95, p. 429–437.

Turner, R.J.W.
1991: Jason stratiform Zn-Pb-barite deposit, Selwyn Basin, Canada (NTS 105-O-1): Geological setting, hydrothermal facies and genesis; *in* Mineral Deposits of the Northern Canadian Cordillera, Yukon-northeastern British Columbia (Field Trip 14), Guidebook: International Association on the Genesis of Ore Deposits, Eighth Symposium, (ed.) J.G. Abbott and R.J.W. Turner; Geological Survey of Canada, Open File 2169, p. 137-175.

Veizer, J., Ala, D., Azmy, K., Bruckschen, P., Buhl, D., Bruhn, F., Carden, G.A.F., Diener, A., Ebneth, S., Godderis, Y., Jasper, T., Korte, C., Pawellek, F., Podlaha, O.G., and Strauss, H.
1999: $^{87}Sr/^{86}Sr$, $\delta^{13}C$ and $\delta^{18}O$ evolution of Phanerozoic seawater; Chemical Geology, v. 161, p. 59-88.

Appendix 1. Geological characteristics of the representative samples within the Prairie Creek area, Northwest Territories.

Zone / showing	Datum	UTM Northing	UTM Easting	DDH or sample #	Sample depth (m)	Host formation	Unit	Type of sulphides	Lithology	Sample description and remarks
3 in SD1	Nad 27	6826316.0	404962.3	PC-92-15	-	Upper Whittaker	OSw3-4	Veins	Quartz-carbonate-sulphide vein in spar rich dolostone	
3 in SD1	Nad 27	6826316.0	404962.3	PC-92-15	298.4	Upper Whittaker	OSw3-3 and/or OSw3-2	Stratabound	Stratabound sulphides in lower chert nodule dolostone or mottled dolostone	Slab of massive py (30%), gn (20%), sph (10%), cherty dol (25%), cal (10%). Generally massive in first half, and after that it becomes cherty dol.
3 in SD1	Nad 27	6826316.0	404962.3	PC-92-15	332.5	Upper Whittaker	OSw3-2	Veins	Quartz-carbonate-sulphide vein in mottled dolostone	Chips of quartz vein and fg to mg pyrite with occ gn. Vein cuts OSw3-4 higher up in ddh, and below cuts OSw3-1.
3 in SD1	Nad 27	6826316.0	404962.3	PC-92-16	-	Upper Whittaker	OSw3-5	Veins	Quartz-carbonate-sulphide vein in upper chert nodule dolostone	
3 in SD1	Nad 27	6826316.0	404962.3	PC-92-16	310.2	Upper Whittaker	OSw3-3	Stratabound	Stratabound sulphides in lower chert nodule dolostone	Typical banded-style sulphides (banding ~45-60º CA) with black chert nodules present throughout. At around 310 m, the sulphides consist of mix of framboidal sph and mg gn. Some layers of sph with minor cal/qtz and layers of gn and some fg sph and py in groundmass. Overall sph (30%), gn (30%), py (30%), jasp (5%), cal/qtz (5%).
3 in SD1	Nad 27	6826316.0	404962.3	PC-92-16	310.6	Upper Whittaker	OSw3-3	Stratabound	Stratabound sulphides in lower chert nodule dolostone	Typical banded-style mx (banding ~45-60º CA) with black chert nodules present throughout. Around 310 m, the sulphides consist of mix of framboidal sph and mg gn. Some framboidal sph in bands with minor cal/qtz and bands of gn and some fine-grained sph and py in groundmass. Overall sph (30%), gn (30%), py (30%), qtz (5%), cal/qtz (5%).
3 in SD1	Nad 27	6826316.0	404962.3	PC-92-16	310.9	Upper Whittaker	OSw3-3	Stratabound	Stratabound sulphides in lower chert nodule dolostone	Contact between recrystallized dolostone and sulphides. Piece of core 5 cm in length.
3 in SD1	Nad 27	6826316.9	404956.4	PC-92-17B	-	Upper Whittaker	OSw3-3	Stratabound	Stratabound sulphides in lower chert nodule dolostone	Overall mas to weakly banded fg py, fine to mg sph, gn along with intevals (bands) and zones (infilled solution cavities) of sparry white cal, dol, and black chert.
3 in SD1	Nad 27	6826316.9	404956.4	PC-92-17B	313.4	Upper Whittaker	OSw3-3	Stratabound	Stratabound sulphides in lower chert nodule dolostone	Pyritic mas sulphides enclosing black cherty (or silicified nodules of host dolostone); the interval (313.1-313.9) is sph-rich; sph is brick red to tan reddish. Sph bands are fg to framboidal textured. Py is fg. Chert is partially replaced by fg grey tan sph. Fg pyrite occurs as mg diss blebs to fine bands.
3 in SD1	Nad 27	6826398.8	405008.6	PC-92-19	237.9	Upper Whittaker	OSw3-5	Veins	Quartz-carbonate-sulphide vein in upper chert nodule dolostone	2 samples: Chips and slab of sulphides within the vein; chips = sph and gn; slab = massive yellow tan sph (68%) with gn as bands (20%) + td (5%), and py (2%).
3 in SD1	Nad 27	6826398.8	405008.6	PC-92-19	250.5	Upper Whittaker	OSw3-5	Veins	Quartz-carbonate-sulphide stringers in upper chert nodule dolostone	Rep sample of OSw3-5 fractured by quartz-dol stringers and small veins.
3 in SD1	Nad 27	6826398.8	405008.6	PC-92-19	274.7	Upper Whittaker	OSw3-4		Lower spar dolostone unit	Rep sample of OSw3-4 fractured by qtz-dol vugs and stringers. Large sph crystal in the middle of a vug; sph and gn surrounded by cg clear dol (dol #2) and this is surrounded by yellowish dol (dol#1).
3 in SD1	Nad 27	6826398.8	405008.6	PC-92-19	289.5-289.8	Upper Whittaker	OSw3-3 or OSw3-2	Stratabound	Stratabound sulphides in lower chert nodule dolostone or mottled dolostone	Lower contact - sulphides and chert nodular dolostone; the lower contact is irregular at 60º CA and defined by red sph/dol. Sph replaces host dolostone, and sparry dol is often at the interface between dolostone and sph.
3 in SD1	Nad 27	6826398.8	405008.6	PC-92-19	313.85	Upper Whittaker	OSw3-2?		Lower chert nodule dolostone or mottled dolostone	Dark grey massive fg to mg dol cut by qtz-dol stringers.
3 in SD1	Nad 27	6826398.8	405008.6	PC-92-19	314	Upper Whittaker	OSw3-3 or OSw3-2	Stratabound	Stratabound sulphides in lower chert nodule dolostone or mottled dolostone	Several intersection of stratabound sul. The upper ones are in OSw3-3 and the lower ones may be in OSw3-2. The sul section is cutting "strata" at angle. Ends at sharp contact with 3 cm mg cx dol band which grades into py and sph.

Appendix 1 continued.

Zone / showing	Datum	UTM Northing	UTM Easting	DDH or sample #	Sample depth (m)	Host formation	Unit	Type of sulphides	Lithology	Sample description and remarks
3 in SD1	Nad 27	6826398.8	405008.6	PC-92-19	315.2	Upper Whittaker	OSw3-3 or OSw3-2	Stratabound	Stratabound sulphides in lower chert nodule dolostone or mottled dolostone	Pieces of core of fg pyrite adjacent to coarse cx dolomite and adjacent to cg gn.
3 in SD1	Nad 27	6826202.1	405004.5	PC-93-23	246.5	Upper Whittaker	OSw3-2	Stratabound	Stratabound sulphides in mottled dolostone	Pyritic sulphide section = Sph 10%, gn 2%, py 50%, white spar 10%, black chert 1%. The white spars form elongated stretched bands (or lenses) giving a zebra texture.
3 in SD1	Nad 27	6826202.1	405004.5	PC-93-23	249.7	Upper Whittaker	OSw3-2	Stratabound	Stratabound sulphides in mottled dolostone	Sph and gn rich towards end of interval. Sph 20%, gn 5%, py 50%, white spar 1% approx 3% chert; bands are ~70°CA.
3 in SD1	Nad 27	6826202.1	405004.5	PC-93-23	252.3	Upper Whittaker	OSw3-2	Stratabound	Stratabound sulphides in mottled dolostone	Pyritic with reddish sph and gn bands: 5% sph, 2% gn, 70% py, 7% chert; discontinuous bands, 65°CA.
3 in SD1	Nad 27	6826202.1	405004.5	PC-93-24	257.1	Upper Whittaker	OSw3-2	Stratabound	Stratabound sulphides in mottled dolostone	Sulphide section = 70% massive sul and 30% dark grey dol. Sul = py (40%), sph (10%), gn (3%); lower contact of sulphides at 50°CA but irregular with fg diss py in a chert band and is discontinuous mas sph rimmed by py band. Sample = fg py and mg sph (red and yellow) in siliceous dolostone (looks like stringers).
3 in SD1	Nad 27	6826203.1	405005.8	PC-93-25	251.4-251.85	Upper Whittaker	OSw3-2	Stratabound	Stratabound sulphides in mottled dolostone	Sulphides with bands of coarse crystalline dolostone at upper contact.
3 in SD1	Nad 27	6826203.1	405005.8	PC-93-25	251.9	Upper Whittaker	OSw3-2	Stratabound	Stratabound sulphides in mottled dolostone	Continuous sample with above. Overall a well mineralized interval with 25% sph, 15% gn, 15% chert, 2% calcite, 2% quartz, and 2% white/grey dol. Coarse sparry calcite (fragments?) is completely surrounded by gn, and gn seems to cut the cal.
3 in SD1	Nad 27	6826203.1	405005.8	PC-93-25	254.5-254.7	Upper Whittaker	OSw3-2	Stratabound	Stratabound sulphides in mottled dolostone	Well mineralized interval with high conc of sph (both reddish-tan and grey sph). Lower contact is very sharp with white dol at 55° CA, which grades into pyritic zone. Interval (254-255.5 m) is chert rich. Overall 20% sph, 3-5% gn, 20% chert, 5% cal and bands of black chert towards the bottom.
3 in SD1	Nad 27	6825981.0	404343.0	PC-93-26	-	Upper Whittaker	Contact of OSw3-3 and OSw3-2	Stratabound	Stratabound sulphides at contact between lower chert nodule dolostone and mottled dolostone	High-grade sph interval. Numerous vuggy qtz-cal-dol bands at approx. 60° CA. Overall approx 35% sph, 15% gn, 5% chert, 5% qtz-cal, well banded.
3 in SD1	Nad 27	6825981.0	404343.0	PC-93-26	-	Upper Whittaker	Contact of OSw3-3 and OSw3-2	Stratabound	Stratabound sulphides at contact between lower chert nodule dolostone and mottled dolostone	Same as above.
3 in SD1	Nad 27	6825981.0	404343	PC-93-26	-	Upper Whittaker	Contact of OSw3-3 and OSw3-2	Stratabound	Stratabound sulphides at contact between lower chert nodule dolostone and mottled dolostone	High-grade gn and sph similar as above. Better defined compositional banding. Banding 60-70°CA = 1-3 cm gn bands.
3 in SD1	Nad 27	6825981.0	404343	PC-93-26	-	Upper Whittaker	OSw3-2	Stratabound	Stratabound sulphides in mottled dolostone	Mottled texture (15% of core is banded); occ spar-infilled vugs with 2-3% gn and sph. Numerous stringers at 45 to 70° CA. Diss py for first 15 cm of interval in dolostone (290.5 to 292.5).
3 in SD1	Nad 27	6826126.4	405092.0	PC-93-27	220.7	Upper Whittaker	OSw3-2		Mottled dolostone	Rep sample of siliceous dolostone with numerous qtz (±dol) stringers, fractures, and some qtz-cemented breccia zones. Mottled texture occurs in lighter grey siliceous zones.
3 in SD1	Nad 27	6826126.4	405092.0	PC-93-27	231.6-231.7	Upper Whittaker	OSw3-2		Mottled dolostone	Weak mottled texture of darker grey spots with diffuse selvage within lighter grey siliceous bands. Numerous white dol-qtz stringers. Diss py, sph in both dol and chert. Sph concentrated on fine fractures (<1%).
3 in SD1	Nad 27	6826126.4	405092.0	PC-93-27	240.6-240.7	Upper Whittaker	OSw3-2	Stratabound	Stratabound sulphides in mottled dolostone	Massive fg py grades into massive fg grey sph bands; colloform red sph with grey rims; last 20 cm of interval has dol fragments in a qtz-rich groundmass + chert + disseminated sph. Overall 15% sph, 1% gn, 60% py, and 20% chert.

Appendix 1 continued.

Zone / showing	Datum	UTM Northing	UTM Easting	DDH or sample #	Sample depth (m)	Host formation	Unit	Type of sulphides	Lithology	Sample description and remarks
3 in SD1	Nad 27	6826126.4	405092.0	PC-93-27	241	Upper Whittaker	OSw3-1		Massive dolostone	Rep sample of dark grey siliceous dolostone with light grey siliceous bands, zones of diss py and numerous fine stringers. Minor black chert nodules and bands.
3 in SD1	Nad 27	6826084.0	405065.5	PC-93-35	223	Upper Whittaker	OSw3-2		Mottled dolostone	Rep sample of OSw3-2. Piece of core ~6 cm in length
3 in SD1	Nad 27	6826084.0	405065.5	PC-93-35	224.8-225.05	Upper Whittaker	OSw3-2	Stratabound	Stratabound sulphides in mottled dolostone	Section of fg mas py and pinkish to yellowish sph cutting cherty dolostone. Pink sph is mixed with py; yellowish sph cut the aggregate of py.
3 in SD1	Nad 27	6826084.0	405065.5	PC-93-35	227.7	Upper Whittaker	OSw3-2	Stratabound	Stratabound sulphides in mottled dolostone	Sample close to upper contact between the silicified dolostone and mas fg py-gn-sph. The contact is marked by a 0.5 cm wide cg white cal band at 75º CA. Sul intersection has a slightly banded whispy appearance, possibly deformed. Overall 40% py, 55% gn, 15% sph. Band generally subparallel at 45-60º CA.
3 in SD1	Nad 27	6826084.0	405065.5	PC-93-35	228.0-228.2	Upper Whittaker	OSw3-2	Stratabound	Stratabound sulphides in mottled dolostone	Bands and agg of fg pyrite and fg pale sph rimming the py; sul are replacing the cherty dolostone.
3 in SD1	Nad 27	6826084.0	405065.5	PC-93-35	-	Upper Whittaker	OSw3-2	Stratabound	Stratabound sulphides in mottled dolostone	
3 in SD1	Nad 27	6826084.0	405065.5	PC-93-35	-	Upper Whittaker	OSw3-2	Stratabound	Stratabound sulphides in mottled dolostone	
3 in SD1	Nad 27	6826084.0	405065.5	PC-93-35	-	Upper Whittaker	OSw3-2	Stratabound	Stratabound sulphides in mottled dolostone	
3 in SD1	Nad 27	6825981.0	404343	PC-93-40	-	Upper Whittaker	OSw3-2	Veins	Quartz-carbonate-sulphide veins in mottled dolostone	Py-sph-rich interval with 10% fg to mg black qtz crystal lath-needles occurring within the reddish sph.
6 in SD4	Nad 27	6823154.6	404363.3	PC-93-41	246.7	Upper Whittaker	OSw3-4	Stratabound	Stratabound sulphides in lower spar dolostone	Stringers present in the upper section of ms. Sample taken in semi-mas stratabound sul section. White qtz vugs at centre of mx. Sul zones connect by fine approx. 1 mm mineralized qtz-sph-py-gn stringers.
6 in SD4	Nad 27	6823154.6	404363.3	PC-93-41	247.75	Upper Whittaker	OSw3-4		Lower spar dolostone unit	Rep sample of mas light grey fossiliferous dolostone with rare sparry dol and qtz infilled-vugs (±fg red sph, gn). Occ chert nodules towards the bottom section.
3 North	Nad 27	6825981.0	404343	PC-93-50	176	Road River		Veins	Quartz-carbonate-sulphide veins in shaly dolostone and shale	Chips of gn from mineralized vein (sph-gn-qtz-cal)
3 North	Nad 27	6825981.0	404343	PC-93-50	176.4	Road River		Veins	Quartz-carbonate-sulphide veins in shaly dolostone and shale	Chips of sph from mineralized vein (sph-gn-qtz-cal); the sph is cg and greyish.
5	Nad 27	6825069.0	404794.8	PC-94-59	-	Upper Whittaker	OSw3-7	Veins	Quartz-carbonate-sulphide vein in banded chert dolostone	Mostly unmineralized vein.
6	Nad 27	6822986.0	404356.6	PC-94-62	300.1	Upper Whittaker	OSw3-2		Mottled dolostone	Fg py in the dolostone; the sample is a mix of very fg py and some dolostone.
6	Nad 27	6822986.0	404356.6	PC-94-62	-	Upper Whittaker				
6	Nad 27	6822986.0	404356.6	PC-94-62	-	Upper Whittaker				
6 in SD4	Nad 27	6823154.6	404363.3	PC-94-64	140.8	Road River			Shaley dolostone and shale	Rep sample of shale.

Appendix 1 continued.

Zone / showing	Datum	UTM Northing	UTM Easting	DDH or sample #	Sample depth (m)	Host formation	Unit	Type of sulphides	Lithology	Sample description and remarks
6 in SD4	Nad 27	6823154.6	404363.3	PC-94-64	145.4	Road River			Shaley dolostone and shale	Vein 1 cm with sparry dol.
6 in SD4	Nad 27	6823154.6	404363.3	PC-94-64	182	Upper Whittaker	OSw3-7		Banded chert dolostone	Rep spl of interbedded chert/dolostone unit.
6 in SD4	Nad 27	6823154.6	404363.3	PC-94-64	197.5	Upper Whittaker	OSw3-7		Banded chert dolostone	Rep spl of interbedded chert/dolostone unit.
6 in SD4	Nad 27	6823154.6	404363.3	PC-94-64	199.2	Upper Whittaker	OSw3-6		Upper spar dolostone	Vugs are filled by qtz and sparry dol.
6 in SD4	Nad 27	6823154.6	404363.3	PC-94-64	203.7	Upper Whittaker	OSw3-6		Upper spar dolostone	Rep spl of upper spar dolostone unit.
6 in SD4	Nad 27	6823154.6	404363.3	PC-94-64	207.6	Upper Whittaker	OSw3-6	Stratabound	Stratabound sulphides in upper spar dolostone unit	Stratabound sulp (sp-gn-py); sample 1 = gn (<2% sph), sample 2 = gn (10%py + sph)
6 in SD4	Nad 27	6823154.6	404363.3	PC-94-64	241.5	Upper Whittaker	OSw3-5		Upper chert nodule dolostone	Rep spl of upper chert nodule dolostone.
6 in SD4	Nad 27	6823154.6	404363.3	PC-94-64	285.7	Upper Whittaker	OSw3-4		Lower spar unit	Rep spl of unit; dol spars and some qtz fill vugs.
6 in SD4	Nad 27	6823154.6	404363.3	PC-94-64	308.4	Upper Whittaker	OSw3-3		Lower chert nodule dolostone	Rep spl of lower chert nodule dolostone.
6 in SD4	Nad 27	6823154.6	404363.3	PC-94-64	329.5	Upper Whittaker	OSw3-2		Mottled dolostone	Sample of OSw3-2 with big vug or vein filled with cal+qtz; fg py diss in the dolostone. Sample of sparry dol may have traces of dolostone.
6 in SD4	Nad 27	6823154.6	404363.3	PC-94-64	330.2	Upper Whittaker	OSw3-2		Mottled dolostone	Rep spl of mottled dolostone.
6 in SD4	Nad 27	6823154.6	404363.3	PC-94-64	338.6	Upper Whittaker	Osw3-1		Massive dolostone	Rep spl of massive grey dolostone.
3 in SD2	Nad 27	6825981.0	404343.0	PC-95-65	432.9			Stratabound	Stratabound sulphides in?	Small spl of fg mas py with vugs or cavities filled by sparry dol.
Zebra showing	Nad 27	6833291.0	410801.2	PC-94-75	197.2	Cadillac ET (~Root River)		MVT	Fine crystalline, vuggy and brecciated dolostone	Vugs filled by sparry dol and rimmed by py.
Zebra showing	Nad 27	6833291.0	410801.2	PC-94-75	204.5	Cadillac ET (~Root River)		MVT	Fine crystalline, vuggy and brecciated dolostone	Vugs filled by sparry dol and rimmed by py.
Zebra showing	Nad 27	6833291.0	410801.2	PC-94-77	73.3-73.4	Cadillac ET (~Root River)		MVT	Fine crystalline, vuggy and brecciated dolostone	Vugs and cavities filled by sparry dol and rimmed by py (some sph?); py is weathered.
Zebra showing	Nad 27	6833291.0	410801.2	PC-94-80	220	Cadillac ET (~Root River)		MVT	Fine crystalline, vuggy and brecciated dolostone	Vugs fillled by sparry dol and rimmed by py (weathered).
3 in SD2	Nad 27	6825981.0	405212.4	PC-94-82	468.8	Upper Whittaker	OSw3-4		Lower spar dolostone unit	Rep spl of silicified dolostone (chips).
3 in SD2	Nad 27	6825981.0	405212.4	PC-94-82	469.6	Upper Whittaker	OSw3-4		Lower spar dolostone unit	Silicified dolostone with stringers of fg py+qtz and fg red sph at contact with massive sul section; cal veins cutting stringers of qtz-py-sph.
3 in SD2	Nad 27	6825981.0	405212.4	PC-94-82	471.2	Upper Whittaker	OSw3-4		Lower spar dolostone unit	Dolostone is crackled with stringers of fg pyrite and fg red sph at contact with mas sul.
3 in SD2	Nad 27	6825981.0	405212.4	PC-94-82	473.9	Upper Whittaker	OSw3-4		Lower spar dolostone unit	Chips of dolostone with spars.
3 in SD2	Nad 27	6825981.0	405212.4	PC-94-82	496.1	Upper Whittaker	OSw3-4	Stratabound	Stratabound sulphides in lower spar dolostone	High grade sph-py-gn and sparry dol; upper contact 70°CA; lower contact irregular but sharp, 80-90°CA.

Appendix 1 continued.

Zone / showing	Datum	UTM Northing	UTM Easting	DDH or sample #	Sample depth (m)	Host formation	Unit	Type of sulphides	Lithology	Sample description and remarks
3 in SD2	Nad 27	6826692.0	405268.0	PC-94-88	-	Upper Whittaker	Contact of OSw3-5 and OSw3-4	Veins	Quartz-carbonate-sulphide veins	Qtz-carbonate-sul vein at contact between OSw3-5 and OSw3-4
3 in SD2	Nad 27	6826692.0	405268.0	PC-94-88	-	Upper Whittaker	OSw3-3	Stratabound	Stratabound sulphides in lower chert nodule dolostone	Looks like py stringers, and qtz-sp-gn stringers at ~45-55º CA.
3	Nad 27	6825981.0	404343.0	PC-95-95	-	Road River		Veins	Quartz-carbonate-sulphide veins in shaly dolostone and shale	HW contact broken, and brecciated. FW contact is with a fairly extensive zone of silicification, mineralization and brecciation.
3	Nad 27	6825981.0	404343.0	PC-95-95	-	Upper Whittaker	OSw3-4	Stratabound	Stratabound sulphides in lower spar unit	The section at around 420.9 and 420.10 m is cg sph and fine gn to smeared banded mas fg sph and gn. Bands at 30-40º CA, 70-80% sul.
4 in SD3	Nad 27	6825745.1	404726.9	PC-95-97	79-79.2	Upper Whittaker	OSw3-2	Stratabound	Quartz-carbonate-sulphide vein in mottled dolostone	Spl is at lower contact = stylolitic-like contact and stringers. Upper contact = rubble. The ms section = massive to semi-massive fg py (50%) reddish-brown sph (35%) and gn band.
4 in SD3	Nad 27	6825694.8	404837.6	PC-95-103	110	Upper Whittaker	Contact of OSw3-3 and OSw3-2	Stratabound	Stratabound sulphides at contact of lower chert nodule dolostone and mottled dolostone	Chips of gn.
4 in SD3	Nad 27	6825694.8	404837.6	PC-95-103	110	Upper Whittaker	Contact of OSw3-3 and OSw3-2	Stratabound	Stratabound sulphides at contact of lower chert nodule dolostone and mottled dolostone	Chips of cg cal in vugs.
4 in SD3	Nad 27	6825694.8	404837.6	PC-95-103	110.3	Upper Whittaker	Contact of OSw3-3 and OSw3-2	Stratabound	Stratabound sulphides at contact of lower chert nodule dolostone and mottled dolostone	Fine pinkish (almost red) sph, brassy py and streaks of gn with minor white spar and pyrobitumen; some banding with variable orientation 30-90º CA. Upper and lower contacts seem parallel to "strata".
3 North	Nad 27	6827664.6	405587.7	PC-95-122	764	Road River		Veins	Quartz-carbonate-sulphide veins in shaly dolostone and shale	Spl of cg yellow-tan sph chips. The interval consists of very high-grade cg sph-gn vein with minor td.
3 North	Nad 27	6827664.6	405587.7	PC-95-122	765.5	Road River		Veins	Quartz-carbonate-sulphide veins in shaly dolostone and shale	Cg yellow-tan sph and intergrowth of cg gn, which cut the sph.
5 in SD5	Nad 27	6824601.7	405040.5	PC-95-124	309.9	Upper Whittaker	OSw3-7	Stratabound	Stratabound sulphides at contact with banded chert dolostone	Chips of massive sul; from 309.9 to 311.2 m, section consists of fg mas agg of py with pink sph, and gn+qtz in veinlets or vugs.
Rico showing	Nad 27	6827849.6	405628.9	PC-95-125	207.7	Cadillac			Dolostone	Rep spl of black to grey dolostone turbidites; thin bedded to laminated.
Rico showing	Nad 27	6827849.6	405628.9	PC-95-125	280	Cadillac			Silty dolostone	Rep spl of silty dolostone.
Rico showing	Nad 27	6827849.6	405628.9	PC-95-125	747	Road River		Veins	Quartz-carbonate-sulphide veins in shaly dolostone and shale	Sph-gn-qtz-td brecciated vein. Indistinct upper and lower contacts.
Rico showing	Nad 27	6827849.6	405628.9	PC-95-125	760	Road River		Veins	Quartz-carbonate-sulphide veins in shaly dolostone and shale	Qtz-gn ±sph vein with cal blobs; darker sulphide (td?) with gn.
Rico showing	Nad 27	6827849.6	405628.9	PC-95-125	762	Road River		Veins	Quartz-carbonate-sulphide veins in shaly dolostone and shale	Chips of cg mas sph (dark tan) from the gn-sph-td-qtz vein.
Rico showing	Nad 27	6827849.6	405628.9	PC-95-125	761.4	Road River		Veins	Quartz-carbonate-sulphide veins in shaly dolostone and shale	Mas ga-sph-td qtz vein; gn forms stringers in mas tan brown colour sph.
3	Nad 27	6826335.0	405042.0	PC-01-130	53	Road River			Shale	Rep spl of blocky and moderately broken grey laminated shale variably crazed with 1-3 mm carb-qtz veinlets. Bedding at 30º CA.
3	Nad 27	6826335.0	405042.0	PC-01-130	82.9	Upper Whittaker	OSw3-7		Banded chert dolostone	Rep spl of bedded chert/dolostone or banded chert member = 1-4 cm banded blue-grey chert bands with chatter marks in grey dolomite-shale.
3	Nad 27	6826335.0	405042.0	PC-01-130	148	Upper Whittaker	OSw3-6		Upper spar unit	Rep spl of upper spar member = 30% coarse white dolospar-cal veins and vugs in a grey fossil trash-rich dolostone.
3	Nad 27	6826335.0	405042.0	PC-01-130	164	Upper Whittaker	OSw3-5		Upper chert nodule dolostone	Rep spl of upper chert nodular member: grey dol with variable ovoid shaped milky grey nodules.

Appendix 1 continued.

Zone / showing	Datum	UTM Northing	UTM Easting	DDH or sample #	Sample depth (m)	Host formation	Unit	Type of sulphides	Lithology	Sample description and remarks
3	Nad 27	6826335.0	405042.0	PC-01-130	182	Upper Whittaker	OSw3-5	Veins	Quartz-carbonate-sulphide veins in upper chert nodule dolostone	Vein of ms cutting core at ~10° CA; the vein is made of cg pale sph with cg gn in the center. Section 181.6 to 183.1: coarse 5 cm wide sph-gn vein stringer sub-paralleling CA, honey colour sph 50%, gn 30%, and carb 20%.
3	Nad 27	6826335.0	405042.0	PC-01-130	257	Upper Whittaker	OSw3-3	Veins	Quartz-carbonate-sulphide veins in lower chert nodule dolostone	Cg sph (beige/tan) and qtz; qtz cut sph.
3	Nad 27	6826335.0	405042.0	PC-01-130	257.5	Upper Whittaker	OSw3-3	Veins	Quartz-carbonate-sulphide veins in lower chert nodule dolostone	Fg to mg py from qtz-carb-sph-gn vein: the py is typically brecciated and streaked texture to sul. Py is mixed with qtz and occ gn.
3	Nad 27	6826335.0	405042.0	PC-01-130	258.6	Upper Whittaker	OSw3-3	Veins	Quartz-carbonate-sulphide veins in lower chert nodule dolostone	Slab of cg pale sph cut by gn.
3	Nad 27	6826335.0	405042.0	PC-01-130	258.6	Upper Whittaker	OSw3-3	Veins	Quartz-carbonate-sulphide veins in lower chert nodule dolostone	Cg cal from qtz-carb-sph-gn vein.
3	Nad 27	6826335.0	405042.0	PC-01-130	269.3	Upper Whittaker	OSw3-3	Stratabound	Stratabound sulphides in lower chert nodule dolostone	Fg py rimming vugs filled by dol in dark dolostone. Spl = fg py (±pink sph), fresh and slightly weathered.
3	Nad 27	6826335.0	405042.0	PC-01-130	272.3	Upper Whittaker	OSw3-3	Stratabound	Stratabound sulphides in lower chert nodule dolostone	Cg of calcite?
3	Nad 27	6826335.0	405042.0	PC-01-130	285.4	Upper Whittaker	OSw3-3	Stratabound	Stratabound sulphides in lower chert nodule dolostone	Spl of mg py with cal and host dolostone.
3	Nad 27	6826335.0	405042.0	PC-01-130	294	Upper Whittaker	OSw3-3	Stratabound	Stratabound sulphides in lower chert nodule dolostone	Small spl of fg mas py mix within the dolostone. Fg py is mixed with fg pink sph and gn; cut by veinlets of cal.
3	Nad 27	6826335.0	405042.0	PC-01-130	295.9	Upper Whittaker	OSw3-3	Stratabound	Stratabound sulphides in lower chert nodule dolostone	Spl of cg sph, gn, and cal; mixture of sph and gn cut by cal.
3	Nad 27	6826335.0	405042.0	PC-01-130	297.3	Upper Whittaker	OSw3-3	Stratabound	Stratabound sulphides in lower chert nodule dolostone	Spl of cg sph, gn, and cal; cal seems to be associated with sulp (possibly contemporaneous).
3	Nad 27	6826335.0	405042.0	PC-01-130	299.7	Upper Whittaker	OSw3-3	Veins	Quartz-carbonate-sulphide veins in lower chert nodule dolostone	Small spl of mas gn from qtz-gn-carb (cal)-sph vein. Sporadic high-grade gn with brecciated qtz fragments.
3	Nad 27	6826335.0	405042.0	PC-01-130	307	Upper Whittaker	OSw3-3	Veins	Quartz-carbonate-sulphide veins in lower chert nodule dolostone	Chips of mg gn mixed with cal or sparry dol - from high-grade gn section (306.7-307.7).
3	Nad 27	6826335.0	405042.0	PC-01-130	307	Upper Whittaker	OSw3-3	Veins	Quartz-carbonate-sulphide veins in lower chert nodule dolostone	Small spl of cg sph and gn mix with qtz - from high-grade gn section (306.7-307.7).
3	Nad 27	6826335.0	405042.0	PC-01-130	307.2	Upper Whittaker	OSw3-3	Veins	Quartz-carbonate-sulphide veins in lower chert nodule dolostone	Small piece of fg mas gn from high-grade gn section (306.7 to 307.7).
3	Nad 27	6826335.0	405042.0	PC-01-130	311.20	Upper Whittaker	OSw3-2	Stratabound	Stratabound sulphides in mottled dolostone	Bands of fg py and fg sph in contact with recrystallized sparry dolostone; the whole sample is brecciated.
3	Nad 27	6826335.0	405042.0	PC-01-130	313.5	Upper Whittaker	OSw3-2	Stratabound	Stratabound sulphides in mottled dolostone	Bands of fg py in agg of fg pinkish sph + fg py; gn and cal fill the remaining spaces.
3	Nad 27	6826335.0	405042.0	PC-01-130	315.2	Upper Whittaker	OSw3-2	Stratabound	Stratabound sulphides in mottled dolostone	Chips of fg to mg pink sph mix with py.
3	Nad 27	6826335.0	405042.0	PC-01-130	317.2	Upper Whittaker	OSw3-2	Stratabound	Stratabound sulphides in mottled dolostone	Agg of fg py cut by veinlets of qtz and 1 veinlet of cg red-pinkish sph+gn.
3	Nad 27	6826405.5	405004.0	PC-01-132	288.5	Upper Whittaker	OSw3-3	Veins	Quartz-carbonate-sulphide veins in lower chert nodule dolostone	White cg (~2 cm) cal crystals.
3	Nad 27	6826405.5	405004.0	PC-01-132	-	Upper Whittaker	OSw3-3	Veins	Quartz-carbonate-sulphide veins in lower chert nodule dolostone	
3	Nad 27	6826405.5	405004.0	PC-01-132	-	Upper Whittaker	OSw3-3	Veins	Quartz-carbonate-sulphide veins in lower chert nodule dolostone	
3	Nad 27	6826405.5	405004.0	PC-01-132	-	Upper Whittaker	OSw3-3	Veins	Quartz-carbonate-sulphide veins in lower chert nodule dolostone	

Appendix 1 continued.

Zone / showing	Datum	UTM Northing	UTM Easting	DDH or sample #	Sample depth (m)	Host formation	Unit	Type of sulphides	Lithology	Sample description and remarks
3	Nad 27	6826405.5	405004.0	PC-01-132	-	Upper Whittaker	OSw3-3	Veins	Quartz-carbonate-sulphide veins in lower chert nodule dolostone	
3	Nad 27	6826405.5	405004.0	PC-01-132	-	Upper Whittaker	OSw3-3	Veins	Quartz-carbonate-sulphide veins in lower chert nodule dolostone	
3	Nad 27	6826405.5	405004.0	PC-01-132	319.5	Upper Whittaker	OSw3-2		Mottled dolostone	Rep spl taken in proximity to the sul zone.
3	Nad 27	6826405.5	405004.0	PC-01-132	320.8	Upper Whittaker	OSw3-2	Stratabound	Stratabound sulphides in mottled dolostone	Section of mas to semi-mas sph-py-gn. Upper contact is approx. parallel to "strata". Spl = chips taken in part in the small beds of recrystallized dolostone.
3	Nad 27	6826405.5	405004.0	PC-01-132	327.5	Upper Whittaker	OSw3-2	Stratabound	Stratabound sulphides in mottled dolostone	Mas sul intersection: Py (75%), cg recrystallized sph (5%), gn (2%) and altered nodules of dolostone; upper contact is a qtz vein, and lower contact is following bedding.
3	Nad 27	6826405.5	405004.0	PC-01-133	-			Veins	Quartz-carbonate-sulphide veins	
3	Nad 27	6826405.5	405004.0	PC-01-133	-			Veins	Quartz-carbonate-sulphide veins	
3	Nad 27	6825981.0	404343.0	PC-04-150	42.5	Upper Whittaker	OSw 3-7		Banded chert dolostone	Rep spl of banded chert dolostone unit, but with no chert nodule.
3	Nad 27	6825981.0	404343.0	PC-04-150	76.8	Upper Whittaker	OSw 3-6		Upper spar unit	Rep spl of upper spar dolostone unit.
3	Nad 27	6825981.0	404343.0	PC-04-150	124	Upper Whittaker	OSw 3-5		Upper chert nodule dolostone	Rep sample of upper chert nodular dolostone unit. The sample has no chert nodule visible.
3	Nad 27	6825981.0	404343.0	PC-04-150	156.6	Upper Whittaker	OSw 3-5		Upper chert nodule dolostone	Rep sample of upper chert nodular dolostone unit. The sample has chert nodule visible.
3	Nad 27	6825981.0	404343.0	PC-04-150	186.6	Upper Whittaker	OSw 3-4		Lower spar unit	Rep sample of lower spar dolostone unit.
3	Nad 27	6825981.0	404343.0	PC-04-150	214.4	Upper Whittaker	OSw 3-3		Lower chert nodule dolostone	Rep sample of lower chert nodular dolostone unit.
3	Nad 27	6825981.0	404343.0	PC-04-150	235.1	Upper Whittaker	OSw3-2		Mottled dolostone	Rep sample of mottled dolostone. Dolostone has fine stringers of py and sph.
3	Nad 27	6825981.0	404343.0	PC-04-150	237.2	Upper Whittaker	OSw3-2	Stratabound	Stratabound sulphides in mottled dolostone	Sul are mainly fg py replacing the sparry dol and the cherty dolostone (beautiful replacement texture).
3	Nad 27	6825981.0	404343.0	PC-04-150	238.15	Upper Whittaker	OSw3-2	Stratabound	Stratabound sulphides in mottled dolostone	Sul section = mas to semi-mas sul, py-rich with pink sph and minor gn. Layers at 90° CA with minor white carbonate spar.
3	Nad 27	6825981.0	404343.0	PC-04-150	238.45	Upper Whittaker	OSw3-2	Stratabound	Stratabound sulphides in mottled dolostone	Sul are fg py and sph showing streatching.
3	Nad 27	6825981.0	404343.0	PC-04-150	238.6	Upper Whittaker	OSw3-2	Stratabound	Stratabound sulphides in mottled dolostone	Sul are agg of fg py+sph replacing the cherty dolostone; gn and later cal fill the remaining spaces.
3	Nad 27	6825981.0	404343.0	PC-04-150	239.5	Upper Whittaker	OSw3-2	Stratabound	Stratabound sulphides in mottled dolostone	Sul section with some open space filling textures: Agg of fg py+sph replacing cherty dolostone; cg sph and py rimmed fg agg of py+sph; gn and cal filled the remaining spaces.
3	Nad 27	6825981.0	404343.0	PC-04-150	270.5	Upper Whittaker	OSw3-2		Mottled dolostone	Rep sample (chips) of moddled dolostone unit with moderate fractures.
3	Nad 27	6825981.0	404343.0	PC-04-150	-	Upper Whittaker	OSw3-2	Stratabound	Stratabound sulphides in mottled dolostone	
3	Nad 27	6825981.0	404343.0	PC-04-150	-	Upper Whittaker	OSw3-2	Stratabound	Stratabound sulphides in mottled dolostone	
3	Nad 27	6825981.0	404343.0	PC-04-150	-	Upper Whittaker	OSw3-2	Stratabound	Stratabound sulphides in mottled dolostone	
3	Nad 27	6825981.0	404343.0	PC-04-150	-	Upper Whittaker	OSw3-2	Stratabound	Stratabound sulphides in mottled dolostone	
3	Nad 27	6825981.0	404343.0	PC-04-150	-	Upper Whittaker	OSw3-2	Stratabound	Stratabound sulphides in mottled dolostone	

Appendix 1 continued.

Zone / showing	Datum	UTM Northing	UTM Easting	DDH or sample #	Sample depth (m)	Host formation	Unit	Type of sulphides	Lithology	Sample description and remarks
3	Nad 27	6825981.0	404343.0	PC-04-150	253.7	Upper Whittaker	OSw3-2	Stratabound	Stratabound sulphides in mottled dolostone	Chips of rep sample of mottled siliceous dolostone.
3	Nad 27	6825981.0	404343.0	PC-04-150	283.3	Upper Whittaker	OSw3-1		Massive dolostone	Small rep sample of grey massive dolostone.
3	Nad 27	6825981.0	404343.0	PC-04-150	263	Upper Whittaker	OSw3-2	Stratabound	Stratabound sulphides in mottled dolostone	Chips of rep sample of mottled siliceous dolostone.
3	Nad 27	6825981.0	404343.0	PC-04-150	241	Upper Whittaker	OSw3-2	Stratabound	Stratabound sulphides in mottled dolostone	Chips of fg to mg py mix with host rock and traces of carbonates.
3	Nad 27	6825981.0	404343.0	PC-04-159	480.6	Upper Whittaker		Veins	Quartz-carbonate-sulphide vein	Cg cal associated with cg gn.
3	Nad 27	6825981.0	404343.0	PC-04-159	482.1	Upper Whittaker		Veins	Quartz-carbonate-sulphide vein	Cg redish tan (with occ darker streaks) sph; traces of gn.
Besa River Fm	Nad 27	N/A	N/A	Besa River Fm	Surface	Besa River			Besa River sediment	Sph grains from 5 cm vug fill with large crystals of orange-red sph + qtz (3-5 mm ~5%) + py (1 mm ~2%).
Rico showing	Nad 83	6831946.8	406649.5	Rico-4	Surface	Arnica		Veins	Quartz-carbonate-sulphide vein in banded cherty dolostone and limestone	Cg silvery yellowish to tan sph in sub-vertical quartz-carbonate-sulphide vein crosscutting the finely crystalline black nodular and banded cherty dolostone and limestone (numerous quartz-carbonate crackle veining).
Rico showing	Nad 83	6831946.8	406649.5	Rico-2	Surface	Arnica		Veins	Quartz-carbonate-sulphide vein in banded cherty dolostone and limestone	Cg silvery yellowish sph with some cg gn.
Rico showing	Nad 83	6831946.8	406649.5	Rico-3	Surface	Arnica		Veins	Quartz-carbonate-sulphide vein in banded cherty dolostone and limestone	Cg sph and fg gn; sample slightly weathered.
Rico showing	Nad 83	6831946.8	406649.5	Rico-1	Surface	Arnica		Veins	Quartz-carbonate-sulphide vein in banded cherty dolostone and limestone	Cg sph and gn; the gn is within a veinlet cutting the sph. Spl slightly weathered.
Rico showing	Nad 83	6831946.8	406649.5	Rico	Surface	Arnica		Veins	Quartz-carbonate-sulphide vein in banded cherty dolostone and limestone	Slab of cg silvery yellowish sph.
8	Nad 83	6820721.3	403662.2	8-1	Surface	Cadillac		Veins	Quartz-carbonate-sulphide veins cutting the Cadillac Fm and possibly the Road River Fm	Sul-rich veins with bands of qtz and bands of sm (±galena) cutting the Cadillac or Road River fms.
8	Nad 83	6820721.3	403662.2	8-2	Surface	Cadillac		Veins	Quartz-carbonate-sulphide veins cutting the Cadillac Fm and possibly the Road River Fm	Sul-rich veins with bands of qtz and bands of sm (±galena) cutting the Cadillac or Road River fms.
8	Nad 83	6820721.3	403662.2	8-3	Surface	Cadillac		Veins	Quartz-carbonate-sulphide veins cutting the Cadillac Fm and possibly the Road River Fm	Sul-rich veins with bands of qtz and bands of sm (±galena) cutting the Cadillac or Road River fms.
5	Nad 83	6825069.0	404794.8	5-3	Surface	Upper Whittaker	OSw3-5	Veins	Quartz-carbonate-sulphide veins in upper chert nodule dolostone	Boulder of sulp-rich veins = mas gn with some qtz fragments; the agg of gn contains fg py and qtz.
5	Nad 83	6825069.0	404794.8	5-1	Surface	Upper Whittaker	OSw3-5	Veins	Quartz-carbonate-sulphide veins in upper chert nodule dolostone	Sul-rich veins = "fragments" of sph and qtz (±dol) in groundmass of gn.
5	Nad 83	6825069.0	404794.8	5-2	Surface	Upper Whittaker	OSw3-5	Veins	Quartz-carbonate-sulphide veins in upper chert nodule dolostone	Sul-rich veins = "fragments" of sph and qtz (±dol) in groundmass of gn.
6	Nad 83	6823154.6	404363.3	6	Surface	Cadillac		Veins	Quartz-carbonate-sulphide veins	Colloform py and ? cut by cg saddle dol vein.

Appendix 1 continued.

Zone / showing	Datum	UTM Northing	UTM Easting	DDH or sample #	Sample depth (m)	Host formation	Unit	Type of sulphides	Lithology	Sample description and remarks
6	Nad 83	6823154.6	404363.3	6-1	Surface	Cadillac		Veins	Quartz-carbonate-sulphide veins	Qtz vein with some stringers of gn and traces of mal in a groundmass of qtz.
6	Nad 83	6823154.6	404363.3	6-2	Surface	Cadillac		Veins	Quartz-carbonate-sulphide veins	Sul-rich veins with band of qtz and "laminae" of gn (gn is parallel to qtz band).
6	Nad 83	6823154.6	404363.3	6-3	Surface	Cadillac		Veins	Quartz-carbonate-sulphide veins	Qtz-carb vein with some stringers of gn and mal.
6	Nad 83	6823154.6	404363.3	6-4	Surface	Cadillac		Veins	Quartz-carbonate-sulphide veins	Vein is in contact with host rock; the qtz-carb vein contains some stringers of gn and ?
7	Nad 83	6822145.4	403910.8	7	Surface	Cadillac		Veins	Quartz-carbonate-sulphide veins	Weathered sample of qtz-carb-sul vein.
7	Nad 83	6822145.4	403910.8	7-1	Surface	Cadillac		Veins	Quartz-carbonate-sulphide veins	Weathered spl of qtz-carb-sul vein; the vein contains mas gn and fragments of qtz.
7	Nad 83	6822145.4	403910.8	7-2	Surface	Cadillac		Veins	Quartz-carbonate-sulphide veins	Qtz-carb-sulp vein with mas gn and fragments of qtz.
Level 930 crosscut 11	Nad 27	6825973	404825	930-1	underground level 930			Veins	Quartz-carbonate-sulphide veins in?	Cg tan sph cut by stringers of qtz and gn.
Level 930 crosscut 11	Nad 27	6825973	404825	930-2 cx 11	underground level 930			Veins	Quartz-carbonate-sulphide veins in?	Cg tan sph and gn; nice texture of mas gn "invading" tan colour sph.
Level 930 crosscut 11	Nad 27	6825973	404825	930-3 cx 11	underground level 930			Veins	Quartz-carbonate-sulphide vein in?	Cg tan sph and gn.
Level 930 crosscut 22	Nad 27	6825973	404825	Underground level 930 cx 22	underground level 930			Veins	Quartz-carbonate-sulphide vein in?	Cg tan to pale grey sph, galena and traces of qtz; gn forms streaks within sph.
Level 930 crosscut 30	Nad 27	6825973	404825	Underground level 930	underground level 930			Veins	Quartz-carbonate-sulphide vein in?	Cg tan sph and gn.
Level 930 crosscut 25	Nad 27	6825973	404825	Underground level 930 cx 25	underground level 930			Veins	Quartz-carbonate-sulphide vein in?	Cg mas gn with qtz fragments.
Level 870	Nad 27	6825722	404582	Underground level 870	underground level 870	Upper Whittaker	OSw3-6		Upper spar dolostone	Rep spl of upper spar dolostone unit with large vugs filled by cal and large sph and gn + traces of py.
Level 870	Nad 27	6825722	404582	Underground "adit"	underground level 870			Veins	Quartz-carbonate-sulphide vein in?	Spl of banded vein with bands of cg sph, cg gn and band of cherty host rock.
Gate showing	Nad 83	6835836.1	400780.6	North Gate vein	Surface	Upper Whittaker		Veins	Quartz-carbonate-sulphide vein	Mas gn and traces of sph and mal in qtz vein.
North Gate (new)	Nad 83	6835732.6	400838.6	North Gate vein - 2	Surface	Upper Whittaker		Veins	Quartz-carbonate-sulphide vein	Mas sph (tan colour) with traces of gn and td in groundmass of qtz. Cg calcite fill spaces.
South Gate showing	Nad 83	6807388.0	390411.3	South Gate vein	Surface	Sunblood?		Veins	Quartz-carbonate-sulphide veins	Various samples of mas gn with some sph and mal.
Road showing	Nad 83	6832497.5	410146.5	Road showing	Surface	Root River		MVT	Grey dolostone	Dolostone with vug filled with saddle dol.
Samantha - lower trench	Nad 83	6842662.5	408600.5	Samantha-1 (lower trench)	Surface	Root River		MVT	Grey dolostone	Light grey dolostone and shale with large bioherms, finely crystalline and generally featureless contain blebs of cg mas gn with some sph.
Samantha - lower trench	Nad 83	6842662.5	408600.5	Samantha showing (lower trench) - SAM 2	Surface	Root River		MVT	Grey dolostone	Light grey dolostone and shale with large bioherms, finely crystalline and generally featureless contain patches of sparry dol.
Samantha - lower trench	Nad 83	6842662.5	408600.5	Samantha showing (lower trench) - SAM 3	Surface	Root River		MVT	Grey dolostone	Dolostone breccia = dolostone fragments enclosed in a sparry dol cement. The dol has a pinkish colour due to oxydation of cleaved surface. SAM 3-1 = sparry dol, SAM 3-2 = frag of host dolostone.

Appendix 1 continued.

Zone / showing	Datum	UTM Northing	UTM Easting	DDH or sample #	Sample depth (m)	Host formation	Unit	Type of sulphides	Lithology	Sample description and remarks
Samantha - lower trench	Nad 83	6842662.5	408600.5	Samantha-2 (lower trench)	Surface	Root River		MVT	Grey dolostone	Cg mas gn with some sph (?).
Samantha - lower trench	Nad 83	6842662.5	408600.5	Samantha (lower trench no 4) - SAM 4	Surface	Root River		MVT	Grey dolostone	CG mas gn.
Zebra - upper showing	Nad 83	6833925.9	410027.5	Zebra-1	Surface	Cadillac ET (~Root River)		MVT	Fine crystalline, fossiliferous vuggy dolostone	Weathered spl of dolostone with cavities filled by colloform py, some sph, and sparry dol.
Zebra - lower showing	Nad 83	6833291.0	410801.2	Zebra-2	Surface	Cadillac ET (~Root River)		MVT	Fine crystalline, vuggy and brecciated dolostone	Weathered brecciated dolostone: Cavities of the dolostone are filled by colloform py, some sph, and sparry dol, and the sul form a nice lace around frags.
Zebra - lower showing	Nad 83	6833291.0	410801.2	Zebra-3	Surface	Cadillac ET (~Root River)		MVT	Fine crystalline, vuggy and brecciated dolostone	Weathered breccia: Cavities of the dolostone are filled by colloform py, some sph, and finally by cg sparry dol; the colloform bands are broken up and the sul are weathered (probably a mix of sph+py).
Zebra - lower showing	Nad 83	6833291.0	410801.2	Zebra-4	Surface	Cadillac ET (~Root River)		MVT	Fine crystalline, vuggy and brecciated dolostone	Weathered brecciated dolostone: Cavities of the dolostone are filled by colloform py, some sph, and sparry dol, and the sul form a nice lace around frags.
6	Nad 83	6823154.6	404363.3	HF-05-03	Surface	Cadillac			Silty dolostone	Crustiform alteration of mas pale brown sph and irregular gn masses. The weathering product is a ribboned colliform sm with abundant vugs and open spaces.
Arnica Fm	Nad 83	N/A	N/A	Arnica Fm	Surface	Arnica			Cherty dolostone	Spl of sparry dol in vertical fracture of the cherty dolostone.

Abbreviations: agg=aggregate, approx=approximative, CA=core axis, cal=calcite, carb=carbonates, cg=coarse grained, coll=colloform, conc=concentration, cp=chalcopyrite, cx=coarse crystalline, diss=disseminated, dol=dolomite, cup=duplicate, fg=fine grained, gn=galena, jasp=jasperoid, mal-malachite, mas=massive, mg=medium grained, ms=massive sulphides, N/A=not available, occ=occasional, po=pyrrhotite, py=pyrite, qtz=quartz, rep=representative, sm=smithsonite, sph=sphalerite, spl=sample, sul=sulphides, td=tetrahedrite, tn=tennantite. All data is in UTM zone 10 and in NTS sheet 95F10.

GEOCHEMICAL INVESTIGATIONS OF HIGH-GRADE QUARTZ-SCHEELITE VEINS OF THE CANTUNG MINE, NORTHWEST TERRITORIES

Jason Yuvan[1], Kevin Shelton[1] and Hendrik Falck[2]
1. Department of Geological Sciences, University of Missouri, Columbia, Missouri 65211-1380
2. Northwest Territories Geoscience Office, P.O. Box 1320 Yellowknife, Northwest Territories X1A 2L9

ABSTRACT

High-grade quartz-scheelite veins (up to 3.7 wt.% WO_3) in the open pit orebody of the Cantung mine, Tungsten, Northwest Territories occur 300 m vertically above a Cambrian limestone-Cretaceous monzogranite contact along which the E-Zone, a world-class tungsten skarn orebody, is developed. The trend of an 80 m wide vein swarm is roughly parallel to the strike and dip of a near-vertical aplite dyke along the edge of the open pit. Adjacent to these quartz-scheelite veins, dark green alteration selvedges overprint earlier light green skarn alteration. This overprint implies that the high-grade quartz-scheelite veins are not part of the early skarn-forming event but represent a distinct, later event.

Oxygen isotope data from vein-hosted quartz-scheelite pairs yield equilibrium depositional temperatures of 430 to 595°C. These temperatures indicate that the high-grade quartz-scheelite veins are related to a deep magmatic hydrothermal system and are likely a distal expression of a protracted skarn-forming event, perhaps related to aplite dyke emplacement. Quartz-scheelite veins did not form in a shallower, cooler, hydrothermal system during uplift.

Primary ore fluids in quartz-scheelite veins from the open pit orebody, in skarn-related quartz veins from the E-Zone orebody, and in aplite dykes are grossly similar H_2O-CO_2-NaCl ± CH_4 fluids. However, two distinct end-member fluids have been documented: aplite-related fluids and skarn-related fluids (in quartz veins from the E-Zone orebody). Fluids in high-grade quartz-scheelite veins contain components of both end-member fluids. High-grade quartz-scheelite veins from the open pit orebody share a common structural attitude with aplite dykes. Fluids in veins from the open pit orebody contain an aplite-related fluid end-member even when occurring up to 70 m from the nearest exposed aplite dyke. Thus, quartz-scheelite veins and aplite dykes in the open pit orebody probably have a genetic relationship in addition to their structural relationship.

The authors envision a conceptual model for the Cantung hydrothermal system in which ore-grade tungsten deposits formed where fluids emerged from the granite and encountered rocks favourable for skarn development (e.g. cleaner 'ore limestone' versus cherty 'swiss cheese limestone'). Due to the folded geometry of the sedimentary sequence, in other areas along the granite contact, the fluids emerging from the granite encountered strata less favourable to skarn development (i.e. argillite). Where these less favourable units were breached by fracture systems, potential skarn-forming fluids (and aplite dykes) gained access to host rocks more conducive to ore development vertically distal to the granite contact. The presence of magmatic ore fluids distal to intrusions is intriguing and has significant implications for mineral resource assessment in the region.

INTRODUCTION

The Cantung mine, Tungsten, Northwest Territories, Canada (Fig. 1) is an unusually large (4 million tonnes of ore) and high-grade (1.6 wt.% WO_3) tungsten skarn deposit (Yukon Geological Survey, 2005) developed in folded and overturned Cambrian limestones above a Cretaceous monzogranite (Mathieson and Clark, 1984; Bowman et al., 1985). Two skarn orebodies have been exploited in the mine, the E-Zone and open pit orebodies. The E-Zone orebody occurs at the granite-limestone contact, and the open pit orebody is located approximately 300 m vertically above the E-Zone orebody (Fig. 2). Due to the folded geometry of the sedimentary rocks, the two skarn orebodies were deposited in the same stratigraphic units.

An 80 m wide en échelon swarm of high-grade quartz-scheelite veins crosscuts the open pit orebody. These veins contain up to 3.7 wt.% WO_3. Adjacent to these quartz-scheelite veins, dark green alteration selvedges overprint earlier light green skarn alteration. This overprint implies that the high-grade quartz-scheelite veins are not part of the early skarn-forming event, but represent a distinct, later event (Yuvan et al., 2005).

In the underground E-Zone orebody, near-vertical aplite dykes that crosscut the skarn ore infrequently grade into quartz veins similar to the high-grade quartz-scheelite veins found in the open pit orebody. Other aplite dykes in the E-Zone orebody are observed to extend upward into massive garnet-pyroxene alteration with abundant scheelite (Yuvan et al., 2004).

Yuvan, J., Shelton, K., and Falck, H., 2007, Geochemical investigations of the high-grade quartz-scheelite veins of the Cantung mine, Northwest Territories, *in* Mineral and Energy Resource Assessment of the Greater Nahanni Ecosystem Under Consideration for the Expansion of the Nahanni National Park Reserve, Northwest Territories; Geological Survey of Canada, Open File 5344, p. 177-190.

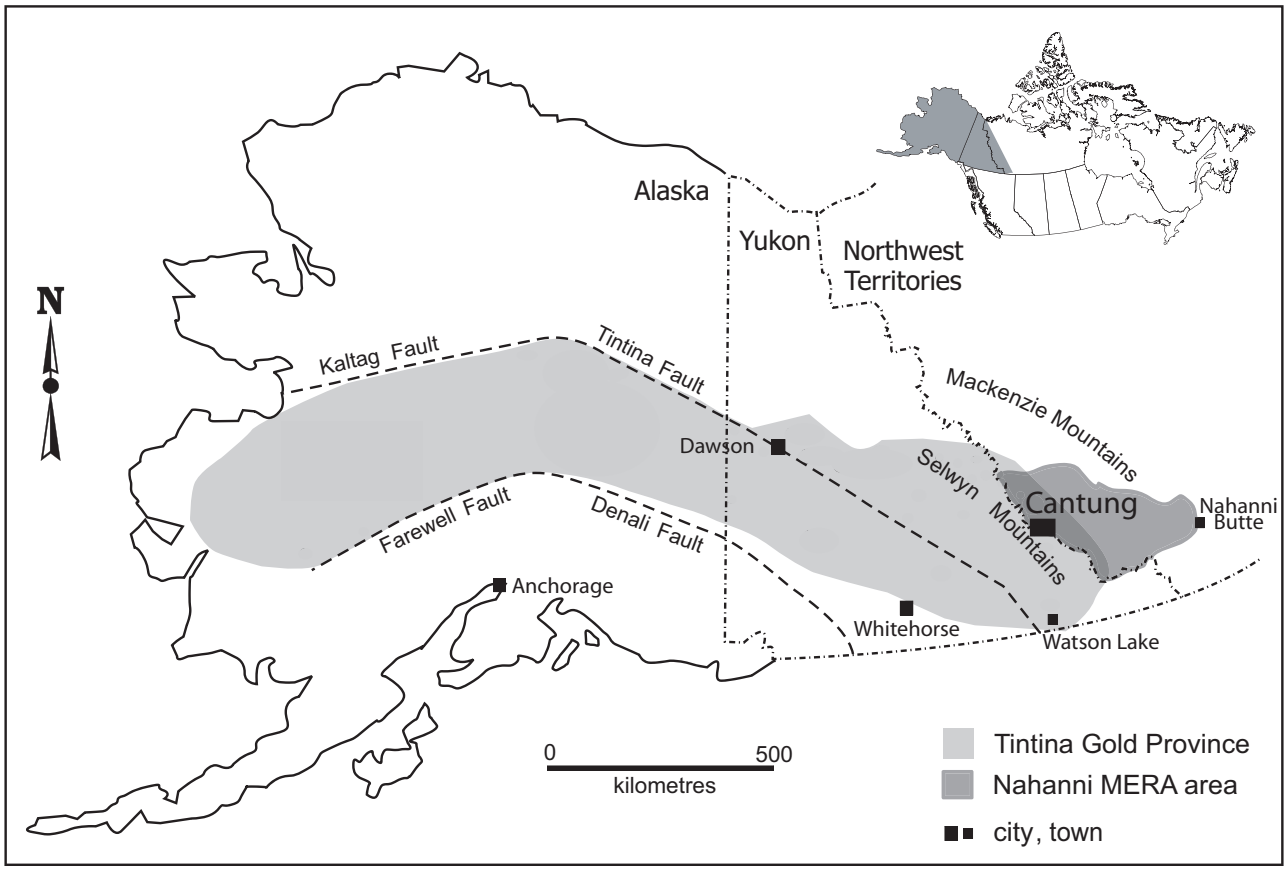


Figure 1. Location of the Cantung mine, Northwest Territories, Canada. Modified after Mortensen et al. (2000) and Rasmussen et al. (2006).

Aplite dykes that crosscut both orebodies share a common structural attitude with quartz-scheelite veins from the open pit orebody, suggesting a possible genetic relationship.

RATIONALE FOR STUDY

Geochemical assessment of high-grade quartz-scheelite veins and examination of their spatial and temporal relationship to aplite dykes tests the possibility that the veins may represent distal products of a protracted magmatic-hydrothermal event. If this idea proves true at Cantung, there are important implications for recognizing similar distal granite-related deposits regionally. Distal exploration targets need not be manifested as massive skarns, but could take on various forms depending on the geometry and chemistry of the host lithologies. Vein and replacement-type deposits in metasedimentary rocks of the Tungsten region frequently have been assumed to represent older ore events. Their origins should be re-evaluated, as some of them could instead represent distal, granite-related deposits.

This report constitutes a portion of a M.Sc. thesis by Jason Yuvan at the Department of Geological Sciences at the University of Missouri-Columbia (Yuvan, 2006).

QUESTIONS ADDRESSED

Specific questions addressed in this assessment includes the following:

1. Did the quartz-scheelite veins form at similar high temperatures and pressures as the skarn ores? Or, do they represent a cooler, shallower hydrothermal system that developed after uplift of the area?
2. Did late skarn-forming fluids form the quartz-scheelite veins or do the veins represent a unique fluid chemistry?
3. Do the quartz-scheelite veins that share a common structural attitude with aplite dykes also share a genetic relationship with them?
4. What are the implications for regional resource assessment if the veins represent a distal expression of a protracted magmatic skarn-forming event?

GEOLOGY

The Cantung mine is located within a polymetallic W-Au province of the Northwest Territories near the Yukon border (Brown, 1961; Lang et al., 2000; Baker et al., 2005). Proterozoic and Cambrian metasedimentary rocks that host ore deposits in the Cantung area include, from oldest to youngest, the lower argillite, the swiss cheese limestone, the ore limestone, and the upper argillite (Fig. 2).

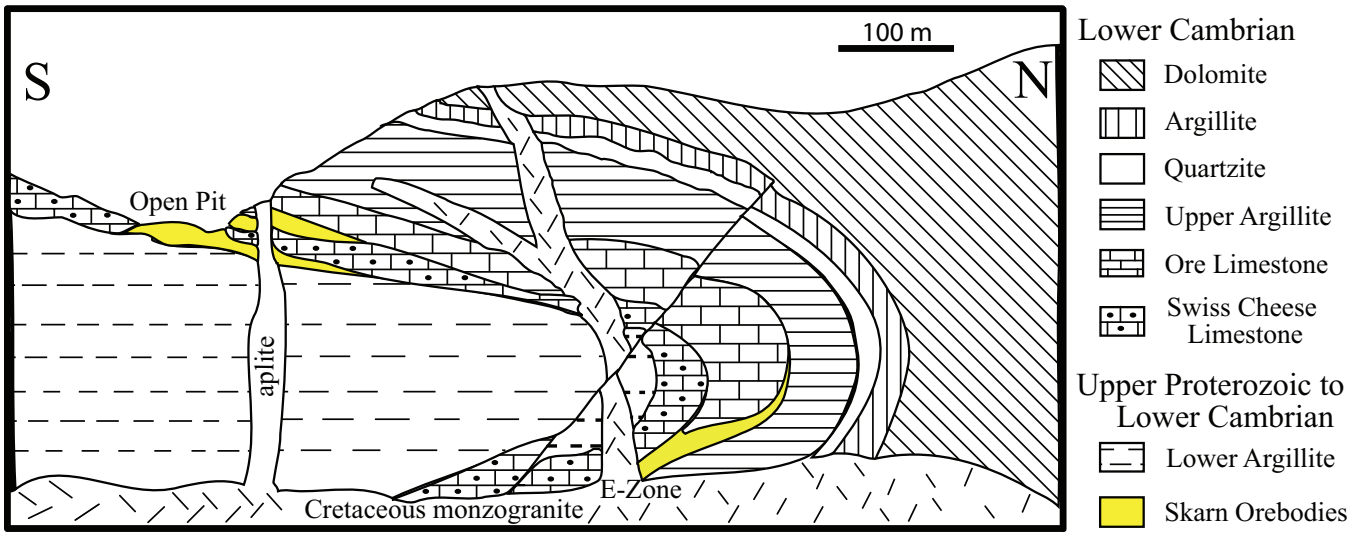


Figure 2. Idealized cross-section of the E-Zone and open pit orebodies at Cantung after Cummings and Bruce (1977). A Cretaceous granite intruded a sequence of folded and overturned Cambrian metasedimentary rocks. The E-Zone and open pit orebodies are separated vertically by approximately 300 m, although they are developed in the same stratigraphic units.

The Upper Proterozoic lower argillite is light brown to dark grey and fine-grained (Zaw, 1976). It is infrequently fractured and crosscut by aplite dykes and quartz veins in the Cantung mine area.

The Lower Cambrian swiss cheese limestone contains massive, boudinaged or nodular calcareous pods and lenses, composed of microcrystalline calcite, intercalated with siltstone (Blusson, 1967; Rasmussen, 2004). The siltstone is composed of cryptocrystalline clay minerals, carbonates, and quartz (Crawford, 1963).

The ore limestone is composed of anhedral, finely crystalline calcite. It is vaguely laminated with dark and light grey to white layers. It is a relatively clean limestone receptive to skarn development.

The upper argillite is brown to grey and interbedded with thin, impure carbonate, mudstone, and sandstone lenses. Carbonate lenses are converted to calc-silicate skarns (Dick and Hodgson, 1982).

Due to differences in reactivity of the metasedimentary units, the unreactive upper and lower argillites appear to act as confining units for ore fluid flow. Where breached by faults and fractures, fluids gain access to more reactive units higher in the section. The more reactive swiss cheese and ore limestones host ore at the contact with the Mine Stock (E-Zone orebody) and approximately 300 m vertically above the contact (open pit orebody).

Skarn Orebodies

E-Zone Orebody

The underground E-Zone orebody is hosted in the ore limestone at the mine stock-ore limestone contact. It occurs on the flat to gently dipping east limb of an overturned anticline and has a tabular cross-section (Blusson, 1967). The E-Zone orebody is approximately 40 to 200 m wide and 450 m in length, containing 4.2 Mt of ore averaging 1.6 wt.% WO_3 (Zaw, 1976; Mathieson and Clark, 1984). Four mineral assemblages were documented in the skarn orebodies and interpreted as facies by Dick (1980) and Dick and Hodgson (1982): garnet-pyroxene, pyroxene-pyrrhotite, amphibole-pyrrhotite, and biotite-pyrrhotite. Scheelite is present in all four assemblages, but its abundance increases with increasing pyrrhotite content.

Open Pit Orebody

The open pit orebody is located approximately 300 m above the E-Zone orebody (Figs. 2 and 3). It is hosted

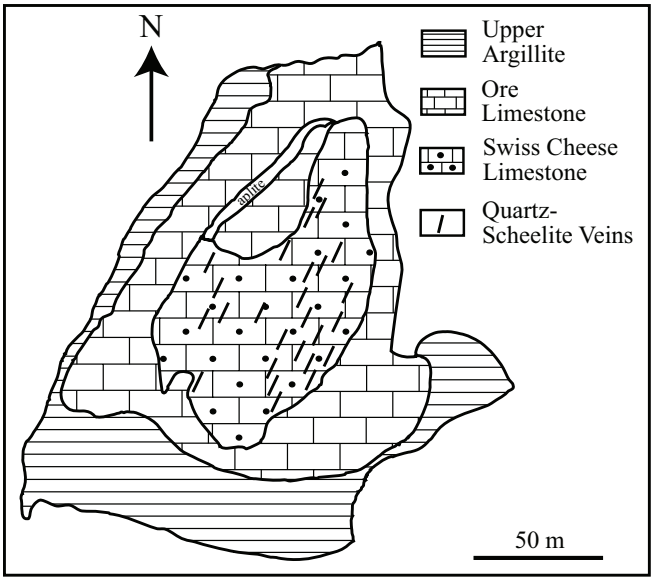


Figure 3. Geologic map of the open pit orebody at Cantung showing the en échelon pattern and trend of the vein swarm. Note the trends of the aplite dyke and quartz-scheelite veins are almost parallel.

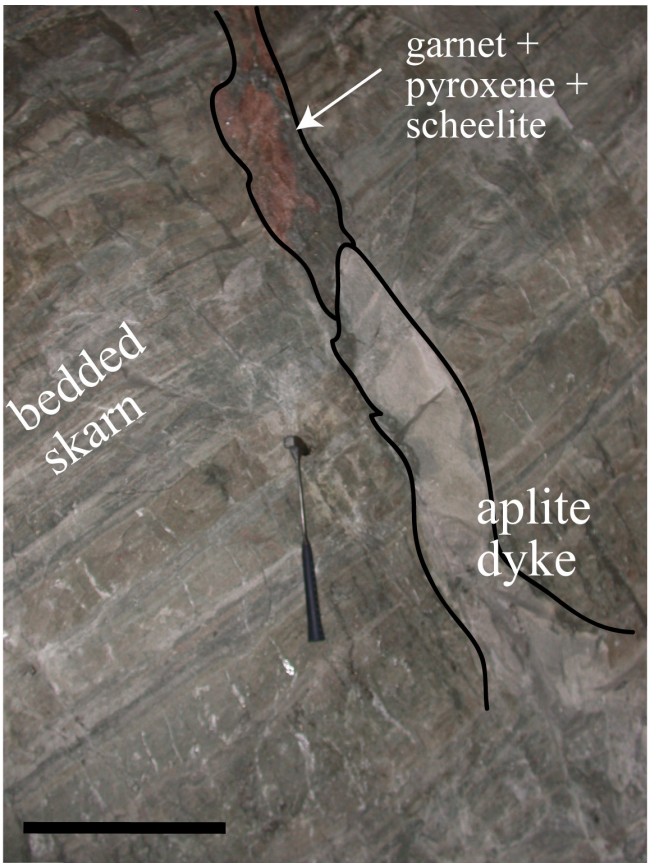


Figure 4. Photograph of aplite dyke crosscutting E-Zone orebody from the 3850 drift. The aplite pinches out and extends upward into pyroxene-garnet alteration with abundant scheelite. Scale bar is 50 cm.

within the base of the ore limestone and in the upper swiss cheese limestone, where calcareous lenses were converted preferentially to skarn. Main ore-bearing skarn zones are tabular in shape and approximately 200 m long, 90 m wide, and up to 25 m thick. Because the orebody is within 120 m of a fault that predates ore formation, Zaw (1976) hypothesized that this fault acted as a conduit for migrating ore fluids. Hodgson (2000), however, stated that a nearby aplite dyke could also be responsible for the influx of ore fluids. In the open pit orebody, scheelite-bearing skarn is dominated by anhydrous garnet-pyroxene mineral assemblages. An 80 m wide en échelon swarm of high-grade quartz-scheelite veins crosscuts the open pit orebody along a 025º trend (Fig. 3).

Igneous Rocks

Mine Stock

The Mine Stock is a monzogranite, consisting of quartz, plagioclase, K-feldspar, and biotite (Rasmussen, 2004). It is an S-type granitoid and conforms to Ishihara's (1977) "ilmenite-series" (Mathieson and Clark, 1984; Christiansen and Keith, 1996). For detailed lithogeochemistry of the intrusion, see Rasmussen et al. (2006).

Dating of the Mine Stock by Rasmussen et al. (2006) yielded a U-Pb zircon age of approximately 98.2 ± 0.4 Ma. Intrusion biotites yielded an $^{40}Ar/^{39}Ar$ cooling age of 95.1 ± 0.4 Ma. The difference in ages was interpreted to indicate slow cooling of the Mine Stock over a time interval of up to 3 m.y. This is sufficient time to develop an extensive magmatic system capable of depositing the world class tungsten skarn at Cantung and later-vein deposits during the waning stages of such a protracted magmatic-hydrothermal skarn-forming event.

Aplite Dykes

Aplite dykes, present as both pre- and post-skarn intrusions (Bowman et al., 1985; Rasmussen, 2004), crosscut the Mine Stock and the open pit and E-Zone orebodies. Aplite dykes crosscutting the E-Zone orebody are less than 2 cm to 1 m thick and are concentrated around the Mine Stock's margins. In the open pit orebody, aplite dykes are 2 to 5 m wide with alteration selvedges of 10 to 20 cm (Rasmussen, 2004).

In the E-Zone and open pit orebodies, aplite dykes are similar geochemically. Aplite dykes contain phenocrysts of quartz, plagioclase, K-feldspar, tourmaline, and biotite, but quartz and tourmaline are the only phenocrysts that have not been altered and which retain sharp grain margins. Potassic, sericitic, calcic, and albitic alteration styles have all been observed within the aplite dykes (Rasmussen, 2004).

Aplite dykes display two interesting features relative to ore. Firstly, aplite dykes from the E-Zone orebody can be seen crosscutting skarn and extending into massive garnet-pyroxene alteration with abundant scheelite (Fig. 4). These aplite dykes could have leached tungsten from deeper in the skarn orebody and concentrated tungsten at higher levels. Alternatively, the aplite dykes

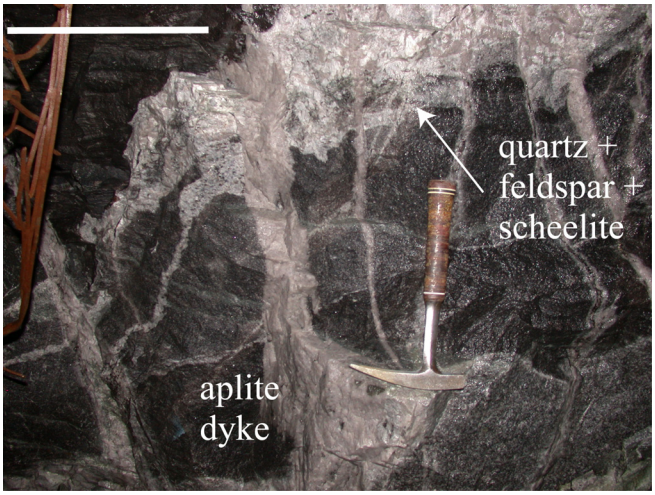


Figure 5. Photograph of aplite dykes grading vertically into quartz-scheelite vein in the E-Zone orebody near the Four Corners area of the 4100 level. These veins are similar to the high-grade quartz-scheelite veins in the open pit orebody. Scale bar is 30 cm.



Figure 6. Photograph of quartz-scheelite vein in the open pit orebody within diopsidic skarn. Note the presence of dark green alteration adjacent to the vein that overprints earlier light green skarn alteration. Rust-coloured veinlet near the vein center is pyrrhotite rich. Scale bar is 10 cm.

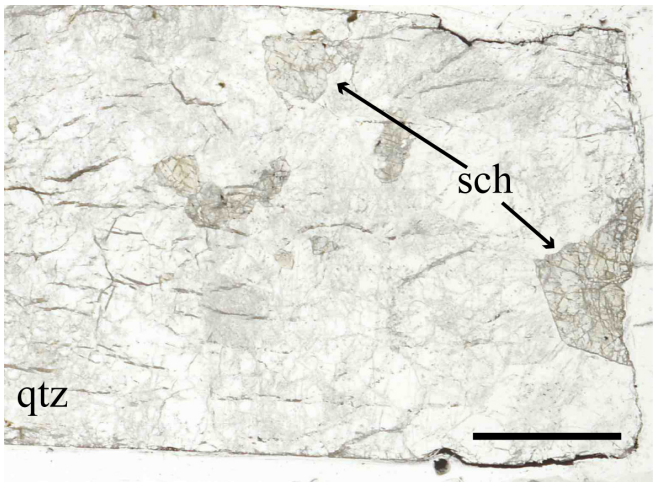


Figure 7. Photograph of polished thin section of high-grade quartz-scheelite vein HF03-17 from the open pit orebody. Note the highly fractured nature of the vein. Dark lineations in quartz are healed fractures containing abundant secondary aqueous brine inclusions. Scale bar is 1 cm. Abbreviations: sch=scheelite; qtz=quartz.

could be bringing in a new, unique source of tungsten. No matter which explanation is correct, these aplite dykes are responsible for localized higher concentrations of tungsten, increasing the economic feasibility of mining the ore. Secondly, some aplite dykes from the E-Zone orebody can be seen grading vertically into quartz-scheelite veins (Fig. 5). These E-Zone quartz veins are similar in mineralogy to the high-grade quartz-scheelite veins crosscutting the open pit orebody and suggest a possible genetic link related to aplite emplacement.

Quartz Veins

Quartz-scheelite veins from the open pit orebody are 10 cm to 1 m wide (Fig. 6). They are usually unzoned or crudely zoned and contain massive, white quartz and lesser amounts of clear quartz, typically where adjacent to scheelite (Fig. 7). Scheelite is up to 2 cm in diameter. It is white to light orange in hand specimen and fluoresces blue under ultraviolet light. Scheelite is found as isolated, fractured, euhedral to subhedral grains or as crystal clusters in the central parts of veins or adjacent to wall rock contacts. Blocky, white alkali feldspar grains are present infrequently in some veins. Sulphides, dominantly pyrrhotite and minor chalcopyrite, occur as pods and filling late veinlets within massive quartz (Fig. 6).

Infrequently, quartz-scheelite veins from the open pit orebody contain biotite-rich masses containing abundant fine-grained scheelite. These are similar mineralogically to biotite-pyrrhotite assemblages in the underground E-Zone skarn orebody and may indicate that the open pit veins are late, distal products related to the magmatic skarn-forming event.

High-grade quartz-scheelite veins from the open pit orebody are steeply dipping (~90°) and have strikes between 000 and 080°, with most near 030° (Fig. 8A). The overall trend of the 80 m wide en échelon vein swarm is approximately 025° (Fig. 3). Aplite dykes, faults, fractures, and sulphide veinlets from the E-Zone and open pit orebodies have strikes between 000 and 080° (Fig. 8B), with most near 030°. If fluids and felsic magmas utilized the same subparallel structural pathways, it is also possible that they may have shared a common genetic relationship.

Vein Alteration

The high-grade quartz-scheelite veins from the open pit orebody have dark green alteration selvedges up to 15 cm wide. This alteration overprints light green alteration associated with development of the earlier open pit skarn (Fig. 6). The dark green alteration adjacent to the veins consists of finer grained diopside, quartz, opaque minerals, and lesser chlorite (Fig. 9A). Earlier, light green skarn alteration consists of coarser grained diopside, quartz, K-feldspar, and calcite with minor epidote, chlorite, and garnet (Fig. 9B).

The overprinting nature of the vein-related alteration indicates that the high-grade quartz-scheelite veins represent a later event distinct from the early skarn-forming event (Yuvan et al., 2005).

Trace Metal Analysis of Veins

Due to their simple mineralogy, consisting dominantly of quartz, scheelite, and pyrrhotite, it is difficult to link the quartz-scheelite veins definitively to a particular event in the protracted history of skarn formation at Cantung. Trace metal concentrations may be more useful in determining the source(s) of metals and fluid(s)

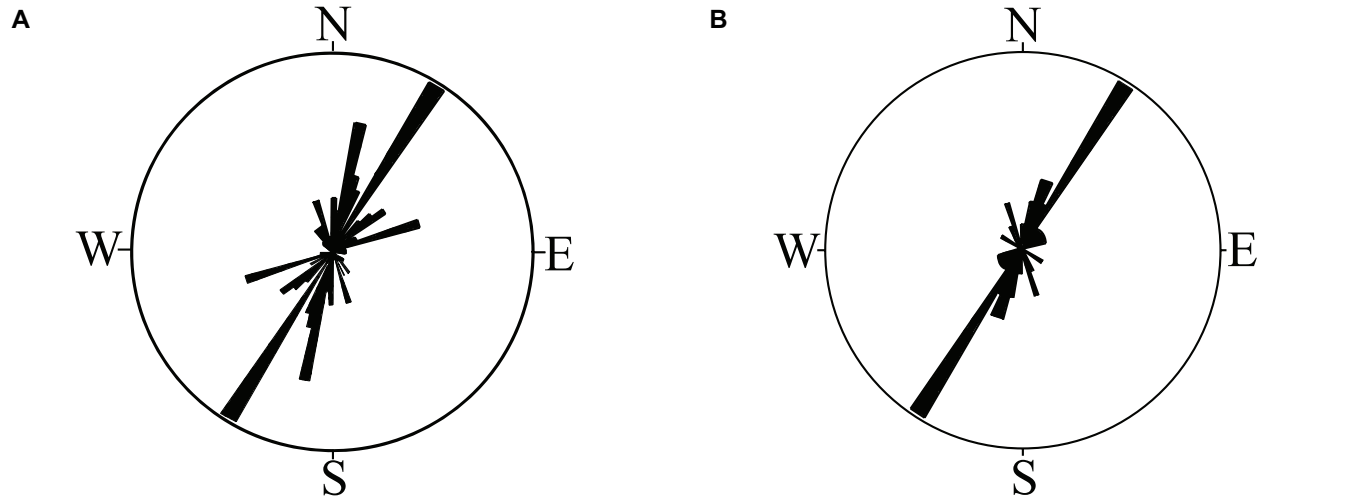


Figure 8. Equal area rose diagrams. **A)** strikes of quartz-scheelite veins from the open pit orebody. Outer circle is 19% of the data. Strikes cluster around 030°. **B)** trends of aplite dykes, fractures, faults, and sulphide veinlets within quartz veins from the E-Zone and open pit orebodies. Outer Circle is 29% of the data. These features also cluster around 030°, similar to the strikes of high-grade quartz-scheelite veins in the open pit orebody. Diagrams made using Stereowin program of Allmendinger (2002).

responsible for deposition of quartz-scheelite veins in the open pit orebody.

Potential metal sources may include magmas and igneous rocks, or metals remobilized from country rocks. Magmatic sources could have metal suites similar to those of the Mine Stock-related E-Zone skarn ores, namely W ± Mo. Alternatively, aplite-related sources could have distinct metal suites (Stern et al., 1986). It is possible that some magmatic metal sources may have metal suites, including Au, Bi, Cu, and Ag, similar to those in regional quartz veins of the Cantung area thought to represent Intrusion Related Gold Deposits (IRGD) (Lang et al., 2000; Baker et al., 2005).

Alternatively, if the quartz-scheelite veins in the open pit orebody at Cantung formed in a shallow, possibly meteoric, hydrothermal system after uplift, metals could have been leached from many different lithologies, including metasedimentary and igneous rocks.

Trace metal concentrations (ppm) and W ore grades (wt.% WO_3) were determined for fourteen quartz-scheelite veins from the open pit orebody by ICP-OES analysis at ACT Labs, Vancouver. Errors are typically 1.0 to 2.0% of the measured concentration.

Interpretation of Trace Metal Values

The authors tested the correlation of various trace metals with tungsten to determine if the trace metals in the quartz-scheelite veins are coming from the same source as the main ore metal at Cantung. A plot of Mo (ppm) and WO_3 (wt.%) has a linear correlation coefficient (R) of 0.71 (Fig. 10A). This strong correlation is common in tungsten ore deposits because of the similar geochemistry of tungsten and molybdenum (Ivanova,

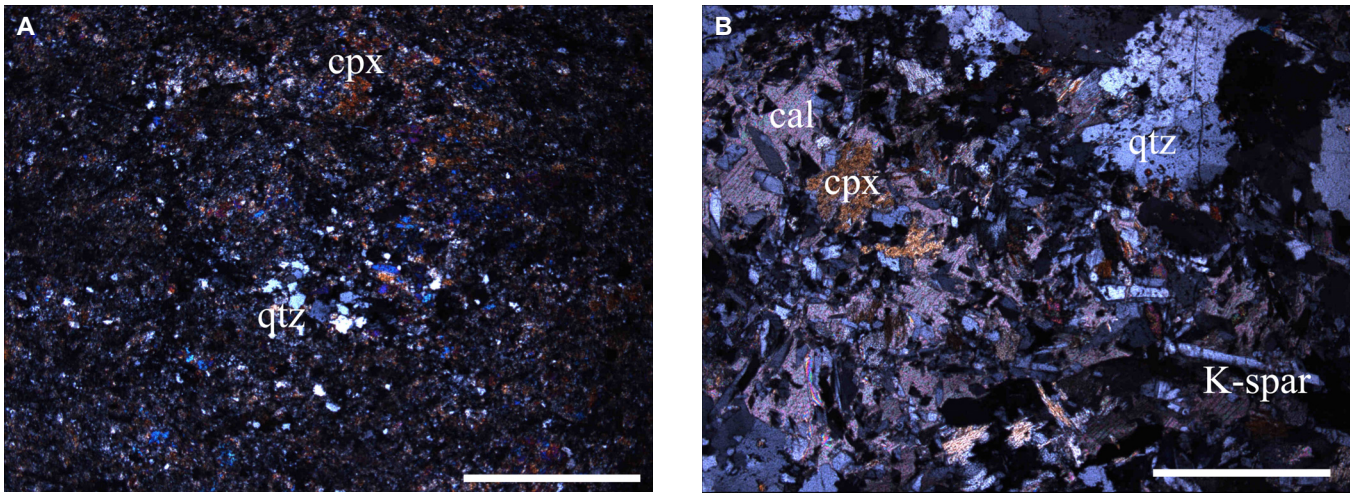


Figure 9. A) Finer grained alteration adjacent to quartz-scheelite vein in the open pit orebody. **B)** Coarser grained skarn alteration 15 cm from the quartz-scheelite veins. Both views under cross-polarized light at 4x. Scale bars are 0.5 mm in length. Abbreviations: cal=calcite; cpx=clinopyroxene; k-spar=potassium feldspar; qtz=quartz.

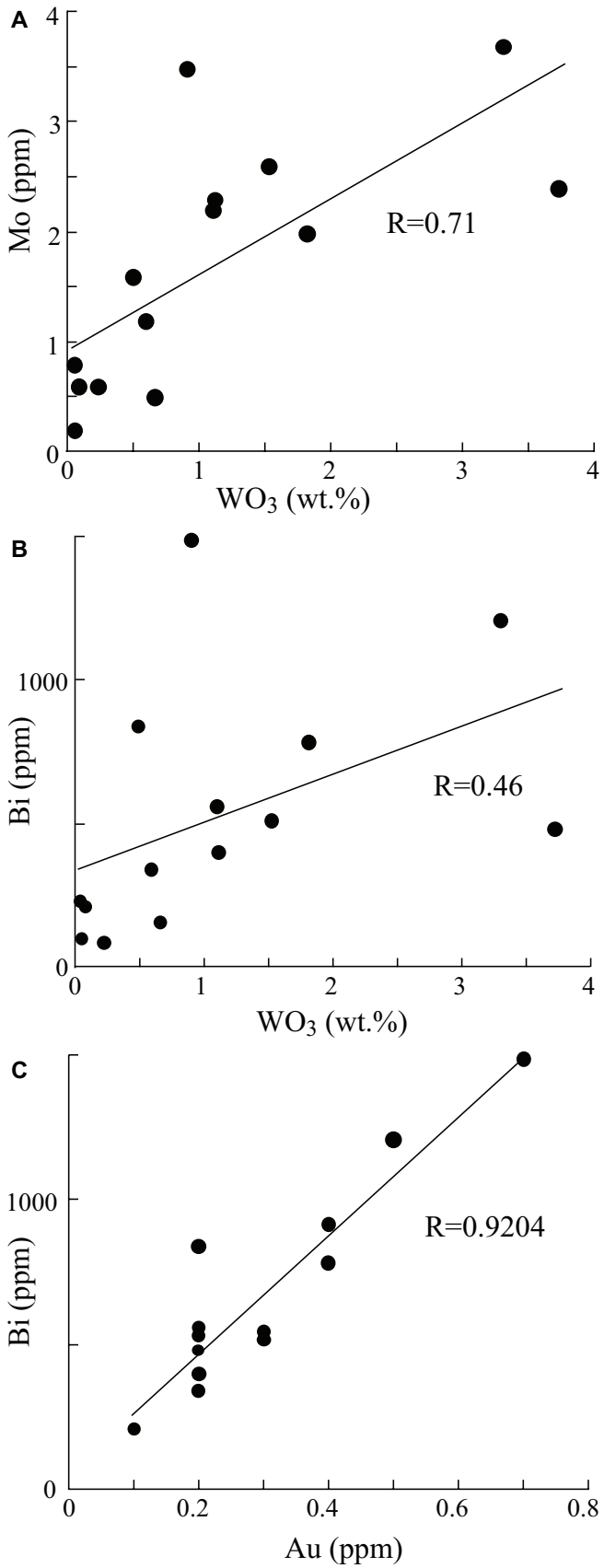


Figure 10. Plots of trace metal contents of high-grade quartz-scheelite veins from the open pit orebody. **A)** Mo (ppm) versus WO_3 (wt %). **B)** Bi (ppm) versus WO_3 (wt.%). **C)** Bi (ppm) versus Au (ppm). R = linear correlation coefficient.

1986). This implies that tungsten and molybdenum likely had a similar source region. A similar correlation should exist for the E-Zone skarn orebody, as molybdenite (MoS_2) and powellite ($CaMoO_4$) are present in minor amounts in the scheelite skarn orebodies at Cantung.

A plot of Bi (ppm) versus WO_3 (wt.%) has an R value of 0.46 (Fig. 10b). The lower correlation coefficient for tungsten and bismuth, compared to that for tungsten and molybdenum, may imply that bismuth was derived from a different source than tungsten (or molybdenum).

By contrast, a plot of Bi (ppm) versus Au (ppm) has the highest correlation, R = 0.92 (Fig. 10C). This correlation implies that the source for bismuth is likely the same as that for gold. Copper and silver have correlation coefficients of 0.59 and 0.69, respectively, when plotted versus Bi. Therefore, Cu and Ag may also reflect a similar source with Bi and Au that is unrelated to the source of tungsten in the Cantung mine.

Mathieson and Clark (1984) reported that bismuth and copper were byproducts of tungsten ores of the E-Zone skarn orebody. We have documented correlated enrichments of Au, Ag, and Cu with Bi in high-grade quartz-scheelite veins of the open pit orebody, 300 m vertically above the E-Zone skarn orebody. We hypothesize that byproduct Bi and Cu (as well as Au and Ag) in the underground E-Zone skarn orebody may be the result of an overprint by a late-stage magmatic-hydrothermal system responsible for the quartz-scheelite veins in the overlying open pit orebody.

FLUID INCLUSIONS IN VEINS AND APLITES

Thirty-seven quartz vein and aplite dyke samples from the open pit and E-Zone orebodies were prepared as 100 μm-thick doubly polished thin sections for fluid inclusion analysis (Yuvan, 2006). The abundance and quality of fluid inclusions resulted in thirty-three of the doubly polished thin sections yielding results.

Microthermometric data were obtained using a FLUID Inc. gas-flow heating/freezing stage calibrated with pure CO_2 and H_2O inclusions (Shelton and Orville, 1980). Temperatures of total homogenization (T_h) have standard errors of ±2°C, and temperatures of melting (T_m of ice, clathrate, and solid CO_2) and homogenization of the carbonic phase ($T_{h\ CO2}$) have standard errors of ± 0.2°C. The composition and density of trapped fluids were determined from thermometric data using the MacFlinCor program (Brown and Hagemann, 1995) and the compiled data of Kerrick and Jacobs (1981), Bodnar and Vityk (1994), and Thiery et al. (1994).

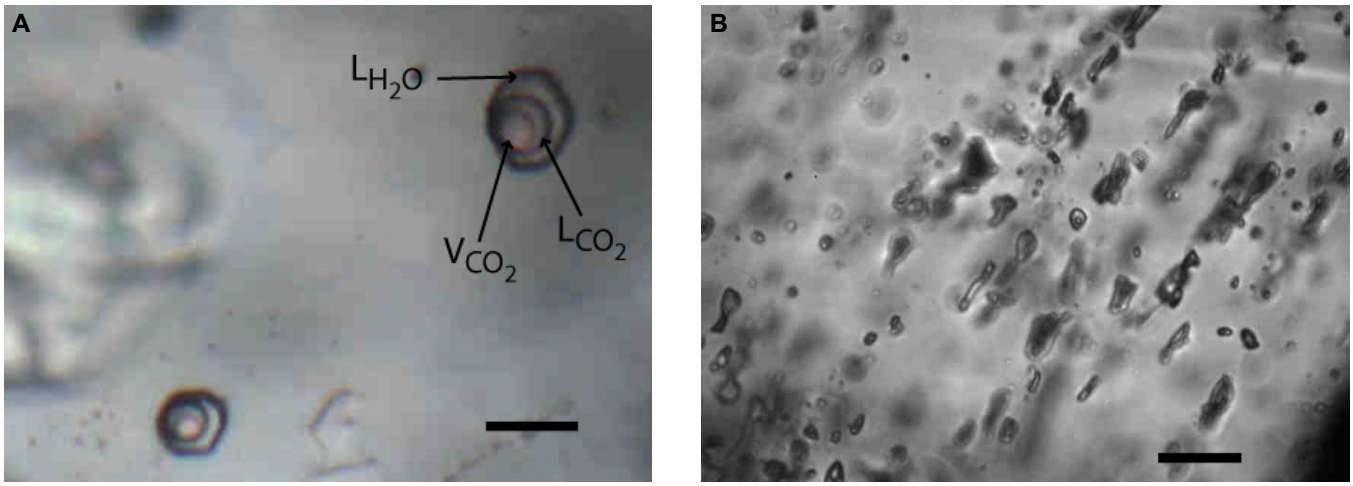


Figure 11. A) Photomicrograph showing primary H_2O-CO_2-NaCl±CH_4 inclusions in scheelite. These three-phase inclusions (vapour CO_2, liquid CO_2, and liquid H_2O) typically have negative crystal shapes. Scale bar is 30 µm. **B)** Two-phase aqueous brine inclusions in vein quartz. Scale bar is 20 µm. These inclusions are typically arranged in linear trails indicating a likely secondary origin. The trails appear to impart a lineation to the samples, similar to those observed in Figure 7.

Occurrence and Compositional Types of Fluid Inclusions

Fluid inclusions were found in quartz and scheelite from quartz veins and in tourmaline and quartz grains from aplite dykes. Two compositional types of fluid inclusions have been identified based on their phase relationships at 20°C and behavior upon cooling: H_2O-CO_2-NaCl±CH_4 and aqueous brine inclusions.

H_2O-CO_2-NaCl±CH_4 Inclusions

These inclusions are present as isolated inclusions and three-dimensional clusters of inclusions in quartz, tourmaline, and scheelite, indicating a primary origin. This fluid type is interpreted to be the ore fluid.

At 20°C, these inclusions consist of two (liquid H_2O + CO_2 dominant liquid) or three phases (liquid H_2O + liquid CO_2 + vapour CO_2). Upon cooling, the two-phase inclusions generated a third phase, vapour CO_2. The volume percentage of liquid + vapour CO_2 in these inclusions is typically between 25 and 55%. Typical XCO_2 + CH_4 values range from 0.02 to 0.30.

These inclusions have more regular shapes than the aqueous brine inclusions and range from less than 5 to 30 µm in length (Fig. 11A). Negative crystal shapes are common among these inclusions, especially when hosted by scheelite.

Aqueous Brine Inclusions

All samples examined contain these two-phase (liquid + vapour) aqueous inclusions (Fig. 11B). Vapour occupies 5 to 30 volume per cent of these inclusions. Aqueous brine inclusions are less than 5 to 20 µm in length, typically near 10 µm. They occur in trails or planes, indicating a secondary origin. Aqueous brine inclusions typically have highly irregular shapes. They are fre-

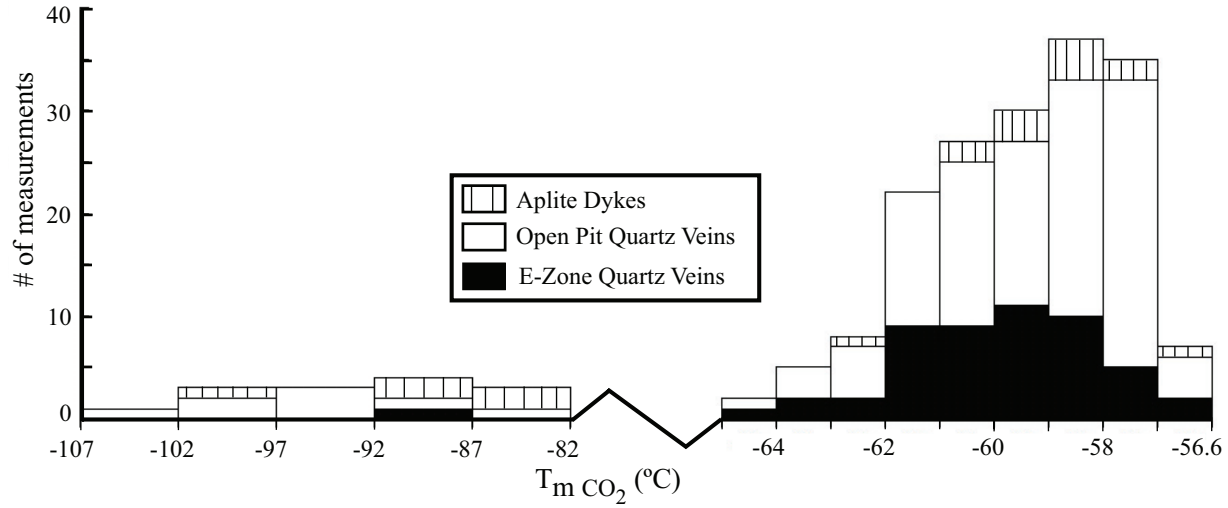


Figure 12. Frequency diagram for the temperature of last CO_2 solid melt ($T_{m\ CO2}$) for primary H_2O-CO_2-NaCl±CH_4 fluid inclusions in aplite dykes, quartz-scheelite veins in the open pit orebody, and quartz veins in the E-Zone orebody. Note the horizontal scale is different for the left and right sides of the diagram.

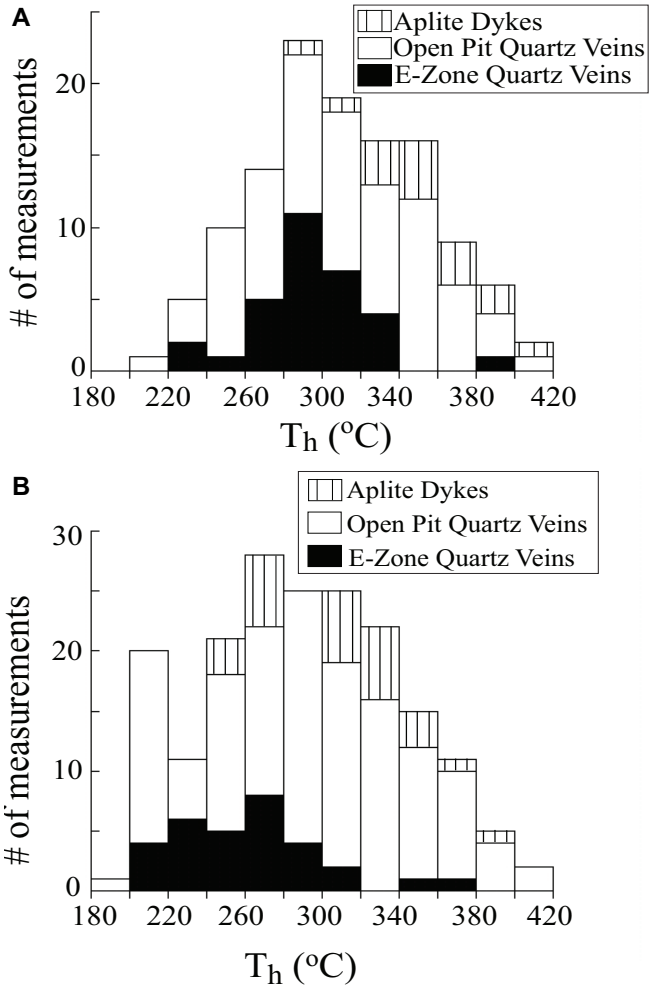


Figure 13. Total homogenization temperatures (Th) for **(A)** H_2O-CO_2-NaCl±CH_4 inclusions and **(B)** aqueous brine inclusions. Diagram includes inclusions that decrepitated as they approached homogenization.

quently elongated in preferred directions and may appear to impart a lineation to the samples (Figs. 7, 11).

Similar aqueous brine inclusions were observed at Cantung by Zaw (1976) and Mathieson and Clark (1984). These inclusions were interpreted by those authors to be the ore fluid, likely because of their overwhelming abundance and ubiquitous occurrence. However, based on textural relationships, we believe that the aqueous brine inclusions are secondary fluids unrelated to ore formation.

Microthermometric Data

Approximately two hundred H_2O-CO_2-NaCl±CH_4 inclusions and three hundred aqueous brine inclusions were measured microthermometrically (Yuvan, 2006).

H_2O-CO_2-NaCl±CH_4 Inclusions

These inclusions contain solid and vapour CO_2 and ice when cooled to approximately -150°C. Upon heating, the first melting of the solid CO_2 ($T_{f\ CO_2}$) occurs between -125.9 and -76.2°C.

Final melting temperatures of the solid CO_2 ($T_{m\ CO_2}$) form two groups, from -64.4 to -56.6°C and -110.6 to -82.1°C (Fig. 12). The carbonic phase of the higher temperature group has XCH_4 values of 0.0 to 0.21, whereas the carbonic phase of the lower temperature group has XCH_4 values of 0.93 to 0.96.

The carbonic phases of H_2O-CO_2-NaCl±CH_4 inclusions in quartz-scheelite veins from the open pit orebody have homogenization temperatures ($T_{h\ CO_2}$) that vary from -86.4 to +28.7°C, dominantly to the liquid phase. The $T_{h\ CO_2}$ values yield carbonic phase densities of 0.28 to 0.91 g/cm^3. Similar inclusions in quartz veins from the E-Zone orebody have $T_{h\ CO_2}$ values of -6.8 to +23.9°C, corresponding to carbonic phase densities of 0.39 to 0.81 g/cm^3. H_2O-CO_2-NaCl±CH_4 inclusions in aplite dykes from the E-Zone and open pit orebodies have $T_{h\ CO_2}$ values of -87.8 to +8.1°C, yielding carbonic phase densities of 0.28 to 0.97 g/cm^3.

Clathrate melting temperatures ($T_{m\ clath}$) are 2.1 to 18.3°C. Methane clathrates are known to melt as high as 18°C (Roedder, 1984). $T_{m\ clath}$ values correspond to fluid salinity values (calculated up to only 10°C, because of the limits of the MacFlinCor program,) of 0.2 to 9.5 wt.% equivalent NaCl (Diamond, 1992; Brown and Hagemann, 1995). The low $T_{f\ CO_2}$ values and $T_{m\ CO_2}$ values, below -56.6°C, along with the high $T_{m\ clath}$ values (>10°C), indicate that other ions, such as H_2S and CH_4, are present in the H_2O-CO_2-NaCl±CH_4 fluid (Collins, 1979; Burruss, 1981).

Total homogenization temperatures (Th) range from 218 to 401°C (Fig. 13A). As they were approaching homogenization, about half of the H_2O-CO_2-NaCl±CH_4 inclusions decrepitated.

Aqueous Brine Inclusions

First ice melting temperatures (T_e) in aqueous brine inclusions range from -49.7 to -21.5°C, which attests to the presence of other salts in addition to NaCl, such as $CaCl_2$ and KCl (Crawford, 1981; Zhang and Frantz, 1989). Final ice melting temperatures ($T_{m\ ice}$) are between -0.4 and -8.8°C, yielding salinity values between 0.7 and 12.6 wt.% equivalent. NaCl. These salinity values are similar to values of 4 to 14 wt.% equivalent. NaCl found by Mathieson and Clark (1984). T_h values, to the liquid phase, range from 188 to 404°C (Fig. 13B).

Interpretation of Fluid Inclusion Data

Primary ore fluids in quartz-scheelite veins from the open pit orebody, quartz veins from the E-Zone orebody, and aplite dykes from both orebodies are grossly similar H_2O-CO_2-NaCl±CH_4 fluids. However, plots of

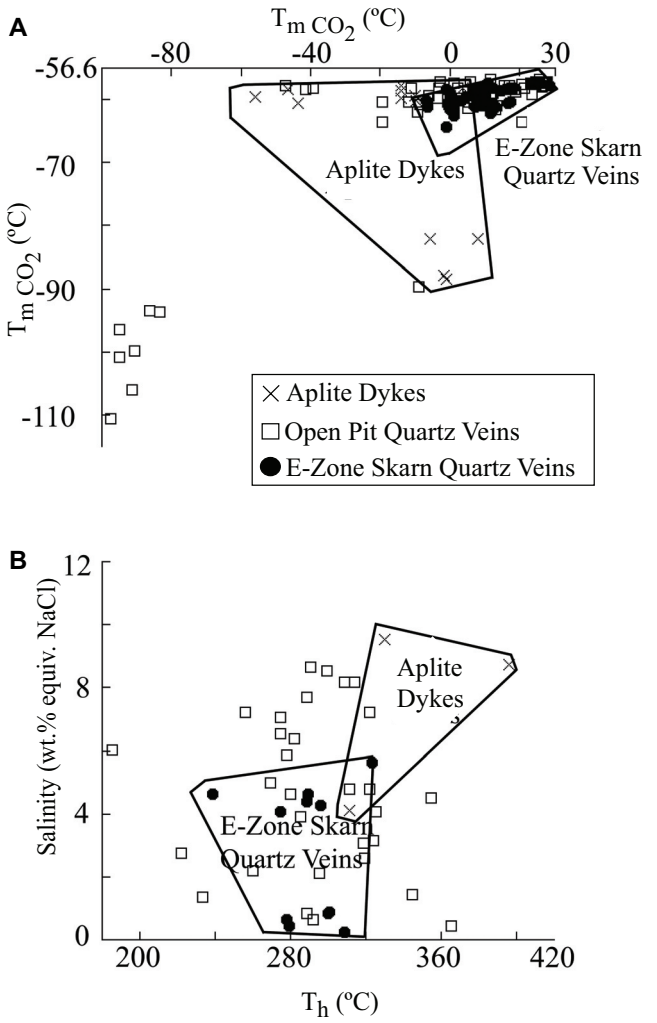


Figure 14. A) $T_{h\ CO_2}$ versus $T_{m\ CO_2}$ values for H_2O-CO_2-NaCl±CH_4 inclusions. Fluids in aplite dykes plot at lower $T_{h\ CO_2}$ values (lower densities) and lower $T_{m\ CO_2}$ values (higher XCH_4). Fluids in skarn-related quartz veins from the E-Zone orebody plot at higher $T_{m\ CO_2}$ values (higher densities) and higher $T_{m\ CO_2}$ values (less XCH_4). Fluids in high-grade quartz-scheelite veins from the open pit orebody overlap both fields outlined by fluids in aplite dykes and quartz veins from the E-Zone orebody. **B)** Salinity versus Th values for H_2O-CO_2-NaCl±CH_4 inclusions. Fluids in aplite dykes and those in skarn-related quartz veins from the E-Zone orebody form distinct end-members. Fluids in high-grade quartz-scheelite veins from the open pit orebody overlap both fields.

$T_{m\ CO_2}$ versus $T_{h\ CO_2}$ (Fig. 14A) and salinity versus T_h values (Fig. 14B), indicate that two distinct end-member fluids exist, a skarn-related fluid and an aplite-related fluid.

Figure 14A is a plot of $T_{m\ CO_2}$ versus $T_{h\ CO_2}$. The vertical axis, $T_{m\ CO_2}$, is dependent on the CH_4 content of the carbonic phase of H_2O-CO_2-NaCl±CH_4 inclusions, with higher XCH_4 values at lower temperatures and lower XCH_4 values at higher temperatures. The horizontal axis, $T_{h\ CO_2}$, is dependent on the density of the carbonic phase of H_2O-CO_2-NaCl±CH_4 inclusions, with lower densities at lower temperatures and higher densities at higher temperatures. Fluids in aplite dykes (from the E-Zone and open pit orebodies) define a broad field at low $T_{m\ CO_2}$ and $T_{h\ CO_2}$ values (higher CH_4, lower density fluid). Fluids in skarn-related quartz veins from the E-Zone orebody are restricted to a narrower field of higher $T_{m\ CO_2}$ and $T_{h\ CO_2}$ values (lower CH_4, higher density fluid). Fluids in high-grade quartz-scheelite veins from the open pit orebody overlap both end-member fluid fields.

Figure 14B is a plot of T_h values versus salinity. Fluids in aplite dykes (from the E-Zone and open pit orebodies) define a field of higher T_h and salinity values. Fluids in skarn-related quartz veins from the E-Zone orebody form a distinct field of lower T_h and salinity values. As in Figure 14A, fluids in high-grade quartz-scheelite veins from the open pit orebody overlap both end-member fluid fields.

Regardless of whether they overlap the aplite dyke field or the skarn-related E-Zone quartz vein field of Figure 14, H_2O-CO_2-NaCl±CH_4 fluid inclusions in high-grade quartz-scheelite veins from the open pit orebody are primary inclusions. This observation requires that both end-member fluids entrapped in the veins were present contemporaneously. The fluid end-members may have been trapped individually, or the fluids may have mixed, with the entrapped fluids consisting of various mixtures of the fluid components. In either scenario, there is an apparent influence of aplite dyke-related fluids on the quartz-scheelite vein swarm even though veins occur up to 70 m laterally from the nearest visible aplite dyke. The authors envision a scenario in which quartz-scheelite veins and aplite dykes utilized the same structures to ascend from the subjacent Mine Stock, so it should be no surprise that the quartz veins entrapped an aplite-related fluid.

Pressure-Temperature Considerations

There is no evidence for unmixing of the ore fluids in the Cantung hydrothermal system. There is a lack of fluid inclusions homogenizing to the vapour phase. Most inclusions have similar vapour to liquid ratios. We did not recognize a high salinity inclusion assemblage or a high $XCO_2 + CH_4$ inclusion assemblage that might be expected from unmixing. The lack of unmixing implies a minimum pressure of 2 kbar for the high-grade quartz-scheelite veins from the open pit orebody (Gehrig, 1980).

Better estimates of pressure can be made using representative isochores for primary H_2O-CO_2-NaCl±CH_4 fluid inclusions in quartz-scheelite veins from the open pit orebody (Fig. 15). Isochores were calculated using the MacFlinCor program (Brown and Hagemann, 1995) and our microthermometric data (Yuvan, 2006). Temperatures are constrained by quartz-scheelite oxygen isotope thermometry (Table 1). Using a temperature range of 430 to 595°C, fluid

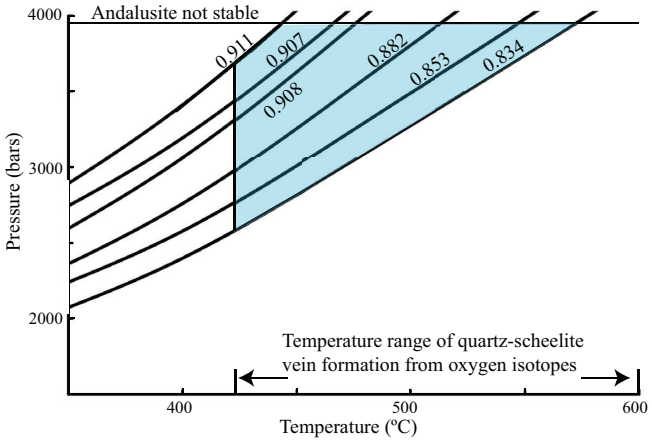


Figure 15. Representative isochores for primary H_2O-CO_2-NaCl±CH_4 fluid inclusions in scheelite from quartz-scheelite veins from the open pit orebody. Combined with temperatures of 430 to 595°C (from oxygen isotope thermometry), these isochores indicate pressures of approximately 2 to 4 kbar for quartz-scheelite vein formation. The shaded area represents pressure and temperature conditions for emplacement of the high-grade quartz-scheelite veins from the open pit orebody.

inclusion isochores yield pressure estimates for quartz-scheelite vein formation of 2 to 4 kbar.

Isochores for H_2O-CO_2-NaCl±CH_4 fluid inclusions in aplite dykes reflect temperatures and pressures similar to those calculated for quartz-scheelite veins from the open pit orebody. The pressure range for quartz-scheelite veins from the open pit orebody and aplite dykes from both orebodies at Cantung corresponds to depths of approximately 6 to 9 km, assuming purely lithostatic pressure conditions. Rasmussen (2004) stated that the Mine Stock was emplaced at a depth of about 6.6 to 12.7 km, comparable to our depth estimates based on fluid inclusions.

Using thermometry and fluid inclusions from E-Zone orebody apatites, Marshall et al. (2003) concluded that the skarn ore formed at temperatures of 400 to 520°C and pressures of approximately 2 to 3 kbar. Similarities in temperature and pressure conditions for the deeper E-Zone skarn orebody and the shallower quartz-scheelite veins from the open pit orebody suggest that no significant uplift and cooling of the magmatic-hydrothermal system had occurred prior to high-grade quartz-scheelite vein formation. Therefore, quartz-scheelite veins at Cantung may be thought of as a distal expression of a protracted magmatic skarn-forming event.

OXYGEN ISOTOPE COMPOSITIONS OF VEINS AND APLITES

Samples of vein-hosted quartz and scheelite and whole-rock aplite from the open pit and E-Zone orebodies were collected for oxygen isotope studies (Table 1). Samples were separated by hand, crushed, sieved between 80 and 100 mesh sizes, and analyzed following the procedures of Clayton and Mayeda (1963). Isotopic data are reported in standard δ notation relative to Vienna SMOW and the standard error for each analysis is approximately ±0.1‰ (Table 1). Four quartz veins and one aplite dyke were collected from the E-Zone skarn orebody. Five high-grade quartz-scheelite veins and two aplite dykes were sampled from the open pit orebody. The authors carefully selected quartz-scheelite pairs in contact with one another from one quartz vein from the E-Zone orebody and three high-grade quartz-scheelite veins from the open pit orebody for isotope thermometry.

Interpretation of Oxygen Isotope Data

Quartz in veins from the E-Zone skarn orebody has $\delta^{18}O$ values of 11.9 to 13.1‰ and quartz from high-grade veins in the open pit orebody has values of 12.2 to 13.1‰. An aplite dyke from the E-Zone orebody has a $\delta^{18}O$ value of 12.4‰ and two aplite dykes from the open pit orebody have values of 9.9 and 11.3‰. Vein-hosted scheelite from the E-Zone skarn orebody has a $\delta^{18}O$ value of 6.8‰, whereas scheelite in veins from the open pit orebody has $\delta^{18}O$ values of 6.6 to 7.2‰.

Ranges of $\delta^{18}O_{water}$ values responsible for quartz vein precipitation were calculated using the quartz-water curve of Clayton et al. (1972) and a temperature range of 430 to 595°C, based on isotope thermometry.

Table 1. Oxygen isotope data for quartz, scheelite, and aplite dyke samples from the Cantung mine.

Sample	Mineral/ Rock	$\delta^{18}O$ (‰)	$\Delta^{18}O_{qtz\text{-}sch}$ (‰)	Isotope T (°C)	$\delta^{18}O_{water}$ (‰)*
E-Zone Orebody					
HF-03-05	quartz	12.1			8.5 - 11.0
HF-03-74	quartz	11.9			10.8
	scheelite	6.8	5.1	595 ± 45	10.8
HF-03-90	quartz	12.9			9.3 - 11.8
HF-03-92	quartz	13.1			9.7 - 12.0
3900Pow	aplite	12.4			9.9 - 11.9
Open Pit Orebody					
HF-03-17	quartz (clear)	12.4			11.0
	scheelite	7.1	5.3	565 ± 45	11.0
	quartz (milky)	12.8			9.2 - 11.7
HF-03-25	quartz	12.9			9.5 - 11.8
Pit Vein 2	quartz	12.8			10.9
	scheelite	7.2	5.6	525 ± 45	10.9
Pit Vein 28	quartz	13.1			9.7
	scheelite	6.6	6.5	430 ± 45	9.7
HF-03-94	quartz	12.2			8.8 - 11.1
HF-03-94-I	aplite	10			7.5 - 9.5
	aplite	9.9			7.4 - 9.5
HF-03-94-II	aplite	10.9			8.4 - 10.5
	aplite	11.3			8.8 - 10.9

Equilibrium isotope temperatures and $\delta^{18}O_{water}$ were calculated using the equations of Wesolowski and Ohmoto (1986), Freidman and O'Neil (1977), and Clayton et al. (1972). *$\delta^{18}O_{water}$ values were calculated at 430 and 595ºC for all samples except those with quartz-scheelite pairs, which were calculated at their own equilibrium temperatures.

The $\delta^{18}O_{water}$ values in equilibrium with quartz veins range from 8.8 to 12.0‰. These values are in good agreement with values of 8.9 to 10.4‰ calculated by Bowman et al. (1985) for waters that deposited the E-Zone skarn orebodies. These values are consistent with waters that equilibrated with igneous and metasedimentary rocks at high temperatures and low water/rock ratios. The fluids that deposited high-grade quartz-scheelite veins of the open pit orebody are likely magmatic-related fluids similar isotopically to those that deposited the underlying E-Zone skarn orebody. There is no isotopic evidence of meteoric water involvement in these vein systems.

ISOTOPE THERMOMETRY

The $\Delta^{18}O_{quartz\text{-}scheelite}$ values for four quartz-scheelite pairs from quartz veins are 5.1 to 6.5‰. Using the oxygen isotope fractionation equations of Clayton et al. (1972) for quartz-water and Wesolowski and Ohmoto (1986) for scheelite-water, calculated equilibrium isotope temperatures for these mineral pairs are 430 to 595 ± 45°C. These calculated temperatures are in good agreement with temperatures of 400 to 520°C suggested for skarn formation by Mathieson and Clark (1984), Bowman et al. (1985), and Marshall et al. (2003).

High-grade quartz-scheelite veins from the open pit orebody are related to a deep, hot, magmatic-hydrothermal system. The veins likely represent a distal expression of the overall skarn-forming event. They are not the result of a cooler, meteoric water system associated with uplift of the area.

CONCEPTUAL MODEL

We envision a conceptual model for the Cantung hydrothermal system in which ore-grade tungsten deposits formed where fluids emerged from the granite and encountered rocks favourable for skarn development (e.g. cleaner 'ore limestone' versus cherty 'swiss cheese limestone'). Due to the folded geometry of the sedimentary sequence, in other areas along the granite contact, the fluids emerging from the granite encountered strata less favourable to skarn development (i.e. argillite). Where these less favourable units were breached by fracture systems, potential skarn-forming fluids (and aplite dykes) gained access to host rocks more conducive to ore development vertically distal to the granite contact.

CONCLUSIONS

There are several conclusions that can be reached from the geochemical assessment of quartz-scheelite veins and aplite dykes from the Cantung mine:

1. Isochores from primary H_2O-CO_2-NaCl±CH_4 inclusions in quartz-scheelite veins from the open pit orebody, constrained by temperature estimates from oxygen isotope thermometry (400-595°C), yield pressures of 2 to 4 kbar. These temperature and pressure estimates are similar to those for the deeper E-Zone skarn orebody (400-520°C and 2-3 kbar). These temperatures and pressures indicate that the high-grade quartz-scheelite veins are related to a deep magmatic-hydrothermal system and are likely a distal expression of a protracted skarn-forming event. Quartz-scheelite veins did not form in a shallower, cooler, hydrothermal system during uplift.
2. Primary ore fluids in quartz-scheelite veins from the open pit orebody, in skarn-related quartz veins from the E-Zone orebody, and in aplite dykes are grossly similar H_2O-CO_2-NaCl±CH_4 fluids. However, two distinct end-member fluids have been documented: aplite-related fluids and skarn-related fluids. Fluids in high-grade quartz-scheelite veins contain components of both end-member fluids.
3. High-grade quartz-scheelite veins from the open pit orebody share a common structural attitude with aplite dykes. Fluids in quartz-scheelite veins contain an aplite-related fluid end-member even when occurring up to 70 meters from the nearest aplite dyke. Thus, quartz-scheelite veins and aplite dykes in the open pit orebody may have a genetic relationship in addition to their structural relationship.
4. High-grade quartz-scheelite veins from the open pit orebody represent a distal expression of a protracted magmatic skarn-forming event. The presence of magmatic ore fluids distal to intrusions is intriguing as it has significant implications for mineral resource assessment in the region.

Implications for Regional Mineral Resource Assessment

The conceptual model proposed for the Cantung magmatic-hydrothermal system can be extrapolated to other regions within the Nahanni MERA study area. We have identified a process and geological environment in which magmatic ore fluids may pass through unreactive lithologies and deposit economic grade mineral deposits at significant distances from their igneous source regions. The documentation of ore-mineralizing fluids distal to the intrusion-country rock contact expands the potential exploration area for ore targets. Distal exploration targets need not be manifested as massive skarns, but could take on various forms depending on the geometry and chemistry of the host lithologies. Vein and replacement-type deposits in metasedimentary rocks of the Nahanni MERA region

frequently have been assumed to represent older ore events. Their origins should be re-evaluated, as some of them could instead represent distal, granite-related deposits.

There is current debate regarding the origin of gold-bearing vein deposits in the Cantung area, specifically whether they are intrusion-related gold deposits (IRGD) or could instead be orogenic (metamorphic) gold deposits. The association of gold mineralization with Cretaceous intrusions of the Tombstone and Mayo plutonic suites of the Tintina Gold Province (Fig. 1) is so prevalent that it has provided a foundation for intrusion-related gold models (Thompson et al., 1999; Lang et al., 2000; Baker, 2002; Baker et al., 2005; Goldfarb et al., 2005).

However, recently, Hart and Lewis (2006) have interpreted some of these deposits as orogenic gold deposits, which may instead be related to metamorphogenic fluid flow focused along faults. In light of our conceptual model for Cantung, the origin of these deposits needs to be re-evaluated. If a distal magmatic model is applicable to deposits of the Nahanni MERA region, it may have important implications for resource management strategies.

REFERENCES

Allmendinger, R.W.
2002: Stereonet/SteroWin, version 1.2 [Computer software].

Baker, T.
2002: Emplacement depth and carbon dioxide-rich fluid inclusions in intrusion-related gold deposits; Economic Geology, v. 97, p. 1111-1117.

Baker, T., Pollard, P.J., Mustard, R., Mark, G., and Graham, J.L.
2005: A comparison of granite-related tin, tungsten, and gold-bismuth deposits: Implications for exploration; Society of Economic Geologist Newsletter, no. 61, p. 5-17.

Blusson, S.L.
1967: Geology and tungsten deposits near the headwaters of the Flat River, Yukon Territory and District of Mackenzie, Canada; Canadian Geological Survey Paper, 67-22, 77 p.

Bodnar, R.J. and Vityk, M.O.
1994: Interpretation of microthermometric data for H_2O-NaCl fluid inclusions, *in* Fluid Inclusions in Minerals: Methods and applications, (ed.) B. De Vino and M.L. Frezzotti; Virginia Polytechnic Institute and State University, Blacksburg, Virginia, p. 11-130.

Bowman, J.R., Covert, J.J., Clark, A.H., and Mathieson, G.A.
1985: The CanTung E Zone scheelite skarn orebody, Tungsten, Northwest Territories: Oxygen, hydrogen, and carbon isotope studies; Economic Geology, v. 80, p. 1872-1895.

Brown, C.J.
1961: The geology of the Flat River Tungsten Deposits; Canada Tungsten Mining Corporation Limited, Canadian Mining and Metallurgical Bulletin, v. 94, p. 510-513.

Brown, P.E. and Hagemann, S.G.
1995: MacFlinCor and its application to fluids in Archean lode-gold deposits; Geochimica et Cosmochimica Acta, v. 19, p. 3943-3952.

Burruss, R.C.
1981: Analysis of phase equilibria in C-O-H-S fluid inclusions; in Fluid Inclusions: Applications to Petrology, (ed.) L.S. Hollister, and M.L. Crawford; Mineralogical Association of Canada, Short Course Handbook, v. 6, p. 39-74.

Christiansen, E.H. and Keith, J.D.
1996: Trace element systematics in silicic magmas: A metallogenic perspective, *in* Trace Element Geochemistry of Volcanic Rocks: Applications for Massive Sulphide Exploration, (ed.) D.A. Wyman; Geological Association of Canada, Short Course notes, v. 12, p. 115-151.

Clayton, R.N. and Mayeda, T.K.
1963: The use of bromine-pentafluoride in the extraction of oxygen from oxides and silicates for isotopic analyses; Geochimica et Cosmochimica Acta, v. 27, p. 43-52.

Clayton, R.N., O'Neil, J.R., and Mayeda, T.K.
1972: Oxygen isotope exchange between quartz and water; Journal of Geophysical Research, v. 77, p. 3057-3067.

Collins, P.L.F.
1979: Gas hydrates in CO_2-bearing fluid inclusions and the use of freezing data for the estimation of salinity; Economic Geology, v. 74, p. 1435-1444.

Crawford, M.L.
1981: Phase equilibria in aqueous fluid inclusions, *in* Fluid Inclusions: Applications to Petrology, (ed.) L.S. Hollister and M.L. Crawford; Mineralogical Association of Canada, Short Course Handbook, v. 6, p. 75-100.

Crawford, W.J.P.
1963: Geology of the Canada Tungsten Mine, SW District of Mackenzie, Canada; M.Sc. thesis, University of Washington, Seattle, United States, 80 p.

Cummings, W.W. and Bruce, D.E.
1977: Canada Tungsten – Change to underground mining and description of mine-mill procedures; Canadian Institute of Mining and Metallurgy, Bulletin, v. 70, p. 94-101.

Diamond, L.
1992: Stability of CO_2 clathrate hydrate + CO_2 liquid + CO_2 vapour + aqueous KCl-NaCl solutions: Experimental determination and application to salinity estimates of fluid inclusions; Geochimica et Cosmochimica Acta, v. 56, p. 273-280.

Dick, L.A.
1980: A Comparative Study of the Geology, Mineralogy and Conditions of Formation of Contact Metasomatic Mineral Deposits in the NE Canadian Cordillera; Ph.D. thesis, Queen's University, Kingston, Ontario, Canada 473 p.

Dick, L.A. and Hodgson, C.J.
1982: The MacTung W-Cu (Zn) contact metasomatic and related deposits of the northeastern Canadian Cordillera; Economic Geology, v. 77, p. 845-867.

Friedman, I. and O'Neil, J.R.
1977: Compilation of stable isotope fractionation factors of geochemical interest; in Data of Geochemistry, (ed.) M. Fleischer; sixth edition, United States Geological Survey, Professional Paper 440-KK, 12 p.

Gehrig, M.
1980: Phasengleichgewichte und PVT-Daten ternärer Mischungen aus Wasser Kohlendioxid und Natriumchlorid bis 3 kbar und 550°C; Ph.D. thesis, Institut für Physikalische Chemie, Universität Karlsruhle, Kalrsruhe, Germany.

Goldfarb, R.J., Baker, T., Dubé, B., Hart, C.J.R., and Gosslin, P.
2005: Distribution, character, and genesis of gold deposits in metamorphic terranes, *in* Economic Geology 100th Anniversary Volume, (ed.) J.W. Hedenquist, J.F.H. Thompson, R.J. Goldfarb and J.P. Richards; p. 407-450.

Hart, C.J.R. and Lewis, L.L.
2006: Gold mineralization in the upper Hyland River area: A non-magmatic origin, *in* Yukon Exploration and Geology 2005, (ed.) D.S. Emond, G.D. Bradshaw, L.L. Lewis, and L.H. Weston; Yukon Geological Survey, p. 109-125.

Hodgson, C.J.
2000: Exploration potential at the Cantung Mine, District of Mackenzie, NWT; Andean Engineering, Cantung Internal Files, 26 p.

Ishihara, S.
1977: The magnetite-series and ilmenite-series granitic rocks; Mining Geology, v. 27, p. 293-305.

Ivanova, G.F.
1986: Geochemistry of tungsten, *in* Geology of Tungsten, (ed.) A.A. Beus; UNESCO, Belgium, p. 11-44.

Kerrick, D.M. and Jacobs, G.K.
1981: A modified Redlich-Kwong equation for H_2O, CO_2, and H_2O-CO_2 mixtures at elevated pressures and temperatures; American Journal of Science, v. 281, p. 735-767.

Lang, J.R., Baker, T., Hart, C.J.R., and Mortensen, J.K.
2000: An exploration model for intrusion-related gold systems; Society of Economic Geologists, Newsletter, no. 40, p. 1-15.

Marshall, D., Falck, H., Mann, B., Kirkham, G., and Mortensen, J.
2003: Geothermometry and fluid inclusion studies of the E-Zone biotite skarn, CanTung Mine, Tungsten, NWT; 31st Annual Yellowknife Geoscience Forum, Abstracts volume, p. 60.

Mathieson, G.A. and Clark, A.H.
1984: The CanTung E-zone scheelite skarn orebody, Tungsten, Northwest Territories: A revised genetic model; Economic Geology, v. 79, p. 883-901.

Mortensen, J.K., Hart, C.J.R., Murphy, D.C., and Heffernan, S.
2000: Temporal evolution of Early and mid-Cretaceous magmatism in the Tintina Gold Belt, *in* The Tintina Gold Belt: Concepts, Exploration, and Discoveries, (ed.) J. Jambor; British Columbia and Yukon Chamber of Mines, Special Volume 2, p. 49-57.

Rasmussen, K.L.
2004: The Aplitic Dykes of the Cantung Mine: Petrography, Geochemistry, and Implications for the Mineralization Process; B.Sc. thesis, University of Calgary, Calgary, Alberta, 128 p.

Rasmussen, K.L., Mortensen, J.K., and Falck, H.
2006: Geochronological and lithogeochemical studies of intrusive rocks in the Nahanni region, southwestern Northwest Territories and southeastern Yukon, *in* Yukon Exploration and Geology 2005, (ed.) D.S. Emond, G.D. Bradshaw, L.L. Lewis, and L.H. Weston; Yukon Geological Survey, p. 287-298.

Roedder, E.
1984: Fluid Inclusions; Mineralogical Society of America, Reviews in Mineralogy, v. 12, 646 p.

Shelton, K.L. and Orville, P.M.
1980: Formation of synthetic fluid inclusions in natural quartz; American Mineralogist, v. 65, p. 1233-1236.

Stern, L.A., Brown Jr., G.E., Bird, D.K., Jahns, R.H., Foord, E.E., Shigley, J.E., and Spaulding Jr., L.B.
1986: Mineralogy and geochemical evolution of the Little Three pegmatite-aplite layered intrusive, Romona, California; American Mineralogist, v. 71, p. 406-427.

Thiery, R., van den Kerkhof, A.M., and Dubessy, J.
1994: vX properties modeling of CH_4-CO_2 and CO_2-N_2 fluid inclusions (T <31°C, P <400 bars); European Journal of Mineralogy, v. 6, p. 753-771.

Thompson, J.F.H., Silltoe, R.H., Baker, T., Lang, J.R., and Mortensen, J.K.
1999: Intrusion-related gold deposits associated with tungsten-tin provinces; Mineralium Deposita, v. 34, p. 323-334.

Wesolowski, D. and Ohmoto, H.
1986: Calculated oxygen isotope fractionation factors between water and the minerals scheelite and powellite; Economic Geology, v. 81, p. 471-477.

Yukon Geological Survey
2005: Canada's Yukon Tungsten; Yukon Geological Survey, Brochure, 4 p.

Yuvan, J.
2006: Fluid Inclusion and Oxygen Isotope Studies of High-Grade Quartz-Scheelite Veins, Cantung Mine, Northwest Territories, Canada: Products of a Late-Stage Magmatic-Hydrothermal Event; M.Sc. thesis, University of Missouri, Columbia, Missouri, 93 p.

Yuvan, J.G., Shelton, K.L., Falck, H, and Marshall, D.
2004: High-grade quartz-scheelite veins in the Cantung Mine, Northwest Territories: A late magmatic-hydrothermal event; Geological Society of America, Annual Meeting, Abstracts with Programs, v. 36, no. 5, p. 355.

Yuvan, J.G., Shelton, K.L., and Falck, H.
2005: A distal expression of a protracted skarn-forming event? Oxygen isotope and fluid inclusion studies of quartz-scheelite veins in the Cantung Mine, NWT; 33rd Annual Yellowknife Geoscience Forum, Abstracts volume, p. 128.

Zaw, U.K.
1976: The CanTung E-Zone Orebody, Tungsten, Northwest Territories: A Major Scheelite Skarn Deposit; Ph.D. thesis, Queens University, Kingston, Ontario, 409 p.

Zhang, Y.G. and Frantz, J.D.
1989: Experimental determination of the compositional limits of immiscibility in the system $CaCl_2$-H_2O-CO_2 at high temperatures and pressures using synthetic fluid inclusions; Chemical Geology, v. 74, p. 289-308.

A REVIEW OF THE LATE CRETACEOUS LITTLE NAHANNI PEGMATITE GROUP AND ASSOCIATED RARE ELEMENT MINERALIZATION IN THE SELWYN BASIN AREA, NORTHWEST TERRITORIES

Elspeth M. Barnes[1], Lee A. Groat[1], and Hendrik Falck[2]

1. Department of Earth and Ocean Sciences, University of British Columbia, 6339 Stores Road, Vancouver, British Columbia V6T 1Z4
2. Northwest Territories Geoscience Office, P.O. Box 1500, Yellowknife, Northwest Territories X1A 2R3

ABSTRACT

The Late Cretaceous Little Nahanni Pegmatite Group (LNPG) is composed of more than 200 subvertical, lithium-cesium-tantalum (LCT) pegmatites, occurring in an area of approximately 55 km^2. The pegmatite group is hosted by Selwyn Basin offshelf facies of the Neoproterozoic to Lower Cambrian Hyland Group and is located between, and subparallel to, major regional northwest-trending structures, such as the March Fault and the Fork Anticline.

Since their discovery in 1961, these coarse-grained, mostly quartz, feldspar, and spodumene pegmatites have been investigated for economic concentrations of rare elements. Whole-rock geochemical analyses indicate granitic compositions and strong peraluminous signatures suggest an S-type affiliation. The depletion in rare earth element (REE) abundance, enrichment of Li, Ta, Cs, Sn, Rb, and Nb, and emplacement into low-pressure metamorphic rocks is typical of LCT pegmatites.

There are similarities between the LNPG dykes and the Greenbushes pegmatite, Australia, which is rich in Sn, Ta, Nb, and Li (Wengzynowski, 2002). However, even closer geochemical comparisons can be made with examples of European late-Variscan, post-orogenic mineralized plutons and pegmatites. One such example, the Beauvoir granite, is suggested as an analog for the plutonic source of the LNPG dykes. Comparison of the setting and ages obtained for the emplacement of the LNPG with this well studied Variscan granite suggests a period of post-orogenic collapse and extension during the late Cretaceous period in this region of the northern Cordillera.

INTRODUCTION

This paper evaluates the published academic and corporate record and looks at the potential of the Little Nahanni Pegmatite Group as an economic resource. Results from the senior author's ongoing doctoral research have been utilized in this assessment. The full extent of these results will be published at a later date.

Granitic pegmatites have been called "the building blocks for our society" (London, 2005) because of their potential to host a variety of minerals crucial to modern industries. Several minerals and rare elements concentrated in these pegmatites can be used for household products. Tantalum, niobium, and tin, which occur in pegmatites as oxide minerals, are used for capacitors and alloys in electronic devices, including televisions, computers, and toys. Lithium (abundant in the silicate minerals petalite and spodumene) is used as an alloy in metal production and as a flux, facilitating lower temperature melting in high-strength ceramics and glasses. It is also a constituent of high-temperature lubricants and pharmaceuticals and is used in the manufacture of rechargeable batteries, such as those found in cell phones. Cesium is used in atomic clocks, drilling fluid, and photoelectric cells and may also be incorporated in smoke detectors.

During their formation, pegmatites can concentrate rare elements to many thousands of times the average crustal abundance. An important control on these concentrations is the nature of the source of the magmatic melt. Researchers believe that LCT pegmatites are the result of extreme fractionation of magma derived from previously untapped crustal sources (Černý, 1991c), although purely anatectic origins (without later fractionation) have also been proposed (Stewart, 1978). This category of pegmatite can display high concentrations of a specific range of incompatible elements that are only present in previously unmelted source rocks. Incompatible elements, such as Cl, F, B, and P, and the compound H_2O are among the first components of pegmatite magma to accumulate, and they preferentially remain in the magma, restricting polymerization and crystal nucleation (Černý, 1991a). As a result of the presence of these incompatible elements, the magma has a low viscosity and can stay fluid at very low magmatic temperatures (<400°C, Sirbescu and Nabelek, 2003). Consequently, if separated from the plutonic source (e.g. along fractures following over-pressurization from the accumulation of volatiles in the magma) the magma can travel for long distances, forming pegmatites several kilometres distant (Baker, 1998). Therefore, pegmatites can occur either proximal to, or

Barnes, E.M., Groat, L.A., and Falck, H., 2007, A review of the Late Cretaceous Little Nahanni Pegmatite Group and associated rare-element mineralization in the Selwyn Basin area, Northwest Territories, *in* Mineral and Energy Resource Assessment of the Greater Nahanni Ecosystem Under Consideration for the Expansion of the Nahanni National Park Reserve, Northwest Territories; Geological Survey of Canada, Open File 5344, p. 191-202.

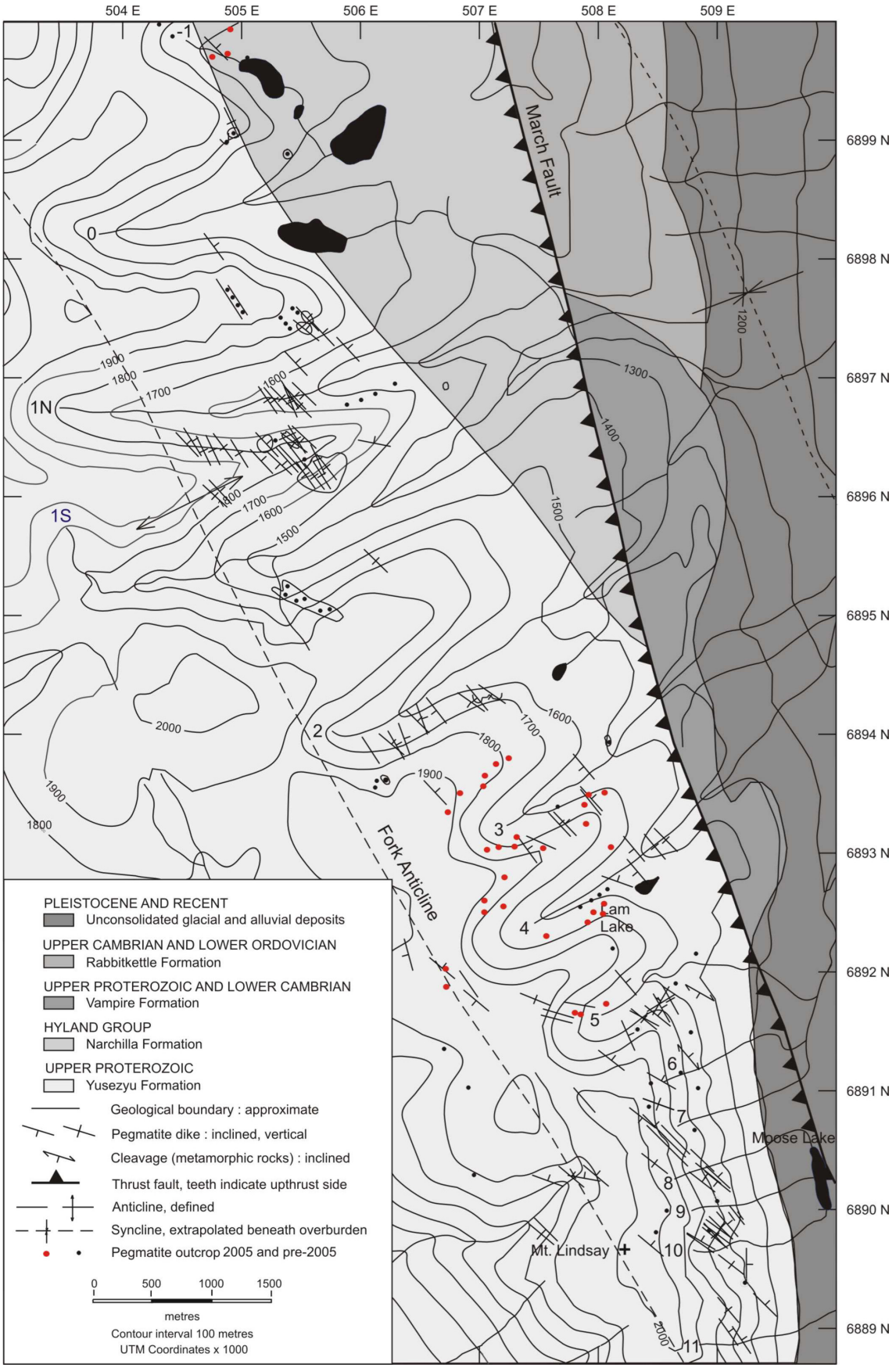


Figure 1. Local geology of the Little Nahanni Pegmatite Group outcrops and structures in the Logan Mountains, Northwest Territories (approximately 62°10'N, 128°55'W; NTS 105 I/2). Amended from Gordey and Anderson (1993) and Groat et al. (2003).

distal from the source pluton (Černý et al., 2005). As the magma travels from the source, it cools and starts to crystallize. Incompatible elements, which include Li, Cs, Be, Nb, and Ta, are not incorporated into minerals that crystallize early on and the concentration of these elements in the remaining magma continues to increase with magmatic fractionation (Černý, 1991a).

The most commonly used scheme of pegmatite classification (Černý, 1991a,b; Černý and Ercit, 2005) combines information on the composition, texture, depth of emplacement, and nature of associated metamorphic rocks. Černý (1991b) defines lithium-cesium-tantalum-enriched ('LCT') pegmatites as family members of the rare-element class of pegmatite, which is typically enriched in Li, Rb, Cs, Be, Ga, Mn, and Y, with Ta concentrations greater than Nb. This class of pegmatite is depleted in rare earth elements and emplaced into low- to moderate-pressure (i.e. ≤2-4 kbar), upper greenschist-facies environments, and has a geochemical signature indicative of extreme fractionation. Under the revised scheme of Černý and Ercit (2005), the LNPG is classified as REL-Li (rare element-lithium class), and as an albite-spodumene type.

Examples of pegmatites exploited for their lithium-cesium-tantalum mineralization include the Tanco pegmatite (Li, Ta, Cs, Be, Rb) at Bernic Lake, Manitoba, the Bikita pegmatite (Li) near Masvingo, Zimbabwe, and the Greenbushes pegmatite (Sn, Ta, Nb, Li) of Western Australia.

LOCATION

The well exposed, late Cretaceous Little Nahanni Pegmatite Group (LNPG), located in the Logan Mountains, Northwest Territories (approximately 62°10'N, 128°55'W, NTS 105 I/2; Fig. 1), offers rare access to extensive lateral and vertical outcrops of a suite of LCT pegmatites (Groat et al., 1994, 2003). The LNPG is the collective name for a cluster of more than 200 granitic pegmatitic dykes in an area of approximately 55 km^2. The pegmatites are exposed on an unnamed ridge (approximately 400 km^2 in area; maximum elevation 2220 m) approximately 80 km northwest of the mining town of Tungsten, Northwest Territories. These subvertical dykes crop out above tree line (1500-1600 m) and have a high aspect ratio, with up to 400 m of vertical exposure and several kilometres along strike length. The site can be accessed in winter via the road to Howard's Pass, which passes within 5 km of the northeast section of the ridge. This road runs along the valley of the Little Nahanni River and can be reached via the all-season Nahanni Range Road. West of the ridge, another track joins the Howard's Pass road to the north and south of the ridge, which could also provide access. During the summer, the area is best accessed by helicopter, although float planes can land at Moose Lake at the southeast corner of the ridge (Fig. 1), from where the pegmatite outcrop can be reached on foot.

Although the location is remote and the topography rugged, the extensive exposure of the dykes provides an almost unparalleled opportunity for field studies of a vertical section of this type of mineralized magmatic system. The LNPG is the focus of the senior author's Ph.D. research, which addresses its petrological, structural, and geochronological aspects and isotopic signature.

PREVIOUS WORK

The pegmatites were discovered in 1961 by D.C. Rotherham of the Canada Tungsten Mining Corporation Ltd. during a regional reconnaissance program (Rotherham, 1962). The unusual mineralogy and abundance of strategic elements were recognized and a series of mineral claims were staked. With the discovery of the mineralization at Cantung at the same time, the exploration focus shifted and the claims lapsed.

In the late 1970s, elevated lithium prices encouraged further mineral exploration and the Cali and Lica claims of the LNPG were staked by Canadian Superior Exploration Ltd. (Ahlborn, 1977; Beavon, 1977) and Cominco Limited (Ahlborn, 1979, 1980). Samples collected by Beavon gave a grade of 1.14% Li_2O (Beavon, 1977). The claims were restaked by Canamera in 1994 but subsequently were allowed to lapse. Currently, the LNPG area is covered by eight adjoining claims. One claim (Cali 1) is leased to V. H. Ahlborn and the other seven claims (Mac 1-7) were staked by Archer Cathro and Associates Ltd. in 2000, on behalf of Strategic Metals Ltd. From an option agreement with Strategic Metals Ltd., War Eagle Mining Company Inc. obtained the right to earn a 100% interest in the property by making additional exploration payments (Wengzynowski, 2002; War Eagle mining Co. Inc., News Release, February 17, 2005).

From 1977 to 1982, the Geological Survey of Canada undertook several studies, including geological mapping and stream sediment surveys, to provide information on the regional geology while specifically targeting intrusive rocks and mineral deposits within the area (Gordey and Anderson, 1993). Several scientific studies have been conducted in the region since 1992 by the Mineralogical Research Group at the University of British Columbia (Groat et al., 1994, 2003; Mauthner et al., 1995; Mauthner, 1996). Groat et al. (1994) outlined the state of pegmatite research in the northern Cordillera and described the mineralogy and the textural zonation across individual pegmatites. Mineralogical, geochemical, and geochronological studies of the dykes were undertaken by Mauthner et

al. (1995) and Mauthner (1996). Mauthner (1996) also constrains the composition of the main mineral phases and discusses some of the textural aspects of the pegmatites. The most recent published work on the LNPG is a comprehensive survey of the geology and mineralogy by Groat et al. (2003).

GEOLOGY

The LNPG lies in the Selwyn Basin area of the northern Cordillera. The Selwyn Basin was a deep-water depositional centre which existed from late Precambrian to mid-Devonian time. The Proterozoic siliciclastic and carbonate passive-margin facies of this basin, the Yusezyu and Narchilla formations of the Hyland Group, form the host rocks for the LNPG pegmatites. During basin formation the eastern margin migrated further eastward, resulting in deep-water offshelf strata commonly overlying shallow-water shelf rocks in the study area (Gordey and Anderson, 1993). The Yusezyu Formation, consisting of at least 3000 m of relatively shallow-water sedimentary rocks (the base is not exposed in the area), is interpreted to represent various submarine-fan clastic deposits (Gordey and Anderson, 1993). The Narchilla Formation conformably overlies the Yusezyu and is composed of deeper water shales with a greater proportion of carbonate strata.

Deep-water deposition of basinal lithologies continued during the Cambrian period with the distinctive nodular, finely bedded limestone of the Rabbitkettle Formation. This in turn was covered by the black shales and fine-grained clastic sediments and fine-grained carbonate beds of the Duo and Steel formations of the Road River Group. Sedimentation flow directions shifted in the late Devonian period with the deposition of the clastic sediments of the Earn Group.

Following deformation, the region was intruded by a number of plutons during the Cretaceous period. Mortensen et al. (2000) include the study area within the boundary of the Tintina Gold Belt, a discontinuous belt of mineralization associated with Cretaceous magmatism which runs several hundred kilometres across the Yukon Territory and into contiguous Alaska (Heffernan and Mortensen, 2000; Mortensen et al., 2000; Hart et al., 2004; Rasmussen et al., 2007). The pegmatites occur on their own, there are no proximal intrusions. The closest intrusions to the LNPG (15-20 km distant) are the Cac, Rudi, and Lened plutons (Lened: 95.0 ± 0.6 Ma, U-Pb, zircon, Rasmussen et al., 2005) which were categorized by Gordey and Anderson (1993) as members of the Selwyn Plutonic Suite (101-93 Ma; K-Ar and Rb-Sr). The two-mica plutons of this suite are typically small (<5.4 km^2) and commonly have associated aplitic or pegmatitic dykes (Fig. 2). The O'Grady batholith, a much larger intrusion (<100 km^2) lies approximately 70 km north of the LNPG (U-Pb, titanite; 92.5 ± 1.8 Ma; Mortensen, unpublished data). This hornblende-bearing pluton incorporates a 10 km long belt of pegmatitic granite, within which lithium mineralization occurs in a localized, 1 km long area (Ercit et al., 2003).

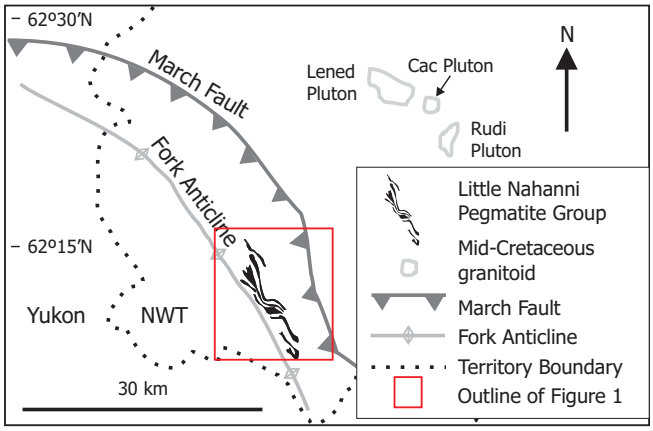


Figure 2. Sketch map of the major structures and Cretaceous intrusions proximal to the Little Nahanni Pegmatite Group.

Initial results from the regional airborne geophysical mapping of the area, using radiometric and magnetic measurements and undertaken as part of the 2004-2006 Nahanni Mineral and Energy Resource Assessment (MERA) in 2005 (Charbonneau, 2007), identified the Lened pluton by its high uranium and potassium signature; the LNPG produced no distinct anomaly using these methods.

Mortensen et al. (2000) described the temporal evolution of Cretaceous magmatism within the Tintina Gold Belt, distinguishing the Tombstone, Tay, and Tungsten plutonic suites, each of which has a distinctive metallogenic association. Hart et al. (2004) included the mid-Cretaceous granitic intrusions proximal to LNPG as members of the ilmenite-series granitoids of the Tungsten Plutonic suite (based on their reduced composition and association with tungsten skarn deposits with less significant Cu, Zn, Sn, and Mo) within the Tombstone Gold Belt, which itself is part of the Tintina Gold Province. In extensive studies of the mineral potential of the regional igneous intrusions, Rasmussen et al. (2005, 2007) suggest that the Tungsten Suite can be categorized as highly evolved, small intrusions which overlie larger and deeper Tay River-Tungsten and Tay River plutons (categories modified from Mortensen et al., 2000 and Hart et al., 2004). As mentioned in Rasmussen et al. (2007) the presence of underlying large plutonic bodies would provide a significant reservoir of metals and other elements which could have strongly influenced the composition of the more evolved, overlying Tungsten intrusive centres.

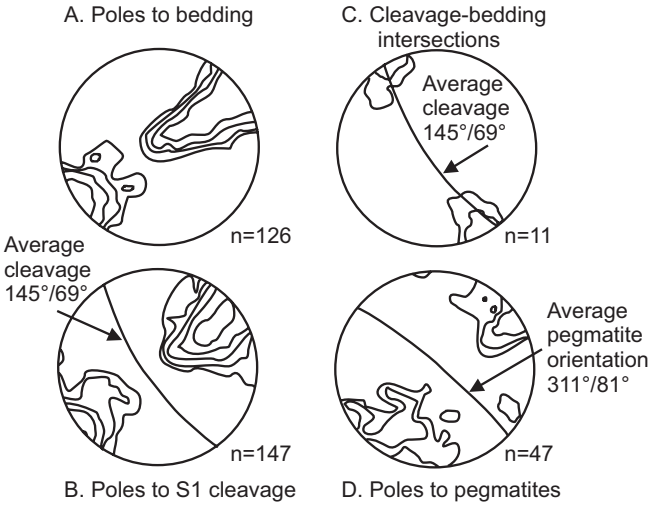


Figure 3. Initial interpretations of the structural fabric of the Fork Anticline and the Little Nahanni Pegmatite Group dykes.

STRUCTURE

The initial formation of the Selwyn Basin is attributed to rifting of the Rodinia supercontinent, followed by basin subsidence that is reflected in the extensive clastic deposits of the Precambrian to Lower Cambrian Yusezu and Narchilla formations (>3.5 km thickness). The earliest evidence of deformation is a gentle warping and stratal discontinuity in the Lower to Middle Cambrian Gull Formation (Gordey and Anderson, 1993).

The March Fault is a significant and long-lived northeast-verging fault separating the Neoproterozoic to Lower Cambrian Narchilla and Gull Lake formations from the Lower Cambrian Vampire Formation to the northeast (Figs. 1, 2; Gordey and Anderson, 1993). Deformation spatially associated with the March Fault during the Cambrian is thought to have been important in the distribution of these lithologies and the warping of the Gull Formation. The eroded remnants of block-faulted and uplifted Hyland Group lithologies (the Yusezu and Narchilla formations) provide the provenance of the clastic material in the Devono-Mississippian Earn Group.

Accretion of the Yukon-Tanana terrane in the mid-Jurassic period initiated a compressive regime with crustal shortening and mountain building replacing sediment accumulation in the Selwyn Basin. After 100 Ma, compressive deformation in the western region of the basin was replaced by an extensional, dextral transcurrent setting (ca. 85 Ma; Mair et al., 2006). The March Fault, in the eastern Selwyn Basin, was reactivated around this time, although the sense of displacement is unknown (Hart and Lewis, 2005).

The Mesozoic orogeny is believed to have influenced the formation of the ridge-forming Fork Anticline (Gordey and Anderson, 1993), located approximately 10 km southwest and almost parallel to the March Fault (Figs. 1, 2). The Fork Anticline is a fairly tight fold and has a strike length of 30 to 40 km (Gordey and Anderson, 1993). Preliminary results from recent mapping of the structural fabric of the Fork Anticline and the LNPG are presented in Figure 3. The poles to bedding (Fig. 3A) illustrate a northwest-trending, asymmetric fold with a more steeply dipping northeast-verging limb. The poles to S1 cleavage (Fig. 3B) show an average orientation of 145°/69° (southwest) and the fold is subhorizontal as indicated by the shallow plunges of the bedding S1 cleavage intersection lineations (Fig. 3C). The poles to the pegmatites (Fig. 3D) show a similar orientation to the S1 cleavage although the pegmatites tend to be slightly steeper in attitude.

A second folding event, evidenced by refolded folds and the development of a shallow, northwest-trending S2 cleavage, is present but not yet well understood.

CHARACTERISTICS OF THE PEGMATITES

The LNPG pegmatites, each typically 1 to 2 m wide (rarely up to 10 m; Fig. 4), are exposed up to 5 km along strike (Wengzynowski, 2002), have vertical exposure of up to 400 m, and occur in seven swarms, each consisting of up to 30 individual pegmatites. The swarms are subparallel, and few crosscutting relationships are observed. The majority of the pegmatites are concordant to semiconcordant to the well bedded Narchilla and Yusezyu formations. The contacts with the host rock are commonly sharp, although calcite-filled fractures within the pegmatites (in carbonate-rich lithologies) or muscovite/tourmaline alteration rims (in siliciclastic lithologies) are observed (Mauthner, 1996). The majority of the dykes are undeformed; however there are localized areas of folding, buckling, and boudinaged dykes suggesting syn- or post-emplacement deformation. The approximate volume of the exposed pegmatitic material is estimated to be greater than 0.16 km^3 (approximately 200 dykes averaging 2 km in length, 1 m in width, and 400 m in height).

Primary mineralogy of the pegmatites includes the silicate minerals quartz, albite, potassium feldspar, spodumene, muscovite, and lepidolite (Li-rich mica). Secondary minerals include albite, muscovite, and zeolites. Accessory minerals, especially oxide and phosphate minerals, are numerous and include rutile, cassiterite, columbite-group minerals (Nb and Ta oxides), apatite, lithiophilite, amblygonite-montebrasite $(Li,Na)AlPO_4(F,OH)$, triploidite $(MnFe)_2(OH)(PO_4)$, as well as beryl, tourmaline (schorl-elbaite), and garnet (spessartine) (Mauthner, 1996). The senior author has also identified berlinite ($AlPO_4$).

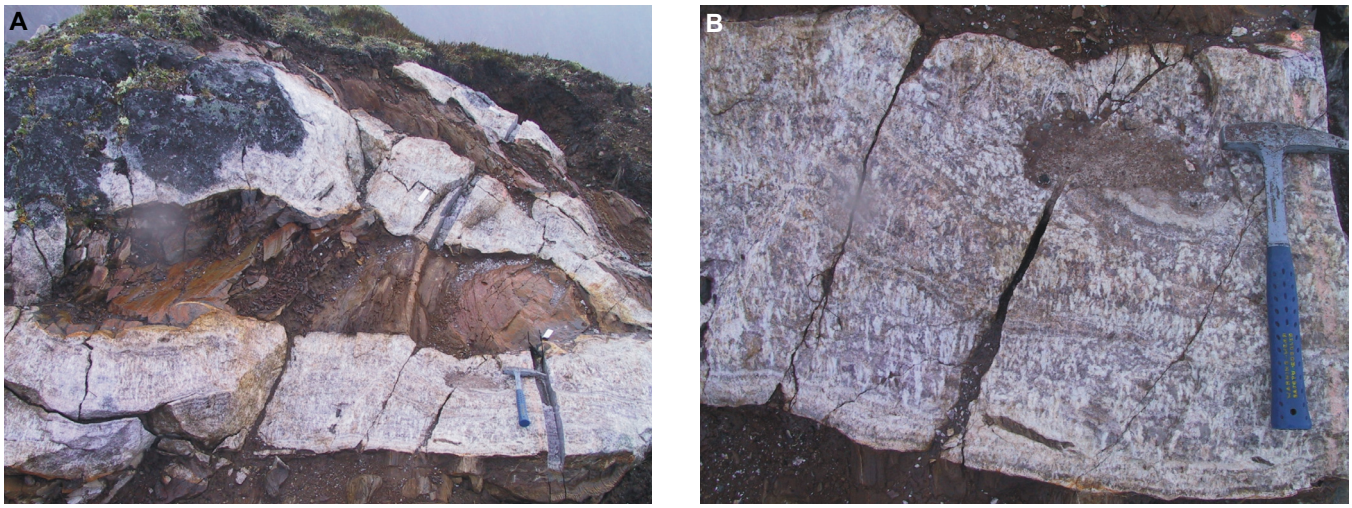


Figure 4. A) A typical, zoned pegmatite outcrop at Little Nahanni Pegmatite Group. **B)** Outcrop showing the crystal-size variations across a single dyke. Hammer for scale. Photographs by D. Kontak.

Groat et al. (2003) divide the LNPG into spodumene-bearing and spodumene-free pegmatites, which differ mineralogically in the abundance of mica and accessory minerals. The spodumene-free pegmatites are richer in mica (muscovite or lepidolite) and phosphate minerals, and are relatively free of aplite. The spodumene-bearing pegmatites display mineral banding consisting of spodumene and quartz (with spodumene laths commonly aligned perpendicular to the contact), which is continuous for no more than a few metres at any occurrence. In contrast, the spodumene-free pegmatites are more commonly represented by textural banding parallel to the contact with aplite (quartz+albite) alternating with pegmatitic layers of K-feldspar+quartz±muscovite±lepidolite. Well developed across dyke zonation, and distinct core zones and cavities are rare. Isolated cavities are small (<5 cm diameter) and occur in the central portion of the pegmatites.

Wengzynowski (2002) differentiated five categories of pegmatites grouped by estimated mineral abundance: (1) spodumene-quartz-feldspar, (2) spodumene-quartz-feldspar-lepidolite, (3) quartz-albite, (4) quartz-feldspar-lepidolite, and (5) quartz-silver mica groups. From extensive assays, selected samples of the spodumene-bearing pegmatites were found to be Ta-Sn poor but to contain moderate to high concentrations of lithium (average 1.43% Li_2O), while the quartz-silver mica pegmatites (spodumene poor) contained the highest concentrations of Sn and Ta.

The abundance of quartz in a pegmatite at one well exposed location was seen to increase with elevation. At lower elevations, the mineralogy of the pegmatite consisted of quartz, albite, potassium feldspar, spodumene, lepidolite, muscovite, garnet, tourmaline, Nb-Ta oxides, and phosphate minerals. At higher elevations (approximately 300 m) the accessory phases were less common, with quartz becoming increasingly abundant. The pegmatite could be traced into a quartz breccia/stockwork system containing only minor amounts of feldspar.

WHOLE ROCK GEOCHEMISTRY

In 2001, a total of 208 whole-rock pegmatite samples (many >10 kg) were collected and analyzed for geochemistry and assay (Wengzynowski, 2002).

The minor and trace elements of twenty-three representative samples from that sample set were re-analyzed in 2005 using the high-resolution ICP-MS at the University of British Columbia. The analysis followed the procedure in Pretorius et al. (2006). The following results include major, minor, and trace element data from both analytical sessions; the minor and trace element data obtained for this study will be available in full on completion of the senior author's Ph.D. studies.

All the samples are strongly peraluminous (1.15-1.85; Maniar and Piccoli, 1989), and the majority can be described as granitic based on their distribution on a total alkali versus silica diagram (Le Bas et al., 1986). Calculation of the CIPW norms (software, B.M. Eglington, Saskatchewan Isotope Laboratory) indicates that the pegmatites are strongly quartz, corundum, orthoclase, and plagioclase normative, with albite much greater than anorthite.

Results from the whole-rock geochemistry data include: K/Rb ratios ranging from 4 to 24 with an average of 12; K/Cs ratios ranging from 58 to 534 and averaging 207; Rb/Cs ratios ranging from 7 to 47 with an average of 16.5; Nb/Ta ratios ranging from 0.6 to 22.6 with an average of 2.4; Li concentrations of 77 to 14161 ppm with an average of 6368 ppm; Cs concentrations of 46.9 to 497.3 ppm with an average of 174 ppm; Ta concentrations 5.3 to 188.4 ppm with an average of 95.7 ppm, (Table 1).

The LNPG samples have very low REE concentrations (0.5-3.6 ppm, average 1.9 ppm) with light REE (LREE) enrichment ranging between La/Er 10.7 to 32.9.

GEOCHRONOLOGY

The mineralogy of the LNPG dykes provides a challenge in determining the age of emplacement. In the absence of more commonly used phases, such as zircon, columbite was dated, using the U-Pb systematics by Mauthner et al. (1995); the result (81.6 ± 0.5 Ma) provides the most robust cooling age for the pegmatites determined so far. This magmatic cooling age of ca. 82 Ma for the LNPG pegmatites is approximately 8 million years younger than the youngest cooling age obtained by Rasmussen et al. (2007) for the regional plutons (as determined by U-Pb geochronology).

Some preliminary results from the senior author's current study include a date (65.89 ± 0.37 Ma, 2σ; Mean Squared Weighted Deviates (MSWD) = 1.09; Fig. 5) determined by step-heating $^{40}Ar/^{39}Ar$ analysis of a muscovite grain from the LNPG pegmatites. A stable plateau was obtained from ten steps corresponding to 74.8% of the released ^{39}Ar gas fraction. This date correlates with others obtained by Mauthner et al. (1995, K-Ar, muscovite and lepidolite, 66-65 Ma) and Rasmussen et al. (2007, $^{40}Ar/^{39}Ar$, biotite, 67-65 Ma), which indicate that a regional reheating event occurred between 67 and 65 Ma, resetting the ages of the micas. The cause of this thermal resetting has yet to be determined.

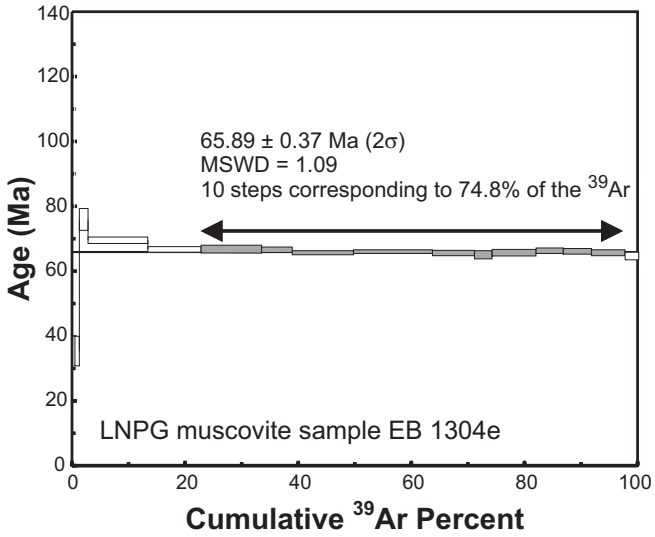


Figure 5. $^{40}Ar/^{39}Ar$ spectra from the analysis of a muscovite sample from the Little Nahanni Pegmatite Group. The heating steps used in calculating the final date are marked with an arrow above the data.

DISCUSSION

Geochemistry

Geochemical evidence for the degree of magmatic fractionation at LNPG is a primary factor in an assessment of the economic potential, as only the most highly evolved magmas are capable of concentrating elements such as lithium, cesium, and tantalum. The following section compares data from LNPG to several other examples of crustal rocks, chosen for the following reasons.

Firstly, the bulk rock compositions of the crust and upper crust (Rudnick and Gao, 2003) and the aplitic dykes associated with regional Cretaceous intrusions (Rasmussen et al., 2007) are compared to the LNPG to qualitatively assess whether the source of the pegmatites had a crustal component and whether the pegmatites have a petrogenetic link with the regional Cretaceous intrusions.

Secondly, the degree of fractionation and element enrichment at LNPG is compared with several examples of LCT pegmatites and other highly evolved intrusions occurring worldwide, including examples of economic LCT pegmatites.

Table 1. Selected elemental ratios and abundances of twenty-three whole-rock samples from the Little Nahanni Pegmatite Group (this study) and the examples mentioned in the text. Beauvoir granite (Raimbault et al., 1995); Greenbushes pegmatite (Partington, 1988); Ehrensfriedorf melt inclusion (Webster et al., 1997); Tanco pegmatite bulk composition (Černý, 2005); North Aubry pegmatite (Tindle et al., 2002; Breaks et al., 2003); Bulk crust (Rudnick and Gao, 2003); Aplite dykes associated with Cretaceous intrusions (Rasmussen et al., 2007). Number in brackets represents the number of samples.

Examples	K/Rb	K/Cs	Rb/Cs	Nb/Ta	Li (ppm)	Cs (ppm)	Ta (ppm)
LNPG (n=23)							
Range	4–24	58-534	7-47	0.6-22.6	77-14161	46.9-497.3	5.3-188.4
Average	12	207	16.5	2.4	6368	174	95.7
Beauvoir granite (6)	6-17	42-145	6-10	0.4-1.1	2201-5762	204-676	39-300
Greenbushes pegmatite (3)	5-20	25-36	5-9	0.7-0.8	955-2873	219-613	158-246
Ehrensfriedorf melt inclusion (1)	10	91	9	NA	NA	393	NA
Tanco pegmatite (composite)	5	9	2	NA	3438	NA	NA
North Aubry pegmatite (3)	6.6-7.9	5.9-32.7	0.9-4.2	0.052-0.199	8538-15967	271-3284	49-2672
Upper continental crust bulk	277	4744	17	13	24	4.9	0.9
Continental crust bulk	305	7472	25	11.4	16	2	0.7
Aplite dykes (9)	NA	NA	17-71	2.6-11.4	NA	6.3	3.2

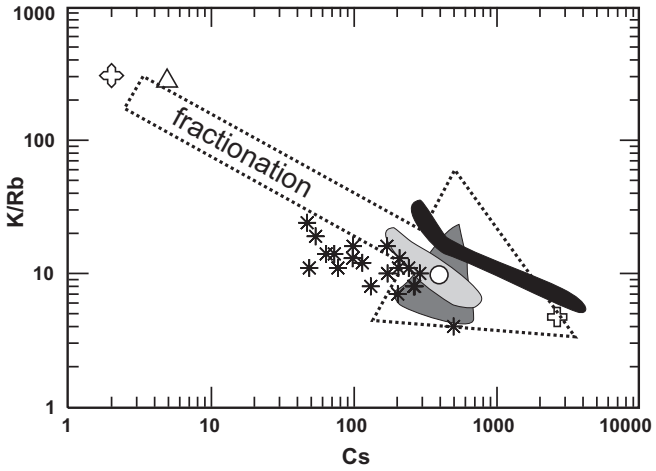


Figure 6. K/Rb ppm versus Cs (ppm). Symbols: star = Little Nahanni Pegmatite Group (this study); black polygon = Superior Province pegmatites (North Aubry) (Tindle et al., 2002; Breaks et al., 2003); pointed cross = bulk continental crust (Rudnick and Gao, 2003); triangle = bulk upper continental crust (Rudnick and Gao, 2003); mid-grey polygon = Greenbushes pegmatite (Partington, 1988); pale grey polygon = Beauvoir granite (Raimbault et al., 1995); circle = Ehrensfriedorf melt inclusion (Webster et al., 1997); cross = Tanco pegmatite bulk composition (Černý, 2005).

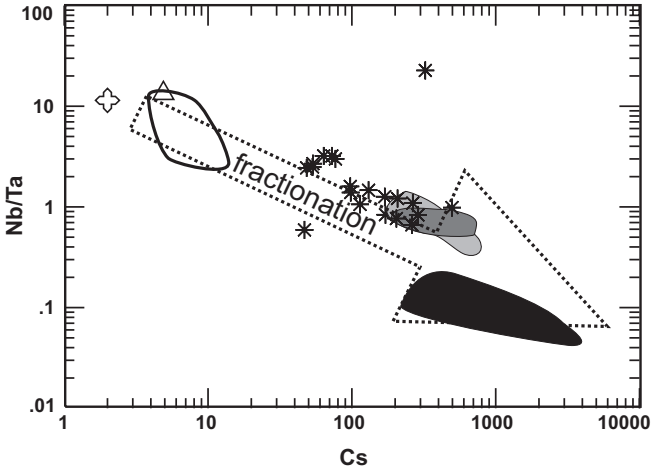


Figure 7. Nb/Ta versus Cs (ppm). Legend: star = Little Nahanni Pegmatite Group (this study); black polygon = Superior Province pegmatites (North Aubry) (Tindle et al., 2002; Breaks et al. 2003); pointed cross = bulk continental crust (Rudnick and Gao, 2003); triangle = bulk upper continental crust (Rudnick and Gao, 2003); mid-grey polygon = Greenbushes pegmatite (Partington, 1988); pale grey polygon= Beauvoir granite (Raimbault et al., 1995); transparent polygon = aplite dykes associated with Cretaceous intrusions proximal to Little Nahanni Pegmatite Group (Rasmussen et al., 2006, 2007).

Whole-rock geochemical analyses of the following selected intrusions were chosen: the North Aubry spodumene pegmatite from the Superior Province (Tindle et al., 2002; Breaks et al., 2003), selected for its high lithium concentration; melt inclusions from the Ehrensfriedorf pegmatite, an evolved peraluminous pegmatite of the Erzebirge region of Germany (Webster et al., 1997); various facies of the Beauvoir rare metal leucogranite in the Massif Central, France (Raimbault et al., 1995); the bulk composition Tanco pegmatite, Manitoba, (Černý, 2005); and the Greenbushes pegmatite, Australia (Partington, 1987; Partington et al., 1995).

As previously mentioned, highly evolved magmas responsible for LCT pegmatites become increasingly enriched in rare elements, such as Li, Cs, Ta, Nb, and Sn, and the degree of magmatic fractionation can be assessed using various elemental ratios such as K/Rb and Nb/Ta (Černý, 1991b).

The twenty-three whole-rock LNPG samples form an array in a diagram of K/Rb vs. Cs (Fig. 6) with decreasing K/Rb ratios and increasing Cs abundance, which is indicative of magmatic evolution (Tindle et al., 2002; Černý, et al. 2005). A straight line through the array to less-evolved compositions originates close to those of bulk crustal values, indicating that the source of the LNPG most likely includes a significant crustal component.

The LNPG data plot close to that from the Beauvoir granite, the Ehrensfriedorf melt inclusion, and the Greenbushes pegmatite. Data from the North Aubry pegmatite (Tindle et al., 2002; Breaks et al., 2003) are slightly more enriched in cesium. The sample from the North Aubry pegmatite, which has the lowest K/Rb ratio, lies proximal to that from the bulk composition of the Tanco pegmatite, which is recognized for its extreme fractionation (Černý, 2005).

A comparison of the Nb/Ta ratio (which decreases with magmatic fractionation) versus Cs (Fig. 7) permits an assessment of the degree of fractionation of the LNPG aplitic dykes associated with the various regional Cretaceous granitic intrusions (data from Rasmussen et al, 2007). The range of data from the LNPG shows a relatively linear fractionation trend that is more similar to the data from the Beauvoir granite than the Greenbushes pegmatite. The North Aubry pegmatite again shows a greater degree of fractionation than this group. The aplitic dykes of the proximal Cretaceous intrusions lie closer to a crustal composition but in line with the general fractionation trend.

The concentrations of lithium, cesium, and tantalum in the examples are compared in Table 1. The LNPG samples have the second highest concentrations of Li, after the North Aubry pegmatite (Tindle et al., 2002; Breaks et al., 2003), and the fourth highest concentration of Cs.

These data illustrate a comparable degree of magmatic fractionation between the LNPG and the economically developed deposits, although not the degree recognized at the North Aubry or Tanco pegmatites. The data indicate that the LNPG may be crustally derived and may also have petrogenetic links with the regional intrusions.

Distribution of Mineralization

The silicate and oxide minerals are both of potential economic significance at LNPG, as they both contain elements of interest. However, the different mineral types have very different distribution patterns within the pegmatites.

The silicate minerals, e.g., spodumene, mica, and feldspar (high in Li, Rb, and Cs), are the main rock-forming minerals, and are therefore ubiquitous and relatively accessible. Spodumene abundance can vary, as can the mica and feldspar compositions. The overall composition of bulk-rock samples from different locations across the system would therefore vary.

In contrast, the oxide minerals, e.g., columbite, tantalite, and cassiterite (enriched in Ta, Nb, and Sn), are accessory minerals, therefore far less abundant. Their concentration is unfocused, and they are disseminated throughout the pegmatites, with a general increase in Nb and Ta oxide mineralization associated with the absence of spodumene (Wengzynowski, 2002).

The Beauvoir Granite

The Beauvoir granite is recognized as sharing several characteristics with rare element-bearing pegmatites (Cuney et al., 1992, 2002), and may be useful as an analog for the plutonic source of the LNPG.

This crustally derived intrusion in the French Massif Central is the youngest and most enriched of several rare element-mineralized, peraluminous leucogranites intruding the thrust sheets of the Variscan Orogeny (Cuney et al., 2002). It was emplaced at ca. 308 Ma during a period of extension and normal faulting at the end, a significant mountain-building period between 390 to 310 Ma. The Beauvoir granite is capped by a small (~0.1 km^2), strongly mineralized Sn-W-Li-Ta-Nb-Be-Na-F-rich cupola. This cupola remained relatively intact, retaining magma that could otherwise have formed pegmatites. It has been mined for kaolin at surface with disseminated cassiterite and columbotantalite extracted as byproducts (Cuney et al., 1992; Raimbault et al., 1995).

Future studies

The discrepancy in the cooling ages between the LNPG and other regional intrusions of older than 10 Ma (Rasmussen et al., 2007) may indicate a period of magmatic fractionation of the plutonic source prior to pegmatite emplacement. Alternatively, this discrepancy may represent a separate magmatic event, perhaps associated with a period of regional extension in the western Selwyn Basin as recognized by Mair et al., (2006). The presence of several dyke swarms at LNPG may indicate several generations of pegmatites, further complicating the magmatic history. Clearly, further geochronological, structural, and petrological studies looking at the geological setting of the pegmatites are fundamental to an accurate evaluation of the potential for regional rare-element mineralization.

Neither the dykes nor the plutonic source of the LNPG show up as distinctive anomalies on maps of the regional airborne geophysical data obtained for the MERA study (radiometric and magnetic; Charbonneau, 2007). However, initial interpretations from a soil sampling program undertaken on behalf of War Eagle Mining Company Inc. in 2006, suggest that dykes may continue below the overburden to the southeast of the ridge, and subsurface studies investigating the location of the plutonic source of LNPG could also make significant advances in our understanding of its formation and mineralization.

CONCLUSION

The Late Cretaceous Little Nahanni Pegmatite Group is the most highly evolved of several small leucogranitic intrusive centres in the area. Its geochemical signature, which is enriched in several rare elements (e.g. Li, Cs, Ta, Nb, and Sn), is comparable to other well known examples of strongly mineralized and economic LCT pegmatites and related intrusions. These examples include the Beauvoir granite, which may serve as a useful analog of the undiscovered plutonic source of the LNPG. However, further studies are required to determine whether the source pluton for the pegmatites retained some of its mineralization in the manner of the cupola of the Beauvoir granite.

The emplacement of the LNPG pegmatites appear to have been influenced by significant regional structures: the March Fault and the Fork Anticline. Whether post-emplacement displacement along the March Fault has affected the distance between the current location of the pegmatites and their plutonic source is unknown.

The relatively small volume of the pegmatitic material and the disseminated nature of the oxide mineralization are recognized, however, given the rarity of the elements concerned and the relatively good access to the dykes, these aspects may not be a hindrance to commercial significance. Until the geology at depth is more clearly understood, the true picture of the full economic potential of the LNPG will remain undetermined.

At present, a zone of the O'Grady batholith (70 km north) presents the only other example of lithium mineralization occurring regionally and, to determine the potential for similar mineralization across the area, further studies on the temporal and petrogenetic link between the pegmatites and the regional Cretaceous intrusions are required.

ACKNOWLEDGEMENTS

The senior author wishes to take this opportunity to thank War Eagle Mining Company Inc. for their generous support of this study, and acknowledge the contribution of an NSERC Discovery Grant awarded to L.A. Groat.

The LNPG lies within the boundaries of the 2004-2006 Nahanni Mineral and Energy Resource Assessment (MERA), and the senior author would also like to thank the Geological Survey of Canada, and Hendrik Falck in particular, for field support during the 2005 field season.

REFERENCES

Ahlborn, V.H.
1977: Assessment Report on Prospecting Permit 105 - I-2; D. C. Rotherham, Feb. 1962, 8 p.
1979: The LICA Pegmatites, Nahanni Spodumene Belt, 1978 Field Investigations; Cominco Rare Metals Exploration Report, 20 p.
1980: Prospecting and Geochemical Survey on Lica Claims, Selwyn Mountains, NWT, Nahanni Mining Division (105I/12, 62º12‘N, 128º50‘W); Cominco Limited, Assessment Report.

Baker, D.R.
1998: The escape of pegmatite dykes from granitic plutons - constraints from new models of viscosity and dyke propagation; Canadian Mineralogist, v. 35, p. 255-263.

Beavon, R.V.
1977: Preliminary Geological Survey of the Cali 1-9, 11 Mineral Claims, Cantung Area, District of Nahanni, NWT; Canadian Superior Exploration Ltd.

Breaks, F.W., Selway, J.B., and Tindle, A.G.
2003: Fertile Peraluminous Granites and Related Rare-Element Mineralization in Pegmatites, Superior Province, northwest and northeast Ontario: Operation Treasure Hunt; Ontario Geological Survey, Open File Report 6099, 179 p.

Černý, P.
1991a: Rare-element granitic pegmatites. Part I: Anatomy and internal evolution of pegmatite deposits; Geoscience Canada, v. 18, p. 49-67.
1991b: Rare-element granitic pegmatites. Part 2: Regional to global environments and petrogenesis; Geoscience Canada, v. 18, p. 68-81.
1991c: Fertile granites of Precambrian rare-element pegmatite fields: is geochemistry controlled by tectonic setting or source lithologies?; Precambrian Research, v. 51, p. 429-468.
2005: The Tanco rare-element pegmatite deposit, Manitoba: Regional context, internal anatomy, and global comparisons, *in* Rare-Element Geochemistry and Mineral Deposits, (ed) R.L. Linnen and I.M. Samson; Geological Association of Canada, Short Course Notes 17, p. 127-158.

Černý, P, and Ercit, T.S.
2005: The classification of granitic pegmatites revisited; Canadian Mineralogist, v. 43, p. 2005-2026.

Černý, P., Masau, M., Goad, B.E., and Ferreira, K.
2005: The Greer Lake leucogranite, Manitoba, and the origin of lepidolite-subtype granitic pegmatites; Lithos, v. 80, p. 305-321.

Charbonneau, B.W.
2007: Evaluation of airborne radiometric and magnetic data in the vicinity of the Nahanni National Park Reserve, Northwest Territories, Canada, *in* Mineral and Energy Resource Assessment of the Greater Nahanni Ecosystem Under Consideration for the Expansion of the Nahanni National Park Reserve, Northwest Territories, (ed.) D.F. Wright, D. Lemkow, and J.R. Harris; Geological Survey of Canada, Open File 5344, p. 99-124.

Cuney, M., Marignac, C., and Weisbrod, A.
1992: The Beauvoir topaz-lepidolite albite granite (Massif Central, France): The disseminated magmatic Sn-Li-Ta-Nb-Be mineralization; Economic Geology, v. 87, p.1766-1794.

Cuney, M., Alexandrov, P., le Carlier de Veslud, C., Cheillitz, A., Raimbault, L., Ruffet, G., and Scaillet, S.
2002: The timing of W-Sn-rare metals mineral deposit formation in the Western Variscan chain in their orogenic setting: The case of the Limousin area (Massif Central, France), *in* The Timing and Location of Major Ore Deposits in an Evolving Orogen, (ed) D.J. Blundell, F. Neubauer, and A. von Quadt; Geological Society of London, Special Publication No. 204, p. 213-228.

Ercit, T.S., Groat, L.A., and Gault, R.A.
2003: Granitic pegmatites of the O’Grady batholith, N.W.T., Canada: A case study of the evolution of the elbaite subtype of rare-element granitic pegmatite; Canadian Mineralogist, v. 41, p. 117-137.

Gordey, S.P. and Anderson, R.G.
1993: Evolution of the Northern Cordilleran Miogeocline, Nahanni Map Area (105I), Yukon and Northwest Territories; Geological Survey of Canada, Memoir 428, 214 p.

Groat, L.A., Mortensen, J.K., Mauthner, M.H.F., Ercit, T.S., and Raudsepp, M.
1994: Geology and geochronology of the Little Nahanni Pegmatite Group, *in* Exploration Overview 1994, Northwest Territories, Mining, Exploration and Geological Investigations, (ed.) R. Kusick and S.P. Goff; Northwest Territories, Geology Division, p. 36-37.

Groat, L.A., Mulja, T., Mauthner, M.H.F., Ercit, T.S., Raudsepp, M., Gault, R.A., and Rollo, H.A.
2003: Geology and mineralogy of the Little Nahanni rare-element granitic pegmatites, Northwest Territories; Canadian Mineralogist, v. 41, p. 139-160.

Hart, C.J.R, and Lewis, L.L.
2005: Gold mineralization in the upper Hyland River area: A non-magmatic origin, *in* Yukon Exploration and Geology 2005, (ed.) D.S. Edmond, G.D. Bradshaw, L.L. Lewis, and L.H. Weston; Yukon Geological Survey, p. 109-125.

Hart, C.J.R., Goldfarb, R.J., Lewis, L.L., and Mair, J.L.
2004: The northern cordilleran mid-Cretaceous plutonic province: Ilmenite/magnetite-series granitoids and intrusion-related mineralization; Resource Geology, v. 54, p. 253-280.

Heffernan, R.S. and Mortensen, J.K.
2000: Age, geochemical, and metallogenic investigations of Cretaceous intrusions in the Tintina gold belt, southeastern Yukon; Geological Society of America, Abstracts with Programs, v. 32, p. 19.

Le Bas, M.J., Le Maitre, R.W., Streckeisen, A., and Zanettin, B.
1986: A chemical classification of volcanic rocks based on the total alkali-silica diagram; Journal of Petrology, v. 27, p. 745-750.

London, D.
2005: Granitic pegmatites: an assessment of current concepts and directions for the future; Lithos, v. 80, p. 281-303.

Mair, J.L., Hart, C.J.R., and Stephens, J.R.
2006: Deformation history of the northwestern Selwyn Basin, Yukon, Canada; Implications for orogen evolution and mid-

Cretaceous magmatism; Geological Society of America Bulletin, v. 118, p. 304-323.

Maniar, P.D. and Piccoli, P.M.
1989: Tectonic discrimination of granitoids; Geological Society of America Bulletin, v. 101, p. 635-643.

Mauthner, M.H.F.
1996: Mineralogy, Geochemistry and Geochronology of the Little Nahanni Pegmatite Group, Logan Mountains, southwestern Northwest Territories; M.Sc. thesis, University of British Columbia, Vancouver, British Columbia, 192 p.

Mauthner, M.H.F., Mortensen, J.K., Groat, L.A., and Ercit, T.S.
1995: Geochronology of the Little Nahanni Pegmatite Group, Selwyn Mountains, southwestern Northwest Territories; Canadian Journal of Earth Sciences, v. 32, p. 2090-2097.

Mortensen, J.K., Hart, C.J.R., Murphy, D.C., and Heffernan, S.
2000: Temporal evolution of Early and mid-Cretaceous magmatism in the Tintina Gold Belt, *in* The Tintina Gold Belt: Concepts, Exploration and Discoveries, (ed.) J. Jambor; British Columbia and Yukon Chamber of Mines, Special Volume 2, p. 49-57.

Partington, G.A.
1987: The geochronology, tectonic environment and structural control on intrusion of the giant rare-metal pegmatite at Greenbushes, Western Australia; Ph.D. thesis, University of Western Australia, Crawley, Western Australia, Australia.

Partington, G.A., McNaughton, N.J., and Williams, I.S.
1995: A review of the geology, mineralization, and geochronology of the Greenbushes Pegmatite, Western Australia; Economic Geology, v. 90, p. 616-635.

Pretorius, W., Weis, D., Williams, G., Hanano, D., Kieffer, B., and Scoates, J.
2006: Complete trace elemental characterisation of granitoid (USGS G-2, GSP-2) reference materials by high resolution inductively coupled plasma mass spectrometry; Geostandards and Geoanalytical Research, v. 30, p. 39-54.

Raimbault, L., Cuney, M., Azencott, C., Duthou, J.-L., and Joron, J.-L.
1995: Geochemical evidence for a multistage magmatic genesis of Ta-Sn-Li mineralization in the granite at Beauvoir, French Massif Central; Economic Geology, v. 90, p. 548-576.

Rasmussen, K.L., Mortensen, J.K., and Falck, H.
2005: Geochronological and lithogeochemical studies of intrusive rocks in the Nahanni region, southwestern Northwest Territories and southeastern Yukon, *in* Yukon Exploration and Geology 2005, (ed.) D.S. Edmond, G.D. Bradshaw, L.L. Lewis, and L.H. Weston; Yukon Geological Survey, p. 287-298.
2007: The potential for intrusion-related mineralization within the South Nahanni River MERA area, Selwyn and Mackenzie Mountains, Northwest Territories, *in* Mineral and Energy Resource Potential of the Proposed Expansion to the Nahanni National Park Reserve, North Cordillera, Northwest Territories, (ed.) D.F. Wright, D. Lemkow, and J. Harris; Geological Survey of Canada, Open File 5344, p. 203-244.

Rotherham, D.C.
1962: Canada Tungsten Mining Corporation Ltd., Hyland River Area, Mackenzie - Geophysics, Geochemistry, Regional Geology; Assessment Report 017568.

Rudnick, R.L. and Gao S.
2003: Composition of the continental crust, Chapter 3.01 *in* Treatise on Geochemistry, (ed.) H. D. Holland and K.K. Turekian; Elsevier, p.1-64.

Sirbescu, M.-L.C. and Nabelek, P.I.
2003: Crustal melts below 400°C; Geology, v. 31, p. 685-688.

Stewart, D.B.
1978: Petrogenesis of lithium-rich pegmatites; American Mineralogist, v. 63, p. 970-980.

Tindle, A.G., Selway, J.B., and Breaks, F.W.
2002: Electron microprobe and bulk analyses of minerals from fertile peraluminous granites and related rare-element pegmatites, Superior Province, Northwest Ontario: Operation Treasure Hunt; Ontario Geological Survey, Miscellaneous Report 127.

Webster, J.D., Thomas, R., Rhede, D., Förster, H.-J., and Seltmann, R.
1997: Melt inclusions in quartz from an evolved peraluminous pegmatite: Geochemical evidence for strong tin enrichment in fluorine-rich and phosphorus-rich residual liquids; Geochimica et Cosmochimica Acta, v. 61, 2589-2604.

Wengzynowski, W.A.
2002: Geological Report on the Mac Property; War Eagle Mining Company Incorporated, 33 p.

THE POTENTIAL FOR INTRUSION-RELATED MINERALIZATION WITHIN THE SOUTH NAHANNI RIVER MERA AREA, SELWYN AND MACKENZIE MOUNTAINS, NORTHWEST TERRITORIES

Kirsten L. Rasmussen[1], James K. Mortensen[1], Hendrik Falck[2], and Thomas D. Ullrich[3]

1. Department of Earth and Ocean Sciences, University of British Columbia, 6339 Stores Road, Vancouver, British Columbia V6T 1Z4
2. Northwest Territories Geoscience Office, P.O. Box 1500, Yellowknife, Northwest Territories X1A 2R3
3. Department of Geological Sciences and Geological Engineering, Queen's University, Kingston, Ontario K7L 3N6

INTRODUCTION

A study of intrusive rocks and the potential for related mineralization in southwestern Northwest Territories (NWT) was initiated as one component of the 2004 to 2006 South Nahanni Mineral and Energy Resource Assessment (MERA II). Magmatism in the study area is confined to the southeastern Selwyn Mountains in the western portion of the Nahanni River watershed near the the Yukon Territories border (Fig. 1). Intrusions in the study area represent the southeastern extent of the Tintina Gold Province, an elongate band of Early to Late Cretaceous magmatism that extends northwest from the study area across the Yukon Territory and into central Alaska. The Tintina Gold Province is characterized by numerous precious and base metal occurrences and deposits that are spatially and genetically related to well defined, metalliferous, Mid- and Late-Cretaceous plutonic suites (Mortensen et al., 2000; Hart et al., 2004a). Several known intrusion-related deposits and occurrences are documented within the study area by the Northern Minerals Database, (Deptartment of Indian Affairs and Northern Development, 2006) (Fig. 2; Appendix 1), but the rugged topography and lack of road access has hindered exploration efforts. The potential for additional intrusion-related mineralization in much of the study area has not been previously investigated in detail despite the presence of widespread intrusion-related mineral occurrences.

The focus of this study is to determine which intrusions within the South Nahanni River MERA area may have the most significant potential for related mineralization. This has been approached through the use of two basic methods: (1) field observations combined with a geochronological, geochemical, and geophysical classification of plutonic suites, and the Pb-isotope chemistry of the intrusions and adjacent mineral occurrences, and, (2) a magmatic fluid composition study involving the detection of enriched versus depleted volatiles within the crystallizing intrusions. The authors conclude with a brief discussion that highlights intrusions with a higher potential for related mineralization within the study area. Additional data is appended: Appendix 1 summarizes the mineral occurrences (plotted on the map in Fig. 2) that are known or inferred to be related to intrusions within the study area, as well as several ambiguous occurrences that may or may not be related to magmatism, and three non-intrusion-related mineral occurrences that were also analyzed. Appendix 2 consists of polished and stained (for K-feldspar) slab images for essentially all of the intrusive samples presented and discussed throughout the body of this paper (i.e. the samples that underwent geochronological and geochemical analysis). Appendices 3, 4, and 5 detail the geochronological, isotope, and microbeam analytical methods employed in this study. Also, a reprint of the paper Rasmussen et al. (2007), which discusses the morphology and composition of placer gold grains collected from the study area, can be found at the end of this volume.

FIELD OBSERVATIONS

Mid-Cretaceous (ca. 100-90 Ma), felsic intrusive rocks underlie a significant portion of the Nahanni MERA area and range from large batholithic bodies to small plugs or stocks, and are associated with contemporaneous to slightly younger felsic and mafic dykes (Fig. 1). Many of the plutons are composed of more than one phase of intrusion; this is established from both internal contacts and textural, mineralogical, and magnetic susceptibility variations, and/or by age variations between different portions of the larger intrusions. Intrusive contacts are shallow- to steep-dipping, but dominantly conformable to the adjacent wall-rock strata, which frequently obscure buried margins of the intrusions (Fig. 3A). Dykes and/or sills are commonly observed along the margins of intrusions, either concentric to the margins of the intrusion (Fig. 3A) or concordant to bedding and local structure (Fig. 3B); such dykes and sills commonly intrude both plutonic and sedimentary rocks.

Most of the Mid-Cretaceous intrusions have a relatively restricted quartzo-feldspathic mineralogy with biotite, ± hornblende or sparse muscovite. Several textural variations, ranging from fine-grained feldspar (-quartz) porphyritic diorite to granite (Fig. 3C), to

Rasmussen, K.L., Mortensen, J.K., Falck, H. and Ullrich, T.D., 2007, The potential for intrusion-related mineralization within the South Nahanni River MERA area, Selwyn and Mackenzie Mountains, Northwest Territories, *in* Mineral and Energy Resource Assessment of the Greater Nahanni Ecosystem Under Consideration for the Expansion of the Nahanni National Park Reserve, Northwest Territories; Geological Survey of Canada, Open File 5344, p. 203-278.

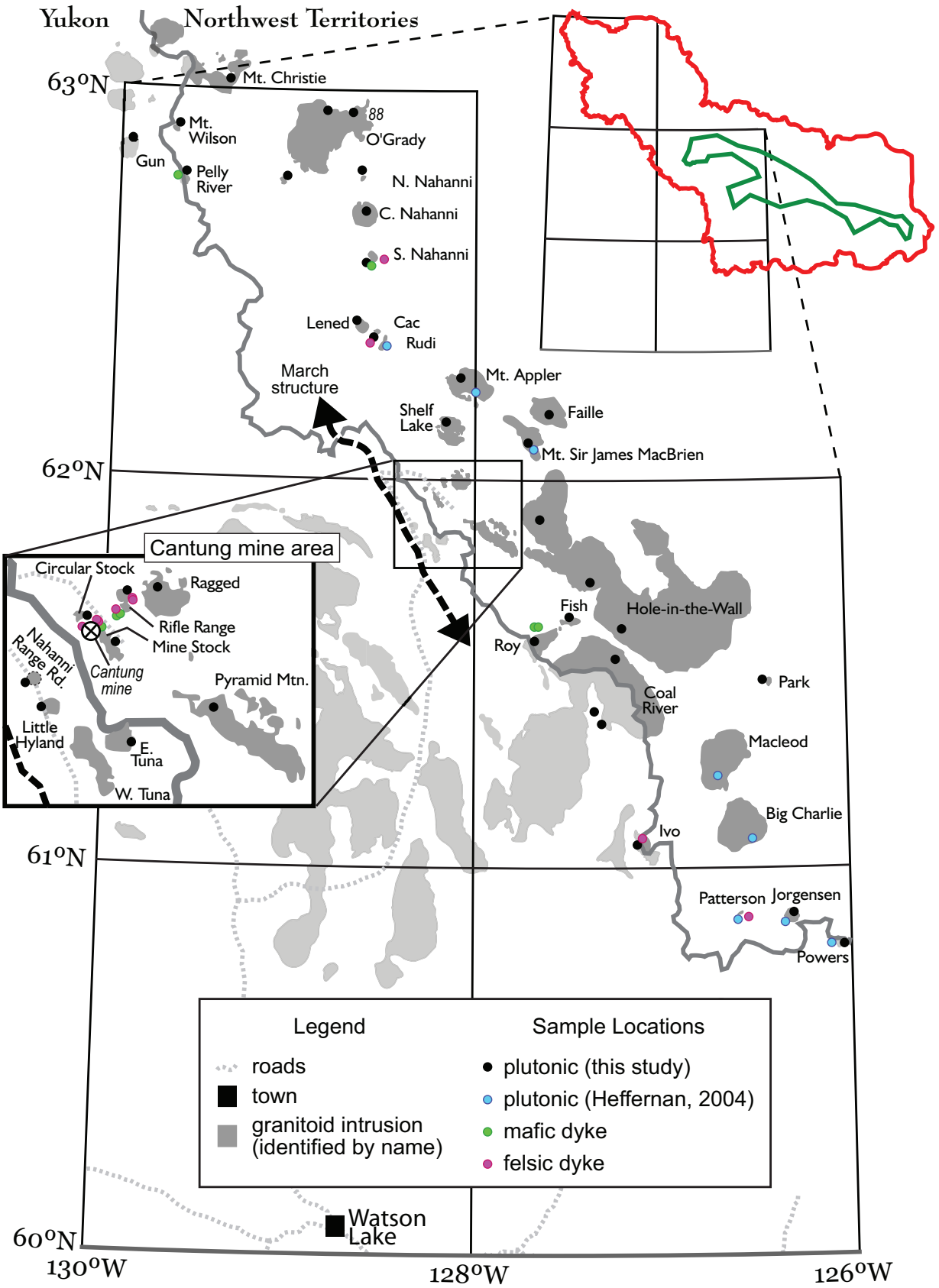


Figure 1. Study area, granitoid intrusions, and sample locations relative to the South Nahanni River watershed (red, upper inset) and the Federal Park Reserve (green, upper inset). Intrusive samples for this study and from Heffernan (2004) are located, and the Cantung mine area is expanded in the lower inset. The Yukon portion of the map is lightly faded, and the base map is modified from Gordey and Makepeace (1999).

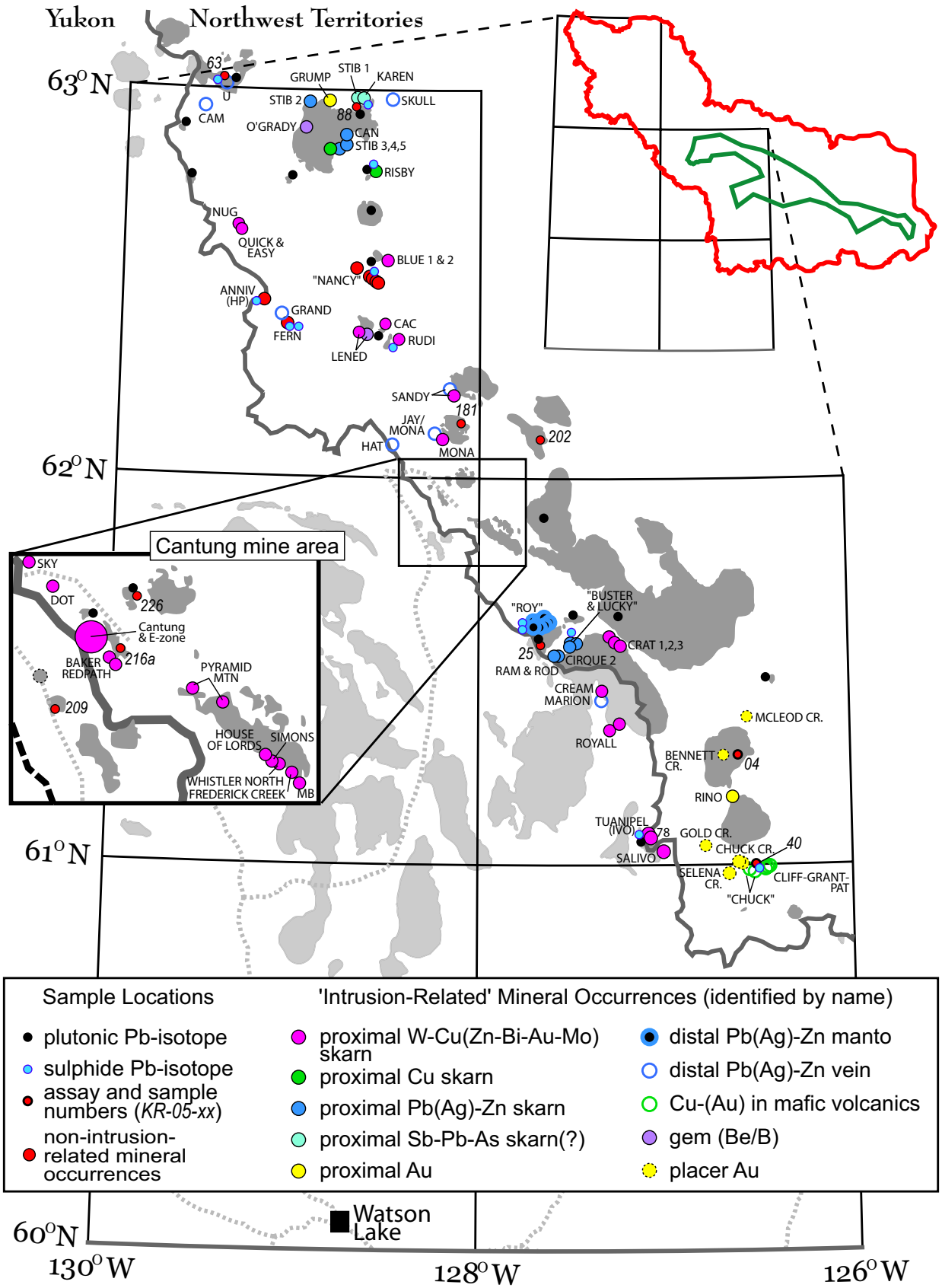


Figure 2. Intrusion-related metallogeny relative to the South Nahanni River watershed (red; upper inset) and the Federal Park Reserve (green; upper inset). 'Intrusion-' and 'non-intrusion'-related mineral occurrences are located and named; locations are taken from the NORMIN database (Gordey and Anderson, 1993; Department of Indian Affairs and Northern Development, 2006). Assay sample locations and Pb-isotope sample locations (plutonic feldspars and mineralization sulphides) are also indicated. The Cantung mine area is expanded in the lower inset, the Yukon portion of the map is lightly faded, and the base map is modified from Gordey and Makepeace (1999).

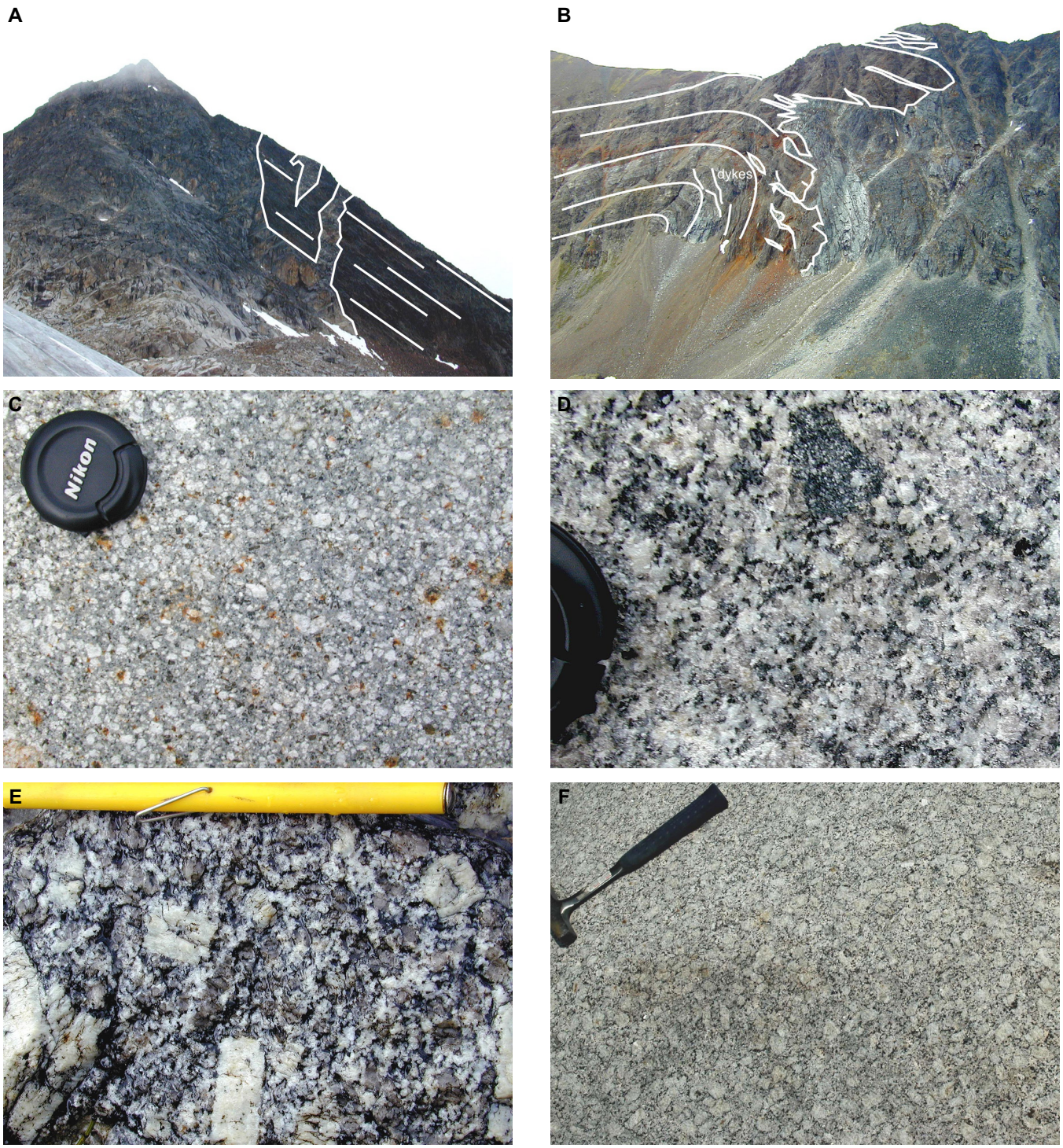


Figure 3. Granitoid field relationships, textures, and evolved phases. **A)** Stepped granite-country rock contact with concentric dykes; bedding is indicated (Rifle Range pluton). **B)** Granite-country rock contact with marginal sill swarms intruding locally folded country rock; folded bedding is indicated and short irregular lines represent dykes (Roy pluton). **C)** Fine-grained feldspar-chlorite-hornblende dioritic porphyry (Powers pluton). **D)** Fine- to medium-grained equigranular, biotite-hornblende-bearing granodioritic phase (North Nahanni pluton). **E)** Medium-to coarse-grained K-feldspar porphyritic monzogranite (South Nahanni pluton). **F)** Medium-grained, hornblende-bearing, K-feldspar cumulate syenitic phase (O'Grady batholith).

fine- to medium-grained granodiorite to monzogranite with sparse to abundant K-feldspar phenocrysts (<0.5 to >4 cm long; Fig. 3D, E) to cumulate K-feldspar syenite (Fig. 3F) are observed within the intrusions. The development of volatile-rich phases in the felsic intrusions, both syn- and post-crystallization, is indicated by the presence of the following:

- leucocratic muscovite-garnet(-tourmaline) phases along the margins of the intrusions (Fig. 3G);



Figure 3 continued. G) Leucocratic marginal phase with biotite-tourmaline-muscovite-(garnet) (Rudi pluton; adjacent to W-skarn). **H)** Tourmaline-quartz vein cutting aplite dyke and leucocratic marginal biotite-muscovite-garnet-bearing phase (Ivo pluton; adjacent to W-skarn). **I)** Small miarolitic cavity infilled by tourmaline (Hole-in-the-Wall batholith). **J)** Large miarolitic cavity with aplitic margin in K-feldspar porphyritic monzogranite (Hole-in-the-Wall batholith). **K)** Sheeted gossanous fractures cutting K-feldspar porphyritic monzogranite (Mt. Appler pluton). **L)** Hydrothermal breccia with clasts of granite, argillite, and unskarnified Swiss Cheese Limestone and Ore Limestone in a rock-flour matrix at the Cantungm mine (Circular Stock).

- quartz(-tourmaline) veins and aplite-pegmatite dykes (Fig. 3H);
- miarolitic cavities infilled with graphic textured tourmaline in batholithic intrusions (Fig. 3I, J);
- sheeted gossanous fractures (Fig. 3K);
- one example of a late-stage, marginal breccia in the Circular stock at the Cantung mine (Fig. 3L); and
- large (>1 m thick), proximal to distal, frequently sulphide-bearing aplite, granite, or quartz diorite dykes.

Table 1. Characteristics of plutonic suites identified in the Nahanni MERA area (based on observations from this study and Hart et al., 2004a and 2005).

Plutonic Suite	Tombstone	Tungsten	TR-Tungsten	Tay River
Intrusions	moderate-large; compositionally zoned with more evolved cores	very small to small; quartz is often pale pink-grey	moderate; quartz is often pale pink-grey	moderate to large; quartz is often dark grey
U-Pb Age Range (Ma)	94-90	99-95	100-96	100-96
Mag. Susc ($x10^{-3}$SI units)	0.3-7.0 (avg = 1.8)	< 0.2 (avg = 0.16)	< 0.3 (may be very high)	typically >5.0
Fe_2O_3/FeO	0.2-1.0	0.0-0.3	0.0-0.35	0.3-0.6 (most ~0.4)
Fe-Ti minerals	magnetite> titanite	ilmenite>> titanite	ilmenite> titanite	magnetite may be present
Alkalinity	alkaline	sub-alkaline	sub-alkaline	sub-alkaline
Aluminosity (ASI)	meta- to slightly peraluminous (0.8-1.16)	moderately peraluminous (1.06-1.20)	peraluminous (0.98-1.14)	lightly peraluminous (0.98-1.14)
Composition	hornblende-biotite-bearing monzonite and **syenite**; lesser qtz monzonite, monzodiorite, monzogabbro, and Si-undersaturated high-K phases	**fine- to medium-grained and weakly K-feldspar porphyritic** leucocratic **biotite-bearing monzogranite**, and quartz monzonite	fine- to medium-grained, weakly K-feldspar porphyritic **biotite-bearing monzogranite, granodiorite,** and quartz monzonite	K-feldspar porphyritic, **biotite-hornblende-bearing granodiorite and monzogranite**
Minor Minerals	local pyroxene	sparse muscovite	possible sparse muscovite; local hornblende	n/a
Associated Intrusive Phases	small tourmaline-infilled miarolitic cavities; coarse cumulate grains are abundant	muscovite-garnet-(±tourmaline)-bearing marginal phases; aplite-pegmatite dykes	aplite-pegmatite dykes; small tourmaline-infilled miarolitic cavities	aplite-pegmatite dykes; feldspar±(quartz or biotite) porphyry phases
Accessory Minerals	epidote, allanite, malanite, apatite, fluorite, zircon	apatite (less abundant) allanite, zircon, monazite	apatite, allanite, zircon, ±monazite	apatite, allanite, zircon
***Th/U**	typically >1	1-2	>/< 1	<1
Metallogeny	proximal Pb(Ag)-Zn, Cu, or Sb-Pb-As skarn; proximal Au and placer Au; distal Pb(Ag)-Zn vein; rare gem (B-elbaite); possible mafic-volcanic-hosted Cu-(Au)	abundant: W-Cu-(Zn-Bi-Au-Mo); distal Pb(Ag)-Zn vein; rare: gem (Be-emerald)	rare proximal Cu or W-Cu-(Zn-Bi-Au-Mo) skarn	proximal Pb(Ag)-Zn or W-Cu-(Zn-Bi-Au-Mo) skarn; rare distal Pb-(Ag)-Zn manto-style

*primitive mantle normalized values (Sun and McDonough, 1989)

Plutonic Suites

In the course of this study, several plutonic suites were identified within the South Nahanni MERA area: the Tombstone suite, the Tungsten suite, a transitional Tay River-Tungsten subsuite (TR-Tungsten), and the Tay River suite (Fig. 4). The Tombstone, Tungsten, and Tay River suites have been previously described (Mortensen et al., 2000; Heffernan, 2004; and Hart et al., 2004a, 2005); however, much of the characterization of these suites is based on studies in the Yukon Territory with limited examination of intrusions from within the MERA area in the Northwest Territories. For this reason, it was uncertain which plutonic suites in the Yukon Territory actually extended over the border to the Northwest Territories, and to which of the suite(s) established in the Yukon Territory the intrusions in the Northwest Territories could be assigned. Although the plutonic suites have been defined for the MERA area in this study largely based on geochronological, geochemical, and geophysical characterization and correlation, a summary of field observations for each suite is given as follows (see also Table 1).

Tay River suite intrusions, as originally defined by Mortensen et al. (2000) and Heffernan (2004), are medium- to coarse-grained, strongly K-feldspar porphyritic (>1 cm; typically 1.5-3 cm), and biotite-hornblende-bearing. These intrusions typically form large batholithic bodies, although a few smaller Tay River suite intrusions are seen flanking the larger intrusions. In this study, rare crosscutting or proximal felsic (aplite or felsic porphyry) and distal mafic (quartz monzodiorite) dykes were locally observed in association with Tay River intrusions, as were sulphide-rich quartz veins or sheeted gossanous fractures near intrusive margins. Although this suite was characterized as 'non-metallogenic' by Mortensen et al. (2000), at least within the study area there are several argentiferous Pb-Zn occurrences, as distal mantos or veins and as proximal skarn, as well as a few tungsten-dominated skarn occurrences, found along the margins of these plutons (Fig. 4). There are also several Tay River suite intrusions located in the southeastern portion of the study area that form very small (<0.5 to 5 km in diameter), very fine-grained to porphyry-textured 'plugs' (Fig. 4). These plugs are typically more mafic than the larger Tay River suite batholiths; the porphyry-textured plugs are plagioclase porphyritic (<0.5 cm).

Tungsten suite intrusions form very small to small (<0.5 to 5 km in diameter), fine- to medium-grained

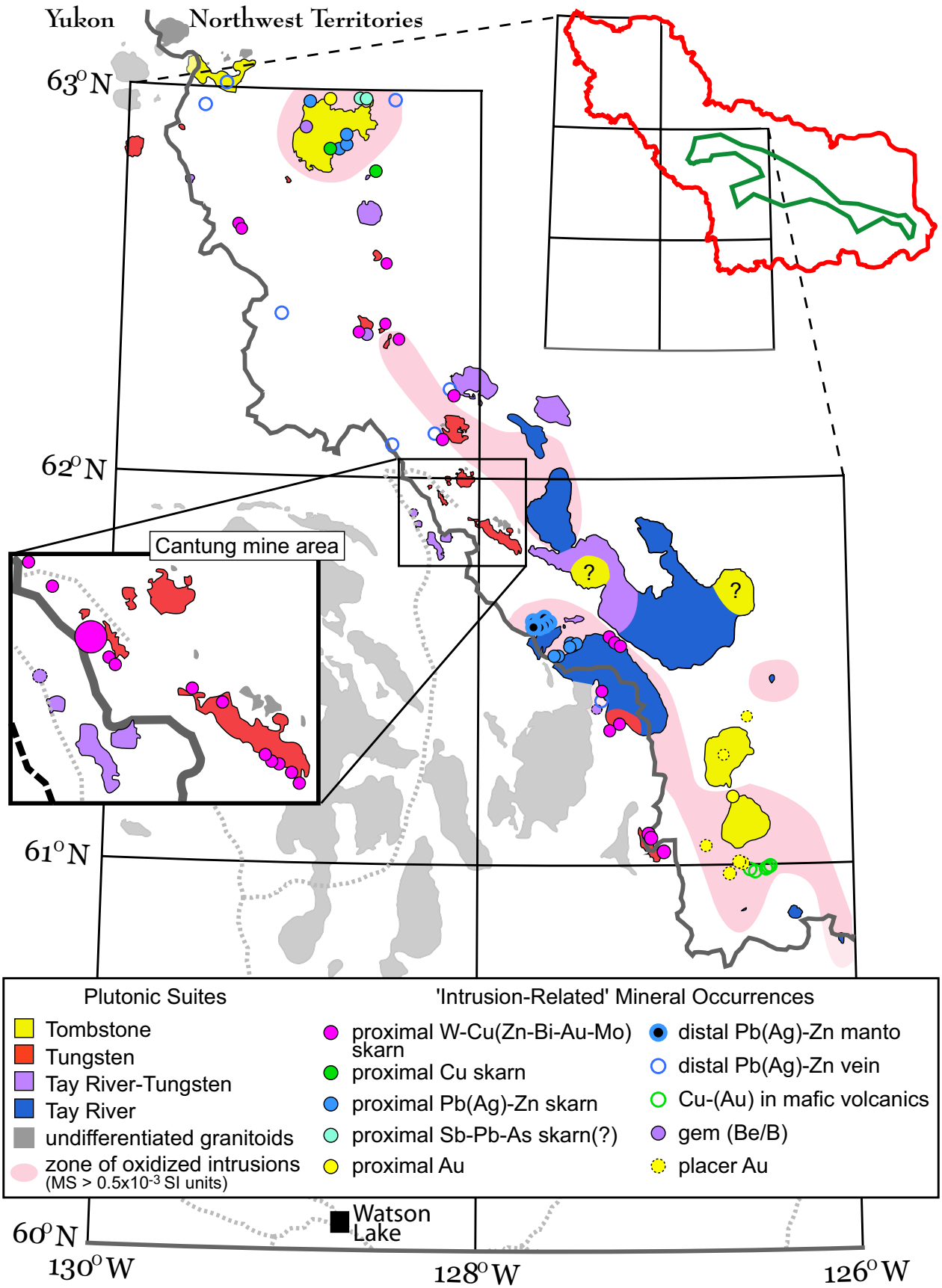


Figure 4. Plutonic suites relative to the South Nahanni River watershed (red, upper inset), the Federal Park Reserve (green, upper inset), and mineral occurrences. The Cantung mine area is expanded in the lower inset, the Yukon portion of the map is lightly faded, and the base map is modified from Gordey and Makepeace (1999).

bodies. These intrusions are usually weakly or sparsely K-feldspar porphyritic, and phenocrysts are frequently <0.5 cm. Biotite and monazite are ubiquitous throughout these intrusions, although rare intrusive phases with additional but sparsely distributed, ragged muscovite are also present in some intrusions (e.g. Lened, Mine Stock). Localized marginal intrusive phases commonly contain muscovite and garnet or tourmaline, tend to be finer grained, and may even be slightly foliated. These marginal phases are typically in direct contact with the majority of the tungsten occurrences in the study area. Aplite and pegmatite dykes may be locally abundant, both crosscutting the intrusions and the country rock, and are usually biotite-muscovite-(garnet or tourmaline)-bearing (Ivo, Rudi, Cac) although some are highly altered and sulphide-bearing (Mine Stock, Rudi). Mafic dykes have also been observed crosscutting these intrusions and the associated mineralization (Mine Stock, Rudi). Sheeted gossanous fractures or quartz veins may be present in this suite, although scheelite and other tungsten minerals are not usually observed in fractures or veins.

The transitional TR-Tungsten sub-suite shares features of both Tungsten and Tay River suite intrusions; these intrusions are typically coarser-grained and more strongly K-feldspar porphyritic, and of intermediate size to both suites. They have only one documented tungsten occurrence and one documented copper occurrence, both skarns (Fig. 4). Overall, Figure 4 also shows a rough spatial distribution whereby the TR-Tungsten suite intrusions are occur near the larger Tay River suite intrusions, in an intermediate position between the exposed Tay River and Tungsten suite intrusions.

Tombstone suite intrusions form moderate-to large-rounded bodies that may or may not be zoned to more felsic cores (Hart et al., 2005). These intrusions are typically medium- to coarse-grained, and hornblende-biotite(-pyroxene)-bearing. K-feldspar phenocrysts are present throughout and, if abundant enough, may form a 'cumulate texture'; magnetite phenocrysts have also been observed. Miarolitic cavities infilled with graphic textured tourmaline may be present in some marginal phases (Fig. 3I) giving the rock a spotted appearance, and although aplite-pegmatite dykes are not abundant, there is at least one report of gem-quality tourmaline hosted in miarolitic cavities of aplite-pegmatite sheets in the southwestern portion of the O'Grady batholith (Fig. 1). Quartz (±tourmaline) veins are relatively abundant, as are sheeted gossanous fractures, particularly near plutonic margins. Porphyry-textured phases may also be observed locally along plutonic or batholithic margins, such as the small intrusive phase associated with an antimony occurrence in the northeastern portion of the O'Grady batholith (Fig. 1).

GEOCHRONOLOGICAL, GEOCHEMICAL, AND GEOPHYSICAL CLASSIFICATION OF PLUTONIC SUITES

Methods and Preliminary Data

Geochronology

Thirty-one intrusive samples were selected for U-Pb analysis, the results are interpreted to be crystallization or emplacement ages (Table 2). Samples selected for analytical work were typically medium-grained and megacrystic or K-feldspar porphyritic intrusive phases, and are inferred to be representative of the intrusion overall. This is consistent with detailed mapping of intrusive phases by Gordey and Anderson (1993) for several plutons in the study area (Lened, Cac, Rudi, and O'Grady), in which the K-feldspar megacrystic phases form the bulk of the intrusions. The two exceptions to the sampling of megacrystic phases for analysis in this study are KR-05-32 (Ivo sample), a marginal fine-grained equigranular muscovite-garnet-bearing monzogranite in proximity to tungsten mineralization, and KR-05-76 (Pelly River), a marginal fine-grained biotite-bearing quartz diorite. The U-Pb data include both zircon (or monazite) ages determined by the isotope dilution thermal ionization mass spectrometry (ID-TIMS) method, and zircon ages determined by the laser ablation inductively coupled plasma mass spectrometry) (LA-ICP-MS) method. $^{206}Pb/^{238}U$ ages are reported for the LA-ICP-MS analyses; however these data presented here are regarded as preliminary as they are currently being improved upon by further analytical work. Results from earlier U-Pb analyses by ID-TIMS methods for ten samples from within the MERA area (Fig. 1), reported by Heffernan (2004), were also compiled with the data from this study in Table 2. Twenty-six of the samples that underwent U-Pb analysis in this study were also dated by $^{40}Ar/^{39}Ar$ analysis of biotite, the results are described as 'cooling ages' (Table 2). An additional five samples collected from mafic dykes observed in proximity to, or crosscutting several intrusions and/or associated mineralization, were also analyzed for argon. ^{40}Ar-^{39}Ar analysis employed laser step-heating and the ages reported here are based on well defined plateau ages for biotite. All geochronological data were obtained at the Pacific Centre for Isotopic and Geochemical Research (PCIGR), University of British Columbia, Vancouver, and errors reported in Table 2 are given at the 2-sigma level. A detailed description of geochronological methods may be found in Appendix 3.

The plutons have a relatively small and continuous range of crystallization ages (inferred by the closure of the U-Pb system in zircon and monazite) and cooling ages (inferred by the closure of the argon system in biotite), between 100 and 90 Ma. Based on the crystal-

Table 2. U-Pb and Ar-Ar geochronology of intrusions within the Nahanni MERA area. Crystallization ages are from U-Pb: KR-05 samples are LA-ICP-MS ages for zircon, and all other samples are ID-TIMS ages for zircon, unless indicated as monazite (-m). Cooling ages are from Ar-Ar data for biotite. 2-sigma errors are in brackets for U-Pb and Ar-Ar ages, and cooling periods are minimum age differences, after accounting for the 2-sigma error between the U-Pb crystallization and Ar-Ar cooling ages. Grey boxes indicate that either no data are available, or that the data are not applicable. Intrusions sampled within proximity to a known mineral occurrence are annotated with the capitalized name of the mineral occurence.

Sample	Location	Plutonic Suite	Crystallization age (Ma)	Cooling age (Ma)	Cooling Period (m.y.)
99-SH-011*	Big Charlie	Tombstone	91.0 (0.3)		
KR-05-198	Hole-in-the-Wall	Tombstone?	91.8 (2.0)	~92	0
KR-05-97b	O'Grady - GRUMP	Tombstone	92.4 (0.4)		
KR-05-62	Mt. Christie - U	Tombstone	93.2 (1.1)	94.4 (0.5)	0
98-HAS-14*	McLeod	Tombstone	93.9 (0.2)		
KR-05-194	Coal River - ROYALL	Tungsten?	90.3 (1.8)	67.0 (0.4)	>4.5
03DM-12	Lened - LENED	Tungsten	95.0 (0.6)	94.5 (0.8)	0
KR-05-148	Rifle Range	Tungsten	96.3 (1.8)	96.6 (0.5)	0
KR-05-143	Circular Stock	Tungsten	96.8 (2.2)	97.6 (0.5)	0
KR-05-68	Mt. Wilson	Tungsten	97.3 (1.7)	96.4 (0.5)	0
KR-05-126	plug southwest of O'Grady	Tungsten	97.7 (1.5)		
KR-05-32	Ivo - IVO	Tungsten	98.0 (1.4)	65.0 (0.5)	>4.5
98-Z-C-028*	Rudi - RUDI	Tungsten	98.0 (1.2)-m		
03M-207	Mine Stock, Cantung mine	Tungsten	98.2 (0.4)	95.1 (0.4)	2.3
03M-204	aplite, cutting Mine Stock	Tungsten	98.3 (0.3)		
03M-203	aplite, along fault, Mine Stock	Tungsten	98.4 (0.3)		
KR-05-110	Cac - CAC	Tungsten	98.7 (0.8)	94.6 (0.5)	2.8
KR-05-113	South Nahanni - BLUE 1& 2	Tungsten	100.3 (1.2)	95.8 (0.5)	2.8
KR-05-164	Hole-in-the-Wall	TR-Tungsten	94.1 (1.2)	95.2 (0.5)	0
98-HAS-02*	Mt. Appler	TR-Tungsten	94.5 (0.9)		
KR-05-26	Fish	TR-Tungsten	95.8 (0.6)	97.2 (0.6)	0
03M-216	Faille	TR-Tungsten	~97.0	96.4 (0.5)	0
99-SH-013*	West Tuna	TR-Tungsten	97.1 (0.2)-m		
KR-05-191	Coal River - MARION	TR-Tungsten	97.3 (1.3)	95.5 (0.5)	0
KR-05-136	North Nahanni - RISBY	TR-Tungsten	98.0 (1.1)	96.8 (0.5)	0
KR-05-76	Pelly River	TR-Tungsten	98.3 (1.2)	97.1 (0.5)	0
KR-05-130	Central Nahanni	TR-Tungsten	98.5 (1.9)	96.0 (0.5)	0.1
KR-05-208	Little Hyland	TR-Tungsten	99.5 (1.3)	89.3 (0.5)	>4.5
KR-05-210	Nahanni Range Road	TR-Tungsten	100.0 (1.3)	86.5 (0.5)	>4.5
99-SH-008*	Coal River (Yukon)	Tay River	95.6 (0.4)		
99-SH-006*	Coal River (Yukon)	Tay River	96.9 (0.4)		
KR-05-196	Coal River - CRAT	Tay River	97.8 (0.9)	94.9 (0.5)	1.5
KR-05-22	Roy - ROY	Tay River	95.7 (1.2)	96.2 (0.5)	0
03M-217	Mt. Sir James McBrien	Tay River	96.8 (0.5)	95.3 (0.5)	0.5
KR-05-43	Park	Tay River	97.0 (0.9)	97.0 (0.5)	0
98-HAS-12*	Patterson	Tay River	97.5 (0.3)		
98-HAS-12a*	felsic dyke, Patterson	Tay River	98.3 (1.6)-m		
03M-218	Hole-in-the-Wall (north)	Tay River	97.5 (0.3)		
98-HAS-06*	Mt. Sir James MacBrien	Tay River	97.7 (0.2)		
KR-05-10	Jorgensen	Tay River	98.2 (1.3)		
KR-05-08	Powers	Tay River	102.4 (2.3)	101.4 (0.6)	0
KR-05-204	mafic dyke, Mine Stock			91.0 (0.8)	
KR-05-77	mafic dyke, Pelly River			95.7 (0.7)	
KR-05-157	mafic dyke, Roy			96.5 (0.7)	
KR-05-213	mafic dyke, Rifle Range			96.7 (0.8)	
KR-05-158	mafic dyke, Roy			97.6 (0.7)	

*data from Heffernan (2004)

lization ages, combined with geochemical and geophysical characteristics (as described below) and earlier work by Heffernan (2004) in the study area, the intrusions analyzed have been classified by this study into several of the plutonic suites previously described by several workers and already established for the Yukon Territory (Mortensen et al., 2000; Hart et al., 2004a and 2005). Those plutonic suites identified in the

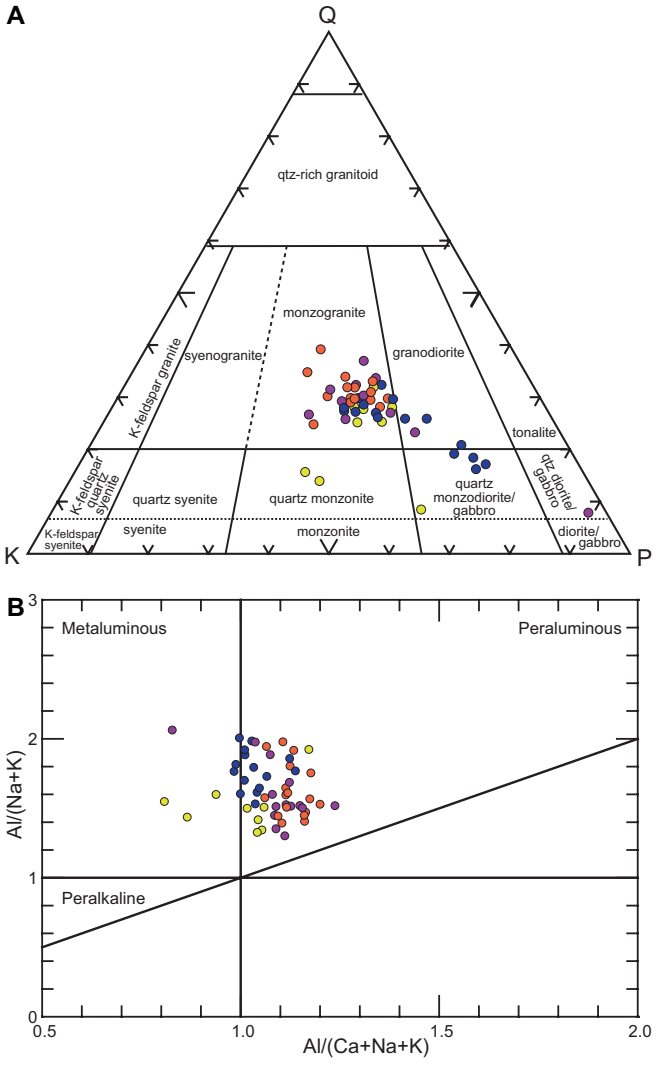


Figure 5. Major element oxides for plutonic samples, based on plutonic suites: Tombstone suite are yellow, Tungsten suite are red, TR-Tungsten subsuite are purple, and Tay River suite are blue. **A)** Quartz-K-feldspar-plagioclase ternary diagram (Streckeisen, 1976). **B)** Aluminosity plot of Shand's Index after Maniar and Piccoli (1989).

study area, as described briefly above, are: the Tombstone suite (94-90 Ma); the Tungsten suite (99-95 Ma); a transitional Tay River-Tungsten subsuite (TR-Tungsten; 100-96 Ma); and, the Tay River suite (102-96 Ma). Associated aplitic dykes and several mafic dykes are essentially coeval to the intrusions, although most crosscut intrusions and/or mineralization, and have for the most part cooled between 98 and 95 Ma.

Several larger intrusions also have a wide range of crystallization ages, such as the Hole-in-the-Wall batholith (97.5, 94.1, or 91.8 Ma; Table 2), which is a result of multiple influxes of magma. The youngest Hole-in-the-Wall age is from a sample of a rounded portion of the batholith that, along with the rounded easternmost lobe of the batholith, was originally mapped as a separate textural phase distinct from the rest of the body (Gabrielse et al., 1973); this younger adjacent phase appears to represent a distinct Tombstone suite intrusion. One other questionable intrusion is the Coal River intrusion at the MARION showing, which also has a young age more typical of Tombstone suite intrusions; however, this intrusion does not display either characteristics in the field or geochemically (see below) that would allow the authors to classify it as Tombstone suite. It should also be noted that one intrusion in the study area closely matches the characteristics that were previously assigned to the Tombstone suite as described by Hart et al. (2005) for the Yukon Territory: the O'Grady batholith in the northernmost portion of the study area. Several other intrusions are very similar geochemically and/or geochronologically to the O'Grady batholith; slight age or geochemical variations in these intrusions have led the authors to extend the definition of the Tombstone suite for the study area to include these bodies.

Lithogeochemistry

Forty plutonic, eleven granitic-aplitic dyke, and seven mafic dyke samples collected during the 2003 and 2005 field seasons were analyzed for major, trace, and rare earth element (REE) composition (Table 3). All major element oxide data were obtained by both X-ray fluorescence (XRF) and inductively coupled plasma atomic emission spectroscopy (ICP-AES) at ALS Chemex Laboratories, North Vancouver; trace and REE data were determined through a combination of ICP-AES and inductively coupled plasma mass spectroscopy (ICP-MS) at the same laboratory. Geochemical data reported by Heffernan (2004) for eight plutonic intrusions within the Nahanni MERA area was also adopted for interpretation. Accuracy and reproducibility of the analyses were monitored by repeat analyses of several in-house standards, and data displayed anomalous and nonrepeatable variations were discarded both from our dataset, and from the data reported by Heffernan (2004). The following geochemical data plots discussed below with reference to the plutonic suites consist only of samples from the large felsic intrusions; compositions of felsic and mafic dykes are tabulated in Table 3 but not plotted.

The normative quartz, K-feldspar, and plagioclase concentrations calculated from the major element data (after Streckeisen, 1976) indicate that most of the intrusions, including all of the Tungsten suite intrusions, in the study area are monzogranitic in composition (Table 3; Fig. 5A), and subalkaline (Irvine and Barager, 1971; not shown). Tombstone suite intrusions may be quartz-poor and alkaline in composition, and the Tay River suite (and TR-Tungsten, to a lesser degree) intrusions trend towards quartz-poor, plagioclase-rich mafic com-

Table 3. Geochemical and geophysical data for intrusive samples in the Nahanni MERA area.

Sample	KR-05-08	KR-05-10	KR-05-22	KR-05-26	KR-05-32	KR-05-33	KR-05-39	KR-05-43	KR-05-47b	KR-05-53	KR-05-59	KR-05-60
Intrusion	Powers	Jorgensen	Roy	Fish	Ivo	aplite, IVO	CHUCK plug	Park	Cirque Lake	aplite, MacPass	Rock Slide Mtn.	aplite, Rock Slide Mtn
***Type**	qtz mzd	qtz mzd	mzg	mzg	mzg	mzg	n/a	grd	mzg	mzg	mzg	mzg
[1]ASI	1.03	1.01	1.04	1.09	1.16	1.23	0.08	1.00	1.12	1.15	1.07	1.13
[2]MS	0.19	8.32	17.3	4.82	0.06	0.03	0.01	16.4	0.13	0.05	0.12	0.05
[3]SiO_2	59.64	62.15	69.95	72.82	74.77	75.21	93.51	63.69	68.18	71.93	68.93	72.1
Al_2O_3	16.17	16.89	14.75	14.01	13.16	13.74	0.38	16.6	15.62	15.02	14.98	14.94
Fe_2O_3	4.0	4.6	2.3	2.0	1.3	0.5	0.4	4.5	3.5	0.9	3.0	0.9
FeO	3.27	3.14	1.34	1.34	1.02	0.32	0.19	2.63	2.75	0.71	2.56	0.77
CaO	4.17	4.26	2.53	1.38	1.09	0.35	2.43	4.61	2.88	1.64	3.37	1.65
MgO	2.39	2.16	0.84	0.32	0.25	0.05	0.04	2.05	1.04	0.1	1.27	0.04
Na_2O	3.48	4.02	3.28	3.27	2.43	3.6	0.16	3.37	2.36	3.06	2.4	3.1
K_2O	2.24	2.17	3.91	4.6	4.95	4.22	0.13	2.52	4.41	4.71	3.6	4.69
TiO_2	0.53	0.71	0.43	0.21	0.21	0.1	0.05	0.56	0.42	0.1	0.51	0.21
MnO	0.09	0.06	0.03	0.07	0.03	0.03	0.01	0.08	0.06	bd	0.05	bd
P_2O_5	0.12	0.13	0.12	0.06	0.03	0.03	0.02	0.12	0.12	0.01	0.09	bd
SrO	0.06	0.1	0.04	0.02	0.02	bd	bd	0.05	0.05	0.02	0.03	0.02
BaO	0.12	0.09	0.07	0.05	0.03	bd	bd	0.07	0.11	0.02	0.06	0.02
LOI	5.27	2.89	0.32	0.51	0.37	0.67	2.16	0.55	0.93	1.37	0.7	0.65
Total	98.27	100.25	98.56	99.35	98.62	98.48	99.24	98.74	99.67	98.85	99	98.35
[4]Cs	2	2	4.5	4.9	3.3	5.9	0.3	2.6	8.1	7.9	7.7	8.2
Rb	111.5	74.4	176.5	217	175	419	5	91.6	204	254	162.5	262
Ba	1050	775	658	389	229	25.4	36.5	750	1040	143.5	634	103.5
Th	10	9	25	34	37	16	1	16	30	5	15	7
U	2.4	2.3	7.1	4.4	3.4	12.4	0.5	2.2	6.8	4.2	1.9	4.2
Nb	14	14	22	28	23	54	2	18	16	15	10	15
K	19800	19600	34700	40800	44700	35000	1200	21400	40600	39700	31500	40900
La	30.4	26.6	57.9	64.8	48.5	12.6	2.4	38.3	60.4	6.3	35.3	7.7
Ce	54.6	49.7	102	118.5	94.7	26	5	64.3	111.5	12.4	69.4	15
Pb	11	9	14	20	26	32	57	16	35	37	33	39
Pr	6	5.7	10.8	12.9	10.7	3	0.5	6.8	12.8	1.5	7.8	1.9
Sr	454	720	335	168.5	85.9	16.4	8.5	463	409	118.5	253	123.5
P	500	620	570	240	100	60	bd	540	580	50	380	80
Nd	21.1	20.4	34.6	44.2	36.8	11	1.8	22.2	44.6	6	28	7.4
Zr	191	195.5	315	281	337	237	477	240	344	147	293	188.5
Sm	3.8	3.8	5.6	7.9	6.8	3.6	0.4	3.7	7.5	2	5.3	2.3
Eu	1	1.1	1.1	1.1	0.6	0.2	0.1	1	1.4	0.4	1	0.5
Ti	2430	3180	1990	1090	750	260	130	2860	2270	350	2760	380
Tl	2.7	2.9	3.5	5.8	4	6.5	0.3	2.7	3.3	0.3	3.7	0.4
Y	18.6	16.7	21	32.4	21.4	41.4	2.3	16	17.4	1.3	20.8	1.7
Yb	1.6	1.6	2.2	3.2	1.8	4.2	0.2	1.7	1.5	bd	1.9	0.1
Lu	0.2	0.3	0.3	0.5	0.3	0.6	bd	0.3	0.2	bd	0.3	bd
Cr	34	14	10	11	5	8	26	18	16	9	23	9
[5]Th/U	1.04	0.98	0.88	1.93	**2.72**	0.32	0.50	1.82	1.10	0.30	**1.97**	0.42
[6]ZST/MST	780.9	780.6	843.1	841.8	871	842.7	336.6	799.9	857.3	787.8	838	809
[6]AST_p	781	835.7	895.5	821.7	734.7	687.9	n/a		808.7	634.4	829.4	
[7]AST_m								854.4				

1 ASI = Aluminosity = Aluminum Saturation Index: Al/(Ca+Na+K)

2 MS = magnetic susceptibility (x10^{-3} SI units)

3 major element concentrations are in %

4 REE concentrations are in ppm

5 Th and U are normalized to the primitive mantle; Sun and McDonough (1989)

6 zircon or monazite, and apatite (for peraluminous samples) saturation temperature (ºC); Harrison and Watson, 1984

7 apatite (for metaluminous samples) saturation temperature (ºC); Bea et al., 1992

bd=below detection limit; grd=granodiorite; mz=monazite; mzg=monzogranite; nd=no data; qtz d=quartz diorite; qtz mz = quartz monzonite; qtz mzd=quartz monzodiorite.

positions (Fig. 5A). Aluminosity of the intrusions ranges from metaluminous to moderately peraluminous (Table 3; Fig. 5B; after Maniar and Piccoli, 1989). Those intrusions with quartz-poor compositions such as quartz monzonite, quartz monzodiorite, and quartz diorite, are also less aluminous (Fig. 5): the quartz-poor

Table 3 continued.

Sample	KR-05-62	KR-05-68	KR-05-71	KR-05-76	KR-05-77	KR-05-87	KR-05-97b	KR-05-106	KR-05-110	KR-05-112	KR-05-113	KR-05-115
Intrusion	Mt. Christie	Mt. Wilson	Gun	Pelly River	mafic dyke, Pelly	KAREN porphyry, O'Grady	O'Grady	aplite, CAC	CAC	mafic dyke, S. Nahanni	South Nahanni	gran. dyke, S. Nahanni
***Type**	qtz mz	mzg	mzg	qtz d	mz	mzg	qtz mz	mzg	mzg	qtz mzd	mzg	mzg
[1]ASI	0.81	1.11	1.06	0.83	0.64	1.17	0.87	1.09	1.11	0.87	1.06	1.05
[2]MS	0.34	0.12	0.16	0.1	0.23	0.15	4.06	0.03	0.15	0.41	0.13	0.59
[3]SiO_2	61.34	68.11	66.73	56.81	50.72	64.76	63.35	73.79	67.5	51.38	69.93	66.42
Al_2O_3	14.37	15.47	15.84	16.61	11.88	15.65	15.09	13.74	15.44	16.14	14.8	15.25
Fe_2O_3	5.1	3.1	3.3	9.8	6.6	3.4	4.4	0.3	3.1	5.9	2.7	3.5
FeO	4.22	2.56	2.76	2.37	5.01	2.69	2.82	0.26	2.57	4.87	2.18	3.08
CaO	4.68	3.39	3.7	6.61	6.74	2.87	3.81	0.81	2.47	6.74	2.51	3.07
MgO	3.64	1.38	1.5	3.12	7.97	2.49	1.99	0.16	0.91	9.02	1.18	1.6
Na_2O	1.93	2.2	2.32	4.65	1.13	2.67	2.15	2.92	2.56	1.96	2.59	2.12
K_2O	5.64	3.88	4	0.37	4.01	3.46	6.44	5.81	4.77	2.89	4.74	5.07
TiO_2	0.74	0.52	0.62	1.04	0.93	0.56	0.57	0.2	0.42	0.78	0.39	0.5
MnO	0.09	0.04	0.04	0.11	0.12	0.07	0.07	bd	0.06	0.07	0.04	0.02
P_2O_5	0.29	0.09	0.1	0.27	0.41	0.1	0.27	0.04	0.18	0.12	0.16	0.21
SrO	0.06	0.03	0.04	0.07	0.05	0.04	0.06	0.01	0.03	0.05	0.04	0.05
BaO	0.12	0.06	0.08	0.01	0.14	0.09	0.13	bd	0.12	0.26	0.08	0.12
LOI	0.72	0.84	0.59	0.42	7.79	2.47	0.43	0.89	0.88	3.94	0.34	1.16
Total	98.69	99.06	98.81	99.94	98.6	98.66	98.73	98.69	98.41	99.32	99.54	99.07
[4]Cs	14.6	13	7.3	9	10.3	7.7	30	12.7	8.5	5	10.8	4.2
Rb	272	184.5	192.5	189	198	134	346	340	205	94.8	228	198.5
Ba	1240	524	721	673	1430	780	1160	86.3	845	2770	681	902
Th	48	20	17	17	39	22	52	6	25	16	37	34
U	12.4	4.3	3.7	5.3	8.4	6.7	14.5	25.2	10.4	5.7	7.9	9.5
Nb	18	9	11	10	20	12	18	24	16	10	16	16
K	50000	33900	34000	33600	35600	29500	59300	50200	42500	24900	41400	44500
La	79.7	43.7	37.8	40.8	45.8	41.5	62.4	7.8	51.4	44.3	49.3	53.2
Ce	152.5	85.2	74.2	80.2	101	76	128	16.8	98.5	83.4	98	108
Pb	41	27	33	33	14	26	48	47	38	6	31	28
Pr	17.4	9.8	8.3	9	13	8.2	14.4	1.9	10.8	9	10.6	11.8
Sr	502	242	271	292	387	346	526	39.9	283	392	335	384
P	1290	460	490	470	1820	460	1210	210	730	600	660	920
Nd	61.2	34.6	28.8	31.6	51.4	27.5	57.9	7.4	40.5	34.5	41.2	46.5
Zr	309	326	313	346	290	227	269	185	272	156.5	274	297
Sm	10.5	6.1	4.9	5.4	9.3	4.8	9.9	2	6.8	5.7	7.2	8.3
Eu	1.8	1	1.1	1.1	1.6	1.1	1.9	0.1	1.4	1.6	1.2	1.5
Ti	3910	2830	3020	2760	5330	3040	3140	380	2340	4720	2160	2730
Tl	4.8	3.3	2.9	2.6	3.6	3.4	4.3	3.1	4.1	3.5	3.8	4.2
Y	24.5	17.8	15.8	14.6	19.1	19.6	20.8	19.8	21.2	16.6	19	20.3
Yb	2.2	1.5	1.4	1.3	1.7	1.8	1.9	3.2	2.2	1.6	1.8	2
Lu	0.3	0.2	0.2	0.2	0.2	0.3	0.3	0.5	0.3	0.2	0.3	0.3
Cr	83	25	21	32	399	47	33	8	11	242	29	33
[5]Th/U	0.97	1.16	1.15	0.80	1.16	0.82	0.90	0.06	0.60	0.70	1.17	0.89
[6]ZST/MST	785.6	850.7	839.3	786.4		818.4	790.3	806.2	833.4		831	831.9
[6]AST_p		793.9	820.1			708.3		793.4	851.2		907.6	909.2
[7]AST_m	928.5		861				943.3					

Tombstone suite intrusions are metaluminous, and several of the more mafic Tay River suite intrusions border on the metaluminous-peraluminous boundary (where aluminousity = ASI = Al / [Ca+Na+K] = 1) defined by Maniar and Piccoli (1991).

Multi-element profiles in Figure 6 are very similar for the Tay River, Tungsten, and Tombstone suites (the transitional TR-Tungsten subsuite is not shown), indicating relatively little variation in magma compositions among intrusive suites. The Tungsten suite intrusions in particular are remarkably homogenous aside from slight variations in specific elements; this homogeneity is even more pronounced for samples from specific areas, such as the Cantung mine area and the Lened-Cac-Rudi-South Nahanni area. When normalized to the primitive mantle of Sun and McDonough (1989), all samples display negative high-field strength element (HFSE includes the elements Nb, Ta, P, and Ti) anomalies. As the HFSE are typically immobile in igneous systems (Rollinson, 1993; Jenner, 1996), such depletions are generally considered to reflect depletions relative to the primitive mantle in the magma source

Table 3 continued.

Sample	KR-05-126	KR-05-130	KR-05-136	KR-05-143	KR-05-148	KR-05-154	KR-05-156	KR-05-157	KR-05-158	KR-05-164	KR-05-175	KR-05-191
Intrusion	plug SW of O'Grady	Central Nahanni	North Nahanni	Circular	Rifle Range	aplitic apophysy, Rifle Range	aplite, Rifle Range	mafic dyke, Roy	mafic dyke, Roy	Hole-in-the-Wall	Lened	Coal River MARION
*Type	mzg	grd	mzg	mzg	mzg	mzg	mzg	qtz mzd	qtz mzd	mzg	mzg	mzg
[1]ASI	1.16	1.04	1.09	1.11	1.10	1.07	1.07	0.86	0.81	1.11	1.12	1.09
[2]MS	0.04	0.22	0.19	0.11	0.12	0.4	0.03	0.68	1.88	0.11	0.14	5.5
[3]SiO_2	71.14	65.08	66.75	69.73	69.22	64.21	75.58	54.05	52.71	70.33	69.63	70.61
Al_2O_3	15.05	16.25	15.97	15.46	15.72	16.07	12.92	16.75	15.74	15	15.35	14.83
Fe_2O_3	0.7	4.1	3.7	2.5	2.1	4.2	0.4	7.2	7.4	1.9	2.9	2.4
FeO	0.64	3.32	2.81	2.06	1.8	3.53	0.45	5.7	5.72	1.53	2.57	1.93
CaO	1.49	4.1	3.47	2.31	1.63	3.54	0.67	6.9	7.25	1.09	2.31	2.1
MgO	0.13	2.26	1.69	0.69	0.54	1.62	0.06	4.98	6.37	0.35	0.89	0.76
Na_2O	3.17	2.76	2.61	3.05	2.77	2.37	2.76	2.16	1.99	2.91	2.75	3.03
K_2O	4.63	3.4	3.79	4.31	6.21	4.27	5.82	3.08	2.71	6.22	4.62	4.45
TiO_2	0.11	0.57	0.47	0.34	0.26	0.53	0.05	0.84	0.81	0.23	0.43	0.33
MnO	0.03	0.06	0.05	0.04	0.03	0.06	bd	0.12	0.11	0.04	0.06	0.03
P_2O_5	0.05	0.12	0.09	0.11	0.1	0.26	0.03	0.45	0.34	0.09	0.16	0.1
SrO	0.02	0.04	0.03	0.02	0.05	0.05	0.01	0.08	0.06	0.01	0.04	0.04
BaO	0.04	0.1	0.07	0.07	0.1	0.13	0.01	0.11	0.11	0.1	0.08	0.08
LOI	1.96	0.35	0.47	0.5	0.41	1.26	0.42	2.79	3.27	0.31	0.6	0.94
Total	98.54	99.24	99.14	99.13	99.14	98.56	98.73	99.51	98.92	98.55	99.78	99.65
[4]Cs	12	10.6	12.4	8.5	7.8	4.7	5.3	8.6	6.1	15.6	8.6	7.3
Rb	240	147.5	163	192	255	162	230	118.5	104	313	218	191
Ba	258	1020	644	710	1080	1080	80.7	1200	1180	930	963	856
Th	6	18	24	20	24	25	4	14	13	18	30	28
U	3.4	5.4	7.4	8.9	7.1	7.9	28.9	3.6	3.4	13.7	4.8	6
Nb	12	14	13	11	18	19	9	19	15	18	17	22
K	38800	28500	32900	35900	54200	37500	48000	26400	23300	50200	39400	37600
La	10.4	41.9	40.2	38	45.6	50.3	6.7	50.4	45.1	30.5	58.3	50.9
Ce	20	78.9	75.4	75	89.5	96.3	13.2	97.8	88.7	61.3	111	92.8
Pb	40	30	37	35	37	16	33	13	5	39	43	18
Pr	2.3	8.4	7.9	8.3	9.7	10.5	1.4	10.8	10	6.8	11.8	9.5
Sr	160.5	364	286	215	339	433	49.6	663	558	113	315	283
P	160	530	420	410	490	1120	160	1960	1520	450	710	460
Nd	9.4	31.5	29.7	31.7	37.3	40.2	5.3	43.9	40.5	25.5	43.7	34.1
Zr	162.5	259	270	260	276	258	216	215	179.5	242	295	274
Sm	2.4	5.4	5.1	6.1	6.5	6.9	1.4	8	7.2	5	7.4	5.7
Eu	0.6	1.2	1	1.1	1.5	1.5	0.3	2	1.8	0.9	1.4	1.3
Ti	390	3220	2780	1660	1360	3180	230	4830	4570	1280	2100	1780
Tl	2.1	3.2	3.8	4	4.1	4.1	3	4.6	4.7	4.7	4.5	3.5
Y	10.6	16	19.6	21.2	21.2	20.2	19.4	22.3	21.8	25.6	21.9	18.1
Yb	0.7	1.6	2	2	2.1	2.1	3.2	2.2	2.2	3	2.2	2.1
Lu	0.1	0.2	0.3	0.3	0.3	0.3	0.5	0.3	0.3	0.4	0.3	0.3
Cr	17	41	27	13	13	19	9	53	178	13	15	17
[5]Th/U	0.44	0.83	0.81	0.56	0.85	0.79	0.03	0.97	0.96	0.33	**1.56**	1.17
[6]ZST/MST	797.9	813.3	826.9	831.6	835.3	818	820.5			826.2	843.3	835.6
[6]ASTp	733.6	841.5	793.6	826.5	818.9	885.6	802.4			816	859.7	845.6
[7]AST_m												

material(s), although they can also be produced by the fractionation of ilmenite, rutile, titanite, or apatite from the magma (Rollinson, 1993). Depletions in the HFSE are typical of magmas resulting from the partial melting of igneous material and are known I-type granites (i.e. granitic magmas derived from partial melting of igneous material, usually volcanic-arc granites found at subduction zones; Christiansen and Keith, 1996).

When normalized to the chondrite of Sun and McDonough (1989), at least two of the Tombstone suite intrusions have relatively enriched light rare earth element (LREE) abundances, when compared to the other plutonic suites. This feature has been interpreted by Hart et al. (2005) to be indicative of an enriched-magma source region, such as the lithospheric mantle above a subducting slab. Most samples from each plutonic suite display negative europium anomalies of varying degrees, from slight to moderately well developed, when normalized to chrondrite compositions. A negative europium anomaly is consistent with crystal fractionation of plagioclase at depth, and gives an indication as to how much fractionation or evolution the

Table 3 continued.

Sample	KR-05-194	KR-05-196	KR-05-198	KR-05-204	KR-05-207	KR-05-208	KR-05-210	KR-05-211	KR-05-212	KR-05-213	KR-05-215
Intrusion	Coal River ROYALL	Coal River CRAT	Hole-in-the-Wall	mafic dyke, Mine Stock	West Tuna	Little Hyland	Nahanni Range Road	aplite dyke, Rifle Range	mafic dyke, Rifle Range	mafic dyke, Rifle Range	Mine Stock (surface)
***Type**	mzg	mzg	mzg	qtz mzd	mzg	mzg	mzg	mzg	qtz mzd	qtz mzd	mzg
[1]ASI	1.16	1.04	1.11	0.77	1.13	1.15	1.24	1.19	0.70	0.73	1.12
[2]MS	0.14	9.01	0.18	nd	0.11	0.11	0.09	0.08	1.22	0.62	0.11
[3]SiO_2	70.19	68.27	68.34	52.18	71.23	72.25	73.27	71.95	52.92	52.85	71.53
Al_2O_3	14.94	15.14	15.1	17.23	15.16	14.61	14.46	14.21	15.6	15.45	15.04
Fe_2O_3	2.9	3.4	3.7	6.2	2.2	2.2	1.8	1.5	6.1	7.8	2.2
FeO	2.31	2.37	3.08	5.31	1.79	1.92	1.41	1.09	4.87	5.96	1.93
CaO	1.42	2.84	2.01	7.26	1.9	1.64	1.19	1.17	8.59	7.67	1.93
MgO	0.71	1.26	0.75	5.33	0.56	0.45	0.4	0.47	7.48	7.86	0.53
Na_2O	2.8	2.89	2.76	1.93	3.45	3.33	3.19	2.83	1.57	2.21	3.26
K_2O	5.26	4.27	4.95	5.56	4	3.89	3.95	4.76	3.77	3.24	4.26
TiO_2	0.54	0.49	0.49	1.03	0.23	0.2	0.17	0.19	0.85	0.85	0.26
MnO	0.05	0.05	0.06	0.19	0.06	0.1	0.07	0.03	0.05	0.12	0.04
P_2O_5	0.19	0.13	0.13	0.61	0.08	0.1	0.07	0.13	0.36	0.36	0.1
SrO	0.02	0.04	0.02	0.06	0.02	0.02	0.01	0.02	0.07	0.06	0.03
BaO	0.04	0.1	0.09	0.21	0.04	0.03	0.02	0.06	0.3	0.13	0.05
LOI	0.57	0.57	0.61	1.45	0.56	0.45	0.71	1.42	1.61	1.2	0.43
Total	99.63	99.46	98.99	99.23	99.49	99.22	99.26	98.74	99.32	99.84	99.66
[4]Cs	12.1	8.4	11.4	17.7	10.2	20.9	15.8	7.2	3.7	7.4	9.8
Rb	237	165	224	309	147.5	262	211	217	104	104	203
Ba	524	1015	883	2160	372	387	247	688	3400	1430	584
Th	34	26	19	18	12	14	13	22	17	16	18
U	5.6	5.2	4.4	7.7	6.1	7.2	5.5	3.8	5	4.8	8.8
Nb	31	19	30	24	9	13	11	15	17	17	11
K	42900	35100	39800	46200	32500	34100	32500	38800	32400	27100	36600
La	58.4	66.6	57.8	59.1	26.2	27.6	24.3	39.4	61.7	57.1	40.6
Ce	108.5	120	104.5	112	50.2	53.9	48	73.8	117.5	111	79.3
Pb	23	9	29	5	27	32	33	30	bd	5	41
Pr	11.7	12	12.3	12.4	5.3	5.6	5	7.5	12.6	12	8.4
Sr	172.5	322	144.5	502	134	128	90.6	174.5	585	547	201
P	760	600	570	2580	340	460	240	540	1890	1780	400
Nd	42.7	41.9	47.6	48.2	20	21.3	18.6	27.2	49.1	46	31.2
Zr	366	277	355	200	199	241	250	196.5	168.5	172.5	268
Sm	7.2	6.4	8.8	8.3	3.8	4.5	4	4.7	8.5	8.3	5.5
Eu	1.2	1.2	1.4	2	0.7	0.7	0.4	0.8	2.4	2.2	1
Ti	2670	2640	2620	5610	1280	1230	960	1000	5080	5000	1490
Tl	4.1	3.7	6.7	4.9	2.8	4.2	3.5	3.2	4.6	4.4	4
Y	19.4	18.8	33.6	23.4	14.6	22.6	18.4	16.4	20.9	20.3	20.9
Yb	1.8	2	3.2	2.2	1.4	2.3	2.1	1.7	1.9	1.8	2
Lu	0.2	0.3	0.5	0.3	0.2	0.3	0.3	0.2	0.3	0.3	0.2
Cr	11	17	14	103	8	10	11	9	224	238	12
[5]Th/U	**1.52**	1.25	1.08	0.58	0.49	0.49	0.59	1.45	0.85	0.83	0.51
[6]ZST/MST	870	827.1	859.5		810	832	844.6	817.8			836.9
[6]AST_p	851.5	882.3	826.7		803.6	816.1	732.2	809.3			836
[7]AST_m											

magma has undergone before emplacement. This feature is usually more pronounced for magmas with a high degree of middle to upper crustal contamination-assimilation, or for S-type granites resulting from partial melting of over-thickened sedimentary rocks in the crust during orogeny (Christiansen and Keith, 1996). Notably, many of the intrusions within the study area, including most of the Tungsten suite intrusions, lack a well developed negative europium anomaly. In fact, several Tay River suite intrusions do not have a negative europium anomaly (inset for Tay River suite, Fig. 6B). The intrusions with a negligible europium anomaly are interpreted to be very close in composition to their source magma and have not undergone significant fractionation of plagioclase or other measures of magma evolution, including significant middle to upper crustal contamination. Furthermore, the same small, plug-like Tay River suite intrusions with a negligible europium anomaly also display a negative rubidium anomaly on the primitive mantle normalized plot (inset, Fig. 6A), as do the mafic dykes samples in the area (not shown). For those Tay River suite intru-

Table 3 continued.

Sample	03M-203	03M-204	03M-207	03M-212	03M-214	03M-215	03M-216	03M-217	03M-218	03M-219	03M-220
Intrusion	aplite dyke, Mine Stock	aplite dyke, Mine Stock	Mine Stock (under-ground)	aplite dyke, Mine Stock	Shelf Lake	Mt. Appler	Faille	Mt. Sir James MacBrien	Hole-in-the-Wall	Rifle Range	Ragged
*Type	mzg	grd	mzg	mzg	mzg	mzg	mzg	mzg	mzg	mzg	mzg
[1]ASI	1.25	1.16	1.18	1.13	1.17	1.16	1.12	1.07	1.05	1.20	1.13
[2]MS	nd	nd	0.18	0.52	0.09	0.09	0.29	2.73	7.28	0.07	0.12
[3]SiO_2	75	74.56	70.5	75.02	70.72	70.97	67.58	67.84	68.19	71.98	66.98
Al_2O_3	14.3	13.92	15.6	13.48	15.3	14.99	15.45	15.61	15.49	14.89	16.03
Fe_2O_3	0.1	0.1	0.1	bd	0.1	0.2	0.5	0.8	0.9	0.2	0.5
FeO	0.82	0.44	2.39	1.11	1.75	1.98	2.65	2.34	2.14	1.72	2.6
CaO	0.86	2.54	2.4	1.22	1.8	1.65	2.53	3.09	2.96	1.47	3.18
MgO	0.17	0.16	0.68	0.16	0.73	0.56	0.92	1.27	1.19	0.61	1.3
Na_2O	2.9	2.8	2.82	2.1	2.86	2.66	2.37	2.5	2.55	2.63	2.74
K_2O	4.74	2.54	3.93	5.79	4.67	5.17	4.86	4.54	4.82	5	3.56
TiO_2	0.1	0.07	0.35	0.13	0.27	0.39	0.43	0.45	0.44	0.36	0.47
MnO	0.03	0.02	0.04	bd	0.03	0.03	0.06	0.06	0.05	0.03	0.05
P_2O_5	0.11	0.15	0.13	0.05	0.2	0.13	0.18	0.18	0.15	0.17	0.13
SrO	nd	nd	nd	nd	nd	nd	nd	nd	nd	nd	nd
BaO	nd	nd	nd	nd	nd	nd	nd	nd	nd	nd	nd
LOI	0.53	2.54	0.41	0.61	0.87	0.33	0.63	0.4	0.39	0.5	1.62
Total	99.77	99.88	99.71	99.79	99.55	99.34	98.68	99.56	99.63	99.82	99.57
[4]Cs	3.2	11.8	7.1	2.3	14.7	10.4	6.7	6.3	4.7	14.2	6.2
Rb	193	146	173	199	212	239	183.5	175.5	187	293	150
Ba	97.9	189.5	666	422	574	508	1285	1250	1155	358	804
Th	6	3	19	23	16	25	33	31	33	21	19
U	21.1	10.8	9.2	7.6	5.3	11.6	4.2	5.8	9.1	6.8	4
Nb	17	6	12	17	17	22	21	20	18	21	12
K	nd	nd	nd	nd	nd	nd	nd	nd	nd	nd	nd
La	10.5	6.6	46.2	39.4	31.5	47.6	85.3	60.6	54.1	38.4	43.6
Ce	22.5	13.3	88	76.3	60.9	93.9	153.5	108.5	97.6	77.3	79.7
Pb	54	23	39	25	43	34	31	25	21	35	35
Pr	2.6	1.5	10	8.6	7	10.3	16.5	11.5	10.3	8.8	9.1
Sr	47.7	146	314	184	253	166	425	458	417	147	351
P	nd	nd	nd	nd	nd	nd	nd	nd	nd	nd	nd
Nd	9.3	5.3	34.3	29	23.5	36.2	55.5	38.7	34.5	30.9	32.1
Zr	186	232	288	467	349	453	576	547	424	354	301
Sm	2.5	1.2	6.3	5.7	4.5	6.6	9	6.2	5.7	5.6	5.5
Eu	0.2	0.4	1.2	0.9	0.9	1	1.7	1.3	1.3	0.8	1.2
Ti	nd	nd	nd	nd	nd	nd	nd	nd	nd	nd	nd
Tl	2.7	1.3	3.1	3.4	2.7	3.3	4.4	3	3	2.3	3.2
Y	1.4	0.8	1.5	1.8	1.4	1.5	2.3	1.5	1.6	1	1.7
Yb	15.5	7.8	17.2	19.2	15.6	17.5	24.2	16.4	16.8	11.9	17.9
Lu	0.2	0.1	0.2	0.3	0.2	0.3	0.4	0.3	0.3	0.2	0.3
Cr	nd	nd	nd	nd	nd	nd	nd	nd	nd	nd	nd
[5]Th/U	0.07	0.07	0.52	0.76	0.75	0.54	**1.96**	1.34	0.91	0.77	1.19
[6]ZST/MST	819.9	835.8	850.1	902.3	869.5	895.1	913.1	899.6	871.2	874.8	846
[6]AST_p	785.5	873.9	803	800.9	851.8	825	844.6	893.3	892.2	829.3	794.8
[7]AST_m											

sive phases in the study area with little evidence for magma evolution or interaction with the middle to upper crust (due to a lack of plagioclase fractionation), the depleted rubidium concentrations represent source-regions compositions. Other studies have noted depleted rubidium concentrations in metamorphic granulite facies terranes (i.e. basement rocks that have undergone partial melting and have produced granitic melts) and have attributed this to result from the removal of rubidium through high degrees of partial melting (>40%) or metamorphic fluid loss in the lower continental crust (Hansen et al., 2002). This rubidium depletion likely indicates a derivation for at least the Tay River suite intrusions from melting in a region already depleted by a prior partial-melting event, or altered by metamorphic fluids.

Previous work on magmatism in the study area (Anderson, 1983; Woodsworth et al., 1991; Gordey and Anderson, 1993) has suggested that the exposed intrusions are a result of partial melting of over-thickened crust in the back-arc region of a subduction zone during terrane accretion. The belt of resulting magmatism

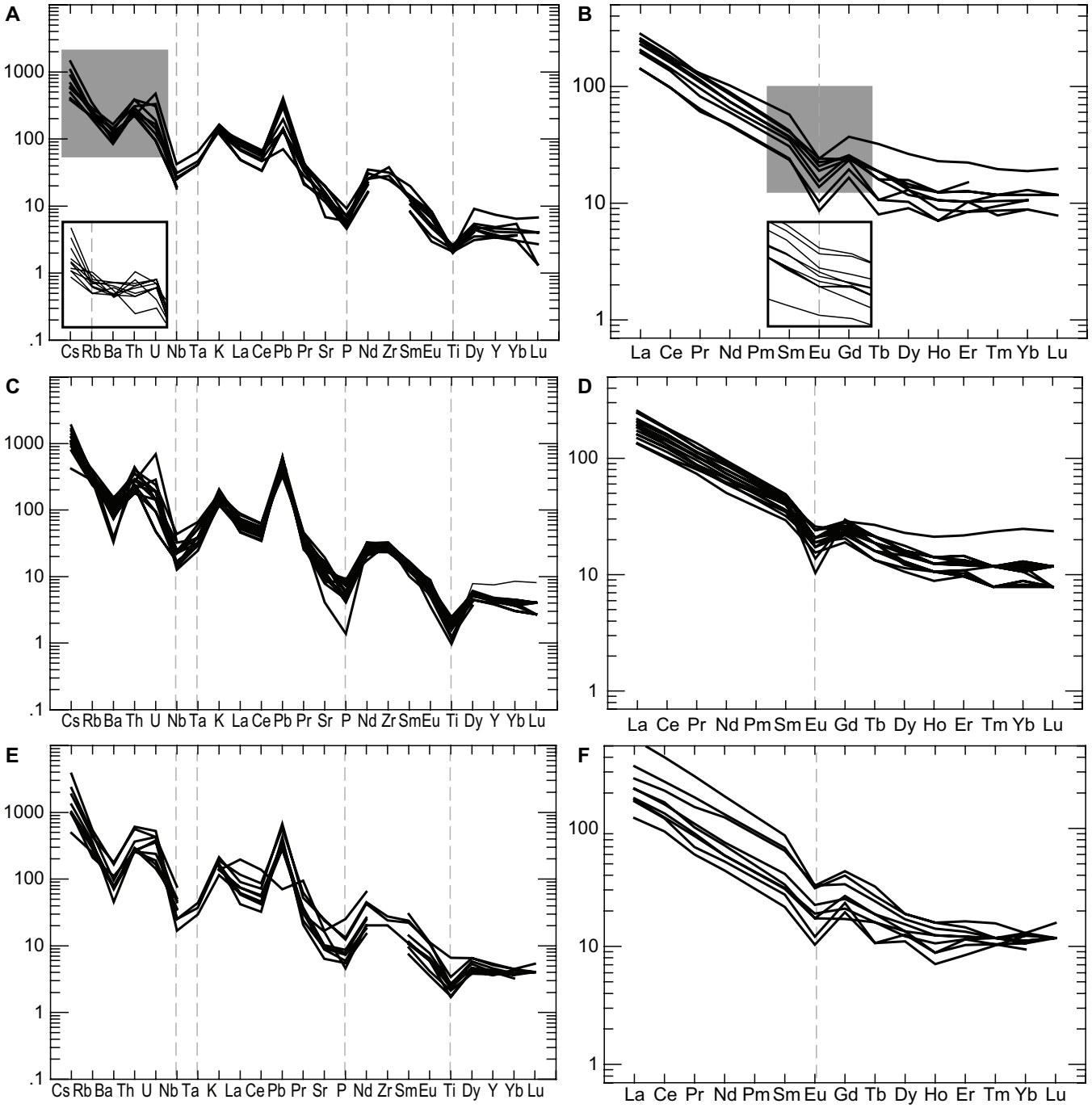


Figure 6. Multi-element plots normalized to the primitive mantle (**A** - Tay River suite, **C** - Tungsten suite, **E** - Tombstone suite) and chondrite **(B -** Tay River suite, **D** - Tungsten suite, **F-** Tombstone suite) compositions of Sun and McDonough (1989) for the plutonic suites. Dashed grey lines indicate anomalies discussed in text, and grey boxes indicate location of samples in insets. Anomalous points due to repeated analytical inconsistencies have been removed (e.g. positive Ta and negative Zr anomalies for all Heffernan (2004) samples; negative Y and positive Yb anomalies for all 2003 samples).

.

was initially termed the Selwyn plutonic suite and described as a post-tectonic, compositionally restricted, metaluminous to peraluminous magmatic belt of granitic, granodioritic, and syenitic compositions (Anderson, 1983). The presence of muscovite in some intrusions, and locally garnet in marginal phases, combined with the tectonic setting resulting in thickened crust, led authors to conclude that the magmatism was derived entirely from partial melting of sedimentary rocks in the crust, and could be considered "S-type" magmatism. A collisional tectonic discrimination diagram (Fig. 7A) from Harris et al. (1986; modified by Rollinson, 1993) suggests that most of the intrusions are post- or late-collisional rather than syncollisional, which is in agreement with the "post-tectonic" descriptor assigned by Anderson (1983). The relaxed or

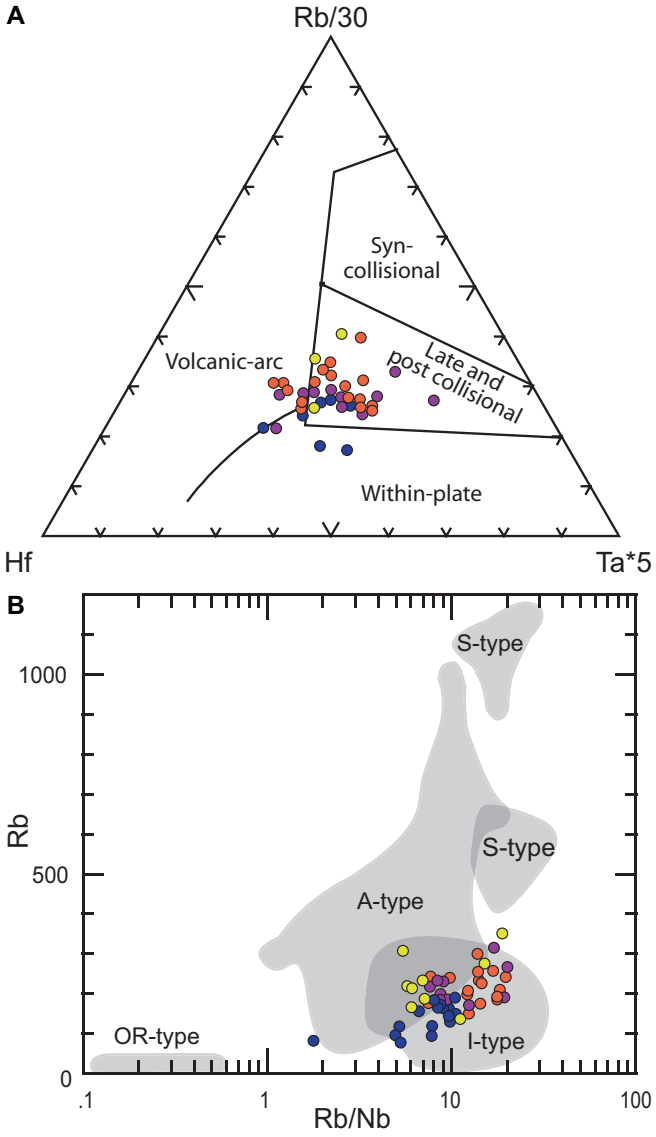


Figure 7. Trace element plots for intrusions in the study area, based on plutonic suites: Tombstone suite samples are yellow, Tungsten suite samples are red, TR-Tungsten subsuite samples are purple, and Tay River suite samples are blue. **A)** Ternary Hf-Rb-Ta tectonic discrimination diagram (modified by Rollinson, 1993, after Harris et al., 1986). **B)** Binary Rb/Nb versus Rb source-rock discrimination diagram (Christiansen and Keith, 1996). Fewer data points in (B) are due to the removal of several samples with analytical inconsistencies for tantalum.

extensional-transtensional tectonic regime post-orogeny is typically when the most voluminous magmatism inboard of a subduction zone occurs (Clemens, 2003). However, the Christiansen and Keith (1996) source material discrimination diagram in Figure 7B, indicates that the intrusions have more of an I-type granite trace element composition rather than that of an S-type granitoid (Christiansen and Keith, 1996). This I-type signature in Figure 7B, combined with the depleted HFSE abundances relative to the primitive mantle of Sun and McDonough (1989) in Figure 6, imply a somewhat different source material from the original S-type granite hypothesis put forward by previous workers. An intermediate to mafic magma source is not unlikely as peraluminous intrusions may still result from fractionation of metaluminous (I-type) magmas (Chappel and White, 1974). Peraluminous granitic melts can also be generated by partial melting of amphibolitic source rocks (Patiño Douce and Beard, 1995) or nonsedimentary, metaluminous protoliths. Partial melting of a mafic to ultramafic igneous material, such as lower crust or possibly even enriched mantle, appears to have had a significant role in the sourcing of these magmas. Partial melts derived from the middle to upper crust may still have interacted with the mafic magmas; however, aside from some xenoliths of mafic igneous material in some intrusions (e.g. Central Nahanni) no evidence for magma mixing was observed in the field. It is uncertain whether crustally derived melts actually formed large volumes of material that assimilated or mixed thoroughly with more mafic melts, or whether this was a relatively insignificant component for the majority of the magmatism in the study area. Certainly the intrusive phases associated with tungsten mineralization that are typically muscovite- and frequently garnet-bearing, have had some significant interaction with the middle to upper crust, but the small surface expression of these intrusive phases (as observed in this study, and as mapped for several plutons associated with tungsten mineralization by Gordey and Anderson, 1993), suggests a limited influence of middle to upper crust in the study area, overall.

It is interesting to note that the majority of the Tombstone suite intrusions plot within the overlapping A-type or 'anorogenic/alkalic/anhydrous granite' field in Figure 7B. A-type granites comprise a wide range of tectonic settings, however these granites all form in extensional settings resulting from rifting or mantle plumes (Christiansen and Keith, 1996). A small subset of these A-type granites are documented to have been emplaced following the termination of a compressional orogeny (Christiansen and Keith, 1996), a setting that agrees well with the interpretation put forward by Hart et al. (2004a, 2005): that the Tombstone suite intrusions comprise a late, alkalic-magmatic event in a region undergoing relaxation, and possibly minor extension, following an earlier compressive regime.

Magnetic Susceptibility

Magnetic susceptibility (MS) measurements for all samples were taken to provide information regarding the relative oxidation state of the intrusions (Table 3). The reported MS values are based on an average of ten randomly oriented readings on fresh, flat surfaces of each sample using a KT-9 Kappameter. Values varied between intrusive phases within a single pluton, although, for the most part all values measured from an

intrusion were either below 0.5 or above 0.5 ($x10^{-3}$ SI units); any larger variation was associated with low volume, marginal phases of a select few intrusions. Following the reasoning described above, the MS of the main or megacrystic intrusive phase from each pluton (also subjected to geochemical and geochronological study) was selected for measurement and interpretation and is regarded as representative of the intrusion as a whole. In addition to identifying and discriminating between various intrusive phases within the plutons, MS measurements allowed the application of the reduced-oxidized classification of Hart et al. (2004a) for intrusions in the northern Cordillera. The majority of the MS values indicate reduced intrusions ($< 0.5x10^{-3}$ SI units) but several intrusions are weakly to strongly oxidized ($> 0.5x10^{-3}$ SI units) with MS values as high as 17.3 $x10^{-3}$ SI units for some of the marginal phases. Based on this oxidized-reduced classification scheme, Tombstone suite intrusions may be both oxidized or reduced, all Tungsten suite intrusions are reduced, TR-Tungsten subsuite intrusions are either reduced or oxidized, and Tay River suite intrusions are typically oxidized (although some reduced intrusive phases were also observed) (Fig. 4).

The field, geochronological, geochemical, and geophysical characteristics of the plutonic suites for the MERA area, as modified and expanded from Hart et al. (2004a, 2005) by this study, are summarized in Table 1.

Thermal History

It is generally accepted that the emplacement of intrusions at relatively high depths (>5 km) allows for a prolonged period of cooling, crystallization, and potential mineralization (Meinert et al., 2005). One commonly used measure of the length of time in which an intrusion 'cools' is the difference between crystallization (zircon or monazite) and cooling (biotite) ages (Coulson et al., 2002; Hart et al., 2004b). Intrusions with lengthier cooling periods, or thermal histories, are more likely to have crystallized at greater depths and/or may have been thermally active for longer periods due to replenishment of the magma chamber. Such intrusions are regarded as more likely to have evolved a magmatic hydrothermal mineralizing system over a long period of time that could result in the deposition of significant quantities of ore metals (Meinert et al., 2005). Short thermal histories (<1 Ma) suggest relatively rapid cooling due to a shallower emplacement of the magma in the crust and reduce the likelihood, but do not eliminate the possibility, of economic intrusion-related mineralization. In fact, several Tombstone suite intrusions in the Yukon Territory that are associated with gold mineralization have cooling periods of 1 to 2 million years (m.y.), as reported by Hart et al. (2004b). If the difference between the crystallization and the cooling (biotite) ages is calculated for the gold-associated intrusions after the 2-sigma errors are taken into account, (as done for the data below) *minimum* estimates of essentially "0" to 1.6 m.y. are obtained. However, the dominant style of mineralization documented in the study area is skarn, particularly reduced tungsten-bearing skarn (Fig. 2, Appendix 1). In most mineral deposit studies and models, reduced tungsten skarns typically form at relatively great depths (1.5-2.5 kbar or approximately 5-8 km; Newberry, 1998), which result in longer cooling periods for the associated intrusions. Such deep settings are hypothesized as necessary for a significant accumulation of at least tungsten metal in the magmatic fluid phase before the release or exsolution of volatile material that transports the metals out of the intrusion and into the surrounding rock (Newberry and Swanson, 1986; Keith et al., 1989).

^{40}Ar-^{39}Ar results for magmatic biotite from for twenty-six plutons are tabulated in Table 2. Most of these data indicate moderately rapid, post-emplacement cooling from magmatic temperatures of 850 to 900ºC (indicated by zircon or monazite saturation thermometry; ZST and MST, respectively; Table 3) to the closure temperature of the argon system in biotite (~300ºC) for the majority of the intrusions. Cooling periods in Table 2 were based on the *minimum* age difference between the U-Pb zircon (or monazite) crystallization age and the Ar-Ar biotite cooling age after 2-sigma errors are taken into account. A thermal history of essentially "0" m.y. was assigned to the six plutons for which the Ar-Ar age was older than the U-Pb age, and for the additional nine plutons for which the Ar-Ar age ± 2-sigma fell within the U-Pb age ± 2-sigma. Examination of Table 2 indicates that cooling periods for at least seventeen of the intrusions are less than about 1.0 m.y., thus, these intrusions were probably not thermally active over a lengthy period of time. Considering that many intrusions in the northern Cordillera examined by Hart et al., (2004b) have cooled within less than 1 m.y., four of the intrusions in Table 2 have relatively prolonged thermal histories that range from 1.0 to 2.8 m.y. A further four intrusions have anomalously long 'apparent' cooling periods (>>4.5 m.y.). The lack of biotite data for the remainder of the intrusions prevented the calculation of the duration of their cooling periods.

One notable intrusion with a relatively extended thermal history is the Mine Stock (2.3 m.y.) at the Cantung mine, which underlies the tungsten skarn orebody. The Cantung deposit is one of the highest grade *known* tungsten skarns (Lentz, 1998, identifies tungsten skarn deposits with 1.4% WO_3 as world class, or within the upper 10th percentile), with over 4.6 million short ton units grading 1.6% WO_3 recovered as of 2004 (B. Mann, pers. comm., 2004). Recent data from Yuvan

et al. (2004) presents pressure estimates of 2 to 3 kilobars for scheelite-mineralized quartz veins located about 500 m above the intrusive stock, which indicates a depth of emplacement for the intrusion of approximately 7 to 10 kilometres. These pressure data are consistent with the longer thermal history detected by the Ar-Ar data and subsequently, a longer duration of the associated magmatic hydrothermal system. Other intrusions within the study area with prolonged thermal histories are the Cac, South Nahanni, and Coal River-Crat plutons.

Surprisingly, one phase of the Lened pluton, which is associated with the second largest tungsten resource within the study area (indicated: 0.75 Mt grading 1.17% WO_3 and 0.15% Cu; Walton, 1998), cooled quickly from emplacement temperatures (indicated by ZST) at approximately 95.0 Ma to the closure temperature of the argon system in biotite, in less than 1 m.y. However, as is the case for almost all of the intrusions in the MERA area, the Lened pluton is composed of several compositional phases (Gordey and Anderson, 1993). It is possible that the intrusive phase selected for geochronological analysis was not directly associated with the tungsten skarn mineralization.

The geochronological data in Table 1 suggest that there were at least two large-scale thermal overprinting events leading to significantly younger Ar-Ar biotite ages for four intrusions: 89 to 86 Ma and 67 to 65 Ma. The earlier (ca. 89-86 Ma) event has reset the biotite ages of the Little Hyland and Nahanni Range Road stocks, near the Cantung mine. These two intrusions are in close proximity to the March Fault (Fig. 1), a Cambrian structural boundary that was reactivated during the Cretaceous and that displays evidence for thrust normal strike-slip movement, as described by Hart and Lewis (2006). Thus, the younger biotite ages may reflect a partial or full re-setting of argon-isotope compositions in mica due to heating during movement along the structure. This is consistent with the very strong foliation observed in the Little Hyland sample (see Appendix 2). The later (ca. 67-65 Ma) event is a thermal overprinting of the biotite ages for the Ivo pluton and the Coal River intrusion at the MARION showing, both directly associated with tungsten skarn mineralization. The Ar-Ar data confirm similar K-Ar ages (D. Archibald, unpub. data; 1981) for two other intrusions associated with tungsten skarn occurrences located in the Yukon Territory (95E-031 and 95E-005; Deklerk and Traynor, 2005): the Salivo intrusion (60.3 ± 1 Ma), which adjoins the Ivo intrusion to the southeast (Fig. 2), and, the Cream stock (69.4 ± 1.2 Ma), which is adjacent to the Coal River batholith at the Marion showing (Fig. 2). As of yet, there is no explanation for this thermal event and it is uncertain as to whether or not the younger thermal event is responsible for the tungsten mineralization, although field evidence suggests that at least the Ivo tungsten skarn is directly related to the Ivo pluton.

Although much of this discussion concerns tungsten mineralization, other intrusions inboard of subduction zones in the back-arc region are also associated with other metals (e.g. intrusion-hosted Au-Bi-[Te-As-Mo-W], proximal W-[Cu-Au], and Cu-Bi-[Au-W], and distal Au-As-Sb-[Hg] deposits) are also emplaced at moderate depths, typically 3 to 8 km (Thompson et al., 1999; Lang and Baker, 2001; Hart et al., 2004b). The shallow end of this range of depths may not be conducive to prolonged cooling histories that would be detectable with the radiometric analytical methods employed by this study (Hart et al., 2004b). Thus, the limitations of the data in this study do not preclude that plutons with an apparent short cooling history may not be related to mineralization. The data can be used as a positive indicator for possible intrusion-related mineralization, particularly tungsten mineralization, (e.g. the prolonged thermal histories for the Mine Stock and Cac plutons, both associated with known W-mineralization), but as was demonstrated for gold-associated Tombstone suite intrusions in Yukon, and intrusions in the study area, not as a negative indicator (e.g. the <1 m.y. thermal history for the North Nahanni pluton that is associated with Cu mineralization).

LEAD ISOTOPE COMPOSITIONS OF INTRUSIONS AND MINERAL OCCURRENCES

A variety of intrusion-related mineral deposits and occurrences are known within the Nahanni MERA area, including several of ambiguous origin. These are located in Figure 2 and summarized in Appendix 1. Lead isotope analyses were done on sulphides sampled from both known intrusion-related and non-intrusion-related mineral occurrences, and of several of the mineral occurrences of ambiguous origin. Mineralized samples were collected from at least eleven locales where an intrusive metal source was suspected, but could not be positively established based on solely field relationships (Fig. 2). These data were compared to Pb-isotope analyses for feldspars from 16 intrusions within the study area and to one galena analysis for a SEDEX mineral occurrence (ANNIV) to help shed light on the possible origin of ambiguous showings throughout the study area (Fig. 2). A mineral occurrence where a sulphide mineral possesses a Pb-isotope composition that plots in relative proximity to the feldspar samples is inferred to be 'intrusion-related' or consist of intrusion-derived sulfur. Sulphide samples with Pb-isotope compositions that did not fall within the field defined by the feldspars were considered to be 'non-intrusion-related.' All Pb-isotope preparation,

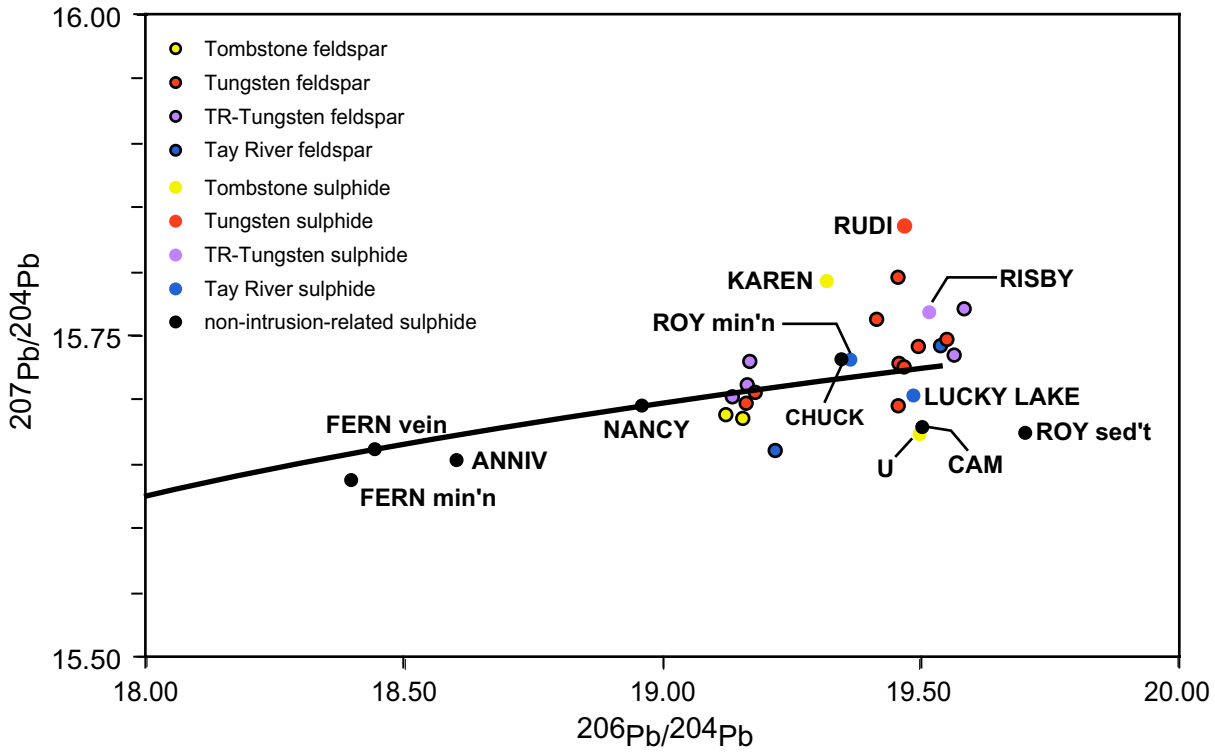


Figure 8. Lead isotope compositions for intrusions within the MERA area and mineral occurrences plotted with the upper crustal Pb evolution model or "shale curve" (indicated by the solid line) for the northern Cordillera (Godwin and Sinclair, 1982).

analysis, and data reduction were done at the PCIGR, University of British Columbia; the methods are described in Appendix 3.

Interpretation

Results from the lead isotope analyses of feldspar and sulphide mineral separates are presented in Table 4 and plotted in Figure 8 with reference to the upper crustal Pb evolution model or "shale curve" of Godwin and Sinclair (1982) for the northern Cordillera. The lead-isotope analyses of feldspars appear to yield a scattered cluster of relatively radiogenic Pb-isotope compositions. Pb-isotope ratios for seven sulphide-bearing samples from six mineral occurrences (Roy, Lucky Lake, U, Cam, Karen, and Chuck) plot within the field defined by the intrusions within the MERA area, indicating that the metals from these mineral showings were probably derived from the Mid-Cretaceous intrusions. Four sulphide-bearing samples from three occurrences (NANCY, ANNIV, and FERN) plot outside the field defined by the intrusions and are best considered as non-intrusion-related. The NANCY showing is described as a northwest-trending zone of stratabound galena and red sphalerite in brecciated and bedded dolomites; the ANNIV showing is galena-sphalerite SEDEX mineralization from the Howard's Pass district; and, the two samples from the FERN showing represent a galena-bearing quartz-carbonate vein, and galena-sphalerite-bearing veins and massive lenses in what is described as a "tremolite skarn." The observation that both FERN samples are less radiogenic, or plot lower on the "shale curve" of Godwin and Sinclair (1982), than the Proterozoic-age Anniv SEDEX mineralization is curious and indicates a much older Pb-reservoir from which the metals were derived. These mineral occurrences are discussed in greater detail by Falck et al. (2007; this volume).

One final observation concerns the Pb-isotope compositions of the intrusions, as represented by feldspar analyses. There are clearly two populations with respect to the $^{206}Pb/^{204}Pb$ ratio: a less radiogenic cluster with ratios of <19.3, and a more radiogenic spread with ratios of >19.3. The former consist of several intrusions found largely within the northwestern portion of the study area: Park, South Nahanni, Central Nahanni, North Nahanni, Pelly River, Mount Wilson, Mount Christie, and O'Grady. None of the sulphides from nearby mineral occurrences plot in proximity to these less radiogenic intrusions, which might indicate that this population may be a result of to analytical error or contamination. If the data are not in error, the bimodal distribution of the feldspar compositions implies two distinct source reservoirs from which the two populations of intrusions are derived. The distinct reservoirs are not related to upper crustal inhomogeneities as the same stratigraphic units are exposed throughout the study area (Gordey and Anderson, 1993). This bimodal data may be a result of distinctly different subsurface isotope reservoirs; however still within the middle to upper crust, as is indicated by the

Table 4. Lead isotopic ratios for intrusions and mineral occurrences within the Nahanni MERA area. Grey indicates questionable data (not plotted).
Sulphide compositions from mineral occurrences.

Sample	Description	Associated Plutonic Suite	Mineral	$^{206}Pb/^{204}Pb$	2s,%	$^{207}Pb/^{204}Pb$	2s,%	$^{208}Pb/^{204}Pb$	2s,%
KR-05-63	U	Tombstone?	galena	19.5042	0.05	15.6788	0.08	39.0145	0.10
KR-05-199h	LUCKY LAKE	Tay River	galena	19.4886	0.05	15.7053	0.08	39.4755	0.10
KR05-139	RISBY	TR-Tungsten	pyrrhotite	19.5211	0.10	15.7694	0.14	39.6125	0.18
HF05-138	IVO	Tungsten	pyrrhotite-pyrite	20.7355	0.09	15.7932	0.14	39.6925	0.18
KR05-120	RUDI	Tungsten	pyrrhotite	19.4746	0.12	15.8387	0.16	39.3101	0.20
HF-05-157	CHUCK	Tombstone	galena	19.3660	0.05	15.7319	0.08	39.4930	0.10
KR-05-61	CAM	Tombstone	galena	19.4895	0.05	15.6756	0.08	38.8689	0.10
KR-05-111	ANNIV	n/a	galena	18.6079	0.05	15.6536	0.08	38.6016	0.10
KR-05-114	NANCY	n/a	sphalerite	18.9674	0.08	15.6965	0.09	39.0774	0.13
KR-05-159	ROY sediment	n/a	pyrite	19.7071	0.05	15.6768	0.08	39.0490	0.10
KR-05-160	ROY mineralization	n/a	galena	19.3693	0.05	15.7322	0.08	39.4814	0.10
KR-05-79	FERN vein	n/a	galena	18.4529	0.07	15.6614	0.09	38.5578	0.11
KR-05-82	FERN mineralization	n/a	galena	18.4029	0.06	15.6382	0.08	38.4643	0.11
KR-05-89	KAREN	n/a	pyrite	19.3202	0.10	15.7939	0.11	39.4898	0.13

Feldspar compositions for intrusions.

Sample	Description	Plutonic Suite	Mineral	$^{206}Pb/^{204}Pb$	2s,%	$^{207}Pb/^{204}Pb$	2s,%	$^{208}Pb/^{204}Pb$	2s,%
KR-05-22	Roy pluton	Tay River	K-feldspar	19.5453	0.05	15.7455	0.08	39.6622	0.10
KR-05-43	Park pluton	Tay River	K-feldspar	19.2203	0.06	15.6614	0.08	39.1873	0.11
KR-05-26	Fish pluton	TR-Tay River	K-feldspar	19.5662	0.11	15.7364	0.13	39.6228	0.14
KR-05-76	Pelly River pluton	TR-Tay River	K-feldspar	19.1482	0.05	15.7029	0.08	39.2916	0.10
KR-05-130	Central Nahanni pluton	TR-Tay River	K-feldspar	19.1742	0.05	15.7324	0.08	39.2057	0.10
KR-05-136	North Nahanni pluton	TR-Tay River	K-feldspar	19.1733	0.05	15.7117	0.08	39.4081	0.10
KR-05-164	Hole-in-the-Wall batholith	TR-Tay River	K-feldspar	19.5881	0.05	15.7730	0.08	39.6577	0.10
KR-05-32	Ivo pluton	Tungsten	K-feldspar	19.4587	0.06	15.6979	0.09	39.4580	0.11
KR-05-32	Ivo pluton	Tungsten	K-feldspar	19.4740	0.71	15.7287	0.71	39.5600	0.72
KR-05-68	Mt. Wilson pluton	Tungsten	K-feldspar	19.1851	0.06	15.7068	0.08	39.2853	0.11
KR-05-110	Cac pluton	Tungsten	K-feldspar	19.4935	0.05	15.7438	0.08	39.5391	0.10
KR-05-113	South Nahanni pluton	Tungsten	K-feldspar	19.1631	0.05	15.6994	0.08	39.2411	0.10
KR-05-126	plug SE of O'Grady	Tungsten	K-feldspar	19.4582	0.05	15.7993	0.08	39.5422	0.10
KR-05-126	plug SE of O'Grady	Tungsten	K-feldspar	19.4189	0.05	15.7658	0.08	39.4413	0.10
KR-05-143	Circular Stock	Tungsten	K-feldspar	19.4615	0.06	15.7324	0.08	39.5141	0.11
KR-05-148	Rifle Range pluton	Tungsten	K-feldspar	19.5551	0.07	15.7519	0.09	39.6135	0.12
KR-05-62	Mt. Christie pluton	Tombstone	K-feldspar	19.1281	0.05	15.6901	0.08	39.1779	0.10
KR-05-97b	O'Grady batholith	Tombstone	K-feldspar	19.1609	0.17	15.6862	0.14	39.1658	0.21

proximity of the samples to the upper crustal "shale curve" of Godwin and Sinclair (1982). At this point it is uncertain as to what the significance this data has for the classification of the plutonic suites in the study area; field observations and geochronological, geochemical, and geophysical properties do not change markedly with the Pb-isotope compositions.

METALLOGENIC CONSIDERATIONS

Metallogenic Associations of the Plutonic Suites

In the Tintina Gold Province, dominantly in the Yukon Territory, metallogenic associations of the Tombstone and Tungsten suites have been previously discussed by Mortensen et al. (2000) and Hart et al. (2004a). These metallogenic associations depend largely on the oxidation state of the intrusion and thus the nature of the source magmas (Ishihara, 1981). The reduced state of the majority of intrusions throughout the MERA area indicates a prospective metallogenic association with tungsten- or antimony-rich mineralization, intrusion-related gold, Pb(Ag)-Zn polymetallic and/or tin vein mineralization (Ishihara, 1981; Hart et al., 2004a). There may also be some potential for mineralization typically associated with oxidized granitoids in the study area (Fig. 4), in particular Cu-Au-Fe(-Mo) min-

Table 5. Assay results (ICP-AES) for prospective intrusion-hosted mineralization in the Nahanni MERA area; anomalous values are shaded pale grey.

Sample	KR-05-04	KR-05-25	KR-05-40	KR-05-63	KR-05-88
Associated plutonic suite	Tombstone	Tay River	proximal to Tombstone suite intrusion	Tombstone	Tombstone
Description	Big Charlie pluton: sheeted gossanous fractures	Roy pluton: sulfide-rich quartz veins	CHUCK showing, silicified aplite plug: mal-sph-gn-bearing vuggy qtz veins	"U" showing, Mt. Christie pluton: apy-gn-py-az-bearing, ribboned-vuggy qtz veins	KAREN showing, O'Grady batholith: strongly oxidized porphyry phase associated with Sb skarn
[1,2]Au	bd	bd	0.005	0.01	bd
Ag	<0.5	<0.5	6.9	54.6	<0.5
As	<5	<5	40	6100	64
Ba	380	270	30	10	820
Be	3.9	4.2	<0.5	0.5	2.6
Bi	<2	<2	<2	43	<2
Cd	<0.5	<0.5	3.7	109	0.6
Co	4	1	2	2	15
Cr	4	5	7	9	48
Cu	13	25	262	24	15
Hg	<0.01	<0.01	0.16	0.04	<0.01
Mo	3	1	<1	<1	1
Ni	<1	<1	4	3	18
Pb	28	25	239	>10000	65
S%	0.02	0.02	0.01	2.22	0.33
Sb	<5	<5	76	1190	10
Sr	160	128	6	25	275
V	27	9	3	4	80
W	<10	10	<10	<10	<10
Zn	48	38	159	4890	39

1 all concentrations in ppm unless otherwise noted
2 bd = below detection limit for Au (0.005 ppm)
apy=arsenopyrite; az=azurite; gn=galena; mal=malachite; py=pyrite; qtz=quartz sph=sphalerite

eralization, and alkalic intrusion-related U-Th-(Cu-Au) enrichment (Ishihara, 1981; Hart et al., 2004a). Metallogenic associations for the Tungsten and Tombstone plutonic suites in the Yukon Territory, as described by Hart et al. (2004a; 2005), are (1) Tungsten suite, W-(Cu-Bi-Au-Mo) skarns in calcareous host rocks, small tin greisens, and distal Pb(Ag)-Zn veins; and the (2) Tombstone suite, U-Th-F occurrences, Au-(Cu-Bi) skarns in calcareous host rock, and tin veins with precious metal enrichments.

Variations on these metallogenic associations in the Yukon Territory are observed for the Tombstone and Tungsten suites within the MERA area, however there are others more specific to the study area documented in the Northern Minerals Database (NORMIN), which are summarized in Table 1 and Appendix 1. The 'intrusion-related' mineral occurrences within the study area detailed in Appendix 1 represent all the known types and styles of mineralization associated with the plutonic suites within the study area. These have been simplified into nine broad categories:

- proximal W-Cu-(Zn-Bi-Au-Mo) skarn;
- proximal Cu skarn;
- proximal Pb(Ag)-Zn skarn;
- proximal Sb-Pb-As skarn(?);
- proximal Au (and placer Au);
- distal Pb(Ag)-Zn manto;
- distal Pb(Ag)-Zn vein;
- gem (Be/Bo); and possibly,
- mafic volcanic-hosted Cu.

Five of the nine categories comprise proximal types of mineralization with variable metal associations, four of which are skarns emplaced into calcareous wall rocks (although the Sb-Pb-As may not be a true 'skarn') and proximal gold (described as a skarn at RINO; Fig. 2). Of the two distal mineralization styles, Pb(Ag)-Zn manto mineralization is not abundant and consists of a cluster of occurrences associated with the Roy pluton

Table 5 continued.

Sample	KR-05-181	KR-05-202	KR-05-209	KR-05-216a	KR-05-226
Associated plutonic suite	Tungsten	Tay River	TR-Tungsten	Tungsten	Tungsten
Description	Shelf Lake pluton: greisenized granite, with py-(apy)-bearing fractures and qtz veins	Mt. Sir James McBrien: greisenized, gossanous, sheeted, scheelite-powellite-bearing fractures	Little Hyland stock: tourmaline-ribboned, scheelite-bearing qtz vein in greisenized granite	surface Mine Stock, Cantung: sheeted, gossanous qtz veins with associated scordierite	Rifle Range pluton: greisenous, gossanous, apy-scheelite-bearing fractures
^{1,2}Au	bd	bd	bd	0.15	bd
Ag	<0.5	<0.5	<0.5	<0.5	<0.5
As	154	22	<5	6	216
Ba	1000	1450	200	40	540
Be	4.5	3.6	4.8	1.3	4.3
Bi	<2	2	6	246	<2
Cd	<0.5	<0.5	<0.5	<0.5	<0.5
Co	6	4	<1	2	1
Cr	10	9	7	3	2
Cu	3	3	4	118	9
Hg	<0.01	0.02	<0.01	<0.01	<0.01
Mo	<1	<1	1	36	<1
Ni	4	1	<1	2	2
Pb	45	37	25	2	43
S%	0.29	0.07	0.13	0.28	0.01
Sb	<5	5	<5	<5	<5
Sr	236	459	51	31	155
V	76	47	12	6	7
W	10	<10	10	<10	<10
Zn	44	44	23	10	10

(Tay River suite); distal base metal veins are much more common throughout the study area and are also associated with other plutonic suites. In addition to the cluster of manto-style sulphide occurrences, the Tay River suite intrusions are also associated with proximal Pb(Ag)-Zn skarn (n=3) and W-Cu-(Zn-Bi-Au-Mo) skarn (n=3). TR-Tungsten suite intrusions are associated with proximal Cu skarn (n=1) and W-Cu-(Zn-Bi-Au-Mo) (n=1) skarn. Tungsten suite intrusions are associated with abundant proximal W-Cu-(Zn-Bi-Au-Mo) skarns (n=14); distal Pb(Ag)-Zn vein (n=2); and one gem (Be-emerald) occurrence hosted within quartz veins in contact-metamorphosed sediments. Finally, Tombstone suite intrusions are associated with distal Pb(Ag)-Zn veins (n=3; including Cam based on a nearly identical Pb-isotope composition with the 'U' occurrence, hosted in a Tombstone suite intrusion; Fig. 8); proximal Pb(Ag)-Zn skarn (n=5; or more specifically, limestone with mineralized fractures that have been grouped into the skarn category); proximal Cu skarn (n=1); proximal Au (n=2; one of which is described as a skarn); proximal Sb-Pb-As skarn(?); several scattered placer Au occurrences centred around two intrusions in the southwestern corner; one gem (Belbaite) occurrence hosted in miarolitic cavities of pegmatite-aplite horizons within the O'Grady batholith; and, several mafic-volcanic-hosted Cu-(Au) occurrences of uncertain origin, although the copper mineralization from the Chuck showing plots in proximity the Pb-isotope compositions of the intrusions (Fig. 8).

Assay Results

Many of the intrusions throughout the MERA area, regardless of plutonic suite, are crosscut by localized, sheeted, gossanous fractures or en echelon quartz veins, some of which carry one or more of the following visible minerals: arsenopyrite and/or scordierite, galena, chalcopyrite and/or copper oxides, sphalerite, scheelite, and gold. Ten of the most prospective of these mineralized zones were analyzed by ICP-AES to determine any anomalous base and precious metal concentrations (Fig. 2; Table 5). The accuracy and reproducibility of these results were monitored by repeat analyses of several in-house standards. A quick review

of the results in Table 5 reveals that gold was only detected in quartz veins associated with two Tombstone suite intrusions, and one Tungsten suite intrusion (at the Cantung mine). The two Tombstone intrusions also display strongly anomalous values of Ag-Cu-Hg-Pb-Zn and Ag-As-Bi-Pb-Sb-Zn; the latter, Tungsten suite intrusion has strongly anomalous concentrations of Bi-Cu-Mo, of which are biproduct or trace metals. These are described in the metallogenic character for the Cantung tungsten deposit by the NORMIN database. Other samples with anomalous values are the Shelf Lake (Tungsten suite), Little Hyland (TR-Tungsten suite), Roy (Tay River suite), and Rifle Range (Tungsten suite) plutons for beryllium, and the Roy and Little Hyland for tungsten. It is also interesting to note that none of the three samples collected from the Tungsten suite intrusions actually contain anomalous tungsten, suggesting that sheeted fractures or veins within this suite of intrusions are not related to any large-scale tungsten mineralizing events.

Tungsten Mineralization in the MERA Area

Initial ID-TIMS U-Pb zircon geochronological results for three separate felsic intrusions sampled underground at the Cantung mine place firm constraints on the timing of tungsten and localized trace molybdenum mineralization (Table 2). The Mine Stock intrusion (sample 03M-207) underlying the orebody and a scheelite- and pyrrhotite-bearing aplite dyke (03M-204) that cuts the intrusion, yield essentially identical zircon crystallization ages of 98.2 ± 0.4 Ma and 98.3 ± 0.3 Ma, respectively (Rasmussen et al., 2006). A biotite-(tourmaline)-bearing felsic dyke (03M-203) that intrudes along one of several low-displacement normal faults and cuts the massive orebody, but does not contain scheelite or pyrrhotite (only trace molybdenite), is slightly younger at 97.4 ± 0.3 Ma (Rasmussen et al., 2006). Combined, these results suggest that the tungsten mineralization largely followed emplacement of the Mine Stock and associated aplite dykes (ca. 98 Ma) and may have occurred over the 2.3 m.y. duration of the thermal history of the Mine Stock, until lower magmatic temperatures were reached (post 95.1 Ma). It is noteworthy that previous work by Hart et al. (2004b) resulted in a sensitive high-resolution ion microprobe (SHRIMP) age for the Mine Stock at Cantung of 96.6 ± 1.2 Ma. This age appears somewhat younger than the ID-TIMS age from this study (98.2 ± 0.4 Ma), but is still within the combined 2-sigma error range.

The age of the Mine Stock intrusion and associated tungsten mineralization (ca. 98 Ma) at Cantung correlates well with the age of mineralization at Mactung, another significant tungsten deposit (reserve: 32 Mt at 0.82% WO_3; Atkinson and Baker, 1986) associated with a Tungsten suite intrusion immediately northwest of the study area. Mineralization at Mactung has been dated by Selby et al. (2003) at 97.5 ± 0.5 Ma, using Re-Os geochronological analysis on molybdenite (closure temperature: ~500 ± 50ºC). However, the age of the Cirque Lake intrusion adjacent to the orebody at Mactung is slightly younger at 96.4 ± 1.0 Ma, as determined by SHRIMP U-Pb analysis (Hart et al., 2004b). This raises the possibility that the SHRIMP analyses are producing anomalously young ages for the plutons at MacTung and Cantung when compared to the ID-TIMS (this study) and Re-Os (Selby et al., 2003) data. Thus, the 98 to 97 Ma interval from crystallization temperatures (~850ºC) to moderate magmatic temperatures (~500ºC) provides an indication of the timing of significant magmatism associated with tungsten mineralization in the study area. Other intrusions in the study area close in age to this event that either have known associated tungsten mineralization, or that may also be prospective for large tungsten deposits based on their age, are Mt. Wilson, the plug southwest of O'Grady, Rudi, Cac, Ivo, and possibly Circular Stock (Table 2). Many other intrusions with related tungsten mineralization are somewhat younger, but for the most part have crystallization ages older than 95 Ma (Table 2), and all intrusions associated with known tungsten mineralization (aside from Ivo, which appears to have been reset) have argon ages for biotite from ca. 94.5 to 96.5 Ma. This constrains a tungsten mineralizing event in the region between 98 to 95 Ma.

Th/U Ratio

The presence of monazite in the Tungsten suite of intrusions is due to enriched thorium relative to uranium. As thorium is slightly more incompatible during crystallization of felsic melts, this occurs in intrusions that have undergone high degrees of crystal fractionation or magma differentiation. A ratio of Th/U of greater than 1 (values are normalized to the primitive mantle; Sun and McDonough, 1989) has been used in this study as a preliminary discriminator of the majority of Tungsten suite intrusions (Table 3; see negative slope from Th to U, Fig. 6). A Th/U ratio greater than or equal to approximately 2.0 is observed for the only two Tungsten suite intrusions analyzed from intrusive phases in direct contact with known mineralization: the underground Mine Stock (adjacent to the E-zone orebody, Cantung), and a garnet-muscovite-bearing marginal phase of the Ivo pluton (adjacent to a tungsten skarn occurrence). Other high ratios (>1.5) are also noted for the Faille, Lened, and Coal River-ROYALL plutons, of which the latter two are associated with tungsten skarn mineralization; this suggests that the intrusive phase sampled at the Faille pluton is also prospective for tungsten mineralization.

Petrogenesis of Tungsten Suite intrusions

It is widely accepted that tungsten mineralization is associated with batholithic, composite, granodiorite to granite intrusions with large K-feldspar phenocrysts in a coarse-grained matrix (Newberry, 1998), due to emplacement and crystallization of such metalliferous intrusions at relatively deep levels in the upper crust (Keith et al., 1989). However, it has been suggested that intrusions actually associated with larger tungsten skarn orebodies tend to be somewhat emplaced at somewhat shallower levels, although still relatively deep in comparison other ore deposit types (Meinert, 1993). As described earlier, Tungsten suite intrusions in the study area are relatively small (frequently <0.5 km across, but up to ~5 km across), fine- to medium-grained granitic bodies lacking in large and/or abundant K-feldspar phenocrysts. However, these intrusions are spatially associated with the slightly older to coeval Tay River suite of composite batholithic intrusions that fit the above description. The Tungsten suite of intrusions is interpreted here to comprise smaller, very highly fractionated and crustally contaminated, and perhaps more highly emplaced (although still relatively deep, >5 km; Newberry, 1998) intrusions overlying or fringing larger, unexhumed to partially exhumed Tay River suite and transitional TR-Tungsten plutons. The geochemical uniformity or homogeneity observed among the Tungsten suite plutons over relatively large areas, described earlier, indicate that these areas could be underlain by an aerially extensive and relatively geochemically and isotopically homogenous magma source, inferred to be unexhumed large plutonic or batholithic bodies similar to those exposed in the study area (Hole-in-the-Wall batholith, Coal River batholith). Such large underlying intrusions could also have provided the more highly-emplaced Tungsten suite of intrusions with a significant metal source.

As discussed earlier, the intrusions in the study area, including Tungsten suite intrusions, do not appear to exhibit typical features of S-type granites despite their initial classification into this category (Gordey and Anderson, 1993). For example: (1) none of the intrusions are strongly peraluminous, or have an aluminosity of greater than 1.3 (Table 3) aside from a few of the aplite dykes and marginal leucocratic phases; (2) alumino-silicate minerals such as cordierite, andalusite, are not observed in the intrusions; (3) the large, coeval, biotite-hornblende-bearing batholiths are not consistent with the mineralogy of S-type intrusions (but more so with I-type intrusions), and (4) only locally developed marginal leucocratic intrusive phases contain garnet, tourmaline, and muscovite (although the Lened or Mine Stock plutons have more widespread but sparse, typically ragged muscovite). These observations, combined with the geochemical data presented earlier, indicate that the intrusions are more likely to be largely sourced from partial melting of a mafic- to ultramafic-source material rather than middle to upper crust.

Newberry (1998) postulated that it is likely that the intrusions underlying the MERA area represent moderately to highly evolved melts similar to the intrusions further to the west in the Yukon Territory and Alaska that have an isotopically primitive magma source. Driver et al. (2000) proposed partial melting of both felsic, upper crustal rocks and intermediate-mafic lower crustal rocks in the genesis of the Mid-Cretaceous Cassiar batholith in the Yukon Territory - British Columbia. However, any significant melting of mafic basement requires temperatures in excess of 900 to 1000°C in order to produce approximately 20 to 40% partial melt (Petford and Gallagher, 2001); these temperatures cannot be produced by orogenic crustal thickening alone (England and Thompson, 1984). One method of generating temperatures high enough to melt mafic basement rocks would be the influx of hot, 'wet' mantle-derived melts, perhaps through mechanisms such as crustal thinning, lower crustal delamination, and/or intra- and under-plating of mantle-derived melts (Petford and Gallagher, 2001; Clemens, 2003). Mortensen et al. (2000) and Hart et al. (2004a; 2005) interpreted some enriched mantle-derived component in the formation of the Tombstone suite intrusions and late mafic dykes, which were emplaced only a few million years after the Tungsten suite and associated TR-Tungsten and Tay River intrusions. This influx of mantle-derived melts could result from the generation of partial melting mantle (and lower crust) due to the increased heat flow observed in the mantle wedge underlying back-arc regions (e.g. Currie and Hyndman, 2006). This anomalously high heat flow has been attributed to small-scale thermal convection resulting from the release of fluids into the mantle wedge above a dehydrating subducting slab. This would subsequently reduce the viscosity of the mantle in this region and allow for more efficient heat transfer from deeper parts of the mantle to the base of the lower crust (Currie and Hyndman, 2006). The increased temperatures (>1200ºC; Currie and Hyndman, 2006) could lead to partial melting of the enriched mantle above the subducting slab, and possibly the mafic or ultramafic lower crust. Thus, the generation of I-type magmas in the back-arc region during the late- or post-collisional stage of orogeny in this region is not unreasonable.

FLUORINE, CHLORINE, AND SULPHUR ANALYSIS OF IGNEOUS APATITE AND BIOTITE

It is generally accepted that some elements, such as chlorine, sulphur, and possibly fluorine, act as ligands or as ionic species that form chemical complexes with

metals in magmatic and hydrothermal systems. In some such systems, a vapour or fluid phase enriched in one or more complexes exsolves or separates from a crystallizing magma body, enabling the transportation, concentration, and precipitation of metals from the intrusion into a structural or chemical trap, and the resultant formation of mineralization. The exsolution of a metalliferous vapour phase is inferred to cause a depletion in the concentration of the ligand in the residual fluid and/or magma within the crystallizing intrusion, which is in turn reflected in the composition of minerals that crystallize from the cooling magma.

Apatite is unique in that it is one of the few minerals with a crystal lattice that will accommodate the substitution of fluorine and chlorine for hydroxyl in the Z-site, and sulphur for phosphorus in the X-site (Pan and Fleet, 2002); it is also relatively resistant to late alteration (Piccoli and Candela, 2002). Biotite is another mineral that allows for halogen accommodation in the crystal structure; however, in contrast to apatite, biotite is susceptible to retrograde-halogen exchange (Piccoli and Candela, 2002). As apatite typically crystallizes early at high temperatures (based on petrography and calculated apatite saturation temperatures, or ASTs; tabulated in Table 3) and biotite crystallizes at lower temperature (Sallet, 2000), the analysis and comparison of halogen concentrations in both minerals helps to establish magmatic fluid compositions from early through late crystallization of the intrusion. The evolution of magmatic volatile chemistry throughout the intrusive cooling process can thus be approximated in order to detect any exsolution of a volatile- and possibly metal-rich phase.

A detailed examination of fluorine, chlorine, and sulphate (as a proxy for sulphur) concentrations in apatite, and of fluorine and chlorine in biotite from selected felsic intrusions was undertaken in an attempt to establish magmatic fluid chemistries of crystallizing intrusions within the MERA area, and to determine the possible implications of magmatic fluid chemistry with respect to the potential for intrusion-related mineralization. Of the representative samples selected for geochronological and geochemical analysis, twenty-two and twenty-four samples were analyzed on the electron-probe micro-analyzer (EPM) for apatite and biotite compositions, respectively. The preparation, analytical microbeam procedures, and data reduction for both apatite and biotite are described in detail in Appendix 3, and the data used for the following plots and interpretations are recorded in Appendix 4.

Results and Interpretation

Apatite

Initial fluorine concentrations (see Appendix 3), and chlorine and sulphate concentrations for each apatite analysis from the intrusions are plotted in Figure 9 using the data documented in Appendix 4). If fluorine is depleted, either chlorine or hydroxyl (determined by stoichiometry) must increase. It should be noted that values of fluorine that approach or exceed 3.75 wt.% will essentially force lower concentrations of chlorine (and hydroxyl). Apatite will accommodate up to 3.75 wt.% fluorine in the Z-site of $Ca_5(PO_4)^3(F,Cl,OH)$, and a quick scan of Figure 9 indicates that many of the intrusions have near end-member 'fluorapatite' compositions. Higher initial concentrations of fluorine in some samples (up to 3.93 wt.% F) are above the upper detection limit (i.e. 3.75 ± 0.04 wt.%) and are possibly due to small analytical errors, in measurement and in data reduction. Another factor that will also result in inflated fluorine values is the presence of carbonate (CO_3^{2-}), which is also retained within apatite as a substitute for hydroxyl but cannot be measured by the EPM (T. Baker, pers. comm., 2006).

In examining Figure 9, the Powers pluton has a wide range of initial fluorine concentrations in apatite, and the Jorgensen pluton has one anomalously high fluorine value. These are the only two intrusions that display any evidence for possible retrograde halogen exchange in apatite. From Figure 9 it is clear that there is an overall increase from the Tay River to the Tungsten suite intrusions in fluorine concentrations, whereas chlorine and sulphate decrease. There is more than one possible explanation for this, including an increased degree of crustal contamination or assimilation (Sallet, 2000), and an increased degree of differentiation (i.e. more evolved) with plutonic suite of the intrusions. Considering that the Tombstone suite intrusions are interpreted to have had some enriched mantle-derived melt component, with limited middle to upper crustal contamination, they are unexpectedly high in fluorine contents, although unlike most of the Tungsten suite intrusions, sulphate is at low but detectable concentrations. One explanation for this would be that the apparent or inflated fluorine concentrations are due to higher carbonate concentrations within apatite, which is not unexpected in magmatism that originated in fluid-rich regions (T. Baker, 2006, pers. comm.). This is consistent with an enriched lithosphere underlying a back-arc region, and from which the Tombstone suite intrusions are interpreted to be largely derived (Hart et al., 2005).

Due to the relatively high fluorine concentrations in the intrusions from the study area, it should again be noted that large enrichments in fluorine approaching 3.75 wt.% are unlikely to be accompanied by any significant enrichment in chlorine due to the 'accommodation problem', described above, in the apatite crystallographic structure. Thus, the most reliable measure of enrichment versus depletion for these intrusions is

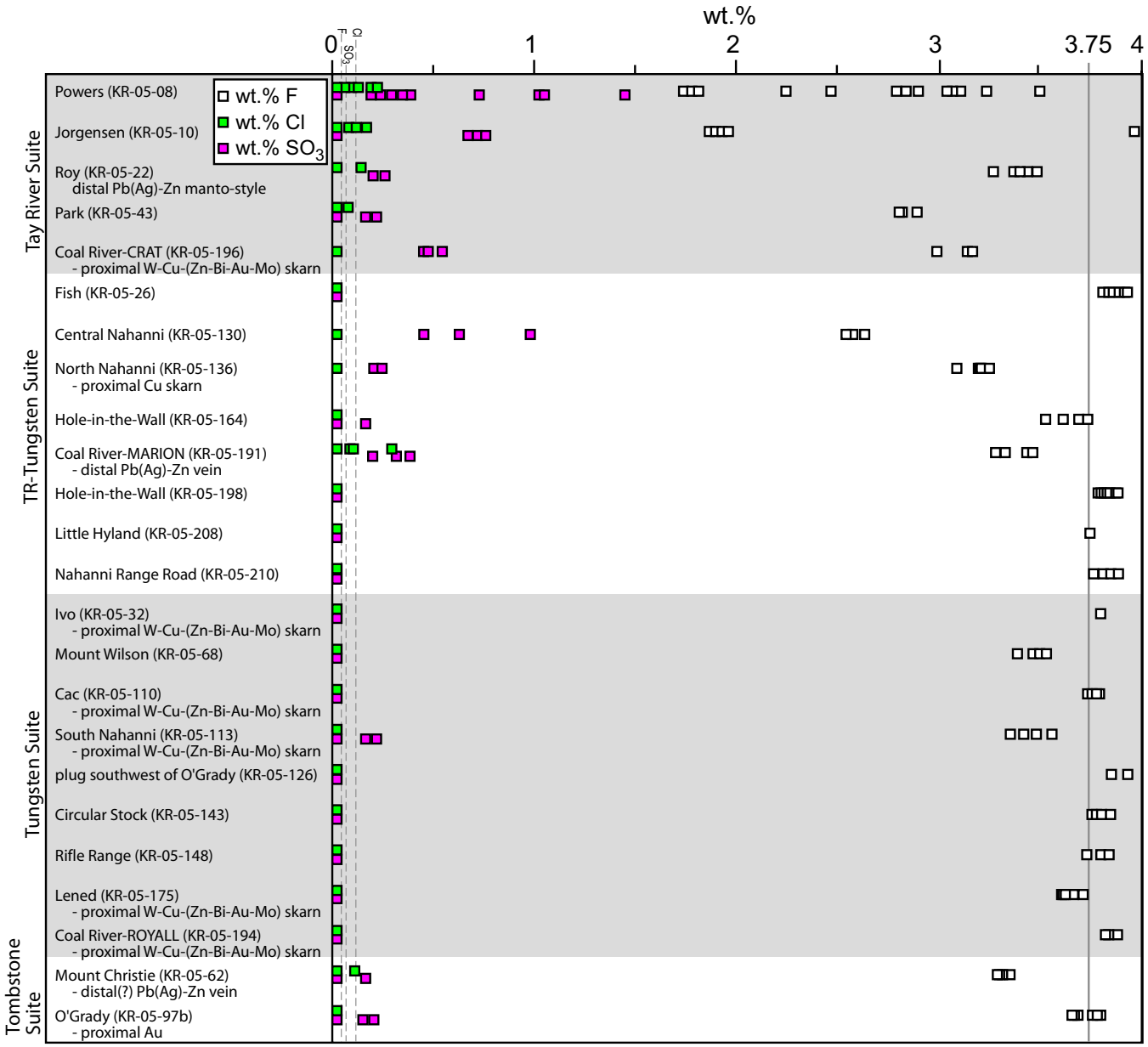


Figure 9. Initial fluorine, chlorine, and sulphate concentrations in apatite for the intrusions; detection limits are indicated by grey dashed lines and the maximum amount of fluorine that may substitute into apatite (3.75 wt.%) is indicated by the solid grey line. Spatially associated mineralization, if present, is described following the classification of types and styles used throughout this paper (Appendix I). Intrusions sampled within proximity to a known mineral occurrence are notated with the name of the mineral occurrence capitalized and a general classification of the type of mineralization.

the fluorine data. Fluorine concentrations are not depleted for the majority of the intrusions, including many associated with mineralization. Even if fluorine was not a significant complex-forming ligand, it would still be expected to be depleted if a any vapour phase was exsolved from the crystallizing intrusions before the crystallization of apatite. Of the intrusions associated with tungsten mineralization only the South Nahanni pluton displays a significant depletion in fluorine in comparison to other Tungsten suite intrusions, although Lened is also somewhat depleted. Though Mt. Wilson has no known-related tungsten mineralization, it also displays a relative depletion in fluorine in comparison to the Tungsten suite intrusions. Possible explanations for this depletion are discussed later; however, the lack of background fluorine concentrations in apatite for each intrusion make it difficult to determine which 'depletions' (or 'enrichments') in fluorine are inherent in the magma composition and which are the result of a release of a volatile phase or possibly late retrograde alteration.

Although the measured fluorine concentrations may be composition-dependant (Sallet, 2000), other intrusions with significantly lower amounts of fluorine are Roy, Park, Coal River-CRAT, Central Nahanni, Coal

River-MARION, and Mount Christie. It would be ideal to identify depleted or enriched fluorine concentrations that are not related to factors affecting the composition of the intrusion, or other factors unrelated to the exsolution of a volatile phase. However, with apatite data available for only one sample from each intrusion at this time, we are currently unable to establish background fluorine (chlorine, and sulphate) concentrations for each intrusion that are independent of composition.

Since both fluorine and chlorine are accommodated in the same crystallographic position in apatite, intrusions that have both depleted fluorine and chlorine concentrations (i.e. F + Cl <3.75 wt.%) could be indicative of an exsolution of a vapour phase detectable by apatite compositions. The rationale for this is that a significant exsolution of a vapour phases from the crystallizing intrusion might have led to a large enough depletion in the remaining fluorine and chlorine within the crystallizing intrusion such that only abundant hydroxyl was available to fill the Z-site in apatite. Similarly, Piccoli and Candela (2002) have suggested, based on their compilation of over 750 published apatite compositional analyses for felsic intrusive systems, that (1) intrusions with large depletions of fluorine and chlorine (and sulphate) are documented to be associated with mineralization in the country rock; (2) intrusions with large enrichments of chlorine and moderate depletions of fluorine and sulphate are documented to be associated with intrusion-hosted mineralization; and (3) intrusions with large enrichments of fluorine and sulphate, and moderate enrichments of chlorine, in apatite are documented to have no association with mineralization.

Upon inspection of Figure 9, a select group of intrusions display combined fluorine and chlorine concentrations that are less than 3.75 wt.%, which could be indicative of related mineralization following the reasoning of Piccoli and Candela (2002), particularly country rock hosted. Most of these intrusions are also relatively depleted in sulphate. Of these intrusions, those that are associated with known mineralization include Coal River near the CRAT occurrence (tungsten), North Nahanni (copper), South Nahanni (tungsten), and Mt. Christie (lead-zinc). Intrusions with a similar combined fluorine-chlorine depletion but no known spatially associated mineralization and that may therefore be considered prospective for associated mineralization are Park, Central Nahanni, and Mt. Wilson. Furthermore, if Tombstone suite intrusions (and possibly intrusions of other plutonic suites) have some component from a fluid-rich source material that could result in the presence of abundant carbonate and artificially inflated fluorine concentrations, there may be other intrusions with potential for related mineralization that cannot be detected by the apatite data alone.

Apatite Composition and Tungsten Mineralization

One unfortunate aspect of the apatite data in Figure 9 is that there is no obvious indicator for intrusion-related tungsten mineralization, such as a notable depletion in either fluorine or combined fluorine-chlorine concentrations, particularly as many of the mineral occurrences in the study area are tungsten-dominant skarns and includes one of the richest known tungsten skarn deposits (Cantung). One explanation for the lack of an observed fluorine depletion is that there was an over abundance of fluorine within the intrusion during crystallization, such that even with the exsolution of a vapour phase enough fluorine remained in the intrusion to fill the Z-site in apatite. Also possible is that the fluorine concentrations are artificially inflated by the presence of carbonate not detected on the EPM. A third, perhaps more likely explanation is that the intrusions, particularly those sampled immediately adjacent to tungsten mineralization (e.g. Ivo), may have exsolved a volatile phase at a lower temperature than that of the AST.

An earlier exsolution of volatile-rich phases has been demonstrated to typically result in predominantly copper mineralization; whereas, a later exsolution of volatile-rich phases from a magma body of the same composition should result in predominantly tungsten mineralization (Newberry and Swanson, 1986). We could thus expect to see a depletion in at least the combined fluorine and chlorine concentrations for intrusions with a significant copper association, which appears to be the case for the North Nahanni pluton: the only intrusion sampled from the study area for apatite analysis with associated and nearby copper mineralization. Similarly, we would also expect that intrusions with related tungsten mineralization may not display any depletion in the apatite composition. Furthermore, most mineral deposit studies and models suggest that (reduced) tungsten skarns typically form at relatively great depths (e.g. 1.5-2.5 kbar or approximately 5-8 km, Newberry, 1998), at which the relatively high-pressure conditions would depress the temperature of volatile-phase exsolution from the associated intrusions. If the release of a volatile phase typically occurs at depressed temperatures (e.g. below the calculated AST for an individual intrusion), we should not expect to see any indicators of volatile exsolution in the apatite composition. At the Cantung deposit within the study area, initial stages of mineralized skarn formation adjacent to the intrusion were interpreted to be between 450 and 500ºC (Mathieson and Clark, 1984): temperatures well below the calculated ASTs for all of the intrusions within the study area (Table 3). Indeed, such deep settings are generally regarded as necessary for a significant accumulation of

at least tungsten metal in the magmatic fluid phase before the release or exsolution of volatile material that transports the metals out of the intrusion and into the surrounding rock (Newberry and Swanson, 1986; Keith et al., 1989). Therefore, it could be hypothesized that those intrusions associated with tungsten mineralization that display a significant combined fluorine and chlorine depletion in apatite are potentially not associated with large volumes of tungsten mineralization (e.g. South Nahanni).

Apatite and Biotite

Data Analysis of Apatite and Biotite

The combination of apatite and biotite data allows for the determination of relative magmatic fluid composition. This is done using the thermodynamic calculations of Zhu and Sverjensky (1991, 1992), which take into account the effect of temperature-dependent compositional variations on halogen concentrations in biotite. The apatite-melt system is also dependent upon temperature, therefore halogen data should be interpreted with the temperature of initial apatite crystallization taken into account (Piccoli and Candela, 2002). The apatite saturation temperature (AST) was calculated, using the method of Bea et al. (1992) for peraluminous ('felsic') samples and the method of Harrison and Watson (1984) for metaluminous ('intermediate') samples (Table 3). This allowed the determination of the temperature at which apatite began to crystallize, and consequently the relative timing or temperature of any halogen and/or sulphur depletion in the crystallizing intrusion. Despite the wide range of largely composition-dependant ASTs in the literature, most apatite has been demonstrated to crystallize within 60 to 100ºC of the calculated AST (Piccoli and Candela, 2002).

For the purpose of modeling activities of fluorine and chlorine in apatite and biotite, an average AST of 850ºC and an average pressure of 2 kilobars (based on the presence of andalusite in most contact metamorphic aureoles) were assumed for apatite. An estimated average temperature of 650ºC at 2 kilobars pressure was adopted for the biotite calculations. The accuracy of these numbers is not critical as Coulson et al. (2001) have shown that despite the temperature dependence of apatite composition, these calculations do not depend greatly upon temperature. Test calculations were done in this study at variable pressures, and the apatite and biotite data were also not found to vary relative to each other.

The calculated activities of fluorine and chlorine are a relative measure of fluorine and chlorine abundance in the crystallizing intrusion at the time of apatite and biotite formation. The HF/HCl activity ratio, a comparison of fluorine versus chlorine concentration, was calculated for the magmatic fluid in each of the intrusions. This HF/HCl data were interpreted to represent independent measures of magmatic fluid composition at the time of apatite and biotite crystallization, respectively, for each intrusion (Munoz and Swenson, 1981; Selby and Nesbitt, 2000; Coulson et al., 2001). The HF/HCl activity ratios have allowed the authors to assess the evolution of magmatic fluids with respect to fluorine and chlorine, in order to (1) constrain the relative timing of exsolution of a volatile-rich vapour, and, (2) to determine which intrusions within the MERA area are most likely to have exsolved a mineralizing vapour phase.

In an effort to provide additional insight into the possible timing of generation of a metalliferous fluid during crystallization of intrusions within the MERA region, HF/HCL activity ratios were calculated for apatite and biotite (tabulated in Appendix 4). A decrease in the ratio from apatite to biotite is thought to be indicative of a decrease in overall halogen activity in the magmatic fluid during crystallization of an intrusion, attributed to the probable release of a volatile or fluid-rich phase (Coulson et al., 2001). Magmatic fluid chemistries were plotted as a log function of the HF/HCl activity ratio for apatite and biotite in Figure 10. Fewer data are plotted in Figure 10 in comparison to Figure 9 due to chlorine concentrations that were "0" wt.%, for which HCl activities are also zero, and the HF/HCl activity ratios cannot be calculated.

Decreasing HF/HCl Activity Ratios

In Figure 10, intrusions associated with mineralization that display a large depletion in the HF/HCl activity ratio from apatite to biotite (i.e, apatite ratios that do not overlap with biotite ratios) are North Nahanni, South Nahanni, Rifle Range, Coal River-Royall, and O'Grady. This depletion is consistent with the release of a significant volatile phase, possibly carrying ore metals, at moderately high temperatures that are intermediate to the crystallization temperatures of apatite and biotite. Other intrusions that have similarly large decreases in the HF/HCl activity ratio but no known related mineralization are Fish and Hole-in-the-Wall as represented by sample KR-05-198. The Park intrusion also displays a significant depletion in the activity ratio, with some data overlap. Based on these large depletions, it is postulated that these three intrusions have some potential for related mineralization. Intrusions with a range of overlapping apatite-biotite data that indicate a negligible to a potentially large depletion are Cac and Lened, both of which are associated with tungsten mineralization. However, until more data is obtained, the authors cannot classify these intrusions relative to the degree of depletion in the activity ratio. Two intrusions that have a notable (non-overlapping apatite-biotite composition) but only moderate

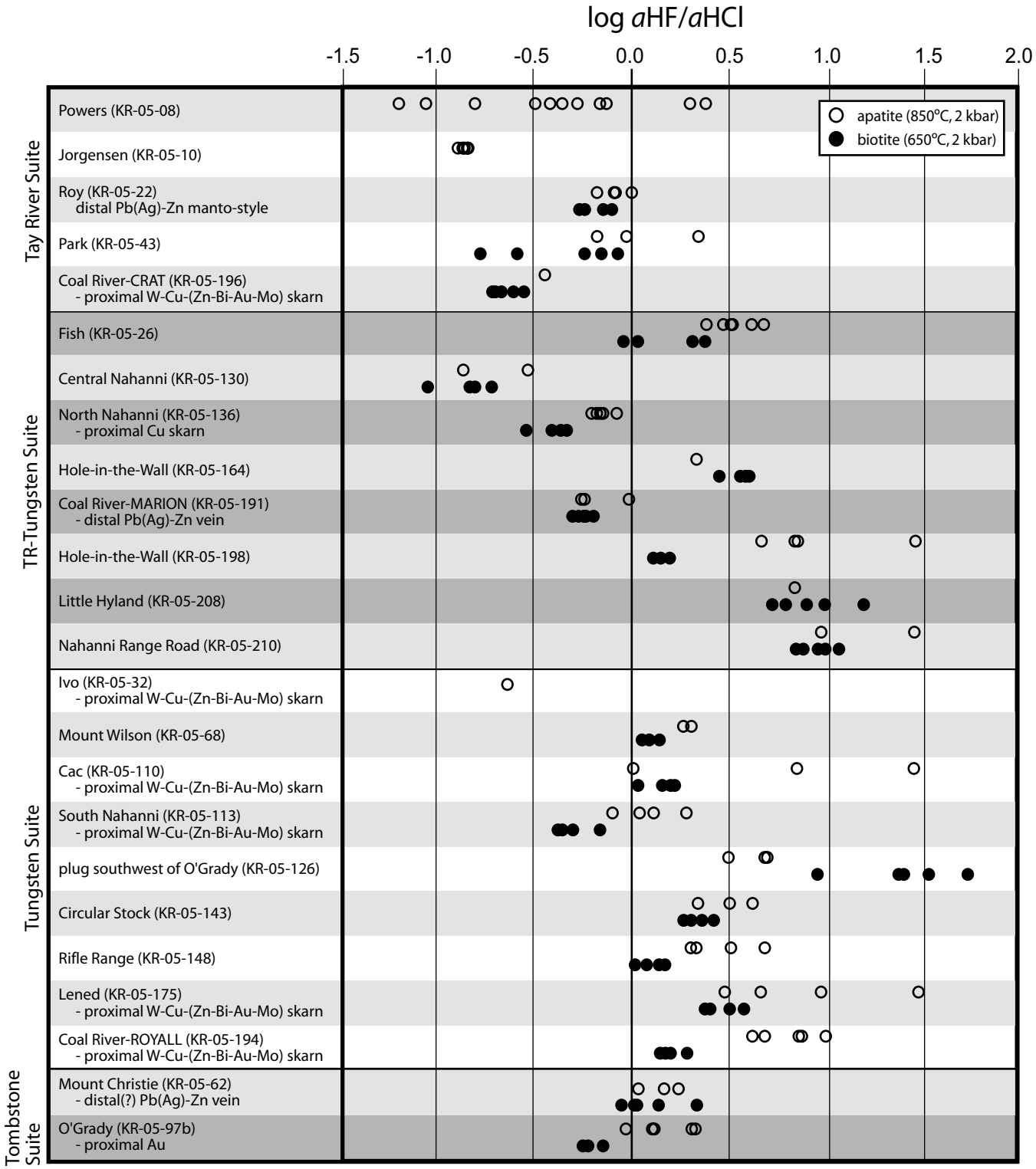


Figure 10. HF/HCl activity ratios in the magmatic fluid as represented by the composition of apatite and biotite. Intrusions sampled within proximity to a known mineral occurrence are notated with the name of the mineral occurrence capitalized and a general classification of the type of mineralization.

depletion in the activity ratio from apatite to biotite are Coal River-CRAT, also associated with mineralization, and Mount Wilson. Of the remaining intrusions, Roy, Central Nahanni, Nahanni Range Road, and Circular Stock display slight depletions of indeterminable significance. Finally, Coal River-MARION, Little Hyland, and Mount Christie do not have any reasonable change in the activity ratio from apatite to biotite, indicating that these intrusions did not exsolve any volatile phase at the temperatures represented; this

reduces their likelihood for related mineralization. Interestingly, the halogen data for biotite in Little Hyland pluton do not appear to have been significantly enriched or depleted during the possible thermal event discussed earlier, which may have lead to the resetting of the Ar-Ar age in the biotite.

Slight depletions in the activity ratio could represent (1) intrusions that exsolved a volatile phase *during* the crystallization of apatite, leading to a temporary depletion in the outer margin of the grain, which would equilibrate with the core through fluorine diffusion and could result in depleted fluorine concentrations overall within individual grains (Pan and Fleet, 2002), or (2) intrusions that gradually exsolved a large amount, or frequently exsolved relatively small amounts of a volatile phase before, during (and potentially after) the crystallization of apatite and/or biotite. The former may be reflected in either a moderately low activity ratio for apatite, or a widely variable activity ratio for apatite (e.g. Lened, Cac), combined with a somewhat more depleted activity ratio in biotite. The second possibility was suggested by Coulson et al. (2001) for the Emerald Lake pluton, Yukon; a Tombstone suite intrusion. The abundance of halogens in the crystallizing Emerald Lake intrusion was tracked by increasingly evolved intrusive phases (syenite to monzonite to granite to pegmatite) and found to decrease gradually over time, even though the activity ratio for each intrusive phase actually increased slightly from apatite to biotite. This overall decrease with time from older and less evolved phases to younger and more evolved phases was interpreted by Coulson et al. (2001) to represent a gradual exsolution of a volatile phase, which resulted in the disseminated and low-grade nature of the uneconomic gold mineralization hosted throughout the pluton. In this latter case, where a volatile phase is released gradually over the course of crystallization of the intrusion, one would expect to see only a slight depletion in the activity ratio from apatite to biotite (Nahanni Range Road, Circular Stock). The results from the Emerald Lake study indicate that, aside from perhaps those samples with variable apatite ratios (e.g. Lened, Cac), slight depletions have little economic significance.

Although the authors were unable to obtain biotite data for the Ivo pluton, it is interesting that the HF/HCl activity ratio for the single apatite analysis is so strongly depleted relative to most of the other intrusions. Notably, Coal River-Crat and Central Nahanni also have highly depleted activity ratios. The Ivo sample was taken from a highly evolved (Th/U > 2) marginal phase in direct contact with the tungsten skarn mineralization. An intrusion with related mineralization is expected to display a decrease in the halogen activity ratios, and such an anomalously low activity ratio could be expected for the intrusive phase responsible for mineralization (i.e. the phase that exsolved all of its volatiles). For such an event to affect apatite concentrations, it would have had to occur before or during the crystallization of apatite at approximately 735ºC (Table 3). These three intrusions with anomalously low activity ratios for apatite, two of which are associated with tungsten skarns, may have released a volatile phase at high temperatures.

Increasing HF/HCl Activity Ratios

There are also two intrusions that display a trend opposite of what was expected: an increase in the HF/HCl activity ratio from apatite to biotite. These include Hole-in-the-Wall, as represented by sample KR-05-164 (based on one apatite data point), and the plug southwest of the O'Grady batholith. As mentioned previously, this effect of slightly increasing activity ratios in the magmatic fluid from apatite to biotite is described by Coulson et al. (2001) to be attributable to the lack of a significant exsolution of a volatile phase. Perhaps a better example of a possible increase in the activity ratio from apatite to biotite is the unnamed plug southwest of O'Grady. This pluton shows a marked increase in the HF/HCl activity ratios from apatite to biotite, which may be due to either an anomalously large enrichment in halogens as the intrusion cooled from apatite- to biotite-forming temperatures, or to late retrograde halogen exchange in biotite. The latter seems to be the most likely given that the plug southwest of O'Grady has been pervasively altered (based on petrographic and field observations), possibly by a late (magmatic) hydrothermal fluid that in itself has potential to generate intrusion-hosted mineralization.

SUMMARY OF INTRUSIVE CHARACTERISTICS THAT ARE FAVOURABLE FOR INTRUSION-RELATED MINERALIZATION WITHIN THE NAHANNI MERA AREA

A review of all the data presented above (i.e. field observations, geochronology, geochemistry, geophysics, Pb-isotope compositions, and magmatic fluid compositions) highlights several characteristics of intrusions that are hypothesized to have an increased potential for related mineralization. Obviously, intrusions that belong to the Tungsten or Tombstone plutonic suites, as defined by geochronological-geochemical methods and field observations, are highly prospective for intrusion-related mineralization as these suites are associated with the majority of the known mineral occurrences in the MERA area (Fig. 4); however, there is still potential for any intrusion not a member of these two suites to be associated with mineralization.

Table 6. Intrusions and factors favourable for intrusion-related mineralization within the Nahanni MERA area; grey indicates insufficient or no data. Intrusions sampled within proximity to a known mineral occurrence are notated with the name of the mineral occurrence capitalized.

Sample	Intrusion	Member of the Tombstone or Tungsten suites (1)	evidence for highly evolved intrusive phases and 'wet' melts (e.g. aplite-pegmatite dykes, veins, miarolitic cavities, mafic dykes) (2)	associated porphyry-textures phases (e.g. apophyses or dykes) (3)	observed gossanous sheeted fractures or en echelon quartz veins **(anomalous values)** (4)	extended thermal histories (e.g. cooling periods >1 Ma) (5)	relatively depleted fluorine, or combined fluorine and chlorine, (<3.75 wt.%) concentrations in apatite[1] (6)
KR-05-08	Powers						
KR-05-10	Jorgensen			x			
KR-05-22	Roy		x		**x**		x
KR-05-26	Fish						
KR-05-32	Ivo	x	x				
KR-05-43	Park						x
KR-05-62	Mt. Christie	x	x		**x**		x
KR-05-68	Mt. Wilson	x					x
KR-05-76	Pelly River		x				
KR-05-97b	O'Grady	x	x	x			
KR-05-110	CAC	x	x			x	
KR-05-113	South Nahanni	x	x			x	x
KR-05-126	plug SW of O'Grady	x					
KR-05-130	Central Nahanni						x
KR-05-136	North Nahanni						x
KR-05-143	Circular Stock	x	x				
KR-05-148	Rifle Range	x	x		**x**		
KR-05-164	Hole-in-the-Wall		x				
KR-05-175	Lened	x	x				x?
KR-05-191	Coal River - MARION						x?
KR-05-194	Coal River - ROYALL	x	x				x
KR-05-196	Coal River - CRAT		x	x		x	x
KR-05-198	Hole-in-the-Wall						
KR-05-208	Little Hyland				**x**		
KR-05-210	Nahanni Range Road						
03M-207	Mine Stock	x	x		**x**	x	
03M-214	Shelf Lake	x	x		**x**		
03M-216	Faille						
03M-217	Mt. Sir James McBrien				x		
03M-218	Hole-in-the-Wall						
03M-220	Ragged	x	x				
03DM-12	Lened	x	x				
99-SH-011*	Big Charlie	x	x		x		
98-HAS-14*	McLeod	x	x		x		
98-HAS-12*	Patterson		x				
98-HAS-02*	Mt. Appler						
98-Z-C-028*	Rudi	x	x				
98-HAS-06*	Mt. Sir James McBrien						
99-SH-013*	West Tuna						

1 note that this may be a negative factor for significant tungsten mineralization (see text)
2 Th/U ratio is normalized to primitive mantle values (Sun and McDonough, 1989)
* samples from Heffernan (2004)
Grt = garnet, Ms = muscovite, Tur = tourmaline

Some features of the more prospective intrusions, regardless of plutonic suite, are

- evidence for highly evolved intrusive phases and 'wet' melts, such as aplite-pegmatite dykes, veins, miarolitic cavities, and mafic dykes;
- associated porphyry textured phases (plutonic apophyses or dykes);
- evidence for extended thermal histories such as $^{40}Ar/^{39}Ar$ biotite ages that are more than one million years younger than the U-Pb crystallization age (the duration of the thermal history here is calculated as a *minimum* as the youngest possible U-Pb age and the oldest possible Ar-Ar age within the confines of the 2-sigma errors);
- sheeted gossanous fractures of en echelon quartz veins with anomalous metal concentrations (an exception to this with respect to the potential for tungsten mineralization are that the fractures and veins assayed from three Tungsten suite intrusions did not contain detectable tungsten);
- depleted fluorine and/or combined fluorine and chlorine (<3.75 wt.% F+Cl) concentrations in apatite that could be indicative of the release of a significant quantity of volatile material at high temperatures (it should be noted that depleted halogen

Table 6 continued.

Sample	Intrusion	a moderate to **large** (overlapping to not overlapping values) depletion in the HF/HCl activity ratio from apatite to biotite; or an anomalously low ratio in apatite (7)	fine-grained, marginal, leucocratic marginal phases (Ms±Grt-Tur-bearing) (8)	[2]Th/U > 1.5 **(or 1.5-2)** (9)	U-Pb age of 98-95 Ma **(98-97 Ma)** (10)	known associated mineralization (**significant, or showngs that have been drilled**) (11)	total points for features favourable for mineralization; see text (12)	potential for intrusion-related mineralization
KR-05-08	Powers						0	low
KR-05-10	Jorgensen						1	low
KR-05-22	Roy					x	3	moderate
KR-05-26	Fish	**x**					2	low
KR-05-32	Ivo	x	x	**x**	**x**	x	12	v. high
KR-05-43	Park	**x**					3	moderate
KR-05-62	Mt. Christie					x	7	high
KR-05-68	Mt. Wilson	x			**x**		6	high
KR-05-76	Pelly River						1	low
KR-05-97b	O'Grady	**x**				x	8	high
KR-05-110	CAC	x	x		**x**	x	12	v. high
KR-05-113	South Nahanni	**x**	x			x	11	v. high
KR-05-126	plug SW of O'Grady				**x**		3	moderate
KR-05-130	Central Nahanni	x				x	5	moderate
KR-05-136	North Nahanni	**x**				x	5	moderate
KR-05-143	Circular Stock		x		**x**		6	high
KR-05-148	Rifle Range	**x**	x		x		9	high
KR-05-164	Hole-in-the-Wall						1	low
KR-05-175	Lened	x	x	x		x	12	v. high
KR-05-191	Coal River - MARION					x	3	moderate
KR-05-194	Coal River - ROYALL	**x**	x	x		x	12	v. high
KR-05-196	Coal River - CRAT	x				x	9	high
KR-05-198	Hole-in-the-Wall	**x**	x				4	moderate
KR-05-208	Little Hyland						1	low
KR-05-210	Nahanni Range Road						0	low
03M-207	Mine Stock		x	**x**	**x**	x	13	v. high
03M-214	Shelf Lake		x				6	high
03M-216	Faille			x			2	low
03M-217	Mt. Sir James McBrien						1	low
03M-218	Hole-in-the-Wall						0	low
03M-220	Ragged		x				5	moderate
03DM-12	Lened		x		x	x	8	high
99-SH-011*	Big Charlie					x	6	high
98-HAS-14*	McLeod						4	moderate
98-HAS-12*	Patterson						1	low
98-HAS-02*	Mt. Appler						0	low
98-Z-C-028*	Rudi		x		**x**	x	8	high
98-HAS-06*	Mt. Sir James McBrien						0	low
99-SH-013*	West Tuna						0	low

concentrations in apatite are not a positive factor with respect to the potential for economic concentrations of tungsten mineralization due to the hypothesized lower temperature of volatile phase exsolution, which is inferred to be below the AST);

- a moderate to large depletion in the activity ratio of HF/HCl from apatite to biotite, where 'moderate' is defined as an obvious depletion with overlapping apatite-biotite values and 'large' is defined by a lack of overlapping apatite-biotite values: this depletion is hypothesized to reflect the exsolution of a volatile-rich, and possible ore-metal-rich, phase from the crystallizing intrusion; and
- an anomalously low HF/HCl activity ratio in apatite, that may indicate an early high-temperature exsolution of a volatile-rich phase.

There are many additional factors that make Tungsten intrusions highly prospective for mineralization, particularly factors that are indicative of associated reduced tungsten skarns.

- very fine-grained, marginal, leucocratic phases (containing muscovite-garnet/tourmaline),
- proximal or distal sulphide-bearing dykes (as observed at Rudi, Cac, Mine Stock, etc.),
- Th/U ratios greater than 1.5, when normalized to the primitive mantle of Sun and McDonough (1989); if Th/U is close to 2.0, then the intrusion is highly prospective for related tungsten mineralization); and
- a crystallization (U-Pb) age within 98 to 95 Ma coincident with the tungsten mineralization at

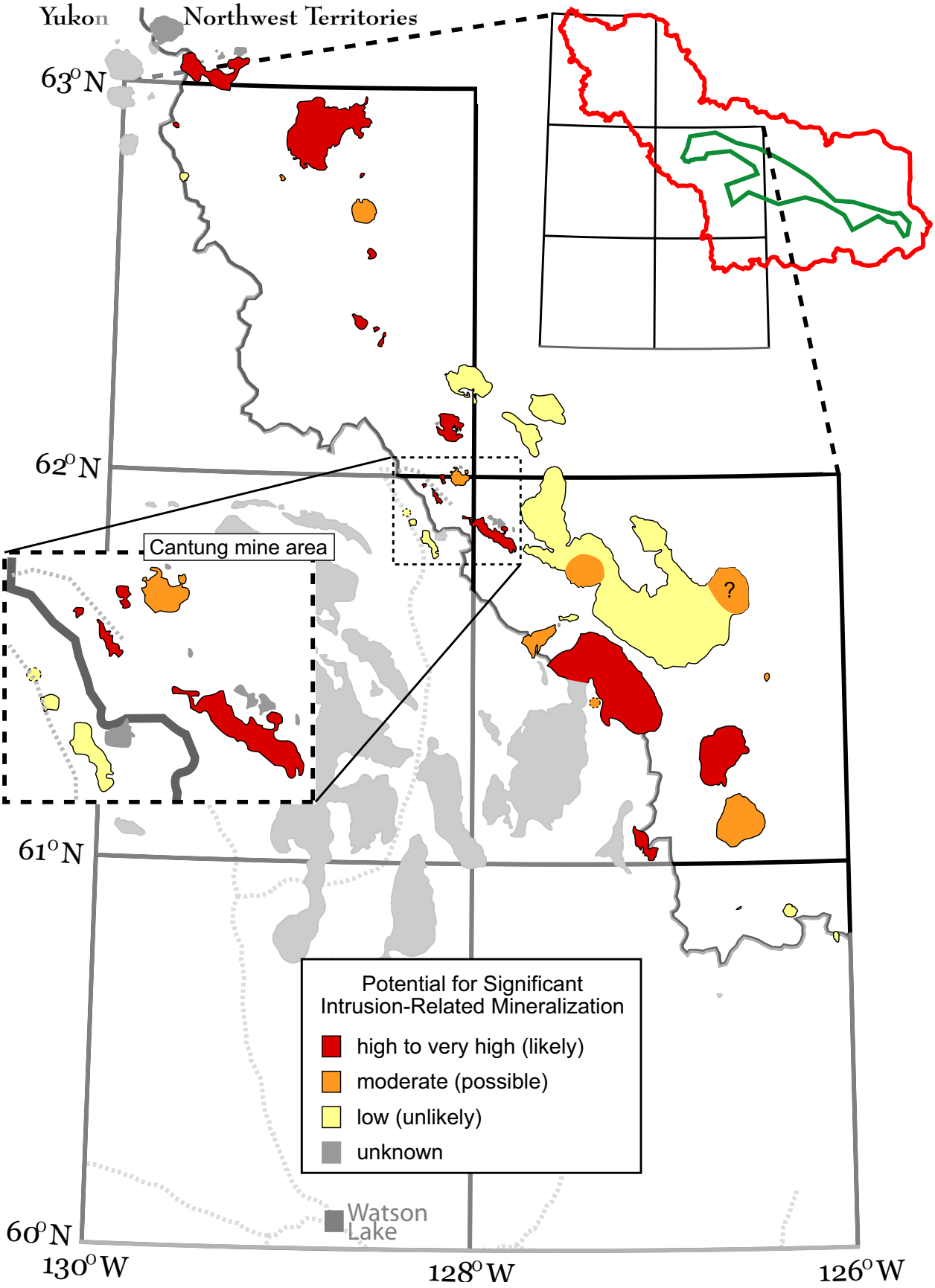


Figure 11. Overall potential for intrusion-related mineralization within the South Nahanni River watershed (red; upper inset), the Federal Park Reserve (green; upper inset); see text for discussion. The Cantung mine area is expanded in the lower inset, the Yukon portion of the map is lightly faded, and the base map is modified from Gordey and Makepeace (1999).

Cantung and MacTung, the two world-class tungsten skarns in the magmatic belt; intrusions closer to the older end of this range (98-97 Ma) are more likely to have evolved a long-lasting magmatic hydrothermal system (as all the Ar-Ar ages from Tungsten suite intrusions are <96.5 Ma), which is observed at Cantung and is an important factor when considering the potential size and grade of any associated mineralization.

TR-Tungsten suite intrusions that are prospective for tungsten mineralization will share features with the Tungsten suite, whereas TR-Tungsten suite intrusions that are prospective for other types of mineralization (e.g. Cu or other base metals) may actually display features that are more similar to the Tay River suite (biotite-hornblende-bearing granodiorite intrusive phases, as is observed at the RISBY Cu-skarn showing, North Nahanni pluton). Aside from the generalized features described above for the intrusions, regardless of plutonic suite, the Tay River suite intrusions do not display any specific features that are indicative of mineralization. Tombstone suite intrusions also do not have any unique features indicative of a potential for related mineralization, aside from possibly the presence of detectable gold in intrusion-hosted quartz veins.

One final feature used to identify intrusions that might have a higher potential for related mineralization is the documentation of known mineral occurrences in association with the intrusion. This is by no means comprehensive as the documented mineral occurrences are in part a reflection of the amount of exploration and property work that has been done in the area, which is limited by the lack of road access in comparison to other areas of the northern Cordillera. For the purpose of identifying intrusions with a relatively high potential for related mineralization, only intrusions with associated mineral occurrences that are 'significant' in size (e.g. were promising enough to warrant drilling) are considered. However, the presence of even small, nearby mineral occurrences indicates that there was some exsolution of metallogenic fluids associated with an intrusion at one time, which is typically regarded as an initial indicator that perhaps more significant mineralization may also be present. A lack of any of the above features do not negate the possibility of associated mineralization, partly as many of the features are from field observations that are limited for some intrusions due to the amount of time spent and area covered on each intrusion; however, a combination of more than one of these features increases the likelihood of intrusion-related mineralization.

Metallogenic Implications

The presence or absence of the factors described above for each intrusive sample is summarized in Table 6. Features that could be indicative of mineralization were assigned a value appropriate to their relative significance: 2 points were given for a feature listed in columns 1, 5, 7, 8, 9, and 11; and 1 point was given for a feature listed in columns 2, 3, 4, 6, and 10. The total number of points was summed in column 12, and a designation of "low", "moderate", "high", or "very high" was assigned to values of: 0-2, 3-5, 6-10, 11+, respectively. Figure 11 displays the potential for related mineralization specific to each intrusion as (1) "high to very high", or likely to have significant associated mineralization, (2) "moderate", and, (3) "low", or unlikely to have significant associated mineralization. Further work to test the validity of the implications of this study appears warranted; however, the data provide a good threshold for the broad characterization of the potential for intrusion-related mineralization within a relatively unknown and under-explored region that hosts voluminous magmatism and abundant associated mineral occurrences.

ACKNOWLEDGEMENTS

Funding for this work was provided by Parks Canada and an NSERC grant to Dr. J.K. Mortensen. The authors would like to thank Dr. I. Coulson for his review of the magmatic fluid composition data. The authors would also like to thank J. Kerswill (Geological Survey of Canada, Ottawa) for his careful and thorough review of this paper; any deficiencies that remain are a result of the authors' inability to implement all of the suggested changes; these will be taken into consideration with respect to future work.

REFERENCES

Anderson, R.G.
1983: Selwyn plutonic suite and its relationship to tungsten skarn mineralization, southeastern Yukon and District of Mackenzie, *in* Current Research, Part B, Geological Survey of Canada, Paper 83-1B, p. 151-163.

Atkinson, D. and Baker, D.J.
1986: Recent developments in the geologic understanding of MacTung, *in* Mineral Deposits of the Northern Cordillera, (ed.) J.A. Morin; Canadian Institute of Mining and Metallurgy Special Volume 37, p. 234-244.

Bea, F., Fershtater, G.B., and Corretge, L.G.
1992: The geochemistry of phosphorus in granite rocks and the effects of aluminium; Lithos, v. 29, p. 43-56.

Chappel, B.W. and White, A.J.R.
1974: Two contrasting granite types; Pacific Geology, v. 8, p.173-174.

Christiansen, E.H. and Keith, J.D.
1996: Trace element systematics in silicic magmas: A metallogenic perspective, *in* Trace Element Geochemistry of Volcanic Rocks: Applications for Massive Sulphide Exploration, Geological Association of Canada, Short Course Notes, (ed.) D.A. Wyman; v. 12, p. 115-151.

Clemens, J.D.
2003: S-type granitic magmas – petrogenetic issues, models and evidence; Earth-Science Reviews, v. 61, p. 1-18.

Coulson, I.M., Dipple, G. M., and Raudsepp, M.
2001: Evolution of HF and HCl activity in magmatic volatiles of the gold-mineralized Emerald Lake pluton, Yukon Territory, Canada; Mineralium Deposita, v. 36, p. 594-606.

Coulson, I.M., Villeneuve, M.E., Dipple, G.M., Duncan, R.A., Russell, J.K., and Mortensen, J.K.
2002: Time-scales of assembly and thermal history of a composite felsic pluton: constraints from the Emerald Lake area, northern Canadian Cordillera, Yukon; Journal of Volcanology and Geothermal Research, v. 114, p. 331-356.

Currie, C.A. and Hyndman, R.D.
2006: The thermal structure of subduction zone back arcs; Journal of Geophysical Research, v. 111, p. 22.

Deer, W.A., Howie, R.A., and Zussman, J.
1992: An Introduction to the Rock-Forming Minerals; Longman Scientif and Technical, Essex, England, 686 p.

Department of Indian Affairs and Northern Development (DIAND)
2006: NORMIN.DB: The Northern Minerals Database; Northwest Territories Geoscience Office, Yellowknife, Northwest Territories.

Deklerk, R. and Traynor, S. (comp.)
2005: Yukon MINFILE 2005 - A Database of Mineral Occurrences; Yukon Geological Survey, CD-ROM.

Driver, L.A., Creaser, R.A., Chacko, T., and Erdmer, P.
2000: Petrogenesis of the Cretaceous Cassiar batholith, Yukon-British Columbia, Canada: Implications for magmatism in the North American cordilleran interior; Geological Society of America Bulletin, v. 112, p. 1119-1133.

England, P. and Thompson, A.B.
1984: Pressure-temperature-time paths of regional metamorphism: Part I. Heat transfer during the evolution of regions of thickened continental crust; Journal of Petrology, v. 25, p. 894-928.

Eyles, N.
1995: Characteristics and origin of coarse gold in Late Pleistocene sediments of the Caribou placer mining district, British Columbia, Canada; Sedimentary Geology, v. 95, p. 69-95.

Gabrielse, H., Roddick, J.A., and Blusson, S.L.
1973: Flat River, Distict of Mackenzie-Yukon Territory; Geological Survey of Canada, Map 1313A, scale 1:250,000.

Godwin, C.I. and Sinclair, A.J.
1982: Average lead isotope growth curves for shale-hosted zinc-lead deposits, Canadian Cordillera; Economic Geology, v. 77, p. 675-690.

Gordey, S.P. and Anderson, R.L.
1993: Evolution of the Northern Cordilleran Miogeocline, Nahanni Map Area (105I), Yukon and Northwest Territories; Geological Survey of Canada, Memoir 428, 214 p.

Gordey, S.P. and Makepeace, A.J. (comp.)
1999: Yukon Digital Geology; Geological Survey of Canada, Open File D3826, and Exploration and Geological Services Division, Yukon, Indian and Northern Affairs Canada, Open File 1999-1, 1 CD-ROM.

Hansen, E., Ahmed, K. ,and Harlov, D.
2002: Rb depletion in biotites and whole rocks across an amphibolite to granulite facies transition zone, Tamil Nadu, South India; Lithos, v. 64 p. 29-47.

Harris, N.B.W., Pearce, J.A., and Tindle, A.G.
1986: Geochemical characteristics of collision-zone magmatism, *in* Collision Tectonics, (ed.) M.P. Coward and A.C. Reis; Special Publication of the Geological Society, v. 19, p. 67-81.

Harrison, T.M and Watson, E.B.
1984: The behavior of apatite during crustal anatexis: Equilibrium and kinetic considerations; Geochimica et Cosmochimica Acta, v. 48, p.1467-1477.

Hart, C.J.R., Goldfarb, R.J., Lewis, L.L., and Mair, J.L.
2004a: The northern cordilleran mid-Cretaceous plutonic province: Ilmenite/magnetite-series granitoids and intrusion-related mineralization; Resource Geology, v. 54, p. 253-280.

Hart, C.J.R., Villeneuve, M.E., Mair, J.L., Selby, D., and Wijns, C.
2004b: Integrated U-Pb SHRIMP and TIMS, Re-Os and Ar-Ar geochronology of mineralizing plutons in Yukon and Alaska: Duration of magmatic-hydrothermal systems; Geology Department and Extension Service, University of Western Australia, v. 33, p. 347-349.

Hart, C.J.R., Mair, J.L., Goldfarb, R.J., and Groves, D.I.
2005: Source and redox controls on metallogenic variations in intrusion-related ore systems, Tombstone-Tungsten belt, Yukon Territory, Canada; Geological Society of America, Special Paper, v. 389, p. 339-356.

Hart, C.J.R. and Lewis, L.L.
2006: Gold mineralization in the upper Hyland River area: A non-magmatic origin, *in* Yukon Exploration and Geology 2005, (ed.) D.S. Emond, G.D. Bradshaw, L.L. Lewis, and L.H. Weston; Yukon Geological Survey, p. 109-125.

Heffernan, R.S.
2004: Temporal, geochemical, isotopic and metallogenic studies of Mid-Cretaceous magmatism in the Tintina Gold Province, southeastern Yukon and southwestern Northwest Territories, Canada; MSc thesis, University of British Columbia, British Columbia, Canada, 83 p.

Irvine, T.N. and Baragar, W.R.A.
1971: A guide to the chemical classification of the common volcanic rocks; Canadian Journal of Earth Sciences, v. 8, p. 523-548.

Ishihara, S.
1981: The granitoid series and mineralization; Economic Geology, 75th Anniversary Volume, p. 458-484.

Jefferson, C.W. and Pare, D.
1991: New placer gold anomalies in the northern Liard Range – southern Ram Plateau area, South Nahanni River region, District of Mackenzie, Northwest Territories, *in* Current Research, Part E, Geological Survey of Canada Paper 91-1E, p. 1-4.

Jefferson, C.W. and Spirito, W.A. (ed.)
2003: Mineral and Energy Resource Assessment of the Tlogotsho Plateau, Nahanni Karst, Ragged Ranges and adjacent areas under consideration for expansion of Nahanni Nation Park Reserve, Northwest Territories; Geological Survey of Canada Open File 1686, 1 CD-ROM.

Jenner, G.A.
1996: Trace element geochemistry of igneous rocks: Geochemical nomenclature and analytical geochemistry, *in* Trace Element Geochemistry of Volcanic Rocks: Applications For Massive Sulphide Exploration, (ed.) D.A. Wyman; Geological Association of Canada, Short Course Notes, v. 12, p. 51-77.

Keith, J.D., van Middelaar, W., Clark, A.H., and Hodgson, C.J.
1989: Granitoid textures, compositions, and volatile fugacities associated with the formation of tungsten-dominated skarn deposits, *in* Reviews in Economic Geology, (ed.) J.A. Whitney and A.J. Naldrett; v. 4, p.235-250.

Knight, J.B., Mortensen, J.K., and Morison, S.R.
1994: Shape and Composition of Lode and Placer Gold from the Klondike District, Yukon, Canada; Exploration and

Geological Services Division, Yukon, Indian and Northern Affairs Canada, Bulletin 3, 142 p.

Knight, J. B., Morison, S. R., and Mortensen, J. K.
1999: The relationship between placer gold particle shape, rimming, and distance of fluvial transport as exemplified by gold from the Klondike district, Yukon Territory, Canada; Economic Geology, v. 94, p. 635-648.

Krogh, T.E.
1982: Improved accuracy of U/Pb zircon ages by the creation of more concordant systems using an air abrasion technique; Geochemica et Cosmochimica Acta, v. 46, p. 63.

Lang, J.R. and Baker, T.
2001: Intrusion-related gold systems: the present level of understanding; Mineralium Deposita, v. 36, p. 477-489.

Lentz, D.R. (comp. and ed.)
1998: Appendix: Grade and tonnage models of skarns, *in* Mineralized Intrusion-Related Skarn Systems, Mineralogical Association of Canada Short Course Series, v. 26, 663 p.

Ludwig, K.R.
1980: Calculation of uncertainties of U/Pb isotopic data; Earth and Planetary Sciences Letters, v. 46, p. 212-220.

Ludwig, K.R.
2003: Isoplot 3.09: A Geochronological Toolkit for Microsoft Excel; Berkeley Geochronology Center, Special Publication No. 4.

Maniar, P.D. and Piccoli, P.M.
1989: Tectonic discrimination of granitoids; Geological Society of America Bulletin, v. 101, p. 635-643.

Mathieson, G.A. and Clark, A.H.
1984: The Cantung E Zone scheelite skarn orebody, Tungsten, Northwest Territories: A revised genetic model; Economic Geology, v. 79, p. 883-901.

Meinert, L.D.
1993: Igneous petrogenesis and skarn deposits, *in* Mineral Deposit Modeling, (ed.) R.V. Kirkam, W.D. Sinclair, R.I. Thorpe, and J.M. Duke; Geological Association of Canada, Special Paper 40, p. 569-583.

Meinert, L.D., Dipple, G.M., and Nicolescu, S.
2005: World skarn deposits, *in* Economic Geology 100th Anniversary Volume, (ed.) J.W. Hedenquist, J.F.H. Thompson, R.J. Goldfarb, J.P.Richards; Society of Economic Geologists, p. 299-336.

Mortensen, J.K., Hart, C.J.R., Murphy, D.C., and Heffernan, S.
2000: Temporal evolution of Early and Mid-Cretaceous magmatism in the Tintina Gold Belt, *in* The Tintina Gold Belt: Concepts, Exploration and Discoveries, (ed.) J. Jambor; British Columbia and Yukon Chamber of Mines, Special Volume 2, p. 49-57.

Mortensen, J.K., Sluggett, C., Liverton, T., and Roots, C.F.
2006: U-Pb zircon and monazite ages for the Seagull and Cassiar batholiths, Wolf Lake map area, southern Yukon, *in* Yukon Exploration and Geology 2005, (ed.) D.S. Emond, G.D. Bradshaw, L.L. Lewis and L.H. Weston; Yukon Geological Survey, p. 257-266.

Mortensen, J.K., Brand, A., and Liverton, T.
in press: Laser ablation ICP-MS U-Pb zircon ages for Cretaceous plutonic rocks in the Logtung and Thirtymile Range areas of southern Yukon, *in* Yukon Exploration and Geology 2006, (ed.) D.S. Emond, L.L. Lewis and L.H. Weston; Yukon Geological Survey.

Munoz, J.L. and Swenson, A.
1981: Chlorite-hydroxyl exchange in biotite and estimation of relative HCl/HF activities in hydrothermal fluids; Economic Geology, v. 76, p. 2212-2221

Newberry, R.J. and Swanson, S.E.
1986: Scheelite skarn granitoids: An evaluation of the roles of magmatic source and process; Ore Geology Reviews, v. 1, p. 57-81.

Newberry, R.J.
1998: W- and Sn-skarn deposits: A 1998 status report, *in* Mineralized Intrusion-Related Skarn Systems, (ed.) D. Lentz; Mineralogical Association of Canada Short Course Series, v. 26, p. 289-335.

Pan, Y. and Fleet, M.E.
2002: Compositions of the apatite group minerals; substitution mechanisms and controlling factors, *in* Phosphates Reviews in Mineralogy and Geochemistry, (ed) M.J. Kohn, J. Rakovan, and J.M. Hughes; v. 48, p. 13-49.

Patiño Douce, A.E. and Beard, J.S.
1995: Dehydration-melting of biotite gneiss and quartz amphibolite from 3 to 15 kbar; Journal of Petrology, v. 36, p.717-738.

Parrish, R., Roddick, J.C., Loveridge, W.D., and Sullivan, R.W.
1987: Uranium-lead analytical techniques at the geochronology laboratory, Geological Survey of Canada, *in* Radiogenic Age and Isotopic Studies, Report 1; Geological Survey of Canada, Paper 8, p. 3-7.

Petford, N. and Gallagher, K.
2001: Partial melting of mafic (amphibolitic) lower crust by periodic influx of basaltic magma; Earth and Planetary Science Letters, v. 193, p.483-499.

Piccoli, P.M. and Candela, P.A.
2002: Apatite in igneous systems, *in* Phosphates - Reviews in Mineralogy and Geochemistry, (ed.) M.J. Kohn, J. Rakovan, and J.M. Hughes; v. 48, p.255-292.

Pouchou, J.L., and Pichoir, F.,
1985: PAP ø(pZ) procedure for improved quantitative microanalysis,.*in* J.T. Armstrong (ed.), Microbeam Analysis;:San Francisco Press, p. 104–106.

Powers, M.C.
1982: Comparison chart for estimating roundness and sphericity; American Geological Institute, Data Sheet 18.

Rasmussen, K.L., Mortensen, J.K. and Falck, H.
2006: Geochronological and lithogeochemical studies of intrusive rocks in the Nahanni region, southwestern Northwest Territories and southeastern Yukon, *in* Yukon Exploration and Geology 2005, (ed.) D.S. Emond, G.D. Bradshaw, L.L. Lewis, and L.H. Weston; Yukon Geological Survey, p. 287-298

Rasmussen, K.L. Mortensen, J.K., and Falck, H.
2007: Morphological and compositional analysis of placer gold in the South Nahanni River drainage, Northwest Territories, *in* Yukon Exploration and Geology 2006, (ed.) D.S. Emond, L.L. Lewis, and L.H. Weston; Yukon Geological Survey, p. 237-250 (and Appendix 2 *in* Mineral and Energy Resource Assessment of the Greater Nahanni Ecosystem Under Consideration for the Expansion of the Nahanni National Park Reserve, Northwest Territories, (ed.) D.F. Wright, D. Lemkow, and J.R. Harris; Geological Survey of Canada, Open File 5344, p. 367-380).

Raudsepp, M.
1995: Recent advances in the electron-probe micro-analysis of minerals for the light elements; The Canadian Mineralogist, v. 33, p. 203-218.

Renne, P.R., Swisher, C.C. III, Deino, A.L., Karner, D.B., Owens, T., and DePaolo, D.J.
1998: Intercalibration of standards, absolute ages and uncertainties in $^{40}Ar/^{39}Ar$ dating; Chemical Geology, v. 145, p. 117-152.

Roddick, J.C.
1987: Generalized numerical error analysis with application to geochronology and thermodynamics; Geochimica et Cosmochimica Acta, v. 51, p. 2129-2135.

Rollinson, H.R.
1993: Using Geochemical Data: Evaluation, Presentation, and Interpretation; Longman Scientific and Technical, Essex, 352 p.

Sallet, R.
2000: Fluorine as a tool in the petrogenesis of quartz-bearing magmatic associations: Applications of an improved F-OH biotite-apatite thermometer grid; Lithos, v. 50, p. 241-253.

Selby, D. and Nesbitt, B.E.
2000: Chemical composition of biotite from the Casino porphyry Cu-Au-Mo mineralization, Yukon, Canada: Evaluation of magmatic and hydrothermal fluid chemistry; Chemical Geology, v. 171, p. 77-93.

Selby, D., Creaser, R.A., Heaman, L.M., and Hart, C.J.R.
2003: Re-Os and U-Pb geochronology of the Clear Creek, Dublin Gulch, and Mactung deposits, Tombstone Gold Belt, Yukon, Canada: Absolute timing relationships between plutonism and mineralization; Canadian Journal of Earth Sciences, v. 40, p.1839-1852.

Spirito, W.A., Jefferson, C.W. and Pare, D.
1988: Comparison of gold, tungsten and zinc in stream silts and heavy mineral concentrates, South Nahanni resource assessment area, District of Mackenzie, *in* Current Research, Part E; Geological Survey of Canada, Paper 88-1E, p. 117-126.

Stacey, J.S. and Kramer, J.D.
1975: Approximation of terrestrial lead isotope evolution by a two-stage model; Earth and Planetary Science Letters, v. 26, p. 207-221.

Stormer, J.C. Jr., Pierson, M.L., and Tacker, R.C.
1993: Variation in F and Cl X-ray intensity due to anisotropic diffusion in apatite during electron microprobe analysis; American Mineralogist, v. 78, p. 641-648.

Streckeisen, A.
1976: To each plutonic rock its proper name; Earth-Science Reviews, v. 12, p. 1-33.

Sun, S.S. and McDonough, W.F.
1989: Chemical and isotope systematics of oceanic basalts: Implications for mantle compositions and processes; *in* Magmatism in Ocean Basins, (ed.) A.D. Saunders, and M.J. Norry; Geological Society, London, Special Publications, v. 42, p. 313-345.

Thirwall, M.F.
2000: Inter-laboratory and other errors in Pb isotopic analyses investigated using a ^{207}Pb-^{204}Pb double spike; Chemical Geology, v. 163, p. 7-25.

Thompson, J.F.H., Sillitoe, R.H., Baker, T., Lang, J.R., and Mortensen, J.K.
1999: Intrusion-related gold deposits associated with tungsten-tin provinces; Mineralium Deposita, v. 34, p. 323-334.

Walton, L.
1998: Geological Report, Lened Property, South Nahanni River Area; Department of Indian Affairs and Northern Development, Northwest Territories, Assessment Report 084048, 34 p.

Woodsworth, G.J., Anderson, R.G., and Armstrong, R.L.
1991: Plutonic regimes, *in* Geology of the Cordilleran Orogen in Canada, (ed.) H. Gabrielse and C.J. Yorath; Geological Survey of Canada, no. 4, p. 491-531.

Youngson, J.H. and Craw, D.
1999: Variation in placer style, gold morphology, and gold particle behavior down gravel bed-load rivers:an example from the Shotover-Arrow-Kawarau-Clutha river system, Otago, New Zealand; Economic Geology, v. 94, p. 615-634.

Yuvan, J.G., Shelton, K.L., Falck, H., and Marshall, D.D.
2004: High-grade quartz-scheelite veins in the Cantung mine, Northwest Territories: A late magmatic-hydrothermal event; 32nd Annual Yellowknife Geoscience Forum, November 16-18, Abstracts volume, p. 85.

Zhu, C. and Sverjensky, D.A.
1991: Partitioning of F-Cl-OH between minerals and hydrothermal fluids; Geochimica et Cosmochimica Acta, v. 55, p. 1837-1858.
1992: Partitioning of F-Cl-OH between biotite and apatite; Geochimica et Cosmochimica Acta, v. 56, p. 3435-3467.

Appendix 1. Mineral deposit types and styles present in the Nahanni MERA area (fORMIN database, Department Indian Affairs and Northern Development, 2006)

Showing Name	Showing ID (NORMIN) or mapsheet	Latitude	Longitude	Metals	Development Stage	Description of Mineralization	Classification	Nearby Plutonic Suite
Intrusion Related								
"ROY"	095ENE0012, 19-24	61.62	127.66	Pb-Zn-Ag-Au-Cu	advanced exploration	arsenopyrite-galena-sphalerite-pyrrhotite-bearing, manto replacement-style sulphides in carbonaceous cherty sediments; minor marcasite, chalcopyrite, cubanite, and possibly native gold; mafic and granite dykes present; associated with faults; indicated reserve at ROY proper: 0.16 Mt at 0.042 oz/t Au, 4.59 oz/t Ag, 5.24% Pb, and 3.11% Zn (EMR Mineral Bulletin MR223)	distal Pb(Ag)-Zn manto sulphide	Tay River
"BUSTER and LUCKY (LAKE)"	095ENW0001, 16, 17	61.55	127.50	Pb-Zn-Ag-Cu-Au	drilled, local examination	galena-sphalerite-chalcopyrite-pyrite-pyrrhotite-bearing, pyroxene skarn adjacent to Coal River batholith; associated QFP dykes; inferred associated faults; trace gold	proximal Pb(Ag)-Zn skarn	Tay River
Cirque 2	095ENE0018	61.53	127.57	Ag-Pb-Zn-Cu-Au	drilled	galena-sphalerite-chalcopyrite-pyrite-pyrrhotite-bearing, (diopside)-garnet skarn adjacent to Coal River batholith; trace gold	proximal Pb(Ag)-Zn skarn	Tay River
RAM and ROD	095ENE0002	61.53	127.58	Pb-Zn-Ag	advanced exploration	galena-sphalerite-bearing skarn and stringers adjacent to Coal River batholith; associated with faults; indicated resource of 1.63 Mt at 5.12% Pb, 5.42% Zn, and 0.71 oz/T Ag (EMR Mineral Bulletin MR223)	proximal Pb(Ag)-Zn skarn	Tay River
CRAT 1	095ENE0027	61.56	127.22	W-Zn	reconnaissance	scheelite-sphalerite-bearing, garnet-diopside skarn with associated QFP dykes; adjacent to Coal River batholith	proximal W-Cu-(Zn-Bi-Au-Mo) skarn	Tay River
CRAT 2	095ENE0028	61.55	127.20	W	reconnaissance	scheelite-bearing, garnet-diopside skarn adjacent to Coal River batholith; intense scheelite mineralization along east-trending faults	proximal W-Cu-(Zn-Bi-Au-Mo) skarn	Tay River
CRAT 3	095ENE0029	61.54	127.18	W-Mo	reconnaissance	scheelite-bearing, garnet-diopside skarn adjacent to Coal River batholith; minor molybdenite	proximal W-Cu-(Zn-Bi-Au-Mo) skarn	Tay River
RISBY	105INE0002	62.78	128.57	Cu	drilled	chalcopyrite, pyrite, pyrrhotite bearing quartz-carbonate stringers and fractures at N. Nahanni contact with quartzite-shale; dissem. pyrite and pyrrhotite in sediments and altered intrusion; small pyrrhotite skarns with <0.5% Cu	proximal Cu skarn	TR-Tungsten
SANDY	105ISE0060	62.22	128.12	W, Pb-Ag-Zn	local examination	scheelite-bearing garnet ± actinolite skarn adjacent to Mt. Appler pluton; minor lead-zinc-silver in pyrite-pyrrhotite-sphalerite-bearing quartz-carbonate veins	proximal W-Cu-(Zn-Bi-Au-Mo) skarn; distal? Pb-Ag)-Zn vein	TR-Tungsten
JAY	105ISE0014	62.09	128.18	Zn-Pb-Ag-Au	local examination	galena-sphalerite-arsenopyrite-bearing quartz veins in sediments; minor gold and silver	distal Pb(Ag)-Zn vein	Tungsten
MONA	105ISE0013	62.10	128.21	Au-Ag-Zn-Pb, W	local examination	galena-sphalerite-arsenopyrite-bearing quartz veins/stockworks in sediments; minor gold and silver; minor scheelite-bearing, pyrrhotite-diopside skarn adjacent to Shelf Lake pluton	distal? Pb(Ag)-Zn vein; proximal W-Cu-(Zn-Bi-Au-Mo) skarn	Tungsten
CAC	105ISE0019	62.34	128.54	W-Cu	drilled	scheelite-bearing, garnet-diopside skarn adjacent to Cac pluton (2 main skarns); minor Cu	proximal W-Cu-(Zn-Bi-Au-Mo) skarn	Tungsten
RUDI	105ISE0061	62.36	128.5	W-Cu	local examination	scheelite-bearing, garnet-diopside skarn adjacent to Rudi pluton (2 main skarns); minor Cu	proximal W-Cu-(Zn-Bi-Au-Mo) skarn	Tungsten

Appendix 1 continued.

Showing Name	Showing ID (NORMIN) or mapsheet	Latitude	Longitude	Metals	Development Stage	Description of Mineralization	Classification	Nearby Plutonic Suite
Cantung Mine and E-zone	105HNE0006, 07	61.95	128.26	W-Cu-Bi-Au-Zn-(Mo)	past producer	scheelite-chalcopyrite-bearing, garnet-diopsite/amphibole-pyrrhotite/biotite skarn adjacent to the Mine Stock intrusion (2 main skarns: Open Pit and E-zone); minor bismuth, gold, zinc; trace molybdenite	proximal W-Cu-(Zn-Bi-Au-Mo) skarn	Tungsten
BAKER	105HNE0002	61.93	128.98	Cu-W-Zn-F	unknown	no details; adjacent to the Mine Stock intrusion	proximal W-Cu-(Zn-Bi-Au-Mo) skarn	Tungsten
PYRAMID MTN	095ENE0015	61.90	127.98	W-Cu-Ag	reconnaissance	scheelite-bearing, diopside skarn (2 main skarns) adjacent to Pyramid Mountain pluton; significant copper and silver values reported	proximal W-Cu-(Zn-Bi-Au-Mo) skarn	Tungsten
HOUSE OF LORD	095ENE0011	61.84	127.91	W	reconnaissance	scheelite-bearing, "dark green" skarn adjacent to Pyramid Mountain pluton	proximal W-Cu-(Zn-Bi-Au-Mo) skarn	Tungsten
SIMONS	095ENE0025	61.84	127.90	W-Cu	reconnaissance	scheelite-chalcopyrite-bearing, garnet skarn adjacent to Pyramid Mountain pluton	proximal W-Cu-(Zn-Bi-Au-Mo) skarn	Tungsten
WHISTLER NORTH	095ENE0005	61.84	127.88	W-Cu	reconnaissance	scheelite-bearing, diopside-amphibole-epidote skarn adjacent to Pyramid Mountain pluton; chalcopyrite and scheelite found on joint surface in intrusion	proximal W-Cu-(Zn-Bi-Au-Mo) skarn	Tungsten
FREDERICK CREEK	095ENE0026	61.83	127.84	W	reconnaissance	scheelite-bearing, diopside-garnet/amphibole skarn adjacent to Pyramid Mountain pluton	proximal W-Cu-(Zn-Bi-Au-Mo) skarn	Tungsten
MB	095ENE0014	61.81	127.81	W	drilled	scheelite-bearing, diopside-garnet skarn adjacent to Pyramid Mountain pluton	proximal W-Cu-(Zn-Bi-Au-Mo) skarn	Tungsten
*BLUE	n/a	62.55	128.57	W	local examination	scheelite-pyrite-pyrrhotite-bearing skarn adjacent to South Nahanni pluton	proximal W-Cu-(Zn-Bi-Au-Mo) skarn	Tungsten
LENED	105ISE0003	62.37	128.63	W-Cu-Au, Be	advanced exploration	scheelite-chalcopyrite-bearing, garnet-diopside/massive pyrrhotite skarn adjacent to Lened pluton (2 main zones); indicated resource of 0.75 Mt at 1.17% WO_3 and 0.15% Cu (Walton, 1998); V-rich beryls (emerald) in	proximal W-Cu-(Zn-Bi-Au-Mo) skarn; gem	Tungsten
78	095ESW0001	61.05	127.05	W	reconnaissance	tungsten-bearing dolomite float at contact with Ivo pluton	proximal W-Cu-(Zn-Bi-Au-Mo) skarn?	Tungsten
TUANIPEL (IVO)	095ESW0002	61.07	127.07	W	local examination	scheelite-pyrrhotite-bearing, "pale calc-silicate" skarn adjacent to Ivo pluton	proximal W-Cu-(Zn-Bi-Au-Mo) skarn?	Tungsten
*SKULL	n/a	62.95	128.50	Pb-Zn-Ag	reconnaissance	lead-zinc-silver vein cutting limestone; near O'Grady batholith	distal Pb(Ag)-Zn vein	Tombstone
*U	n/a	62.99	129.49	Pb-Zn-Cu	reconnaissance	galena-sphalerite-arsenopyrite-pyrite-bearing quartz vein cutting Mt. Christie pluton; azurite staining	distal? Pb(Ag)-Zn vein	Tombstone
O'GRADY	105INE0023	62.89	128.98	tourmaline	local examination	Li-rich tourmaline (e.g. elbaite) in miarolitic pockets in pegmatite horizons/sills/dykes within the O'Grady batholith	gem	Tombstone
"SITE"	095DNE0004-6	60.97	126.66	Au	reconnaissance	gold (and scheelite) in gravel placer deposit near Big Charlie pluton	placer Au	Tombstone
MCLEOD	095ESE0008	64.10	126.53	Au	reconnaissance	gold in gravel placer deposit near McLeod pluton	placer Au	Tombstone

Appendix 1 continued.

Showing Name	Showing ID (NORMIN) or mapsheet	Latitude	Longitude	Metals	Development Stage	Description of Mineralization	Classification	Nearby Plutonic Suite
1035 and 1063 (GOLD	095ESE0020, 19	61.67	126.80	Au-Zn	reconnaissance	stream sediment sample with anomalous gold and zinc near Big Charlie pluton	placer Au	Tombstone
BENNETT	095ESE0007	61.27	126.67	Au	reconnaissance	gold in gravel placer deposit within McLeod pluton	placer Au	Tombstone
GRUMP	105INE0026	62.94	128.71	Au	drilled	pyrrhotite and pyrite dissem. in siliceous sediments at the O'Grady contact; 1 anomalous gold assay (0.025 oz/t)	proximal Au	Tombstone
RINO	095ESE0016	61.17	126.65	Ag-Au	local examination	skarn adjacent to Big Charlie pluton; reports of local W-Mo or Pb-Zn enrichments but no assays values returned	proximal Au	Tombstone
*CAN	n/a	62.87	128.73	Cu-Pb-Zn	local examination	galena-sphalerite-chalcopyrite-arsenopyrite-pyrite-(stibnite)-bearing skarn adjacent to O'Grady contact (2 skarn zones)	proximal Pb(Ag)-Zn skarn	Tombstone
STIB 2	105INE0027	62.97	128.89	Zn	local examination	fracture-hosted and disseminated sphalerite in limey sediments at contact with O'Grady	proximal Pb(Ag)-Zn skarn	Tombstone
STIB 3	105INE0028	62.85	128.83	Cu	reconnaissance	pods of pyrrhotite with minor disseminated chalcopyrite in skarn; adjacent to the O'Grady contact.	proximal Cu skarn	Tombstone
STIB 4	105INE0029	62.85	128.77	Pb-As-Zn	reconnaissance	galena, arsenopyrite, and sphalerite-bearing fractures in limestones at O'Grady contact	proximal Pb(Ag)-Zn skarn	Tombstone
STIB 5	105INE0030	62.86	128.73	Pb-As-Zn	reconnaissance	galena, arsenopyrite, and sphalerite-bearing fractures in limestones at O'Grady contact	proximal Pb(Ag)-Zn skarn	Tombstone
KAREN	105INE0011	62.97	128.66	Pb-Zn-As-Sn-Sb	local examination	massive pyrite, arsenopyrite, stibnite, sphalerite, and galena in gossanous limestone; adjacent to a felsic, porphyry-textured phase of O'Grady batholith	proximal Sb-Pb-As skarn?	Tombstone
STIB 1	105INE0022	62.96	128.65	Sb-Pb-As	reconnaissance	stibnite, boulangerite (Pb-Sb-S), jamesonite (Pb-Fe-Sb-S), galena, and arsenopyrite in limestone adjacent to O'Grady contact	proximal Sb-Pb-As skarn?	Tombstone
"CHUCK"	095DNE0007-10	60.98	126.56	Au-Cu	reconnaissance	bornite-malachite-chalcopyrite dissem. in highly silicified, intermediate-mafic, Lower Cambrian volcanics; minor gold with the copper; stream sediment samples with anomalous gold near bedrock shownings and near Big Charlie pluton	placer Au; mafic volcanic hosted Cu	Tombstone; Lower Cambrian volcanics
CAM	105INW0021	62.92	129.56	Pb-Ag-Cu-Au	local examination	Ag- and galena-bearing quartz-carbonate veins in sediments; no proximal intrusion; minor Cu, trace Au	distal Pb(Ag)-Zn vein	Tombstone?
NUG	105INW0023	62.64	129.3	W-Zn-Ni-Bi	local examination	scheelite- (up to 50% of vein material) and wolframite-bearing quartz veins in hornfelsed sediments with minor disseminated scheelite in sediments; no proximal intrusion; chalcopyrite, bismuthinite/bismuth, arsenopyrite, pyrite, and pyrrhotite also in veins	proximal? W-Cu-(Zn-Bi-Au-Mo) skarn?	?
QUICK & EASY	105INW0022	62.62	129.28	W-Cu	local examination	scheelite-bearing quartz veins and vugs in hornfelsed sediments with minor disseminated scheelite in sediments; no proximal intrusion	proximal? W-Cu-(Zn-Bi-Au-Mo) skarn?	?
SKY	105ISE0059	62.02	128.29	W	local examination	no details	proximal? W-Cu-(Zn-Bi-Au-Mo) skarn?	?
DOT	105HNE0008	61.98	128.28	W	local examination	no details	proximal? W-Cu-(Zn-Bi-Au-Mo) skarn?	?
Uncertain Origin								
CLIFF-GRANT-PAT	095ESE004,17; 095DNE0001	61.00		Cu	local examination	disseminated bornite-malachite-(chalcopyrite)-(covellite?) in intermediate-mafic, volcaniclastic, Lower Cambrian volcanics; also along cleavage/foliation/fracture planes	mafic volcanic hosted Cu	Tombstone; Lower Cambrian volcanics

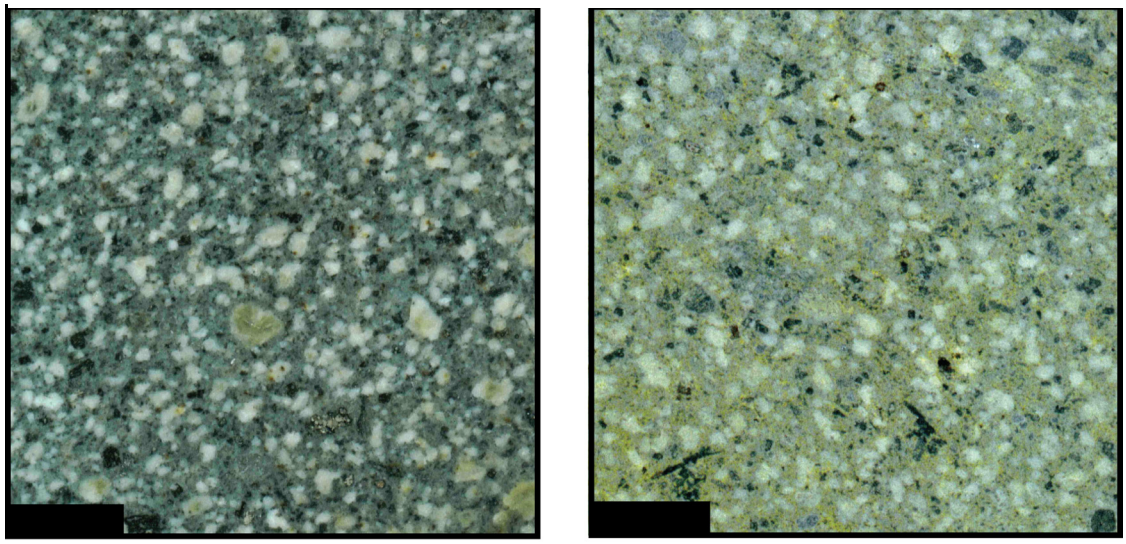
Appendix 1 continued.

Showing Name	Showing ID (NORMIN) or mapsheet	Latitude	Longitude	Metals	Development Stage	Description of Mineralization	Classification	Nearby Plutonic Suite
*HAT	n/a	62.67	128.47	Cu-Pb-Zn	local examination	malachite-azurite-(tetrahedrite)-bearing quartz veins in sediments	distal Pb(Ag)-Zn vein?	?
*GRAND	n/a	62.38	129.08	Pb-Zn-Cu	local examination	dissem. galena-sphalerite in sediments and in quartz vein; no proximal intrusion	distal Pb(Ag)-Zn vein?	?
Non-intrusion Related								
"NANCY"	105INE0010, 31, 32, 63, 64	62.5	128.6	Zn-Pb-Cu-(Ag)	local examination	stratabound NW-trending Pb-Zn mineralization in brecciated and bedded dolomites	?	n/a
ANNIV (Howard's Pass)	105ISW0018	62.45	129.21	Pb-Zn-Ag	advanced exploration	strataform disseminated galena and sphalerite in cherty-phosphatic-carbonaceous-limey shales/mudstones; indicated resource of 61 Mt at 5.4% Zn, and 2.1% Pb (ANNIV; EMR Mineral Bulletin MR223)	SEDEX Pb-Zn	n/a
***FERN**	n/a	62.36	129.03	Pb-Zn	local examination	galena-sphalerite-bearing veins and massive lenses in tremolite 'skarn'; no proximal intrusion	?	n/a

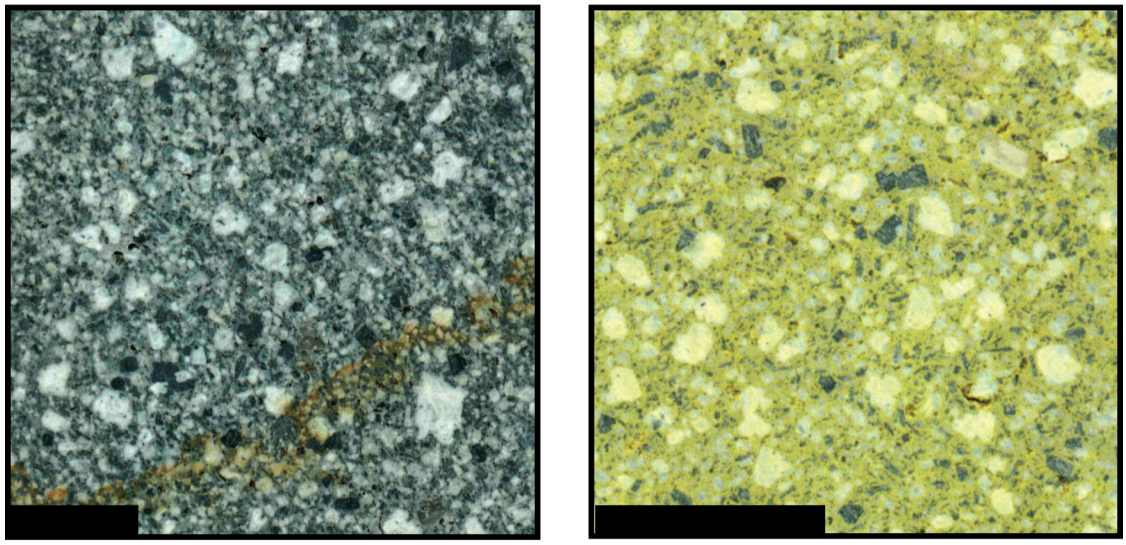
*additional showings listed in Gordey and Anderson (1993)

bolded = confirmed "intrusion-related" or "non-intrusion-related" by Pb-isotopic composition

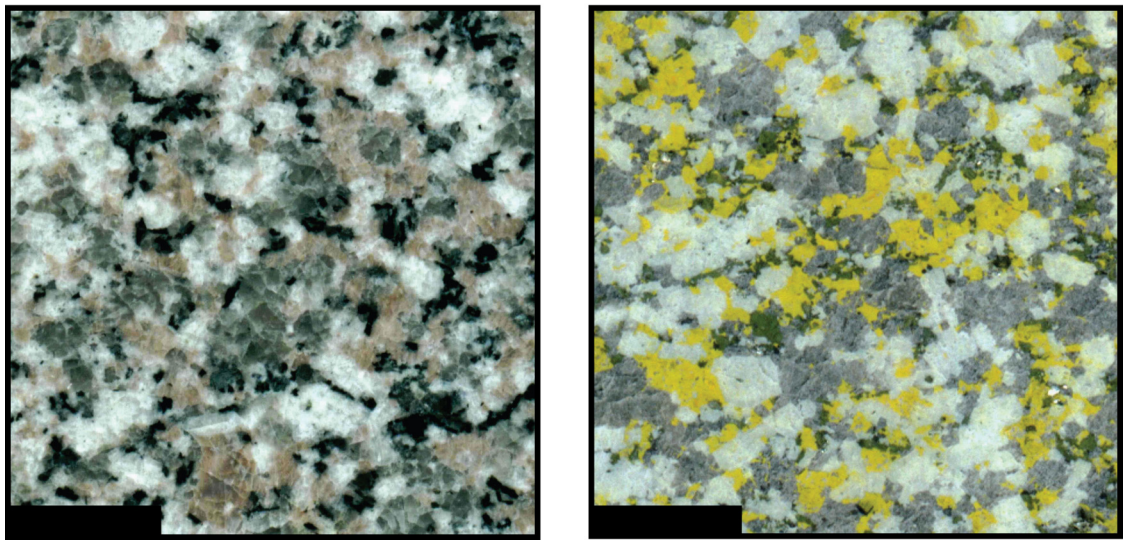
KR-05-08. Powers - porphyritic (plagioclase)-chlorite-hornblende-quartz monzodiorite.



KR-05-10. Jorgenson - porphyritic (plagioclase)-chlorite-hornblende quartz.

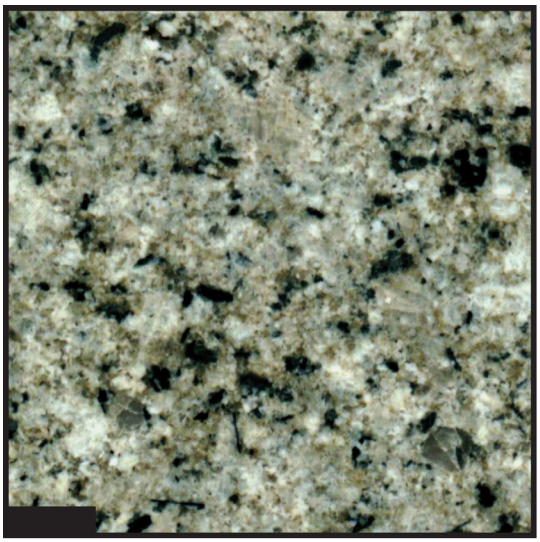


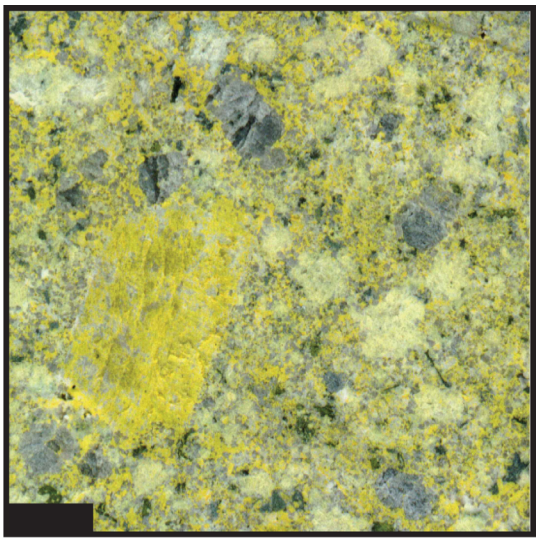
KR-05-22. Roy pluton - biotite-hornblende monzogranite.



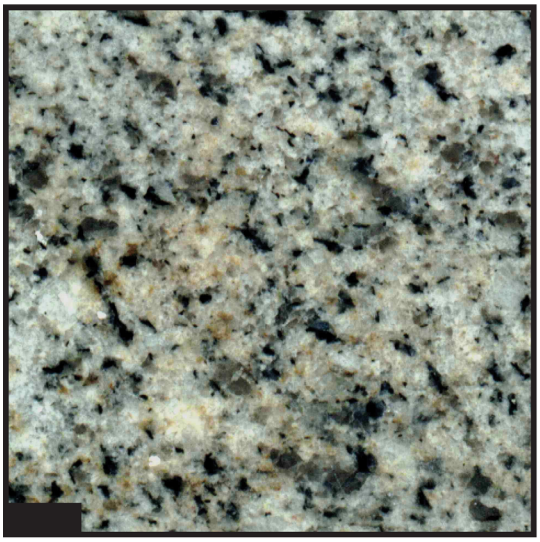
Appendix 2. Intrusive textures from polished and stained slabs for most of the intrusions in the Nahanni MERA area; K-feldspar is bright to dark yellow and plagioclase is white to pale yellow. Black bar represents 1 cm in length.

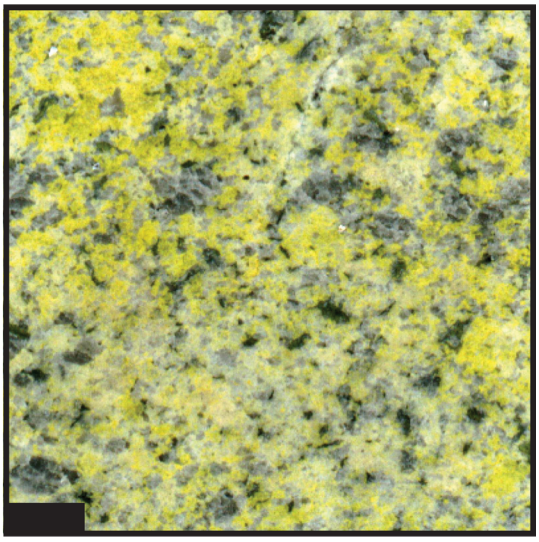
KR-05-26. Fish - porphyritic (quartz, plagioclase, sparse K-feldspar)-biotite monzogranite.





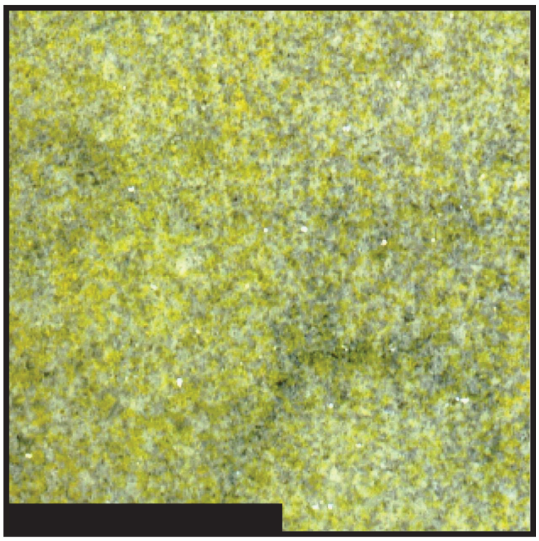
KR-05-32. Ivo - biotite-muscovite-garnet monzogranite.





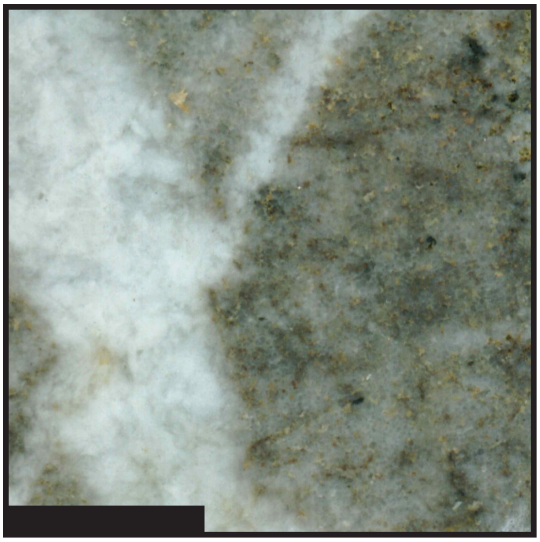
KR-05-33. Ivo -aplite dyke.

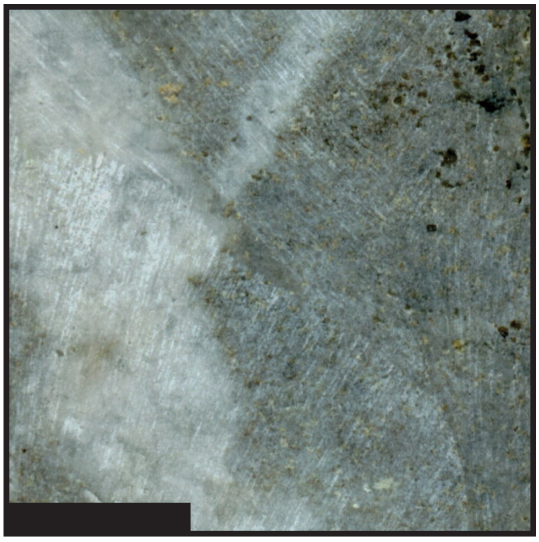




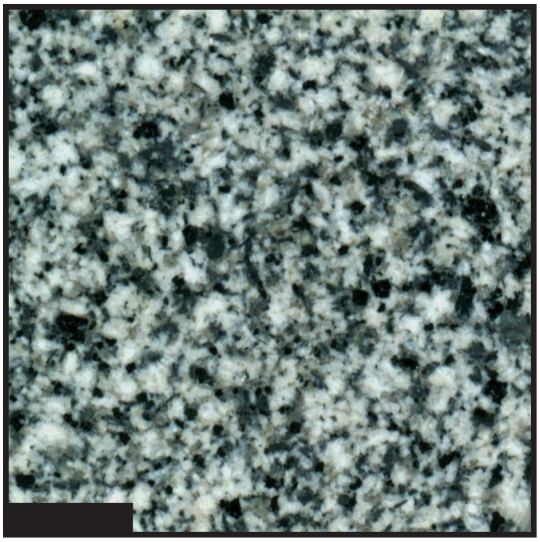
Appendix 2 contined.

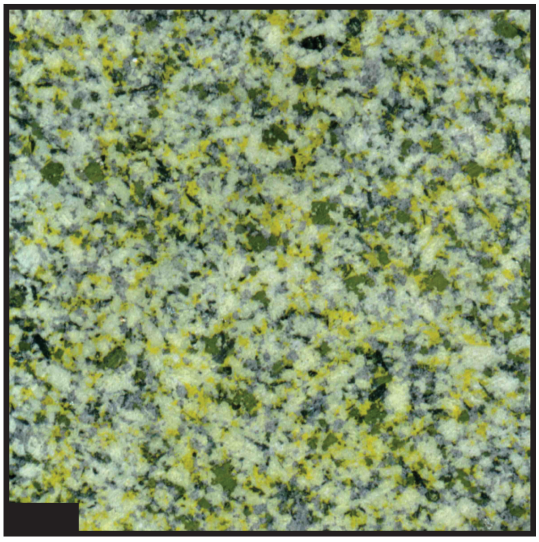
KR-05-39. Chuck plug - silica-flooded aplitic dyke/plug.



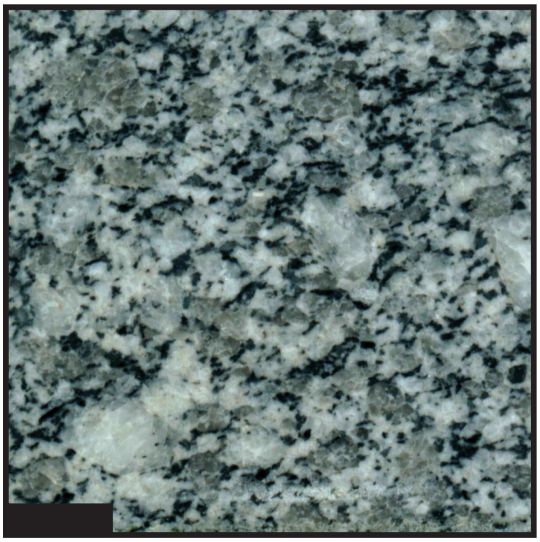


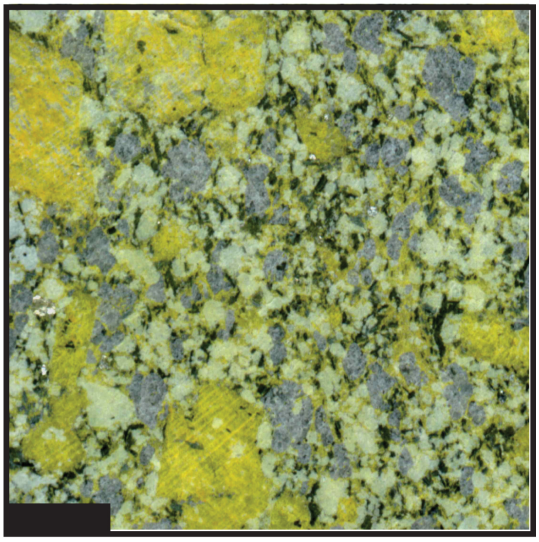
KR-05-43. Park - biotite-hornblende granodiorite.





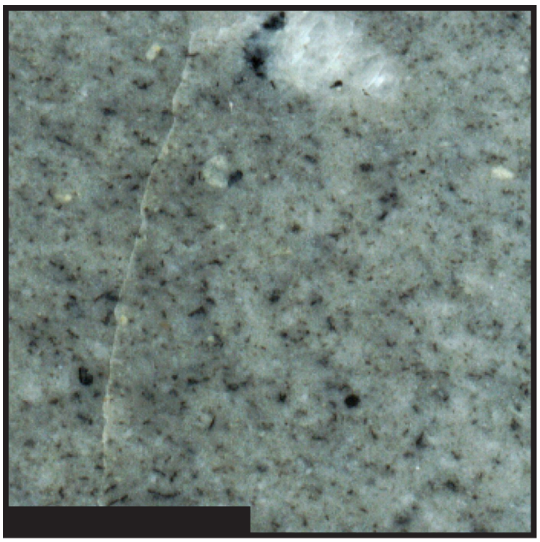
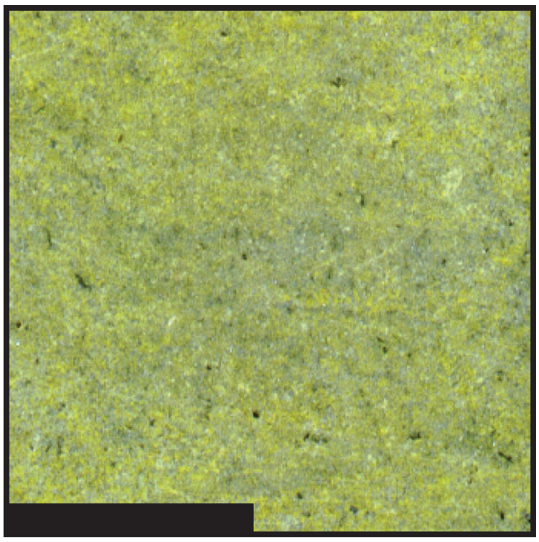
KR-05-47b. Cirque Lake - porphyritic (K-feldspar)-biotite-muscovite monzogranite.



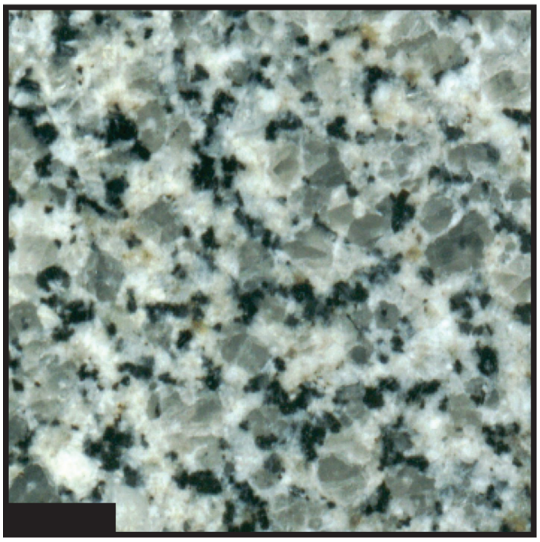
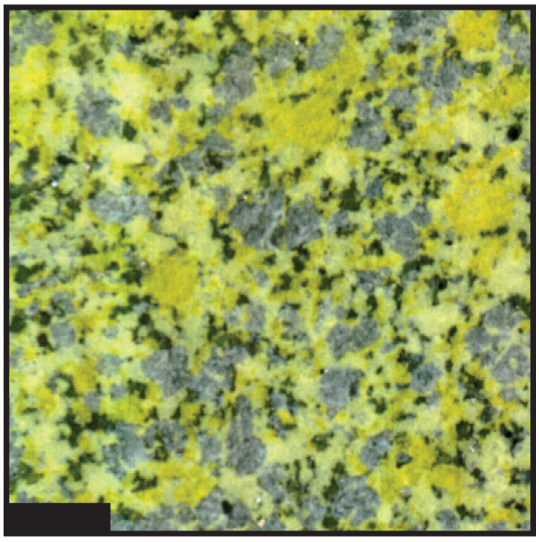


Appendix 2 contined.

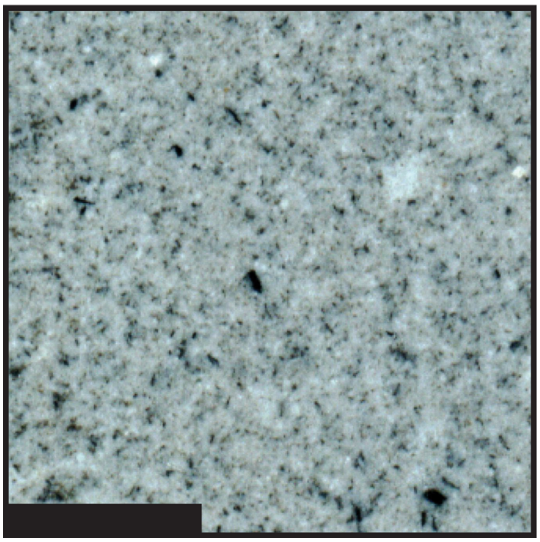
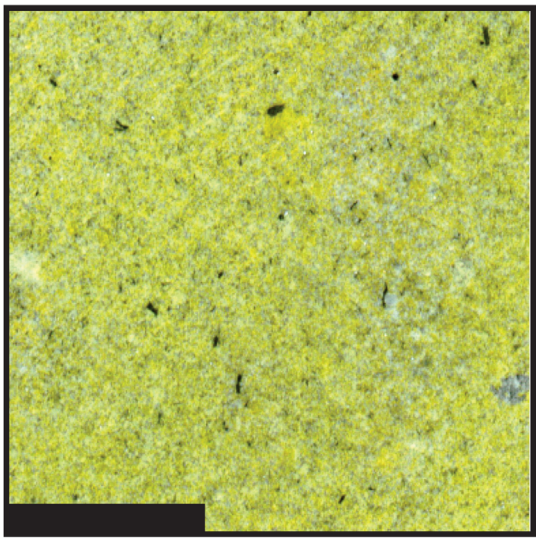
KR-05-53. Cirque Lake and Rockslide Mountain -aplite dyke.

KR-05-59. Rockslide Mountain - biotite monzogranite.

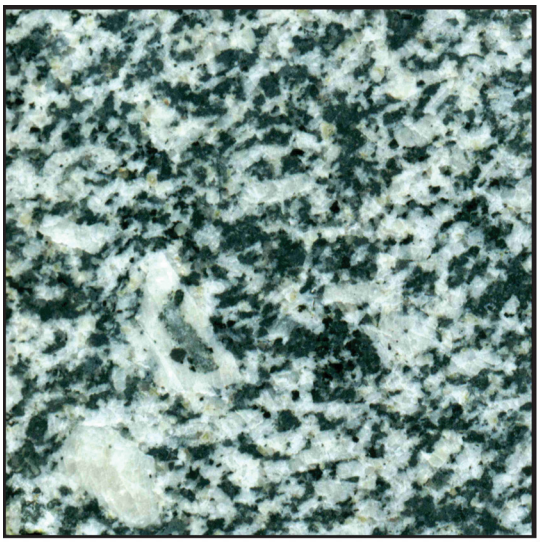



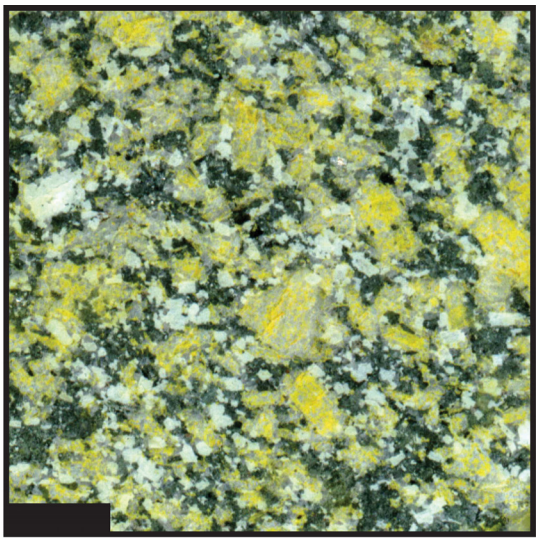
KR-05-60. Rockslide Mountain -aplite dyke.

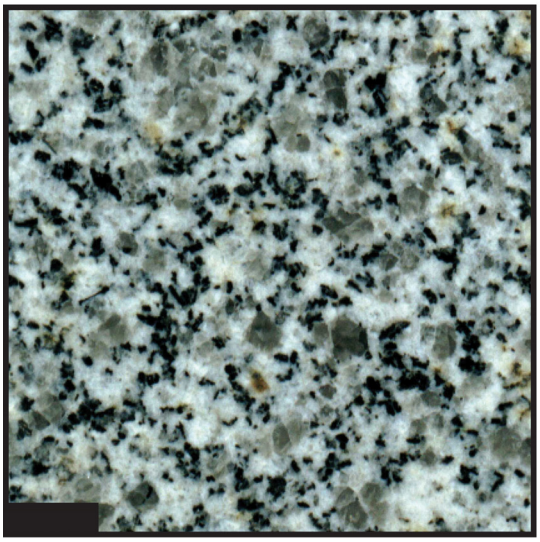
Appendix 2 contined.

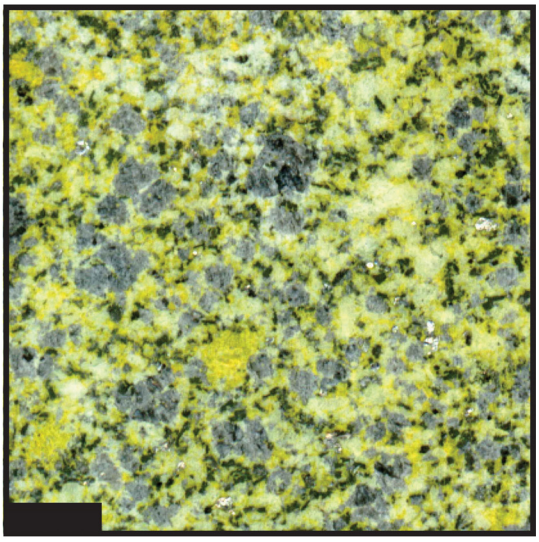
KR-05-62. Mt. Christie - porphyritic (K-feldspar)-biotite-hornblende-quartz monzonite.



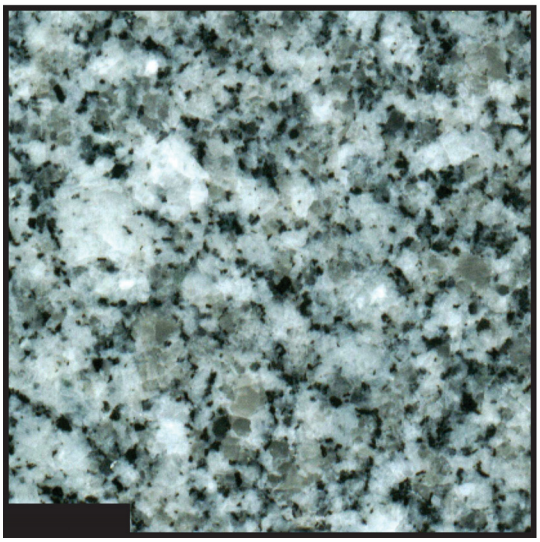


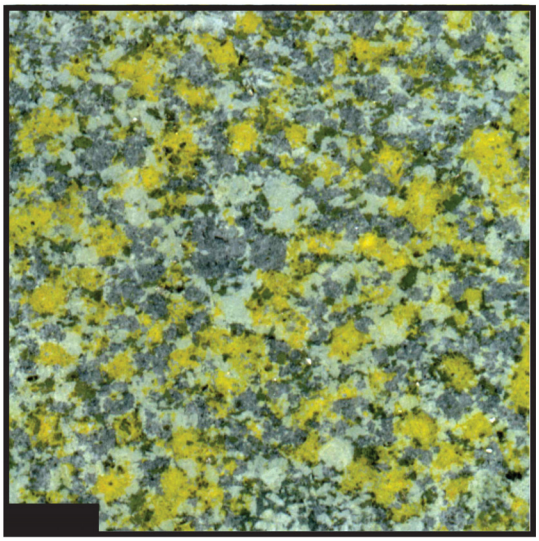
KR-05-68. Mt. Wilson - biotite monzogranite.





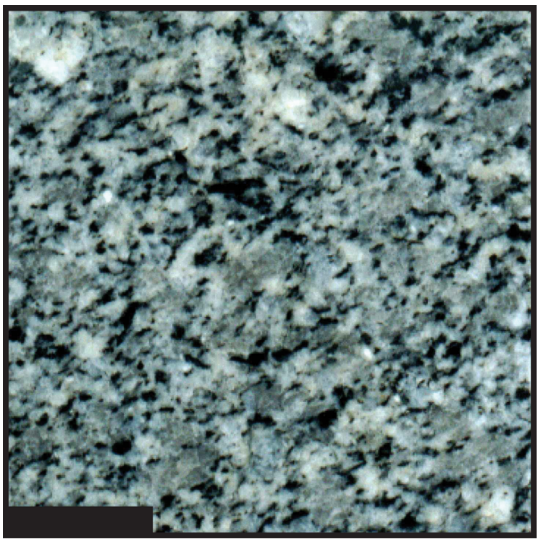
KR-05-71. Gun - biotite monzogranite.

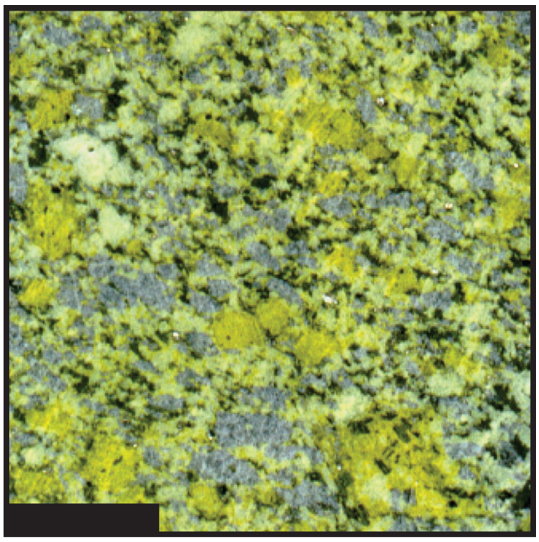




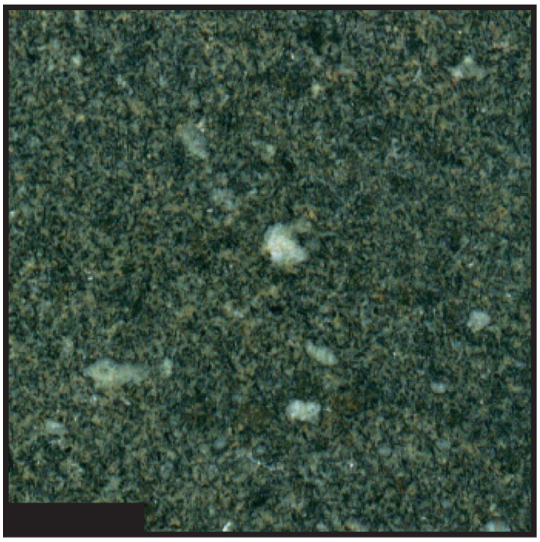
Appendix 2 contined.

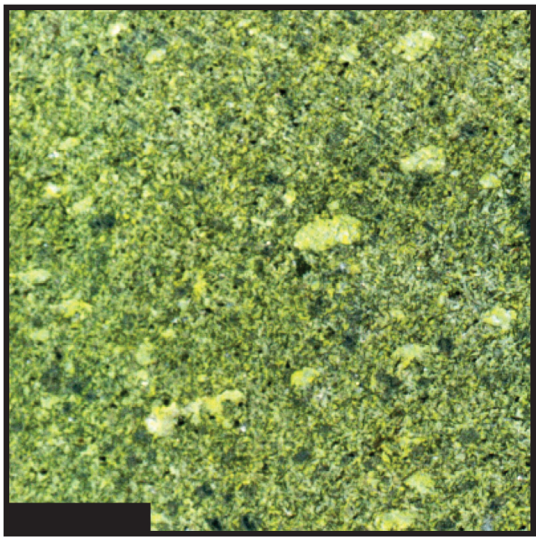
KR-05-76. Pelly River - biotite-quartz monzonite.



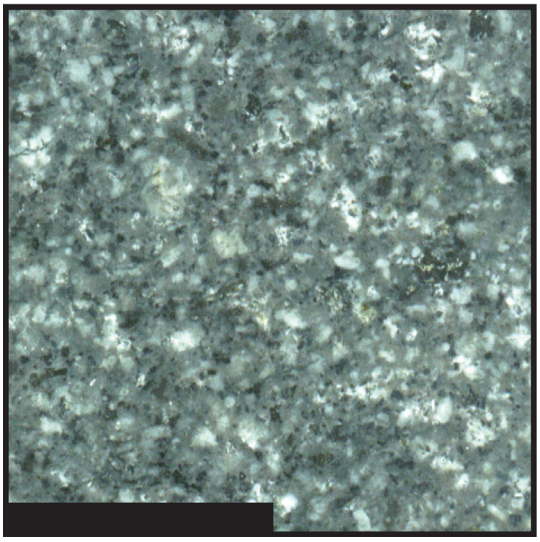


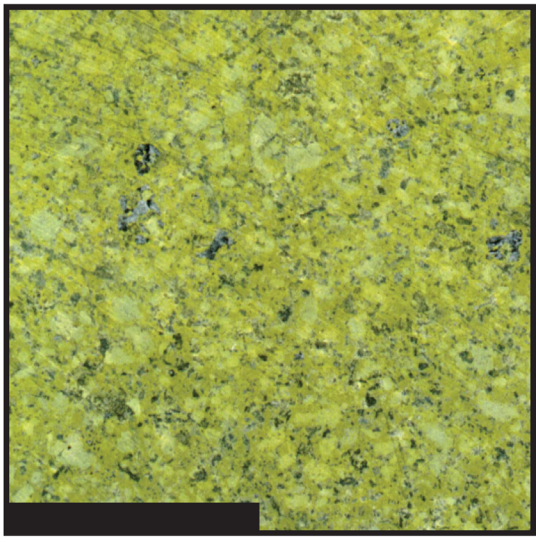
KR-05-77. Pelly River - biotite monzonite (mafic dyke).





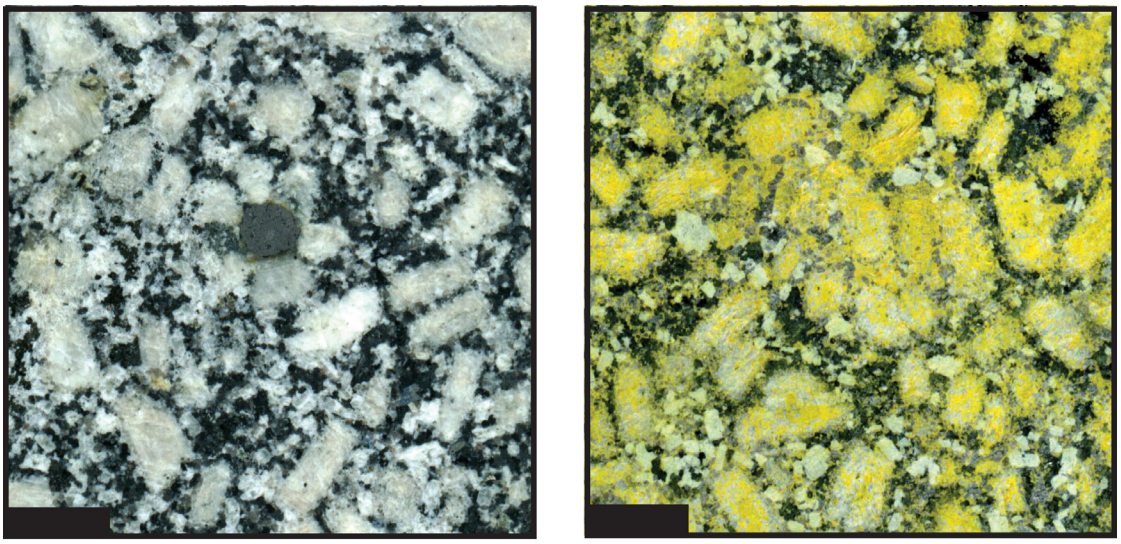
KR-05-87. KAREN (O'Grady apophysy) porphyritic (plagioclaiser)-biotite monzogranite.



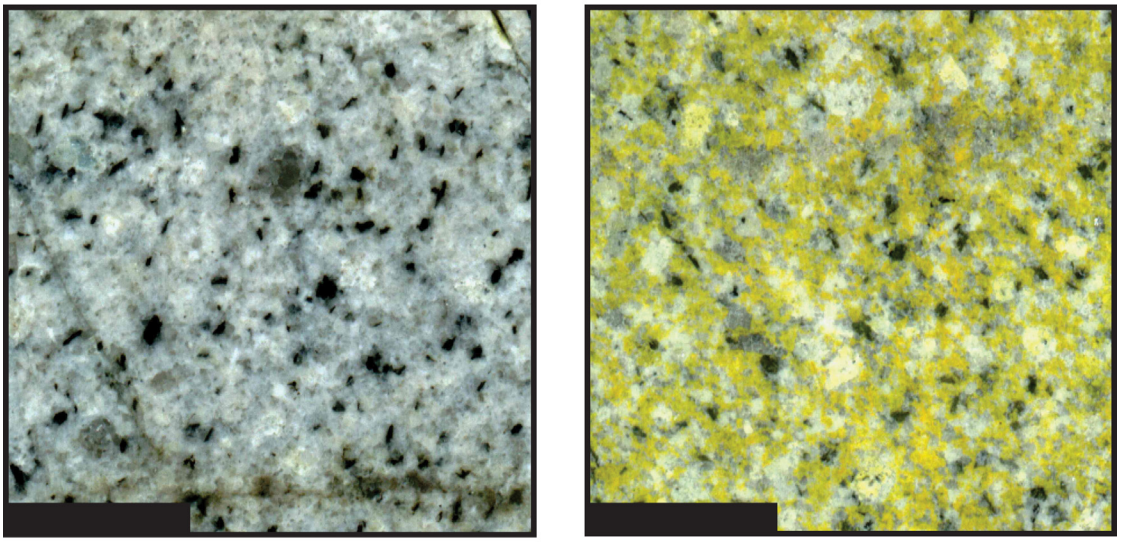


Appendix 2 contined.

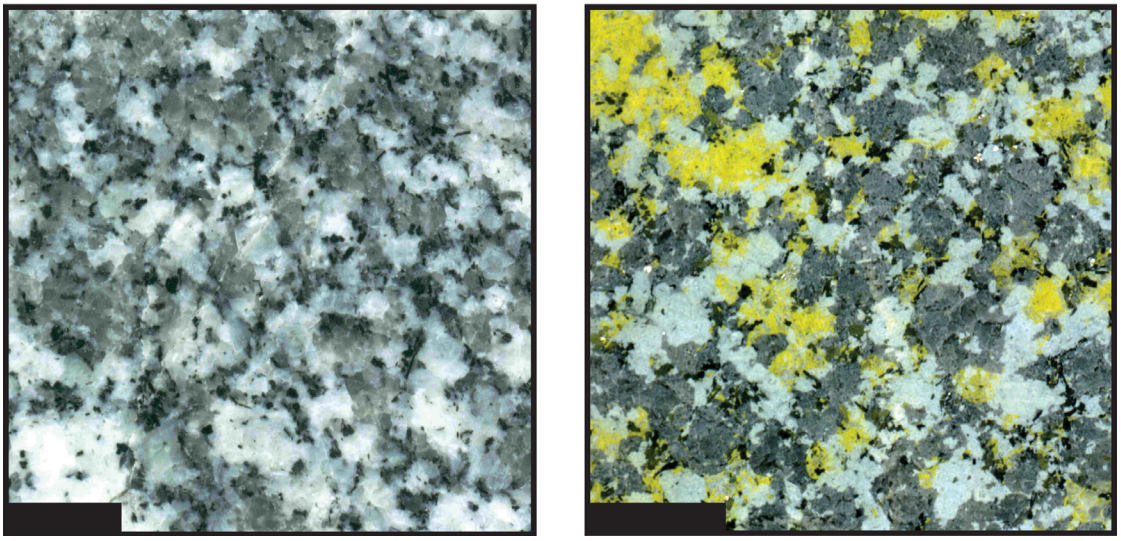
KR-05-97b. O'Grady - porphyritic (crowded K-feldspar)-biotite-hornblende-pyroxene-quartz monzonite.



KR-05-106. CAC - aplite dyke.

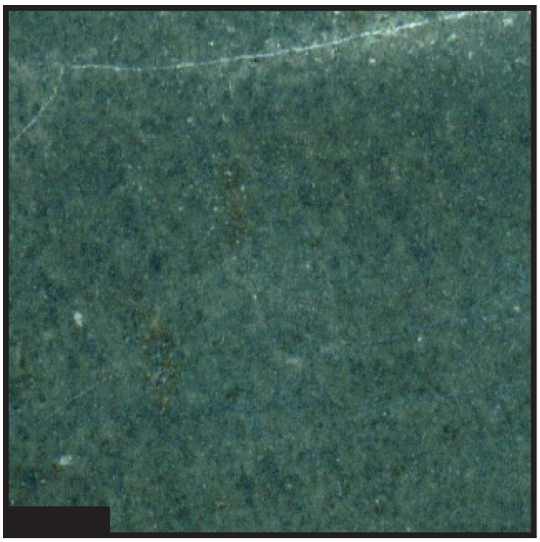
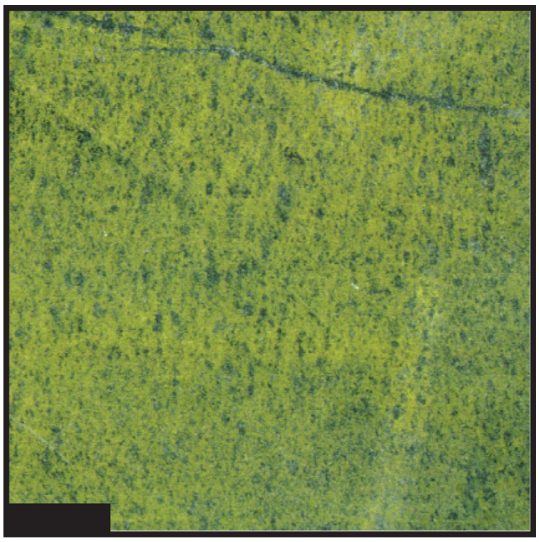


KR-05-110. CAC - porphritic (sparse K-feldspar)-biotite monzogranite.

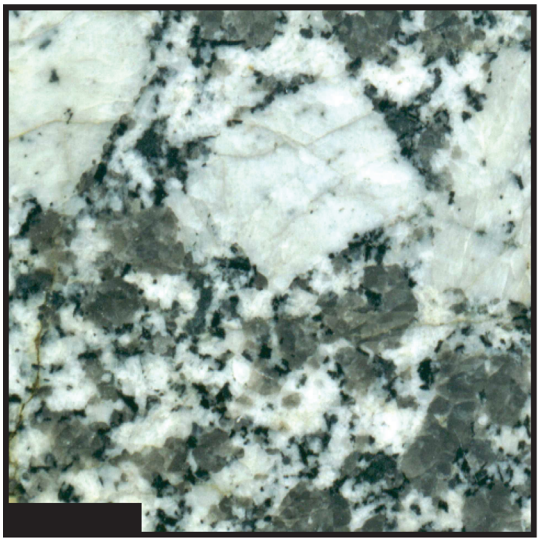
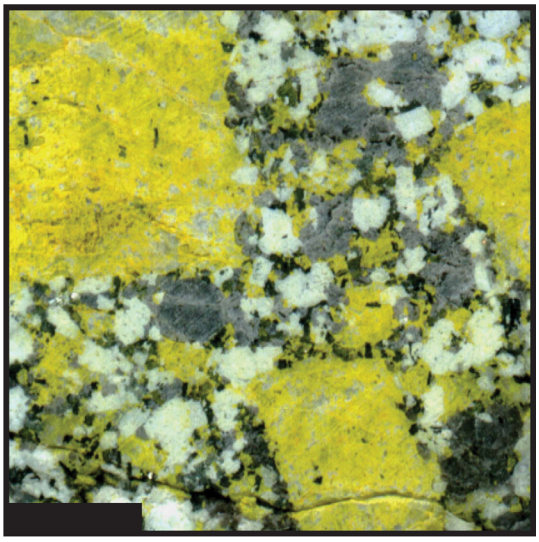


Appendix 2 contined.

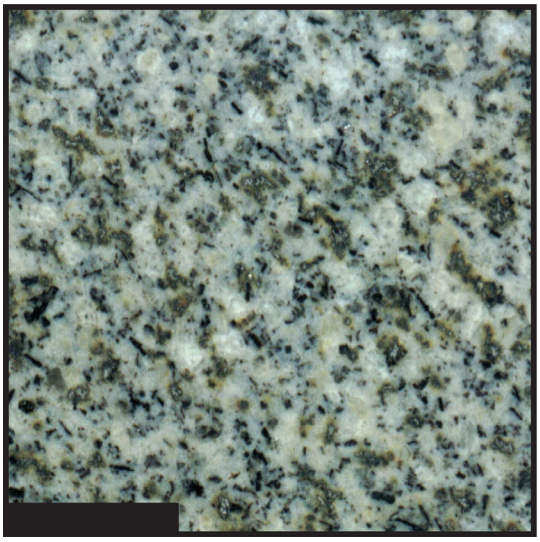
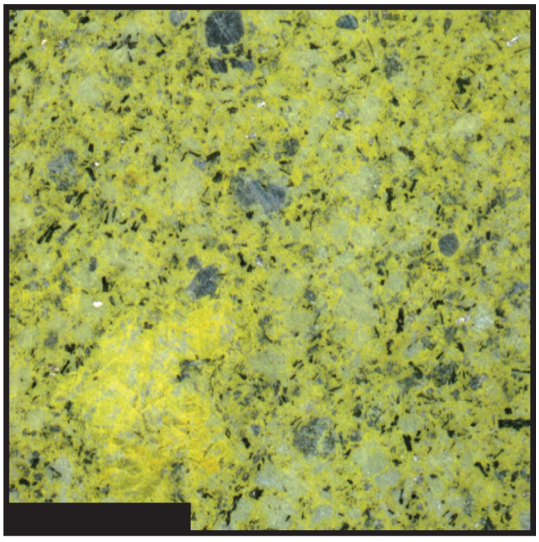
KR-05-112. South Nahanni - altered biotite/chlorite-quartz monzonite (mafic dyke).

KR-05-113. South Nahanni - porphyritic (K-feldspar)-biotite monzogranite

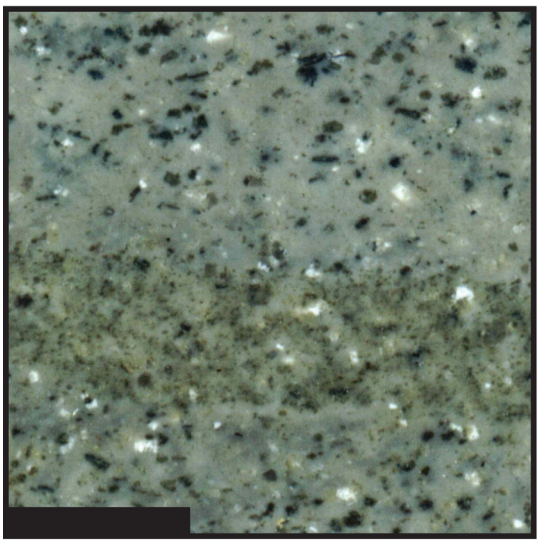



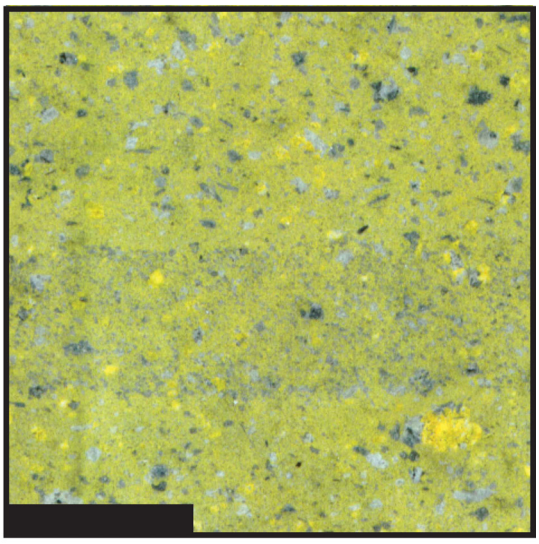
KR-05-115.South Nahanni - biotite monzogranite (dyke/plug).

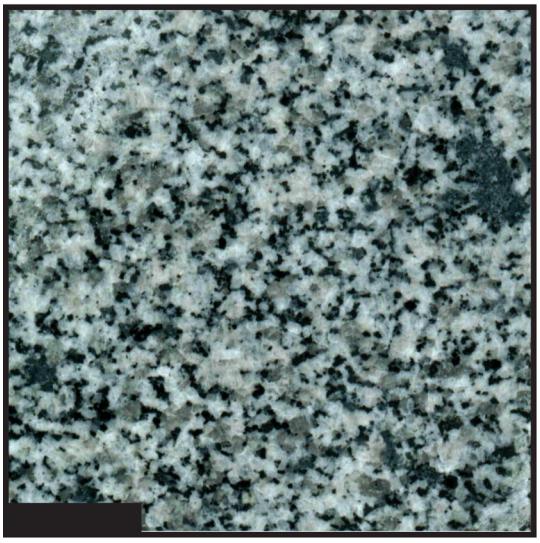
Appendix 2 contined.

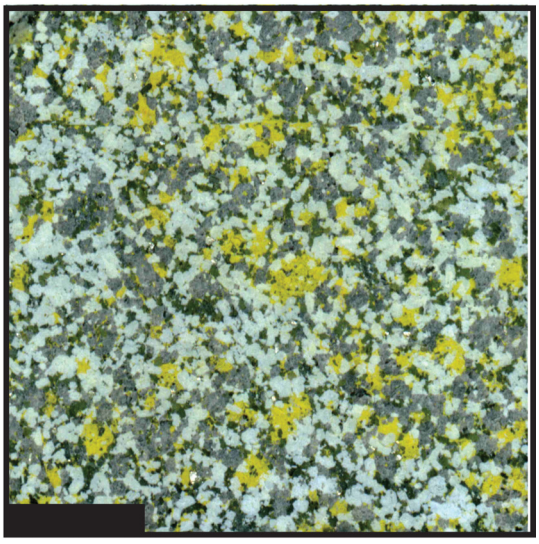
KR-05-126. Plug southwest of O'Grady - altered biotite-muscovite monzogranite.



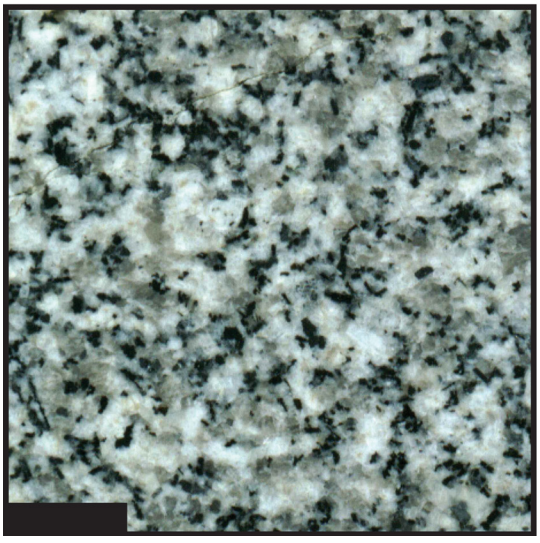


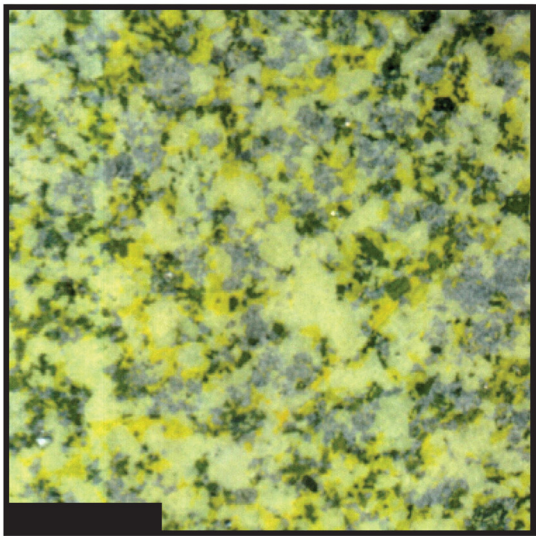
KR-05-130. Central Nahanni - biotite-hornblende granodiorite.





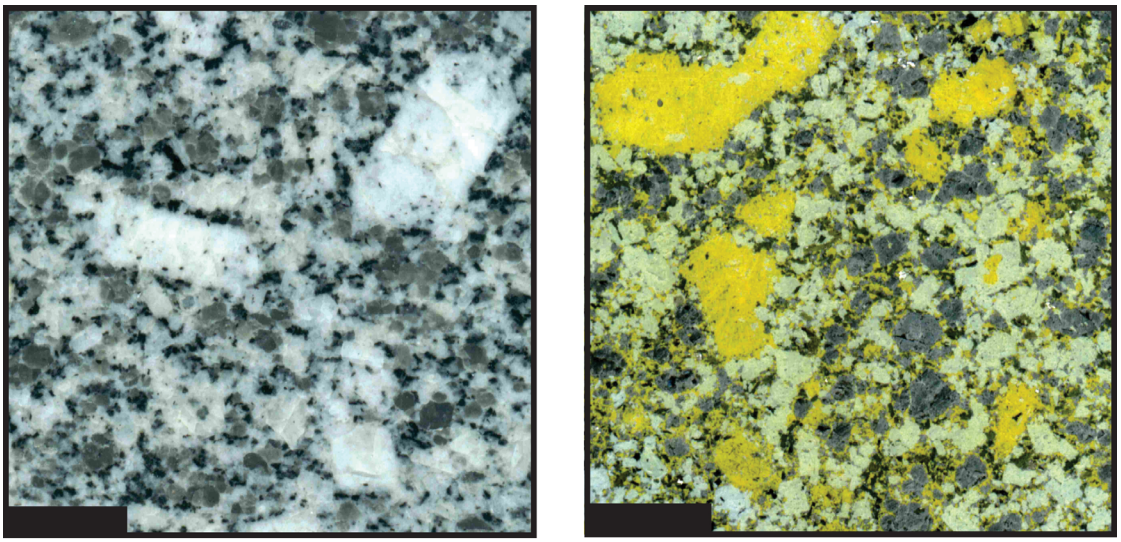
KR-05-136. North Nahanni - biotite monzogranite.



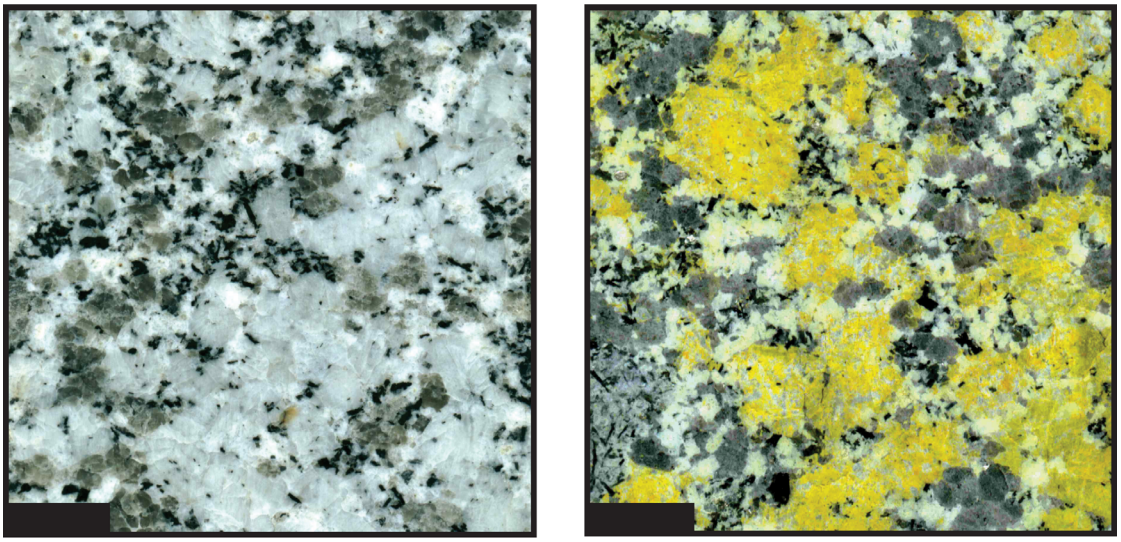


Appendix 2 contined.

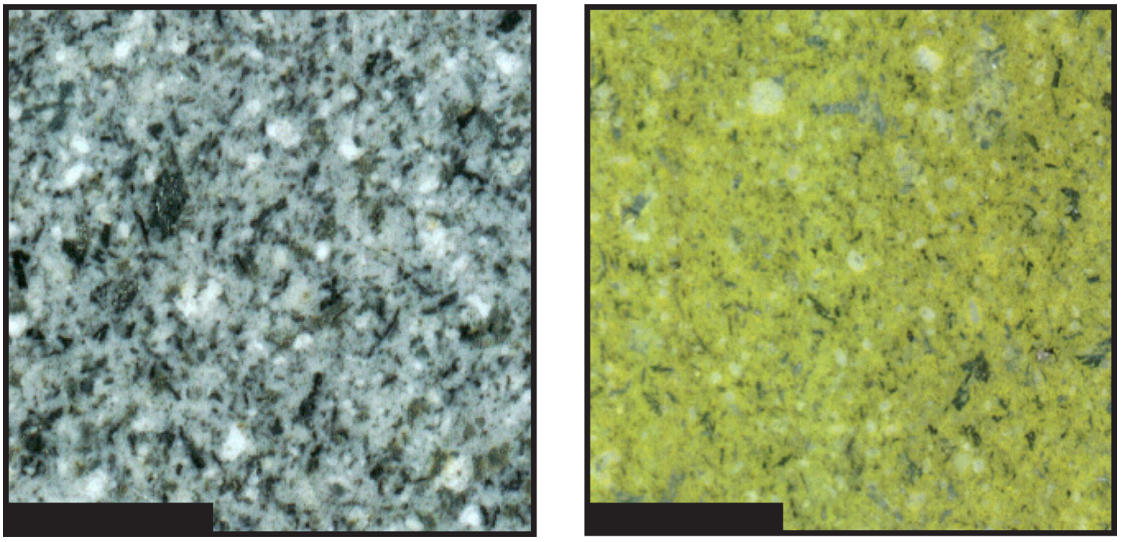
KR-05-143. Circular Stock - porphyritic (K-feldspar)-biotite monzogranite.



KR-05-148. Rfile Range - porphyritic (K-feldspar)-biotite monzogranite

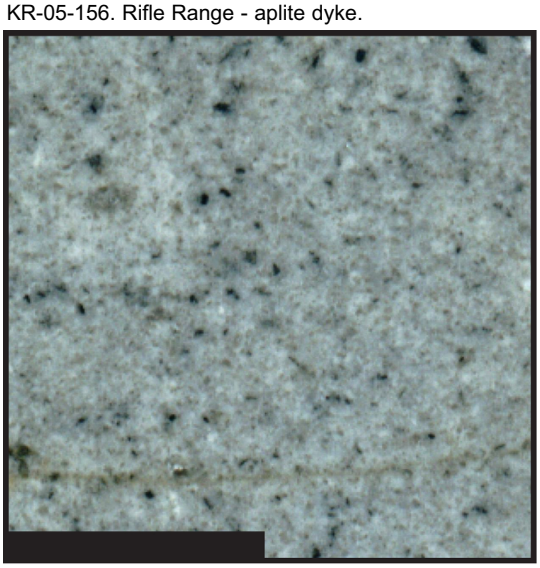


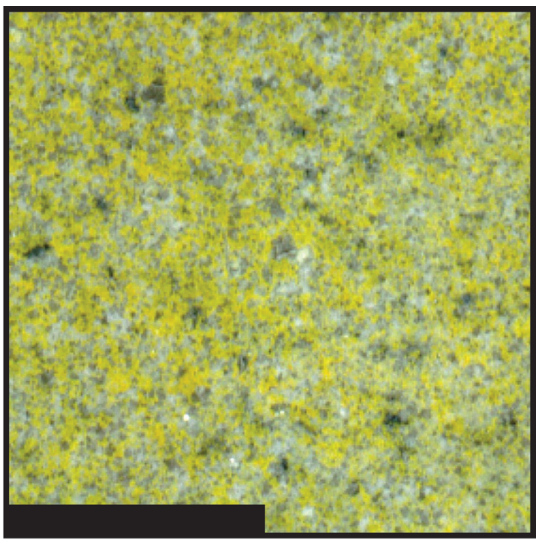
KR-05-154 Rifle Range - biotite monzogranite (apophysydyke).



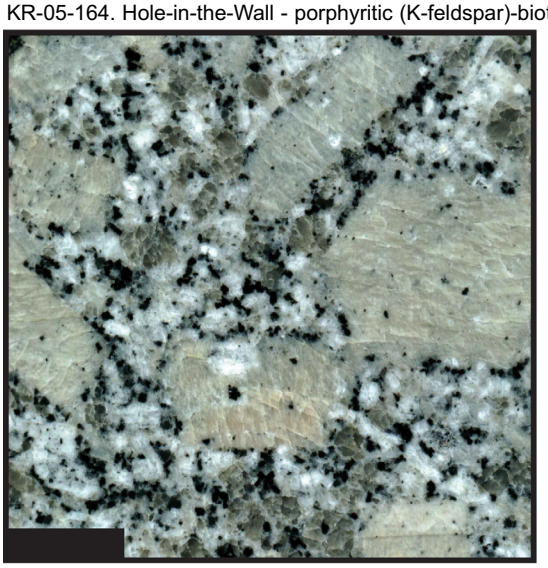
Appendix 2 contined.

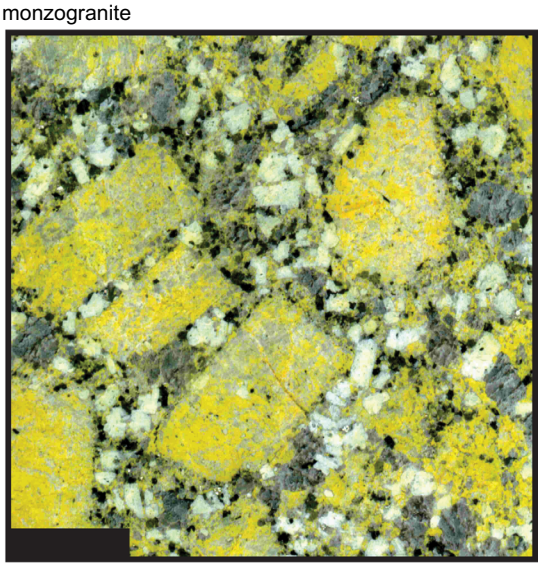
KR-05-156. Rifle Range - aplite dyke.



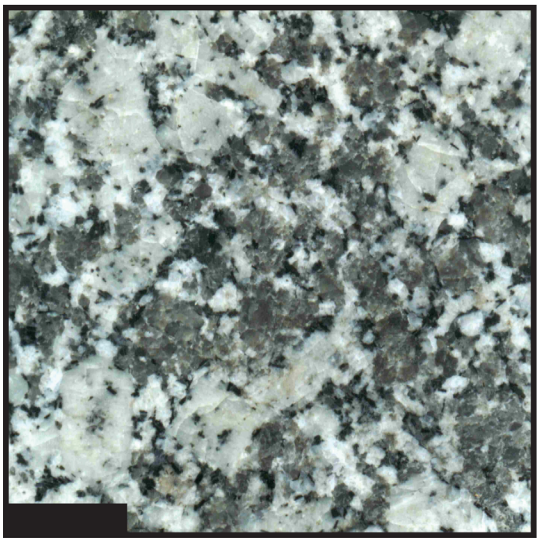


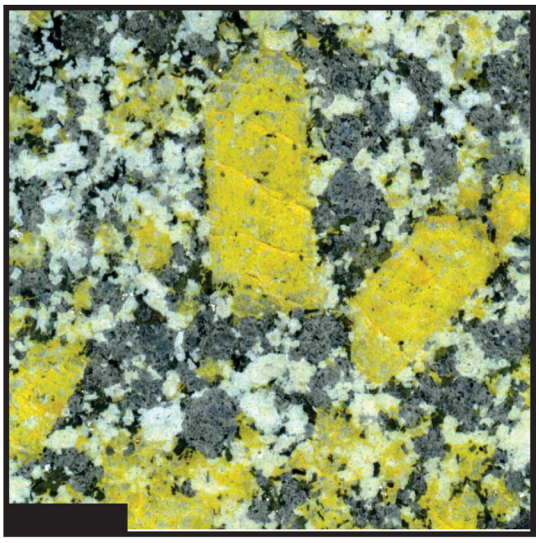
KR-05-164. Hole-in-the-Wall - porphyritic (K-feldspar)-biotite monzogranite





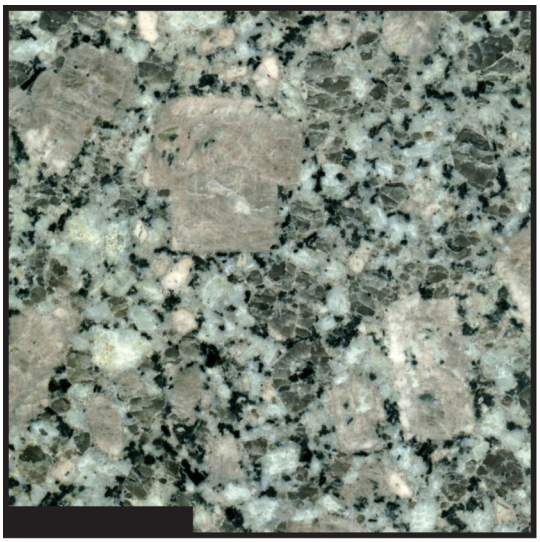
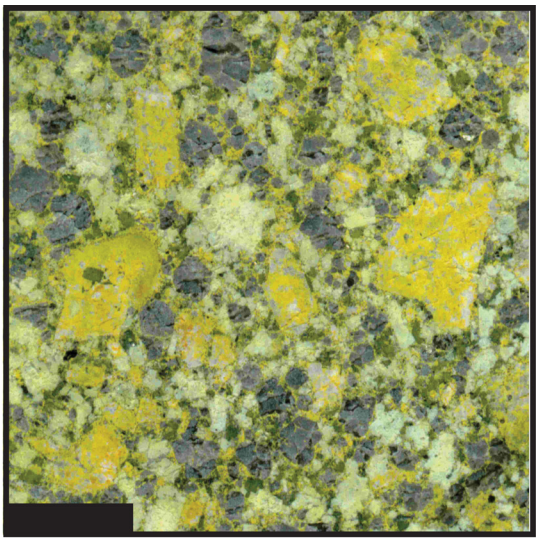
KR-05-175. Lened - porphyritic (K-feldspar)-biotite-muscovite monzogranite.



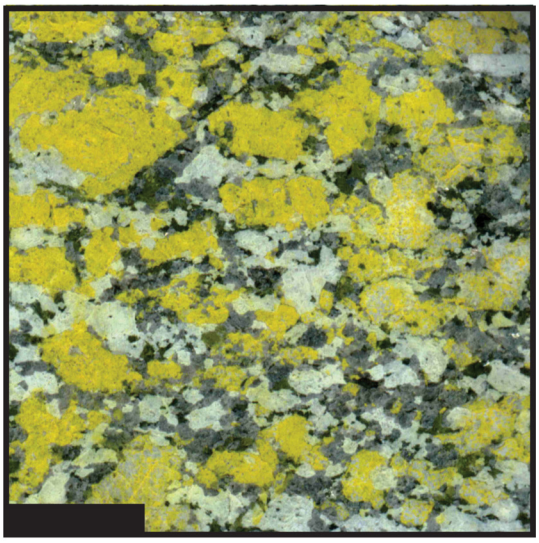


Appendix 2 contined.

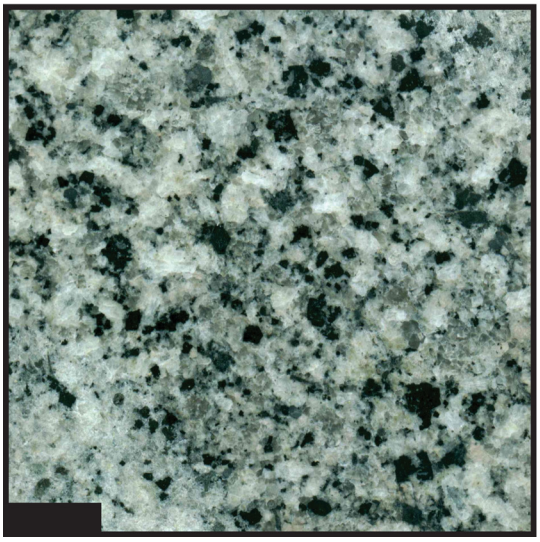
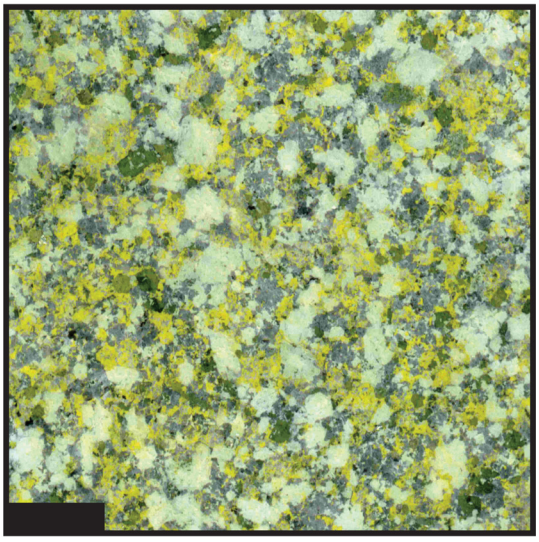
-KR-05-191. MARION (Coal River) - porphyritic (K-feldspar)-biotite monzogranite

KR-05-194. ROYALL (Coal River) - porphyritic (K-feldspar)-biotite monzogranite.

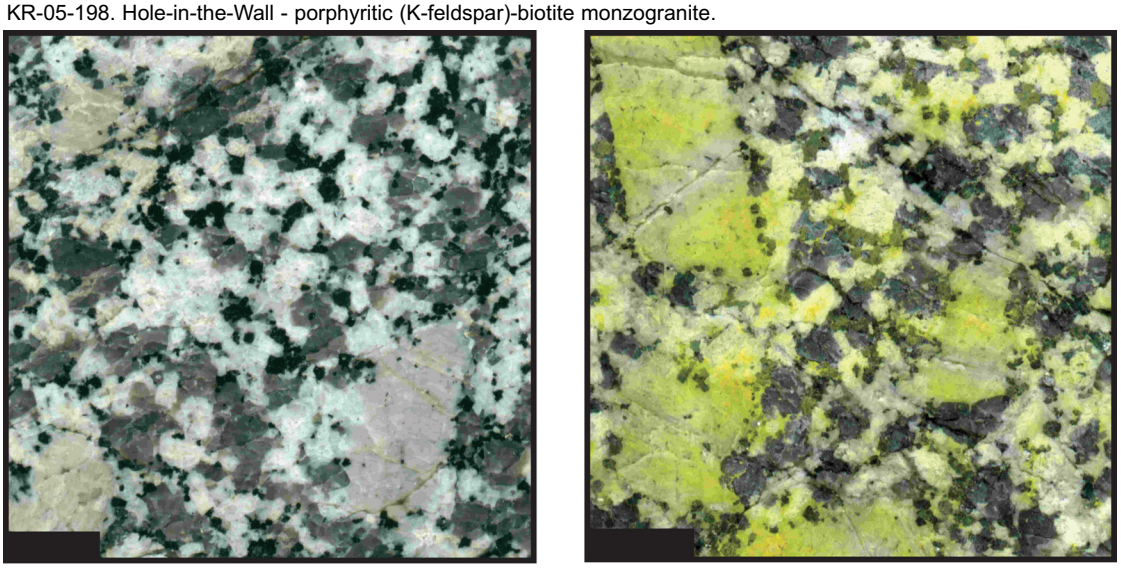



KR-05-196. Coal River - porphyritic (K-feldspar)-biotite-hornblende monzogranite.

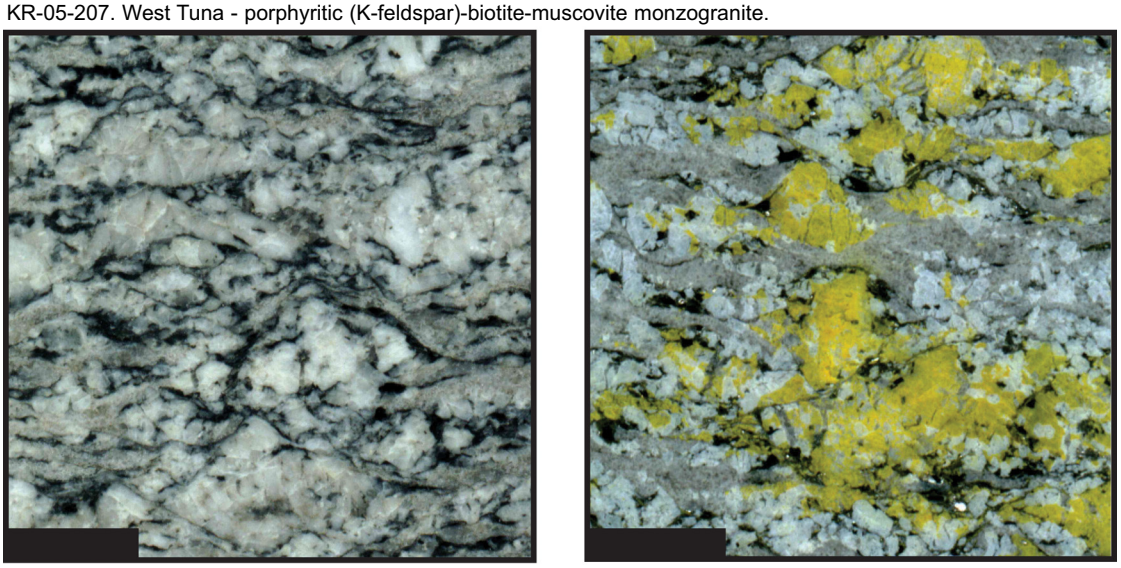



Appendix 2 contined.

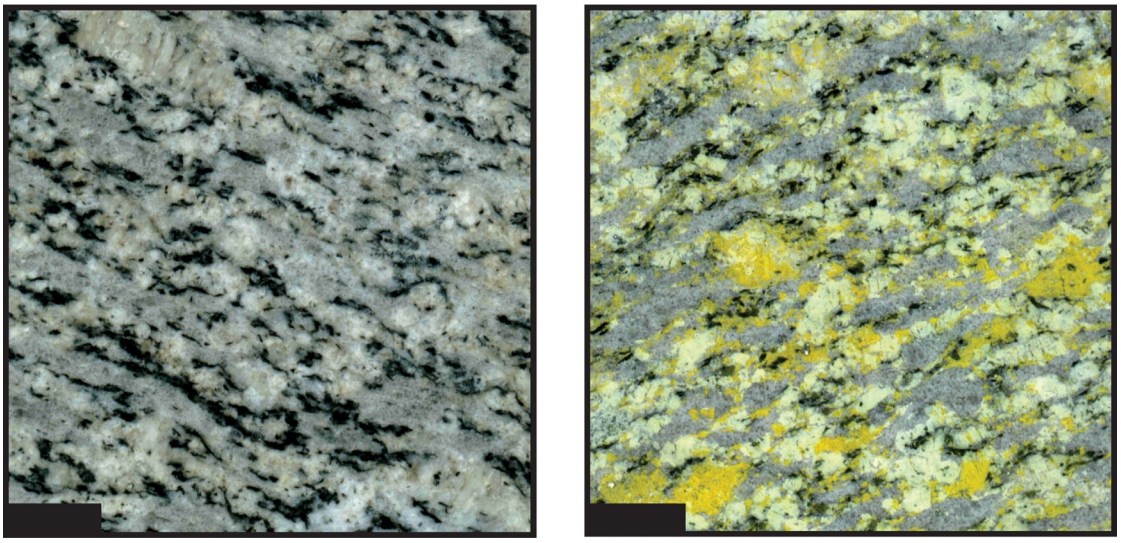
KR-05-198. Hole-in-the-Wall - porphyritic (K-feldspar)-biotite monzogranite.



KR-05-207. West Tuna - porphyritic (K-feldspar)-biotite-muscovite monzogranite.

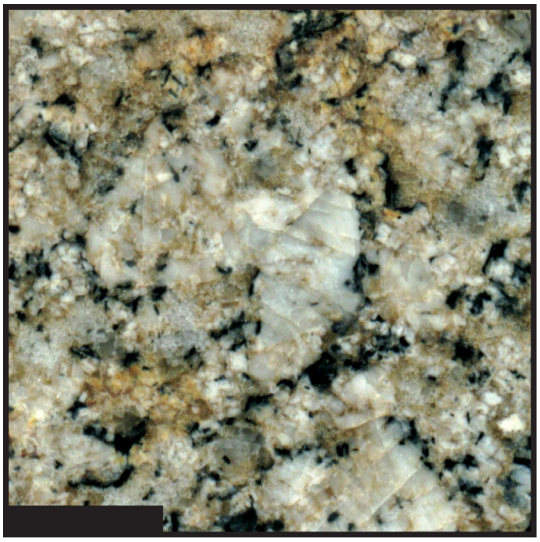
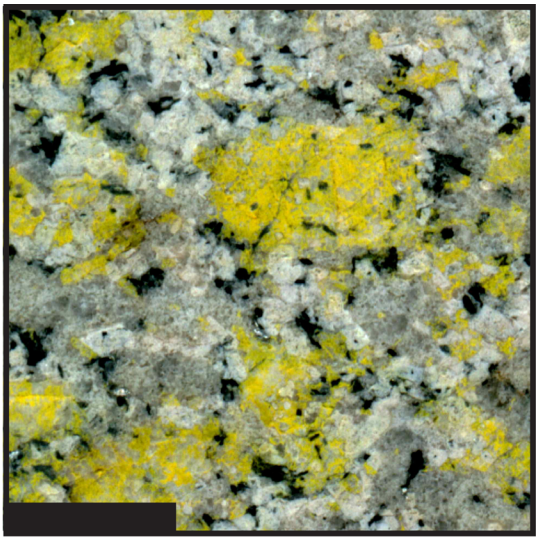


KR-05-208. Little Hyland - porphyritic (K-feldspar)-biotite-muscovite monzogranite.

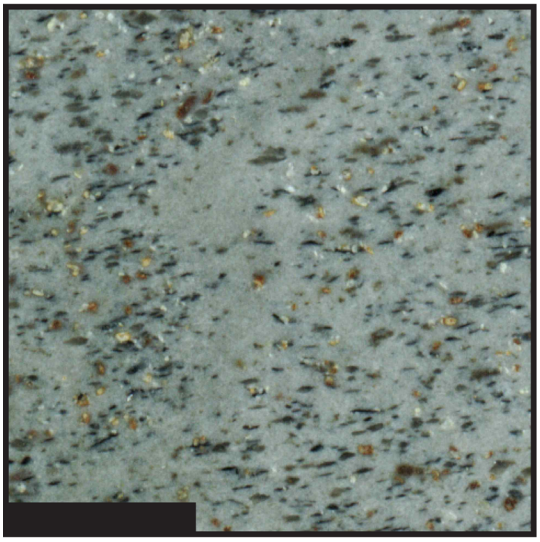
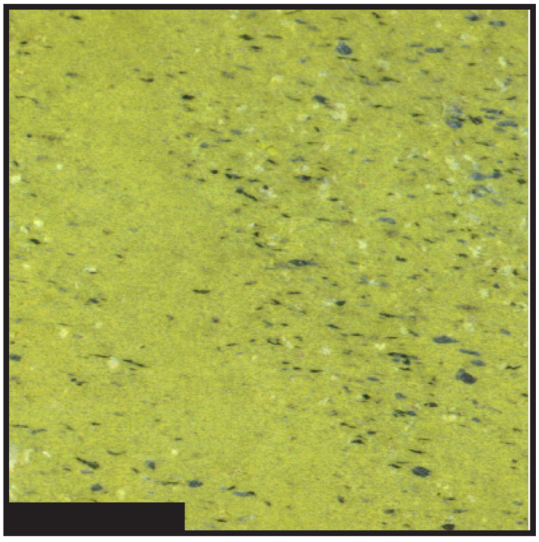


Appendix 2 contined.

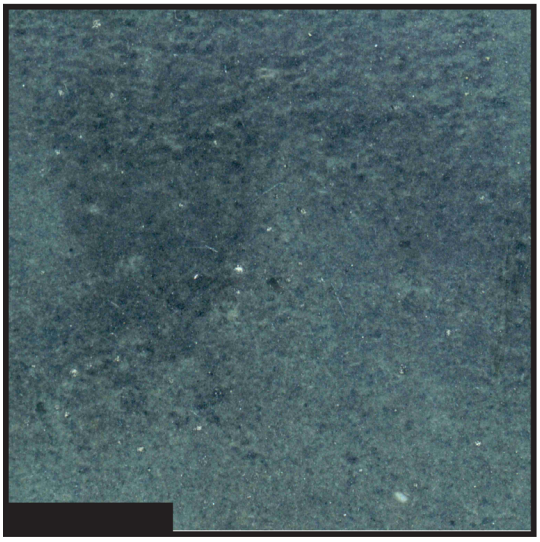
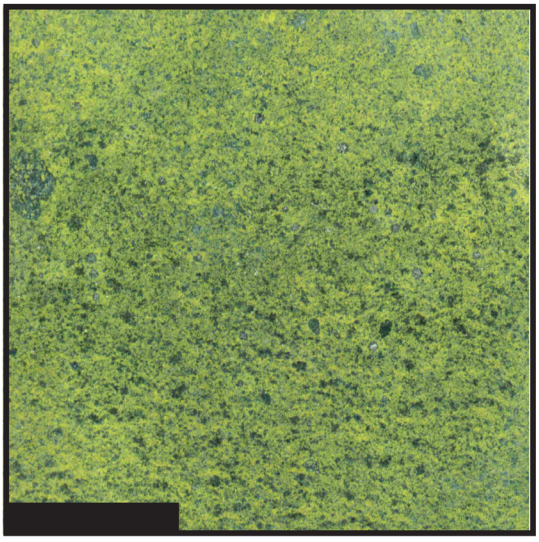
-KR-05-210. Nahanni Range Road - porphyritic (K-feldspar)-biotite monzogranite

KR-05-211. Rifle Range - altered aplite dyke.

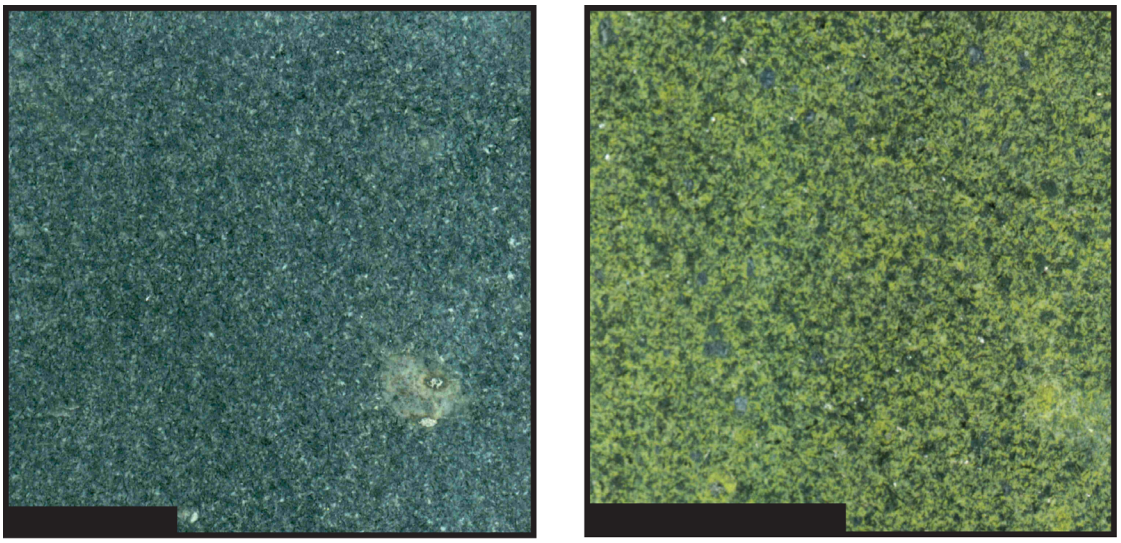



KR-05-212. Rifle Range - biotite/chlorite-quartz monzodiorite (altered mafic dyke).

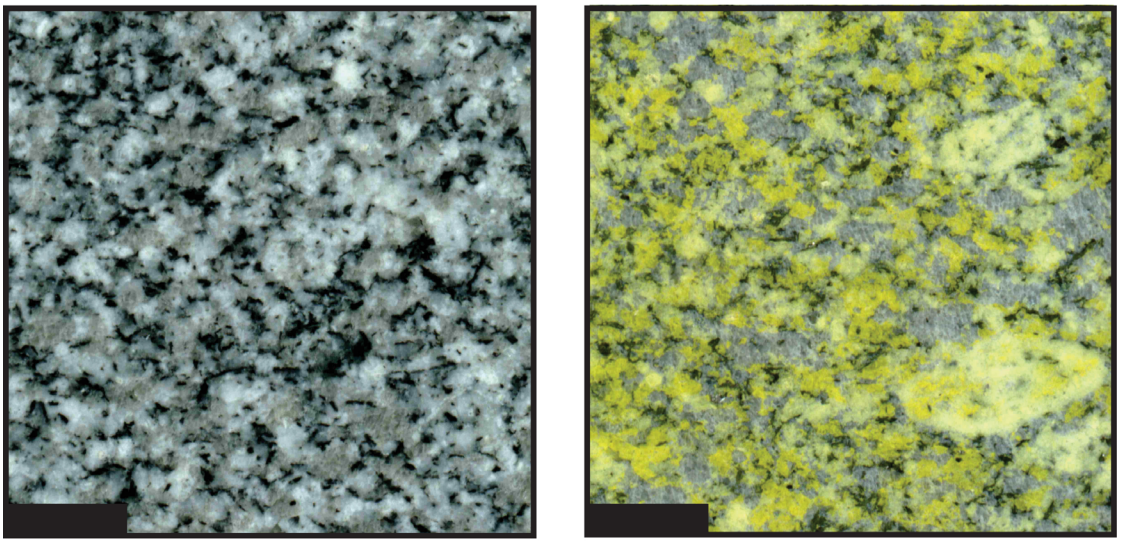



Appendix 2 contined.

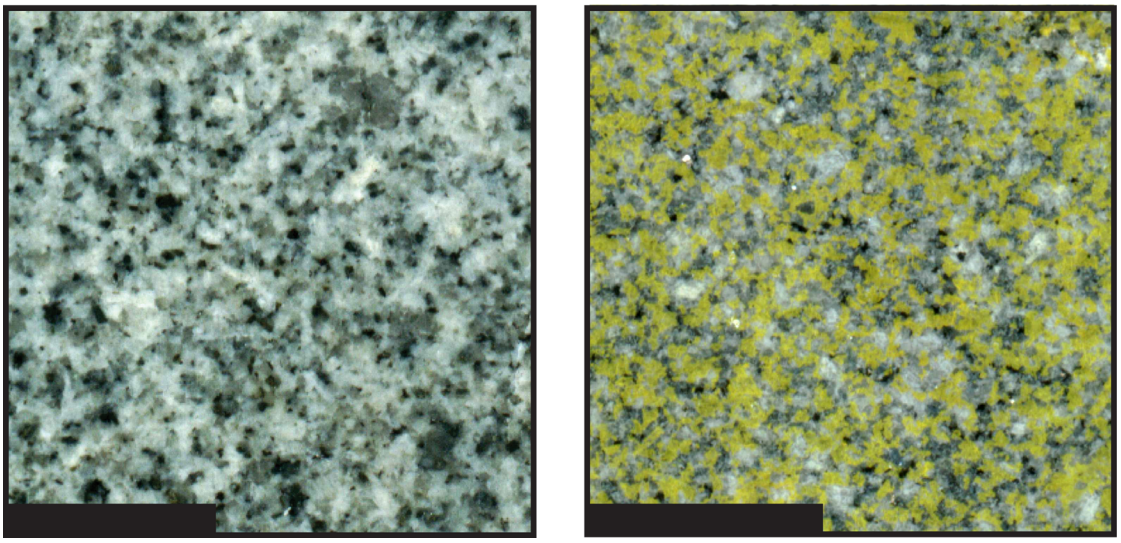
KR-05-213. Rifle Range - biotite/chlorite-quartz monzodiorite (altered mafic dyke).



.KR-05-215. Mine Stock - porphyritic (sparse K-feldspar)-biotite-muscovite monzogranite.

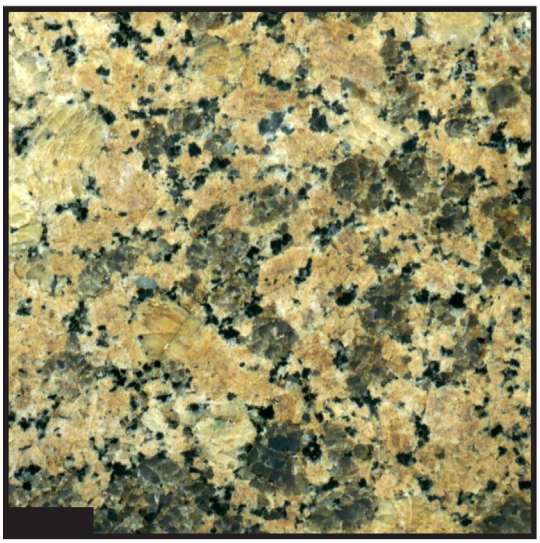
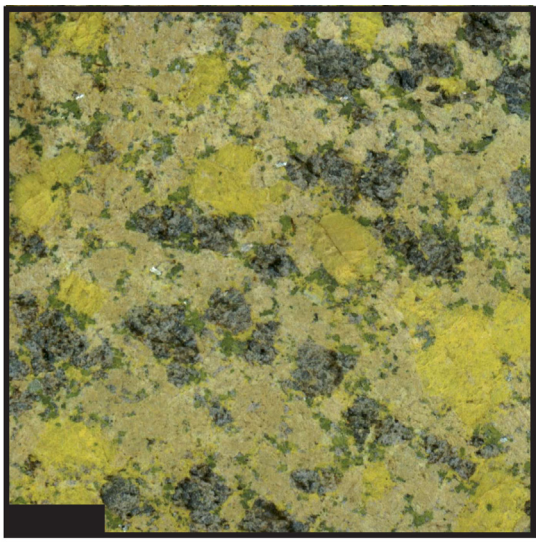


03-CH-123-b. Pyramid Mtn - biotite-muscovite monzogranite.

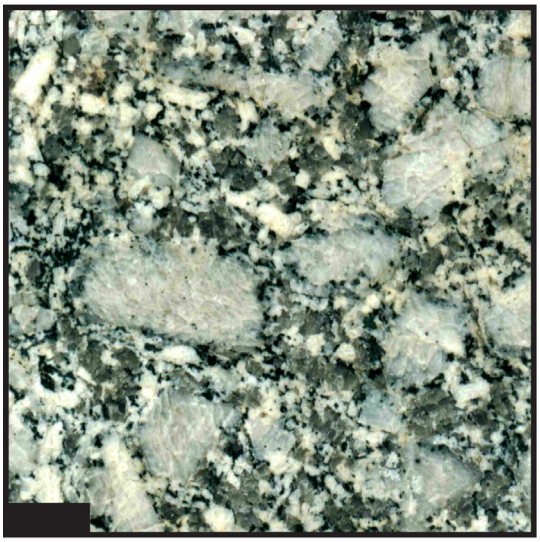
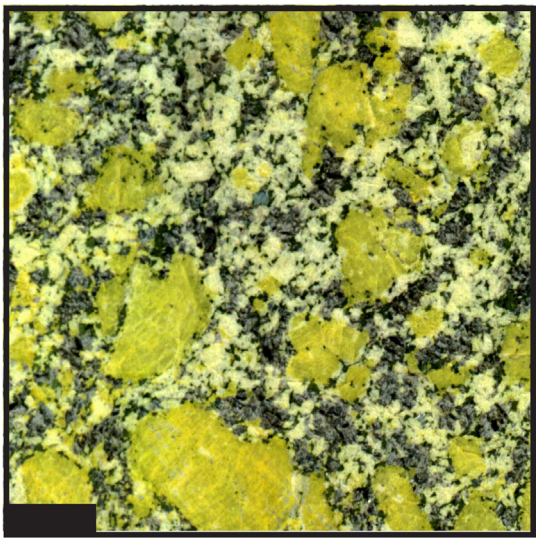


Appendix 2 contined.

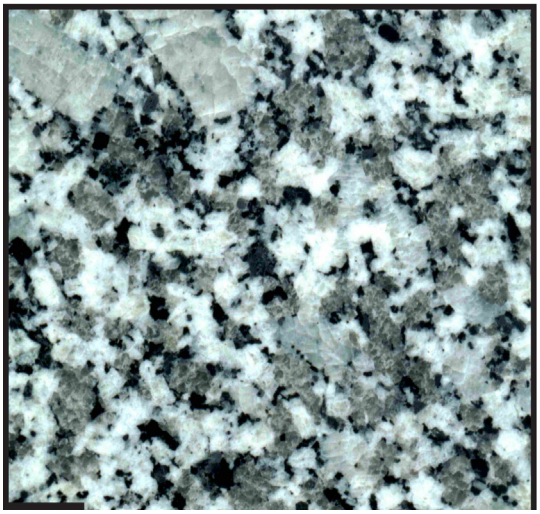
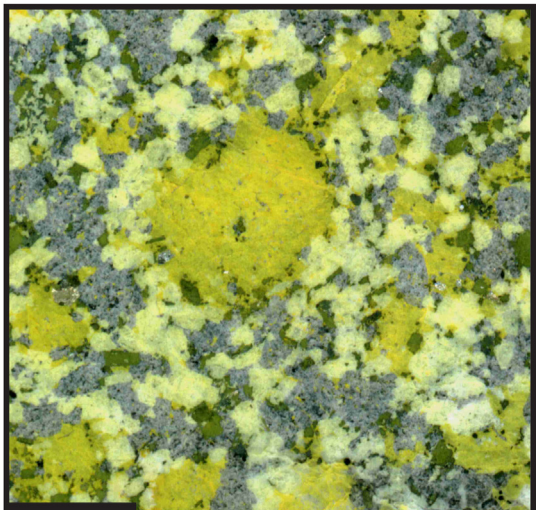
KR-05-04. Big Charlie - porphyritic (K-feldspar)-biotite-hornblende granodiorite.

KR-05-13. McLeod - porphyritic (K-feldspar)-biotite-hornblende granodiorite.

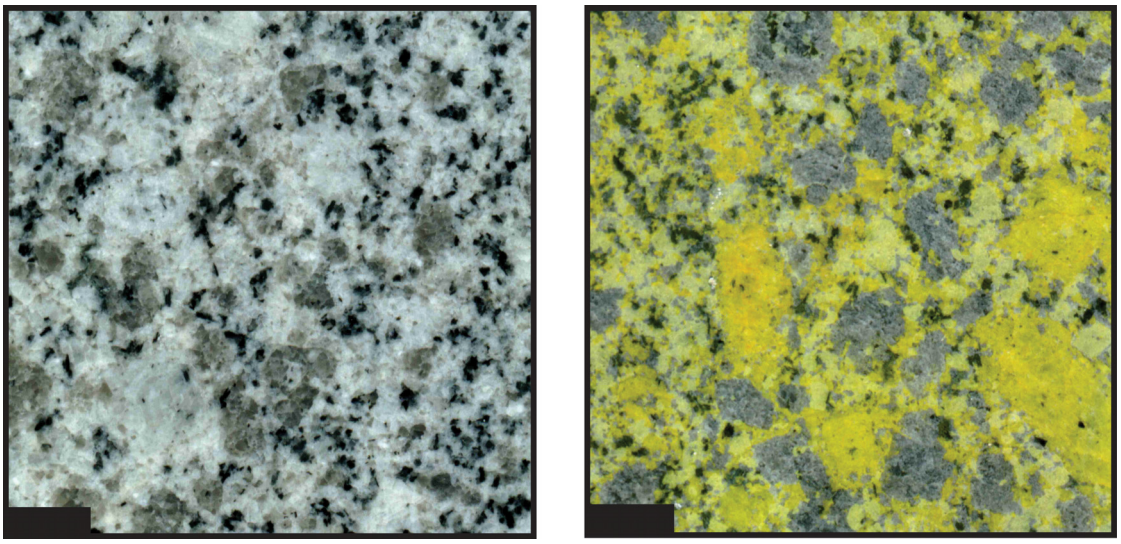



KR-05-200. Mt. Sir James McBrien - porphyritic (K-feldspar)-biotite-hornblende.

Appendix 2 contined.

KR-05-122. RUDI - porphyritic (K-feldspar)-biotite monzogranite.



Appendix 2 contined.

APPENDIX 3
ANALYTICAL METHODS

U-Pb Geochronology

Isotope Dilution Thermal Ionization Mass Spectrometry (ID-TIMS)

Zircon and other accessory phases were separated from samples using conventional crushing, grinding, and wilfley table techniques, followed by final concentration using heavy liquids and magnetic separations. Mineral fractions for analysis were selected based on grain quality, size, magnetic susceptibility and morphology. All zircon fractions were air-abraded prior to dissolution to minimize the effects of surface-correlated Pb-loss, using the technique of Krogh (1982).

Zircons were then washed with warm ultra-pure 3N HNO_3, (monazite grains were washed with 1N HNO_3), rinsed with ultra-pure water and sub-boiled acetone, and weighed (to ±2 μg). Zircons were dissolved in 300 μL PTFE or PFA microcapsules with ~100 μL of sub-boiled 29N HF and ~15 μL of sub-boiled 14N HNO_3 in the presence of a mixed $^{233\text{-}235}$U-205Pb tracer for 40 hours at 240°C. Dissolution took place in stainless steel Parr bombs with 250 mL teflon PTFE liners. Sample solutions were then dried to salts at approximately 125°C and re-bombed in ultra-pure ~200 μL 3.1N HCl for 12 hours at 210°C. Monazites were dissolved in approximately 1 mL of sub-boiled 6.2 N HCl for a minimum of 72 hours in 3.5 ml PFA screw top beakers on a hot plate at ~125°C, also in the presence of a mixed $^{233\text{-}235}$U-^{205}Pb tracer. These solutions (monazites) were then dried to salts on a hot plate at roughtly 125°C and redissolved in approximately 0.5 mL 3.1 HCl on a hot plate at around 125°C.

Lead and uranium separation for both zircon and monazite employed ion-exchange column techniques similar to those described by Parrish et al. (1987). Lead and uranium were eluted sequentially into the same beaker followed by the addition of approximately 10μL of 0.6N ultra-pure phosphoric acid. Each sample was loaded onto a single-zone refined rhenium filament using a phosphoric acid-silica gel emitter ($SiCl_4$). Isotopic ratios were measured using a modified single collector VG-54R thermal ionization mass spectrometer equipped with an analogue Daly photomultiplier. Both uranium and lead, respectively, were run at 1450°C, in peak-switching mode on the Daly detector. The uranium fractionation was determined directly on individual runs using the $^{233\text{-}235}$U tracer, and lead isotopic ratios were corrected for fractionation of 0.37%/amu, based on replicate analyses of the NBS-981 lead standard and the values recommended by Thirlwall (2000). Uranium analytical blanks were less than 1 pg, and lead less than 3 pg. Common lead isotopic compositions are derived from the model of Stacey and Kramers (1975), and all analytical errors were numerically propagated through the entire age calculation using the technique of Roddick (1987). Concordia intercept ages and associated errors were calculated using a modified version the York-II regression model (wherein the York-II errors are multiplied by the mean squared weighted deviates(MSWD)) and the algorithm of Ludwig (1980). All ages are quoted at the 2-sigma level of uncertainty. All sample preparation, analysis, and data reduction were done at the Pacific Centre for Isotopic and Geochemical Research (PCIGR), University of British Columbia.

Laser Ablation Inductively Coupled Plasma Mass Spectrometry (LA-ICP-MS)

Laser ablation inductively coupled plasma mass spectrometry (LA-ICP-MS) dating has recently been established as a routine procedure at the PCIGR, University of British Columbia. The following description of the method used for this study is modified from Mortensen et al. (2006; in press). Zircons were separated using conventional mineral separation methods (see ID-TIMS description), sectioned in an epoxy grain mount along with grains of internationally accepted standard zircon (FC-1, ca. 1100 Ma zircon standard, and Sakinaw, ca. 116 Ma in-house zircon standard), and brought to a 1 micron polish. The grains are examined using high-contrast back-scattered electron (BSE) imaging that makes it possible to detect the presence of altered zones or inherited cores within the zircon. The highest quality portions of each grain (free of fractures, alteration, inclusions, or cores) were selected for analysis. The surface of the mount was then washed for approximately 10 minutes with dilute nitric acid and rinsed in ultra-clean water.

Analyses were carried out using a New Wave 213 nm Nd-YAG laser coupled to a Thermo Finnigan Element2 hig- resolution ICP-MS. Ablation took place within a New Wave "Supercell" ablation chamber that is designed to achieve very high-efficiency entrainment of aerosols into the carrier gas. Helium was used as the carrier gas for all experiments. Gas flow rates, together with other parameters such as torch position, were optimized prior to beginning a series of analyses. Data was collected in mixed analog and ion-counting modes, with the strongest isotopic peaks (^{238}U and ^{232}Th) counted in analog mode, and the remaining weaker peaks in ion-counting mode (Mortensen et al., in press). The mixed modes have resulted in substantially stronger ion beams and much improved counting statistics, leading to better precision and accuracy on individual analyses (Mortensen et al., in press). A 15 to 25 micron spot with 60% laser power, and line scans (2 micron/s; 5 microns depth) were used rather than spot analyses in order to avoid within-run elemental

fraction. Each analysis consisted of a 7-second background measurement (laser off) followed by an approximately 28 second data acquisition period with the laser firing. Standard and unknown materials were analyzed at a ratio of approximately 1:1 to 1:2 for each sample.

Data were reduced using the GLITTER software package, developed by the GEMOC group at Macquarrie University, which can subtract background measurements, propagate all analytical errors, and calculate isotopic ratios and ages. This application generates a time-resolved record of each laser shot. The time-resolved signal from each line analysis was carefully examined, and portions of the signal that reflect the effects of post-crystallization lead-loss, or the presence of older inherited zircon cores were excluded from the calculation of the final isotopic ratios. Final ages for contiguous populations of relatively young (Phanerozoic) zircons were based on a weighted average of the calculated $^{206}Pb/^{238}U$ ages for 10 to 20 individual analyses for each sample. The final interpretation and plotting of the analytical results employed ISOPLOT 3.00 software (Ludwig, 2003). All sample preparation, analysis, and data reduction were done at the Pacific Centre for Isotopic and Geochemical Research (PCIGR), the University of British Columbia.

Ar-Ar Geochronology

Mineral separates were hand-picked, washed in acetone, dried, wrapped in aluminum foil, and stacked in an irradiation capsule with similar-age samples and neutron flux monitors (Fish Canyon Tuff sanidine, 28.02 Ma; Renne et al., 1998). The samples were irradiated on February 15 through 17, 2006 at the McMaster Nuclear Reactor in Hamilton, Ontario, for 90 MWH, with a neutron flux of approximately $3x10^{16}$ neutrons/cm^2. Analyses (n=57) of 19 neutron flux monitor positions produced errors of <0.5% in the J value.

The samples were analyzed on March 7 through 14, 2006, at the Noble Gas Laboratory, PCIGR, University of British Columbia, Vancouver, British Columbia. The mineral separates were step-heated at incrementally higher powers in the defocused beam of a 10W CO_2 laser (New Wave Research MIR10) until fused. The gas evolved from each step was analyzed by a VG5400 mass spectrometer equipped with an ion-counting electron multiplier. All measurements were corrected for total system blank, mass spectrometer sensitivity, mass discrimination, radioactive decay during and subsequent to irradiation, as well as interfering argon from atmospheric contamination and the irradiation of calcium, chlorine, and potassium. Isotope production ratios were: $(^{40}Ar/^{39}Ar)_K = 0.0302 \pm 0.00006$, $(^{37}Ar/^{39}Ar)_{Ca} = 1416.4 \pm 0.5$, $(^{36}Ar/^{39}Ar)_{Ca} = 0.3952 \pm 0.0004$, $Ca/K = 1.83 \pm 0.01(^{37}Ar_{Ca}/^{39}Ar_K)$.

The plateau and correlation ages were calculated using Isoplot ver.3.09 (Ludwig, 2003). Errors are quoted at the 2-sigma (95% confidence) level and are propagated from all sources except mass spectrometer sensitivity and age of the flux monitor. The best statistically-justified plateau and plateau age were picked based on the following criteria:

- Three or more contiguous steps comprising more than 50% of the ^{39}Ar;
- Probability of fit of the weighted mean age greater than 5%;
- Slope of the error-weighted line through the plateau ages equals zero at 5% confidence;
- Ages of the two outermost steps on a plateau are not significantly different from the weighted-mean plateau age (at 1.8 sigma, six or more steps only); and,
- Outermost two steps on either side of a plateau must not have nonzero slopes with the same sign (at 1.8 sigma, nine or more steps only).

All sample preparation, analysis, and data reduction were done at the Pacific Centre for Isotopic and Geochemical Research (PCIGR), the University of British Columbia.

Pb-Isotope Compositions

Pb-isotopic analysis followed the procedure described by Heffernan (2004), which is as follows. Sulphide grains were picked from handcrushed/ground grab samples of mineralization. Approximately 10 to 50 milligrams of sulphide minerals were leached in dilute HCl acid to remove surface contamination, then dissolved in dilute nitric acid. Samples of galena required no leaching and were directly dissolved in dilute hydrochloric acid. Relatively fresh, inclusion-free feldspar grains were picked from a >600 mesh crushed and ground separate, then reground and sieved to 100-200 mesh fraction. Plagioclase separates were first leached in dilute HCl, then in a mixture of dilute Hf and HBr, and subsequently dissolved in concentrated Hf.

Separation and purification of Pb from both sulphide and feldspar samples employed ion exchange column techniques. Samples were converted to bromide, the solution was passed through ion exchange columns in HBr and the lead was eluted in 6N HCl. The total procedural blank on the trace lead chemistry was 100 to 110 pg. Approximately 10 to 25 ng of the lead in chloride form was loaded onto a rhenium filament using a phosphoric acid-silica gel emitter, and isotopic compositions were determined on a Faraday collector in peak-switching mode using a modified VG54R thermal ionization mass spectrometer. The measured ratios were corrected for instrumental mass fractionation of 0.12%

per mass unit based on repeated measurements of the NBS SRM 981 standard and the values recommended by Thirwall (2000). Mass fractionation and analytical errors were numerically propagated throughout all calculations and are presented at the 2-sigma level. All Pb-isotopic sample preparation, geochemical separation, isotopic analysis, and data correction/reduction were done at the PCIGR, University of British Columbia.

Electron-Probe Micro-Analyzer (EPM) Techniques

Apatite

Apatite grains were separated from crushed material from each of the 25 felsic intrusions sampled in 2005 for geochemistry and geochronology, however apatite grains were only recovered from 24 samples. Between 5 and 20 large and relatively pristine (whole and unfractured, inclusion-free, etc.) apatite grains were selected from each sample for possible analysis. The grains were mounted in epoxy with the long axis of each grain parallel to the surface of the mount; in this orientation, the c-axis is perpendicular to the beam during EPM analysis. This orientation significantly reduces the degree of fluorine diffusion to the grain surface along the c-axis during analysis and minimizes inflated fluorine concentrations (Stormer et al., 1993).

The apatite grains were then analyzed in wavelength-dispersion mode on a fully automated CAMECA SX-50 instrument, operating in the wavelength-dispersion mode following a variation on the methods of Stormer et al. (1993) and Coulson et al. (2001); repeated short analyses (n=5 at 100 seconds each) were done on the same spot for each grain to track any increase in measured fluorine and to allow extrapolation back to initial fluorine concentrations. EPM analyses of apatite were done with the operating conditions in the following description. The matrix (cations) were analyzed with: an excitation voltage of 15 kV; a beam current of 10 nA; and spot diameter, 10 mm. Peak and background times, respectively, were 10 and 5 seconds for magnesium, aluminium, phosphorus, chlorine, calcium, manganese, iron, and strontium; 20 and 10 seconds for sulfur; and 50 and 25 seconds for fluorine. For the elements considered, the following standards, X-ray lines, and crystals were used to monitor data quality: topaz, F*Kα*, PC1 (W/Si); albite, Na*Kα*, TAP; grossular, Al*K*α, TAP; diopside, Mg*Kα*, TAP; apatite, PKa, TAP; apatite, CaKa, PET; barite, S*Kα*, PET; synthetic rhodonite, Mn*Kα*, LIF; synthetic fayalite, Fe*Kα*, LIF; and $SrTiO_3$, SrLa, TAP. A second pass on the same spot for chlorine and fluorine analysis used an excitation voltage of 10 kV, a beam current of 5 nA, a peak count time of 60 seconds, a background count time of 30 seconds, and a spot diameter of 10 mm. The following standards, X-ray lines, and crystals were used in the second pass: apatite, F*Kα*, PC1 (W/Si); scapolite, and Cl*Kα*, PET. Data reduction was done using the 'PAP' Φ(ρZ) (phi-rho-Z) method (Pouchou and Pichoir 1985). Detection limits for fluorine, chlorine, and sulphur were 0.04, 0.15, and 0.08 wt%, respectively. Between one and fifteen apatite grains from each sample were analyzed.

The fluorine concentration appears to increase very little, if at all, with time during EPM analysis. For any fluorine increase with time, the 5 spot analyses on each grain allowed apparent fluorine concentrations to be translated to actual *initial* fluorine concentrations at the beginning of the analysis (at t=0) using a linear regression to the initial concentration of fluorine (Stormer et al., 1993; Raudsepp, 1995). This linear regression permits the direct interpretation of halogen concentrations within the apatite grains for each of the intrusions. Analyses with anomalously high or low fluorine concentrations, or with inconsistent linear regressions were discarded; only analyses with the total weight percent of the components between 98.00 and 100.99% were used for plotting and interpretation purposes, except for sample KR-05-32 for which only one analysis was available. Analytical data used for interpretation are presented in Appendix 4. All sample preparation and micro-beam analysis were done at the University of British Columbia.

Biotite

Polished thin sections were obtained for each of the representative samples from 24 of the felsic intrusions sampled in 2005. Each section was examined in transmitted light on a microscope and in BSE mode on the SEM. Fresh, euhedral to subhedral, primary biotite grains (with c-axes parallel to the thin section) were analyzed on a fully automated CAMECA SX-50 instrument, operating in the wavelength-dispersion mode following the methods of Stormer et al. (1993) and Coulson et al. (2001).

At least five analyses of 120 seconds each were completed on 2 to 5 grains from each sample. EPM analyses of mica were done under the following operating conditions: an excitation voltage of 15 kV; a beam current of 10 nA; a spot diameter of 10 mm. Peak and background count times, respectively, were 40 and 20 seconds for fluorine and chlorine, and 20 and 10 seconds for all other elements. Data reduction was done using the 'PAP' Φ(ρZ) method (Pouchou and Pichoir, 1985). For the elements considered, the following standards, X-ray lines, and crystals were used: synthetic phlogopite, F*Kα*, PC1 (W/Si); albite, Na*Kα*, TAP; kyanite, Al*Kα*, TAP; synthetic phlogopite, Mg*Kα*, TAP; synthetic phlogopite, SiKa, TAP; scapolite, Cl*Kα*, PET; synthetic phlogopite, K*Kα*, PET; diopside, Ca*Kα*, PET; rutile, Ti*Kα*, PET; synthetic magne-

siochromite, Cr*Kα*, LIF; synthetic rhodonite, Mn*Kα*, LIF; synthetic fayalite, Fe*Kα*, LIF; and barite, BaLa, PET. Detection limits for fluorine and chlorine in biotite were 0.06 and 0.15 wt.%, respectively, and only analyses with the total weight percent of the components between 98.00 and 100.99% were used for plotting and interpretation purposes. Analytical data used for interpretation are presented in Appendix 5. All sample preparation and micro-beam analysis were done at the University of British Columbia.

Appendix 4. Apatite compositions for intrusions in the Nahanni MERA area. Compositions were calculated for eight cations; H_2O was determined by stoichiometry assuming 1 (F,OH,Cl). Activity ratios (log aHF/aCl) were calculated following the methods of Zhu and Sverjensky (1991, 1992); analytical details and standards are described in the Appendix 3 text.

	KR-05-08	KR-05-08	KR-05-08	KR-05-08	KR-05-08	KR-05-08	KR-05-08	KR-05-08	KR-05-08	KR-05-08	KR-05-08	KR-05-08	KR-05-08	KR-05-10
F	3.05	2.80	2.47	1.75	2.84	3.23	2.25	1.77	2.90	3.10	3.04	3.50	3.10	1.94
Cl	0.20	0.28	0.39	1.03	0.33	0.07	0.74	1.45	0.39	0.23	0.30	0.09	0.22	0.74
SO_3	0.01	0.04	0.04	0.12	0.05	0.04	0.21	0.23	0.12	0.08	0.08	0.06	0.06	0.16
CaO	55.09	55.15	55.34	54.13	54.72	54.56	54.34	54.28	54.98	55.54	55.29	55.60	55.02	53.77
P_2O_5	41.38	41.84	42.05	41.83	41.72	42.07	41.23	41.13	41.96	42.25	41.49	41.51	41.83	41.31
MgO	0.05	0.06	0.04	0.08	0.02	0.02	0.05	0.06	0.08	0.08	0.08	0.06	0.19	0.10
FeO	0.05	0.04	0.02	0.19	0.05	0.03	0.26	0.12	0.08	0.04	0.03	0.20	0.26	0.22
Al_2O_3	0.04	0.05	0.01	0.00	0.01	0.01	0.03	0.00	0.04	0.02	0.03	0.06	0.09	0.01
MnO	0.12	0.08	0.09	0.15	0.08	0.02	0.07	0.15	0.05	0.12	0.10	0.03	0.07	0.16
SrO	0.00	0.00	0.00	0.00	0.00	0.01	0.00	0.00	0.00	0.00	0.00	0.00	0.00	0.00
H_2O	0.27	0.38	0.51	0.67	0.33	0.22	0.50	0.54	0.30	0.26	0.26	0.10	0.26	0.64
O=F	-1.28	-1.18	-1.04	-0.74	-1.20	-1.36	-0.95	-0.75	-1.22	-1.31	-1.28	-1.47	-1.31	-0.82
O=Cl	-0.05	-0.06	-0.09	-0.23	-0.07	-0.02	-0.17	-0.33	-0.09	-0.05	-0.07	-0.02	-0.05	-0.17
Total	98.93	99.48	99.83	98.98	98.88	98.90	98.57	98.66	99.59	100.37	99.35	99.72	99.74	98.06
F^-	0.818	0.747	0.657	0.472	0.763	0.868	0.608	0.479	0.774	0.820	0.812	0.931	0.825	0.527
Cl^-	0.029	0.040	0.056	0.149	0.048	0.010	0.107	0.210	0.056	0.033	0.043	0.013	0.031	0.108
S^{6+}	0.001	0.003	0.003	0.008	0.003	0.003	0.013	0.015	0.008	0.005	0.005	0.004	0.004	0.010
Ca^{2+}	5.006	4.987	4.989	4.941	4.982	4.965	4.972	4.978	4.971	4.979	5.005	5.011	4.960	4.946
P^{5+}	2.971	2.989	2.995	3.017	3.002	3.025	2.981	2.980	2.998	2.993	2.968	2.956	2.980	3.002
Mg^{2+}	0.006	0.008	0.005	0.010	0.003	0.003	0.006	0.008	0.010	0.010	0.010	0.008	0.024	0.013
Fe^{2+}	0.004	0.003	0.001	0.014	0.004	0.002	0.019	0.009	0.006	0.003	0.002	0.014	0.018	0.016
Al_{3+}	0.004	0.005	0.001	0.000	0.001	0.001	0.003	0.000	0.004	0.002	0.003	0.006	0.009	0.001
Mn^{2+}	0.009	0.006	0.006	0.011	0.006	0.001	0.005	0.011	0.004	0.009	0.007	0.002	0.005	0.012
Sr^{2+}	0.000	0.000	0.000	0.000	0.000	0.000	0.000	0.000	0.000	0.000	0.000	0.000	0.000	0.000
H^+	0.153	0.213	0.287	0.380	0.189	0.122	0.285	0.311	0.170	0.147	0.145	0.056	0.144	0.366
O^{2-}	12.113	12.204	12.285	12.420	12.198	12.165	12.285	12.311	12.184	12.147	12.108	12.000	12.125	12.390
log a_{HF}/a_{HCl}	-0.110	-0.289	-0.491	-1.059	-0.359	0.379	-0.805	-1.202	-0.419	-0.165	-0.284	0.295	-0.135	-0.872

Appendix 4 continued.

	KR-05-10	KR-05-10	KR-05-10	KR-05-10	KR-05-22	KR-05-22	KR-05-22	KR-05-22	KR-05-22	KR-05-26	KR-05-26	KR-05-26	KR-05-26	KR-05-26
F	1.90	1.86	1.86	1.96	3.43	3.47	3.40	3.44	3.38	3.86	3.88	3.94	3.82	3.85
Cl	0.67	0.74	0.73	0.70	0.22	0.18	0.21	0.22	0.26	0.07	0.08	0.05	0.06	0.06
SO_3	0.18	0.14	0.10	0.14	0.06	0.09	0.02	0.01	0.05	0.06	0.03	0.04	0.05	0.03
CaO	54.52	54.74	54.27	54.13	53.97	54.35	54.45	53.69	54.20	53.79	53.61	54.12	54.33	54.31
P_2O_5	41.72	41.90	41.99	41.91	41.59	41.66	41.69	41.95	41.92	41.60	41.63	42.12	42.05	40.95
MgO	0.13	0.08	0.12	0.12	0.06	0.03	0.04	0.02	0.09	0.07	0.07	0.05	0.03	0.08
FeO	0.20	0.22	0.19	0.15	0.04	0.01	0.05	0.07	0.04	0.15	0.11	0.14	0.11	0.13
Al_2O_3	0.02	0.01	0.00	0.01	0.02	0.03	0.01	0.00	0.01	0.02	0.02	0.01	0.01	0.02
MnO	0.11	0.21	0.12	0.13	0.20	0.12	0.13	0.16	0.17	0.19	0.24	0.18	0.21	0.28
SrO	0.00	0.00	0.00	0.01	0.00	0.00	0.00	0.00	0.00	0.00	0.01	0.00	0.01	0.00
H_2O	0.70	0.71	0.70	0.65	0.07	0.07	0.09	0.06	0.09	0.00	0.00	0.00	0.00	0.00
O=F	-0.80	-0.78	-0.78	-0.83	-1.44	-1.46	-1.43	-1.45	-1.42	-1.63	-1.63	-1.66	-1.61	-1.62
O=Cl	-0.15	-0.17	-0.16	-0.16	-0.05	-0.04	-0.05	-0.05	-0.06	-0.02	-0.02	-0.01	-0.01	-0.01
Total	99.20	99.65	99.13	98.93	98.16	98.50	98.61	98.12	98.73	98.17	98.03	98.98	99.06	98.08
F^-	0.510	0.497	0.500	0.527	0.929	0.936	0.916	0.933	0.911	1.044	1.051	1.057	1.025	1.041
Cl^-	0.096	0.106	0.105	0.101	0.032	0.026	0.030	0.032	0.038	0.010	0.012	0.007	0.009	0.009
S^{6+}	0.011	0.009	0.006	0.009	0.004	0.006	0.001	0.001	0.003	0.004	0.002	0.003	0.003	0.002
Ca^{2+}	4.953	4.954	4.938	4.935	4.953	4.969	4.972	4.934	4.946	4.930	4.921	4.920	4.938	4.975
P^{5+}	2.995	2.996	3.019	3.019	3.016	3.009	3.008	3.046	3.023	3.013	3.019	3.026	3.020	2.964
Mg^{2+}	0.016	0.010	0.015	0.015	0.008	0.004	0.005	0.003	0.011	0.009	0.009	0.006	0.004	0.010
Fe^{2+}	0.014	0.016	0.013	0.011	0.003	0.001	0.004	0.005	0.003	0.011	0.008	0.010	0.008	0.009
Al_{3+}	0.002	0.001	0.000	0.001	0.002	0.003	0.001	0.000	0.001	0.002	0.002	0.001	0.001	0.002
Mn^{2+}	0.008	0.015	0.009	0.009	0.015	0.009	0.009	0.012	0.012	0.014	0.017	0.013	0.015	0.020
Sr^{2+}	0.000	0.000	0.000	0.000	0.000	0.000	0.000	0.000	0.000	0.000	0.000	0.000	0.000	0.000
H^+	0.394	0.397	0.395	0.372	0.039	0.038	0.053	0.035	0.052	0.000	0.000	0.000	0.000	0.000
O^{2-}	12.410	12.409	12.436	12.419	12.071	12.065	12.068	12.105	12.093	11.982	11.981	11.990	12.009	11.910
log a_{HF}/a_{HCl}	-0.835	-0.889	-0.882	-0.843	-0.097	-0.004	-0.075	-0.095	-0.180	0.459	0.382	0.619	0.496	0.503

Appendix 4 continued.

	KR-05-26	KR-05-26	KR-05-32	KR-05-43	KR-05-43	KR-05-43	KR-05-62	KR-05-62	KR-05-62	KR-05-62	KR-05-68	KR-05-68	KR-05-68	KR-05-97b
F	3.85	3.90	3.81	2.90	2.82	2.81	3.30	3.30	3.31	3.36	3.47	3.54	3.50	3.80
Cl	0.06	0.04	0.03	0.07	0.16	0.22	0.16	0.10	0.12	0.12	0.10	0.09	0.09	0.10
SO_3	0.01	0.06	0.01	0.08	0.09	0.09	0.08	0.02	0.12	0.02	0.01	0.03	0.02	0.01
CaO	54.51	54.87	53.45	54.50	53.81	54.74	55.73	55.67	55.56	55.57	53.72	53.57	53.30	54.83
P_2O_5	40.86	41.39	41.61	41.81	41.97	41.91	41.38	41.34	40.96	41.71	42.23	42.39	41.73	41.78
MgO	0.11	0.06	0.03	0.01	0.02	0.03	0.07	0.12	0.08	0.10	0.09	0.10	0.07	0.01
FeO	0.09	0.11	0.07	0.04	0.04	0.05	0.05	0.04	0.09	0.08	0.39	0.41	0.27	0.05
Al_2O_3	0.05	0.02	0.00	0.02	0.01	0.01	0.04	0.07	0.06	0.06	0.01	0.01	0.01	0.02
MnO	0.21	0.18	0.44	0.04	0.16	0.17	0.03	0.08	0.08	0.03	0.48	0.56	0.52	0.10
SrO	0.01	0.00	0.00	0.00	0.00	0.00	0.00	0.00	0.00	0.00	0.00	0.00	0.00	0.00
H_2O	0.00	0.00	0.00	0.37	0.37	0.38	0.18	0.19	0.17	0.16	0.09	0.07	0.06	0.00
O=F	-1.62	-1.64	-1.60	-1.22	-1.19	-1.18	-1.39	-1.39	-1.39	-1.41	-1.46	-1.49	-1.47	-1.60
O=Cl	-0.01	-0.01	-0.01	-0.02	-0.04	-0.05	-0.04	-0.02	-0.03	-0.03	-0.02	-0.02	-0.02	-0.02
Total	98.13	98.98	97.84	98.60	98.23	99.18	99.59	99.52	99.13	99.77	99.11	99.25	98.08	99.08
F^-	1.040	1.045	1.035	0.781	0.763	0.753	0.879	0.879	0.885	0.893	0.932	0.950	0.950	1.018
Cl^-	0.009	0.006	0.004	0.010	0.023	0.032	0.023	0.014	0.017	0.017	0.014	0.013	0.013	0.014
S^{6+}	0.001	0.004	0.001	0.005	0.006	0.006	0.005	0.001	0.008	0.001	0.001	0.002	0.001	0.001
Ca^{2+}	4.988	4.981	4.919	4.972	4.935	4.968	5.027	5.022	5.033	5.005	4.888	4.870	4.900	4.978
P^{5+}	2.954	2.969	3.026	3.014	3.041	3.005	2.949	2.946	2.932	2.968	3.036	3.045	3.031	2.997
Mg^{2+}	0.014	0.008	0.004	0.001	0.003	0.004	0.009	0.015	0.010	0.013	0.011	0.013	0.009	0.001
Fe^{2+}	0.006	0.008	0.005	0.003	0.003	0.004	0.004	0.003	0.006	0.006	0.028	0.029	0.019	0.004
Al_{3+}	0.005	0.002	0.000	0.002	0.001	0.001	0.004	0.007	0.006	0.006	0.001	0.001	0.001	0.002
Mn^{2+}	0.015	0.013	0.032	0.003	0.012	0.012	0.002	0.006	0.006	0.002	0.035	0.040	0.038	0.007
Sr^{2+}	0.000	0.000	0.000	0.000	0.000	0.000	0.000	0.000	0.000	0.000	0.000	0.000	0.000	0.000
H^+	0.000	0.000	0.000	0.209	0.213	0.216	0.098	0.107	0.098	0.090	0.054	0.037	0.037	0.000
O^{2-}	11.895	11.919	12.007	12.241	12.287	12.236	12.035	12.033	12.013	12.047	12.110	12.109	12.087	11.970
log a_{HF}/a_{HCl}	0.503	0.681	0.333	-0.039	-0.188	0.022	0.238	0.156	0.160	0.263	0.304	0.304		0.302

Appendix 4 continued.

	KR-05-97b	KR-05-97b	KR-05-97b	KR-05-97b	KR-05-110	KR-05-110	KR-05-110	KR-05-113	KR-05-113	KR-05-113	KR-05-113	KR-05-126	KR-05-126	KR-05-126
F	3.69	3.78	3.67	3.68	3.79	3.75	3.78	3.42	3.35	3.57	3.48	3.93	3.98	3.85
Cl	0.21	0.15	0.15	0.09	0.01	0.03	0.00	0.22	0.16	0.10	0.14	0.04	0.04	0.06
SO_3	0.01	0.01	0.03	0.03	0.08	0.02	0.03	0.04	0.03	0.04	0.01	0.03	0.02	0.03
CaO	54.92	55.08	55.04	55.43	53.69	54.13	54.13	54.44	53.88	55.39	55.48	55.48	55.42	55.47
P_2O_5	41.20	40.77	40.75	41.44	41.66	42.37	42.26	42.28	42.55	41.95	42.06	41.78	41.52	41.77
MgO	0.07	0.08	0.04	0.09	0.01	0.01	0.02	0.01	0.01	0.06	0.11	0.13	0.09	0.10
FeO	0.08	0.07	0.01	0.01	0.13	0.06	0.07	0.09	0.11	0.03	0.02	0.14	0.11	0.20
Al_2O_3	0.02	0.05	0.03	0.05	0.01	0.00	0.01	0.00	0.01	0.03	0.04	0.06	0.04	0.05
MnO	0.07	0.10	0.03	0.09	0.22	0.17	0.15	0.06	0.11	0.09	0.10	0.17	0.11	0.11
SrO	0.00	0.00	0.00	0.01	0.00	0.00	0.00	0.00	0.01	0.00	0.01	0.00	0.00	0.00
H_2O	0.00	0.00	0.00	0.01	0.00	0.00	0.00	0.09	0.13	0.06	0.10	0.00	0.00	0.00
O=F	-1.55	-1.59	-1.55	-1.55	-1.60	-1.58	-1.59	-1.44	-1.41	-1.50	-1.47	-1.65	-1.68	-1.62
O=Cl	-0.05	-0.03	-0.03	-0.02	0.00	-0.01	0.00	-0.05	-0.04	-0.02	-0.03	-0.01	-0.01	-0.01
Total	98.67	98.46	98.17	99.36	98.00	98.95	98.86	99.16	98.91	99.80	100.05	100.10	99.65	100.01
F^-	0.992	1.017	0.991	0.982	1.028	1.008	1.016	0.918	0.902	0.950	0.923	1.041	1.058	1.021
Cl^-	0.030	0.022	0.022	0.013	0.001	0.004	0.000	0.032	0.023	0.014	0.020	0.006	0.006	0.009
S^{6+}	0.001	0.001	0.002	0.002	0.005	0.001	0.002	0.003	0.002	0.003	0.001	0.002	0.001	0.002
Ca^{2+}	5.004	5.022	5.036	5.013	4.933	4.929	4.931	4.949	4.914	4.991	4.986	4.977	4.992	4.984
P^{5+}	2.966	2.937	2.946	2.961	3.024	3.048	3.042	3.037	3.066	2.987	2.987	2.962	2.955	2.965
Mg^{2+}	0.009	0.010	0.005	0.011	0.001	0.001	0.003	0.001	0.001	0.008	0.014	0.016	0.011	0.013
Fe^{2+}	0.006	0.005	0.001	0.001	0.009	0.004	0.005	0.006	0.008	0.002	0.001	0.010	0.008	0.014
Al_{3+}	0.002	0.005	0.003	0.005	0.001	0.000	0.001	0.000	0.001	0.003	0.004	0.006	0.004	0.005
Mn^{2+}	0.005	0.007	0.002	0.006	0.016	0.012	0.011	0.004	0.008	0.006	0.007	0.012	0.008	0.008
Sr^{2+}	0.000	0.000	0.000	0.000	0.000	0.000	0.000	0.000	0.000	0.000	0.000	0.000	0.000	0.000
H^+	0.000	0.000	0.000	0.005	0.000	0.000	0.000	0.051	0.075	0.036	0.057	0.000	0.000	0.000
O^{2-}	11.932	11.877	11.914	11.953	12.023	12.065	12.053	12.111	12.178	12.023	12.040	11.910	11.884	11.930
log a_{HF}/a_{HCl}	-0.041	0.105	0.094	0.318	1.452	0.841	n/a	-0.102	0.033	0.272	0.104	0.679	0.686	0.495

Appendix 4 continued.

	KR-05-130	KR-05-130	KR-05-136	KR-05-136	KR-05-136	KR-05-136	KR-05-136	KR-05-136	KR-05-143	KR-05-143	KR-05-143	KR-05-148	KR-05-148	KR-05-148
F	2.57	2.63	3.22	3.24	3.20	3.22	3.09	3.08	3.81	3.80	3.76	3.74	3.73	3.80
Cl	0.97	0.45	0.20	0.25	0.23	0.26	0.24	0.24	0.05	0.09	0.06	0.10	0.09	0.06
SO_3	0.02	0.02	0.02	0.04	0.02	0.02	0.01	0.05	0.02	0.02	0.06	0.01	0.03	0.02
CaO	55.32	54.67	53.97	54.61	54.64	54.30	55.50	55.34	53.97	53.54	53.62	52.88	53.43	53.16
P_2O_5	41.32	41.62	42.45	42.34	42.52	41.59	41.33	41.45	41.73	41.35	41.49	42.16	42.14	41.80
MgO	0.08	0.11	0.06	0.03	0.05	0.04	0.12	0.08	0.08	0.07	0.09	0.07	0.07	0.06
FeO	0.03	0.07	0.08	0.07	0.03	0.09	0.08	0.08	0.23	0.31	0.30	0.41	0.39	0.30
Al_2O_3	0.04	0.06	0.03	0.01	0.01	0.02	0.05	0.04	0.01	0.01	0.02	0.03	0.02	0.02
MnO	0.08	0.11	0.09	0.13	0.09	0.16	0.11	0.21	0.39	0.45	0.44	0.82	0.93	0.82
SrO	0.00	0.00	0.00	0.00	0.00	0.00	0.00	0.00	0.00	0.00	0.00	0.00	0.00	0.01
H_2O	0.31	0.40	0.18	0.17	0.20	0.16	0.25	0.26	0.00	0.00	0.00	0.00	0.00	0.00
O=F	-1.08	-1.11	-1.36	-1.36	-1.35	-1.36	-1.30	-1.30	-1.60	-1.60	-1.58	-1.57	-1.57	-1.60
O=Cl	-0.22	-0.10	-0.05	-0.06	-0.05	-0.06	-0.05	-0.05	-0.01	-0.02	-0.01	-0.02	-0.02	-0.01
Total	99.44	98.94	98.90	99.47	99.59	98.45	99.43	99.47	98.67	98.02	98.24	98.62	99.24	98.44
F^-	0.688	0.706	0.866	0.866	0.855	0.869	0.824	0.822	1.026	1.030	1.017	1.011	1.001	1.028
Cl^-	0.139	0.065	0.029	0.036	0.033	0.038	0.034	0.034	0.007	0.013	0.009	0.014	0.013	0.009
S^{6+}	0.001	0.001	0.001	0.003	0.001	0.001	0.001	0.003	0.001	0.001	0.004	0.001	0.002	0.001
Ca^{2+}	5.016	4.974	4.919	4.948	4.943	4.967	5.015	5.002	4.924	4.918	4.915	4.841	4.860	4.870
P^{5+}	2.960	2.992	3.057	3.031	3.040	3.006	2.951	2.960	3.008	3.001	3.005	3.050	3.028	3.026
Mg^{2+}	0.010	0.014	0.008	0.004	0.006	0.005	0.015	0.010	0.010	0.009	0.011	0.009	0.009	0.008
Fe^{2+}	0.002	0.005	0.006	0.005	0.002	0.006	0.006	0.006	0.016	0.022	0.021	0.029	0.028	0.021
Al_{3+}	0.004	0.006	0.003	0.001	0.001	0.002	0.005	0.004	0.001	0.001	0.002	0.003	0.002	0.002
Mn^{2+}	0.006	0.008	0.006	0.009	0.006	0.012	0.008	0.015	0.028	0.033	0.032	0.059	0.067	0.059
Sr^{2+}	0.000	0.000	0.000	0.000	0.000	0.000	0.000	0.000	0.000	0.000	0.000	0.000	0.000	0.000
H^+	0.173	0.229	0.105	0.098	0.113	0.093	0.142	0.144	0.000	0.000	0.000	0.000	0.000	0.000
O^{2-}	12.118	12.222	12.194	12.150	12.175	12.106	12.071	12.093	11.987	11.969	11.995	12.056	12.035	12.012
log a_{HF}/a_{HCl}	-0.865	-0.524	-0.085	-0.179	-0.147	-0.201	-0.176	-0.177	0.606	0.339	0.493	0.299	0.326	0.498

Appendix 4 continued.

	KR-05-148	KR-05-164	KR-05-175	KR-05-175	KR-05-175	KR-05-175	KR-05-191	KR-05-191	KR-05-191	KR-05-194	KR-05-194	KR-05-194	KR-05-194	KR-05-194
F	3.83	3.69	3.63	3.62	3.66	3.71	3.47	3.43	3.28	3.88	3.89	3.88	3.82	3.84
Cl	0.04	0.09	0.04	0.06	0.02	0.01	0.19	0.31	0.32	0.05	0.04	0.02	0.03	0.03
SO_3	0.03	0.01	0.02	0.01	0.01	0.02	0.12	0.10	0.30	0.03	0.03	0.02	0.03	0.03
CaO	54.16	52.57	53.16	53.52	53.86	53.96	54.09	54.18	54.40	54.62	54.46	54.62	54.90	54.71
P_2O_5	41.06	41.47	42.08	41.53	41.91	41.45	41.86	41.75	40.73	42.22	42.07	41.85	41.34	41.21
MgO	0.12	0.06	0.06	0.05	0.05	0.05	0.04	0.04	0.04	0.02	0.03	0.02	0.01	0.06
FeO	0.31	0.60	0.25	0.20	0.26	0.21	0.09	0.05	0.17	0.04	0.05	0.06	0.04	0.06
Al_2O_3	0.06	0.00	0.03	0.02	0.01	0.00	0.01	0.01	0.01	0.02	0.01	0.02	0.00	0.05
MnO	0.91	1.26	0.59	0.67	0.66	0.66	0.24	0.20	0.21	0.20	0.10	0.17	0.08	0.12
SrO	0.00	0.00	0.00	0.00	0.00	0.00	0.00	0.00	0.00	0.00	0.00	0.00	0.00	0.00
H_2O	0.00	0.00	0.02	0.02	0.02	0.00	0.06	0.05	0.11	0.00	0.00	0.00	0.00	0.00
O=F	-1.61	-1.55	-1.53	-1.52	-1.54	-1.56	-1.46	-1.44	-1.38	-1.63	-1.64	-1.63	-1.61	-1.62
O=Cl	-0.01	-0.02	-0.01	-0.01	0.00	0.00	-0.04	-0.07	-0.07	-0.01	-0.01	0.00	-0.01	-0.01
Total	98.90	98.18	98.34	98.16	98.92	98.51	98.67	98.61	98.12	99.43	99.03	99.02	98.63	98.49
F^-	1.028	1.002	0.983	0.981	0.985	1.001	0.936	0.926	0.889	1.036	1.043	1.040	1.027	1.034
Cl^-	0.006	0.013	0.006	0.009	0.003	0.001	0.027	0.045	0.046	0.007	0.006	0.003	0.004	0.004
S^{6+}	0.002	0.001	0.001	0.001	0.001	0.001	0.008	0.006	0.019	0.002	0.002	0.001	0.002	0.002
Ca^{2+}	4.927	4.837	4.877	4.915	4.908	4.934	4.941	4.954	4.993	4.943	4.947	4.960	5.002	4.990
P^{5+}	2.951	3.015	3.050	3.013	3.018	2.995	3.021	3.016	2.954	3.019	3.019	3.003	2.976	2.970
Mg^{2+}	0.015	0.008	0.008	0.006	0.006	0.006	0.005	0.005	0.005	0.003	0.004	0.003	0.001	0.008
Fe^{2+}	0.022	0.043	0.018	0.014	0.018	0.015	0.006	0.004	0.012	0.003	0.004	0.004	0.003	0.004
Al_{3+}	0.006	0.000	0.003	0.002	0.001	0.000	0.001	0.001	0.001	0.002	0.001	0.002	0.000	0.005
Mn^{2+}	0.065	0.092	0.043	0.049	0.048	0.048	0.017	0.014	0.015	0.014	0.007	0.012	0.006	0.009
Sr^{2+}	0.000	0.000	0.000	0.000	0.000	0.000	0.000	0.000	0.000	0.000	0.000	0.000	0.000	0.000
H^+	0.000	0.000	0.011	0.010	0.013	0.000	0.037	0.030	0.065	0.000	0.000	0.000	0.000	0.000
O^{2-}	11.905	12.011	12.091	12.032	12.041	11.992	12.085	12.067	12.035	11.997	11.993	11.972	11.941	11.929
log a_{HF}/a_{HCl}	0.674	0.327	0.654	0.477	0.956	1.440	-0.020	-0.247	-0.274	0.610	0.680	0.980	0.850	0.852

Appendix 4 continued.

	KR-05-196	KR-05-198	KR-05-198	KR-05-198	KR-05-198	KR-05-198	KR-05-198	KR-05-208	KR-05-210	KR-05-210
F	3.16	3.81	3.79	3.87	3.87	3.85	3.82	3.75	3.77	3.85
Cl	0.47	0.04	0.03	0.01	0.03	0.04	0.04	0.03	0.01	0.02
SO_3	0.04	0.01	0.00	0.00	0.01	0.02	0.00	0.01	0.02	0.02
CaO	53.90	54.23	54.30	54.41	54.70	55.17	55.11	53.23	52.76	53.89
P_2O_5	41.78	41.90	41.92	42.28	41.97	41.74	41.33	41.73	41.95	41.73
MgO	0.05	0.02	0.04	0.02	0.11	0.07	0.10	0.09	0.06	0.06
FeO	0.08	0.05	0.03	0.07	0.06	0.06	0.04	0.19	0.41	0.12
Al_2O_3	0.01	0.01	0.01	0.01	0.04	0.03	0.06	0.04	0.01	0.02
MnO	0.20	0.12	0.10	0.07	0.12	0.10	0.16	1.47	2.00	0.77
SrO	0.00	0.00	0.00	0.00	0.00	0.00	0.00	0.00	0.00	0.00
H_2O	0.13	0.00	0.00	0.00	0.00	0.00	0.00	0.00	0.00	0.00
O=F	-1.33	-1.60	-1.60	-1.63	-1.63	-1.62	-1.61	-1.58	-1.59	-1.62
O=Cl	-0.11	-0.01	-0.01	0.00	-0.01	-0.01	-0.01	-0.01	0.00	0.00
Total	98.39	98.58	98.62	99.11	99.27	99.45	99.04	98.95	99.40	98.85
F^-	0.855	1.027	1.021	1.037	1.034	1.027	1.022	1.009	1.012	1.035
Cl^-	0.068	0.006	0.004	0.001	0.004	0.006	0.006	0.004	0.001	0.003
S^{6+}	0.003	0.001	0.000	0.000	0.001	0.001	0.000	0.001	0.001	0.001
Ca^{2+}	4.943	4.951	4.954	4.940	4.953	4.985	4.997	4.854	4.798	4.909
P^{5+}	3.027	3.022	3.022	3.033	3.003	2.980	2.961	3.006	3.014	3.004
Mg^{2+}	0.006	0.003	0.005	0.003	0.014	0.009	0.013	0.011	0.008	0.008
Fe^{2+}	0.006	0.004	0.002	0.005	0.004	0.004	0.003	0.014	0.029	0.009
Al_{3+}	0.001	0.001	0.001	0.001	0.004	0.003	0.006	0.004	0.001	0.002
Mn^{2+}	0.014	0.009	0.007	0.005	0.009	0.007	0.011	0.106	0.144	0.055
Sr^{2+}	0.000	0.000	0.000	0.000	0.000	0.000	0.000	0.000	0.000	0.000
H^+	0.076	0.000	0.000	0.000	0.000	0.000	0.000	0.000	0.000	0.000
O^{2-}	12.123	12.008	12.013	12.018	11.975	11.947	11.921	12.002	12.014	11.977
log a_{HF}/a_{HCl}	-0.461	0.673	0.847	1.456	0.852	0.673	0.671	0.842	1.445	0.978

Appendix 5. Biotite compositions for intrusions in the Nahanni MERA area. Compositions were calculated for 18 cations following Deer, Howie, and Zussman (1992), H_2O is from stoichiometry, and Ca and Cr were not detected. Activity ratios (log a_{HF}/a_{Cl}) were calculated following the methods of Zhu and Sverjensky (1991, 1992); Aaalytical details and standards are described in the text.

	KR-05-22	KR-05-22	KR-05-22	KR-05-22	KR-05-22	KR-05-26	KR-05-26	KR-05-26	KR-05-26	KR-05-26	KR-05-43	KR-05-43	KR-05-43	KR-05-43	KR-05-43	KR-05-62	KR-05-62	KR-05-62
F	0.54	0.69	0.6	0.62	0.51	1.06	1.08	1.07	0.75	0.52	0.08	0.11	0.1	0.11	0.1	0.3	0.46	0.42
Na_2O	0.07	0.08	0.05	0.12	0.08	0.09	0.13	0.17	0.09	0	0.12	0.06	0.08	0.03	0.08	0.05	0.07	0.1
MgO	11.95	12.95	13.1	12.94	12.4	6.42	6.68	6.22	6.38	5.75	11.79	11.93	12.08	12.07	11.84	10.63	11.32	11.18
Al_2O_3	13.98	13.72	13.59	13.6	13.95	12.73	12.91	12.76	13.04	13.62	14.18	13.99	14.12	13.92	14.44	14.42	14.11	14.36
SiO_2	36.63	37.62	37.47	37.58	37.62	35.89	35.73	36.11	35.96	34.96	36.55	37.48	37.01	37.5	36.99	37.46	38.31	37.31
Cl	0.22	0.19	0.21	0.15	0.2	0.28	0.29	0.26	0.41	0.39	0.1	0.03	0.04	0.03	0.08	0.08	0.05	0.1
K_2O	9.68	10.18	9.73	9.72	9.61	9.19	9.25	9.02	9.18	8.34	9.72	9.88	9.69	9.63	9.58	9.9	9.94	9.62
TiO_2	4.24	3.76	4.17	4.35	4.3	4	3.55	4.11	3.54	2.28	3.99	3.89	4	3.79	3.77	3.67	3.72	3.83
MnO	0.43	0.45	0.47	0.49	0.47	1.29	1.35	1.33	1.22	0.98	0.47	0.42	0.48	0.36	0.43	0.3	0.16	0.22
FeO	19.12	17.57	17.63	17.75	19.04	26.57	26.87	27.39	26.15	29.28	19.55	18.78	18.97	18.93	18.7	20.77	18.69	19.67
H_2O	1.72	1.73	1.73	1.73	1.74	1.64	1.65	1.66	1.64	1.62	1.72	1.72	1.72	1.72	1.71	1.72	1.72	1.71
O=F	-0.23	-0.29	-0.25	-0.26	-0.21	-0.45	-0.45	-0.45	-0.32	-0.22	-0.03	-0.05	-0.04	-0.05	-0.04	-0.13	-0.19	-0.18
O=Cl	-0.05	-0.04	-0.05	-0.03	-0.05	-0.06	-0.07	-0.06	-0.09	-0.09	-0.02	-0.01	-0.01	-0.01	-0.02	-0.02	-0.01	-0.02
Total	98.31	98.61	98.51	98.81	99.66	98.73	98.98	99.6	98	97.46	98.23	98.24	98.32	98.05	97.72	99.19	98.36	98.34
F^-	0.299	0.377	0.329	0.339	0.278	0.611	0.619	0.613	0.434	0.304	0.044	0.061	0.055	0.061	0.055	0.165	0.254	0.232
Na^+	0.024	0.027	0.017	0.04	0.027	0.032	0.046	0.06	0.032	0	0.041	0.02	0.027	0.01	0.027	0.017	0.024	0.034
Mg^{2+}	3.114	3.337	3.385	3.335	3.184	1.745	1.806	1.679	1.741	1.586	3.064	3.094	3.131	3.137	3.087	2.758	2.943	2.915
Al^{3+}	2.88	2.795	2.776	2.771	2.831	2.735	2.759	2.724	2.813	2.97	2.914	2.869	2.893	2.86	2.976	2.957	2.9	2.96
Si^{4+}	6.404	6.502	6.494	6.497	6.479	6.542	6.48	6.54	6.582	6.468	6.372	6.521	6.435	6.538	6.469	6.519	6.681	6.527
Cl^-	0.065	0.056	0.062	0.044	0.058	0.086	0.089	0.08	0.127	0.122	0.03	0.009	0.012	0.009	0.024	0.024	0.015	0.03
K^+	2.159	2.245	2.151	2.144	2.111	2.137	2.14	2.084	2.144	1.969	2.162	2.193	2.149	2.142	2.137	2.198	2.211	2.147
Ti^{4+}	0.558	0.489	0.544	0.566	0.557	0.548	0.484	0.56	0.487	0.317	0.523	0.509	0.523	0.497	0.496	0.48	0.488	0.504
Mn^{2+}	0.064	0.066	0.069	0.072	0.069	0.199	0.207	0.204	0.189	0.154	0.069	0.062	0.071	0.053	0.064	0.044	0.024	0.033
Fe^{2+}	2.795	2.54	2.555	2.566	2.742	4.05	4.075	4.148	4.003	4.53	2.851	2.732	2.758	2.76	2.735	3.023	2.726	2.878
H^+	2	2	2	2	2	2	2	2	2	2	2	2	2	2	2	2	2	2
O^{2-}	26.13	26.04	26.15	26.17	26.22	26.03	25.9	26.04	26.11	26.07	26.22	26.32	26.29	26.36	26.33	26.28	26.37	26.29
log a_{HF}/a_{HCl}	-0.246	-0.155	-0.269	-0.110	-0.252	0.315	0.310	0.375	0.012	-0.048	-0.773	-0.060	-0.238	-0.143	-0.573	0.019	0.330	0.024

Appendix 5 continued.

	KR-05-62	KR-05-62	KR-05-68	KR-05-68	KR-05-68	KR-05-68	KR-05-68	KR-05-97b	KR-05-97b	KR-05-97b	KR-05-97b	KR-05-97b	KR-05-110	KR-05-110	KR-05-110	KR-05-110	KR-05-110	KR-05-113
F	0.29	0.4	0.28	0.24	0.21	0.34	0.29	0.63	0.63	0.63	0.67	0.67	0.34	0.32	0.29	0.28	0.3	0.36
Na_2O	0.06	0.04	0.14	0.11	0.11	0.07	0.09	0	0.06	0.06	0.06	0	0.06	0.07	0.05	0.07	0.06	0.04
MgO	10.21	10.5	11	10.69	10.68	10.97	10.7	11.02	10.64	10.73	10.73	10.94	7.3	7.12	7.26	7.07	7.02	9.92
Al_2O_3	14.03	14.4	15.3	15.49	15.57	14.8	15	12.85	12.91	12.84	12.84	12.84	15.91	15.62	15.8	16.26	16.12	13.69
SiO_2	37.05	36.6	36.8	36.3	36.49	36.61	36.9	38.02	37.83	37.64	37.26	37.36	35.81	35.56	35.6	35.11	35.29	36.25
Cl	0.1	0.08	0.06	0.06	0.04	0.07	0.07	0.27	0.24	0.29	0.31	0.29	0.1	0.1	0.09	0.13	0.11	0.27
K_2O	9.82	9.74	9.51	9.64	9.68	9.57	9.57	9.74	9.56	9.71	9.73	9.65	9.52	9.45	9.53	9.55	9.58	9.67
TiO_2	3.63	3.26	3.63	3.56	3.63	3.14	3.27	4.44	4.53	4.5	4.65	4.33	3.64	3.62	3.7	3.79	3.63	3.49
MnO	0.18	0.2	0.31	0.32	0.32	0.32	0.27	0.21	0.3	0.27	0.24	0.28	0.45	0.5	0.61	0.54	0.4	0.29
FeO	21.54	20.6	20.5	20.69	20.34	19.9	20.1	20.39	20.21	20.56	20.35	20.27	24.13	24.05	24.3	23.22	23.18	22.44
H_2O	1.71	1.69	1.73	1.72	1.72	1.7	1.71	1.71	1.7	1.7	1.69	1.69	1.68	1.67	1.68	1.66	1.66	1.69
O=F	-0.12	-0.17	-0.12	-0.1	-0.09	-0.14	-0.12	-0.27	-0.27	-0.27	-0.28	-0.28	-0.14	-0.13	-0.12	-0.12	-0.13	-0.15
O=Cl	-0.02	-0.02	-0.01	-0.01	-0.01	-0.02	-0.02	-0.06	-0.05	-0.07	-0.07	-0.07	-0.02	-0.02	-0.02	-0.03	-0.02	-0.06
Total	98.48	97.5	99.1	98.8	98.69	97.42	97.9	98.95	98.31	98.69	98.27	98.04	98.79	97.99	98.8	97.58	97.25	97.94
F^-	0.161	0.22	0.15	0.132	0.116	0.19	0.16	0.35	0.352	0.351	0.375	0.375	0.192	0.182	0.16	0.16	0.171	0.202
Na^+	0.02	0.01	0.05	0.037	0.037	0.024	0.03	0	0.021	0.02	0.021	0	0.021	0.024	0.02	0.024	0.021	0.014
Mg^{2+}	2.677	2.77	2.84	2.776	2.773	2.883	2.81	2.882	2.805	2.818	2.83	2.889	1.939	1.909	1.93	1.899	1.892	2.629
Al^{3+}	2.908	2.99	3.13	3.18	3.196	3.075	3.11	2.657	2.69	2.666	2.678	2.681	3.341	3.311	3.31	3.453	3.434	2.868
Si^{4+}	6.515	6.48	6.38	6.324	6.356	6.454	6.47	6.671	6.689	6.631	6.593	6.618	6.381	6.395	6.36	6.326	6.379	6.444
Cl^-	0.03	0.02	0.02	0.018	0.012	0.021	0.02	0.08	0.072	0.087	0.093	0.087	0.03	0.03	0.03	0.04	0.034	0.081
K^+	2.203	2.2	2.1	2.142	2.151	2.152	2.15	2.18	2.156	2.182	2.196	2.181	2.164	2.168	2.17	2.195	2.209	2.193
Ti^{4+}	0.48	0.43	0.47	0.466	0.476	0.416	0.43	0.586	0.602	0.596	0.619	0.577	0.488	0.49	0.5	0.514	0.494	0.467
Mn^{2+}	0.027	0.03	0.05	0.047	0.047	0.048	0.04	0.031	0.045	0.04	0.036	0.042	0.068	0.076	0.09	0.082	0.061	0.044
Fe^{2+}	3.168	3.05	2.97	3.014	2.963	2.934	2.96	2.992	2.988	3.029	3.011	3.003	3.596	3.617	3.63	3.499	3.504	3.336
H^+	2	2	2	2	2	2	2	2	2	2	2	2	2	2	2	2	2	2
O^{2-}	26.24	26.2	26.3	26.22	26.27	26.22	26.3	26.28	26.34	26.24	26.21	26.22	26.34	26.34	26.3	26.36	26.37	26.1
log a_{HF}/a_{HCl}	-0.046	0.134	0.060	0.086	0.065	0.149	0.147	-0.221	-0.149	-0.235	-0.248	-0.229	0.216	0.185	0.188	0.029	0.145	-0.375

Appendix 5 continued.

	KR-05-113	KR-05-113	KR-05-113	KR-05-113	KR-05-126	KR-05-126	KR-05-126	KR-05-126	KR-05-126	KR-05-130	KR-05-130	KR-05-130	KR-05-130	KR-05-130	KR-05-136	KR-05-136	KR-05-136	KR-05-136
F	0.38	0.36	0.38	0.35	2.93	2.96	1.22	3.07	3.2	0.13	0.17	0.15	0.07	0.13	0.16	0.17	0.16	0.14
Na_2O	0	0.08	0	0.08	0.33	0.26	0.14	0.32	0.32	0.03	0.06	0.03	0.08	0.05	0.05	0.1	0.09	0.06
MgO	10.16	10	10.23	9.94	5.14	5.15	4.39	6.08	6.38	11.49	11.79	11.83	11.69	11.44	11	10.86	10.96	10.45
Al_2O_3	13.69	13.84	13.54	13.78	18.84	18.94	19.72	17.33	17.35	14.01	13.46	14.03	14.06	14.24	14.05	14.07	14.09	14.13
SiO_2	37.01	36.2	36.81	36.48	36.61	36.33	36.26	36.39	36.23	37.28	38.05	37.34	37.01	36.56	36.78	36.75	36.77	36.6
Cl	0.28	0.25	0.17	0.23	0.09	0.04	0.11	0.08	0.06	0.22	0.28	0.2	0.2	0.22	0.11	0.11	0.11	0.14
K_2O	9.86	9.72	9.82	9.57	9.69	9.6	9.52	9.58	9.77	9.64	9.87	9.54	9.48	9.49	9.42	9.49	9.49	9.67
TiO_2	3.56	3.63	3.56	3.65	3.03	3.04	2.72	3.38	3.53	3.75	3.38	3.47	3.78	3.51	3.38	3.48	3.24	3.75
MnO	0.33	0.34	0.36	0.3	0.62	0.68	0.6	0.54	0.41	0.22	0.23	0.29	0.27	0.12	0.46	0.39	0.35	0.4
FeO	22.55	22.22	21.84	22.41	21.73	21.84	21.32	22.06	22.2	20.23	20.17	19.66	20.55	20.66	20.58	21.03	21.09	21.85
H_2O	1.71	1.69	1.7	1.69	1.67	1.67	1.65	1.67	1.68	1.72	1.73	1.72	1.72	1.71	1.7	1.71	1.71	1.71
O=F	-0.16	-0.15	-0.16	-0.15	-1.23	-1.25	-0.51	-1.29	-1.35	-0.05	-0.07	-0.06	-0.03	-0.05	-0.07	-0.07	-0.07	-0.06
O=Cl	-0.06	-0.06	-0.04	-0.05	-0.02	-0.01	-0.02	-0.02	-0.01	-0.05	-0.06	-0.05	-0.05	-0.05	-0.02	-0.02	-0.02	-0.03
Total	99.36	98.14	98.22	98.36	99.44	99.29	97.15	99.23	99.92	98.65	99.1	98.16	98.86	98.05	97.67	98.14	98.05	98.86
F^-	0.211	0.202	0.212	0.196	1.66	1.681	0.702	1.744	1.804	0.072	0.093	0.083	0.038	0.072	0.089	0.094	0.089	0.078
Na^+	0	0.027	0	0.027	0.115	0.091	0.049	0.111	0.111	0.01	0.02	0.01	0.027	0.017	0.017	0.034	0.031	0.02
Mg^{2+}	2.654	2.641	2.696	2.622	1.373	1.378	1.191	1.628	1.695	2.987	3.047	3.081	3.03	2.991	2.892	2.845	2.871	2.729
Al^{3+}	2.827	2.89	2.821	2.874	3.978	4.008	4.23	3.669	3.645	2.879	2.75	2.888	2.881	2.943	2.92	2.914	2.918	2.917
Si^{4+}	6.484	6.414	6.508	6.456	6.559	6.523	6.6	6.537	6.459	6.5	6.596	6.522	6.435	6.411	6.486	6.458	6.461	6.411
Cl^-	0.083	0.075	0.051	0.069	0.027	0.012	0.034	0.024	0.018	0.065	0.082	0.059	0.059	0.065	0.033	0.033	0.033	0.042
K^+	2.204	2.197	2.215	2.161	2.215	2.199	2.211	2.195	2.222	2.144	2.183	2.126	2.103	2.123	2.119	2.127	2.127	2.161
Ti^{4+}	0.469	0.484	0.473	0.486	0.408	0.411	0.372	0.457	0.473	0.492	0.441	0.456	0.494	0.463	0.448	0.46	0.428	0.494
Mn^{2+}	0.049	0.051	0.054	0.045	0.094	0.103	0.093	0.082	0.062	0.032	0.034	0.043	0.04	0.018	0.069	0.058	0.052	0.059
Fe^{2+}	3.304	3.292	3.229	3.317	3.256	3.279	3.245	3.314	3.31	2.95	2.924	2.872	2.988	3.03	3.035	3.09	3.099	3.201
H^+	2	2	2	2	2	2	2	2	2	2	2	2	2	2	2	2	2	2
O^{2-}	26.12	26.09	26.15	26.16	25.95	25.95	26.59	25.79	25.68	26.29	26.23	26.28	26.26	26.21	26.27	26.23	26.21	26.21
log a_{HF}/a_{HCl}	-0.369	-0.350	-0.175	-0.306	1.391	1.723	0.968	1.369	1.524	-0.829	-0.837	-0.729	-1.055	-0.812	-0.408	-0.344	-0.384	-0.525

Appendix 5 continued.

	KR-05-136	KR-05-143	KR-05-143	KR-05-143	KR-05-143	KR-05-143	KR-05-148	KR-05-148	KR-05-148	KR-05-148	KR-05-148	KR-05-164	KR-05-164	KR-05-164	KR-05-164	KR-05-164	KR-05-175	KR-05-175
F	0.18	0.4	0.42	0.41	0.45	0.42	0.52	0.43	0.36	0.42	0.55	0.48	0.5	0.54	0.44	0.51	0.3	0.34
Na_2O	0.07	0.07	0.1	0.05	0.12	0.1	0.18	0.06	0.1	0.11	0.09	0.06	0.07	0.05	0.09	0.07	0.07	0.1
MgO	10.9	6.76	6.68	6.67	6.77	6.5	6.58	6.68	6.44	6.72	6.92	5.88	5.96	6.14	5.92	6.41	7.26	7.48
Al_2O_3	14.24	18	17.87	17.68	17.69	17.8	16.27	16.8	17.14	16.72	16.46	18.32	18.42	17.83	18.57	18.16	17.78	17.16
SiO_2	36.66	35.99	35.77	35.79	36.06	35.77	35.35	35.88	35.21	35.42	35.89	35.49	35.15	35.97	34.76	35.96	35.56	36.32
Cl	0.13	0.11	0.12	0.1	0.12	0.09	0.2	0.2	0.19	0.17	0.2	0.08	0.09	0.09	0.1	0.08	0.04	0.06
K_2O	9.46	10.08	9.56	9.91	9.86	9.78	9.4	9.64	9.34	9.54	9.49	9.95	9.86	9.85	9.97	10.01	9.73	9.93
TiO_2	3.46	2.67	3.18	3.48	3.28	3.43	3.51	3.24	3.06	3	3.11	2.99	3.06	3.28	3.11	2.91	3.16	3.47
MnO	0.28	0.44	0.46	0.48	0.45	0.48	0.52	0.47	0.55	0.5	0.53	0.28	0.34	0.39	0.32	0.39	0.52	0.54
FeO	21.82	23.39	23.04	22.92	22.78	22.87	24.34	24.53	25.29	25.2	24.34	23.35	24.03	23.93	23.75	23.19	22.73	22.07
H_2O	1.72	1.7	1.69	1.69	1.7	1.69	1.67	1.69	1.68	1.69	1.68	1.68	1.69	1.69	1.68	1.7	1.69	1.7
O=F	-0.08	-0.17	-0.18	-0.17	-0.19	-0.18	-0.22	-0.18	-0.15	-0.18	-0.23	-0.2	-0.21	-0.23	-0.19	-0.21	-0.13	-0.14
O=Cl	-0.03	-0.02	-0.03	-0.02	-0.03	-0.02	-0.05	-0.05	-0.04	-0.04	-0.05	-0.02	-0.02	-0.02	-0.02	-0.02	-0.01	-0.01
Total	98.88	99.44	98.69	99.02	99.12	98.78	98.29	99.47	99.2	99.3	98.99	98.35	98.96	99.51	98.5	99.25	98.76	99.06
F^-	0.099	0.223	0.236	0.23	0.252	0.236	0.296	0.241	0.203	0.236	0.31	0.271	0.281	0.303	0.248	0.285	0.168	0.19
Na^+	0.024	0.024	0.034	0.017	0.041	0.034	0.063	0.021	0.035	0.038	0.031	0.021	0.024	0.017	0.031	0.024	0.024	0.034
Mg^{2+}	2.839	1.774	1.771	1.763	1.785	1.722	1.763	1.767	1.71	1.78	1.838	1.567	1.581	1.621	1.575	1.689	1.915	1.965
Al^{3+}	2.932	3.735	3.745	3.694	3.688	3.729	3.447	3.512	3.598	3.501	3.456	3.86	3.862	3.723	3.907	3.784	3.707	3.564
Si^{4+}	6.404	6.337	6.36	6.345	6.378	6.358	6.355	6.365	6.271	6.293	6.394	6.345	6.253	6.372	6.205	6.357	6.29	6.401
Cl^-	0.038	0.033	0.036	0.03	0.036	0.027	0.061	0.06	0.057	0.051	0.06	0.024	0.027	0.027	0.03	0.024	0.012	0.018
K^+	2.108	2.264	2.168	2.241	2.225	2.218	2.156	2.182	2.122	2.162	2.157	2.269	2.238	2.226	2.27	2.257	2.196	2.233
Ti^{4+}	0.455	0.354	0.425	0.464	0.436	0.459	0.475	0.432	0.41	0.401	0.417	0.402	0.409	0.437	0.418	0.387	0.42	0.46
Mn^{2+}	0.041	0.066	0.069	0.072	0.067	0.072	0.079	0.071	0.083	0.075	0.08	0.042	0.051	0.059	0.048	0.058	0.078	0.081
Fe^{2+}	3.188	3.444	3.426	3.398	3.37	3.4	3.659	3.639	3.767	3.745	3.627	3.491	3.575	3.545	3.545	3.428	3.363	3.253
H^+	2	2	2	2	2	2	2	2	2	2	2	2	2	2	2	2	2	2
O^{2-}	26.2	26.29	26.42	26.4	26.38	26.43	26.27	26.31	26.27	26.2	26.26	26.38	26.31	26.38	26.29	26.35	26.37	26.41
log a_{HF}/a_{HCl}	-0.386	0.294	0.273	0.361	0.292	0.419	0.166	0.079	0.046	0.156	0.171	0.603	0.553	0.557	0.451	0.573	0.559	0.399

Appendix 5 continued.

	KR-05-175	KR-05-175	KR-05-175	KR-05-191	KR-05-191	KR-05-191	KR-05-191	KR-05-191	KR-05-194	KR-05-194	KR-05-194	KR-05-194	KR-05-196	KR-05-196	KR-05-196	KR-05-196	KR-05-196	KR-05-198
F	0.28	0.28	0.32	0.5	0.48	0.43	0.37	0.44	0.68	0.61	0.61	0.62	0.27	0.25	0.24	0.29	0.26	0.58
Na_2O	0.09	0.07	0.11	0.14	0.14	0.1	0.11	0.09	0.06	0.06	0.11	0.1	0.1	0.15	0.13	0.15	0.17	0.04
MgO	7.3	7.24	7.21	12.03	12.04	10.92	11.39	11.32	6.51	6.61	6.79	6.67	10.86	10.75	10.19	10.84	10.22	6.22
Al_2O_3	17.46	17.33	17.3	13.2	13.34	13.35	13.59	13.36	16.66	16.17	16.56	16.29	13.25	13.31	13.36	13.27	13.23	13.24
SiO_2	35.53	35.88	35.65	37.05	36.88	37	36.27	37.14	36.52	36.2	36.46	36.31	36.86	36.95	36.78	36.9	36.8	36.23
Cl	0.06	0.04	0.06	0.21	0.22	0.21	0.15	0.18	0.2	0.25	0.21	0.24	0.26	0.33	0.36	0.33	0.31	0.22
K_2O	9.68	9.94	9.63	9.33	9.5	9.37	9.42	9.81	9.89	9.85	9.53	9.65	9.66	9.38	9.53	9.53	9.62	9.37
TiO_2	3.38	3.45	3.48	3.99	4.14	4.02	4.17	3.99	3.38	3.58	3.29	3.36	4.23	4.45	4.58	4.56	4.47	4.05
MnO	0.43	0.52	0.41	0.45	0.41	0.39	0.32	0.46	0.39	0.42	0.38	0.29	0.35	0.39	0.39	0.49	0.47	0.5
FeO	23.09	22.49	22.48	19.69	19.73	21.33	20.51	21.13	23.02	23.57	23.16	22.59	21.1	21.52	21.46	20.35	21.28	27.45
H_2O	1.69	1.7	1.68	1.71	1.71	1.71	1.7	1.72	1.68	1.68	1.68	1.66	1.7	1.71	1.7	1.7	1.7	1.66
O=F	-0.12	-0.12	-0.13	-0.21	-0.2	-0.18	-0.16	-0.19	-0.29	-0.26	-0.26	-0.26	-0.11	-0.11	-0.1	-0.12	-0.11	-0.24
O=Cl	-0.01	-0.01	-0.01	-0.05	-0.05	-0.05	-0.03	-0.04	-0.05	-0.06	-0.05	-0.05	-0.06	-0.07	-0.08	-0.07	-0.07	-0.05
Total	98.86	98.83	98.24	98.06	98.34	98.63	97.82	99.46	98.69	98.7	98.53	97.52	98.47	99.03	98.56	98.25	98.46	99.26
F^-	0.157	0.157	0.18	0.277	0.266	0.239	0.206	0.242	0.384	0.345	0.345	0.354	0.15	0.139	0.134	0.162	0.145	0.332
Na^+	0.031	0.024	0.038	0.048	0.047	0.034	0.038	0.03	0.021	0.021	0.038	0.035	0.034	0.051	0.045	0.051	0.058	0.014
Mg^{2+}	1.926	1.909	1.914	3.147	3.14	2.862	2.994	2.934	1.734	1.764	1.81	1.796	2.848	2.811	2.684	2.851	2.692	1.676
Al^{3+}	3.641	3.612	3.63	2.73	2.75	2.766	2.825	2.737	3.508	3.411	3.489	3.467	2.747	2.752	2.782	2.759	2.755	2.821
Si^{4+}	6.287	6.346	6.347	6.501	6.451	6.505	6.396	6.456	6.525	6.479	6.518	6.557	6.485	6.482	6.498	6.509	6.502	6.55
Cl^-	0.018	0.012	0.018	0.062	0.065	0.063	0.045	0.053	0.061	0.076	0.064	0.073	0.078	0.098	0.108	0.099	0.093	0.067
K^+	2.185	2.243	2.187	2.089	2.12	2.102	2.119	2.176	2.254	2.249	2.173	2.223	2.168	2.099	2.148	2.145	2.168	2.161
Ti^{4+}	0.45	0.459	0.466	0.527	0.545	0.532	0.553	0.522	0.454	0.482	0.442	0.456	0.56	0.587	0.609	0.605	0.594	0.551
Mn^{2+}	0.064	0.078	0.062	0.067	0.061	0.058	0.048	0.068	0.059	0.064	0.058	0.044	0.052	0.058	0.058	0.073	0.07	0.077
Fe^{2+}	3.417	3.326	3.347	2.889	2.886	3.136	3.025	3.072	3.44	3.528	3.462	3.412	3.105	3.157	3.171	3.002	3.144	4.15
H^+	2	2	2	2	2	2	2	2	2	2	2	2	2	2	2	2	2	2
O^{2-}	26.36	26.39	26.42	26.16	26.12	26.2	26.16	26.1	26.38	26.32	26.4	26.41	26.2	26.25	26.28	26.27	26.25	26.22
log a_{HF}/a_{HCl}	0.382	0.501	0.408	-0.262	-0.302	-0.255	-0.232	-0.207	0.275	0.137	0.193	0.144	-0.562	-0.679	-0.703	-0.649	-0.608	0.192

Appendix 5 continued.

	KR-05-198	KR-05-198	KR-05-198	KR-05-198	KR-05-208	KR-05-208	KR-05-208	KR-05-208	KR-05-208	KR-05-210	KR-05-210	KR-05-210	KR-05-210	KR-05-210
F	0.46	0.5	0.49	0.47	0.51	0.52	0.55	0.55	0.75	0.69	0.64	0.55	0.55	0.59
Na_2O	0.07	0.04	0.02	0.07	0.07	0.04	0.04	0.03	0.04	0.04	0.01	0.06	0.04	0.05
MgO	6.02	6.04	6.14	6.03	5.25	5.16	5.32	5.34	6	5.45	5.68	5.37	5.32	5.39
Al_2O_3	13.34	13.42	13.31	13.09	17.29	17.94	18.06	18.26	17.17	17.74	18.21	18.13	18.37	18.79
SiO_2	35.98	35.7	36.27	36.42	35.45	35.22	35.81	35.46	36.4	34.93	35.59	35.14	35.64	35.6
Cl	0.18	0.22	0.23	0.22	0.07	0.04	0.05	0.06	0.03	0.05	0.04	0.03	0.05	0.06
K_2O	9.32	9.37	9.62	9.62	9.66	9.68	9.87	9.9	9.82	9.67	9.89	9.79	9.86	9.81
TiO_2	4.14	4.13	4.25	4.05	3.2	2.54	2.35	2.1	2.65	2.41	1.9	2.07	2.48	2.42
MnO	0.45	0.52	0.43	0.49	1.23	1.02	1.07	1.03	0.99	1	1.12	0.89	0.88	0.96
FeO	27.84	27.37	27.56	28.03	24.28	25.5	25.04	24.49	23.62	25.06	24.81	24.74	24.61	24.22
H_2O	1.66	1.65	1.67	1.67	1.66	1.68	1.69	1.68	1.68	1.67	1.69	1.67	1.68	1.69
O=F	-0.19	-0.21	-0.21	-0.2	-0.21	-0.22	-0.23	-0.23	-0.32	-0.29	-0.27	-0.23	-0.23	-0.25
O=Cl	-0.04	-0.05	-0.05	-0.05	-0.02	-0.01	-0.01	-0.01	-0.01	-0.01	-0.01	-0.01	-0.01	-0.01
Total	99.26	98.81	99.77	99.96	98.45	99.11	99.6	98.66	98.86	98.4	99.3	98.22	99.26	99.32
F^-	0.263	0.287	0.279	0.267	0.291	0.294	0.309	0.311	0.424	0.393	0.36	0.313	0.31	0.332
Na^+	0.025	0.014	0.007	0.024	0.024	0.014	0.014	0.01	0.014	0.014	0.003	0.021	0.014	0.017
Mg^{2+}	1.623	1.636	1.646	1.615	1.41	1.377	1.409	1.425	1.597	1.463	1.505	1.439	1.412	1.428
Al^{3+}	2.844	2.873	2.822	2.771	3.672	3.784	3.782	3.852	3.614	3.764	3.814	3.841	3.855	3.936
Si^{4+}	6.508	6.485	6.524	6.543	6.389	6.303	6.363	6.346	6.5	6.288	6.325	6.316	6.346	6.327
Cl^-	0.055	0.068	0.07	0.067	0.021	0.012	0.015	0.018	0.009	0.015	0.012	0.009	0.015	0.018
K^+	2.151	2.171	2.207	2.205	2.221	2.21	2.237	2.26	2.237	2.221	2.242	2.245	2.24	2.224
Ti^{4+}	0.563	0.564	0.575	0.547	0.434	0.342	0.314	0.283	0.356	0.326	0.254	0.28	0.332	0.324
Mn^{2+}	0.069	0.08	0.066	0.075	0.188	0.155	0.161	0.156	0.15	0.152	0.169	0.135	0.133	0.145
Fe^{2+}	4.211	4.158	4.146	4.211	3.659	3.816	3.721	3.666	3.527	3.773	3.687	3.719	3.665	3.6
H^+	2	2	2	2	2	2	2	2	2	2	2	2	2	2
O^{2-}	26.25	26.22	26.23	26.2	26.38	26.27	26.28	26.26	26.32	26.18	26.18	26.22	26.32	26.32
$\log a_{HF}/a_{HCl}$	0.184	0.137	0.099	0.103	0.719	0.987	0.896	0.787	1.159	0.952	0.983	1.061	0.874	0.842

RADIOGENIC ISOTOPE STUDIES OF Pb-Zn MINERALIZATION IN THE HOWARDS PASS AREA, SELWYN BASIN

Brian L. Cousens
Ottawa-Carleton Geoscience Centre, Carleton University, 1125 Colonel By Drive, Ottawa, ON K1S 5B6

INTRODUCTION

The lead-zinc deposits of the Howards Pass area, Selwyn Basin, are collectively one of the few giant to supergiant sedimentary-exhalative (SEDEX) deposits in the world (Goodfellow, 2004). In addition to the Howards Pass properties, Pb-Zn economic deposits are also found in the Anvil mining district of the central Yukon and the Gataga region of northern British Columbia, all within the Selwyn Basin (Fig. 1; Abbott et al., 1986; Nelson et al., 2002; Héon, 2003; Goodfellow, 2006).

SEDEX deposits form from the discharge of hydrothermal solutions on or within sediments deposited on the seafloor (Fig. 2). The important ore minerals are sphalerite (Zn-Fe sulphide) and galena (Pb sulphide). The ore minerals are layered within the sediment pile, often rhythmically banded and intergrown with sediment particles on a very fine scale. Other hydrothermal minerals, such as barite, chert, or rare carbonate, are found interbedded with the Pb-Zn mineralization. The formation of SEDEX deposits is a function of several regional- to local-scale geological variables, including the nature of the basin hosting the deposits, the role of extension in continental rifting, heat from local magmatism, the presence of faults to act as conduits for hydrothermal fluids, significant rates of sedimentation, and oceanographic water conditions.

In Alaska, northern British Columbia, the Yukon, and the Northwest Territories, SEDEX deposits of the Selwyn Basin range in age from Early Cambrian to Carboniferous (summarized in Goodfellow, 2006). The DY, Swim, Faro, Vangorda, and Grum deposits of the Anvil district are hosted in Early Cambrian sedimentary rocks and minor volcanic rocks that are intruded by Cretaceous plutons. The rocks of the Anvil District are metamorphosed from greenschist to amphibolite grade, and have undergone as many as five deformation events. The Howards Pass deposits (OP, Anniv, XY) form an elongate "corridor" of mineralization that straddles the Yukon-Northwest Territories border. The deposits are hosted in early Silurian black shales of the Road River Group. Stratigraphically above the Howards Pass occurrences are the Tom and Jason deposits at Macmillan Pass, hosted within late Devonian coarse clastic sedimentary rocks of the Earn Group. Alkalic basalt volcanic rocks occur within the stratigraphic units hosting the Pb-Zn-barite mineralization. SEDEX deposits of the Gataga district, also known as the Kechika Trough of northern British Columbia, are hosted within late Devonian carbonaceous shale and chert of the lower Earn Group. The Gataga district includes six known Pb-Zn occurrences, including the 38 million tonne Cirque deposit. The Red Dog deposit of Alaska is situated within Mississippian to Permian black shales of the Arctic Alaska Basin, and the ore horizon is overlain by barite-rich rocks.

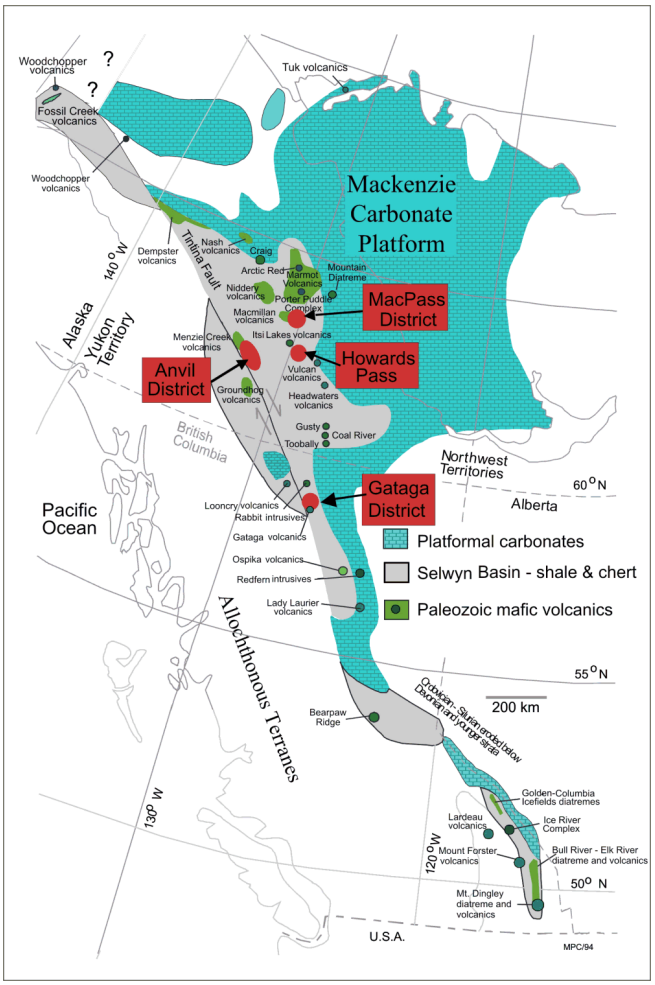


Figure 1. Location of Pb-Zn mining districts in the Selwyn Basin (grey area), Yukon Territory, and northern British Columbia (Goodfellow, 2006). The Red Dog deposit is located just northwest of the upper left map area.

Cousens, B., 2007, Radiogenic isotope studies of Pb-Zn mineralization in the Howards Pass area, Selwyn Basin, *in* Mineral and Energy Resource Assessment of the Greater Nahanni Ecosystem Under Consideration for the Expansion of the Nahanni National Park Reserve, Northwest Territories, (eds.) D.F. Wright, D. Lemkow, and J.R. Harris; Geological Survey of Canada, Open File 5344, p. 279-292.

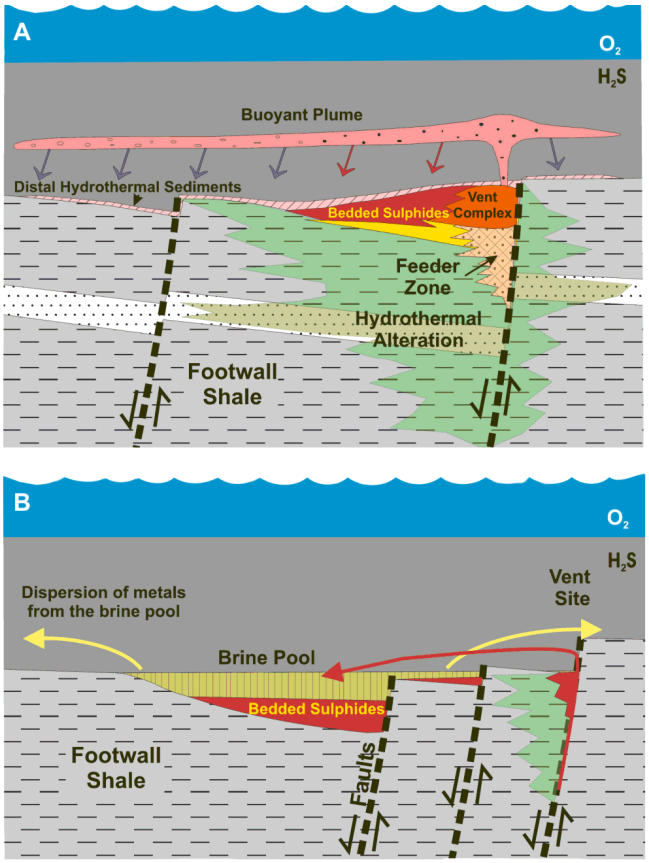


Figure 2. Models for the deposition of SEDEX Pb-Zn mineralization (Goodfellow, 2006). In model A, hydrothermal fluids form a "vent-proximal" deposit but also disperse metals through the water column via a buoyant plume (e.g. Sullivan; Tom, and Jason). In model B, "vent-distal" deposits form as hydrothermal fluids cascade from upper to lower basins (e.g. Howards Pass, and Anniv).

RADIOGENIC ISOTOPES AND ORE DEPOSITS

Lead (Pb) isotopes are useful in dating Pb-bearing ore deposits and in evaluating potential source rocks for mineralizing fluids (Stacey and Kramers, 1975; Godwin and Sinclair, 1982; Godwin et al., 1982; Cousens et al., 2002, 2006; Nelson et al., 2002). The extremely high abundances of Pb in sphalerite and galena make Pb isotopic ratios difficult to modify during deformational events that occur subsequent to ore deposition. Thus Pb isotopes have been used in the past to define the details of metallogenic evolution for mineral deposits at the deposit, district, and regional scales (e.g. Godwin et al., 1982; Nelson et al., 2002).

Many ore deposits are hosted by carbonate rocks or include carbonate as a gangue mineral. Strontium (Sr) is a minor constituent of these carbonates, and thus Sr isotopes can potentially yield information on mineralizing fluids. Of particular interest is the contrast between Sr isotope ratios in seawater (Burke et al., 1982) and those in hydrothermal fluids that are generally rock-dominated (Albarède et al., 1981; Ridley et al., 1994; Davis et al., 2003). Like Pb, Sr isotopes can be used to track sources of hydrothermal fluids at scales from the deposit to a sedimentary basin.

Of the three most commonly measured radiogenic isotopes, the neodymium (Nd) isotope system is the most useful in older rocks due to the low mobility of the rare earth elements Sm and Nd during low- to medium-grade metamorphism. Nd isotopes are commonly used in ore deposit studies to evaluate the tectonic setting and petrogenesis of the host rocks and to investigate the effects of alteration on host-rock geochemistry. In the case of sedimentary rocks, Nd isotopes are an invaluable tool in establishing the provenance of the sedimentary particles. In many cases, it has been possible to link widely spaced sedimentary packages to source rocks thousands of kilometres distant, or to find contrasting sources for sedimentary packages in close proximity to one another (Patchett and Gehrels, 1998; Yamashita and Creaser, 1999).

PROJECT GOALS

The goals of this study are to evaluate the effectiveness of the following:

1. Using Nd isotopes to evaluate the provenance of sedimentary rocks in the Howards Pass area of the Selwyn Basin. In particular, is there a significant shift in sediment source between the Road River Group, host to the XY deposit, and the overlying Earn Group, host to the Tom/Jason deposits?
2. Using Pb isotopes to evaluate the continuity of ore horizons in the "zinc corridor" of the Howards Pass area. This impacts the model for ore deposition and exploration models for the region.
3. Using Pb isotopes to compare the ore minerals with local host rocks. Could local sediments have been a partial source of Pb and other metals for the deposits? How well do Pb isotopes distinguish mineralized from unmineralized rocks; can Pb isotopes be used as a vector to mineralization?
4. Using Sr isotopes to evaluate the sources for hydrothermal ore fluids. Was seawater an active component during the formation of carbonates associated with mineralization, or is Sr in carbonates rock-dominated and derived primarily from deep-seated rock sources? This distinction impacts exploration potential if proximity to a fault conduit is a critical aspect of the mineralization.

FIELD WORK AND LABORATORY TECHNIQUES

In July of 2005, eight days were spent at the Pacifica Resources camp on the ANNIV property, Howards Pass (see claim map with sample locations, Figure 3). A total of 45 rock samples were collected (Table 1) for

Table 1. Sample locations.

Sample Number	Area	Unit	NAD83E	NAD83N
05-HP-1	XY	Active Member	491116	6925098
05-HP-2	XY	Limstone concretion	491834	6924845
05-HP-3	ANNIV	Active Member	472173	6937433
05-HP-4	ANNIV	Limestone concretion	472313	6937381
05-HP-5	ANNIV	A46-289 Active Member	474700	6935800
05-HP-6	ANNIV	A35-402 mudstone	472700	6937000
05-HP-7	ANNIV	A35-412 mudstone	472700	6937000
05-HP-8	ANNIV	A55-352 flaggy mudstone	474100	6936000
05-HP-9	ANNIV	A55-945 Active Member	474100	6936000
05-HP-10	ANNIV	A51-874 mudstone	?	?
05-HP-11	ANNIV	A18-175 pyritic mudstone	472700	6937100
05-HP-12	ANNIV	A18-20 laminated mudstone	472700	6937100
05-HP-13	ANNIV	A18-228 Active Member	472700	6937100
05-HP-14	ANNIV	A18, limestone concretion	472700	6937100
05-HP-15	ANNIV	A19-475 mudstone	472150	6937500
05-HP-16	ANNIV	A69-156 Active Member	471800	6937500
05-HP-17	ANNIV	A69-78 limestone	471800	6937800
05-HP-18	ANNIV	A18-272 mudstone	472150	6937500
05-HP-19	ANNIV	A37-525 mudstone	475500	6936200
05-HP-20	ANNIV	Rabbittkettle limestone	472057	6938076
05-HP-21	ANNIV	Upper cherty mudstone	471886	6937217
05-HP-22	XY	Iron Creek formation	490198	6926777
05-HP-23	XY	Backside siliceous mudstone	490279	6926319
05-HP-24	XY	Backside siliceous mudstone	490326	6926141
05-HP-25	XY	Flaggy mudstone	490231	6926101
05-HP-26	XY	Limestone concretion	490231	6926054
05-HP-26	XY	Active Member	490056	6925987
05-HP-27	XY	Upper siliceous mudstone	490041	6925946
05-HP-28	XY	Lower cherty mudstone	490030	6926017
05-HP-29	XY	Flaggy mudstone	490352	6925716
05-HP-30	XY	Active Member	490862	6925686
05-HP-31	XY	Lower calcareous member	491074	6925453
05-HP-32	XY	Lower cherty mudstone	491626	6924908
05-HP-33	XY	Rabbittkettle limestone	491365	6924861
05-HP-34	CMC	Cherty mudstone	495993	6925222
05-HP-35	CMC	Mineralized cherty mudstone	496132	6925150
05-HP-36	CMC	Fetid limestone	496209	6924871
05-HP-37	CMC	Cherty mudstone, mineralized?	496125	6923917
05-HP-38	GRAND/NOR	Cherty mudstone	494057	6917688
05-HP-39	GRAND/NOR	Quartz vein, galena	494103	6917676
05-HP-40	GRAND/NOR	Black shale	494103	6917676
05-HP-41	GRAND/NOR	Pyritic mudstone	494742	6917463
05-HP-42	GRAND/NOR	Pyritic mudstone, galena	495027	6917219
05-HP-43	GRAND/NOR	Pyricitic sandstone, galena	495104	6917286
05-HP-44	GRAND/NOR	Pyritic sandstone	496143	6916189
05-HP-45	BRODEL	Mudstone, spahelrite-galena	486359	6929187
BC-05-01	OP-11-67.9m	Galena stringer	466900	6940700
BC-05-02	OP-11-65.0m	Active member, laminated	466900	6940700
BC-05-03	DON-04-178m	Active Member, laminated	478100	6934600
BC-05-04	BRODEL-05-56.6m	Active Member, laminated	485500	6929300
BC-05-05	BRODEL-07-213.3m	Galena stringer	486350	6929000
BC-05-06	BRODEL-07-230.5m	Active Member, laminated	486350	6929000
105I-816052	XY/BRODEL H71	Active Member	486118	6929074
105I-816160	ANNIV A26	Active Member	472100	6936230
105I-796002	XY DDH42	Earn sandstone	489460	6925820
105I-796015	XY DDH42	Earn black shale	489460	6925820
105I-796018	XY DDH42	Road River Upper Mudstone	489460	6925820
105I-796047	XY DDH42	Road River Lower carbonaceous shale	489460	6925820
105I-796098	XY DDH42	Road River lower siliceous shale	489460	6925820
105I-796110	XY DDH42	Road River lower mudstone	489460	6925820
105O-798071	North of Jason Deposit	shale	417400	7013850
ORO103	ORO 180	silty limestone	460013	6942736
ORO122	ORO 180	baritic silty shale	460013	6942736
105I-SL0108	Summit Lake	siltstone	476000	6909000

Note: UTM coordinates using NAD83 datum

Table 2. Isotopic Data.

Sm-Nd Isotopic Data

Sample	Nd (ppm)	Sm (ppm)	$^{147}Sm/^{144}Nd$	$^{143}Nd/^{144}Nd$ (meas)	$^{143}Nd/^{144}Nd$ init	ε_{Nd}	T (CHUR)
105I-796002	5.11	0.96	0.1133	0.511987	0.511705	-8.65	1188
105I-796015	22.51	4.49	0.1205	0.511882	0.511582	-11.1	1508
105I-796018	37.78	9.30	0.1489	0.511947	0.511877	-11.2	2191
105I-796047	16.57	3.40	0.1240	0.512087	0.511778	-7.23	1155
105I-796098	17.61	3.59	0.1233	0.511758	0.511451	-13.6	1822
105I-796110	21.86	3.72	0.1028	0.511388	0.511132	-19.8	2021
105O-798071	30.98	5.28	0.1031	0.511743	0.511487	-12.9	1454
ORO103	11.85	2.12	0.1082	0.511495	0.511226	-18	1962
ORO122	29.62	4.29	0.0875	0.511819	0.511601	-10.7	1143
105I-SL0108	29.64	4.28	0.0874	0.511746	0.511528	-12.1	1243

Notes: Nd, Sm by isotope dilution. "meas" = measured ratio. init = initial ratio at 380 Ma. "εNd" = epsilon Nd, calculated at 380 Ma. T (CHUR) = Model age using a Chondrite Uniform Reservoir model. Error in epslion Nd value is +/- 0.5 epsilon units.

Sr Isotopic Data

Sample	Locality	$^{87}Sr/^{86}Sr$	2-sigma
05-HP-02 concretion	XY	0.710253	0.000012
05-HP-04 concretion	ANNIV	0.710510	0.000016
05-HP-14 concretion	ANNIV	0.712083	0.000009
05-HP-17 limestone	ANNIV	0.715780	0.000007
05-HP-20 Rabbitkettle	ANNIV	0.711349	0.000006
05-HP-26 concretion	XY	0.713199	0.000006
05-HP-33 Rabbitkettle	XY	0.711696	0.000006
05-HP-36 Fetid Limestone	CMC	0.709912	0.000007

Notes: 2-sigma = within-run 2-sigma analytical uncertainty. Concretion = carbonate concretion from Active member.

isotopic and trace element analysis. This sample set was supplemented by the collection of rock samples from Wayne Goodfellow of the Geological Survey of Canada (GSC), from which ten samples of sedimentary rocks were chosen for Nd isotopic analysis and four for Pb and Sr isotopic analysis. In addition, six samples of drill core from Pacifica Resources Fall 2005 drill campaign were obtained for Pb isotopic analysis. Isotopic data from this study are listed in Table 2. Host-rock samples collected in 2005 and a suite of sedimentary rock samples from the GSC, totaling 104 samples, were submitted for trace element analysis by inductively coupled plasma masss spectrometry (ICP-MS). The following describes the radiogenic isotope chemistry and mass spectrometry procedures at Carleton University. All chemistry was performed in Class 100 fume hoods in a clean laboratory.

Sulphides: Small chips of sulphide or sulphide-rich sedimentary rock were placed in a Savillex screw-cap vial and immersed in 3N HNO_3 that preferentially dissolved sulphide minerals over silicate minerals. After 12 to 24 hours of immersion, the acid was pipeted out of the vial, centrifuged, dried down, and the residue redissolved in 1N HBr.

Silicate Rocks: For Pb and Nd isotopic analysis, between 100 and 200 milligrams of crushed rock powder were dissolved in 50% HF-12N HNO_3, then attacked with 8N HNO_3, and finally 6N HCl. The

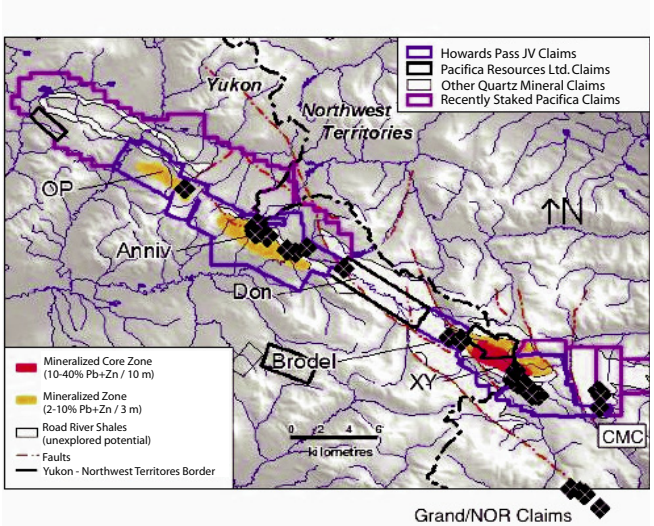


Figure 3. Sample Location map for Pb and Sr isotopic analyses, Howards Pass Area. Sample Location indicated by black diamonds. Claim map courtesy of Pacifica Resources.

Table 2 continued. Pb Isotopic Data

Sample	$^{208}Pb/^{204}Pb$	2-sigma	$^{207}Pb/^{204}Pb$	2-sigma	$^{206}Pb/^{204}Pb$	2-sigma
05-HP-01	38.737	0.005	15.685	0.002	18.670	0.002
05-HP-03	38.819	0.009	15.721	0.005	18.660	0.004
05-HP-05	38.580	0.010	15.675	0.003	18.537	0.002
05-HP-06	38.637	0.003	15.679	0.001	19.135	0.001
05-HP-07	38.649	0.036	15.725	0.014	19.855	0.018
05-HP-08	40.644	0.038	15.724	0.014	20.320	0.020
05-HP-09	38.571	0.016	15.668	0.007	18.606	0.008
05-hp-10	38.652	0.015	15.690	0.006	19.297	0.008
05-HP-11	38.585	0.003	15.664	0.001	18.593	0.001
05-HP-12	38.600	0.009	15.668	0.003	18.573	0.004
05-HP-13	38.627	0.007	15.678	0.002	18.579	0.003
05-HP-15	38.682	0.010	15.745	0.004	20.265	0.005
05-HP-16	38.621	0.003	15.673	0.001	18.575	0.001
05-HP-17	38.603	0.004	15.681	0.001	18.949	0.002
05-HP-18	38.704	0.016	15.700	0.005	18.630	0.003
05-HP-19	38.782	0.017	15.724	0.006	18.617	0.005
05-HP-26	38.907	0.112	15.741	0.044	18.725	0.048
05-HP-30	39.202	0.032	15.849	0.014	18.777	0.021
05-HP-37	38.698	0.002	15.690	0.001	18.826	0.001
05-HP-38	38.602	0.007	15.680	0.002	18.444	0.002
05-HP-39	38.594	0.012	15.677	0.004	18.451	0.003
05-HP-41	38.637	0.006	15.690	0.002	18.457	0.001
05-HP-42	38.616	0.004	15.687	0.001	18.459	0.001
BC-05-01	38.629	0.004	15.671	0.003	18.593	0.002
BC-05-02	38.607	0.003	15.670	0.001	18.574	0.001
BC-05-03	38.729	0.004	15.705	0.001	18.601	0.001
BC-05-04	38.595	0.004	15.664	0.002	18.625	0.002
BC-05-05	38.804	0.008	15.723	0.002	18.715	0.002
BC-05-06	38.718	0.007	15.696	0.002	18.687	0.002
XY ORE	38.716	0.008	15.701	0.002	18.605	0.002
05-HP-35	38.742	0.003	15.693	0.001	18.876	0.001
05-HP-43	38.777	0.020	15.733	0.014	18.486	0.011
05-HP-44	38.726	0.028	15.662	0.010	18.673	0.013
05-HP-45	38.781	0.028	15.722	0.008	18.612	0.006
05-HP-21	39.075	0.002	15.699	0.001	19.716	0.001
05-HP-22	39.374	0.002	15.729	0.001	19.766	0.001
05-HP-23	39.194	0.002	15.701	0.001	19.236	0.001
05-HP-24	38.769	0.002	15.712	0.001	19.230	0.001
05-HP-25	38.729	0.009	15.699	0.003	18.712	0.002
05-HP-27	38.728	0.006	15.687	0.002	18.732	0.002
05-HP-28	38.884	0.009	15.732	0.003	18.704	0.002
05-HP-29	39.943	0.001	15.730	0.001	20.356	0.001
05-HP-31	39.192	0.002	15.840	0.001	21.597	0.001
05-HP-32	38.645	0.002	15.685	0.001	19.020	0.001
05-HP-34	38.781	0.002	15.752	0.001	19.982	0.001
05-HP-40	38.618	0.007	15.697	0.002	18.668	0.002
105I-816052	38.824	0.010	15.930	0.003	22.840	0.003
105I-816160	38.739	0.017	15.716	0.007	18.635	0.008
05-HP-26	38.756	0.011	15.699	0.003	18.824	0.003
05-HP-33	38.727	0.008	15.688	0.002	18.717	0.002

Notes: 2-sigma: within-run 2-sigma analytical uncertainty. Note that reproducubility of standard NBS981 should be used as the best estimate of analytical uncertaintiy for Pb isotopes (see text).

residue is taken up in 1N HBr for Pb separation, or 2.5N HCl for Nd chemistry.

Carbonate Rocks: For Pb isotopic analysis, approximately 100 mg of carbonate was dissolved in 2.5N HCl, dried down, and the residue redissolved in 1N HBr for Pb separation. For Sr isotopic analysis, approximately 10 mg of carbonate was dissolved in weak HCl, dried down, and the residue redissolved in 2.5N HCl for Sr separation.

Lead was separated in Bio-Rad 10 ml polyethylene columns and Dowex AG1-8X anion resin, using 1N HBR to elute other elements and 6N HCl to elute Pb. The collected Pb solution was dried, redissolved in 1N HBr, and the above procedure was repeated with a small volume resin bed. Total procedural blanks for Pb are <300 picograms and are insignificant. Samples were loaded onto single Re filaments with H_3PO_4 and silica gel, and were run at filament temperatures of 1175 to 1225°C in a Thermo-Finnigan TRITON mass spectrometer. All mass spectrometer runs were corrected for fractionation using NIST SRM981. The average ratios measured for SRM981 are $^{206}Pb/^{204}Pb$ = 16.892 ± 0.010, $^{207}Pb/^{204}Pb$ = 15.431 ± 0.013, and $^{208}Pb/^{204}Pb$ = 36.512 ± 0.038 (2 standard deviations of the mean), based on 20 runs between April 2005 and February 2006. The fractionation correction is +0.124%/amu (based on the values of Todt et al., 1984).

For Sr separation, the sample, dissolved in 2.5N HCl, is pipetted into a 14 ml Bio-Rad borosilicate glass chromatography column containing 3.0 ml of Dowex AG50-X8 cation resin. Rb and Sr are eluted in succession using 2.5 N HCl. The rare earth elements (including Nd and Sm) are then eluted using 6N HCl. The REE solution is dried and the residue dissolved in 0.26N HCl. Total procedural blanks for Sr are <450 picograms. Sr is loaded onto a single Ta filament with H_3PO_4 and is run at filament temperatures of 1450 to 1520°C. Isotope ratios are normalized to $^{86}Sr/^{88}Sr$ = 0.11940 to correct for fractionation. Two standards are run at Carleton, NIST SRM987 ($^{87}Sr/^{86}Sr$ = 0.710245 ± 0.000016, n=25, April 2005 – February 2006) and the Eimer and Amend (E&A) $SrCO_3$ ($^{87}Sr/^{86}Sr$ = 0.708012 ± 0.000020, n=5, April 2005 – February 2006).

For Sm-Nd separation, the REE residue is dissolved in 0.26N HCl and loaded into a 14 ml Bio-Rad borosilicate glass chromatographic column containing a 2 cm high bed of Teflon powder coated with HDEHP (di(2-ethylhexyl) orthophosphoric acid, Richard et al., 1976). Nd is eluted using 0.26N HCl, followed by Sm in 0.5N HCl.

Total procedural blanks for Nd are <350 picograms. Samples are spiked with a mixed ^{148}Nd-^{149}Sm spike prior to dissolution. Concentrations are precise to ±1%, but $^{147}Sm/^{144}Nd$ ratios are reproducible to 0.5%. Samples are loaded with H_3PO_4 on one side of a Re double filament, and run at temperatures of 1750 to 1800°C. Isotope ratios are normalized to 146Nd/144Nd = 0.72190. Analyses of the United States Geological Survey standard BCR-1 yield Nd = 29.02 ppm, Sm = 6.68 ppm, and $^{143}Nd/^{144}Nd$ = 0.512668 ± 0.000020 (n=4). Thirteen runs of the La Jolla standard average $^{143}Nd/^{144}Nd$ = 0.511848 ± 0.000005 (February 2005 – February 2006). Five runs of the Carleton University in-house Nd metal standard yield an average $^{143}Nd/^{144}Nd$ = 0.511820 ± 0.000003 over the same time period.

STUDY OF SEDIMENT PROVENANCE USING Sm-Nd ISOTOPE SYSTEMATICS

Sedimentary rocks are composed of rock particles typically derived from more than one source. The trace element and isotopic composition of sedimentary rocks are commonly used to distinguish between potential sediment sources, or to determine the relative contributions of multiple sources to sedimentary basins (e.g. Jenner et al., 1981; Patchett et al., 1984; Patchett and Gehrels, 1998; Yamashita and Creaser, 1999).

The Sm-Nd isotopic system is particularly well suited to evaluate the sources of sediments. Both are rare earth elements that are actually fairly abundant in sedimentary rocks, and the ratio of the parent isotope Sm to the daughter isotope Nd is usually not affected by greenschist- to lower amphibolite-grade metamorphism. Thus the Sm-Nd system will faithfully record the average isotopic composition of detritus accumulating in the sedimentary basin. Changes in the dominant source of detritus will result in significant changes in Nd isotopic composition, particularly if there is a large age difference between source rocks.

^{147}Sm decays to ^{143}Nd with a half-life of 106 billion years. Due to the extremely long half-life of ^{147}Sm, the ratio of $^{143}Nd/^{144}Nd$ is commonly expressed in epsilon units, defined as

$$\varepsilon_{Nd}{}^t = \{((^{143}Nd/^{144}Nd)_{sample}{}^t) / (^{143}Nd/^{144}Nd)_{CHUR}{}^t)) - 1\} \times 10^4$$

where t = time of sediment deposition and CHUR is the Chrondrite Uniform Reservoir, commonly considered to represent the composition of the Bulk Earth (DePaolo, 1988). By default, $\varepsilon_{Nd}CHUR^t = 0$ at all times, and thus on diagrams of $\varepsilon_{Nd}{}^t$ versus time the isotopic evolution of CHUR is a horizontal line with an $\varepsilon_{Nd}{}^t$ of zero. We can estimate the average age of detritus accumulated in the sedimentary rock of interest by backtracking the isotopic evolution of the sedimentary rock back to a hypothetical source composition, yielding a "model age" for the source (e.g. Bennett and DePaolo, 1987; DePaolo et al., 1991). In this way, we

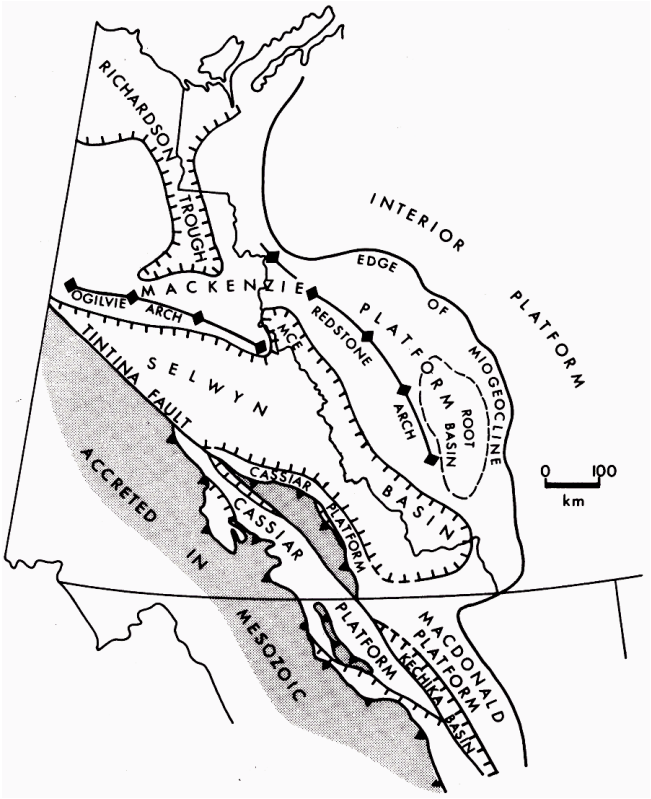


Figure 4. Tectonic elements of the Selwyn Basin. Diagram by S. Gordey, from Héon (2003).

can distinguish Archean from Proterozoic sources of detritus to the Selwyn Basin.

The Selwyn Basin was a centre of deep-water, passive margin sedimentation located southwest of a major carbonate platform (Mackenzie Platform) from Late Precambrian to Devonian time (Figs. 4, 5). From Cambrian through Silurian time, migration of the Mackenzie shelf edge resulted in the interstratification of basinal and platformal rocks along with the formation of small subbasins within the platform. Passive margin sedimentation ended during the Mid-Devonian, and coarse-grained clastic sediments were deposited across the former shelf edge (Héon, 2003).

In the Howards Pass area, one of the oldest exposed units is the wavy banded limestones of the Rabbitkettle Formation (Fig. 6). This unit is a significant marker unit across the Selwyn Basin. The Rabbitkettle limestone can be traced to the northeast onto the Mackenzie Platform. Sedimentary features indicate an offshelf, quiet water depositional environment, perhaps marking a significant rifting event along the continental margin. Overlying the Rabbitkettle Formation are the dominantly black shales of the Road River Group, which host the Howards Pass Pb-Zn deposit ("Active member"; Figs. 5, 6). These fine-grained clastic sediments were deposited under generally anoxic conditions that became oxic in the upper Silurian. The change to oxic conditions is marked by orange-weathering, pyritic mudstones and siltstones with whispy horizontal burrows. Overlying the Road River Group are the coarse clastic, submarine fan deposits of the Earn Group (Fig. 6). The Earn Group includes bedded barite horizons, such as those associated with the Tom and Jason deposits. Unlike the deep-water Road River Group, rocks of the Earn Group included abundant paleocurrent indicators that are aligned east to southeast.

The goal of the Sm-Nd isotopic analyses is to evaluate the sources of sediment to the Rabbitkettle, Road River, and Earn Groups in the Howards Pass area (Fig. 7). A total of ten samples were chosen. Six samples were collected from diamond drillhole DDH42 at the centre of the XY deposit (Fig. 7), including two from the Earn Group, one from the orange-weathering bioturbated hanging wall mudstone at the top of the Road River Group, and three footwall shales and siltsones from the lower Road River Group. Two samples are from a stratigraphic section named ORO180 at the northwest end of the XY deposit (Fig. 7), one from the lower Earn Group and the other from the Rabbitkettle Formation (a silty limestone). The remaining two samples are outcrop samples, one from Earn Group rocks at the Jason deposit, Macmillan Pass, and the other from the lower Earn Group near Summit Lake, southwest of the XY deposit. The Sm-Nd data are shown in Table 1.

All of the analyzed samples of sedimentary rock have low present-day ε_{Nd}, ranging from -10.4 to -24.4. Age-corrected to their Nd isotopic composition at 380 Ma, which is the time of sediment deposition, ε_{Nd}^{t} values are still highly negative, ranging from -7.2 to -19.8. Two trends are visible in DDH 42 (Fig. 8, ε_{Nd}^{380} and T_{CHUR} vs. stratigraphic height). Firstly, the Rabbitkettle limestone and lower Road River shale have amongst the

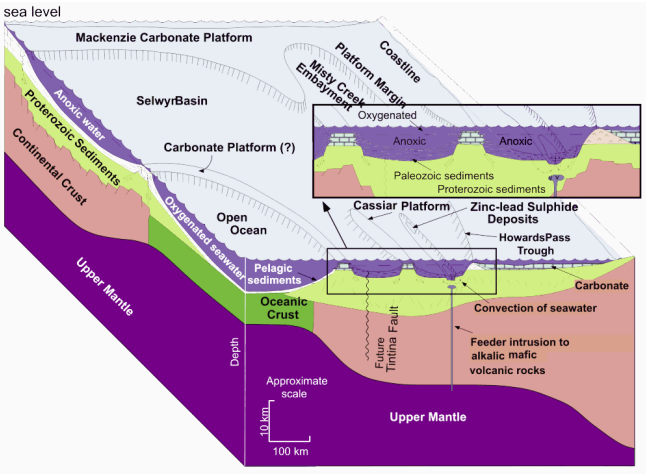


Figure 5. Block diagram showing the relationships between the Mackenzie carbonate platform, the Selwyn Basin, and an open ocean to the southwest during the early and middle Silurian (Goodfellow, 2007).

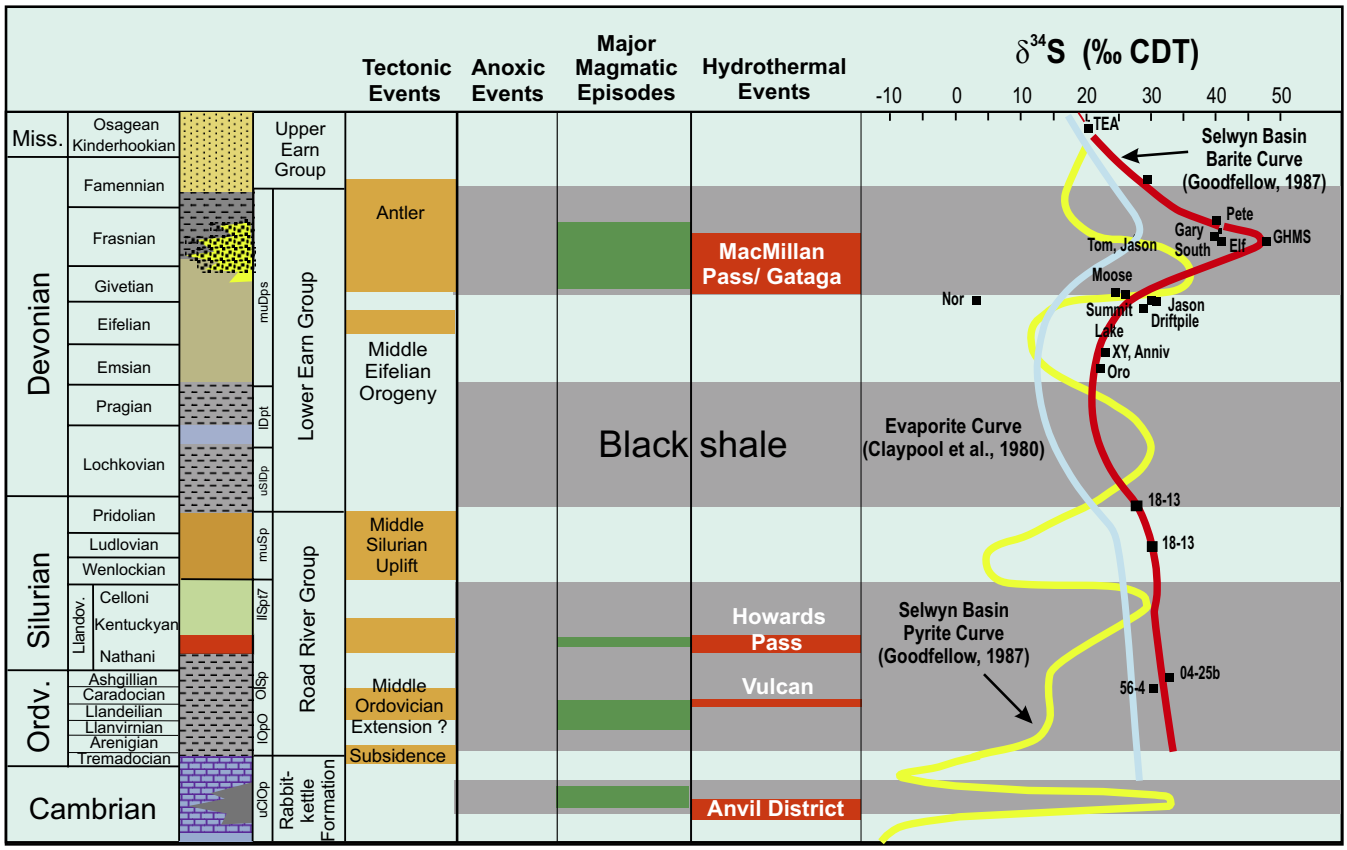


Figure 6. Stratigraphy of the Selwyn Basin in the Howards Pass area (Goodfellow, 2007). In the colour stratigraphic column on the left, the Active Member is shown in red. Also shown are major tectonic, anoxic, magmatic, and hydrothermal events, as well as variations in sulphur isotopic compositions in rocks and minerals of the basin.

most negative ε_{Nd}^{380} values, but that ε_{Nd}^{380} values become less negative moving up towards the Active Member. Secondly, the upper Road River and the Earn Group are much more homogeneous in isotopic composition than the lower Road River Group. Earn Group sedimentary rocks from the Jason, Summit Lake, and Oro areas are very similar isotopically to Earn Group rocks from DDH 42. ε_{Nd}^{380} for Earn Group rocks fall in the mid-range of values for the lower Road River Group.

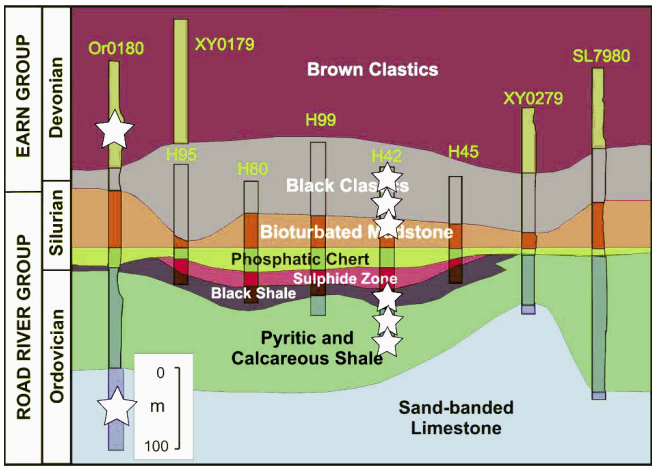


Figure 7. Cross-section through the XY deposit, Howards Pass (Goodfellow and Jonasson, 1986; Goodfellow, 2004). "Sand-banded limestone" is the Rabbitkettle Formation, and "Brown Clastics" is the Earn Group. All other units are Road River Group. Stars indicate sample locations for Nd isotopic work.

Model ages generally follow ε_{Nd}^{380} values (Figs. 8, 9). The Rabbitkettle and lower Road River Group have early Proterozoic model ages that decrease to late Proterozoic going upsection towards the Active Member. The Upper Road River orange-weathering mudstone has Sm-Nd systematics that are different from all of the other samples; these rocks have an intermediate present-day ε_{Nd} but, as a result of their high Sm/Nd ratio, have the oldest model age. It is important to note that model ages reflect not only the average age of detritus in the sedimentary rock, but also its composition.

In Figure 9, the isotopic evolution envelope for Archean granitoids from the Slave province is compared to the evolution lines for Selwyn Basin sedimentary rocks. The Selwyn rocks all have ε_{Nd} values higher than Archean rocks. Granitoids from the Wopmay Orogen typically have ε_{Nd} values, calculated at 380 Ma, of between -25 and -15 (V. Jackson and V. Bennett, pers. comm., 2005). The least radiogenic of the Selwyn samples overlap with the Wopmay Orogen

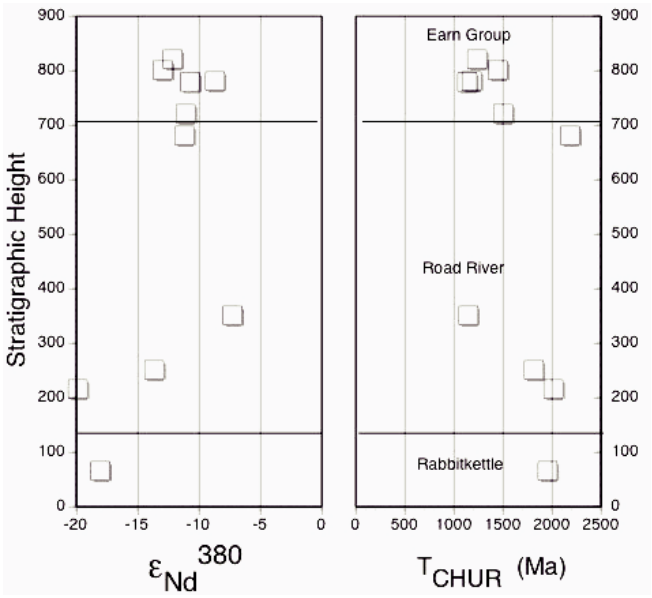


Figure 8. ε_{Nd}^{380} (at 380 Ma) and CHUR model ages (T_{CHUR}) plotted against stratigraphic height (metres) in DDH 42 and ORO180 sections. Additional Earn Group samples from outcrops in the Jason and Summit Lake areas are plotted around the ORO180 samples but the exact height relationship between the outcrop and drillhole samples is not known.

ε_{Nd} values, but most of the Earn Group sedimentary rocks are more radiogenic than Wopmay granitoids.

The Nd isotopic data indicate that Archean detritus is not a dominant component of the Selwyn Basin sedimentary rocks, but Paleoproterozoic detritus from the Wopmay Orogen may be important volumetrically. Proterozoic sedimentary rocks underlie the Selwyn Basin sequence and extend to the east beneath the Mackenzie carbonate platform (Goodfellow, 2004), indicating that detritus derived from the east was being shed westward prior to deposition of the deep water Selwyn Basin sediments. Since no Proterozoic sediment source is thought to have existed west of the Selwyn Basin at this time (see Fig. 6 in Goodfellow, 2004), this implies that the sediment source must have been to the east. The low ε_{Nd} values of the silty limestone from the Rabbitkettle Formation appears to be consistent with this implication, in that the bulk of the rare earth element budget in the limestone should be in the silty portion of the rock that would represent fine detritus wafting over the Mackenzie Platform from the east.

Although the Rabbitkettle and Road River sedimentary rocks overlap in model age with Wopmay rocks, the Earn Group samples are slightly less radiogenic and have model ages younger than those of the Wopmay granitoids. The Earn Group samples appear to include a more radiogenic component that may be derived from local, coeval alkalic volcanic rocks. The low Sm/Nd ratios (steep evolution lines in Fig. 9) of the Earn Group samples suggests that this more radiogenic component is felsic in composition, compared to the lower Sm/Nd ratio of all but one of the Road River sedimentary rocks, which is consistent with a less felsic detrital composition.

Paleocurrent direction in the Earn Group suggests that sediment was shed from the west and northwest. This requires either uplift of Selwyn Basin sequences in the northern Yukon or the development of a new volcanic arc west of Selwyn Basin during the Devonian (Yukon-Tanana terrane?, Héon, 2003). Although Earn and Road River Group Nd isotopic ratios overlap and would be consistent with simple uplift of Road River sedimentary rocks and reworking to form Earn Group turbidites, the apparently younger model ages for the Earn Group would fit nicely with the addition of a felsic arc volcaniclastic component from an island arc to the west.

There are no unequivocal Nd isotopic distinctions between sedimentary formations/groups in the Howards Pass area based on the Nd analytical work to date. Further work is required in order to evaluate the apparent decrease in ε_{Nd} values with increasing stratigraphic height in the lower Road River Group, in particular to see if this trend continues upwards through the Active Member and to see where ε_{Nd} values increase again up towards the orange-weathering mudstone at the top of the Road River. Further evaluation of the apparent model age difference between the Road River and Earn group sedimentary rocks would improve our understanding of the tectonic setting of the Earn Group.

STUDY OF THE ROLES OF SEAWATER AND HYDROTHERMAL FLUIDS IN CARBONATE FORMATION

Strontium (Sr) is an abundant trace element in seawater and is also abundant in hydrothermal waters due to

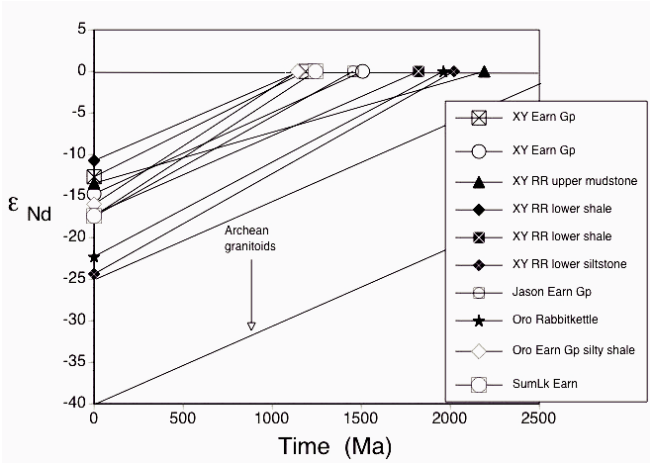


Figure 9. Time versus ε_{Nd} for sedimentary rocks of the Selwyn Basin. Present-day ε_{Nd} values are extrapolated back to where their isotopic composition is equal to that of CHUR (ε_{Nd} = 0), and the time at which each line meets the CHUR line is the model age (T_{CHUR}). RR = Road River Group.

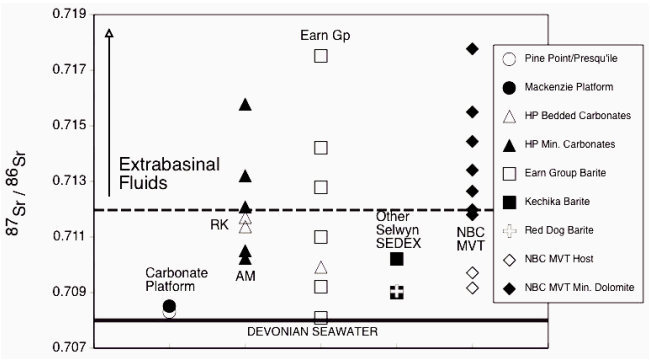


Figure 10. Plot of Sr isotope ratios in carbonates and hydrothermal barite deposits of the Selwyn Basin and nearby Mackenzie Platform. Howards Pass (HP) bedded carbonates include Rabbitkettle limestones (RK) and the fetid limestone of the Earn Group, whereas "HP Min. Carbonates" are carbonate/phosphatic nodules and carbonate-rich layers associated with the Active Member (AM) at the XY and ANNIV deposits (this study). NBC MVT = northern British Columbia Mississippi Valley-type Pb-Zn deposits; dashed line is lower limit of fluid compositions expected for extrabasinal fluids with Precambrian Sr sources (Machel and Cavell (1999). Other carbonate and barite data from Nelson et al. (2002) and Goodfellow (2004).

scavenging of Sr from plagioclase feldspar (e.g. Seyfried et al., 1988). The Sr isotopic composition of seawater varies as a balance between continental runoff (high $^{87}Sr/^{86}Sr$ ratio) and seafloor hydrothermal vent output (low $^{87}Sr/^{86}Sr$ ratio), and the isotopic variation of seawater over time has been determined from isotopic analysis of shells of marine organisms (Burke et al., 1982). Hydrothermal springs in continental environments, however, will have high Sr isotopic ratios more consistent with continental crust sources only.

Previous Sr isotopic studies have shown that measured $^{87}Sr/^{86}Sr$ ratios in carbonate and barite units of the Selwyn and Kechica basins are higher than that of Devonian seawater (Fig. 10). Carbonate units that predate but host Pb-Zn deposits, such as carbonates from the Pine Point area, the Presqu'ile barrier, and the Mackenzie Platform, are only slightly more radiogenic than seawater. At Howards Pass, the Rabbitkettle limestone is moderately radiogenic compared to seawater but below the calculated cutoff for having a fluid source from outside of the shale basin (dashed line, Fig. 10). Concretions and carbonate-rich layers of the Active Member have a wide range of Sr isotope ratios that straddle the extrabasinal fluid dashed line, as do hydrothermal barite horizons in the Earn Group. In the Kechika Trough and the Red Dog deposit, hydrothermal barite layers are less radiogenic than carbonates associated with the Pb-Zn mineralization at Howards Pass.

The observation that bedded carbonate units in the Robb Lake Mississippi Valley-type deposit in northern British Columbia are more radiogenic than Devonian seawater led Nelson et al. (2002) to conclude that Sr in these units had been modified during diagenesis by addition of seawater that included a component derived from compaction of underlying siliciclastic rocks. The Rabbitkettle limestone in the Howards Pass area has even higher $^{87}Sr/^{86}Sr$ ratio than the Robb Lake case, perhaps also due to diagenetic alteration. The Rabbitkettle Formation is both underlain and overlain by clastic rocks with more radiogenic Sr than seawater (although no Sr isotopic analyses of these sedimentary rocks are available), and diagenetic or metamorphic addition of Sr is inevitable. It is also possible that the silty component in the Rabbitkettle units has contributed some radiogenic Sr during dissolution of the carbonate for isotopic analysis, although no silicate residue was observed after dissolution of the limestone in weak HCl.

Limestone concretions within the Active Member of the Road River Group at Howards Pass vary considerably in isotopic composition. The large range is possibly the product of the diagenetic addition of radiogenic strontium from adjacent clastic rocks where the proportion of clastic-derived Sr exchanged with the concretion was highly variable. If so, then the isotopic composition of Sr added to the concretions was greater than 0.716, which is the highest $^{87}Sr/^{86}Sr$ ratio measured in the concretions. Given the high Sr content of carbonate rocks, it is unlikely that this added component would completely overwhelm an original Sr isotopic composition. In this case, the measured $^{87}Sr/^{86}Sr$ ratios of the carbonate concretions should be close to their original isotopic ratio. An alternative explanation to a diagenetic origin for high $^{87}Sr/^{86}Sr$ raito is that the concretions inherited Sr that was a variable mixture of seawater and hydrothermal fluid Sr. Most of the concretions in the Howards Pass Pb-Zn deposits and many of the barite horizons in the Earn Group are therefore dominated by a hydrothermal fluid component with high $^{87}Sr/^{86}Sr$ ratios (see also Goodfellow, 2004).

The Sr isotopic composition of the carbonate concretions of the Active Member suggests that even though no fault conduit or vent complex has been identified close to the XY deposit, mineralizing fluids were rock-dominated and derived their Sr from old, radiogenic rocks. Thus a fluid vent must exist somewhere in the XY area that exhaled these fluids onto the seafloor and into the sediment pile. The discovery of such a vent or conduit may lead to further identification of prospective areas for SEDEX exploration.

Pb ISOTOPIC COMPOSITION OF SULPHIDES AND HOST ROCKS, HOWARDS PASS

Pb isotope ratios in sulphide minerals represent an average isotopic composition of source rocks sampled for metals by hydrothermal fluids (e.g. Stacey and Kramers, 1975; Thorpe, 1982). Pb isotopes can also be used to define genetically related groups of ore

deposits with similar Pb isotope ratios. Below, the similarities and differences in Pb isotopic composition between individual Pb-Zn deposits or showings in the Howards Pass area are evaluated.

In Figure 11, Pb isotope ratios in galena and sphalerite from the major orebodies and showings of the Howards Pass area, including OP, ANNIV, XY, Brodel, and Don, all show the same isotopic characteristics. They show variations in both $^{208}Pb/^{204}Pb$ and $^{207}Pb/^{204}Pb$ ratios, which are large relative to variations in $^{206}Pb/^{204}Pb$ ratios. All are hosted in the Road River Group. New data from this study overlap with previous Pb isotopic studies that primarily focused on the XY deposit (summarized in Morganti, (1979) and Godwin and Sinclair (1982)). Galena and pyrite from the Grand/NOR property, located south of the XY deposit and hosted in the Earn Group, have Pb isotopic compositions distinct from those of Road River-hosted deposits, and in particular $^{206}Pb/^{204}Pb$ ratios are measurably lower. The CMC showing, hosted in a folded wedge of Road River Group within Earn Group sediments, has measurably higher $^{206}Pb/^{204}Pb$ ratios than the major Howards Pass showings.

The Pb isotope ratios in Howards Pass siliceous and carbonate rocks are shown in Figure 12. Rock units similar in composition to Howards Pass sulphides are shown in open symbols, and these units include all of the carbonates including the Rabbitkettle limestone. Most of the siliceous units (solid symbols) range to much higher Pb isotope ratios than the sulphides, as expected given the much higher U/Pb ratio in silicates compared to sulphides. Some of the mudstones may be mineralized, levering their Pb isotopic composition towards the field of HP mineralization in Figure 12.

Figure 13 compares the Pb isotopic data from this study at Howards Pass with other Pb data from Pb-Zn deposits from the Selwyn Basin. Also shown is an average crustal evolution curve (Stacey and Kramers, 1975) and the growth curve for shale-hosted Pb-Zn deposits of the Canadian Cordillera (Godwin and Sinclair, 1982). The shale curve indicates the Pb isotopic evolution of sediments deposited on the western margin of North America that were derived primarily from upper crustal rocks of the western Canadian Shield (Godwin and Sinclair, 1982). The Howards Pass samples form a linear array that begins on the shale growth curve and extends to more radiogenic compositions, implying a second source of Pb besides that represented by the shale curve. Note that the Tom and Jason deposits of the Earn Group are extremely similar isotopically to the Howards Pass deposits, even though the Tom and Jason are considered to be much younger in age. Sulphides in the Anvil area are older than those at Howards Pass, as expected.

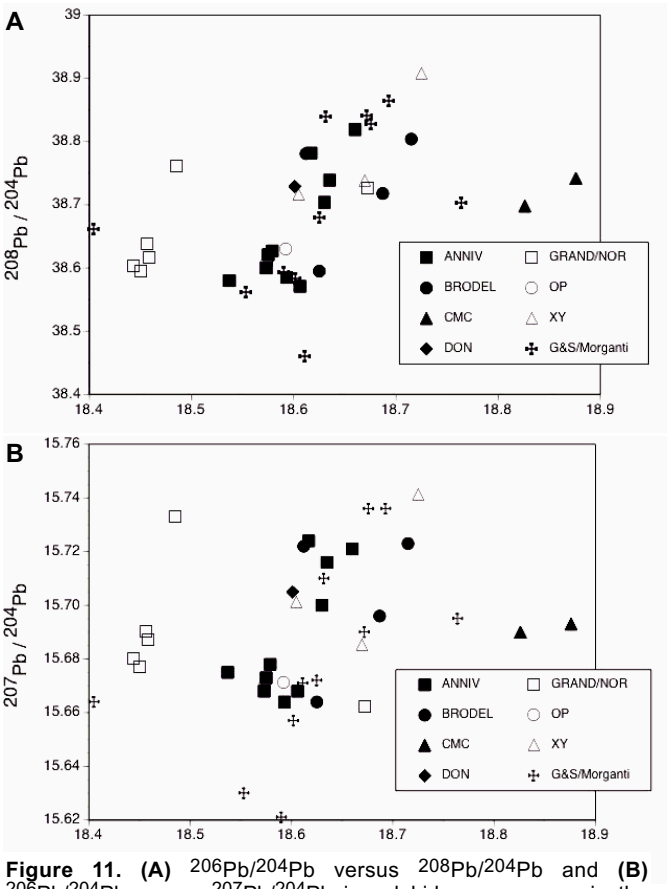


Figure 11. (A) $^{206}Pb/^{204}Pb$ versus $^{208}Pb/^{204}Pb$ and **(B)** $^{206}Pb/^{204}Pb$ versus $^{207}Pb/^{204}Pb$ in sulphide occurrences in the Howards Pass area. Previous Pb isotopic data from Morganti (1979) and Godwin and Sinclair (1982) (G&S) are shown as crosses. Uncertainties are $^{208}Pb/^{204}Pb$ = +/- 0.038; $^{207}Pb/^{204}Pb$ = +/- 0.013; $^{206}Pb/^{204}Pb$ = +/- 0.010.

From the Pb isotopic data, several conclusions can be drawn. Firstly, all of the Howards Pass mineralized zones (OP, ANNIV, Brodel, XY) overlap in isotopic composition. Thus, if each mineralized zone represents a different brine pool within a local subbasin in this part of the Selwyn Basin (Goodfellow, 2004), either each pool was connected or hydrothermal fluids that vented into each subbasin were identical isotopically (i.e. similar source rocks but multiple fault conduits; Fig. 2B). Thus all of the mineralized zones are linked and appear to represent a single depositional event (however protracted in time). The likelihood of finding other mineralized bodies along the strike of the OP-XY corridor would appear to be high if more subbasins existed at the time of the mineralizing event.

Secondly, two end-member components in the hydrothermal fluids can be recognized (Fig. 13). The first, plotting close to the shale growth curve, is identified as Proterozoic sedimentary rock sources similar to those of the Sullivan deposit in the southern Cordillera. The second plots well above this curve at high $^{207}Pb/^{204}Pb$ (Fig. 13) ratios. Other Pb-Zn deposits within the Yukon, such as those in the Wolverine area,

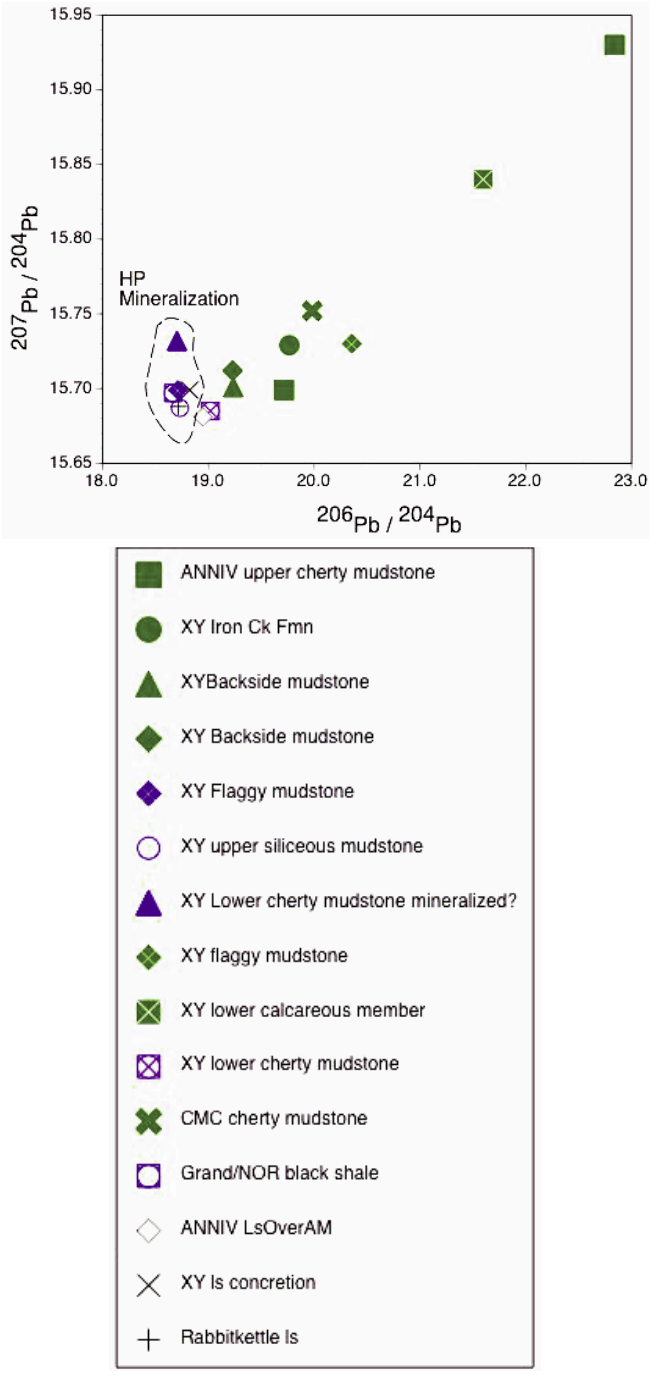


Figure 12. $^{206}Pb/^{204}Pb$ (present-day) versus $^{207}Pb/^{204}Pb$ in silicate and carbonate rocks in the Howards Pass area. Isotopic compositions of sulphide minerals from Figure 11B are enclosed within the dashed field. Ck = Creek; "LsOverAM" = limestone over Active Member; ls = limestone.

also form arrays between the shale growth curve and a more radiogenic component (D. Layton-Matthews, pers. comm., 2005). The origin of this radiogenic component is unclear, but requires a very old source, perhaps Archean in age, with a high U/Pb ratio.

Thirdly, it is unclear why the GRAND/NOR sulphides, hosted in the Earn Group, should plot at lower $^{206}Pb/^{204}Pb$ ratios than Howards Pass deposits hosted in the Road River Group (Fig. 11). This implies that the GRAND/NOR sulphides are older than the XY/ANNIV sulphides, based on the shale curve model, yet they are hosted in younger Earn Group rocks. One possibility is that the shale model is not appropriate for Earn Group mineralization, and that a new Pb source (derived from the west?) was introduced during the Devonian. In contrast, sulphides in the CMC showings have higher $^{206}Pb/^{204}Pb$ ratios, yet are hosted in Road River-age rocks similar to the XY deposit. CMC sulphides may have been reset isotopically during intense folding of Road River and abundant Earn Group sedimentary rocks, and perhaps some of the mineralization at CMC was mobilized from surrounding Earn Group rocks.

SUMMARY

This study has outlined several important points in the origin of SEDEX deposits in the Selwyn Basin and the potential for the discovery of additional mineralized zones in the Howards Pass area.

Firstly, the Sm-Nd study shows significant variation in the age, composition, and source of sediments to the Selwyn Basin in the Howards Pass area. Model ages range from early to late Proterozoic. Road River Group shales, probably derived from Proterozoic rocks the east, vary considerably in isotopic composition from base to top, but Earn Group clastic rocks are isotopically more homogeneous. Earn Group rocks also carry isotopic and rare earth element characteristics that are best explained by the increased importance of relatively juvenile, felsic volcanic detritus shed from the west or northwest. The Yukon-Tanana terrane may be the source of these sediments.

Sr isotopic compositions in carbonate units and carbonate-phosphate concretions within mineralized zones

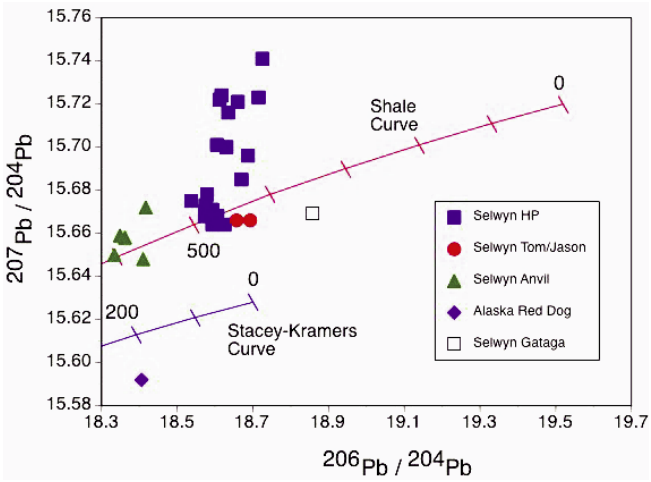


Figure 13. Comparison of Pb isotopic data from the Howards Pass and other Selwyn Basin SEDEX deposits with the average crustal evolution curve (lower) of Stacey and Kramers (1975) and the shale evolution curve (upper) of Godwin and Sinclair (1982). Ticks are spaced 100 Ma apart.

in the Howards Pass area are all more radiogenic than Devonian seawater. Although diagenetic exchange of Sr may occur between host shales and carbonates, we favour a rock-dominated hydrothermal fluid source for the radiogenic Sr. Sr isotope ratios may reflect mixing between seawater Sr and hydrothermal Sr, dominated by the hydrothermal component. Trace element concentration data (analyses are underway) are required to develop a mixing model to test this hypothesis.

Pb isotopic data from sulphides and host rocks of the Howards Pass Pb-Zn deposits and showings indicate that the main prospects (OP, ANNIV, Brodel, XY, and Don) formed from isotopically identical hydrothermal fluids, supporting a cogenetic model in linked sub-basins within the Selwyn Basin. A roughly linear Pb isotopic array suggests two Pb sources, one lying close to the shale evolution curve for the northern Cordillera, the other having much higher $^{207}Pb/^{204}Pb$ and $^{208}Pb/^{204}Pb$ ratios. The probability of connectivity between the deposits is high, as is the probability of extension of the Pb-Zn mineralization to the northwest and southeast. No feeder system (fault conduit, vent complex) has yet been identified for the XY deposit, but the dominance of hydrothermal Sr in carbonate concretions in the Active Member suggests that the feeder system must be nearby. Showings in the Grand/NOR claims, hosted in the Earn Group, have unexpectedly low Pb isotope ratios, which infer an older age than Road River-hosted sulphides. Alternatively, the source of Pb for Grand/NOR showings is not the typical sedimentary source modeled by the shale curve. This may apply also to the Tom and Jason deposits at Macmillan Pass, which are also hosted in Earn Group clastics that also have anomalously low Pb isotope ratios for their age.

ACKNOWLEDGEMENTS

This work was supported by Hendrik Falck and Danny Wright at the Geological Survey of Canada. I sincerely appreciate the support of Pacifica Resources for field work, a home, and great food at the ANNIV camp. In particular, I thank the camp managers, Geoff and JJ, for their interest in the project and access to core samples. Sm-Nd analyses were carried out by Vishal Gupta, Integrated Sciences Program, Carleton University. Sample preparation and lab chemistry were ably handled by Anatoliy Franchuk and Jacqueline Dohaney, and assistance in the mass spectrometry lab was provided by E.A. Spencer. John Blenkinsop was instrumental (no pun intended) in keeping the Triton operating at peak efficiency. This is the Ottawa-Carleton Geoscience Centre, Isotope Geochemistry and Geochronology Research Centre Contribution Number 45.

REFERENCES

Abbott, J.G., Gordey, S.P., and Tempelman-Kluit, D.J.
1986: Setting of stratiform, sediment-hosted lead-zinc deposits in Yukon and northeastern British Columbia, *in* Mineral Deposits of the Canadian Cordillera, (ed.) J. A. Morin; The Canadian Institute of Mining and Metallurgy, Special Volume 37, p. 1-18.

Albarède, F., Michard, A., Minster, J.F., and G. Michard, G.
1981: $^{87}Sr/^{86}Sr$ ratios in hydrothermal waters and deposits from the East Pacific Rise at 21°N; Earth Planetary Science Letters, v. 55, p. 229-236.

Bennett, V.C. and DePaolo, D.J.
1987: Proterozoic crustal history of the western United States as determined by neodymium isotopic mapping; Geological Society of America Bulletin, v. 99, p. 674-685.

Burke, W.H., Denison, R.E., Hetherington, E.A., Koepnick, R.B., Nelson, H.F., and Otto, J.B.
1982: Variation of seawater 87Sr/86Sr throughout Phanerozoic time; Geology, v. 10, p. 516-519.

Claypool, G.E., Holser, W.T., Kaplan, I.R., Sakai, H., and Zak, I.
1980: The age curves of sulfur and oxygen isotopes in marine sulfate and their mutual interpretation; Chemical Geology, v. 28, p. 3-4.

Cousens, B., Blenkinsop, J., and Franklin, J.
2002: Lead isotope systematics of sulfide minerals in the Middle Valley hydrothermal system, northern Juan de Fuca Ridge, Geochemistry Geophysics Geosystems, v. 3, p. 1029.

Cousens, B.L., Falck, H., van Hees, E.H., Farrell, S., and Ootes, L.
2006: Pb isotopic compositions of sulphide minerals from the Yellowknife gold camp: Metal sources and timing of mineralization, *in* Gold in the Yellowknife Greenstone Belt, Northwest Territories: Results of the EXTECH III Multidisciplinary Research Project, (ed.) C.D. Anglin, H. Falck, D.F. Wright, and E.J. Ambrose; Geological Association of Canada, Mineral Deposits Division, Special Paper 3, St. Johns, Newfoundland, p. 286-300.

Davis, A.S., Clague, D.A., Zierenberg, R.A., Wheat, C.G., and Cousens, B.L.
2003: Sulfide formation related to changes in the hydrothermal system on Loihi Seamount, Hawaii, following the seismic event in 1996; Canadian Mineralogist, v. 41, p. 457-472.

DePaolo, D.J.
1988: Neodymium Isotope Geochemistry; Springer-Verlag, Berlin, 154 p.

DePaolo, D.J., Linn, A.M., and Schubert, G.
1991: The continental crustal age distribution: Methods of determining mantle separation ages from Sm-Nd isotopic data and application to the southwestern United States; Journal of Geophysical Research, v. 96, p. 2071-2088.

Godwin, C.I. and Sinclair, A.J.
1982: Average lead isotope growth curves for shale-hosted zinc-lead deposits, Canadian Cordillera; Economic Geology, v. 77, p. 675-690.

Godwin, C.I., Sinclair, A.J., and Ryan, B.D.
1982: Lead isotope models for the genesis of carbonate-hosted Zn-Pb, shale-hosted Ba-Zn-Pb, and silver-rich deposits in the northern Canadian Cordillera; Economic Geology, v. 77, p. 82-94.

Goodfellow, W.D.
1987: Anoxic stratified oceans as a source of sulphur in sediment-hosted stratiform Zn-Pb deposits (Selwyn Basin, Yukon, Canada); Chemical Geology, v. 65, p. 359-382.
2004: Geology, genesis and exploration of SEDEX deposits, with an emphasis on the Selwyn Basin, Canada, *in* Sediment-

Hosted Pb-Zn Sulphide Deposits: Attributes and Models of Some Major Deposits of India, Australia and Canada, (ed.) M. Deb and W.D. Geoodfellow; Narose Publishing House, Delhi, p. 24-99.

2006: Metallogeny of the Selwyn Basin, *in* Mineral Deposits of Canada: A Synthesis of Major Deposit-Types, District Metallogeny, the Evolution of Geological Provinces, and Exploration Methods, (ed.) W.D. Goodfellow; Geological Association of Canada, Mineral Deposits Division, Special Publication, in press.

Goodfellow, W.D., and Jonasson, I.R.

1986: Environment of formation of the Howards Pass (XY) Zn-Pb deposit, Selwyn Basin, Yukon, *in* Mineral Deposits of the Canadian Cordillera, (ed.) J.A. Morin; The Canadian Institute of Mining and Metallurgy, Special Volume 37, p. 19-50.

Héon, D.

2003: Selwyn Basin Metallogeny;
http://www.geology.gov.yk.ca/metallogeny/selwyn/intro.html.

Jenner, G.A., Fryer, B.J., and McLennan, S.M.

1981: Geochemistry of the Archean Yellowknife Supergroup; Geochimica Cosmochimica Acta, v. 45, p. 1111-1129.

Machel, H.G. and Cavell, P.A.

1999: Low-flux, tectonically-induced squeegee fluid flow ("hot flash") into the Rocky Mountain foreland basin; Bulletin of Canadian Petroleum Geology, v. 47, p. 510-533.

Morganti, J.M.

1979: The Geology and Ore Deposits of the Howards Pass Area, Yukon and Northwest Territories: The Origin of Basinal Sedimentary Stratiform Sulphide Deposits; Ph.D. thesis, University of British Columbia, Vancouver , British Columbia, 317 p.

Nelson, J., Paradis, S., Christensen, J., and Gabites, J.

2002: Canadian Cordillera Mississippi Valley-type deposits: A case for Devonian-Mississippian back-arc hydrothermal origin; Economic Geology, v. 97, p. 1013-1036.

Patchett, P.J. and Gehrels, G.E.

1998: Continental influence on Canadian Cordilleran terranes from Nd isotopic study, and significance for crustal growth processes; Journal of Geology, v. 106, p. 269-280.

Patchett, P.J., White, W.M., Feldmann, H., Kielinczuk, S., and Hofmann, A.W.

1984: Hafnium/rare earth element fractionation in the sedimentary system and crustal recycling into the Earth's mantle; Earth and Planetary Science Letters, v. 69, p. 365-378.

Richard, P., Shimizu, N., and Allègre, C.J.

1976: $^{143}Nd/^{146}Nd$, a natural tracer: An application to oceanic basalts; Earth and Planetary Science Letters, v. 31, p. 269-278.

Ridley, W.I., Perfit, M.R., Jonasson, I.R., and Smith, M.F.

1994: Hydrothermal alteration in oceanic ridge volcanics: A detailed study at the Galapagos Fossil Hydrothermal Field; Geochimica Cosmochimica Acta, v. 58, p. 2477-2494.

Seyfried, W.E., Jr., Berndt, M.E., and Seewald, J.S.

1988: Hydrothermal alteration processes at mid-ocean ridges: Constraints from diabase alteration experiments, hot-spring fluids, and composition of the oceanic crust; Canadian Mineralogist, v. 26, p. 787-804.

Stacey, J.S. and Kramers, J.D.

1975: Approximation of terrestrial lead isotope evolution by a two-stage model; Earth and Planetary Science Letters, v. 26, p. 207-221.

Thorpe, R.I.

1982: Lead isotope evidence regarding Archean and Proterozoic metallogeny in Canada; Revista Brasileira de Geosciencias, v. 12, p. 510-521.

Todt, W., Cliff, R.A., Hanser, A., and Hofmann, A.W.

1984: ^{202}Pb -^{205}Pb spike for Pb isotopic analysis; Terra Cognita, v. 4, p. 209.

Yamashita, K. and Creaser, R.A.

1999: Geochemical and Nd isotopic constraints for the origin of late Archean turbidites from the Yellowknife area, Northwest Territories, Canada; Geochimica Cosmochimica Acta, v. 63, p. 2579-2598.

MODELLING MINERAL POTENTIAL FOR THE GREATER NAHANNI ECOSYSTEM USING GIS-BASED ANALYTICAL METHODS

J. R. Harris[1], D. Lemkow[1], D. F. Wright[1], and H. Falck[2]
1. Geological Survey of Canada, 601 Booth Street, Ottawa, Ontario K1A 0E8
2. Northwest Territories Geoscience Office, P.O. Box 1500, Yellowknife, Northwest Territories X1A 2R3

ABSTRACT

Mineral potential within the Greater Nahanni Ecosystem was modelled in a Geographic Information System (GIS) for four different deposit models: 1) SEDEX -stratiform shale-hosted sedimentary-exhalative Zn-Pb-Ag, 2) 'carbonate-fault' - carbonate-hosted zinc-lead-silver associated with major faults, 3) 'intrusion-related' - includes skarn, rare metals and gemstones), and 4) Carlin-type gold as lode and/or derived placer deposits. This mineral-potential modelling study integrates data collected during two Mineral and Energy Resource Assessment (MERA) projects. The results have contributed to the process of determining the geographic boundaries of the proposed expansion of the Nahanni National Park Reserve.

Four mineral potential maps were produced (one for each model) using a data-modified knowledge-driven approach. A weighting scheme, based on integrated mineral deposit and regional geological knowledge, was derived for the various evidence maps for each deposit model. The four potential maps, plus a fifth map of hydrocarbon potential based on the Nahanni MERA 1 assessment, were then combined into a final mineral-potential map using two algorithms: an additive operator and a maximum operator. Prediction plots of the four deposit models show that partial data sets provide reasonable predictions of the remaining known data.

Several areas within the study area were identified as having very high mineral potential. For SEDEX zinc-lead-silver type deposits, five areas were identified: A) Howards Pass at the northwest end of the 'zinc corridor'; B) another strand of this corridor northwest of the Cantung mine; C) the Meilleur River Embayment; D) Selena Creek; and E) east of Prairie Creek. For carbonate-fault zinc-lead-silver deposits, five areas are highlighted: F) Prairie Creek; G) Broken Skull Fault; H) Selena Creek; I) Howards Pass; and J) southeast of the Cantung mine. For intrusion-related deposits, three areas stand out: K) Selena Creek; L, M, N) a broad zone intruded by the Tay River plutonic suite including Cantung; and O) O'Grady Batholith. Finally, for the Carlin-type lode and/or placer gold deposits, six areas have high ratings: P) Selena Creek; Q, R, S) a broad linear zone of intrusions dividing and overlapping the 'zinc corridor'; T) surrounding the Mount Hamilton pluton; and U) in and around the O'Grady batholith. High natural gas potential was assessed under the MERA 1 project in the southeast corner of the study area, over the untested Etanda Dome and Twisted Mountain Anticline, as well as over the partially explored Mattson Anticline.

INTRODUCTION

This paper documents the application of a GIS (Geographic Information System)-based data-modified knowledge-driven approach to synthesize the results of multiple thematic studies, model mineral and energy potential, and submit the comprehensive transformed results to the national park planning process for the Greater Nahanni Ecosystem (Fig. 1). One single and three composite deposit models represent the key known and suspected mineral deposit types in the study area: 1) SEDEX - stratiform shale-hosted sedimentary-exhalative Zn-Pb-Ag, 2) 'carbonate-fault' - carbonate-hosted base-metals associated with major faults, 3) 'intrusion-related' - includes skarn, rare metals, and gemstones), and 4) 'Carlin-type' gold as lode and/or derived placer. The composite models are not formally recognized deposit types in the literature, but are informal amalgamations of several deposit types used specifically for this resource assessment, because their component types have so many attributes in common. These composite models are defined in the Deposit Models section below.

This work was part of the formal Mineral and Energy Resource Assessment (MERA) process (Government of Canada, 1995). An initial MERA 1 study was conducted for three smaller regions adjacent to the existing Nahanni National Park Reserve between 1985 and 1988 (Jefferson and Spirito, 2003). The current MERA 2 study covers an expanded region including the entire catchment for the Nahanni River (Fig. 1). The initial MERA study is referred to as MERA 1 and the current MERA study is referred to as MERA 2 throughout this paper. Under MERA 1, the focus was in three specific areas (Fig. 1) with the objective of upgrading the geological knowledge base (Jefferson et al., 2003), acquiring geochemical data for stream sediments (Spirito and Jefferson, 2003) and spring waters (Hamilton et al., 2003), compiling and transferring mineral occurrence data to the Northern Minerals Database (Normin.db; Department of Indian and Northern Affairs, 2006), and

Harris, J.R., Lemkow, D., Wright, D.F., and Falck, H., 2007, Modelling mineral potential for the Greater Nahanni Ecosystem using GIS-based analytical methods, *in* Mineral and Energy Resource Assessment of the Greater Nahanni Ecosystem Under Consideration for the Expansion of the Nahanni National Park Reserve, Northwest Territories, (eds.) D.F. Wright, D. Lemkow, and J.R. Harris; Geological Survey of Canada, Open File 5344, p. 293-326.

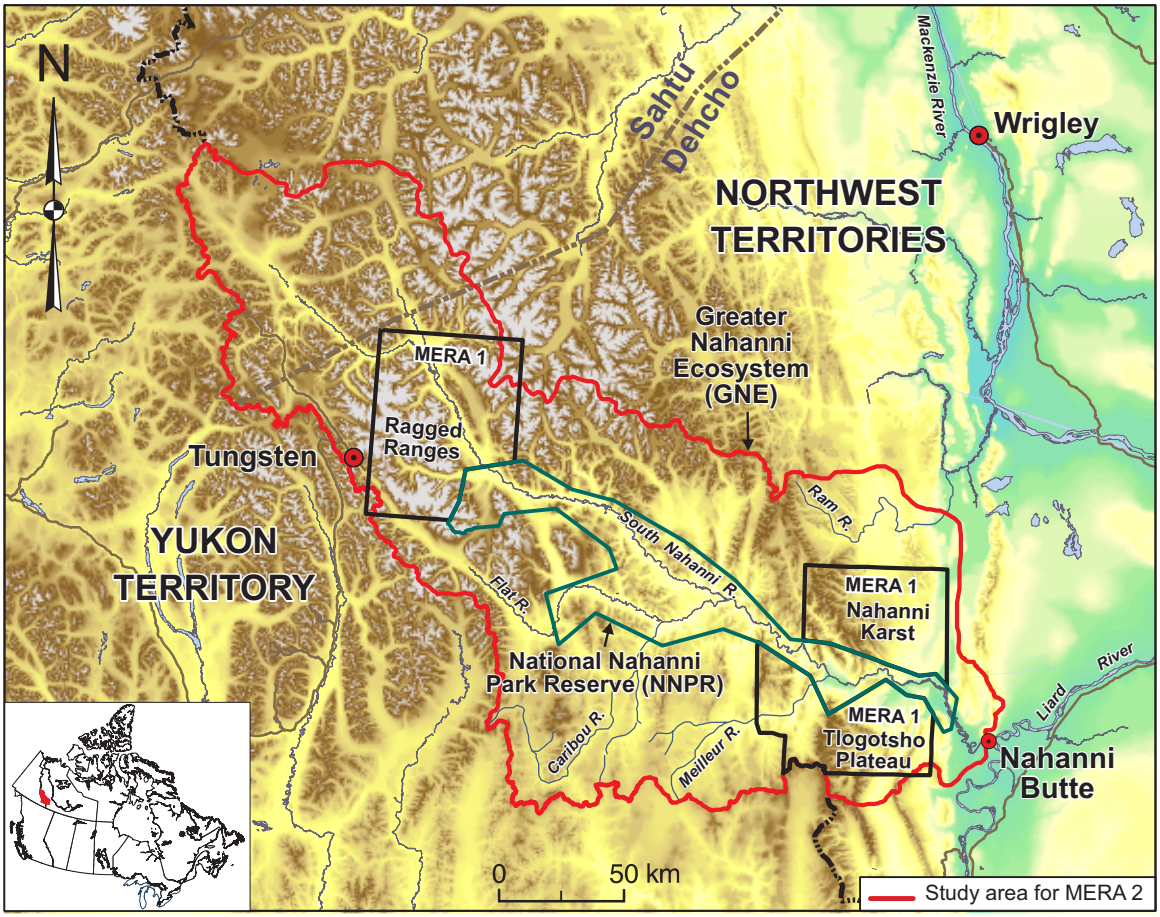


Figure1. Index and regional geographic context of the Nahanni MERA 2 study area. The MERA 1 study areas are Nahanni Karst, Ragged Ranges, and the Tlogotsho Plateau.

conducting structural play analysis for hydrocarbons (Osadetz et al., 2003). Under MERA 2, regional surveys of stream sediment and water (McCurdy et al., 2007) and spring water (Caron et al., 2007) brought a much larger area to match national standards of methodology and density, although duplication in the MERA 1 study areas was avoided except for calibrations. In addition, a new 1:1,000,000 digital geological base was adapted (Okulitch, in prep. a,b), five thematic mineral deposit studies (Barnes et al., 2007; Cousens, 2007; Paradis, 2007; Rasmussen et al., 2006, 2007; Yuvan et al., 2007), and a three-part airborne geophysical survey (Carson et al., 2007a,b,c; Charbonneau, 2007) established mineral-potential parameters for the most important occurrences in the study area. All of the primary data from these studies were compiled (see Data Collection section below) and archived in GIS format by Lemkow et al. (2007). In both MERA 1 and MERA 2, each component study generated qualitative prognostications of mineral potential from the perspective of mainly one type of knowledge; these all became part of the holistic knowledge base that helped to build the four representative mineral deposit models (see the Deposit Models section below) used for the GIS analysis.

The purpose of this GIS analysis is to derive relative mineral-potential maps as systematically, seamlessly, and quantitatively as possible from the entire suite of mineral deposit studies completed under MERA 1 and MERA 2. This study modelled the complete range of primary to synthesized topical geological and geochemical data in a GIS database to more fully consider their geological context and determine background values for different geological settings and thereby objectively defining anomalousness. The relative mineral- and energy-potential values presented here are in the context of the study area only, and there is no intent in this report to imply absolute values of potential for undiscovered mineral resources. The results generated from the GIS mineral deposit modelling were transferred with full spatial integrity to Parks Canada for use in their GIS modelling related to defining park boundary options.

Background on Geographic Information System Methods

One of the major strengths of GIS modelling is the ability to integrate and combine multiple layers (evidence maps) of geoscience data into mineral prospec-

tivity maps[1] showing areas that are potentially favourable for the presence of undiscovered mineral deposits (e.g. Chung and Agterberg, 1980; Bonham-Carter et al., 1988; Harris, 1989; Agterberg et al., 1990; Agterberg, 1992; Bonham-Carter, 1994; Rencz et al., 1994; Harris et al., 1995, 2001, 2006; Wright and Bonham-Carter, 1996; Raines, 1999; Wilkinson et al., 1999; Harris and Sanborn-Barrie, 2006). These capabilities make GIS an extremely useful tool for resource assessment and mineral exploration.

Numerous modelling methods for producing mineral potential maps using a GIS have been developed over the past ten years. These methods can be divided into two basic categories: data-driven and knowledge-driven techniques, for which reviews can be found in Bonham-Carter (1994) and Wright and Bonham-Carter (1996).

For any study area, data-driven approaches require that a prior knowledge (expressed in terms of a prior probability) exists in the form of known mineral deposits, prospects, or showings. Spatial relationships between the input data, as captured on evidence maps, and the locations of the mineral occurrences (the 'training set') are used to establish the importance (weight) of features on each evidence map. In other data-driven approaches, training areas can be established over each mineral deposit from which characteristic signatures of mineralization can be calculated from the various evidence layers (e.g. geochemistry, geophysics) used in the modelling process. Methods, such as logistic regression (Chung and Agterberg, 1980), weights of evidence (WofE) (Bonham-Carter, 1994), decision tree analysis (Reddy and Bonham-Carter, 1991) and neural networks (Singer and Kouda, 1996, 1999; Harris and Pan, 1999; Brown et al., 2000), are examples of data-driven approaches.

Knowledge-driven approaches are subjective to the extent that they rely on input from a geologist or team of geologists to rate the relative importance of evidence layers as they relate to each mineral deposit analogue or model being used. The subjective aspect is compensated for by the advantage of incorporating the accumulated knowledge and expertise of one or more geologists in the modelling process. Examples of knowledge-driven approaches include Boolean logic, index overlays (Harris, 1989), analytical hierarchy process (Harris et al., 1995, 2001), and fuzzy logic (An et al., 1991).

A data-modified knowledge-driven approach (see below) was used in this study because only one producing mine (Canada Tungsten, Fig. 1) is present in the study area. This is not a sufficient training set, since production histories are required to make reliable mineral-potential maps for all deposit models by data-driven techniques. Furthermore, mineral deposit knowledge would be better incorporated directly into the mineral-potential modelling process by using a knowledge-driven technique. This knowledge-driven technique consisted of a simple weighting system in which each type of evidence for each model was assigned a relative weight (reflecting importance) ranging in value from 1 to 10. However, it should be noted that data-driven methods make use of the location of mineral deposits with respect to individual evidence maps to derive the weights for each evidence map (see Bonham-Carter, 1994). In this study, even though the weights for each evidence map were subjectively derived, the location of mineral occurrences of a given deposit type were divided into four classes (defined resources, advanced prospects, showings, and anomalies), assigned a weight, and incorporated as evidence maps in the modelling process. Thus information on mineral occurrences was incorporated in the modelling process, albeit using a different strategy than that used for data-driven approaches. We refer to this method as a data-modified knowledge-driven approach.

One primary potential map was produced for each of the four deposit models that were defined for this study. This was done by combining the weighted evidence maps for each model, using a simple additive technique (weighted index-overlay), followed by normalization, to give each of the four deposit maps equal weight. The knowledge decisions for all four models were made with the aid of the mineral deposit studies cited. Particular weight was given to evidence derived from the studies supported by Nahanni MERA 2 that focused on significant local mineral occurrences by Barnes et al. (2007), Charbonneau (2007), Cousens (2007), Paradis (2007), Rasmussen et al. (2007), and Yuvan et al. (2007).

Hydrocarbon resource potential was not assessed in the Nahanni MERA 2 but was fully assessed by Osadetz et al. (2003) and reaffirmed based on new exploration knowledge by Osadetz (pers. comm., 2007). Three areas with significant hydrocarbon potential within the Greater Nahanni Ecosystem were identified in the southeast portion of the study area: Twisted Mountain Anticline, Mattson Anticline, and the Etanda Dome (Fig 2). A hydrocarbon potential map comprising these three areas was constructed and converted to a binary map in which all three areas were given a high weight.

The four primary mineral potential maps and the fifth hydrocarbon potential map were then combined into a single overall potential map by use of another simple arithmetic operator ('MAX'). This takes the

1 Also referred to as a 'potential' or a 'favourability' map in the GIS literature.

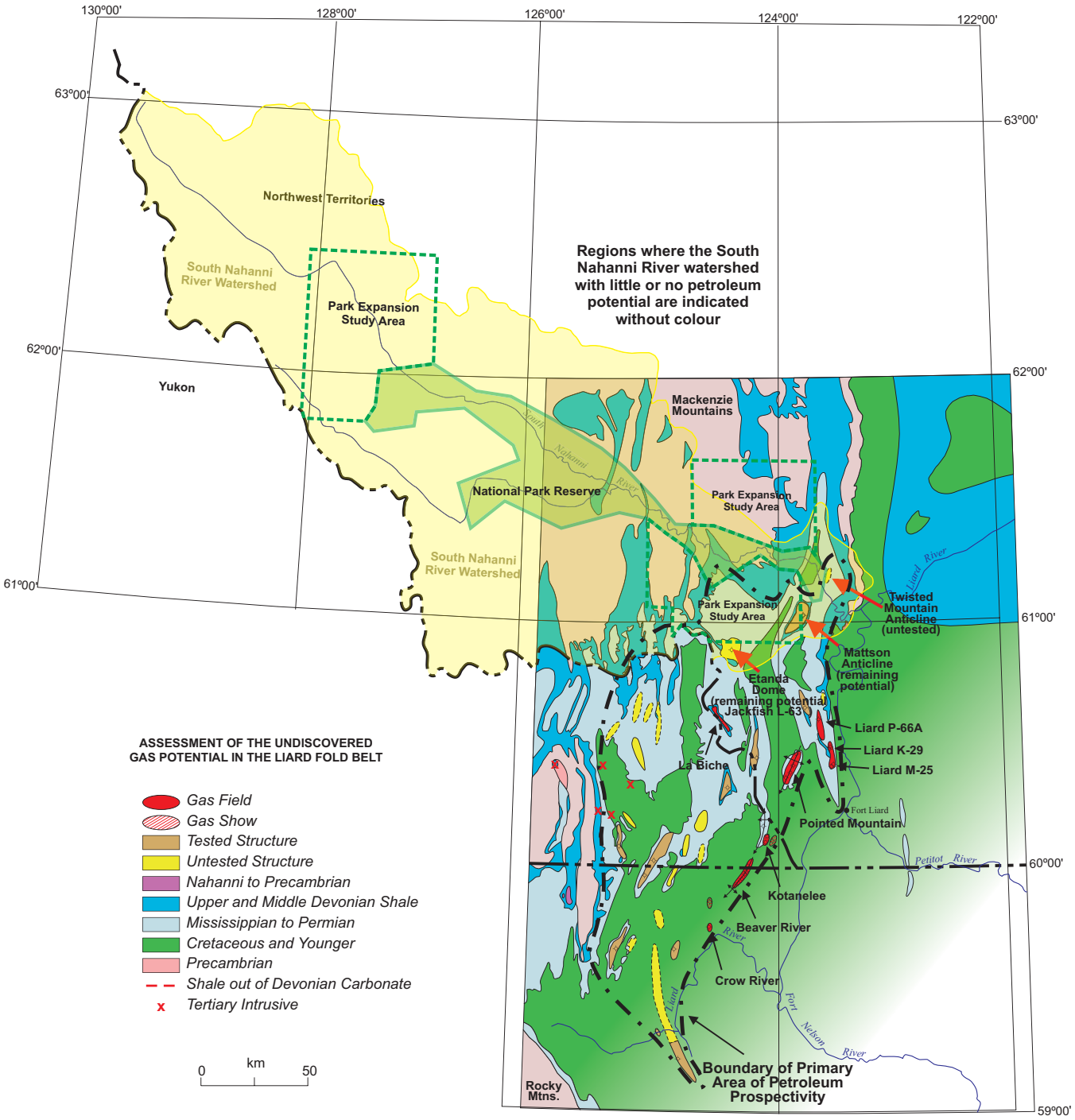


Figure 2. Hydrocarbon-potential map, from Osadetz et al. (2003), MERA 1. Three of the areas they assessed as having high potential for hydrocarbons (Twisted Mountain Anticline, Mattson Anticline, and Etanda Dome indicated by bold red arrows) are within the study area (South Nahanni River Watershed, outlined by yellow line and pale yellow shading).

maximum value from each of the five normalized potential maps on a cell-to-cell basis. The rationale behind the MAX operator is that high potential for any one deposit model is sufficient on its own. If the additive function was to be used at this stage, the normalization process would subdue a high potential rating that is based on only one deposit model compared to a similar high potential rating that is derived for two or more deposit models.

The assessment process used in this study employs GIS quantitative spatial analysis techniques of the data-modified, knowledge-driven weighted data sets to produce semi-quantitative relative mineral potential maps. This differs from all previous MERA assessments, which employed a completely subjective and much less systematic 'light table' approach whereby analogue maps were overlaid and judged with respect to mineral potential. A powerful asset of the new GIS approach is

to provide direct input to the GIS-based park planning system that does a cost-benefit analysis of biotic, physiographic, and ecosystem attributes, which are of importance to modern park sustainability and in order to develop boundary options for public consultation purposes.

Study Area

The area being assessed for this study is located in the southwestern corner of the Northwest Territories (Fig. 1). It includes the entire length and catchment area of the South Nahanni River and a small extension to the northeast that includes the Ram Plateau. This assessment area is known as the Greater Nahanni Ecosystem (GNE). It is approximately 400 km long and 150 km across, from latitude 63º00' to 60º45'N and from longitude 123º50' to 129º45'W. The total area of the GNE is approximately 39,000 km^2. In this assessment, the existing Nahanni National Park Reserve was excluded from the area of data collection, and as a result the additive-modelling process automatically produces an artificially depressed mineral potential within its boundaries.

Geological Setting

In paleogeographic terms, this region was situated on the western margin of the North American Craton from more than 800 million years ago until the Middle Devonian, about 350 million years ago. Along this margin, the sedimentary rocks of the western two-thirds of this region were deposited in the shaly, deep-marine Selwyn Basin, whereas the eastern third of the strata are shallow marine carbonate shelf facies of the MacDonald Platform. After this time, conglomerate and black shale were derived from colliding terranes to the west and silty shale was derived from distal orogens to the east. These two different shaly successions were roughly coeval and their interface in the central part of the study area is poorly known. The western part of the study area was uplifted due to continued mountain building in the west, and a mixture of foreland shale, limestone, and coaly sandstone were deposited in the southern and eastern areas.

The next geological phase of this region was dominated by structural and igneous activity. The Mackenzie Mountains were produced by compressional folding and thrusting of the above sedimentary units during the Jurassic (ca. 170 Ma) to Cretaceous (ca. 100 Ma). Major granitoid batholiths (termed Selwyn plutonic suite by Gordey and Anderson, 1993) intruded these rocks from about 100 to 94 Ma during collision of an island arc with western North America. The majority of the plutons are quartzofeldspathic and have accessory minerals within a narrow range of compositions that permit the plutons to be classified as biotite-muscovite ('two-mica'), biotite-hornblende, or biotite (Gordey and Anderson, 1993). Rasmussen et al. (2007) abandoned the local 'Selwyn plutonic suite' nomenclature in the process of documenting the Tombstone, Tungsten, Tay River (each of which has a distinct age range, distribution, composition and metallogeny) and transitional Tungsten-Tay River plutonic suites. Right-lateral strike-slip motion along major faults began in the Tertiary (ca. 40 Ma) and continues today.

The present landscape and exposed rock units (Fig. 3) are a result of recent weathering and erosion by water and ice during and after tectonic uplift. The eastern section of the study area is a dissected plateau exposing broadly folded karst (vertical dissolution of carbonate rocks by rain water produced sinkholes and caves) on the north side of the Nahanni River, and coal-bearing sandstone and shale with minor limestone on the south side. Continental glaciers carried till and mud east from the Canadian Shield into the eastern part of the study area. Mountain glaciers carved the U-shaped valleys and cirques into the Selwyn Ranges (Duk-Rodkin et al., 2007). More details on the geology of the study area are provided by Jefferson et al. (2003), Falck (2007), and Okulitch (in prep. a,b).

Data Collection

A critical component of the Nahanni MERA 2 project was to compile existing data along with data collected during the MERA 2 project into a digital, georeferenced GIS database. A comprehensive digital database covering the entire study area is essential to conduct mineral and energy resource assessment and model mineral potential using GIS-based analytical methods. In total, the current GIS database contains over 200 layers of digital geoscience data, including bedrock geology, surficial geology, geochemistry, geophysics, mineral deposits, and topographic data (Lemkow et al., 2007).

A selection of the bedrock geology, compiled by Okulitch (in prep a, b) at a scale of 1:1,000,000, is included in the digital GIS database. The bedrock geology map (Fig. 3) is a simplified classification of the major bedrock lithological groupings based on Okulitch (in prep. a, b). This fundamental framework locates key geological attributes associated with the four deposit models, which in turn highlight the most likely deposit types to be found in the study area. These lithologic attributes include primary sedimentary rock types, products of diagenetic alteration (e.g. Manetoe facies; Morrow et al., 1990), structure (faults and folds), and intrusive rock types (granitic plutons). All of these lithologic attributes provide indirect evidence for sources, transport, and deposition of elements that may have formed mineral deposits.

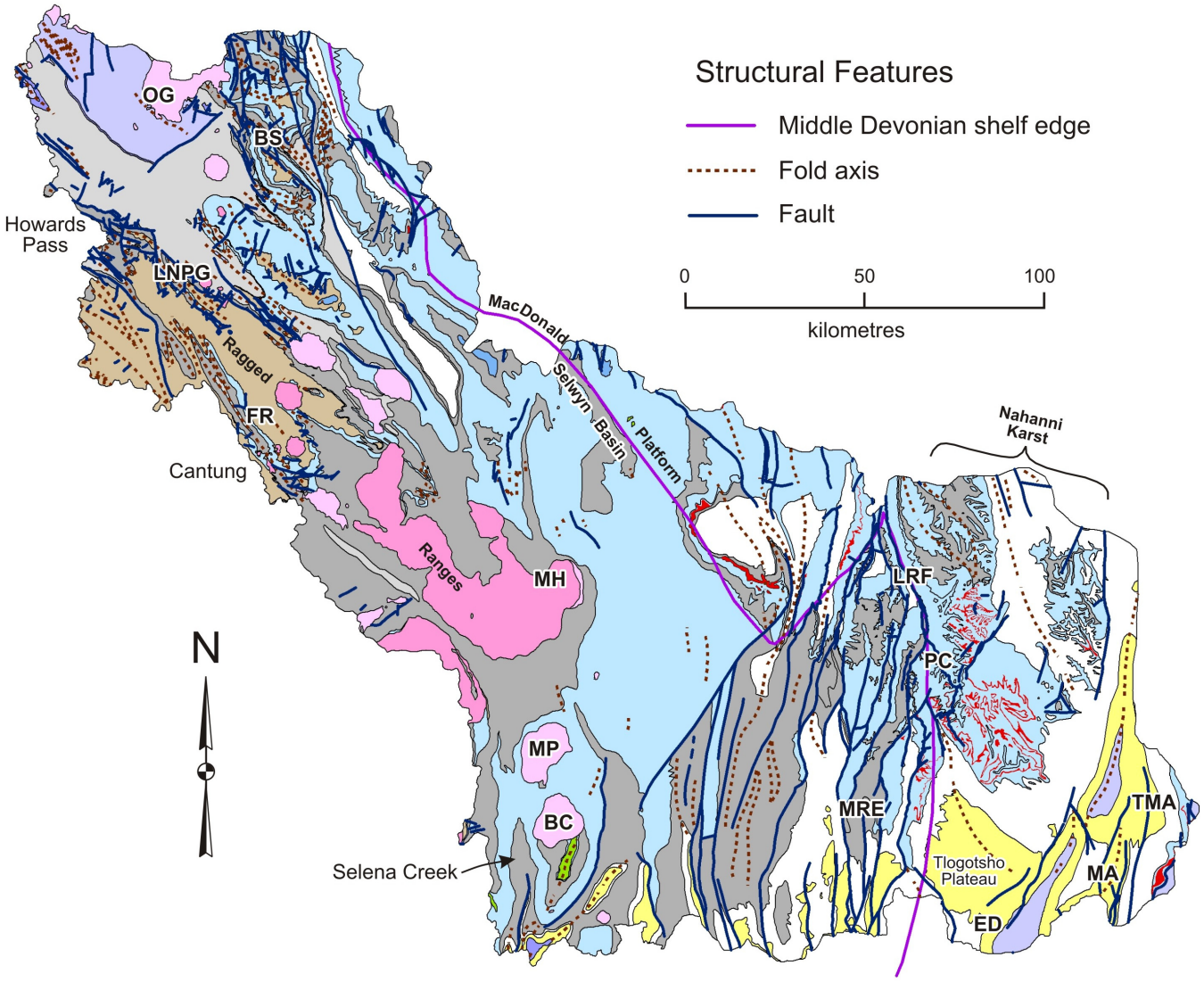


Figure 3. Geology used for spatial modelling of the Nahanni MERA 2 study area, after Jefferson and Spirito (2003), Okulitch (in prep. a, b), and Rasmussen et al. (2007). Units are combined in different ways (favourable rock units) for different mineral deposit models, as listed in Tables 2 to 5. BC = Big Charlie pluton, BS = Broken Skull River area, ED = Etanda Dome, FR = Flat River, LNPG = Little Nahanni Pegmatite Group, LRF = Leif Ridge Fault, MA = Mattson Anticline, MH = Mount Hamilton pluton, MP = McLeod pluton, MRE = Meilleur River Embayment, OG = O'Grady Batholith, PC = Prairie Creek, and TMA = Twisted Mountain Anticline. See opposite page for the legend.

A total of 2463 stream sediment samples and 2068 stream water samples were collected (Fig. 4A) by various surveys within the Greater Nahanni Ecosystem and geochemically analyzed to help model mineral potential. Over half of these samples (1374 stream sediment and 1378 stream water samples) were collected by McCurdy et al. (2007) during the 2004 and 2005 field seasons; these were combined with additional geochemical data for stream sediments and waters from previous surveys: 396 sediment samples from the first Nahanni MERA (Jefferson and Spirito, 2003), and 693 sediment samples and 683 water samples from previous National Geochemical Reconnaissance surveys (Friske et al., 2001; Day et al., 2005). All of these data are included in the GIS database (Lemkow et al., 2007) and were spatially analysed herein.

Detailed public-domain airborne geophysical data were not available for the study area prior to this MERA study. As part of the Nahanni MERA 2 project, three airborne surveys were flown at 135 m nominal terrain clearance along lines spaced at 500 m, for a total of 16,000 line kilometres over three areas (Figure 4B). These areas were considered most likely to generate conflicts between mineral potential and park values. The geophysical data provide additional evidence to help build the mineral deposit knowledge base, refine the mineral potential modelling, and may help resolve future planning issues. For each area, ten types of data were generated: total radioactivity, potassium (K, %), equivalent uranium (eU, ppm), equivalent thorium (eTh, ppm), eU/eTh, eU/K, eTh/K, ternary radioactive plots (K, eU, eTh), residual magnetic total field (nT), and calculated magnetic vertical gradient (nT/m). Key

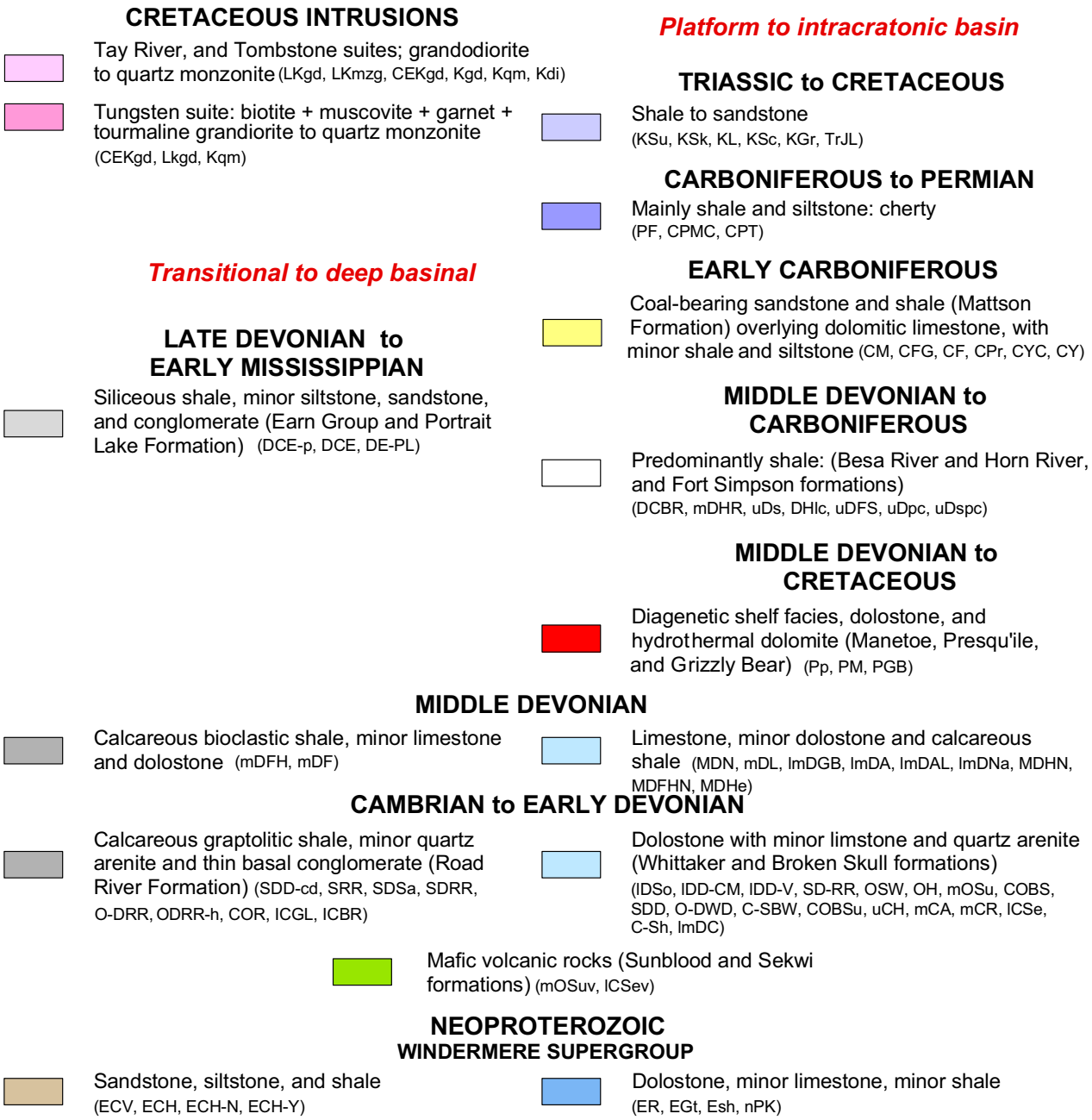


Figure 3 continued. Legend for the geological map of the Nahanni MERA 2 study area on the opposite page.

aspects of these surveys are discussed and illustrated by Charbonneau (2007). The full primary data sets have been published (Carson et al., 2007a,b,c) and are included in the GIS database (Lemkow et al., 2007).

Spring water geochemistry can be an effective tool for investigating regional compositional trends and for indirectly detecting buried mineral deposits that were transected by subterranean flow paths. Spring-water geochemistry surveys, reported by Hamilton et al. (2003) and Caron et al. (2007), contributed to the Nahanni MERA 1 and MERA 2 studies, respectively. Ninety-two different springs were sampled during 5ERA 1 and 79 during MERA 2, for a total of 157 different spring locations (this number does not include field duplicates, triplicates, laboratory blanks or the 16 springs that were sampled during MERA 1 and resampled in MERA 2). This data was compiled and integrated for this GIS analysis. Anomalous springs are listed in Table 1 and were derived from the compiled studies; these are shown in Figure 4C.

Mineral deposit data (Fig. 4D) were compiled and rationalized for the Nahanni MERA 1 over the entire watershed (Jefferson and Spirito, 2003). This data, a significant contribution to the NORMIN database (Department of Indian Affairs and Northern Development, 2006), was augmented by mineral

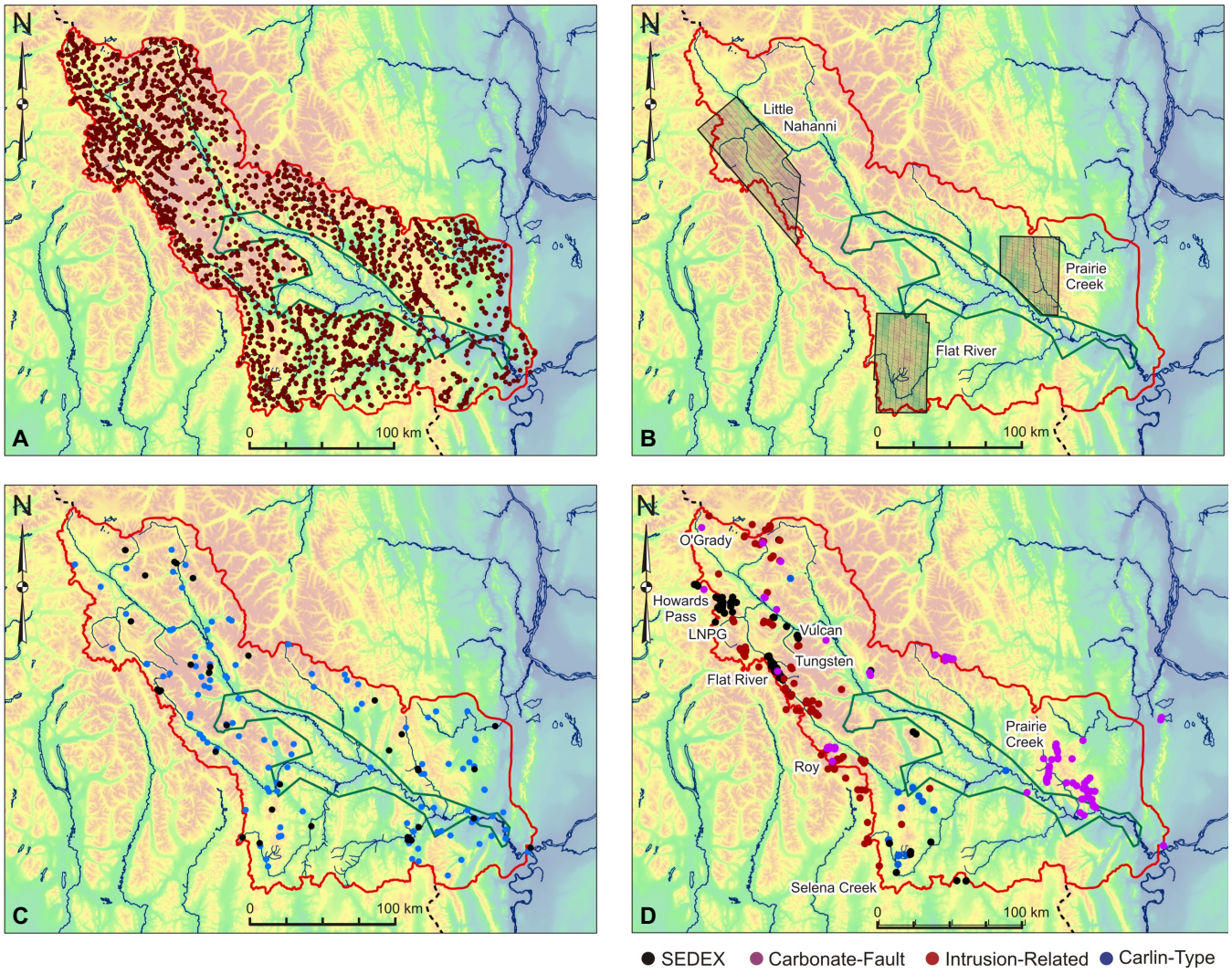


Figure 4. Locations of data collected for the Nahanni MERA 1 and 2 studies. **A)** Locations of stream sediment and stream water samples collected by Spirito and Jefferson (2003) in MERA 1 areas and by McCurdy et al. (2007) for MERA 2 under the National Geochemical Reconnaissance (NGR) program. **B)** Locations of geophysical surveys as reported by Charbonneau (2007). **C)** Locations of spring water sample sites, from Hamilton et al. (2003) for the MERA 1 areas, and from Caron et al. (2007) for MERA 2. Anomalous springs (Table1) are shown by black dots. **D)** Locations of mineral occurrences from the NORMIN database. See further discussion in the text for an explanation of the deposit models.

deposit studies conducted as part of the Nahanni MERA 2 project (Barnes et al., 2007; Cousens, 2007; Paradis, 2007; Rasmussen et al., 2006, 2007; Yuvan et al., 2007). All known mineral showings in the study area, as determined from the NORMIN database and the current MERA study, were classified into the four deposit models outlined in the following section.

DEPOSIT MODELS

Overview

Four different deposit models were designed to incorporate the most important mineral deposit types for this region (Fig. 4D), using the minimum number of GIS operations. The SEDEX (stratiform sediment-hosted exhalative Zn-Pb-Ag) model is a single deposit type that is well documented and dominant in the region. The three other models are composites of two or more deposit types with spatial and genetic affinities, carbonate-fault, intrusion-related, and Carlin-type gold (Carlin or other types of intrusion-related lode-gold and/or derived placer deposits).

SEDEX Model

The SEDEX mineral-potential map created in this study is based on a well known set of attributes, which have been summarized by Carne and Cathro (1982), Lydon (1995), J. Lydon (pers. comm., 2005), and Cousens (2007). These include favourable host lithology (black, graphitic, siliceous shale with rapid lateral facies changes including conglomerate tongues), structural features (known faults, and faults inferred from facies changes), as well as direct and indirect pathfinder elements that are detected by stream sediment, stream water, and spring water geochemistry sur-

Table 1. Anomalous springs compiled from Nahanni MERA 1 (Hamilton et al., 2003) and MERA 2 (Caron et al., 2007) studies. Duplicate samples and analyses are listed together. MERA 1 elements are listed in decreasing order of abundance; anomalousness was determined in context for classified springs; 'elevated' elements (above average) were not anomalous. MERA 2 elements are listed in order as reported by the laboratory. All MERA 2 elements were considered 'anomalous'; and no 'elevated' elements were interpreted. 'Surface formation' and 'significant subsurface' were determined by either GIS location (this paper) and/or by field geological knowledge (MERA 1 and 2 spring studies). In some cases, the significant subsurface information is interpreted from the spring water geochemistry.

Sample	MERA	Name	Host rock	Surface formation	Significant subsurface	Anomalous elements	Elevated metals	Model	Summary of anomalous criteria used
86-012	1	unnamed	shale	Earn Group	Rabbitkettle Formation argillaceous limestone	Zn, Ni	Co, Cu, Cd, U	SEDEX	acidic, high SO_4, and shale near intrusions
86-015	1	Glacier Lake	shale	Earn Group	Road River Group; near instrusive contact; hornfels signature	Zn, Ni	Fe, Mn, Co	SEDEX	acidic, high SO_4, and shale near intrusions
C-420937	2	Glacier Lake	shale	Earn Group	Road River Group; near instrusive contact; hornfels signature	Fe, Zn, Tl	na	SEDEX	elevated TDS, 3 anomalous elements, Ficklin and Piper diagrams
86-018	1	CanTung West	quartz monzonite	Tay River Plutonic Suite	quartz monzonite	W, Mo, F	As, Au	Intrusion	thermal, related to quartz monzonite
C-420957	2	West Cantung	limestone, siltstone	Sekwi Formation	quartz monzonite	Cs, Li, V, B, Ga	na	Intrusion	5 anomalous elements
86-019, 020	1	CanTung Mine	silty limestone, limestone	Sekwi Formation	quartz monzonite	W, Mo, As	F, Ag	Intrusion	thermal springs related to quartz monzonite
86-021	1	unnamed	shaly carbonate	Back Bone Ranges Formation	Sheepbed Formation; shale, siltstone	As	Fe, Mn, U	Carlin-Placer, Carbonate-Fault	high TDS, carbonate terrane; Used in GIS for both models
86-025	1	northwest Glacier Lake	Shale	Earn Group	Road River Group; near instrusive contact	Zn	Mn, Fe	SEDEX	acidic, high SO_4, and shale near intrusions
86-038	1	unnamed	quartz monzonite; shale	O'Grady Batholith; Mt. Christie Formation	O'Grady Batholith	W, As, Mo	F	Intrusion	thermal spring related to quartz monzonite
86-042	1	unnamed	shale, major fault	Portrait Lake and Funeral formaitons	Lower Paleozoic calcareous shale and shaly limestone; plutonic elemental signature (Aronoff et al., 1989)	Zn, Ni	Fe, Mn, Cd, Cu, Co	SEDEX	acidic, high SO_4, shales near intrusions
86-067	1	Prairie Creek Mine	dolostone, karst, fault	Whittaker Formation	Lower Paleozoic calcareous shale and shaly limestone, limestone, quartzite, dolostone	Zn, Cu, Cd, Sb	Ni, Co	SEDEX	high TDS spring, carbonate terrane
C-453841	2	Prairie Creek	faulted limestone, quartzite, dolostone	Whittaker Formation	faulted limestone, quartzite, dolostone, calcareous shale	Sb, NO_2	na	Carbonate-Fault	2 anomalous elements and Ficklin diagram
C-453839	2	Prairie Creek Mine Shaft	dolostone, karst, fault	Whittaker Formation	Lower Paleozoic calcareous shale and shaly limestone, limestone, quartzite, dolostone	Cu, Zn, Pb, Cd, Sb, Tl, Se	na	Carbonate-Fault	7 anomalous elements and Ficklin diagram
86-072A	1	Meilleur River	silty, non-calcareous shale	Fort Simpson, Besa River formations	Arnica Formation: dolostone, limestone, minor shale	Zn, Ni, Co, Cd, Au	Mn, Fe, Cu, U	SEDEX	acidic, high SO_4, metalliferous

Table 1 continued.

Sample	MERA	Name	Host rock	Surface formation	Significant subsurface	Anomalous elements	Elevated metals	Model	Summary of anomalous criteria used
87-073A	1	unnamed	silty, non-calcareous shale	Fort Simpson, Besa River formations	dolostone, limestone, minor shale	Zn, Ni, Co, Cd, Au	Mn	SEDEX	acidic, high SO_4, and metalliferous
C-420946	2	Meilleur River	silty, non-calcareous shale	Fort Simpson, Besa River formations	Arnica formation: dolostone, limestone, minor shale	Cs, Rb, Br	na	SEDEX	3 anomalous elements
87-082	1	White Aster	carbonate, shale, near fault	Sombre and Arnica formations	deep fault; flowed through Arnica Formation dolomite	Zn	As, Mo, W	SEDEX	high TDS spring, carbonate terrane, and high lead in precipitate
87-107	1	unnamed	mudstone beneath Nahanni Butte thrust	Lepine Formation	mudstone, shale in footwall to thrust containing Nahanni Butte vein Zn-Cu occurrence	Zn		Carbonate-Fault	low TDS; outside but buffer overlaps study area
87-111	1	Arnica Fm	silty, non-calcareous shale near fault	Besa River Formation	along same deep fault as White Aster, contact between Arnica dolomite and Besa River shale	Zn, Ni	Mo, U	SEDEX	high TDS spring, carbonate terrane
87-112	1	unnamed	silty, non-calcareous shale	Besa River Formation	Arnica Formation: dolostone, limestone, minor shale	Fe , Mn, Zn, Ni, Co, As		SEDEX	acidic, high SO_4, metalliferous
87-125	1	unnamed	karsted bioclastic limestone along fault	Headless and Nahanni formations	karsted bioclastic limestone along fault	Zn	Mo	SEDEX	moderate TDS, carbonate terrane
C-420979	2	Bougere	chert, siliceous shale, conglomerate	Prevost Fm, Earn Group	chert, siliceous shale, conglomerate, (Earn Group); limestone, silty limestone; (Haywire and Sapper formtions)	Al, Mn, Ni, Cu, Zn, Co, Ga, Ag	na	SEDEX	high TDS, 8 anomalous elements, Ficklin and Piper diagrams
C-453847	2	Brimstone	argillaceous limestone	Rabbitkettle Formation	limestone and quartz monzonite	Fe, Mn, Cr, Rb, Se, Be	na	Intrusion	6 anomalous elements
C-453842/44	2	Broken Skull's Upper Pool	shale, thin bioclastic limestone, near faults	Funeral Formation	Sapper Formation, silty limestone; plutonic or granitoid basement elemental signature	Pb, Cs, Rb, B, Br	na	Intrusion	5 anomalous elements
C-453861	2	Cimitar	karsted limestone, silty shale, near fault	Headless, Nahanni and Horn River formations	karsted limestone; plutonic or granitoid basement elemental signature	Sr, U, Tl	na	Intrusion	3 anomalous elements and Ficklin diagram
C-453858	2	Cowgirl	limestone, dolostone, near fault margin of Prairie Creek embayment	Camsell, Sombre, Bear Rock, Arnica, Grizzly formations	growth-faulted limestone, calcareous shale, plutonic or granitoid basement elemental signature	V, Tl	na	Intrusion	2 anomalous elements and Ficklin diagram
C-453853	2	Galena	faulted limestone, quartzite, dolostone	Cadillac and Whittaker formations	faulted limestone, plutonic or granitoid basement elemental signature	Pb, U, Tl, Se	na	Intrusion	4 anomalous elements and Ficklin diagram

Table 1 continued.

Sample	MERA	Name	Host rock	Surface formation	Significant subsurface	Anomalous elements	Elevated metals	Model	Summary of anomalous criteria used
C-420936	2	Grizzle Bear	limestone, dolostone, quartz arenite	Haywire Formation	limestone, dolostone, quartz arenite, plutonic or granitoid basement elemental signature	Cr, Cs, Rb, Br	na	Intrusion	4 anomalous elements
C-420952	2	Hole in the Wall	quartz monzonite	Selwyn Plutonic Suite	quartz monzonite	Mo, As, V, Ga	na	Intrusion	4 anomalous elements
C-453880	2	Interpluton	quartz monzonite	Tombstone Plutonic Suite	quartz monzonite	Ga	na	Intrusion	high TDS, 1 anomalous element, and Piper diagram
C-420944	2	Kraus (Clausen)	karsted diagenetically altered dolostone	Manetoe Facies	Manetoe Facies, Headless and Nahanni limestone; plutonic or granitoid basement elemental signature	Cr, Cs, Li, Rb, Sr, V, B	na	Intrusion	7 anomalous elements
C-420932	2	Nahanni Headwaters	shale	Mt. Christie Formation	Permian and Devono-Mississippian shale, O'Grady Batholith	Cs, Mo, As, Li, B, Sb, Ga	na	Intrusion	elevated TDS, 7 anomalous elements, and Piper diagram
C-420930	2	Nahanni North (Lened Creek)	sandstone, argillaceous limestone	Vampire and Rabbitkettle formations	argillaceous limestone, skarn, quartz monzonite, Tay River Suite	Cs, Mo, Li, B, Ga	na	Intrusion	5 anomalous elements
C-453891	2	Orange Creek	calcareous shale, limestone, at fault contact	Sunblood Formation and Road River Group	calcareous shale, limestone, at fault contact	Al, Mn, Ni, Cu, Zn, Cd, Co, Cr, Li, U, Tl, Ga, Be	na	SEDEX	high TDS, 15 anomalous elements, and Ficklin and Piper diagrams
C-453894	2	Persistent (Last Minute)	limestone, siltstone, sandstone, near cross faults	Sekwi Formation	limestone, siltstone, quartz arenite; plutonic Tungsten Suite elemental signature	Cd, Cs, As, Rb, Ba, Tl	na	Carlin-Placer	6 anomalous elements
C-453849	2	Sibbeston	limestone, dolostone, near fault margin of Prairie Creek embayment	Camsell, Sombre, Bear Rock, Arnica, Grizzly formations	growth-faulted limestone, calcareous shale, plutonic or granitoid basement elemental signature	Tl, Ga	na	Intrusion	2 anomalous elements and Ficklin diagram
C-453873	2	Smurf	calcareous shale	Road River Group	Road River Group calcareous shale; Sunblood dolostone; near instrusive contact with Tombstone suite	V, Se	na	Intrusion	2 anomalous elements, and Ficklin diagram
C-420947	2	Wildmint	dolostone, limestone	Sunblood Formation	Road River Group calcareous shale; Sunblood dolostone; near instrusive contact with various plutonic suites	Cs, Li, B, Ga	na	Intrusion	4 anomalous elements
C-453856	2	Wrigley	limestone	Camsell, Sombre, Bear Rock, Arnica, Grizzly formations	limestone, calcareous shale, plutonic or granitoid basement elemental signature	Mo, U, V, Tl, Se	na	Intrusion	5 anomalous elements and Ficklin diagram

Table 2. Evidence layers for the GIS modelling of the SEDEX mineral potential map. These layers are based on a set of attributes summarized by Carne and Cathro (1982), Lydon (1995), J. Lydon (pers. comm., 2004), and Cousens (2007).

Favourable rock units:

1. Transitional to deep basinal strata (Cambrian to Early Devonian + Middle Devonian to Early Mississippian are established producers) – **weight 10**.
2. Basinal Windermere strata (theoretically a producing rock package) – **weight 3**.

Structural Features:

3. Cambrian and Ordovician volcanic units (like faults, represents deep crustal structure favouring hydrothermal fluid flow) – **weight 10**.
4. Volcanic,10 km buffer *outside units* – **weight 3**.
5. Growth faults (north-northwesterly faults along Broken Skull River, structures along the carbonate-shale facies change (#5), and parallels to the northeasterly Leith Ridge and Fort Norman structures are interpreted as Laramide expressions of deep crustal weaknesses by steeply dipping breaks discordant to regional fold and thrust trends); 3 km buffer – **weight 2**.
6. Carbonate-shale facies change (Ordovician-Devonian platform edge from Morrow and Cook (1987) represents depositional structure favourable for SEDEX-type mineralization); 3 km buffer –**weight 2**.
7. All other faults (mainly southwest-dipping thrusts); 2 km buffer – **weight 1**.

Geochemistry; anomalous direct and indirect pathfinder elements listed:*

8. Stream sediment, direct: Ag, Cu, Pb, and Zn. Each element map was normalized to provide equal influence and then all elements were summed and the mean value was calculated; this map was divided into a five-class map reflecting high to low concentration. Class thresholds were based on natural breaks in the data histogram – **weights of 10, 7, 2, 1, and 0** by class.
9. Stream sediment, indirect: As, Ba, Bi, Cd, Cr, F, Hg, Mn, Mo, Ni, P, Sb, and V. Each element map was normalized to provide equal influence and then all elements were summed and the mean value was calculated; this map was divided into a five-class map reflecting high to low concentration. Class thresholds based on natural breaks in the data histogram – **weights of 6, 4, 2, 1, and 0** by class.
10. Stream water, direct: Ag, Cu, Pb, and Zn. Each element map was normalized to provide equal influence and then all elements were summed and the mean value was calculated; this map was divided into a five-class map reflecting high to low concentration. Class thresholds were based on natural breaks in the data histogram – **weights of 10, 7, 2, 1, and 0** by class.
11. Stream water, indirect: As, Ba, Cd, Cr, F, Mn, Mo, Ni, P, Sb, and V, and low pH. Each element map was normalized to provide equal influence and then all elements were summed and the mean value was calculated; this map was divided into a five-class map reflecting high to low concentration. Class thresholds were based on natural breaks in the data histogram – **weights of 6, 4, 2, 1, and 0** by class.
12. Spring water sample sites (Table 1: all SEDEX from Table 5.12 of Hamilton et al. (2003) and selected springs from Table 6 of Caron et al. (2007)) anomalous in one or more of fourteen pathfinder elements. Direct pathfinder elements Ag, Cu, Pb, and Zn, and indirect elements, As, Ba, Cd, Cr, Mn, Mo, Ni, Sb, and V; and low pH. Buffer = 3 km, **weight = 2**.
13. pH – determined from water chemistry. The data were interpolated and the map was divided into eight classes reflecting acid to basic conditions – **weights of 10, 9, 8, 7, 4, 3, 2, and 0**.
14. Mineral occurrences of the SEDEX type were assigned to one of four categories: defined resources **(weight 10)**, advanced prospect **(weight 7)**, showing **(weight 4),** and anomaly (**weight 2**), buffer = 3 km.

A total of seventeen evidence maps were used for producing the SEDEX mineral-potential map.

* Anomalous cutoffs were determined by separate statistical analysis of the frequency distribution of the results for samples in each of the rock units used for each deposit model. The 'buffer' for each sample is calculated by interpolation within a data-determined zone of influence. Each sample location is assigned to a rock unit based on a straightforward spatial intersection. Although most individual stream catchment areas and spring water flow paths intersect multiple rock types, their relative proportions were NOT taken into account in determining the background rock influence on each sample. In a few cases, the location is just inside a rock unit that did not contribute significantly to the sample medium. Stream water pH data were included in stream sediment geochemistry as well as stream water geochemistry for spatial modelling (see discussion in text under SEDEX Model).

veys, and the locations of SEDEX-type mineral occurrences (Table 2).

SEDEX deposits are most likely to occur within the early Cambrian to Middle Devonian Selwyn Basin that comprises the deep-water euxinic (oxygen-poor) portions of the western North American passive margin

sedimentary sequence. Two main districts at Macmillan Pass and Howards Pass are defined by linear belts of such occurrences near the margins of the Selwyn Basin. The only past-producing SEDEX deposits in the Selwyn Basin are those of the Anvil District, which are hosted by basal Cambrian shaly strata near Whitehorse, Yukon. However, the deposits in the Howards Pass district contain some of the largest base metal accumulations in the world.

Carbonate-Fault Model

The composite carbonate-fault deposit model accounts for the spatial association of zinc-lead-silver deposits of at least three types with an associated district-scale fault, which are exemplified by their joint occurrence in the Prairie Creek district (Paradis, 2007): vein quartz-carbonate, SEDEX, and Mississippi Valley-type. Fluids trapped during sedimentation, combined with fluids derived from deeply buried basement rocks, may have leached metals from basement rocks as they flowed along more permeable zones, driven by pressure due to increased burial near basin centres, by differential tectonic uplift or subsidence, or by thermal convection. Where the fluids encountered fault zones in competent rocks, the permeability would have been locally enhanced, thereby focusing the fluids. As these fluids passed through other layers, including different aquifers, reaction with the wall rock or mixing with fluids from other aquifers may have altered the parameters of the fluid sufficiently for metals to precipitate. The Manetoe diagenetic alteration facies (Morrow et al., 1990) is an example of the alteration of carbonate layers due to basinal fluids. Mississippi Valley-type (MVT) base-metal deposits, such as those of the classic past-producing Pine Point district, are typically associated with this style of alteration. Faults, especially reactivated vertical growth faults, may locally facilitate fluid transportation and mixing, as is found at Pine Point as well as in variants of MVT deposits, such as the Irish-type of carbonate-hosted Zn-Pb-Ag deposits. Faults may also have allowed great fluctuations in fluid pressure regimes, facilitating the formation of breccias, stockworks, and veins.

Favourable rock units, structural features, geochemistry, and the location of carbonate-fault-associated mineral occurrences (Table 3) were used to produce a mineral-potential map.

Intrusion-Related Model, Including a Variety of Skarn, Rare Metal, and/or Gemstone Types

Intrusions provide both primary metalliferous fluids and heat for metal redistribution and reconcentration. In addition to mineral concentrations that are direct products of the magma (rare element-bearing pegmatites and gemstones), the introduction of magmatic and meteoric fluids, driven by the heat energy from the intrusion and their interaction with reactive host rocks, can produce many different styles of mineral deposits. These include the extensive skarn family, manto, chimney, epithermal, endoskarn, porphyry, and high-temperature replacement deposits. A wide range of metal assemblages and rare metals are associated with the intrusion-related family of deposits, including one or more of W, Cu, Zn, Pb, Ag, Au, As, Sb, Li, Ta, Cs, and Sn (refer to Barnes et al., 2007). For this Nahanni MERA 2 GIS analysis, gold (Au) is treated separately, as described in the next section.

In order to form intrusion-associated metal concentrations, a number of additional factors are important to optimize the effects of heat energy and chemical reactions with host rocks. Fluid pathways are essential to channel fluids through and away from metal sources and focus them in zones where the deposition of metals can build up economic concentrations. Because the plutons intruded deformed sedimentary rocks, such pathways were generally along pre-existing structures (faults, fold axes, and permeable strata), which may also have constrained the upward ascent of magma to form the intrusions.

Another critical aspect of these deposits is that the focusing parameters under which metals are carried in solution must have changed in order to form an ore deposit rather than disperse the metals distally from the source and dilute them. Mechanisms to focus precipitation include chemical reaction with the wall rock, such as changes in pH (acidity), Eh (oxidation), trace element contents, cooling of the fluid, and/or depressurization. For example, a hot, acidic, high-pressure fluid passing through a carbonate unit will be cooled and neutralized. This explains why limestone, dolomite, and calcareous shale layers are common hosts to skarn. Skarn deposits tend to be best developed in the first relatively pure limestone layer in a mixed stratigraphic assemblage that the hydrothermal fluids encounter on their ascent from the related intrusion.

Depressurization of mineralizing fluid related to an active fault system can also be important; thus, the presence of faults as a transport mechanism and a concentration mechanism is also an important factor for localizing intrusion-related deposits. Ponding due to physical ‘traps’ may also concentrate metals, as the movement of fluids is impeded giving them time to cool.

Some deposits are located within a pluton, caused by ingress of fluid from country rock, concentrating alteration within the upper portion of the pluton (termed endoskarn). Endoskarn may be recognized by the presence of metamorphosed remnants of wall rock preserved in the pluton as roof pendants. Such alteration introduces more potassium into the pluton, result-

Table 3. Evidence layers for the GIS modelling of the carbonate-fault mineral potential map. These layers are based on a set of attributes for three spatially associated types of zinc-lead-silver massive sulphides deposits: stratabound, Mississippi Valley-type, and vein quartz-carbonate of the Prairie Creek camp (as summarized by Paradis, 2007).

Favourable rock units:

1. Diagenetic facies consisting of vuggy recrystallized dolostone of the Devonian to the Cretaceous Manetoe (PM), Presqu'ile (Pp), and Grizzly Bear (PGB) formations – **weight 10**.
2. All Middle Devonian, strata, limestone, dolostone, and shale – **weight 5**.
3. Cambrian to Early Devonian platformal limestone and dolostone – **weight 5**.
4. Cambrian to Early Devonian transitional to deep basinal shale – **weight 2**.
5. Buffer around Diagenetic Facies: 3 km buffer only around Cambrian to Early Devonian platformal units (#3 above) to 5 – **weight 5**.

Structural Features:

6. Growth faults (as for SEDEX): 3 km buffer – **weight 2**.
7. Carbonate-shale facies change (as for SEDEX): 3 km buffer – **weight 2**.
8. All other faults (as for SEDEX): 2 km buffer – **weight 1**.

Geochemistry; anomalous direct and indirect pathfinder elements listed:*

9. Stream sediment, direct evidence: Ag, Cu, Pb, Zn. Each element map was normalized to provide equal influence and then all the elements were summed and the mean value was calculated; this map was divided into a five-class map reflecting high to low concentrations. Class thresholds were based on natural breaks in the data histogram – **weights of 10, 7, 2, 1, and 0** by class.
10. Stream sediment, indirect evidence: Cd, F, Hg, Sb. Each element map was normalized to provide equal influence and then all the elements were summed and the mean value was calculated; this map was divided into a five-class map reflecting high to low concentrations. The class thresholds were based on natural breaks in the data histogram – **weights of 6, 4, 2, 1, and 0** by class.
11. Stream water, direct: Ag, Cu, Pb, Zn. Each element map was normalized to provide equal influence and then all elements were summed and the mean value was calculated; this map was divided into a five-class map reflecting high to low concentration. Class thresholds were based on natural breaks in the data histogram – **weights of 10, 7, 2, 1, and 0** by class.
12. Stream water, indirect: Cd, F, Sb. Each element map was normalized to provide equal influence and then all the elements were summed and the mean value was calculated; this map was divided into a five-class map reflecting high to low concentration. Class thresholds were based on natural breaks in the data histogram – **weights of 6, 4, 2, 1, 0** by class.
13. Spring water sample sites (Table 1: Prairie Creek mine water from Table 5.12 of Hamilton et al. (2003) and selected anomalous springs from Table 6 of Caron et al. (2007)) anomalous in one or more of six pathfinder elements, direct: Ag, Cu, Pb, Zn; and indirect: Cd and Sb. Buffer = 3 km – **weight 2**.
14. Mineral occurrences of the Carbonate-Fault type were assigned to one of four categories: defined resources **(weight 10)** and showing (**weight 4);** buffer = 3 km.

A total of seventeen evidence maps were used for producing the SEDEX mineral-potential map.

* Anomalous cutoffs were determined by separate statistical analysis of the frequency distribution of the results for samples in each of the rock units used for each deposit model. The 'buffer' for each sample is calculated by interpolation within a data-determined zone of influence. Each sample location is assigned to a rock unit based on a straightforward spatial intersection. Although most individual stream catchment areas and spring water flow paths intersect multiple rock types, their relative proportions were NOT taken into account in determining the background rock influence on each sample. In a few cases, the location is just inside a rock unit that did not contribute significantly to the sample medium. Stream water pH data were included in stream sediment geochemistry as well as stream water geochemistry for spatial modelling (see discussion in text under SEDEX Model).

ing in crystallization of potassic feldspar, muscovite, and/or sericite clay, and is registered by high K/U and K/Th ratios. Gamma-ray spectrometer data is useful for detecting potassium enrichment, and thereby targeting alteration associated with such deposits. Gamma-ray data were acquired in three strategic areas (Fig. 4B), and interpreted and reported by Charbonneau (2007). The gamma-ray data (K channel) were used as a signature of potassic alteration.

Skarn deposits in the Canadian Cordillera are abundant, diverse, and economically significant. In the study region, skarn occurrences are localized where the mid Cretaceous Tay River (100-96 Ma), Tungsten (99-95 Ma), and Tombstone (94-90 Ma) plutonic suites discordantly intrude the lowest and/or thickest limestone unit of an upper Proterozoic to lower Paleozoic shelf carbonate-pelite sequence. The broad thermal aureole at the contact between a Cretaceous quartz monzonite

stock of the Tungsten suite and a Lower Cambrian limestone unit is the setting of the world-class Cantung mine. A belt of W-Cu (Zn, Mo) mineralized skarn follows an arcuate trend of generally small mid Cretaceous granitoid plutons in these suites from the southwestern Northwest Territories to the Dublin Gulch District of Yukon and on into Alaska. This trend contains some of the largest and highest grade resources of skarn tungsten in the world, mainly in the Cantung mine and in the Mac Tung deposit at Macmillan Pass, as well as important gold and gemstone resources (Rasmussen et al., 2007). Thus, proximity to a pluton, especially where in contact with an appropriate carbonate unit, is an important vector for intrusion-related deposits.

Favourable host lithology, distance to plutons of various types, structural features, favourable pathfinder elements in stream sediments, stream waters, and springs, and the locations of intrusion-related mineral occurrences (Table 4) were used to produce an intrusion-related mineral-potential map.

Carlin-Type Model

Carlin-type gold is a special, possibly intrusion-related deposit model that for this study comprises at least two basic genetic hypotheses. Recent research has determined many of the associated empirical factors involved in these highly economic and commonly very large gold deposits (Poulsen, 1996; Cline et al., 2005; Emsbo et al., 2006). The characteristics of these gold deposits range from stratiform disseminations, breccia zones, sinter, and vein stockworks to bonanza-style vein systems. Richards (1989) and Rowan (1989) recognized some of the geochemical attributes of such deposits in the Selena Creek area. Work under MERA 2 reported by Charbonneau (2007) and McCurdy et al. (2007) focused on this area to further test the premise that As, Sb, Hg, Ti +/- Ba-bearing placer-gold occurrences here were derived from one or more Carlin-type lode-gold deposits.

Depending on the deposit being examined, the genesis of Carlin-type gold has been ascribed to a number of different mechanisms. The varied appearances and settings of the different deposits have resulted in a range of hypotheses describing their possible origins; these are summarized here by two generalized hypotheses. The first hypothesis emphasizes the common proximity of the deposits to granitoid intrusions (plutons), which are considered to have been the thermal engines that drove fluid flow and were themselves the source for much of the fluid that carried the gold and associated trace metals.

The second hypothesis for Carlin-type deposits emphasizes the regional linear trends of the gold deposits that geologists have divided into regional 'trends' (i.e. The Carlin trend, the Battle Mountain trend, etc.). According to this hypothesis, the plutons were not responsible for the heat, but were simply accessories. Instead, the extensional tectonic regime resulted in high heat flow that mobilized metal-bearing fluids to form the deposits. The fluids themselves were derived from meteoric water that penetrated the crust along deep-seated fracture systems created by the same extensional tectonism.

The metal contents of Carlin-type deposits, regardless of their hypothetical origins, tend to be distinctive with As, Sb, Hg, Ti, and Ba accompanying Au and Ag. The suite of pathfinder elements is controlled by the geochemistry of the transporting fluids, especially at the cool temperatures at which these deposits tend to form.

The host rocks are primarily impure carbonate strata, typically argillaceous limestone and dolostone, which were effective at channelling fluids while at the same time providing the reactive elements ($CaCO_3$) to alter the pH of the transporting fluids, resulting in the precipitation of sulphide minerals.

Active fault systems are also thought to play a role in the formation of Carlin-type deposits by localizing and concentrating deposits along fault traces with a reduction in ore thickness away from the fault zones. The faults act as fluid conduits transporting and concentrating fluids from large regions into focused flow zones. Intersections of conjugate fault systems where permeability is the greatest are highly prospective zones.

Deformation structures such as anticlines may also play a significant role in the formation of Carlin-type deposits. Although these structures may not have been active during the mineralization events, folding and modification of the sedimentary sequence in many cases resulted in an increase in permeability, especially in the dilational, anticlinal axis zones.

In the search for the Carlin-type of deposit, the presence of other mineral deposits is often used as a vector, including linear strings of seemingly unrelated metal concentrations. Long-lived, deep-seated crustal sutures along which continents may have amalgamated are commonly the locus of a variety of metal-bearing fluids derived from intrusive and extrusive magma, regional metamorphic events, and from the surface. As such deeply buried structures are rarely exposed and difficult to identify using geophysical techniques, they are often identified by the linear pattern formed by the deposits themselves.

More direct indicators of Carlin-type deposits are fine-grained placer-gold deposits with pathfinder elements that represent weathered and locally transported lode-gold deposits. Placer-gold occurrences in many

Table 4. Evidence layers for the GIS modelling of the intrusion-related mineral potential map. These layers are based on a set of attributes for skarn tungsten or zinc-lead-silver, rare metals, and/or gemstones (excludes Carlin-type gold) and are modelled after Dawson et al. (1992), Barnes et al. (2007), Rasmussen et al. (2007), and Yuvan et al. (2007).

Favourable rock units

1. High-to very high-potential granitic bodies (include hornfels): 1, 5, and 20 km buffers; inside and outside of margins only, **weights of 10, 5, and 2**, respectively.
2. Moderate-potential granitic bodies (include hornfels): 1, 5, and 10 km buffers; inside and outside of margins only, **weights of 5, 2, and 1**, respectively.
3. Low-potential granitic bodies: 1 and 5 km buffers, **weights of 3 and 1**, respectively.
4. Shaly limestone units. Sedimentary units within a 20 km buffer of all granite bodies are weighted 1 to 10 for skarn potential, based on the presence of impure limestone units, with the #10 rank going to heterogeneous units (Vampire and Sekwi). Sedimentary unit values are added to the buffer values of the respective plutons.

Structural Features

5. Fault-density map based on line-density algorithm (assigned weights based on low, medium, and high fault density) – **weights of 5, 3, and 1**, respectively.

Geochemistry

6. Stream sediment, direct: Cu, Pb, W, and Zn. Each element map was normalized to provide equal influence and then all the elements were summed and the mean value was calculated; this map was divided into a five-class map reflecting high to low concentration. Class thresholds based on natural breaks in the data histogram – **weights of 10, 7, 2, 1, and 0** by class.
7. Stream sediment, indirect, Ag, As, Au, Bi, Sb, Sn, and Te. Each element map was normalized to provide equal influence and then all the elements were summed and the mean value was calculated; this map was divided into a five-class map reflecting high to low concentration. Class thresholds were based on natural breaks in the data histogram – **weights of 6, 4, 2, 1, and 0** by class.
8. Stream water, direct: Cu, Pb, W, and Zn. Each element map was normalized to provide equal influence and then all the elements were summed and the mean value was calculated; this map was divided into a five-class map reflecting high to low concentration. Class thresholds were based on natural breaks in the data histogram – **weights of 10, 7, 2, 1, and 0** by class.
9. Stream water, indirect: Ag, As, Au, Bi, Sb, Sn, and Te. Each element map was normalized to provide equal influence and then all the elements were summed and the mean value was calculated; this map was divided into a five-class map reflecting high to low concentration. Class thresholds were based on natural breaks in the data histogram – **weights of 6, 4, 2, 1, and 0** by class.
10. Spring-water sample sites (Table 1), three 'tungsten skarn' from Table 5.12 of Hamilton et al. (2003) and selected springs from Table 6 of Caron et al. (2007) anomalous in one or more of six direct pathfinder elements: W, Cu, Pb, Zn; and eight indirect, Ag, As, Au, Bi, F, Sb, Sn, and Te. Buffer = 3 km – **weight 2**.
11. Mineral occurrences of the Intrusion type (after Rasmussen et al. (2007) and Department of Indian Affairs and Northern Development (2006)) were assigned to one of four categories: defined resources **(weight 10)**, advanced prospect **(weight 5)**, showing (**weight 2**), and anomaly **(weight 1)**. Buffer = 3 km.

A total of fourteen evidence maps were used for producing the Intrusion mineral-potential map.

***** Anomalous cutoffs were determined by separate statistical analysis of the frequency distribution of the results for samples in each of the rock units used for each deposit model. The 'buffer' for each sample is calculated by interpolation within a data-determined zone of influence. Each sample location is assigned to a rock unit based on a straightforward spatial intersection. Although most individual stream catchment areas and spring water flow paths intersect multiple rock types, their relative proportions were NOT taken into account in determining the background rock influence on each sample. In a few cases, the location is just inside a rock unit that did not contribute significantly to the sample medium. Stream water pH data were included in stream sediment geochemistry as well as stream water geochemistry for spatial modelling (see discussion in text under SEDEX Model).

places have provided the first evidence of the presence of Carlin and other types of lode-gold deposits.

The westernmost Nahanni River region has been identified as one of the most prospective in Canada for hosting Carlin-type deposits (Richards, 1989; Rowan, 1989; Poulsen, 1996; Rasmussen et al., 2007). All of the elements identified as critical to the formation of a fine-grained disseminated sediment-hosted gold deposit (Carlin-type) discussed above have been identified in the study area, except for the regional extensional tectonism.

Favourable rock units, structural features, potassium anomalies detected by airborne gamma-ray spectrometer data, and the locations of intrusion-associated placer- and lode-gold mineral occurrences (Table 5) along with favourable stream sediment, stream water,

Table 5. Evidence layers for the GIS modelling of the Carlin-type and/or placer mineral-potential map. These layers are based on a set of attributes for intrusion-related lode-gold and associated placer deposits (after Cline et al., 2005; Emsbo et al., 2006).

Favourable rock units

1. High-to very high-potential granitic bodies (includes hornfels): 1, 5 and 20 km buffers; inside and outside of margins only - **weights 10, 5, and 2,** respectively.
2. Moderate-potential granitic bodies (includes hornfels): 1, 5, and 10 km buffers; **weights 5, 2, and 1,** respectively (inside and outside of margins only).
3. Low-potential granitic bodies: 1 and 5 km buffers - **weights 3 and 1,** respectively.
4. Reactive limestone units. Carlin-type uses same sedimentary units and additive weighting as for skarn.

Structural features

5. Growth faults as for SEDEX, within 20 km of granite bodies, treat as vertical: 2 km buffer each side – **weight 1**.
6. All other faults, within 20 km of granite bodies, 2 km buffer down-dip to southwest – **weight 1**.
7. Fault intersections, within 20 km of granite bodies, treat as vertical: 2 km buffer – **weight 2**.
8. Anticlines: 2 km buffer – **weight 1**.
9. Volcanic units regardless of age: 5 km buffer – **weight 2**.

Geochemistry – anomalous direct and indirect pathfinder elements listed

10. Stream sediment, direct: Au. (interpolated map – divided into five classes based on high to low concentration) – **weights of 10, 8, 2, 1, and 0**.
11. Stream sediment, key indirect: As, Sb, Hg, and Te. Each element map was normalized to provide equal influence and then all the elements were summed and the mean value was calculated; this map was divided into a five-class map reflecting high to low concentration. Class thresholds based on natural breaks in the data histogram – **weights of 6, 4, 2, 1, and 0** by class.
12. Stream sediment, possible indirect: Ag, Ba, Cs, Cu, Fe, Mo, Pb, Se, Si, Te, Tl, W, and Zn. Each element map was normalized to provide equal influence and then all the elements were summed and the mean value was calculated; this map was divided into a five-class map reflecting high to low concentration. Class thresholds were based on natural breaks in the data histogram – **weights of 4, 3, 2, 1, and 0** by class.
13. Stream water, key indirect: As, Sb, Hg, and Te. Each element map was normalized to provide equal influence and then all the elements were summed and the mean value was calculated; this map was divided into a five-class map reflecting high to low concentration. Class thresholds were based on natural breaks in the data histogram – **weights of 6, 4, 2, 1, and 0** by class.
14. Stream water, possible indirect: Ag, Ba, Cs, Cu, Fe, Mo, Pb, Se, Si, Te, Tl, W, and Zn. Each element map was normalized to provide equal influence and then all the elements were summed and the mean value was calculated; this map was divided into a five-class map reflecting high to low concentration. Class thresholds based on natural breaks in the data histogram – **weights of 4, 3, 2, 1, and 0** by class.
15. Springs (Table 1) with carlin-type signature anomalous in Ag, Sb, As, Au, Ba, Hg, Ti, and Tl. Buffer = 3 km – **weight 2**.
16. Placer-gold occurrences only where they fit Rasmussen et al. (2007) local derivation criteria: around Selwyn Plutonic Suite and within buffer of springs with Carlin signature. Buffer = 5 km – **weight 5**.
17. Lode mineral occurrences of Carlin and other granite-related types (after Cline et al., 2005, and Department of Indian Affairs and Northern Development, 2006; Rasmussen et al., 2007) were assigned to one of two categories: showing **(weight 2**), or anomaly (**weight 1**); 3 km buffer.
18. Airborne gamma-ray spectrometry should detect potassic alteration zones that may be expressed as illite, dickite, or potassium feldspar. Binary map of anomalous potassium concentration – **weight 1**.
19. pH (acidity) was sampled from stream water chemistry (data were interpolated and map was divided into eight classes reflecting acid to basic conditions – **weights of 10, 9, 8, 7, 4, 3, 2, and 0**.

A total of twenty evidence maps were used for producing the Carlin mineral-potential map.

* Anomalous cutoffs were determined by separate statistical analysis of the frequency distribution of the results for samples in each of the rock units used for each deposit model. The 'buffer' for each sample is calculated by interpolation within a data-determined zone of influence. Each sample location is assigned to a rock unit based on a straightforward spatial intersection. Although most individual stream catchment areas and spring water flow paths intersect multiple rock types, their relative proportions were NOT taken into account in determining the background rock influence on each sample. In a few cases, the location is just inside a rock unit that did not contribute significantly to the sample medium. Stream water pH data were included in stream sediment geochemistry as well as stream water geochemistry for spatial modelling (see discussion in text under SEDEX Model).

and spring water geochemistry were used to produce a Carlin-type mineral-potential map.

APPLIED METHODOLOGY

Overview: Production of Mineral-Potential Maps

Figure 5 provides a summary of the modelling process used to produce the various potential maps. For each deposit model, vectors to mineralization were selected based on the exploration criteria discussed above, in concert with exploration knowledge of the area. Evidence maps (thematic data layers) were created based on these vectors and each map was weighted (see Tables 2 to 5). It should be noted that weighted mineral occurrences for each style of mineralization were used as evidence maps in the modelling process, thus leading to what we have termed a data-modified knowledge-driven process. The evidence maps were then combined using an arithmetic operation (addition) to create a final potential map for each deposit model. Each of these additive potential maps were normalized to a numeric scale of 1 to 50 to ensure each had equal weight before integration into the final potential map. The hydrocarbon map was also normalized so that each of the three high-potential areas had a weight of 50, reflecting their high potential for hydrocarbons (K. Osadetz, pers. comm., 2007)

These four individual potential maps (one for each model) were divided into five classes based on natural breaks in the histograms, with 5 being the highest mineral potential. The four multi-class maps and the fifth hydrocarbon potential map (already converted into one class of very high potential) were then combined into one final mineral-potential map using a MAX operator as outlined in Figure 5. The final step was to partition the geologically based mineral-potential map into drainage-defined planning units developed by Parks Canada for park planning purposes.

A prediction graph for the final additive potential map was generated for each of the four deposit models to assess how well the map predicts the individual occurrences as organized by deposit type. These graphs were produced by plotting cumulative area against the number of deposits predicted (see Chung and Fabbri, 2003; Harris and Sanborn-Barrie, 2006; Harris et al., 2006).

Space does not permit showing the individual evidence maps for all four models. However, to demonstrate the methodology, a complete set of evidence maps is shown in Figure 6 and explained for the SEDEX model only.

SEDEX Model

A total of 17 weighted evidence maps (Table 2; Fig. 6) were used to create an additive SEDEX mineral-poten-

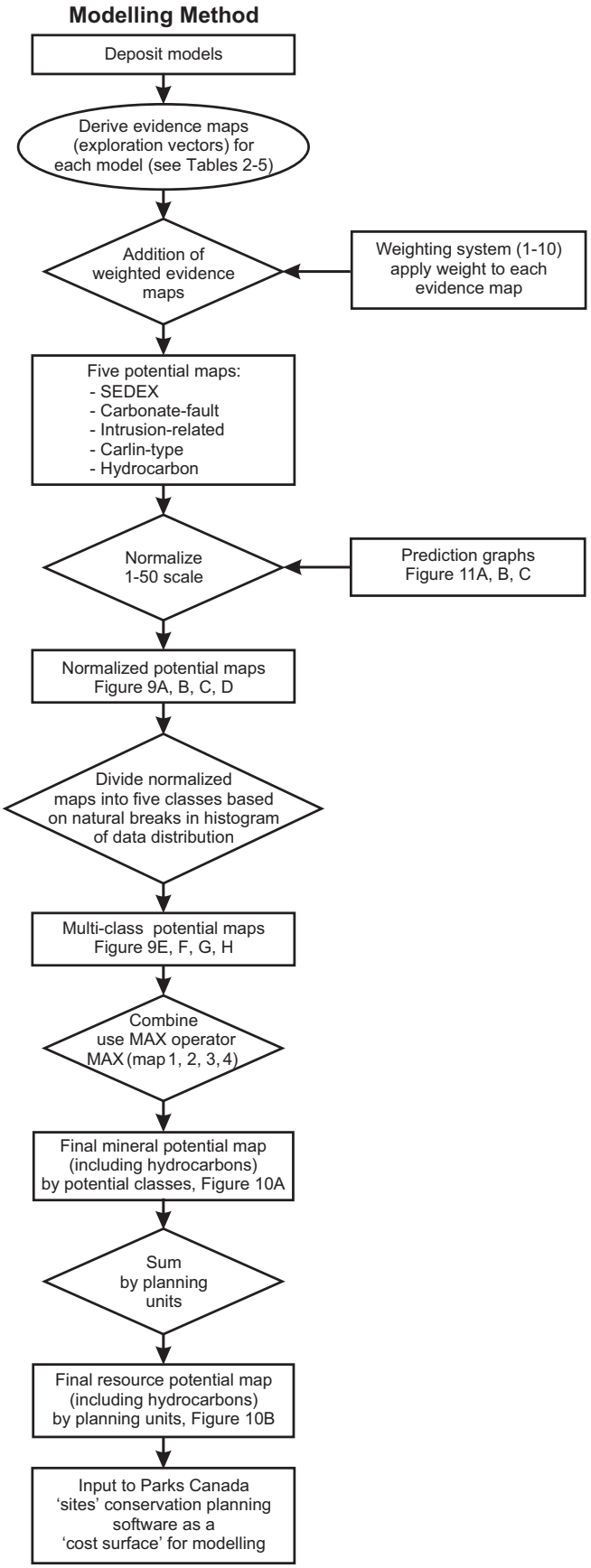


Figure 5. Flow chart for the GIS-modelling operations reported in this paper.

tial map (see the Final Model section below). The individual evidence maps are described below.

Favourable Rock Packages

Favourable rock packages included Cambrian to mid-Devonian transitional to deep basinal strata (Fig. 6A), which are established SEDEX hosts, and basinal Neoproterozoic Windermere Supergroup strata (shaly sandstone) (Fig. 6B), which may have been the source of metals to form the overlying SEDEX deposits as well as having potential to host SEDEX deposits in their own right. The former rock package is highly weighted (see Table 2), whereas the latter is assigned a lower weight due to its speculative genetic ties to the SEDEX model.

The early Silurian portion of the generally black, calcareous, graptolitic, Cambrian to Silurian shale in the Road River Group hosts the Howards Pass deposits. These collectively represent one of the few giant to super giant SEDEX-type camps of the world. Of similar age but different in lithology, the carbonaceous cherty black shale of the Whittaker Formation also hosts similar stratabound zinc and lead sulphide minerals at Prairie Creek (one of the three types that constitute the fault-associated composite model). The total extent of the SEDEX portion of Prairie Creek is not known, but its presence supports the concept of a broader mineralizing event in the late Silurian. A second series of SEDEX-type mineral deposits, characterized by the Tom and Jason deposits in the Macmillan Pass area, is hosted by late Devonian to Mississippian siliceous black shale and conglomerate of the Earn Group. All of the Cambrian to Mississippian basinal strata together constitutes the highly weighted first lithological evidence map.

East of the Earn Group tract, contemporaneous grey silty shale units, the Besa River and Horn formations, are not known to host mineral deposits. Neither do they display facies changes such as siliceous or highly carbonaceous zones, or conglomerate. Therefore, these units are characterized as an unfavourable rock package and given no weight in this analysis.

Structural Features

Cambrian and Ordovician volcanic units (Fig. 6C), as well as proximity to these units (Fig. 6D), are modelled in a similar fashion to faults, in that they represent deep crustal zones of weakness that may have channelled hydrothermal fluid flow. Growth faults (Fig. 6E) are interpreted as Laramide expressions of northeast-trending deep crustal offsets, such as the Leith Ridge and Fort Norman structures (Aitken and Pugh, 1984). These are interpreted as zones of weakness that caused subtle lateral facies changes and could have focused the transport of hydrothermal fluids during sedimentation. They are now interpreted as reactivated, with steeply dipping cross-faults that are discordant to northwesterly regional fold and thrust trends.

All other faults (excluding growth faults) (Fig. 6F) are mainly southwest-dipping thrusts, some of which may have been primary depositional extensional faults that could have channelled mineralizing fluids but were reversed during the compressional Laramide deformation that formed the Selwyn and Mackenzie mountains.

A major carbonate-shale facies change (Fig. 6G) along the Ordovician to Devonian platform edge is interpreted as yet another favourable location for the development of structures that could have transported hydrothermal fluids. It is interpreted in the GIS models as having been localized by a combination of extensional and transecting deep crustal structures that were active during sedimentation (i.e. growth faults).

Stream Sediment and Stream Water Geochemistry

Elements considered to reflect both direct and indirect evidence for SEDEX deposits (Table 2) were extracted from the stream sediment and water geochemical data sets (Fig. 4A). Variograms were constructed for each pathfinder element in order to determine a 'zone of influence' around each sample point (see Harris et al., 2001). The zone of influence (typically 3 km) was used as a search radius for an inverse distance-weighted (IDW) algorithm used to interpolate the data over selected favourable rock units. An advantage of this approach, which utilizes a fixed radius, is that areas characterized by a low density of sample points are not interpolated, thus reducing the introduction of artifacts and thereby increasing the certainty in the interpolation process. The interpolated map of each element was then normalized from either ppm or ppb to byte data (0-255) so that in the additive processes of combining the data all of the included elements would be equally weighted, preventing any one element dominating based on a wider data distribution range. A map showing mean normalized concentration was then produced by summing the normalized interpolated element maps and dividing by the number of elements. For example, the evidence map of direct SEDEX pathfinder elements obtained from stream sediment data was created by using the following formula:

$$(nAg + nCu + nPb + nCu) / 4,$$

where n = normalized value

This map was then broken into five classes based on natural breaks in the histograms of the normalized data. The classes were assigned weights of 10, 7, 2, 1, and 0 for the highest to lowest mean concentrations, respectively. The entire data processing method (applied to the geochemical data for all deposit models) is summarized in Figure 7.

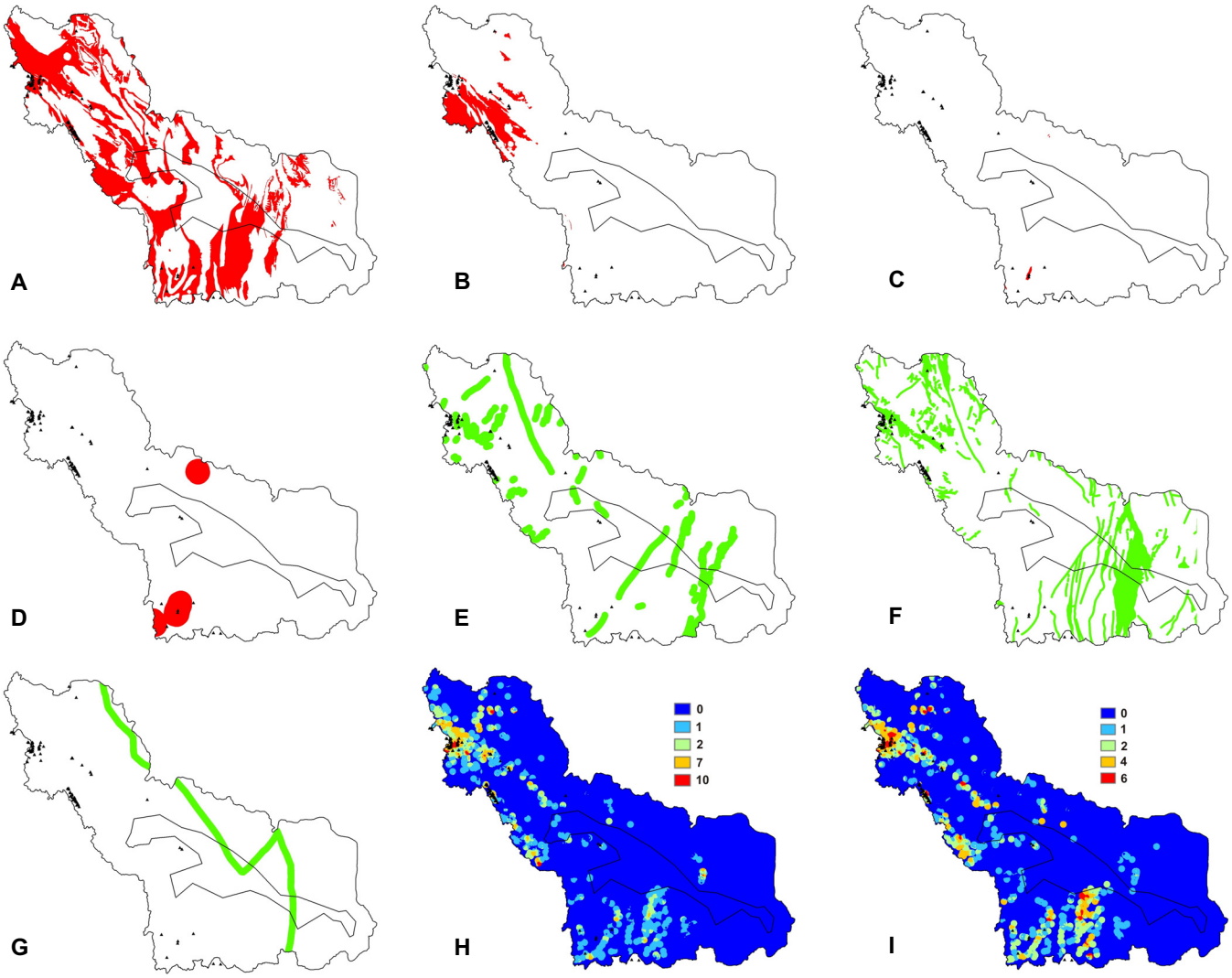


Figure 6. Evidence maps used for modelling the SEDEX deposit type. **A)** Transitional to deep basinal strata, weight = 10. **B)** Basinal Windermere strata, weight = 3. **C)** Cambrian to Ordovician volcanic units, weight = 10. **D)** Three kilometre buffer around volcanic units, weights = 5. **E)** Three kilometre buffer around growth faults, weight = 2. **F)** Two kilometre buffer around faults, weight = 1. **G)** Carbonate-shelf facies change, 3 km buffer, weight =1. **H)** Stream sediment geochemistry, direct indicators. **I)** Stream sediment geochemistry, indirect (pathfinder) indicators.

This same process was repeated for the indirect SEDEX pathfinder elements As, Ba, Cd, Cr, F, Mn, Mo, Ni, Sb, and U. However, the lower weights assigned to the five class normalized mean map (6, 4, 2, 1, 0) reflect the lower predictive power of the indirect pathfinder elements.

The same process was applied to the water geochemical data, excluding those pathfinder elements that could not be determined in water due to low concentrations (see Table 2). Figure 6H, I, J, and K show the final five class normalized mean maps for the direct and indirect elements from the stream sediment and water geochemical data used to produce the SEDEX mineral potential map

pH (Acidity of Stream Water)

The pH is lowered by the oxidation of sulphidic minerals under aqueous conditions to produce sulphuric acid. The pH in turn influences the transport of metals in water and their adsorption onto particulate matter in stream sediments. Low pH (acidic) water has enhanced capacity to transport most metals and may thereby enhance their geochemical expression. In neutral to alkaline environments, the chemical mobility of many metals, including Zn, Ag, and Pb and to a lesser extent As and Cd, is severely restricted (Plant and Raiswell, 1994). Conversely, metals such as U, Mo, and V are relatively mobile. Figure 3 of McCurdy et al. (2007) illustrates pH values from the various surveys used to evaluate mineral potential. As the pH of stream waters exceeds 7.0 in much of the survey area due to the dominance of limestone, the geochemical dispersion of many elements is reduced in these areas. It is expected that pH will tend to be buffered consistently within rock units except for anomalous sites.

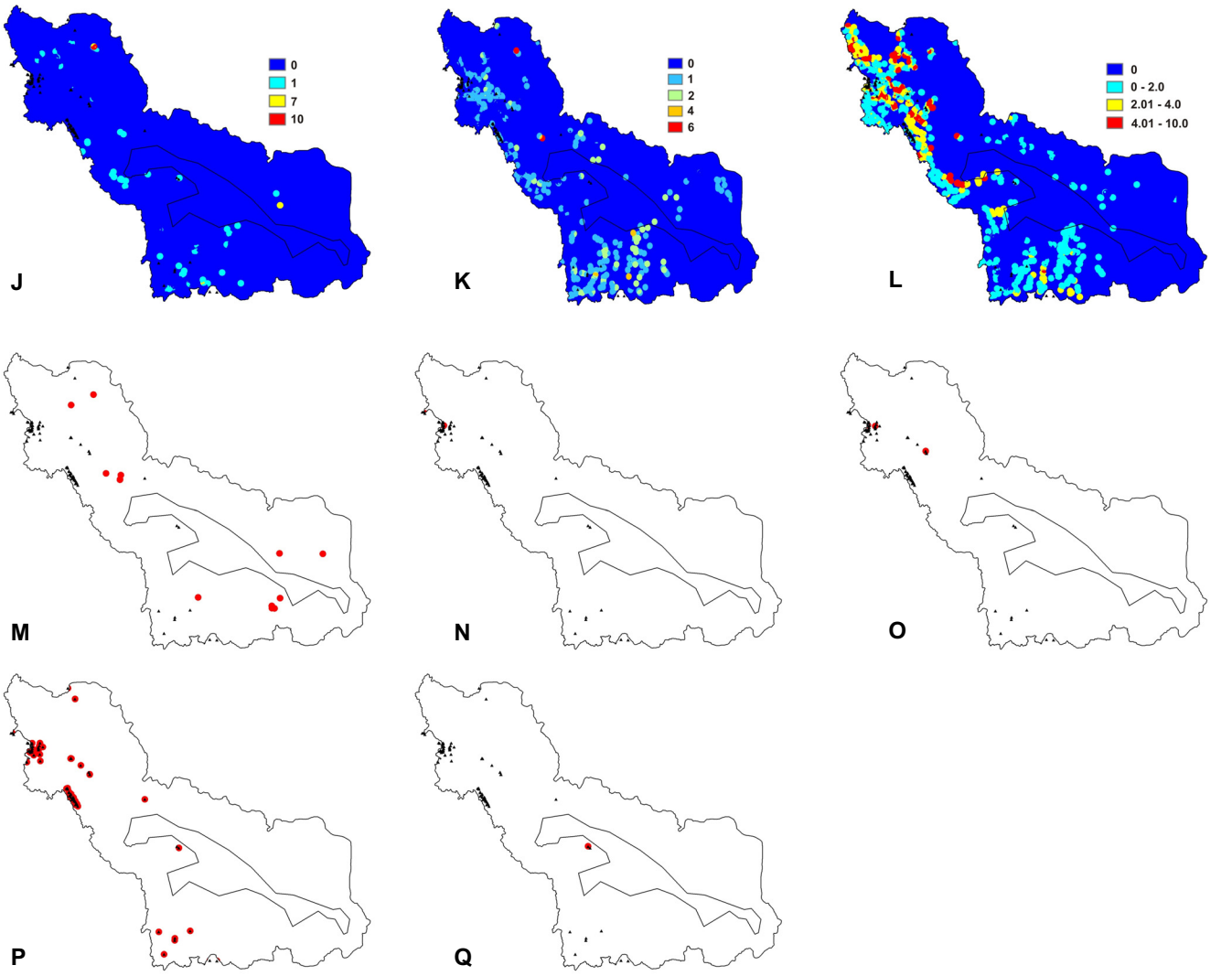


Figure 6 continued. J) Stream water geochemistry, direct indicators. **K)** Stream water geochemistry, indirect (pathfinder) indicators. **L)** pH, water geochemistry. **M)** Three kilometre buffer around anomalous springs, weight = 2. **N)** Three kilometre buffer around SEDEX occurrences, defined resources, weight = 10. **O)** Three kilometre buffer around SEDEX occurrences, advanced prospect, weight = 7. **P)** Three kilometre buffer around SEDEX occurrences, showings, weight = 4. **Q)** Three kilometre buffer around SEDEX occurrences, anomalies, weight = 2.

Using the above knowledge, a map of pH was produced from the water geochemical data using the following method. The point data were interpolated using inverse distance weighting with a 3 km fixed search radius, as determined from a variogram (Fig. 7). This interpolated map was then divided into eight equal classes based on quartiles with the following weights: 10, 9, 8, 7, 4, 3, 2, and 0, representing extremely acidic to basic pH conditions, respectively (Fig. 6L). The more acidic conditions were given a higher weight to reflect more favourable environments, assuming that the cause of the acidity was sulphide minerals such as sphalerite (zinc +/- silver), galena (lead +/- silver) and tetrahedrite (copper + silver), recognizing that pyrite and carbonaceous shale that contain no base metals also reduce pH.

Spring Water Geochemistry

Spring water sample sites were subjectively classified as favourable for SEDEX mineral deposits (Table 1), based on anomalous pathfinder elements (all SEDEX anomalous springs from Table 5.12 of Hamilton et al.(2003) and selected anomalous springs characterized as SEDEX from Table 6 of Caron et al. (2007)). Ag, Cu, Pb, and Zn were considered as direct evidence pathfinder elements and As, Ba, Cd, Cr, Mn, Mo, Ni, Sb, and V; and low pH as indirect evidence. Those sites considered as anomalous for one or more elements indicating SEDEX mineralization were buffered to 3 km and assigned a weight of two (Fig. 6M).

Mineral Occurrences

Mineral occurrences of the SEDEX-type were assigned to one of four categories: defined resources (weight 10), advanced prospect (weight 7), showing (weight 4), and anomaly (weight 2). The weighted points were then buffered to 3 km representing a zone of influence (Fig. 6N-Q).

Carbonate-Fault Model

A total of 15 weighted evidence maps (Table 3) were used to create an additive carbonate-fault mineral-potential map. This map indicates relative potential for the presence of undiscovered zinc-lead-silver massive sulphide deposits that fit this composite model, as described above in the deposit model overview section. The evidence maps are as follows.

Favourable Rock Units

Favourable host rocks include dolostone of the Devonian to Cretaceous Manetoe, Presqu'ile, and Grizzly Bear formations (diagenetic facies) (weight 10), middle Devonian strata (weight 5), Cambrian to early Devonian carbonate platform strata (limestone, dolostone) (weight 5), Cambrian to early Devonian calcareous shale (weight 2.), and proximity to the diagenetic facies listed above (3 km buffer and weight 5).

The Manetoe and Presqu'ile facies are diagenetic and/or hydrothermal alteration products of carbonate lithofacies (limestone and dolostone) that constitute the Mackenzie Platform (Morrow et al., 1990). This style of alteration is associated with reef-related dolomite diagenesis and with the passage of hydrothermal fluids, an alteration style that is present in and around significant carbonate-hosted base metal deposits in western Canada, i.e., Pine Point, Robb Lake, and near Prairie Creek (Paradis, 2007).

Structural Features

Growth faults (3 km buffer and weight 2), all other faults (2 km buffer and weight 1), and the trend of the facies change between the Devonian carbonate and shale assemblages, as per the SEDEX model (2 km buffer and weight 1) were used as evidence maps for the presence of undiscovered carbonate-fault-related deposits. As for the SEDEX deposit model, these features were likely to have focused the flow of hydrothermal fluids.

Stream Sediment and Stream Water Geochemistry

Four evidence maps were created based on direct and indirect elements for carbonate-fault-related mineralization from the stream sediment and stream water geochemical data. The processing and weighting strategy was the same as that described for the SEDEX model, however, different suites of pathfinder elements were used, as is listed in Table 3.

Spring Water Geochemistry

Spring water sample sites were subjectively classified as favourable for carbonate-fault deposits based on anomalous pathfinder elements (Prairie Creek mine water from Table 5.12 of Hamilton et al. (2003) and selected anomalous springs from Table 6 of Caron et al. (2007)). Ag, Cu, Pb, and Zn were considered direct pathfinder elements and Cd and Sb as indirect. Those considered anomalous for one or more of these elements were assigned a weight of 2 with a 3 km buffer.

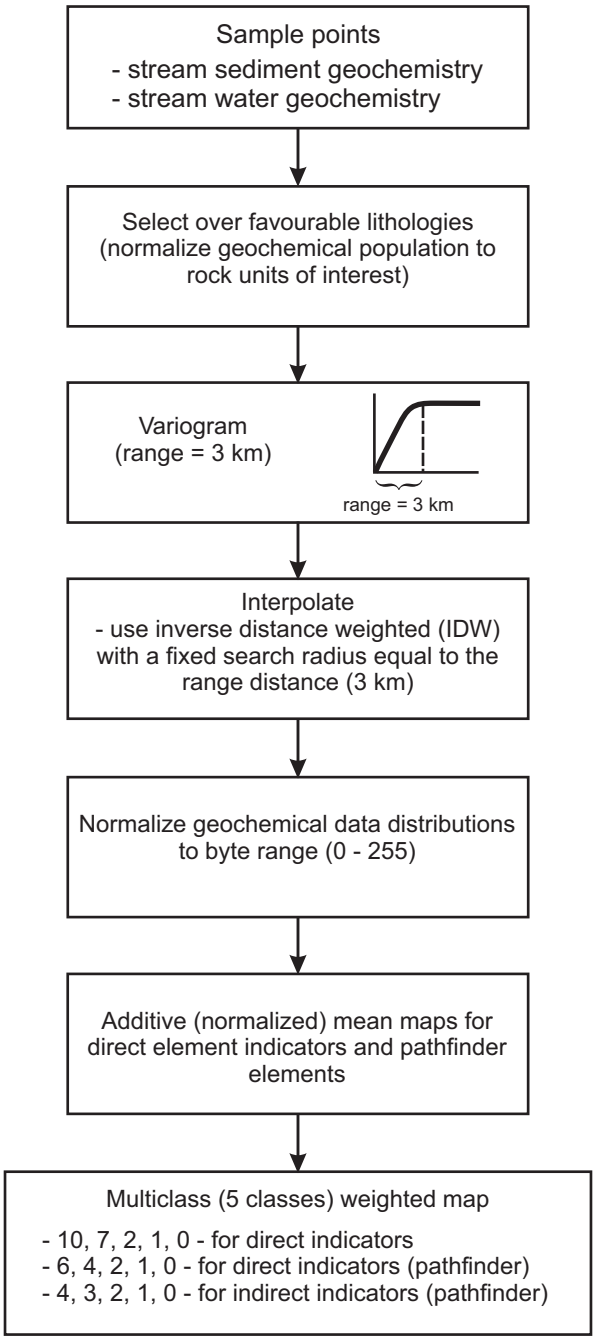


Figure 7. GIS modelling process to determine a zone of influence around sample points for interpolation of geochemical data between sites of stream sediment, stream water, and spring water samples.

Mineral Occurrences

Mineral occurrences classified in the carbonate-fault model were assigned to one of two categories: defined resources (weight 10) or showing (weight 4). These

classified points were buffered to 3 km reflecting a potential zone of influence.

Intrusion-Related Model

A total of fourteen weighted evidence maps (Table 4) were used to create an additive intrusion-related mineral potential map. These are described below.

Favourable Rock Units

Each intrusion (pluton) was assigned to one of three groups, based on qualitative geological assessment of their potential (high, medium, or low) to host or be spatially associated with undiscovered intrusion-related deposits, following the classification of Rasmussen et al. (2007). Additional geological knowledge provided by Barnes et al. (2007) and Yuvan et al. (2007) was also considered. For modelling purposes, any mapped hornfels associated with the margin of a pluton was included as part of that pluton, based on the assumption that hornfels (contact metamorphosed sedimentary rock) was caused by a shallowly underlying portion of a pluton below the hornfels. The plutons were buffered at three different distance intervals and within each pluton itself. The proximal zone (1 km buffer outside and inside each pluton) was assigned the highest weight.

Shaly limestone units situated within 20 km of any pluton were also weighted for their potential to host undiscovered skarn deposits (Fig. 8). Units thought to have the highest potential for skarn deposits are defined by their content of impure limestone. The highest rank of 10 was assigned to the heterogeneous limestone-bearing units (Vampire and Sekwi formations) that include the immediate host of the Cantung mine.

Structural Features

A fault density map was produced from a vector file of faults using a line density algorithm in the GIS database. The basic premise is that faults acted as conduits for mineralizing fluids, either from the plutons themselves or remobilized from the host rocks as a result of pluton emplacement. This algorithm produces a density map based on the number of faults within a 5 by 5 km neighbourhood. This map was divided into three classes: high, medium, and low density to which were assigned weights of 5, 3, and 1, respectively.

Stream Sediment and Stream Water Geochemistry

Two multi-class additive and normalized maps were produced showing direct and indirect pathfinder elements from the stream sediment data. Two maps were similarly produced from the water geochemical data. The same geochemical processing method described for the SEDEX model (Fig. 7), using a different suite

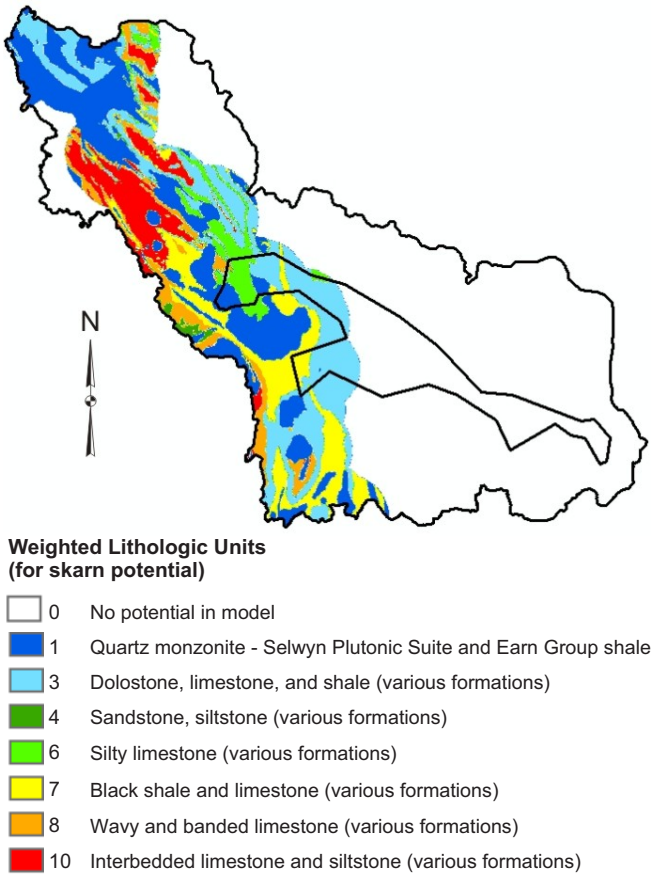


Figure 8. Rated geology within the areas of influence of intrusions, used for modelling intrusion-related and Carlin-type gold deposit potentials. Cool colours are assigned to low potential and hot colours to high potential.

of elements for direct and indirect evidence (see Table 4), was adopted for the intrusion-related model.

Spring Water Geochemistry

Spring-water sample sites were subjectively classified as favourable for intrusion-related mineralization based on anomalous pathfinder elements (three examples labelled 'tungsten skarn' from Table 5.12 of Hamilton et al. (2003) and selected anomalous springs from Table 6 of Caron et al. (2007)). Direct pathfinder elements include W, Cu, Pb, Zn; and indirect pathfinder elements include Ag, As, Au, Bi, F, Sb, Sn, and Te. In the SEDEX model, a 3 km buffer around each anomalous sample point was produced and a weight of 2 was assigned for this evidence map.

Mineral Occurrences

Mineral occurrences of the intrusion-related model (Department of Indian Affairs and Northern Development, 2006; Barnes et al., 2007; Rasmussen et al., 2007; Yuvan et al., 2007) were assigned to one of four categories: defined resources (weight 10), advanced prospect (weight 5), showing (weight 2), and anomaly (weight 1). In the SEDEX model, each

weighted occurrence was buffered to a distance of 3 km, representing a zone of influence.

Carlin-Type Model

A total of twenty weighted evidence maps (Table 5) were used to create an additive mineral-potential map for undiscovered Carlin-type lode gold and/or related placer deposits. The evidence maps are described below.

Favourable Rock Units

Many researchers feel that Carlin-type mineral deposits share a strong association with the late Cretaceous plutons (e.g. Poulsen, 1996; Tombstone Suite of Rasmussen et al., 2006, 2007). In the Nevada, carbonate units are essential as host rocks for Carlin-type mineralization. Thus, the same three pluton groups and variegated limestone units, with the same buffering and weighting strategies as the intrusion-related model, were applied to the Carlin-type model.

Structural Features

With the initiation of fluid systems, transportation corridors were also needed to focus fluid flow. Additional dilational zones, such as anticline axes, may have enhanced permeability and therefore are also an important structural feature to model. Thus, as with the intrusion-related model, growth faults within 20 km of a granite body were buffered to 2 km and assigned a weight of 1. All other faults were buffered to a distance of 2 km but only on the down-dip side (i.e. toward the southwest) and weighted as 1. Fault intersections were buffered to 2 km with a weight of 2 and within 20 km of a granite body. Anticlinal axes were buffered to 2 km with a weight of 1. A 5 km buffer (weight 2) was assigned to all volcanic units and the units themselves were weighted 2. Regardless of the age of extrusion, volcanic units are modelled as indicating deep-seated basement structures. All of the above structural evidence maps highlight features that may have served as conduits for mineralizing fluids.

Stream Sediment and Stream Water Geochemistry

Three evidence maps were created from the stream sediment data; one based on direct pathfinder elements, one on indirect pathfinder elements, and one on possible pathfinder elements. The same processing and weighting strategy described for the SEDEX model was also used for the Carlin-type model. The only exception was the addition of a possible pathfinder map whose five normalized classes are assigned weights of 4, 3, 2, 1, and 0. This map was ranked lower due its lower predictive power. The only stream sediment element used for direct evidence was Au.

The same procedure was repeated for the stream water geochemical data using a modified suite of elements (Table 5). Only two evidence maps, indirect pathfinder and possible pathfinder, were produced from the water geochemical dataset, because no direct evidence (Au) was analyzed.

pH

The same strategy and weights used to create pH evidence maps for the SEDEX and intrusion-related models were applied to the Carlin-type model.

Spring Water Geochemistry

Springs with a ‘Carlin signature’ in anomalous pathfinder elements (Ag, Sb, As, Au, Ba, Hg, Ti, Tl; Table 1) were buffered to a distance of 3 km and assigned a weight of 2.

Placer-Gold Occurrences

Placer-gold occurrences are historically the first direct indicator in the discovery history of many Carlin-type deposits and these were selected from the mineral deposits database (Department of Northern Affairs and Northern Development, 2006). Given the importance of intrusions to the composite Carlin-type model used in this analysis, placer-gold occurrences were included in the model only where they fit local derivation criteria within the buffer of a pluton or a spring with plutonic characteristics; thus, not all of the eastern Nahanni gold occurrences were included. A 5 km buffer around each placer gold occurrence with a weight of 5 was employed to create the evidence map.

Lode-Gold Occurrences

Lode-gold occurrences that are compatible with the Carlin-type model (after Cline et al., 2005; Department of Indian Affairs and Northern Development, 2006; Rasmussen et al., 2007) were assigned to one of two categories, showing (weight 2) or anomaly (weight 1), and each group of points was buffered to 3 km, creating two evidence maps.

FINAL MODEL

The four additive-normalized potential maps are shown in Figure 9A to 9D and their associated five-class potential maps are shown in Figure 9E to 9H (see Fig. 5 and previous discussion for method). The five-class maps (Fig. 9E-H) and the single-class hydrocarbon-potential map of Osadetz et al. (2003) were used to create the final potential map using the equation MAX (Carlin-type, carbonate-fault, intrusion-related, SEDEX, Hydrocarbon), where the input maps listed between the brackets represent the additive mineral potential maps normalized to 50 classes and the

Hydrocarbon anomaly map classified into two classes, very low potential and very high potential.

This final potential map (Fig. 10A) was used as the basis for selecting conservation areas, as it formed the 'cost layer; that was used in the site selection process undertaken by Parks Canada. Figure 10B shows a map of Parks Canada's planning units where each planning unit was assigned the maximum value underlying it between 1 and 5 based on Figure10A.

The rationale for using a MAX operator was to ensure that a planning unit was labelled high potential (thus a high cost), even if only one of the four potential maps showed the area or even part of the area to be of high potential. Thus, the planning units coloured red in Figure 10B represent areas where one or more of the five potential maps indicate high mineral or energy resource potential. This strategy provides a comprehensive estimate of mineral potential.

Validation

Prediction plots (Fig. 11) were calculated for each of the individual potential maps. Figure 11A was derived from Figure 9A to D, the multi-class potential maps; Figure 11B from Figure 9E to H; and Figure 11C, the potential map displayed by planning units, from Figure 10B. These prediction plots show the number of mineral occurrences (includes all categories discussed in Tables 2 to 5) predicted as a per cent of the total number of occurrences of that type, versus per cent area, ranging from high to low potential. Only mineral prospects assigned to a particular deposit model were selected for inclusion in the prediction graph for that deposit model (Fig. 11A). Each of the individual models is at best only moderately predictive, although all four models predict 100% of the associated mineral occurrences in approximately 30% of the high-potential area.

Considering the top 5% of the highest potential areas, the SEDEX model is the best predictor, with approximately 80% of the SEDEX-style mineral occurrences being predicted. The intrusion-related model is next best, predicting about 60%, the Carlin-type model slightly weaker at 40%, and the carbonate-fault model is the least predictive, with only 30% success (Fig. 11A).

Considering the top 1% of the high-potential area, the SEDEX model is again the best, predicting close to 50% of the SEDEX occurrences. The intrusion-related and carbonate-fault models predict 20% of its style of mineral occurrences, whereas the Carlin-type model predicts only 11%.

On the final potential map (Fig. 10B), 40 to approximately 70% of the various mineral occurrences fall within the top two potential classes (Fig. 10B), which is a reasonable result, although a perfect model would predict closer to 100%. When MAX summation by planning units is included, the results increase from 25 to almost 100% (Fig. 11C) of the occurrences that fall within the top two levels (coloured red and orange on Fig. 10B). These are better results and can be reasonably used as a cost layer in the conservation area selection process.

Geological Interpretation

This section relates the areas of highest quantitative GIS model potential, in qualitative terms, to mineral deposit models and the geological and geochemical evidence supporting them. In a number of places there is overlap between the evidence for different deposit models and their quantitative GIS model results. Areas of interest referred to below are keyed to Figure 9.

SEDEX Zinc-Lead-Silver Model

Five areas of interest on the final SEDEX potential map (Fig. 9A-E) are discussed below.

Area A, in the northwest section of the study area, contains some of the Howards Pass deposits, and is a high-potential area. It forms the northwest part of a southeast-northwest-trending linear zone within the study area, informally known as the 'zinc corridor', extending from the northwest end of the existing park reserve and the Flat River Valley to the Howards Pass deposits. A separate subparallel strand of this corridor contains a high-potential zone (area B) northwest of the Cantung deposit.

Area C represents a broad area of relatively high potential in the Meilleur River Embayment of the Selwyn Basin, hosted by the Road River Group but partially masked by the younger Besa River Formation. This area is generally under-explored due to its remoteness but was previously highlighted by the Nahanni MERA 1, along the western edge of the Tlogotsho Plateau. The Meilleur River Embayment had earlier been identified as an important eastern extension of the Selwyn Basin by Morrow and Cook (1987). Despite the lack of exploration interest, this MERA 2 study has quantitatively reinforced evidence that the Meilleur River Embayment has relatively high potential for the presence of undiscovered SEDEX deposits based on the added favourability of stream sediment, stream water, and spring water geochemistry, northeasterly growth faults associated with the Leith Ridge basement structure, and favourable rock units throughout the area.

Area D in the vicinity of the Selena Creek deposit represents an area of relatively high potential, very much like that of Area C, and underlain by the Road River Group within the Selwyn Basin proper. This area is characterized by rolling vegetated hills with little exposure except where dissected by deep canyons.

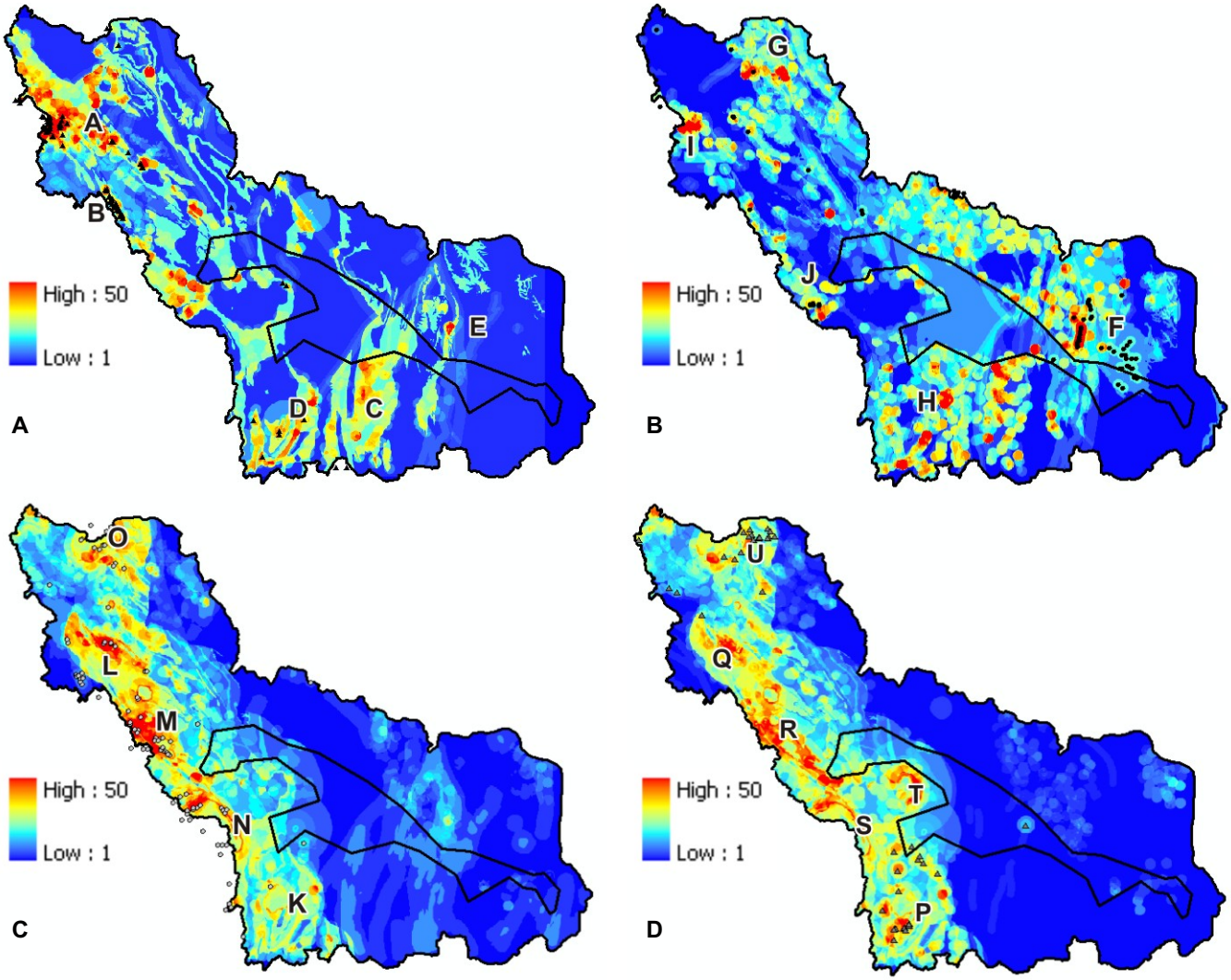


Figure 9. Final resource-potential maps for the four mineral deposit models analyzed by GIS in this paper. The locations of mineral occurrences assigned to each of the deposit models are shown for reference. The four maps shown in **(A)** SEDEX, **(B)** carbonate-fault, **(C)** intrusion-related, and **(D)** Carlin-type are the result of the additive-normalized process of combining multiple evidence maps for each deposit type.

Some zinc showings have been identified by the limited exploration efforts in this area. The regional northeasterly trend of high mineral potential from the Prairie Creek to Meilleur River areas continues toward the southwest into this area, parallel to the deep-seated Leith Ridge structure.

Area E represents the northeastern extension of the Leith Ridge trend established by areas C and D, into the MacDonald Platform. This area is enhanced in potential by the growth fault attribute contributed by the carbonate-shale facies change that trends northerly along the Prairie Creek sub-embayment of the Meilleur River Embayment. Stream sediment, stream water, and spring water geochemical data further support this designation.

Carbonate-Fault Model

Figure 9B and F show mineral-potential maps for the carbonate-fault zinc-lead-silver deposit model. A large area around the Prairie Creek deposit (Area F) containing many fault-related prospects has been classified as high potential based on this model. This rating is supported by favourable stream sediment chemistry, a high density of mapped faults, and the presence of diagenetically altered limestone and dolostone units (Manetoe facies).

The Broken Skull area (Area G) is in the vicinity of the Broken Skull Fault, which is interpreted as a reactivated growth fault due to lithological changes across it (see Fig. 3). A number of anomalous hot springs in this area, combined with geochemistry suggestive of mantle fluids, supports the inference that this fault is long-lived and deep-seated. This area is also characterized by anomalous stream sediment geochemistry.

Area H, in the vicinity of the Selena Creek deposit, is classified as higher in potential due to anomalous sediment geochemistry, favourable rock units, and the presence of a number of north-trending faults. Some SEDEX prospects have been identified in this area and

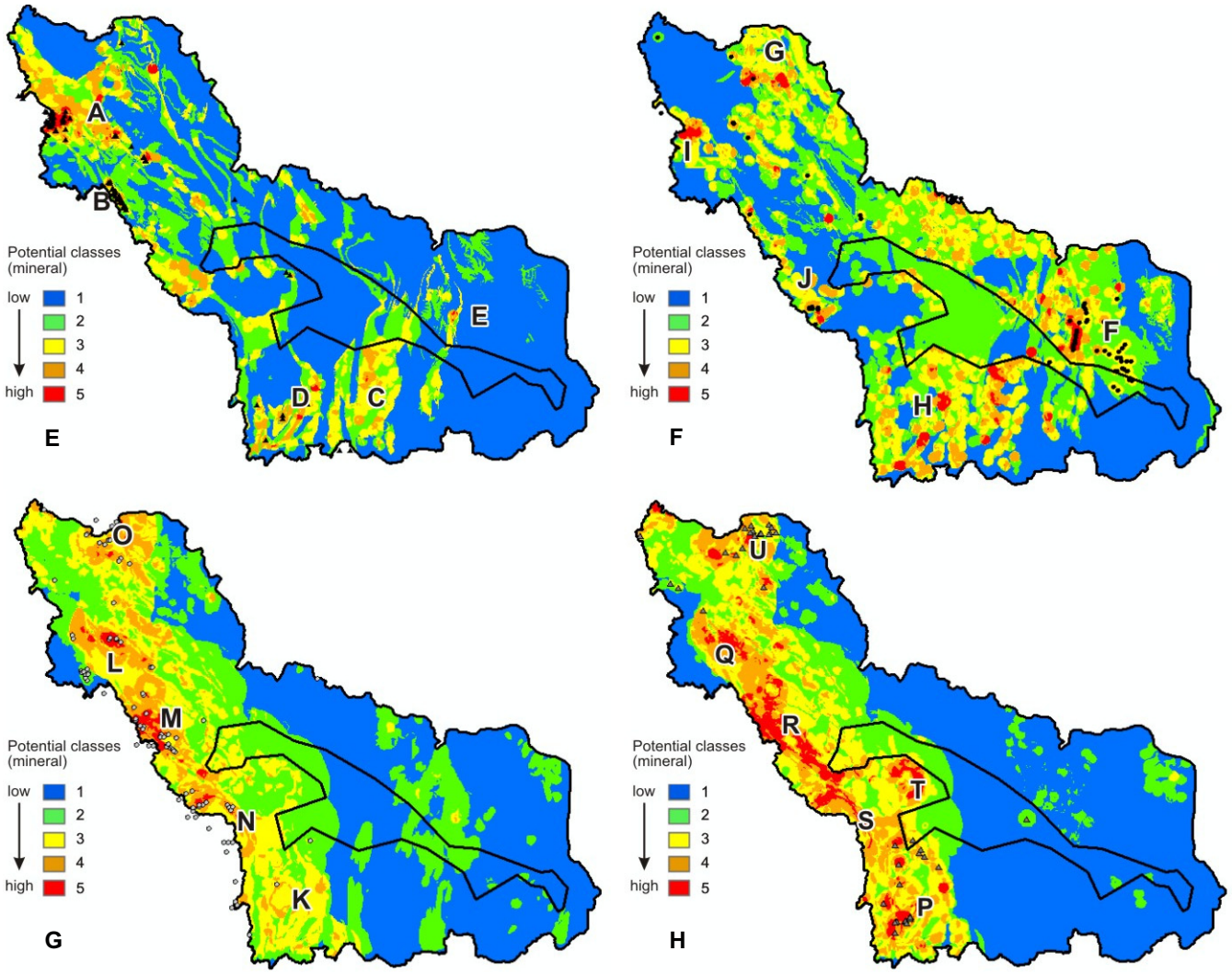


Figure 9 continued. The simplified five-class maps used to create the final additive potential map are shown in **(E)** SEDEX, **(F)** carbonate-fault, **(G)** intrusion-related, and **(H)** Carlin-type. The areas of highest potential are indicated by single unique capital letters and are explained in the text.

also the high potential for intrusion-related mineralization may reflect overlaps in the genetic models. The plutons in this vicinity may have acted as heat sources for remobilizing mineralized fluids along major faults.

Areas I (Howards Pass) and J (southeast of Cantung) are located along the western strand of the zinc corridor, defined here primarily by anomalous stream sediment geochemistry, favourable basinal shale packages, and a high density of faults.

A southeast-northwest-trending divide is apparent between the high potential zones F and G in strata of the Mackenzie Platform, and areas H, I, and J within the Selwyn Basin which may reflect an overlap of intrusion-related models with SEDEX parameters. There are some examples of carbonate-fault occurrences in the southwestern area, but most of these show evidence of higher temperatures, favouring classification as intrusion-related instead.

Intrusion-Related Model

Figure 9C and 9G shows the intrusion-related mineral-potential map. Obvious high-potential areas are restricted to the western portion of the region, in proximity to the plutons. Area K, around and to the north of Selena Creek, is modelled as high in potential by virtue of its proximity to the McLeod and Big Charlie plutons, intersecting carbonate units, anomalous geochemistry (particularly stream sediment), anomalies in spring waters, and anomalous geophysical signatures. This area also contains a number of skarn occurrences.

Area L-M-N is a broad zone of high potential related directly to the Tay River plutonic suite. Its favourability is supported in part by anomalous stream sediment geochemistry, as well as carbonate units within the pluton buffers.

Area O is centred near O'Grady Lakes/Moose Ponds, covering the O'Grady Batholith of the Tombstone plu-

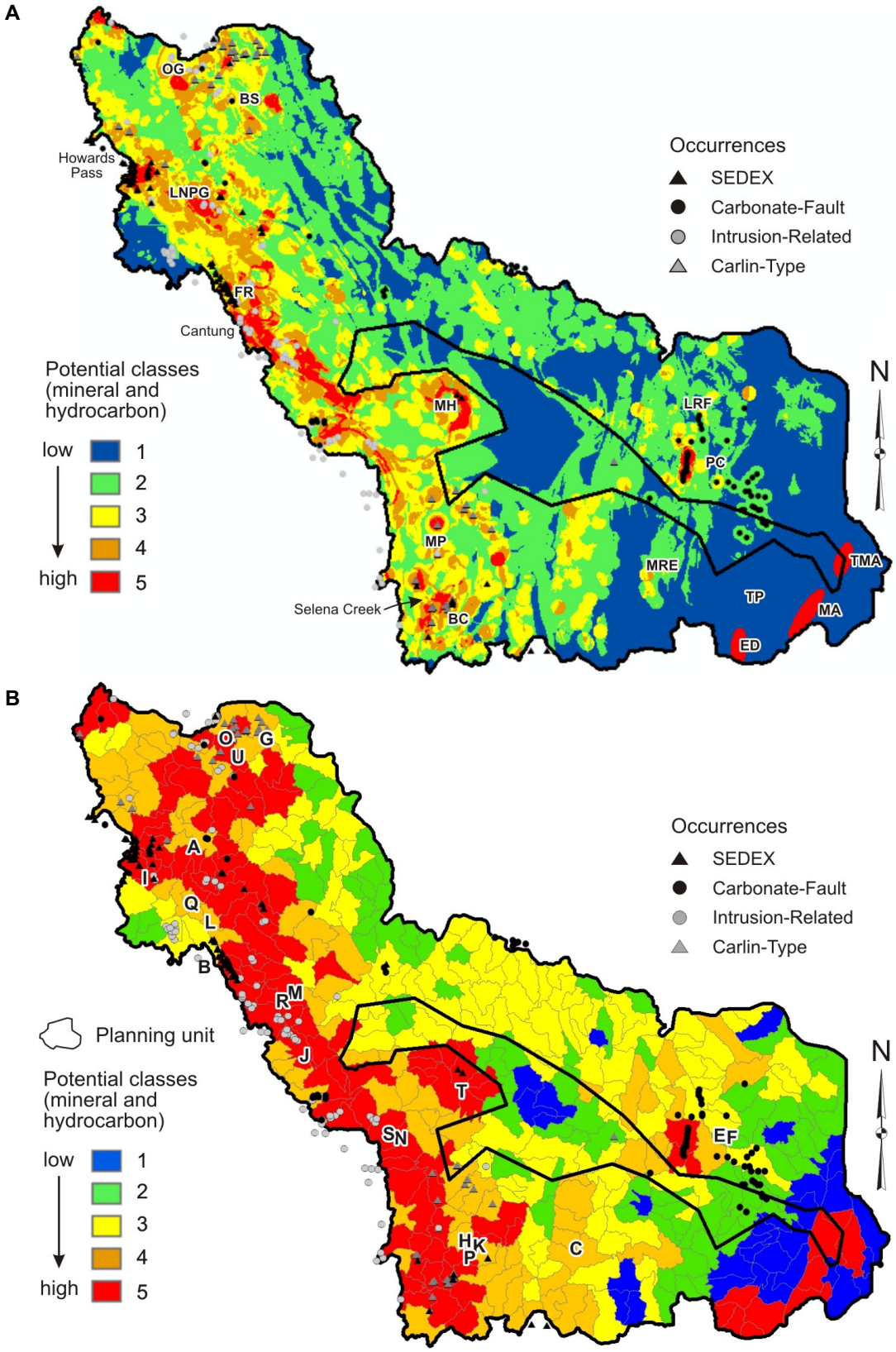


Figure 10. Final additive mineral potential maps. Mineral occurrences by type are shown for reference. **A)** Continuous potential map generated by combining the maximum values of the individual potential maps for each deposit model as well as the potential map for hyrdocarbons. BC = Big Charlie pluton, BS = Broken Skull River area, ED = Etanda Dome, FR = Flat River, LNPG = Little Nahanni Pegmatite Group, LRF = Leif Ridge Fault, MA = Mattson Anticline, MH = Mount Hamilton pluton, MP = McLeod pluton, MRE = Meilleur River Embayment, OG = O'Grady Batholith, PC = Prairie Creek, TMA = Twisted Mountain Anticline, TP = Tlogotsho Plateau. **B)** Resource potential apportioned to park planning units using the MAX operator. See text for explanation. Unique letters refer to deposit model areas of interest, as described in the Results section of the text.

tonic suite and a number of high-ranking intrusion-related mineral prospects. In addition to anomalous stream sediment geochemistry, the pluton-buffered areas also contain favourable carbonate units and several intrusion-related anomalies represented by pathfinder elements in spring waters.

Carlin-Type Model

Figure 9D and 9H shows the Carlin-type Au-potential map. An expansive area of high potential occurs in the vicinity of the Selena Creek placer deposit (Area P). This area has been classified as high potential based on a series of placer-gold showings, favourable pathfinder elements (As, Sb, Hg, Ti, and Ba accompanying Au and Ag), lithology, proximity to plutons, and position at the southern end of a regional trend of existing gold prospects and deposits extending to Alaska.

The linear zinc corridor (Area Q-R-S), which contains both the Howards Pass and the Cantung regions, is divided and partly overlapped by the high-potential area for Carlin-type gold mineralization based on the proximity to plutons, a high density of anticlines, and a trend of numerous occurrences that includes the world-class Cantung mine. This area illustrates an overlap in parameters with the intrusion-related model.

The high-potential rating of Area T is a result of the intersection of the Mount Hamilton pluton buffer with favourable carbonate lithology, anomalous geochemical data from stream sediment, stream water, and springs, as well as minor placer-gold occurrences.

Area U, around and to the east of the O'Grady batholith, is similar to Area T with the added influence of favourable structural parameters, such as faults parallel to the Broken Skull River.

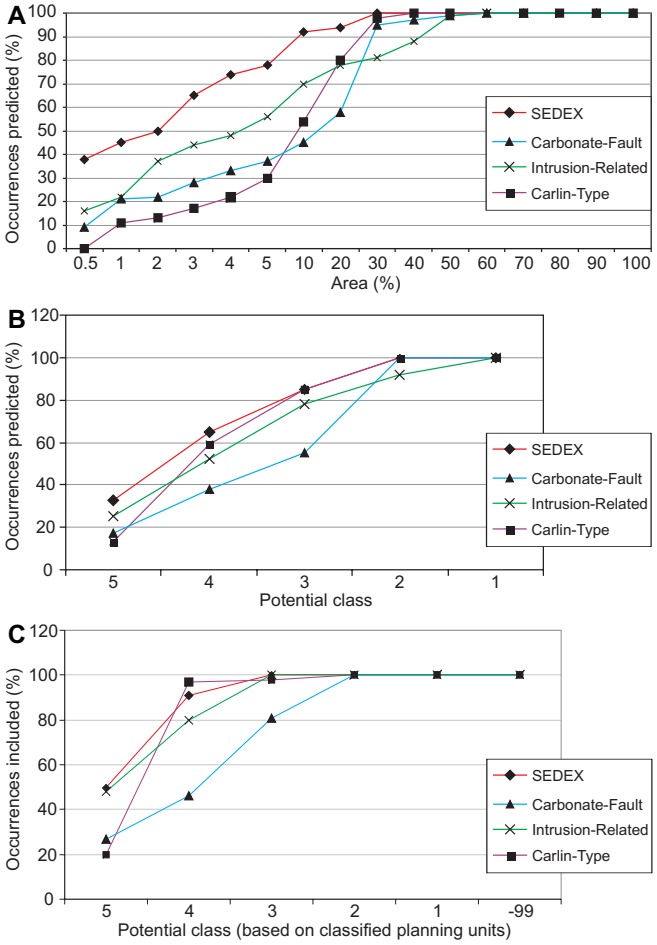


Figure 11. Prediction graphs for each of the four deposit models in this GIS study, showing how well the final additive potential maps (Figs. 9, 10) predict the individual occurrences classified by deposit type. **A)** Prediction plot from individual mineral-potential maps for each of the four deposit models (Fig. 9). **B)** Prediction plot based on the five-class mineral-potential map (Fig. 10A). **C)** Prediction plot based on the planning units map (Fig. 10B).

DISCUSSION AND SUMMARY

Figure 10A summarizes the total mineral and energy potential based on all of the models discussed above. Twelve percent of the park expansion study area is characterized by moderate to high nonrenewable resource potential, with restricted areas of very high potential. The high-potential ratings are consistent with previously published, aerially or topically restricted resource assessments by Jefferson and Spirito (2003) and Lariviere et al. (2006). Although still not all-encompassing, this GIS analysis achieves more comprehensive and objective results than the previous assessments by incorporating broader and more advanced sampling and analytical techniques for the field and laboratory geochemistry, by enhanced regional geological and geophysical knowledge, and by quantitative spatial modelling in a GIS that applies state-of-the-art integration methods to combine a knowledge-driven weighted data set of deposit models with the geochemical and geological data. The mineral potential maps are constrained by the present knowledge base, by the use of only four enhanced composite deposit models that, together with the Hydrocarbon map, represent all nonrenewable resource types known or thought to be important in the Nahanni Park area, a limited number of evidence maps used to produce each map, and a subjective knowledge-driven weighting system for evidence layers.

This entire resource assessment process is knowledge-driven and the maps generated represent "our best estimate' of relative mineral potential given the limitations discussed above, although experiments to generate data-driven weightings show that the knowledge-driven estimates are reasonable. These maps would likely change in various areas with increased exploration knowledge, the availability of more (uniformly distributed) geoscience data for additional evidence maps, and further data-driven modelling to refine the weighting systems.

Harris, J.R., Wilkinson, L., Heather, K., Fumerton, S., Bernier, M., and Dahn, R.
2001: Gold potential of the Swayze Greenstone Belt, Ontario: Application of GIS technology; Natural Resources Research, v. 10, p. 91-124.

Harris, J.R., Sanborn-Barrie, M., Panagapko, D., Skulski, T., and Parker, J.R.
2006: Gold prospectivity maps of the Red Lake greenstone belt: Application of GIS technology; Canadian Journal of Earth Sciences, v. 43, p. 865 -893.

Jefferson, C.W. and Spirito, W. (ed.)
2003: Non-Renewable Mineral and Energy Resource Potential of the Proposed Extensions to Nahanni National Park Reserve, Northern Cordillera, Northwest Territories; Geological Survey of Canada, Open File 1686, 253 p.

Jefferson, C.W., Spirito, W.A., and Hamilton, S.M.
2003: Geological setting, Chapter 3 *in* Non-Renewable Mineral and Energy Resource Potential of the Proposed Extensions to Nahanni National Park Reserve, Northern Cordillera, Northwest Territories, (ed.) C.W. Jefferson and W. Spirito; Geological Survey of Canada, Open File 1686, p. 3-1 to 3-21.

Lariviere, J.M., Eddy, B.G., Udell, A., and Slack, T.
2006: Mackenzie Valley Mineral Potential Map; Northwest Territories Geoscience Office, Open File 2006-03, scale 1:1,500,000.

Lemkow, D., Harris, J.R., and Slack, T. (comp.)
2007: Digital geoscience database: A contribution to the mineral and energy resource assessment of the greater Nahanni ecosystem, Northwest Territories, Appendix 4 *in* Mineral and Energy Resource Assessment of the Greater Nahanni Ecosystem Under Consideration for the Expansion of the Nahanni National Park Reserve, Northwest Territories, (ed.) D.F. Wright, D. Lemkow, and J.R. Harris; Geological Survey of Canada, Open File 5344.

Lydon, J.
1995: Sedimentary exhalative sulphides (SEDEX), *in* Geology of Canadian Mineral Deposit Types No. 8, (ed.) O.R. Eckstrand, W.D. Sinclair, and R.I. Thorpe; Geological Survey of Canada, p. 130-152 (also Geological Society of America, The Geology of North America, v. P-1).

McCurdy, M.W., McNeil, R.J., Friske, P.W.B., Day, S.J.B, Wilson, R.S.
2007: Stream sediment geochemistry in the proposed extension to the Nahanni Park Reserve, *in* Mineral and Energy Resource Potential of the Proposed Expansion to the Nahanni National Park Reserve, North Cordillera, Northwest Territories, (ed.) D.F. Wright, D. Lemkow, and J. Harris; Geological Survey of Canada, Open File 5344, p. 75-98.

Morrow, D.W. and Cook, D.G.
1987: The Prairie Creek Embayment and Lower Paleozoic Strata of the Southern Mackenzie Mountains; Geological Survey of Canada, Memoir 412, 195 p.

Morrow, D.W., Cumming, G.L., and Aulstead, K.L.
1990: The Gas-Bearing Devonian Manetoe Facies, Yukon and Northwest Territories; Geological Survey of Canada, Bulletin 400, 87 p.

Okulitch, A.
in prep a: Geology of the Redstone River Area, National Earth Science Series, Geological Atlas; National Resources Canada, Map NP-9/10-G, scale 1:1 million.

In prep b: Geology of the Ross River Area, National Earth Science Series, Geological Atlas; ational Resources Canada, scale 1:1 million.

Osadetz, K.G., Chen, Z., and Morrow, D.W.
2003: Petroleum resource assessment of the Tlogotsho Plateau, Nahanni Karst, and adjacent areas under consideration for expansion of Nahanni National Park Reserve, Northern Cordillera and District of Mackenzie, *in* Non-Renewable Mineral and Energy Resource Potential of the Proposed Extensions to Nahanni National Park Reserve, Northern Cordillera, Northwest Territories, (ed.) C.W. Jefferson and W. Spirito; Geological Survey of Canada, Open File 1686, p. 8-1 to 8-36.

Paradis, S.
2007: Isotope geochemistry of the Prairie Creek carbonate-hosted zinc-lead-silver deposit, southern Mackenzie Mountains, Northwest Territories, *in* Mineral and Energy Resource Assessment of the Greater Nahanni Ecosystem Under Consideration for the Expansion of the Nahanni National Park Reserve, Northwest Territories, (ed.) D.F. Wright, D. Lemkow, and J.R. Harris; Geological Survey of Canada, Open File 5344, p. 131-176.

Poulsen, K.H.
1996: Carlin-type gold deposits and their potential occurrence in the Canadian Cordillera, *in* Cordillera and Pacific Margin; Geological Survey of Canada, Current Research 1996-A, p. 1-9.

Plant, J.A. and Raiswell, R.W.
1994: Modifications to the geochemical signatures of ore deposits and their associated rocks in different surface environments, *in* Handbook of Exploration Geochemistry, v. 6: Drainage Geochemistry, (ed.) M. Hale and J.A. Plant; Elsevier, p. 73-109.

Raines, G.L.
1999: Evaluation of weights of evidence to predict epithermal gold deposits in the Great Basin of the western United States; Natural Resources Research, v. 8, p. 257-276.

Rasmussen, K.L., Mortensen, J.K., and Falck, H.
2006: Morphological and compositional analysis of placer gold in the South Nahanni River drainage, Northwest Territories; Yukon Exploration and Geology 2006, p. 237-250

Rasmussen, K.L., Mortensen, J.K., Falck, H. and Ullrich, T.D.
2007: The potential for intrusion-related mineralization within the South Nahanni River MERA area, Selwyn and Mackenzie Mountains, Northwest Territories, *in* Mineral and Energy Resource Assessment of the Greater Nahanni Ecosystem Under Consideration for the Expansion of the Nahanni National Park Reserve, Northwest Territories, (ed.) D.F. Wright, D. Lemkow, and J.R. Harris; Geological Survey of Canada, Open File 5344, p. 203-278.

Reddy, R.K.T. and Bonham-Carter, G.F.
1991: A decision-tree approach to mineral potential mapping in Snow Lake area, Manitoba; Canadian Journal of Remote Sensing, v. 17, p. 191-200.

Rencz, A.N., Harris, J.R., Watson G.P., and Murphy, B.
1994: Data integration for mineral exploration in the Antigonish Highlands, Nova Scotia: Canadian Journal of Remote Sensing, v. 20, p. 258-267.

Richards, B.G.
1989: Report on the Selena Creek placer property, Nahanni Mining Division, Northwest Territories, Latitude: 60º55'N; Longitude: 126º40'W; unpub. report for Sirius Resource Corporation and Verdstone Gold Corporation; Dynamin Engineering Limited, Vancouver, 19 p.

Rowan, L.
1989: Similarities of geological environment and potential for Carlin-style mineralization at Selena Creek; INAC Assessment Files, November 27, 1989., unpub. memorandum.

Singer, D.A. and Kouda R.
1996: Application of feedforward neural network in search for Kuoroko deposits in the Hokuroku district, Japan; Mathematical Geology, v. 28, p. 1017-1023.

1999: A comparison of the weights-of-evidence method and probabilistic neural networks; Natural Resources Research, v. 8, p. 287-298.

Spirito, W.A. and Jefferson, C.W.
2003: Regional surficial geochemistry, *in* Non-Renewable Mineral and Energy Resource Potential of the Proposed Extensions to Nahanni National Park Reserve, Northern Cordillera, Northwest Territories, (ed.) C.W. Jefferson and W. Spirito; Geological Survey of Canada, Open File 1686, p. 4-1 to 4-79.

Wilkinson, L., Harris, J.R., and Grunsky, E.C.
1999: Building a Lithogeochemical Dataset for GIS Analysis: Methodology Problems and Solutions; Geological Survey of Canada, Open File Report 3788, 44 p.

Wright, D.F. and Bonham-Carter, G.F.
1996: VHMS favourability mapping with GIS-based integration models, Chisel Lake-Anderson Lake area, *in* EXTECH I: A Multidisciplinary Approach to Massive Sulphide Research in the Rusty Lake- Snow Lake Greenstone Belts, Manitoba, (ed.) G.F. Bonham-Carter, A.G. Galley, and G.E.M. Hall; Geological Survey of Canada, Bulletin 426, p. 339-376.

Yuvan, J., Shelton, K., and Falck, H.
2007: Geochemical investigations of the high-grade quartz-*in* Mineral and Energy Resource Assessment of the Greater Nahanni Ecosystem Under Consideration for the Expansion of the Nahanni National Park Reserve, Northwest Territories, (ed.) D.F. Wright, D. Lemkow, and J.R. Harris; Geological Survey of Canada, Open File 5344, p. 177-190.

Harris, J.R., Wilkinson, L., Heather, K., Fumerton, S., Bernier, M., and Dahn, R.
2001: Gold potential of the Swayze Greenstone Belt, Ontario: Application of GIS technology; Natural Resources Research, v. 10, p. 91-124.

Harris, J.R., Sanborn-Barrie, M., Panagapko, D., Skulski, T., and Parker, J.R.
2006: Gold prospectivity maps of the Red Lake greenstone belt: Application of GIS technology; Canadian Journal of Earth Sciences, v. 43, p. 865 -893.

Jefferson, C.W. and Spirito, W. (ed.)
2003: Non-Renewable Mineral and Energy Resource Potential of the Proposed Extensions to Nahanni National Park Reserve, Northern Cordillera, Northwest Territories; Geological Survey of Canada, Open File 1686, 253 p.

Jefferson, C.W., Spirito, W.A., and Hamilton, S.M.
2003: Geological setting, Chapter 3 *in* Non-Renewable Mineral and Energy Resource Potential of the Proposed Extensions to Nahanni National Park Reserve, Northern Cordillera, Northwest Territories, (ed.) C.W. Jefferson and W. Spirito; Geological Survey of Canada, Open File 1686, p. 3-1 to 3-21.

Lariviere, J.M., Eddy, B.G., Udell, A., and Slack, T.
2006: Mackenzie Valley Mineral Potential Map; Northwest Territories Geoscience Office, Open File 2006-03, scale 1:1,500,000.

Lemkow, D., Harris, J.R., and Slack, T. (comp.)
2007: Digital geoscience database: A contribution to the mineral and energy resource assessment of the greater Nahanni ecosystem, Northwest Territories, Appendix 4 *in* Mineral and Energy Resource Assessment of the Greater Nahanni Ecosystem Under Consideration for the Expansion of the Nahanni National Park Reserve, Northwest Territories, (ed.) D.F. Wright, D. Lemkow, and J.R. Harris; Geological Survey of Canada, Open File 5344.

Lydon, J.
1995: Sedimentary exhalative sulphides (SEDEX), *in* Geology of Canadian Mineral Deposit Types No. 8, (ed.) O.R. Eckstrand, W.D. Sinclair, and R.I. Thorpe; Geological Survey of Canada, p. 130-152 (also Geological Society of America, The Geology of North America, v. P-1).

McCurdy, M.W., McNeil, R.J., Friske, P.W.B., Day, S.J.B, Wilson, R.S.
2007: Stream sediment geochemistry in the proposed extension to the Nahanni Park Reserve, *in* Mineral and Energy Resource Potential of the Proposed Expansion to the Nahanni National Park Reserve, North Cordillera, Northwest Territories, (ed.) D.F. Wright, D. Lemkow, and J. Harris; Geological Survey of Canada, Open File 5344, p. 75-98.

Morrow, D.W. and Cook, D.G.
1987: The Prairie Creek Embayment and Lower Paleozoic Strata of the Southern Mackenzie Mountains; Geological Survey of Canada, Memoir 412, 195 p.

Morrow, D.W., Cumming, G.L., and Aulstead, K.L.
1990: The Gas-Bearing Devonian Manetoe Facies, Yukon and Northwest Territories; Geological Survey of Canada, Bulletin 400, 87 p.

Okulitch, A.
in prep a: Geology of the Redstone River Area, National Earth Science Series, Geological Atlas; National Resources Canada, Map NP-9/10-G, scale 1:1 million.

In prep b: Geology of the Ross River Area, National Earth Science Series, Geological Atlas; ational Resources Canada, scale 1:1 million.

Osadetz, K.G., Chen, Z., and Morrow, D.W.
2003: Petroleum resource assessment of the Tlogotsho Plateau, Nahanni Karst, and adjacent areas under consideration for expansion of Nahanni National Park Reserve, Northern Cordillera and District of Mackenzie, *in* Non-Renewable Mineral and Energy Resource Potential of the Proposed Extensions to Nahanni National Park Reserve, Northern Cordillera, Northwest Territories, (ed.) C.W. Jefferson and W. Spirito; Geological Survey of Canada, Open File 1686, p. 8-1 to 8-36.

Paradis, S.
2007: Isotope geochemistry of the Prairie Creek carbonate-hosted zinc-lead-silver deposit, southern Mackenzie Mountains, Northwest Territories, *in* Mineral and Energy Resource Potential of the Proposed Expansion to the Nahanni National Park Reserve, North Cordillera, Northwest Territories, (ed.) D.F. Wright, D. Lemkow, and J. Harris; Geological Survey of Canada, Open File 5344, p. 131-176.

Poulsen, K.H.
1996: Carlin-type gold deposits and their potential occurrence in the Canadian Cordillera, *in* Cordillera and Pacific Margin; Geological Survey of Canada, Current Research 1996-A, p. 1-9.

Plant, J.A. and Raiswell, R.W.
1994: Modifications to the geochemical signatures of ore deposits and their associated rocks in different surface environments, *in* Handbook of Exploration Geochemistry, v. 6: Drainage Geochemistry, (ed.) M. Hale and J.A. Plant; Elsevier, p. 73-109.

Raines, G.L.
1999: Evaluation of weights of evidence to predict epithermal gold deposits in the Great Basin of the western United States; Natural Resources Research, v. 8, p. 257-276.

Rasmussen, K.L., Mortensen, J.K., and Falck, H.
2006: Morphological and compositional analysis of placer gold in the South Nahanni River drainage, Northwest Territories; Yukon Exploration and Geology 2006, p. 237-250

Rasmussen, K.L., Mortensen, J.K., Falck, H. and Ullrich, T.D.
2007: The potential for intrusion-related mineralization within the South Nahanni River MERA area, Selwyn and Mackenzie Mountains, Northwest Territories, *in* Mineral and Energy Resource Potential of the Proposed Expansion to the Nahanni National Park Reserve, North Cordillera, Northwest Territories, (ed.) D.F. Wright, D. Lemkow, and J. Harris; Geological Survey of Canada, Open File 5344, p. 203-278.

Reddy, R.K.T. and Bonham-Carter, G.F.
1991: A decision-tree approach to mineral potential mapping in Snow Lake area, Manitoba; Canadian Journal of Remote Sensing, v. 17, p. 191-200.

Rencz, A.N., Harris, J.R., Watson G.P., and Murphy, B.
1994: Data integration for mineral exploration in the Antigonish Highlands, Nova Scotia: Canadian Journal of Remote Sensing, v. 20, p. 258-267.

Richards, B.G.
1989: Report on the Selena Creek placer property, Nahanni Mining Division, Northwest Territories, Latitude: 60º55'N; Longitude: 126º40'W; unpub. report for Sirius Resource Corporation and Verdstone Gold Corporation; Dynamin Engineering Limited, Vancouver, 19 p.

Rowan, L.
1989: Similarities of geological environment and potential for Carlin-style mineralization at Selena Creek; INAC Assessment Files, November 27, 1989., unpub. memorandum.

Singer, D.A. and Kouda R.
1996: Application of feedforward neural network in search for Kuoroko deposits in the Hokuroku district, Japan; Mathematical Geology, v. 28, p. 1017-1023.

1999: A comparison of the weights-of-evidence method and probabilistic neural networks; Natural Resources Research, v. 8, p. 287-298.

Spirito, W.A. and Jefferson, C.W.
2003: Regional surficial geochemistry, *in* Non-Renewable Mineral and Energy Resource Potential of the Proposed Extensions to Nahanni National Park Reserve, Northern Cordillera, Northwest Territories, (ed.) C.W. Jefferson and W. Spirito; Geological Survey of Canada, Open File 1686, p. 4-1 to 4-79.

Wilkinson, L., Harris, J.R., and Grunsky, E.C.
1999: Building a Lithogeochemical Dataset for GIS Analysis: Methodology Problems and Solutions; Geological Survey of Canada, Open File Report 3788, 44 p.

Wright, D.F. and Bonham-Carter, G.F.
1996: VHMS favourability mapping with GIS-based integration models, Chisel Lake-Anderson Lake area, *in* EXTECH I: A Multidisciplinary Approach to Massive Sulphide Research in the Rusty Lake- Snow Lake Greenstone Belts, Manitoba, (ed.) G.F. Bonham-Carter, A.G. Galley, and G.E.M. Hall; Geological Survey of Canada, Bulletin 426, p. 339-376.

Yuvan, J., Shelton, K., and Falck, H.
2007: Geochemical investigations of the high-grade quartz-scheelite veins of the Cantung mine, Northwest Territories, *in* Mineral and Energy Resource Potential of the Proposed Expansion to the Nahanni National Park Reserve, North Cordillera, Northwest Territories, (ed.) D.F. Wright, D. Lemkow, and J. Harris; Geological Survey of Canada, Open File 5344, p. 177-190.

APPENDIX 1

A Review of the Bedrock Geology of the Nahanni River Region and Its Context in the Northern Cordillera

H. Falck

Northwest Territories Geoscience Office, P.O. Box 1500, Yellowknife, Northwest Territories X1A 2R3

SUMMARY

The Nahanni region is defined by the watershed of the Nahanni River which has its headwaters in the eastern Selwyn Mountains. The river transects the southern Mackenzie Mountains as it flows east toward the Liard River. The rocks exposed and underlying these mountains have been deposited since early Proterozoic time and continue to be affected by geological forces today. The basement to the region consists of a series of cratonic terranes that collided and merged with the Canadian Shield during the early and middle Proterozoic since about 2.1 billion years ago. This basement collage was covered by a thick wedge of clastic and carbonate sedimentary rocks, in a large deltaic system starting approximately 1800 Million years ago (Ma). At 750 Ma, the paleo-continent began a protracted major rifting event that lasted until about 600 Ma. Continent-sized blocks including Australia and Siberia were broken off of North America and the Nahanni region was cut by major faults. These faults, such as the Liard and Fort Norman lines, formed controlling structures for much of the subsequent geological history, defining the position of ancient shorelines as well as favourable sites for sediment-hosted mineral deposits. Movements on these faults were not singular events, as periodic reactivation formed topographic highs and depressions.

After rifting, the Nahanni region became part of a long-lived passive continental margin. In the eastern part of the area, the uplifted margin developed a carbonate platform similar to that found today in the Bahamas. To the west, a deeper water basin resembling the Gulf of Mexico developed, into which fine-grained sediments were deposited. Fossils of some of the earliest animal life forms that lived during this period (ca. 580 Ma) are preserved in siltstone units of the Vampire Ranges. The Mackenzie Platform carbonate, and the deeper water Selwyn Basin shale environments persisted until the Jurassic Era, 170 Ma. Over this extended period, distant tectonic events provided new sediment sources. Fluctuations in sea level combined with local uplifts developed arches such as the Redstone Arch, formed local basins such as the Meilleur and Prairie Creek embayments, and adjusted the location of the divide between the basin and platformal settings, all within the persistent overall passive margin setting.

By 170 Ma, tectonic movements of the Pacific plate had transported a large volcanic island arc (similar to Indonesia today) westward, until it collided with the margin of North America. The slow collision raised the seafloor, transforming it into mountain ranges west of the Nahanni region while pushing layers of sedimentary rocks toward the east, termed the Laramide Orogeny. These thrust sheets rode on low angle faults and were stacked and folded as the orogeny proceeded. Erosion by rivers flowing from the west transported sediment from the newly-formed mountains and deposited them in a series of deltas into a western interior seaway that extended from the Arctic Ocean to the Gulf of Mexico. Plants growing on these deltas became buried in the sand and mud to form the coal seams on the eastern side of the Nahanni region. Beneath the mountains, the orogeny generated sufficient heat to melt the base of the structurally thickened sedimentary rock succession. The molten rock rose through the surrounding rocks and cooled near the surface to form the large granitic plutons that are the core of the Ragged Ranges.

The tectonic forces responsible for the mountain building persisted, and additional terranes collided obliquely in the Cenozoic Era, starting at 65 Ma. The resultant tearing motions created large strike-slip faults that moved the western side of North America northward by over 400 kilometres. These forces are still active, as evidenced by the frequent earthquakes in the Nahanni region and detailed surveys using Global Positioning Satellites (GPS) that have shown the mountains to be growing and Whitehorse moving toward Yellowknife at 3 to 5 millimetres per year.

While tectonic events have been uplifting the mountains, the current landscape of craggy spires and deep valleys are mainly the product of the last ice age (2 Ma to 10,000 years ago). Glaciers formed in the highlands of the western Nahanni region then flowed across the mountain ranges towards the Mackenzie lowlands where they encountered the westward-advancing Laurentide continental ice sheet. During the course of this ice age, glaciers advanced and retreated and the zone of interaction shifted, allowing the Laurentide ice

Falck, H., 2007, Appendix 1. A review of the bedrock geology of the Nahanni River region and its context in the Northern Cordillera, *in* Mineral and Energy Resource Assessment of the Greater Nahanni Ecosystem Under Consideration for the Expansion of the Nahanni National Park Reserve, Northwest Territories, (ed.) D.R. Wright, D. Lemkow, and J.R. Harris; Geological Survey of Canada, Open File 5344, p. 327-365.

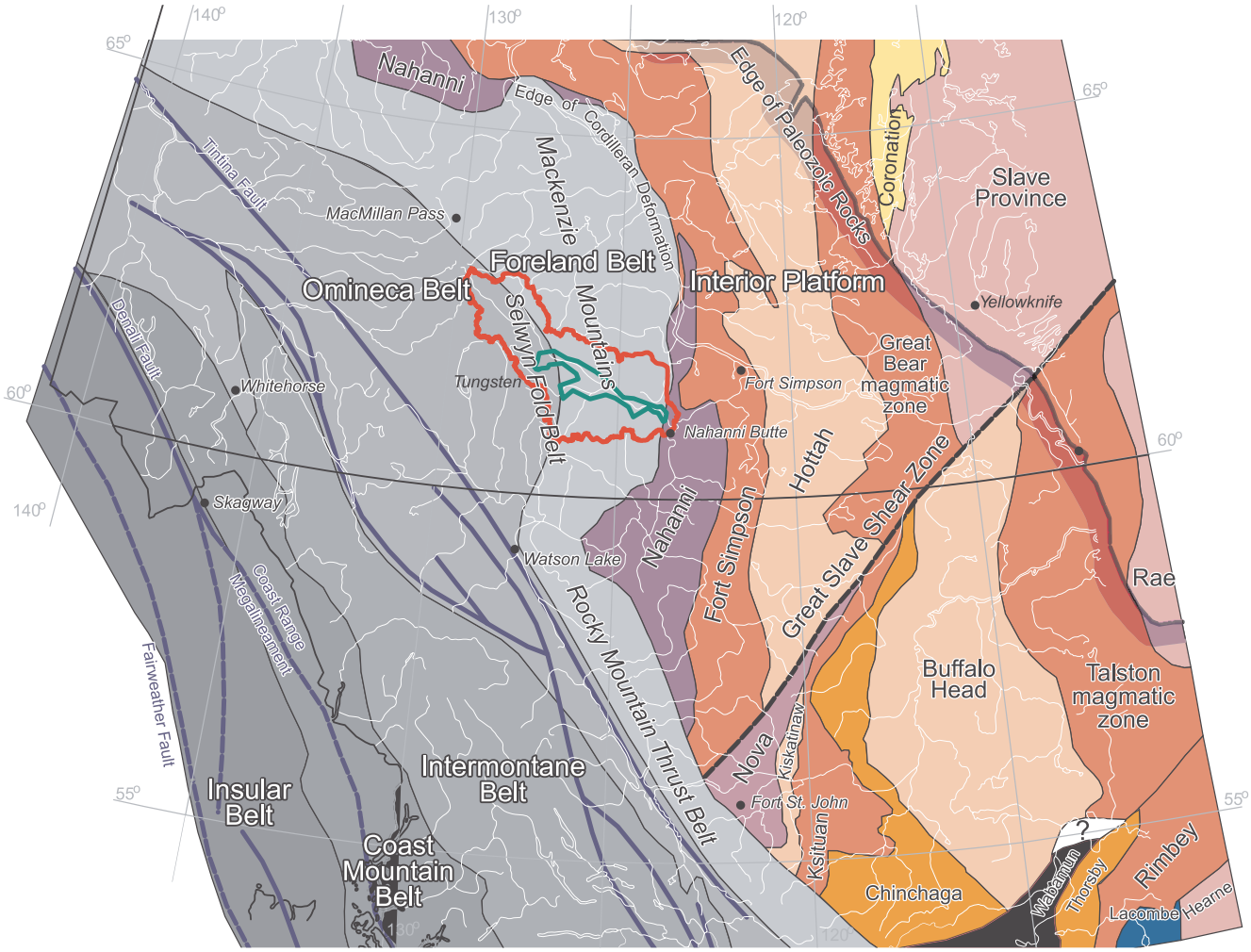


Figure 1-1. Geology of the Northern Cordillera showing the Archean to Proterozoic basement elements, mostly covered by Paleozoic strata of the Interior Platform and the major tectonomorphologic Insular, Coast, Intermontane, Omineca, and Foreland belts (after Gabrielse, 1992 and Cook and Erdmer, 2005). Major Proterozoic structures are in black and Paleozoic structures in dark blue. The study area is outlined in red and the Nahanni National Park Reserve in green.

sheets at times to flow into the mountains, reaching well past the front ranges. The cold temperatures combined with abundant water have sculpted the landscape to form the spires of the Ragged Ranges, deep U-shaped valleys and tarn lakes. At warmer times, precipitation has dissolved carbonate rocks by vertically descending flow, creating sink holes, collapse breccias and seasonal lakes (poljes) in the Nahanni Karst terrain in the Ram Plateau. Melting of the glaciers formed large glacial lakes trapped behind dams of stagnant ice and moraines. Failure of the ice dams and subsequent torrential outflow events excavated the spectacular gorges that the Nahanni River now follows. Less dramatic but more common are the large outwash plains and broad alluvial plains deposited as the glaciers retreated to the upper reaches of the mountains. Geological forces are still active in the Nahanni region. Rivers and glaciers continue to erode the rising mountains, sculpting the landscape, while landslides and slope failures form new lakes, building the ever changing character of the Nahanni region.

REGIONAL OVERVIEW

The geology of the Nahanni River study area is the product of major tectonic events that affected the entire Canadian Cordillera and in some cases the western half of North America. Although some of the tectonism taken place directly within the bounds of the study area, most of the forces and processes that have acted on the rocks in the Nahanni River areas originated from events that took place far outside of it, such as the growth of the North American continent from Paleoproterozoic time to the present. These had a profound controlling influence on the geology of the Nahanni study area. This section will summarize the major, seemingly disparate events to assist in understanding the foundations upon which the study area geology rests, leading to the current interpretation of the depositional setting of the rocks and the tectonomagmatic events that affected them. Much of this account has been summarized from Gabrielse and Yorath (1992) with the inclusion of results from more recent research, especially that of the Central Foreland

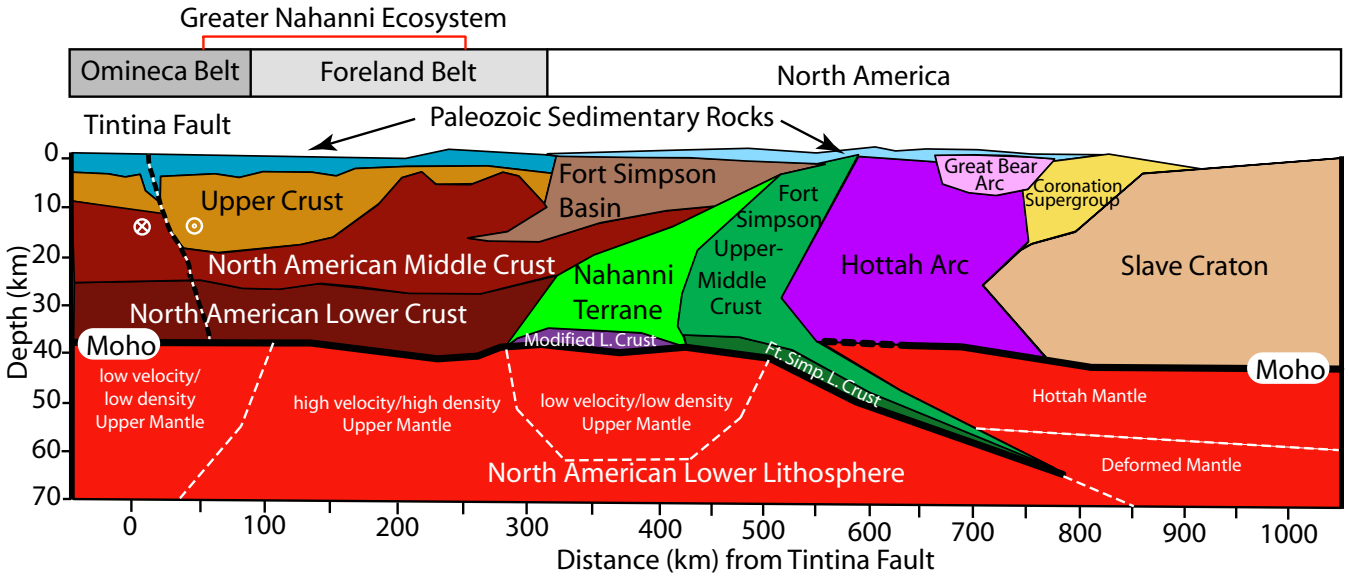


Figure 1-2. Interpreted cross-section for the transition between the North American Craton and the Cordillera based on the SNORCLE Lithoprobe Line. The circular symbols adjacent to the Tintina Fault indicate strike-slip motion with the block marked by X moving away from the viewer. The vertical exaggeration is 3.2:1 (from Welford et al., 2001). L. Crust = lower crust.

NATMAP Project (Lane, 2004, 2005) and the Lithoprobe SNORCLE Transect (Cook and Erdmer, 2005).

The geology of the Nahanni region has been shaped by a series of tectonic processes that controlled the growth and form of the ancient continental margin of North America (Fig. 1). This margin was built on a Paleoproterozoic core of amalgamated Archean cratons (Fig. 2). Collisions with other cratons and crustal elements such as island arcs punctuated an early history otherwise dominated by uplift, erosion and the transport of sediment off the cratons into thick oceanward-prograding stratigraphic sequences (Hoffmann, 1989; Cook and Erdmer, 2005) (Fig. 3A). During the late Mesoproterozoic to Neoproterozoic the tectonic setting of North America changed from amalgamation as part of the Nuna supercontinent to rifting of cratonic blocks and establishing the Pacific margin of North America (Fig. 3B) as it separated from Antarctica-Australia-North China-Siberia (Gabrielse and Yorath, 1992; Sears and Price, 2000).

After separation of large continental fragments from ancestral North America, the tectonics of the western margin became much more quiescent as a miogeoclinal passive margin developed. Based on tectonic subsidence curves, the transition from rift to post-rift cooling and subsidence was in latest Proterozoic or Early Cambrian time (Bond and Kominz, 1984). This timing is supported by the character of Lower Cambrian strata that indicates nearly synchronous deposition of thick relatively clean sandstone units along the length of the Cordilleran margin. The eastern limit of deposition of these strata appears to be controlled by a pronounced flexure in the cratonic margin (Gabrielse and Yorath, 1992). To the west, the sandstone beds pass into finer grained clastic rocks of probable continental slope setting. This model of a single rift event is however, an oversimplification of the stratigraphic record of the miogeocline, which is far too complex to be accounted for by a single rifting event. Many authors have suggested that separation of portions of the ancestral continent over a protracted period is more likely (Sears and Price, 2000; Eyles and Januszczak, 2004).

The development of the miogeocline following Neoproterozoic to Early Cambrian rifting was characterized by the growth of carbonate platforms on a westerly sloping shelf (Fig. 3B,C). Topographic irregularities related to rifting became embayments and subbasins on the western edge of this passive margin. Thick carbonate and clean quartz-dominated clastic rocks dominate the shelf strata, whereas the clastic-starved deep-water embayments and basins were filled by thin successions of fine-grained calcareous and cherty shale and siltstone (Morrow and Cook, 1987). Olistostromal deposits and other slope deposits are located near the shelf margins, along tectonically elevated arches, intra-platform ridges and reefal shoals. Between Early Ordovician and Middle Devonian time, more than 4000 m of dominantly carbonate strata were deposited in the easterly-trending Meilleur River Embayment of the Selwyn Basin and Root Basin. Continuing extension attributed to broad crustal attenuation between the Cordilleran and Franklinian miogeoclines may have contributed to the periodic development of these small rift basins. Much of the activity was concentrated near the shelf to off-shelf transition zone where the basement may have been substantially attenuated and weakened during Neoproterozoic rifting

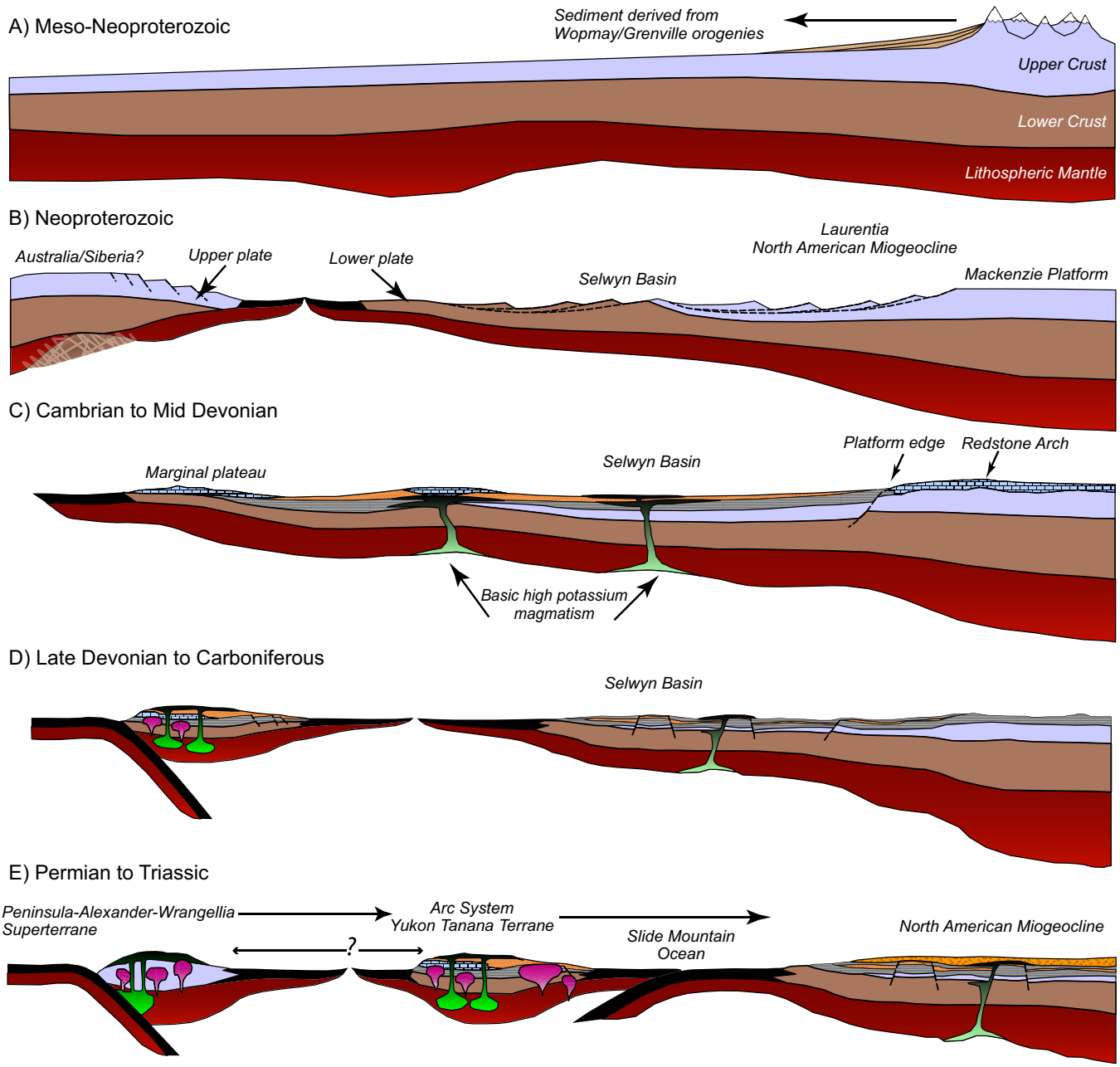


Figure 1-3. Schematic evolution of the margin of northwestern North America. **A)** Amalgamated smaller terranes with cratonic North America formed the basement to a thick sequence of clastic sediment. **B)** The western margin of Laurentia began to rift again and Selwyn Basin developed on the broad lower plate of the asymmetric rift system (Cecile et al., 1997). **C)** The region stabilized from the Ediacaran to the Devonian with deposition of the carbonate-dominated Mackenzie Platform, marginal plateaux and outboard shoals, and the shale-dominated Selwyn Basin. Local potassic magmatism included volcanism. **D)** Rifting during the Early Devonian to Early Mississippian opened the Slide Mountain Ocean west of the Nahanni Region and this basin filled with sediment derived from the north. E) The Slide Mountain Ocean closed, Yukon Tanana Terrane collided with North America, the Omineca and Foreland belts formed, and the amalgamated Peninsula-Alexander-Wrangellia Superterrane collided with the Yukon Tanana Terrane (from Mair et al., 2006).

(Gordey and Anderson, 1993). Several important Ordovician and Silurian stratiform Pb-Zn-barite deposits are found in areas with rift histories and intersecting faults, such as the Howards Pass district (Morganti, 1979; Goodfellow et al., 1983; Goodfellow and Jonasson, 1986).

Apart from localized rifting, the miogeocline remained stable from the Late Cambrian to the mid-Devonian (Gordey and Anderson, 1983). Transition zones between shelf and basin sequences migrated in response to eustatic changes, but the passive margin sequence persisted. This depositional pattern changed in the Late Devonian to the Mississippian, when the westerly derived Earn Group clastic wedge prograded eastward into the area. This was later covered by Mississippian and Pennsylvanian clastic rocks whose source lay more to the north. The distal Earn Group shale lapped over the carbonate platform toward the

east beyond the Selwyn Basin, interfingering in the middle of the Nahanni River study area with black Besa River and un-named shales of the Mackenzie Valley. These were overlapped by the Horn River and Fort Simpson shales that were derived from the northeast, and whose equivalents extend northerly to the Arctic Platform (Gordey et al., 1987). This time period records the westward prograding collisional Ellesmerian Orogeny in the Arctic, at the same time as the establishment of a major subduction zone off western North America (Fig. 3D) that persists to the present. As uplift and accompanying minor plutonism took place in northern Yukon, so did extensive deformation and uplift in the Arctic Archipelago, generating a pronounced unconformity in the northern islands. The widespread northerly-derived clastic wedge of which the Besa River, Horn River and Fort Simpson shale units are a distal part may represent the products of this erosion.

The change from a stable extensional to a compressive orogenic margin tectonic setting is recorded along much of the Cordillera. This event in the western United States is termed the "Antler Orogeny" (Nilsen and Stewart, 1980). There, and extending to northern British Columbia, deep basinal fan strata and mafic volcanic strata (e.g. the Sylvester Allochthon of northern B.C.) were emplaced over the passive margin strata (Smith et al., 1993). Correlative clastic units in the southern Cordillera, such as the Exshaw Formation, display many similar attributes to the Earn Group in northeastern B.C. and the Mackenzie Mountains including, most notably, a western derivation (Savoy et al., 2000). This abrupt change in sedimentation pattern has been attributed to a number of factors, including rifting, regional strike-slip faulting and the response to the compressive regime and uplift in northern Yukon created by the Ellesmerian Orogeny in addition to the Antler Orogeny in the southern Cordillera (Gordey et al., 1987). However Smith et al. (1993) suggested that a single Antler deformation with flexural extension in the northern Cordillera could explain the different sediment source areas (cf. Gordey et al., 1987).

One distinction is that thrust faults have been identified in the south as an important contractional tectonic element contributing to the formation of the sedimentary sequence. Equivalent thrust faults of this age have not been identified north or east of the Sylvester Allochthon in the northern Cordillera (Gordey et al., 1987). The widespread deposition of coarse- to fine-grained clastic rocks was also coeval with localized rifting and alkaline volcanism in the northern Cordillera (Goodfellow et al., 1995). Alkalic intrusive rocks and carbonatites have been documented in many places along the shelf to basin facies boundary (Pigage and Mortensen, 2004).

After the Ellesmerian and Antler orogenies, Permian uplift and erosion along a northeast-trending zone from Alaska to the northern Richardson Mountains and along the eastern Cordillera (Gabrielse and Yorath, 1992) resulted in a profound regional unconformity. A second regional unconformity is located at the base of the Triassic. Whereas tectonic causes have been suggested to explain these widespread erosive events, an alternative hypothesis is that these unconformities, especially the widespread sub-Permian unconformity, formed as a response to lower sea level due to extensive Late Carboniferous to Permian glaciation (Bamber et al., 1992; Bowring et al., 1998).

The main structural elements of the Cordillera were developed from the Early Jurassic to the Paleogene (Gabrielse and Yorath, 1992). This period marked a change in the tectonic regime from the miogeoclinal passive sequence to one of terrane amalgamation, in which crustal terranes associated with the Pacific plates collided with ancestral North America (Colpron et al., 2007) (Fig. 3E). The amalgamation and accretion of terranes resulted in the formation of four morphotectonic belts from east to west: Foreland, Omineca, Intermontane and Coastal (Gabrielse et al., 1992).

The Omineca and Foreland belts formed during the collision of the Intermontane Superterrane with the western margin of North America. Prior to this collision, the superterrane consisted of a series of smaller exotic terranes that amalgamated independently. This composite terrane encountered the North American craton when the relative motions associated with the oceanic plates in the Pacific Ocean changed. The effects of the impact were focused along a zone defined by highly metamorphosed and subsequently uplifted rocks of the Omineca belt. The age of this collision is constrained by deformed and metamorphosed Late Triassic strata and Middle Jurassic granitoid plutons that crystallized at 160 to 180 Ma and cut the highly deformed and regionally metamorphosed Omineca Belt (Tempelman-Kluit, 1979; Dusel-Bacon et al., 2002; Colpron et al., 2007).

During this collision, the miogeoclinal sequence was detached from its basement, folded and stacked by imbricate thrust faults, and transported eastward over the edge of the craton, developing the Foreland Belt (Gabrielse and Yorath, 1992). Imbricate thrust sheets and related cylindrical folds form the dominant northwesterly-trending structural fabric in the Foreland Belt. The intense imbrication of lower Paleozoic strata has been calculated to represent a pre-mid-Cretaceous contraction of at least 50%, representing crustal shortening of possibly 200 km or more (Gordey and Anderson, 1993). The advancing thrust sheets were eroded to form a large clastic sedimentary wedge in the foredeep moat east of the rising mountains. The foredeep pro-

gressively migrated eastward in advance of the deformation front, as each successive thrust sheet stepped eastward. Consequently, a single eastern limit of the deformation and the western extent of deposition are difficult to define (Aitken and Cook, 1974).

By the Early Cretaceous, widespread S-type granitic plutons characterized by $^{87}Sr/^{86}Sr$ ratios of 0.710 to 0.740 were emplaced, concurrent with minor volcanism and regional metamorphism (Gabrielse and Yorath, 1992). Slightly younger mid-Cretaceous plutons are characterized by I-type granitic rocks with $^{87}Sr/^{86}Sr$ of less than 0.706 (generally less than 0.7045). The emplacement of the plutons post-dated most of the contractional deformation as all regional contractional structures are cut by undeformed plutons. The eastern limit of the Cretaceous plutonism is parallel to but far west of the eastern limit of Foreland Belt deformation. The parallelism of the two features suggests a coupled relationship in which the generation of plutons resulted from an over-thickened crust caused by westward under-thrusting of the craton. The isotopic compositions of the Omineca plutons suggest sialic material as a melt source (Gabrielse and Yorath, 1992; Hart et al., 2004; Rasmussen, 2007).

The Cordilleran Orogeny was succeeded by collision of the Insular Superterrane (Alexander and Wrangellia terranes) with North America in mid-Cretaceous time (Monger et al., 1982; Gabrielse and Yorath, 1992; Colpron et al., 2007). The resultant deformation and metamorphism produced the Coast Belt, a suture zone dominated by long-lived plutonism, and major shear zones in the Omineca Belt. As the Coast Belt evolved from an island-arc terrane into a plutonic-metamorphic welt, the impact renewed uplift in the Omineca Belt. Rocks at depths of more than 20 km during Middle Jurassic tectonism were uplifted more than 13 to 14 km and intruded by mid-Cretaceous granite. The deformation also formed broad anticlinoria and synclinoria throughout the Cordillera in previously deformed and regionally metamorphosed rocks. Transform motion generated major crustal faults including the Tintina Fault (Gabrielse and Yorath, 1992; Murphy and Mortensen, 2003). Most of the movement on this fault was not completed until the Eocene (40 Ma), after much of the deformation and thermal events related to the Insular collision had ceased.

A second clastic wedge was shed eastward into the foredeep of the rising orogen in response to the renewed uplift (Yorath et al., 1992). While most of the newly derived sediment was transported eastward toward the foredeep, sub-basins within the amalgamated terranes and along their boundaries were also filled. These basins developed either as a direct response to the process of terrane amalgamation and collision or followed the collisional events as a consequence of crustal attenuation, thermal subsidence and lithospheric flexure. The prolonged tectonism fed sediment into a third clastic wedge in the foredeep of the Foreland Belt during Late Cretaceous to Paleocene time.

In the Paleogene, two small terranes collided with North America and each successive collision contributed to the ongoing uplift and deformation (Gabrielse and Yorath, 1992). The effects of the amalgamation were quite intense in the southern Cordillera with a high degree of crustal shortening in the Omineca and Foreland belts. In the north, deformation is suspected to have been largely restricted to dextral transcurrent movement on abundant northwest-trending faults, although precise ages of these movements have not been established (Gabrielse and Yorath, 1992; Murphy and Mortensen, 2003). Local clastic sediment filled small extensional basins created by this dextral strain regime (Long, 1986).

In the southern Cordillera, widespread granitic magmatism extended from 55 to 45 Ma in the Coast and Omineca Belts (Gabrielse and Yorath, 1992). These plutons post-dated the last episode of compressional deformation and sedimentation east of the Insular Belt (Hyndman et al., 2005b). The change from contraction to extension was in response to the change from orthogonal to oblique subduction of the Farallon plate. Changes in the relative motions among the Farallon, Kula, Pacific and North American plates during the late Mesozoic and Paleogene appear to have resulted in uplift and extension east of the Insular Belt. The uplift was associated with extensive erosion and deposition of thick non-marine to marine strata along the western flank of the Insular Belt. Continued motion of the oceanic plates along the western continental margin compressed this sequence into an accretionary wedge along a subduction zone in the Gulf of Alaska. Changes in direction and in relative velocity were significant and triggered additional uplift or magmatism. The highest mountains in Canada, in the northwestern British Columbia, are the product of oblique subduction of the Yakutat Terrane beneath the continental margin (Hyndman et al., 2005b). Subduction was along the Fairweather Fault, which in turn is part of the modern Pacific-North American transform plate boundary. Additional major right-lateral strike-slip faults, including the Tintina and Rocky Mountain fault systems, define northwestward movements of more than 1500 km related to continuing plate interaction (Murphy and Mortensen, 2003). Although faults formed in the mid-Cretaceous, it was not until the influence of the Kula plate was encountered that lateral motions predominated. The plate motion combined with the rapid west to southwest motion of the North American Plate rela-

tive to the Kula and Juan de Fuca plates resulted in large-scale dextral faulting.

The fault movements continue (Cassidy et al., 2005; Hyndman et al., 2005a,b). While the present landscape in the Nahanni region has been sculpted during glaciation and appears static, the influence of tectonic motions is still evident. Recent GPS measurements demonstrate active compression in the region between Whitehorse and Yellowknife. The concentration of hot springs and thermal anomalies in petroleum wells indicates anomalously high heat flow, and recent earthquakes show that the Mackenzie Mountains are one of the more tectonically active regions in Canada, an area of continuing mountain building processes (Majorowicz et al., 2005).

GEOLOGY OF THE STUDY AREA

Archean and Paleoproterozoic

The compositions of Archean to Proterozoic crystalline basement are critical to understanding subsequent development of the geology. The basement is often cited as the source of melts for plutons, as well as the fluids and metals responsible for the formation of mineral deposits. The basement is cut by the regional scale crustal faults described above, many of which were initiated early and reactivated periodically throughout the geological history of the region. These faults and related fractures locally served as concentrators and conduits of mineralizing fluids and were also important geological controls on the nature of overlying sedimentary deposits and localized post-depositional alteration. Thus, a discussion of the exposed strata in the study area must start with an understanding of the older basement units and the development of the North American craton (Figs. 1, 2).

The western part of the craton grew through three major orogenic episodes, interspersed by episodes of cratonic fragmentation and continental breakup. Accretion of the Slave Province began at 4.2 Ga (Iizuka et al., 2006) and was largely complete by 2.50 Ga. Subsequent breakup events reduced the Slave Craton between 2.6 to 2.2 Ga (Bleeker, 2003). The western margin of the Slave Craton formed a depositional locus for a passive margin sequence belonging to the Coronation Supergroup at about 1.97 Ga (Hoffman, 1989) (Fig. 2). The Wopmay Orogen records the accretion of a collage of terranes to the western margin of the Slave province between 2.1 and 1.84 Ga (Hildebrand et al., 1987). The Hottah Terrane, formed between 1.94 and 1.89 Ga (Housh et al., 1989), collided with the Coronation margin as part of the Calderian Orogeny about 1.90 to 1.88 Ga. This collision folded the sedimentary rocks of the Coronation Supergroup and thrust them onto the Slave Craton (Hildebrand et al., 1987). Continuing eastward subduction nd partial melting of the oceanic lithosphere beneath the Hottah terrane generated the Great Bear magmatic arc, commencing at 1.88 Ga (Hoffman and Bowering, 1984; Villeneuve et al., 1991). This plutonism continued until 1.84 Ga when the Fort Simpson terrane collided with the western margin of the Hottah terrane resulting in regional transcurrent faulting of the Wopmay Orogen (Hoffman and Bowering, 1984; Hoffman, 1987).

The Fort Simpson terrane and the adjacent Nahanni terrane are hidden beneath a thick sequence of Proterozoic and Paleozoic strata in the Western Canada Sedimentary Basin but were distinguished by their aeromagnetic characteristics (Hoffman, 1989; Villeneuve et al., 1991; Cook et al., 1992). Initial interpretation of the magnetically positive, curvilinear anomaly of the Fort Simpson terrane, which extends from northern Alberta into the Northwest Territories and trends northwest beyond Great Bear Lake, was as an accreted magmatic arc. Villeneuve et al. (1991) suggested that the magmatic arc was fed by anatexis of the adjacent Nahanni terrane during collision with the Hottah terrane. Two drill cores in the Fort Simpson terrane intersect massive biotite monzogranitic basement with a U-Pb crystallization age of 1845 Ma (Villeneuve et al., 1991). On the basis of similar isotopic results, Ross (1991) suggested correlation with basement gneiss along the eastern edge of the southern Cordillera. As the Fort Simpson magmatic arc is slightly younger than the Hottah terrane, it is thought to have formed while the Fort Simpson terrane collided with the previously amalgamated terranes, perhaps at 1.84 Ga when Great Bear magmatism ceased. The nature of the Nahanni terrane remains enigmatic, as no drill core has been recovered from it. Nd model ages do suggest that a component of the Nahanni terrane consisted of 2.0 to 2.4 Ga crust (Villeneuve et al., 1991).

The extended period of compression and mountain building of the Wopmay Orogeny was followed by quiescence, then rifting (Fig. 3B). Stable margin sedimentation dominated between 1.84 to 1.76 Ga, forming the westward-thickening Fort Simpson-Wernecke basin (Cook et al., 1992; Cook and Erdmer, 2005). The basin margin was preserved as a west-facing crustal ramp delineated in the southern Northwest Territories by the Lithoprobe seismic reflection survey and traced to the Mackenzie Delta by gravity and industry seismic reflection surveys (Cook et al., 2005). The north-south portion of the Fort Simpson Basin was largely filled by clastic sediment, as was the adjacent Wernecke basin to the northwest. The estimated thickness of the Wernecke Supergroup is 15 to 20 km (Delaney, 1981).

These Archean to Proterozoic elements constituted a stable and rigid basement upon which the younger strata in the Mackenzie Mountains were deposited and

by which the younger strata were largely protected from subsequent tectonic events until the ca. 40 to 80 Ma Laramide Orogeny that involved significant basement-cover intercalation by mechanisms still poorly understood (English and Johnston, 2004).

Young et al. (1979) identified regional unconformities that divide the thick Proterozoic sedimentary package of the Mackenzie Mountains region into sequences A, B, and C, whose nomenclature has been revised and refined several times (e.g. Delaney, 1981; Jefferson and Parrish, 1989; Rainbird et al., 1996). The latest Proterozoic strata of the Windermere Supergroup (Sequence C) were overlain during the transition to Cambrian time by the Hyland Group or the Vampire and Backbone formations, and all of these strata were formed in place as part of the continent of Laurentia (Thorkelson et al., 2005).

The oldest exposed strata in the Mackenzie Mountains and in the Wernecke and Ogilvie mountains to the west are of Paleoproterozoic age, exposed in the cores of anticlines and soles of thrust faults formed during the Laramide Orogeny, and assigned to sequence A. The Wernecke Supergroup was deposited in two siliciclastic cycles capped by carbonate rocks. The uppermost carbonate unit, the Gillespie Lake Group, has a cumulative thickness of nearly 4.6 kilometres indicating a long period of gradual subsidence starved of detritus. Possible tectonic settings were a long-lived intracratonic basin or a passive continental margin (Thorkelson et al., 2005; Cook and Erdmer, 2005). The Wernecke Supergroup was uplifted and deformed during the Racklan Orogeny (Gabrielse, 1967) in Yukon and its correlative, the Forward Orogeny in the Northwest Territories (Cook and MacLean, 1995; MacLean and Cook, 2004). This event may have been coincident with the emplacement of the 1.71 Ga Bonnet Plume intrusions (Thorkelson et al., 2001), or was as late as 1.60 Ga (Thorkelson et al., 2005). This deformation may represent the far-field effects of the Yavapai and Mazatal orogenies in southern Laurentia or a more proximal collision with Australia (Thorkelson et al., 2005).

Mesoproterozoic

After the Racklan Orogeny, extension and hydrothermal alteration at 1.60 Ga formed the Wernecke Breccias in northern Yukon and similar breccias in the Richardson Mountains of the Northwest Territories (Hunt et al., 2005). A subsequent quiescent period was interrupted at 1.38 Ga by extension and rifting recorded by mafic volcanic rocks of the Hart River Group and siliciclastic strata of the Pinguicula Group in Yukon. Either the Dismal Lakes Group (still Sequence A) or parts of the lower Shaler Group (Sequence B) may be correlated with this depositional phase, in the

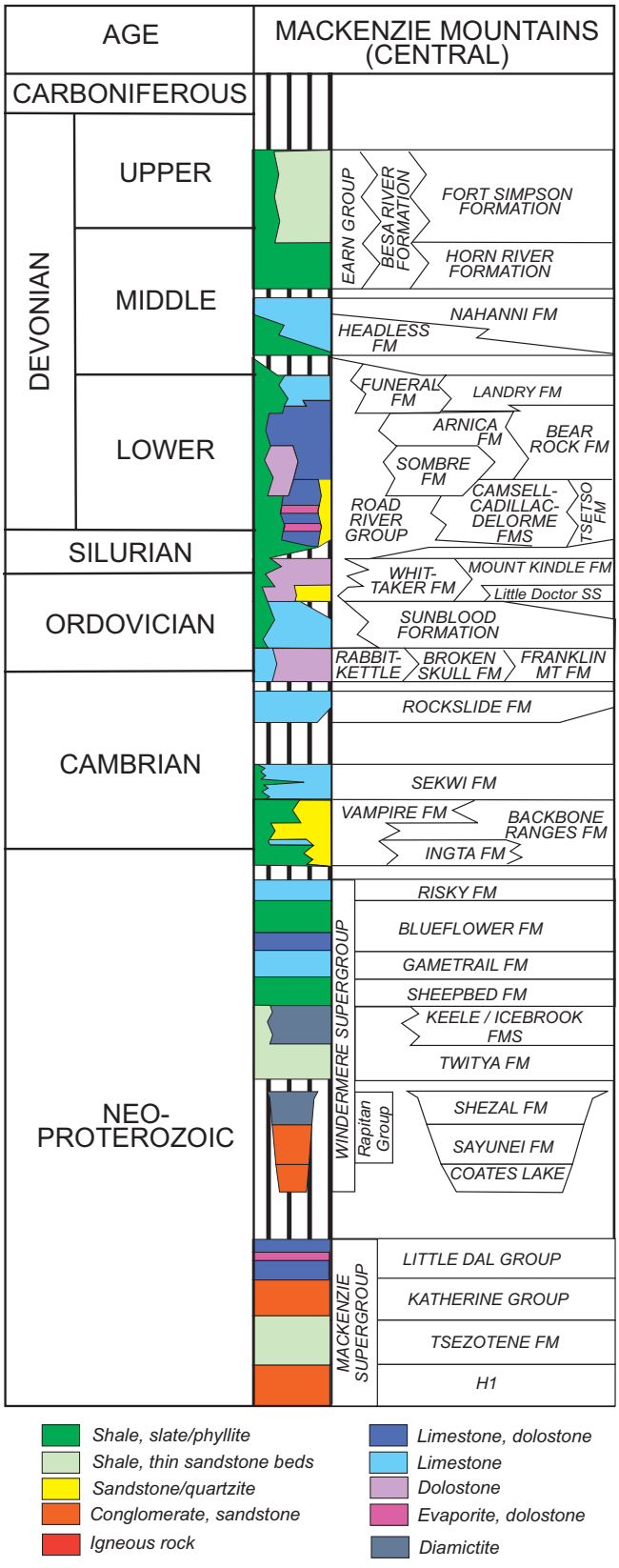


Figure 4. Simplified stratigraphic column from the Neoproterozoic to the Upper Devonian in the Nahanni region (From Dewing et al., 2006).

Northwest Territories (Cook and MacLean, 1995; Rainbird et al., 1997). A 100 Ma period of stability was punctuated in northwestern Laurentia by contemporaneous extrusion of the Coppermine River Group flood basalts and intrusion of the major Mackenzie dyke swarm that radiated across much of western North America from the Muskox Intrusion at ca. 1272 Ma (Rainbird et al., 1997; Buchan and Ernst, 2004). A mantle plume may have fed the major Mackenzie igneous event that marks the end of Sequence A.

Neoproterozoic

Extensional tectonics resumed in the Neoproterozoic as early as 1 Ga with deposition of Mackenzie Mountains Supergroup (Fig. 4) and the correlative Shaler Supergroup (all Sequence B of Young et al., 1979) on the stable western margin of Laurentia while mountains rising in the Grenville Orogen along eastern Laurentia at ca 1.10 Ga fed big rivers that flowed across the craton toward the northwest (Rainbird et al., 1992) (Fig. 4). Deposition of intercalated shallow marine siliciclastic and stromatolitic carbonate strata continued on the northwest margin of Laurentia, past 0.78 Ga when it was punctuated by a minor mafic volcanic event in Mackenzie Mountains (Jefferson and Parrish, 1989) to about 0.723 to 0.718 Ga (Heaman et al., 1992) when it was terminated by eruption of the Natkusiak basalt and intrusion of major sills and dykes of the continent-scale Franklin magmatic event.

Correlative lithological units in stratigraphic successions similar to Sequence B have been identified throughout northern Canada and Alaska, as well as Siberia and Australia. These separate localities have been hypothesized to have been part of Kanatia supercontinent (Young, 1995; Sears and Price, 2000). Correlations are based a consistent order of key marker units, and transitions in the stable platformal successions. A lower marine clastic assemblage was succeeded by a platformal carbonate assemblage that was followed by a marine delta to braided fluvial clastic assemblage overlain by an upper carbonate platform assemblage. Distinctive marker units include an orange-weathering stromatolite biostrome that has been correlated from the upper Katherine Group in Mackenzie Mountains to the Aok Formation at the top of the Rae Group in the Amundsen Basin (Jefferson and Young, 1988) and a thick gypsum/anhydrite formation that separates major carbonate units of the Little Dal Group (Narbonne and Aitken, 1995) and correlates with the Minto Inlet Formation on Victoria Island (Young et al., 1979). Further evidence for the supercontinent assemblage include correlations determined by sequence stratigraphy, biostratigraphy, geochemistry and geochronology, especially that of detrital zircons (Narbonne and Aitken, 1995; Rainbird et al., 1996, 1997). The entire Sequence B has been interpreted as a series of continent-scale transgression-regression cycles on a second-order global scale ending with the deposition of rift-related basalts (Rainbird et al., 1996).

Deposition of the Mackenzie Mountains Supergroup was locally interrupted by the Corn Creek Orogeny, a tectonic event, which may have been restricted to the Wernecke Mountains region (Thorkelson et al., 2005). Later localized tectonism and rifting during the Hayhook Event after ca. 780 Ma (Jefferson and Parish, 1989) may have been responsible for the deposition of the rift-hosted and fault-bounded Coates Lake Group in the Mackenzie Mountains (Fig. 5). The stratigraphic position of the Coates Lake Group is contentious due to unconformable contacts with both the underlying Mackenzie Mountains Supergroup and the overlying Windermere Supergroup and the presence of sabkha dolostone, red beds and evaporites like those of the older Gypsum Formation. The Coates Lake Group consists of three formations preserved in a series of subbasins with copper sulphide deposits stratabound between the upper two formations (Chartrand et al., 1989; Jefferson and Parish, 1989). The basal Thundercloud Formation comprises sabkha dolostone with minor quartzarenite, overlain by bedded sulphate evaporites. This assemblage resembles the Killian Formation on Victoria Island that is near the top of the Shaler Supergroup, overlying the platformal Wynniatt Formation that has been correlated with the Upper Carbonate Formation of the Little Dal Group (Jefferson and Parrish, 1989). The Thundercloud Formation is gradationally overlain by the Redstone River Formation: thick alluvial braid plain red mudstone with abundant desiccation cracks that is laterally equivalent to thin locally derived basin-margin conglomerate. At the transition between the Redstone River Formation and overlying Coppercap Formation at Coates Lake, a series of up to seven grey cryptalgal dolostone beds, discontinuous gypsum beds and tan dolomitic mudstone units are interbedded with red mudstone. The lowest three of up to seven carbonate beds contain copper sulphide minerals grading up to 2% Cu. The upper carbonate beds contain dominantly pyrite. The remainder of the Coppercap Formation is carbonaceous calcareous shale grading upward to allodapic limestone in two shallowing- and coarsening-up sequences capped by local stromatolite biotherms. The copper-rich Coates Lake Group has been considered to be a localized basal portion of the Windermere Supergroup (Eisbacher, 1981; Aitken, 1991; Narbonne and Aitken, 1995; James et al., 2001) even though its bedded evaporites and copper metallogeny are more similar to underlying units in Sequence B (Jefferson and Parrish, 1989).

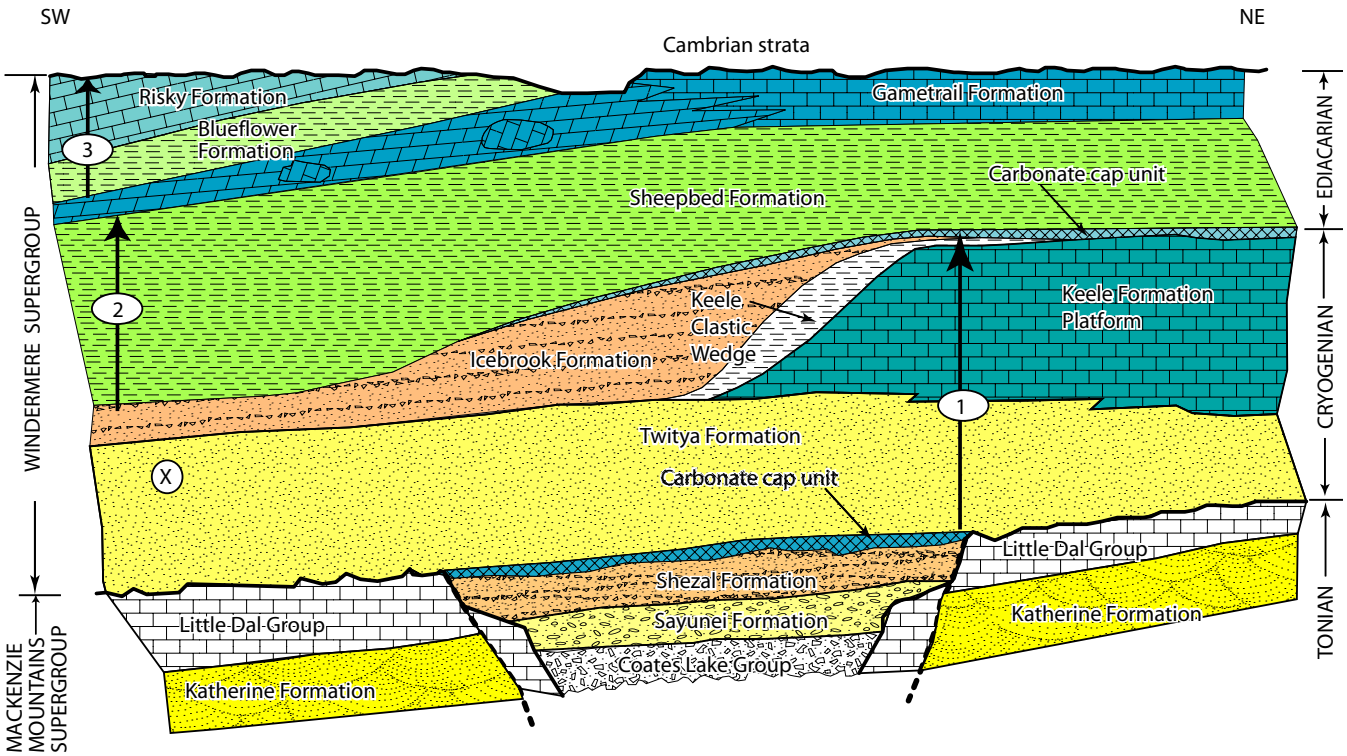


Figure 5. Schematic cross-section of the Mackenzie and Windermere supergroups showing the relationships of their components in the Mackenzie and Selwyn mountains. The numbers refer to individual grand cycles and the circled 'X' in the Twitya Formation indicates the stratigraphic position of the lowest Ediacaran-type soft-bodied animal fossils (from James et al., 2001).

More typical deposits of the Windermere Supergroup are diamictite, rhythmite and iron formation of the Rapitan Group that unconformably overlies the incipient rift-hosted Coates Lake Group. Fault tectonics are much more significant than for underlying units - the basal unconformity of the Rapitan Group cuts down to lower parts of the Little Dal Group and includes glaciogenic strata correlated with the Sturtian glaciation of Australia (ca. 730 Ma, Young, 1992, 2002). The Rapitan Group is covered by a thin-bedded limestone cap unit. Clast compositions in the diamictic layers are largely comparable to local underlying strata but a small number of "Stranger Stones" of more distal origins have been identified. A leucogranite dropstone with a zircon U-Pb age of 755 ± 18 Ma provides a maximum age of deposition for the Rapitan Group (Ross and Villeneuve, 1996). Glacial marine deposits have been identified in the Proterozoic stratigraphy along the length of the North American Cordillera and, together with iron formation, have been correlated with similar sequences in Australia (Sturtian), India and Antarctica (Bell and Jefferson, 1987; Young, 1992, 2002; Halverson et al., 2005).

Overlying the rift-related, Sturtian glaciogenic strata are passive-margin deposits that have been grouped into kilometre-thick, upward shoaling, shale to carbonate transitional sequences, termed "grand cycles" by Aitken (1978) (Fig. 5). These sequences are interpreted as a series of stacked clinoforms (MacNaughton et al., 2000). The cyclic clinoforms represent a series of prograding shelf margins, starting with deep-water turbiditic siliciclastic or carbonate-dominated mudstone with isolated carbonate clasts. The mudstone grades upward into shallow-water carbonate deposits that are capped by grainstone, stromatolites, and cryptalgeal laminite (Narbonne and Aitken, 1995).The first such grand cycle begins with approximately 900 m of Twitya Formation clastic rocks overlain by approximately 600 m of Keele Formation carbonate, succeeded by a series of shallow-water siliciclastic clastic units and the Icebrook Formation, a second glaciogenic unit correlated with the Marinoan glacial event in Australia (James et al., 2001, 2005). The Twitya-Keele sequence records mixed siliciclastic-carbonate deposition with stromatolites and hummocky cross-stratification on a storm-dominated shelf, shallower than fair-weather wave base. The overlying Icebrook Formation diamictite sheets contain limestone clasts almost entirely derived from the Keele Formation. The Icebrook Formation is 'capped' by a thin regionally extensive "Teepee Dolostone" (Eisbacher, 1981) that has been subdivided into the Ravensthroat and Hayhook formations (James et al., 2001). The Ravensthroat Formation and the upper layers of the Twitya Formation are distinguished as carbonate rocks formed in a shallow-marine cold-water environment, similar to the carbonate cap on the older Rapitan Group. Distinctive features of the upper Twitya and the

Ravensthroat formations include glendonites with stellate or radiating pseudomorphs of ferroan dolomite after ikaite ($CaCO_3 \cdot 6H_2O$) (James et al., 2005).

The siliciclastic Twitya Formation is noteworthy for its fossil record - circular annuli and disc impressions at the base of turbiditic beds (Hofman et al., 1990). These Ediacaran–type fossils identified below the glacial strata of the Marinoan glaciation may represent the oldest known Ediacaran fauna, and some of the earliest evidence of complex animal life on earth (James et al., 2001).

As with the Sturtian Rapitan Group, comparisons of the Icebrook Formation with other Marinoan-age strata have indicated a globally distributed glaciogenic sequence (Young, 1995. 2002; Knoll et al., 2000; Halverson et al., 2005). This records a second period during which much of the Earth was covered by ice sheets, a hypothesis supported by carbon isotope curves, paleomagnetic evidence and marked reductions in biodiversity (Hoffman et al., 1998; Knoll et al., 2004). These diversity changes in the faunal record of fossils and fossil traces are well documented in the Windermere Supergroup (Baudet et al., 1989; Narbonne et al., 1994; Narbonne and Aitken, 1995).

The fragmentation of Nuna into Laurentia and the Australian, Indian, Antarctican and Siberian blocks has been suggested as the driver for development of widespread global ice sheets ("Snowball Earth"; Young, 1995; Hoffman et al., 1998, Sears and Price, 2000). Fragmentation is supported by bimodal magmatism with radiometric ages in the range of 720 to 780 Ma associated with local coarse clastic rocks and thickened stratigraphy along the interpreted rift margins of Nuna. These intrusive and volcanic rocks have been interpreted to represent the onset of one rifting event, but the spread of younger ages of similar rocks may be evidence that the rifting was a complex series of events (Colpron et al, 2002; Pyle and Barnes, 2003; Pigage and Mortensen, 2004).

Deeper water shale of the Sheepbed Formation overlies the Icebrook and Hayhook Formation and constitutes the basal unit of the second of three Grand Cycles in the Windermere Supergroup of Mackenzie Mountains. The carbonate cap of the third cycle is the Risky Formation, a distinctive marker correlated with the middle member of the Backbone Ranges Formation and the top of the Yusezyu Formation. Karst breccia near the top of the Risky Formation is interpreted as evidence for uplift and unconformity just prior to the Cambrian (Narbonne et al., 1994) - the end of Windermere Supergroup deposition and the close of the Proterozoic.

Neoproterozoic to Paleozoic Transition

The sedimentary record in the Mackenzie Mountains, from the initial rift sequence of the Coates Lake Group, through the fault-associated glacio-tectonic deposits of the Rapitan Group, to the Grand Cycles of the latest Neoproterozic and the Precambrian-Cambrian transition, is one of supercontinent breakup and gently subsiding continental shelf during three global glaciations. The shape of this rifted continental margin (the Cordilleran Miogeocline of Cecile et al., 1997) and associated controlling faults were major controls on sedimentation and ore deposits in the Nahanni Region from the Neoproterozoic to at least Early Devonian time (Fig. 6). The sedimentary facies deposited in the miogeocline form two contrasting belts roughly parallel to the continental margin. The northeastern belt, referred to as the inner miogeocline, is dominated by shallow water siliciclastic carbonate platform deposits (Mackenzie Platform of Cecile et al., 1997). The southwestern belt preserves deeper water off-shelf facies, or outer miogeocline, and is termed the Selwyn Basin. The transitional boundary between the Selwyn Basin and Mackenzie Platform marks the shelf edge or hinge line (Fig. 3C).

A thick succession of strata accumulated in the Cordilleran Miogeocline from the Neoproterozoic to the Devonian (Fig. 4) while progradation of the shoreline was balanced by subsidence of the continental margin due to thermal relaxation and sediment loading. The gradual sinking of the crust was however, punctuated by periods of extension, local uplifts, volcanism and tectonic instability. Several major unconformities and breaks in the sedimentary succession record periodic thermal uplift during the Neoproterozoic to Cambrian transition. In places such as the Redstone and Mackenzie Arches, erosion removed older strata and formed widespread unconformities. Uplifts in the northern Cordillera appear to have coincided with rifting in the southern Cordillera where uplift was also followed by thermal subsidence in the Early Cambrian (MacNaughton et al., 2000).

Variations in the balance between uplift and crustal subsidence resulted in changes to the position of the shelf edge and interfingering of shelf and offshelf facies. Local extensional tectonism developed fault-bounded basins; some faults were conduits for mafic sills, dykes and isolated volcanic units (Goodfellow et al., 1995). Important northeast-trending structural elements such as the Fort Norman Line, Leith Ridge Fault, Beaver River Structure, and Liard Line obliquely transect crystalline basement structural-metamorphic belts (Fig. 6) (e.g. Aitken and Pugh, 1984; Cecile et al., 1997; Morrow and Miles, 2000). These lines also delineate distinct regions of Paleozoic deposition. For example, a wide area north of the Liard line is the outer Selwyn Basin, whereas to the south is a zone of high crustal attenuation and sediment accumulation known as the Liard Basin. The Liard Line offsets aeromag-

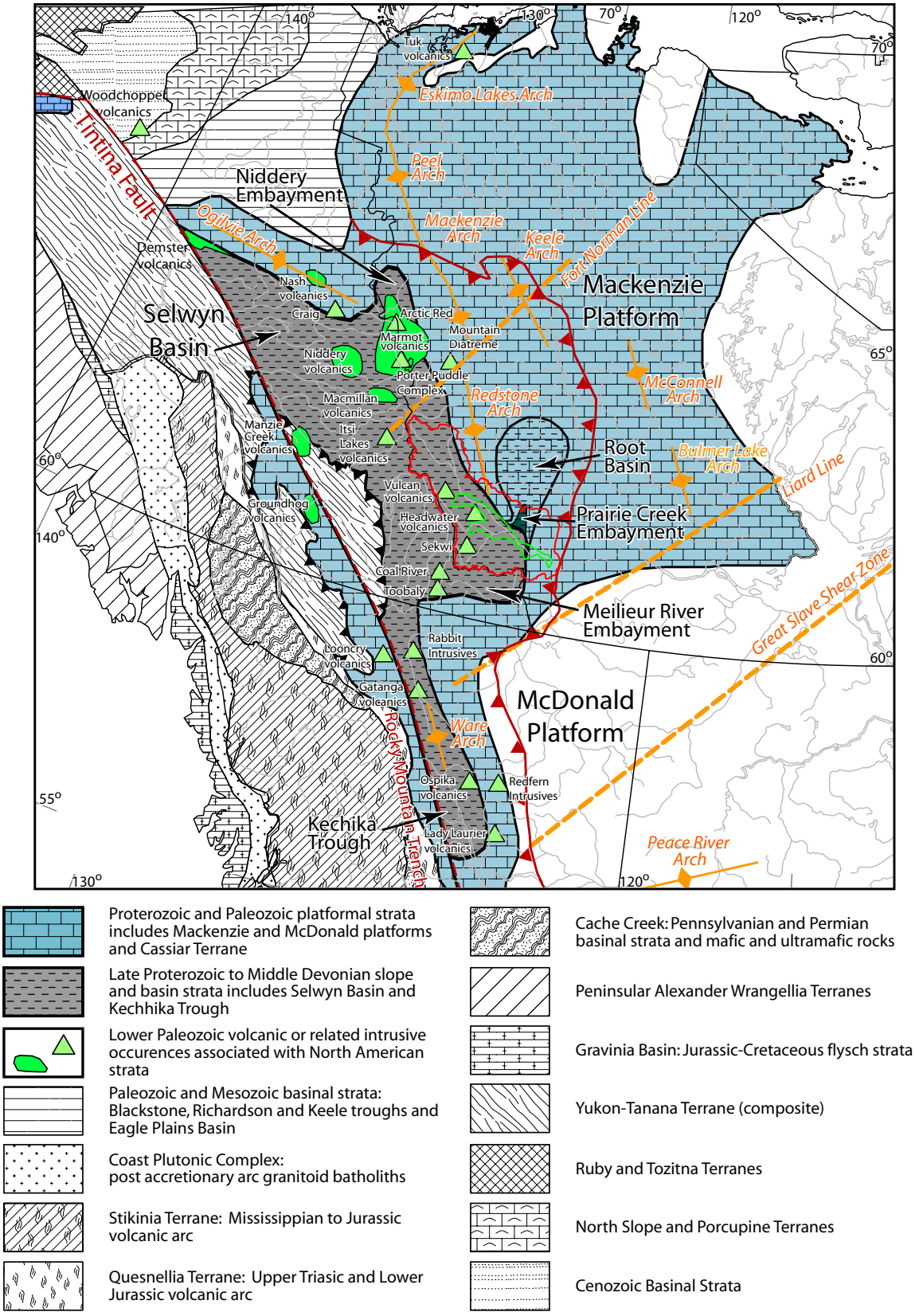


Figure 6. Distribution of the Mackenzie and MacDonald platforms (carbonate shelves) and the Selwyn Basin and embayments (deep-water shale and turbidite) (after Morrow and Cook, 1987; Gabrielse and Yorath, 1992; Cecile et al., 1997; Cecile, 2000; and Mair et al., 2006). Green symbols and green-shaded areas are lower Paleozoic alkalic and potassic volcanic rocks (after Goodfellow et al., 1995). Orange lines show major structural paleographic features, such as arches and hypothetical transform faults (after Cecile et al., 1997). Red lines are Cretaceous and younger structural elements (line bordered with triangles locates the edge of Cordilleran deformation) and the Nahanni MERA 2 study area. Green line outlines the Nahanni National Park Reserve.

netic domains, coincides with thickness and facies changes in the Mackenzie Mountains Supergroup, and is interpreted as a transform fault offsetting the passive margin during the Neoproterozoic. It may have been reactivated by Ordovician extension that deepened the depression and localized mafic volcanic centres. Profound changes in the basement across the Liard Line have been interpreted to represent a fault zone across which the rifting of the ancient continental margin underwent a reversal of crustal asymmetry (Cecile et al., 1997).

The Leith Ridge Fault defines the linear edge of the Prairie Creek embayment (Morrow and Cook, 1987), the edge of the Sombre Formation and the Caribou River, and is exposed far to the northeast in the Leith Ridge, an outlier of the craton (Kerans et al., 1981).

The hypothetical Beaver River structure extends through the southern end of the Nahanni thrust and may have formed part of the north side of the Liard Basin. Offsets on these various structural elements appear to have developed repeatedly over time since the Proterozoic. Dextral displacement of 10 to 20 km during the Laramide Orogeny has been suggested along parts of this zone, and stratigraphic differences across it indicate earlier movements possibly coincident with the Jura-Cretaceous Columbian Orogeny (Morrow and Miles, 2000). Local and intermittent extension along these structural elements may have resulted in the development of secondary rift basins such as the Misty Creek Embayment, the Richardson and Blackstone Troughs, the Root River Basin and the Prairie Creek and Meilleur River embayments. In addition to the basinal depocentres, the region has distinct northwest-trending arches (Mackenzie and Redstone) that were tectonically active during sedimentation, as recorded by thinner stratigraphy and irregular changes in the position of facies boundaries and was reactivated as Laramide structural culminations (Morrow and Cook, 1987; Gordey and Anderson, 1993; Cecile et al., 1997; Héon, 2003).

Ediacaran to Middle Devonian (Figs. 4, 7)

In order to clarify the complex distribution of Ediacaran to Middle Devonian strata, the units are described as three assemblages that reflect, from northeast to southwest, the shelf facies of the Mackenzie Platform, a central belt composed of the interstratified margins of the Mackenzie Platform shelf facies and a belt of offshelf (western miogeocline) facies of the Selwyn Basin (Gordey and Anderson, 1993).

The Mackenzie Platform consists mainly of dolostone with some limestone and lesser amounts of quartz sandstone and shale. These shallow-marine formations include the Ediacaran to Middle Cambrian Ingta, Backbone Ranges, Sekwi and Avalanche; the Cambro-Ordovician Haywire and Broken Skull; the Ordovician Sunblood; the Siluro-Devonian Delorme, Camsell, Sombre and Arnica; and the Devonian Landry, Headless and Nahanni.

The Selwyn Basin is represented by mainly calcareous shale with subordinate shaly limestone chert and siltstone. There is little evidence of coarse terrigenous input except for an orange-brown-weathering bioturbated Silurian siltstone to fine sandstone. Deeper water strata include the Ediacaran Yusezyu and Narchilla formations, the Lower Cambrian Gull Lake Formation, part of the Cambro-Ordovician Rabbitkettle Formation, the Ordovician Duo Lake and Steel formations and the Siluro-Devonian Sapper, Grizzly Bear, Natla and Funeral formations (Gordey and Anderson, 1993).

Between the Mackenzie Platform and Selwyn Basin, the transitional zone of intercalated basinal, platformal and slope facies is thickest and most laterally extensive in the Liard Basin, including the Meilleur River and Prairie Creek embayments. On the platform adjacent to these embayments, an unusually thick package of Silurian to Devonian strata is also preserved. The embayments and thicker platform successions reflect rapid subsidence controlled in part by local rifting that extended the Selwyn Basin into the platform area (Morrow and Cook, 1987).

Ephemerally uplifted regions on the flanks of rifts such as the Redstone Arch fostered deposition of the shallow-water Sunblood carbonate platform. The Sunblood Formation is overlain by the Mount Kindle - Root River assemblage, including the Esbataottine and Whittaker formations and Road River Group. The shelf edge shifted to the east and submergence of the Redstone Arch was accompanied by deepening of the Meilleur River Embayment and the Root River Basin. As the basins filled, the deep-water facies assemblage was succeeded by the Prairie Creek Assemblage, restricted to a local depression that was filled by the clastic Cadillac Formation and detrital components of the Sombre and Arnica formations. Gradual filling of the tectonic basins was followed by deposition of the Funeral-Headless assemblage marking the return to a simpler shelf to basin transition by the Middle Devonian (Morrow and Cook, 1987).

Ediacaran to Middle Devonian of the Mackenzie Platform (Figs. 4, 7)

The shelf facies overlying the Ediacaran Risky Formation is best exposed northeast of the Broken Skull River and lies unconformably on the Windermere Supergroup. The eastern facies of these Ediacaran to Placentian strata is light coloured quartzite with abundant crossbeds, localized channels, and sparse trace fossils. This is overlain by and grades laterally into the

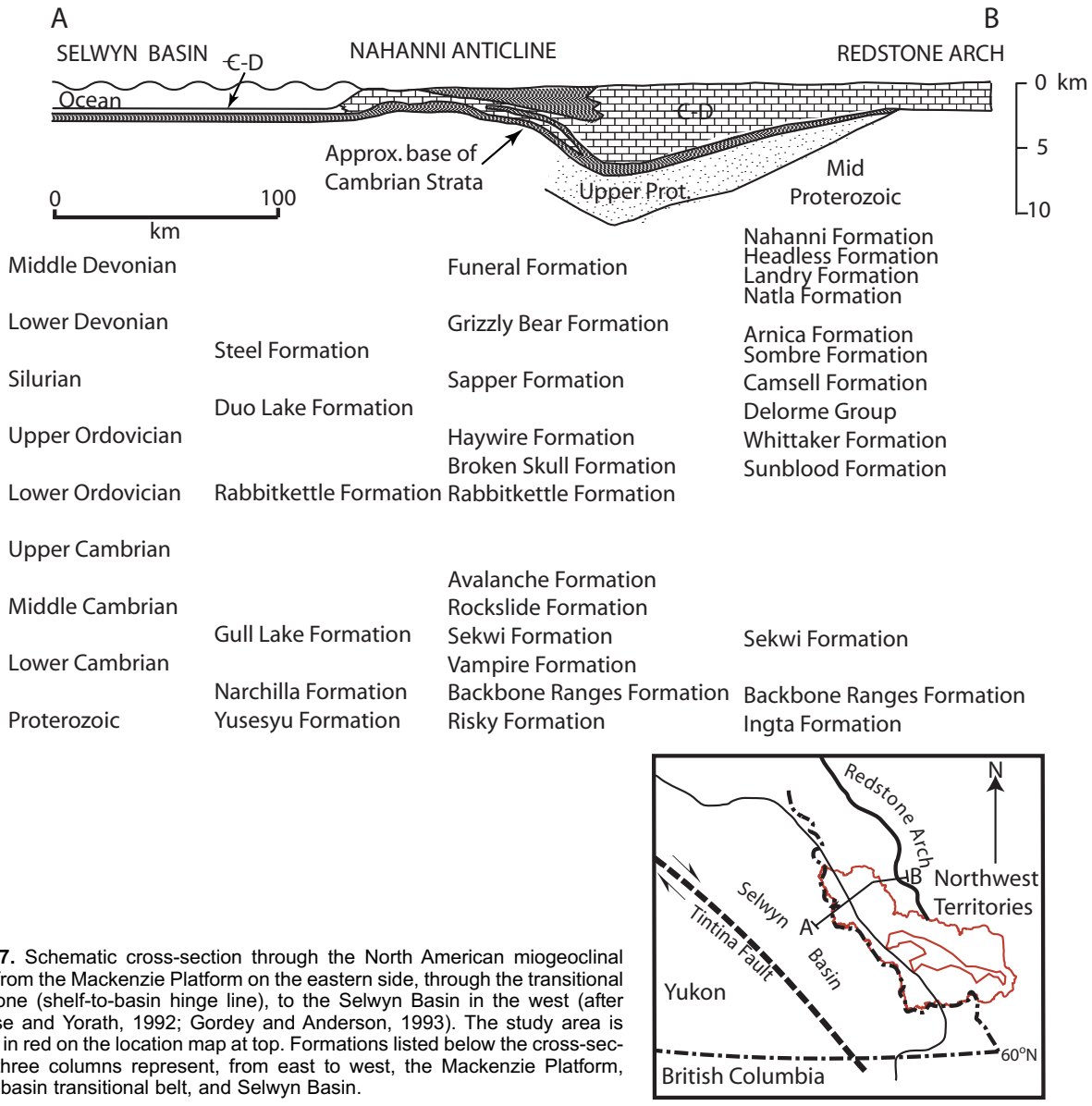


Figure 7. Schematic cross-section through the North American miogeoclinal margin from the Mackenzie Platform on the eastern side, through the transitional slope zone (shelf-to-basin hinge line), to the Selwyn Basin in the west (after Gabrielse and Yorath, 1992; Gordey and Anderson, 1993). The study area is outlined in red on the location map at top. Formations listed below the cross-section in three columns represent, from east to west, the Mackenzie Platform, shelf-to-basin transitional belt, and Selwyn Basin.

non-marine to marine quartz sandstone and siltstone of the Backbone Ranges Formation, and dark grey siltstone and shale interbedded with light brown, very fine-grained quartzite of the Vampire Formation. The Backbone Ranges Formation was deposited in a complex array of fluvial braid plain, braid-delta, nearshore, and shallow shelf environments. The braided stream deltas emptied onto a northwest-trending basin margin. The finer grained Vampire Formation represents a shoreface to open shelf setting in a delta front. Rapid deposition is supported by abundant slump structures (MacNaughton et al., 1997a,b). The Vampire Formation is transitional westward into the Narchilla Formation of the Hyland Group (Gordey and Anderson, 1993). The Narchilla Formation consists of apple-green shale and siltstone with abundant planar laminated bedding. Trace fossils have only been reported from the base and the top of the unit. The Ingta Formation, mapped more towards the platformal side of the region, may be an eastward extension of the Narchilla Formation. The fine-grained siliciclastic Ingta Formation records shallow- water shelf, nearshore, and fluvio-deltaic deposition (Gordey and Anderson, 1993). Although volcanic rocks of this age have not been identified in the Nahanni region, similar siliciclastic strata in the rift bounded Misty Creek Embayment enclose mafic tuff and flows of the Marmot Formation (Cecile, 1997).

Siltstone of the Vampire Formation grades up-section into the carbonate-dominated Sekwi Formation, an important regional marker. The first definite Cambrian trace fossils, Rusophycus Sp. were identified in the middle of the Vampire Formation by Fritz et al. (1983) and Fallotaspis Zone trilobites in the upper layers (Fritz, 1980). Hard-shell fossils, such as trilobites of the Nevadella and Bonnia-Olenellus zones and

Archeocyathids, are more common in the transition to the carbonate Sekwi Formation (Fritz, 1972; Narbonne and Aitken, 1995). However, the fossil record may reflect the change in the depositional environment more than the ages of the strata. Preservation of trace fossils is preferential in fine-grained siliciclastic strata whereas shelly fossils survive better in carbonate-rich environments (Fritz, 1980). In the southwestern corner of the study area the Sekwi Formation also contains a lens of interstratified pillow and massive basalt flows, tuffaceous breccia and local coarse-grained gabbro sills.

Dolostone of the Avalanche and Franklin Mountain formations overlies the Sekwi Formation. The Franklin Mountain Formation is dominant on the eastern side of the Nahanni region whereas the contemporary Avalanche Formation is best exposed in the central Nahanni area. The Avalanche Formation is also the lateral equivalent of the Rockslide Formation of the central Nahanni Region, with shallower water facies such as oncolites and quartz sandstone beds in grey to white dolostone, suggestive of a subtidal or peritidal environment. In contrast, the Rockslide Formation was deposited in relatively deep water with slump structures indicating slope failures. Both contain abundant Middle Cambrian trilobites (Fritz, 1972; Gordey and Anderson, 1993; Morrow, 1999).

Repeated transgressive-regressive cycles have been identified in the Mackenzie Platform. In the Late Cambrian a widespread transgression is represented by the Franklin Mountain Formation, mostly fine-grained microcrystalline dolomite in four members, some upper portions rhythmically laminated with pisolitic lenses. The Franklin Mountain Formation can be divided into four members. The lowest member is olive grey argillaceous and shaly limestone with local halite casts in the shale, and dolostone including pale yellow to orange, finely crystalline, conglomeratic and stromatolitic. The second and thicker member is well bedded silty dolostone. The third member is thick-bedded coarsely crystalline dolostone with drusy quartz and bedded chert. The fourth member, a porous limestone, is absent in many sections due bevelling by the unconformity beneath the Mount Kindle Formation. The paucity of fossils and the nature of the strata suggest a shallow, peritidal depositional setting (Morrow, 1999). Conodont fauna indicate Late Cambrian to Middle Ordovician deposition (Barnes et al., 1991).

The Franklin Mountain Formation grades westward into the Broken Skull Formation and the basinal Rabbitkettle Formation. The Broken Skull Formation is buff-, orange-, yellow-, and brown-weathering sandy dolostone and limestone with an upper member of grey-weathering dolostone to limestone.

The Franklin Mountain Formation is also laterally equivalent to the Sunblood Formation in the transitional shelf-basin sequence and both units are truncated by an unconformity that is overlain by the Whittaker Formation (Morrow and Cook, 1987).

The Sunblood Formation is a distinctive bright reddish-orange colour and forms ridges at Sunblood Mountain, the backdrop to the popular access point at Virginia Falls. The banded grey- to yellowish weathering dolostone, grey mottled limestone, greyish to orange-weathering sandstone and siliceous dolostone were deposited in shallow water with some intertidal beds. Fossil remains of trilobites, brachiopods and conodonts indicate a Middle Ordovician age (Barnes et al., 1991). The distribution of the Sunblood Formation appears to be centered near the trace of the Redstone Arch suggesting that this structure, which has its greatest development during the Devonian, may have been a shoal as early as the Ordovician. In the Glacier Lake area, the Sunblood Formation also contains a prominent but discontinuous series of basaltic to andesitic volcanic flows up to 50 m thick (Gordey and Anderson, 1993). A regionally extensive unconformity separates the Sunblood Formation from the overlying Whittaker Formation. There is a lateral facies change to the deeper water Rabbitkettle Formation to the west of the Nahanni River where the Sunblood Formation is unconformably overlain by the Road River Group (Mako and Shanks, 1984).

The initial Paleozoic depositional cycle was terminated by regression and erosion ending by the late Middle Ordovician. The second depositional cycle recorded transgression from the Late Ordovician to Early Silurian, with deposition of dark grey to brownish grey, thin to thickly bedded, fine to medium dolostone with local coral reefs of the Mount Kindle Formation. Basinal sections include a lower member of dark grey chert and reefoid dolostone. On the southern Mackenzie Platform similar rocks are called the Whittaker Formation (Morrow and Cook, 1987).

The Esbataottine Formation was defined by Ludvigson (1975) as thinly bedded argillaceous limestone conformably overlying the Sunblood Formation at Sunblood Mountain. However, Morrow and Cook (1987) suggest that this name be discontinued because these beds are a continuation of the lowest member of the Whittaker Formation.

The Whittaker Formation is an important stratigraphic unit in the Prairie Creek Embayment but it also is widespread in the Mackenzie Platform (Douglas and Norris, 1961). It correlates with the Mount Kindle Formation in the northern Mackenzie Mountains, the Haywire Formation in the Central Nahanni region, and the Sapper and Road River formations in the Selwyn Basin (Gordey and Anderson, 1993). Three divisions are regionally distributed: a lower unit of dark grey silty and sandy limestone, a middle unit of white to

dark grey dolomitic sandstone to quartzarenite sandstone and an upper unit of dark grey cherty dolostone. Detailed mapping by geologists of San Andreas Resources Corporation near the Prairie Creek mine, in the Prairie Creek Embayment, has identified seven distinct subunits in the OSw3 lithofacies (Taylor, 1995; see Table 2 of Paradis, 2007). Conodont fauna suggest Middle Ordovician deposition (Barnes et al. 1991).

Over much of the study region, the Whittaker Formation is overlain by a thin extension of the Road River Group, a major component of the Selwyn Basin. Renewed uplift restored shallower water conditions across the Mackenzie Platform and led to deposition of the Delorme Group, mainly distinctive orange-weathering, finely crystalline dolostone and limestone. In the Prairie Creek region, the group has distinctly greater siliciclastic content, comprising the Root River Formation (light grey dolomite overlain by orange, dolomitic sandstone), and the Vera Formation (green and orange striped argillaceous limestone). The low-diversity biostratigraphic assemblage dominated by the deeper water, thin-shelled pentamerid species changes gradually to large-shelled pentamerids and spiriferids indicating shallower water (Jin and Chatterton, 1997). Delorme Group strata are correlative to the Steel Formation of the Road River Group in the Selwyn Basin.

The Camsell Formation, grey to black, fine-grained limestone to dolostone, conformably overlies the Delorme Group. Locally, the shallow-water carbonate is interbedded with the argillaceous Vera Formation. Core samples from a well south of the Nahanni region indicate that the Camsell Formation also contains anhydrite siltstone beds that are consistent with a shallow water evaporitic environment but rarely exposed. The Camsell Formation is correlative with the Sapper Formation in the central Nahanni region (Morrow and Cook, 1987).

The Middle Devonian Sombre Formation is thick-bedded dolostone conformably overlying the Camsell Formation. Three members include a fine- to medium-grained crystalline dolostone, a fetid bioclastic crystalline dolostone and an amphora-rich, black dolostone. These members are correlative with the Grizzly Bear and Sapper formations and the Portrait Lake Formation of the Earn Group in the deeper water portions of the Selwyn Basin (Gordey and Anderson, 1993).

Cherty black dolostone of the Arnica Formation conformably overlies the Sombre Formation and is more extensive than the underlying two carbonate units. The paucity of fossils and featureless nature of the Arnica Formation has been attributed to peritidal deposition. Conodonts define a late Early Devonian age. Parts of the Camsell and Sombre formations have been mapped as Arnica Formation. As such, correlative units in the central Nahanni region include the Grizzly Bear and Sapper formations (Morrow and Cook, 1987).

The platformal Funeral, Landry, Headless and Nahanni formations marked the filling of the Prairie Creek Embayment during the Middle Devonian, but continuing subsidence re-established the Root River Basin. Massive erosion-resistant limestone of the Landry Formation forms a basin-rimming marginal facies deposited concurrently and interbedded with the more argillaceous limestone of the Funeral Formation in the central portion of the basin. The overlying recessive Headless Formation consists of argillaceous subtidal lime wackestone with abundant corals, echinoderm debris, bryozoa, brachiopods, and trilobites compatible with an open marine shelf setting. The transgression is correlative with the Horn River and Hare Indian shale formations to the east and north of the study area.

The Headless Formation is gradationally overlain by the Nahanni Formation, recording upward shoaling and westward expansion of an open marine carbonate shelf. The cliff-forming Nahanni Formation is thick to massive bedded blue-grey lime wackestone to packstone. This is the youngest preserved unit of the Mackenzie Platform sequence and appears to be equivalent to the Hume Formation in the northern Mackenzie Mountains (Gordey and Anderson, 1993). At the southern edges of the Mackenzie Platform, the Nahanni Formation is the reservoir rock for the Beaver River, Pointed Mountain, and Kotaneelee gas fields (Osadetz et al., 2003).

Ediacaran to Middle Devonian of the Shelf to Basin Transition (Figs. 4, 7)

South of the Broken Skull River, Gordey and Anderson (1993) defined a transitional succession marking the boundary between the Mackenzie Platform and the Selwyn Basin. From the Ediacaran to Middle Devonian, intercalated shelf and off-shelf strata are variably dominated by either end member. As with the platformal sequence, Backbone Ranges Formation sandstone and deep water Vampire Formation siltstone grade conformably into deep water carbonate of the Sekwi Formation and underlie the interstratified zone.

The widespread Sekwi Formation averages 700 m in thickness and consists of lime mudstone and wacke in thinly bedded to nodular limestone, intercalated with thick bedded dolostone, limy siltstone and shale. Variegated siltstone and sandstone are included east of the main carbonate unit. This excellent nearshore to basin record for the Lower Cambrian was deposited along the northeastern platformal margin of the Selwyn Basin (Gordey and Anderson, 1993). Diachronously overlying the Sekwi Formation are black graptolitic shale and dark platy limestone of the Road River Group. On the eastern margin of the Selwyn Basin a sharp but conformable contact separates the Sekwi

Formation from deep-water limestone of the Rockslide Formation. The Sekwi Formation hosts a number of lead-zinc showings (Carrière and Sangster, 1999) and the Cantung tungsten deposit along the Flat River (Blusson, 1968).

The Gull Lake Formation is the coeval outer slope and basinal equivalent of the Sekwi Formation (Gordey and Anderson, 1993). The lower member is orange to rust brown, slightly limy slate, siltstone and very fine-grained sandstone. At the base a discontinuous layer of limestone conglomerate has a maximum thickness of several tens of metres. The upper member is grey-weathering limy mudstone. Archeocyathids, as in the Sekwi Formation, are found in conglomerate clasts. The contact with the underlying Narchilla Formation is abrupt but no significant hiatus is suspected (Gordey and Anderson, 1993). The total extent of the Gull Lake Formation is uncertain as a regional unconformity at the base of the Upper Cambrian Rabbitkettle Formation has removed it in many places.

In the Selwyn Basin, the Road River Group includes dark grey to black shale units of the Hess River, Steel and Duo Lake formations, and represents the Lower to Middle Cambrian (Gordey and Anderson, 1993; Cecile, 2000). The basinal deposits are separated from the platformal shelf deposits by platy dark limestone of the Rockslide Formation and dolomite of the Avalanche Formation. The Rockslide Formation contains dark grey, planar-laminated limestone with interbedded black shale and isolated, thin quartzite beds predominantly in its upper part. Penecontemporaneous breccias and slump structures suggest shelf slope deposition. The lateral shallow-water equivalent of the Rockslide Formation is the Avalanche Formation - buff-weathering, thin- to thick-bedded dolostone. The contact between the Rockslide and the Avalanche formations shifted to the west through time as demonstrated by changes in the thickness of the sections of the underlying Rockslide Formation. This transitional sequence has also been removed from many areas in the southern Selwyn Basin at the unconformity beneath the Rabbitkettle Formation (Gordey and Anderson, 1993).

The Upper Cambrian to Lower Ordovician Rabbitkettle Formation overlies the Lower Cambrian sequences over much of the Nahanni Region. Its distinctive nodular, wavy-banded limestone with abundant medium grey siltstone layers lacks black shale. The paucity of fossils and uniform character of the limestone indicate a deeper water depositional setting for this regional marker unit. Widely distributed throughout the northern Cordillera, it displays slightly different characteristics and thicknesses across the region. At the type section near the headwaters of the Rabbitkettle River the unit is over 1200 m thick but 200 km northwest in the Niddery Lake area, only 60 m are present (Cecile, 2000). Ripple and herring-bone cross lamination in basal members of the formation indicate initial shallow marine deposition, possibly intertidal, but the balance was deposited in deep water (Gordey and Anderson, 1993). Its age has been constrained by trilobites, graptolites and conodonts as Dresbachian (Late Cambrian) to early Tremadocian (Early Ordovician) (Orchard and McCracken, 1991; Pratt, 1992; Jackson and Norford, 2004). The Broken Skull Formation, a more fossiliferous shallow-water equivalent, is on the eastern margin of the Selwyn Basin. The Rabbitkettle Formation is also transitional into the Haywire Formation east of the Lened area (Jefferson et al., 2003) and the Sunblood Formation near Bologna Creek (Mako and Shanks, 1984).

The conformable and diachronous nature of the contact between the Rabbitkettle Formation and the overlying Duo Lake Formation of the Road River Group, and similarities with the Road River Group in the Richardson Trough region and the Misty Creek Embayment, north of the study area have prompted some authors to conclude that the Rabbitkettle Formation should be classified as part of the Road River Group (Cecile, 2000). This is supported by the biostratigraphy (Jackson and Norford, 2004). To the north and east of the Nahanni Region, the Rabbitkettle Formation interfingers with the Franklin Mountain Formation on the Mackenzie Platform. To the southeast of the Broken Skull River, the amount of shale and siltstone in the Rabbitkettle Formation increases and it is difficult to distinguish from shale units of the Road River Group, although its position above the pronounced unconformity is still recognizable. The slope and basinal limestone portions of the Rabbitkettle Formation are overlain by shale and chert of the Ordovician Duo Lake or Haywire formations.

The Late Cambrian to Early Ordovician Broken Skull Formation is white to dark grey-weathering, thick-bedded sandy dolostone and limestone, widely exposed in the northeastern portion of the Nahanni River area. Locally, the Broken Skull Formation overlies the Rabbitkettle Formation with a sharp but conformable contact. Oncolites and minor quartz sand indicate shallow water deposition in contrast to the deeper water environment of the Rabbitkettle Formation (Gordey and Anderson, 1983). The Broken Skull Formation is considered to correlate with the Sunblood Formation, but does not contain the thick black lower dolomite characteristic of the Sunblood in the Prairie Creek Embayment (Morrow and Cook, 1987).

The Haywire Formation comprises a lower tongue of sandy carbonate overlain by more dominant light grey medium to thick-bedded limestone. A small mem-

ber of interstratified amygdaloidal basaltic and volcaniclastic tuff is near the type section at Haywire Lake in the Central Nahanni region (Gordey and Anderson, 1993). The Haywire Formation overlies different units in various ways. In the type section it unconformably overlies the Avalanche Formation. Southwest of the South Nahanni River the Haywire Formation rests directly on the Vampire Formation. The Haywire Formation correlates with the Broken Skull, Rabbitkettle and Sunblood formations and possibly part of the Whittaker Formation, and may represent the outer shelf extension of these units. Conodont faunas suggest deposition during the Middle to Late Ordovician (Barnes et al., 1991).

Following deposition of the Rabbitkettle Formation and related units, regional crustal flexure combined with local rifting formed the semi-circular Meilleur River Embayment (Bassett and Stout, 1967), an eastward extension of the Selwyn Basin into the Mackenzie Platform in the central portion of the study area. Minor in the Early Ordovician, it expanded into the Middle Ordovician when it was partially replaced by platformal carbonate strata of the Sunblood Formation.

Overlying the Sunblood Formation, thinly bedded argillaceous and silty limestone (obsolete Esbataottine Formation) is basal Whittaker Formation (Morrow and Cook, 1987). A return to basinal settings during the Late Ordovician to Early Silurian filled the Meilleur and adjoining Prairie Creek embayments with thin-bedded shaly limestone and shale. In the Late Silurian, reactivation of rifting expanded the embayment eastward, with deposition of up to 700 m of carbonate-rich orange-weathering siltstone of the Cadillac Formation. To the northeast the broader Root River Basin formed at the same time and accumulated shale of the Root River Formation. The Meilleur Embayment and the Root River Basin deepened, with continued deposition of interfingered Whittaker Formation and Road River Group. Eventually the distinction between the sub-basins and the Selwyn Basin disappeared and the Road River Group was deposited across the entire depression, (Morrow and Cook, 1987).

Deposition of the Road River Group was interrupted by marked regression at the end of the early Late Silurian. Widespread sub-aerial exposure coincided with the deposition of the Cadillac Formation of the Delorme Formation carbonate mudstone and orange-weathering sandstone. Marked variations in total thickness throughout the miogeocline may have been influenced by the formation of fault scarps along the margins of the Root Basin and the Redstone Arch. Deposition of the Cadillac and Delorme formations continued though the period of regression concurrently with the Road River Group in the main Selwyn Basin. The shallow Root River Basin was filled by brightly coloured argillaceous to skeletal lime wackestone of the Vera Formation. Deposited below wave base, the fossil assemblage of brachiopods and trilobites suggests that much of the Root Basin area remained in the photic zone. Additional shallowing of sea level led to widespread deposition of yellow-weathering arenaceous dolostone of the Tsetso Formation. This Late Silurian regression resulted in sandy and mudcracked intertidal deposits on the shelf, but restricted circulation in the Root Basin caused accumulation of up to 1500 m of anhydrite and dolostone of the Camsell Formation (Morrow and Cook, 1987; Fritz et al., 1992).

Complexities of these transitional strata reflect variable paleotopography combined with changes in global sea level. The region was inundated in the middle Emsian, eliminating siliciclastic input with a shift from sandy orange-yellow-weathering sandy units to blue-grey carbonate units. This gradual shift was recorded by interfingering of the Camsell Formation and overlying Sombre Formation (Morrow and Cook, 1987).

The Sombre Formation, which comprises light grey dolostone with light grey lamination and local mudstone, records a broad peritidal carbonate shoal that bordered the shelf. Laterally and above to the east, dark brown to grey fossiliferous, medium- to thick-bedded, dominantly subtidal dolostone of the Arnica Formation was deposited inshore of the shoal belt in lagoons. East of the Arnica and Sombre formations, the laterally equivalent Bear Rock Formation is anhydrite interbedded with mudcracked dololutite (Fritz et al., 1992).

While the Sombre and Arnica formations covered much of Root Basin, deep-water calcareous dark grey shale of the Road River Group persisted in the Prairie Creek and Meilleur River embayments. Hemipelagic strata dominated in the basin centers, but large blocks of limestone slumped into the basin by gravity flows along the fault margins during local instabilities (Morrow and Cook, 1987).

North and west from the Meilleur Embayment and the Root Basin, the Sapper Formation is a transitional zone of recessive grey to tan-orange limestone in two discrete members. The lower limestone is grey-weathering; black, very fine crystalline limestone with black to grey-brown chert. The upper member is buff- to tan-weathering, platy, silty limestone. Conodonts, graptolites, and shelly fossils indicate deposition from the Late Ordovician to Middle Devonian, equivalent to the Portrait Lake Formation of the Road River Group. The Sapper Formation was included in the Road River Group by Jefferson et al. (2003) although Gordey and Anderson (1993) had excluded it based on the calcareous nature of the siltstone that is distinct from siliceous siltstone of the Road River Group.

The Grizzly Bear Formation, crinoidal limestone that weathers dark grey to black, conformably overlies the Sapper Formation. Distinctive twin-ossicle crinoids mark this stratum separating the Sapper and Funeral formations and record a shallow platformal setting but sedimentary structures indicate beneath wave-base. Stromatoporoids and corals in growth position represent offshore shoals in otherwise moderately deep water. The Grizzly Bear Formation correlates with the upper Sombre, the Arnica and lower Natla formations on Mackenzie Platform. West of the Redstone arch, these units are overlain by massive limestone of the Natla Formation (Gordey and Anderson, 1993).

The Middle Devonian Natla Formation is recessive-weathering bioclastic limestone that weathers sooty black, distinct from the underlying Arnica and overlying Headless and/or Landry formations. Slump structures and fossils suggest an offshore slope environment at maximum transgression (Gordey and Anderson, 1993).

Regional regression coincident with deepening of the Root Basin then caused argillaceous to silty limestone of the Funeral Formation to fill Root Basin and its orange-weathering dolomitic limestone facies to drape Redstone Arch during the Middle Devonian. At about the same time, the Headless and Landry formations were deposited on Mackenzie Platform and the Portrait Lake Formation filled Selwyn Basin. The scarcity of fossils and lack of wave-produced sedimentary features indicate an open-marine, off-shelf setting. The Landry Formation, a pelletal lime wackestone and packstone with few fossils other than ostracodes, defines the laterally equivalent carbonate margin and correlates with the Dunedin Formation to the south (Fritz et al., 1992).

Widespread regional transgression is recorded by the recessively weathering Headless Formation that grades into Nahanni Formation in an upward shoaling progression that expanded the carbonate shelf westward (Fritz et al., 1992).

Ediacaran to Middle Devonian of the Selwyn Basin (Figs. 4, 7)

The Selwyn Basin is located west of the Mackenzie Platform and transitional assemblages, and includes the Meilleur River, Prairie Creek and Misty Creek embayments. These deeper water basinal deposits are the facies equivalents to the platformal and transitional sequences that locally interfinger with the deeper water deposits. The oldest exposed basin strata are rusty shale of the Vampire Formation, coeval with the Neoproterozoic Yusezyu Formation and Lower Cambrian Narchilla Formation of the Hyland Group (Gordey and Anderson, 1993; Hart and Lewis, 2005).

The Yusezyu Formation (formerly termed ‘Grit unit’) is interbedded conglomerate, quartz rich grit, and tabular shale. Locally the Yusezyu Formation is dominated by finer grained strata but the coarser grit is the defining characteristic. Minor limestone is near the top. The Yusezyu Formation is sharply and conformably overlain by maroon and green argillite, grey shale and lesser grit and sandstone of the Narchilla Formation. These two formations of the Hyland Group are interpreted as a broad slope to basin turbidite fan coeval with the Vampire Formation (Mair et al., 2006) fed by the deltaic system of the Backbone Ranges Formation (Gordey and Anderson, 1993).

The Hyland Group is overlain by the Gull Lake Formation, which consists of brown- to buff-weathering blue-grey shale with minor limestone conglomerate. Archeocyathids as clasts (also found in the Sekwi Formation, Fritz et al., 1983) may represent debris flows from the coeval platformal Sekwi Formation onto the basin slope to off-shelf area (Gordey and Anderson 1993; Hart and Lewis, 2005).

Above the Early Cambrian, the northern and southern parts of the Selwyn basin have distinctly different lithofacies. In the north, shale with minor shaly limestone to limestone beds is overlain by a succession of siliceous shale and chert. Minor volcanic strata include the Early and Middle Ordovician Marmot Formation in the Misty Creek Embayment. Overall the basinal sequence contains no detritus from the platform.

To the south, limestone and shale of the Rabbitkettle Formation are overlain by Duo Formation shale, argillaceous shale and argillaceous limestone and calcareous shale beds. A regional unconformity beneath the Rabbitkettle Formation truncates the Gull Lake and Sekwi formations along the western and central portions of the study area. The widespread limestone Rabbitkettle Formation is in turn conformably overlain by the Road River Group deposited from the Middle Ordovician to the Early Devonian. The Road River Group was originally identified by Jackson and Lenz (1962) as a graptolitic black shale and chert in the Richardson Mountains. Gabrielse et al. (1973) extending the name to the Selwyn Basin in the Nahanni region. It was raised to group status by Gordey and Anderson (1993) who defined the Duo Lake and Steel formations. The lower boundary of the group was defined at the top of the Rabbitkettle Formation, but this conformable contact is only rarely exposed and often disturbed by thrust faults. The upper contact of the group is defined at the top of the Steel Formation.

The Duo Lake Formation consists mainly of recessive, black, siliceous shale. Thin beds of chert and minor limestone beds are common in the approximately 300 m thick unit. Bedded chert contains small

spherical nodules thought to be poorly preserved radiolaria. The quiet off-shelf setting below wave base was starved from clastic input. The Duo Formation hosts extensive lead-zinc sulphide SEDEX deposits in the Howards Pass to Summit Lake area. Morganti (1979) described the finely laminated mineralized "Active member" as part of the Howards Pass Formation but Gordey and Anderson (1993) reinstated the Road River Group terminology. Late Llandovery (Early Silurian) graptolites near the SEDEX deposits are consistent with conodont ages for beds immediately overlying the "Active member" (Norford and Orchard, 1985). Graptolites in the Duo Lake Formation range from Late Tremadoc (Early Ordovician) to late Early Silurian (Jackson and Norford, 2004).

Widespread Upper Silurian mudstone (Steel Formation) is one of the marker units in the Road River Group. This siliciclastic light grey to dark grey dolomitic mudstone is up to 140 m thick, and weathers orange due to ubiquitous finely disseminated pyrite and ferroan dolomite. Wispy laminations and discontinuous bedding are abundant burrows and bioturbation. Thin bedding and lack of other sedimentary features indicate deep-water deposition (Cecile 2000). Graptolites and sparse conodonts are late Wenlock to earliest Devonian (Norford and Orchard, 1985; Gordey and Anderson, 1993).

Shale units of the Road River Group are preserved from northeastern British Columbia (Jefferson et al., 1983; Pyle and Barnes 2003) into northern Yukon (Cecile 2000). The Duo Formation is equivalent to parts of the Haywire, Sunblood, Whittaker, and Mount Kindle formations. The Steel Formation correlates with the Sapper Formation, the uppermost Whittaker Formation and some of the lower Delorme Group.

Middle Devonian to Carboniferous (Mississippian) (Figs. 4, 8, 9)

Commencing in the mid-Devonian, the pattern of passive margin sedimentation in the Selwyn Basin and carbonate deposition on the Mackenzie Platform was terminated by the Antler Orogeny, a time of regional uplift and erosion followed by subsidence of the continental margin. Extensional and wrench tectonics caused block faulting, rifting, localized volcanism and uplift in previously basinal areas, causing deposition of siliciclastic debris derived from the west to northwest. Black turbiditic shale, siltstone and chert pebble conglomerate were deposited in a regional basinal transgression across the Selwyn Basin and distal shale-siltstone units lapped over the Mackenzie Platform during the Frasnian to earliest Mississippian (Gordey et al., 1987). The earliest sedimentation included radiolarian chert and black siliceous shale associated with SEDEX zinc-lead-silver deposits of the Mac Pass District in Yukon and Gataga District of northeastern British Columbia. Siliciclastic sediment spread to the south and east from uplifted sources in northern Yukon, to the east from uplifted western portions of Selwyn Basin (Fig. 8, and to the west and south from the Arctic (Ellesmerian Orogeny)).

In the northern Cordillera, deposits related to Devono-Mississippian tectonism are called the Earn Group (Campbell, 1967) and divided into two mappable formations (Gordey et al., 1982). The lower, Portrait Lake Formation represents quiet marine deposition with little clastic input other than local sediment gravity flows. The overlying Prevost Formation is a medium- to coarse-grained clastic facies deposited by turbidite channel and debris flows.

The Middle to Late Devonian Portrait Lake Formation was deposited predominantly in structurally controlled sub-basins distributed across the region of the previous Selwyn Basin. Gun-blue-weathering black siliceous shale and chert dominate, with local turbiditic arenite, wacke, pebbly mudstone and pebble conglomerate. Coarse clasts are composed of reworked black to white chert and quartz. Fine lamination, graded bedding, carbonaceous composition and the lack of bioturbation record a euxinic paleo-environment below wave base, with coarse detritus transported by gravity flows in submarine fan channels from rugged nearby mountains (Winn and Bailes, 1987). Groove casts record paleoflow to the east and southeast (Fig. 8).

Sedimentation was influenced locally by block faulting, accompanied by felsic and mafic volcanism, and in the lower Portrait Lake Formation was synchronous with numerous Zn-Pb-Ag-Ba deposits in several camps (Carne, 1979; Jefferson et al., 1983; Lydon et al., 1985). Abrupt facies, thickness variations and structural complexity indicate local graben (Cecile, 2000), commonly termed third-order basins, that preferentially host ore deposits (e.g. Macmillan Pass area: Carne, 1979; Winn and Bailes, 1987). Thickness changes across the faults and paleocurrents parallel to fault traces record syn-sedimentary deformation. Near the top of the Portrait Lake Formation a regionally distributed bedded barite unit (Lydon et at., 1985) lacks base metals yet may be an indicator of broad-scale tectonism. Conodonts indicate mid-Devonian to Early Mississippian deposition (Irwin and Orchard, 1991). The Portrait Lake Formation correlates in part with the Delorme, Camsell, Sombre, Arnica, Natla, Landry, Headless and Nahanni formations.

The latest Devonian to mid-Mississippian Prevost Formation consists of brown-weathering shale, resistant grey- to brown-weathering chert pebble conglomerate and chert lithic sandstone. Its sharp basal contact suggests scouring by sediment gravity flows marking the progradation of a turbidite fan complex from the

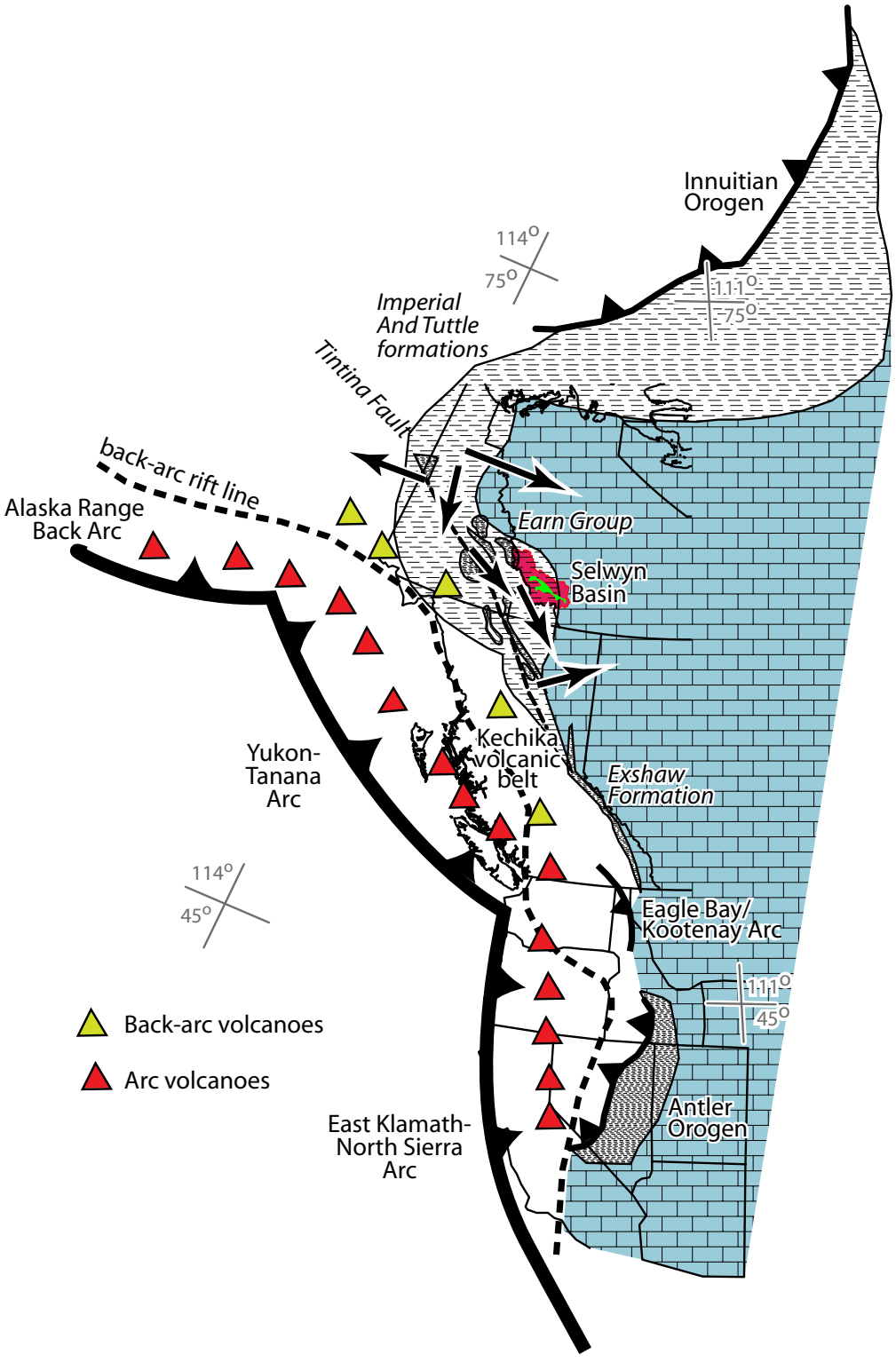


Figure 8. Middle Devonian paleogeography showing the paleocurrent directions for the Earn Group and equivalent units. The study area is filled in red, enclosing the Nahanni National Park Reserve in green. After Gordey et al. (1987), Smith et al. (1993), and Colpron et al. (2007).

west. Much of the chert pebble conglomerate could have been derived locally from the Road River Group (Carne, 1979). Sedimentary features include massive to graded bedding with local turbiditic Bouma sequences. Correlative clastic strata include the Hare Indian, Canol, and Imperial formations in the northern Cordillera and the Besa River, Horn, Muskwa and the Fort Simpson formations (Hadley and Jones, 1990) in the southern and eastern portions of the study area.

In the eastern Nahanni region, the Besa River Formation was deposited as part of the major transgression that submerged the carbonate platform

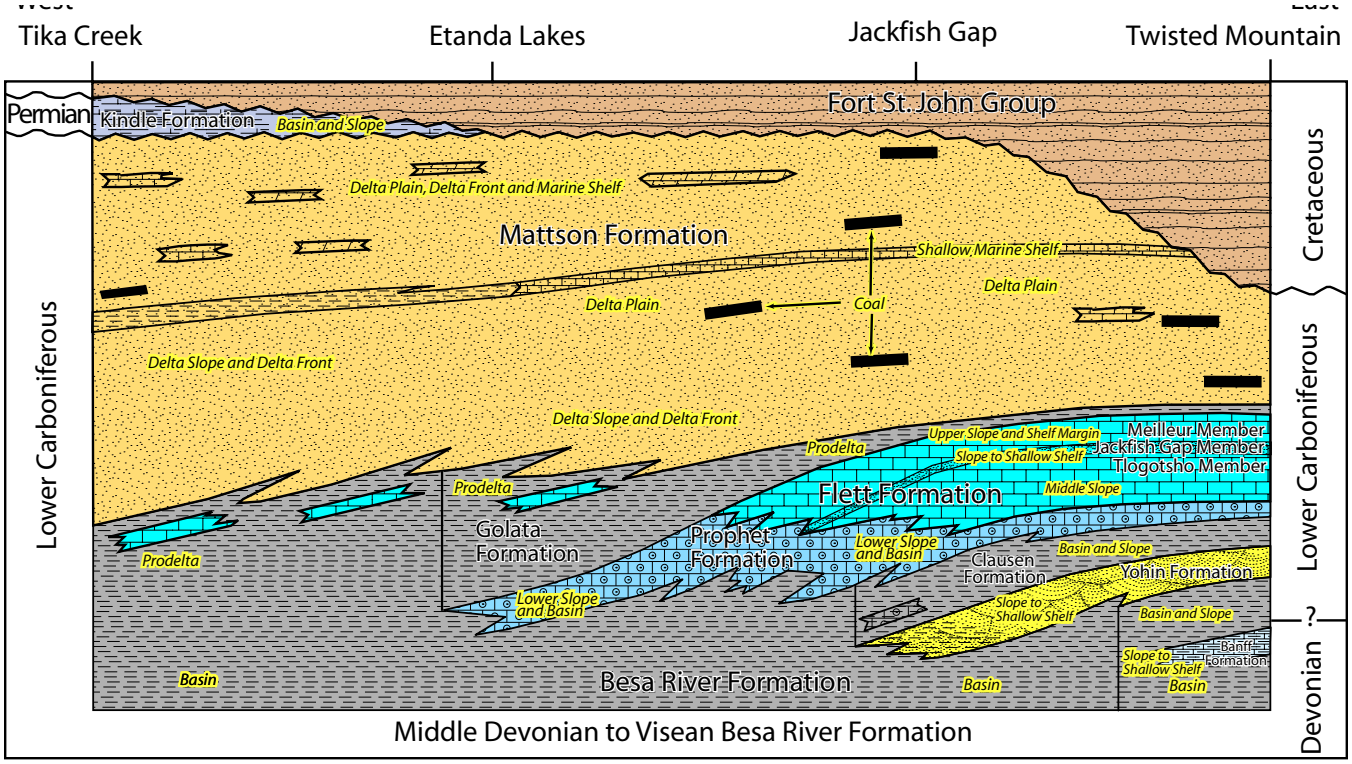


Figure 9. Schematic cross-section of the Upper Devonian to Cretaceous strata in the Liard Basin between Tika Creek, Yukon, and Twisted Mountain, Northwest Territories. Depositional settings for the units are indicated in the fine print (adapted from Richards, 1989).

(Pelzer, 1966). Its widespread deposition across northeastern British Columbia, southeastern Yukon, and southwestern Northwest Territories was concurrent with the coarse siliciclastic strata of the Portrait Lake Formation. The Besa River Formation shares many of the characteristics of the Provost Formation and some find it hard to distinguish the two (Bamber et al., 1992; Gordey, 1992). The Besa River consists of dark grey to black, thin-bedded to massive shale containing minor amounts of sandstone, limestone, chert, argillite and calcareous shale (Lowey, 1990). The local barite concretions reported by Gabrielse and Blusson (1969) are likely in the Earn Group, not Besa River. Similar to the Earn Group but lacking chert pebble conglomerate, these slightly more calcareous shale units may represent distal turbidite deposits in a pro-delta setting. Contacts with overlying units tend to be gradational. Brachiopods, ammonites, and conodonts suggest that deposition took place from the Middle Devonian to Late Mississippian. The fine-grained platy Besa River Formation, as for the Road River and Earn groups, is a structurally weak unit that commonly is a décollement zone for thrust faults (McMechan, 2002; Hinds and Spratt, 2005; Hynes and Dixon, 2005).

Carboniferous (Mississippian) to Triassic (Fig. 9)

Erosion, especially prior to the Permian, removed much of the upper Paleozoic record in the Mackenzie Mountains. The record is patchy in the western portion of the study area but in the east a more complete record of marine shelf sedimentation has been preserved such as in the Liard Basin (Bamber et al., 1992)

From the Carboniferous to the Triassic, marine shelf sedimentation resumed across the miogeocline (Fig. 9). Similar to the early Paleozoic, two contrasting belts of strata were deposited along the length of the entire Cordillera. An eastern facies of marine platform and ramp carbonate is interbedded with shallow marine to continental detrital deposits, both of which grade laterally into and interfinger with a basinal shale assemblage to the west (Bamber et al., 1992).

During the late stages of Besa River Formation deposition, carbonate platformal sedimentation resumed on the western edge of the craton to form the Banff, Pekisko, Flett, and Prophet limestone units. To the west, the deep water Prophet Trough superseded the Selwyn Basin. Shale and deep-water facies of the Besa River and overlying Golata formations are widely distributed but thin westward due to reduced sedimentation rates in the starved basin. Unlike the lower Paleozoic sequence, the carbonate platform also received substantial amounts of clastic material in the form of deltaic to shallow marine clastic sediment. During Carboniferous time, the carbonate-clastic deposits prograded westward over portions of the basinal trough strata, resulting in a broad transitional zone that migrated southwesterly. A brief eastward trans-

gression deposited Golata Formation shale over the platform. This was overlapped westerly by the thick, siliciclastic, deltaic Mattson Formation that covered both the carbonate platform and the Prophet Trough (Richards, 1989).

The Banff and Pekisko carbonates did not prograde into the study area. Addition of coarse clastic material defines the Yohin Formation but it also demonstrates transitional contacts with the basinal sequence. The Yohin Formation is partly coeval with and younger than the Banff Formation to the southeast, and comprises approximately 160 m of silty sandstone, siltstone and mixed skeletal limestone deposited in a shallowing-upward slope to shallow marine environment. The Clausen Formation, 150 to 200 m of black shale interbedded with siltstone (Richards, 1989; Bamber et al., 1992), conformably overlies the Yohin Formation and interfingers with the basinal Golata Formation shale.

Carbonate deposition of the Prophet and Flett formations resumed above the Clausen Formation. The Prophet Formation consists of cherty spicularite and spicule-rich limestone with minor shale, thickens toward the west, and displaces part of the Flett Formation. The Flett Formation, also referred to as the Debolt Formation (Monahan, 2000), is dominantly grey limestone: abundant skeletal fragments in lime packstone and grainstone with intervals of cross-stratified sandstone and siltstone. Shale of the Jackfish Gap Member (Hynes and Dixon, 2005) marks the middle of the Flett Formation. The upper Flett Formation consists of grainstone. Large paleochannels are common in the slope sections of the Yohin, Flett, and Prophet formations. The Clausen, Yohin, Prophet, and Flett formations represent a series of facies transitions between reef deposits with cratonic deltaic input to the east, and more basinward slope and off reef deposits to the west (Richards, 1989). The Golata Formation is thin and slightly coarser grained than the Besa River Formation, comprising mainly shale and mudstone, interlaminated with fine sand, recording a basinal to prodelta environment.

Fine-grained strata of the Golata Formation coarsen upward and are overlain by quartz arenite with minor chert arenite of the Mattson Formation. The Mattson Formation prograded westward into the Prophet Trough (Richards, 1989).The sand was derived from the north and was deposited in a progression of slope to shallow marine shelf to delta-plain units divided in some areas into three members. The middle member is a significant hydrocarbon reservoir rock. Periodic subaerial exposure is recorded in these fluvial facies containing significant coal measures (Long, 1986; Morrow et al., 1993; Potter et al, 1993) that mark a shift in the depositional environment from platformal to continental sedimentation.

North of the Liard Basin, erosion has removed most of the Carboniferous deposits. The upper Earn Group is abruptly and locally unconformably overlain by quartzose sandstone with shaly interbeds of the Tischu Group (Cecile, 2000). The best example of this relationship is exposed near Mount Wilson where grey- to white-weathering quartz sandstone interbedded with black shale and siliceous shale overlies blue grey shale of the upper Earn Group. A shallow-marine shelf setting was suggested with the coarser sandstone beds representing storm generated sediment gravity flows. Conodont biostratigraphy indicates that deposition continued throughout the Carboniferous. This allows correlation to the Mattson Formation in the Liard Basin area (Bamber et al., 1992; Gordey and Anderson, 1993).

The Tsichu Group is both overlain by and partly a facies equivalent of the Mount Christie Formation, buff- to orange-weathering shale and chert with minor sandstone. Based on limited sedimentary structures, the depositional setting is below wave base with the addition of minor clastic horizons either due to shoaling or sediment gravity flows. Poorly constrained conodonts ages are as late as Early Permian to Middle Permian. Correlations with the upper Mattson, Kindle and Fantasque formations in the Liard Basin have been suggested (Gordey and Anderson, 1993).

The Permian is poorly preserved in the study area, being represented by a thin succession of mainly shallow-marine to basinal siliciclastic strata with silty to sandy carbonate (Butrenchuk, 1988) (Fig. 9). The Kindle Formation is best preserved in Liard Basin, where it rests disconformably on Carboniferous strata and displays a marked facies change from east to west. The easternmost portion consists of neritic sandstone, shale, and carbonate units in the Interior Platform, passing westward into dark grey rhythmically bedded siltstone with minor glauconite, shale and limestone. Farther west, slope to basinal silty carbonate, siltstone, and shale include 60 m of phosphatic siltstone. The preserved thickness of this assemblage varies due to differential erosion related to the unconformity beneath the Fantasque Formation (Bamber et al., 1992; Monahan, 2000).

The Fantasque Formation (not shown in figures) comprises slope to basinal deposits including spicular phosphatic, locally glauconitic chert, shale, and siltstone, and is distributed from northern British Columbia to the southern Mackenzie Mountains. A lag deposit of phosphate nodules, chert nodules, and pebbles marks the disconformity at the base of the Fantasque Formation. Above this the medium to dark grey, bedded chert of eastern sections grades westward through an intermediate facies of interbedded chert, siliceous mudstone, shale, and siltstone, into basinal

shale and siliceous mudstone. A 1 m siltstone bed near the top of the formation contains large phosphatic nodules (Butrenchuk, 1988; Bamber et al., 1992). The Fantasque Formation is a reservoir for gas pools in areas where it has been structurally modified (Monahan, 2000).

Preservation of Triassic rocks is also poor in most of the study area but those that remain, especially in the Liard Basin area are of particular interest because they are known to contain petroleum reservoirs (Monahan, 2000). Thicknesses are greater Foreland Belt from the Fort St. John basin northward into the Liard Basin where the Grayling and Toad formations are a westward-thickening succession of siliciclastic, carbonate and lesser evaporitic rocks deposited in a wave-dominated shelf (Gibson, 1992; Utting et al., 2005).

The Grayling Formation is recessive dark grey, shaly- to flaggy-weathering dolomitic siltstone, silty shale, and lesser calcareous siltstone to very fine sandstone. The massive to faintly laminated bedding and abundant load structures or basal tool marks are typical of storm-generated deposits. The Grayling Formation disconformably overlies chert and siliceous mudstone of the Permian Fantasque Formation, and has a poorly defined upper contact with the Toad Formation generally determined by the first sandstone beds (Utting et al., 2005).

The Toad Formation is dark grey, thin- to medium-bedded, shaly- to flaggy-weathering, very calcareous siltstone, silty limestone, and silty shale with minor amounts of dolostone and calcareous sandstone. The hummocky to swaley cross stratification and abundant isolated lenses of sandstone encased in finer grained strata represent turbidity or storm-generated offshore currents in relatively shallow waters of a regressive setting. In the Fort St. John basin, the Toad Formation is gradationally overlain by the Liard Formation but in the study area the overlying units have been removed by a sub-Cretaceous unconformity and the unit is disconformably overlain by the Fort St. John Group (Gibson, 1992; Utting et al., 2005).

In the northern part of the study area, isolated scattered exposures of thin-bedded, ripple cross-laminated calcareous siltstone, sandstone and shale of the Jones Lake Formation (Gordey and Anderson, 1993) contain Triassic conodonts and are correlated with the Toad Formation. The Jones Lake Formation disconformably overlies the Mount Christie Formation. Abundant ripple cross-lamination probably represents sub-tidal deposition on a shallow-marine shelf in a shallowing environment related to ongoing uplift (Gibson, 1992).

Late Jurassic and Cretaceous

During the Jurassic, the western margin of the North American craton collided with an island arc system (Yorath, 1992; Gabrielse and Yorath, 1992) resulting in intense deformation, regional metamorphism, granitic magmatism, uplift and erosion. The Omineca and Foreland tectonic belts were established during this collision. The Omineca Belt is a regional tectonic "welt" and the Foreland Belt a series of troughs and basins that developed east of the rising orogen. Deformation was concentrated in the Omineca Belt; overlap and compressional thickening of crustal rocks resulted in widespread plutonic activity.

Early to middle Cretaceous granitic magmas intruded the deformed rocks of the Selwyn Basin, forming large batholiths to small stocks in three major suites: Tombstone, Tungsten and Tay River defined by age and metallogenic similarities (Mortenson et al. 2000; Hart et al., 2004, 2005; Heffernan, 2004; Barnes et al., 2007; Rasmussen et al., 2007) (formerly Selwyn Plutonic Suite; Anderson, 1988; Gordey and Anderson, 1993). Most plutons consist of quartz-feldspar with biotite, ± hornblende or rare muscovite but these suites range from fine-grained, dioritic, quartz-feldspar porphyry phases through fine- to medium-grained equigranular granodiorite-monzogranite with sparse to abundant K-feldspar phenocrysts to cumulate K-feldspar syenite. Multiple phases are common especially in the larger intrusions. Intrusive contacts are shallow to steeply dipping, but dominantly conformable to the wallrock strata.

A consequence of the island arc collision and related uplift was the accommodation in synorogenic foreland basins of stratigraphic successions derived from miogeoclinal strata and the adjacent Omineca Belt. This process began as Proterozoic to lower Paleozoic sequences were folded and detached from their basement. Detached sections were stacked and carried northeastward over the craton in an advancing thrust-and-fold belt. The foreland basins were linear crustal moats caused by loading of the craton by the structurally thickened basinal and platformal strata. As the deformation front advanced eastward, these foreland clastic basins were filled, then in turn uplifted and eroded into the next basin to the east (Gabrielse and Yorath, 1992).

North of the newly formed Mackenzie Mountains, a broad inland marine shelf covered the region. This bordered the continent scale, shallow but rapidly subsiding intra-cratonic Western Interior Seaway that accommodated the Martin House, Arctic Red-Horton River and Sans Sault formations during the Early Cretaceous (Dixon, 1986, 1999). This succession consisted of basal glauconitic sandstone and a series of alternating thick bedded, concretionary, fossiliferous, silty mudstone-dominated, then sandstone-dominated siliciclastic rocks (Dixon, 1999).

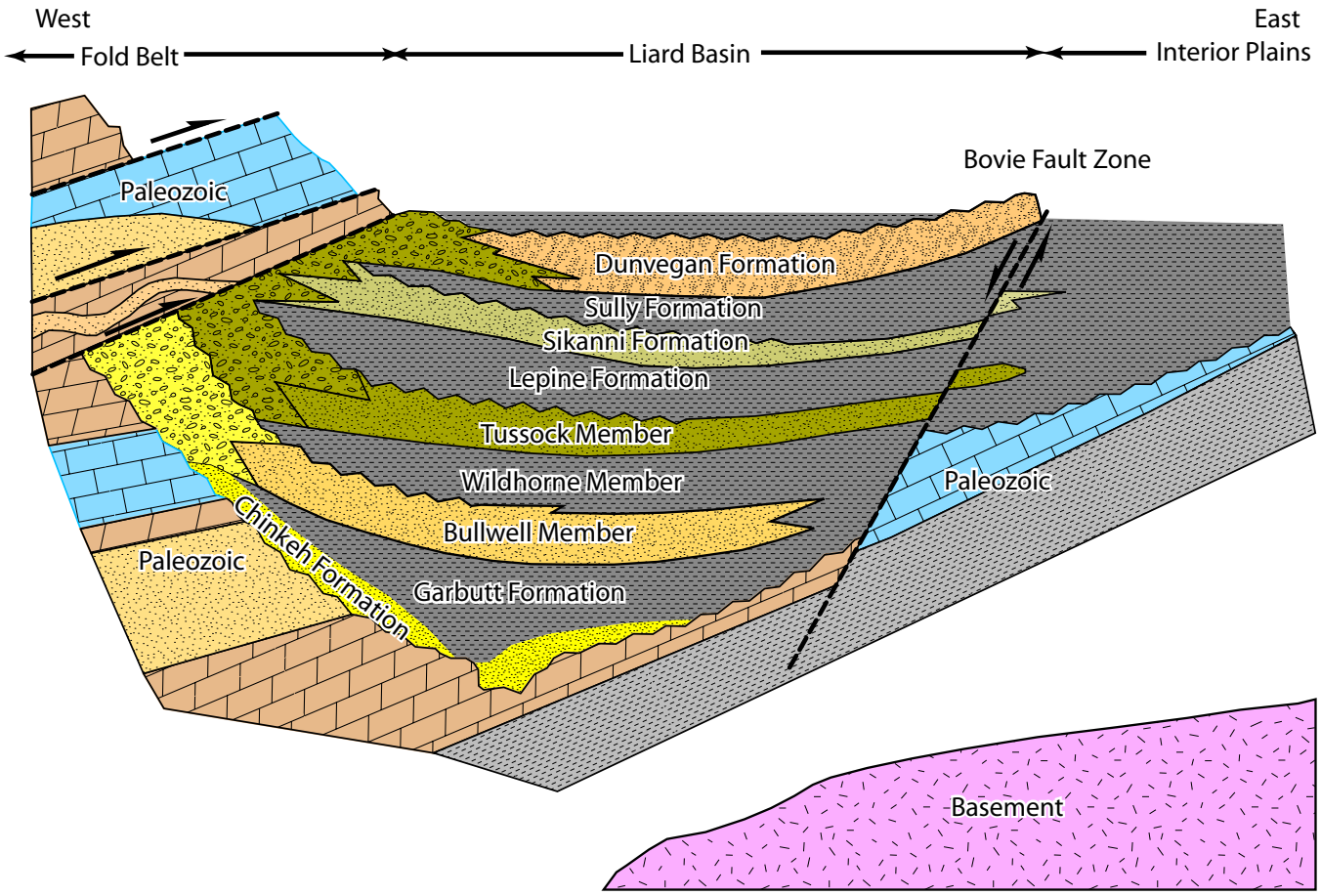


Figure 10. Schematic cross-section showing stratigraphic relationships and structural elements of the Liard Basin (Leckie et al., 1991).

To the south of the Mackenzie Mountains, a long-lived depocentre in the Liard Basin area was bounded by the Liard Line to the north and the Bovie Fault to the east-southeast (MacLean and Morrow, 2004) (Fig. 10). Active subsidence and sedimentation during the Cretaceous was balanced by the high rate of uplift to the west. Whereas many regions display substantial unconformities recording widespread regressions, the Liard Basin contains a relatively complete record of deposition. Episodic uplift formed a clastic wedge derived from the west, while subsidence accompanied by fluctuations in the sea level allowed marine incursions (Stott, 1982; Jowett and Schröder-Adams, 2005). The resultant clastic wedge comprises four cycles of marine shale grading upward to coarse sandstone and conglomerate included in the Fort St. John Group and the Dunvegan Formation, as well as extensive coal deposits (Stott et al., 1992).

Locally preserved at the base of this clastic wedge is the upward-fining Chinkeh Formation of conglomerate, sandstone, and shale. Meandering stream deposits, in many places capped by coaly shale or coal, filled a local, probably fault-bounded trough from the northwest. The unconformity at the base of the Chinkeh Formation developed after deposition of the Triassic Grayling and Toad formations. Burial of the Chinkeh Formation was to a depth of over 2000 m as indicated by coal rank. Uplift since the beginning of the Paleogene has returned it to the surface around the margins of the Liard Basin (Leckie et al., 1991). The Chinkeh Formation west of the Bovie Lake Fault (MacLean and Morrow, 2004) is a known gas reservoir, considered to be a significant petroleum play in the region (Osadetz et al., 2003; Monahan, 2000).

Mudstone and siltstone of the Garbutt Formation overlie the Chinkeh Formation. Wave ripples and hummocky cross stratification are common in sandier beds, and bentonite layers have been identified near the base (Stott, 1982). Large slump structures indicate high rates of sedimentation in a shallow marine setting where storms disturbed the seafloor (Leckie and Potocki, 1998). The Garbutt Formation coarsens upward into the Scatter Formation, whose sandstone and shale members also record wave activity during lowering of sea level and deposition on a shallow marine shelf to shoreface. The Bulwell and Tussock sandstone members record shallower water while shale of the Wildhorn Member suggests periods of deeper water (Leckie and Potocki, 1998). The fine to very fine sandstone members commonly contain up to 50% glau-

conite. Their upper contacts tend to be abrupt but bases are gradational with underlying shale members (Leckie et al., 1991).

The overlying Lepine Formation marks regression in the Liard Basin. This dark grey mudstone is distinguished from the underlying shaly Scatter members by its sideritic concretions and a distinctively radioactive horizon near the base. Based on sparse forminifera and ammonites and well logs, this thick marine shale sequence can be correlated with the upper Buckingham and Hassler formations in the Peace River region of Alberta. The paucity of biota in the Lepine Formation, despite favourable offshore to shelf environments, may have been caused by restricted circulation in the Interior Seaway north of the Liard Region (Jowett and Schr öder-Adams, 2005).

Fine sandstone with mudstone of the Sikanni Formation, deposited in deltaic and wave-dominated shelf settings, rests on the Lepine Formation. The Sikanni Formation appears to be derived locally from northwest of the Liard Basin and is overlain by the Sully Formation. The Sully Formation strongly resembles the Lepine Formation in that it consists of mudstone with sideritic concretions (Leckie et al., 1991) and it represents a re-incursion of deeper water marine conditions (Stelck and Hedinger, 1983).

After deposition of the Sully Formation, the balance between subsidence, uplift and sedimentation changed again. A regressive phase is recorded by the Dunvegan Formation as a wedge of quartz arenite and quartz-quartzite-chert-pebble conglomerate (Stott, 1982) deposited by broad deltaic fan that prograded gradationally over the Sully mudstone from the Liard Basin well into central Alberta. Fossils tend to be sparse in many of the higher energy facies but lacustrine, floodplain deposits preserve an abundance of dinosaur tracks (Plint et al., 2001). These settings are also associated with paleosols and coal-rich layers. A widespread unconformity at the top of the Dunvegan Formation (Stott et al., 1992) has removed much of this stratigraphy from the MERA 2 study area.

During the latest Cretaceous, the tectonic evolution of the Cordillera shifted from compression to extension. In response to continuing uplift in the Cordillera, widespread eastward-prograding alluvial-deltaic deposits with associated coal and fossil beds supplanted marine conditions in the continental interior. In the Mackenzie Mountains, the Dunvegan Formation, which grades into the Slater River Formation (Dixon, 1986; Stott et al., 1992), represents the onset of this shift but much of the overlying stratigraphic record has been removed by erosion. In the Alberta Basin to the south, this period is recorded by the Wapiti Formation of coarse-grained alluvial strata in the west, grading eastward into marine shale. Coal seams up to 3 m thick were buried to depths of 900 to 1900 m (Nurkowski, 1984).

Paleogene

The shift back to an extensional tectonic regime during the Late Cretaceous to Paleogene produced numerous small fault-controlled basins filled by Eocene strata in the Coal and Rock River areas, in association with major dextral strike- slip faults in the Omineca and Intermontane belts (Wright and Miller, 1986). Mudstone with minor conglomerate and sandstone, and coal in lenticular pods accumulated as overbank deposits in a coarse-grained fluvial setting (Long, 1986). Coal seams up to 30 m thick are preserved near the margins of the paleovalley. These valley fills are commonly obscured by glacial overburden but some are up to 1000 m thick, controlled by northerly trending faults (Wright and Miller, 1986).

The youngest intrusive episode in the region formed the Ting Creek Intrusive Suite, the Pool Creek Syenite and the Beaver River Alkaline Complex (Rowins and Francis, 1995; Symons et al, 2003) (Fig. 11). Biotite phenocrysts from the Ting Creek Suite were dated by the K-Ar method at 53 ± 2 Ma (Stevens et al., 1982), similar to the 51.8 ± 0.2 Ma date derived from zircon in a biotite phase of the Pool Creek Syenite (Pigage and Mortensen, 2004). An older alkaline complex may have preceded the Early Tertiary within the same locality. Igneous zircon grains ranging in age from 640 to 650 Ma have also been identified in phases of the Pool Creek Complex. Although no alkaline complexes have been identified within the study area, the small size of such intrusions makes them easy to miss during reconnaissance mapping.

The extensional and thermal events that generated these unusual intrusions are still in effect, based on anomalous thermal levels identified in the region through borehole measurements (Majorowicz et al., 2005). Heat-flow values between 100 to 140 mW/m^2 are highly anomalous in contrast to typical cratonic values of 33 mW/m^2. High heat-flow values have been attributed to thinning of the Proterozoic sedimentary cover sequence over the crystalline basement. High regional organic thermal maturity values suggest that high heat flow persisted into the Neogene, and that extension initiated in the Paleogene may still affect the region (Nurkowski, 1984; Leckie et al., 1991).

METAMORPHISM

All rocks in the study area have been compacted, lithified during burial, and subject to increased heat and pressure during the Laramide Orogeny. Regional metamorphism does not generally exceed sub-greenschist facies, except for Precambrian rocks being mainly greenschist facies. Paleozoic and some Mesozoic strata

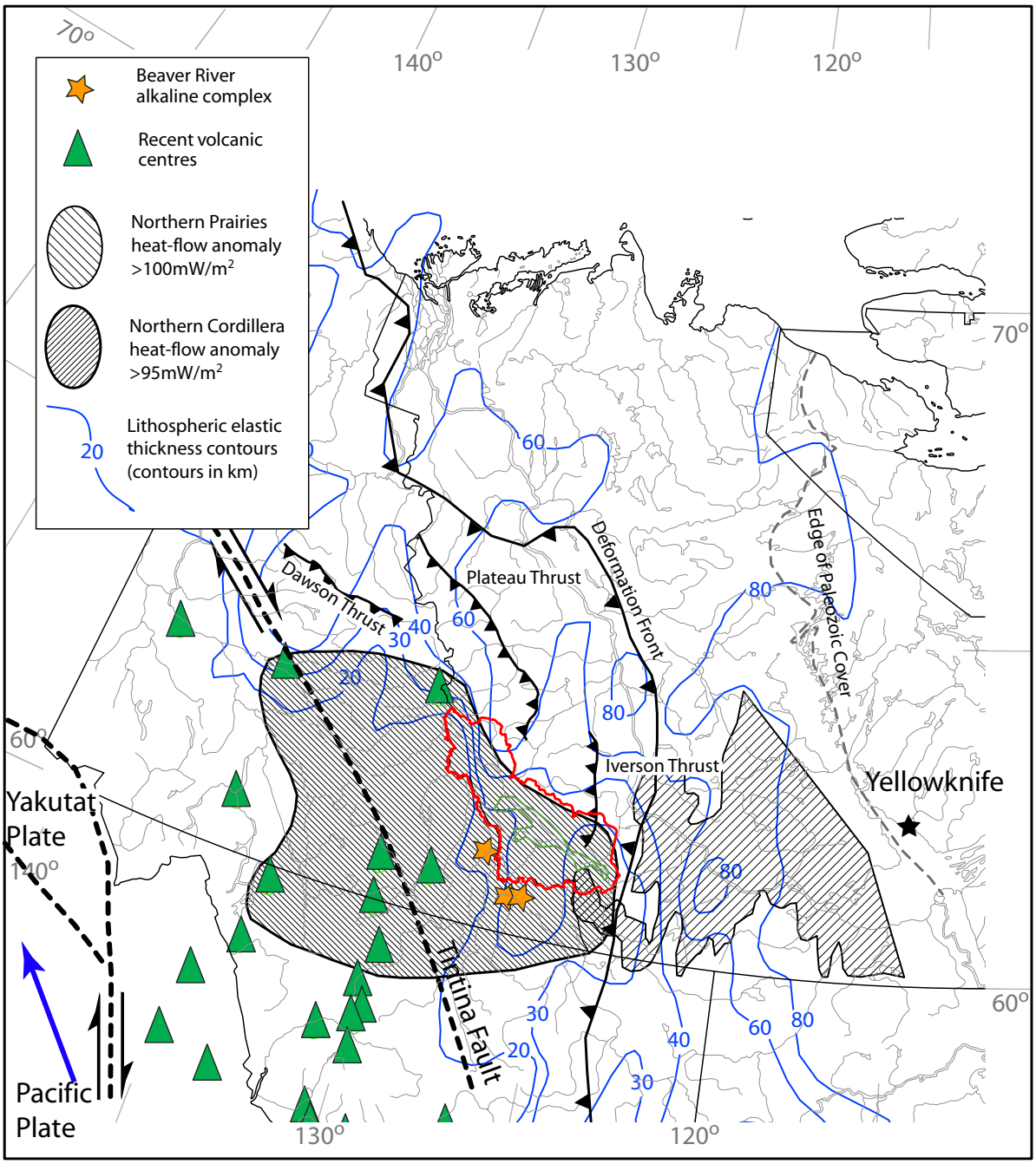


Figure 11. Heat-flow anomalies in the Northern Cordillera superimposed on contours of the effective elastic lithospheric thickness (Majorowicz et al., 2005). Also shown are locations of the Eocene Beaver River alkaline intrusive suite (Pigage and Mortensen, 2004), and Recent volcanic centres (Hyndman et al., 2005). These elements illustrate the ongoing high levels of thermal activity in the study area (outlined in red; Nahanni National Park Reserve in green).

are at prehnite-pumpellyite facies; zeolite is common in Cenozoic strata. Foliation and cleavage are poorly developed i.e., pelitic rocks have slaty cleavage and some Precambrian rocks have chlorite or even biotite foliation. Cretaceous strata of the Interior Platform, including the Wapiti Formation, are commonly at zeolite grade, containing carbonate, illite, montmorillonite, chlorite, and interstratified clay minerals (Gordey and Anderson, 1983; Greenwood et al., 1992).

One of the more pronounced metamorphic changes in the study area is that of the Manetoe alteration facies (Fig. 12). Initially, the Manetoe was mapped as a stratigraphic layer (Douglas and Norris, 1961) and then considered to be a depositional facies, possibly a reef or barrier reef (Noble and Ferguson, 1971). More detailed mapping demonstrated that this distinctive white, massive and coarsely crystalline dolomite has a distinctly crosscutting relationship with several formations of the platformal shelf sequence. The Manetoe facies is best

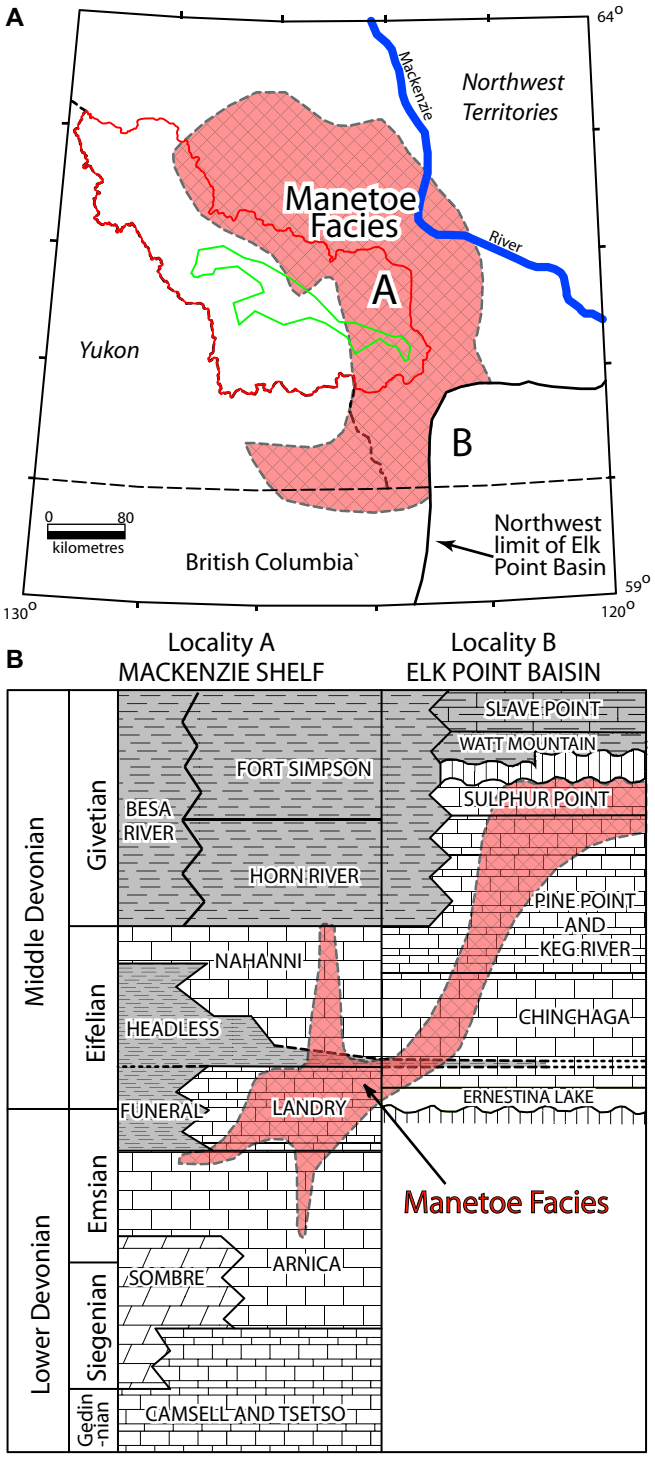


Figure 12. A) Geographic distribution of Manetoe facies alteration (pink hatched pattern) in the study area (red outline) and the Nahanni National Park Reserve (green outline). **B)** Schematic cross-section of the Lower to Middle Devonian Platform showing the cross-cutting nature of the Manetoe and Presqu'ile facies (from Morrow et al., 1990).

developed in the Arnica Formation but also extends into the Headless, Landry and Nahanni formations. Coarsely crystalline dolomite fills open spaces ranging from large cave-like collapse structures, breccias to disseminated vugs in leached carbonate units. Significantly, the Manetoe facies does not extend above the Arnica and Landry formations in areas where the Headless Formation is thick and shaly. In contrast, where the Headless Formation is thin or absent, the Manetoe extends well up into the Nahanni Formation. These observations led to the conclusion that the Manetoe dolomite represents a high-temperature diagenetic event superimposed upon these older strata (Morrow and Cook, 1987).

The Manetoe facies is part of a suite of dolomitic alteration associated with petroleum reservoirs and zinc-lead±silver deposits interpreted as Mississippi Valley, Irish, and sedimentary-exhalative types. The development of the Manetoe facies has been attributed to a number of different hydrodynamic flow drivers including topographic recharge, tectonic or burial compaction, mixing of aquifers, and thermal convection (Garven and Freeze, 1984; Morrow et al., 1990; Morrow, 1998; Davies and Smith, 2006). While still in debate, the Manetoe facies displays many attributes that support thermal convection with structural control (Morrow, 1998; Davies and Smith, 2006).

Hydrothermal diagenesis is the result of fluids accessing a host formation through a fault or adjacent aquifer systems under conditions such that the fluids are at least 5ºC warmer than the host unit. Such alteration is best developed in shallow settings before deep burial. Chemical reactions between the fluid and the host formation, especially when accompanied by fluctuating hydrostatic pressure, fractured impermeable units to produce voids and permeability. Fault systems associated with diagenetic alteration act not only as conduits but may provide transient pressures that promote the propagation of fine fractures. Fluids related to rapid formation of saddle dolomite are commonly saline brines with elevated magnesium concentrations, but the brines can also precipitate quartz, sulphate minerals, authigenic clay minerals and sulphide minerals (Davis and Smith, 2006).

The timing of alteration in the Nahanni region is poorly constrained. Morrow et al. (1990), and Morris and Nesbitt (1998) used lead and hydrogen isotopes, as well as Rb-Sr age determinations for the Pine Point deposit (361 ± 13 Ma from Nakai et al., 1993) to suggest that the alteration is Late Devonian to Carboniferous. On the other hand, Garven and Freeze (1984) and Symons et al. (1993) interpreted paleomagnetic data from the Nahanni and Pine Point deposits in terms of fluids driven by uplift during the Laramide Orogeny in the Late Cretaceous.

Intrusion of the Selwyn Plutonic Suite developed pronounced contact metamorphic aureoles (Gordey and Anderson, 1993). In pelitic rocks of the Selwyn Basin sequence, hornfels aureoles including pyritic alteration are up to 3 km wide. The wider aureoles are

interpreted as products of shallowly dipping underlying plutons. Isograds are difficult to define but inner zones contain andalusite and biotite. Carbonate units are recrystallized to marble, in a number of places including bi-metasomatic skarns of alternating green diopside and red garnet layers. Interaction between pluton-derived fluids and the carbonate host marbles in many places produced assemblages with crosscutting and overprinting relationships. Geothermometric and geobarometric studies of the alteration assemblages constrained peak metamorphic conditions to below 610ºC and 320 MPa close to the plutons (Marshall et al., 2004; Yuvan et al., 2007).

Metamorphism is also defined by alteration in coal. Coalification of Carboniferous to Upper Cretaceous seams appears to have taken place prior to Late Cretaceous Laramide deformation. Coal rank ranges from sub-bituminous C to high volatile bituminous B. Initial interpretations of the coal rank showed increases from east to west (Nurkowski, 1984; Kalkreuth et al., 1989). Modelling has suggested that this is related to the duration and depth of burial beneath the Upper Cretaceous-Paleogene foredeep deposits (Kalkreuth et al., 1989). This general pattern may have been modified by regional variations in heat flow related to Late Eocene extension (England and Bustin, 1985; Kalkreuth et al., 1989; Majorowicz et al., 2005; Utting et al., 2005).

The source and development of petroleum in the Liard Basin region does not follow the pattern established in the Foreland Belt. Petroleum was generated south of 60º concurrent with tectonic imbrication associated with local source rocks in the footwalls of thrusts. Maturation models of the Liard Basin suggest that all potential Paleozoic source rocks are in the wet gas to over-mature zone, with some oil potential in the Mesozoic succession (Potter et al., 1993). An early heating event during the Late Devonian resulted in generation of liquid hydrocarbons during the late Paleozoic to early Mesozoic. Gas in the Manetoe reservoirs may in part represent breakdown of previously generated oil from the overlying Besa River Formation (Morrow et al., 1993; Potter et al., 1993; Osadetz et al., 2005). Organic maturity studies have also outlined several areas of low organic maturity including one near the confluence of the South Nahanni and Liard rivers. Here the Mattson Formation has been metamorphosed only to zeolite facies (Greenwood et al., 1992; Potter et al., 1993). The marked decrease in thermal maturity above the Nahanni Formation constrains the thermal event in this area to Late Devonian (Fig. 13).

To the south of the Nahanni Region in the Northern Rocky Mountain Trench area, an Eocene thermal event has reset K-Ar ages in amphibole. This required temperatures in excess of 500ºC (Greenwood et al., 1992), consistent with the presence of a coeval suite of alkaline intrusions and anomalously high heat flow in and near the study area (Majorowicz et al., 2005).

STRUCTURE

The dominant structural elements of the Northern Cordillera are the major tectonomorphologic Insular, Coast, Intermontane, Omineca, and Foreland belts (Gabrielse, 1992). Most of the structural elements identified in the study area developed after the Mid-Jurassic, although some evidence of earlier structures has been locally preserved (see Gordey and Anderson, 1993). During the initial collision at ca. 170 Ma, the Intermontane Superterrane, including the Yukon-Tanana terrane, was accreted to the North American Plate (Tempelman-Kluit, 1979; Dusel-Bacon et al., 2002). The Omineca Belt is the suture zone of this collision. During the Late Cretaceous, a second collision accreted the Insular Superterrane (Alexander and Wrangellia terranes) to North America. The collision caused extensive uplift and deformation in the interior of the orogen, producing the Coast Mountain Belt, a second suture zone dominated by long-lived plutonism (Gabrielse, 1992) (Fig. 1).

The Nahanni study area transects the eastern part of the Omineca Belt and the entire Foreland Belt in the southern Selwyn and Mackenzie mountains respectively. The latter are arcuate, over 950 km long, and bounded on the east by undeformed strata of the Interior Plains (Hyndman et al., 2005). The two belts display contrasting structural styles as exposed in the Selwyn and Mackenzie mountains. The eastern margin of the Selwyn Belt coincides with the abrupt facies change in the Upper Ordovician to Devonian platformal strata, from competent carbonate units in the east, to incompetent argillaceous units in the west. Selwyn Fold Belt elements include regional-scale thrust faults, imbricate fault zones, chevron and other angular folds with vergence from northward through eastward to westward. Axial-planar slaty cleavage, locally intense, detailed folds, and zones of closely spaced imbricate thrusts are common. Strata in places were thickened substantially by multiple imbricate thrust faults, which are difficult to recognize, especially in siliceous shale, chert and mudstone where unique stratigraphic units cannot be defined (Gordey and Anderson, 1993; Cecile, 2000).

The Mackenzie Mountains feature cratonward-vergent thrust faults; narrow, locally en echelon, doubly plunging, faulted anticlines; and broad, flat-bottomed synclines. Resistant Paleozoic carbonate units are exposed in anticlines whereas recessive Devonian shale underlies most synclines. The large, upright folds are 25 to 60 km along strike with amplitudes of about 1 to 2 km and half wavelengths between 5 and 9 km.

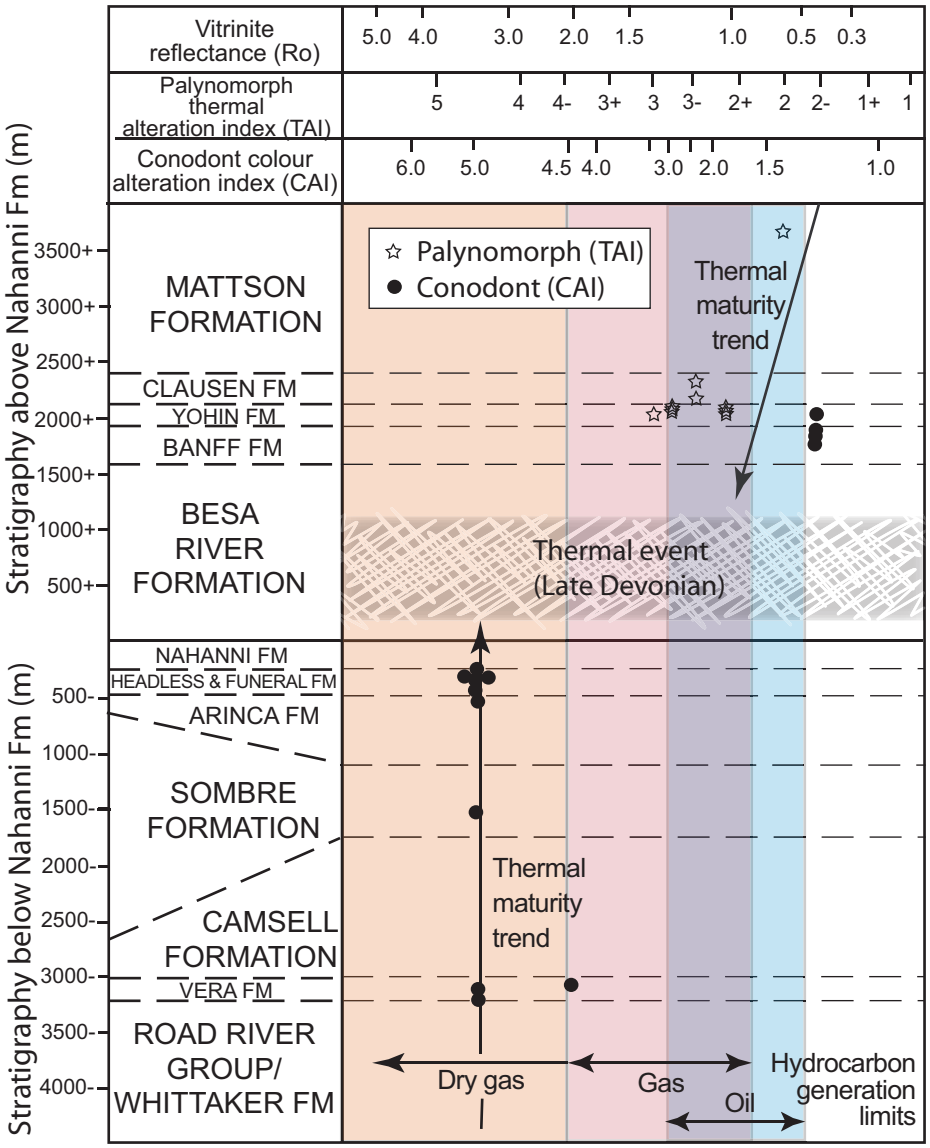


Figure 13. Thermal maturation values from conodont and palnyomorphic studies plotted against stratigraphic position from the Road River Group to the Mattson Formation (from Morrow et al., 1993).

Hinge zones are round and limb dips in the order of 40º. Small folds and slaty cleavage are uncommon (Gordey and Anderson, 1993).

These broad concentric folds suggest deep detachment surfaces in the northern Mackenzie Mountains and shallow ones in the south. Gordey (1981) calculated a detachment level at about 9 km below sea level. At least four levels of detachment have been identified. The shallowest detachment is the Plateau Thrust Fault; deeper detachments extend to the Saline River Formation in the Franklin Mountains, east of the Mackenzie River. The dominant structure at surface is the Plateau Fault, which appears to have detached along a Mesoproterozoic gypsum layer in the Little Dal Group over a distance of 270 km. The hanging-wall strata remained relatively undeformed during a lateral displacement of at least 35 km that placed the Proterozoic Little Dal Group on top of Devonian shale (Cecile and Cook, 1981).

Deformation progressed from west to east in stages from the Early Cretaceous to Paleocene, preceding the emplacement of mid-Cretaceous plutons in the Selwyn Mountains but continuing until rocks as young as Paleocene were faulted and folded in the Franklin Mountains to the east. The limbs of many folds are cut by eastward- and westward-directed right-lateral wrench faults with moderate displacements. Many dextral strike-slip faults may have been localized by Precambrian faults as suggested by regional alignments (MacLean and Cook, 1992; Gordey and Anderson, 1993).

Following the Late Cretaceous, plate interactions did not cause regional deformation in the study area. Continued subduction and modest collisions with small blocks such as the Yakutat block caused continent-

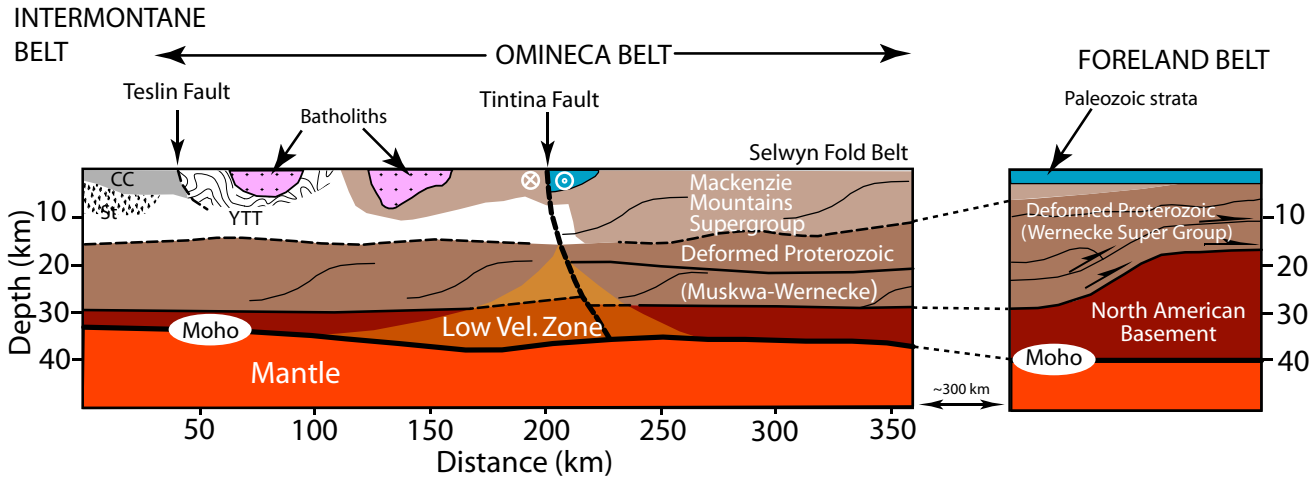


Figure 14. Interpretation of crustal structure in the Nahanni River region, based on Lithoprobe SNORCLE line 3, by Creaser and Spence (2005). The Tintina Fault, rooted at the Moho, has strike-slip motion (cross in circle indicates motion away from the viewer). CC = Cache Creek Terrane; St = Stikine Terrane; YTT = Yukon Tanana Terrane.

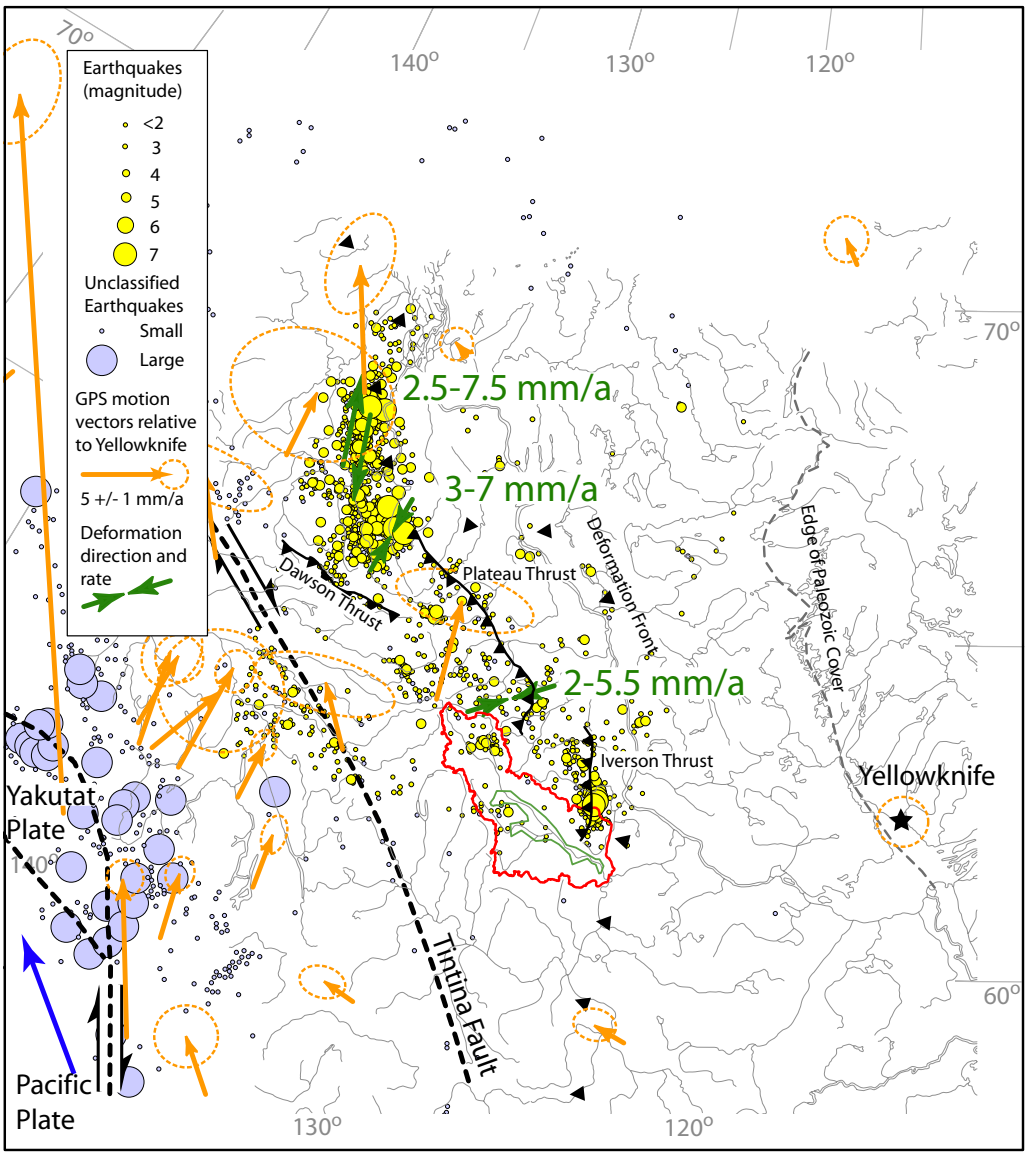


Figure 15. GPS motion vectors (orange) and seismicity (yellow and grey circles) of the Northern Cordillera (from Hyndman et al., 2005b). The vectors represent estimates for the motion of stations relative to Yellowknife. The green arrows indicate the direction and magnitude of deformation with respect to the major regional structures (black).

scale strike-slip crustal faults west of the study area (Hyndman et al., 2005b). These faults, including the Tintina Fault, were initiated during the Late Cretaceous but may have experienced their greatest offsets since the Cenozoic (from 65 to 10 Ma). Total displacement on the Tintina Fault is at least 425 km and may be as much as 800 km (Gabrielse, 1992; Murphy and Mortensen, 2003). Recent geophysical studies have described a complex anastomosing fault zone over 30 km wide extending vertically approximately 20 km into the mid-crust and passing into a diffuse ductile zone to the Moho at 35 km (Clowes et al., 2005; Snyder et al., 2005)(Fig. 14).

Earthquake activity in the Mackenzie Mountains attests to continuing deformation. GPS measurements suggest that Whitehorse at N79ºE is moving toward Yellowknife at 5.2 ± 2.3 mm/a (Fletcher and Frymueller, 1999; Hyndman et al., 2005a,b) (Fig. 15). Paleomagnetic data indicate that this motion has been consistent for at least the last 42 Ma since crystallization of the Beaver River alkaline complex (Symons et al., 2003). Ongoing interaction with the Yakutat tectonic block riding on the Pacific oceanic plate that is subducting beneath the North American continent has been suggested as the driving force behind the deformation (Lewis et al., 2002; Mazzotti and Hyndman, 2002). The movement is being transmitted through the upper crust along shallowly north-dipping thrust faults that extend to the Foreland. The GPS velocity, if constant for 42 Ma, indicates between 80 and 315 km of displacement (Hyndman et al., 2005b). Palinspastic restoration of mapped structures suggests shortening was on the order of 55 km or less (Gordey, 1981) but this disparity could be explained by variable rates of plate movement or uncertainties in the measurement of paleomagnetic poles (Symons et al., 2003). In any case, the motion is significant and continuing. As a result the Foreland Belt is one of the most seismically active zones in Canada, with earthquakes of magnitudes greater than 3.0 taking place five times more frequently than observed for the Rocky Mountains. These include some of the largest earthquakes in Canada, with magnitudes of 6.0 to 7.0 (Cassidy et al., 2005; Hyndman et al., 2005b).

REFERENCES

Aitken, J.D.
1978: Revised models for depositional Grand Cycles, Cambrian of the southern Rocky Mountains Canada; Bulletin of Canadian Petroleum Geology, v. 26, p. 515-542.
1991: Two Late Proterozoic glaciations, Mackenzie Mountains, northwestern Canada; Geology, v. 19, p. 445-448.

Aitken, J.D. and. Cook D.G.
1974: Carcajou Canyon Map Area, District of Mackenzie, Northwest Territories; Geological Survey of Canada, Paper 74-13, 28 p.

Aitken, J.D. and Pugh, D.C.
1984: The Fort Norman and Leith Ridge structures: Major buried Precambrian features underlying Franklin Mountains and Great Bear and Mackenzie Plains; Bulletin of Canadian Petroleum Geology, v. 32, p.139-147.

Anderson, R.G.
1988: An overview of Mesozoic plutonic suites and their associated mineralisation in the northern Cordillera*, in* Recent Advances in the Geology of Granite-Related Mineral Deposits, (ed.) R.P. Taylor and D.F. Strong; Canadian Institute of Mining and Metallurgy and Petroleum, Special Volume 39, p. 96-113.

Bamber, E.W., Henderson, C.M., Richardson, B.C., and McGugan, A.
1992: Carboniferous and Permian stratigraphy of the Foreland Belt*, in* Geology of the Cordilleran Orogeny in Canada, (ed.) H. Gabrielse and C.J. Yorath; Geological Survey of Canada, Geology of Canada, No. 4, DNAG v. G-2, p. 242-265.

Barnes, C., Zailiang, J., and Pohler, S.M.L.
1991: A review of Ordovician conodont paleontology of the Canadian Cordillera*, in* Ordovician to Triassic Conodont Paleontology of the Canadian Cordillera; Geological Survey of Canada, Bulletin 417, p. 27-37.

Barnes, E.M., Groat, L.A., and Falck, H.
2007: A review of the late Cretaceous Little Nahanni Pegmatite Group and associated rare-element mineralization in the Selwyn Basin area, Northwest Territories, in Mineral and Energy Resource Assessment of the Greater Nahanni Ecosystem Under Consideration for the Expansion of the Nahanni National Park Reserve, Northwest Territories, (ed.) D.F. Wright, D. Lemkow, and J.R. Harris; Geological Survey of Canada, Open File 5344, p. 191-202.

Bassett, H.G. and Stout, J.G.
1967: Devonian of Western Canada*, in* International Symposium on the Devonian System, (ed.) D.H. Oswald; Society of Petroleum Geologists, v. 1, p. 717-752.

Baudet, D., Aitken J.D., and Vanguestaine, M.
1989: Palynology of uppermost Proterozoic and lowermost Cambrian formations, central Mackenzie Mountains, northwestern Canada; Canadian Journal of Earth Sciences, v. 26, p. 129-148.

Bell, R.T. and Jefferson, C.W.
1987: An hypothesis for an Australian-Canadian connection in the Late Proterozoic and the birth of the Pacific Ocean*, in* An International Congress of the Geology, Structure, Mineralisation and Economics of the Pacific Rim; The Australasian Institute of Mining and Metallurgy, Proceedings of the Pacific Rim Congress,1987, Parkville, Victoria, p. 39-50.

Bleeker, W.
2003: The late Archean Record: A puzzle in ca. 35 pieces; Lithos, v. 71, p.99-134.

Blusson, S.L.
1968: Geology, Vicinity of Canada Tungsten Mine, Yukon Territory and District of Mackenzie; Geological Survey of Canada, Preliminary Map 4-1967.
1971: Sekwi Mountain Map Area; Geological Survey of Canada, Paper 71-22.

Bond, G.C. and Kominz, M.A.
1984: Construction of tectonic subsidence curves for the early Paleozoic miogeocline, southern Canadian Rocky Mountains: Implications for subsidence mechanisms, age of breakup and crustal thinning; Geological Society of America Bulletin, v. 95, p. 155-173.

Bowring, S. A., Erwin, D.H., Jin, Y.G., Martin, M.W., Davidek, K., and Wang, W.
1998: U/Pb zircon geochronology and tempo of the end-Permian mass extinction; Science, v. 280, p. 1039-1045.

Buchan, K.L. and Ernst, R.E.
2004: Diabase dyke swarms and related units in Canada and adjacent regions; Geological Survey of Canada, Map 2022A, 39 p.

Butrenchuk, S.B.
1988: Phosphate Inventory: Northeastern British Columbia*, in* Canada/British Columbia Mineral Development Agreement, British Columbia Ministry of Energy Mines and Petroleum Resources, Geological Fieldwork 1987, Paper 1988-1, p. 397-411.

Campbell, R.B.
1967: Reconnaissance Geology of Glenlyon Map Area, Yukon Territory (105L); Geological Survey of Canada, Memoir 352, 92 p.

Carne, R.C.
1979: Geological setting and stratiform lead-zinc-barite mineralization, Tom Claims, Yukon Territory; Department of Indian Affairs and Northern Development, Open File Report EGS 1979-4, 30 p.

Carrière, J.J. and Sangster, D.F.
1999: A Multidisciplinary Study of Carbonate-Hosted Zinc-Lead Internalization in the Mackenzie Platform (a.k.a. Blackwater and Lac de Bois platforms) Yukon and Northwest Territories, Canada; Geological Survey of Canada, Open File 3700, 15 p.

Cassidy, J.F., Rogers, G.C., and Ristau, J.
2005: Seismicity in the vicinity of the SNORCLE corridors of the northern Canadian Cordillera; Canadian Journal of Earth Sciences, v. 42, p. 1137-1148.

Cecile, M.P.
2000: Geology of the Northeastern Niddery Lake Map Area, East-central Yukon and Adjacent Northwest Territories; Geological Survey of Canada, Bulletin 553, 102 p.

Cecile, M.P and Cook, D.G.
1981: Structural Cross-Section Northern Selwyn and Mackenzie Mountains, Yukon and District of Mackenzie; Geological Survey of Canada, Open File 807.

Cecile, M.P., Morrow, D.W., and Williams, G.K.
1997: Early Paleozoic (Cambrian to Early Devonian) tectonic framework, Canadian Cordillera; Bulletin of Canadian Petroleum Geology, v. 45, p. 654-674.

Chartrand, F.M., Brown, A.C., and Kirkham, R.V.
1989: Diagenesis, Sulphides and Metal Zoning in the Redstone Copper Deposit, Northwest Territories*, in* Sediment-Hosted Stratiform Copper Deposits, (ed.) R.W.Boyle, A.C. Brown, C.W. Jefferson, E.C. Jowett, and R.V. Kirkham; Geological Association of Canada, Special Paper 36, p. 189-206.

Clowes, R.M., Hammer, P.T., Fernandez-Viejo, G., and Welford, J.K.
2005: Lithospheric structure in northwestern Canada from Lithoprobe seismic refraction and related studies: A synthesis; Canadian Journal of Earth Sciences, v. 42, p. 1277-1293.

Colpron, M., Logan, J.M., and Mortensen, J.K.
2002: U-Pb zircon ages constraint for late Neoproterozoic rifting and initiation of the lower Paleozoic margin of western Laurentia; Canadian Journal of Earth Sciences, v. 39, p. 133-143.

Colpron, M., Nelson, J.L., and Murphy, D.C.
2007: Northern Cordilleran terranes and their interactions through time; GSA Today, v. 17, p. 4-10.

Cook, D.G.
1992: Mackenzie Mountains, Franklin Mountains and Colville Hills*, in* Geology of the Cordilleran Orogeny in Canada, (ed.) H. Gabrielse and C.J. Yorath; Geological Survey of Canada, Geology of Canada No. 4, DNAG v. G-2, p. 642-647.

Cook, D.G. and Maclean, B.C.
1995: The intracratonic Paleoproterozoic Forward Orogeny, and implication for regional correlation, Northwest Territories, Canada; Canadian Journal of Earth Sciences, v. 32, p. 1991-2008.

Cook, F.A. and Erdmer, P.
2005: An 1800 km cross-section of the lithosphere through the northwestern North American plate: Lessons from 4.0 billion years of Earth's history; Canadian Journal of Earth Sciences, v. 42, p. 1295-1311.

Cook, F.A., Dredge, M., and Clark, E.A.
1992: The Proterozoic Fort Simpson structural trend in northwestern Canada; Geological Society of America Bulletin, v. 104, p. 1121-1137.

Cook, F.A., Hall, K.W., and Lynn, C.E.
2005: The edge of northwestern North America at ~1.8 Ga; Canadian Journal of Earth Sciences, v.42, p. 983-997.

Creaser, B. and Spence, G.
2005: Crustal Structure across the northern Cordillera, Yukon Territory, from seismic wide-angle studies: Omineca Belt to Intermontane Belt; Canadian Journal of Earth Sciences, v. 42, p. 1187-1203.

Davies, G.R. and Smith, L.B.
2006: Structurally controlled hydrothermal dolomite reservoir facies: An overview; American Association of Petroleum Geologists, Bulletin, v. 90, p. 1641-1690.

Delaney, G.D.
1981: The mid Proterozoic Wernecke Supergroup, Wernecke Mountains, Yukon Territory*, in* Proterozoic Basins of Canada, (ed.) F.H.A. Campbell; Geological Survey of Canada, Paper 82-10, p 1-24.

Dewing, K., Sharp, R.J., Ootes, L., Turner, E.C., and Gleeson, S.
2006: Geological assessment of known Zn-Pb showings, Mackenzie Mountains, Northwest Territories; Geological Survey of Canada, Current Research, 2006-A4, 12 p.

Dixon, J.
1986: Cretaceous to Pleistocene Stratigraphy and Paleogeography, Northern Yukon and Northwestern District of Mackenzie; Bulletin of Canadian Petroleum Geology, v. 34, p. 49-70.
1999: Mesozoic-Cenozoic Stratigraphy of the Northern Interior Plains and Plateaux, Northwest Territories; Geological Survey of Canada, Bulletin 536, 56 p.

Douglas, R.J.W. and Norris, D.K.
1961: Camsell Bend and Root River Map Areas, District of Mackenzie; Geological Survey of Canada, Paper 61-33.

Dusel-Bacon, C., Lanphere, M.A., Sharp, W.D., Layer, P.W., and Hansen, V.L.
2002: Mesozoic thermal history and timing of structural events for the Yukon-Tanana Upland, east-central Alaska: $^{40}Ar/^{39}Ar$ data from metamorphic and plutonic rocks; Canadian Journal of Earth Sciences, v. 39, p. 1013-1051.

Eisbacher, G.H.
1981: Sedimentary tectonics and glacial record in the Windermere Supergroup, Mackenzie Mountains, northwestern Canada; Geological Survey of Canada, Paper 80-27, 40 p.

England, T.D.J and R.M Bustin, R.M.
1985: Effect of thrust faulting on organic maturation in the southeastern Canadian Cordillera; Organic Geochemistry, v. 10, p. 609-616.

English, J.M. and Johnston, S.T.
2004: The Laramide Orogeny: What were the driving forces? International Geology Review 46, p. 833-838.

Eyles, N. and Januszczak, N.
2004: 'Zipper-rift': A tectonic model for Neoproterozoic glaciations during the breakup of Rodinia after 750 Ma; Earth Science Reviews, v. 65 p. 1-73.

Fletcher, H.J. and Frymueller, J.T.
1999: New GPS constrains on the motion of the Yakutat block; Geophysical Research Letters, v. 26, p. 3029-3032.

Fritz, W.H.
1972: Lower Cambrian Trilobites from the Sekwi Formation Type Section Mackenzie Mountains, Northwestern Canada; Geological Survey of Canada, Bulletin 212, 58 p.
1980: International Precambrian-Cambrian Boundary Working Group's 1979 field study to Mackenzie Mountains, Northwest Territories, Canada, *in* Current Research Part A; Geological Survey of Canada Paper 80-1A, p.41-45.

Fritz, W.H., Narbonne, G., and Gordey, S.P.
1983: Strata and trace fossils near the Precambrian-Cambrian boundary, Mackenzie, Selwyn and Wernecke Mountains, Yukon and Northwest Territories, *in* Current Research, Part B; Geological Survey of Canada Paper 83-1B, p. 365-375.

Fritz, W.H., Cecile, M.P., Norford, B.S., Morrow, D., and Geldsetzer, H.H.J.
1992: Cambrian to Middle Devonian assemblages, *in* Geology of the Cordilleran Orogeny in Canada, (ed.) H. Gabrielse and C.J. Yorath; Geological Survey of Canada, Geology of Canada No. 4, Decade of North American Geology (DNAG), v. G-2, p. 151-218.

Gabrielse, H.
1967: Tectonic evolution of the northern Canadian Cordillera; Canadian Journal of Earth Sciences, v .4, p. 271-298.
1992: Structural Styles, *in* Geology of the Cordilleran Orogeny in Canada, (ed.) H. Gabrielse and C.J. Yorath; Geological Survey of Canada, Geology of Canada No. 4, Decade of North American Geology (DNAG), v. G-2, p. 571-675.

Gabrielse, H. and Blusson, S. L.
1969: Geology of Coal River map Area, Yukon Territory and District of Mackenzie [95d]; Geological Survey of Canada, Paper 68-38, 22 p.

Gabrielse, H. and C.J. Yorath
1992: Tectonic synthesis, *in* Geology of the Cordilleran Orogeny in Canada, (ed.) H. Gabrielse and C.J. Yorath; Geological Survey of Canada, Geology of Canada No. 4, Decade of North American Geology (DNAG), v. G-2, p. 679-705.

Gabrielse, H., Blusson, S.L., and Roddick, J.A.
1973: Geology of Flat River, Glacier Lake and Wrigley Lake map-areas, District of Mackenzie and Yukon Territory; Geological Survey of Canada, Memoir 366 (Parts I and II), 421 p.

Gabrielse, H., Monger, J.W.H., Wheeler, J.O., and Yorath, C.J.
1992: Morphogeological belts, tectonic assemblages and terranes, *in* Geology of the Cordilleran Orogeny in Canada, (ed.) H. Gabrielse and C.J. Yorath; Geological Survey of Canada, Geology of Canada No. 4, Decade of North American Geology (DNAG), v. G-2, p. 15-38.

Garven, G. and Freeze, R.A.
1984: Theoretical analysis of the role of groundwater flow in the genesis of stratabound ore deposits: 2. Quantitative results; American Journal of Science, v. 284, p. 1125-1174.

Gibson, D.W.
1992: Triassic strata of the Foreland Basin, *in* Geology of the Cordilleran Orogeny in Canada, (ed.) H. Gabrielse and C.J. Yorath; Geological Survey of Canada, Geology of Canada No. 4, Decade of North American Geology (DNAG), v. G-2, p. 265-276.

Goodfellow, W.D. and Jonasson, I.R.
1986: Environment of formation of the Howards Pass (XY) Zn-Pb deposits, Selwyn Basin, Yukon and Northwest Territories, *in* Mineral Deposits of Northern Cordillera, (ed.) J.A. Morin; Canadian Institute of Mining and Metallurgy and Petroleum, Special Volume 37, p. 19-50.

Goodfellow, W.D., Jonasson, I.R., and Morganti, J.M.
1983: Zonation of chalcophile elements about the Howards Pass (XY) Zn-Pb deposit Selwyn Basin,Yukon; Journal of Geochemical Exploration, v. 19, p 503-542.

Goodfellow, W.D., Cecile, M.P., and Leybourne, M.I.
1995: Geochemistry, petrogenesis, and tectonic setting of lower Paleozoic alkalic and potassic volcanic rocks, Northern Canadian Miogeocline; Canadian Journal of Earth Sciences, v. 32, p 1236-1254.

Gordey, S.P.
1981: Geology, Nahanni, Yukon Territory and District of Mackenzie, maps and sections; Geological Survey of Canada, Open File 780.
1992: Devonian-Mississippian clastics of the Foreland and Ominica belts, *in* Geology of the Cordilleran Orogeny in Canada, (ed.) H. Gabrielse and C.J. Yorath; Geological Survey of Canada, Geology of Canada No. 4, Decade of North American Geology (DNAG), v. G-2, p. 230-242.

Gordey, S.P. and Anderson, R.G.
1993: Evolution of the Northern Cordilleran Miogeocline, Nahanni Map Area (105I), Yukon and Northwest Territories; Geological Survey of Canada, Memoir 428, 214 p.

Gordey, S.P., Abbott, J.G., and Orchard, M.J.
1982: Devono-Mississippian (Earn Group) and younger Strata in east-central Yukon, *in* Current Research, Part B; Geological Survey of Canada, Paper 82-1B, p. 93-100.

Gordey, S.P., Abbott, J.G., Tempelman-Kluit, D.J., and Gabrielse, H.
1987: "Antler" clastics in the Canadian Cordillera; Geology, v. 15, p. 103-107.

Greenwood, H.J., Woodsworth, G.J., Read, P.B., Ghent, E.D., and Evenchick, C.A.
1992: Metamorphism, *in* Geology of the Cordilleran Orogeny in Canada, (ed.) H. Gabrielse and C.J. Yorath; Geological Survey of Canada, Geology of Canada No. 4, Decade of North American Geology (DNAG), v. G-2, p. 533-570.

Hadley, M.G. and Jones, B.
1990: Lithostratigraphy and nomenclature of Devonian Strata in the Hay River area, Northwest Territories; Bulletin of Canadian Petroleum Geology, v. 38, p. 332-356.

Halverson, G.P., Hoffman, P.F., Schrag, D.P., Maloof, A.C., Hugh, A., and Rice, N.
2005: Toward a Neoproterozoic composite carbon-isotope record; Geological Society of America Bulletin, v. 117, p. 1181-1207.

Hart, C.J.R. and Lewis, L.L.
2005: Gold Mineralization in the upper Hyland River area: A non-magmatic origin, *in* Yukon Exploration and Geology 2005, (ed.) D.S. Emond, G.D. Bradshaw, L.L. Lewis, and L.H. Weston; Yukon Geological Survey, p. 109-125.

Hart, C. J.R., Goldfarb, R.J., Lewis, L.L., and Mair, J.L.
2004: The northern Cordilleran mid-Cretaceous plutonic province: Ilmenite/magnetite-series granitoids and intrusion-related mineralization; Resource Geology, v. 54, p. 253-280.

Hart, C.J.R., Mair, J.L., Goldfarb, R.J., and Groves, D.I.
2005: Source and redox controls on metallogenic variations in intrusion-related ore systems, Tombstone-Tungsten belt,

Yukon Territory, Canada; Geological Society of America, Special Paper, v. 389, p. 339-356.

Heaman, L.M., LeCheminant, A.N., and Rainbird, R.H.
1992: Nature and timing of Franklin igneous events, Canada: Implications for a late Proterozoic mantle plume and break-up of Laurentia; Earth and Planetary Science Letters, v. 109, p. 117-131.

Heffernan, R.S.
2004: Temporal, geochemical, isotopic and metallogenic studies of mid- Cretaceous magmatism in the Tintina Gold Province, southeastern Yukon and southwestern Northwest Territories, Canada; M.Sc. thesis, University of British Columbia, Vancouver, British Columbia, 83 p.

Héon, D.
2003: Selwyn Basin Metallogeny, Yukon Geology Website http://www.geology.gov.yk.ca/metallogeny/selwyn/intro.html#intro.

Hildebrand, R.S., Hoffman, P.F., and Bowering, S.A.
1987: Tectono-magmatic evolution of the 1.9 Great Bear Magmatic Zone, Wopmay Orogen, northwestern Canada; Journal of Volcanology and Geothermal Research, v. 32, p. 99-118.

Hinds, S.J. and Spratt, D.A.
2005: Stratigraphy, structure and tectonic history of the Pink Mountain Anticline Trutch (94G) and Halfway River (94B) map areas, northeastern British Columbia; Bulletin of Canadian Petroleum Geology, v. 53, p. 84-98.

Hoffman, P.F.
1987: Continental transform tectonics: Great Slave Lake shear zone (ca. 1.9 Ga), northwest Canada; Geology, v. 15, p. 785-788.
1989: Precambrian Geology and tectonic history of North America*, in* The Geology of North America – An overview, (ed.) A.W. Bally and A.R. Palmer; Geological Society of America, Boulder, Colorado, v. A, p. 447-512.

Hoffman, P.F. and Bowering, S.A.
1984: Short-lived 1.9 Ga continental margin and its destruction, Wopmay Orogeny, northwest Canada; Geology, v. 12, p. 68-72.

Hoffman, P.F., Kaufman, A.J., Halverson, G.P., and Schrag, D.P.
1998: A Neoproterozoic Snowball; Earth Science, v. 281, p. 1342-1346.

Hofman, H.J., Narbonne, G.M., and Aitken, J.D.
1990: Ediacaran remains from intertillite beds in northwestern Canada; Geology, v. 18, p. 1199-1202.

Housh, T., Bowering, S.A., and Villeneuve, M.
1989: Lead Isotopic study of early Proterozoic Wopmay Orogen, NW Canada: Role of continental crust in arc magmatism; Journal of Geology, v. 97, p. 735-747.

Hunt, J., Baker, T., and Thorkelson, D.
2005: Regional-scale Proterozoic IOCG-mineralized breccia systems: Examples from the Wernecke Mountains, Yukon, Canada; Mineralium Deposita, v. 40, p. 492-512.

Hyndman, R.D., Cassidy, J.F., Adams, J., Rogers, G.C., and Mazzotti, S.
2005a: Earthquakes and Seismic Hazard in the Yukon-Beaufort-Mackenzie; Canadian Society of Exploration Geophysicists Recorder, May 2005, p. 32-66.

Hyndman, R.D., Flueck, P., Mazzotti, S., Lewis, T.J., Ristau, J., and Leonard, L.
2005b: Current Tectonics of the northern Canadian Cordillera; Canadian Journal of Earth Sciences, v. 42, p. 1117-1136.

Hynes, G.F. and Dixon, J.M.
2005: Geological Mapping and analogue modeling of the Liard, Kotaneelee and Tlogotsho Ranges, Northwest Territories; Bulletin of Canadian Petroleum Geology, v. 53, p. 67-83.

Iizuka, T., Horie, K., Komiya, T., Maruyama, S., Hirata, T., Hidaka, H., and Windley, B.F.
2006: 4.2 Ga zircon xenocryst in an Acasta gneiss from northwestern Canada: Evidence for early continental crust; Geology, v. 34, p. 245-248.

Irwin, S.E.B. and M.J. Orchard
1991: Upper Devonian – Lower Carboniferous conodont biostratigraphy of the Earn Group and overlying units, northern Canadian Cordillera*, in* Ordovician to Triassic Conodont Paleontology of the Canadian Cordillera; Geological Survey of Canada, Bulletin 417, p. 185-213.

Jackson, D.E. and Lenz, A.C.
1962: Zonation of Ordovician and Silurian graptolites of northern Yukon Canada; American Association of Petroleum Geologists Bulletin, v. 46, p. 30-45.

Jackson, D.E. and Norford, B.S.
2004: Biostratigraphical and ecostratigraphical significance of Tremadoc (Ordovician) graptolite faunas from the Misty Creek Embayment and Selwyn Basin in Yukon and Northwest Territories; Canadian Journal of Earth Sciences, v. 41. p. 331-348.

James, N.P., Narbonne, G.M., and Kyser, T.K.
2001: Late Neoproterozoic cap carbonates, northwestern Canada: Precipitation and global glacial meltdown; Canadian Journal of Earth Sciences, v. 38, p. 1229-1262.

James, P., Narbonne, G.M., Dalrymple, R.W., and Kyser, T. K.
2005: Glendonites in Neoproterozoic low-latitude, interglacial, sedimentary rocks, northwest Canada: Insights into the Cryogenian ocean and Precambrian cold-water carbonates; Geology, v. 33, p. 9-12.

Jefferson, C.W. and Parish, R.R.
1989: Late Proterozoic stratigraphy, U-Pb zircon ages and rift tectonics, Mackenzie Mountains, northwestern Canada; Canadian Journal of Earth Sciences, v. 26, p. 1784-1801.

Jefferson, C.W. and Young, G.M.
1988: Late Proterozoic orange-weathering stromatolite biostrome, Mackenzie Mountains and western Arctic Canada*, in* Reefs in Canada and Adjacent Areas, (ed.) H. Geldsetzer; Canadian Society of Petroleum Geologists, Memoir 13, p. 72-80.

Jefferson, C.W., Kilby, D.B., Piagage, L.C., and Roberts, W.J.
1983: The Cirque barite zinc-lead deposits, northeastern British Columbia*, in* Sediment-Hosted Stratiform Lead-Zinc Deposits, (ed.) D.F. Sangster; Mineralogical Association of Canada, Short Course Handbook, p. 121-140.

Jefferson, C.W., Spirito, W.A., and Hamilton, S.M.
2003: Geological setting, Chapter 3 *in* Non-Renewable Mineral and Energy Resource Potential of the Proposed Extensions to Nahanni National Park Reserve, Northern Cordillera, Northwest Territories, (ed.) C.W. Jefferson and W. Spirito; Geological Survey of Canada, Open File 1686, p. 3-1 to 3-21.

Jin, J. and Chatterton, B.D.E.
1997: Latest Ordovician-Silurian articulate brachiopods and biostratigraphy of the Avalanche Lake area, southwestern District of Mackenzie, Canada; Palaeontographica Canadiana, v. 13, p. 52-59.

Jowett, D.M.S. and Schröder-Adams, C.J.
2005: Paleoenvironments and regional stratigraphic framework of the Middle-Upper Albian Lepine Formation in the Liard Basin, Northern Canada; Bulletin of Canadian Petroleum Geology, v. 53, p. 25-50.

Kalkreuth, W., Langenberg, W., and McMechan, M.
1989: Regional Coalification pattern of Lower Cretaceous coal-bearing strata, Rocky Mountain Foothills and foreland

Canada-implications for future exploration; International Journal of Coal Geology, v. 13, p. 261-302.

Kerans, C., Ross, G.M., Donaldson, J.A., and Geldsetzer, H.J.
1981: Tectonism and depositional history of the Helikian Hornby Bay and Dismal Lakes groups, District of Mackenzie*, in* Proterozoic Basins of Canada, (ed.) F.H.A. Campbell; Geological Survey of Canada, Paper 81-10, p. 157-182.

Knoll, A.H., Walter, M., Narbonne, G., and Christie-Blick, N.
2004: The Ediacaran Period: A New Addition to the Geological Time Scale; Unpublished report of the Terminal Proterozoic Subcommission of the International Commission on Stratigraphy. 35 p. Http://www.stratigraphy.org/ediacaran/Knoll_et_al_2004a.pdf

Lane, L.S.
2004: Central Foreland NATMAP: Stratigraphic and Structural Evolution of the Central Foreland; Bulletin of Canadian Petroleum Geology, v. 52, p. 273-275.
2005: Central Foreland NATMAP: Stratigraphic and Structural Evolution of the Central Foreland; Bulletin of Canadian Petroleum Geology, v. 53, p. 1-4.

Leckie, D.A. and Potocki, D.J.
1998: Sedimentology and petrography of marine shelf sandstones of the Cretaceous Scatter and Garbutt formations, Liard Basin, northern Canada; Bulletin of Canadian Petroleum Geology, v. 46, p. 30-50.

Leckie, D.A., Potocki, D.J., and Visser, K.
1991: The Lower Cretaceous Chinkeh Formation: A frontier-type play in the Liard Basin of Western Canada; American Association of Petroleum Geologists Bulletin, v. 75, p. 1324-1352.

Lewis, T.J., Hyndman, R.D., and Flueck, P.
2002: Thermal Controls on present tectonic in northern Canadian Cordillera; Lithoprobe Report 82, p. 15-16.

Long, D.G.F.
1986: Coal in Yukon*, in* Mineral Deposits of the Northern Cordillera, (ed.) J.A. Morin; Canadian Institute of Mining and Metallurgy and Petroleum, Special Volume 37, p. 311-318.

Lowey, G.W.
1990: Occurrence of turbidites in the Besa River Formation (Devonian-Mississippian), Northwest Territories; Bulletin of Canadian Petroleum Geology, v. 38, p. 426-428.

Ludvigsen, R.
1975: Ordovician formations and faunas, southern Mackenzie Mountains; Canadian Journal of Earth Sciences, v. 12, p. 663-697.

Lydon, J.W., Goodfellow, W.D., and Jonasson, I.
1985: A General Genetic Model for Stratiform Baritic Deposits of the Selwyn Basin, Yukon Territory and District of Mackenzie*, in* Current Research, Part A; Geological Survey of Canada, Paper 85-1A, p.651-660.

Maclean, B.C. and Cook, D.G.
1992: The influence of Proterozoic structures on the development of Laramide structures, northern Interior Plains Northwest Territories, Canada; Bulletin of Canadian Petroleum Geology, v.40, p. 207-221.
2004: Revisions to the Paleoproterozoic Sequence A, based on reflection seismic data across the western plains of the Northwest Territories, Canada; Precambrian Research, v. 129, p. 271-289.

MacLean, B.C. and Morrow, D.W.
2004: Bovie Structure: Its evolution and regional context; Bulletin of Canadian Petroleum Geology, v. 52, p. 302-324.

MacNaughton, R., Dalrymple, R., and Narbonne, G.M.
1997a: Early Cambrian braid-delta deposits, Mackenzie Mountains, northwestern Canada; Sedimentology, v. 44 p. 587-609.
1997b: Multiple orders of relative sea-level change in an earliest Cambrian passive-margin succession, Mackenzie Mountains, Northwestern Canada; Journal Sedimentary Research, v. 67, p. 622-637.

MacNaughton, R.B., Narbonne, G.M., and Dalrymple, R.W.
2000: Neoproterozoic slope deposits, Mackenzie Mountains, northwestern Canada: Implications for passive-margin development and Ediacaran faunal ecology; Canadian Journal of Earth Sciences, v. 37, p. 997-1020.

Mair, J.L., Hart, C.R., and Stephens, J.R.
2006: Deformation history of the northwestern Selwyn Basin, Yukon, Canada: Implications for orogen evolution and mid-Cretaceous Magmatism; Geological Society of America Bulletin, v. 118, p. 304-323.

Majorowicz, J.A., Jessop, A.M., and Lane, L.S.
2005: Regional heat flow pattern and lithospheric geotherms in northeastern British Columbia and adjacent Northwest Territories, Canada; Bulletin of Canadian Petroleum Geology, v. 53 p. 51-66.

Mako, D.A. and Wayne C. Shanks, W.C. III
1984: Stratiform sulfide and barite-fluorite mineralization of the Vulcan prospect, Northwest Territories: Exhalation of basinal brines along a faulted continental margin; Canadian Journal of Earth Sciences, v. 21, p. 78-91.

Marshall, D.D., Groat, L.A. Falck, H., Giuliani, G., and Neufeld, H.
2004: The Lened emerald prospect, Northwest Territories, Canada: Insights from fluid inclusions and stable isotopes with implications from Northern Cordilleran Emerald; Canadian Mineralogist, v. 42, p. 1523-1539.

Mazzotti, S. and Hyndman, R.D.
2002: Yakutat collision and strain transfer across the northern Cordillera; Geology, v. 30, p. 495-498.

McMechan, M.E.
2002: Structural Geometry in the Carbon Creek area of the Rocky Mountain Fold and Thrust belt, Northeastern British Columbia; Bulletin of Canadian Petroleum Geology, v. 50, p. 407-418.

Monahan, P.
2000: Stratigraphy and potential hydrocarbon objectives of Mississippian to lower Cretaceous strata in the eastern Liard Basin area; Government of British Columbia, Crown Publications Inc. Inventory #667, 1 CD-ROM.

Monger, J.W.H., Price, R.A., and Tempelman-Kluit, D.J.
1982: Tectonic accretion and the origin of two metamorphic and plutonic welts in the Canadian Cordillera; Geology, v. 10, p. 70-75.

Morganti, J.M.
1979: The Geology and Ore Deposits of the Howards Pass Area, Yukon and Northwest Territories: The Origin of Basinal Sedimentary Stratiform Sulphide Deposits; Ph.D. thesis, University of British Columbia, Vancouver, British Columbia, 317 p.

Morris, G.A. and Nesbitt, B.E.
1998: Geology and timing of paleohydrological events in the Mackenzie Mountains, Northwest Territories, Canada*, in* Dating a. nd Duration of Fluid Flow and Fluid-Rock interaction, (ed.) J. Parnell; Geological Society, London, Special Publications, v. 144, p. 161-172.

Morrow, D.W.
1998: Regional Subsurface dolomitization: models and constraints; Geoscience Canada, v. 25, p. 57-70.

1999: Lower Paleozoic Stratigraphy of Northern Yukon Territory and Northwestern District of Mackenzie; Geological Survey of Canada, Bulletin 538, p. 202.

Morrow, D.W. and Cook, D.G.
1987: The Prairie Creek Embayment and Lower Paleozoic Strata of the Southern Mackenzie Mountains, Geological Survey of Canada, Memoir 412, 195 p.

Morrow, D.W. and Miles, W.C.
2000: The Beaver River Structure: A cross strike discontinuity of possible crustal dimensions in the southern Mackenzie Fold Belt, Yukon and Northwest Territories, Canada; Bulletin of Canadian Petroleum Geology, v. 48, p. 19-29.

Morrow, D.W., Cumming, G.L., and Koepnick, R.B.
1986: Manetoe Facies – A gas-bearing, megacrystalline, Devonian dolomite, Yukon and Northwest Territories, Canada; American Association of Petroleum Geologists Bulletin, v. 70, p. 702-720.

Morrow, D.W., Cumming, G.L., and Aulstead, K.L.
1990: The Gas-Bearing Devonian Manetoe Facies, Yukon and Northwest Territories; Geological Survey of Canada, Bulletin 400, 54 p.

Morrow, D.W., Potter, J., Richards, B., and Goodarzi, F.
1993: Paleozoic burial and organic maturation in the Liard Basin region, Northern Canada; Bulletin of Canadian Petroleum Geology, v. 41 p. 17-31.

Mortensen, J.K., Hart, C.J.R., Murphy, D.C., and Heffernan, S.
2000: Temporal evolution of early and mid-Cretaceous magmatism in the Tintina Gold Belt*, in* The Tintina Gold Belt: Concepts, Exploration and Discoveries, (ed.) J.L. Jambor; British Columbia and Yukon Chamber of Mines, Special Volume. 2, p. 49-57.

Murphy, D.C. and Mortensen, J.K.
2003: Late Paleozoic and Mesozoic features constrain displacement on Tintina Fault and limit large-scale orogen-parallel displacement in the Northern Cordillera; Geological Association of Canada Annual General Meeting, Program with Abstracts, v. 28, p. 151.

Nakai, S., Halliday, A.N., Kesler, S.E., Jones, H.D., Kyle, J.R., and Lane, T.E.
1993: Rb-Sr dating of sphalerites from Mississippi Valley-type (MVT) ore deposits; Geochimica et Cosmochimica Acta, v. 57, p. 417–427.

Narbonne, G.M. and Aitken, J.D.
1995: Neoproterozoic of the Mackenzie Mountains, northwestern Canada; Precambrian Research, v. 73, p. 101-121.

Narbonne, G.M., Kaufman, A.J., and Knoll, A.H.
1994: Integrated chemostratigraphy and biostratigraphy of the Windermere Supergroup, northwestern Canada: Implications for Neoproterozoic correlations and the early evolution of animals; Geological Society of America Bulletin, v. 106, p. 1281-1292.

Nilsen, T.H. and Stewart, J.H.
1980: The Antler orogeny-Mid-Paleozoic tectonism in western North America; Geology, v. 8, p. 298-302.

Noble, J.P.A and Ferguson, R.D.
1971: Facies and Faunal Relations at the edge of Early Mid Devonian Carbonate shelf, South Nahanni River Area, NWT; Bulletin of Canadian Petroleum Geology, v. 19, p. 570-588.

Norford, B.S. and Orchard, M.J.
1985: Early Silurian Age of Rocks Hosting Lead-Zinc Mineralization at Howards Pass, Yukon Territory and District of Mackenzie; Local Biostratigraphy of Road River Formation and Earn Group; Geological Survey of Canada, Paper 83-18, 35 p.

Nurkowski, J.R.
1984: Coal quality, coal rank variation and its relation to reconstructed overburden, Upper Cretaceous and Tertiary Plains Coals, Alberta, Canada; American Association of Petroleum Geologists Bulletin, v. 68, p. 1967-2001.

Orchard, M.J. and A.D. MacCracken (ed.)
1991: Ordovician to Triassic Conodont Paleontology of the Canadian Cordillera; Geological Survey of Canada, Bulletin 417, 435 p.

Osadetz, K.G., Chen, Z., and Morrow, D.
2003: Petroleum resource assessment of the Tlogotsho Plateau, Nahanni Karst and adjacent areas under consideration for expansion of the Nahanni National Park Reserve, Northern Cordillera and District of Mackenzie*, in* Non-Renewable Mineral and Energy Resource Potential of the Proposed Extensions to Nahanni National Park Reserve, Northern Cordillera, Northwest Territories, (ed.) C.W. Jefferson and W. Spirito; Geological Survey of Canada, Open File 1686, p. 8-1 to 8-36.

Osadetz, K.G., Maclean. B.C., Morrow, D.W. and Hannigan, P.K.
2005: Petroleum Resource Assessment, Peel Plateau and Plain, Yukon Territory, Canada; Geological Survey of Canada, Open File 4841, 94 p.

Paradis, S.
2007: Isotope geochemistry of the Prairie Creek carbonate-hosted zinc-lead-silver deposit, southern Mackenzie Mountains, Northwest Territories, in Mineral and Energy Resource Assessment of the Greater Nahanni Ecosystem Under Consideration for the Expansion of the Nahanni National Park Reserve, Northwest Territories, (ed.) D.F. Wright, D. Lemkow, and J.R. Harris; Geological Survey of Canada, Open File 5344, p. 131-176.

Pelzer E.E.
1966: Mineralogy, Geochemistry and Stratigraphy of Besa River Shale, British Columbia; Bulletin of Canadian Petroleum Geology, v. 14, p.273-321.

Pigage, L.C. and Mortensen, J.K.
2004: Superimposed Neoproterozoic and Early Tertiary alkaline magmatism in the La Biche River area, southeast Yukon Territory; Bulletin of Canadian Petroleum Geology, v. 52, p. 325-342.

Plint, G.A., McCarthy, P.J., and Faccini, U.F.
2001: Nonmarine sequence stratigraphy: Up dip expression of sequence boundaries and systems tracts in a high-resolution framework, Cenomanian Dunvegan Formation, Alberta foreland basin, Canada; American Association of Petroleum Geologists Bulletin, v. 85, p. 1967-2001.

Potter, J., Richards, B., and Cameron, A.R.
1993: The petrology and origin of coals from the Lower Carboniferous Mattson Formation, southwestern District of Mackenzie, Canada, International Journal of Coal Geology, v. 24, p. 113-140.

Pratt, B.R.
1992: Trilobites of the Marjuman and Steptoean stages, (Upper Cambrian), Rabbitkettle Formation, southern Mackenzie Mountains, northwest Canada; Palaeontographica Canadiana, v. 9, 179 p.

Pyle, L. and Barnes, C.R.
2003: Lower Paleozoic stratigraphic and biostratigraphic correlations in the Canadian Cordillera: Implications for tectonic evolution of the Laurentian margin; Canadian Journal of Earth Sciences, v. 40, p. 1739-1753.

Rainbird, R.H., Heaman, L.M, and Young, G.M.
1992: Sampling Laurentia: Detrital zircon geochronology offers evidence for and extensive Neoproterozoic river system

originating from Grenville Orogen; Geology, v. 20, p. 351-354.

Rainbird, R.H., Jefferson, C.W., and Young, G.M.
1996: The early Neoproterozoic sedimentary Succession B of northwestern Laurentia: Correlations and paleogeographic significance; Geological Society of America Bulletin, v. 108, p. 454–470.

Rainbird, R.H., McNicoll, V.J. Theriault, R.J. Heaman, L.M., Abbot, J.G., Long, D.G.F., and Thorkelson, D.J.
1997: Pan-continental river system draining Grenville Orogen recorded by U-Pb and Sm-Nd geochronology of Neoproterozoic quartz arenite and mudrocks, Northwestern Canada; Journal of Geology, v. 105, p. 1-18.

Rasmussen, K.L., Mortensen, J.K., Falck, H. and Ullrich, T.D.
2007: The potential for intrusion-related mineralization within the South Nahanni River MERA area, Selwyn and Mackenzie Mountains, Northwest Territories, in Mineral and Energy Resource Assessment of the Greater Nahanni Ecosystem Under Consideration for the Expansion of the Nahanni National Park Reserve, Northwest Territories, (ed.) D.F. Wright, D. Lemkow, and J.R. Harris; Geological Survey of Canada, Open File 5344, p. 203-278.

Richards, B.C.
1989: Uppermost Devonian and Lower Carboniferous Stratigraphy, Sedimentation, and Diagenesis, Southwestern District of Mackenzie and Southeastern Yukon Territory; Geological Survey of Canada, Bulletin 390, 135 p.

Ross, G.M.
1991: Precambrian Basement in the Canadian Cordillera: An Introduction; Canadian Journal of Earth Sciences, v. 28, p. 1133-1139.

Ross, G.M. and Villeneuve, M.
1996: Geochronology of Stranger Stone in Neoproterozoic Lithoprobe Report #50; Report of the 1996 Combined Meeting March 1-3, 1996, University of Calgary, p. 18-19.

Rowins, S.M. and D.M. Francis
1995: The late Tertiary to Recent Beaver River Alkaline Complex, southeastern Yukon; Geological Society of America, 1995 Annual Meeting Abstracts with Program, p. A46.

Savoy, L.E., Stevenson, R.K., and Mountjoy, E.W.
2000: Provenance of Upper Devonian-Lower Carboniferous Miogeoclinal strata, southeastern Canadian Cordillera: Link between tectonics and sedimentation; Journal of Sedimentary Research, v. 70, p. 181-193.

Sears, J.W. and Price, R.A.
2000: New look at the Siberian connection: No Sweat; Geology, v. 28, p. 423-426.

Smith, M.T., Dickinson, W.R., and Gehrels, G.E.
1993: Contractional nature of Devonian-Mississippian Antler tectonism along the North American continental margin; Geology, v. 21, p. 21-24.

Snyder, D.B., Roberts, B.J., and Gordey, S.P.
2005: Contrasting seismic characteristics of three major faults in northwestern Canada; Canadian Journal of Earth Sciences, v. 42, p. 1223-1237.

Stelck, C.R. and Hedinger, A.S.
1983: Foraminifera of the lower part of the Sully Formation (Upper Albian), northeastern British Columbia; Canadian Journal of Earth Sciences, v. 20, p. 1248-1259.

Stevens, R.D., Delabio, R.N., and Lechance, G.R.
1982: Age determinations and geological studies, K-Ar isotopic ages, Report 15; Geological Survey of Canada, Paper 81-2, p. 23.

Stott, D.F.
1982: Lower Cretaceous Fort St. John Group and Upper Cretaceous Dunvegan Formation of the Foothills and Plains of Alberta, British Columbia, District of Mackenzie and Yukon Territory; Geological Survey of Canada, Bulletin 328, 124 p.

Stott, D.F., Yorath, C.J., and Dixon, J.
1992: The Foreland Belt: Upper Jurassic to Paleogene assemblages, *in* Geology of the Cordilleran Orogeny in Canada, (ed.) H. Gabrielse and C.J. Yorath; Geological Survey of Canada, Geology of Canada No. 4, Decade of North American Geology (DNAG), v. G-2, p. 335-344.

Symons, D.T.A., Pan, H., Sangster, D.F., and Jowett, E.C.
1993: Paleomagnetism of the Pine Point Zn-Pb Deposits; Canadian Journal of Earth Sciences, v. 30, p. 1028-1036.

Symons, T.A., Erdmer, E., and McCausland, P.J.A.
2003: New 42 Ma cratonic North American paleomagnetic pole form the Yukon underscores another Cordilleran paleomagnetism-geology conundrum; Canadian Journal of Earth Sciences, v. 40, p. 1321-1334.

Taylor, A.B.
1995: Geological Summary of the Northern Sector Pb-Zn Trend on the Prairie Creek Property, N.W.T.; San Andreas Resources Corporation, internal document, 32 p.

Tempelman-Kluit, D J.
1979: Transported Cataclasite, Ophiolite and Granodiorite in the Yukon: Evidence of Arc-Continent Collision; Geological Survey of Canada, Paper 79-14, 27 p.

Thorkelson, D.J., Mortensen, J.K., Creaser, R.A., Davidson, G.J., and Abbot, J.G.
2001: Early Proterozoic magmatism in Yukon, Canada: Constraints on the evolution of northwestern Laurentia; Canadian Journal of Earth Sciences, v. 38, p.1479-1494.

Thorkelson, D.J., Abbot, J.G., Mortensen, J.K., Creaser, R.A., Villeneuve, M.E., McNicoll, V.J., and Layer, P.W.
2005: Early and Middle Proterozoic evolution of Yukon, Canada; Canadian Journal of Earth Sciences, v. 42, p. 1045-1071.

Utting, J., Zonnenveld, J.P., McNaughton, R.B., and Fallas, K.M.
2005: Palynostratigraphy, lithostratigraphy and thermal maturity of the Lower Triassic Toad and Grayling, and Monteny formations of western Canada, and comparisons with coeval rocks of the Sverdrup Basin, Nunavut; Bulletin of Canadian Petroleum Geology, v. 53, p. 5-24.

Villeneuve, M.E. and Theriault, R.J.
1991: U-Pb ages and Sm-Nd signature of two subsurface granites from the Fort Simpson magnetic high, northwest Canada; Canadian Journal of Earth Sciences, v. 28, p. 1003-1008.

Welford, J.K., Clowes, R.M., Ellis, R.M. Spence, G.D., Asudeh, I., and Hajnal, Z.
2001: Lithospheric structure across the craton-Cordilleran British Columbia; Canadian Journal of Earth Sciences, v. 38, p. 1169-1189.

Winn, R.D. and Bailes, R.J.
1987: Stratiform lead-zinc sulfides, mudflows, turbidites: Devonian sedimentation along a submarine fault scarp of extensional origin, Jason deposit, Yukon territory, Canada; Geological Society of America Bulletin, v. 98, p. 528-539.

Wright, J. and Miller, D.C.
1986: Rock River coal basin: Geology, gravity survey and interpretation, *in* Mineral Deposits of the Northern Cordillera; (ed.) J.A. Morin; Canadian Institute of Mining and Metallurgy and Petroleum, Special Volume 37, p. 362-371.

Yorath, C.J., Stott, D.F., Dixon, J., Gabrielse, H., Anderson, R.G., Souther, J.G., Woodsworth, G.J., Tipper, H.W., Monger, J.W.H., Sutherland Brown, A., Campbell, R.B., and Dodds, C. J.

1992: Upper Jurassic to Paleogene assemblages, *in* Geology of the Cordilleran Orogeny in Canada, (ed.) H. Gabrielse and C.J. Yorath; Geological Survey of Canada, Geology of Canada No. 4, Decade of North American Geology (DNAG), v. G-2, p. 329-371.

Young, G.M.

1992: Late Proterozoic stratigraphy and the Canada-Australia connection; Geology, v. 20, p. 215-218.

1995: Are Neoproterozoic glacial deposits preserved on the margins of Laurentia related to the fragmentation of two supercontinents?; Geology, v. 23, p. 153-156.

2002: Stratigraphic and tectonic settings of Proterozoic glaciogenic rocks and banded iron formations: Relevance to the snowball Earth debate; Journal of African Earth Sciences, v. 35, p.451-466.

Young, G. M., Jefferson, C.W., Delaney, G.D., and Yeo, G.M

1979: Middle and late Proterozoic evolution of the northern Canadian Cordillera and Shield; Geology, v. 7, p. 125-128.

Yuvan, J., Shelton, K., and Falck, H.

2007: Geochemical investigations of the high-grade quartz-scheelite veins of the Cantung mine, Northwest Territories, in Mineral and Energy Resource Assessment of the Greater Nahanni Ecosystem Under Consideration for the Expansion of the Nahanni National Park Reserve, Northwest Territories, (ed.) D.F. Wright, D. Lemkow, and J.R. Harris; Geological Survey of Canada, Open File 5344, p. 177-190.

APPENDIX 2

Previously published in Yukon Exploration and Geology 2006, (ed.) D.S. Emond, L.L. Lewis, and H. Weston: Yukon Geological Survey, p. 237-250. Reprinted with permission from the Yukon Geological Survey.

Morphological and compositional analysis of placer gold in the South Nahanni River drainage, Northwest Territories

K.L. Rasmussen[1] and J.K. Mortensen[2]
Department of Earth and Ocean Sciences, University of British Columbia

H. Falck[3]
Geological Survey of Canada/Northwest Territories Geoscience Office

Rasmussen, K.L., Mortensen, J.K. and Falck, H., 2007. Morphological and compositional analysis of placer gold in the South Nahanni River drainage, Northwest Territories. *In:* Yukon Exploration and Geology 2006, D.S. Emond, L.L. Lewis and L.H. Weston (eds.), Yukon Geological Survey, p. 237-250.

ABSTRACT

Placer gold has been reported in small amounts throughout the South Nahanni river drainage; however, the original source of the gold is uncertain. This study focuses on two types of placer gold in the area: (1) locally abundant grains derived from near Selena Creek, and (2) scattered grains recovered from streams throughout the South Nahanni drainage area. A shape analysis of all gold grains was completed and representative grains from each sample population were selected for imaging on the scanning electron microscope, along with analysis for Au-Ag-Cu-Hg values on the electron microprobe. The gold grains are typically >700 fineness and mercury is below detection levels (<0.20%). Approximately half the grains analysed from the Selena Creek area registered near to, or slightly greater than, detection levels of copper (<0.04%), whereas the majority of grains from the isolated showings had copper contents below detection levels. The results are compared with published morphological and compositional data for placer and lode gold in other regions.

RÉSUMÉ

La présence d'or placérien a été signalée en petite quantité dans l'ensemble du bassin versant de la rivière Nahanni Sud dans les Territoires du Nord-Ouest, mais une grande conjecture persiste quant à son origine. Cette étude est focalisée sur les deux types d'or placérien trouvés dans la région : 1) les grains abondants par endroits près du ruisseau Selena et 2) les grains épars récupérés dans des cours d'eau dans l'ensemble du bassin. Une analyse de la forme de tous les grains d'or a été effectuée et des grains représentatifs de chaque population échantillonnée ont été sélectionnés à des fins d'imagerie au microscope électronique à balayage suivie d'analyses pour Au-Ag-Cu-Hg à la microsonde électronique. De manière caractéristique le titre des grains est supérieur à 700 et leur teneur en mercure est inférieure aux seuils de détection (< 0,20 %). Approximativement la moitié des grains provenant de la région du ruisseau Selena ne présentaient que des concentrations de cuivre légèrement supérieures aux seuils de détection (< 0,04 %), alors que la majorité des grains provenant d'indices isolées renfermaient des concentrations de cuivre inférieures aux seuils de détection. Les résultats obtenus sont comparés aux données de morphologie et de composition publiées pour l'or placérien et l'or filonien provenant d'autres régions.

[1]*6339 Stores Road, Vancouver, British Columbia, Canada, V6T 1Z4, krasmuss@eos.ubc.ca*

[2]*jmortens@eoc.ubc.ca*

[3]*P.O. Box 1500, 4601-B 52nd Avenue, Yellowknife, NT, Canada, X1A 2R3*

Rasmussen, K.L. Mortensen, J.K., and Falck, H., 2007, Appendix 2. Morphological and compositional analysis of placer gold in the South Nahanni River drainage, Northwest Territories, *in* Mineral and Energy Resource Assessment of the Greater Nahanni Ecosystem Under Consideration for the Expansion of the Nahanni National Park Reserve, Northwest Territories, (ed.) D.F. Wright, D. Lemkow, and J.R. Harris; 0eological Survey of Canada, Open File 5344, p. 367-380 (also Yukon Exploration and Geology 2006, (ed.) D.S. Emond, L.L. Lewis, and L.H. Weston; Yukon Geological Survey, p. 237-250).

INTRODUCTION

Since the 1920s, the South Nahanni River has been known as a 'dangerous river' by the people entering the region for various reasons (e.g., trapping, route to the Klondike, adventure, etc.), including the prospectors who were searching for gold in the area. An account of their efforts has been partially preserved by the names of the lakes, creeks and felsic intrusions, many of which are named after many of the early prospectors; Deadman and Headless valleys give some indication of the fates of those who did not survive their time in the region. The stories are also documented in books such as R.M. Patterson's "Dangerous River" (1953) and P. Berton's "The Mysterious North" (1956). Certainly the fate of the McLeod Brothers, who are alleged to have been discovered without their heads in the early 1900s after reportedly having found a mother-lode, or a 'good prospect', made for much speculation as to the cause of their deaths (e.g., cannibal Indian tribes, eight-foot-tall sasquatches, scavenging grizzly bears), and even more so with respect to the location of their lost gold mine (Turner, 1975).

While literature on the legends abounds (with varying degrees of exaggeration), the geological understanding of the source of the placer gold has lagged far behind. A study of placer gold-grain morphology and composition for the South Nahanni River watershed of the Selwyn and Mackenzie mountains, Northwest Territories, was undertaken in order to investigate the nature of, and to make inferences as to the origin of, the placer gold (Fig. 1). The study was initiated as part of the Mineral and Energy Resource Assessment (MERA II) conducted by the Geological Survey of Canada for Parks Canada over the 2004-2005 field seasons (Falck and Wright, 2007, in press). The purpose of the MERA II was to evaluate the precious- and base-metal potential of the South Nahanni River area; however, the question as to the source of scattered deposits of placer gold in the area was not fully addressed. This study aims to develop a preliminary characterization of the known placer gold in the area, in order to determine whether or not the gold is locally derived. This study will also make suggestions for possible mineral deposit settings from which the gold may have been derived (e.g., intrusion-related skarns or sheeted veins, Carlin-type sediment-hosted disseminated, orogenic vein, etc.).

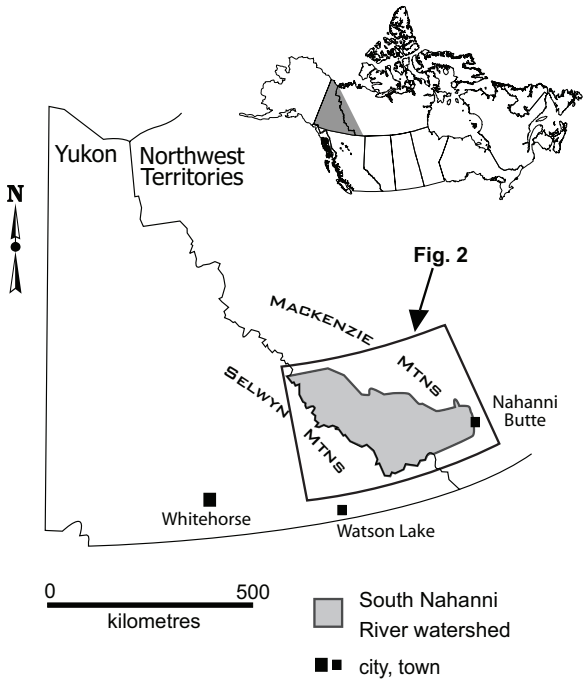


Figure 1. *Location of the South Nahanni River watershed in the Selwyn and Mackenzie mountains, southwestern Northwest Territories (adapted from Mortensen et al., 2000).*

To characterize and determine the source of the placer gold in the area, samples from two 'types' of placer occurrences were investigated:

(1) Locally abundant placer gold grains were recovered from Chuck Creek, in the Selena Creek area (referred to as the 'Chuck sample'). This sample was collected adjacent to the intermediate to mafic volcanic rocks hosting the Chuck copper (-gold) mineral showings documented in the Northern Minerals Database[4] (NORMIN) (Fig. 2). This area also has several known placer gold occurrences, as documented in NORMIN. Locations of these placer occurrences are shown in Figure 2. Gold grains were panned from a sample of light-coloured, clay-rich material with small limestone fragments. In the field, this material underlies an immature, cobble-boulder lag in the streambed. It is uncertain whether the clay-rich material is an oxidized till forming a basal layer of the creek, or part of an underlying linear feature, such as a fault (T. Christie and H. Smith, writ. comm., 2006). The gold grains were separated by hand from a concentrate composed predominantly of ilmenite-magnetite-barite, but includes specular hematite and an iron- and/or calcium-rich garnet (no sulphide minerals were present).

[4]*NWT Geoscience Office, Government of the Northwest Territories, 2006. Northern Minerals Database (NORMIN), www.nwtgeoscience.ca/normin*

(2) A collection of placer gold grains referred to as 'isolated samples' (36 grains from 8 sample locations and 18 unidentified/unlocated grains) were recovered from approximately 450 stream silt and heavy mineral concentrate (HMC) samples (Fig. 2). These samples were collected during the 1985-1987 field seasons for an earlier Mineral and Energy Resource Assessment (MERA I) conducted over the Ragged Ranges and Nahanni Karst and Tlogotsho Plateau regions (Spirito *et al.*, 1988; Jefferson and Pare, 1991) of the watershed (Fig. 2).

The distribution of the isolated samples is biased due to the limited HMC sample coverage within the entire South Nahanni River watershed. Areas that are not represented by the 'isolated placer gold samples', and which are thought to have a high potential for locally derived placer gold, are the southwestern corner where several placer gold occurrences are documented in NORMIN and where the Chuck sample is located, as well as the northern portion of the field area that has at least one primary intrusion-associated gold showing documented in NORMIN (Fig. 2). We are also restricted by the relatively small number of gold grains included in the isolated

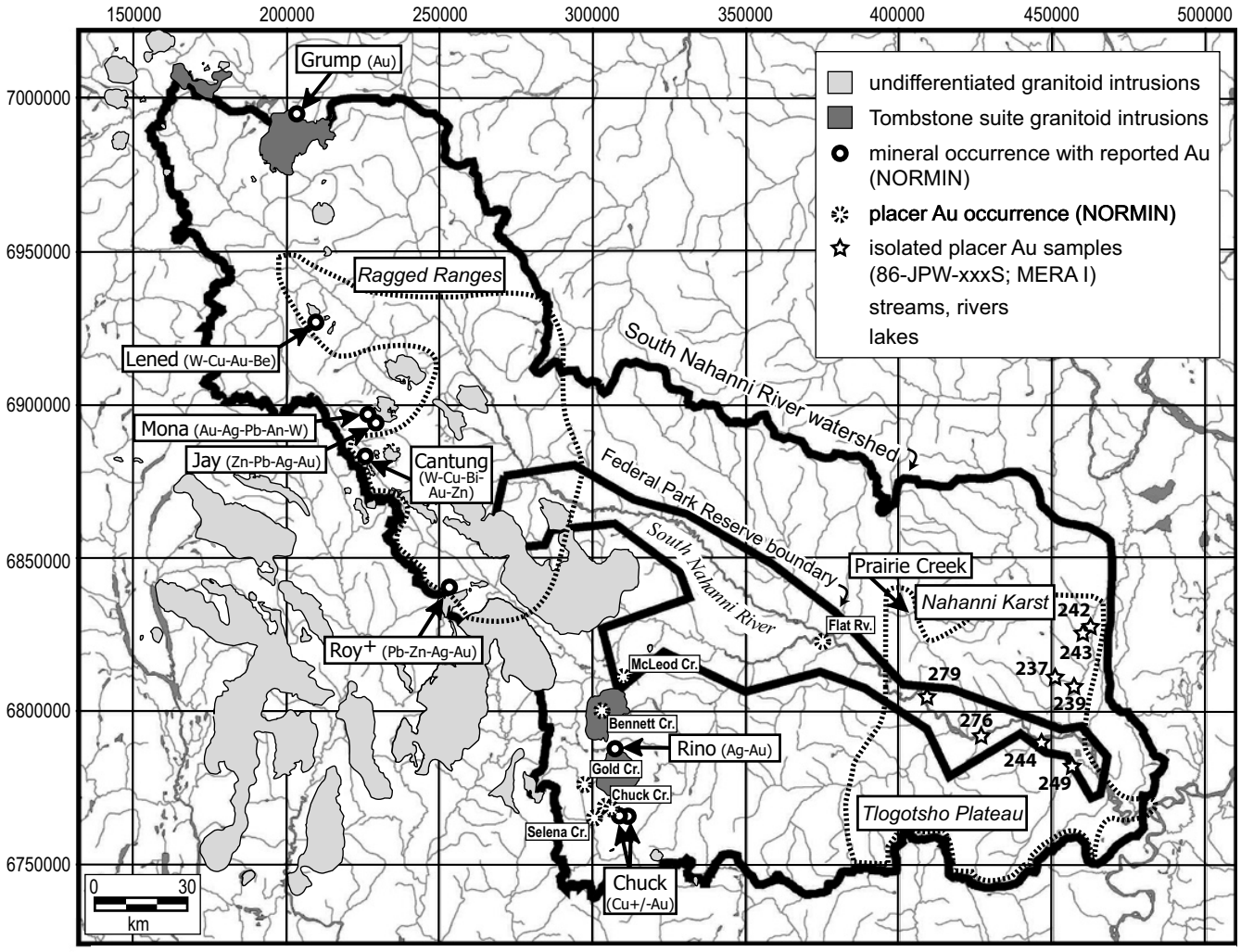


Figure 2. *Map of the South Nahanni River watershed area (Heffernan, 2004; Rasmussen et al., 2006). Approximate Ragged Ranges and Nahanni Karst-Tlogotsho Plateau HMC sampling regions from the MERA I are outlined by dashed black lines (Spirito et al., 1988). Locations of lode and placer gold occurrences (NORMIN) are also shown. Isolated samples of placer gold grains collected by C.W. Jefferson within Nahanni MERA I areas and made available for this study are represented by star symbols (Spirito et al.1988; Jefferson and Spirito, 2003). The map grid is NAD 83, Zone 10 UTM coordinates.*

samples. A larger sample size is preferred in order to statistically characterize gold grain morphologies and compositions. This, in turn, limits the inferences we can make regarding the source of these samples. The Chuck sample, however, consisted of enough grains (>250) to completely characterize the placer gold morphology and composition for the Chuck placer gold showing.

PREVIOUS WORK IN THE SOUTH NAHANNI RIVER WATERSHED

Prospecting in the South Nahanni River region began near the turn of the 20th century, most likely as a result of historical reports by local First Nations (Dene) groups. The Dene discovered and mined large gold nuggets from local streambeds (as described by R.M. Patterson in "Dangerous River", 1953). This prospecting along the river and its tributaries has continued sporadically up until present day and has resulted in the filing of assessment work on six placer gold occurrences in the Nahanni region (Fig. 2; NORMIN). The majority of follow-up work was conducted on the five showings in the southwestern corner of the South Nahanni River watershed, which consist of the McLeod Creek, Bennett Creek, Gold Creek, Chuck Creek and Selena Creek placer occurrences (Fig. 2). The placer deposits were discovered either by prospectors panning, or during large regional stream sediment surveys (Gallup, 1973; Lenters, 1984). Following discovery, only a limited amount of work was conducted on these showings and consisted mainly of test pits on the placer deposits and minor prospecting to identify the source of the gold. Investigations of a select few of the claims included soil sampling and geophysical surveys, as well as geological mapping and prospecting (White and Cruz, 1973; Vulimiri and Crooker, 1989). The most comprehensive documented work has been in the Selena Creek area (Fig. 2), where there has been prospecting of two copper showings in the creek headwaters (McDougall, 1976; Stammers, 1983; Vulimiri, 1986) combined with several investigations of the placer gold deposits (Rowan and von Kursell, 1989; Cairns*et al.*, 1995).

Although anecdotal evidence suggests that small-scale placer gold testing and mining by individuals has taken place historically throughout the southwestern corner of the South Nahanni River watershed, records in NORMIN detailing exploration in the Selena Creek area only date from the early 1980s. The following geological summary of the Chuck occurrences is sourced from the NORMIN assessment files 095DNE0007 to 095DNE0010. From this area, anomalous placer gold and bedrock-hosted gold and copper (malachite, bornite and chalcopyrite) values were reported. The lode occurrences are hosted in intensely sericitized and locally highly silicified, intermediate to mafic volcanic rocks of the Lower Cambrian Sekwi Formation. The volcanic rocks are overlain by the calcareous Rabbitkettle Formation and crop out in the core of the southwest-plunging Caribou anticline. More recent work that has resulted in the completion of a second MERA in the South Nahanni River watershed (Falck and Wright, 2007, in press), as well as ideas proposed by Emsbo *et al.* (2006), have highlighted the possibility that the gold in the southwestern portion of the watershed may be derived from a Carlin-type gold deposit in the sedimentary and/or volcanic strata.

The results of the MERA I, conducted from 1986-1987 (Spirito *et al.*, 1988), also addressed the source of placer gold grains recovered by HMC sampling throughout the Ragged Ranges (none of which were available for this study), Nahanni Karst and Tlogotsho Plateau areas. The lack of evidence for continental glaciation in the western half of the South Nahanni River watershed led Spirito*et al.* (1988) to suggest that placer gold recovered from the Ragged Ranges area was locally sourced from intrusion-related vein or skarn mineralization. The most prospective suite of intrusions for hosting gold mineralization is the Tombstone suite (Fig. 2), which has a known affinity for gold mineralization both in the study area (Fig.2) and elsewhere in Yukon (Mortensen *et al.*, 2000; Hart *et al.*, 2005). Some anomalous gold values are also associated with the tungsten skarns related to Tungsten suite intrusions (as documented in NORMIN) in the western part of the study area; however, no gold grains have been reported in proximity to the larger tungsten skarn occurrences, such as Lened or Cantung (Fig. 2), despite HMC sampling in that area. Unfortunately, none of the placer gold grains recovered from the western portion of the field area during the MERA I were available for this study.

Spirito *et al.* (1988) suggested two other possible sources for the fine placer gold recovered from isolated sample locations in the Nahanni Karst and Tlogotsho Plateau areas, south and east of the Prairie Creek minesite (Fig. 2). One hypothesis is that gold may have been locally derived from tetrahedrite-bearing sulphide veins with heterogeneous gold concentrations, such as those that crosscut base metal occurrences at Prairie Creek (Fig. 2). The spatial location of gold-bearing samples, that is,

following a northerly trend not paralleled by till deposits, and at the intersection of north- and northwest-trending faults where gold-bearing quartz veins may occur, was thought to support such a local provenance for the gold grains (Jefferson and Pare, 1991; Jefferson and Spirito, 2003). Alternatively, gold may have been derived from the greenstone-hosted gold mineralization in the Precambrian basement of the Canadian Shield. This gold is believed to have been transported by continental glaciers from the east and concentrated by glaciofluvial reworking. The latter possibility has recently taken precedence based on the presence of granite clasts and garnet grains in glacial till, the lack of other precious- or base-metals with the gold, and the random locations of gold anomalies (Jefferson and Spirito, 2003).

ANALYTICAL TECHNIQUES

The shapes of gold grains were studied using image analysis employing ImageJ software, with which minor, intermediate and major axes lengths of grains were measured. This allowed the calculation of various flatness indices such as the Cailleux flatness index[5] (Cailleux and Tricard, 1959) as well as a statistical comparison of grain size and the degree of flattening each gold particle has undergone. Representative grains selected from the Chuck sample and all grains from the isolated placer samples were subsequently imaged with the minor axis of each grain parallel to the surface of the slide, using the secondary electron (SE) detector on the scanning electron microscope (SEM) in order to document surficial textures and particle morphologies (e.g., folding, crystallinity, etc.). Following SE imaging, a representative population of the Chuck sample (~180 grains) and all grains from the isolated samples were mounted in epoxy with the long axis of each grain perpendicular to the surface of the slide. The grain mounts were then brought to a high polish using 1 µ diamond paste, and analysed for gold, silver, copper and mercury on a fully automated CAMECA SX-50 electron microprobe (EMP) operating in wavelength-dispersion mode. The operating conditions were as follows: excitation voltage, 20 kV; beam current, 20 nA, peak count time, 40 s; background count time, 20 s; and spot diameter, 5 µ. The standards, X-ray lines, and crystals used for gold, silver, copper and mercury were as follows: Au element, AuMa, PET; Ag element, AgLa, PET; Cu element, CuKa, LIF; and HgTe, HgMb, PET. Data reduction was done using the 'PAP' (phi-rho-Z) method of Pouchou and Pichoir (1985). Detection limits for gold, silver, copper and mercury, respectively, were 0.30, 0.15, 0.07, 0.30 (wt% minimum), and 0.20, 0.10, 0.04, 0.20 (wt% limit). No sulphide inclusions were observed in any grains using the backscattered electron detector (BSE) on the EMP.

RESULTS

Chuck gold grains display relatively consistent morphologies, with somewhat flattened, smoothed grain outlines and limited local folding (Fig3a-f). Some grains, however, display complicated shapes with delicate protrusions; sub-spherical grains are rare. Gold grains from the isolated samples tend to have a more variable range of morphology, including commonly folded protrusions and/or grain margins (Fig. 3g-l). Some of these grains display smoothed but relict crystalline shapes, whereas others are almost spherical. Chuck gold grains also display less complex surficial textures than the isolated samples, which have abundant smear and groove marks, scratches, and dents (Fig. 3). It should be noted, however, that the isolated samples have been handled much more frequently with tweezers, which may explain some of the scratch marks or dents. Gold grains from the isolated samples also tend to be smaller in size compared to those grains from the Chuck sample (Fig. 3). Furthermore, the minor and major axes typically measure <0.05 mm and <0.20 mm respectively for gold grains of the isolated samples, while the gold grains from the Chuck sample have minor and major axes measuring <0.15 mm and <0.50 mm, respectively (Fig. 4).

Gold grains from the Chuck sample have a range of low Cailleux flatness index values, typically between one and six, which do not appear to be a function of gold fineness[6] (Fig. 5a). The gold fineness values are relatively high, typically from 800 to 975. In the Chuck sample, copper and mercury were typically below standard detection levels (wt% minimum), but approximately one-third contain copper concentrations between 0.04 (wt% limit) to 0.11 wt% (Fig.5b). At copper concentrations above 0.04%, there is a clear covariant relationship between copper and gold fineness for gold grains of the Chuck sample. Despite the range of grain morphology

[5]Cailleux flatness index is a simple measure of the mass redistribution a malleable particle undergoes due to hammering and/or folding during transport in fluvial systems (Youngson and Craw, 1999); if (a), (b) and (c) are the lengths of the long, intermediate and short axes of a particle, respectively, the Cailleux flatness index = (a + b) / 2c

[6]fineness = Au/(Au + Ag)∗ 1000, if Au and Ag are in wt%

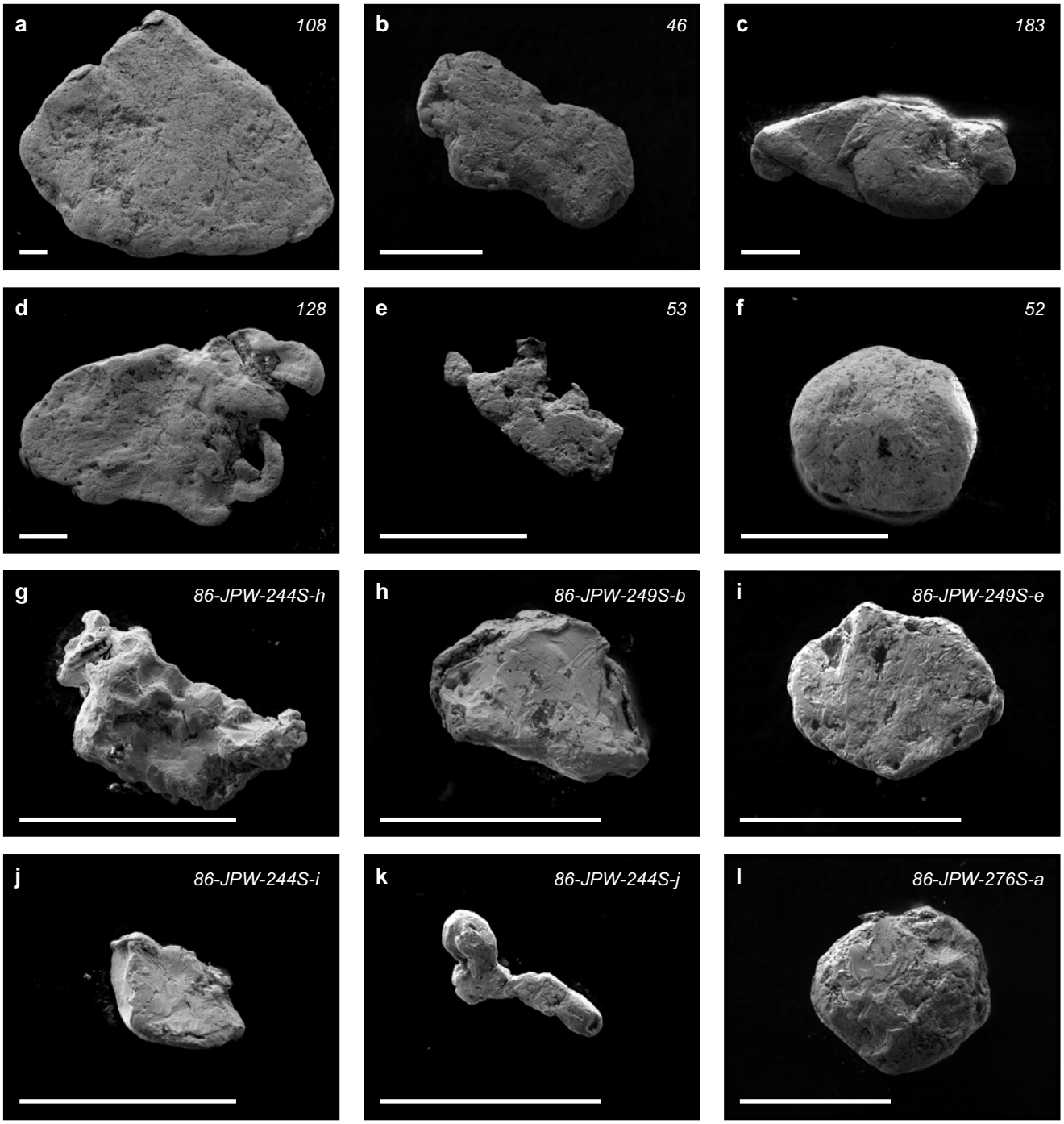


Figure 3. *Placer gold grain morphologies for grains from the Chuck sample (a-f) and grains from the isolated sample locations (g-l). Grain numbers for the Chuck sample, as well as sample number and grain letter for the isolated samples are noted; the minor axis of each grain is perpendicular to the surface and the white bar represents 200 microns.*

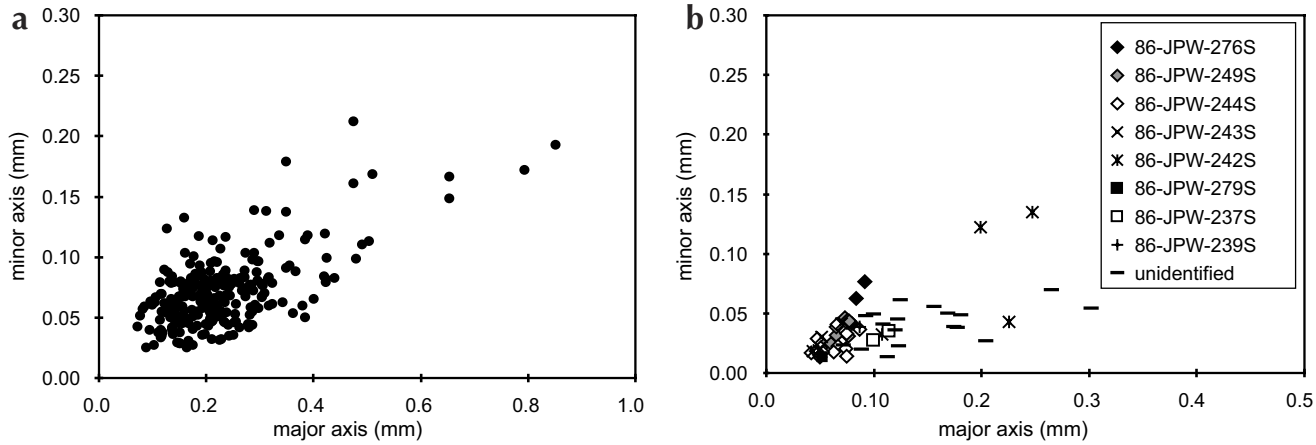


Figure 4. *(**a**) Plot of minor axis vs. major axis for gold grains from the Chuck sample; **(b)** plot of minor axis vs. major axis for gold grains from isolated samples; note the different scales on the x-axis.*

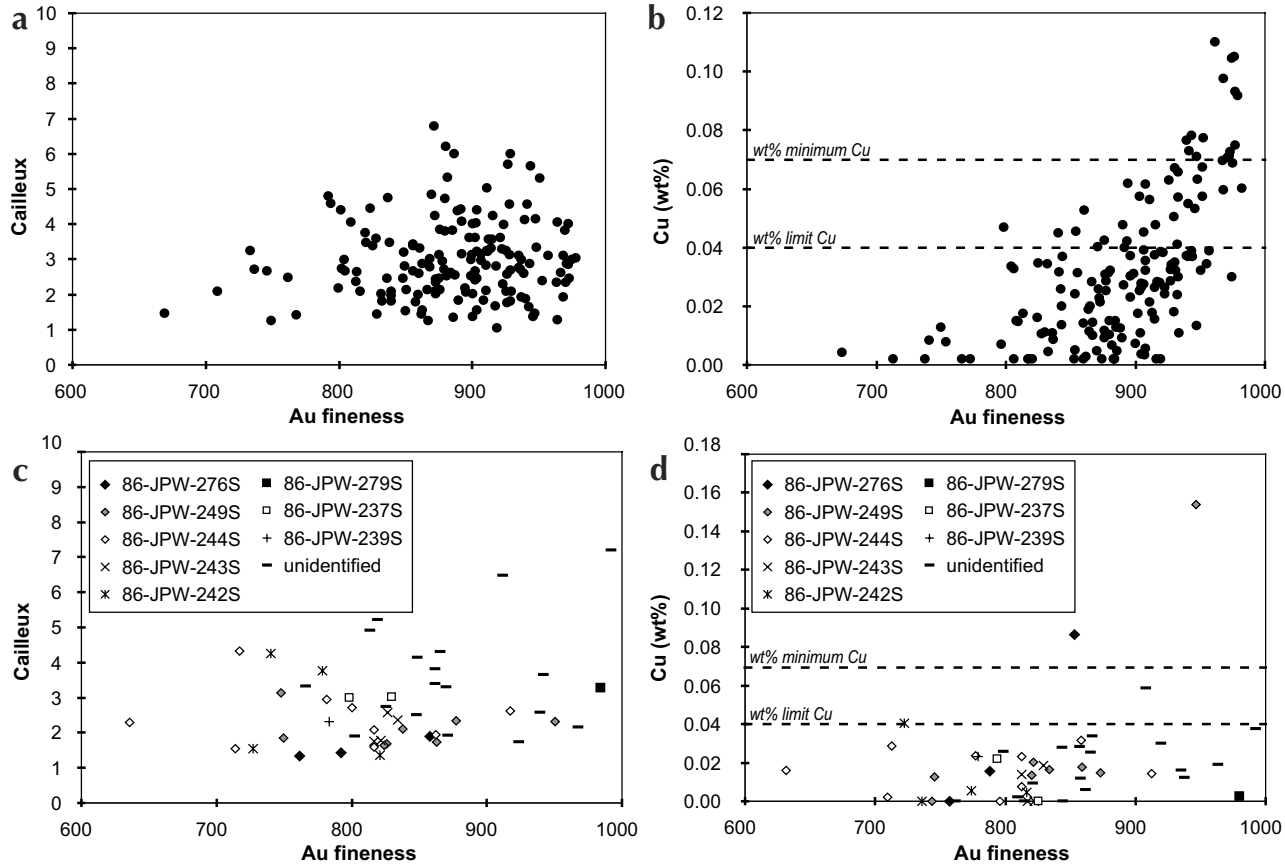


Figure 5. *(**a**) Plot of Cailleux flatness index vs. gold fineness for the Chuck sample; **(b)** plot of copper content vs. gold fineness for the Chuck sample; **(c)** plot of Cailleux flatness index vs. gold fineness for isolated samples; **(d)** plot of copper content vs. gold fineness for isolated sample locations.*

observed, placer gold from the isolated samples are relatively consistent with respect to the Cailleux flatness index, typically between one and five for samples with known locations (Fig. 5c). Gold fineness values are also high, from 700 to 950, but have a greater range than the Chuck sample. Mercury (not shown) and copper were not detected by EMP analysis in the majority of these grains (Fig. 5d).

DISCUSSION

TRANSPORT DISTANCE

Measurements of the degree of flattening is one of the most useful parameters in determining approximate distances of transport for placer gold grains in fluvial systems (e.g., Knight *et al.*, 1999a; Youngson and Craw, 1999). Detailed work on placer gold grain morphologies from known lode sources in the Klondike District, western Yukon, and the Otago Schist Belt of South Island, New Zealand, has resulted in semi-quantitative curves relating observed transport distances to the degree of flattening of a population of gold grains (Knight *et al.*, 1999a; Youngson and Craw, 1999). The Shotover/Arrow-Kawarau-Clutha fluvial system in Otago, New Zealand, transects a back-arc region currently undergoing active exhumation, but with relatively low topographic gradients and low levels of precipitation (Youngson and Craw, 1999). This setting is similar to the tectonic regime experienced in the Selwyn and MacKenzie mountains from the mid-Jurassic through to at least the Cretaceous (e.g., Gordey and Anderson, 1993). Placer gold in Otago is sourced from sparse quartz veins hosted in schistose metasedimentary rocks of the Otago Schist. Youngson and Craw (1999) have shown that the Cailleux flatness index of placer gold grains increases with transport distance in the Otago Schist Belt. Flatness index ranges from approximately 1 (spherical or cubic) to just over 130 (highly flattened and folded discoids, or elongate/irregularly folded discoids, or sub-spherical/ellipsoidal) for the most far-traveled grains in Otago. Based on the data compiled by Youngson and Craw (1999), gold grains with maximum Cailleux flatness values of less than seven are found in proximal primitive-placer zones and are largely undeformed; they have traveled 1 to 10 km from the lode gold source. Furthermore, grains with maximum Cailleux flatness values of 1 to 3 are found in primary or colluvial sources and have crystalline and delicate morphologies; they in turn have traveled less than 1 km from the lode gold source. Although the distances determined in the Otago study apply specifically to Otago placer gold (Youngson and Craw, 1999), the validity of their data is extended to our study area based on a similar tectonic and geographic regime.

The majority of gold grains in the Chuck sample have variable, but anomalously low, Cailleux flatness indices of <7, indicating that they have been transported very little distance (e.g., 1-10 km) in a fluvial environment. Similarly, gold from the isolated samples also have anomalously low Cailleux flatness values, which for many of the samples is <3. The limited flattening of the grains could also indicate a local provenance rather than the glacially transported hypothesis first suggested by Spirito *et al.* (1988) for the isolated samples. Other possibilities are: (1) grains reworked from a local primitive paleoplacer; or (2) grains sourced from a nearby primary lode gold source (Youngson and Craw, 1999). Due to the statistically small number of grains recovered, each of the isolated samples cannot be fully or statistically characterized with respect to the degree of flattening, although the lack of highly flattened grains or higher Cailleux flatness index values significantly lowers the likelihood that the grains have traveled more than 10 km in a fluvial system, regardless of whether or not glacial transport was involved at some point in time.

POSSIBLE LODE GOLD SOURCES

As discussed previously, several possible lode sources have been suggested for the placer gold grains in the South Nahanni river watershed, including:

(1) intrusion-related mineralization, either in intrusion-hosted vein systems (similar to the Dublin Gulch deposit west of Mayo, Yukon; e.g., Mortensen *et al.*, 2000), or possibly disseminated in skarn, or siliceous contact aureoles (Spirito *et al.*, 1988);

(2) a Carlin-type lode source for at least the Chuck samples (e.g., Emsbo *et al.*, 2006; Falck and Wright, 2007, in press);

(3) tetrahedrite-bearing sulphide veins cross-cutting fault-controlled base-metal mineralization such as at Prairie Creek (Spirito *et al.*, 1988; Jefferson and Pare, 1991); and/or

(4) glacially transported gold derived from orogenic quartz veins in the Slave craton to the east (Spirito *et al.*, 1988; Jefferson and Spirito, 2003).

Other possibilities include epithermal-related mineralization and gold formed within the fluvial system

by chemically or microbially induced precipitation (authigenic). A derivation of placer gold from an epithermal lode is rejected because of the relative homogeneity and high levels of gold fineness for all the samples in the study area; a gold fineness range of 0-1000 is typically present in most epithermal systems. This is even the case within individual deposits, due to variable temperatures, mixing of mineralizing fluids and changing sulphidation states (McCready *et al.*, 2003; Shikazono and Shimizu, 1986, 1987; Morrison *et al.*, 1991; Knight *et al.*, 1999b; Chapman and Mortensen, 2006). The absence of pristine, sharply crystalline gold grains with very high fineness cores (>980; e.g., McCready *et al.*, 2003) eliminates the possibility of authigenic gold (e.g., Loen, 1994; McCready *et al.*, 2003).

Western portion of drainage

As described above, an intrusion-related lode source for placer gold in the western portion of the study area has been proposed for isolated placer gold grains (not available for analysis) by Spirito *et al.* (1988), and there is a spatial association between placer gold showings and Tombstone suite intrusions in the southwestern portion of the study area (Fig. 2). Specific to the Chuck sample, the increased or measurable copper concentrations in the gold grains are not unexpected as the gold was sampled from a creek near the Chuck lode copper (-gold) occurrences. The relationship of increasing copper concentration with gold fineness (as is demonstrated by the plot in Figure 5b) has been described by other researchers (e.g., Knight and McTaggart, 1990) and is explained as a copper-saturation curve in copper-poor and gold-rich mineralizing systems (Knight *et al.*, 1999b). This increase in copper with gold fineness indicates some form of environmental variation during formation of the lode gold source, perhaps a change in temperature, or pH over time. The occurrence of relatively high fineness gold, measurable copper and low mercury (not shown) is relatively consistent with various intrusion-related sources for gold (Fig. 6a) from several placer camps in the Stewart River map area, western Yukon (Dumula and Mortensen, 2002). Furthermore, the presence of Fe- and/or Ca-rich garnet in the heavy minerals collected with the gold grains and limestone fragments indicates some form of silicate-fluid reaction with iron-rich and/or calcareous rocks during the initial gold mineralizing event(s); this in turn could also point towards a skarn-type lode source adjacent to an intrusion. Anomalous gold values are also reported in the NORMIN database for the Rino skarn occurrence, which is adjacent to a Tombstone suite intrusion near the Chuck sample location (Fig. 2). However, the lack of typical intrusion-derived or contact aureole minerals such as titanite, zircon, pyrite, pyrrhotite, andalusite, etc., observed in the heavy minerals panned from the Chuck sample, or as inclusions within the Chuck gold grains, does not lend support to a proximal, intrusive derivation for the gold (Loen, 1994).

Another possible gold source for the Chuck gold grains is nearby, or adjacent, Carlin-type mineralization. Emsbo *et al.* (2006) suggested that the association of gold with specific Tombstone suite intrusions throughout Yukon and Alaska (a continuation of the belt of Tombstone suite intrusions that crops out in the study area) is analogous to the Carlin-type mineralization trend in southwestern USA. This inference is based largely on a similar tectonic regime to that of northern Nevada (Emsbo *et al.*, 2006) where the majority of large Carlin-type gold deposits are hosted in a distal back-arc environment with far-ranging, deep-seated (transpressional?) structures, spatially and temporally associated with magmatism (Hart *et al.*, 2005; Rasmussen *et al.*, 2006; Gabrielse *et al.*, 2006, in press). Carlin-type gold deposits (summarized from Li and Peters, 1998) are commonly found near, but outside, the contact aureole of felsic intrusions and are typically hosted in impure carbonate-argillite strata; however, they may be hosted in intermediate to mafic volcanic rocks or felsic plutonic rocks. These deposits are generally associated with structurally controlled zones of silicification, sericitization, stockwork, and/or brecciation. Gold mineralization is very fine grained (micron scale, or ~0.01 mm), has a range of gold fineness (typically >500), and is disseminated in the host rock with limited associated sulphide minerals, although arsenic-mercury-antimony-bearing minerals are commonly observed. Base metals such as copper are usually not reported with Carlin-type gold; however, copper mineralization has been observed in association with gold at some Carlin-type deposits in China and Nevada (Li and Peters, 1998). The copper measured in the Chuck sample gold grains may be derived from the intermediate to mafic volcanic rocks and remobilized along the same structures that carry Carlin-type fluids. The intensely sericitized, and locally silicified, intermediate to mafic volcanic rocks hosting anomalous copper (-gold) mineralization and the overlying Rabbitkettle Formation limestones are both possible hosts for a Carlin-type deposit. Despite the lack of any associated sulphide minerals with the Chuck sample, and the relatively large gold-grain size compared to those grains of most Carlin-type gold deposits (particularly in the southwestern USA), this option remains a viable possibility for the source of

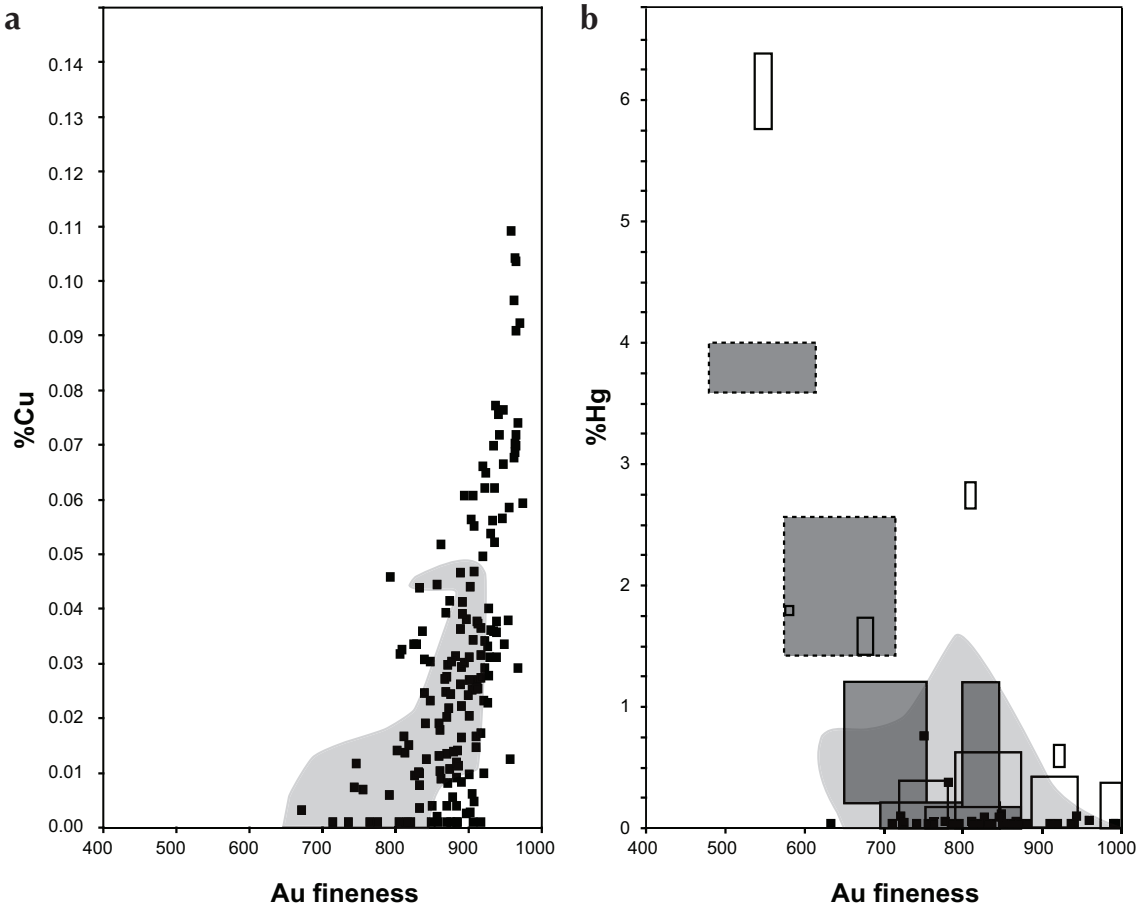


Figure 6. ***(a)*** *Plot of copper content vs. gold fineness for intrusion-related gold and the Chuck placer gold sample. The compositional field of intrusion-related gold from the Stewart River map area (Dumula and Mortensen, 2002) is indicate by the pale grey underlay, and compositions exhibited by the Chuck sample are indicated by small black squares;* ***(b)*** *plo of mercury content vs. gold fineness for orogenic and intrusion-related gold, and the isolated placer gold samples. Compositional fields of Archean greenstone-hosted orogenic gold in the Yellowknife Greenstone Belt, Slave craton are indicated by unfilled black outlines (data from Armstrong and Gochnauer, 2000; Gochnauer, unpublished data, 2001), compositional fields for Mesozoic orogenic gold from Yukon are indicated by dark grey boxes (dashed fields are inferred from a few data points; data from Knight* et al.*, 1999b), compositions of intrusion-related gold from the Stewart River map area are indicated by the pale grey underlay (Dumula and Mortensen, 2002), and the compositions exhibited by isolate samples of placer gold are indicated by small black squares.*

the placer gold due to the many other similarities listed above. At this time, the lack of access to compositional data for gold from Carlin-type mineralization does not allow for a compositional comparison with the Chuck sample.

Eastern portion of drainage

Studies of placer gold deposits have documented the presence of quartz and commonly pyrite, as well as other sulphide or silicate inclusions in gold grains sourced from orogenic veins (e.g., Loen, 1994; Knight *et al.*,1999b). Sulphide inclusions (e.g., pyrite, chalcopyrite and galena; Loen, 1994) are common in gold grains sourced from intrusion-related deposits. Therefore, it is plausible that gold associated with tetrahedrite-bearing sulphide veins could contain inclusions of tetrahedrite, and possible galena, sphalerite and Cu-sulphides from the base-metal veins that they postdate. However, it should also be noted

that the size and abundance of inclusions tends to decrease with increasing transport distance due to the effects of 'hammering' of the gold grains (Mortensen *et al.*, 2005). The lack of mineral inclusions (sulphide, silicate, or carbonate) in the isolated samples of gold grains, as viewed under the EMP, does not discount the possibility of a distal, intrusion-related source, especially for isolated samples collected from the South Nahanni River (Fig.2). A more proximal, vein-derived source as described above can not be discounted by the absence of inclusions, particularly if the small size of the grains and the relatively flat or spherical nature of some of the grains are as a result of increased transport distances rather than primary features of the lode gold source (Mortensen *et al.*, 2005). Figure 6b demonstrates that gold compositions of the isolated samples in the study area overlap with placer gold compositions in the Stewart River map area that have an intrusion-related lode source (Dumula and Mortensen, 2002), although the absence of copper in most of the grains from the isolated samples (Fig. 5d) is inconsistent with the range of low copper concentrations observed in the Stewart River placer gold (Fig. 6a). Several mineral occurrences with anomalous gold concentrations are present in the study area. These are typically adjacent to granitoid intrusions (Fig2; as documented in NORMIN). The isolated samples, however, are not spatially associated with granitoid intrusions, nor are they from tributaries that currently drain valleys containing granitoid intrusions, with the exception of samples 86-JPW- 276S and -279S located on the South Nahanni River. These two samples do not have Cailleux flatness indices indicative of the great distances of travel in a fluvial system (i.e., >12 for more than 100 km travel; Youngson and Craw, 1999) necessary for these samples to have been sourced from intrusion-related mineralization (Fig. 5c). Unfortunately, the lack of compositional data for gold from the tetrahedrite-bearing veins in the study area does not allow for a similar compositional comparison.

Another possibility for the origin of the isolated gold grains is a glacially transported, distal source from Archean greenstone gold deposits in the Precambrian shield (Spirito *et al.*, 1988; Jefferson and Spirito, 2003). Gold grains transported by southwest-flowing continental ice sheets would be deposited within glacial till as poorly concentrated and poorly sorted, relatively large and/or irregular grains displaying crystalline outlines and low degrees of flattening due to their initial glacial transport in host rock clasts. Striations, grooves, crush marks and folded grain edges would also be common (Herail *et al.*, 1989). It is also possible, however, for gold grains with a nearby lode source to have some, or all, of these features (Loen, 1994; Youngson and Craw, 1999). Most gold grains from the isolated samples have relatively low Cailleux flatness values and range in morphology from delicate with relict crystallinity, to partially or entirely flattened and rounded grains, to almost spherical grains. These grains also display much more complex surficial textures, such as scratch and smear marks, dents, and more frequently folded grain margins than the Chuck sample. All of these observations are consistent with glacially transported material.

Gold compositions of the isolated samples in the study area are compared with available data for multiple Archean greenstone-hosted orogenic gold deposits in the Yellowknife greenstone belt (YGB), Slave craton, NWT (Armstrong and Gochnauer, 2000; Gochnauer, unpublished data, 2001; Fig 6b). Results of EMP analyses of gold, silver and mercury for *in situ* gold from the Archean deposits indicate that gold fineness and mercury concentration form several distinct compositional fields (Fig. 6b); gold fineness typically ranges from 720 to 1000 and mercury is typically <0.5%, although a couple of individual deposits of lower gold fineness (500 to 750) have anomalously high mercury concentrations (Gochnauer, unpublished data, 2001). Copper was not measured for the YGB lode gold. The lack of mercury in several of the YGB deposits, with the exception of two grains from the isolated samples, combined with an overlapping range of gold fineness (Fig. 6b), allows for a viable Archean-derived and glacially transported model for the placer gold. Although Yukon orogenic gold has not been proposed as a possible lode source, compositional fields of several lode gold deposits in the Klondike region, Yukon (Knight *et al.*, 1999b) also overlap with many of the placer gold grain compositions (Fig. 6b). This compositional overlap with orogenic gold from the Klondike indicates that the same, or a similar, Mesozoic mineralizing event could also be regarded as a possible lode gold source for the isolated placer gold samples. Ultimately, whether there are one or more sources of gold for the isolated placer gold occurrences, the lack of a statistically valid population for each sample does not allow us to make any inferences as to the original gold source(s), aside from describing compositional similarities or dissimilarities between the placer gold and gold from specific lodes.

FUTURE WORK

Further imaging of gold grains using the back-scattered electron detector (BSE) will be carried out on the polished grain mounts in order to document the nature and thicknesses of high gold-fineness rims and any mineral inclusions that were not obvious under the EMP. The identification of particular sulphide, sulphate, or silicate mineral phases or combinations thereof will be important in addressing the possible lode gold sources, particularly with respect to Carlin-type gold for the Chuck sample and glacially transported Archean greenstone-derived gold for the isolated samples. Additional analyses on the grains will include laser ablation inductively coupled plasma mass spectrometry methods to determine trace-element signatures by measuring lower concentrations of copper and mercury, and trace amounts of other elements such as arsenic, bismuth, tellurium, antimony, chromium, arsenic, tungsten, rubidium, strontium, tin, barium, etc. (e.g., Outridge *et al.*, 1998). This compositional data, combined with a statistical Kernal Density estimation (KDE) of shape and trace element composition, will accurately define specific populations within a sample group. This, in turn, will allow stronger inferences as to the distance of travel the grains have undergone and the most prospective lode gold deposit-type(s) (e.g., intrusion-related, Carlin-type, Archean greenstone, etc.) for the placer gold in the South Nahanni River watershed. The more detailed work will be particularly useful for the Chuck sample. This work is expected to take place early in 2007.

ACKNOWLEDGEMENTS

Funding for this project was provided by an NSERC Discovery Grant to Dr. J.K. Mortensen (University of British Columbia). We are very grateful to C. Jefferson (GSC Ottawa) for contributing the placer gold grains obtained during the MERA I, and Archer Cathro & Associates Ltd. for contributing the Chuck placer sample. Access to unpublished gold compositional data for the Yellowknife Greenstone Belt was kindly provided by J. Armstrong (currently with Stornoway Diamond Corporation) and K. Gochnauer (Department of Indian and Northern Affairs Canada). We also thank E. Crawford (University of British Columbia) for his help with the image analysis process he is currently developing, and to L. Ootes (Northwest Territories Geoscience Office), who provided many useful comments and a review of this manuscript.

REFERENCES

Armstrong, J.P. and Gochnauer, K., 2000. A preliminary discussion of intra and inter sample variation in gold fineness from a variety of Au-showings, EXTECH-III field area. *In:* Abstract volume - 28th Annual Yellowknife Geoscience Forum; Yellowknife, Northwest Territories, Nov 22-24; p. 5-6.

Berton. P., 1956 (reprinted 1989). The Mysterious North. McClelland and Stewart Ltd., Toronto, Ontario, 391 p.

Cailleux, A. and Tricart, J., 1959. Initiation à l'étude des sables et des galets, vol. 1, Paris, Centre de Documentation Universitaire, 369 p.

Cairns, S., Roman, R. and Adams L., 1995. Report on prospecting and sampling on claims Peter 1, X and Gilbert, District of MacKenzie, NWT. Department of Indian Affairs and Northern Development, Assessment Report 83599, 113 p.

Chapman, R.J. and Mortensen, J.K., 2006. Application of microchemical characterization of placer gold grains to exploration for epithermal gold mineralization in regions of poor exposure. Journal of Geochemical Exploration, vol. 91, p. 1-26.

Dumula, M.R. and Mortensen, J.K., 2002. Composition of placer and lode gold as an exploration tool in the Stewart River map area, western Yukon. *In:* Yukon Exploration and Geology 2001, D.S. Emond, L.H. Weston and L.L. Lewis (eds.), Exploration and Geological Services Division, Yukon Region, Indian and Northern Affairs Canada, p. 87-102.

Emsbo, P., Groves, D.I., Hofstra, A.H. and Bierlein, F.P., 2006. The giant Carlin gold province: a protracted interplay of orogenic, basinal, and hydrothermal processes above a lithospheric boundary. Mineralium Deposita, vol. 41, no. 6, p. 517-525.

Falck, H. and Wright, D.F. (eds.), 2007 (in press). Mineral and Energy Resource Potential of the Proposed Expansion to the Nahanni National Park Reserve, Northern Cordillera, Northwest Territories. Geological Survey of Canada Open File 5344. 1 CD-ROM.

Gabrielse, H., Murphy, D.C. and Mortensen, J.K., 2006 (in press). Cretaceous and Cenozoic dextral orogen-parallel displacements, magmatism, and paleogeography, north-central Canadian Cordillera. *In:* Paleogeography of the North American Cordillera: Evidence For and Against Large-Scale Displacements, J.W. Haggart, R.J. Enkin and J.W.H. Monger (eds.), Geological Association of Canada, Special Paper 46, p. 255-276.

Gallup, W.B., 1973. Geology of the Nahanni placer claims, Flat River, NWT; Windfall, Binker and Epler Groups. Department of Indian Affairs and Northern Development Assessment Report 80393, 19 p.

Gordey, S.P. and Anderson, R.L., 1993. Evolution of the northern cordilleran miogeocline, Nahanni map area (105I), Yukon and Northwest Territories. Geological Survey of Canada, Memoir 428, 214 p.

Hart, C.J.R., Mair, J.L., Goldfarb, R.J. and Groves, D.I., 2005. Source and redox controls on metallogenic variations in intrusion-related ore systems, Tombstone-Tungsten belt, Yukon Territory, Canada. Geological Society of America, Special Paper, vol. 389, p. 339-356.

Heffernan, R.S., 2004. Temporal, geochemical, isotopic and metallogenic studies of mid-Cretaceous magmatism in the Tintina Gold Province, southeastern Yukon and southwestern Northwest Territories, Canada. Unpublished MSc thesis, University of British Columbia, British Columbia, Canada, 83 p.

Herail, G., Fornar, G., Viscarra, G. and Miranda, V., 1990. Morphological and chemical evolution of gold grains during the formation of a polygenetic fluviatile placer: the Mio-Pleistocene Tipuani placer example (Andes, Bolivia). Chronique de la Recherche Minière, vol. 500, p. 41-49.

Jefferson, C.W. and Pare, D., 1991. New placer gold anomalies in the northern Liard Range – southern Ram Plateau area, South Nahanni River region, District of Mackenzie, Northwest Territories. Current Research, Part E, Geological Survey of Canada Paper 91-1E, 4 p.

Jefferson, C.W. and Spirito, W.A. (eds.), 2003. Mineral and Energy Resource Assessment of the Tlogotsho Plateau, Nahanni Karst, Ragged Ranges and adjacent areas under consideration for expansion of Nahanni Nation Park Reserve, Northwest Territories. Geological Survey of Canada Open File 1686, 1 CD-ROM.

Knight, J.B. and McTaggart, K.C., 1990. Lode and placer gold of the Coquihalla and Wells areas, British Columbia. British Columbia Ministry of Energy, Mines and Petroleum Resources, Exploration in British Columbia 1989, Paper 1990-1, p. 387-394.

Knight, J.B., Morison, S.R. and Mortensen, J.K., 1999a. The relationship between placer gold particle shape, rimming, and distance of fluvial transport as exemplified by gold from the Klondike district, Yukon Territory, Canada. Economic Geology, vol. 94, p. 635-648.

Knight, J.B., Morison, S.R. and Mortensen, J.K., 1999b. Lode and placer gold composition in the Klondike district, Yukon Territory, Canada: implications for the nature and genesis of Klondike placer and lode gold deposits. Economic Geology, vol. 94, p. 649-664.

Lenters, M.H., 1984. Report on prospecting and geochemical sampling permits 969, 970, 971, 972, Flat River Prospect. Department of Indian Affairs and Northern Development Assessment Report 81741, 26 p.

Li, Z. and Peters, S.G., 1998. Comparative geology and geochemistry of sedimentary-rock-hosted (Carlin-Type) gold deposits in the People's Republic of China and in Nevada, USA. United States Geological Survey Open-File Report 98–466, 104 p.

Loen, J.S., 1994. Origin of placer gold nuggets and history of formation of glacial gold placers, Gold Creek, Granite County, Montana. Economic Geology, vol. 89, p. 91-104.

McCready, A.J., Parnell, J. and Castro, L., 2003. Crystalline placer gold from the Rio Neuquen, Argentina: Implications for the gold budget in placer gold formation. Economic Geology, vol. 98, p. 623-633.

McDougall, G., 1976. Report on the Deb property. Department of Indian Affairs and Northern Development Assessment Report 80508, 81 p.

Morrison, G.W., Rose, W.J. and Jaireth, S., 1991. Geological and geochemical controls on the silver content (fineness) of gold in gold-silver deposits. Ore Geology Reviews, vol. 6, no. 4, p. 333-364.

Mortensen, J.K., Hart, C.J.R., Murphy, D.C. and Heffernan, S., 2000. Temporal evolution of Early and mid-Cretaceous magmatism in the Tintina Gold Belt. *In:* The Tintina Gold Belt: Concepts, Exploration and Discoveries, J. Jambor (ed.), British Columbia and Yukon Chamber of Mines, Special Volume 2, p. 49-57.

Mortensen, J.K., Chapman, R., LeBarge, W. and Jackson, L., 2005. Application of placer and lode gold geochemistry to gold exploration in western Yukon. *In:* Yukon Exploration and Geology 2004, D.S. Emond, L.L. Lewis and G.D. Bradshaw (eds.), Yukon Geological Survey, p. 205-212.

Outridge, P.M., Doherty, W. and Gregoire, D.C., 1998. Determination of trace elemental signatures in placer gold by laser ablation – inductively coupled plasma – mass spectrometry as a potential aid for gold exploration. Journal of Geochemical Exploration, vol. 60, p. 229-240.

Patterson, R.M., 1953 (reprint 1999). Dangerous River: Adventure on the Nahanni. Boston Mill Press, Erin, Ontario, 276 p.

Pouchou, J.-L. and Pichoir, F., 1985. "PAP" (phi-rho-Z) procedure for improved quantitative microanalysis. *In:* Microbeam Analysis, J.T. Armstrong (ed.), San Francisco Press, San Francisco, California, p. 104-106.

Rasmussen, K.L., Mortensen, J.K. and Falck, H., 2006. Mid-Cretaceous granitoids in the southwestern Northwest Territories and southeastern Yukon: implications for magma source regions, tectonic setting, and metallogeny. *In:* Abstract volume - 34th Annual Yellowknife Geoscience Forum, Yellowknife, Northwest Territories, Nov. 21-23, p. 46.

Rowan, L.G. and von Kursell, A.H., 1989. Geological report on the evaluation survey of the Selena Creek property, Nahanni Mining District, NWT. Department of Indian Affairs and Northern Development Assessment Report 82830, 77 p.

Samusikov, V.P. and Petrova, N.I., 1983. Correlations between the content of silver, antimony and copper in native gold (deposits of the Yana-Kolyma belt as examples). Chemical Abstracts, vol. 101, p. 114-234.

Shikazono, N. and Shimizu, M., 1986. Compositional variations in gold-silver series minerals from some gold deposits in the Korean Peninsula. Kozan Chishitsu, vol. 36, no. 200, p. 545-553.

Shikazono, N. and Shimizu, M., 1987. The silver/gold ratio of native gold and electrum and the geochemical environment of gold vein deposits in Japan. Mineralium Deposita, vol. 22, no. 4, p. 309-314.

Spirito, W.A., Jefferson, C.W. and Pare, D., 1988. Comparison of gold, tungsten and zinc in stream silts and heavy mineral concentrates, South Nahanni resource assessment area, District of Mackenzie. Current Research, Part E, Geological Survey of Canada Paper 88-1E, p. 117-126.

Stammers, M.A., 1983. Geological and geochemical report on the Chuck 1 and 2 claims, Nahanni Mining District, NWT. Department of Indian Affairs and Northern Development Assessment Report 81665, 27 p.

Turner, D., 1975. Nahanni. Hancock House Publishing, Blaine, Washington, 286 p.

Vulimiri, M.R., 1986. Geological report on the Chuck 1 mineral claim, Caribou River area, Nahanni Mining District, NWT. Department of Indian Affairs and Northern Development Assessment Report 82082, 17 p.

Vulimiri, M.R. and Crooker, G.E., 1989. Geological, geophysical and geochemical report on the Chuck 1 mineral claim, Caribou River Area, Nahanni Mining District, NWT. Department of Indian Affairs and Northern Development Assessment Report 82859, 36 p.

White, G.E. and Cruz, E.D., 1973. Geochemical, geophysical report, Andrew and Becker, Rino Claims, East Skinboat Lake, NWT. Department of Indian Affairs and Northern Development Assessment Report 82032, 16 p.

Youngson, J.H. and Craw, D., 1999. Variation in placer style, gold morphology, and gold particle behavior down gravel bed-load rivers: an example from the Shotover-Arrow-Kawarau-Clutha river system, Otago, New Zealand. Economic Geology, vol. 94, p. 615-634.

APPENDIX 3

UNIVERSITY OF CALGARY

Spring Geochemistry: A Tool for Mineral Exploration in

the South Nahanni River Basin, NWT

by

Marie-Eve Caron

A THESIS

SUBMITTED TO THE FACULTY OF GRADUATE STUDIES

IN PARTIAL FULFILMENT OF THE REQUIREMENTS FOR THE

DEGREE OF MASTER OF SCIENCE

DEPARTMENT OF GEOLOGY AND GEOPHYSICS

CALGARY, ALBERTA

JANUARY, 2007

© Marie-Eve Caron 2007

Caron, M-E., 2007, Appendix 3. Spring geochemistry: A tool for mineral exploration in the South Nahanni River basin of the Mackenzie Mountains, Northwest Territories, *in* Mineral and Energy Resource Assessment of the Greater Nahanni Ecosystem Under Consideration for the Expansion of the Nahanni National Park Reserve, Northwest Territories, (ed.) D.F. Wright, D. Lemkow, and J.R. Harris; Geological Survey of Canada, Open File 5344, p. 381-547 (also M..Sc. thesis, University of Calgary, Alberta, 152 p.).

UNIVERSITY OF CALGARY

FACULTY OF GRADUATE STUDIES

The undersigned certify that they have read, and recommend to the Faculty of Graduate Studies for acceptance, a thesis entitled "Spring Geochemistry: A Tool for Mineral Exploration in the South Nahanni River Basin, NWT" submitted by Marie-Eve Caron in partial fulfilment of the requirements of the degree of MASTER OF SCIENCE.

Supervisor, M. Cathryn Ryan, Department of Geology and Geophysics

Co-Supervisor, Stephen E. Grasby, Department of Geology and Geophysics

Bernhard Mayer, Department of Geology and Geophysics

Ralph Cartar, Department of Biological Sciences

Jan 17/07

Date

Abstract

Geochemical data from over 200 springs within the remote 37,000 km^2 South Nahanni River Basin of the Mackenzie Mountains, Northwest Territories, were used to evaluate the economic mineral potential of the region which is proposed for a national park designation. Trace element analyses were evaluated using three different approaches (the sum of trace element concentrations as a percentage of total dissolved solids, identifying individual elevated trace elements, and the inverse use of the Ficklin Diagram). Two out of the three approaches detected the two known deposits of the area, Prairie Creek and Tungsten, but not with the same method in each case, indicating that a multi-pronged approach is best. The springs are elevated in trace elements in comparison to mineral deposit related waters around the world. Silica geothermometry determined the average depth of circulation of the springs to be 2.1 km in the warm or hot springs and ranging from 4.7 km to less than 200 m for the entire dataset, indicative of the accessibility of the predicted mineralized zones. These simple statistical and graphing methods can identify mineralized zones quickly and efficiently in a largely under-explored area.

Acknowledgements

I would like to thank my co-supervisors, Stephen E. Grasby and M. Cathryn Ryan, for all the time, guidance, mentorship, patience and advice that they gave. I would like to thank my internal and external committee members, Ralph Cartar and Bernhard Mayer, for the detailed manuscript review and thoughtful questioning. Thank you to my neutral chair, Stephen Hubbard, for giving up a morning of his time to watch over my thesis defence. For field assistance, I would like to thank a number of people and organizations: my co-worker and field assistant, offering constant enthusiasm and good humour, Melanie Myden; the staff of Great Slave Helicopters (especially Glenn Sibbeston, our pilot, and his base manager); the staff of Canadian Zinc at Prairie Creek Mine (especially Alan Taylor and his staff); and the other Nahanni MERA II team members: Hendrik Falck, Kirsten Rasmussen, Danny Wright and Suzanne Paradis. I would like to thank all the people who gave valuable GIS assistance, from providing data to explaining how ARCMAP works: especially Kelly Pierce and Todd Slack at the NWT Geoscience Office, and Paul Wozniak at the GSC-Calgary. This work could not have been done without the careful analysis of samples in a variety of laboratories: University of Calgary Isotope Laboratory (especially Stephen Taylor and his staff), University of Victoria Isotope Laboratory (especially Paul Eby and his staff), GSC Laboratories in Ottawa (especially Raymond Boisvert and his staff), GSC Isotope Laboratory in Quebec (especially Martine Savard and her staff), and the helium isotope analysis that was done by Nick Utting and Ian Clark at the University of Ottawa. I also spent time with a variety of different people having discussions about the geology of the area, different procedures

and logistics, and practicing my oral presentations; in no particular order, these people are: Stewart Hamilton, Andrew Okulitch, Rod Smith, Karen Fallas, Dave Morrow, Hamed Sanei, Laurence Bentley, Masaki Hayashi, Maurice Shevalier, Peggy Ferguson, James Roy, Jennette Baker, Jean-Francois Caron, Anita Liu, Sandra Gilbert, My Le, Chris Horack, and Sandy Hemstock. Last but not least, I would like to thank my parents for all their continued support throughout my university career.

Table of Contents

Approval Page ii
Abstract iii
Acknowledgements iv
Table of Contents vi
List of Tables viii
List of Figures and Illustrations x
Epigraph xv

CHAPTER ONE: INTRODUCTION 1
1.1 Nahanni National Park History 1
1.2 The MERA Process 2
1.3 Areas of Interest 2
1.4 Spring Study Overview 3

CHAPTER TWO: BACKGROUND 5
2.1 The Watershed-Scale Approach to Mineral Exploration 5
2.1 Geochemical Exploration 6
2.2 Climate of SNRB 9
2.3 Geologic Overview of SNRB 10
2.3.1 Topographical Features 10
2.3.2 Sedimentary Geology 12
2.3.3 Igneous Geology 14
2.3.4 Known Mineral Occurrences 15
2.4 Groundwater Geochemistry 17
2.4.1 Carbonates 18
2.4.2 Salt Deposits 18
2.4.3 Shales 19
2.4.4 Sandstones 20
2.4.5 Plutonic Rocks 20
2.5 Depth of Circulation 21
2.5.1 Groundwater Flow in Mountainous Terrain 22
2.5.2 Heat Flow 23
2.5.3 Geothermometry 24
2.6 Overview of Spring Study 26

CHAPTER THREE: METHODS 27
3.1 Field Methods 27
3.1.1 Note about Terminology 29
3.2 Laboratory Methods 29
3.2.1 Percent Error 30
3.2.2 Charge Balance 31
3.3 Geothermometry Approach 31
3.4 Determination of Dominant Major Ions in Aquachem 32
3.5 Trace Element Data Analysis 33
3.5.1 Total Trace Elements 33

3.5.2 Individual Trace Elements....34
3.5.3 Ficklin Diagram....35

CHAPTER FOUR: RESULTS & DISCUSSION....36
4.1 Oxygen and Hydrogen Isotopes In Water....37
4.2 Temperature, pH and Major Ions....38
4.3 Total Dissolved Solids....43
4.4 Sulphur-Related Isotopes....46
4.4.1 Sulphide Oxidation....47
4.4.2 Bacterial Sulphate Reduction (BSR)....48
4.4.3 Evaporite Dissolution....49
4.5 Trace Element Analysis....50
4.5.1 Total Trace Elements....50
4.5.2 Individual Trace Elements....54
4.5.3 Ficklin Diagram....55
4.5.4 Summary of Indicator Springs....55
4.5.5 Circulation Depth Estimates....57
4.5.5.1 Geothermometry....57
4.5.5.2 Summary and Significance of Circulation Depth Estimates....59
4.6 Summary of Results....59

CHAPTER FIVE: CONCLUSION....63

APPENDIX A: TABLES OF MERA I AND II DUPLICATES....111

APPENDIX B: DISCUSSION ON GEO-AVAILABILITY OF METALS....114

APPENDIX C: MERA I SPRING LOCATIONS....116

APPENDIX D: MERA II SPRING LOCATIONS....117

APPENDIX E: PH-TEMPERATURE SCATTER PLOT OF SNRB SPRINGS....118

APPENDIX F: HCO_3-SO_4 SCATTER PLOT AND ALTERNATE PIPER PLOT....119

APPENDIX G: MAJOR ION SCATTER PLOTS (R > 0.5)....120

APPENDIX H: TABLES OF SPRING GROUPINGS WITH ELEVATED TOTAL TRACE ELEMENTS (T.E. > 0.9%)....121

APPENDIX I: SIGNS OF DEEP CIRCULATION – C AND HE ISOTOPES AND FAULTS/FRACTURES....123
I.1. Carbon Isotopes....125
I.2. Helium Isotopes....126

APPENDIX J: EXTRA BACKGROUND GEOLOGY NOTES....128

APPENDIX K: CONFIDENCE INTERVALS AT THE 0.05 SIGNIFICANCE LEVEL 130

List of Tables

Table 3.1 Field Measurements Conducted 80

Table 3.2 Sample Descriptions Summary 81

Table 3.3 Methods and Limits of Detection for Trace Elements 82

Table 3.4: Isotope Methods Summary 83

Table 4.1: Description of bedrock geology from which MERA II springs discharge from based on Okulitch (2005). 84

Table 4.2: Field Parameters from MERA II springs (2003-2005 field seasons). 85

Table 4.3: Major Ions of 2003-2005 Springs. All units in ppm unless otherwise noted. Charge balance data in bold is above 10% and with stars (*) has metals included to balance the charge. 87

Table 4.4a: Most common trace elements (Fe, Al, Mn, Ni, Cu, Zn, Pb, Cd, Co and Cr) from MERA I and II springs. All units in µg/L unless otherwise noted. Bolded numbers were determined to be elevated using the individual trace element method. 89

Table 4.4b: Moderately common trace elements (Cs, Mo, As, Li, Rb, Sr, Ba, U, V, B and Sb) from MERA I and II springs. All units in µg/L unless otherwise noted. Bolded numbers were determined to be elevated using the individual trace element method. 92

Table 4.4c: Least common trace elements (Tl, Ga, Se, Br, Ag, Be, Sc, Ti, Bi, In and NO_2) from MERA I and II springs. All units in µg/L unless otherwise noted. Bolded numbers were determined to be elevated using the individual trace element method. 95

Table 4.5: Isotope ratios of MERA II samples. Note: 1.81E+0.3 signifies 1.81×10^3 or 1810 in scientific notation. Gaseous springs are marked with a bubble (^{o}). All units are in permil notation (‰) unless otherwise noted. 98

Table 4.6: Correlation matrix of MERA I and II springs. Strong (> 0.7) and moderate (0.7 > r > 0.5) linear correlation coefficients are in bold and listed for surface temperature (Temp), Si-geothermometry predicted temperature (Geotherm), pH, Eh, major ions, stable isotopes and total trace elements as percent of total dissolved solids (% T.E.). Total number of samples: 221. 100

Table 4.7: Frequency distribution of springs tallied for lithology, pH, temperature, total dissolved solids (TDS), sulphide oxidation and total trace elements (TTE). . 101

Table 4.8A: Br/Cl ratios of SNRB springs with detectable Br concentrations, compared to world salt deposit averages according to Worden (1996). 102

Table 4.8B: Anhydrite- and gypsum-containing formations of the SNRB with their associated ages and sulphate isotope values based on age description by Okulitch (2005) and world average Palaeozoic sulphate isotope curves by Claypool et al. (1980). 102

Table 4.9: Summary of Indicator Springs - % total trace elements, # of individual elevated trace elements, Ficklin Diagram groupings (from Figure 4.8; groupings described as footnote), geochemical groupings (from Figure 4.2) and estimate of depth of circulation (from Si-geothermometry, Section 4.5.5). Summary of indicator springs near the two known mines is tabulated as footnote. 103

Table 4.10: Cut-off values used to determine elevated individual trace elements, compared with select deposit-related waters. Units are in µg/L. Description of deposits follows as footnote. 107

Table 4.11: Geothermometry results for select MERA II springs. Appropriate silica sampling was only performed in MERA II study. Warm and hot springs were analyzed with geothermometry, with some cold ones for comparison (e.g.: Bougere, Brimstone). MERA II springs not listed here are assumed to circulate < 200 m in depth. 110

Appendix A – Table 1: Number of times springs were sampled for MERA I and II. ... 111

Appendix A – Table 2: Major ions, TDS and % total trace elements of field duplicates of MERA I and II springs. All units are in ppm unless otherwise noted. 112

Appendix H – Table 1: List of cold (T < 12 ºC) and basic (pH > 7) springs with elevated total trace elements (i.e.: Group 1 of Figure 4.2) and their associated lithological grouping based on Okulitch (2005) descriptions. 121

Appendix H – Table 2: List of cold (T < 12 ºC) and acidic (pH < 7) springs with elevated total trace elements (i.e.: Group 2 of Figure 4.2) and their associated lithological grouping based on Okulitch (2005) descriptions. 122

Appendix H – Table 3: List of hot (T > 40 ºC) and basic (pH > 7) springs with elevated total trace elements (i.e.: Group 3 of Figure 4.2) and their associated lithological grouping based on Okulitch (2005) descriptions. 122

Appendix I - Table 1: Helium Isotopes Results 126

List of Figures and Illustrations

Figure 1.1 (previous page): Location and Description of the South Nahanni River Basin (SNRB). A) NWT permafrost zones (bold font and solid lines; NRCan, 1995), eco-zones (italic font and dashed lines; Wiken, 1986; CCEA, 2006), with SNRB highlighted in blue and MacMillan Pass and Howard's Pass mineral deposit locations marked with stars; B) SNRB physiographic regions (after GSC, 1986) with the platformal carbonate / basinal shale facies boundary as described by Gabrielse et al. (1965); C) SNRB map sheets, Sahtu/Deh Cho First Nations groups, waterways, infrastructure and current Nahanni National Park (NNP) boundary. Mineral and Energy Resource Assessment (MERA) I and II areas are marked as dotted boxes and as the outline of the watershed, respectively. Beaver River Structure (BSR) is marked with a dashed line as proposed by Morrow and Miles (2000). 67

Figure 2.1: Major bedrock lithological groupings based on Okulitch (2005) overlaid with MERA I & II springs, Nahanni National Park (NNP) boundary, major faults and folds and outlined by the current proposed park expansion area of the South Nahanni River Basin (SNRB). Springs discharge mostly near faults, folds and/or contacts between major bedrock types. Springs are symbolized for temperature, pH, and total trace elements as described in Figure 4.2. Springs with elevated total trace elements (T.E. > 0.9 %) cluster in three groups: sandstone-related, pluton-related and fault related. 68

Figure 4.1: Hydrogen and oxygen stable isotope ratios of SNRB springs plotted to compare with the Yellowknife meteoric water line (YMWL; IAEA/WMO, 1998). 69

Figure 4.2: Piper plot of SNRB springs' major ions. Springs with elevated trace element percentages (T.E. > 0.9 %) have filled symbols and fall into three distinct groups: 1) Cold, basic and HCO_3-SO_4-rich; 2) Cold, acidic, and SO_4-rich; and 3) Hot, basic and Na-rich. There are no warm springs (except for Tungsten mine water drainage) and no acidic hot springs (n/a) that have elevated total trace elements. Dotted rectangles in the lower left-hand triangle highlight the linear trend of warm springs from Ca to Na richness, and the two clusters of hot springs: Ca-rich on the left and Na-rich on the right. These symbols are also used in Figures 2.1, 4.3, 4.4, 4.5 and 4.8. 70

Figure 4.3: B/Cl scatter plot of SNRB springs overlaid with fields based on waters from Iceland in Arnorsson and Andresdottir (1995). B/Cl ratios are determined by the meteoric source water, dissolution from rock, mixing with seawater, magma degassing or concentration of B by phase separation. Springs falling on the seawater ratio line are assumed to be flowing through evaporites, while springs falling near the magma degassing line are assumed to be flowing much deeper; both clusters are all hot or warm springs. The five springs that fall on or near the seawater ratio line are, from left to right: Tabletop, Redstone Junction #1, Deca, Ekwi and Kraus. The six springs that are near the 'magma degassing'

area are, from left to right: Broken Skull, Nahanni North, West Cantung, Tulita, Nahanni Headwaters, and Wildmint. Symbols are the same as described in Figure 4.2. 71

Figure 4.4 (previous page): A) $\delta^{18}O_{SO4}$ and B) $\delta^{34}S_{SO4}$ plotted vs. sulphate concentration in MERA II springs. Springs are overlaid with corresponding world average Paleozoic evaporite values (upper beige box; Claypool et al., 1980) and pyrite $\delta^{34}S$ values from black shales in the Mackenzie Mountains (lower grey box; Al-Aasm et al., 1996). Ranges associated with evaporite-containing formations of the SNRB are based on age descriptions from Okulitch (2005). Springs show signs of evaporite dissolution (ED) and sulphide oxidation (SO) along trends described by van Stempvoort and Krouse (1994) and Clark and Fritz (1997). Warm or hot springs tend to show evaporitic or bacterial sulphate processes, while cold springs tend to show sulphide oxidation. Data are only available for MERA II samples. Springs symbols are the same as described in Figure 4.2. 73

Figure 4.5: Sulphate and water $\delta^{18}O$ scatter plot overlaid with the sulphide oxidation field of van Stempvoort and Krouse (1994). Data are only available for MERA II samples, and symbols are the same as described in Figure 4.2. Thirty-seven springs show signs of sulphide oxidation, of which six have total trace elements > 0.9% and discharge mostly from shale (Bougere, Glacier Lake, Orange Creek, Red Mini, Nahanni Headwaters and Cathedral). Similar to Figure 4.4, cold springs tend to fall in the field of sulphide oxidation, while warm or hot springs tend to fall outside this field. 'Limit I' signifies 100 % of oxygen in sulphate is derived from H_2O while above 'Limit II', oxygen is derived from other sources (e.g.: air). Sulphate reduction typically results in $\delta^{34}S_{SO4}$ values above 'Limit II' (van Stempvoort and Krouse, 1994). 74

Figure 4.6: A) Sulphate and sulphide $\delta^{34}S$ of SNRB springs with expected $\delta^{34}S_{SO4}$ ranges from 5 local evaporite-containing formations based on their known ages (Okulitch, 2005) and age-corresponding world $\delta^{34}S_{SO4}$ average (Claypool et al., 1980). Only samples with available $\delta^{34}S_{HS}$ data are included, indicating fractionation with $\delta^{34}S_{SO4}$ and therefore bacterial sulphate reduction. B) $\Delta\delta^{34}S_{SO4\text{-}HS}$ vs. temperature and concentration of sulphate. Kinetic fractionation, i.e.: bacterial sulphate reduction is occurring in the samples with available $\delta^{34}S_{HS}$ data because of the increase in fractionation with temperature and sulphate concentration. 75

Figure 4.7: Trace element statistics for SNRB springs: maximum, minimum, average, and sum of average and 1 x standard deviation concentrations (stdev) for all MERA I and II springs. The number next to each element refers to the total of springs with detectable concentrations of that element. Some elements are very common (e.g.: Fe) and while some elements are uncommon (e.g.: Ag). Correspondingly, different cut-off values were used to determine which elements

were elevated in each spring, which are listed in Table 4.4a-c and compared to deposit-related waters in Table 4.10. 76

Figure 4.8: Ficklin Diagram showing MERA I and II springs grouped by total trace elements >0.9% with the same symbols as in Figure 4.2. Springs showing sulphide oxidation as indicated by $\delta^{18}O_{SO4}$ and $\delta^{34}S_{SO4}$ values are circled. Many springs fall into fields labeled E-K as delineated from mine water drainage geochemistry from known mineral deposits in Colorado (Plumlee et al., 1994; descriptions listed below). Increasing buffering capacity increases with pH towards the right, and sulphide-related base metal content increases towards the top. 77

Figure 4.9 A-E: Solubility diagrams of 5 SNRB springs at different modeled temperature intervals, used to determine temperature at maximum depth of circulation as per Pang and Reed (1998). Lack of convergence at the equilibrium line [log (AP/KT) = 0] indicates effects of mixing with fresh meteoric waters and carbon dioxide degassing in the springs. "Log AP/KT" as labeled by the Solmineq88 program (Kharaka et al., 1988) is also known as "log Q/K" in Pang and Reed (1998) or as the 'saturation index' in Appelo and Postma (1999); Sub-saturation is reflected below the equilibrium line (where log (AP/KT) < 0), and super-saturation above the equilibrium line (where log (AP/KT) > 0; Appelo and Postma, 1999). 78

Figure 4.10: Illustration of the variety of spring types in the SNRB. 1) Deep, gaseous water mixing with shallow meteoric water; 2) shallow, cold and acidic water discharging from tops of plutons; 3) shallow, cold and without signs of evaporite dissolution; 4) warm with signs of evaporite dissolution; 5) hot, basic, Na-rich and high in total trace elements discharging from deformation halos around plutons; 6) hot, basic, Ca-rich and low in total trace elements discharging from faults far from plutons; 7) cold, basic, low in total trace element, HCO_3-rich water discharging from carbonate; and 8) cold, acidic, high in total trace element, SO_4-rich water discharging from sulphide-containing shale. Diagram is not to scale. Depth of gaseous spring circulation is approximately 5 km and evaporites are present at depths below approximately 300 m. Shape of plutons was modified from Hamilton et al. (1990). More types of springs exist that can fit on this diagram. 79

Appendix B - Comparison of SNRB spring and pluton (Rasmussen, MERA II report – in press) geochemistry with world igneous average (Hem, 1985). In most cases, spring geochemistry reflects rock abundance of that element, except with As, Cr, Ga, Pb, V, Cs, Cu and U. Differences can be accounted for by varying weathering effects, mineral properties, sorption and/or geochemical conditions (Smith and Huyck, 1999). 114

Appendix C: Map of MERA I springs based on data from Hamilton (1990) and Jefferson and Spirito (2003). 116

Appendix D: Map of MERA II springs with individual elevated trace elements, % total trace element (T.E.), geochemical groups from Piper Diagram (Group 1-3; Figure 4.2), and Ficklin Diagrams groups (Group E-K; Figure 4.8) for each indicator spring if applicable..... 117

Appendix E: Scatter plots of pH vs. temperature of SNRB springs with symbols relating to the bedrock lithology from which springs discharge (A), and Figure 4.2 (B). Similarly, scatter plots of pH vs. % total trace elements with symbols relating to lithology (C) and Figure 4.2 (D). Lithological groups are based on Okulitch (2005). More than half of basic springs are discharging from carbonates or calcareous shale, while more than half of acidic springs are discharging from siliceous shales. Springs with total trace elements > 0.9% cluster in cold or hot groups and acidic or basic groups. There are no warm or hot acidic springs, nor any warm springs with above average total trace elements (> 0.9 % T.E.) - except for 86-020 from MERA I, a discharge from inside Tungsten Mine. 118

Appendix F: Scatter plots of HCO_3 and SO_4 with symbols relating to the bedrock lithology from which springs discharge from (A; Okulitch, 2005) and Figure 4.2 groups (B). Piper plot shows the springs grouped by lithology (C). Shales tend to be relatively richer in sulphate, while carbonates tend to be richer in bicarbonate, although there is a large amount of overlap. 119

Appendix G: Scatter plots of different major ions in the SNRB with corresponding R values. Most of the data generally line up with the 1:1 slope lines. Symbols are the same as those in the piper plot of Figure 4.2. 120

Appendix I-1: $\delta^{13}C$ of four different gaseous components (free and aqueous CO_2 and CH_4) in SNRB springs. Some $\delta^{13}C_{CO2(g)}$ values fall in the mantle zone as previously defined by Irwin and Barnes (1980), Giggenbach et al. (1991) and Whiticar (1999). Spring names with stars (*) are gaseous, i.e.: continuously discharging gas bubbles. BS = Broken Skull, U = Upper Pool, L = Lower Pool, 03 = sampled in 2003, Champ. = Champagne, FF = Flat Fruit, GB = Grizzle Bear, dup = field duplicate, g = gaseous, aq = aqueous. 123

Appendix I-2: Exploring SNRB bicarbonate trends. Diagrams in A & B show typical fractionations according to Fritz and Clark (1997). A) $\delta^{13}C_{CaCO3}$ and $\delta^{13}C_{HCO3}$ – Dissolved bicarbonate $\delta^{13}C$ is strongly correlated to that of precipitated bicarbonate found at spring outlets. B) $\delta^{13}C_{CO2(aq)}$ and $\delta^{13}C_{HCO3}$ – Dissolved carbon dioxide $\delta^{13}C$ is strongly correlated to that of dissolved bicarbonate. C) $\delta^{13}C_{HCO3}$ and $[HCO_3]$ as ppm – Similar trends are found in springs of the southern Cordillera, showing a significant contribution of high $\delta^{13}C$ bicarbonate to high alkalinity waters (Grasby et al., 2000). 124

Appendix K-1: Confidence intervals at the 0.05 significance level for pH, total trace elements (T.E.) and total dissolved solids (TDS) in springs divided by bedrock lithology from which they discharge according to Okulitch (2005). 130

Appendix K-2: Confidence intervals at the 0.05 significance level for cations in springs divided by bedrock lithology from which they discharge according to Okulitch (2005). 131

Appendix K-3: Confidence intervals at the 0.05 significance level for anions in springs divided by bedrock lithology from which they discharge according to Okulitch (2005). 132

Appendix K-4: Confidence intervals at the 0.05 significance level for pH, total trace elements (T.E.) and total dissolved solids (TDS) in springs divided by temperature groupings. 133

Appendix K-5: Confidence intervals at the 0.05 significance level for cations in springs divided by temperature groupings. 134

Appendix K-6: Confidence intervals at the 0.05 significance level for anions in springs divided by temperature groupings. 135

Epigraph

"Water science is the foundation of management decision making."

Milburn, 1996

Chapter One: Introduction

The primary goal of this thesis is to assess the economic mineral potential of the South Nahanni River Basin (SNRB) by examining the geochemistry of groundwater springs for evidence of mineralization. This work forms one component of a federal government Mineral and Energy Resource Assessment study (MERA; see below), which also includes airborne geophysics, stream sediment sampling and hard rock geology exploration. A new multi-pronged method was developed using spring trace element geochemistry in order to assess mineral potential over a large area within a short time frame and modest budget. A side-benefit of this thesis is to provide part of what could be an environmental baseline of aqueous geochemical data. Given that Nahanni waters, sediments, fish, and caribou have already naturally elevated metals levels (Halliwell and Catto, 2003), it is important to characterize the natural background concentrations of a variety of chemical constituents which could be used to detect environmental impacts if any development were to occur in the future.

1.1 Nahanni National Park History

Most of the SNRB falls within the Deh Cho First Nations' land settlement areas and its upper headwaters are within the Sahtu's (Figure 1.1). Nahanni National Park Reserve was first designated by the Canadian Government in 1976 to protect the SNRB, which is located in the Mackenzie Mountains, Northwest Territories. It became a World Heritage Site in 1978. During the same time period three areas were chosen for possible future

national park expansion: the Ragged Range, the Tlogotsho Plateau and the Nahanni Karst. As a consequence, a MERA study (MERA I, see section 1.1) was conducted in those areas (Jefferson and Spirito, 2003). A recent proposal to include the entire watershed of the South Nahanni River in the National Park Reserve has automatically triggered a second, larger MERA study (MERA II).

1.2 The MERA Process

The MERA process, established in 1980, is the primary means whereby the Department of Indian and Northern Affairs Canada, Parks Canada, Natural Resources Canada and the territorial governments co-operate in conducting assessments of mineral and energy resources that would be removed from potential production through creation of a National Park (ICCM, 2005). Since the 1994 Whitehorse Accord, decisions to withdraw any lands from resource extraction must be based on all relevant technical, environmental, social and economic information, including information on energy and mineral potential that is gained through unbiased resource assessments (ICCM, 2005). The main goal of the MERA process is to help people make land use decisions with full knowledge of what is in the land in question.

1.3 Areas of Interest

The SNRB is primarily located in the Mackenzie Mountains east of the continental divide Figure 1.1A). The western side of the basin is characterized by the Selwyn Range of the Mackenzie Mountains and the Logan Mountains' saw-toothed Ragged Range, and the

eastern side of the basin is characterized by the Funeral, Headless, Caribou and Tlogotsho ranges, and the Hyland and Liard plateaus. The eastward progression of land between the mountains and the Mackenzie River is formed by the Mackenzie Plains. The Ram Plateau, which is dominated by karst features, borders the north-eastern corner of the current National Park (UNEP-WCMC, 2002). Physiographic regions of the SNRB are indicated in Figure 1.1B (GSC, 1986).

1.4 Spring Study Overview

Geochemical analyses of over 200 springs within the 37,000 km^2 SNRB since the 1980's are included in this assessment. This study includes 83 new water samples obtained during the 2003-05 field seasons, which are collated with 126 samples from the 1986-87 field seasons in the separate, non-overlapping, MERA I field areas (Hamilton, 1990; Jefferson and Spirito, 2003; Figure 1.1C). The spring geochemistries are used as tracers to elucidate the types and locations of mineral deposits in the SNRB. Specifically, the origin of the waters and their associated deposit types (e.g.: evaporites vs. sulphides) are assessed using stable isotopes (C, S, O, H), local bedrock types are related to springs' major ions, mineralized zones are predicted using three different data analysis techniques, and depth of mineralized zones are estimated using silica geothermometry.

Influencing factors on groundwater geochemistry in the SNRB are presumed to be temperature (indirectly, depth of circulation) and lithology of bedrock through which the springs are discharging and circulating. The resulting spring waters have geochemistry

characterized by variations in pH, TDS, major ions, and total trace elements. General trends are described over a large and geologically complex area, where the rock type is approximated based on previous studies. Overall, this is a reconnaissance-type project, where a large area is studied very quickly in order to identify zones where further, more detailed study is required.

Chapter Two: Background

A new geochemical exploration approach was developed in order to quickly identify mineralized zones in an area as large as Vancouver Island, given a limited budget and a total of 4 weeks of field work (split over two field seasons). Naturally discharging ground waters (i.e.: springs) of the SNRB were sampled and analyzed as indicators of mineralization in the local bedrock, with one of the largest datasets of springs known in the literature. The methodology was adapted from previous studies that largely focused on environmental impact assessments of mines, such as compiled by Plumlee et al. (1994).

2.1 The Watershed-Scale Approach to Mineral Exploration

> "An important next step in the development of geoenvironmental mineral-deposit models will be the shift to watershed- or ecosystem-based focus, where the deposits are considered not only in the context of their geology, but also in the context of their surrounding watersheds."
>
> -- Plumlee, 1999.

Ideally, mineral resource assessments, preferably at a regional or watershed-scale, are the first reconnaissance step in exploration and mine development (Plumlee and Logsdon, 1999). More detailed sub-regional environmental or prospect evaluations should follow, for example, determining local sub-watershed delineations, climate, stream chemistry, rock units, faults and fractures that may control flow, mine prospects, un-mined deposits, extent of metal mobility away from mineralized areas, and biological/ecological data –

i.e., potential receivers of impacts (Plumlee and Logsdon, 1999). This approach is considered to be a holistic one, as opposed to looking at just one piece of the ecosystem or watershed at a time. Geochemical characterization of entire ecosystems has been recommended to better understand mine impacts, pre- and post-mining. It has even been recommended to map world-wide geochemical patterns in many overlapping mediums to better understand our planet, one watershed at a time (Fortescue, 1992; Smith and Huyck, 1999).

The current SNRB study is well-aligned with these ideal development practices. It represents one of the largest compilations of spring geochemistry. The collected data could be used as part of a baseline study in an impact assessment if development were to occur because the SNRB is currently an area with little or no human impact.

2.1 Geochemical Exploration

Geochemical mapping is a common tool for regional reconnaissance, especially for large, under-explored areas such as the SNRB. Commonly used media include stream sediments (e.g.: Avila et al., 2005), lakes (e.g.: base metal exploration in the northern Canadian Shield; Cameron, 1978) and stream water samples (e.g.: Mingqi et al., 1995; Kelley and Taylor, 1997; Tosiani et al., 2004; Banks et al., 2004; Olias et al., 2004). Groundwater is another useful medium because it also is known to reflect bedrock geochemistry in particular during winter stream base flow conditions (i.e.: stream sampling in winter base flow conditions is equivalent to sampling spring water in

summer; Whitfield et al., 1996) and shallow (<50 m) wells (Deering et al., 1983). The usefulness of groundwater as a reconnaissance tool for large areas such as the SNRB is confirmed by Deering et al. (1983), where geochemical trends were more significant at the regional (~19 000 km^2) than local (~100 km^2) scale in shallow ground waters near mineral deposits of north-western Ohio.

Hydrochemical prospecting is not a new idea – broad discussions can be found in Runnells (1984), and groundwater sampling and anomaly-determination techniques have been described in detail in Giblin (2001). Mineral deposit models and their related geochemistries are well-established, as shown by Cox and Singer (1986) and Seal II and Foley (2002). More recently, hydro-geochemistry has also been incorporated into geochemical models (Plumlee et al., 1994; du Bray, 1995; Plumlee, 1999; Wanty et al., 2006). Primary factors affecting deposit-drainage water chemistry are: extent of exposure of the deposit, the grade of mineralization, amount of carbonate rocks (which buffers pH and reduces the tendency for minerals to be dissolved), and proportion of Fe-sulphides in the ore (Kelley and Taylor, 1997). Sometimes hydro-geochemical data have been incorporated into regional geochemical descriptions, with natural water being one of the foci that also include soils, sediments and mine drainage (e.g.: King, 1995; Miller, 2002).

One of the most directly applicable hydro-geochemical ore deposit models is the Ficklin Diagram (Plumlee et al., 1994 & 1999) which will be used here to infer local mineralized

zones of the SNRB, but is normally utilized to predict environmental impact of mineral deposits, such as acid-consuming or producing tendencies. This is done by plotting the sum of six key sulphide-related metals vs. pH, and comparing the spring geochemistry to fields of mine waters of known deposits.

Similar to the Ficklin Diagram approach described above, most other hydro-geochemical studies have been designed to predict environmental impacts of mines (Plumlee and Logsdon, 1999), rather than for exploration purposes. The U.S. Geological Survey has done extensive surveys of stream and spring samples in watersheds close to mined regions in order to improve the understanding of the local processes and environmental impacts (Miller, 2002; Wanty et al., 2006). Local studies have found significant geochemical trends which can predict mining potential, such as the Mississippi Valley-type deposits that were associated with elevated Pb-Zn concentrations (>20 ppb) in 143 spring samples over zones approximately 100 km^2 in size in Arkansas, U.S.A. (Steele and Dilday, 1985). There are many more examples from around the world in the literature of local, environmentally-oriented, hydro-geochemical studies that include, but are not limited to: Cu-Ni mines in Minnesota (Siegel and Ericson, 1980); Cu mine in Sweden (Sanden et al., 1997); Pb-Zn ore deposits in New Brunswick (Leybourne et al., 1998); Au, Cu-Mo, and Au-bearing iron-skarn deposits in Wrangell - St. Elias National Park in Alaska (Eppinger et al., 2000); antimony deposit in Denali National Park in Alaska (Eppinger et al., 2002); pit lake inflows of high grade Cu-Zn-Ag-Mn veins in Montana (Pellicori et al., 2005); groundwater samples from sulphide mine tailings in northern

Manitoba (Sidenko and Sherriff, 2005); acid mine drainage in Japan (Ohkuni et al., 2004); abandoned mine in Colorado (Verplanck et al., 2004); and Ag and Au-rich veins that have been mined since 1548 in Mexico (Carrillo-Chavez et al., 2003).

Hydro-geochemical prospecting has generally been restricted to areas with developed well networks. In Australia, water analysis from wells has been used as an effective exploration tool to map out anomalies in groundwater chemistry (Giblin, 2001; de Caritat and Kirste, 2005). Similarly, elevated strontium concentrations from a study with one-hundred shallow wells (<50 m) sampled in a 19 000 km^2 area rich in carbonates and evaporites were linked to Mississippi Valley-type deposits (Deering et al., 1983).

2.2 Climate of SNRB

The SNRB encompasses two eco-zones: taiga plain to the southeast and taiga cordillera to the northwest (Figure 1.1A). Its climate is cold continental with wide monthly variations in temperature and precipitation, and long cold winters and short warm summers (Staple and Wall, 1996). Recorded temperatures at Fort Liard are maximum (34 °C) in the summer months (June-August) and minimum (–46.7 °C) in the winter (Parks Canada, 2001). In the headwaters of the basin, average summer temperatures range between 6 to 17 °C, with 60-90 mm average monthly precipitation, and an average winter lows of -21 ºC in January (Staple and Wall, 1996; Parks Canada, 2001). Most of the annual precipitation (530 mm) falls in the summer (Staple and Wall, 1996). Parks Canada and Environment Canada have weather monitoring stations at Nahanni Butte,

Fort Simpson and Tungsten. The vegetation is consistent with habitat that is well drained but usually moist through most of the growing season, i.e.: both wet and dry (UNEP-WCMC, 2002). The SNRB has both continuous and extensive discontinuous permafrost zones (Figure 1.1A).

2.3 Geologic Overview of SNRB

The geology of the SNRB is well-summarized by Gordey and Anderson (1993) and includes 5 major components: Late Precambrian to Middle Devonian platform-basin assemblage, Devono-Mississippian turbidite basin assemblage, Mississippian to Triassic clastic shelf assemblage, regional Jurassic-Cretaceous deformation, and granitic intrusions of the Mid-Cretaceous Selwyn Plutonic Suite crosscutting the regional structure. Not included in Gordey and Anderson (1993) is the modern shortening of the Mackenzie Mountains at an average of 4 mm/yr (Hyndman et al., 2005). A simplified geology map of the SNRB, based on Okulitch (2005), is presented in Figure 2.1.

2.3.1 Topographical Features

Overall, the SNRB encompasses two main topographical regions: 1) the relatively flat south-eastern region which is characterized by broadly folded karstic terrain, shallowly-incised topography, and inferred faults; and 2) the mountainous north-western region with more complex structure (including igneous intrusions of the Cretaceous Selwyn Plutonic Suite) and strong glacially-eroded terrain.

Distinct, separate features of the SNRB are often discussed in regards to the proposed National Park expansion. These are highlighted in Figure 1.1B as: the eastern edge of the Selwyn Mountains, the southern area of the Mackenzie Mountains, the Liard and Hyland plateaus near the southern edge of the SNRB next to the British Columbia/Yukon border, the Tlogotsho Plateau in the southeastern part of the SNRB, the Nahanni Karst in the northeastern part of the SNRB (including the Ram Plateau), the Ragged Ranges in the western side of the SNRB with its Cretaceous igneous intrusions and tall peaks (such as the Logan Mountains that include the "Cirque of the Unclimbables"), and the Mackenzie Plain which borders the eastern edge of the Mackenzie Mountains towards the Mackenzie River.

The regional physiography of the SNRB is characterized by glacially eroded terrain, karst terrain, and muted, shallowly incised topography (Ford, 1973; Duk-Rodkin et al., 2004). The region has been glaciated in the past and the Cordilleran / Laurentide Ice sheet boundary is found in the Wrigley map area, north of the SNRB, as indicated by glacial erratics such as granitic boulders from the Canadian Shield (Gabrielse et al., 1965). Northern parts of the SNRB were not covered by continental glaciers; this area was the boundary region between mountain and continental glaciations, where an ice-free corridor probably occurred during the last ice age (Ford, 1976; Duk-Rodkin and Lemmen, 2000; Halliwell and Catto, 2003). Nahanni National Park is described as having the largest variety of landscapes of any Canadian national park due to having Cordilleran ice sheet influences on its western side, Laurentide ice sheet influence on its

eastern side, and a completely unglaciated central area that allowed the formation of 3200-4500 ft high cliffs by the South Nahanni River over a million years (Ford, 1976).

Extensive karst topography, solution channels, caves and sinkholes occur in carbonate rocks, particularly in the Nahanni Karst/Ram Plateau area, caused by chemical dissolution and re-precipitation of the naturally soluble carbonate minerals by rainwater and snow-melt (Brook and Ford, 1980).

2.3.2 Sedimentary Geology

The Mackenzie Mountains are comprised mainly of sedimentary rocks, including Neoproterozoic (~800 Ma) to Late Cretaceous (~100 Ma) platformal to basinal shale sedimentary strata. Proterozoic strata are comprised of the Windermere and Mackenzie Mountain Supergroups, which are exposed in the Ragged Ranges of the western side of the SNRB, but not on the eastern side. They are dominantly platformal and basinal strata (carbonates, shales, and shaly facies), with some units hosting skarn deposits where they are intruded by plutons (e.g.: Tungsten/Cantung Mine).

Palaeozoic strata are subdivided into the carbonate-dominated/platformal (Rabbitkettle, Sunblood, Whittaker, Nahanni, Arnica and Headless formations) and shale-dominated/basinal (Road River Group and Cadillac and Funeral formations) facies. This significant facies change occurs in the Devonian rocks in the Ragged Ranges - from mainly carbonate strata in the east to graptolitic shales to the west (Gabrielse et al., 1965;

Figure 1.1B). The Cambrian to Early Devonian package comprises platformal carbonate strata, and Selwyn Basin shales to shaly carbonates (Road River Group, Prairie Creek Embayment strata) on the Devonian Shale side of the Devonian Carbonate/Devonian Shale facies boundary (Gabrielse et al., 1965).

The Selwyn Basin, mostly found in the western side of the SNRB, is a well known geological province that spans the Yukon and part of the NWT. A basin formed by passive margin sedimentation, it is characterized by thick accumulations of clastic sediments, with a significant component of deepwater black shales and cherts. These basinal rocks interfinger with, and are bound by, shallower water platformal carbonates. Spatially, the Selwyn Basin grades into the platformal facies of the Mackenzie Platform towards the east, is bound to the north by the Dawson Fault, and is offset to the southwest by the Tintina Fault (Heon, 2003). In the SNRB, Late Devonian to Jurassic rocks include basinal shales, cherts and turbiditic sandstones to conglomerates of the Earn Group in the Ragged Ranges area of the Selwyn Basin.

In the Tlogotsho Plateau/Nahanni Karst area of the eastern side of the SNRB, the package includes shales and cherts of the Besa River and Fort Simpson Formations, carboniferous shallow marine carbonates and continental sandstones with coal measures (Mattson Formation), and basinal cherts and mudstones of Permian and Triassic ages. Late Jurassic to Late Cretaceous fine-to-coarse clastic rocks record a complex interplay of

continental to marine deposition and include important coal measures in the region (Stott, 1982).

2.3.3 Igneous Geology

The sedimentary rocks of the SNRB were intruded by minor Devonian (350 Ma) granitoid rocks and all were folded and thrust faulted during the collision of an island arc with western North America, spanning the Jurassic (~170 Ma) to Cretaceous. During this collisional event the Selwyn and westernmost Mackenzie Mountains were intruded by major Cretaceous granitoid batholiths interpreted to be a result of syn- to post-collisional partial melting of miogeoclinal strata within the thickened crustal material (Woodsworth et al., 1991). Most of the mid-Cretaceous intrusions have relatively restricted mineralogies, classified as biotite-hornblende-bearing, biotite-bearing, and biotite-muscovite-bearing plutons (Anderson, 1983). Compressive and right lateral strike-slip adjustments continued throughout the Tertiary (~40 Ma) and to the present (e.g. the 1985 Nahanni Earthquake) in the SNRB (Hyndman et al., 2005; Gendzwill, 1994).

Plutonism in the area is temporally related to crustal shortening during the mid-Jurassic to Palaeocene formation of the Mackenzie Mountains. Granitic pegmatites are associated with many of the plutons of the Cretaceous Selwyn Plutonic Suite, both with hornblende and non-hornblende bearing plutonic rocks, mostly between 89-95 Ma as an emplacement age (Mauthner et al., 1995).

2.3.4 Known Mineral Occurrences

The area around the Yukon/NWT border is host of world-renowned sedimentary-exhalative (SEDEX) deposits of zinc, lead, and silver (barite) such as Faro, Howard's Pass and the Tom and Jason deposits of Macmillan Pass. Howard's and MacMillan passes are the closest to the SNRB and are shown in Figure 1.1A. These deposits are hosted in Cambrian to Devonian rocks of the Selwyn Basin and of the Earn Group (Heon, 2003). The Earn Group is host to numerous strata bound barite/base metal deposits (Gordey et al., 1982). The Selwyn Basin and Earn Group are primarily located across the Yukon Territory, but both continue into the SNRB, both large components of the western shale facies in Figure 1.1B, indicating the high potential for mineralization of a largely unexplored area.

Across the Yukon, the Earn Group is host to a total of twenty-five mineral prospects, twelve of which are hosting known mineralization (Yukon Geological Survey, 1996). The most commonly identified deposit types are zinc-lead sedimentary exhalative deposits or copper-skarn deposits. The most important deposit within all of the Yukon to date is the Howard's Pass zinc-lead sedimentary exhalative deposit hosted by Road River Formation rocks near the Yukon/NWT border. Drilling programs from 1982 indicated reserves for the Howard's Pass deposits are approximately 113.4 million tones, averaging 5.4% zinc and 2.1% lead. Inferred reserves for both deposits are in excess of 362.9 million tones (Yukon Geological Survey, 1996).

Magmatism in the SNRB region, which defines the eastern extent of the Tintina Gold Province, is generally associated with tungsten mineralization and/or gold-copper-antimony-bismuth-lead-zinc metal occurrences (Rasmussen et al., 2006). Known mineral deposits near or in the SNRB include the Lened tungsten skarn in the platformal Rabbitkettle formation (located near Howard's Pass between the Cantung and Mactung tungsten deposits along the Yukon - Northwest Territories border), Tungsten (also known as Cantung Mine, located at the western end of the SNRB), and the lead-zinc vein deposit of Prairie Creek (at the eastern end of the SNRB) hosted in the Whittaker Formation (Hamilton, 1990). Tungsten skarn deposits are preferentially associated with biotite-muscovite-bearing plutons where they contact argillaceous limestone of various ages (Gordey and Anderson, 1993).

Cantung Mine is a base metal (W-Cu) skarn deposit and the only tungsten mine in Canada, currently holding 12% of the world's tungsten reserves (ITIA, 2005). Prairie Creek Mine (owned by Canadian Zinc Corporation), which never came into production but is almost fully complete in terms of infrastructure (including a mill), is currently under permit approval processes and is trying to re-open since its closure in 1982. It is one of Canada's largest Pb-Zn deposits at 11.8 million tonnes with 12.5% Zn, 10.1% Pb, 161g/t Ag and 0.4% Cu (GNWT, 2005). It is the highest grade Mississippi Valley-type deposit (Pb + Zn as weight %), and is in the top six for total geological resources (production + remaining) in Canada (Hannigan, 2006).

Placer gold potential also exists in Ragged Ranges and northern Liard Range-southern Ram Plateau area (Hamilton et al., 1988; INAC, 2001). Southeast of Nahanni National Park Reserve, towards Fort Liard, world class natural gas deposits have been discovered within Devonian and Carboniferous dolostones, shales, sandstones and limestones (NEB, 1996; Robinson and Irwin, 2000).

2.4 Groundwater Geochemistry

Groundwater often reflects the rock-types that it flows through. There are the 5 major rock types which occur in the SNRB based on groupings from Okulitch (2005): carbonates, salts, shales, sandstone and plutons (Table 4.1 shows the units related to MERA II springs). Salt deposits in the SNRB are usually minor units interbedded within carbonates (Okulitch, 2005). The governing principles which guide the environmental signatures of these rock types in groundwater are explained in detail in Freeze and Cherry (1979), Stumm and Morgan (1981), and Appelo and Postma (1999). Groundwaters in complex or stratified sedimentary systems, such as the SNRB, exhibit complex spatial patterns that are difficult to interpret, even with good stratigraphic and groundwater flow information (Freeze and Cherry, 1979); geochemistry of the discharge waters can be affected by the order the rocks are encountered in, their ion exchange or redox reactions and flow direction (Freeze and Cherry, 1979). Regardless, bedrock geology is the dominant controlling factor in mountainous headwaters geochemistry (Miller, 2002) and expected geochemical trends from the SNRB's major bedrock geology types are as follows.

2.4.1 Carbonates

Carbonate rocks, such as limestone and dolomite, are found throughout the SNRB and their waters are usually dominated by Ca-Mg-HCO_3 (Hem, 1985). They can often be explained in terms of equilibrium reactions, with silica or clay as a minor constituent (Hem, 1985; Freeze and Cherry, 1979). Limestone often contains gypsum and sodium chloride (Hem, 1985) as found in certain units of the SNRB (Okulitch, 2005).

Many springs of the SNRB have cyanobacteria growing near their outlets, creating mats that may influence calcium carbonate precipitation (also known as travertine or tufa) when the spring water is rich in calcium and bicarbonate, and such as is observed in other hot springs in western Canada (e.g.: Pentecost, 2003). The degassing of carbon dioxide as per the following reaction causes this precipitation:

$Ca^{2+} + 2HCO_3^- \leftrightarrow H_2O + CaCO_3 + CO_2$

2.4.2 Salt Deposits

Salts, also known as evaporites, include gypsum, anhydrite, $MgSO_4$, NaCl, Na_2CO_3. They are highly soluble and typically cause waters to have very high TDS (typically above 1000 ppm; Hem, 1985; Freeze and Cherry, 1979). Many units of the SNRB are interbedded with gypsum or anhydrite, such as the Bear Rock, Tetso, Mount Cap, Saline River, Little Dal Group and Redstone River formations (Okulitch, 2005).

2.4.3 Shales

Shales include fine-grained sedimentary rocks, which are mainly composed of clay minerals and other particulate matter that was formed by chemical reactions between water and silicates (Hem, 1985). The conversion from clay to shale typically occurs during compaction and/or tectonic activity (Freeze and Cherry, 1979). Water flowing through shales tends to have higher TDS due to longer water/rock interaction (less permeable, less connected pores; Hem, 1985). Shales can contain layers of coarser material that can hold or transmit more water. Sulphide mineral presence is common in shales and coal-bearing sandstones, which are deposited in reducing environments (Hem, 1985). Clays have a large cation exchange capacity, potentially having a large effect on the dominant cations (Na, Mg, Ca, and K) (Hem, 1985; Freeze and Cherry, 1979). Sulphides could be present in SNRB rock formations such as shales from the Besa River Formation (Okulitch, 2005).

Pyrite oxidation, which occurs in pyrite-bearing rocks, increases sulphate concentrations and reduces the pH of the water. Low pH conditions mobilize heavy metals that have been sorbed or fixed on solid phases and also increases their solubility (Freeze and Cherry, 1979; Igarashi et al., 2003). Pyrite oxidation is governed by the following reaction:

$Fe_2S + 7/2O_2 + H_2O \Rightarrow Fe^{2+} + 2SO_4^{2-} + 2H^+$

2.4.4 Sandstones

Sandstones can be dominated by quartz, garnet, tourmaline and zircon rock fragments (Hem, 1985) but their geochemistry also depends on their original material, cement type, or lack of previous weathering such as remaining feldspars. The cements are most commonly calcium carbonate, silica, ferric hydroxide or ferrous carbonate, with mixtures with other materials such as clay (Hem, 1985; Freeze and Cherry, 1979). Co-precipitation of metals is very possible, and/or cation (e.g.: Ca, Mg, Na, K) and anion (e.g.: OH^-/F^-) exchange on particle surfaces (Hem, 1985). Sandstones can stay in reducing conditions for long periods of time and therefore may contain reduced mineral species such as pyrite which can later be oxidized. Coal-bearing sandstones in the SNRB include an unnamed Eocene clastic unit, and the Wapiti, Summit Creek, Little Bear and Mattson formations (Okulitch, 2005). In particular, the Mattson Formation is a resistant unit of quartz arenite with some sandy shale sections, and minor siltstone, limestone and coal (Okulitch, 2005).

2.4.5 Plutonic Rocks

Igneous rocks are dominantly composed of silicates, such as quartz and alumino-silicates (such as feldspars and micas) whose weathering is governed by the Goldich weathering sequence (Goldich, 1938; Freeze and Cherry, 1979). Plagioclase is usually the first mineral to be weathered. Nesbitt and Young (1984) predict that rocks are first stripped of CaO and Na_2O before K_2O. On average, waters that flow through igneous rocks tend to have relatively higher Si, Al, Fe, Na, and K concentrations, but lower Ca and Mg

concentrations than those flowing through carbonates (Hem, 1985; Stumm and Morgan, 1981). The weathering of albite to kaolinite or gibbsite is an acid consuming reaction (Appelo and Postma, 1999).

Groundwater flowing through igneous rocks can differ greatly in its geochemical signature depending on its depth of circulation, e.g.: shallow, Ca-HCO_3-rich, dilute systems such as in the Stripa granite in Sweden (Nordstrom et al., 1989) or deep, hot, metalliferous, high pH springs throughout Europe (Michard, 1990).

Igneous rocks are also often linked to mineralized zones. In areas intruded by granitic masses, metal concentration in specific local zones is common (e.g.: Zolotarev, 1984). Groundwater can also flow through the igneous rocks and concentrate metals by re-depositing them downstream. For example, a cave within granites in the southwestern states has birnessite (manganese IV oxide) being precipitated in its speleothems, due to the manganese mineralization upstream of the cave (Finlayson and Webb, 1988).

2.5 Depth of Circulation

Identified mineralized zones can be evaluated in terms of accessibility by approximating depth of circulation of indicator springs. Combining knowledge of large scale faults and fractures, geothermometry-estimated spring reservoir temperatures and geothermal gradients can be a useful tool for approximating depth of water circulation.

2.5.1 Groundwater Flow in Mountainous Terrain

Flow in mountainous terrain is controlled by surface topography, geology, climate and regional heat flux, of which water table elevation can be a sensitive indicator (Forster and Smith, 1988). Looking at the regional geology overlain with spring locations (Figure 4.1), it is noticeable that most springs outflow from faults or contacts between major units. This indicates a preference for groundwater flow along high permeability pathways, consistent with the southern Cordillera (Grasby and Hutcheon, 2001) and modeling work of Caine et al. (1996). Even in low heat-flow settings, these high permeability windows can allow the development of thermal springs if the water circulates deep enough and rises faster than it cools (Grasby and Hutcheon, 2001). There is a critical range of permeabilities which favour the formation of thermal springs: 10^{-16} to $10^{-14}m^2$ (Smith and Forster, 1990; Lopez and Smith, 1995) typical of large-scale faults and fractures.

The structural and seismic setting of the Mackenzie Mountains, an active tectonic compressional belt, is a good setting for deeply circulating springs, which usually discharge from large scale faults and fracture systems. Stratigraphic and structural features in most sedimentary mountainous systems can locally and regionally affect groundwater flow patterns (Mayo et al., 2003; Allen and Michel, 1998; Janes, 1998; Huntoon, 1981; Mayo et al., 1985 ; Mayer and Sharp, 1998). Currently, northern Cordillera GPS-estimated velocities of horizontal compression are ~4 mm/yr relative to the craton (Hyndman et al., 2005). The largest recorded earthquake in the Canadian

Cordillera occurred in the Mackenzie Mountains on December 22nd 1985 with a 6.9 magnitude, whose compressional force is believed to be coincident with the principal tectonic stress during orogenesis (Gendzwill, 1994).

In particular relevance to groundwater springs which typically discharge from faults and fractures, the Nahanni Thrust Fault, parallel to the Beaver River Structure (BRS; Figure 1.1C), shows minor amounts of mineralization in its fracture fillings such as pyrite, galena, sphalerite, and copper-containing minerals (Morrow and Miles, 2000). The BRS can therefore be used as a sign that mineralized zones exist within faults and fractures throughout the SNRB.

It is likely that different geochemical signatures can be identified, perhaps from overlapping flow zones, such as "shallow" vs. "deep" systems. In the SNRB, it is assumed that springs flowing from deeper systems are likely a) flowing near or from faults or fractures, b) are gaseous, or c) have higher temperatures as indicated by Si-geothermometry. A more detailed description of estimating depth of circulation follows.

2.5.2 Heat Flow

The normal geothermal gradients of the Cordillera, even in low heat-flow settings, are sufficient for thermal springs to develop, simply due to the existence of brittle faults that provide high permeability flow paths for deep-circulating meteoric water (Grasby and Hutcheon, 2001). There is high heat flow in the northern Canadian Cordillera, estimated

to be 105 ± 22 mW/m^2 (Lewis et al., 2003). Estimated Moho temperatures range between 800-1000 °C, with 32-35 km crust thickness in higher elevations; this is a thinner crust and weaker lithosphere compared to the Slave Craton (Lewis et al., 2003). The geothermal gradient is estimated to be 23-31 °C/km (Hyndman et al., 2005).

Many thermal springs in Canada occur in or near Tertiary or younger plutons, suggesting these young intrusive bodies have a relatively high thermal aura (Souther and Halstead 1973), but the older SNRB plutons (mid-Cretaceous in age) are unlikely to be a significant heat source. Heat flow thus differs with pluton ages. For example, in the Idaho Batholith there are two ages of plutons: Tertiary and Cretaceous. The area near and within the younger pluton has a geothermal gradient of 32°C/km vs. 25°C/km near the older pluton, resulting in a heterogeneous heat flow field (Druschel and Rosenberg, 2001).

2.5.3 Geothermometry

Chemical species, such as silica, K or Na, are controlled by temperature-dependent mineral reactions. Chemical geothermometers can be applied to estimate the reservoir temperature if the water in which they are dissolved discharges at surface relatively quickly, without re-equilibrating to lower-temperature conditions (Fournier and Truesdell, 1973; Truesdell, 1976; Tonani, 1980; Arnorsson, 1983; D'Amore et al., 1987; Nieva and Nieva, 1987; Giggenbach, 1988; Kharaka and Mariner, 1989; Tole et al., 1993; Pang and Reed, 1998).

The application of silica geothermometers is the most appropriate for estimating temperatures of Na-HCO_3 type springs (Choi et al., 2005). Since low temperature Na/K ratios are controlled by mineral dissolution or precipitation, they may cause erroneous results (Mutlu and Gulec, 1998). When the two different silica and Na/K-geothermometers agreed, it was assumed that it was the most reasonable estimate for the spring reservoir temperature in Choi et al. (2005). Cation geothermometers are notoriously slow to equilibrate at the low temperatures of non-thermal groundwaters, supporting silica geothermometry for the many SNRB colder springs. Grasby and Hutcheon (2001) also show that silica is the best geothermometer for carbonate rocks.

Other types of errors can occur in the estimates when at deep crustal conditions, quartz solubility decreases as the NaCl content of the fluid increases, and drops very sharply with the addition of CO_2; thus, if immiscible brine–CO_2 fluids exist in the deep crust, silica will partition strongly into the brine (Walther and Orville, 1983; Newton and Manning, 2000a, b). This was considered negligible for our purposes in the SNRB because even the six high pCO_2 springs of our study had total dissolved solids that ranged between 950 to 2400 ppm and none are dominated by NaCl. Ekwi spring is the only spring strictly dominated by NaCl and had the highest total dissolved solids at 15 000 ppm, but is located outside of the SNRB and included only as comparison. Common dissolved salts generally have an insignificant effect on quartz solubility in natural groundwaters such as in the SNRB because dissolved silica exists predominantly as a

neutral species (H_4SiO_4). World-wide reservoir temperatures for CO_2-rich springs typically range between 100-170ºC (Choi et al., 2005) such as is expected in the SNRB. The extreme case of high temperature (>250°C) or high salt content is not considered applicable here.

2.6 Overview of Spring Study

A watershed-scale approach to the method of geochemical exploration is being used as a quick reconnaissance tool for a large, under-explored area using easily-accessed, naturally discharging groundwater (i.e.: springs). First, major rock types of the SNRB, which were determined by grouping units based on a compilation by Okulitch (2005), are linked to local spring geochemistry. Secondly, a common method of predicting environmental impacts for different mineral deposits (i.e.: a Ficklin Diagram) is being used in a new way by studying the natural environmental signatures and predicting potential mineralized zones. Other methods based on Giblin (2001) and comparisons with geochemistry of deposit-related waters are used to identify indicator springs of mineralized zones within the SBRB, making this analysis a multi-pronged approach. Lastly, in order to judge the accessibility of mineralized zones, estimates of depth of circulation of springs are made using the geological setting of the SNRB and its regional geothermal gradient.

Chapter Three: Methods

3.1 Field Methods

Previously known springs were located using previous reports such as Brandon (1965), Souther and Halstead (1973), Crandall and Sadlier-Brown (1976), and Hamilton et al. (1988), Hamilton (1990) and Jefferson and Spirito (2003), and in some cases were re-sampled. Previously sampled springs from the MERA I study (Hamilton, 1990; Jefferson and Spirito, 2003) were included, where possible, in many of the analyses of this thesis. New spring locations were found by sighting from a helicopter in the summer months (June, July or August). A bare patch of ground within a vegetated area, a spot of colouring (usually a red or white zone of precipitate, or a bright green patch of algae), and creeks flowing out of mountains or starting from nowhere, were some of the visual clues used. Creeks starting from below patches of snow or ice were avoided since their main source was likely freshly melted water, although a few were sampled simply for comparison. At each spring, a GPS location was obtained, and Eh, pH, electrical conductivity, dissolved oxygen and temperature were measured as close to the outlet as possible (see Table 3.1 for a list of instruments used).

A typical, complete water sample included (Table 3.2): cations and trace elements (samples field acidified to a pH < 2 with ultra pure nitric acid – $HNO_{3(aq)}$), anions, alkalinity, $\delta^{34}S$ analysis on sulphates (field precipitation of $BaSO_4$ by adding barium chloride - $BaCl_2 \cdot 2H_2O$), $\delta^{34}S$ analysis on sulphides only if they were detectable by smell

($CdS_{(s)}$ was precipitated by adding cadmium acetate - $(CH_3COO)_2Cd{\cdot}2H_2O_{(s)}$), dissolved inorganic carbon $\delta^{13}C$ analysis ($HgCl_{(s)}$ was added to inhibit micro-organisms), silica (with dilution factor of 6 to inhibit precipitation, using doubly distilled water), $\delta^{18}O$ and $\delta^{2}H$ (lids sealed tightly with paraffin wax to prevent evaporation), dissolved gases with tightly sealed lids (which were sealed underwater, and covered in paraffin wax), and free gases only when bubbles were seen at the spring outlet (a sample bottle was filled with water, held upside down over the bubbles, where they were funnelled into the bottle so that the gas could displace the water, then tightly sealed underwater and covered with paraffin wax). Sulphide samples were taken at the spring, preserved with Sulphur-Anti-Oxidant Buffer (SAOB) and measured with a sulphide probe at the base camp only when sulphides were detectable by smell.

All samples were filtered using 0.45μm filter paper, except those listed in Table 3.2. The filter apparatus was rinsed with distilled water once and with filtered sample water 3 times, in between each spring. Cation sample bottles were rinsed three times with filtered sample water before being used, and the anion and alkalinity bottles were rinsed once. The samples were kept in coolers and fridges until laboratory analysis. Additionally, samples were also taken of any mineral precipitates present for x-ray diffraction and $\delta^{13}C$ analysis of $CaCO_{3(s)}$.

3.1.1 Note about Terminology

The terms “major ions” and “trace elements” are used throughout this report, even though they may not be representative of their respective element concentrations in particular springs. For example, when total trace elements add up to more than 10% in a sample, they are not “trace” elements anymore, but for simplicity will still be referred to as such. In this report, major ions are therefore Na, K, Ca, Mg, Cl, HCO_3, and SO_4, while everything else is considered trace elements.

3.2 Laboratory Methods

In total, 95 samples were analysed for MERA II. Analyses included 7 laboratory duplicates (Champagne Creek, Deca, Galena, Mossy, Clark Lake, Cascade, Persistent), 5 field duplicates (Champagne, Broken Skull Upper Pool, Sombre, Dookie, Blue Bells), one field triplicate (Dookie), one trip blank and one laboratory blank. Ten of the water samples are surface water, one is direct mine water, three are seeps and the rest are springs. A list of field duplicate samples taken from both MERA studies combined (i.e.: from 1986-2005 field seasons) is shown in Appendix A with their respective major ions, TDS and % total trace elements.

Alkalinity was measured using an Orion 960 Autotitrator with $H_2SO_{4(aq)}$ and ROSS pH electrode. Anions, cations and trace elements were analyzed at the Geological Survey of Canada Laboratories in Ottawa. Anions were measured using Ion Chromatography (IC-110). The cations and trace elements were measured using Inductively Coupled Plasma emission spectrometry / mass spectrometry (ICP-ES / ICP-MS 120) as described in Table

3.3. The limits of detection for the anions, cations and trace elements are listed in their respective tables in Chapter 4, and the trace elements detection limits are also listed in Table 3.3.

Oxygen and deuterium isotopes in water were analyzed by the Geological Survey of Canada Laboratory in Quebec, and sulphur and oxygen isotopes in sulphate were analyzed at the University of Calgary Isotope Laboratory using continuous flow and dual inlet isotope ratio mass spectrometry. Stable isotope composition ($^{18}O/^{16}O$, D/H, $^{34}S/^{32}S$) are expressed in the usual δ notation:

$$\delta(‰) = [(R_{sample} - R_{standard})/(R_{standard})] \times 10^3,$$

where R is the ratio of heavy to light isotope abundances. Reference materials, standards, and uncertainty of isotope measurements are described in Table 3.4.

3.2.1 Percent Error

Percent error for MERA II samples using duplicates, triplicates and blanks was determined as follows: The triplicate % error was calculated as (standard deviation)/(average), while duplicates were calculated by (A-B)/(A+B). The overall error of major ions is 3%. All major ions were undetected in both blanks, except for 0.3ppm Ca in the field blank (which is 0.4% of the average Ca value in the duplicates and triplicates; therefore negligible and within overall % error). The overall error of trace elements is 7%. All trace elements detected in the field blank were, on average, 2.1% of the average concentrations of samples for each element, and 1.4% in the lab blank, therefore field- and laboratory- introduced errors are negligible and within the overall %

error. Cu and Pb concentrations were high in both blanks due to the boiler used to make the distilled water, but this effect was not found in the samples. A compilation of duplicate MERA I and II samples is listed in Appendix A.

3.2.2 Charge Balance

All 93 MERA II samples have <10% in charge balance error except for seven springs which are within 15%, and three which are within 20% (Table 4.3). Ninety percent of MERA II samples to have a charge balance < 10% and the rest < 20%, indicating good sample quality for the most part.

3.3 Geothermometry Approach

The Solmineq88 program (Kharaka et al., 1988) was used to create geothermometry graphs and solubility diagrams. Inputs included spring temperature, pH, and concentrations in mg/L of Na, K, Mg, Ca, Cl, SO_4, SiO_2, Fe, Al, alkalinity (as HCO_3) and Eh potential (mV). Outputs of the model included estimated reservoir temperatures using seven different geothermometers: a) quartz conductive (if water is boiling or steaming); b) quartz adiabatic (if no steam is lost); c) chalcedony with SiO_2; d) alfa-cristobalite with SiO_2; e) amorphous silica (if amorphous silica saturation); f) log(Na/K) (if in-situ temperature is >150 °C); and g) log(Na/K)+1/3*log($Ca^{0.5}$/Na) (if temperature is <100 °C).

Generally, high-temperature reservoirs are usually studied with the quartz geothermometer, and low-temperature (<100?C) with chalcedony (Fournier, 1981).

Relatively young silica (ex: Iceland) may be present as chalcedony, whereas well-crystallized, older silica is more likely present as quartz (Xilai et al., 2002). In the SNRB, it is assumed that chalcedony is the most applicable geothermometer (as opposed to quartz, amorphous silica or cristobalite) because it is in a normal, low-temperature setting. The chalcedony Si-geothermometer was also used by Gulley (1993) on the Rabbitkettle Hot Springs, on the western end of the current Nahanni National Park, because 1) using silica-geothermometers eliminates the errors associated with CO_2 degassing in carbonate-dominated areas and 2) chalcedony is the accepted geothermometer for low temperature systems according to Fournier (1981) such as in the SNRB.

The method of plotting select mineral solubilities at different temperatures (Pang and Reed, 1998) was also applied to 5 warm springs.

3.4 Determination of Dominant Major Ions in Aquachem

Water type in Aquachem is calculated as follows:

- All concentrations are converted to meq/L.
- Values are then transformed from meq/L to meq %.
- All parameters which are below a certain limit (10%) are removed.
- The remaining ions are considered **Major ions**. These ions are ordered according to their percentage. Cations are ordered first, followed by the anions.

The result is the **Water Type** string (e.g. Ca-Mg-HCO_3) for each spring. These water-type strings were used to group springs in Table 4.7 along with lithology, pH, temperature, total dissolved solids and total % trace elements.

3.5 Trace Element Data Analysis

A multi-pronged approach was developed to detect mineralized zones through indicator springs in the SNRB. Mineralized zones are identified by above-average total trace elements, individual elevated trace elements and Ficklin Diagram groupings. This methodology is tested by: 1) comparing the results to the two known deposits of the area (Tungsten and Prairie Creek), 2) testing the consistency of detected zones of elevated trace elements with current deposit models for the region (e.g.: Earn Group shales, halos of alteration around plutons), and 3) comparing the elevated cut-off values with mineral deposit related waters around the world. Most of these comparisons are done by visual inspection of data plots, descriptive statistics and partitions as described in the literature in other similar studies of the hydrogeology discipline. Ultimately, these results can only be tested with detailed field studies and drilling programs.

3.5.1 Total Trace Elements

Total trace element concentrations were normalized after Giblin (2001) by dividing them each by TDS, and were labelled as 'elevated' if they were above the average of the SNRB (0.9%). These elevated springs were then plotted on a Piper Diagram where geochemical groupings were identified and linked to major ions, pH, temperature and a bedrock geology map (Figures 4.3, 4.9). This method can detect a variety of potential

deposit types, because it lumps all the trace elements into one parameter. It may also be an indicator to the size of the deposit.

3.5.2 Individual Trace Elements

Elevated individual trace elements were identified and counted for each spring by using averages and standard deviations, and highlighted in bold font (Table 4.4a-c). Descriptive statistical results (minimum, maximum, average, average + 1 standard deviation of concentrations) for each trace element in the SNRB springs were plotted, and elevated trace elements were identified using six different approaches depending on the element and its distribution (as listed at the end of Table 4.4 a-c, based on Figure 4.9). For example, some elements are only detected in a few springs (e.g.: Ag), therefore all springs with detectable concentrations are considered elevated in that element, even if their concentrations are below average. On the other hand, some elements are very common (e.g.: Cu or Zn) and therefore need a higher cut-off to be defined as "elevated". Additionally, some element distributions may be skewed to the left or right of a normal distribution, also affecting the cut-off value. Cut-off values which were used for each element include: 50%, 100% and 150% of the average, and the average plus 50%, 100% and 150% of the standard deviation (Table 4.4a-c). The aim was to find the approximately top fifteen springs (about the 7^{th} percentile) for each element.

A large variety of combinations and permutations of elevated elements in the environment can indicate different mineral deposits. For example, a possible deposit as

indicated by elevated Ag is a sedimentary exhalative deposit, if seen in combination with Cu, Au, Zn, Sn, Pb, As, Sb, S, C, NH_3, Ba, Mn and Fe (Cox and Singer, 1986). As another example, sedimentary manganese deposits leave a geochemical signature of Ba, Mn, P and Pb (du Bray, 1995). Because these signatures have been found in rocks, they may not be the same in water, depending on the pH, Eh and salinity (a more detailed discussion on the geo-availability of metals can be found in Appendix B). Geochemical signatures from deposit models by Cox and Singer (1986) have, on average, nine elevated elements, although some have as few as one or as many as nineteen.

3.5.3 Ficklin Diagram

A Ficklin Diagram, where pH is plotted vs. the sum of the concentrations of six key sulphide-related metals, was used to characterize spring waters with high mineralization potential (Figure 4.8; Plumlee et al., 1994). This method allows for the comparison of spring waters of the SNRB with mine waters from known mineral deposits in Colorado (n = 50). The higher the pH of the water, the more buffering the system, and the higher the sum of the six key metal concentrations, the higher the base-metal content of the deposit (Plumlee, 1999). Overall, the Ficklin Diagram is a tool which gives a different total trace element perspective which is specific to sulphide-related metals.

Chapter Four: Results & Discussion

In this section, major ion geochemistry and stable isotopes (O, H, S and C) of SNRB springs are related to each other and compared to the local bedrock map in order to identify broad geochemical trends. Trace element spring geochemistry as an indicator of mineralized zones is identified using three approaches: total trace elements, individual trace elements, and the Ficklin Diagram (Plumlee et al., 1994). Finally, the depth of circulation of the springs, as an indicator of accessibility of mineralized zones, is estimated using silica geothermometry.

A broad range of spring water characteristics is observed within the SNRB. The springs are classified into basic geochemical types based on groupings as shown in the Piper Diagram of Figure 4.2 and typical cut-off values used in the literature. These partitions include major ions (Na + K, Ca, Mg, Cl, SO_4, HCO_3 as determined in Aquachem), acidity (pH ± 7.0), surface temperature (cold (T < 12 ºC), warm (12 < T < 40 ºC) and hot (T > 40 ºC)), salinity (saline if TDS ≥ 900 ppm; Freeze and Cherry, 1979), sulphate origin using isotopes (where $\delta^{18}O < -5‰$ indicates sulphide oxidation; van Stempvoort and Krouse, 1994) and elevated total trace element concentrations (defined as above the average of the SNRB as percentage of total dissolved solids, i.e.: > 0.9%; further discussed in Section 4.5.1). Springs were grouped based on the bedrock geology at each spring outlet using a 1:1,000,000 map (Okulitch, 2005; Figure 2.1 & Table 4.1). Field parameters and water analyses for samples taken in the 2003-2005 field seasons are shown in Tables 4.2-

4.5. A correlation coefficient matrix was used to determine strong ($r > 0.7$) and moderate ($0.5 < r < 0.7$) trends between field parameters, major ion geochemistry, stable isotopes, Si-geothermometry-estimated temperatures, and total trace elements as is commonly used in aqueous geochemistry as a first approximation (Hem, 1970; Table 4.6). The samples from MERA I and II projects are shown on a map and labelled by name in Appendices C and D, respectively.

4.1 Oxygen and Hydrogen Isotopes In Water

Oxygen and hydrogen isotopes in ground water are commonly used to determine the source of the water when compared to local precipitation data (e.g.: Clark et al., 1980). The SNRB spring waters oxygen and hydrogen isotope values are strongly correlated ($r = 0.75$; Table 4.6) and plot parallel to the closest available meteoric dataset, the Yellowknife Meteoric Water Line (YMWL). Both the spring values and the YMWL have a slope of 6.7 (IAEA/WMO, 1998; Figure 4.1), indicating a meteoric source for all springs in this study. The SNRB data points cluster near the middle of the range of the YMWL. Even given the topographical differences between the west (higher, sharper peaks and glaciers) and east sides (rolling hills) of the SNRB, there is no significant difference between the average d-excess of the western (confidence interval = 3.1 ± 0.98; with 0.05 significance level) and eastern (confidence interval = 3.1 ± 0.91; with 0.05 significance level) sides. The y-intercept is slightly lower in the SNRB, possibly because of differing meteorological regimes (i.e.: from western vs. eastern Canada) between SNRB and Yellowknife (Fritz et al., 1987; Peng et al., 2004). In Canada, western air masses typically originate from the Pacific Ocean, while eastern air masses come from

the Gulf of Mexico or the Atlantic Ocean; Arctic air streams can cover all of the country in the winter (Fritz et al., 1987). Additionally, the Mackenzie Mountains are located where the Arctic and Pacific air masses converge, where a "low" in the $\delta^{18}O$ values relative to the rest of the north of Canada is observed (Fritz et al., 1987). A similar "finger" of low $\delta^{18}O$ is seen in the regional map of North America by IAEA (2001) in the approximate location of the Mackenzie Mountains, with more current data. The lowest values of $\delta^{18}O$ in the Mackenzie River Basin are found in the Mackenzie Mountains of the N.W.T., which is different from other parts of the basin due to higher altitude precipitation, greater snowfall, and higher runoff/precipitation ratios (Hitchon and Krouse, 1972). Similar to the data obtained near Fort Simpson in the Liard River Basin (Gibson and Prowse, 2002), groundwater samples of the SNRB cluster in the middle of the data range for the local meteoric water line (in our case, Yellowknife) indicating recharge is an average of year-round precipitation (snow and rain) and glacial melt water.

4.2 Temperature, pH and Major Ions

Broad, regional geochemical trends can be identified by studying the major ions, pH and temperatures of the spring waters. These trends can also be linked to major bedrock types. Two distinct groups of springs are defined by temperature in the SNRB, cold and warm/hot, where the cold springs are further subdivided based on pH (warm/hot springs are all near-neutral or basic and not dividable by pH). This gives three major groups of springs: 1) cold & acidic, 2) cold & basic and 3) warm/hot & basic (Table 4.7; Appendix

E). These temperature and pH groups are related to the bedrock from which they discharge: the largest group of cold and acidic springs discharges from shales (15 in total; all but three are either siliceous or siliceous and calcareous) while the others are from a mixture of carbonates (12), plutons (6) and clastics (4). The largest group of warm/hot, basic springs discharges from carbonates (33) while the others are from a mixture of shale (14 in total; all but three are calcareous, the others are either siliceous or siliceous and calcareous), clastics (9) and plutons (8; Table 4.7; Appendix E). The cold and basic springs are mostly discharging from carbonates (65) or from shales (36 in total; from both calcareous or siliceous and calcareous shales (half and half), with only one from siliceous shale). This suggests that although there is a large degree of overlap (30 of 70 springs are discharging from shales with both siliceous and calcareous components), springs discharging from calcareous shale show similar characteristics to those discharging from carbonates such as limestone and dolostone.

Confidence intervals at the 0.05 significance level show that temperature has a strong effect in the spring geochemistry. Total trace elements are elevated in only cold and hot springs, but not warm springs. Cold springs have the lowest total dissolved solids and have lower pH than warm springs. Warm or hot springs have more Na and K than cold springs, while cold or warm springs have more Ca, Mg and SO_4 than hot springs. Warm springs have significantly higher total dissolved solids, and higher Cl and HCO_3 concentrations than cold or hot springs.

All hot springs and most of the warm springs are located in the north-western side of the basin. Hot or warm springs tend to be found near large faults or contacts between main lithological groups (Figure 2.1). On the other hand, cold springs are found throughout the SNRB, but still are located dominantly near faults or contacts between major rock types (Figure 2.1). If the main source of heat of springs is the background heat flow, it can be inferred that the cold and acidic springs circulate at shallower levels compared to the warm or hot springs. The lack of acidic warm or hot springs could be due to the fact that deeper-circulating springs are more likely to flow through carbonate rocks and therefore be buffered, similar to the deep, high pH springs discharging from plutons in Europe (Michard, 1990). Also, the presence of plutons on the western side of the basin adds another source of buffering because weathering of feldspars to clays is often an acid-consuming reaction (Appelo and Postma, 1999).

On a Piper Diagram, the cold springs tend to be dominated by mixtures of sulphate-bicarbonate anions and calcium-magnesium cations, while warm or hot springs tend to be dominated by sodium-bicarbonate waters, with higher proportions of higher concentrations of chloride (Figure 4.2). Two main hot spring clusters can be discerned: Na-HCO_3 dominated and Ca-HCO_3 dominated. In the southern Cordillera, hot spring geochemistry is controlled by clay weathering and ion-exchange reactions (Cody, 1989; Grasby et al., 2000), which could explain the trends observed in the SNRB hot springs from the cold springs. Sodium concentrations in western Canadian hot springs are controlled by the ion exchange equilibrium reaction between smectite and kaolinite,

while calcium is controlled by an ion exchange reaction between smectite and laumonite or kaolinite (Cody, 1989), both ion-exchange reactions. Similarly, Na/K ratios are controlled by K-feldspar/albite weathering with illite and smectite, while Ca/Mg ratios are controlled by weathering to smectite (Grasby et al., 2000). Similar controls were found in Kacandes and Grandstaff (1989) which show that major ion ratios are consistent with 1:1 ion-exchange reactions such as listed above in modeling compositions of geothermal reservoir fluids. Since the Na-rich hot springs in the SNRB tend to occur near the plutons on the western side of the basin, they could be showing effects of igneous rock weathering. Na is the most commonly leached ion from feldspar weathering: albite weathering to k-feldspar consumes K and releases Na, while waikarite + quartz weathering to albite + water consumes Na and releases Ca (and vice versa) – also both temperature-dependent reactions (Fournier, 1981).

A tally of the bedrock geology from which the SNRB springs discharge from shows some common trends between geology (clastics, carbonates, plutons, shales) and geochemistry (major ions, pH, temperature, TDS and trace elements; Table 4.7; Appendix F). Most springs discharge from carbonates (107) or shales (70), and the rest are from clastics (21) or plutons (17). Shales are further subdivided into siliceous (e.g.: cherty) or calcareous (e.g.: fossiliferous) or a mixture of both. Most shales have full or partial calcareous compositions while a small number (12) are solely siliceous, according to Okulitch (2005). Confidence intervals at the 0.05 significance level show that springs discharging from siliceous shales and plutons have very similar characteristics: both have higher total

trace elements (followed by carbonates then clastics), lower pH, and lower K, Ca, Cl, and HCO_3 concentrations than all the other bedrock groups. Overall, sulphate concentrations are highest in waters discharging from shales, and shales with both siliceous and calcareous components have the lowest $\delta^{18}O_{SO4}$ values than all the other groups, consistent with sulphide oxidation (to be discussed later on). Plutons have the lowest Mg and SO_4 concentrations. Springs discharging from shales with full or partial calcareous compositions have higher total dissolved solids than all other groups. Calcareous shales have significantly higher Ca and Mg concentrations than all other groups. Although there are no warm, acidic springs in the SNRB, there are shallow, cold and acidic surficial springs and deep and warm or hot basic springs that discharge from plutons.

The exceptions to the trends found in the geology groupings as described above can be explained by local variations within the major groups. For example, while acidic springs dominantly discharge from siliceous shales and basic springs from carbonates or calcareous shales, a few acidic springs discharge from carbonates and often are accompanied by high total trace elements – this is unusual because they should be buffered by the carbonate rocks. These springs (86-049, 86-069, 86-025, and 86/87-012) discharge from formations such as Haywire, Flett, Sapper and Rabbitkettle, which all have terms in their descriptions such as: “argillaceous limestone”, “minor shale”, “black limestone” and “impure limestone”, suggestive of interbedded parts that wouldn’t necessarily buffer an acidic spring within carbonate rock. In these cases of non-matching

geochemistry between springs and bedrock group, one must realize that the groupings leave out smaller-scale variations because they were determined by using only the first term of the description based on Okulitch (2005). This occurrence has also been observed in the southern Cordillera, where the acidic Paint Pots mineral springs (pH < 4) discharge from a contact between units of interbedded limestone, dolostone and shale, grouped as "argillaceous limestone" (van Everdingen, 1972). Although the lithological groupings serve a useful purpose for the regional assessment of the SNRB with consistent trends overall, they do not account for local-scale variations such as those that have just been discussed and exceptions to dominant trends are found in almost all the groupings.

4.3 Total Dissolved Solids

Although springs' total dissolved solids (TDS) may not specifically show signs of mineralization, they can be useful to characterize major ion trends and therefore deepen the understanding of the regional geochemistry. Major ions which correlate to TDS in the SNRB are, in order of strength of relationship as indicated by their correlation coefficient (r), $Ca > Mg > SO_4 > HCO_3 > K > Cl$ (Table 4.6). Although HCO_3 is the most common dominant anion, SO_4 is the largest contributor to higher TDS. The most strongly correlated major ions are Na and Cl, Mg and SO_4, K and Cl, Ca and HCO_3, and Ca and SO_4 which generally plot as mmol/l with slopes of 1 (Appendix G), suggesting they are derived from weathering of minerals. For example, NaCl, $CaCO_3$, and $CaSO_4$ salts have been documented in previous spring studies in the area as listed in the methods section, but it is also possible that $MgSO_4$ or KCl salts are also present. Mg is strongly correlated with Ca (r = 0.73), suggesting a common dolomitic influence. Most Na and

Cl-rich springs are warm or hot (>12 ºC), and likely flowing through deeper salt deposits that have avoided the usual dissolution due to shallow meteoric water circulation. In this way, TDS can be a sign of deeper circulation but not exclusively, if the water happens to be flowing in a salt poor area (e.g. plutonic rocks).

Chlorine/boron ratios have been used to determine salt sources in groundwaters (Arnorsson and Andresdottir, 1995). Most SNRB springs with detectable boron concentrations are warm or hot (boron data are only available for MERA II springs; Figure 4.3). Five springs fall near the line of typical seawater ratio (straight solid line; Figure 4.3), which also have higher $\delta^{18}O_{SO4}$ values compared to other springs, indicating possible evaporitic sources of SO_4 (see sulphur-related isotopes section). A few springs are near the area of magma degassing/phase separation, indicating relatively deeper flow (lower curved line; Figure 4.3). The two springs elevated in total trace elements with detectable boron concentrations seem to have very different origins: 1) Cathedral, which is cold, low in Cl and likely from a shallow circulation system, and 2) Nahanni Headwaters, which is hot, elevated in Cl and likely from a deeper circulation system since it plots near the 'magma degassing or phase separation' zone (Figure 4.3). Overall, the B/Cl plot illustrates the variety and complexities within springs of the SNRB: mostly warm or hot springs have detectable boron concentrations, some of which plot on the seawater ratio line (implying seawater evaporite dissolution) or near the magma degassing line (implying deep circulation). Only two springs with above-average total trace elements have detectable boron concentrations and have very different

characteristics, indicating that the B/Cl plot does not consistently predict mineralized zones.

Another parameter commonly used to determine origin of salts in groundwater is the ratio of bromine/chlorine (in ppm; e.g. Boschetti et al., 2005). Where high volumes of water flow through rock, such as groundwater springs, congruent dissolution of evaporites typically results in high chlorine concentrations and low Br/Cl ratios (Land and Prezbindowski, 1981; Worden, 1996). Mixing of different formation waters (Carpenter, 1978) or K-salt (e.g.: sylvite) dissolution (Hanor, 1994) may also explain waters enriched in chlorine relative to sea water evaporation. The mean groundwater Br/Cl ratio in the United Kingdom, for example, ranges from 2.6 to 5.15 x 10^{-3}, while seawater is 3.47 x 10^{-3} (Edmunds, 1996). Of the 93 MERA II samples analyzed for Br, the five with detectable bromide concentrations have Br/Cl ratios that range from 5.9 to 9.0 x 10^{-3} (standard deviation = 1.1 x 10^{-3}; Table 4.8A), consistent with the world average of Palaeozoic salt deposits (n = 383, Br/Cl = 8.47 x 10^{-3}; Worden, 1996). In comparison, Mesozoic and Tertiary world average Br/Cl salt deposits are outside the SNRB range (1.6 x 10^{-2} and 3.1 x 10^{-3}, respectively; Worden, 1996). These four springs all have relatively deep estimated circulation depths compared to other SNRB springs (geothermometry section), supporting the idea that there are deeper evaporites or salts in the SNRB that is being dissolved by groundwater sampled at the springs. The only anhydrite-containing unit within the Camsell Formation is found only at 2150 m below ground level, is 120 m thick, and above which solution-collapse limestone breccias are found (Morrow and

Cook, 1987). The other youngest anhydrite-containing formation is the Bear Rock Formation (Okulitch, 2005) which is similar in age to the Camsell (lower to middle Devonian). This is also suggestive of an active upper layer (because of observations of solution collapse breccias, and lack of evaporites at shallow levels) and a deeper level only reached by deeper-circulating springs that reach relatively un-weathered anhydrite layers. Overall, the Br/Cl ratios of the SNRB are consistent with Palaeozoic salt deposits and supporting the idea that there are un-weathered evaporites below shallow ground levels.

4.4 Sulphur-Related Isotopes

Recent groundwater studies have used sulphate isotopes to identify mineralized zones by identifying signs of sulphide oxidation (Kirste et al., 2003; de Caritat et al., 2005). Groundwater isotope values of S (and Sr and Pb) have been found to match known mineral deposit signatures when compared to background evaporitic or meteoric sources (de Caritat et al., 2005). Similarly, it is important to distinguish between the different sulphur processes in the SNRB springs because they can indicate zones of sulphide mineralization or a lack thereof, such as in the case of evaporite dissolution or bacterial sulphate reduction. This is done by studying sulphate concentrations and their corresponding sulphur and oxygen isotope values.

The average sulphate concentration of SNRB spring waters is 200 mg/L (standard deviation = 400 mg/L, minimum = 0, and maximum = 2000 mg/L). Springs with sulphate concentrations above the average + 1 standard deviation are considered to have

'high' sulphate concentrations (> 600 mg/L; outliers in Figure 4.4), also above the sulphate drinking water guideline (CCME, 2006). Values of $\delta^{34}S_{SO4}$ in the SNRB groundwater range from -11.3 ‰ to 32‰ (average = 13.1‰, standard deviation = 9.4‰, n = 72), and values of $\delta^{18}O_{SO4}$ range from -15.2 to 13.7‰ (average = -4.7‰, standard deviation = 8.0‰, n = 55). The $\delta^{18}O_{SO4}$ and $\delta^{34}S_{SO4}$ values and sulphate concentrations together are used as a first approximation to group the SNRB springs into three end member regions. The $\delta^{18}O_{SO4}$ values falling below -5 ‰ are considered to be in the 'sulphide oxidation field' (van Stempvoort and Krouse, 1994), while higher values can be indicative of evaporite dissolution or bacterial sulphate reduction (Clark and Fritz, 1997). The $\delta^{34}S_{SO4}$ values falling below the Palaeozoic average of 12.9 ‰ are also seen as sulphide oxidation indicators (Claypool et al., 1980). Sulphides in the Mackenzie Mountains have $\delta^{34}S_{SO4}$ values as high as 5.3‰ (Al-Aasm et al., 1996). These processes are illustrated by arrows in Figure 4.4.

4.4.1 Sulphide Oxidation

Of the 72 available $\delta^{34}S$ values for MERA II springs, 24 springs have both $\delta^{34}S < 12.9$ ‰ (average of Palaeozoic evaporites; Figure 4.4; Claypool et al., 1980) and $\delta^{18}O < -5$ ‰ (sulphide oxidation field; Figure 4.5; van Stempvoort and Krouse, 1994), indicating presence of sulphides at those locations. All of these springs discharge from shale- or sandstone-containing formations, or from the carbonate Whittaker Formation which is associated with the samples near Prairie Creek Mine, and are circled in Figure 4.8. Six springs with sulphide oxidation have above-average total trace elements and similar $\delta^{34}S$

values to those of pyrite in the Mackenzie Mountains (-11.1 to 5.3 ‰; Al-Aasm et al., 1996). Similar sulphide oxidation signatures ($\delta^{34}S < 12.5$ ‰), with associated relatively low $\delta^{18}O_{SO4}$ values, were observed in Palaeozoic sedimentary rocks overlying Proterozoic metamorphic rocks of Australia near known deposits (Kirste et al., 2003).

4.4.2 Bacterial Sulphate Reduction (BSR)

Although none of the BSR-related springs are elevated in total trace elements, they make up a significant portion of springs in the SNRB and are an important part of the natural resources of the area. Ten MERA II springs appear to have undergone BSR, which are dominantly warm or hot and flow through mostly carbonates and some shale and clastics. The source of the sulphate is likely evaporite dissolution, after which point the sulphur is reduced to hydrogen sulphide gas, as illustrated in Figure 4.4 by elevated $\delta^{34}S_{SO4}$ values. Springs with sulphide oxidation did not have signs of BSR, therefore by exclusion BSR springs have $\delta^{34}S_{SO4}$ above -5l (van Stempvoort and Krouse, 1994). Bacterially mediated sulphate reduction (BSR) is usually accompanied by strong S fractionation and generally limited to temperatures of below 100°C, such as is found in the SNRB, while thermochemical sulphate reduction (TSR) is generally limited to temperatures above 120 to 145 °C (e.g., Bildstein et al., 2001; Ohmoto et al., 1990).

Sulphide isotope ratios were only measured (where they were detected by smell) in seven springs from the MERA II study, and their $\delta^{34}S_{HS}$ values range from -30 ‰ to 15 ‰. Significant sulphur isotope fractionation between sulphate and sulphides in some of these

springs suggest BSR (which can cause fractionations ranging up to -70‰; Brunner and Bernasconi, 2005; Figure 4.6A). This process is also similarly observed in the thermal and mineral springs of the southern Cordillera (van Everdingen, 1972; Grasby and Hutcheon, 2001).

Using the limited MERA II sulphide data, the fractionation (i.e.: $\Delta^{34}S_{SO4\text{-}HS}$ values) increases linearly with concentration ($r^2 = 0.90$) and temperature ($r^2 = 0.76$; Figure 4.6B), suggesting the fractionation is kinetic (i.e.: bacterial) since equilibrium fractionation would decrease with increasing temperature (Fritz and Fontes, 1980). The correlation between fractionation and sulphate concentration could be caused by bacteria being more selective when high SO_4 concentrations are present (Fritz et al., 1989), or by different bacteria at higher warmth or depths, because a significant trend with temperature is observed (Figure 4.6B) and different bacteria are known to have differing fractionation (e.g.: Detmers et al., 2001).

4.4.3 Evaporite Dissolution

There are many evaporite-containing formations in the SNRB from which springs could obtain their elevated TDS values and distinct geochemical patterns (Table 4.8B). Values of $\delta^{18}O_{SO4}$ in the SNRB are moderately and positively correlated to TDS, temperature, K, and Ca (Table 4.6). In other words, warmer springs have higher TDS and are associated with higher $\delta^{18}O_{SO4}$ values. Twenty-five springs have $\delta^{34}S$ values consistent with average Palaeozoic evaporites (between 15 and 30 ‰; Figure 4.4;

Claypool et al., 1980). The five definite evaporitic springs are also high in TDS (> 900 ppm), outflow from carbonates, and have elevated sulphate concentrations and positive $\delta^{18}O_{SO4}$ values. Possible sources of evaporites in the SNRB are therefore anhydrite and gypsum containing formations as listed in Table 4.8B and described by Okulitch (2005), to which Kraus Hot Springs was linked by Souther and Halstead (1973).

4.5 Trace Element Analysis

Three different methods of detecting mineralized zones were evaluated using springs' trace element concentrations (see Table 4.4 a-c for raw data): total trace elements, individual trace elements, and a Ficklin Diagram. As a check of internal consistency, waters from the two major known deposits in the SNRB were analysed. This multi-method approach (of which results are summarized in Table 4.9) allowed for both world-class deposits (Prairie Creek and Tungsten) to be successfully detected with at least two out of the three different methods in each case. Notably, they were not detected by each method, showing the need for a multi-method approach.

4.5.1 Total Trace Elements

Normalizing total trace element concentrations as a percentage of total dissolved solids (Giblin, 2001) provides a simple means to indicate which springs have elevated trace elements, above background concentrations, and potentially mineralized zones (Table 4.9). In this study of the SNRB, these are springs that have above average total trace elements (0.9 %) and range from 0.01 to 11.3%. Trace element totals are moderately and negatively correlated to pH (r = -0.56), where many springs with elevated total trace

elements tend to be acidic (Table 4.6; Appendix E). Importantly, Tungsten mine water is positively identified with this method, with total trace elements at 1.00%, while Prairie Creek was not at 0.81%.

On a major-ion Piper Diagram, springs with > 0.9 % total trace elements cluster into three distinct groups (Figure 4.2). When temperature and pH are also added as factors, the groups can be defined as follows, where 'n' is the number of springs in that group: Group 1 - a sulphate-bicarbonate linear distribution, basic (pH ~ 8), and cold (< 12 ºC) springs which discharge mostly from carbonate and calcareous or siliceous/calcareous shale (n = 18); Group 2 - sulphate-rich, acidic (pH ~ 3), and cold (< 12 ºC) springs which discharge mostly from siliceous or siliceous/calcareous shale (n = 21); and Group 3 - sodium-bicarbonate dominated, basic and hot (> 40 °C) springs which discharge near plutons from a variety of bedrock types (n = 5). Only the coldest and hottest waters of the SNRB have elevated total trace elements, while springs with moderate temperatures between 12-40 °C have total trace elements below 0.9% (Appendix E).

Two main features of these groups will be important for potential environmental impact of development: buffering capacity and relative depth of circulation as indicated by surface temperature. The hot and cold basic spring groups with elevated total trace elements both have relatively higher alkalinity and are dominantly associated with carbonates, while the cold acidic spring group tends to be more SO_4-rich and associated with siliceous shales (Figure 4.2; Appendix F). The hot and cold basic springs have more

buffering capacity, and their exploitation would have a lower risk of acid mine drainage than the cold acidic group, which has little to no internal buffering capacity. The temperature of the basic and acidic cold springs with elevated total trace elements suggests that the mineralized zone is not as deeply buried and potentially more accessible for exploration and extraction purposes. Geothermometry will also be evaluated in this context.

Overall, the Na-rich hot springs have significantly higher values of total trace elements (confidence interval of 1.13 ± 0.30 % with 0.05 significance level) than Ca-rich ones (confidence interval of 0.31 ± 0.13 % with 0.05 significance level). Of the Ca-rich hot springs, three out of four discharge from carbonates (the other from calcareous shale) while the Na-rich hot springs discharge from one pluton, one clastic, two shale and two carbonate bedrock groups. It is possible that Ca-rich hot springs flow through more carbonate rocks which buffer the pH and do not release as many metals, or that carbonate rocks in the SNRB are not as metalliferous as the other rock types. Na-rich hot springs tend to originate out of plutonic rock (Hole-in-the-Wall), near a contact with plutonic rock (Nahanni North and Nahanni Headwaters) or from the Flat River Valley (West Cantung, Cantung East and Cantung, a.k.a. Tungsten Mine water), which is bordered on each side by plutons and likely underlain by them as well. It is therefore likely that the Na-rich waters in hot springs originate from the plutons or the alteration halo near the plutons. These same Na-rich hot springs were described as having a ‘granitic’ influence, as opposed to the others as having a ‘sedimentary’ origin (Crandall and Sadlier-Brown,

1976). The differing origin of Na and Ca rich hot springs is further observed in the B/Cl plot (Figure 4.3), where the Na-rich hot springs all fall near the 'magma degassing' line, suggesting deep circulation, and in the sulphur isotope section (Figure 4.4) where the Ca-rich hot springs all have $\delta^{34}S_{SO4}$ values that indicate bacterial sulphate reduction. Overall, Na-rich, pluton-related hot springs do show higher mineralization potential whereas the Ca-rich hot springs do not (summary of features in Appendix H).

A similar trend as described above is seen in the spatial distribution of mineralized springs. Comparing the springs with elevated total trace elements and the geology map simplified from Okulitch (2005) allows for the delineation of three main clusters (Figure 2.1):

1) pluton-related springs (Selwyn Plutonic Suite);

2) sandstone-related springs (Mattson Formation); and

3) springs near major faults and fractures, mostly on the western side of the basin near the Flat River Valley and Broken Skull River.

The pluton-related springs are not necessarily discharging directly from the plutons themselves, but instead often within a certain radius around them and usually within 5 km of the contact with the country rock. Contact aureoles of metamorphism up to 1 mile in diameter have been documented by Blusson (1968) where these springs with elevated total trace elements are found. Tungsten mine is located within one of these halos of deformation (Blusson, 1968). The elevated total trace elements of the springs clustered near the Mattson Formation can be explained by the pyritic nature of the sandstone and

its coal deposits south of the basin (Stott, 1982; sandstone group in Figure 2.1). Lastly, the cluster of springs near faults and fractures may be explained by the observed presence of mineralization in these types of structures in other places in the basin (e.g.: Morrow and Miles, 2000).

4.5.2 Individual Trace Elements

This is a relative method, where elevated zones of individual trace elements are chosen by sampling groundwater wells throughout an area to define background concentrations (Giblin, 2001; Chapter 3 of this thesis). Descriptive statistics of trace elements in SNRB springs show that some elements are more common or present in higher concentrations, such as iron (Figure 4.7). The relatively-chosen cut-off values of the SNRB are similar to concentrations observed in waters related to known deposits around the world and their acid mine drainages (Table 4.10), and quite conservative in comparison. Both known deposits of the SNRB have positively identified trace elements with this method, demonstrating its usefulness for a variety of deposit types (a summary of the deposits and their associated waters can be found at the bottom of Table 4.9). For example, Tungsten mine water (MERA I sample # 86-020) is elevated in Ag, and Stinky Drift (a sulphide-smelling seep from inside a mine shaft at Tungsten Mine) is elevated in Tl. Comparatively, the hot spring flowing next to Tungsten Mine (i.e.: West Cantung) has five elevated trace elements: Cs, Li, V, B and Ga. Prairie Creek mine water is elevated in seven elements (Cu, Zn, Pb, Cd, Sb, Tl and Se) and two nearby creeks are elevated in Pb (Harrison Creek) and Sb (Prairie Creek).

4.5.3 Ficklin Diagram

The Ficklin Diagram was designed specifically to predict environmental impacts of mining, i.e.: the buffering capacity of an area and its potential released trace element concentrations using 6 indicator metals, for different deposit types for both natural and man-made acid drainage (Plumlee, 1999). In the SNRB, this approach was adapted by using the natural environmental conditions to predict the deposit types (Figure 4.8). The springs are listed with their corresponding groups in Table 4.9 as defined by Plumlee et al. (1994). As a test of internal consistency, Prairie Creek mine water from the eastern side of the SNRB plots exactly in the right type of deposit in Figure 4.8, demonstrating the usefulness of this approach. Above the sum of the six key metals where known deposits exist (> 0.3 ppm), mostly cold springs are found, and springs with available sulphide-oxidation data ($\delta^{34}S$ and $\delta^{18}O$ of sulphate as discussed in Section 4.4.1) plot in or around delineated fields. Non-sulphide-related Tungsten mine water does not plot in any given area as defined by Plumlee et al. (1994), demonstrating the method's limitations for non-sulphidic deposits or at low metal concentrations (below 0.03 ppm of the sum of six key metals).

4.5.4 Summary of Indicator Springs

Springs indicative of mineralized zones were identified using three different methods: 1) above-average total trace elements as a percentage of total dissolved solids (>0.9 %); 2) individual elevated trace elements using basic statistics to determine "cut-offs" such as averages and standard deviations and comparing to mine waters of known deposits around the world; and 3) a Ficklin Diagram by comparing springs to Groups E-K based

on Plumlee et al. (1994). Prairie Creek and Tungsten, two world-class mineral deposits, were detected in two out of three methods, but not by all three, demonstrating the need to utilize a multi-pronged approach.

Springs with > 0.9 % total trace elements clustered in three distinct geochemical groupings according to pH, major ion geochemistry, temperature and lithological groupings on a major ion Piper Diagram and overlaying on the regional geology map based on Okulitch (2005). Out of a total 200 samples, five indicator springs were hot, basic, Na-rich and discharging near plutons (Group 3), 18 indicator springs were cold, basic, SO_4-HCO_3-rich and discharging from mostly calcareous shale and carbonate rock (Group 1), and 21 indicator springs were found to be cold, acidic, SO_4-rich and discharging mostly from siliceous shale (Group 2); (Appendix H). Springs with elevated total trace elements tended to discharge near plutons (western side of SNRB), faults and fractures (throughout), and from rocks that are in contact with the Mattson Formation (eastern side of SNRB). Cold and basic indicator springs are likely more accessible mineralized zones with a higher buffering potential. Thirty-six springs were found to have more than three elevated individual trace elements, and 49 springs plotted within determined mineralized areas in the Ficklin Diagram (7 in group E, 5 in F, one in G, three in H, 17 in I, one in J, 8 in K and 7 in either I, J or K; Table 4.9). Both known deposits of Prairie Creek and Tungsten are in areas with high buffering potential as indicated by the Ficklin Diagram (Figure 4.8).

4.5.5 Circulation Depth Estimates

Estimates of springs' depth of circulation can determine the relative accessibility of mineralized zones and are found by using a combination of Si-geothermometry and solubility diagrams for select MERA II springs.

4.5.5.1 Geothermometry

As expected, geothermometry-predicted temperatures, surface temperatures, Si-concentrations are all strongly correlated (Table 4.6), demonstrating the well-integrated nature of this approach. Based on an assumed geothermal gradient of 23 ºC/km (Hyndman et al., 2005), the average depth of circulation of the analyzed springs in the SNRB is 2.1 km, the deepest being 4.7 km at Brimstone Spring and the shallowest being near 0.2 km at Cotton (Table 4.11). Corresponding temperatures at depth range from 5.5 ºC to 108 ºC, with an average of 48 ºC. These are considered minimum estimates of the system's highest temperatures since dilution and re-equilibration of waters would only lower the calculated temperatures (Grasby and Hutcheon, 2001) and advective heat flow along faults would lower the geothermal gradient (Forster and Smith, 1988). All other springs are assumed to flow at less than 200 m in depth due to cold temperatures and low silica concentrations.

The estimates of depth of circulation obtained via Si-geothermometry compare to other work done on some of the previously analyzed springs. A previous analysis of Kraus Hot Spring, using a combination of the understanding of the local geology and a tritium age of 30 ± 10 yrs old, predicted the depth of circulation as being 1.5 km (Brandon, 1965)

which is within the same range of our own estimate of 2.3 km. Similarly, Rabbitkettle Hot Springs were estimated to circulate approximately 1 km at depth by Gulley (1993), similar to our own estimate of 1.1 km. High pCO_2 springs of the Flat River Valley were estimated to flow 3-5 km at depth by Hamilton et al. (1990), similar to our estimated 4.7 km depth of circulation for Brimstone but different from our estimated 0.9 km for Flat Fruit, both high pCO_2 springs. It is possible that Flat Fruit's deep fluids mixed with a larger component of fresh meteoric waters than Brimstone, diluting the Si concentrations. Relatively high permeability and porosity was found in a 4 km deep borehole by Stober and Bucher (2005), showing that water can still flow even at such depths. Local maximum depth of water circulation, as defined by the ductile-brittle transition zone typically found at depths of 10-15 km, can be affected by local rock type, water content and geothermal gradient (Stober and Bucher, 2005).

Solubility diagrams of five warm springs, as per Pang and Reed (1998), confirm that there are effects of mixing with fresh meteoric waters and carbon dioxide degassing in the SNRB because of the lack of convergence at a single point of the curves (Figure 4.9 a-e). Similar trends in Choi et al. (2005) were also interpreted to show mixing between a geothermal-component with a cooler groundwater during ascent of the fluid. Most of the solubility curves equilibrate below 200 °C, which is within the same range of the Si-geothermometry-estimated temperatures in the SNRB. This method is therefore not useful for geothermometry purposes in the SNRB, but does show that there is mixing between shallow and deep water in some of the springs.

4.5.5.2 Summary and Significance of Circulation Depth Estimates

The springs' estimated depth of circulation can be used as an indication of accessibility of potential mineralized zones, i.e.: shallower springs are potentially more accessible relative to deep-flowing springs. These are listed in decreasing order according to Si-geothermometry-predicted circulation in Table 4.11 and in conjunction with mineralized springs in Table 4.9. The order in Table 4.11 is supported by other previous local studies (Brandon, 1965; Hamilton et al., 1990; and Gulley, 1993), solubility curves as per Pang and Reed (1998), and the presence of large-scale faults/folds/fractures. Springs with deep circulation signs that have mineralization potential may still be relatively accessible if the source of their signature is from the shallow meteoric water component mixing in, because indications of deeper waters mixing with shallow meteoric waters are evident throughout the study area, as described in other studies in a similar setting (Hamilton et al., 1990; Choi et al., 2005; and Crossey et al., 2006).

4.6 Summary of Results

All SNRB springs are meteoric in origin as indicated by the similar slope between their hydrogen and oxygen water isotopes with the local meteoric water line. They tend to discharge from fractures, faults or contacts between major lithological groups. Warm or hot springs are always near neutral or basic and mostly found on the western side of the basin, while cold springs are found throughout the basin and can be either acidic or basic, depending on the bedrock type they discharge from. Hot or warm springs tend to flow more deeply therefore are more likely to flow through some type of carbonate rock and

be well-buffered. Most acidic springs tend to discharge from siliceous shale or from the tops of plutons, and most basic ones discharge from carbonates or calcareous shale. Congruent dissolution of salts in deeper evaporite deposits are thought to underlay the SNRB, which explains the overall high correlation of salts (NaCl, $MgSO_4$, etc.) in the warm springs. This is corroborated by chlorine/boron and bromine/chlorine ratios and by sulphur isotopes. On the other hand, Na-rich hot springs are also more likely to be related to the plutonic rock geochemistry due to weathering of clays and/or feldspars and ion-exchange reactions, and plot on the 'magma degassing' area of the plot by van Stempvoort and Krouse (1994). The Ca-rich hot springs are discharging mostly from faults in carbonate rocks, and show signs of bacterial sulphate reduction.

Evidence for sulphide oxidation, as indicated by sulphate S and O isotopes, was found in springs discharging from a variety of lithological groups, and was sometimes associated with elevated sulphate concentrations and trace elements from shale. Springs with above average total trace elements as a percentage of total dissolved solids typically cluster in three main groups when plotted on a Piper Diagram and a bedrock geology map. On the Piper Diagram, there are springs that are cold, sulphate-bicarbonate rich, basic and discharging from mostly carbonates and calcareous shales (Group 1), cold, sulphate-rich, acidic, and mostly discharging from siliceous shales (Group 2), and hot, sodium-rich, basic and discharging from or near plutons (Group 3). On the SNRB geology map, these springs with elevated total trace elements cluster near sandstones on the eastern side of

the basin, near plutons on the western side of the basin, and/or are fault/fracture-related in carbonate/shale rocks throughout the basin.

Numerous mineralized springs were also identified by plotting concentrations of six key elements and pH on a Ficklin Diagram overlaid with geochemical fields of known deposits as defined by Plumlee et al. (1994). This method successfully and correctly identified waters related to Prairie Creek mine. Other indicator springs were identified by analysing individual trace elements, which identified a number of trace elements for each of the two known deposits in the SNRB and many other springs. Springs with signs of sulphide oxidation as suggested by $\delta^{34}S$ and $\delta^{18}O$ values of sulphate plotted in or within delineated fields of the Ficklin Diagram above a sum of 0.03 ppm, underlying the use of this diagram for the purpose of exploring for sulphide-related deposits.

Applying silica-geothermometry on the warm and hot springs determined the average depth of circulation to be 2.1 km, with the maximum being 4.7 km at Brimstone and the minimum being 0.2 km at Cotton (standard deviation = 1.2 km, n = 32). Solubility diagrams as per Pang and Reed and the gas isotopes also pointed to signs of deep fluids mixing with a shallow, fresh component. All hot or warm springs are located on or near large faults and fracture systems, suggesting that these more permeable structures are pre-requisites for deep fluid circulation. All other springs are assumed to have shallow (< 200 m) circulation depths. The large variety of circulation depth of springs in the SNRB with their associated geochemical characteristics is illustrated in Figure 4.10.

A summary of the results from the three detection methods used is listed in Table 4.9 for each spring along with its estimated circulation depth, which can be used to prioritize more detailed exploration work. The springs are listed first by order of geochemical group (1, 2 or 3), then by the number of individual elevated trace elements, and lastly by total trace elements (as above average as % of total dissolved solids). The priority for future exploration should focus on a combination of the shallowest, most buffering and most mineralized springs (such as 'Group 1', i.e.: cold and basic springs with above average total trace element). Depending on the type of deposit one may be exploring for, different indicator spring types may be prioritized depending on their individual elevated trace elements or Ficklin Diagram grouping.

Chapter Five: Conclusion

The economic potential of the SNRB was assessed and characterized using spring geochemistry based on a watershed-scale, multi-component analysis method which was newly developed as part of this work, using 200 springs that were sampled and geochemically analyzed since the 1980's over an area of 37 000 km^2. In addition to the primary goal of identifying potentially economic mineralized zones, this dataset could also be included as part of a collection of baseline data during pre-mining activity in a region naturally elevated in dissolved trace elements and metals. These results have already been incorporated into the larger MERA report (in press) in order to develop an economic potential map for the region. This map will be used in the negotiations to make final decisions on land status as part of the national park expansion process between the Deh Cho, Sahtu, Parks Canada and the local mining industries.

Specifically, this study recommends three simple statistical and graphing methods that can identify mineralized zones quickly and efficiently in a largely under-explored area. The methods include summing trace elements concentrations as a percentage of total dissolved solids, identifying individual elevated trace elements and confirming their identities by comparing them with mine waters from known deposits around the world using a Ficklin Diagram (Plumlee et al., 1994). These methods test a new concept of using a Ficklin Diagram for the purpose of mineral exploration as opposed to predicting environmental impacts. The identified springs can be used as indicators to the overall elevated mineral potential of the region, and potentially guide future field work. Overall,

the large sample size used in the analyses allows for a large, regional, watershed-based understanding of the South Nahanni River Basin geochemistry and its related mineral potential.

The methods developed in this work are adaptable for a variety of geologic terraines, which can be used for future MERA (or similar) assessments, in addition to regional geochemical prospecting and environmental baseline studies.

The major findings of this work therefore include:

1) Springs are a great tool for regional geochemical studies because they are relatively easy and inexpensive to sample, and are natural groundwater 'outcrops' which retain characteristics of the rocks they flow through.
2) Springs that are elevated in total or individual trace elements above background concentrations, can be used as indicators to the overall elevated mineral potential of the region, and ideally guide future field work and/or decision making. The SNRB has high mineral potential when compared to other studies from around the world.
3) The Ficklin Diagram can be adapted for the purpose of mineral exploration, aside from its original purpose of predicting environmental impacts (as designed by Plumlee et al., 1994) and can distinguish between sulphide or non-sulphide-related mineralization;

4) A multi-method approach can identify mineralized zones quickly and efficiently in a large, under-explored area, while single methods of data analysis can lead to non-detection of major world class deposits;
5) The large sample size used in these analyses allowed for a comprehensive, regional, watershed-based understanding of the South Nahanni River Basin geochemistry and its related mineral potential.
6) 'Success' was achieved by the detection of the two known deposits of the area. Further study is needed to confirm the presence of the other mineralized zones as predicted by the methods in this thesis, such as comparing the results with the other MERA II sections or more detailed field work in those areas of higher potential.

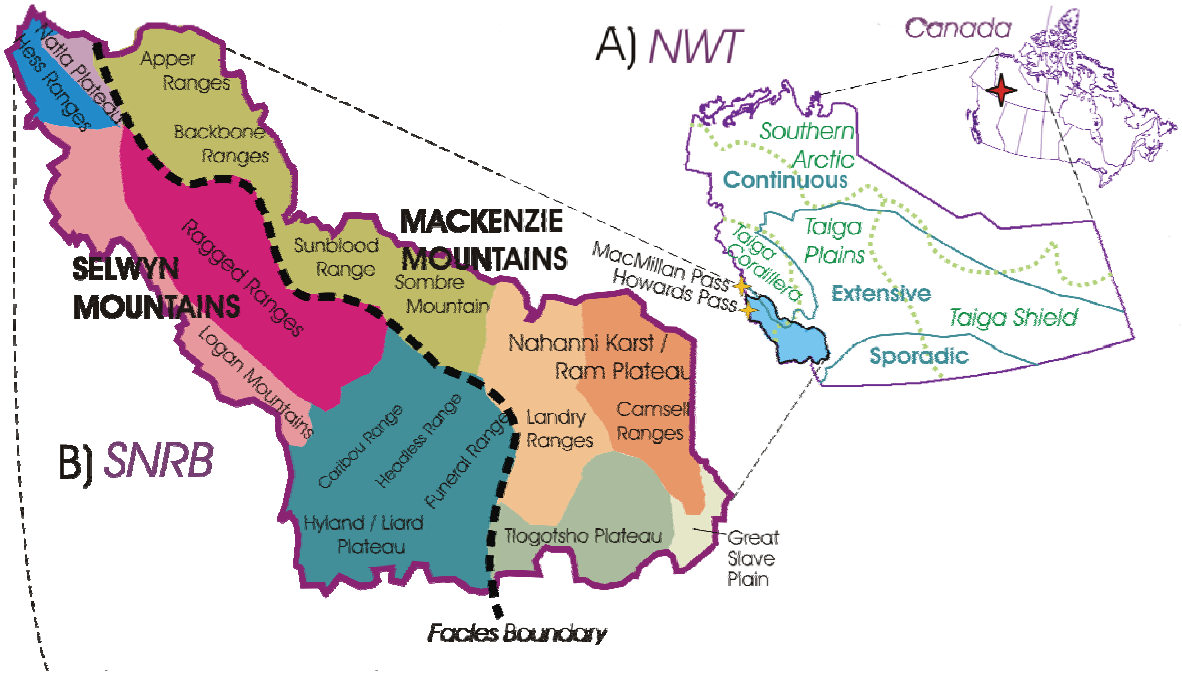

A) NWT
Canada
Southern Arctic
Continuous
Taiga Plains
Taiga Cordillera
Extensive
Taiga Shield
Sporadic
MacMillan Pass
Howards Pass
B) SNRB
SELWYN MOUNTAINS
MACKENZIE MOUNTAINS
Ragged Ranges
Logan Mountains
Sunblood Range
Sombre Mountain
Backbone Ranges
Upper Ranges
Nahanni Karst / Ram Plateau
Landry Ranges
Camsell Ranges
Caribou Range
Headless Range
Funeral Range
Hyland / Liard Plateau
Tlogotsho Plateau
Great Slave Plain
Facies Boundary

Figure 1.1 (previous page): Location and Description of the South Nahanni River Basin (SNRB). A) NWT permafrost zones (bold font and solid lines; NRCan, 1995), eco-zones (italic font and dashed lines; Wiken, 1986; CCEA, 2006), with SNRB highlighted in blue and MacMillan Pass and Howard's Pass mineral deposit locations marked with stars; B) SNRB physiographic regions (after GSC, 1986) with the platformal carbonate / basinal shale facies boundary as described by Gabrielse et al. (1965); C) SNRB map sheets, Sahtu/Deh Cho First Nations groups, waterways, infrastructure and current Nahanni National Park (NNP) boundary. Mineral and Energy Resource Assessment (MERA) I and II areas are marked as dotted boxes and as the outline of the watershed, respectively. Beaver River Structure (BSR) is marked with a dashed line as proposed by Morrow and Miles (2000).

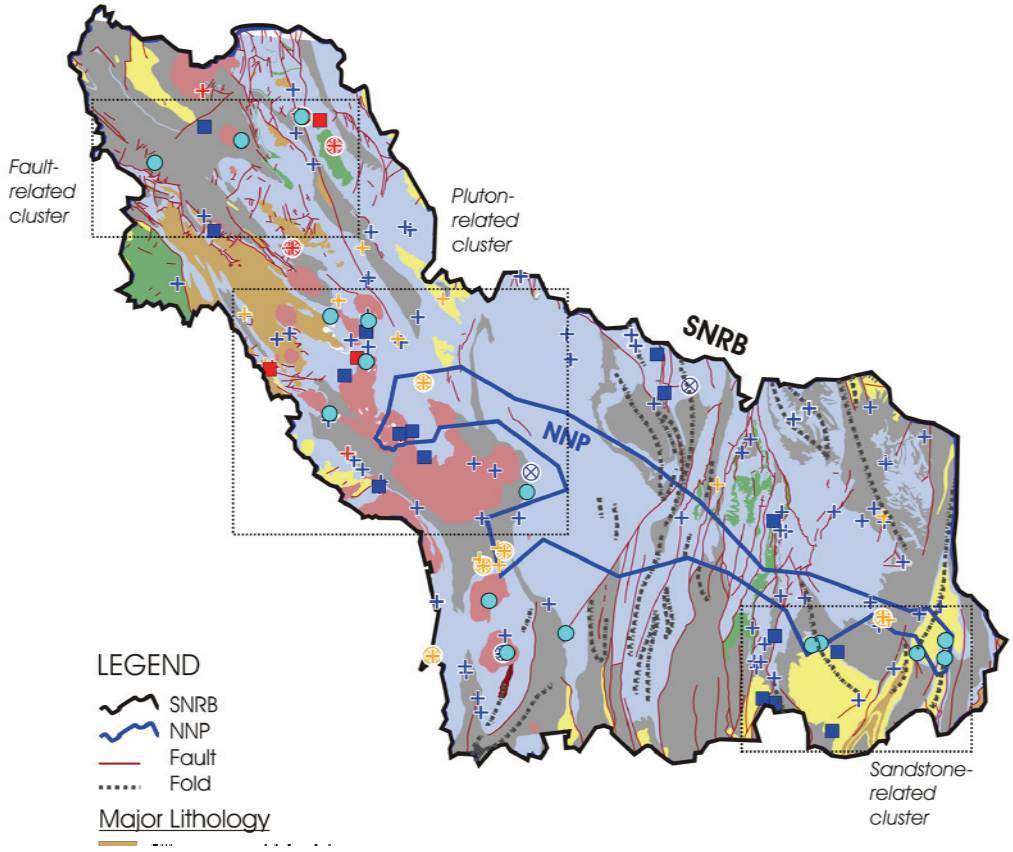


Figure 2.1: Major bedrock lithological groupings based on Okulitch (2005) overlaid with MERA I & II springs, Nahanni National Park (NNP) boundary, major faults and folds and outlined by the current proposed park expansion area of the South Nahanni River Basin (SNRB). Springs discharge mostly near faults, folds and/or contacts between major bedrock types. Springs are symbolized for temperature, pH, and total trace elements as described in Figure 4.2. Springs with elevated total trace elements (T.E. > 0.9 %) cluster in three groups: sandstone-related, pluton-related and fault related.

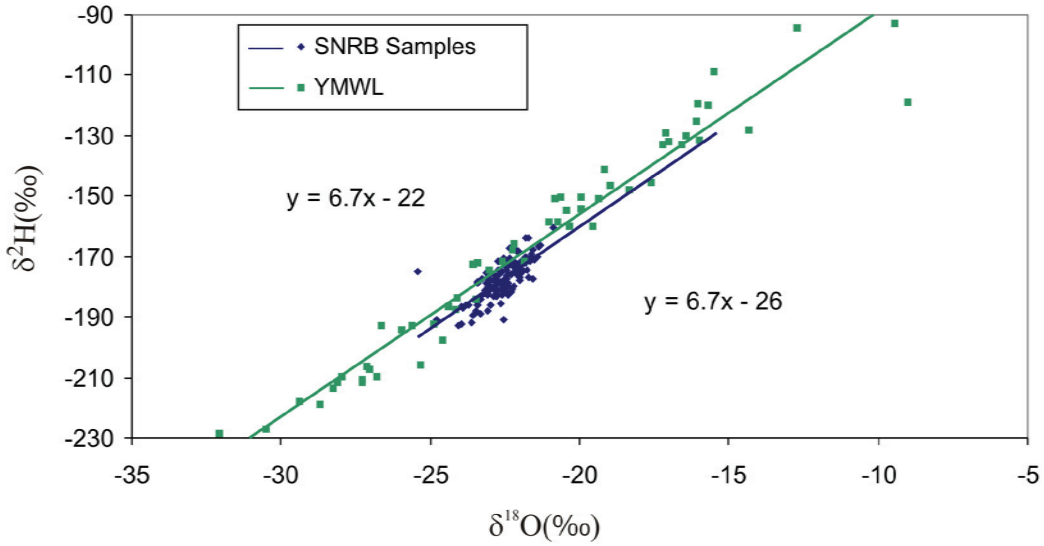


Figure 4.1: Hydrogen and oxygen stable isotope ratios of SNRB springs plotted to compare with the Yellowknife meteoric water line (YMWL; IAEA/WMO, 1998).

Figure 4.2: Piper plot of SNRB springs' major ions. Springs with elevated trace element percentages (T.E. > 0.9 %) have filled symbols and fall into three distinct groups: 1) Cold, basic and HCO_3-SO_4-rich; 2) Cold, acidic, and SO_4-rich; and 3) Hot, basic and Na-rich. There are no warm springs (except for Tungsten mine water drainage) and no acidic hot springs (n/a) that have elevated total trace elements. Dotted rectangles in the lower left-hand triangle highlight the linear trend of warm springs from Ca to Na richness, and the two clusters of hot springs: Ca-rich on the left and Na-rich on the right. These symbols are also used in Figures 2.1, 4.3, 4.4, 4.5 and 4.8.

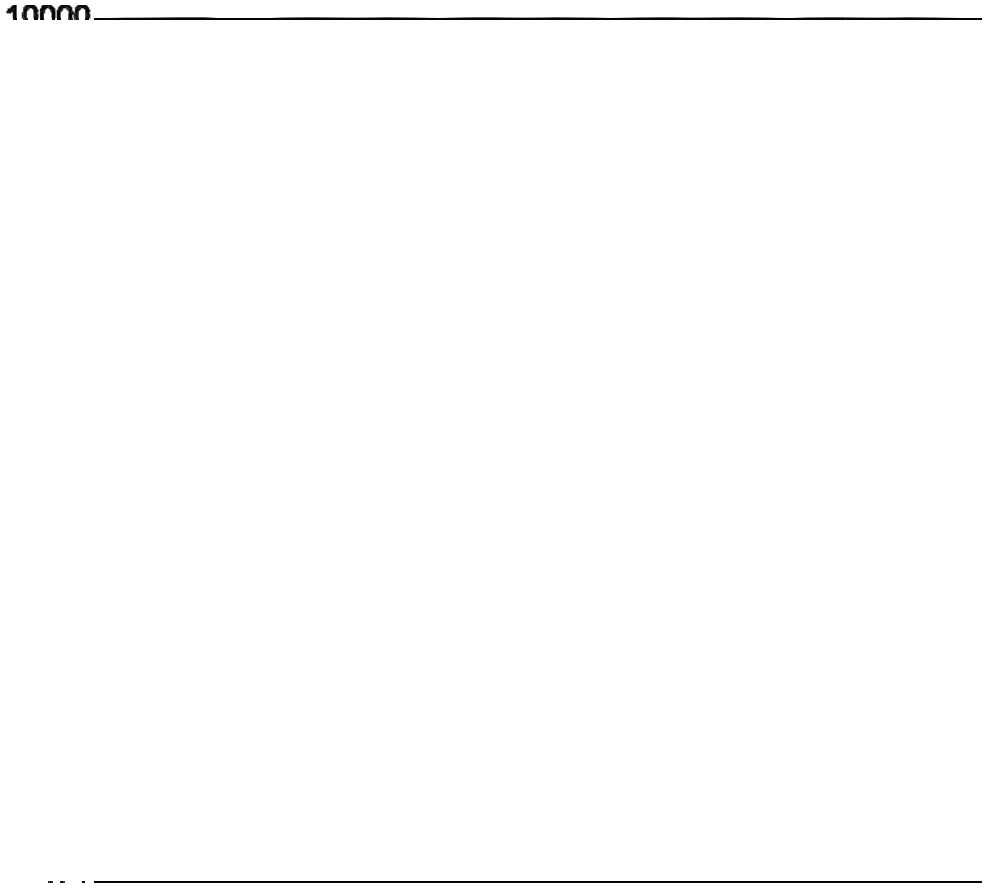


Figure 4.3: B/Cl scatter plot of SNRB springs overlaid with fields based on waters from Iceland in Arnorsson and Andresdottir (1995). B/Cl ratios are determined by the meteoric source water, dissolution from rock, mixing with seawater, magma degassing or concentration of B by phase separation. Springs falling on the seawater ratio line are assumed to be flowing through evaporites, while springs falling near the magma degassing line are assumed to be flowing much deeper; both clusters are all hot or warm springs. The five springs that fall on or near the seawater ratio line are, from left to right: Tabletop, Redstone Junction #1, Deca, Ekwi and Kraus. The six springs that are near the 'magma degassing' area are, from left to right: Broken Skull, Nahanni North, West Cantung, Tulita, Nahanni Headwaters, and Wildmint. Symbols are the same as described in Figure 4.2.

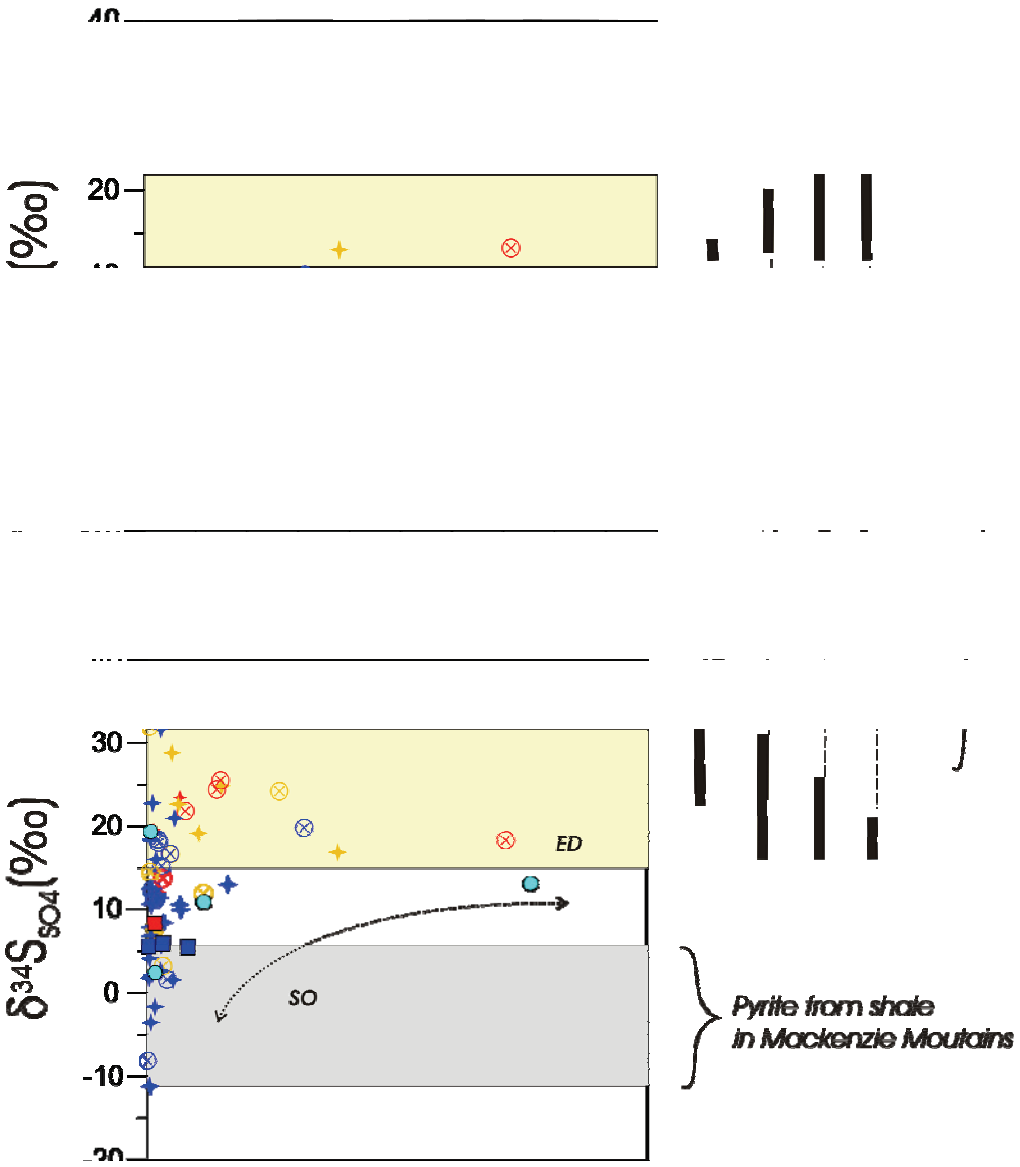

40
20
(‰)
30
20
10
0
-10
-20
$\delta^{34}S_{SO4}$ (‰)
ED
SO
Pyrite from shale
in Mackenzie Moutains

Figure 4.4 (previous page): A) $\delta^{18}O_{SO4}$ and B) $\delta^{34}S_{SO4}$ plotted vs. sulphate concentration in MERA II springs. Springs are overlaid with corresponding world average Paleozoic evaporite values (upper beige box; Claypool et al., 1980) and pyrite $\delta^{34}S$ values from black shales in the Mackenzie Mountains (lower grey box; Al-Aasm et al., 1996). Ranges associated with evaporite-containing formations of the SNRB are based on age descriptions from Okulitch (2005). Springs show signs of evaporite dissolution (ED) and sulphide oxidation (SO) along trends described by van Stempvoort and Krouse (1994) and Clark and Fritz (1997). Warm or hot springs tend to show evaporitic or bacterial sulphate processes, while cold springs tend to show sulphide oxidation. Data are only available for MERA II samples. Springs symbols are the same as described in Figure 4.2.

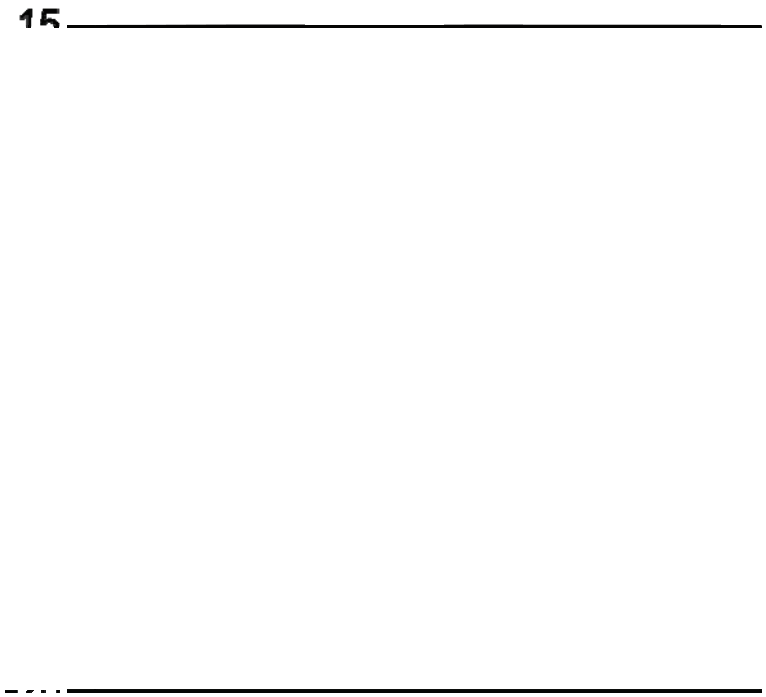


Figure 4.5: Sulphate and water $\delta^{18}O$ scatter plot overlaid with the sulphide oxidation field of van Stempvoort and Krouse (1994). Data are only available for MERA II samples, and symbols are the same as described in Figure 4.2. Thirty-seven springs show signs of sulphide oxidation, of which six have total trace elements > 0.9% and discharge mostly from shale (Bougere, Glacier Lake, Orange Creek, Red Mini, Nahanni Headwaters and Cathedral). Similar to Figure 4.4, cold springs tend to fall in the field of sulphide oxidation, while warm or hot springs tend to fall outside this field. 'Limit I' signifies 100 % of oxygen in sulphate is derived from H_2O while above 'Limit II', oxygen is derived from other sources (e.g.: air). Sulphate reduction typically results in $\delta^{34}S_{SO4}$ values above 'Limit II' (van Stempvoort and Krouse, 1994).

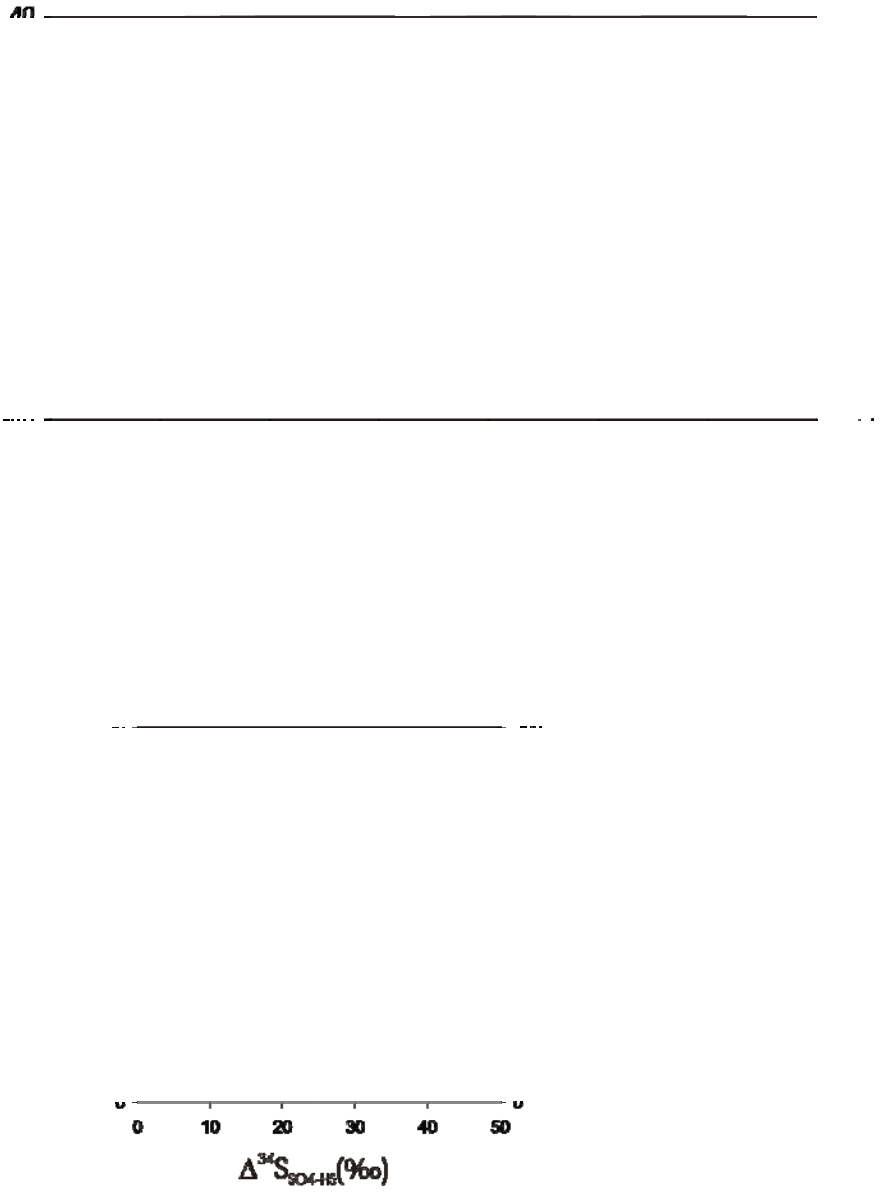


Figure 4.6: A) Sulphate and sulphide $\delta^{34}S$ of SNRB springs with expected $\delta^{34}S_{SO4}$ ranges from 5 local evaporite-containing formations based on their known ages (Okulitch, 2005) and age-corresponding world $\delta^{34}S_{SO4}$ average (Claypool et al., 1980). Only samples with available $\delta^{34}S_{HS}$ data are included, indicating fractionation with $\delta^{34}S_{SO4}$ and therefore bacterial sulphate reduction. B) $\Delta\delta^{34}S_{SO4-HS}$ vs. temperature and concentration of sulphate. Kinetic fractionation, i.e.: bacterial sulphate reduction is occurring in the samples with available $\delta^{34}S_{HS}$ data because of the increase in fractionation with temperature and sulphate concentration.

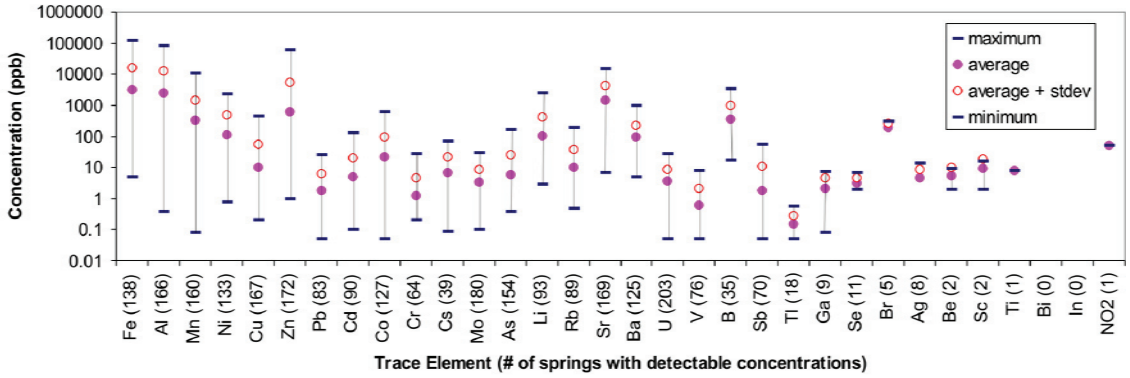


Figure 4.7: Trace element statistics for SNRB springs: maximum, minimum, average, and sum of average and 1 x standard deviation concentrations (stdev) for all MERA I and II springs. The number next to each element refers to the total of springs with detectable concentrations of that element. Some elements are very common (e.g.: Fe) and while some elements are uncommon (e.g.: Ag). Correspondingly, different cut-off values were used to determine which elements were elevated in each spring, which are listed in Table 4.4a-c and compared to deposit-related waters in Table 4.10.

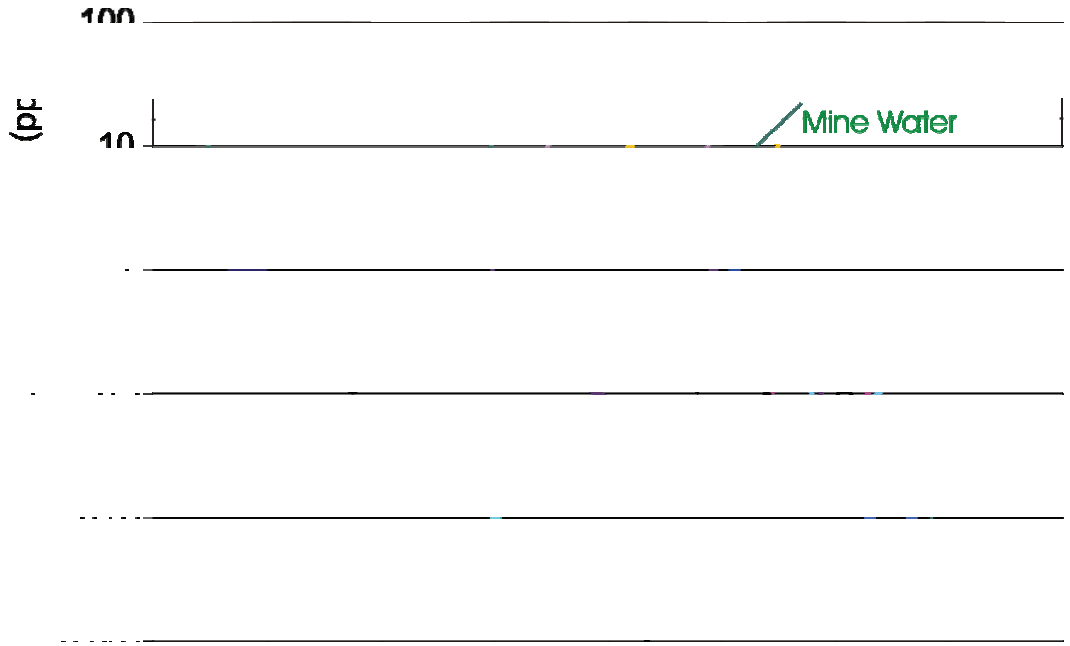


Figure 4.8: Ficklin Diagram showing MERA I and II springs grouped by total trace elements >0.9% with the same symbols as in Figure 4.2. Springs showing sulphide oxidation as indicated by $\delta^{18}O_{SO4}$ and $\delta^{34}S_{SO4}$ values are circled. Many springs fall into fields labeled E-K as delineated from mine water drainage geochemistry from known mineral deposits in Colorado (Plumlee et al., 1994; descriptions listed below). Increasing buffering capacity increases with pH towards the right, and sulphide-related base metal content increases towards the top.

Ficklin Diagram Groups (Plumlee et al., 1994)

E	Pyrite- and base metal-rich polymetallic veins and disseminations in wallrock with low acid-buffering capacity
F	Pyrite-rich, base metal-poor veins and disseminations in wallrock with low acid-buffering capacity
G	Pyrite- and base metal-rich polymetallic veins that are carbonate-rich or occur in wallrock altered to contain carbonate
H	Pyrite- and base metal-rich, polymetallic replacements and veins in carbonate-rich sediments
I	Polymetallic veins with moderate to low pyrite and base metal content that are carbonate-rich or occur in carbonate-rich wallrock
J	Pyrite-poor polymetallic replacements in carbonate-rich sediments
K	Pyrite-poor, Au-Te veins and breccias with carbonate gangue

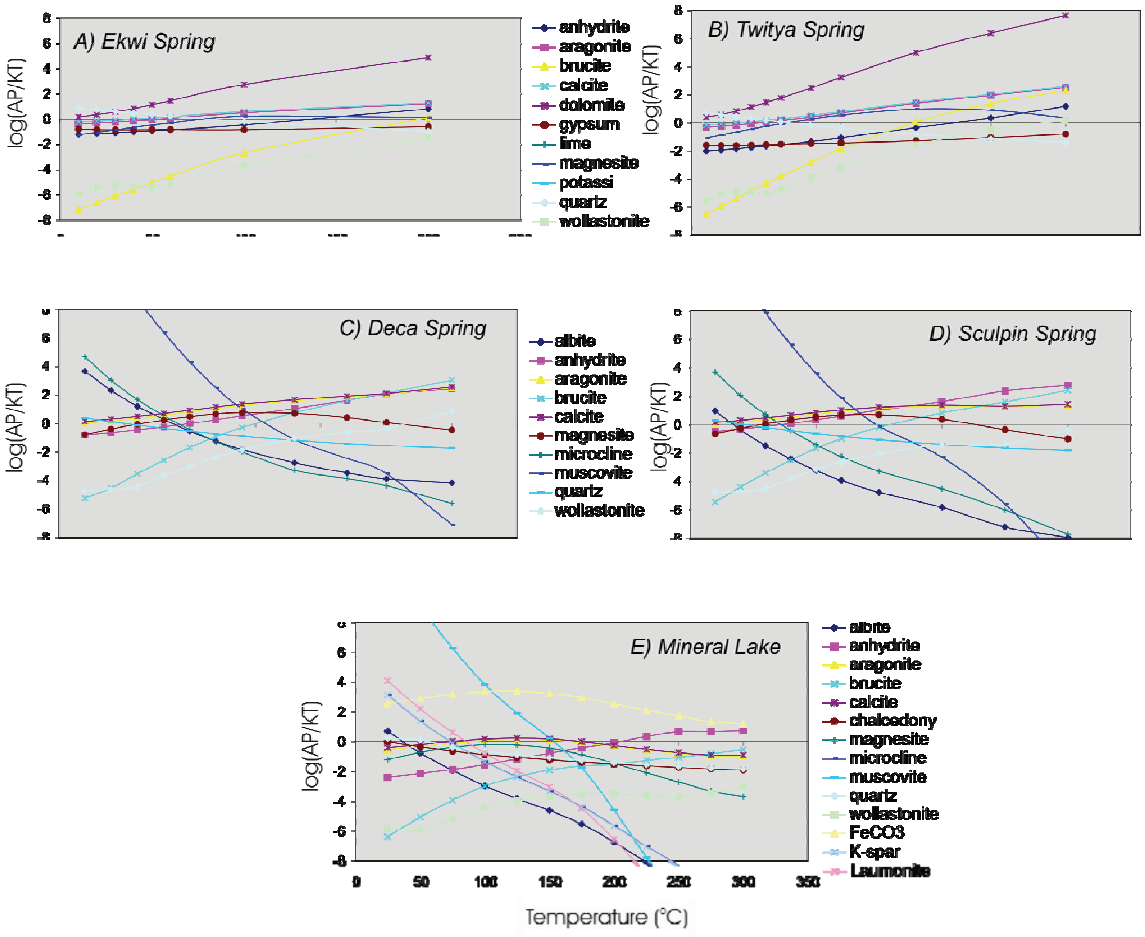


Figure 4.9 A-E: Solubility diagrams of 5 SNRB springs at different modeled temperature intervals, used to determine temperature at maximum depth of circulation as per Pang and Reed (1998). Lack of convergence at the equilibrium line [log (AP/KT) = 0] indicates effects of mixing with fresh meteoric waters and carbon dioxide degassing in the springs. "Log AP/KT" as labeled by the Solmineq88 program (Kharaka et al., 1988) is also known as "log Q/K" in Pang and Reed (1998) or as the 'saturation index' in Appelo and Postma (1999); Sub-saturation is reflected below the equilibrium line (where log (AP/KT) < 0), and super-saturation above the equilibrium line (where log (AP/KT) > 0; Appelo and Postma, 1999).

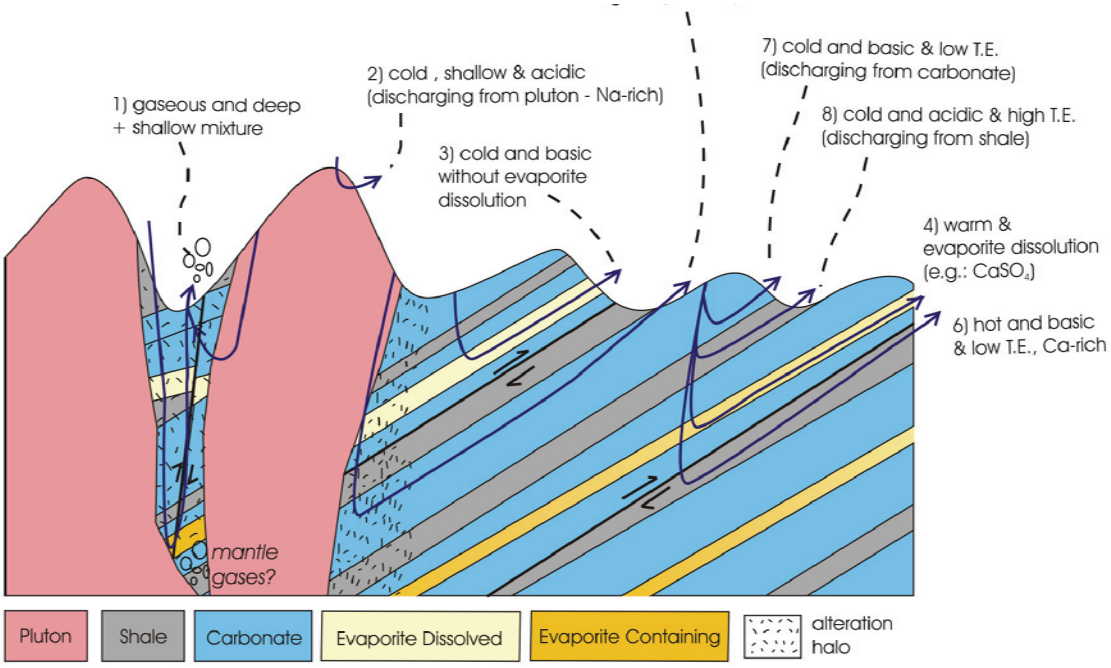


Figure 4.10: Illustration of the variety of spring types in the SNRB. 1) Deep, gaseous water mixing with shallow meteoric water; 2) shallow, cold and acidic water discharging from tops of plutons; 3) shallow, cold and without signs of evaporite dissolution; 4) warm with signs of evaporite dissolution; 5) hot, basic, Na-rich and high in total trace elements discharging from deformation halos around plutons; 6) hot, basic, Ca-rich and low in total trace elements discharging from faults far from plutons; 7) cold, basic, low in total trace element, HCO_3-rich water discharging from carbonate; and 8) cold, acidic, high in total trace element, SO_4-rich water discharging from sulphide-containing shale. Diagram is not to scale. Depth of gaseous spring circulation is approximately 5 km and evaporites are present at depths below approximately 300 m. Shape of plutons was modified from Hamilton et al. (1990). More types of springs exist that can fit on this diagram.

Table 3.1 Field Measurements Conducted

Parameter Measured	Instrument Used
pH	Orion 290A meter; ThermoOrion Perphect ROSS 8202BN electrode
Electrical Conductivity (EC)	Conductivity meter Orion 125; conductivity cell
Eh (redox potential)	Orion 290A meter; ThermoOrion 9678BN Combination redox electrode
Dissolved Oxygen (DO)	ThermoOrion DO meter 830A, probe included
GPS Location	Garmin 12CX (hand held)
Temperature	Recorded from DO, pH and EC meters
Sulphide concentration	Orion 900200 D/junc. Ref. Electrode; Orion 9416BN Sulphide electrode

Table 3.2 Sample Descriptions Summary

Sample Purpose	Amount (ml)	BOTTLE MATERIAL*	FILTERED (0.45μM)	Additive (purpose explained in text)
Anions	125	HDPE	Yes	None
Cations & Trace Elements	125	HDPE	Yes	Ultra pure nitric acid – $HNO_{3(aq)}$
Alkalinity	125	HDPE	Yes	None
Sulphate Isotopes	250	HDPE	Yes	Barium chloride - $BaCl_2 \cdot 2H_2O_{(s)}$
Sulphide Isotopes	1000	Amber PET	No	Cadmium acetate - $(CH_3COO)_2Cd \cdot 2H_2O_{(s)}$
DIC Isotopes	60	Amber Glass	Yes	Mercuric chloride - $HgCl_{(s)}$
Silica	10	HDPE	Yes	50ml of doubly distilled water
O&H Isotopes	30	HDPE	Yes	Paraffin wax on lid
Dissolved Gases	2 x 125	Amber Glass with Septum Lid	No	None
Free Gases	2 x 125	Amber Glass with Septum Lid	No	None
Sulphide	30	HDPE	No	30ml of Sulphur-Anti-Oxidant-Buffer (SAOB)

*HDPE = High Density Polyethylene **PET = Polyethylene Terephthalate

Table 3.3 Methods and Limits of Detection for Trace Elements

ICP emission spectrometry (METHOD ICPES-120)		ICP mass spectrometry (METHOD ICPMS-120)	
Element	Limit of Determination (ppb)	Element	Limit of determination (ppb)
Al	5.5	Ag	0.2
As	12.0	Al	0.5
B	9.5	As	1.0
Ba	0.6	Ba	0.5
Be	0.1	Be	1.0
Ca	2.8	Bi	0.2
Cd	0.3	Cd	0.5
Co	3.1	Co	0.2
Cr	29.0	Cr	2.0
Cu	0.4	Cs	0.2
Fe	1.9	Cu	0.5
Li	0.6	Ga	0.2
K	12.0	Hg	0.2
Mg	1.1	In	0.2
Mn	0.2	Mn	0.2
Na	12.1	Mo	0.5
Ni	1.6	Ni	1.0
Pb	9.4	Pb	0.2
Sc	0.3	Rb	0.2
Se	23.8	Sb	0.2
Si	3.3	Se	2.0
Sr	0.2	Tl	0.2
Ti	0.4	U	0.2
V	1.0	V	0.2
Zn	0.32	Zn	2.0

Table 3.4: Isotope Methods Summary

Isotope	Accuracy and Precision	Standard	Preparation Process	Instrument Type	Method References	Machine Name
$\delta^{34}S$ in sulphides and sulphates	+/-0.7 ‰	V-CDT[1]	chemical oxidation and gas generation	EA-C-IRMS[4]	Coplen and Krouse, 1998.	Carlo Erba *NA 1500* elemental analyzer interfaced to a magnetic-sector mass analyzer
$\delta^{18}O$ in sulphates	+/-0.5 ‰	V-SMOW[2]	Pyrolysis and gas generation	TC/EA-C-IRMS[4]		TCEA pyrolysis reactor interfaced to a magnetic-sector mass analyzer
$\delta^{13}C$ of CO_2 and CH_4 gases	+/-0.2 ‰	V-PDB[3]		GC-C-IRMS[4]		HP 6890 gas chromatogram interfaced to a high temperature combustion reactor which in-turn is interfaced to a Finnigan Mat Delta+XL mass spectrometer via a open split reaction with carbonates / gas injection
Carbonate and Aqueous DIC $\delta^{13}C$	+/-0.2 ‰	V-PDB[3]		D-IRMS[5]	Coplen et al., 1983; Friedman and O'Neil, 1977; McCrea, 1950; Rosenbaum and Sheppard, 1986.	VG Sira 903
$\delta^{2}H$ in H_2O	+/-2 ‰	V-SMOW[2]	Zn or Cr reduction	D-IRMS[5]	Coleman et al, 1982; Friedman, 1953; Nelson and Dettman, 2001; Gehre et al., 1996; Donnelly et al, 2001.	Micromass 602
$\delta^{18}O$ in H_2O	+/-0.2 ‰	V-SMOW[2]	equilibration with CO_2	D-IRMS[5]	Epstein and Mayeda, 1953; Horita et al., 1993; O'Neil et al., 1975; Sofer, 1972.	Micomass SIRA II

[1]Canyon Diablo Troilite [2]Standard Mean Ocean Water [3]Peedee Belemnite
[4]Continuous Flow-Isotope Ratio Mass Spectrometry [5]Dual Inlet-Isotope Ratio Mass Spectrometry
EA = elemental analyzer

Table 4.1: Description of bedrock geology from which MERA II springs discharge from based on Okulitch (2005).

Major Grouping	Geology Unit	Unit Description	Associated Springs
Limestone / Dolostone	mOSu	Sunblood Formation: dolostone, limestone.	Wildmint, Clearwater Creek, Cascade, Cartman
	OSW	Whittaker Formation: lower grey limestone, middle white quartzite, upper dark grey cherty dolostone	South Redstone, Prairie Creek Mine Shaft, Harrison Creek, Prairie Creek, Galena Creek
	PM	Manetoe Facies: grey coarse-grained massive vuggy diagenetic dolostone.	Kraus (Clausen)
	SDRR	Root River Formation: light yellowish grey dolostone	Mel's Pool
	COBS	Broken Skull Formation: dolostone, limestone; basal sandstone, sandy dolostone.	Dookie, Boulder
	COR	Rabbitkettle Formation: wavy banded silty limestone; platy impure limestone, siltstone, limestone.	Brimstone, North Cantung, Glacier Lake, Stinky Drift, Tiny
	CSH	Haywire Formation: dolomitic, cherty and argillaceous limestone	Moore's, Grizzle Bear
	lCSe	Sekwi Formation: limestone, calcareous silstone, sandstone, sandy & silty dolostone, argillite, minor quartzite & limestone	West Cantung, Blue Bells, Persistence, Stinky
	lmDC	Camsell, Sombre, Bear Rock, Arnica, Natla, Grizzly Bear, Funeral, Headless, Landry, Hume and Nahanni Formations: Limestone, dolostone, shale, siltstone and sandstone.	Tabletop, Meilleur River, Sibbeston, Sombre, Wrigley, Cowgirl, Mossy, Crack
	lmDA	Arnica Formation: dolostone: finely crystalline thick-bedded grey finely porous	Sculpin
	mCR	Rockslide Formation: dark grey sooty argillaceous limestone and calcareous siltstone, shale.	Grasby
	mDHN	Headless and Nahanni Formations: grey shale and limestone / bioclastic limestone.	Veil, Big Veil, Cimitar
	PLD	Little Dal Group: basal varicloured mudstone, subordinate sandstone; grainstone, lime mudstone, stromatolotic biostromes and bioherms passing northwards in lime rhythmites, shale, siltstone; dolomitic grainstone, laminite, stromatolites, calcareous siltite all interbedded with dolostone and minor gypsum and local breccia; gypsum, anhydrite, minor quartz sandstone, siltstone, claystone; red, green and grey shale, very fine-grained sandstone, peritidal carbonate; dolomitic stromatolitic peritidal carbonate, mudrock; basaltic lava	Ekwi, Deca
Pluton	Kqm	Hole-In-the-Wall Batholith, Selwyn Plutonic Suite: Quartz monzonite, granodiorite.	n/a
	Kqm2	Skinboat Plutons, Selwyn Plutonic Suite: Quartz monzonite, granodiorite.	Hole-in-the-Wall, Overflow, Jacson, Darkness, Interpluton Seep, Meltwater, Waterfall, Half Spring,
Shale	CPMC	Mount Christie: burrowed, interbedded greenish grey cherty shale and green shale; thin to medium bedded, light grey-green to black chert; black siliceous slate and siltstone; minor quartzite, limestone and dolostone; locally abundant, large grey barite nodules	Nahanni Headwaters
	DCBR	Besa River Formation: shale: dark grey, pyritic, siliceous; calcareous shale, siltstone, calcareous siltstone, silty limestone and limestone	Smurf, Clark Lake, Selena, Caribou, Chance, Orange Creek, Caribou River
	DCE	Earn Group (marine): chert, cherty mudstone, black shale, silty shale, argillite.	Tulita, Cotton, Red Mini, Muddy, Red Steel, Bougere
	mDF	Funeral Formation: grey thin-bedded argillaceous bioclastic shale.	Corridor Creek, Broken Skull, Brigade
	ODRR	Road River Formation: black calcareous graptolitic shale, grey argillaceous limestone	Mineral Lake, Cordes Vertes, Rabbitkettle, Flat Fruit, Descente, Softie, Karst
	uDFS	Fort Simpson Formation: green and grey shale, siltstone, limestone	Cowboy, Ram Plateau, Cathedral, Quickie
Siltstone/ Mudstone	ECv	Vampire Formation: siltstone, grey fine-grained sandstone	Nahanni North
Stratified Clastics	ECH	Hyland Group: Lower dark shale & slate, gritty quartzite, calcarenite, quartz pebble conglomerate; Upper sandstone, maroon green & buff shale & slate.	Champagne, Champagne Creek
	PCssc	Neohadrynian and/or Lower Paleozoic: grey to brown fine-grained sandy dolostone, medium to coarse-grained sandstone	Redstone Junction #1

Table 4.2: Field Parameters from MERA II springs (2003-2005 field seasons).

Informal Name of Water Sample	Water Type	UTM Zone	Easting (m)	Northing (m)	Year Sampled	Sulfide[1] (ppm)	Eh[2] (mV)	pH[2]	EC[3] (µS/cm)	T[4] (°C)	TDGP[5] (% sat'n)	DO[6] (ppm)
CCME Drinking Water Guideline						*<=0.05**	*n/a*	*6.5-8.5**	*n/a^*	*<=15**	*n/a*	*n/a*
CCME Recreation Guideline								*6.5-8.5*		*<=30*		
Tulita	spring	09V	457358	7075426	2004	45	nd	7.05	966	24.7	101	0.65
Sculpin	spring	09V	484585	7089847	2004	0.0	nd	7.03	2	17.1	105	0.52
Deca	spring	09V	527633	7113365	2004	0.9	125	7.10	40800	21.6	127	2.2
Ekwi	spring	09V	537294	7104066	2004	0.0	10.4	6.69	18300	40.8	127	0.23
Mineral Lake	spring	09V	622470	6806505	2004	n/a	-58	6.68	776	18.3	105	0.13
Brimstone	spring	09V	583173	6830761	2004	0.1	11.5	5.89	8200	6.2	114	2.1
Cordes Vertes	spring	09V	571388	6841735	2004	0.0	88.0	7.22	600	8.2	97	8.2
Tabletop	spring	10V	355313	7030440	2004	0.0	76.7	7.67	827	38.5	102	2.7
South Redstone	spring	10V	352412	7033921	2004	0.0	97.5	7.51	767	51.2	138	nd
Redstone Junction #1	spring	10V	365506	7047713	2004	0.1	140	7.36	1274	15.4	105	3.4
Cotton	spring	09V	474514	6951213	2004	0.1	366	3.77	0	12.5	nd	7.0
Red Mini	spring	09V	493635	6937404	2004	0.1	403	3.94	144	4.2	nd	9.9
Muddy	spring	09V	512709	6920298	2004	0.1	130	6.84	342	2.3	99	9.3
Grasby	spring	09V	539903	6967578	2004	0.1	44.9	7.27	455	3.2	100	9.6
Red Steel	spring	09V	542374	6952471	2004	0.1	92.4	6.65	127	0.8	100	10.4
Bougere	spring	09V	523354	6948113	2004	0.3	344	4.31	547	2.7	102	10.5
Champagne	spring	09V	505562	6895664	2004	0.2	115	6.43	436	5.9	101	6.4
Champagne Creek	surface	09V	505562	6895664	2004	0.1	nd	nd	nd	nd	nd	nd
Broken Skull Upper Pool (2003)	spring	09V	544141	6958547	2003	nd	nd	nd	nd	nd	nd	nd
North Cantung / Zenchuck Creek	spring	09V	530149	6887223	2003	n/a	124	7.61	367	20.9	nd	nd
Moore's	spring	09V	544845	6911991	2003	n/a	-191	6.75	871	48.2	nd	nd
Nahanni North / Lened Creek	spring	09V	516600	6915433	2003	34	-363	8.66	579	56.1	nd	nd
Nahanni Headwaters	spring	09V	508211	6964253	2003	n/a	-149	8.30	503	63.6	nd	nd
Broken Skull	spring	09V	544141	6958547	2003	20	-160	6.38	2200	46.4	nd	nd
Grizzle Bear	spring	09V	556331	6949262	2003	n/a	-79	6.78	1371	42.6	nd	nd
Glacier Lake	spring	09V	573552	6884820	2003	n/a	-204	7.11	944	3.5	nd	nd
Rabbitkettle	spring	09V	595449	6868956	2003	n/a	nd	5.74	1896	21.1	nd	nd
Kraus / Clausen	spring	10V	443147	6791497	2003	61	nd	6.54	11870	36.7	nd	nd
Meilleur River	spring	10V	397576	6778381	2003	25	nd	6.63	1845	36.9	nd	nd
Wildmint	spring	09V	629391	6812339	2003	43	nd	6.63	1243	30.0	nd	nd
Stinky Drift	spring	09V	541638	6869584	2003	nd	nd	8.76	1013	16.6	nd	nd
Hole in the wall	spring	09V	589113	6849731	2003	n/a	nd	8.43	211	40.2	nd	nd
Flat Fruit	spring	09V	573499	6839393	2003	n/a	nd	6.29	4030	9.3	nd	nd
West Cantung	spring	09V	541638	6869584	2003	nd	nd	8.39	460	41.3	nd	nd
Prairie Creek Mine Shaft	mine	10V	404598	6825669	2005	0.5	149	7.15	1185	1.4	nd	n/a
Harrison Creek	surface	10V	404760	6825676	2005	0.6	136	8.23	645	8.2	nd	n/a
Prairie Creek	surface	10V	404733	6825262	2005	0.7	160	8.08	498	9.1	nd	n/a
Broken Skull Upper Pool (2005)	spring	09V	544141	6958547	2005	0.3	112	7.18	1346	27.9	nd	6.3
Broken Skull Lower Pool (2005)	spring	09V	544141	6958547	2005	7.9	-286	6.46	1340	46.3	nd	0.80
Cowboy	spring	10V	396251	6854569	2005	0.7	230	7.87	352	1.3	nd	11.4
Sibbeston	spring	10V	384613	6838707	2005	0.8	235	7.65	340	16.9	nd	4.6
Corridor Creek	seep	10V	411544	6861536	2005	0.2	197	8.82	265	3.8	nd	11.0
Veil	spring	10V	444167	6845930	2005	0.6	203	8.17	414	4.8	nd	11.0
Big Veil	spring	10V	443995	6846719	2005	n/a	254	8.37	446	4.8	nd	7.9
Galena	spring	10V	404768	6824888	2005	0.5	235	8.01	779	2.3	nd	3.6
Sombre	spring	10V	363265	6884608	2005	0.5	229	8.67	169	0.3	nd	11.3
Wrigley	spring	10V	374780	6873478	2005	0.7	258	6.15	624	2.5	nd	7.8
Mel's Pool	waterfall	10V	371922	6826904	2005	0.3	2.62	7.53	138	2.7	nd	12.5
Cowgirl	spring	10V	393366	6849954	2005	n/a	178	7.37	463	2.0	nd	7.7
Brigade	spring	10V	417004	6865784	2005	0.4	2.89	7.55	576	3.3	nd	10.2
Ram Plateau	waterfall	10V	438705	6865933	2005	0.3	3.08	7.52	134	2.6	nd	11.6
Cimitar	spring	10V	457861	6855539	2005	n/a	*5.80*	6.79	1960	11.9	nd	0.27
Cathedral	spring	10V	365815	6871064	2005	0.2	3.91	7.55	473	2.0	nd	10.8
Mossy	spring	10V	355469	6887488	2005	0.2	3.69	7.61	409	1.4	nd	8.4
Crack	spring	10V	354083	6891379	2005	n/a	*-1.50*	7.83	279	4.0	nd	*7.2*
Quickie	seep	10V	362240	6867252	2005	n/a	2.11	7.98	453	7.0	nd	10.3
Clearwater Creek	surface	09V	646454	6881852	2005	0.2	310	8.66	292	5.8	nd	10.8
Dookie	surface	09V	626201	6909591	2005	0.1	283	8.78	298	4.1	nd	10.2
Boulder	spring	09V	644261	6890647	2005	n/a	258	8.79	159	0.8	nd	11.4
Overflow	spring	09V	633581	6776726	2005	0.0	312	4.85	5	1.7	nd	10.3
Smurf	spring	09V	619206	6770435	2005	n/a	289	7.39	354	2.7	nd	10.5
Clark Lake	spring	09V	646722	6795048	2005	n/a	53	7.49	473	3.3	nd	2.8
Jacson	spring	09V	632059	6776080	2005	n/a	280	6.87	13	1.8	nd	11.1
Darkness	spring	09V	632175	6776410	2005	n/a	292	6.40	23	1.0	nd	10.0
Selena	seep	09V	624764	6759725	2005	n/a	88.8	7.24	708	7.6	nd	3.3

Table 4.2 (continued from previous page): Field parameters from MERA II springs (2003-2005 field seasons).

Informal Name of Water Sample	Water Type	UTM Zone	Easting (m)	Northing (m)	Year Sampled	Sulfide[1] (ppm)	Eh[2] (mV)	pH[2]	EC[3] (µS/cm)	T[4] (°C)	TDGP[5] (% sat'n)	DO[6] (ppm)
CCME Drinking Water Guideline						*<=0.05**	*n/a*	*6.5-8.5**	*n/a^*	*<=15**	*n/a*	*n/a*
CCME Recreation Guideline								*6.5-8.5*		*<=30*		
Caribou	spring	09V	619689	6768728	2005	n/a	215	7.75	377	3.8	nd	10.1
Chance	spring	09V	619815	6768439	2005	n/a	400	7.66	431	2.0	nd	11.5
Interpluton	seep	09V	625583	6794379	2005	n/a	260	4.41	16	4.1	nd	9.8
Tiny	spring	09V	607475	6792433	2005	n/a	225	7.64	252	1.4	nd	11.4
Blue Bells	spring	09V	606845	6773246	2005	n/a	193	7.41	380	7.6	nd	6.5
Cascade	spring	09V	626373	6754797	2005	n/a	291	7.37	356	4.0	nd	8.9
Meltwater	seep	09V	632361	6782647	2005	n/a	264	7.44	63	3.7	nd	8.0
Waterfall	surface	09V	615834	6842094	2005	n/a	259	6.90	26	9.8	nd	9.0
Descente	spring	09V	620423	6823148	2005	n/a	278	7.49	57	0.8	nd	11.1
Softie	spring	09V	635352	6833829	2005	n/a	287	5.53	18	6.3	nd	6.3
Cartman	spring	09V	636224	6840955	2005	n/a	256	6.34	30	1.7	nd	10.7
Half Spring	spring	09V	623424	6840327	2005	n/a	243	7.60	155	4.5	nd	11.3
Orange Creek	surface	09V	653663	6785389	2005	n/a	219	4.65	3260	1.9	nd	*7.7*
Caribou River	surface	09V	653624	6785282	2005	n/a	190	7.93	355	9.3	nd	12.8
Karst	spring	09V	549539	6942051	2005	n/a	285	7.93	163	3.7	nd	*13.0*
Persistent	spring	09V	607144	6773277	2005	n/a	127	6.07	661	20.5	nd	2.4
Stinky	spring	09V	607101	6773258	2005	2.3	-60.3	6.74	761	24.1	nd	*1.0*

[1]Sulfide concentration <1ppm is considered negligible

[2]Normalized to 25°C

[3]Electrical Conductivity

[4]Temperature

[5]Total Dissolved Gas Pressure (% saturation)

[6]Dissolved Oxygen

n/a = not applicable (ex: no smell of sulfide)

nd = no data available (ex: test not performed)

unstable reading

CCME Drinking Water Guidelines:
Federal-Provincial-Territorial Committee on Drinking Water. "Guidelines for Candadian Drinking Water Quality Summary Table". Health Canada, Government of Canada, March 2006.

CCME Recreation Guidelines:
Federal-Provincial Working Group on Recreational Water Quality of the Federal-Provincial Advisory Committee on Environmental and Occutpational Health. "Guidelines for Canadian Recreational Water Quality". Health and Welfare Canada, Government of Canada, 1992.

***Aesthetic Guideline Only**

***n/a* = guideline not available**

^TDS <=500*

Table 4.3: Major Ions of 2003-2005 Springs. All units in ppm unless otherwise noted. Charge balance data in bold is above 10% and with stars (*) has metals included to balance the charge.

Name of Spring	Ca^{2+}	Mg^{2+}	K^{+}	Na^{+}	Si^{4+}	HCO_3^{-}	SO_4^{2-}	Cl^{-}	NO_3^{-}	F^{-} (ppb)	Charge
CCME Drinking Water Guideline	*n/a*	*n/a*	*n/a*	*<=200**	*n/a*	*n/a*	*<=500**	*<=250**	*45*	*1.5*	**Balance (%)**
Tulita	68	22	12	110	8.40	389	118	45.9	<0.05	2.61E+03	0.75
Sculpin	440	130	1.0	1.6	4.44	220	1.50E+03	<1	<0.50	<500	-3.0
Deca	270	59	5.2	420	5.40	261	944	471	<0.50	<500	-0.68
Deca (lab dup)	nd	nd	nd	nd	5.46	nd	nd	nd	nd	nd	nd
Ekwi	220	49	72	4800	12.0	663	1.78E+03	7503	<2.50	<2500	-7.0
Mineral Lake	120	29	2.8	6.4	4.32	327	78.3	1.59	<0.05	342	**10.7**
Brimstone	630	55	8.2	44	36	1813	69.3	4.09	<0.05	2.71E+03	9.8
Cordes Vertes	92	20	0.95	7.0	2.52	458	14.7	0.40	0.431	<50	-8.7
Tabletop	73	23	1.4	60	13.2	188	150	85.2	0.198	178	-2.6
South Redstone	77	21	1.3	48	15.6	172	162	68.5	0.148	157	-2.8
Redstone Junction #1	110	38	2.1	100	10.8	172	252	144	0.741	239	3.6
Cotton	0.93	1.2	0.27	0.27	3.72	0.0	15.6	0.1	<0.05	<50	**-15.1**
Red Mini	4.7	1.5	0.83	0.7	5.58	0.0	38.0	<0.1	<0.05	<50	**-10.4***
Muddy	37	15	1.7	1.4	5.58	79.9	99.0	<0.1	0.63	136	-2.9
Grasby	64	17	0.85	1.9	2.64	297	29.3	0.29	0.813	<50	-7.7
Red Steel	17	2	0.26	1.0	2.40	0.0	21.6	<0.1	1.214	<50	**12.4***
Bougere	2.8	37	0.32	0.29	7.20	0.0	279	<0.1	0.288	<50	0.87*
Champagne	83	1	1.6	2.4	2.58	223	52.7	<0.1	0.296	<50	-4.2
Champagne (field dup)	79	0.93	1.6	2.1	2.76	218	52.3	<0.1	0.296	<50	-5.8
Champagne Creek	72	0.57	1.6	0.96	2.22	169	55.8	0.10	0.116	<50	-2.7
Champagne Creek (lab dup)	72	0.58	1.6	0.97	nd	169	54.9	0.14	<0.05	<50	nd
North Cantung / Zenchuck Creek	26	14	0.56	0.58	4.92	201	8.64	0.21	729	197	**-16.6**
Moore's	74	23	4.1	2.2	21	279	73.4	0.48	<50	286	-2.8
Nahanni North / Lened Creek	1.6	0.059	1.1	76	25.8	146	57.4	1.11	157	2.87E+03	-2.9
Nahanni Headwaters	2.9	0.01	1.6	65	34.2	101	31.9	10.3	<50	8.16E+03	7.3
Broken Skull Upper Pool (2003)	160	50	32	56	15.6	387	345	22.0	<50	2.25E+03	4.1
Grizzle Bear	110	26	23	22	16.2	229	188	26.8	290	680	4.3
Glacier Lake	75	17	0.84	1.3	7.80	64.5	199	0.14	<50	436	0.17
Rabbitkettle	200	40	5.1	4.1	6.60	447	34.8	0.57	<50	235	0.91*
Kraus / Clausen	410	74	81	940	12.6	236	656	1695	<500	<500	3.1
Meilleur River	150	46	14	30	18.6	317	277	23.9	<50	467	5.3
Wildmint	17	2.5	1.2	130	16.8	187	114	29.4	6590	8.31E+03	3.6
Stinky Drift	130	26	2.8	1.5	7.80	346	29.4	0.30	208	291	-4.8*
Hole in the wall	1.6	0.061	0.63	26	25.8	72.3	5.74	1.14	<50	1.88E+03	-4.1
Flat Fruit	500	52	6.0	27	5.70	581	35.1	1.56	454	631	1.6*
West Cantung	8	1.2	1.2	57	21	140	31.5	5.89	<50	5.00E+03	-1.8
Prairie Creek Mine Shaft	150	65	1.1	0.91	1.86	315	396	0.39	0.407	<50	-2.0
Harrison Creek	75	39	0.79	0.91	1.50	223	161	0.19	1.041	<50	-0.09
Prairie Creek	58	23	0.47	1.8	1.32	193	74.8	<0.1	0.269	67.0	1.5
Broken Skull's Upper Pool (2005)	160	50	32	51	13.2	439	366	21.6	<0.05	1.70E+03	-0.94
Broken Skull's Lower Pool (2005)	160	49	31	50	15.0	440	364	21.2	<0.05	1.77E+03	-1.3
Cowboy	45	15	0.22	0.72	1.08	157	35.3	<0.1	0.561	<50	3.1
Sibbeston	44	16	0.58	1.3	4.74	168	29.8	0.91	0.765	1.31E+03	2.4
Corridor Creek	35	11	0.16	0.64	0.66	122	22.7	0.14	0.635	129	3.9
Veil	65	14	0.6	5.6	1.68	186	62.4	0.72	0.647	307	3.1
Big Veil	65	14	0.6	5.6	1.68	188	64.2	0.69	0.729	300	2.3
Galena	110	40	1.0	1.8	1.74	283	155	0.49	0.115	53.0	6.0
Galena (lab dup)	120	44	1.1	2.2	nd	283	144	0.58	0.101	<50	**12.0**
Sombre	22	8.3	0.07	0.040	0.17	94.5	4.15	<0.1	0.398	1.19E+03	4.2
Sombre (field dup)	22	8.2	0.080	0.040	bdl	94.6	4.13	<0.1	0.497	907	3.9
Wrigley	95	19	0.43	0.84	1.74	244	113	0.26	1.376	337	-0.16
Mel's Pool	27	4.1	0.17	0.35	1.56	73.4	1.25	<0.1	<0.05	<50	**16.2**

Table 4.3 (continued from previous page): Major Ions from 2003/04/05 Springs. All units in ppm unless otherwise noted. Charge balance data in bold is above 10% and with stars (*) has metals included to balance the charge.

Name of Spring	Ca^{2+}	Mg^{2+}	K^{+}	Na^{+}	Si^{4+}	HCO_3^{-}	SO_4^{2-}	Cl^{-}	NO_3^{-}	F^{-} (ppb)	Charge
CCME Drinking Water Guideline	*n/a*	*n/a*	*n/a*	*<=200**	*n/a*	*n/a*	*<=500**	*<=250**	*45*	*1.5*	**Balance (%)**
Cowgirl	70	14	0.23	0.49	1.38	190	64.9	0.18	0.581	66.0	2.0
Brigade	68	29	0.50	4.1	1.92	198	127	0.27	1.317	133	0.59
Ram Plateau	23	3.4	0.45	0.30	1.02	61.3	7.42	<0.1	<0.05	<50	**11.2**
Cimitar	370	63	2.5	13	4.32	287	780	14.6	<0.05	<500	6.4
Cathedral	55	19	0.31	6.1	1.08	178	73.2	0.17	0.963	370	1.3
Mossy	46	21	0.26	0.21	0.90	167	54.2	0.16	0.666	350	2.0
Mossy (lab dup)	51	24	0.34	0.33	nd	167	56.1	<0.1	0.497	333	7.5
Crack	34	15	0.14	0.16	0.84	136	14.8	0.14	0.51	86.0	7.0
Quickie	61	19	0.30	4.2	1.50	174	67.7	0.18	0.646	145	5.7
Clearwater Creek	39	12	0.32	0.27	0.96	112	37.8	0.14	0.464	<50	5.7
Dookie	30	17	0.19	0.099	0.96	97.6	62.9	<0.1	0.39	<50	-0.17
Dookie (field dup)	31	17	0.19	0.12	0.84	83.8	63.2	<0.1	0.393	<50	4.6
Dookie (field trip)	31	17	0.19	0.11	0.78	81.7	63.8	<0.1	0.384	<50	5.0
Boulder	20	7.4	0.09	0.07	0.53	75.8	5.47	0.11	0.543	<50	8.2
Overflow	0.66	0.078	0.11	0.54	1.14	4.0	<0.05	<0.1	<0.05	<50	0.08
Smurf	62	6.8	0.45	0.84	2.40	220	8.37	<0.1	<0.05	<50	-1.0
Clark Lake	81	11	0.64	0.35	2.04	187	21.4	0.14	<0.05	<50	**17.3**
Clark Lake (lab dup)	89	12	0.72	0.45	nd	187	21.3	<0.1	<0.05	<50	**21.9**
Jacson	1.4	0.13	0.20	0.51	1.08	5.7	0.32	<0.1	0.347	<50	1.1
Darkness	2.4	0.15	0.26	0.91	1.92	9.7	0.73	<0.1	0.758	<50	-2.0
Selena	130	14	0.77	1.2	2.22	188	131	0.15	<0.05	<50	**14.1**
Caribou	57	12	0.64	0.77	2.58	200	11.9	0.11	0.483	<50	4.6
Chance	67	13	0.49	0.66	2.46	181	17.6	0.11	0.766	<50	**14.3**
Interpluton	1.6	0.17	0.36	0.70	2.94	8.0	<0.05	<0.1	<0.05	<50	0.90
Tiny	38	7.7	1.2	0.62	2.22	127	2.55	<0.1	<0.05	<50	9.6
Blue Bells	43	20	1.8	2.2	3.30	187	11.9	0.70	0.716	451	8.2
Blue Bells (field dup)	42	20	1.8	2.2	3.30	188	11.9	0.71	0.793	456	7.3
Cascade	55	11	0.41	0.48	1.98	166	14.4	0.11	0.425	<50	9.7
Cascade (lab dup)	60	12	0.45	0.59	nd	166	13.7	<0.1	0.35	<50	**14.3**
Meltwater	9.4	0.27	0.78	0.47	1.74	36.6	0.56	<0.1	<0.05	<50	-7.0
Waterfall	3.1	0.17	0.74	0.81	2.16	14.2	0.20	<0.1	<0.05	<50	-3.1
Descente	4.9	1.8	0.39	0.63	2.52	19.5	7.97	<0.1	0.218	<50	-6.4
Softie	1.7	0.5	<0.02	1.1	4.02	8.9	<0.05	<0.1	<0.05	<50	8.7
Cartman	1.7	1.2	0.24	0.86	3.72	15.5	0.66	<0.1	<0.05	<50	-8.1
Half Spring	27	2.6	0.89	2.3	3.18	85.4	12.3	0.15	0.579	536	0.43
Orange Creek	380	170	1.6	0.89	4.44	0.0	1913	<0.5	<0.5	<500	-9.3
Caribou River	56	11	0.69	0.87	1.92	164	41.9	<0.1	0.143	<50	2.7
Karst	23	8.1	0.13	0.10	0.60	89.3	10.5	<0.1	0.299	<50	3.9
Persistent	79	34	8.4	12	nd	397	11.8	5.35	<0.05	1.46E+03	4.0
Persistent (lab dup)	83	38	9.3	13	6.6	397	11.1	4.97	<0.05	1.44E+03	8.0
Stinky	93	37	9.7	15	8.4	457	10.7	6.52	<0.05	1.80E+03	4.2
Field Blank (2005)	0.3	0.011	<0.02	<0.02	<0.06	nd	<0.05	<0.1	<0.05	<50	nd
Calgary Lab Blank (2005)	<0.005	<0.002	<0.02	<0.02	<0.06	nd	<0.05	<0.1	<0.05	<50	nd

CCME Drinking Water Guidelines:
Federal-Provincial-Territorial Committee on Drinking Water. "Guidelines for Candadian Drinking Water Quality Summary Table". Health Canada, Government of Canada, March 2006.

***Aesthetic Guideline Only**
***n/a* = guideline not available**
nd = no data
bdl = below detection limit
**Silica concentration was determined by diluting 10ml of sample water with 50ml of distilled water.
The determined concentration of the diluted sample was multiplied by 6 for the reported values.
Note: 1.46E+03 indicates scientific notation for 1.46 x 10^3 or 1460

Table 4.4a: Most common trace elements (Fe, Al, Mn, Ni, Cu, Zn, Pb, Cd, Co and Cr) from MERA I and II springs. All units in μg/L unless otherwise noted. Bolded numbers were determined to be elevated using the individual trace element method.

element	Fe	Al	Mn	Ni	Cu	Zn	Pb	Cd	Co	Cr
Name of Spring *detection limit (MERA II)*	*3*	*0.2*	*0.05*	*0.2*	*0.2*	*0.32*	*0.05*	*0.1*	*0.05*	*0.2*
detection limit (MERA I)	*4*	*100*	*5*	*2*	*2*	*5*	*2*	*2*	*2*	*n/a*
CCME Drinking Water Guideline (mg/L)	*<=0.3**	*n/a*	*<=0.05**	*n/a*	*<=1.0**	*<=5.0**	*0.010*	*0.005*	*n/a[c]*	*0.05*
MERA II Samples										
Tulita	bdl	0.6	5.60	0.8	0.6	3	bdl	0.1	0.08	0.9
Sculpin	84	0.8	2.50	9.9	bdl	6	0.06	0.1	0.56	0.4
Deca	bdl	0.8	0.94	5.7	3.3	4	0.08	0.1	0.34	**4.4**
Ekwi	170	3.9	17.0	2.8	2.5	2	0.09	bdl	0.25	**2.9**
Mineral Lake	1.30E+03	0.4	12.0	3.9	0.2	1	bdl	bdl	0.21	**1.8**
Brimstone[1]	**1.54E+04**	120	**1.34E+03**	9.7	0.5	7	bdl	0.9	1.90	**6.9**
Cordes Vertes	13	0.8	0.25	2.2	0.3	2	0.05	0.3	0.13	**1.6**
Tabletop	bdl	0.7	0.08	1.2	0.4	2	bdl	0.4	0.06	**1.6**
South Redstone	bdl	1.1	0.08	1.2	1.3	6	0.42	0.1	0.07	**1.1**
Redstone Junction #1	bdl	0.6	0.10	2.0	0.8	3	0.06	0.1	0.11	2.5
Cotton	300	600	23.0	19.0	2.0	56	0.74	1.3	3.90	bdl
Red Mini	140	2.0E+03	94.0	70.0	14.0	72	0.23	2.2	11.0	bdl
Muddy	bdl	7.0	0.27	13.0	0.3	29	bdl	0.4	0.05	0.2
Grasby	bdl	0.7	bdl	1.3	bdl	1	bdl	1.8	0.08	0.6
Red Steel	5	12.0	0.28	1.9	0.7	3	bdl	2.3	bdl	0.2
Bougere	26	**2.4E+04**	**930**	**1.3E+03**	**28.0**	**2.3E+03**	0.22	4.4	**390**	bdl
Champagne	180	5.9	150	2.1	0.4	4	bdl	3.8	0.21	0.8
Champagne (dup)	150	9.9	120	1.9	0.3	2	bdl	2.8	0.18	0.6
Champagne Creek	28	22.0	1.10	1.6	0.3	2	bdl	4.2	0.11	0.4
Champagne Creek (dup)	28	19.0	1.00	1.4	0.2	2	bdl	3.8	0.10	0.3
North Cantung (Zenchuck Creek)	bdl	0.60	bdl	0.3	0.7	3	0.36	bdl	bdl	0.2
Moore's	110	39.0	14.0	1.0	0.7	2	0.43	0.1	0.20	0.3
Nahanni North (Lened Creek)	77	70.0	0.79	0.2	0.5	2	0.08	bdl	0.05	bdl
Nahanni Headwaters	5	24.0	0.23	bdl	0.5	2	bdl	bdl	bdl	0.4
Broken Skull	65	2.40	3.20	1.9	0.5	1	0.10	bdl	0.13	0.8
Grizzle Bear	14	0.60	26.0	1.2	0.2	2	0.05	bdl	0.30	**1.1**
Glacier Lake	**1.70E+04**	6.40	530	1.9E+02	bdl	**679**	bdl	2.1	28.0	bdl
Rabbitkettle	10	0.40	4.50	4.0	bdl	8	bdl	bdl	0.29	0.8
Kraus (Clausen)	11	4.70	27.0	3.3	5.8	3	0.07	bdl	0.37	**27**
Meilleur River	17	5.10	14.0	2.0	0.3	2	bdl	bdl	0.13	0.8
Wildmint	bdl	1.50	49.0	1.2	0.8	1	0.07	0.1	0.26	1.2
Stinky Drift	23	3.40	1.20	1.6	bdl	7	0.12	bdl	0.12	0.6
Hole in the wall	17	36.0	0.37	bdl	0.4	2	bdl	0.1	bdl	0.4
Flat Fruit	9	2.70	94.0	6.3	0.9	5	0.05	0.1	0.47	bdl
West Cantung	34	4.00	0.79	bdl	0.5	3	bdl	0.2	bdl	0.4
Prairie Creek Mine Shaft	bdl	1.0	4.60	15.0	**16.0**	**6.90E+03**	**16.0**	**41**	0.46	0.2
Harrison Creek	bdl	2.0	0.11	1.9	0.8	30	**3.50**	0.3	0.08	0.2
Prairie Creek	bdl	1.3	0.36	2.0	0.7	80	0.82	0.2	0.06	bdl
Broken Skull's Upper Pool	5	4.6	11.0	2.1	1.2	20	**2.30**	0.2	0.27	0.4
Broken Skull's Lower Pool	120	4.1	5.10	2.8	0.5	4	0.64	0.2	0.19	0.6
Cowboy	bdl	1.8	0.05	1.3	0.2	2	0.48	0.3	0.05	0.2
Sibbeston	bdl	2.6	0.08	2.9	0.2	33	1.00	0.2	0.05	0.2
Corridor Creek	bdl	2.4	bdl	0.8	0.2	2	0.15	bdl	0.05	0.2
Veil	bdl	0.8	0.07	2.8	0.3	10	0.11	0.2	0.08	0.2
Big Veil	bdl	1.3	2.10	3.0	0.9	10	0.40	0.2	0.08	0.2
Galena	bdl	1.7	0.18	6.1	0.9	350	**2.60**	0.6	0.12	0.3
Galena (lab dup)	bdl	1.3	0.15	5.9	1.3	350	2.00	0.6	0.11	0.2
Sombre	bdl	4.4	0.09	0.3	bdl	2	0.50	bdl	bdl	bdl
Sombre (field dup)	bdl	5.0	0.18	0.6	0.3	9	0.65	0.1	bdl	bdl
Wrigley	bdl	0.9	0.16	20.0	0.5	42	0.27	0.2	0.11	0.4
Mel's Pool	130	62.0	1.50	4.8	2.4	10	0.78	0.3	0.13	0.2
Cowgirl	bdl	1.2	0.06	8.6	0.5	19	0.19	0.1	0.07	0.2
Brigade	bdl	0.9	0.08	1.2	0.2	2	0.19	bdl	0.07	bdl
Ram Plateau	120	72.0	1.30	3.1	5.6	4	0.29	0.1	0.16	0.3
Cimitar	840	3.5	150	37.0	0.2	64	0.24	0.1	4.90	0.4
Cathedral	11	7.2	0.44	1.3	0.2	4	0.44	0.1	0.07	0.3
Mossy	15	4.6	0.20	1.0	0.3	5	0.34	0.1	0.06	0.2
Mossy (lab dup)	4	4.4	0.20	1.0	0.5	5	0.33	0.1	0.06	bdl
Crack	bdl	2.8	0.10	1.7	0.3	4	0.34	0.1	0.05	0.2
Quickie	bdl	2.8	0.11	2.4	0.5	2	0.19	0.1	0.08	0.2
Clearwater Creek	bdl	14.0	1.40	1.4	0.2	2	0.26	0.1	0.15	bdl
Dookie	bdl	40.0	220	14.0	0.4	4	0.54	0.1	11.0	bdl
Dookie (field dup)	18	46.0	220	14.0	0.4	3	0.22	bdl	11.0	bdl
Dookie (field trip)	bdl	70.0	220	14.0	0.4	3	0.10	bdl	11.0	bdl
Boulder	bdl	5.2	0.65	0.5	0.2	1	0.18	bdl	0.10	bdl
Overflow	31	170	1.90	0.3	0.6	3	0.52	0.1	0.10	bdl
Smurf	bdl	2.6	0.23	6.5	0.6	46	0.11	0.9	0.09	0.3
Clark Lake	1.30E+03	1.1	35.0	1.7	0.3	4	0.27	bdl	0.14	0.2
Clark Lake (lab dup)	1.30E+03	1.2	35.0	1.5	0.5	4	0.28	bdl	0.14	bdl
Jacson	bdl	26.0	0.37	bdl	0.4	2	0.35	bdl	bdl	bdl
Darkness	bdl	28.0	0.52	0.2	0.4	2	0.20	0.1	bdl	bdl
Selena	470	0.8	110	35.0	14.0	120	1.50	0.3	1.20	0.3
Caribou	150	2.3	0.95	1.3	0.2	4	0.08	0.1	0.08	0.4
Chance	bdl	1.9	0.10	1.4	0.3	3	0.14	0.1	0.09	0.4
Interpluton	57	340	1.20	0.3	1.3	3	0.34	0.1	0.06	bdl
Tiny	bdl	7.3	0.20	0.8	2.6	2	0.38	bdl	0.07	0.4
Blue Bells	bdl	2.0	0.09	0.8	0.3	4	0.17	bdl	0.06	0.3
Blue Bells (field dup)	bdl	2.2	0.13	0.8	0.2	2	0.21	bdl	0.06	0.3
Cascade	bdl	1.5	0.06	1.2	0.5	4	0.22	bdl	0.07	0.3
Cascade (lab dup)	bdl	1.1	0.06	1.1	0.6	4	0.22	bdl	0.07	0.2
Meltwater	18	54.0	0.31	0.3	3.9	1	0.50	bdl	0.07	bdl

Table 4.4a (continued): Most common trace elements (Fe, Al, Mn, Ni, Cu, Zn, Pb, Cd, Co and Cr) from MERA I and II springs. All units in µg/L unless otherwise noted. Bolded numbers were determined to be elevated using the individual trace element method.

element	Fe	Al	Mn	Ni	Cu	Zn	Pb	Cd	Co	Cr
Name of Spring ***detection limit (MERA II)***	*3*	*0.2*	*0.05*	*0.2*	*0.2*	*0.32*	*0.05*	*0.1*	*0.05*	*0.2*
detection limit (MERA I)	*4*	*100*	*5*	*2*	*2*	*5*	*2*	*2*	*2*	*n/a*
CCME Drinking Water Guideline (mg/L)	*<=0.3**	*n/a*	*<=0.05**	*n/a*	*<=1.0**	*<=5.0**	*0.010*	*0.005*	*n/a* [c]	*0.05*
Waterfall	10	26.0	0.94	bdl	0.9	3	0.22	0.1	bdl	bdl
Descente	bdl	6.2	0.17	bdl	0.2	1	0.10	0.1	bdl	bdl
Softie	96	58.0	3.40	0.4	0.9	3	0.08	0.1	0.09	bdl
Cartman	bdl	4.5	0.40	bdl	bdl	1	bdl	bdl	bdl	bdl
Half Spring	10	14.0	2.90	0.7	0.6	2	0.05	0.1	0.05	bdl
Orange Creek	bdl	**8.3E+04**	**1.10E+04**	**1.9E+03**	**430**	**4.50E+03**	0.99	**14**	**620**	**8.0**
Caribou River	26	78.0	13.0	9.4	1.1	18	0.14	0.4	0.81	0.2
Karst	bdl	12.0	0.51	0.5	0.2	1	0.05	bdl	0.05	bdl
Persistent	16	9.9	200	1.5	0.4	11	0.20	**12**	0.43	0.3
Persistent (lab dup)	14	9.7	200	1.4	0.4	12	0.19	**12**	0.42	0.3
Stinky	bdl	11.0	220	1.9	0.7	4	0.26	1.4	0.87	0.2
Field Blank	bdl	0.5	0.76	0.7	**18.0**	6	**7.40**	bdl	bdl	bdl
Calgary Lab Blank	bdl	0.2	bdl	0.3	**31.0**	4	**4.50**	0.1	bdl	bdl
MERA I Samples (as reported by Hamilton, 1990)										
86-1	129	100	13	<2	3	8		<2	<2	
86-4	361	600	12	<2	4	<5		3	3	
86-6	<20	100	<10	<2	<2	<5		<2	<2	
86-7	<20	bdl	<10	<2	3	<5		<2	<2	
86-9	33	bdl	<10	<2	<2	<5		<2	<2	
86-10	108		12	16	3	<5		<2	5	
86-11	<20	100	<10	<2	5	10		<2	<2	
86-12	<20	4100	135	101	10	366		5	28	
87-012B	<5	400	3	35	3	220	<5	5	<2	
87-12	60	3500	80	130	15	305	<5	5	13	
87-012C	103	800	45	75	3	445	<5	**10**	5	
86-13	<20	bdl	<10	<2	3	<5		<2	<2	
86-15	**14416**	200	430	173	<2	**652**		3	23	
86-17	**20766**	400	**1503**	<2	11	<5		3	<2	
87-17	58	100	**1498**	<2	3	8	<5	<2	<2	
86-18	<20	bdl	<10	<2	4	<5		<2	<2	
87-18	<5	bdl	3	<2	<2	<2	<5	<2	<2	
87-018B		bdl								
86-19	199	200	37	<2	<2	<5		<2	<2	
86-20	65	bdl	<10	<2	5	<5		<2	<2	
86-21	243	700	165	<2	4	<5		<2	<2	
86-22	33	bdl	<10	<2	4	<5		<2	<2	
86-23	<20	bdl	<10	<2	13	<5		<2	6	
86-24	<20	bdl	<10	<2	<2	<5		<2	<2	
86-25	147	7000	169	<2	<2	**3936**		<2	<2	
86-26	<20	bdl	<10	<2	<2	<5		<2	<2	
86-27	26	bdl	<10	<2	4	<5		<2	<2	
87-27	15	bdl	<2	<2	<2	5	<5	<2	<2	
86-28	<20	bdl	<10	<2	<2	<5		<2	<2	
86-29	24	100	<10	<2	4	7		<2	13	
86-30	1710	200	15	<2	4	<5		<2	5	
86-31	<20	bdl	<10	<2	<2	<5		3	5	
86-32	460	200	23	<2	<2	<5		<2	3	
86-33	36	100	<10	11	13	<5		3	<2	
87-33	<5	bdl	<2	<2	<2	<2	<5	<2	<2	
87-34	<5	bdl	<2	<2	<2	<2	<5	<2	<2	
86-35	972	700	10	63	**16**	7		<2	**40**	
86-36	645		534	168	4	**640**		<2	**46**	
86-37	**19082**	200	425	8	3	306		<2	<2	
86-38	26	bdl	<10	<2	5	8		<2	<2	
86-40	65	300	<10	8	5	<5		3	<2	
86-41	440	500	<10	3	6	6		<2	<2	
86-42	5816	**8000**	225	273	**25**	**1488**		**39**	29	
86-43	138	200	30	<2	<2	5		<2	6	
86-44	91	100	<10	<2	3	<5		<2	<2	
86-45	57	bdl	<10	<2	4	6		<2	<2	
86-46	36	100	<10	<2	3	10		<2	<2	
86-47	72	200	<10	<2	3	13		<2	<2	
86-48	451	500	11	<2	5	<5		3	11	
86-49	**122307**	**28400**	856	233	<2	331		3	**50**	
86-50	91	300	16	23	<2	92		3	<2	
86-51	79	bdl	<10	<2	<2	8		<2	<2	
86-52	57	200	<10	<2	4	<5		<2	<2	
86-53	72	100	<10	4	3	8		<2	15	
87-53	5	bdl	<2	<2	<2	<2	<5	<2	<2	
86-54	3194	500	152	<2	4	19		<2	<2	
86-55	**15850**	300	587	125	6	412		<2	18	
86-56	33	300	34	16	4	<5		<2	8	
86-57	161	300	521	8	4	<5		<2	10	
86-58	28	200	158	<2	5	<5		<2	4	
87-58	<5	bdl	275	<2	<2	8	**8**	<2	<2	
86-59	480	100	157	<2	<2	<5		<2	3	
86-60	120	100	<10	8	6	<5		<2	3	
87-60	<5	bdl	<2	<2	3	<2	<5	<2	<2	
86-61	1817	bdl	123	3	6	<5		<2	<2	
86-62	9721	bdl	707	13	6	<5		<2	13	

Table 4.4a (continued 2): Most common trace elements (Fe, Al, Mn, Ni, Cu, Zn, Pb, Cd, Co and Cr) from MERA I and II springs. All units in µg/L unless otherwise noted. Bolded numbers were determined to be elevated using the individual trace element method.

element	Fe	Al	Mn	Ni	Cu	Zn	Pb	Cd	Co	Cr
Name of Spring *detection limit (MERA II)*	*3*	*0.2*	*0.05*	*0.2*	*0.2*	*0.32*	*0.05*	*0.1*	*0.05*	*0.2*
detection limit (MERA I)	*4*	*100*	*5*	*2*	*2*	*5*	*2*	*2*	*2*	*n/a*
CCME Drinking Water Guideline (mg/L)	*<=0.3**	*n/a*	*<=0.05**	*n/a*	*<=1.0**	*<=5.0**	*0.010*	*0.005*	*n/a[c]*	*0.05*
86-63	852	600	75	4	**19**	30		3	6	
86-64	129	500	57	<2	**16**	13		3	<2	
87-64	163	200	85	<2	8	13	**25**	<2	<2	
86-65	136	100	<10	6	4	10		<2	6	
86-66	67	100	<10	3	9	40		<2	<2	
86-67	337	300	92	65	**448**	**61877**		**135**	9	
86-68	81	100	<10	<2	8	14		3	<2	
86-69	**51793**	**30300**	**1180**	115	6	86		<2	**58**	
86-70	2870	6900	**1294**	94	11	67		<2	**45**	
86-71	**21517**	**21500**	**1047**	103	**18**	187		<2	**46**	
86-072A	136	**43000**	**2824**	**2318**	14	**4977**		**34**	**170**	
86-072B	1402	**57200**	**5396**	**2311**	**49**	**5351**		**30**	**405**	
87-072B	470	**29200**	**3568**	**1120**	15	**2350**	**5**	**13**	**268**	
87-072BH		**28800**								
87-073A	10	100	15	**768**	<2	**1613**	**13**	3	<2	
87-073B	13	**15000**	**3818**	**1513**	3	**2713**	<5	**15**	**95**	
87-073C	<5	200	18	**633**	<2	155	<5	3	<2	
86-74	465	500	653	16	11	58		4	10	
86-75	337	bdl	<10	<2	9	36		<2	<2	
86-76	158	bdl	10	8	6	<5		<2	<2	
86-77	96	bdl	11	<2	10	23		<2	<2	
86-78	**63347**	100	**1180**	34	5	15		<2	18	
86-79	1942	bdl	101	<2	8	6		<2	4	
86-80	9820	3500	217	11	9	12		<2	5	
86-81	705	bdl	222	5	4	9		<2	<2	
86-82	159	200	23	<2	9	44		<2	<2	
87-82	<5	bdl	3	<2	<2	18	<5	<2	<2	
87-82	H	bdl	0.1			<.1				
87-082B		bdl								
86-83	5179	300	437	<2	11	15		<2	4	
87-100	80	2900	108	38	8	98	<5	<2	3	
87-101	<5	bdl	<2	<2	<2	38	<5	<2	<2	
87-102	<5	bdl	<2	<2	<2	<2	<5	<2	<2	
87-103	6363	500	305	<2	<2	3	<5	<2	5	
87-104	<5	bdl	<2	<2	<2	<2	<5	<2	<2	
87-105	35	1100	48	13	3	50	<5	<2	3	
87-106	<5	bdl	<2	<2	<2	<2	<5	<2	3	
87-107	<5	bdl	<2	<2	3	565	<5	<2	<2	
87-108	65	800	83	<2	<2	10	<5	<2	<2	
87-109	5373	bdl	250	<2	<2	3	<5	<2	<2	
87-110	2013	bdl	190	<2	3	8	<5	<2	3	
87-111	10	bdl	<2	80	<2	353	<5	<2	<2	
87-112	**>20000**	200	**3098**	**303**	5	538	<5	<2	**60**	
87-112H		200								
87-113	18	bdl	<2	5	<2	28	<5	<2	<2	
87-114	<5	bdl	8	<2	<2	3	<5	<2	<2	
87-115	8	bdl	<2	<2	3	3	<5	<2	<2	
87-116	105	200	<2	<2	3	5	<5	<2	<2	
87-117	<5	bdl	<2	<2	<2	<2	<5	<2	<2	
87-118	<5	bdl	<2	<2	<2	10	<5	<2	<2	
87-119	<5	bdl	<2	<2	<2	10	**5**	<2	<2	
87-120	<5	bdl	<2	<2	<2	5	<5	<2	<2	
87-121	3763	**14700**	313	50	8	58	<5	<2	<2	
87-122	250	bdl	78	<2	3	3	**15**	<2	<2	
87-123	123	100	230	<2	8	8	**20**	<2	<2	
87-124	50	bdl	<2	<2	<2	<2	<5	<2	<2	
87-125	<5	bdl	<2	<2	<2	58	<5	<2	<2	
87-126	523	500	10	<2	3	10	<5	<2	<2	
87-127	33	bdl	10	<2	3	40	<5	<2	<2	
87-128	115	200	<2	<2	<2	5	<5	<2	3	
AVERAGE (PPM)	**3113**	**2541**	**318**	**109**	**10**	**608**	**2**	**5**	**21**	**1**
STANDARD DEVIATION	**12745**	**9736**	**1096**	**377**	**47**	**4737**	**4**	**15**	**77**	**3**
AVE+0.5*STDEV	**9485**	**7410**	**866**	**298**	**33**	**2976**	**4**	**13**	**59**	**3**
AVE+STDEV	**15858**	**12278**	**1414**	**486**	**57**	**5345**	**6**	**20**	**98**	**5**
MAX	**122307**	**83000**	**11000**	**2318**	**448**	**61877**	**25**	**135**	**620**	**27**
MIN	**5**	**0**	**0**	**1**	**0**	**1**	**0**	**0**	**0**	**0**
Criteria Cut-Off Used to Determine Anomalousness:	> 10 000	> 7500	> 880	> 300	> 15	> 622	> 2	> 5	> 31	> 1
Definition of Criteria (to obtain approx. top 15 springs):	ave+0.5stdev	ave+0.5stdev	ave+0.5stdev	ave+0.5stdev	1.5*ave	ave	ave	ave	1.5*ave	ave

Footnotes:

bdl = below detection limit

nd = no data available

CCME Drinking Water Guidelines Available at:

Federal-Provincial-Territorial Committee on Drinking Water. "Guidelines for Candadian Drinking Water Quality Summary Table". Health Canada, Government of Canada, March 2006.

***n/a* = guideline not available**

***Aesthetic Guideline Only**

[c]Maximum 100 Platinum-Cobalt Units for Recreational Aesthetics of Colour

CCME Recreation Guidelines Are Available at:

Federal-Provincial Working Group on Recreational Water Quality of the Federal-Provincial Advisory Committee on Environmental and Occutpational Health. "Guidelines for Canadian Recreational Water Quality". Health and Welfare Canada, Government of Canada, 1992.

Table 4.4b: Moderately common trace elements (Cs, Mo, As, Li, Rb, Sr, Ba, U, V, B and Sb) from MERA I and II springs. All units in μg/L unless otherwise noted. Bolded numbers were determined to be elevated using the individual trace element method.

element	Cs	Mo	As	Li	Rb	Sr	Ba	U	V	B	Sb
Name of Spring — detection limit (MERA II)	*0.05*	*0.1*	*0.2*	*1*	*0.05*	*1*	*0.6*	*0.05*	*0.05*	*16*	*0.05*
detection limit (MERA I)	*n/a*	*0.1*	*0.3*	*n/a*	*n/a*	*100*	*100*	*0.01/0.1*	*n/a*	*n/a*	*0.3*
CCME Drinking Water Guideline (mg/L)	*n/a*	*n/a*	*0.025*	*n/a*	*n/a*	*n/a*	*1.0*	*0.02*	*n/a*	*5*	*0.006*
MERA II Samples											
Tulita	**7.50**	bdl	3.0	**910**	19.0	1.50E+03	**780**	0.13	0.27	**920**	bdl
Sculpin	bdl	0.6	0.9	15	1.20	**1.40E+04**	10	0.38	0.06	24	bdl
Deca	1.40	0.2	0.4	64	9.20	1.90E+03	22	0.40	1.00	130	bdl
Ekwi	**20.0**	0.2	0.9	**630**	**110**	3.10E+03	30	0.05	bdl	**800**	0.05
Mineral Lake	1.20	2.1	1.8	24	9.10	1.30E+03	47	2.80	0.25	37	bdl
Brimstone[1]	1.00	0.4	0.9	160	**33.0**	2.40E+03	110	0.63	0.19	25	0.05
Cordes Vertes	0.67	0.2	bdl	25	2.70	470	98	0.61	0.18	22	0.06
Tabletop	0.26	1.6	0.8	13	2.00	3.70E+03	44	0.67	0.51	18	bdl
South Redstone	0.42	1.6	1.8	13	1.90	2.50E+03	27	0.42	0.36	bdl	bdl
Redstone Junction #1	0.35	1.0	0.5	18	3.00	2.40E+03	31	0.88	0.62	28	bdl
Cotton	0.14	bdl	bdl	8	0.93	7	13	0.05	bdl	bdl	0.10
Red Mini	0.16	bdl	bdl	3	2.50	25	56	0.12	bdl	bdl	0.18
Muddy	0.09	0.2	bdl	17	4.50	79	19	0.54	0.05	bdl	bdl
Grasby	bdl	0.6	bdl	3	1.70	260	56	0.62	0.06	bdl	bdl
Red Steel	bdl	0.4	bdl	bdl	0.49	85	170	0.05	bdl	bdl	0.06
Bougere	0.39	bdl	bdl	150	0.66	8	37	0.48	bdl	bdl	bdl
Champagne	0.46	0.2	0.8	150	3.90	350	6.0	1.40	0.05	bdl	bdl
Champagne (dup)	0.43	0.1	0.8	130	3.80	310	6.0	1.40	bdl	bdl	bdl
Champagne Creek	0.39	0.1	1.0	16	3.90	270	5.2	1.50	0.05	bdl	bdl
Champagne Creek (dup)	0.37	0.1	0.8	17	3.60	270	5.0	1.60	0.05	bdl	bdl
North Cantung (Zenchuck Creek)	0.15	0.6	0.5	5	0.78	78	35	1.50	0.14	bdl	bdl
Moore's	1.60	1.4	2.6	25	9.90	470	120	1.50	0.25	48	0.18
Nahanni North (Lened Creek)	**11.0**	**16.0**	bdl	**500**	16.0	22	5.5	bdl	0.09	**600**	bdl
Nahanni Headwaters	**68.0**	**30.0**	**87.0**	**480**	18.0	71	4.6	bdl	0.15	**1.60E+03**	**1.30**
Broken Skull	**4.50**	0.1	1.2	92	**57.0**	3.30E+03	43	0.10	0.22	**380**	bdl
Grizzle Bear	**5.80**	0.2	5.1	110	**34.0**	1.40E+03	50	0.05	0.24	220	0.05
Glacier Lake	0.99	3.8	1.0	69	4.00	190	9.1	2.30	0.13	bdl	0.15
Rabbitkettle	0.56	2.9	0.3	38	9.80	620	180	6.30	bdl	34	0.78
Kraus (Clausen)	**65.0**	0.1	14.0	**1.30E+03**	**200**	**1.30E+04**	44	1.60	**8.30**	**1.40E+03**	bdl
Meilleur River	**4.40**	2.6	5.2	250	**28.0**	1.60E+03	44	2.00	0.32	230	bdl
Wildmint	**17.0**	0.4	0.7	**2.50E+03**	13.0	180	0.7	1.50	0.35	**3.40E+03**	bdl
Stinky Drift	0.47	1.5	0.9	16	8.10	1.00E+03	78	3.70	0.28	24	0.10
Hole in the wall	2.30	**19.0**	**19.0**	210	4.20	8	2.1	6.70	**7.00**	160	0.39
Flat Fruit	**4.50**	bdl	0.2	150	18.0	1.70E+03	160	1.30	0.05	110	bdl
West Cantung	**30.0**	11.0	1.7	**570**	17.0	38	160	1.20	**2.10**	**760**	0.24
Prairie Creek Mine Shaft	bdl	1.5	0.8	12	0.91	450	36	6.20	bdl	bdl	**56**
Harrison Creek	bdl	2.9	bdl	11	0.41	280	65	12.0	0.08	bdl	0.39
Prairie Creek	bdl	3.0	0.2	12	0.25	260	66	5.40	0.26	bdl	**0.95**
Broken Skull's Upper Pool	**4.00**	0.2	0.6	87	**55.0**	3.50E+03	53	0.15	0.26	**390**	0.06
Broken Skull's Lower Pool	**4.30**	0.1	1.1	85	**52.0**	3.50E+03	60	0.15	0.13	**390**	bdl
Cowboy	bdl	2.1	bdl	11	0.16	190	93	2.40	0.59	bdl	bdl
Sibbeston	bdl	3.0	2.2	10	0.83	680	81	3.40	0.96	bdl	1.00
Corridor Creek	bdl	0.9	bdl	11	0.08	290	20	1.10	0.09	bdl	bdl
Veil	bdl	4.6	0.3	19	0.36	320	83	4.90	0.11	bdl	0.07
Big Veil	bdl	4.7	0.3	18	0.37	320	83	4.90	0.12	bdl	0.11
Galena	bdl	1.9	0.3	13	0.90	320	54	**16.0**	0.09	bdl	0.74
Galena (lab dup)	bdl	1.9	0.2	14	0.92	330	54	**16.0**	0.10	bdl	0.73
Sombre	bdl	0.2	bdl	7	bdl	2.00E+03	97	0.98	bdl	bdl	bdl
Sombre (field dup)	bdl	0.2	bdl	5	bdl	2.00E+03	97	0.93	bdl	bdl	bdl
Wrigley	bdl	**26.0**	bdl	7	0.20	2.20E+03	120	**16.0**	**7.10**	bdl	0.39
Mel's Pool	bdl	1.6	0.5	2	0.08	52	21	0.18	0.43	bdl	0.16
Cowgirl	bdl	8.5	bdl	6	0.10	170	32	6.60	**3.60**	bdl	0.16
Brigade	bdl	3.5	bdl	15	0.40	1.60E+03	45	2.40	bdl	30	bdl
Ram Plateau	bdl	0.5	0.3	3	0.28	280	21	0.13	0.13	bdl	0.21
Cimitar	bdl	5.9	0.5	34	2.10	**8.50E+03**	13	**16.0**	0.06	29	bdl
Cathedral	bdl	3.7	bdl	6	0.23	**4.60E+03**	110	3.60	0.23	32	0.09
Mossy	bdl	0.8	bdl	3	0.15	1.90E+03	54	2.60	0.42	bdl	bdl
Mossy (lab dup)	bdl	0.8	bdl	9	0.15	2.00E+03	50	2.50	0.43	bdl	bdl
Crack	bdl	1.8	0.2	2	0.07	34	23	1.90	**2.70**	bdl	0.10
Quickie	bdl	11.0	0.2	6	0.15	1.10E+03	120	7.40	0.66	bdl	0.22
Clearwater Creek	bdl	2.3	bdl	4	0.36	82	11	2.50	0.07	bdl	0.12
Dookie	bdl	0.3	bdl	7	0.10	25	12	0.15	bdl	bdl	bdl
Dookie (field dup)	bdl	0.2	bdl	11	0.09	25	12	0.16	bdl	bdl	bdl
Dookie (field trip)	bdl	0.2	bdl	11	0.08	25	11	0.16	bdl	bdl	bdl
Boulder	bdl	0.1	bdl	7	0.05	11	3.3	0.14	bdl	bdl	0.05
Overflow	bdl	bdl	bdl	7	0.42	4	5.6	0.16	0.09	bdl	bdl
Smurf	bdl	4.2	0.7	9	0.62	160	210	2.40	**2.80**	bdl	0.82
Clark Lake	bdl	3.5	1.1	9	1.60	130	140	1.70	0.05	bdl	bdl
Clark Lake (lab dup)	bdl	3.6	1.1	14	1.60	130	150	1.60	0.05	bdl	bdl
Jacson	bdl	0.2	bdl	7	0.89	6	3.7	0.24	0.07	bdl	bdl
Darkness	bdl	0.4	bdl	7	0.96	11	3.5	1.60	0.10	bdl	bdl
Selena	bdl	7.4	4.1	10	0.61	370	78	6.90	bdl	24	0.29
Caribou	bdl	3.4	0.3	9	0.13	160	130	1.70	0.33	bdl	0.40
Chance	bdl	2.2	0.3	9	0.60	180	150	1.30	0.44	bdl	0.17
Interpluton	bdl	0.1	bdl	7	0.65	10	9.3	1.40	0.18	bdl	0.08
Tiny	bdl	0.5	0.5	8	0.51	84	24	0.85	0.29	bdl	0.11
Blue Bells	0.69	0.3	3.2	23	6.50	150	21	0.78	0.06	bdl	0.08
Blue Bells (field dup)	0.70	0.3	3.2	23	6.40	150	20	0.77	0.07	22	0.09
Cascade	bdl	0.9	0.4	8	0.41	130	92	0.85	0.12	bdl	0.22
Cascade (lab dup)	bdl	0.9	0.3	12	0.40	130	91	0.88	0.11	bdl	0.22
Meltwater	bdl	bdl	bdl	7	1.70	37	6.3	0.11	0.22	bdl	0.17
Waterfall	bdl	0.9	0.4	7	0.72	9	3.9	0.65	0.11	bdl	0.12
Descente	bdl	0.1	0.4	8	0.24	13	2.2	bdl	0.09	bdl	0.07
Softie	bdl	bdl	0.3	7	0.06	10	5.5	0.06	0.14	bdl	0.09

Table 4.4b (continued): Moderately common trace elements (Cs, Mo, As, Li, Rb, Sr, Ba, U, V, B and Sb) from MERA I and II springs. All units in µg/L unless otherwise noted. Bolded numbers were determined to be elevated using the individual trace element method.

element	Cs	Mo	As	Li	Rb	Sr	Ba	U	V	B	Sb
Name of Spring *detection limit (MERA II)*	*0.05*	*0.1*	*0.2*	*1*	*0.05*	*1*	*0.6*	*0.05*	*0.05*	*16*	*0.05*
detection limit (MERA I)	*n/a*	*0.1*	*0.3*	*n/a*	*n/a*	*100*	*100*	*0.01/0.1*	*n/a*	*n/a*	*0.3*
CCME Drinking Water Guideline (mg/L)	*n/a*	*n/a*	*0.025*	*n/a*	*n/a*	*n/a*	*1.0*	*0.02*	*n/a*	*5*	*0.006*
Cartman	bdl	0.1	0.2	7	bdl	8	2.1	bdl	0.12	23	0.07
Half Spring	bdl	2.9	0.3	13	0.24	110	9.6	3.80	0.15	bdl	0.10
Orange Creek	bdl	0.4	bdl	**280**	2.10	990	19	**26.0**	0.14	33	0.10
Caribou River	bdl	3.0	0.3	9	0.58	170	83	1.80	0.28	bdl	0.35
Karst	bdl	0.2	0.3	7	0.09	29	15	0.24	0.06	23	bdl
Persistent	**4.10**	0.7	**50.0**	87	**32.0**	650	**240**	0.87	0.07	90	0.10
Persistent (lab dup)	**4.10**	0.7	**51.0**	110	**32.0**	670	**260**	0.83	0.08	110	0.09
Stinky	**4.80**	0.3	**120**	100	**37.0**	770	**380**	1.00	0.14	110	0.07
Field Blank	bdl	bdl	bdl	7	bdl	bdl	1.2	bdl	bdl	bdl	bdl
Calgary Lab Blank	bdl	bdl	bdl	6	bdl	bdl	0.1	bdl	bdl	bdl	bdl
MERA I Samples (as reported by Hamilton, 1990)											
86-1		1.8	0.3			700	200	6.4			
86-4		0.2	1.4			bdl	bdl	0.4			
86-6		0.6	0.5			400	bdl	1.92			
86-7		0.7	<.2			100	bdl	0.84			
86-9		1.2	<.2			200	bdl	4.4			
86-10		7.3						14.2			
86-11		3.8	0.5			bdl	bdl	3.6			
86-12		0.6	0.8			bdl	bdl	4.4			
87-012B		3	<.3			bdl	bdl	1.7			0.4
87-12		1	<.3			bdl	bdl	1.6			<.3
87-012C		0.1	<.3			bdl	bdl	2.8			<.3
86-13		1	**32.9**			100	bdl	0.92			
86-15		2.1	1.4			200	bdl	2.38			
86-17		<.1	0.4			2900	200	0.6			
87-17		<.1	<.3			2300	100	0.5			<.3
86-18		8	1.8			bdl	200	0.92			
87-18		9.1	1.9			bdl	100	1.4			<.3
87-018B		9.9	1.8			bdl	100				<.3
86-19		8.1	5.2			100	bdl	0.96			
86-20		1.1	<.2			bdl	bdl	0.24			
86-21		0.4	**99.3**			**5600**	bdl	7.8			
86-22		2.5	0.7			200	200	1.2			
86-23		4	2.4			200	100	6.2			
86-24		8	0.3			200	100	5.7			
86-25		<.1	0.4			bdl	bdl	4			
86-26		4.3	1			200	200	2.8			
86-27		1.2	0.8			1200	100	2.4			
87-27		1.7	0.8			1000	bdl	3.8			0.4
86-28		2	0.2			200	100	0.96			
86-29		0.6	0.5			1400	100	3.6			
86-30		1.6	1.2			1500	bdl	4			
86-31		0.9	0.3			1700	100	3.2			
86-32		1.4	2.4			500	100	1.64			
86-33		**19**	0.2			bdl	bdl	0.66			
87-33		**18.8**	0.3			bdl	bdl	1.3			<.3
87-34		9.5	2.1			bdl	bdl	**28**			<.3
86-35		<.1	0.5			300	bdl	0.44			
86-36		<.1						0.4			
86-37		0.4	2.2			500	bdl	4			
86-38		**30**	**163.5**			bdl	bdl	0.4			
86-40		<.1	1.5			4000	bdl	3.8			
86-41		0.1	0.8			4000	bdl	5.2			
86-42		<.1	0.6			200	100	3.2			
86-43		0.1	5.2			1800	bdl	5			
86-44		0.5	0.6			100	bdl	2.4			
86-45		<.1	0.3			bdl	bdl	0.24			
86-46		3.1	1.2			200	200	3.2			
86-47		3	0.6			300	bdl	3.4			
86-48		1.4	<.2			bdl	bdl	3.6			
86-49		<.1	<.2			700	bdl	4.4			
86-50		2.4	1			200	bdl	2.6			
86-51		0.6	0.6			bdl	bdl	2.8			
86-52		10	**23.7**			bdl	bdl	7.4			
86-53		**21**	**25.5**			bdl	bdl	7.2			
87-53		**20.3**	**20.9**			bdl	bdl	6.6			0.4
86-54		0.5	4			bdl	bdl	2			
86-55		1.7	0.9			800	100	6.6			
86-56		0.7	0.5			3300	bdl	4.68			
86-57		<.1	0.2			2500	bdl	3			
86-58		<.1	<.2			2000	200	1.44			
87-58		0.2	0.38			200		<.3			<.3
86-59		<.1	<.2			500	100	0.66			
86-60		**19**	0.5			bdl	bdl	0.27			
87-60		**17.8**				bdl	bdl	1.2			
86-61		0.6	0.5			100	bdl	0.74			
86-62		<.1	<.2			bdl	bdl	0.1			
86-63		0.2	7.2			**15000**	bdl	**15.6**			
86-64		<.1	1.4			**15300**	bdl	5.4			
87-64		0.7	0.3			**14100**	bdl	**15.2**			<.3
86-65		0.6	0.12			bdl		1.2			0.3
86-66		1.7	0.1			bdl		2			0.6
86-67		0.6	0.49			bdl		3.8			**49.6**
86-68		<.1	0.11			100		2			0.2
86-69		<.1	0.28			bdl		3			<.2

Table 4.4b (continued 2): Moderately common trace elements (Cs, Mo, As, Li, Rb, Sr, Ba, U, V, B and Sb) from MERA I and II springs. All units in µg/L unless otherwise noted. Bolded numbers were determined to be elevated using the individual trace element method.

element	Cs	Mo	As	Li	Rb	Sr	Ba	U	V	B	Sb
Name of Spring *detection limit (MERA II)*	*0.05*	*0.1*	*0.2*	*1*	*0.05*	*1*	*0.6*	*0.05*	*0.05*	*16*	*0.05*
detection limit (MERA I)	*n/a*	*0.1*	*0.3*	*n/a*	*n/a*	*100*	*100*	*0.01/0.1*	*n/a*	*n/a*	*0.3*
CCME Drinking Water Guideline (mg/L)	*n/a*	*n/a*	*0.025*	*n/a*	*n/a*	*n/a*	*1.0*	*0.02*	*n/a*	*5*	*0.006*
86-70		<.1	0.2			500	bdl	3.12			
86-71		<.1	1.3			1000	bdl	2.4			
86-072A		<.1	0.4			**5300**	bdl	5.4			
86-072B		0.8	1.9			**4500**	bdl	**26**			
87-072B		0.3				3200	bdl	13.2			
87-072BH						3100	bdl				
87-073A		0.4	1.32			bdl		<.3			<.3
87-073B		0.4	2.18			bdl		<.3			<.3
87-073C		0.3	1.36			bdl		<.3			<.3
86-74		0.8	0.8			3500	100	4.4			
86-75		0.3	0.3			bdl	bdl	2.4			
86-76		2.5	0.4			100	100	2.4			
86-77		2.7	3.4			200	**600**	4.6			
86-78		<.1	0.8			200	bdl	0.66			
86-79		<.1	1.5			bdl	bdl	0.92			
86-80		<.1	0.4			bdl	bdl	0.44			
86-81		3.9	4.5			400	bdl	2.4			
86-82		4.5	10.9			1400	bdl	5			
87-82		4.6				1600	bdl	14			
87-82						1500	bdl				
87-082B		4.5				1500	bdl				
86-83		3	12.7			1700	bdl	5.4			
87-100		<.1	<.3			bdl	bdl	3.5			<.3
87-101		5.5	0.9			bdl	bdl	6.9			<.3
87-102		0.6	<.3			200	bdl	2.5			<.3
87-103		0.1	12.6			700	bdl	0.5			0.3
87-104		0.5	14.9			bdl	bdl	0.3			0.4
87-105		<.1	<.3			bdl	bdl	0.7			<.3
87-106		0.3	0.3			bdl	bdl	0.7			<.3
87-107		1.8	0.7			300	100	5.8			0.7
87-108		<.1	<.3			bdl	bdl	<.1			<.3
87-109		<.1	0.3			bdl	bdl	0.8			<.3
87-110		6	1.2			1300	bdl	**20**			<.3
87-111		11	<.3			800	bdl	**27.9**			<.3
87-112		0.2	7.7			3400	bdl				
87-112H						3400	bdl				
87-113		6.7	0.5			200	100	11.2			<.3
87-114		5.5	<.3			200	bdl	7.9			<.3
87-115		10.2	0.3			700	bdl	4.7			0.4
87-116		0.4	0.4			1100	bdl	14.4			<.3
87-117		1.1	<.3			bdl	bdl	1.4			<.3
87-118		1	<.3			bdl	bdl	1.4			<.3
87-119		1.1	0.4			bdl	200	3.1			0.4
87-120		1.4	<.3			200	100	6			<.3
87-121		<.1	<.3			bdl	bdl	2.5			<.3
87-122		0.3	2.4			2900	bdl	**16.8**			0.4
87-123		0.3	<.3			**12300**	bdl	6.6			<.3
87-124		4.6	0.5			bdl	**1000**	0.7			0.4
87-125		**15.3**	<.3			300	bdl	12.2			0.6
87-126		2.8	0.3			100	200	1.7			0.4
87-127		1.2	<.3			600	**300**	4.2			<.3
87-128		2.3	0.8			200	**300**	7.6			0.4
AVERAGE	**7**	**3**	**6**	**105**	**10**	**1427**	**94**	**4**	**1**	**316**	**1.66**
STANDARD DEVIATION	**15**	**5**	**20**	**315**	**26**	**2731**	**133**	**5**	**2**	**634**	**8**
AVE+0.5*STDEV	**14**	**6**	**16**	**262**	**23**	**2792**	**160**	**6**	**1**	**633**	**5.9**
AVE+STDEV	**22**	**9**	**26**	**419**	**36**	**4157**	**226**	**9**	**2**	**950**	**10.1**
MAX	**68**	**30**	**164**	**2500**	**200**	**15300**	**1000**	**28**	**8**	**3400**	**56**
MIN	**0**	**0**	**0**	**3**	**0**	**7**	**5**	**0**	**0**	**18**	**0**
Criteria Cut-Off Used to Determine Anomalousness:	> 3.5	> 12	> 16	> 266	> 23	> 4200	> 231	> 15	> 1	> 350	> 0.9
Definition of Criteria (to obtain approx. top 15 springs):	0.5*ave	ave+1.5stdev	ave+0.5stdev	ave+0.5stdev	ave+0.5stdev	ave+stdev	ave+stdev	ave+1.5stdev	ave	ave	ave*0.5

Footnotes:

bdl = below detection limit

nd = no data available

CCME Drinking Water Guidelines Available at:

Federal-Provincial-Territorial Committee on Drinking Water. "Guidelines for Candadian Drinking Water Quality Summary Table". Health Canada, Government of Canada, March 2006.

***n/a* = guideline not available**

***Aesthetic Guideline Only**

[C]Maximum 100 Platinum-Cobalt Units for Recreational Aesthetics of Colour

CCME Recreation Guidelines Are Available at:

Federal-Provincial Working Group on Recreational Water Quality of the Federal-Provincial Advisory Committee on Environmental and Occutpational Health. "Guidelines for Canadian Recreational Water Quality". Health and Welfare Canada, Government of Canada, 1992.

Table 4.4c: Least common trace elements (Tl, Ga, Se, Br, Ag, Be, Sc, Ti, Bi, In and NO_2) from MERA I and II springs. All units in μg/L unless otherwise noted. Bolded numbers were determined to be elevated using the individual trace element method.

element	Tl	Ga	Se	Br	Ag	Be	Sc	Ti	Bi	In	NO_2
Name of Spring *detection limit (MERA II)*	*0.05*	*0.05*	*2*	*50*	*0.05*	*1*	*1*	*1*	*0.05*	*0.05*	*50*
detection limit (MERA I)	*n/a*	*n/a*	*n/a*	*n/a*	*2*	*n/a*	*n/a*	*n/a*	*n/a*	*n/a*	*n/a*
CCME Drinking Water Guideline (mg/L)	*n/a*	*n/a*	*0.01*	*n/a*	*n/a*	*n/a*	*n/a*	*n/a*	*n/a*	*n/a*	*3.2*
MERA II Samples											
Tulita	bdl	bdl	bdl	**317**	bdl	bdl	**2**	bdl	bdl	bdl	<500
Sculpin	bdl	bdl	bdl	<500	bdl	bdl	bdl	bdl	bdl	bdl	<500
Deca	bdl	bdl	bdl	<500	bdl	bdl	bdl	bdl	bdl	bdl	bdl
Ekwi	**0.10**	bdl	bdl	<2500	bdl	bdl	bdl	bdl	bdl	bdl	bdl
Mineral Lake	bdl	bdl	bdl	bdl	bdl	bdl	bdl	bdl	bdl	bdl	bdl
Brimstone[1]	bdl	bdl	**2**	bdl	bdl	**2**	bdl	bdl	bdl	bdl	bdl
Cordes Vertes	bdl	bdl	bdl	bdl	bdl	bdl	bdl	bdl	bdl	bdl	bdl
Tabletop	0.05	bdl	bdl	bdl	bdl	bdl	bdl	bdl	bdl	bdl	bdl
South Redstone	0.06	bdl	bdl	bdl	bdl	bdl	bdl	bdl	bdl	bdl	bdl
Redstone Junction #1	bdl	bdl	bdl	bdl	bdl	bdl	bdl	bdl	bdl	bdl	bdl
Cotton	0.05	bdl	bdl	bdl	bdl	bdl	bdl	bdl	bdl	bdl	bdl
Red Mini	0.06	bdl	bdl	bdl	bdl	bdl	bdl	bdl	bdl	bdl	bdl
Muddy	bdl	bdl	bdl	bdl	bdl	bdl	bdl	bdl	bdl	bdl	bdl
Grasby	bdl	bdl	**2**	bdl	bdl	bdl	bdl	bdl	bdl	bdl	bdl
Red Steel	bdl	bdl	**5**	bdl	bdl	bdl	bdl	bdl	bdl	bdl	bdl
Bougere	bdl	**0.08**	bdl	bdl	**14.00**	bdl	bdl	bdl	bdl	bdl	bdl
Champagne	bdl	bdl	bdl	bdl	bdl	bdl	bdl	bdl	bdl	bdl	bdl
Champagne (dup)	bdl	bdl	bdl	bdl	bdl	bdl	bdl	bdl	bdl	bdl	bdl
Champagne Creek	bdl	bdl	**2**	bdl	bdl	bdl	bdl	bdl	bdl	bdl	bdl
Champagne Creek (dup)	bdl	bdl	bdl	bdl	bdl	bdl	bdl	bdl	bdl	bdl	bdl
North Cantung (Zenchuck Creek)	bdl	bdl	bdl	bdl	bdl	bdl	bdl	bdl	bdl	bdl	nd
Moore's	bdl	bdl	bdl	bdl	bdl	bdl	bdl	bdl	bdl	bdl	nd
Nahanni North (Lened Creek)	bdl	**7.50**	bdl	bdl	bdl	bdl	bdl	bdl	bdl	bdl	nd
Nahanni Headwaters	bdl	**2.60**	bdl	bdl	bdl	bdl	bdl	bdl	bdl	bdl	nd
Broken Skull	bdl	bdl	bdl	bdl	bdl	bdl	bdl	bdl	bdl	bdl	nd
Grizzle Bear	bdl	bdl	bdl	**157**	bdl	bdl	bdl	bdl	bdl	bdl	nd
Glacier Lake	**0.58**	bdl	bdl	bdl	bdl	bdl	bdl	bdl	bdl	bdl	nd
Rabbitkettle	bdl	bdl	bdl	bdl	bdl	bdl	bdl	bdl	bdl	bdl	nd
Kraus (Clausen)	bdl	bdl	bdl	<500	bdl	bdl	bdl	bdl	bdl	bdl	nd
Meilleur River	bdl	bdl	bdl	**215**	bdl	bdl	bdl	bdl	bdl	bdl	nd
Wildmint	bdl	**1.50**	bdl	bdl	bdl	bdl	bdl	bdl	bdl	bdl	nd
Stinky Drift	**0.14**	bdl	bdl	bdl	bdl	bdl	bdl	bdl	bdl	bdl	nd
Hole in the wall	bdl	**4.90**	bdl	bdl	bdl	bdl	bdl	bdl	bdl	bdl	nd
Flat Fruit	bdl	bdl	bdl	bdl	bdl	bdl	bdl	bdl	bdl	bdl	nd
West Cantung	bdl	**1.70**	bdl	bdl	bdl	bdl	bdl	bdl	bdl	bdl	nd
Prairie Creek Mine Shaft	**0.37**	bdl	**7**	bdl	bdl	bdl	bdl	bdl	bdl	bdl	bdl
Harrison Creek	bdl	bdl	bdl	bdl	bdl	bdl	bdl	bdl	bdl	bdl	bdl
Prairie Creek	bdl	bdl	bdl	bdl	bdl	bdl	bdl	bdl	bdl	bdl	**52**
Broken Skull's Upper Pool	bdl	bdl	bdl	**149**	bdl	bdl	bdl	bdl	bdl	bdl	bdl
Broken Skull's Lower Pool	bdl	bdl	bdl	**145**	bdl	bdl	bdl	bdl	bdl	bdl	bdl
Cowboy	bdl	bdl	bdl	bdl	bdl	bdl	bdl	bdl	bdl	bdl	bdl
Sibbeston	**0.07**	**0.07**	bdl	bdl	bdl	bdl	bdl	bdl	bdl	bdl	bdl
Corridor Creek	bdl	bdl	bdl	bdl	bdl	bdl	bdl	bdl	bdl	bdl	bdl
Veil	bdl	bdl	**3**	bdl	bdl	bdl	bdl	bdl	bdl	bdl	bdl
Big Veil	bdl	bdl	**3**	bdl	bdl	bdl	bdl	bdl	bdl	bdl	bdl
Galena	**0.10**	bdl	**3**	bdl	bdl	bdl	bdl	bdl	bdl	bdl	bdl
Galena (lab dup)	**0.08**	bdl	bdl	bdl	bdl	bdl	bdl	bdl	bdl	bdl	bdl
Sombre	bdl	bdl	bdl	bdl	bdl	bdl	bdl	bdl	bdl	bdl	bdl
Sombre (field dup)	bdl	bdl	bdl	bdl	bdl	bdl	bdl	bdl	bdl	bdl	bdl
Wrigley	**0.13**	bdl	**2**	bdl	bdl	bdl	bdl	bdl	bdl	bdl	bdl
Mel's Pool	bdl	bdl	bdl	bdl	bdl	bdl	bdl	bdl	bdl	bdl	bdl
Cowgirl	**0.12**	bdl	bdl	bdl	bdl	bdl	bdl	bdl	bdl	bdl	bdl
Brigade	bdl	bdl	bdl	bdl	bdl	bdl	bdl	bdl	bdl	bdl	bdl
Ram Plateau	bdl	bdl	bdl	bdl	bdl	bdl	bdl	bdl	bdl	bdl	bdl
Cimitar	**0.32**	bdl	bdl	bdl	bdl	bdl	bdl	bdl	bdl	bdl	bdl
Cathedral	bdl	bdl	bdl	bdl	bdl	bdl	bdl	bdl	bdl	bdl	bdl
Mossy	bdl	bdl	bdl	bdl	bdl	bdl	bdl	bdl	bdl	bdl	bdl
Mossy (lab dup)	bdl	bdl	bdl	bdl	bdl	bdl	bdl	bdl	bdl	bdl	bdl
Crack	bdl	bdl	bdl	bdl	bdl	bdl	bdl	bdl	bdl	bdl	bdl
Quickie	bdl	bdl	**3**	bdl	bdl	bdl	bdl	bdl	bdl	bdl	bdl
Clearwater Creek	bdl	bdl	bdl	bdl	bdl	bdl	bdl	bdl	bdl	bdl	bdl
Dookie	bdl	bdl	bdl	bdl	bdl	bdl	bdl	bdl	bdl	bdl	bdl
Dookie (field dup)	bdl	bdl	bdl	bdl	bdl	bdl	bdl	bdl	bdl	bdl	bdl
Dookie (field trip)	bdl	bdl	bdl	bdl	bdl	bdl	bdl	bdl	bdl	bdl	bdl
Boulder	bdl	bdl	bdl	bdl	bdl	bdl	bdl	bdl	bdl	bdl	bdl
Overflow	bdl	bdl	bdl	bdl	bdl	bdl	bdl	bdl	bdl	bdl	bdl
Smurf	bdl	bdl	**3**	bdl	bdl	bdl	bdl	bdl	bdl	bdl	bdl
Clark Lake	bdl	bdl	bdl	bdl	bdl	bdl	bdl	bdl	bdl	bdl	bdl
Clark Lake (lab dup)	bdl	bdl	bdl	bdl	bdl	bdl	bdl	bdl	bdl	bdl	bdl
Jacson	bdl	bdl	bdl	bdl	bdl	bdl	bdl	bdl	bdl	bdl	bdl
Darkness	bdl	bdl	bdl	bdl	bdl	bdl	bdl	bdl	bdl	bdl	bdl
Selena	bdl	bdl	bdl	bdl	bdl	bdl	bdl	bdl	bdl	bdl	bdl
Caribou	bdl	bdl	bdl	bdl	bdl	bdl	bdl	bdl	bdl	bdl	bdl
Chance	bdl	bdl	bdl	bdl	bdl	bdl	bdl	bdl	bdl	bdl	bdl
Interpluton	bdl	**0.05**	bdl	bdl	bdl	bdl	bdl	bdl	bdl	bdl	bdl
Tiny	bdl	bdl	bdl	bdl	bdl	bdl	bdl	bdl	bdl	bdl	bdl
Blue Bells	bdl	bdl	bdl	bdl	bdl	bdl	bdl	bdl	bdl	bdl	bdl
Blue Bells (field dup)	bdl	bdl	bdl	bdl	bdl	bdl	bdl	bdl	bdl	bdl	bdl
Cascade	bdl	bdl	bdl	bdl	bdl	bdl	bdl	bdl	bdl	bdl	bdl
Cascade (lab dup)	bdl	bdl	bdl	bdl	bdl	bdl	bdl	bdl	bdl	bdl	bdl
Meltwater	bdl	bdl	bdl	bdl	bdl	bdl	bdl	bdl	bdl	bdl	bdl

Table 4.4c (continued): Least common trace elements (Tl, Ga, Se, Br, Ag, Be, Sc, Ti, Bi, In and NO_2) from MERA I and II springs. All units in µg/L unless otherwise noted. Bolded numbers were determined to be elevated using the individual trace element method.

element	Tl	Ga	Se	Br	Ag	Be	Sc	Ti	Bi	In	NO_2
Name of Spring *detection limit (MERA II)*	*0.05*	*0.05*	*2*	*50*	*0.05*	*1*	*1*	*1*	*0.05*	*0.05*	*50*
detection limit (MERA I)	*n/a*	*n/a*	*n/a*	*n/a*	*2*	*n/a*	*n/a*	*n/a*	*n/a*	*n/a*	*n/a*
CCME Drinking Water Guideline (mg/L)	*n/a*	*n/a*	*0.01*	*n/a*	*n/a*	*n/a*	*n/a*	*n/a*	*n/a*	*n/a*	*3.2*
Waterfall	bdl	bdl	bdl	bdl	bdl	bdl	bdl	bdl	bdl	bdl	bdl
Descente	bdl	bdl	bdl	bdl	bdl	bdl	bdl	bdl	bdl	bdl	bdl
Softie	bdl	bdl	bdl	bdl	bdl	bdl	bdl	bdl	bdl	bdl	bdl
Cartman	bdl	bdl	bdl	bdl	bdl	bdl	bdl	bdl	bdl	bdl	bdl
Half Spring	bdl	bdl	bdl	bdl	bdl	bdl	bdl	bdl	bdl	bdl	bdl
Orange Creek	**0.25**	**0.23**	bdl	<500	bdl	**9**	**16**	**8**	bdl	bdl	<500
Caribou River	bdl	bdl	bdl	bdl	bdl	bdl	bdl	bdl	bdl	bdl	bdl
Karst	bdl	bdl	bdl	bdl	bdl	bdl	bdl	bdl	bdl	bdl	bdl
Persistent	**0.10**	bdl	bdl	bdl	bdl	bdl	bdl	bdl	bdl	bdl	bdl
Persistent (lab dup)	**0.09**	bdl	bdl	bdl	bdl	bdl	bdl	bdl	bdl	bdl	bdl
Stinky	0.06	bdl	bdl	bdl	bdl	bdl	bdl	bdl	bdl	bdl	bdl
Field Blank	bdl	bdl	bdl	bdl	bdl	bdl	bdl	bdl	bdl	bdl	bdl
Calgary Lab Blank	bdl	bdl	bdl	bdl	bdl	bdl	bdl	bdl	bdl	bdl	bdl
MERA I Samples (as reported by Hamilton, 1990)											
86-1					<2						
86-4					<2						
86-6					<2						
86-7					<2						
86-9					<2						
86-10					<2						
86-11					<2						
86-12					<2						
87-012B											
87-12											
87-012C											
86-13					<2						
86-15					<2						
86-17					<2						
87-17											
86-18					<2						
87-18											
87-018B											
86-19					**3**						
86-20					**3**						
86-21					<2						
86-22					<2						
86-23					<2						
86-24					<2						
86-25					<2						
86-26					<2						
86-27					**4**						
87-27											
86-28					<2						
86-29					<2						
86-30					**3**						
86-31					<2						
86-32					<2						
86-33					<2						
87-33											
87-34											
86-35					<2						
86-36					<2						
86-37					<2						
86-38					<2						
86-40					<2						
86-41					<2						
86-42					<2						
86-43					<2						
86-44					<2						
86-45					<2						
86-46					<2						
86-47					<2						
86-48					<2						
86-49					<2						
86-50					<2						
86-51					<2						
86-52					<2						
86-53					<2						
87-53											
86-54					<2						
86-55					<2						
86-56					<2						
86-57					<2						
86-58					<2						
87-58											
86-59					<2						
86-60					<2						
87-60											
86-61					<2						
86-62					<2						
86-63					<2						
86-64					<2						
87-64											

Table 4.4c (continued 2): Least common trace elements (Tl, Ga, Se, Br, Ag, Be, Sc, Ti, Bi, In and NO_2) from MERA I and II springs. All units in μg/L unless otherwise noted. Bolded numbers were determined to be elevated using the individual trace element method.

element	Tl	Ga	Se	Br	Ag	Be	Sc	Ti	Bi	In	NO_2
Name of Spring *detection limit (MERA II)*	*0.05*	*0.05*	*2*	*50*	*0.05*	*1*	*1*	*1*	*0.05*	*0.05*	*50*
detection limit (MERA I)	*n/a*	*n/a*	*n/a*	*n/a*	*2*	*n/a*	*n/a*	*n/a*	*n/a*	*n/a*	*n/a*
CCME Drinking Water Guideline (mg/L)	*n/a*	*n/a*	*0.01*	*n/a*	*n/a*	*n/a*	*n/a*	*n/a*	*n/a*	*n/a*	*3.2*
86-65					<2						
86-66					<2						
86-67					**3**						
86-68					<2						
86-69					<2						
86-70					<2						
86-71					<2						
86-072A					**4**						
86-072B					<2						
87-072B											
87-072BH											
87-073A											
87-073B											
87-073C											
86-74					<2						
86-75					<2						
86-76					<2						
86-77					<2						
86-78					<2						
86-79					<2						
86-80					<2						
86-81					<2						
86-82					<2						
87-82											
87-82											
87-082B											
86-83					**3**						
87-100											
87-101											
87-102											
87-103											
87-104											
87-105											
87-106											
87-107											
87-108											
87-109											
87-110											
87-111											
87-112											
87-112H											
87-113											
87-114											
87-115											
87-116											
87-117											
87-118											
87-119											
87-120											
87-121											
87-122											
87-123											
87-124											
87-125											
87-126											
87-127											
87-128											
AVERAGE	**0.146**	**1.868**	**2.847**	**172**	**3.425**	**4.000**	**6.333**	**4.500**	**0.000**	**0.000**	**35.067**
STANDARD DEVIATION	**0.139**	**2.524**	**1.674**	**89**	**3.571**	**4.359**	**8.386**	**n/a**	**0.000**	**0.000**	**n/a**
AVE+0.5*STDEV	**0.216**	**3.130**	**3.684**	**216**	**5.210**	**6.179**	**10.527**	**n/a**	**0.000**	**0.000**	**n/a**
AVE+STDEV	**0.286**	**4.392**	**4.521**	**261**	**6.996**	**8.359**	**14.720**	**n/a**	**0.000**	**0.000**	**n/a**
MAX	**0.580**	**7.500**	**7.000**	**317**	**14.000**	**9.000**	**16.000**	**8.000**	**0.050**	**0.050**	**52.000**
MIN	**0.050**	**0.080**	**2.000**	**317**	**14.000**	**2.000**	**2.000**	**0.000**	**0.000**	**0.000**	**0.000**
Criteria Cut-Off Used to Determine Anomalousness:	> 0.07	>0	>0	>0	>0	>0	>0	>0	>0	>0	>0
Definition of Criteria (to obtain approx. top 15 springs):	ave*0.5	anything detectable	anything detectable	anything detectable	anything detectable	anything detectable	anything detectable	anything detectable	anything detectable	anything detectable	anything detectable

Footnotes:
bdl = below detection limit
nd = no data available
CCME Drinking Water Guidelines Available at:
Federal-Provincial-Territorial Committee on Drinking Water. "Guidelines for Candadian Drinking Water Quality Summary Table". Health Canada, Government of Canada, March 2006.
***n/a* = guideline not available**
***Aesthetic Guideline Only**
[C]**Maximum 100 Platinum-Cobalt Units for Recreational Aesthetics of Colour**
CCME Recreation Guidelines Are Available at:
Federal-Provincial Working Group on Recreational Water Quality of the Federal-Provincial Advisory Committee on Environmental and Occutpational Health. "Guidelines for Canadian Recreational Water Quality". Health and Welfare Canada, Government of Canada, 1992.

Table 4.5: Isotope ratios of MERA II samples. Note: 1.81E+0.3 signifies 1.81×10^3 or 1810 in scientific notation. Gaseous springs are marked with a bubble (^{0}). All units are in permil notation (‰) unless otherwise noted.

	WATER		AQ SULPHUR			AQ CARBON		FREE GASES		DISSOLVED GASES		TUFA	
	$\delta^{18}O_{H2O}$	$\delta^{2}H_{H2O}$	$\delta^{34}S_{SO4}$	$\delta^{18}O_{SO4}$	$[SO_4]$	$\delta^{13}C_{HCO3(aq)}$	$[HCO_3]$	$\delta^{13}C_{CH4}$	$\delta^{13}C_{CO2}$	$\delta^{13}C_{CH4}$	$\delta^{13}C_{CO2}$	$\delta^{13}C_{CaCO3}$	$\delta^{18}O_{CaCO3}$
SAMPLE NAME Unit					ppm		ppm						
Precision and Accuracy	*0.04*	*0.4*	*0.3*	*0.5*		*0.2*		*0.5*	*0.5*	*0.5*	*0.5*	*0.2*	*0.2*
Prairie Creek Mine Shaft	-22.4	-173.6	12.8	-13.7	396	-19.9	315						
Harrison Creek	-23.1	-176.8	9.8	-12.7	161	-6.3	223						
Prairie Creek (downstream of mine)	-22.8	-176.4	8.2	-12.2	74.8	-3.8	193						
Broken Skull Upper Pool (2005) °	-23.1	-178.9	24.7	3.7	366	-4.3	439		-5.1		-8.5		
Broken Skull Lower Pool (2005)	-24.0	-186.5	25.4	3.4	364	0.5	440				-8.3		
Cowboy	-22.7	-176.0	-1.8	-14	35.3	-4.1	157						
Sibbeston	-22.0	-173.8	7.4	-5.9	29.8	-3.3	168				-13.8		
Corridor Creek	-23.0	-177.5	2.1		22.7	-1.2	122						
Veil	-22.4	-172.7	2.4	-7.9	62.4	-5.3	186				-16		
Big Veil	-21.8	-170.5	2.5	-6.8	64.2	-6.5	188				-16.2		
Galena Creek	-22.5	-176.2	10.4	-9.5	150	-6.9	283						
Sombre	-21.8	-164.0	5.4		4.15	2.9	94.5				-7.2		
Sombre (field dup)	-21.3	-166.2			4.13	5.5	94.6				-6.8		
Wrigley	-22.5	-178.3	16.6	-9.7	113	-8.9	244						
Mel's Pool	-21.4	-166.7			1.25	-8.0	73.4						
Cowgirl	-23.0	-175.3	5.6	-8.7	64.9	-6.6	190						
Brigade	-22.1	-172.4	1.4	-15.2	127	-5.8	198						
Ram Plateau	-21.8	-172.1	-11.3	-6.3	7.42	-7.2	61.3						
Cimitar	-21.9	-172.8	19.7	9.9	780	-9.5	287				-16.4		
Cathedral	-22.2	-174.4	5.7	-10.8	73.2	-5.9	178						
Mossy	-22.3	-175.9	11.3	-5.9	55.2	-4.0	167						
Crack	-22.7	-178.4	-3.7		14.8	-3.0	136						
Quickie	-21.8	-171.1		-8.3	67.7	-6.3	174						
Clearwater Creek	-25.4	-175.2	15.9	-11.7	37.8	-1.2	112						
Dookie	-23.1	-177.1	31.6	-11.7	62.9	2.0	97.6						
Dookie (field dup)	-23.1	-175.6	31.5	-12.3	63.2	0.7	83.8						
Dookie (field trip)	-23.3	-177.5	31.8	-11.9	63.8	0.5	81.7						
Boulder	-22.7	-174.4	1.7		5.47	2.6	75.8						
Overflow	-21.7	-163.9	6.3		0.00		4.0						
Smurf	-21.8	-174.5			8.37	-10.3	220						
Clark Lake	-21.9	-171.0	22.6	-7.1	21.4	-8.6	187						
Jacson	-20.9	-160.3			0.32		5.7						
Darkness	-22.1	-172.2	-8.2		0.73	-15.3	9.7						
Selena	-21.6	-167.9	20.8	-9.8	131	-8.3	188						
Caribou	-22.1	-174.9	12.4		11.9	-9.1	200						
Chance	-22.0	-172.8			17.6	-8.4	181					-6.5	-19.0
Interpluton Seep		-168.9			0.00		8.0						
Tiny	-22.7	-171.6			2.55	-11.0	127						
Blue Bells	-22.6	-175.0	18.3		11.9	-5.9	187				-15.2		
Blue Bells (field dup)	-22.8	-177.6	18.2		11.9	-5.1	188						
Cascade	-22.3	-173.2	6.7		14.1	-6.5	166				-16.9		
Meltwater	-22.3	-167.4			0.56	-9.8	36.6						
Waterfall	-23.4	-178.4			0.20		14.2						

Table 4.5 (continued): Isotope ratios of MERA II samples. Note: 1.81E+0.3 signifies 1.81×10^3 or 1810 in scientific notation. Gaseous springs are marked with a bubble (°). All units are in permil notation (‰) unless otherwise noted.

	WATER		AQ SULPHUR			AQ CARBON		FREE GASES		DISSOLVED GASES		TUFA	
SAMPLE NAME Unit	$\delta^{18}O_{H2O}$	$\delta^{2}H_{H2O}$	$\delta^{34}S_{SO4}$	$\delta^{18}O_{SO4}$	$[SO_4]$ ppm	$\delta^{13}C_{HCO3(aq)}$	$[HCO_3]$ ppm	$\delta^{13}C_{CH4}$	$\delta^{13}C_{CO2}$	$\delta^{13}C_{CH4}$	$\delta^{13}C_{CO2}$	$\delta^{13}C_{CaCO3}$	$\delta^{18}O_{CaCO3}$
Precision and Accuracy	*0.04*	*0.4*	*0.3*	*0.5*		*0.2*		*0.5*	*0.5*	*0.5*	*0.5*	*0.2*	*0.2*
Descente	-22.6	-170.9	4.0		7.97	-6.5	19.5						
Softie	-22.4	-172.8			0.00	-17.5	8.9						
Cartman	-22.8	-176.5			0.66	-17.0	15.5						
Half Spring	-22.6	-185.6	10.5		12.3	-6.6	85.4						
Orange Creek	-21.7	-171.7	12.9	-15.1	1.91E+03	-8.1	0.0						
Caribou River	-21.8	-170.5	11.6	-12.7	41.9	-8.1	164						
Karst	-22.5	-171.1	7.7		10.5	1.5	89.3						
Persistent	-22.9	-178.0	14.4		11.5	-0.5	397						
Stinky	-23.2	-182.2	31.9		10.7	-1.9	457				-8.7		
Twitya	-24.1	-193.0	28.6	2.8	118	-9.3	389			-49.2	-17.8	-9.2	-26.2
Sculpin	-23.9	-192.3	24.0	13.7	1.50E+03	-2.4	220				-10.3	1.3	-21.8
Deca °	-23.5	-189.7	16.7	12.8	944	-1.8	261		-10.4		-9.5	2.2	-21.4
Ekwi	-23.6	-191.8	18.2	13.1	1.78E+03	-1.2	663				-8.1	2.5	-22.8
Mineral Lake	-22.8	-183.0	3.1	-7.4	78.3	-4.0	327				-12.5	-0.8	-20.2
Brimstone °	-23.2	-181.1	15.1	-2.9	69.3	3.0	1.81E+03		-3.3		-3.6	10.5	-18.1
Cordes Vertes	-22.5	-178.4	12.3		14.7	2.4	458				-5.8	2.1	-20.8
Tabletop	-23.0	-179.5	22.5	7.3	150	-2.9	188				-13.6	-2.5	-25.8
South Redstone	-22.5	-177.5	23.3	8.3	162	-5.3	172				-13.1	-3.3	-27
Redstone Junction #1	-22.6	-175.2	19.0	1.6	252	-5.6	172				-13.7	-3.5	-21.3
Cotton	-22.2	-172.0	19.2		15.6		0.0						
Red Mini	-22.8	-179.5	2.3	-10	38.0		0.0						
Muddy	-23.0	-178.2	1.5	-9.7	99.0	-9.8	79.9				-18.1		
Grasby	-23.1	-178.2	19.0	-6.8	29.3	-8.5	297				-17.0	-6.5	-19.7
Red Steel	-22.5	-174.6	12.2	-11.6	21.6	-14.1	0.0				-21.1		
Bougere	-22.4	-170.5	10.7	-7.2	279		0.0				-22.1		
Champagne °	-22.1	-168.2	18.3	-9.5	52.7	-2.6	223	-81.1	-2.7		-8.8		
Champagne ° (field dup)	-22.1	-168.3	18.3	-9.5	52.3	-2.1	218						
Champagne Creek	-22.0	-172.1	17.9		55.8	-5.3	169				-13.6		
North Cantung (Zenchuck Creek)	-22.4	-182.7			8.64	-15.7	201						
Moore's	-22.6	-182.9	13.6	-1.3	73.4	-6.3	279						
Nahanni North (Lened Creek)	-23.3	-188.7	11.9	-7.9	57.4	-12.6	146						
Nahanni Headwaters	-22.8	-181.1	8.1	-8.7	31.9	-8.9	101						
Grizzle Bear °	-23.5	-188.2	21.7	6.2	188	-4.0	229	-40.4	-6.18				
Glacier Lake	-23.1	-182.7	5.3	-6.9	199	-7.5	64.5					-3.8	-19.2
Rabbitkettle	-22.5	-181.6	7.7	2.5	34.8	-1.5	447						
Kraus (Clausen)	-21.7	-176.9	24.1	6.5	656	-8.5	236						
Meilleur River	-22.3	-181.6	11.8	-5.1	277	-10.1	317					-5.9	-24.1
Wildmint	-22.5	-190.9	16.5	-12.2	114	-6.2	187						
Stinky Drift	-22.3	-180.6	6.2	2.5	29.4	-4.9	346						
Hole in the wall	-22.6	-181.2			5.74	-15.1	72.3						
West Cantung	-22.5		19.4	-6.9	31.5	-9.5	140						
Broken Skull Upper Pool (2003) °	-23.5	-188.3	24.3	4.4	345	-3.5	387	1.8	-5.1				
Broken Skull Upper Pool (2004) °						-3.5		-0.1					
Flat Fruit (2003) °	-21.5	-177.4	11.1	4.8	35.1	1.6	581						
Flat Fruit (2004) °									-2.47				
Flat Fruit (2005) °									-0.5		-0.2		

Table 4.6: Correlation matrix of MERA I and II springs. Strong (> 0.7) and moderate (0.7 > r > 0.5) linear correlation coefficients are in bold and listed for surface temperature (Temp), Si-geothermometry predicted temperature (Geotherm), pH, Eh, major ions, stable isotopes and total trace elements as percent of total dissolved solids (% T.E.). Total number of samples: 221.

	Temp	Geotherm.	Si	pH	% T.E.	Eh	TDS	Na	K	Ca	Mg	Cl	SO_4	HCO_3	$\delta^{18}O$	$\delta^{2}H$	$\delta^{13}C$	$\delta^{18}O_{SO4}$
Temp	1.00	**0.72**	**0.75**	0.15	-0.09	**-0.63**	0.25	0.22	0.28	0.02	-0.02	0.21	0.03	0.08	-0.26	**-0.55**	-0.03	**0.53**
Geotherm.		1.00	**0.94**	0.33	-0.07	**-0.50**	0.26	0.13	0.24	0.13	0.07	0.08	0.03	0.24	-0.22	-0.42	-0.18	0.10
Si			1.00	0.09	0.10	**-0.59**	0.24	0.09	0.14	0.18	-0.02	0.06	-0.01	0.24	-0.39	**-0.54**	-0.05	0.32
pH				1.00	**-0.56**	-0.12	0.07	-0.01	0.03	0.00	-0.12	-0.02	-0.27	0.19	-0.01	-0.04	0.20	-0.17
% T.E.					1.00	0.16	-0.10	-0.07	-0.11	-0.10	0.03	-0.08	0.15	-0.30	0.02	0.07	-0.06	-0.14
Eh						1.00	-0.47	-0.11	-0.35	-0.27	-0.19	-0.07	-0.13	-0.30	0.24	**0.53**	-0.01	-0.36
TDS							1.00	0.35	0.44	**0.68**	**0.66**	0.42	**0.63**	**0.50**	-0.13	-0.49	0.26	**0.58**
Na								1.00	**0.57**	0.22	0.13	**0.97**	0.36	0.20	-0.08	-0.23	0.10	0.38
K									1.00	**0.46**	0.28	**0.66**	0.29	0.23	-0.05	-0.22	0.10	**0.52**
Ca										1.00	**0.73**	0.27	**0.54**	**0.62**	-0.01	-0.22	0.23	**0.52**
Mg											1.00	0.16	**0.88**	0.23	0.02	-0.15	0.12	0.37
Cl												1.00	0.39	0.17	-0.07	-0.21	0.13	0.40
SO_4													1.00	0.01	0.00	-0.15	0.03	0.44
HCO_3														1.00	-0.07	-0.28	0.31	0.29
$\delta^{18}O$															1.00	**0.75**	-0.19	-0.23
$\delta^{2}H$																1.00	-0.04	**-0.55**
$\delta^{13}C$																	1.00	0.27
$\delta^{18}O_{SO4}$																		1.00
$\delta^{34}S_{SO4}$																		

Table 4.7: Frequency distribution of springs tallied for lithology, pH, temperature, total dissolved solids (TDS), sulphide oxidation and total trace elements (TTE).

	Clastics* (n = 21)		Carbonates (n = 107)		Plutons (n = 17)		Siliceous Shales (n = 12)		Calcareous Shales (n = 28)		Both Shales** (n = 30)	
	#	%	#	%	#	%	#	%	#	%	#	%
Acidic (pH < 7)	4	19	21	20	6	38	8	67	6	21	4	13
Cold (T < 12 °C)	8	42	72	68	9	53	7	58	16	57	28	93
Warm (12-40 °C)	4	21	29	27	0	0	3	25	10	36	0	0
Hot (T > 40 °C)	7	37	5	5	8	47	2	17	2	7	0	0
High TDS (> 900 ppm)	3	15	25	23	0	0	2	17	12	43	13	43
Sulphide Oxidation ($\delta^{18}O_{SO4}$ < -5 ‰)	2	67	20	67	0	0	5	83	2	33	8	100
High TTE (> 0.9 %)	5	24	17	16	10	63	8	67	4	14	8	27

*Clastics includes: arenite, siltstone and mudstone

**Both shales = having both siliceous and calcareous parts

Note: % was adjusted to the number of available data for the corresponding parameter

n = number of springs discharging from the corresponding bedrock group

Table 4.8A: Br/Cl ratios of SNRB springs with detectable Br concentrations, compared to world salt deposit averages according to Worden (1996).

Spring	Br/Cl ratio
Tulita	6.9 x 10-3
Grizzle Bear	5.9 x 10-3
Meilleur	9.0 x 10-3
BS Upper Pool	6.9 x 10-3
BS Lower Pool	6.8 x 10-3
SNRB Average	7.1 x 10-3
SNRB Standard Deviation	1.1 x 10-3
Paleozoic Average (Worden, 1996)	8.5 x 10-3
Mesozoic Average (Worden, 1996)	1.6 x 10-3
Tertiary Average (Worden, 1996)	3.1 x 10-3

Table 4.8B: Anhydrite- and gypsum-containing formations of the SNRB with their associated ages and sulphate isotope values based on age description by Okulitch (2005) and world average Palaeozoic sulphate isotope curves by Claypool et al. (1980).

Formation (Okulitch et al, 2005)	Age (million years ago) (Okulitch et al, 2005)	$\delta^{34}S$ (‰) (Claypool et al., 1980)	$\delta^{18}O$ (‰) (Claypool et al., 1980)
Bear Rock	387-418 Early-Mid Devonian	25-30 to 15-20	12-19
Tetso	387-418 (?) Late Silurian - Mid Devonian (?)	25-30 to 15-20	12-19
Mount Cap & Saline River	500-509 Middle Cambrian	22-33	11-13
Redstone River	723 Early Neohadrynian	15-20	11-22
Little Dal Group	723-1000 Paleohadrynian	15-25	11-22

Table 4.9: Summary of Indicator Springs - % total trace elements, # of individual elevated trace elements, Ficklin Diagram groupings (from Figure 4.8; groupings described as footnote), geochemical groupings (from Figure 4.2) and estimate of depth of circulation (from Si-geothermometry, Section 4.5.5). Summary of indicator springs near the two known mines is tabulated as footnote.

Spring	% Trace Elements	# of Anomalous Elements	List of Anomalous Elements	Ficklin Diagram Group	Geo-Chemical Group	Estimated Depth of Circulation (km)
86-072A (near Meilleur River)	2.16	8	Al, Mn, Ni, Zn, Cd, Co, Sr, Ag	G	1	
86-67 (Prairie Creek Mine Water)	4.68	5	Cu, Zn, Cd, Sb, Ag	H	1	
Glacier Lake	4.87	3	Fe, Zn, Tl	I	1	1.4
86-78	5.96	2	Fe, Mn	I	1	
86-15 (Glacier Lake)	2.78	2	Fe, Zn	I	1	
86-17	1.44	2	Fe, Mn		1	
86-35	1.14	2	Cu, Co	IJK	1	
86-37	2.28	1	Fe	I	1	
86-55	1.47	1	Fe	I	1	
Cathedral	1.41	1	Sr		1	<0.2
86-54	5.12			K	1	
86-62	4.89				1	
86-48	3.21				1	
87-012B	2.26			I	1	
Sombre (field dup)	1.60				1	<0.2
Sombre	1.59				1	<0.2
87-103	1.53				1	
86-4	1.20				1	
Softie	1.13				1	<0.2
87-109	1.05				1	
Orange Creek	4.00	15	Al, Mn, Ni, Cu, Zn, Cd, Co, Cr, Li, U, Tl, Ga, Be, Sc, Ti	E	2	<0.2
86-072B (near Meilleur River)	3.24	9	Al, Mn, Ni, Cu, Zn, Cd, Co, Sr, U	E	2	
Bougere	8.20	8	Al, Mn, Ni, Cu, Zn, Co, Ga, Ag	E	2	1.3
87-072B (near Meilleur River)	1.16	7	Al, Mn, Ni, Zn, Pb, Cd, Co	E	2	
86-71	3.07	5	Fe, Al, Mn, Cu, Co	F	2	
86-69 (Twisted Mountain)	5.59	4	Fe, Al, Mn, Co	F	2	
86-42	4.36	4	Al, Cu, Zn, Cd	E	2	
86-49	11.32	3	Fe, Al, Co		2	
86-36	1.17	2	Zn, Co	E	2	
86-70	1.01	2	Mn, Co	I	2	
87-121	3.85	1	Al	F	2	
86-25	3.52	1	Zn	E	2	
Interpluton	3.04	1	Ga		2	<0.2
87-072BH (near Meilleur River)	1.93	1	Al		2	
86-80	5.93				2	
Red Mini	4.63			F	2	0.9
Cotton	4.47			F	2	0.2
Overflow	3.33				2	
87-108	3.32				2	
87-100	2.43				2	
86-12	1.99				2	
87-105	1.30			IJK	2	
Nahanni Headwaters	0.93	7	Cs, Mo, As, Li, B, Sb, Ga		3	4.4
87-53 (Hole-in-the-Wall)	1.93	2	Mo, As		3	
86-53 (Hole-in-the-Wall)	1.72	2	Mo, As	K	3	
87-33 (Nahanni North)	0.92	1	Mo		3	
87-60 (Cantung East)	2.07	1	Mo		3	
86-52 (Hole-in-the-Wall)	1.71	1	As		3	
86-20 (Tungsten Mine Water)	1.00	1	Ag		3	
87-18 (West Cantung)	1.95				3	
87-018B (West Cantung)	1.90				3	
86-18 (West Cantung)	1.71				3	

Table 4.9 (continued): Summary of Indicator Springs.

Spring	% Trace Elements	# of Anomalous Elements	List of Anomalous Elements	Ficklin Diagram Group	Geo-Chemical Group	Estimated Depth of Circulation (km)
Prairie Creek Mine Shaft	0.81	7	Cu, Zn, Pb, Cd, Sb, Tl, Se	H		<0.2
Kraus (Clausen)	0.39	7	Cr, Cs, Li, Rb, Sr, V, B			2.3
87-073B	0.73	6	Al, Mn, Ni, Zn, Cd, Co			
Brimstone	0.73	6	Fe, Mn, Cr, Rb, Se, Be			4.7
Tulita	0.57	6	Cs, Li, Ba, B, Br, Sc			1.5
Persistent (lab dup)	0.26	6	Cd, Cs, As, Rb, Ba, Tl			n/a
Persistent	0.26	6	Cd, Cs, As, Rb, Ba, Tl			n/a
Ekwi	0.03	6	Cr, Cs, Li, Rb, B, Tl			2.3
West Cantung	0.60	5	Cs, Li, V, B, Ga			3.2
Wrigley	0.51	5	Mo, U, V, Tl, Se	I		<0.2
Broken Skull's Upper Pool	0.38	5	Pb, Cs, Rb, B, Br			2.7
Nahanni North (Lened Creek)	0.28	5	Cs, Mo, Li, B, Ga			3.6
Broken Skull's Lower Pool	0.39	4	Cs, Rb, B, Br			2.7
Hole in the wall	0.37	4	Mo, As, V, Ga			3.7
Grizzle Bear	0.22	4	Cr, Cs, Rb, Br			2.8
87-112	0.15	4	Fe, Mn, Ni, Co	I		
Galena	0.13	4	Pb, U, Tl, Se	J		<0.2
Wildmint	0.09	4	Cs, Li, B, Ga			2.9
Cimitar	0.63	3	Sr, U, Tl	I		<0.2
Broken Skull	0.37	3	Cs, Rb, B			2.7
Meilleur River	0.28	3	Cs, Rb, Br			3.1
86-63	0.26	3	Cu, Sr, U	I		
87-64	0.18	3	Pb, Sr, U			
87-073A	0.15	3	Ni, Zn, Pb	H		
86-21	0.37	2	As, Sr			
87-122	0.31	2	Pb, U			
Sibbeston	0.31	2	Tl, Ga	K		<0.2
87-123	0.30	2	Pb, Sr			
86-64	0.25	2	Cu, Sr			
Smurf	0.15	2	V, Se	IJK		<0.2
Prairie Creek	0.14	2	Sb, NO2	IJK		<0.2
Galena (lab dup)	0.13	2	U, Tl	J		<0.2
Cowgirl	0.08	2	V, Tl	K		<0.2
86-60	0.89	1	Mo			
87-012C	0.84	1	Cd	I		
87-124	0.79	1	Ba			
86-33	0.73	1	Mo			
Tabletop	0.63	1	Cr			2.3
Red Steel	0.63	1	Se			<0.2
Sculpin	0.61	1	Sr			0.3
86-30	0.54	1	Ag			
86-19	0.53	1	Ag			
Mineral Lake	0.48	1	Cr			0.5
South Redstone	0.45	1	Cr			2.7
87-128	0.39	1	Ba			
Quickie	0.38	1	Se			<0.2
86-83	0.38	1	Ag			
86-77	0.31	1	Ba	K		
86-27	0.30	1	Ag			
87-17	0.25	1	Mn			
87-110	0.20	1	U			
Stinky Drift	0.16	1	Tl			1.2
87-34	0.15	1	U			
87-58	0.15	1	Pb			
87-127	0.15	1	Ba			
87-119	0.14	1	Pb			
Flat Fruit	0.14	1	Cs			0.9
Veil	0.13	1	Se			<0.2
Big Veil	0.13	1	Se			<0.2
Champagne Creek	0.12	1	Se			<0.2
87-111	0.11	1	U			
Cordes Vertes	0.11	1	Cr			n/a
87-073C	0.11	1	Ni	I		
86-13	0.10	1	As			
Deca	0.09	1	Cr			0.8
Harrison Creek	0.08	1	Pb			<0.2
87-125	0.08	1	Mo	IJK		
Grasby	0.08	1	Se			n/a
Crack	0.04	1	V			<0.2

Table 4.9 (continued 2): Summary of Indicator Springs.

Spring	% Trace Elements	# of Anomalous Elements	List of Anomalous Elements	Ficklin Diagram Group	Geo-Chemical Group	Estimated Depth of Circulation (km)
Mossy (lab dup)	0.69					<0.2
Mossy	0.68					<0.2
86-61	0.59					
Clark Lake	0.53					<0.2
Clark Lake (lab dup)	0.53					<0.2
Ram Plateau	0.53					<0.2
87-126	0.49					
Jacson	0.49					<0.2
86-11	0.46					
86-31	0.45					
Brigade	0.39					<0.2
86-41	0.39					
87-12	0.38					
86-79	0.37					
86-74	0.37			I		
86-29	0.37					
86-81	0.36					
86-40	0.35					
Darkness	0.33					<0.2
86-43	0.31					
86-32	0.31					
Redstone Junction #1	0.30					2.0
Waterfall	0.30					<0.2
86-50	0.30			IJK		
86-59	0.28					
Stinky	0.28					n/a
87-082B	0.27					
Mel's Pool	0.27			K		<0.2
Selena	0.27			I		<0.2
Meltwater	0.26					<0.2
86-57	0.25					
86-1	0.25					
86-75	0.25			K		
87-107	0.24			I		
87-27	0.24					
Champagne	0.23					n/a
86-58	0.22					
86-82	0.22					
Champagne (dup)	0.21					n/a
86-76	0.20					
86-9	0.20					
Cartman	0.19					<0.2
87-82	0.19					
87-82	0.19					
Dookie (field trip)	0.19					<0.2
86-44	0.18					
Dookie (field dup)	0.18					<0.2
86-56	0.18					
87-115	0.18					
86-10	0.18					
Moore's	0.18					3.3
Corridor Creek	0.17					<0.2
86-6	0.17					
86-46	0.17					
Caribou	0.16					<0.2
Dookie	0.16					<0.2
86-47	0.16					
Caribou River	0.15					<0.2
87-104	0.15					
86-26	0.15					
86-22	0.14					
87-116	0.14					
86-28	0.14					
86-7	0.14					
86-68	0.14					
Half Spring	0.13					<0.2
Rabbitkettle	0.12					1.1
Chance	0.12					<0.2
86-45	0.12					
Cowboy	0.12					<0.2
87-120	0.12					
Champagne Creek (dup)	0.12					<0.2

Table 4.9 (continued 3): Summary of Indicator Springs.

Spring	% Trace Elements	# of Anomalous Elements	List of Anomalous Elements	Ficklin Diagram Group	Geo-Chemical Group	Estimated Depth of Circulation (km)
86-65	0.12			K		
87-112H	0.12					
87-113	0.11					
86-23	0.10					
86-24	0.10					
86-66	0.10			IJK		
Cascade	0.10					<0.2
Cascade (lab dup)	0.10					<0.2
Blue Bells (field dup)	0.09					<0.2
Descente	0.08					<0.2
87-114	0.08					
Blue Bells	0.08					<0.2
Tiny	0.07					<0.2
Muddy	0.07			I		0.9
87-102	0.07					
Karst	0.07					<0.2
86-51	0.06					
Clearwater Creek	0.06					<0.2
87-106	0.05					
87-118	0.04					
87-101	0.04					
87-117	0.03					
Boulder	0.03					<0.2
North Cantung (Zenchuck Creek)	0.01					1.3

Ficklin Diagram Groups (Plumlee et al., 1994)

E	Pyrite- and base metal-rich polymetallic veins and disseminations in wallrock with low acid-buffering capacity
F	Pyrite-rich, base metal-poor veins and disseminations in wallrock with low acid-buffering capacity
G	Pyrite- and base metal-rich polymetallic veins that are carbonate-rich or occur in wallrock altered to contain carbonate
H	Pyrite- and base metal-rich, polymetallic replacements and veins in carbonate-rich sediments
I	Polymetallic veins with moderate to low pyrite and base metal content that are carbonate-rich or occur in carbonate-rich wallrock
J	Pyrite-poor polymetallic replacements in carbonate-rich sediments
K	Pyrite-poor, Au-Te veins and breccias with carbonate gangue

Testing the Multi-Method Approach using the two Known Deposits of the SNRB

Sample	Total Trace Elements	Individual Trace Elements	Ficklin Diagram Group	Geo-Chemical Group
Tungsten Mine Water	1.00%	Ag	n/a	3
Stinky Drift	0.16%	Tl	n/a	n/a
West Cantung	1.42%	Cs, Li, V, B, Ga	n/a	3
Prairie Creek Mine Water	0.81%	Cu, Zn, Pb, Cd, Sb, Tl, Se	H	n/a
Prairie Creek	0.14%	Sb, NO_2	IJK	n/a
Harrisson Creek	0.08%	Pb	n/a	n/a
Galena	0.13%	Pb, U, Tl, Se	J	n/a
Galena (lab dup)	0.13%	U, Tl	J	n/a

Table 4.10: Cut-off values used to determine elevated individual trace elements, compared with select deposit-related waters. Units are in μg/L. Description of deposits follows as footnote.

	Fe	Al	Mn	Ni	Cu	Zn	Pb	Cd	Co	Cr
Criteria Cut-Off Used to Determine Anomalousness in SNRB	> 10,000	> 7,500	> 880	> 300	> 15	> 622	> 2	> 5	> 31	> 1
Criteria Statistic Description	ave+0.5stdev	ave+0.5stdev	ave+0.5stdev	ave+0.5stdev	1.5*ave	ave	ave	ave	1.5*ave	ave
Leybourne et al., 1998	6 to 4,600	2 to 281	11 to 440	1 to 6	1 to 7.8	2 to 2,300	0.2 to 530	0.5 to 6.1	0 to 2.7	0.2 to 2.7
Kennecott Site (Eppinger et al., 2000)	10	10 to 50	0.01 to 15	0.01-1	0.2-80	0.05	0.05-0.1	0.01	0.01-0.1	0.2-0.8
Bremner Site (Eppinger et al., 2000)	10	2 to 30	0.04-80	0.01-10	0.3-20	0.03-10	0.02	0.01-0.2	0.01-7	0.2
Gold Hill Site (Eppinger et al., 2000)	10	2 to 100	0.003-1	0.4-1	0.2-8	0.03-4	0.03-0.2	0.01	0.02-0.05	0.2
Orange Hill and Bond Creek Sites (Eppinger at al., 2000)	10 to 3,000	10 to 100,000	0.007-15,000	0.01-200	0.2-20,000	20-20,000	0.03-10	0.1-100	0.01-900	0.3-3
Nabesna Site (Eppinger et al., 2000)	10-1,500,000	0.003-100,000	0.005-7,000	0.01-100	0.3-30,000	0.02-7,000	0.03-150	0.01-100	0.01-900	0.2-30
Siegel and Ericson, 1980	0-67,000	0-280	10-26,000	1-120	0.6-190	3.9-620	0.1-18	0-8.4	0.1-46	0-5.5
Pellicori et al., 2005	1,450-311,000	<300-42,700	1,300-6,500	n/a	<2-13,400	1,100-114,000	n/a	n/a	n/a	n/a
Sidenko and Sherriff, 2005	1,200,000	n/a	n/a	3,000	45	300	n/a	n/a	n/a	n/a
Ohkuni et al., 2004	9,500									
Big Colorado Mine (Verplanck et al., 2004)	892-242	210	n/a	1	0.44	17	0.01	0.074	0.9	n/a
Carrillo-Chavez et al., 2003	3 to 80	n/a	n/a	n/a	10-100	30-800	1 to 10	n/a	n/a	n/a

Table 4.10 (continued): Cut-off values used to determine elevated individual trace elements, compared with select deposit-related waters. Units are in μg/L. Description of deposits follows as footnote.

	Cs	Mo	As	Li	Rb	Sr	Ba	U	V	B	Sb
Criteria Cut-Off Used to Determine Anomalousness in SNRB	> 3.5	> 12	> 16	> 266	> 23	> 4,200	> 231	> 15	> 1	> 350	> 0.9
Criteria Statistic Description	0.5*ave	ave+1.5stdev	ave+0.5stdev	ave+0.5stdev	ave+0.5stdev	ave+stdev	ave+stdev	ave+1.5stdev	ave	ave	ave*0.5
Leybourne et al., 1998	n/a	0.5 to 19	13 to 110	2 to 1,800	0.34 to 3.7	2.1 to 610	12 to 550	0.01 to 0.92	0.01 to 0.18	n/a	n/a
Kennecott Site (Eppinger et al., 2000)	n/a	0.07-20	0.1-8	0.05-2	n/a	30-300	0.6-40	0.07-0.8	0.6-2	30-100	0.01
Bremner Site (Eppinger et al., 2000)	n/a	0.2-1.5	0.1-1.5	0.04-1	n/a	40-100	2 to 30	0.2-0.3	0.07	5	0.01
Gold Hill Site (Eppinger et al., 2000)	n/a	0.1-0.9	0.1-2	1 to 9	n/a	10 to 300	3 to 30	0.01-0.3	0.05	4-200	0.01-0.2
Orange Hill and Bond Creek Sites (Eppinger at al., 2000)	n/a	0.07-200	0.1-0.3	1 to 40	n/a	200-6,000	3 to 80	0.4-20	0.05	4 to 80	0.01-70
Nabesna Site (Eppinger et al., 2000)	n/a	0.03-20	0.1-5,000	0.03-20	n/a	15-1,000	0.01-40	0.03-40	0.06-20	4-200	0.01-1
Siegel and Ericson, 1980	n/a	n/a	n/a	n/a	n/a	n/a	n/a	n/a	n/a	n/a	n/a
Pellicori et al., 2005	n/a	n/a	8-750	n/a	n/a	n/a	n/a	n/a	n/a	n/a	n/a
Ohnuki et al., 2004	n/a	n/a	90	n/a	n/a	n/a	n/a	n/a	n/a	n/a	n/a
Big Colorado Mine (Verplanck et al., 2004)	n/a	n/a	n/a	8	n/a	8	0.03	n/a	n/a	n/a	n/a
Carrillo-Chavez et al., 2003	n/a	n/a	7 to 20	n/a	n/a	n/a	n/a	n/a	n/a	n/a	n/a

Table 4.10 (continued 2): Cut-off values used to determine elevated individual trace elements, compared with select deposit-related waters. Units are in μg/L. Description of deposits follows as footnote.

	Tl	Ga	Se	Br	Ag	Be	Sc	Ti	Bi	In
Criteria Cut-Off Used to Determine Anomalousness in SNRB	> 0.07	>0	>0	>0	>0	>0	>0	>0	>0	>0
Criteria Statistic Description	ave*0.5	anything detectable	anything detectable	anything detectable	anything detectable	anything detectable	anything detectable	anything detectable	anything detectable	anything detectable
Leybourne et al., 1998	n/a	n/a	n/a	n/a	n/a	n/a	n/a	0.05 to 1.52	n/a	n/a
Kennecott Site (Eppinger et al., 2000)	n/a	n/a	n/a	n/a	0.05	0.02	0.02	0.04	n/a	n/a
Bremner Site (Eppinger et al., 2000)	n/a	n/a	0.1	n/a	0.005	0.02	0.02-0.5	0.07	n/a	n/a
Gold Hill Site (Eppinger et al., 2000)	n/a	n/a	0.2-3	n/a	0.004-0.07	0.02	0.02-1	0.05-0.9	n/a	n/a
Orange Hill and Bond Creek Sites (Eppinger at al., 2000)	n/a	n/a	0.1-7	n/a	0.006-0.02	0.02-2	0.03-20	0.05-10	n/a	n/a
Nabesna Site (Eppinger et al., 2000)	n/a	n/a	0.1-9	n/a	0.004-1	0.02-0.9	0.06-10	0.05-200	n/a	n/a

Description of References used in Table 4.10:

Eppinger et al., 2000 — *Kennecott stratabound copper mines (Alaska)*
Eppinger et al., 2000 — *Bremner Disctrict Historic Mine gold polytmetallic veins (Alaska)*
Eppinger et al., 2000 — *Gold Hill gold placer mines (Alaska)*
Eppinger et al., 2000 — *Orange Hill and Bond Creek undisturbed porphyry copper-molybdenum deposits (Alaska)*
Eppinger et al., 2000 — *Nabesna Historic Mine gold-bearing iron skarn deposits (Alaska)*
Leybourne et al., 1998 — *undisturbed Zn-Pb massive sulphide deposits, Bathurst Mining Camp (New Brunswick)*
Siegel and Ericson, 1980 — *Cu-Ni mining region (Minnesota)*
Pellicori et al., 2005 — *Berkeley Pit Lake of high grade Cu-Zn-Pb-Ag-Mn veins (Montana)*
-largest Superfund complex in US in terms of areal extent
-mined from 1870-1982
-320 million tons of ore, >700 million tons of waste rock
-10,000km of interconnected mine workings
-lake is 220m deep with 110 billion liters of acidic mine water
-concentrations shown here are from the monitoring wells around the pit lake
Sidenko and Sherrif, 2005 — *Groundwater samples from within two sulphide mine tailings (northern Manitoba)*
Ohkuni et al., 2004 — *Acid mine discharge water (Japan)*
Verplanck et al., 2004 — *Abandoned Big Colorado mine water (Colorado)*
Carrillo-Chavez et al., 2003 — *Silver and gold exploitation from low-sulphidation quartz and calcite-rich epithermal veins since 1548 (Mexico)*

Table 4.11: Geothermometry results for select MERA II springs. Appropriate silica sampling was only performed in MERA II study. Warm and hot springs were analyzed with geothermometry, with some cold ones for comparison (e.g.: Bougere, Brimstone). MERA II springs not listed here are assumed to circulate < 200 m in depth.

			Geothermometer-predicted Temperature			
Name of Spring	Surface Temperature	Predicted* Depth of Circulation (km)	quartz adiabatic	silica chalcedony*	silica alfa-cristobalite	log(Na/K) + 1/3*log(Ca^0.5/Na)
Brimstone	6.2	4.67	130.4	107.5	83.8	159.6
Nahanni Headwaters	63.6	4.41	125.8	101.4	78.3	115.4
Hole in the wall	40.2	3.69	112.8	84.8	63.2	106.7
Nahanni North (Lened Creek)	56.1	3.60	111.4	82.9	61.5	100.8
Moore's	48.2	3.33	106.3	76.6	55.7	260.8
West Cantung	41.3	3.23	104.4	74.2	53.6	101.2
Meilleur River	36.9	3.07	101.5	70.6	50.2	217.2
Wildmint	30.0	2.85	97.4	65.5	45.6	77.8
Grizzle Bear	42.6	2.77	96.0	63.8	44.0	270.3
Broken Skull	46.4	2.70	94.6	62.1	42.5	244.0
South Redstone	51.2	2.68	94.3	61.7	42.1	94.6
Tabletop	38.5	2.34	87.9	53.9	34.9	92.3
Kraus (Clausen)	36.7	2.30	87.1	53.0	34.1	176.1
Ekwi	40.8	2.30	87.1	52.9	34.0	124.3
Redstone Junction #1	15.4	1.97	80.8	45.3	27.1	92.1
Tulita	24.7	1.52	72.1	35.0	17.6	166.7
Glacier Lake	3.5	1.39	69.5	32.0	14.9	181.6
Bougere	2.7	1.26	66.9	29.0	12.1	214.4
North Cantung (Zenchuck Creek)	20.9	1.25	66.8	28.8	12.0	198.1
Stinky Drift	16.6	1.21	66.0	27.9	11.1	244.8
Rabbitkettle	21.1	1.12	64.2	25.8	9.2	234.9
Flat Fruit	9.3	0.89	59.6	20.5	4.3	162.2
Red Mini	4.2	0.85	58.7	19.5	3.3	234.1
Muddy	2.3	0.85	58.7	19.5	3.3	228.1
Deca	21.6	0.81	57.9	18.6	2.5	85.2
Mineral Lake	18.3	0.46	50.9	10.6		185.1
Sculpin	17.1	0.32	48.0	7.4		167.9
Cotton	12.5	0.24	46.4	5.5		215.3
Cordes Vertes	8.2	n/a	35.4			131.5
Champagne	5.9	n/a	37.0			196.7
Grasby	3.2	n/a	36.7			170.2
Red Steel	0.8	n/a	34.1			144.1
Champagne Creek	nd	n/a	32.0			231.6
AVERAGE	**24.6**	**2.1**	**76.5**	**47.7**	**33.6**	**168.6**
standard deviation	**18.3**	**1.2**	**27.1**	**28.6**	**24.2**	**57.8**

APPENDIX A: TABLES OF MERA I AND II DUPLICATES

Appendix A – Table 1: Number of times springs were sampled for MERA I and II.

Note: all other springs were sampled once only. (M.R. = Meilleur River)

	1986	1987	2003	2004	2005	TOTAL
Rabbitkettle (001)	1		1			2
not named (012)	1	3				4
Glacier Lake (015)	1		1			2
not named (017)	1	1				2
Cantung West (018)	1	2	1			4
Cantung Mine (019, 020)	2		1			3
Wildmint (027)	1	1	1			3
Moore's (032)	1		1			2
Nahanni North (033, 034)	1	2	1			4
Nahanni Headwaters (038)	1		1			2
Broken Skull (040, 041)	2		1		2	5
Grizzly Bear (043)	1		1			2
Cantung North (044)	1		1			2
Hole-in-the-Wall (052, 053)	2	1	1			4
Flat Fruit (058)	1	1	1			3
Cantung East (060)	1	1				2
Kraus (063, 064)	2	1	1			4
Prairie Creek Mine (067)	1				1	2
Meilleur (072, 073)	2	5	1			8
M.R. metaliferous tufa (082, 111, 112)	1	6				7
Champagne				2		2
Sombre					2	2
Dookie					3	3
Blue Bells					2	2

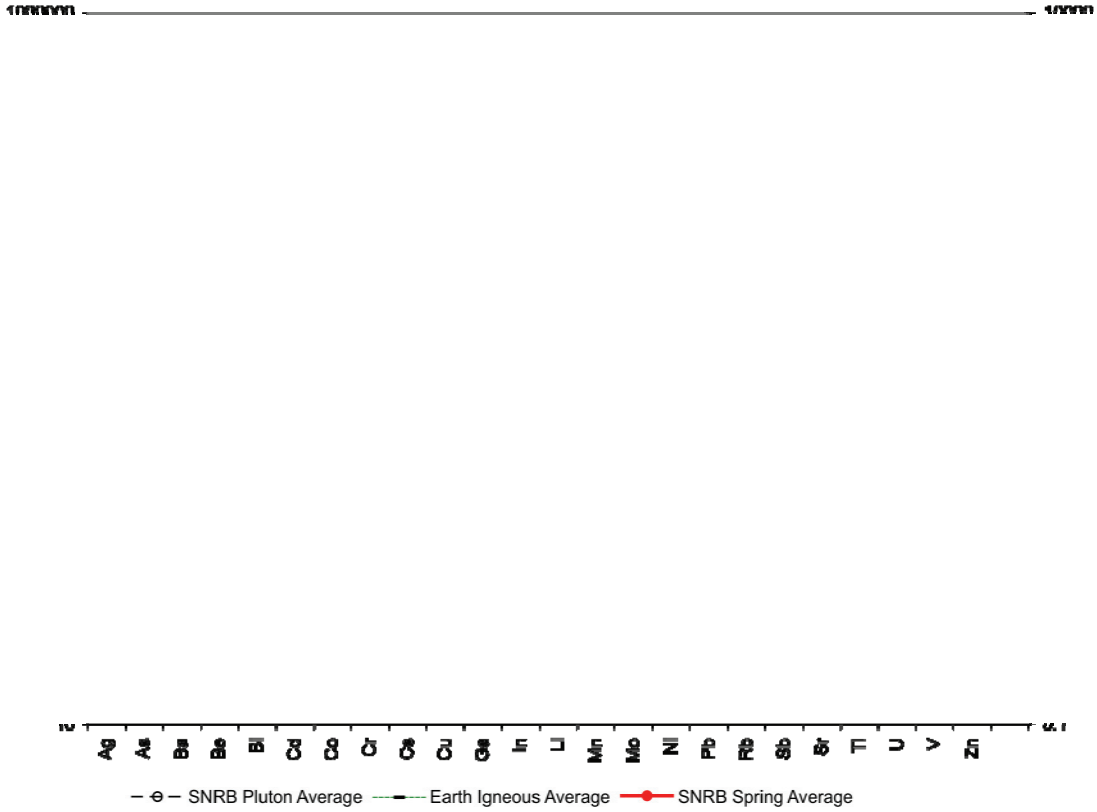
Appendix A – Table 2: Major ions, TDS and % total trace elements of field duplicates of MERA I and II springs. All units are in ppm unless otherwise noted.

Name of Spring	% T.E.	TDS	Ca^{2+}	Mg^{2+}	K^{+}	Na^{+}	Si^{4+}	HCO_3^{-}	SO_4^{2-}	Cl^{-}	F^{-} (ppb)
Rabbitkettle	0.12	732	200	40	5.1	4.1	6.60	447	35	0.57	235
86-001	0.25	609	231	46	4.9	4.0	7.48	290	33	1.21	530
86-012	1.99	99	25	5.0	0.5	1.0	9.35	0.1	68	0.16	120
87-012	0.38	106	19	4.0	0.5	0.5	7.95	0.1	81	1.27	130
87-012B	2.26	106	26	3.0	0.5	0.5	5.14	13	63	0.10	50
87-012C	0.84	103	22	4.0	0.5	0.5	7.48	0	75	0.12	150
Glacier Lake	4.87	358	75	17	0.8	1.3	7.80	64	199	0.14	436
86-015	2.78	361	92	15	0.7	1.0	10	64	188	0.35	580
86-017	1.44	1703	791	68	8.1	60	44	718	55	3.05	920
87-017	0.25	1720	635	55	6.5	46	34	925	50	2.74	560
West Cantung	0.60	245	8.0	1.2	1.2	57	21	140	32	5.89	4997
86-018	1.71	207	8.0	0.5	1.0	60	22	105	26	6.48	4090
87-018	1.95	189	6.0	0.5	0.5	50	18	101	25	6.59	4270
87-018B	1.90	208	7.0	0.5	0.5	55	20	109	28	7.48	4710
Stinky Drift (Cantung Mine shaft spring)	0.16	536	130	26	2.8	1.5	7.80	346	29	0.30	291
86-019	0.53	185	36	4.0	0.3	22	12	28	92	2.09	1100
86-020	1.00	352	4.0	3.0	0.9	115	18	144	60	25.2	9310
Wildmint	0.09	481	17	2.5	1.2	130	17	187	114	29.4	8310
86-027	0.30	495	155	34	2.7	1.0	9.35	272	30	0.40	310
87-027	0.24	517	128	27	1.5	1.0	7.48	331	28	0.48	330
Moore's	0.18	456	74	23	4.1	2.2	21	279	73	0.48	286
86-032	0.31	419	93	29	3.8	2.0	24	208	82	0.91	420
Nahanni North / Lened Creek	0.28	283	1.6	0.1	1.1	76	26	146	57	1.11	2874
86-033	0.73	258	2.0	0.5	1.0	80	29	104	69	1.44	2950
87-033	0.92	235	2.0	0.5	0.5	69	25	101	61	1.48	2940
87-034	0.15	188	39	2.0	0.5	7.0	5.14	118	21	0.23	310
Nahanni Headwaters	0.93	212	2.9	0.0	1.6	65	34	101	32	10.3	8157
86-038	2.27	201	3.0	0.5	1.5	68	39	80	38	11.0	7790
Broken Skull Upper Pool (2003)	0.37	1051	160	50	32.0	56	16	387	345	22.0	2250
Broken Skull's Upper Pool (2005)	0.38	1120	160	50	32.0	51	13	439	366	21.6	1699
Broken Skull's Lower Pool (2005)	0.39	1115	160	49	31.0	50	15	440	364	21.2	1771
86-040	0.35	1139	216	67	33.3	66	19	338	396	23.4	1520
86-041	0.39	1082	218	68	33.7	68	19	282	389	23.6	1530
Grizzle Bear	0.22	625	110	26	23.0	22	16	229	188	26.8	680
86-043	0.31	676	139	35	23.2	26	20	202	219	32.2	910
North Cantung / Zenchuck Creek	0.01	251	26	14	0.6	0.6	4.92	201	8.6	0.21	197
86-044	0.18	206	35	19	0.8	0.5	10	132	19	0.38	150

Appendix A – Table 2 (continued): Major ions, TDS and % total trace elements of field duplicates of MERA I and II springs. All units are in ppm unless otherwise noted.

Name of Spring	% T.E.	TDS	Ca^{2+}	Mg^{2+}	K^{+}	Na^{+}	Si^{4+}	HCO_3^{-}	SO_4^{2-}	Cl^{-}	F^{-} (ppb)
Hole-in-the-Wall	0.37	107	1.6	0.1	0.6	26	26	72	5.7	1.14	1876
86-052	1.71	103	1.0	0.5	0.6	30	32	61	7.9	2.03	2620
86-053	1.72	107	1.0	0.5	0.5	31	33	63	8.7	2.18	2770
87-053	1.93	89	1.0	0.5	0.5	28	27	51	6.6	1.90	2770
86-055	1.47	1070	425	53	3.4	10	12	447	126	5.25	660
Flat Fruit	0.14	1203	500	52	6.0	27	5.70	581	35	1.56	631
86-058	0.22	1280	647	66	5.6	32	7.01	488	38	3.76	530
87-058	0.15	1280	484	51	4.0	25	6.08	686	27	3.10	1600
86-060	2.07	231	2.0	0.5	1.3	75	38	112	30	10.5	6530
87-060	0.89	217	2.0	0.5	1.0	67	32	107	29	10.3	6770
Kraus / Clausen	0.39	4092	410	74	81.0	940	13	236	656	1695	<500
86-063	0.26	4809	610	114	88.1	601	14	195	854	2347	830
86-064	0.25	4837	617	116	84.4	601	14	225	860	2333	820
87-064	0.18	5480	502	92	172.5	1252	11	265	829	2368	0
Prairie Creek Mine Shaft	0.14	929	150	65	1.1	0.9	1.86	315	396	0.39	<50
86-067	4.68	916	182	67	0.5	0.5	2.80	272	393	1.17	200
86-072A	2.16	3479	613	310	2.5	18	5.61	115	2404	16.8	490
86-072B	3.24	2988	413	268	2.1	18	8.88	0.1	2285	2.47	480
87-072B	1.16	1876	253	151	1.5	18	6.54	0.1	1451	2.02	1300
87-072BH	1.93	422	253	149	2.0	18	6.08				0
87-073A	0.15	2399	363	212	2.5	20	3.27	191	1610	1.09	3800
87-073B	0.73	1988	299	175	3.0	20	4.67	0.1	1490	1.00	3500
87-073C	0.11	2365	354	206	3.5	18	2.80	275	1508	1.00	3400
Meilleur River	0.28	857	150	46	14.0	30	19	317	277	23.9	467
86-082	0.22	964	171	54	13.8	31	19	289	373	31.5	990
87-082	0.19	935	151	46	8.5	30	17	378	297	24.8	790
87-082B	0.27	834	131	45	8.0	29	16	306	291	24.0	760
87-082H	n/a	230	147	45	8.0	30	16				0
87-111	0.11	1007	278	31	1.0	0.5	3.27	322	374	0.23	400
87-112	0.15	2983	397	160	3.5	254	2.34	32	2122	14.9	1130
87-112H	0.12	827	402	161	4.0	260	2.34				0
Champagne	0.23	364	83	1.0	1.6	2.4	2.58	223	53	0.00	<50
Champagne (field dup)	0.21	354	79	0.9	1.6	2.1	2.76	218	52	0.00	<50
Sombre	1.59	129	22	8.3	0.1	0.0	0.17	95	4.2	0.00	1193
Sombre (field dup)	1.60	129	22	8.2	0.1	0.0	bdl	95	4.1	0.00	907
Dookie	0.16	208	30	17	0.2	0.1	0.96	98	63	0.00	<50
Dookie (field dup)	0.18	195	31	17	0.2	0.1	0.84	84	63	0.00	<50
Dookie (field trip)	0.19	194	31	17	0.2	0.1	0.78	82	64	0.00	<50
Blue Bells	0.08	266	43	20	1.8	2.2	3.30	187	12	0.70	451
Blue Bells (field dup)	0.09	266	42	20	1.8	2.2	3.30	188	12	0.71	456

APPENDIX B: DISCUSSION ON GEO-AVAILABILITY OF METALS



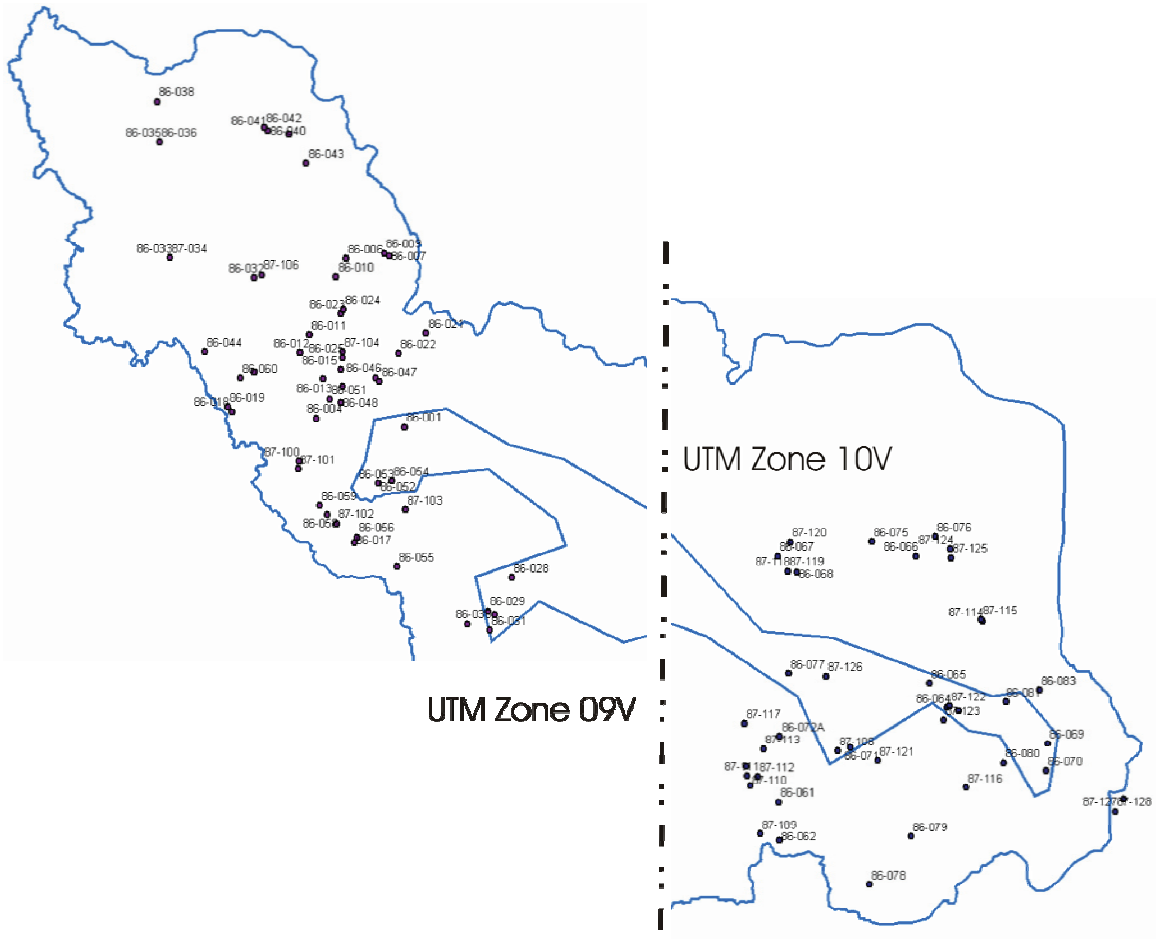
Appendix B - Comparison of SNRB spring and pluton (Rasmussen, MERA II report – in press) geochemistry with world igneous average (Hem, 1985). In most cases, spring geochemistry reflects rock abundance of that element, except with As, Cr, Ga, Pb, V, Cs, Cu and U. Differences can be accounted for by varying weathering effects, mineral properties, sorption and/or geochemical conditions (Smith and Huyck, 1999).

Controls on geo-availability of metals have been listed in Smith and Huyck (1999) as initial abundance or total metal content in the rock, access of weathering agents / degree of weathering, mineral properties (e.g.: solubility), and geochemical conditions (e.g.: pH and Eh). Most of the average trace element concentrations of the spring waters in the SNRB match very closely to that of the local plutonic rock geochemistry (Figure B1), indicating that total metal content of the rocks is the main factor in spring trace element

geochemistry. There are some differences too – springs sometimes peak or trough at different elements than the rocks at certain elements (troughs at As, Cr, Ga, Pb, V; peaks at Cs, Cu, U). These differences could be accounted by weathering effects, mineral properties, geochemical conditions and sorption (Smith and Huyck, 1999). For example, As is mobile in acidic (pH < 3) and oxidizing conditions, but immobile in neutral pH's regardless of the redox conditions; Cr and Pb are mobile under most conditions except with the presence of abundant iron-rich particulates or hydrogen sulphide; Ga is only mobile in acidic conditions; V and U are only mobile in acidic conditions or in the absence of iron-rich particulates; Cs is somewhat mobile in any conditions; and Cu is most mobile under oxidizing & acidic conditions or reducing & neutral conditions (Smith and Huyck, 1999 and references therein).

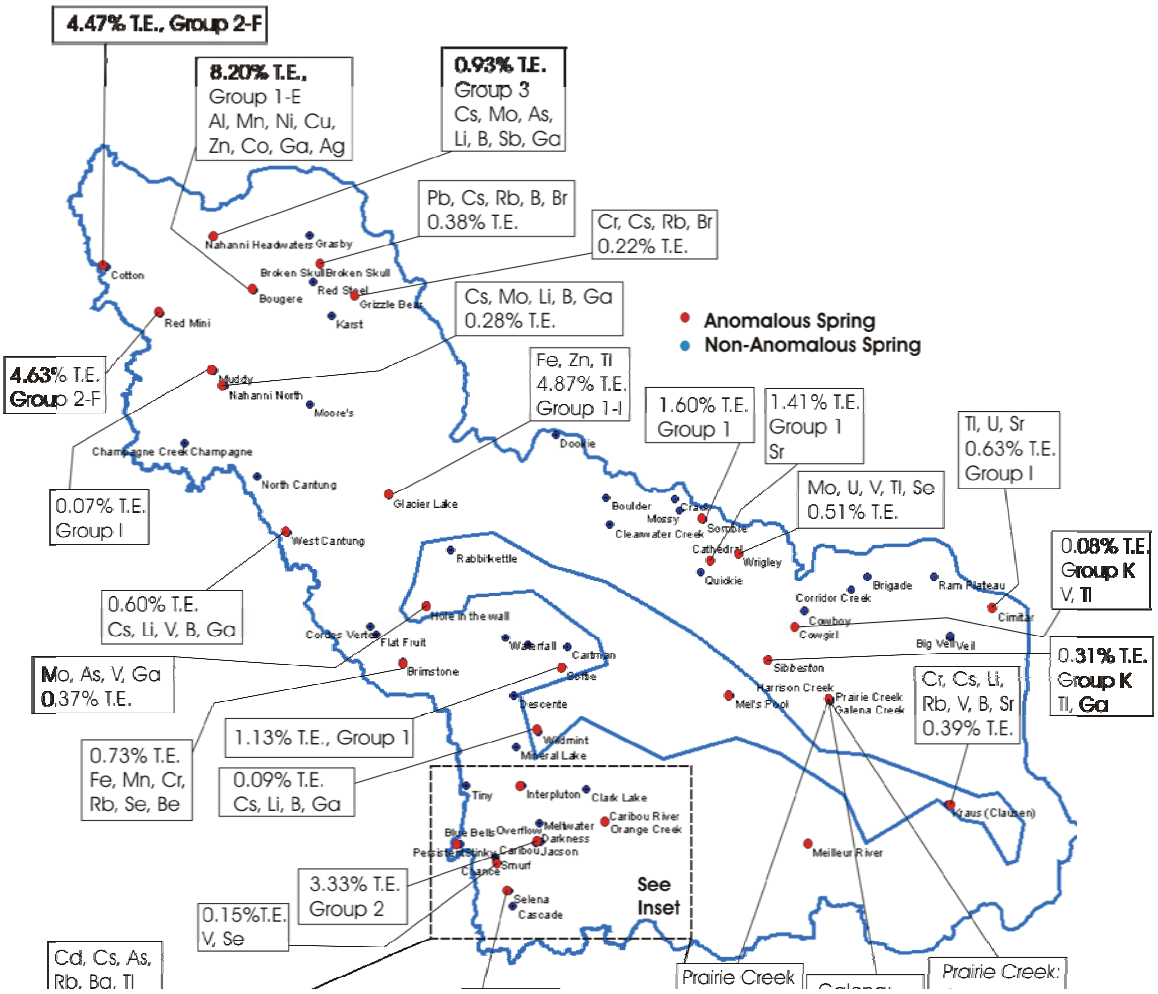
Relative comparisons between springs can still reflect mineralized zones vs. background levels in the SNRB because the differences in the geo-availability factors are assumed to be relatively constant / negligible in this regional study or taken under account when determining cut-off values. For example, someone might argue that acidity of springs releases more metals therefore explains why many acidic springs are metalliferous, but one must recall that acidity in itself is a sign of the presence of sulphides (as discussed in the background section). The resulting trace element concentrations then may tell you what kind of sulphide it is (e.g.: pyrite if mostly Fe, chalcopyrite if Fe + Cu, arsenopyrite if Fe + As, etc.).

APPENDIX C: MERA I SPRING LOCATIONS



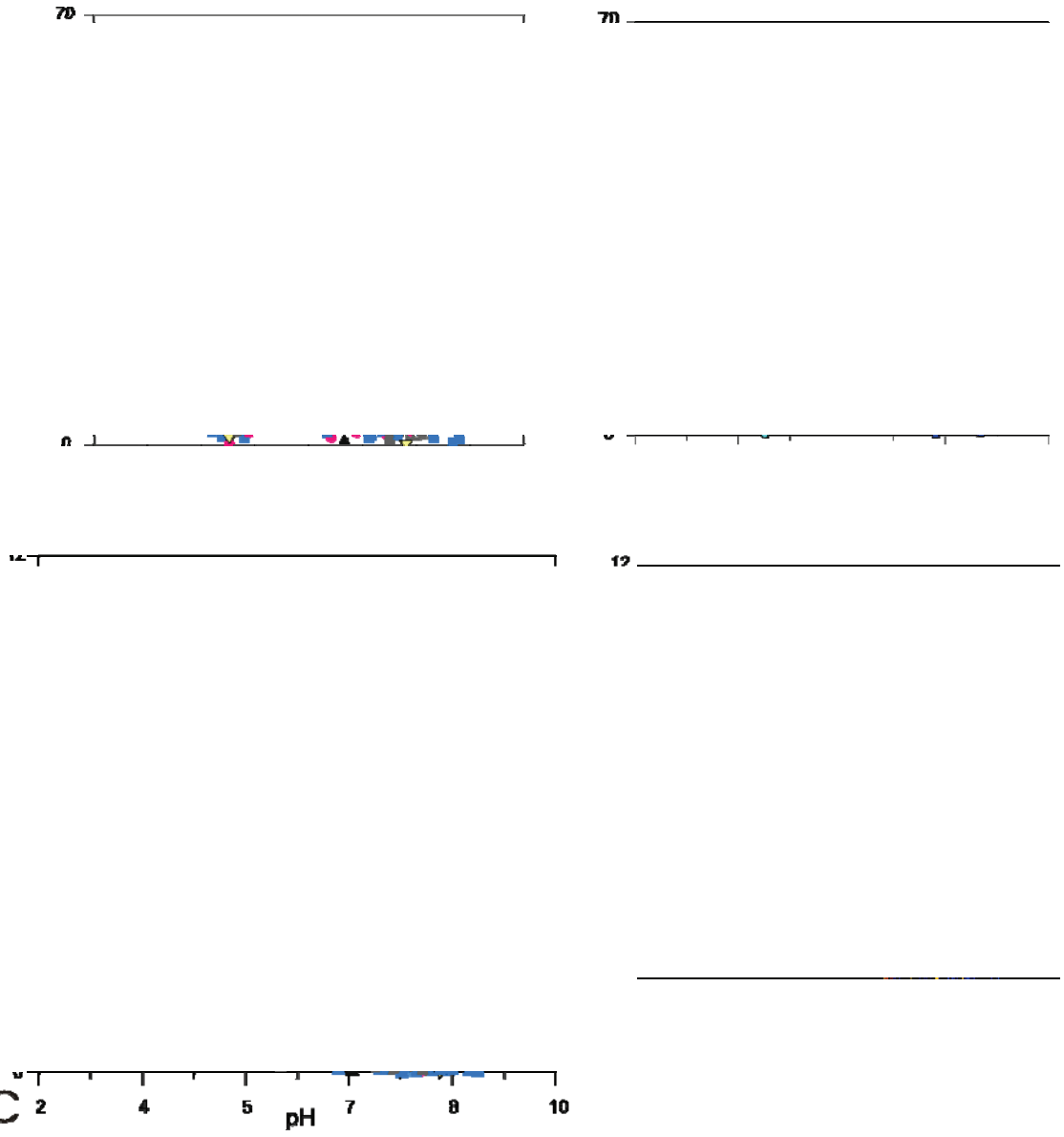
Appendix C: Map of MERA I springs based on data from Hamilton (1990) and Jefferson and Spirito (2003).

APPENDIX D: MERA II SPRING LOCATIONS



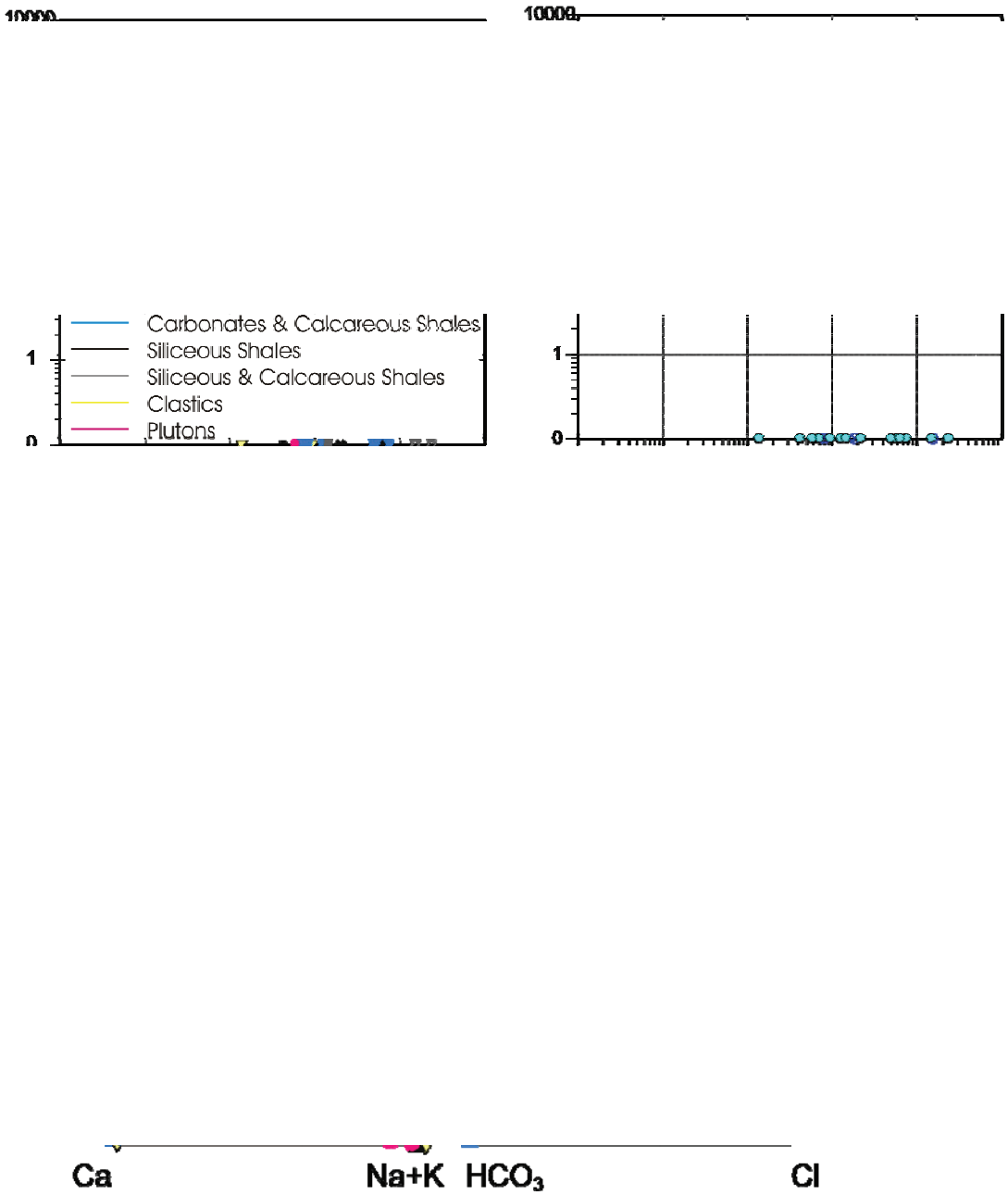
Appendix D: Map of MERA II springs with individual elevated trace elements, % total trace element (T.E.), geochemical groups from Piper Diagram (Group 1-3; Figure 4.2), and Ficklin Diagrams groups (Group E-K; Figure 4.8) for each indicator spring if applicable.

APPENDIX E: PH-TEMPERATURE SCATTER PLOT OF SNRB SPRINGS



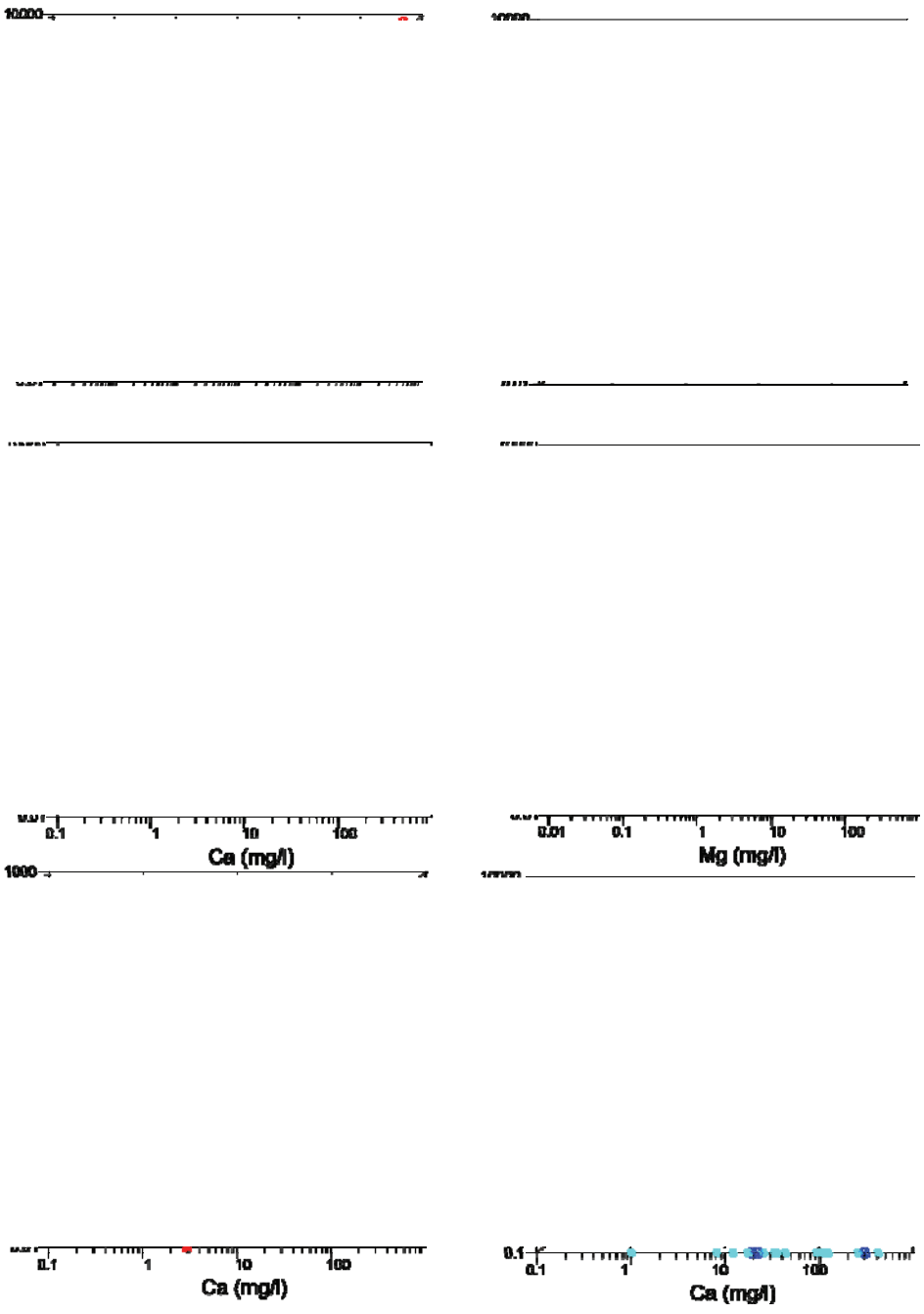
Appendix E: Scatter plots of pH vs. temperature of SNRB springs with symbols relating to the bedrock lithology from which springs discharge (A), and Figure 4.2 (B). Similarly, scatter plots of pH vs. % total trace elements with symbols relating to lithology (C) and Figure 4.2 (D). Lithological groups are based on Okulitch (2005). More than half of basic springs are discharging from carbonates or calcareous shale, while more than half of acidic springs are discharging from siliceous shales. Springs with total trace elements > 0.9% cluster in cold or hot groups and acidic or basic groups. There are no warm or hot acidic springs, nor any warm springs with above average total trace elements (> 0.9 % T.E.) - except for 86-020 from MERA I, a discharge from inside Tungsten Mine.

APPENDIX F: HCO_3-SO_4 SCATTER PLOT AND ALTERNATE PIPER PLOT



Appendix F: Scatter plots of HCO_3 and SO_4 with symbols relating to the bedrock lithology from which springs discharge from (A; Okulitch, 2005) and Figure 4.2 groups (B). Piper plot shows the springs grouped by lithology (C). Shales tend to be relatively richer in sulphate, while carbonates tend to be richer in bicarbonate, although there is a large amount of overlap.

APPENDIX G: MAJOR ION SCATTER PLOTS (R > 0.5)



Appendix G: Scatter plots of different major ions in the SNRB with corresponding R values. Most of the data generally line up with the 1:1 slope lines. Symbols are the same as those in the piper plot of Figure 4.2.

APPENDIX H: TABLES OF SPRING GROUPINGS WITH ELEVATED TOTAL TRACE ELEMENTS (T.E. > 0.9%)

Appendix H – Table 1: List of cold (T < 12 ºC) and basic (pH > 7) springs with elevated total trace elements (i.e.: Group 1 of Figure 4.2) and their associated lithological grouping based on Okulitch (2005) descriptions.

Spring Name (MERA I and II)	Lithological Grouping	Formation	*Shale Type*
Cathedral	Shale	Fort Simpson	*siliceous & calcareous*
Sombre (I & II)	Carbonate	lmDC	
Glacier Lake	Carbonate	Rabbitkettle Fm	
86-004	Carbonate	Rabbitkettle Fm	
86-015 (Glacier Lake)	Carbonate	Rabbitkettle Fm	
86-017	Carbonate	Rabbitkettle Fm	
86-035	Carbonate	Rabbitkettle Fm	
86-037	Shale	Earn Group	*siliceous*
86-048	Carbonate	Haywire Fm	
86-054	Carbonate	Sapper Fm	
86-055	Carbonate	Sapper Fm	
86-062	Shale	Besa River Fm	*siliceous & calcareous*
86-067 (Prairie Creek Mine Water)	Shale	Road River Fm	*calcareous*
86-078	Shale	Besa River Fm	*siliceous & calcareous*
87-103	Carbonate	Sapper Fm	
87-109	Clastic	Mattson Fm	

GROUP 1 SUMMARY
11 carbonates
4 siliceous & calcareous shales
1 calcareous shales
1 siliceous shale
1 clastic

Appendix H – Table 2: List of cold (T < 12 ºC) and acidic (pH < 7) springs with elevated total trace elements (i.e.: Group 2 of Figure 4.2) and their associated lithological grouping based on Okulitch (2005) descriptions.

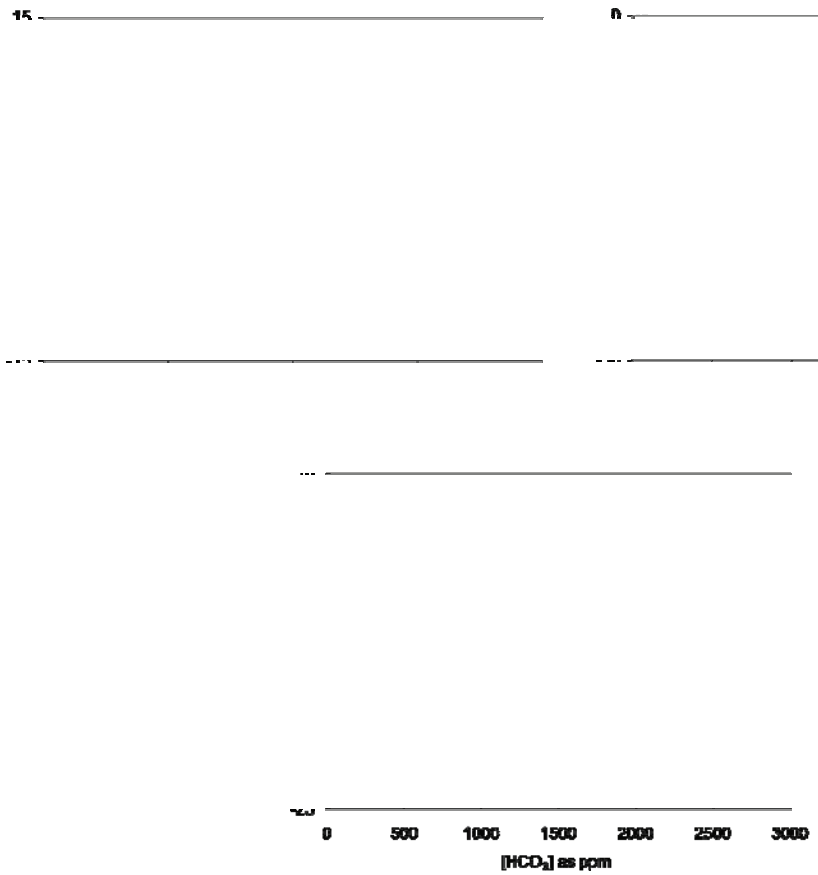
Spring Name (MERA I and II)	Lithological Grouping	Formation	*Shale Type*	GROUP 2 SUMMARY
Cotton	Shale	Earn Group	*siliceous*	7 siliceous shale
Red Mini	Shale	Earn Group	*siliceous*	3 siliceous & calcareous shale
Bougere	Shale	Earn Group	*siliceous*	5 carbonate
Overflow	Pluton	Kqm		1 calcareous shale
Interpluton	Pluton	Kqm		3 pluton
Orange Creek	Shale	Besa River Fm	*siliceous & calcareous*	2 clastic
86-025	Carbonate	Sapper Fm		
86-036	Shale	Earn Group	*siliceous*	
86-042	Shale	Hume Fm	*siliceous*	
86-049	Carbonate	Haywire Fm		
86-069 (Twisted Mountain)	Carbonate	Flett Fm		
86-070	Carbonate	Flett Fm		
86-071	Shale	Yohin & Clausen	*siliceous*	
86-072B / 87-072B (near Meilleur River)	Shale	Fort Simpson Fm	*siliceous & calcareous*	
86-080	Clastic	Mattson Fm		
87-100	Pluton	Kqm		
87-105	???	???		
87-108	Clastic	Mattson Fm		
87-121	Shale	Yohin & Clausen	*siliceous*	
Softie	Shale	Road River Fm	*calcareous*	
86-072A (near Meilleur River)	Shale	Fort Simpson Fm	*siliceous & calcareous*	
86-012 / 86-012B	Carbonate	Rabbitkettle Fm		

Appendix H – Table 3: List of hot (T > 40 ºC) and basic (pH > 7) springs with elevated total trace elements (i.e.: Group 3 of Figure 4.2) and their associated lithological grouping based on Okulitch (2005) descriptions.

	Spring Name (MERA I and II)	Lithological Grouping	Formation	% T.E.	GROUP 3 SUMMARY
	Nahanni North / Lened Creek / 86-033 / 87-033	Clastic	ECv	0.52	1 clastic (4 x)
	Nahanni Headwaters / 86-038	Shale	CPMC	**0.93**	1 siliceous shale (2 x)
	Hole-in-the-Wall / 86-052 / 87-052 / 86-053 / 87-053	Pluton	Kqm2	**1.43**	1 calcareous shale (2 x)
Na-Rich	West Cantung / 86-018 / 87-018	Carbonate	ICSe	**1.42**	1 pluton (5 x)
	86-060 / 87-060 (Cantung East)	Shale	O-DRR	**1.48**	2 carbonates
	86-020 (Cantung Mine Water)	Carbonate	ICSe	**1.00**	
	Average			1.13±0.30	
	South Redstone	Carbonate	OSW	0.45	
	Moore's / 86-032	Carbonate	CSH	0.18	
Ca-Rich	Broken Skull Upper Pool / 86-040 / 87-041	Shale	mDF	0.38	
	Grizzle Bear / 86-043	Carbonate	CSH	0.22	
	Average			0.31±0.13	
NaCl	Ekwi	Carbonate	PLD	0.03	

APPENDIX I: SIGNS OF DEEP CIRCULATION – C AND HE ISOTOPES AND FAULTS/FRACTURES

Appendix I-1: $\delta^{13}C$ of four different gaseous components (free and aqueous CO_2 and CH_4) in SNRB springs. Some $\delta^{13}C_{CO2(g)}$ values fall in the mantle zone as previously defined by Irwin and Barnes (1980), Giggenbach et al. (1991) and Whiticar (1999). Spring names with stars (*) are gaseous, i.e.: continuously discharging gas bubbles. BS = Broken Skull, U = Upper Pool, L = Lower Pool, 03 = sampled in 2003, Champ. = Champagne, FF = Flat Fruit, GB = Grizzle Bear, dup = field duplicate, g = gaseous, aq = aqueous.



Appendix I-2: Exploring SNRB bicarbonate trends. Diagrams in A & B show typical fractionations according to Fritz and Clark (1997). A) $\delta^{13}C_{CaCO3}$ and $\delta^{13}C_{HCO3}$ – Dissolved bicarbonate $\delta^{13}C$ is strongly correlated to that of precipitated bicarbonate found at spring outlets. B) $\delta^{13}C_{CO2(aq)}$ and $\delta^{13}C_{HCO3}$ – Dissolved carbon dioxide $\delta^{13}C$ is strongly correlated to that of dissolved bicarbonate. C) $\delta^{13}C_{HCO3}$ and [HCO_3] as ppm – Similar trends are found in springs of the southern Cordillera, showing a significant contribution of high $\delta^{13}C$ bicarbonate to high alkalinity waters (Grasby et al., 2000).

I.1. Carbon Isotopes

SNRB gas-discharging springs have $\delta^{13}C$ values that can help pinpoint the source of the gas as plotted in Figure I-1. The aqueous CO_2 is closely inter-related to aqueous bicarbonate and solid calcium carbonate $\delta^{13}C$ values (Figure I-2) following naturally expected fractionations (Clark and Fritz, 1997). On the other hand, mantle-derived CO_2 has been documented as having values of $\delta^{13}C_{CO2(g)}$ between -4 and -8 ‰ (e.g.: Irwin and Barnes, 1980; Giggenbach et al., 1991; Whiticar, 1999) with some reports of mantle degassing being as high as -3.4 ‰ (Hamilton et al., 1990). Values above this range are typical of metamorphic decarbonation reactions, likely related to the plutonic intrusions into the country rock in the SNRB (Hamilton et al., 1990). Therefore, Grizzle Bear (GB) and Broken Skull (BS) could potentially be mantle-derived CO_2 (Figure I-1). The springs are thought to be a mixture of 3-5 km deep fluids and shallow, <35 year old, meteoric water (Hamilton et al, 1990). Similar gaseous springs with confirmed mantle sources in the Grand Canyon area of the United States have corresponding $\delta^{13}C_{CO2}$ values between -1.0 and -4.6 ‰, meaning that Brimstone, Champagne and Flat Fruit gaseous SNRB springs may also be included as having a mantle-derived component due to this comparison.

Additionally, Broken Skull's unusually high $\delta^{13}C_{CH4}$ (duplicates at 1.8 and -0.1‰) also suggests a mantle source (Whiticar, 1999). Hamilton et al. (1990) proposes a model for the mixing of both metamorphic and mantle-source carbon in the high pCO_2 springs of the SNRB. The other $\delta^{13}C_{CH4}$ values of -40, -49, and -81 ‰ are typical of thermogenic

methane (Grizzle Bear) and biogenic methane (Twitya and Champagne); (Whiticar, 1999).

I.2. Helium Isotopes

Helium samples were collected in 30 cm lengths of 0.95 mm diameter copper tubes sealed with cold welds, which were submerged in the springs near the gas discharges holes for 1 week, and analyzed by Dr. Ian Clark and Nicolas Utting at the University of Ottawa using high-sensitivity branch-tube mass spectrometry. Results are reported as R/R_A, and by definition, $R/R_A = (^3He/^4He_{(sample)})/(^3He/^4He_{(air)})$.

Appendix I - Table 1: Helium Isotopes Results

Spring Name	R/R_A*
Broken Skull Hot Spring	0.13
Tungsten Hot Spring	0.14
Flat Fruit Cold Spring	1.57
Brimstone Cold Spring	1.27

Excess ^3He ($R/R_A > 0.1$) is known to be indicative of mantle-derived fluids (Welhan et al., 1979; Giggenbach et al., 1993; Crossey et al., 2006), such as in the sampled gaseous springs listed above in Table 1. Fault-related, high pCO_2 springs in the Grand Canyon of the United States were found to be a mixture of deep mantle-derived fluids with shallow meteoric water (Crossey et al., 2006), with similar R/R_A values to what is found in the SNRB. Pure mantle gas discharges have been associated with R/R_A values as high as 16 in Yellowstone National Park and Iceland (Welhan et al., 1988). Crossey at al. (2006) emphasize that mantle-derived helium (^3He) is more common than people are aware, and is present in a wide variety of thermal and non-thermal springs world-wide.

I.3. Location of Springs near Large Linear Features

Springs on or near faults, fractures, folds and major contacts potentially circulate more deeply than other springs (e.g.: Flat River Valley). Actually, most springs in the SNRB are located near one of the above, as also described by Hamilton et al. (1988), Hamilton et al. (1990) and Gulley (1993) and as shown in Figure 2.1. The exceptions are: Waterfall, Half Spring, Darkness, Jacson, Clearwater Creek, Boulder, Interpluton Seep, 86-081, 86-062, 86-038, 86-047, 82-046, 86-060, 86-035, 86-036, 86-009, and 86-007. These springs are considered to be the shallowest of springs.

APPENDIX J: EXTRA BACKGROUND GEOLOGY NOTES

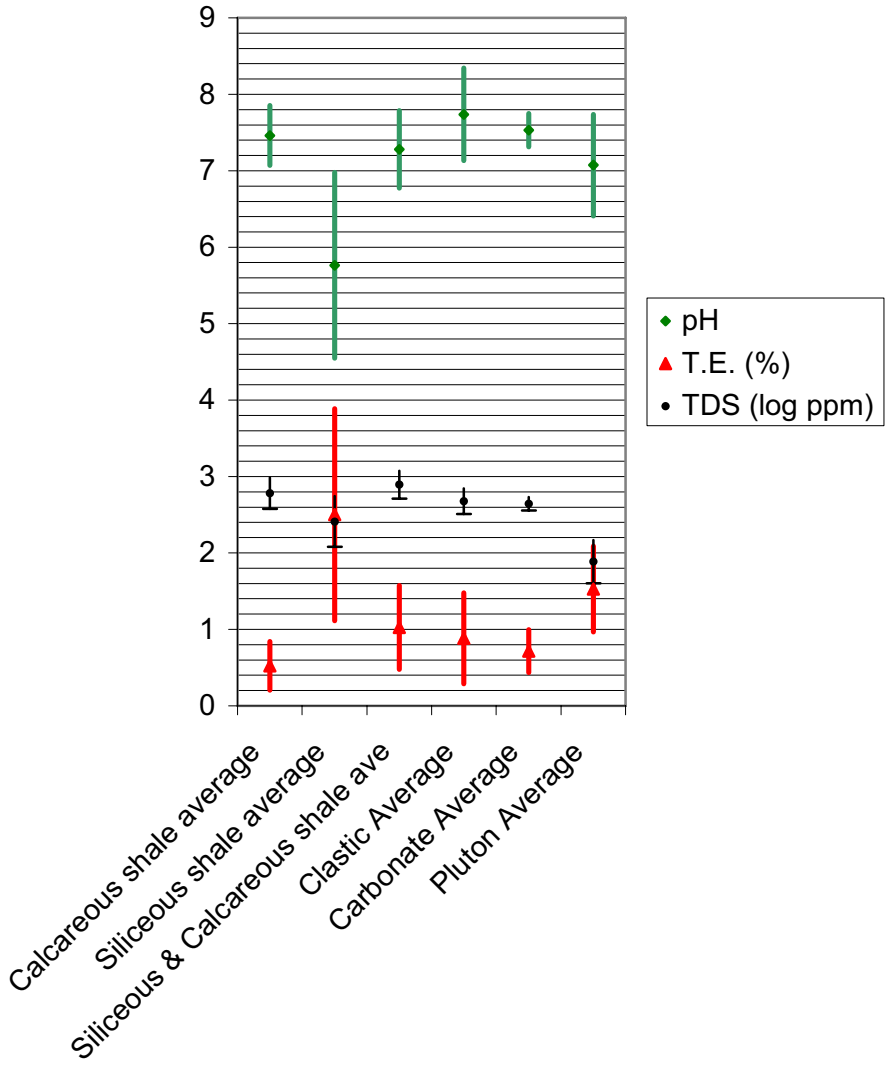
Tight, upright to strongly overturned folds are common in the south-eastern part of the Selwyn Basin, particularly in the incompetent basinal shale strata where they are pushed against the relatively competent buttress of the west flank of the Redstone Arch (a regional cross-section by R.J.W. Douglas and H. Gabrielse is available in Douglas (1970). The ability of a great volume of incompetent sediments to accommodate compressive stress may be a cause of the structural style differences between Mackenzie Mountains and Rocky Mountains (Gabrielse et al., 1965). There is a deep detachment in Proterozoic strata beneath the Mackenzie Mountains, which has been related to the much shallower detachment in Upper Cambrian salt beds beneath the northern Franklin Mountains (Cook and MacLean, 1999).

Continental heat flux is very complex, and is a sum of mantle flux, contributions of radiogenic elements in the crust, and the transient effect of recent tecto-magnetic events. After an orogeny it usually takes at least 200 millions years for complete cooling to occur. The heat flow depends on the history of the orogenic region and the amount of radioactive elements in the crust. Due to the lessening of these elements from weathering and decay the amount of heat released from the crust decreases with time (Hamdani, 1997).

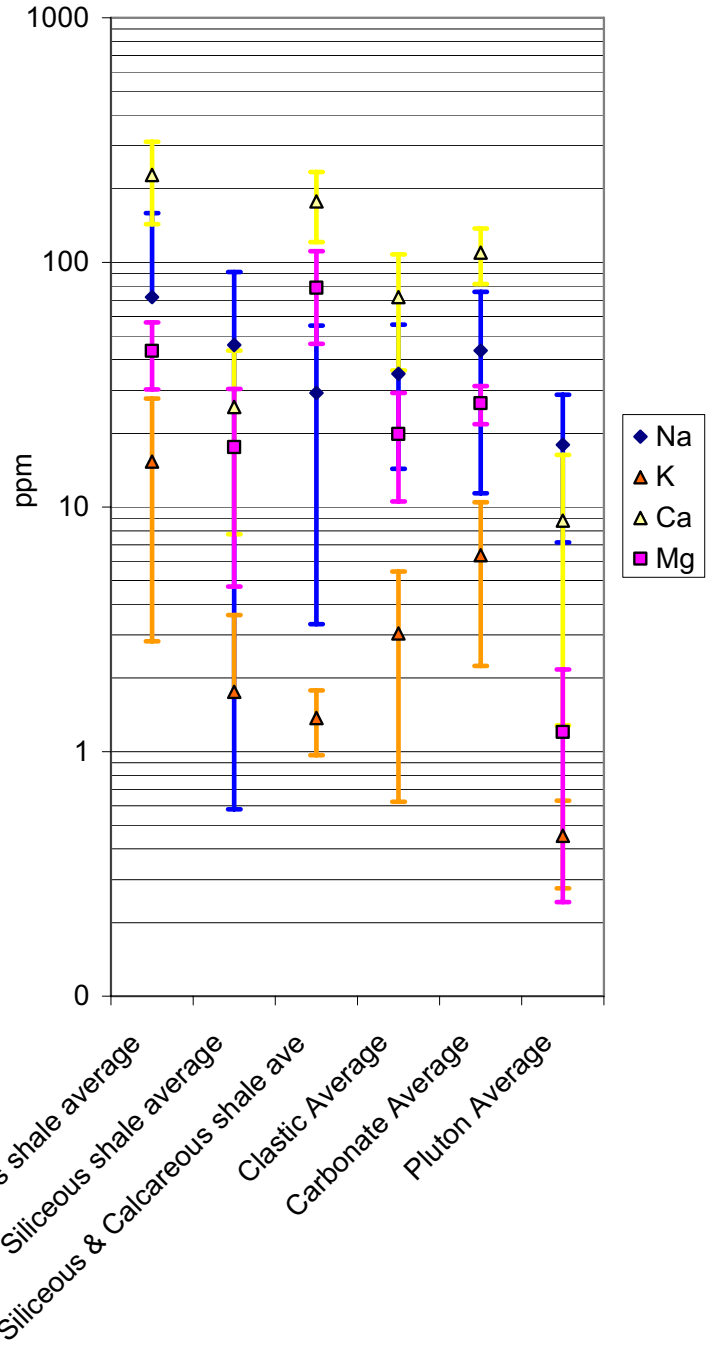
A mechanism that has been proposed to explain the rising of granitic magma in the continental crust such as the Cretaceous Selwyn Plutonic Suite in the Mackenzie

Mountains, includes basaltic magma as a heat source (Nelson, 2003). The basaltic magma is generated in the mantle, and then rises into the continental crust. But, because basaltic magma has a high density it may stop in the crust and crystallize, releasing heat into the surrounding crust. This raises the geothermal gradient and may cause wet partial melting of the crust to produce rhyolitic or granitic magmas (Nelson, 2003). Most of this magma appears to result from wet melting of continental crust, and usually contains quartz, feldspar, hornblende, biotite, and muscovite, indicating high water content.

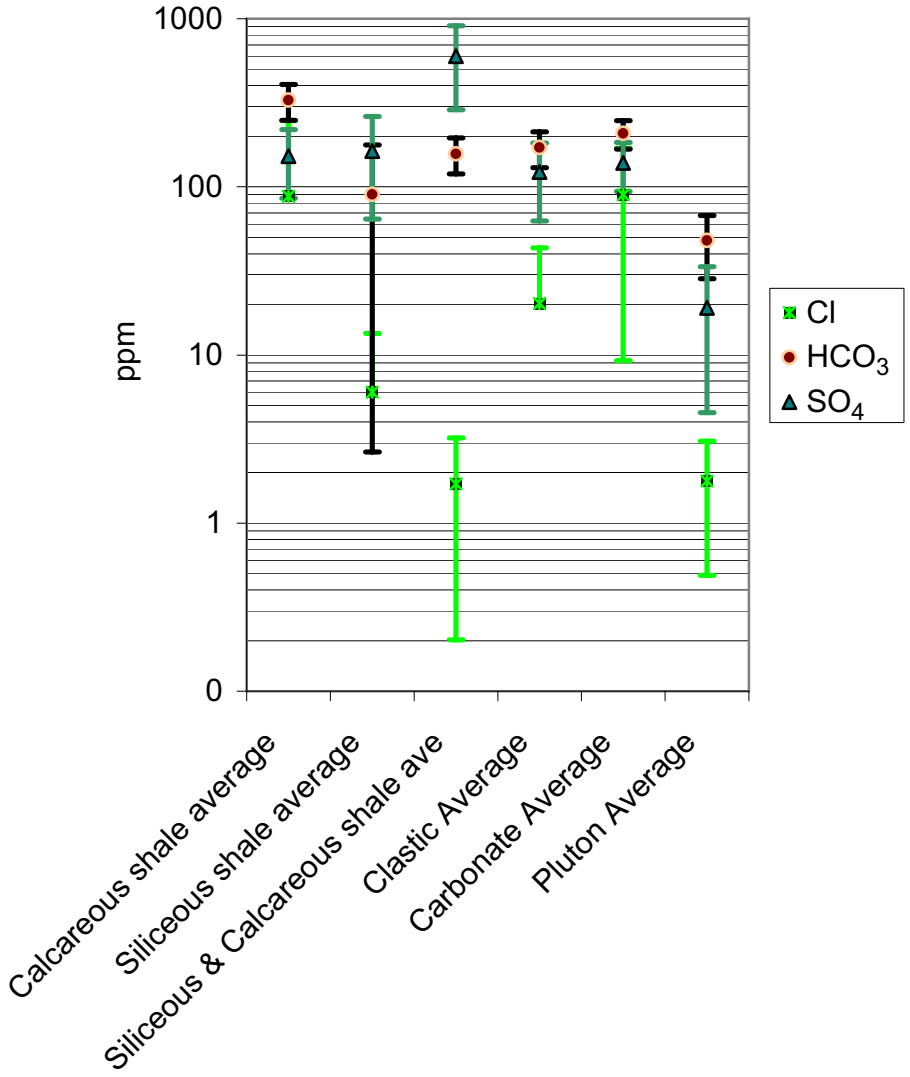
APPENDIX K: CONFIDENCE INTERVALS AT THE 0.05 SIGNIFICANCE LEVEL



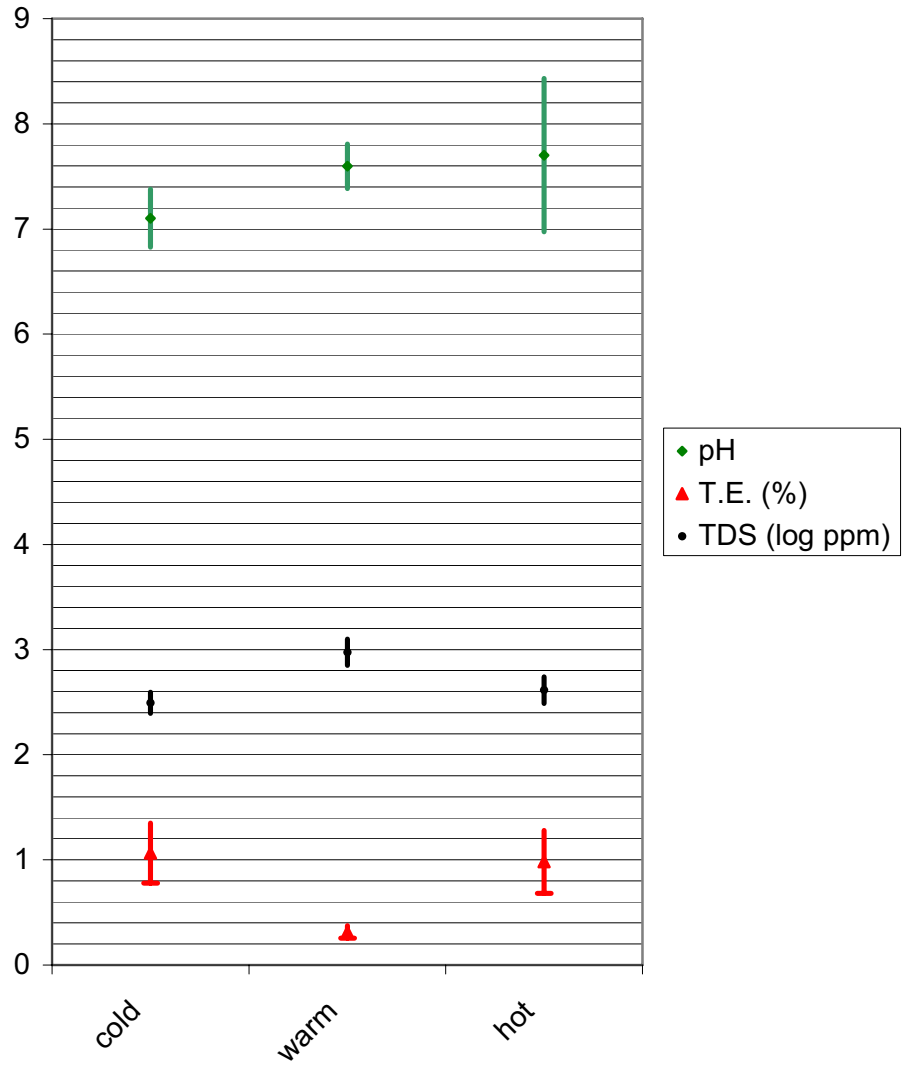
Appendix K-1: Confidence intervals at the 0.05 significance level for pH, total trace elements (T.E.) and total dissolved solids (TDS) in springs divided by bedrock lithology from which they discharge according to Okulitch (2005).



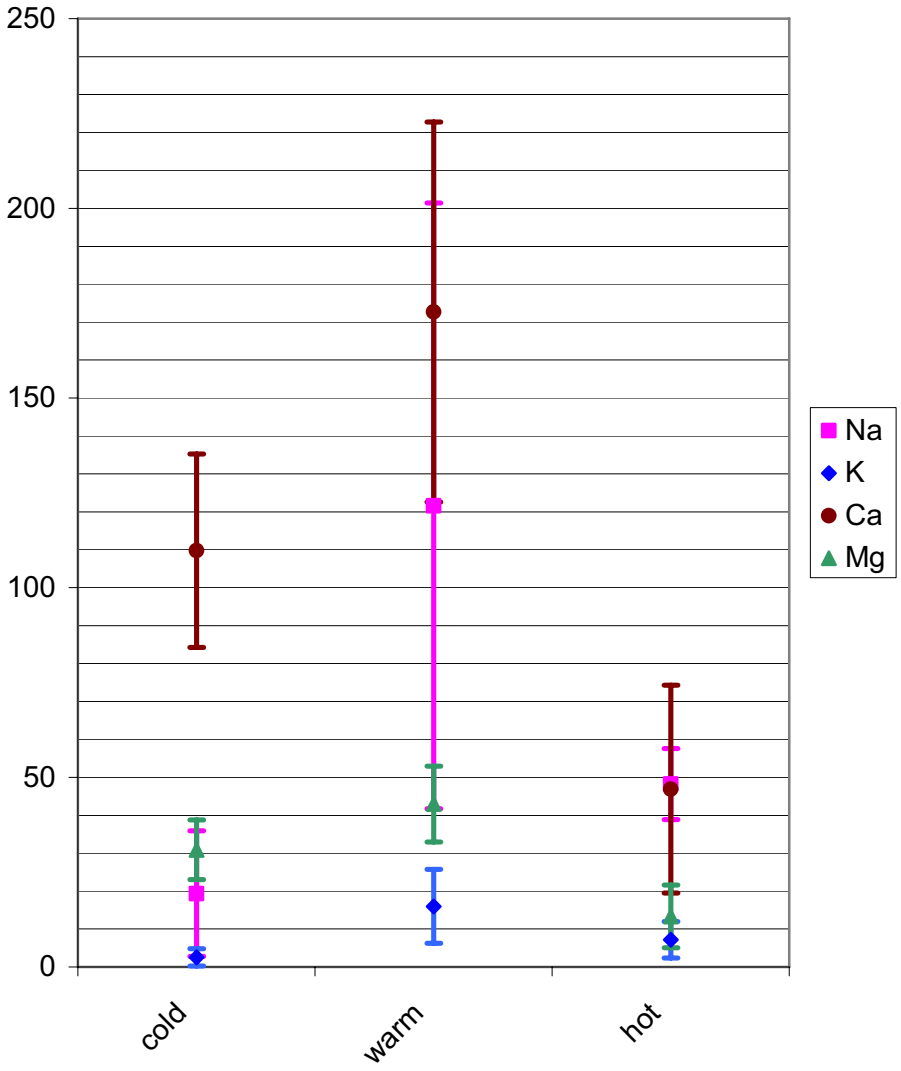
Appendix K-2: Confidence intervals at the 0.05 significance level for cations in springs divided by bedrock lithology from which they discharge according to Okulitch (2005).



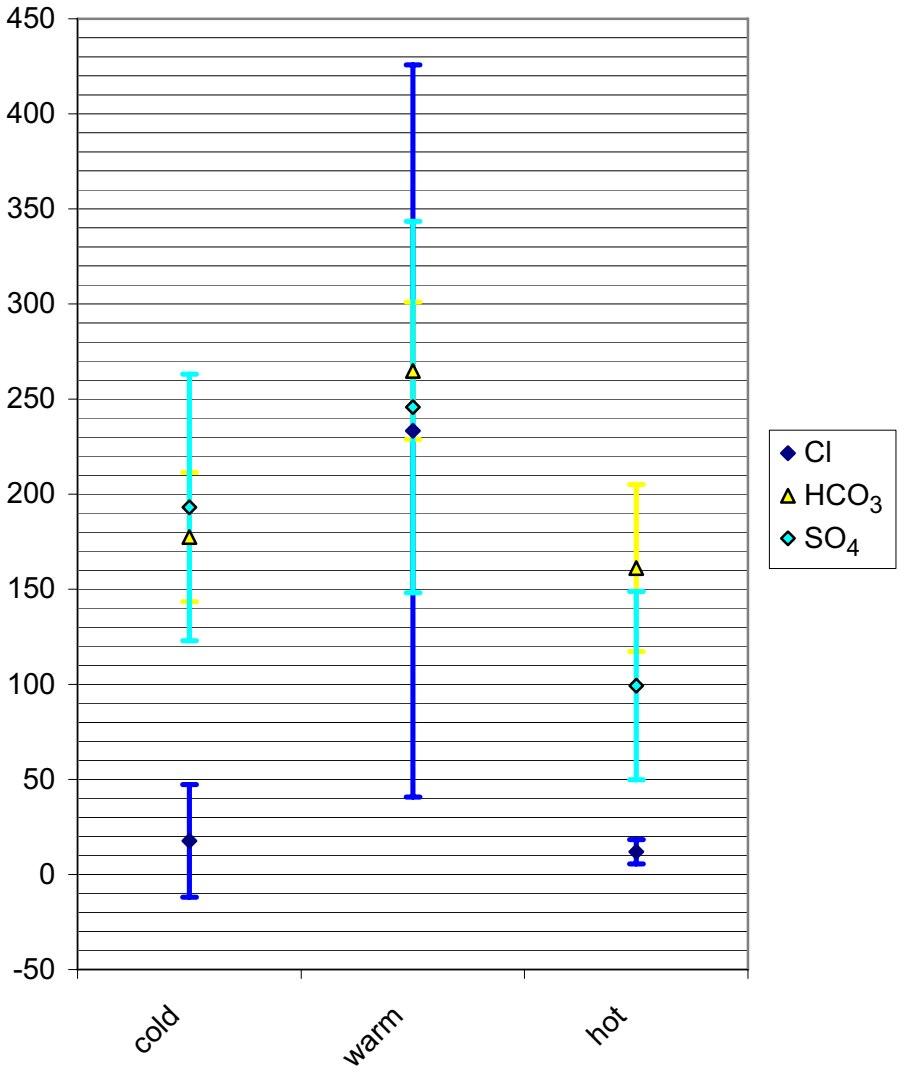
Appendix K-3: Confidence intervals at the 0.05 significance level for anions in springs divided by bedrock lithology from which they discharge according to Okulitch (2005).



Appendix K-4: Confidence intervals at the 0.05 significance level for pH, total trace elements (T.E.) and total dissolved solids (TDS) in springs divided by temperature groupings.



Appendix K-5: Confidence intervals at the 0.05 significance level for cations in springs divided by temperature groupings.



Appendix K-6: Confidence intervals at the 0.05 significance level for anions in springs divided by temperature groupings.

Bibliography

Al-Aasm, I.S., Morad, S., Durocher, S. and Muir, I. 1996. Sedimentology, C-S-Fe relationships and stable isotopic compositions in Devonian black mudrocks, Mackenzie Mountains, Northwest Territories, Canada. Sedimentary Geology 106: 279-298.

Allen, D.M., and Michel, F.A. 1998. Evaluation of multi-well test data in a faulted aquifer using linear and radial flow models. Groundwater 36: 938–948.

Anderson, R.G., 1983. Selwyn plutonic suite and its relationship to tungsten skarn mineralization, southeastern Yukon and District of Mackenzie. Current Research, Part B, Geological Survey of Canada, Paper 83-1B, p. 1151-163.

Appelo, C.A.J. and Postma, D. 1999. Geochemistry, groundwater and pollution. A.A. Balkema Publishers, Rotterdam, Netherlands. 536 pp.

Arnorsson, S., 1983. Chemical equilibria in Icelandic geothermal systems. Implications for chemical geothermometry investigations. Geothermics 12, 119– 128.

Arnorsson, S. and Andresdottir, A. 1995. Processes controlling the distribution of boron and chlorine in natural waters in Iceland. Geochimica et Cosmochimica Acta 59: 4125-4146.

Avila, P.F., Santos Oliveira, J.M., Ferreira da Sila, E. and Cardoso Fonseca, E. 2005. Geochemical signatures and mechanisms of trace elements dispersion in the area of the Vale das Gatas mine (Northern Portugal). Journal of Geochemical Exploration 85: 17-29.

Banks, D., Markland, H., Smith, P.V., Mendez, C., Rodriguez, J., Huerta, A., and Saether, O.M. 2004. Distribution, salinity and pH dependence of elements in surface waters of the catchment areas of the Salars of Coipasa and Uyuni, Bolivian Altiplano. Journal of Geochemical Exploration 84: 141-166.

Bildstein, O., Worden, R.H. and Brosse, E. 2001. Assessment of anhydrite dissolution as the rate-limiting step during thermochemical sulfate reduction. Chemical Geology 176: 173-189.

Blusson, S. L. 1968. Geology and Tungsten deposits near the headwaters of Flat River, Yukon Territory and Southwestern District of Mackenzie, Canada. Geological Survey of Canada Paper 67-22.

Boschetti, T., Venturelli, G., Toscani, L., Barbieri, M. and Mucchino, C. 2005. The Bagni di Luca thermal waters (Tuscany, Italy): an example of Ca-SO4 waters with high Na/Cl and low Ca/SO4 ratios. Journal of Hydrology 307: 270-293.

Brandon, L.V. 1965. Groundwater and Water Supply in the District of Mackenzie, Yukon Territory, and Adjoining Parts of British Columbia. Geological Survey of Canada Paper 64-39, 102pp.

Brook, G.A. and Ford, D.C. 1980. Hydrology of the Nahanni Karst, Northern Canada, and the Importance of Extreme Summer Storms. Journal of Hydrology 46: 103-121.

Brunner, B. and Bernasconi, S.M. 2005. A revised isotope fractionation model for dissimilatory sulfate reduction in sulfate reducing bacteria. Geochimica et Cosmochimica Acta 69: 4759-4771.

Caine, J.S., Evans, J.P. and Forster, C.B. 1996. Fault zone architecture and permeability structure. Geology 24: 1025-1028.

Cameron, E.M. 1978. Hydrogeochemical methods for base metal exploration in the northern Canadian Shield. Journal of Geochemical Exploration 10: 219-243.

Canadian Council on Ecological Areas (CCEA) and Environment Canada. Ecozones of Canada. Available online at http://www.ccea.org/ecozones/. First published by Wiken, 1986. Last updated 2006. Last accessed on April 8, 2006.

Carpenter, A.B. 1978. Origin and chemical evolution of brines in sedimentary basins. Oklahoma Geological Survey Circulation 79: 589-606.

Carrillo-Chavez, A., Morton-Bermea, O., Gonzalez-Partida, E., Rivas-Solorzano, H., Oesler, G., Garcia-Meza, V., Hernandez, E., Morales, P. and Cienfuegos, E. 2003. Environmental geochemistry of the Guanajuato Mining District, Mexico. Ore Geology Reviews 23: 277-297.

CCME (Canadian Council of Ministers of the Environment) 2006. Guidelines for Canadian Drinking Water Quality Summary Table. Committee on Drinking Water, Health Canada, Government of Canada, March 2006.

Choi, H-S., Koh, Y-K., Bae, D-S., Park, S-S., Hutcheon, I. and Yun, S-T. 2005. Estimation of deep-reservoir temperature of CO_2-rich springs in Kangwon district, South Korea. Journal of Volcanology and Geothermal Research 141, 77-89.

Clark, I.D. and Fritz, P. Environmental Isotopes in Hydrogeology. Lewis Publishers, New York © 1997.

Clark, I.D., Fritz, P. and Michel, F. 1980. Isotope Hydrogeology and Geothermometry of the Mount Meager Geothermal Area – Final Report. Office of Research Administration, University of Waterloo, Incorporating the Waterloo Research Institute, Project No. 707-10-03. Prepared for Energy, Mines and Resources, Open File 1015.

Claypool, G.E., Holser, W.T., Kaplan, I.R., Sakai, H. and Zak, I. 1980. The age curves of sulfur and oxygen isotopes in marine sulfate and their mutual interpretation. Chemical Geology 28: 199-260.

Cody, J. 1989. Geochemistry of the thermal springs of the Rocky Mountains, southern Alberta and British Columbia. University of Calgary Undergraduate Thesis, 28 pp.

Coleman, M.L., Shepherd, T.J., Durham, J.J., Rouse, J.E., Moore, G.R., 1982, Reduction of water with zinc for hydrogen isotope analysis. Analytical Chemistry 54: 993-995.

Cook, D.G. and MacLean, B.C. 1999. The Imperial anticline, a fault-bend fold above a bedding-parallel thrust ramp, Northwest Territories, Canada. Journal of Structural Geology 21:215-228.

Coplen, T.B. and Krouse, H.R. 1998. Sulphur isotope data consistency improved. Nature (London) 392 (6671) p.32.

Coplen, T.B., Kendall, C. and Hopple, J., 1983. Comparison of stable isotope reference samples. Nature (London), 302: 236-238.

Cox, D.P. and Singer, D.A. (editors) 1986. Mineral Deposit Models. U.S. Geological Survey Bulletin 1693, 379p.

Crandall, J.T. and Sadlier-Brown, T.L. 1976. Data on geothermal areas: Cordilleran Yukon, Northwest Territories, and adjacent British Columbia. Departmrnt of Supply and Services, Department of Energy, Mines and Resources, Canada. Contract Number 1SQ5-0136.

Crossey, L.J., Fischer, T.P., Patchett, P.J., Karlstrom, K.E., Hilton, D.R., Newell, D.L., Huntoon, P., Reynolds, A.C. and de Leeuw, G.A.M. 2006. Dissected hydrologic system at the Grand Canyon: Interaction between deeply derived fluids and plateau aquifer waters in modern springs and travertine. Geology 34: 25-28.

D'Amore, F., Fancelli, R., Caboi, R., 1987. Observations on the application of chemical geothermometers to some hydrothermal systems in Sardinia. Geothermics 16, 271– 282.

De Caritat, P. and Kirste, D. 2005. Hydrogeochemistry applied to mineral exploration under cover in the Curnamona Province. MESA Journal 37: 13-17.

De Caritat, P., Kirste, D., Carr, G., and McCullogh, M. 2005. Groundwater in the Broken Hill region, Australia: recognizing interaction with bedrock and mineralisation using S, Sr and Pb isotopes. Applied Geochemistry 20: 767-787.

Deering, M.F., Mohr, E.T., Sypniewski, B.F. and Carlson, E.H. 1983. Regional hydrogeochemical patterns in ground water of northwestern Ohio and their relation to Mississippi Valley-type mineral occurrences. Journal of Geochemical Exploration 19: 225-241.

Detmers J., Brüchert V., Habicht K. S., and Kuever J. (2001) Diversity of sulfur isotope fractionations by sulfate-reducing prokaryotes. Applied and Environmental Microbiology 67: 888–894.

Donnelly, T., Waldron, S., Tait, A., Dougans, J., Bearhop, S., 2001: Hydrogen isotope analysis of natural abundance and deuterium-enriched waters by reduction over chromium on-line to a dynamic dual inlet isotope-ratio mass spectrometer, 2001; 15: 1297-1303.

Douglas, R.J.W. (Editor) 1970. Geology and Economic Minerals of Canada. Geological Survey of Canada, Economic Geology Report No. 1 © Crown Copyrights, Ottawa, Canada.

Druschel, G.K and Rosenberg, P.E. 2001. Non-magnatic fracture-controlled hydrothermal systems in the Idaho Batholith: South Fork Payette geothermal system. Chemical Geology 173: 271-291.

Du Bray, E.A. (editor) 1995. Preliminary Compilation of Descriptive Geoenvironmental Mineral Deposit Models. U.S. Geological Survey Open-File Report 95-931.

Duk-Rodkin, A. and Lemmen, D.S. 2000. The physical environment of the Mackenzie Valley, Northwest Territories: a base line for the assessment of environmental change. Bulletin – Geological Survey of Canada, Report 547: 11-20.

Duk-Rodkin, A., Barendregt, R.W., Froese, D.G., Weber, F., Enkin, R., Smith, R.I., Zazula, G.D., Waters, P. and Klassen, R. 2004. Timing and extent of Plio-Pleistocene glaciations in north-western Canada and east-central Alaska. In: Quaternary Glaciations - Extent and Chronology, Part II (J. Ehlers and P.L. Gibbard, eds.), pp. 313-345.

Edmunds, W.M. 1996. Bromine geochemistry of British groundwaters. Mineralogical Magazine 60:275-284.

Eppinger, R.G., Briggs, P.H., Crock, J.G., Meier, Al.L., Sutley, S.J. and Theodorakos, P.M. 2002. Environmental-geochemical study of the Slate Creek antimony deposit,

Kantisha Hills, Denali National Park and Preserve, Alaska. U.S.Geological Survey Professional Paper 1662: 123-141.

Eppinger, R.G., Briggs, P.H., Rosenkrans, D. and Ballestrazze, V. 2000. Environmental Geochemical Studies of Selected Mineral Deposits in Wrangell-St.Elias National Park and Preserve, Alaska. U.S. Geological Survey Professional Paper 1619, 47 p.

Epstein, S. and T. K. Mayeda, 1953. Variation of ^{18}O content of waters from natural sources. Geochimica et Cosmochimica Acta, 4: 213-224.

Finlayson, B.L. and Webb, J.A. 1988. Evolution of groundwater in Californian granites: Evidence from speleothems. Geological Society of America Bulletin 100: 639-643.

Ford, D.C. 1973. Development of the Canyons of the South Nahanni River, N.W.T., CJES, 10: 366-378.

Ford, D.C. 1976. Evidences of multiple glaciation in South Nahanni National Park, Mackenzie Mountains, Northwest Territories. Canadian Journal of Earth Sciences 13:1433-1445.

Fortescue, J.A.C. 1992. Landscape geochemistry – Retrospect and prospect – 1990. Applied Geochemistry 7: 1-53.

Forster, C., and Smith, L. 1988. Groundwater flow systems in mountainous terrain 2: Controlling factors. Water Resources Research 24: 1011–1023.

Fournier, R.O. 1981. Application of water geochemistry to geothermal exploration and reservoir engineering. *In:* Rybach, L. and Muffler, L.J.P. (editors) 1981. Geothermal Systems: Principles and Case Histories. Chichester, John Wiley & Sons Limited, p. 109-143.

Fournier, R.O., Truesdell, A.M., 1973. An empirical Na–K–Ca geothermometer for natural waters. Geochimica et Cosmochimica Acta 43: 1543–1550.

Freeze, R.A. and Cherry, J.A. 1979. Groundwater. Prentice-Hall, Inc., Englewood Cliffs, New Jersey, 604 pp.

Friedman, I., 1953. Deuterium content of natural water and other substances: Geochimica et Cosmochimica Acta 4: 89-103.

Friedman, I. and O'Neil, J.R . 1977. Compilation of stable isotope fractionation factors of geochemical interest. *In*: Data of Geochemistry. U.S. Geological Survey Professional Paper 440-KK, 6th ed.

Fritz, P. and Fontes, J.C. (editors) 1980. Handbook of Environmental Isotope Geochemistry: Volume 1 – The Terrestrial Environment. Elsevier Scientific Publishing Company, New York © 1980.

Fritz, P., Drimmie, R.J., Drimmie, S.K., Frape, O'Shea, K. 1987. The isotopic composition of precipitation and groundwater in Canada. IAEA, Vienna (Austria) p. 539-550.

Fritz, P., Basharmal, G.M., Drimmie, R.J., Ibsen, J., and Qureshi, R.M.` 1989. Oxygen isotope exchange between sulphate and water during bacterial reduction of sulphate. Chemical Geology (Isotope Geoscience Section) 79: 99–105.

Gabrielse, H. 1966. Tectonic evolution of the Northern Canadian Cordillera. Canadian Journal of Earth Sciences, 4: 271-298.

Gabrielse, H., Roddick, J.A., and Blusson, S.L. 1965. Flat River, Glacier Lake, and Wrigley Lake, District of Mackenzie and Yukon Territory. Geological Survey of Canada Paper 64-52.

Gehre, M., Hoefling, R., Kowski, P., and Strauch, G. 1996. Sample Preparation Device for Quantitative Hydrogen Isotope Analysis Using Chromium Metal. Analytical Chemistry 68: 4414-4417.

Gendzwill, D.J. 1994. Earthquakes and a review of seismicity in the Canadian North. Musk-Ox, 40: 31-46.

Giblin, A. 2001. Groundwaters – Geochemical Pathfinders to Concealed Ore Deposits. CSIRO Exploration and Mining, Australia, 79 p.

Gibson, J.J. and Prowse, T.D. 2002. Stable isotopes in river ice: identifying primary over-winter streamflow signals and their hydrological significance. Hydrological Processes 16: 873–890.

Giggenbach, W.F. 1988. Geothermal solute equilibria. Derivation of Na-K-Mg-Ca geoindicators. Geochimica et Cosmochimica Acta 52: 2749-2765.

Giggenbach, W.F., Sano, Y. and Schminke, H.U. 1991. CO_2-rich gases from Lakes Nyos and Monoun, Cameroon; Lacher See, Germany; Dieng, Indonesia, and Mt. Gambier, Australia – variations on a common theme. Journal of Volcanology and Geothermal Research 45: 311-323.

Giggenbach, W.F., Sano, Y. and Wakita, H. 1993. Isotopic composition of helium, and CO_2 and CH_4 contents in gases produced along the New Zealand part of a convergent plate boundary. Geochimica et Cosmochimica Acta 57: 3427-3455.

GNWT (Minerals, Oil and Gas Division, Department of Industry, Tourism and Investment, Government of Northwest Territories). 2005. A Guide to Mineral Deposits of the Northwest Territories. 204 pp. Available at: http://www.iti.gov.nt.ca/mog/pdf/2005_mindeposits.pdf. Last accessed Oct. 26, 2006.

Goldich, S.S. 1938. A study in rock weathering. Journal of Geology 46: 17-58.

Gordey, S.P., Abbott, J.G. and Orchard, M.J. 1982. Devono—Mississippian (Earn Group) and younger strata in east-central Yukon. *In:* Current Research, Part B, Geological Survey of Canada, Paper 82-1B, p. 93-100.

Gordey, S.P. and Anderson, R.G. 1993. Evolution of the northern Cordilleran Miogeocline, Nahanni Map area (105I), Yukon and Northwest Territories. Geological Survey Memoir 428.

Grasby, S.E. and Hutcheon, I. 2001. Controls on the distribution of thermal springs in the southern Canadian Cordillera. Canadian Journal of Earth Sciences 38(3): 427-440.

Grasby, S.E., Hutcheon, I. and Krouse, H.R. 2000. The influence of water-rock interaction on the chemistry of thermal springs in western Canada. Applied Geochemistry 15: 439-454.

GSC (Geological Survey of Canada). 1986. Physiographic Map of the Canadian Cordillera. Surveys and Mapping Branch Map 1701A.

Gulley, A.L. 1993. Rabbitkettle Hotsprings, Nahanni National Park Reserve, N.W.T.: A Hydrogeological Study. M.Sc. Thesis with the Faculty of Graduate Studies and Research, Carleton University, Ottawa, Canada. 178pp.

Halliwell, D., and Catto, S. 2003. How and why is aquatic quality changing at Nahanni National Park Reserve, NWT, Canada? Environmental Monitoring and Assessment 88: 243-281.

Hamdani, Y. 1997. Flux de chaleur continental. Université du Québec à Montréal (UQAM). Available at: http://www.unites.uqam.ca/terre/flux_de_chaleur/heatc.html. Last accessed on August 25, 2005.

Hamilton, S.M. 1990. The application of spring water geochemistry and hydrogeology to a non-renewable resource assessment of the South Nahanni River area, NWT. M.Sc. Thesis, Ottawa-Carleton Geoscience Center & Department of Earth Sciences, Carleton University, April 1990.

Hamilton, S.M., Michel, F.A. and Jefferson, C.W. 1988. Groundwater geochemistry, South Nahanni resource assessment area, District of Mackenzie. Current, Part E, Geological Survey of Canada, Paper 88-1E, p. 127-136.

Hamilton, S.M., Michel, F.A. and Jefferson, C.W. 1990. CO_2-rich ground waters of the Flat River Valley, NWT. *In:* Prowse, T.D. and Ommanney, C.S.L. (editors) 1990. Northern Hydrology: Selected Perspectives, Proceedings of the Northern Hydrology Symposium, 10-12 July 1990, Saskatoon, Saskatchewan. Edited by Prowse, T.D. and Ommanney, C.S.L.

Hannigan, P.K., 2006. Introduction; in Potential for Carbonate-hosted Lead-zinc Mississippi Valley-type Mineralization in Northern Alberta and Southern Northwest Territories: Geoscience Contributions, Targeted Geoscience Initiative, (ed.) P.K. Hannigan; Geological Survey of Canada, Bulletin 591, p. 9-40.

Hanor, J.S. 1994. Physical and chemical controls on the composition of waters in sedimentary basins. Marine and Petroleum Geology 11: 31-45.

Hem, J.D. 1985. Study and Interpretation of the Chemical Characteristics of Natural Water. U.S. Geological Survey Water-Supply Paper 1473.

Heon, D. (compiler) 2003. Selwyn Basin Metallogeny: An overview of the significant geological features of a world famous SEDEX basin. Yukon Geological Survey. Available at: http://www.geology.gov.yk.ca/metallogeny/selwyn/intro.html. Last accessed January, 2007.

Hitchon, B. and Krouse, H.R. 1972. Hydrogeochemistry of surface waters of the Mackenzie River drainage basin, Canada—III. Stable isotopes of oxygen, carbon and sulphur. Geochimica et Cosmochimica Acta 36: 1337–1357.

Horita, J., Wesolowski, D., and Cole, D. 1993. The activity-composition relationship of oxygen and hydrogen isotopes in aqueous salt solutions: I. Vapor-liquid water equilibration of single salt solutions from 50 to 100 ^{o}C.: Geochimica et Cosmochimica Acta 57: 2797-2817.

Huntoon, P.W. 1981. Fault controlled ground-water circulation under the Colorado River, Marble Canyon, Arizona. Ground Water 19: 20–27.

Hyndman, R.D., Fluck, P., Mazzotti, S., Lewis, T.J., Ristau, J., and Leonard, L. 2005. Current tectonics of the northern Canadian Cordillera. Canadian Journal of Earth Sciences 42: 1117-1136.

IAEA, 2001. GNIP Maps and Animations, International Atomic Energy Agency, Vienna. Available at http://isohis.iaea.org. Last updated September 2002. Last accessed August 2006.

IAEA/WMO, 1998. Global Network of Isotopes in Precipitation. The GNIP Database. Released October 3rd, 1999. Available at http://isohis.iaea.org. Last accessed August 2006.

ICCM (International Council on Mining and Metals), 2005. Canada's mineral and energy resource assessments. Available at: http://www.icmm.com/casestudy.php?rcd=6. Last accessed on Feb. 7, 2006.

Igarashi, T., Hataya, R. and Oyama, T. 2003. Estimation of pyrite oxidation rate by sulfate ion discharged from a catchment. Journal of Geochemical Exploration 77: 151-165.

INAC (Indian and Northern Affairs Canada – Affaires indiennes et du Nord Canada), 2001. Petroleum Exploration in Northern Canada: A Guide to Oil and Gas Exploration and Potential - Chapter 2 – Mackenzie Valley, Southern Territories and Interior Plains. Available at http://ainc-inac.gc.ca/oil/bkgd/prospectus/index_e.html. Last accessed on Oct. 23, 2006.

Irwin, W.P. and Barnes, I. 1980. Tectonic relations of carbon dioxide discharges and easrthquakes. Journal of Geophysical Research 86(B6): 3115-3121.

ITIA (International Tungsten Industry Association), 2005. About Tungsten Resources. Available online at http://www.itia.org.uk/. Last accessed on April 10th, 2006.

Janes, S.D. 1998. Anisotropic groundwater migration in structurally deformed sedimentary bedrock terrains. American Association of Petroleum Geologist Bulletin 81:849–850.

Jefferson, C.W. and Spirito, W.A. (editors) 2003. Mineral and Energy Resource Assessment of the Tlogotsho Plateau, Nahanni Karst, Ragged Ranges and Adjacent Areas Under Consideration for Expansion of Nahanni National Park Reserve, Northwest Territories. Geological Survey of Canada, Open File 1686.

Kacandes, G.H. and Grandstaff, D.E. 1989. Differences between geothermal and experimentally derived fluids: how well do hydrothermal experiments model the composition of geothermal reservoir fluids? Geochimica et Cosmochimica Acta 53: 343-358.

Kelley, K.D. and Taylor, C.D. 1997. Environmental geochemistry of shale-hosted Ag-Pb-Zn massive sulfide deposits in northwest Alaska: natural background concentrations of metals in water from mineralized zones. Applied Geochemistry 12: 397-409.

Kharaka, Y.K., Gunter, W.D., Aggarwal, P.K., Perkins, E.H. and Debraal, J.D. 1988. SOLMINEQ.88: A computer program for Geochemical Modeling of Water-Rock Interactions. USGS Water Resources Investigation report 88-4227 and Alberta Research Council Information Series No. 104.

Kharaka, Y.K., Mariner, R.H., 1989. Chemical geothermometers and their application to formation waters from sedimentary basins. *In*: Naeser, N.D., McCulloch, T. (Eds.), Thermal History of Sedimentary Basins. Springer Verlag, New York, pp. 99–117.

King, T.V.V. (editor) 1995. Environmental Considerations of Active and Abandoned Mine Lands: Lessons from Summitville, Colorado. U.S. Geological Survey Bulletin 2220, 43pp.

Kirste, D., de Caritat, P. and Dann, R. 2003. The application of the stable isotopes of sulfur and oxygen in groundwater sulfate to mineral exploration in the Broken Hill region of Australia. Journal of Geochemical Exploration 78-79: 81-84.

Land, L.S. and Prezbindowski, D.R. 1981. The origin and evolution of saline formation water, Lower Cretaceous carbonates, south-central Texas, U.S.A., Journal of Hydrology 54: 51-74.

Lewis, T.J., Hyndman, R.D. and Flück, P. 2003. Heat flow, heat generation, and crustal temperatures in the northern Canadian Cordillera. Journal of Geophysical Research, 108(B6): 2316-2334.

Leybourne, M.I., Goodfellow, W.D. and Boyle, D.R. 1998. Hydrogeochemical, isotopic, and rare earth element evidence for contrasting water-rock interactions at two undisturbed Zn-Pb massive sulphide deposits, Bathurst Mining Camp, N.B., Canada. Journal of Geochemical Exploration 64: 237-261.

Lopez, D.L. and Smith, L. 1995. Fluid flow in fault zones: Analysis of the interplay of convective circulation and topographically driven groundwater flow. Water Resources Research, 32: 3227-3235.

Mauthner, M.H.F., Mortensen, J.K., Groat, L.A. and Ercit, T.S. 1995. Geochronology of the Little Nahanni pegmatite group, Selwyn Mountains, southwestern Northwest Territories. Canadian Journal of Earth Sciences 32: 2090-2097.

Mayer, J.R., and Sharp, J.M., Jr. 1998. Fracture control of regional ground-water flow in a carbonate aquifer in a semi-arid region. Geological Society of America Bulletin 110(2): 269–283.

Mayo, A.L., Morris, T.H., Peltier, S., Petersen, E.C., Payne, K., Holman, L.S., Tingey, D., Fogel, T., Black, B.J., and Gibbs, T.D. 2003. Active and inactive groundwater flow systems: Evidence from a stratified, mountainous terrain. Geological Society of America Bulletin 115: 1456-1472.

Mayo, A.L., Muller, A.B., and Ralston, D.R. 1985. Hydrogeochemistry of the Meade thrust allochthon southeastern Idaho, and its relevance to the stratigraphic and structural groundwater flow control. Journal of Hydrology 76: 27–61.

McCrea, J.M. 1950. On the isotopic chemistry of carbonates and a paleotemperature scale. Journal of Chemical Physics 18: 849-857.

Michard, G. 1990. Behavior of major elements and some trace elements (Li, Rb, Cs, Sr, Fe, Mn, W, F) in deep hot waters from granitic areas. Chemical Geology 89: 117-134.

Milburn, D. (editor) 1996. Introduction. *In*: Proceedings of the hydro-ecology workshop on the arctic environmental strategy on water. Banff, May 1996.

Miller, W.R. 2002. Influence of Rock Composition on the Geochemistry of Stream and Spring Waters from Mountainous Watersheds in the Gunnison, Uncompahgre, and Grand Mesa National Forests, Colorado. U.S. Geological Survey Professional Paper 1667, 58 p.

Mingqi, W., Tianxiang, R., Yinhan, L., and Shuxing, L. 1995. Stream water, an ideal medium for rapidly locating polymetallic mineralization in forest-swamp terrain: a case study in the Da Hinggan Mts., northern Heilongjiang, China. Journal of Geochemical Exploration 55: 257-264.

Morrow, D.W. and Cook, D.G. 1987. The Prairie Creek Embayment and Lower Paleozoic Strata of the Southern Mackenzie Mountains. Geological Survey of Canada Memoir 412.

Morrow, D.W. and Miles, W.C. 2000. The Beaver Structure: a cross-strike discontinuity of possible crustal dimensions in the southern Mackenzie Fold Belt, Yukon and Northwest Territories, Canada. Bulletin of Canadian Petroleum Geology, 48: 19-29.

Mutlu, H. and Gulec, N. 1998. Hydrogeochemical outline of thermal waters and geochemistry applications in Anatoia (Turkey). Journal of Volcanology and Geothermal Research 85: 495-515.

NRCan (Natural Resources Canada), 1995. The National Atlas of Canada 5th edition: "Canada Permafrost" Sheet, MCR 4177. Available online at http://atlas.gc.ca/site/english/maps/archives/5thedition/environment/land/mcr4177. Last accessed on Apr. 8, 2006.

NEB (National Energy Board), 1996. A Natural Gas Resource Assessment of Southeast Yukon and Northwest Territories, Canada; Report by National Energy Board, June 1996, 140p.

Nelson, S.A. 2003. Magmas, Igneous Rocks, Volcanoes and Plutons. Tulane University. Available at: http://www.tulane.edu/~sanelson/geol111/igneous.htm. Last accessed on August 25, 2005.

Nelson, S.T., Dettman D., 2001. Improving hydrogen isotope ratio measurements for on-line chromium reduction systems. Rapid Communications in Mass Spectrometry 15: 2301-2306.

Nesbitt, H.W. and Young, G.M., 1984. Prediction of some weathering trends of plutonic and volcanic rocks based on thermodynamic and kinetic considerations. Geochimica et Cosmochimica Acta, 48: 1523-1534.

Newton R. C. and Manning C. E. (2000a) Quartz solubility in H_2O–NaCl and H_2O–CO_2 solutions at deep crust–upper mantle pressures and temperatures: 2–15 kbar and 500–900 8C. Geochimica et Cosmochimica Acta 64: 2993–3005.

Newton R. C. and Manning C. E. (2000b) Metasomatic phase relations in the system CaO–MgO–SiO_2–H_2O–NaCl at high temperature and pressures. International Geological Review 42: 152–162.

Nieva, D., Nieva, R., 1987. Developments in geothermal energy in Mexico: Part 12. A cationic composition geothermometer for prospection of geothermal resources. Heat Recovery Systems CHP 7: 243– 258.

Nordstrom, D.K., Ball, J.W., Donahoe, R.J. and Whittemore, D. 1989. Groundwater chemistry and water-rock interactions at Stripa. Geochimica et Cosmochimica Acta 53: 1727-1740.

Ohmoto, H., Kaiser, C.J. and Geer, K.A., 1990. Systematics of sulphur isotopes in recent marine sediments and ancient sediment-hosted basemetal deposits. In: Herbert, H.K. and Ho, S.E., Editors, 1990. Stable Isotopes and Fluid Processes in Mineralization. Publication **V**ol. 23, University of Western Australia, Geology Department and Extension Service, Perth, West. Aust., Australia, pp. 70–120.

Ohkuni, T., Sakamoto, F., Kozai, N., Ozaki, T., Yoshida, T., Narumi, I., Wakai, E., Sakai, T. and Francis, A. 2004. Mechanisms of arsenic immobilization in a biomat from mine discharge water. Chemical Geology 212: 279-290.

Okulitch, A.V. (compiler) 2005. Bedrock Geology, Redstone River, Yukon Territory, Northwest Territories; Geological Survey of Canada, Map NP-9/10-G, scale 1:1 000 000 (National Earth Science Series, Geological Atlas).

Olias, M., Nieto, J.M., Sarmiento, A.M., Ceron, J.C. and Canovas, C.R. 2004. Seasonal water quality variations in a river affected by acid mine drainage: the Odiel River (South West Spain). Science of the Total Environment 333: 267-281.

O'Neil, J.R., Adami, L.H., Epstein, S. 1975. Revised value for the ^{18}O fractionation factor between CO_2 and water at 25^{o}C: Journal of Research of the U.S. Geological Survey 3: 623-624.

Pang, Z-H. and Reed, M. 1998. Theoretical chemical thermometry on geothermal waters: Problems and methods. Geochimica et Cosmochimica Acta Vol. 62: 1083-1091.

Parks Canada. 2001. Nahanni National Park Reserve. Natural Resource Conservation Section, Parks Canada, Winnipeg. 9pp.

Pellicori, D.A., Gammons, C.H. and Poulson, S.R. 2005. Geochemistry and stable isotope composition of the Berkeley pit lake and surrounding mine waters, Butte, Montana. Applied Geochemistry 20: 2116-2137.

Peng, H., Mayer, B., Harris, S. and Krouse, R. 2004. A 10-yr record of stable isotope ratios of hydrogen and oxygen in precipitation at Calgary, Alberta, Canada. Tellus 56B:147-159.

Pentecost, A. 2003. Cyanobacteria associated with hot spring travertines. Canadian Journal of Earth Sciences 40: 1447-1457.

Plumlee, G.S., Smith, K.S. and Ficklin, W.H. 1994. Geoenvironmental Models of Mineral Deposits and Geology-Based Mineral-Environmental Assessments of Public Lands. U.S. Geological Survey Open-File Report 94-203, 9 p.

Plumlee, G.S. 1999. The environmental geology of mineral deposits; *in* Filipek, L.H., Plumlee, G.S. (editors) 1999. The environmental geochemistry of mineral deposits, Part A: Processes, techniques and Health Issues: Society of Economic Geologists, Inc., Reviews in Economic Geology, vol. 6A, pp. 71-116.

Plumlee, G.S. and Logsdon, M.J. 1999. An Earth-System Toolkit for Environmentally Friendly Mineral Resource Development; *In* Filipek, L.H., Plumlee, G.S. (editors) 1999.

The environmental geochemistry of mineral deposits, Part A: Processes, techniques and Health Issues: Society of Economic Geologists, Inc., Reviews in Economic Geology, vol. 6A, pp. 1-27.

Plumlee, G.S., Smith, K.S., Montour, M.R., Ficklin, W.H. and Mosier, E.L. 1999. Geological Controls on the Composition of Natural Waters and Mine Waters. *In* Filipek, L.H., Plumlee, G.S. (editors) 1999. The environmental geochemistry of mineral deposits, Part B: Case Studies and Research Topics: Society of Economic Geologists, Inc., Reviews in Economic Geology, vol. 6B, pp. 373-432.

Rasmussen, K.L., Mortensen, J.K., Falck, H. 2006. Geochronological and lithogeochemical studies of intrusive rocks in the Nahanni region, southwestern Northwest Territories and southeastern Yukon. *In*: Yukon Exploration and Geology 2005, D.S. Edmond, G.D. Bradshaw, L.L. Lewis and L.H. Weston (editors), Yukon Geological Survey, p. 287-298.

Robinson, J. and Irwin, D. (compilers). 2000. Mineral Deposits and Petroleum Resources of the Northwest Territories (map). Minerals, Oil and Gas Division; Department of Resources, Wildlife and Economic Development; Government of the Northwest Territories. Available at http://www.enr.gov.nt.ca/maps/index.htm. Last accessed on Oct. 26, 2006.

Rosenbaum, J. and Sheppard, S.M.F. 1986. An isotopic study of siderites, dolomites and ankerites at high temperatures. Geochimica et Cosmochimica Acta Vol 50: 1147-1150.

Runnells, D.D. (chairman) 1984. Workshop 3: Hydrochemistry in Mineral Exploration. Journal of Geochemical Exploration 21: 129-131.

Sanden, P., Karlsson, S., Duker, A., Ledin, A., and Lundman, L. 1997. Variations in hydrochemistry, trace metal concentration and transport during a rain storm event in a small catchment. Journal of Geochemical Exploration 58: 145-155.

Seal II, R.R. and Foley, N.K. (editors) 2002. Progress on Geoenvironmental Models for Selected Mineral Deposit Types. U.S. Geological Survey Open File Report 02-195, Chapters A-L.

Sidenko, N.V. and Sherriff, B.L. 2005. The attenuation of Ni, Zn and Cu, by secondary Fe phases of different crystallinity from surface and ground water of two sulfide mine tailings in Manitoba, Canada. Applied Geochemistry 20: 1180-1194.

Siegel, D.I. and Ericson, D.W. 1980. Hydrology and Water Quality of the Copper-Nickel Study Region, Northeastern Minnesota. U.S. Geological Survey Water-Resource Investigation 80-739, 87 p.

Smith, L. and Forster, C. 1990. Fluid flow, heat transfer, and thermal springs in mountainous terrain, Memoirs of the 22nd Congress of International Association of Hydrologists (IAH), Lauzanne, Switzerland, August 27 – September 1, 1990, 22, pp. 616–623,

Smith K.S. and Huyck, H.L.O. 1999. An overview of the abundance, relative mobility, bioavailability, and human toxicity of metals. *In* Filipek, L.H., Plumlee, G.S. (editors) 1999. The environmental geochemistry of mineral deposits, Part A: Processes, techniques and Health Issues: Society of Economic Geologists, Inc., Reviews in Economic Geology, vol. 6A, pp. 29-70.

Sofer, Z.a.G.J.R. 1972. Activities and concentrations of oxygen-18 in concentrated aqueous salt solutions: analytical and geochemical implications: Earth and Planetary Science Letters 15: 232-238.

Souther, J.G. and Halstead, E.C. 1973. Mineral and Thermal Waters of Canada. Geological Survey of Canada, Department of Energy, Mines and Resources, Paper 73-18.

Staple, T., and Wall, G. 1996. Climate Change and Recreation in Nahanni National Park Reserve. Canadian Geographer, Summer 1996, 40-2.

Steele, K.F. and Dilday, T.F. 1985. Hydrogeochemical exploration for Mississippi Valley-type deposits, Arkansas, USA. Journal of Geochemical Exploration 23: 71-79.

Stober, I. And Bucher, K. 2005. The upper continental crust, an aquifer and its fluid: hydraulic and chemical data from 4 km depth in fractured crystalline basement rocks at the KTB test site. Geofluids 5:8-19.

Stott, D.F. 1982. Lower Cretaceous Fort St. John Group and Upper Cretaceous Dunvegan Formation of the foothills and plains of Alberta, British Columbia, District of Mackenzie and Yukon Territory; Geological Survey of Canada, Bulletin 328, 124p.

Stumm, W. and Morgan, J.J. 1981. Aquatic Chemistry: An Introduction Emphasizing Chemical Equilibria in Natural Waters. © John and Wiley Sons, Inc.

Tole, M.P., Armannsson, H., Pang, Z., Arnorsson, S., 1993. Fluid/ mineral equilibrium calculations for geothermal fluids and chemical geothermometry. Geothermics 22: 17–37.

Tonani, F., 1980. Some remarks on the application of geochemical techniques exploration. Proceedings, Advances in European Geothermal Research, 2nd Symposium, Strasbourg, pp. 428–443.

Tosiani, T., Loubet, M., Viers, J., Valladon, M., Tapia, J., Marrero, S., Yanes, C., Ramirez, A. and Dupre, B. 2004. Major and trace elements in river-borne materials from the Cuyuni basin (southern Venezuela): evidence for organo-colloidal control on the dissolved load and element redistribution between the suspended and dissolved load. Chemical Geology 211: 305-334.

Truesdell, A.H., 1976. Summary of Section III. Geochemical techniques in exploration. Proceedings, Second United Nations Symposium on the Development and Use of Geothermal Resources, San Francisco, pp. 53–79.

UNEP-WCMC (United Nations Environment Program World Conservation Monitoring Center), 2002. "World Heritage Sites – Nahanni National Park Reserve, Canada, NWT." Available at: http://www.unep-wcmc.org/. First published in 1982, last updated 2002. Last accessed on Feb. 2nd, 2006.

Van Everdingen, R.O. 1972. Thermal and Mineral Springs in the Southern Rocky Mountains of Canada. Water Management Service, Environment Canada, 151p.

Van Stempvoort, D.R. and Krouse, H.R. 1994. Controls of d18O in sulphate: Review of Geochemistry of Sulphide Oxidation. In: Alpers, C.N., Blowes, D.W. (Eds) American Chemical Society Symposium Series 550: 446-480.

Verplanck, P.L., Nordstrom, D.K., Taylor, H.E. and Kimball, B.A. 2004. Rare earth element partitioning between hydrous ferric oxides and acid mine water during iron oxidation. Applied Geochemistry 19: 1339-1354.

Walther, J. V. and Orville, P. M. 1983. The extraction-quench technique for determination of the thermodynamic properties of solute complexes. Application to quartz solubility in fluid mixtures. American Mineralogist 68: 731–741.

Wanty, R.B., Berger, B.R., Tuttle, M.L., Briggs, P.H., Meier, A.L., and Crock, J.G. 2006. Hydrogeochemical Investigations in the Osgood Mountains, North-Central Nevada. U.S. Geological Survey Bulletin 2210-B.

Welhan, J.A., Poreda, R., Lupton, J.E. and Craig, H. 1979. Gas Chemistry and Helium Isotopes at Cerro Prieto. Geothermics 8: 241-244.

Welhan, J.A., Poreda, R.J., Rison, W. and Craig, H. 1988. Helium isotopes in geothermal and volcanic gases of the Western United States, I. Regional variability and magmatic origin. Journal of Volcanology and Geothermal Research 34: 185-199.

Whitfield, P.H., Whitley, W., Wade, N.L., and Regnier, R. 1996. Controls on chemistry of Yukon streams during winter baseflow. *In:* Proceedings of the hydro-ecology workshop on the arctic environmental strategy action on water. Banff, May 1996.

Whiticar, M.J. 1999. Carbon and hydrogen isotope systematics of bacterial formation and oxidation of methane. Chemical Geology 161: 291-314.

Wiken, E.B. 1986. Terrestrial Ecozones of Canada. Ecological Land Classification, Series No. 19. Environment Canada. Hull, Quebec. 26pp. + map.

Woodsworth, G.J., Anderson, R.G. and Armstrong, R.L., 1991. Plutonic regimes. *In:* Geology of the Cordilleran Orogen in Canada, GSC Geology of Canada, H. Gabrielse and C.J. Yorath (eds.), no. 4, p. 491-531.

Worden, R.H. 1996. Controls on halogen concentrations in sedimentary formation waters. Mineral. Mag. 60:259-274.

Xilai, Z., Armannsson, H., Yongle, Li., Hanxue, Q. 2002. Chemical equilibria of thermal waters for the application of geothermometers from the Guanzhong basin, China. Journal of Volcanology and Geothermal Research, Vol. 113, 119-127.

Yukon Geological Survey. 1996. 105I – Nahanni River, Yukon GEOPROCESS File, Scale 1:250 000 map. Open File 2002. Available at: http://www.geology.gov.yk.ca/publications/openfile/2002/of2002_8d_geoprocess_file/documents/map_specific/105i.pdf. Last accessed Oct. 23, 2006.

Zolotarev, V.G. 1984. Formation of geochemical fields of concentration in the thermal gradient fields of intrusive bodies. Journal of Geochemical Exploration, 21: 229-237.

APPENDIX 4

Digital geoscience database: A contribution to the mineral and energy resource assessment of the Greater Nahanni Ecosystem, Northwest Territories

D. Lemkow, J.R. Harris, and T. Slack (Compilers)
Geological Survey of Canada, 601 Booth Street, Ottawa, Ontario K1A 0E8

Appendix 4 contains the 2-D GIS database with over 200 geoscience data sets in shapefile format as well as grid, images, and excel tables, which provide a scientific framework for the Greater Nahanni Ecosystem and immediate area. The data sets were compiled from scientific or various surveys and research studies conducted for MERA 2 but include data from MERA 1 as well as from other public sources. Data sets include geochemistry (stream, spring, whole rock, and isotope), geophysics (aeromagnetic, radiometric, and gravity), geology (bedrock and surficial), structural, mineral deposit, base, watershed, and digital elevation and Landsat imagery. A metadata file is included. This can be used with any software that recognizes shape file formats. This database was created using ESRI ArcMap version 9.2. Some of ESRI files e.g. '.lyr' files will not open in earlier versions.

The data are located on the DVD in the directory
\Appendix_4

Lemkow, D., Harris, J.R., and Slack, T., 2007, Appendix 4. Digital geoscience database: A contribution to the Mineral and Energy Resource Assessment of the greater Nahanni ecosystem, Northwest Territories, *in* Mineral and Energy Resource Assessment of the Greater Nahanni Ecosystem Under Consideration for the Expansion of the Nahanni National Park Reserve, Northwest Territories, (ed.) D.F. Wright, D. Lemkow, and J.R. Harris; Geological Survey of Canada, Open File 5344.